



*pharmaceutics*

Special Issue Reprint

---

# Kinase Inhibitor for Cancer Therapy

---

Edited by  
Francesca Musumeci

[mdpi.com/journal/pharmaceutics](https://mdpi.com/journal/pharmaceutics)



# **Kinase Inhibitor for Cancer Therapy**



# **Kinase Inhibitor for Cancer Therapy**

Editor

**Francesca Musumeci**



Basel • Beijing • Wuhan • Barcelona • Belgrade • Novi Sad • Cluj • Manchester

*Editor*

Francesca Musumeci  
Department of Pharmacy  
University of Genoa  
Genoa  
Italy

*Editorial Office*

MDPI  
St. Alban-Anlage 66  
4052 Basel, Switzerland

This is a reprint of articles from the Special Issue published online in the open access journal *Pharmaceutics* (ISSN 1999-4923) (available at: [www.mdpi.com/journal/pharmaceutics/special\\_issues/Kinase\\_Inhibitor\\_Cancer](http://www.mdpi.com/journal/pharmaceutics/special_issues/Kinase_Inhibitor_Cancer)).

For citation purposes, cite each article independently as indicated on the article page online and as indicated below:

Lastname, A.A.; Lastname, B.B. Article Title. <i>Journal Name</i> <b>Year</b> , <i>Volume Number</i> , Page Range.
--

**ISBN 978-3-7258-1290-5 (Hbk)**

**ISBN 978-3-7258-1289-9 (PDF)**

**[doi.org/10.3390/books978-3-7258-1289-9](https://doi.org/10.3390/books978-3-7258-1289-9)**

© 2024 by the authors. Articles in this book are Open Access and distributed under the Creative Commons Attribution (CC BY) license. The book as a whole is distributed by MDPI under the terms and conditions of the Creative Commons Attribution-NonCommercial-NoDerivs (CC BY-NC-ND) license.

# Contents

**Francesca Musumeci and Silvia Schenone**

Unlocking Potential and Limits of Kinase Inhibitors: The Highway to Enhanced Cancer Targeted Therapy

Reprinted from: *Pharmaceutics* **2024**, *16*, 625, doi:10.3390/pharmaceutics16050625 . . . . . 1

**Jieun Bang, Mihyeon Jun, Soyun Lee, Hyuk Moon and Simon Weonsang Ro**

Targeting EGFR/PI3K/AKT/mTOR Signaling in Hepatocellular Carcinoma

Reprinted from: *Pharmaceutics* **2023**, *15*, 2130, doi:10.3390/pharmaceutics15082130 . . . . . 4

**Patrycja Wińska, Monika Wielechowska, Mirosława Koronkiewicz and Paweł Borowiecki**

Synthesis and Anticancer Activity of Novel Dual Inhibitors of Human Protein Kinases CK2 and PIM-1 †

Reprinted from: *Pharmaceutics* **2023**, *15*, 1991, doi:10.3390/pharmaceutics15071991 . . . . . 21

**Rebeca Carrión-Marchante, Celia Pinto-Díez, José Ignacio Klett-Mingo, Esther Palacios, Miriam Barragán-Usero, M. Isabel Pérez-Morgado, et al.**

An Aptamer against MNK1 for Non-Small Cell Lung Cancer Treatment

Reprinted from: *Pharmaceutics* **2023**, *15*, 1273, doi:10.3390/pharmaceutics15041273 . . . . . 47

**Ana Monfort-Vengut and Guillermo de Cárcer**

Lights and Shadows on the Cancer Multi-Target Inhibitor Rigosertib (ON-01910.Na)

Reprinted from: *Pharmaceutics* **2023**, *15*, 1232, doi:10.3390/pharmaceutics15041232 . . . . . 66

**Amineh Ghaderi, Mohammad-Ali Okhovat, Jemina Lehto, Luigi De Petris,**

**Ehsan Manouchehri Doulabi, Parviz Kokhaei, et al.**

A Small Molecule Targeting the Intracellular Tyrosine Kinase Domain of ROR1 (KAN0441571C) Induced Significant Apoptosis of Non-Small Cell Lung Cancer (NSCLC) Cells

Reprinted from: *Pharmaceutics* **2023**, *15*, 1148, doi:10.3390/pharmaceutics15041148 . . . . . 82

**Andrea Rodríguez-Agustín, Víctor Casanova, Judith Grau-Expósito, Sonsoles Sánchez-**

**Palomino, José Alcamí and Núria Climent**

Immunomodulatory Activity of the Tyrosine Kinase Inhibitor Dasatinib to Elicit NK Cytotoxicity against Cancer, HIV Infection and Aging

Reprinted from: *Pharmaceutics* **2023**, *15*, 917, doi:10.3390/pharmaceutics15030917 . . . . . 98

**Marina Ferreira Candido, Mariana Medeiros, Luciana Chain Veronez, David Bastos,**

**Karla Laissa Oliveira, Julia Alejandra Pezuk, et al.**

Drugging Hijacked Kinase Pathways in Pediatric Oncology: Opportunities and Current Scenario

Reprinted from: *Pharmaceutics* **2023**, *15*, 664, doi:10.3390/pharmaceutics15020664 . . . . . 121

**Federica Poggialini, Chiara Vagaggini, Annalaura Brai, Claudia Pasqualini, Emmanuele Crespan, Giovanni Maga, et al.**

Biological Evaluation and In Vitro Characterization of ADME Profile of In-House Pyrazolo[3,4-*d*]pyrimidines as Dual Tyrosine Kinase Inhibitors Active against Glioblastoma Multiforme

Reprinted from: *Pharmaceutics* **2023**, *15*, 453, doi:10.3390/pharmaceutics15020453 . . . . . 208

**Chunying Peng, Katrin Rabold, Mihai G. Netea, Martin Jaeger and Romana T. Netea-Maier**

Influence of Lenvatinib on the Functional Reprogramming of Peripheral Myeloid Cells in the Context of Non-Medullary Thyroid Carcinoma

Reprinted from: *Pharmaceutics* **2023**, *15*, 412, doi:10.3390/pharmaceutics15020412 . . . . . 223

<b>Samantha Sabetta, Davide Vecchiotti, Letizia Clementi, Mauro Di Vito Nolfi, Francesca Zazzeroni and Adriano Angelucci</b> Comparative Analysis of Dasatinib Effect between 2D and 3D Tumor Cell Cultures Reprinted from: <i>Pharmaceutics</i> <b>2023</b> , <i>15</i> , 372, doi:10.3390/pharmaceutics15020372 . . . . .	240
<b>Antonios G. X. Trochopoulos, Yana Ilieva, Alexander D. Kroumov, Lyudmila L. Dimitrova, Ivanka Pencheva-El Tibi, Stanislav Philipov, et al.</b> Micellar Curcumin Substantially Increases the Antineoplastic Activity of the Alkylphosphocholine Erufosine against TWIST1 Positive Cutaneous T Cell Lymphoma Cell Lines Reprinted from: <i>Pharmaceutics</i> <b>2022</b> , <i>14</i> , 2688, doi:10.3390/pharmaceutics14122688 . . . . .	253
<b>Andrea Astolfi, Francesca Milano, Deborah Palazzotti, Jose Brea, Maria Chiara Pismataro, Mariangela Morlando, et al.</b> From Serendipity to Rational Identification of the 5,6,7,8-Tetrahydrobenzo[4,5]thieno[2,3- <i>d</i> ]pyrimidin-4(3 <i>H</i> )-one Core as a New Chemotype of AKT1 Inhibitors for Acute Myeloid Leukemia Reprinted from: <i>Pharmaceutics</i> <b>2022</b> , <i>14</i> , 2295, doi:10.3390/pharmaceutics14112295 . . . . .	274
<b>Amineh Ghaderi, Wen Zhong, Mohammad Ali Okhovat, Johanna Aschan, Ann Svensson, Birgitta Sander, et al.</b> A ROR1 Small Molecule Inhibitor (KAN0441571C) Induced Significant Apoptosis of Mantle Cell Lymphoma (MCL) Cells Reprinted from: <i>Pharmaceutics</i> <b>2022</b> , <i>14</i> , 2238, doi:10.3390/pharmaceutics14102238 . . . . .	290
<b>Michael E. Stokes, Matthew D. Surman, Veronica Calvo, David Surguladze, An-Hu Li, Jennifer Gasperek, et al.</b> Optimization of a Novel Mandelamide-Derived Pyrrolopyrimidine Series of PERK Inhibitors Reprinted from: <i>Pharmaceutics</i> <b>2022</b> , <i>14</i> , 2233, doi:10.3390/pharmaceutics14102233 . . . . .	303
<b>Mina Ardestani, Zahra Khorsandi, Fariba Keshavarzipour, Siavash Iravani, Hojjat Sadeghi-Aliabadi and Rajender S. Varma</b> Heterocyclic Compounds as Hsp90 Inhibitors: A Perspective on Anticancer Applications Reprinted from: <i>Pharmaceutics</i> <b>2022</b> , <i>14</i> , 2220, doi:10.3390/pharmaceutics14102220 . . . . .	323
<b>Lucie Čermáková, Jakub Hofman, Lenka Laštovičková, Lucie Havlíčková, Ivona Špringrová, Eva Novotná and Vladimír Wsól</b> Bruton's Tyrosine Kinase Inhibitor Zanubrutinib Effectively Modulates Cancer Resistance by Inhibiting Anthracycline Metabolism and Efflux Reprinted from: <i>Pharmaceutics</i> <b>2022</b> , <i>14</i> , 1994, doi:10.3390/pharmaceutics14101994 . . . . .	348
<b>Suhair Sunoqrot, Sundos Aliyeh, Samah Abusulieh and Dima Sabbah</b> Vitamin E TPGS-Poloxamer Nanoparticles Entrapping a Novel PI3K $\alpha$ Inhibitor Potentiate Its Activity against Breast Cancer Cell Lines Reprinted from: <i>Pharmaceutics</i> <b>2022</b> , <i>14</i> , 1977, doi:10.3390/pharmaceutics14091977 . . . . .	364
<b>Men Thi Hoai Duong and Hee-Chul Ahn</b> Fragment-Based and Structural Investigation for Discovery of JNK3 Inhibitors Reprinted from: <i>Pharmaceutics</i> <b>2022</b> , <i>14</i> , 1900, doi:10.3390/pharmaceutics14091900 . . . . .	382
<b>Felipe Pantoja Mesquita, Pedro Filho Noronha Souza, Emerson Lucena da Silva, Luina Benevides Lima, Lais Lacerda Brasil de Oliveira, Caroline Aquino Moreira-Nunes, et al.</b> Kinase Inhibitor Screening Displayed <i>ALK</i> as a Possible Therapeutic Biomarker for Gastric Cancer Reprinted from: <i>Pharmaceutics</i> <b>2022</b> , <i>14</i> , 1841, doi:10.3390/pharmaceutics14091841 . . . . .	394

<b>Igor Valentim Barreto, Caio Bezerra Machado, Davi Benevides Almeida, Flávia Melo Cunha de Pinho Pessoa, Renan Brito Gadelha, Laudreísa da Costa Pantoja, et al.</b> Kinase Inhibition in Multiple Myeloma: Current Scenario and Clinical Perspectives Reprinted from: <i>Pharmaceutics</i> <b>2022</b> , <i>14</i> , 1784, doi:10.3390/pharmaceutics14091784 . . . . .	<b>405</b>
<b>Lorenzo Monteleone, Barbara Marengo, Francesca Musumeci, Giancarlo Grossi, Anna Carbone, Giulia E. Valenti, et al.</b> Anti-Survival Effect of SI306 and Its Derivatives on Human Glioblastoma Cells Reprinted from: <i>Pharmaceutics</i> <b>2022</b> , <i>14</i> , 1399, doi:10.3390/pharmaceutics14071399 . . . . .	<b>421</b>
<b>Juan Carlos Lacal, Rosario Perona, Javier de Castro and Arancha Cebrián</b> Choline Kinase $\alpha$ Inhibitors MN58b and RSM932A Enhances the Antitumor Response to Cisplatin in Lung Tumor Cells Reprinted from: <i>Pharmaceutics</i> <b>2022</b> , <i>14</i> , 1143, doi:10.3390/pharmaceutics14061143 . . . . .	<b>433</b>
<b>Ahmed M. Shawky, Faisal A. Almalki, Ashraf N. Abdalla, Ahmed H. Abdelazeem and Ahmed M. Gouda</b> A Comprehensive Overview of Globally Approved JAK Inhibitors Reprinted from: <i>Pharmaceutics</i> <b>2022</b> , <i>14</i> , 1001, doi:10.3390/pharmaceutics14051001 . . . . .	<b>446</b>





Editorial

# Unlocking Potential and Limits of Kinase Inhibitors: The Highway to Enhanced Cancer Targeted Therapy

Francesca Musumeci \* and Silvia Schenone

Department of Pharmacy, University of Genoa, Viale Benedetto XV, 3, 16132 Genoa, Italy; silvia.schenone@unige.it  
\* Correspondence: francesca.musumeci@unige.it

Kinases are a family of enzymes comprising over five hundred members, which, when overexpressed or hyperactivated, are implicated in the pathogenesis of numerous hematological and solid cancers. This evidence has spurred extensive research into molecules with targeted anti-cancer activity and led to the approval of the first monoclonal antibody, trastuzumab, in 1998 and the first small-molecule kinase inhibitor, imatinib, in 2001. Since then, the search for new kinase inhibitors has attracted the attention of scientists, as they can provide a powerful approach to mitigating the side effects associated with traditional antineoplastic agents and enabling convenient oral administration in the case of small-molecule inhibitors. The impact of targeted cancer therapy is underscored by the approval of over 70 kinase inhibitors, with approximately 25 new compounds emerging in the past five years [1,2]. Traditionally, small-molecule kinase inhibitors are classified into six types: type I inhibitors, which target the ATP-binding pocket of active kinases; type II inhibitors, which target the ATP-binding pocket of inactive kinases; type III inhibitors, allosteric inhibitors that bind a site adjacent to the ATP-binding pocket; type IV inhibitors, allosteric inhibitors that bind a site distant from the ATP-binding pocket; type V inhibitors, bivalent inhibitors; and type VI inhibitors, covalent inhibitors. Most currently approved kinase inhibitors belong to types I and II. Some examples of other types of kinase inhibitors include trametinib (a type III allosteric inhibitor targeting MEK1/2), asciminib (a type IV allosteric inhibitor targeting Bcr-Abl), and afatinib (a type VI covalent inhibitor targeting EGFR).

The fervent interest in kinase inhibitors from the academic and industrial world points toward a promising expansion of this field in the coming decades. This enthusiasm is driven by the untapped potential of targeting kinases alongside the pressing need to address current limitations.

Notably, despite significant progress, only approximately 20% of the kinome has been targeted to date, indicating vast opportunities for discovering novel treatment options once the roles of additional kinases are elucidated. Furthermore, ongoing research points out allosteric inhibition as a powerful approach to reduce adverse effects and fight resistance to the drug due to mutations in the active site of the enzyme. In this context, developing novel types of allosteric inhibitors, such as compounds targeting pseudokinase domains or extracellular domains, is a promising new route [2,3].

Regarding the current limitations of kinase inhibitors, major issues can be identified in the onset of mutations that confer drug resistance and the general suboptimal pharmacokinetic profiles exhibited by small-molecule kinase inhibitors.

Drug resistance poses a significant challenge to the long-term efficacy of kinase inhibitors, as treatment with most approved drugs is eventually interrupted following prolonged use. Resistance can arise through various mechanisms, with gene mutations being the most prevalent cause. Mutations in the catalytic domain frequently confer resistance to type I and II kinase inhibitors. This evidence encouraged, and is still encouraging, the search for new efficacious approaches [4].

First, the most intuitive strategy plans the design and synthesis of compounds that are also active against resistant isoforms. The approval of ponatinib is a pertinent example,

**Citation:** Musumeci, F.; Schenone, S. Unlocking Potential and Limits of Kinase Inhibitors: The Highway to Enhanced Cancer Targeted Therapy. *Pharmaceutics* **2024**, *16*, 625. <https://doi.org/10.3390/pharmaceutics16050625>

Received: 12 April 2024  
Revised: 29 April 2024  
Accepted: 30 April 2024  
Published: 7 May 2024



**Copyright:** © 2024 by the authors. Licensee MDPI, Basel, Switzerland. This article is an open access article distributed under the terms and conditions of the Creative Commons Attribution (CC BY) license (<https://creativecommons.org/licenses/by/4.0/>).

as it is a multitargeted covalent kinase inhibitor that is able to inhibit the T315I Bcr-Abl gatekeeper mutation.

Second, as previously mentioned, the development of allosteric inhibitors constitutes another exciting opportunity to bypass resistance related to mutations in the catalytic domain. In particular, combining an ATP-competitive inhibitor and an allosteric inhibitor often led to improved efficacy compared to the single-agent regimen [3].

Third, the development of antibody–drug conjugates (ADCs) has been highlighted. An ADC comprises a monoclonal antibody and cytotoxic agent attached by a linker. The rationale behind the design of this class of compounds lies in the synergy between the highly specific targeting ability of monoclonal antibodies and the potent cytotoxic activity of the attached agents. Gemtuzumab ozogamicin (Mylotarg<sup>®</sup>) was the first ADC approved by the FDA in 2000. Since then, about 15 ADCs have been released. Notably, Fam-trastuzumab deruxtecan (Enhertu<sup>®</sup>) is an ADC targeting the HER kinase and incorporates the topoisomerase I inhibitor DXd as its cytotoxic agent. It was approved in 2019 as a second-line treatment for patients with unresectable or metastatic HER2-positive breast cancer [5].

Fourth, a recent approach gaining attention is synthetic lethality, which exploits the concept that in certain tumors, the expression of two or more genes is altered, and targeting both synthetic lethal factors enables the selective killing of cancer cells. The most relevant example of synthetic lethality is the use of the poly(ADP-ribose) polymerase inhibitor olaparib in the treatment of breast cancer associated with BRCA1/2 mutations [6]. However, kinase inhibitors also present an opportunity to leverage the concept of synthetic lethality. For instance, cyclin-dependent kinases (CDKs) are being investigated as synthetic lethal players when combined with specific oncogenes, such as MYC, TP53, and RAS [7].

At the same time, the poor suboptimal pharmacokinetic profile generally associated with kinase inhibitors has prompted the search for efficient drug delivery systems. In this frame, nanoformulations offer an effective tool to improve the absorption, distribution, metabolism, and excretion (ADME) properties and, consequently, the bioavailability of kinase inhibitors. Nanocarriers include liposomes, micelles, gold and polymeric nanoparticles, bovine serum albumin, and metal–organic frameworks. Notably, the nanoparticle surface can be functionalized with specific ligands, such as antibodies or peptides, capable of recognizing particular proteins on the surface of cancer cells, thus facilitating active targeting. This approach enables the selective release of the drug to the neoplastic cells, thereby enhancing therapeutic efficacy while minimizing off-target effects. Moreover, nanodelivery represents an effective strategy for overcoming resistance mechanisms [8].

The Special Issue features a comprehensive overview of the latest developments in kinase inhibitor research across various fronts, including *in silico* studies, the synthesis and identification of new compounds, drug delivery methods, overcoming resistance mechanisms, the potential to target specific kinases or use selected inhibitors, and biological and pharmacokinetic evaluations. Herein, an overview of the most innovative articles is reported. Čermáková et al. (contribution 1) provided deep insight into the ability of Bruton's tyrosine kinase inhibitor zanubrutinib to modulate cancer resistance by inhibiting anthracycline metabolism and efflux, suggesting a new combination therapy including both the drugs. Sunoqrot et al. (contribution 2) proposed vitamin E TPGS-ploxamer nanoparticles to deliver the new PI3K $\alpha$  inhibitor R19 in breast cancer cell lines. The research carried out by the authors showed that the formulation possessed enhanced activity compared to R19 alone, good cancer cell selectivity, and high biocompatibility, paving the way for clinical translation. Poggialini et al. (contribution 3) performed a study to identify new candidates for glioblastoma (GBM) treatment since this tumor still has a poor prognosis. Starting from the in-house library of pyrazolo[3,4-*d*]pyrimidines, they performed extensive research, including enzymatic assays of Src/Bcr-Abl kinases, *in vitro* tests on four GBM cell lines, and a deep ADME evaluation that led to the discovery of a compound (namely derivative 5 of the paper) as a suitable candidate for *in vivo* evaluation. Sabetta et al. (contribution 4) analyzed the effect of dasatinib in 2D monolayer cultures of prostate cancer and glioblastoma cell lines and the corresponding 3D spheroids and

3D bioprinting models. Three-dimensional cell models better resemble tumor complexity associated with drug resistance than two-dimensional models and, for this reason, are gaining increasing attention in preclinical studies. In this work, the authors took a step forward in this field, identifying that the 3D bioprinted model utilizing an alginate–gelatin hydrogel was endowed with improved feasibility, reproducibility, and scalability than the classical 3D spheroid model.

Overall, this Special Issue offers a panoramic view of the current state of the field. Each contribution showcases the multifaceted approaches researchers are employing to unlock the power of kinase inhibition for cancer treatment. These studies contribute valuable data to the scientific community and pave the way for translating the findings into clinical applications.

**Conflicts of Interest:** The authors declare no conflicts of interest.

#### List of Contributions

1. Cermáková, L.; Hofman, J.; Laštovičková, L.; Havlíčková, L.; Špringrová, I.; Novotná, E.; Wsól, V. Bruton's Tyrosine Kinase Inhibitor Zanubrutinib Effectively Modulates Cancer Resistance by Inhibiting Anthracycline Metabolism and Efflux. *Pharmaceutics* **2022**, *14*, 1994. <https://doi.org/10.3390/PHARMACEUTICS14101994>.
2. Sunoqrot, S.; Aliyeh, S.; Abusulieh, S.; Sabbah, D. Vitamin E TPGS-Poloxamer Nanoparticles Entrapping a Novel PI3K $\alpha$  Inhibitor Potentiate Its Activity against Breast Cancer Cell Lines. *Pharmaceutics* **2022**, *14*, 1977. <https://doi.org/10.3390/PHARMACEUTICS14091977>.
3. Poggialini, F.; Vagaggini, C.; Brai, A.; Pasqualini, C.; Crespan, E.; Maga, G.; Perini, C.; Cabella, N.; Botta, L.; Musumeci, F.; et al. Biological Evaluation and In Vitro Characterization of ADME Profile of In-House Pyrazolo[3,4-*d*]pyrimidines as Dual Tyrosine Kinase Inhibitors Active against Glioblastoma Multiforme. *Pharmaceutics* **2023**, *15*, 453. <https://doi.org/10.3390/PHARMACEUTICS15020453>.
4. Sabetta, S.; Vecchiotti, D.; Clementi, L.; Di Vito Nolfi, M.; Zazzeroni, F.; Angelucci, A. Comparative Analysis of Dasatinib Effect between 2D and 3D Tumor Cell Cultures. *Pharmaceutics* **2023**, *15*, 472. <https://doi.org/10.3390/PHARMACEUTICS15020372>.

#### References

1. Attwood, M.M.; Fabbro, D.; Sokolov, A.V.; Knapp, S.; Schiöth, H.B. Trends in Kinase Drug Discovery: Targets, Indications and Inhibitor Design. *Nat. Rev. Drug Discov.* **2021**, *20*, 839–861. [CrossRef] [PubMed]
2. Roskoski, R. Properties of FDA-Approved Small Molecule Protein Kinase Inhibitors: A 2024 Update. *Pharmacol. Res.* **2024**, *200*, 107059. [CrossRef] [PubMed]
3. Lu, X.; Smaill, J.B.; Ding, K. New Promise and Opportunities for Allosteric Kinase Inhibitors. *Angew Chem. Int. Ed. Engl.* **2020**, *59*, 13764–13776. [CrossRef] [PubMed]
4. Zhong, L.; Li, Y.; Xiong, L.; Wang, W.; Wu, M.; Yuan, T.; Yang, W.; Tian, C.; Miao, Z.; Wang, T.; et al. Small Molecules in Targeted Cancer Therapy: Advances, Challenges, and Future Perspectives. *Signal Transduct. Target. Ther.* **2021**, *6*. [CrossRef]
5. Fu, Z.; Li, S.; Han, S.; Shi, C.; Zhang, Y. Antibody Drug Conjugate: The “Biological Missile” for Targeted Cancer Therapy. *Signal Transduct. Target. Ther.* **2022**, *7*, 93. [CrossRef] [PubMed]
6. Li, S.; Topatana, W.; Juengpanich, S.; Cao, J.; Hu, J.; Zhang, B.; Ma, D.; Cai, X.; Chen, M. Development of Synthetic Lethality in Cancer: Molecular and Cellular Classification. *Signal Transduct. Target. Ther.* **2020**, *5*, 241. [CrossRef] [PubMed]
7. Li, K.; You, J.; Wu, Q.; Meng, W.; He, Q.; Yang, B.; Zhu, C.; Cao, J. Cyclin-Dependent Kinases-Based Synthetic Lethality: Evidence, Concept, and Strategy. *Acta Pharm. Sin. B* **2021**, *11*, 2738–2748. [CrossRef] [PubMed]
8. Xu, W.; Ye, C.; Qing, X.; Liu, S.; Lv, X.; Wang, W.; Dong, X.; Zhang, Y. Multi-Target Tyrosine Kinase Inhibitor Nanoparticle Delivery Systems for Cancer Therapy. *Mater. Today Bio* **2022**, *16*, 100358. [CrossRef]

**Disclaimer/Publisher's Note:** The statements, opinions and data contained in all publications are solely those of the individual author(s) and contributor(s) and not of MDPI and/or the editor(s). MDPI and/or the editor(s) disclaim responsibility for any injury to people or property resulting from any ideas, methods, instructions or products referred to in the content.

Review

# Targeting EGFR/PI3K/AKT/mTOR Signaling in Hepatocellular Carcinoma

Jieun Bang <sup>†</sup>, Mihyeon Jun <sup>†</sup>, Soyun Lee <sup>†</sup>, Hyuk Moon and Simon Weonsang Ro <sup>\*</sup>

Department of Genetics and Biotechnology, College of Life Sciences, Kyung Hee University, Yongin-si 17104, Republic of Korea; qkdwldms612@khu.ac.kr (J.B.); mihyeonjun@khu.ac.kr (M.J.); lsoyun15@khu.ac.kr (S.L.); hmoon@khu.ac.kr (H.M.)

<sup>\*</sup> Correspondence: simonro@khu.ac.kr; Tel.: +82-31-201-5640; Fax: +82-31-204-8116

<sup>†</sup> These authors contributed equally to this work.

**Abstract:** Hepatocellular carcinoma (HCC) poses a significant global health concern, with its incidence steadily increasing. The development of HCC is a multifaceted, multi-step process involving alterations in various signaling cascades. In recent years, significant progress has been made in understanding the molecular signaling pathways that play central roles in hepatocarcinogenesis. In particular, the EGFR/PI3K/AKT/mTOR signaling pathway in HCC has garnered renewed attention from both basic and clinical researchers. Preclinical studies *in vitro* and *in vivo* have shown the effectiveness of targeting the key components of this signaling pathway in human HCC cells. Thus, targeting these signaling pathways with small molecule inhibitors holds promise as a potential therapeutic option for patients with HCC. In this review, we explore recent advancements in understanding the role of the EGFR/PI3K/AKT/mTOR signaling pathway in HCC and assess the effectiveness of targeting this signaling cascade as a potential strategy for HCC therapy based on preclinical studies.

**Keywords:** hepatocellular carcinoma; EGFR/PI3K/AKT/mTOR signaling; animal models; targeted therapy

**Citation:** Bang, J.; Jun, M.; Lee, S.; Moon, H.; Ro, S.W. Targeting EGFR/PI3K/AKT/mTOR Signaling in Hepatocellular Carcinoma. *Pharmaceutics* **2023**, *15*, 2130. <https://doi.org/10.3390/pharmaceutics15082130>

Academic Editors: Fabiana Quaglia and Xiaowei Zeng

Received: 25 July 2023

Revised: 7 August 2023

Accepted: 10 August 2023

Published: 14 August 2023



**Copyright:** © 2023 by the authors. Licensee MDPI, Basel, Switzerland. This article is an open access article distributed under the terms and conditions of the Creative Commons Attribution (CC BY) license (<https://creativecommons.org/licenses/by/4.0/>).

## 1. Introduction

Liver cancer presents a significant global health challenge due to its rising incidence and mortality rates. According to the World Health Organization, liver cancer accounted for approximately 800,000 deaths, positioning it as the fourth leading cause of cancer-related mortality [1]. Liver cancer comprises a heterogeneous group of malignant tumors with varying histologic characteristics and poor prognoses. Among these, hepatocellular carcinoma (HCC) represents the most prevalent primary liver cancer, accounting for approximately 80% of cases, followed by cholangiocarcinoma (CC), which contributes to 10–20% of primary liver cancers [2,3].

Existing treatment modalities for HCC offer limited success, with a considerably low 5-year survival rate. Surgical resection or local ablation therapy is typically favored for early-stage HCC; however, tumor recurrence occurs in approximately 70% of patients within 5 years [1,4]. For advanced HCC, systemic therapy is recommended as the standard treatment option, but the overall prognosis has been unsatisfactory [1,2].

HCC is a heterogeneous tumor with diverse phenotypic and genetic characteristics, and its tumorigenesis involves a range of molecular mechanisms [5,6]. Extensive research on the molecular pathogenesis of HCC has identified several critical signaling pathways involved in tumor initiation, promotion, and metastasis. These pathways include the mitogen-activated protein kinase/extracellular signal-regulated kinase (MAPK/ERK), Wnt/ $\beta$ -catenin, Hedgehog (HH), Hippo-YAP/TAZ, and phosphatidylinositol 3-kinase/AKT/mammalian target of rapamycin (PI3K/AKT/mTOR) signaling pathways. Recently,

we have extensively reviewed the roles of MAPK/ERK, Wnt/ $\beta$ -catenin, HH, and Hippo-YAP/TAZ signaling in HCC development together with preclinical and clinical studies targeting signaling pathways in HCC [7,8].

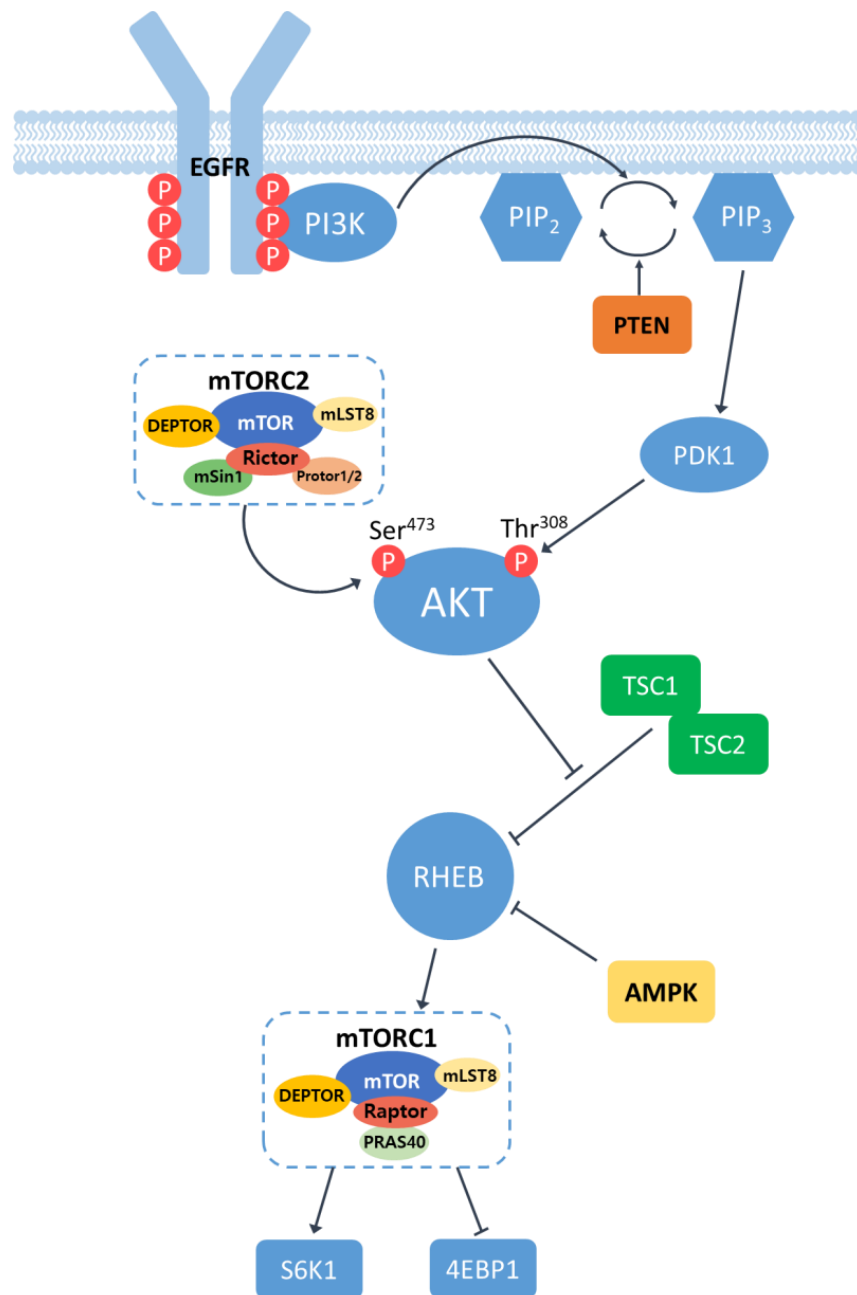
In this review, our aim is to provide an overview of the tumor-promoting effects exerted by the PI3K/AKT/mTOR signaling pathway in hepatocellular carcinoma (HCC), which is primarily triggered by the epidermal growth factor receptor (EGFR). Additionally, we discuss the results from recent preclinical and clinical studies that target the EGFR/PI3K/AKT/mTOR signaling cascade as a potential therapeutic approach for treating HCC.

## 2. Role of EGFR/PI3K/AKT/mTOR Signaling Pathway in HCC

### 2.1. Overview of EGFR/PI3K/AKT/mTOR Signaling Pathway

Epidermal Growth Factor Receptor (EGFR) is a cell surface receptor that belongs to the ErbB family of receptor tyrosine kinases. EGFR is activated by binding specific ligands, such as the epidermal growth factor (EGF) or transforming growth factor- $\alpha$  (TGF- $\alpha$ ). Ligand binding induces receptor dimerization, leading to the activation of the intrinsic kinase activity of EGFR. The catalytic domain of EGFR kinases carries out a transphosphorylation process by which an array of tyrosine residues at the c-terminal cytoplasmic domain of EGFR are phosphorylated by its dimerized partner. Phosphotyrosine (pY) at the cytoplasmic domain of an activated EGFR acts as a docking site for proteins containing Src homology 2 (SH2) domains, such as Phosphatidylinositol 3-kinase (PI3K). The SH2 domain of PI3K binds to phosphorylated tyrosine residues on EGFR, bringing PI3K in close proximity to the plasma membrane. Upon recruitment, PI3K converts phosphatidylinositol-4,5-disphosphate (PIP<sub>2</sub>) in the plasma membrane into phosphatidylinositol-3,4,5-trisphosphate (PIP<sub>3</sub>) [9,10]. This conversion is carried out by the lipid kinase activity of the catalytic subunit of PI3K. The conversion of PIP<sub>2</sub> to PIP<sub>3</sub> can be antagonized by lipid phosphatase PTEN that converts PIP<sub>3</sub> into PIP<sub>2</sub> [11]. PIP<sub>3</sub> serves as a docking site for proteins containing pleckstrin homology (PH) domains, such as the serine/threonine kinase AKT (also known as protein kinase B). Thus, the presence of PH domains in AKT allows the serine/threonine kinase to be recruited to the plasma membrane where AKT is phosphorylated at two critical residues: Thr308 by phosphoinositide-dependent kinase 1 (PDK1) and Ser473 by the mammalian target of rapamycin complex 2 (mTORC2). These phosphorylation events lead to the full activation of AKT [12]. Fully activated AKT phosphorylates numerous downstream effectors, including proteins involved in cell survival, protein synthesis, metabolism, and cell-cycle progression. One of the key targets of activated AKT is the mammalian target of rapamycin (mTOR), which exists in two complexes: mTORC1 and mTORC2 (Figure 1).

The mammalian target of rapamycin (mTOR) is a serine/threonine protein kinase that regulates tumor growth, proliferation, metabolism, cell growth, and immunity [13]. mTOR has two complexes, which are mTORC1 and mTORC2. mTORC1 consists of mTOR, which is a regulator-associated protein of mTOR (Raptor), the DEP domain-containing mTOR interacting protein (DEPTOR), mammalian lethal with SEC13 protein 8 (mLST8), and the proline-rich AKT substrate 40 (PRAS40). mTORC2 contains the rapamycin-insensitive companion of mTOR (Rictor), DEPTOR, mLST8, Rictor-1 (Protor-1), Protor-2, and mammalian stress-activated protein kinase-interacting protein 1 (mSin1). mTORC1 is involved in cell growth and proliferation through nutritional sensing, and mTORC2 regulates the rebuilding of cytoskeletons and cell survival [14]. To activate mTORC1, RHEB, a small GTPase, is required. However, RHEB is usually inactivated by TSC1/2, a GTPase-activating protein (GAP) inhibitor [15]. The activated AKT can inhibit TSC1/2 and let RHEB be activated, resulting in the activation of mTORC1 and its downstream targets. Active mTORC1 increases protein synthesis by phosphorylating the eukaryotic translation inhibition factor 4E binding protein1 (4EBP1) and ribosomal proteins S6 kinase 1/2 (S6K1/2). Considering that these cellular processes are closely involved in carcinogenesis, it is no surprise that the dysregulation of the mTOR pathway has been observed in multiple human solid tumors [16].



**Figure 1.** Schematic illustration of EGFR/PI3K/AKT/mTOR signaling pathway. Receptor dimerization induces the phosphorylation of tyrosine residues at the c-terminal cytoplasmic domain of EGFR. PI3K binds to phosphorylated tyrosine residues on EGFR and converts phosphatidylinositol-4,5-disphosphate (PIP<sub>2</sub>) in the plasma membrane into phosphatidylinositol-3,4,5-trisphosphate (PIP<sub>3</sub>), leading to the recruitment and subsequent phosphorylation of AKT by PDK1 and mTORC2. Phosphorylated AKT, in turn, leads to the activation of mTORC1 by regulating the activity of RHEB. Active mTOR induces the phosphorylation and activation of S6K1 and 4EBP1.

## 2.2. Activation of EGFR/PI3K/AKT/mTOR Signaling Pathway in HCC

The EGFR/PI3K/AKT/mTOR signaling pathway is a major pathway in diverse types of cancers. This pathway actively regulates various aspects of cellular processes, including cell proliferation, survival, migration, and metabolism. It also plays a pivotal role in regulating the tumor microenvironment via angiogenesis and the recruitment of inflammatory cells [17]. Also, the EGFR/PI3K/AKT/mTOR signaling is significantly involved in therapy response and metastasis [18,19]. Considering the multifaceted roles in

carcinogenesis, it is no surprise that the signaling pathway is commonly upregulated in a variety of human cancers [20].

In HCC, the EGFR/PI3K/AKT/mTOR pathway is abnormally activated in approximately 50% of cases, and this dysregulated activation is involved in various cellular processes, including cell proliferation, tumor cell differentiation, autophagy, metabolism, and the epithelial–mesenchymal transition (EMT) [14]. EGFR overexpression occurs in 68% of human HCC cases and significantly correlates with metastasis, poor patient survival, and aggressive tumors [21]. Moreover, EGFR ligands are overexpressed in human liver cancer cells and tumor tissues [22]. In higher stages of HCC, this signaling pathway is associated with vascular invasion, poor differentiation, and reduced survival rates [23]. Additionally, it has been reported that 40% of HCC patients who underwent orthotopic liver transplantation exhibited elevated mTOR activity [24].

PTEN suppresses AKT activation by converting PIP3 to PIP2. The loss of tumor suppressor PTEN and reduced expression of PTEN are primarily observed in the majority of patients with HCC in the early stages [25,26]. Somatic mutations in PTEN have been reported in HCC tissues [27,28]. Moreover, Fujiwara et al. observed 12 allelic losses of PTEN in 37 patients with HCC [29]. Loss-of-function mutations in TSC1/2 were found in approximately 20% of patients with HCC, which serves as another major suppressor of the EGFR/PI3K/AKT/mTOR signaling pathway [30].

### 3. In Vitro Studies Investigating EGFR/PI3K/AKT/mTOR Signaling in HCC Cell Lines

#### 3.1. Tumorigenic Roles of EGFR/PI3K/AKT/mTOR Signaling in HCC Cells

The activation of the EGFR/PI3K/AKT/mTOR pathway has been observed in various cancer types. Although ligand binding to EGFR is the natural process, which induces the dimerization of the receptors and subsequent phosphorylation of the cytoplasmic tails, the overexpression of EGFR alone can lead to the enhanced formation of its dimerization and activation of the downstream signaling pathway in the absence of its ligands. EGFR overexpression can be achieved through various mechanisms [31]. In addition to gene amplification and the epigenetic upregulation of the EGFR gene, changes in positive or negative regulators of EGFR can also affect its abundance in cancer cells. For example, NT5DC2 suppresses the ubiquitination of EGFR, preventing its ubiquitin-mediated proteasome degradation and leading to increased EGFR levels. In HCC cell lines, such as MHCC97H and PLC/RLF/5, the upregulated NT5DC2-induced overexpression of EGFR and the activation of the downstream PI3K/AKT/mTOR signaling pathway occurs [32]. Similarly, Song et al. reported that 14-3-3 $\sigma$  can interact with EGFR and stabilize the receptor, prolonging the activation of EGFR signaling in Huh7 and HepG2 cells [33]. Tropomodulin 3 (TMOD3), a member of the pointed-end capping protein family, is significantly upregulated in HCCs and is correlated with poor survival in patients with HCC. In various HCC cell lines, including Huh-7 and Hep3B, TMOD3 was found to facilitate the phosphorylation of the cytoplasmic tail of EGFR, triggering the activation of the downstream PI3K/AKT/mTOR signaling cascade [34].

In addition to the EGF/EGFR-mediated activation of the PI3K/AKT/mTOR signaling pathway, various molecules can contribute to eliciting this pathway. Recently, DEAD/DEAH box helicase 11 (DDX11) and Apelin (APLN) were identified as activators of the PI3K/AKT/mTOR signaling pathway in HCC. The overexpression and/or knockdown of these molecules substantially altered the PI3K/AKT/mTOR signaling in HCC cell lines and significantly affected the tumorigenic potentials of HCC cells [35,36]. Alpha-fetoprotein (AFP), which is strongly correlated with the aggressiveness of HCC, is a serum biomarker routinely used for the diagnosis and prognosis of HCC. Recently, Wang et al. investigated the role of AFP in HCC using two HCC cell lines. They reported that AFP interacted with PTEN, a negative regulator of AKT, and activated the PI3K/AKT/mTOR signaling pathway [37]. The role of claudin-6 (CLDN6) was investigated in HepG2 cells, where CLDN6 was found to activate the EGFR/PI3K/AKT/mTOR signaling pathway. The knockdown of CLDN6 led to decreases in the proliferation, migration, and invasion



of HepG2 cells [38]. MicroRNAs (miRNAs) can also contribute to the activation of the EGFR/PI3K/AKT/mTOR signaling pathway. For example, miR-494-3p is correlated with aggressive clinicopathological characteristics and poor prognosis in HCC patients. Lin et al. showed that miR-494-3p bound to the 3'UTR of PTEN mRNA and repressed its translation in two HCC cell lines, SMMC7721 and HCCLM3 [39]. Notably, the suppression of PTEN expression by the ectopic expression of miR-494-3p led to the activation of the PI3K/AKT/mTOR pathway and enhanced the metastasis potentials of HCC cells [39]. Another in vitro study using the PLC/PRF/5 HCC cell line showed that the Mac-2-binding protein glycan isomer (M2BPGi) activated mTOR and exerted tumor-promoting effects on HCC [40].

### 3.2. Anti-Tumor Effects of Targeting EGFR/PI3K/AKT/mTOR Pathway in HCC Cells

Given that the EGFR/PI3K/AKT/mTOR signaling pathway exerts strong tumor-promoting effects on HCC, it is reasonable to attempt to inhibit this pathway for the treatment of HCC. EGFR is a direct target of miRNA-133b. The overexpression of miRNA-133b significantly suppressed EGFR protein expression and led to decreased activities of PI3K, AKT, and mTOR in the HepG2 cells [41]. Of note, the inhibition of the EGFR/PI3K/AKT/mTOR pathway via the overexpression of miRNA-133b induced the activation of caspase-3/-8 and apoptotic cell deaths in HepG2 cells. Methyltransferase like 14 (METTL14) can destabilize EGFR mRNA via an N6-methyladenosine (m6A) RNA methylation. METTL14 is significantly downregulated in HCC and is associated with the poor prognosis of HCC patients [42]. Similarly, an m6A-binding protein, YTH-Domain Family Member 2 (YTHDF2), binds to m6A sites in 3'UTR of EGFR mRNA and promotes the degradation of EGFR mRNA in HCC cells. In HCC cells such as HEP3B and SMMC7721, the overexpression of YTHDF2 suppressed cell proliferation via destabilizing EGFR mRNA and, thus, acting as a tumor suppressor [43]. In summary, inhibiting EGFR by the overexpression of endogenous EGFR suppressors such as miRNA-133b, METTL14, and YTHDF2 led to the subsequent inactivation of the downstream PI3K/AKT/mTOR signaling pathway and effectively reduced the malignancy of HCC cells by inducing cell apoptosis and suppressing cell proliferation.

In line with the observations in HCC cells characterized by the overexpression of endogenous suppressors of EGFR, the pharmacological inhibition of EGFR in HCC cell lines elicited similar effects. Specifically, it led to the suppression of cell proliferation and the induction of apoptosis in HCC cells through the downregulation of PI3K, p-AKT, and p-mTOR. For instance, the treatment of HepG2 cells with GW2974, an EGFR inhibitor, induced the attenuation of the downstream PI3K/AKT/mTOR signaling pathway, resulting in decreased cell proliferation and increased apoptosis in HCC cells [41]. Moreover, the inhibition of EGFR using erlotinib demonstrated inhibitory effects on the migratory capabilities and cell proliferation of HCC cells [32,44]. Similarly, the administration of EGFR inhibitors AG1478 and Gefitinib led to a reduction in cell proliferation, decreased invasion, and enhanced apoptosis in HCC cells [38,45].

In addition to targeting EGFR, the inhibition of its downstream effectors, such as PI3K, AKT, and/or mTOR, exerted similar tumor-suppressing effects on HCC cells (Table 1). Its treatment with LY294002 or Wortmannin, potent inhibitors of PI3K, downregulated the phosphorylated levels of AKT and induced apoptosis in HCC cells such as MHCC97 and Huh7 [46]. The treatment of HCC cells with a PI3K inhibitor 740Y-P showed similar effects [47]. These results consistently show that the inhibition of PI3K leads to the suppression of tumor growth and the induction of apoptosis. Cell cycle arrest was also observed in HCC cells when they were treated with inhibitors of PI3K. For example, the treatment of Huh7 and HepG2 cells with copanlisib induced cell-cycle arrest via the downregulation of CDK4/6 and cyclin D1, although this treatment had a minor effect on apoptosis [48].

**Table 1.** The inhibition of the EGFR/PI3K/AKT/mTOR pathway in HCC cell lines.

Drug	Target	HCC Cell Line	Phenotype	Reference
erlotinib	EGFR	MHCC97H, PLC/RLF/5	reduced cell proliferation	[32]
		Huh7	reduced migration	[44]
AG1478	EGFR	HepG2	reduced cell proliferation and invasion	[38]
gefitinib	EGFR	Huh7	induced apoptosis	[45]
GW2974	EGFR	HepG2	reduced cell proliferation, induced apoptosis	[41]
copanlisib	PI3K	Huh7, HepG2	induced apoptosis, inhibited cell growth, inducing cell cycle arrest	[45,48]
LY294002	PI3K	MHCC97-H	induced apoptosis	[49]
		Huh7, Mahlavu	suppressed cell growth, induced apoptosis	[46]
wortmannin	PI3K	Huh7, Mahlavu	suppressed cell growth, induced apoptosis	[46]
		HepG2	induced apoptosis	[46]
740Y-P	PI3K	SMMC-7721, MHCC-97H	reduced cell proliferation, induced apoptosis	[47]
MK2206	AKT	Hep3B, Huh7, PLC/RLF/5	growth-inhibitory, induced apoptosis	[50]
		HepG2	anti-proliferative	[51]
AKT inhibitor VIII	AKT	Huh7, Mahlavu	suppressed cell growth, induced apoptosis	[46]
rapamycin	mTOR	Hep3B	prevent enrichment of CSCs	[52]
RAD001 (everolimus)	mTOR	Hep3B, Huh7, PLC/RLF/5	growth-inhibitory, induced apoptosis	[50]
BEZ235	PI3K/mTOR	Hep3B, Huh7, PLC/RLF/5	growth-inhibitory, induced apoptosis	[50]
lenvatinib	AKT/mTOR	Hep3B, HepG2	reduced cell proliferation, migration	[53]

MK2206 effectively interacts with the pleckstrin–homology (PH) domain of AKT and hinders its recruitment in the plasma membrane, inhibiting PDK1 binding and the subsequent activation of AKT [54]. MK2206 has shown strong potency in inhibiting AKT [55]. Similar to the findings in HCC cells treated with PI3K inhibitors, treatment with MK2206 also induced growth inhibition and apoptosis in HCC cells [50,51]. The AKT Inhibitor VIII, which also blocks the activity of AKT through binding to the pleckstrin homology (PH) domain in AKT, suppressed cell growth and induced apoptosis in HCC cells [46].

Recent studies have indicated that mTOR plays a critical role in maintaining stemness-related functions in cancer stem cells (CSCs), and the inhibition of mTOR leads to the sensitization of CSCs to radiation therapy in breast cancer [56]. In line with these findings, treatment with rapamycin, the prototypic mTOR inhibitor, significantly reduces the frequency of CD133+/EpCAM+ cells in Hep3B and Huh7, which are widely considered liver cancer stem cell populations [52]. RAD001, also known as everolimus, is an inhibitor of mTOR. Its binding to the FK506-binding protein12 (FKBP12) allows the RAD001–FKBP12 complex to interact with mTOR, which subsequently inhibits S6K1 and 4EBP1 phosphorylation by mTOR. Treatment with RAD001 resulted in the induction of apoptosis [50], as well as a decrease in cell proliferation in diverse HCC cell lines, including Hep3B, Huh7, and HepG2 [50,51].

The PI3K/mTOR dual inhibitor BEZ235 induced growth inhibition and apoptosis in HCC cells [50]. Similarly, the treatment of HCC cells with Lenvatinib, which targets both AKT and mTOR, exhibited inhibitory effects on cell proliferation and migration [53]. In summary, targeting the EGFR/PI3K/AKT/mTOR signaling pathway via the inhibition of EGFR, PI3K, AKT, and/or mTOR has consistently shown anti-tumor effects on HCC cells in vitro (Table 1).

### 3.3. Targeting EGFR/PI3K/AKT/mTOR Signaling on Sorafenib-Resistant HCC Cells

Sorafenib is the first-line systemic therapeutic for patients with advanced HCC, which inhibits both receptor tyrosine kinases (RTKs) and RAF [57]. However, the development of resistance to drugs and disease progression are nearly inevitable during the course of treatment [58]. Sorafenib resistance appears to be associated with the activation of PI3K/AKT/mTOR signaling [59]. Therefore, the combination of sorafenib and an inhibitor of the EGFR/PI3K/AKT/mTOR signaling pathway has been proposed as an effective therapeutic approach [45,51,60].

Copanlisib, a PI3K inhibitor, down-regulates downstream targets of AKT, leading to cell-cycle arrest and the suppression of cell proliferation, although it has a minimal effect on apoptosis [48,61]. Copanlisib counteracted sorafenib-induced AKT phosphorylation and synergistically enhanced anti-tumor effects on HCC when combined with sorafenib [48]. Likewise, combined treatment with sorafenib and capsaicin, an inhibitor of the PI3K/AKT/mTOR signaling pathway, also showed enhanced anti-tumor effects in Hep3B and HuH7 cells [62].

Lenvatinib is another first-line treatment for HCC which also inhibits RTKs. The combination of lenvatinib and copanlisib effectively suppressed the phosphorylation of AKT, which had been induced by treatment with lenvatinib. Copanlisib enhanced pro-apoptotic effects on HCC cell lines that were resistant to Lenvatinib [45]. Moreover, the sequential treatment of Huh7 cells with rapamycin, an mTOR inhibitor, following treatment with sorafenib substantially increased the sensitivity of HCC cells to sorafenib and decreased the frequency of liver cancer stem cell (CSC)-like cells, which are considered primary cells resistant to chemotherapy [52].

In summary, the combination of sorafenib or lenvatinib with agents targeting PI3K/AKT/mTOR signaling can enhance the anticancer activity of RTK inhibitors and is expected to overcome the emergence of therapy-resistant cells.

## 4. Animal Studies Investigating EGFR/PI3K/AKT/mTOR Signaling in HCC

### 4.1. Animal Models for HCC Induced by Activated EGFR/PI3K/AKT/mTOR Signaling

Studies have demonstrated the induction of hepatocarcinogenesis through the modification of genes involved in the PI3K/AKT/mTOR signaling pathway (Table 2). PTEN functions as a negative regulator of PI3K/AKT/mTOR signaling because it counteracts PI3K-mediated AKT activation (Figure 1). For the inactivation of PTEN, specifically in the liver, genetically engineered mice were used that carried two *Pten* alleles flanked by loxP sites as well as the *Cre* transgene under the promoter of albumin. These mice (referred to as “AlbCre; *Pten*<sup>fl/fl</sup> mice”) were prone to the development of HCC as well as intrahepatic cholangiocarcinoma (ICC). Tumors from the mice exhibited significant increases in the phosphorylated level of AKT, confirming the activation of the PI3K/AKT/mTOR signaling in *Pten*-deleted livers [63].

**Table 2.** Mouse models for HCC induced by activated EGFR/PI3K/AKT/mTOR signaling.

Gene	Mouse Model	Phenotype/Tumor Type	Ref.
<i>Pten</i>	Alb-Cre; <i>Pten</i> <sup>fl/fl</sup>	ballooning, steatosis/ICC, HCC	[63]
	sgPten	lipid accumulation/no tumor	[64]
	sgPten/c-Met	lipid accumulation/HCA, HCC	

Table 2. Cont.

Gene	Mouse Model	Phenotype/Tumor Type	Ref.
AKT	HA-myr-AKT1 HA-myr-AKT1/V5-c-Met	hepatic steatosis, proliferation/HCC rapid liver tumor growth	[65]
	myr-AKT1 myr-AKT1/N-RasG12V	hepatocyte proliferation/HCA (12 w), HCC (6 m) spotty and pale color/nodular lesions (~4 w)	[66]
Tsc1/Tsc2	Alb-Cre; <i>Tsc1</i> <sup>fl/fl</sup>	dysplastic foci, nodules, hepatomas/HCC	[67]
	Alb-Cre; <i>Tsc1</i> <sup>fl/fl</sup>	moderate tumor incidence rate/HCC	[68]
	Alb-Cre; <i>Tsc1</i> <sup>fl/fl</sup> Alb-Cre; <i>Tsc1</i> <sup>fl/fl</sup> / <i>Pten</i> <sup>fl/fl</sup>	no steatosis/HCC, ICC hepatomegaly (early), large tumor (14 w)/HCC	[63]

ICC, intrahepatic cholangiocarcinoma; HCA, hepatocellular adenoma; HCC, hepatocellular carcinoma.

Recently, simple liver-specific transgenesis has been developed that allows the liver in adult mice to be transfected with DNA. This methodology, called hydrodynamic tail vein injection or simply HTVI, employs the application of physical force through the rapid injection of a large volume of DNA solution into the lateral tail vein. This process generates increased pressure within the vena cava, propelling the DNA solution into the large hepatic vein and eventually reaching the hepatic tissue and hepatocytes [69,70]. For genome editing in the liver using the CRISPR/Cas system, plasmids containing Cas9 and sgRNA are delivered to the liver via the HTVI method [71]. Using CRISPR-based gene editing combined with the HTVI method, the *Pten* gene was ablated in a subset of hepatocytes in murine livers [64]. In this setting, however, the tumor failed to develop in mice (referred to as “sgPten mice”). The discrepancy in these results between sgPten and AlbCre; *Pten*<sup>fl/fl</sup> mice were thought to be partially due to the lower frequency of hepatocytes having undergone the loss of PTEN in sgPten mice compared with that in AlbCre; *Pten*<sup>fl/fl</sup> mice. Moreover, in the case of the latter, the *Pten* gene was deleted during early embryogenesis, as opposed to sgPten mice, in which the deletion was induced in adult livers. Considering massive cell divisions during embryonic and fetal development, the deletion of *Pten* in embryos is expected to create a more favorable tissue environment for hepatocarcinogenesis [72]. Although the tumor failed to develop in the sgPten mice, concomitant c-Met overexpression in the liver led to the formation of hepatic adenomas (HCA) as well as HCC [64].

Plasmids delivered to the liver via HTVI remain as episomes in the nucleus and, thus, are prone to degradation. To overcome this limitation, the *Sleeping Beauty* transposon system is often coupled with HTVI, which allows genes of interest to be integrated into the genome. The HTVI of transposons encoding an activated form of AKT (myr-AKT1) alone induced HCC after 24 weeks post-HTVI [65,66]. Notably, the simultaneous expression of myr-AKT1 and c-Met significantly accelerated HCC development, causing complete lethality by 8 weeks post-HTVI [65]. Likewise, the co-expression of myr-AKT1 and N-RasG12V led to the rapid emergence of HCC [66]. The studies indicate that oncogenic AKT synergistically cooperated with another oncogene in the development of HCC.

TSC1 is an upstream inhibitor of mTOR which suppresses an mTOR activator, RHEB (Figure 1). The liver-specific knockout of *Tsc1* using a similar method, as described in AlbCre; *Pten*<sup>fl/fl</sup> mice, resulted in the development of HCC by the age of 9–10 months old [67]. Similar experiments using AlbCre; *Tsc1*<sup>fl/fl</sup> mice conducted by other groups also showed HCC development with a minor presence of ICC by 40 weeks of age. Tumors from AlbCre; *Tsc1*<sup>fl/fl</sup> mice consistently exhibited the activation of mTOR signaling [63,68]. Of note, the concomitant deletion of both *Tsc1* and *Pten* in the liver gave rise to the rapid induction of HCC, usually around the age of 14 weeks, showing the simultaneous deletion of the two major negative regulators of PI3K/AKT/mTOR signaling strongly enhanced the signaling pathway and carcinogenesis in the liver [63].

#### 4.2. Preclinical Animal Studies Targeting EGFR/PI3K/AKT/mTOR Signaling in HCC

Since the activation of the EGFR/PI3K/AKT/mTOR signaling pathway significantly contributes to HCC development, various inhibitors of this signaling pathway have been administered to murine models of HCC to investigate their effects on HCC in vivo (Table 3). MUC15 is a member of the high-molecular-weight glycoprotein family of Mucins. It has been shown to bind to EGFR and induce EGFR degradation, subsequently suppressing the downstream PI3K/AKT/mTOR signaling pathway [73]. In xenograft models of HCC, mice transplanted with HCCLM3 cells overexpressing MUC15 displayed fewer and smaller tumors, leading to increased survival rates compared to the control mice transplanted with HCC cells overexpressing the green fluorescent protein (GFP): an inert protein. Additionally, the degradation of EGFR by MUC15 resulted in fewer lung metastases in the MUC15 group compared to the control [73]. RHEB, as an activator of mTOR, was also targeted in a xenograft model of HCC. When human HCC cells, which were manipulated to express short hairpin RNA downregulating RHEB (RHEB-shRNA), were transplanted to immune-deficient mice, they grew more slowly than tumor cells expressing the control of shRNA in vivo [74].

**Table 3.** HCC suppression in xenograft models by targeting EGFR/PI3K/AKT/mTOR signaling.

Agent	Target	Administration Route	HCC Cell Line Transplanted	Phenotype	Ref.
MUC15	EGFR	NA	HCCLM3	delayed tumor formation, higher survival rate	[73]
RHEB-shRNA	RHEB	NA	SMMC-7721	decrease in tumor growth	[74]
DZW-310	PI3K	OA	Hep3B	decrease in tumor growth	[75]
MK2206	AKT	IP	Hep3B, Huh7	decrease in tumor growth	[50]
ZJQ-24	AKT/mTOR	OA	HepG2	Tumor cell death/reduced tumor growth	[76]
RAD001	mTOR	OA	Patient-derived HCCs	decrease in tumor growth	[77]
rapamycin	mTOR	OA	HepG2	no effects	[78]
rapamycin + bevacizumab	mTOR + VEGF	OA + IP	HepG2	decreased tumor size/increased survival	[78]
metformin	mTOR	IP	Bel-7402	decrease in tumor growth	[79]
miRNA-199a-3p	mTOR	IV	Huh7	decreased tumor growth/increased survival	[80]
miRNA-99a	mTOR	IT	SMMC-LTNM	reduction in tumor size	[81]

NA, not applicable; OA, oral administration; IP, intraperitoneal; IV, intravenous; IT, intertumoral.

The pharmacological inhibition of PI3K, AKT, or mTOR has exerted similar anti-cancer effects in xenograft models of HCC. Recently, a novel small-molecule inhibitor of PI3K, DZW-310, was developed. The administration of the drug to a Hep3B xenograft tumor model resulted in a significant decrease in tumor growth [75]. As observed in in vitro studies using HCC cells (see above in Section 3.2), administration with an AKT inhibitor, MK2206, led to the growth inhibition of tumors in xenograft models transplanted with Hep3B and Huh7 [50]. A novel dual inhibitor was developed that simultaneously inhibited AKT and mTOR. The compound, ZJQ-24, suppressed tumor growth in HepG2 xenograft mice in a dose-dependent manner [76].

Rapamycin (sirolimus) and its derivatives, RAD001 (also known as everolimus), function as highly selective allosteric inhibitors of mTORC1. They bind tightly to its primary target, the FK506-binding protein12 (FKBP12), which allows the complex to associate with the FKBP-rapamycin binding domain (FRB domain) of mTOR, which is located proximal to the active site of mTOR kinase. The formation of the FKBP12–rapamycin–mTOR complex

restricts the access of mTOR substrates and, thus, inhibits the phosphorylation and activation of S6K1 and 4EBP1 [82,83]. In patient-derived HCC xenograft models, treatment with RAD001 led to a significant reduction in tumor growth in a dose-dependent manner [77]. Molecular analysis confirmed significant decreases in the phosphorylated levels of S6K1 and 4EBP1, while the level of phosphorylated mTOR was not altered. RAD001-induced growth suppression was associated with the inhibition of cell proliferation via the downregulation of Cdk-6, Cdk-2, Cdk-4, cdc-25C, cyclin B1 and c-Myc [77]. Treatment with rapamycin alone in the HepG2 xenograft model, however, showed no significant benefit to animal survival compared to the control mice treated with the vehicle [78]. Instead, combination therapy with rapamycin and bevacizumab, a monoclonal antibody targeting the vascular endothelial growth factor (VEGF), led to reduced tumor sizes as well as prolonged survival in xenograft mice. Although the discrepancy in the results between RAD001 and rapamycin treatments was not clear, it was speculated that xenograft mice transplanted with HCC directly derived from patients might better represent the characteristics of human HCC compared to those transplanted with HepG2, which had been long maintained in the tissue culture in vitro. Metformin inhibits mTOR via the activation of AMPK: a strong suppressor of mTOR. It is noteworthy that treatment with metformin also retarded tumor development in HCC xenograft models transplanted with Bel-7402 cells [79].

Recently, there has been increasing interest in applying the RNA interference (RNAi) approach to HCC therapy [84–86]. A variety of short interfering RNAs (siRNAs), as well as miRNAs have been tested for anti-cancer effects in HCC cells in vitro, targeting the major components of the EGFR/PI3K/AKT/mTOR signaling pathway. For example, miRNAs targeting EGFR, such as miRNA-137, miRNA-302b, and miRNA-486-3p, have consistently shown anti-proliferative effects on HCC cells, including HepG2, Huh7, and SMMC-7721 [87–89]. Likewise, PI3K and AKT were downregulated in HepG2 cells using miRNA-124 and miRNA-149, respectively, which led to decreases in the proliferation and migration of HCC cells [90,91]. In particular, attempts have been made to inhibit mTOR using miRNA in vivo. The intravenous injection of miRNA-199a-3p encapsulated in nanoparticles efficiently reduced the growth of tumors in HCC xenograft mice [80]. In this study, target delivery to the liver was achieved by conjugating lactobionic acid (LA) with nanoparticles, the receptor of which was overexpressed in HCC cells. In another study, the intratumoral injection of cholesterol-conjugated miR-99a, which targets mTOR, led to a reduction in tumor mass in xenograft mice bearing HCC [81]. With the recent improvements in the stability of RNA, nanoparticle technology, and targeted delivery, RNAi-based therapy is expected to arise as a promising approach to target the EGFR/PI3K/AKT/mTOR signaling specifically and effectively in HCC in vivo.

## 5. Clinical Studies Targeting EGFR/PI3K/AKT/mTOR Signaling

Given the significant roles of the EGFR/PI3K/AKT/mTOR pathway in human cancer, there has been a strong emphasis on investigating its clinical potential by targeting the major components of the EGFR/PI3K/AKT/mTOR signaling pathway using specific small-molecule inhibitors. For instance, copanlisib, an inhibitor specific to PI3K, was administered to patients with cancers carrying an activating mutation in PI3K (NCT02465060) [92]. In a similar vein, a phase II clinical trial evaluated the efficacy of the allosteric AKT inhibitor MK-2206 (NCT01239355) [93]. Both clinical studies, however, were prematurely terminated due to discouraging results, including various adverse side effects (Table 4).

Various drugs have been employed to inhibit mTOR in clinical studies of HCC [94]. In the phase I/II study, patients with advanced HCC were given everolimus at 10 mg/day as a single agent. The treatment failed to consistently show effectiveness, as only two patients (8%) were progression-free at 24 weeks (NCT00516165). HCC patients treated with the mTOR inhibitor sirolimus (rapamycin) exhibited significantly longer overall survival (OS) compared to the control group [95]. A phase II clinical study demonstrated that sirolimus extended the survival of patients with HCC after liver transplantation (NCT01374750). Onatasertib (CC-223), an orally administered mTOR inhibitor, has been found to induce mitochondrial dysfunction in HCC cell lines [96]. In an open-label phase II trial (NCT03591965), researchers explored the

use of onatasertib in subjects with hepatitis B virus (HBV)-positive HCC who had previously undergone at least one line of therapy. Another completed phase I/II study investigated AZD8055, a novel ATP-competitive mTOR kinase inhibitor, evaluating its safety, tolerability, pharmacokinetics, and preliminary efficacy [97]. Overall, although some clinical trials have shown that mTOR inhibitors can provide a survival benefit in patients with advanced HCC, especially when they were intolerant to sorafenib (a standard first-line therapy for advanced HCC), not all trials have demonstrated a significant improvement in overall survival with the treatment of an mTOR inhibitor.

**Table 4.** Clinical trials targeting the EGFR/PI3K/Akt/mTOR signaling pathway in HCC.

Agent	Target	Phase	Clinical Outcomes	Adverse Events (Side Effects)	NCT #
Copanlisib	pan-class I PI3K	II	discontinuation due to disease progression	hyperglycemia (63%), fatigue (40%), diarrhea (37%), hypertension (33%), nausea (33%), maculopapular rash (30%)	02465060
MK-2206	AKT	II	early termination for discouraging results	anemia (73.33%), hyperglycemia (60.00%), hypoalbuminemia (46.67%), hyperbilirubinaemia (13.33%)	01239355
everolimus (RAD001)	mTOR	I/II	only 2 patients (8%) responded to treatment	hyperglycemia (42.86%), diarrhea (39.29%), hyponatremia (32.14%)	00516165
sirolimus (rapamycin)	mTOR	II	MOS of 21.1 m vs. 14.1 m for control (survival benefit over control)	dyslipidaemia, oral mucositis, diarrhea	01374750
onatasertib (CC-223)	mTOR	II	preliminary antitumor activity	diarrhea (60.38%), hyperglycaemia (60.38%), thrombocytopenia (30.19%), hyperbilirubinaemia (11.32%)	03591965
AZD8055	mTOR	I/II	not yet determined	increased aspartate aminotransferase (22%), fatigue (16%)	00999882
rapamycin + bevacizumab	mTOR + VEGF	I	no survival benefit over bevacizumab-only treatment	hyperglycaemia (83%), thrombocytopenia (75%), fatigue (46%), mucositis (46%), anorexia (42%), Diarrhea (33%)	00467194
erlotinib + bevacizumab	EGFR + VEGF	II	no improvement over sorafenib-treated group	increased alkaline phosphatase (38.30%), hypoalbuminemia (29.79%)	00881751
temsirolimus + sorafenib	mTOR + RTK	II	no survival benefit over sorafenib-only group	hypophosphatemia (60.71%), diarrhea (28.57%), anemia (10.71%)	01687673

MOS, mean overall survival; VEGF, vascular endothelial growth factor; RTK, receptor tyrosine kinase.

The combinatory inhibition of mTOR and VEGF using rapamycin and bevacizumab significantly reduced tumor growth in xenograft models of HCC [78] (Table 3). A phase I clinical trial explored the combination of rapamycin with bevacizumab at the maximum tolerated dose in patients with HCC, demonstrating a complete response in one case and stable disease states in the majority, although this combinatory treatment did not show significant improvements in overall survival compared to patients treated with bevacizumab only (NCT00467194). Phase I/II clinical trials are ongoing to further investigate the efficacy of the combination therapy in HCC [94]. Erlotinib is an EGFR inhibitor that effectively suppresses the phosphorylation of its downstream effectors, such as AKT and mTOR. The combined inhibition of EGFR and VEGF using erlotinib and bevacizumab showed similar anti-cancer effects in patients with advanced HCC (NCT00881751) [98].

In an attempt to improve outcomes, a single-arm phase II trial combined temsirolimus and sorafenib to exploit mTOR inhibition along with sorafenib's effects on HCC [99]. However, it failed to achieve an improvement in overall survival compared to the control group, who were treated with sorafenib only (NCT01687673). Despite this setback, ongoing research continues to explore drug combinations, and several clinical studies are underway [100,101].

It is noteworthy that while mTOR inhibitors, as well as other therapeutics targeting the EGFR/PI3K/AKT/mTOR pathway, have shown some promise in preclinical studies, their efficacy in patients with advanced HCC remains uncertain. These findings highlight the complexity of targeting the EGFR/PI3K/AKT/mTOR pathway in HCC and underscore the need for further investigation to identify more effective treatment approaches.

## 6. Perspectives and Conclusions

A comprehensive understanding of the molecular pathway leading to carcinogenesis is crucial for predicting patient responses to targeted therapies, significantly impacting clinical decision-making. The development of HCC is a complex process involving various alterations in multiple signaling cascades [5,6]. Among the various oncogenic signals, the EGFR/PI3K/AKT/mTOR pathway stands out as it is activated in over 50% of HCC cases, making it a crucial target for patients with this condition. Research has emphasized the pivotal role of the EGFR/PI3K/AKT/mTOR cascade in the development of HCC. Promisingly, preclinical studies using human HCC cells have consistently demonstrated the effectiveness of targeting the key components of this signaling pathway. Such interventions have been shown to suppress the proliferation of tumor cells *in vitro* and inhibit the growth of HCC *in vivo*, offering hope for potential therapeutic approaches.

While preclinical studies have shown promise in targeting the PI3K/AKT/mTOR pathway, clinical trials have not consistently demonstrated a significant improvement in patient outcomes. The overall response rate and survival benefits observed in clinical studies targeting the EGFR/PI3K/AKT/mTOR signaling pathway have been modest or disappointing. These less-than-satisfactory outcomes could be attributed, in part, to the significant toxicities and adverse effects caused by PI3K/AKT/mTOR inhibitors, negatively impacting patients' quality of life and leading to treatment discontinuation. Notably, adverse effects routinely observed in administering these inhibitors include decreased liver functions, as determined by increased alkaline phosphatase (ALP) and aspartate aminotransferase (AST) levels, hypoalbuminemia, thrombocytopenia, and hyperbilirubinemia (Table 4). The side effects on the liver exerted by PI3K/AKT/mTOR inhibitors are especially detrimental to HCC patients who already have pre-existing liver damage.

In this sense, successful therapy for HCC should enable the efficient targeting of the EGFR/PI3K/AKT/mTOR pathway with minimal toxicities and adverse effects. One promising approach is the targeted delivery of drugs to HCC using polymeric nanoparticles (PNPs) [86,102]. In other words, for HCC-targeted delivery, inhibitors of EGFR/PI3K/AKT/mTOR signaling are encapsulated in PNPs that are conjugated with targeting ligands specific to HCC cells. For example, the asialoglycoprotein receptors (ASGP-R) and Glypican-3 (GPC3) are overexpressed in HCC and are considered highly specific markers for HCC [103,104]. Conjugating monoclonal antibodies or ligands that specifically recognize ASGP-R or GPC3 with PNPs are expected to allow the encapsulated drugs to be specifically delivered to HCC, minimizing various side effects and drug-related toxicities commonly found in the systemic delivery of these inhibitors for EGFR/PI3K/AKT/mTOR signaling. Thus, there is hope for the future as new drugs and therapeutic approaches are anticipated to be developed.

**Funding:** This work was supported by a National Research Foundation of Korea (NRF) grant, 2019R1A2C2009518 (awarded to S.W.R.) which was funded by the Korea government (MSIT).

**Institutional Review Board Statement:** Not applicable.

**Informed Consent Statement:** Not applicable.

**Data Availability Statement:** Not applicable.

**Conflicts of Interest:** The authors declare no conflict of interest.



## References

1. Llovet, J.M.; Kelley, R.K.; Villanueva, A.; Singal, A.G.; Pikarsky, E.; Roayaie, S.; Lencioni, R.; Koike, K.; Zucman-Rossi, J.; Finn, R.S. Hepatocellular carcinoma. *Nat. Rev. Dis. Prim.* **2021**, *7*, 6. [CrossRef]
2. Singal, A.G.; Lampertico, P.; Nahon, P. Epidemiology and surveillance for hepatocellular carcinoma: New trends. *J. Hepatol.* **2020**, *72*, 250–261. [CrossRef]
3. Banales, J.M.; Marin, J.J.G.; Lamarca, A.; Rodrigues, P.M.; Khan, S.A.; Roberts, L.R.; Cardinale, V.; Carpino, G.; Andersen, J.B.; Braconi, C.; et al. Cholangiocarcinoma 2020: The next horizon in mechanisms and management. *Nat. Rev. Gastroenterol. Hepatol.* **2020**, *17*, 557–588. [CrossRef]
4. Villanueva, A. Hepatocellular Carcinoma. *N. Engl. J. Med.* **2019**, *380*, 1450–1462. [CrossRef]
5. Llovet, J.M.; Bruix, J. Molecular targeted therapies in hepatocellular carcinoma. *Hepatology* **2008**, *48*, 1312–1327. [CrossRef]
6. Dimri, M.; Satyanarayana, A. Molecular Signaling Pathways and Therapeutic Targets in Hepatocellular Carcinoma. *Cancers* **2020**, *12*, 491. [CrossRef]
7. Moon, H.; Ro, S.W. MAPK/ERK Signaling Pathway in Hepatocellular Carcinoma. *Cancers* **2021**, *13*, 3026. [CrossRef]
8. Park, H.; Park, H.; Baek, J.; Moon, H.; Ro, S.W. Target Therapy for Hepatocellular Carcinoma: Beyond Receptor Tyrosine Kinase Inhibitors and Immune Checkpoint Inhibitors. *Biology* **2022**, *11*, 585. [CrossRef]
9. Fruman, D.A.; Rommel, C. PI3K and cancer: Lessons, challenges and opportunities. *Nat. Rev. Drug Discov.* **2014**, *13*, 140–156. [CrossRef]
10. Osaki, M.; Oshimura, M.; Ito, H. PI3K-Akt pathway: Its functions and alterations in human cancer. *Apoptosis* **2004**, *9*, 667–676. [CrossRef]
11. Thorpe, L.M.; Yuzugullu, H.; Zhao, J.J. PI3K in cancer: Divergent roles of isoforms, modes of activation and therapeutic targeting. *Nat. Rev. Cancer* **2015**, *15*, 7–24. [CrossRef]
12. Gao, Y.; Moten, A.; Lin, H.K. Akt: A new activation mechanism. *Cell Res.* **2014**, *24*, 785–786. [CrossRef]
13. Saxton, R.A.; Sabatini, D.M. mTOR Signaling in Growth, Metabolism, and Disease. *Cell* **2017**, *169*, 361–371. [CrossRef]
14. Sun, E.J.; Wankell, M.; Palamuthusingam, P.; McFarlane, C.; Hebbard, L. Targeting the PI3K/Akt/mTOR Pathway in Hepatocellular Carcinoma. *Biomedicines* **2021**, *9*, 1639. [CrossRef]
15. Ma, X.M.; Blenis, J. Molecular mechanisms of mTOR-mediated translational control. *Nat. Rev. Mol. Cell Biol.* **2009**, *10*, 307–318. [CrossRef]
16. Laplante, M.; Sabatini, D.M. mTOR signaling in growth control and disease. *Cell* **2012**, *149*, 274–293. [CrossRef]
17. He, Y.; Sun, M.M.; Zhang, G.G.; Yang, J.; Chen, K.S.; Xu, W.W.; Li, B. Targeting PI3K/Akt signal transduction for cancer therapy. *Signal Transduct. Target. Ther.* **2021**, *6*, 425. [CrossRef]
18. Liu, R.; Chen, Y.; Liu, G.; Li, C.; Song, Y.; Cao, Z.; Li, W.; Hu, J.; Lu, C.; Liu, Y. PI3K/AKT pathway as a key link modulates the multidrug resistance of cancers. *Cell Death Dis.* **2020**, *11*, 797. [CrossRef]
19. Peng, Y.; Wang, Y.; Zhou, C.; Mei, W.; Zeng, C. PI3K/Akt/mTOR Pathway and Its Role in Cancer Therapeutics: Are We Making Headway? *Front. Oncol.* **2022**, *12*, 819128. [CrossRef]
20. Yu, L.; Wei, J.; Liu, P. Attacking the PI3K/Akt/mTOR signaling pathway for targeted therapeutic treatment in human cancer. *Semin. Cancer Biol.* **2022**, *85*, 69–94. [CrossRef]
21. Harada, K.; Shiota, G.; Kawasaki, H. Transforming growth factor- $\alpha$  and epidermal growth factor receptor in chronic liver disease and hepatocellular carcinoma. *Liver* **1999**, *19*, 318–325. [CrossRef]
22. Ito, Y.; Takeda, T.; Sakon, M.; Tsujimoto, M.; Higashiyama, S.; Noda, K.; Miyoshi, E.; Monden, M.; Matsuura, N. Expression and clinical significance of erb-B receptor family in hepatocellular carcinoma. *Br. J. Cancer* **2001**, *84*, 1377–1383. [CrossRef]
23. Zhou, L.; Huang, Y.; Li, J.; Wang, Z. The mTOR pathway is associated with the poor prognosis of human hepatocellular carcinoma. *Med. Oncol.* **2010**, *27*, 255–261. [CrossRef]
24. Sieghart, W.; Fuereder, T.; Schmid, K.; Cejka, D.; Werzowa, J.; Wrba, F.; Wang, X.; Gruber, D.; Rasoul-Rockenschaub, S.; Peck-Radosavljevic, M.; et al. Mammalian target of rapamycin pathway activity in hepatocellular carcinomas of patients undergoing liver transplantation. *Transplantation* **2007**, *83*, 425–432. [CrossRef]
25. Villanueva, A.; Chiang, D.Y.; Newell, P.; Peix, J.; Thung, S.; Alsinet, C.; Tovar, V.; Roayaie, S.; Minguez, B.; Sole, M.; et al. Pivotal role of mTOR signaling in hepatocellular carcinoma. *Gastroenterology* **2008**, *135*, 1972–1983.e11. [CrossRef]
26. Chen, D.; Li, Z.; Cheng, Q.; Wang, Y.; Qian, L.; Gao, J.; Zhu, J.Y. Genetic alterations and expression of PTEN and its relationship with cancer stem cell markers to investigate pathogenesis and to evaluate prognosis in hepatocellular carcinoma. *J. Clin. Pathol.* **2019**, *72*, 588–596. [CrossRef]
27. Kawamura, N.; Nagai, H.; Bando, K.; Koyama, M.; Matsumoto, S.; Tajiri, T.; Onda, M.; Fujimoto, J.; Ueki, T.; Konishi, N.; et al. PTEN/MMAC1 mutations in hepatocellular carcinomas: Somatic inactivation of both alleles in tumors. *Jpn. J. Cancer Res.* **1999**, *90*, 413–418. [CrossRef]
28. Yao, Y.J.; Ping, X.L.; Zhang, H.; Chen, F.F.; Lee, P.K.; Ahsan, H.; Chen, C.J.; Lee, P.H.; Peacocke, M.; Santella, R.M.; et al. PTEN/MMAC1 mutations in hepatocellular carcinomas. *Oncogene* **1999**, *18*, 3181–3185. [CrossRef]
29. Fujiwara, Y.; Hoon, D.S.; Yamada, T.; Umeshita, K.; Gotoh, M.; Sakon, M.; Nishisho, I.; Monden, M. PTEN/MMAC1 mutation and frequent loss of heterozygosity identified in chromosome 10q in a subset of hepatocellular carcinomas. *Jpn. J. Cancer Res.* **2000**, *91*, 287–292. [CrossRef]

30. Ho, D.W.H.; Chan, L.K.; Chiu, Y.T.; Xu, I.M.J.; Poon, R.T.P.; Cheung, T.T.; Tang, C.N.; Tang, V.W.L.; Lo, I.L.O.; Lam, P.W.Y.; et al. TSC1/2 mutations define a molecular subset of HCC with aggressive behaviour and treatment implication. *Gut* **2017**, *66*, 1496–1506. [CrossRef]
31. Wang, C.; Liao, Y.; He, W.; Zhang, H.; Zuo, D.; Liu, W.; Yang, Z.; Qiu, J.; Yuan, Y.; Li, K.; et al. Elafin promotes tumour metastasis and attenuates the anti-metastatic effects of erlotinib via binding to EGFR in hepatocellular carcinoma. *J. Exp. Clin. Cancer Res.* **2021**, *40*, 113. [CrossRef]
32. Li, K.S.; Zhu, X.D.; Liu, H.D.; Zhang, S.Z.; Li, X.L.; Xiao, N.; Liu, X.F.; Xu, B.; Lei, M.; Zhang, Y.Y.; et al. NT5DC2 promotes tumor cell proliferation by stabilizing EGFR in hepatocellular carcinoma. *Cell Death Dis.* **2020**, *11*, 335. [CrossRef]
33. Song, J.; Liu, Y.; Liu, F.; Zhang, L.; Li, G.; Yuan, C.; Yu, C.; Lu, X.; Liu, Q.; Chen, X.; et al. The 14-3-3 $\sigma$  protein promotes HCC anoikis resistance by inhibiting EGFR degradation and thereby activating the EGFR-dependent ERK1/2 signaling pathway. *Theranostics* **2021**, *11*, 996–1015. [CrossRef]
34. Zheng, H.; Yang, Y.; Hong, Y.G.; Wang, M.C.; Yuan, S.X.; Wang, Z.G.; Bi, F.R.; Hao, L.Q.; Yan, H.L.; Zhou, W.P. Tropomodulin 3 modulates EGFR-PI3K-AKT signaling to drive hepatocellular carcinoma metastasis. *Mol. Carcinog.* **2019**, *58*, 1897–1907. [CrossRef]
35. Chen, H.; Wong, C.C.; Liu, D.; Go, M.Y.Y.; Wu, B.; Peng, S.; Kuang, M.; Wong, N.; Yu, J. APLN promotes hepatocellular carcinoma through activating PI3K/Akt pathway and is a druggable target. *Theranostics* **2019**, *9*, 5246–5260. [CrossRef]
36. Yu, Y.; Zhao, D.; Li, K.; Cai, Y.; Xu, P.; Li, R.; Li, J.; Chen, X.; Chen, P.; Cui, G. E2F1 mediated DDX11 transcriptional activation promotes hepatocellular carcinoma progression through PI3K/AKT/mTOR pathway. *Cell Death Dis.* **2020**, *11*, 273. [CrossRef]
37. Wang, S.; Zhu, M.; Wang, Q.; Hou, Y.; Li, L.; Weng, H.; Zhao, Y.; Chen, D.; Guo, J.; Ding, H.; et al. Publisher Correction: Alpha-fetoprotein inhibits autophagy to promote malignant behaviour in hepatocellular carcinoma cells by activating PI3K/AKT/mTOR signalling. *Cell Death Dis.* **2019**, *10*, 214. [CrossRef]
38. Huang, L.; Zhao, C.; Sun, K.; Yang, D.; Yan, L.; Luo, D.; He, J.; Hu, X.; Wang, R.; Shen, X.; et al. Downregulation of CLDN6 inhibits cell proliferation, migration, and invasion via regulating EGFR/AKT/mTOR signalling pathway in hepatocellular carcinoma. *Cell Biochem. Funct.* **2020**, *38*, 541–548. [CrossRef]
39. Lin, H.; Huang, Z.P.; Liu, J.; Qiu, Y.; Tao, Y.P.; Wang, M.C.; Yao, H.; Hou, K.Z.; Gu, F.M.; Xu, X.F. MiR-494-3p promotes PI3K/AKT pathway hyperactivation and human hepatocellular carcinoma progression by targeting PTEN. *Sci. Rep.* **2018**, *8*, 10461. [CrossRef]
40. Dolgormaa, G.; Harimoto, N.; Ishii, N.; Yamanaka, T.; Hagiwara, K.; Tsukagoshi, M.; Igarashi, T.; Watanabe, A.; Kubo, N.; Araki, K.; et al. Mac-2-binding protein glycan isomer enhances the aggressiveness of hepatocellular carcinoma by activating mTOR signaling. *Br. J. Cancer* **2020**, *123*, 1145–1153. [CrossRef]
41. Wang, X.; Zeng, J.; Wang, L.; Zhang, X.; Liu, Z.; Zhang, H.; Dong, J. Overexpression of microRNA-133b is associated with the increased survival of patients with hepatocellular carcinoma after curative hepatectomy: Involvement of the EGFR/PI3K/Akt/mTOR signaling pathway. *Oncol. Rep.* **2017**, *38*, 141–150. [CrossRef] [PubMed]
42. Shi, Y.; Zhuang, Y.; Zhang, J.; Chen, M.; Wu, S. METTL14 Inhibits Hepatocellular Carcinoma Metastasis Through Regulating EGFR/PI3K/AKT Signaling Pathway in an m6A-Dependent Manner. *Cancer Manag. Res.* **2020**, *12*, 13173–13184. [CrossRef] [PubMed]
43. Zhong, L.; Liao, D.; Zhang, M.; Zeng, C.; Li, X.; Zhang, R.; Ma, H.; Kang, T. YTHDF2 suppresses cell proliferation and growth via destabilizing the EGFR mRNA in hepatocellular carcinoma. *Cancer Lett.* **2019**, *442*, 252–261. [CrossRef]
44. Xu, Y.; Xu, H.; Li, M.; Wu, H.; Guo, Y.; Chen, J.; Shan, J.; Chen, X.; Shen, J.; Ma, Q.; et al. KIAA1199 promotes sorafenib tolerance and the metastasis of hepatocellular carcinoma by activating the EGF/EGFR-dependent epithelial-mesenchymal transition program. *Cancer Lett.* **2019**, *454*, 78–89. [CrossRef] [PubMed]
45. Sun, D.; Liu, J.; Wang, Y.; Dong, J. Co-administration of MDR1 and BCRP or EGFR/PI3K inhibitors overcomes lenvatinib resistance in hepatocellular carcinoma. *Front. Oncol.* **2022**, *12*, 944537. [CrossRef]
46. Buontempo, F.; Ersahin, T.; Missiroli, S.; Senturk, S.; Etro, D.; Ozturk, M.; Capitani, S.; Cetin-Atalay, R.; Neri, M.L. Inhibition of Akt signaling in hepatoma cells induces apoptotic cell death independent of Akt activation status. *Investig. New Drugs* **2011**, *29*, 1303–1313. [CrossRef]
47. Gong, C.; Ai, J.; Fan, Y.; Gao, J.; Liu, W.; Feng, Q.; Liao, W.; Wu, L. NCAPG Promotes The Proliferation Of Hepatocellular Carcinoma Through PI3K/AKT Signaling. *Onco Targets Ther.* **2019**, *12*, 8537–8552. [CrossRef]
48. Ye, L.; Mayerle, J.; Ziesch, A.; Reiter, F.P.; Gerbes, A.L.; De Toni, E.N. The PI3K inhibitor copanlisib synergizes with sorafenib to induce cell death in hepatocellular carcinoma. *Cell Death Discov.* **2019**, *5*, 86. [CrossRef]
49. Song, L.; Luo, Y.; Li, S.; Hong, M.; Wang, Q.; Chi, X.; Yang, C. ISL Induces Apoptosis and Autophagy in Hepatocellular Carcinoma via Downregulation of PI3K/AKT/mTOR Pathway in vivo and in vitro. *Drug Des. Dev. Ther.* **2020**, *14*, 4363–4376. [CrossRef]
50. Ou, D.L.; Lee, B.S.; Lin, L.I.; Liou, J.Y.; Liao, S.C.; Hsu, C.; Cheng, A.L. Vertical blockade of the IGF1R-PI3K/Akt/mTOR pathway for the treatment of hepatocellular carcinoma: The role of survivin. *Mol. Cancer* **2014**, *13*, 2. [CrossRef]
51. Grabinski, N.; Ewald, F.; Hofmann, B.T.; Staufer, K.; Schumacher, U.; Nashan, B.; Jücker, M. Combined targeting of AKT and mTOR synergistically inhibits proliferation of hepatocellular carcinoma cells. *Mol. Cancer* **2012**, *11*, 85. [CrossRef]
52. Kahraman, D.C.; Kahraman, T.; Cetin-Atalay, R. Targeting PI3K/Akt/mTOR Pathway Identifies Differential Expression and Functional Role of IL8 in Liver Cancer Stem Cell Enrichment. *Mol. Cancer Ther.* **2019**, *18*, 2146–2157. [CrossRef] [PubMed]
53. Zhao, Z.; Song, J.; Zhang, D.; Wu, F.; Tu, J.; Ji, J. Oxyphosphocarpine suppresses FGFR1-overexpressed hepatocellular carcinoma growth and sensitizes the therapeutic effect of lenvatinib. *Life Sci.* **2021**, *264*, 118642. [CrossRef] [PubMed]

54. Cheng, Y.; Zhang, Y.; Zhang, L.; Ren, X.; Huber-Keener, K.J.; Liu, X.; Zhou, L.; Liao, J.; Keihack, H.; Yan, L.; et al. MK-2206, a novel allosteric inhibitor of Akt, synergizes with gefitinib against malignant glioma via modulating both autophagy and apoptosis. *Mol. Cancer Ther.* **2012**, *11*, 154–164. [CrossRef]
55. Hirai, H.; Sootome, H.; Nakatsuru, Y.; Miyama, K.; Taguchi, S.; Tsujioka, K.; Ueno, Y.; Hatch, H.; Majumder, P.K.; Pan, B.S.; et al. MK-2206, an allosteric Akt inhibitor, enhances antitumor efficacy by standard chemotherapeutic agents or molecular targeted drugs in vitro and in vivo. *Mol. Cancer Ther.* **2010**, *9*, 1956–1967. [CrossRef]
56. Lai, Y.; Yu, X.; Lin, X.; He, S. Inhibition of mTOR sensitizes breast cancer stem cells to radiation-induced repression of self-renewal through the regulation of MnSOD and Akt. *Int. J. Mol. Med.* **2016**, *37*, 369–377. [CrossRef] [PubMed]
57. Llovet, J.M.; Hernandez-Gea, V. Hepatocellular carcinoma: Reasons for phase III failure and novel perspectives on trial design. *Clin. Cancer Res.* **2014**, *20*, 2072–2079. [CrossRef] [PubMed]
58. Niu, L.; Liu, L.; Yang, S.; Ren, J.; Lai, P.B.S.; Chen, G.G. New insights into sorafenib resistance in hepatocellular carcinoma: Responsible mechanisms and promising strategies. *Biochim. Biophys. Acta Rev. Cancer* **2017**, *1868*, 564–570. [CrossRef]
59. Samarin, J.; Laketa, V.; Malz, M.; Roessler, S.; Stein, I.; Horwitz, E.; Singer, S.; Dimou, E.; Cigliano, A.; Bissinger, M.; et al. PI3K/AKT/mTOR-dependent stabilization of oncogenic far-upstream element binding proteins in hepatocellular carcinoma cells. *Hepatology* **2016**, *63*, 813–826. [CrossRef]
60. Gedaly, R.; Angulo, P.; Chen, C.; Creasy, K.T.; Spear, B.T.; Hundley, J.; Daily, M.F.; Shah, M.; Evers, B.M. The role of PI3K/mTOR inhibition in combination with sorafenib in hepatocellular carcinoma treatment. *Anticancer Res.* **2012**, *32*, 2531–2536.
61. Schneider, P.; Schön, M.; Pletz, N.; Seitz, C.S.; Liu, N.; Ziegelbauer, K.; Zachmann, K.; Emmert, S.; Schön, M.P. The novel PI3 kinase inhibitor, BAY 80-6946, impairs melanoma growth in vivo and in vitro. *Exp. Dermatol.* **2014**, *23*, 579–584. [CrossRef] [PubMed]
62. Dai, N.; Ye, R.; He, Q.; Guo, P.; Chen, H.; Zhang, Q. Capsaicin and sorafenib combination treatment exerts synergistic anti-hepatocellular carcinoma activity by suppressing EGFR and PI3K/Akt/mTOR signaling. *Oncol. Rep.* **2018**, *40*, 3235–3248. [CrossRef] [PubMed]
63. Kenerson, H.L.; Yeh, M.M.; Kazami, M.; Jiang, X.; Riehle, K.J.; McIntyre, R.L.; Park, J.O.; Kwon, S.; Campbell, J.S.; Yeung, R.S. Akt and mTORC1 have different roles during liver tumorigenesis in mice. *Gastroenterology* **2013**, *144*, 1055–1065. [CrossRef] [PubMed]
64. Xu, Z.; Hu, J.; Cao, H.; Pilo, M.G.; Cigliano, A.; Shao, Z.; Xu, M.; Ribback, S.; Dombrowski, F.; Calvisi, D.F.; et al. Loss of Pten synergizes with c-Met to promote hepatocellular carcinoma development via mTORC2 pathway. *Exp. Mol. Med.* **2018**, *50*, e417. [CrossRef] [PubMed]
65. Hu, J.; Che, L.; Li, L.; Pilo, M.G.; Cigliano, A.; Ribback, S.; Li, X.; Latte, G.; Mela, M.; Evert, M.; et al. Co-activation of AKT and c-Met triggers rapid hepatocellular carcinoma development via the mTORC1/FASN pathway in mice. *Sci. Rep.* **2016**, *6*, 20484. [CrossRef]
66. Ho, C.; Wang, C.; Mattu, S.; Destefanis, G.; Ladu, S.; Delogu, S.; Armbruster, J.; Fan, L.; Lee, S.A.; Jiang, L.; et al. AKT (v-akt murine thymoma viral oncogene homolog 1) and N-Ras (neuroblastoma ras viral oncogene homolog) coactivation in the mouse liver promotes rapid carcinogenesis by way of mTOR (mammalian target of rapamycin complex 1), FOXM1 (forkhead box M1)/SKP2, and c-Myc pathways. *Hepatology* **2012**, *55*, 833–845. [CrossRef]
67. Menon, S.; Yecies, J.L.; Zhang, H.H.; Howell, J.J.; Nicholatos, J.; Harputlugil, E.; Bronson, R.T.; Kwiatkowski, D.J.; Manning, B.D. Chronic activation of mTOR complex 1 is sufficient to cause hepatocellular carcinoma in mice. *Sci. Signal.* **2012**, *5*, ra24. [CrossRef]
68. Luo, Y.D.; Fang, L.; Yu, H.Q.; Zhang, J.; Lin, X.T.; Liu, X.Y.; Wu, D.; Li, G.X.; Huang, D.; Zhang, Y.J.; et al. p53 haploinsufficiency and increased mTOR signalling define a subset of aggressive hepatocellular carcinoma. *J. Hepatol.* **2021**, *74*, 96–108. [CrossRef]
69. Chen, X.; Calvisi, D.F. Hydrodynamic transfection for generation of novel mouse models for liver cancer research. *Am. J. Pathol.* **2014**, *184*, 912–923. [CrossRef]
70. Ju, H.L.; Han, K.H.; Lee, J.D.; Ro, S.W. Transgenic mouse models generated by hydrodynamic transfection for genetic studies of liver cancer and preclinical testing of anti-cancer therapy. *Int. J. Cancer* **2016**, *138*, 1601–1608. [CrossRef]
71. Cho, K.; Ro, S.W.; Seo, S.H.; Jeon, Y.; Moon, H.; Kim, D.Y.; Kim, S.U. Genetically Engineered Mouse Models for Liver Cancer. *Cancers* **2019**, *12*, 14. [CrossRef]
72. Moon, H.; Park, H.; Chae, M.J.; Choi, H.J.; Kim, D.Y.; Ro, S.W. Activated TAZ induces liver cancer in collaboration with EGFR/HER2 signaling pathways. *BMC Cancer* **2022**, *22*, 423. [CrossRef]
73. Wang, R.Y.; Chen, L.; Chen, H.Y.; Hu, L.; Li, L.; Sun, H.Y.; Jiang, F.; Zhao, J.; Liu, G.M.; Tang, J.; et al. MUC15 inhibits dimerization of EGFR and PI3K-AKT signaling and is associated with aggressive hepatocellular carcinomas in patients. *Gastroenterology* **2013**, *145*, 1436–1448.e12. [CrossRef]
74. Liu, F.; Pan, Z.; Zhang, J.; Ni, J.; Wang, C.; Wang, Z.; Gu, F.; Dong, W.; Zhou, W.; Liu, H. Overexpression of RHEB is associated with metastasis and poor prognosis in hepatocellular carcinoma. *Oncol. Lett.* **2018**, *15*, 3838–3845. [CrossRef]
75. Wu, Y.; Xu, X.; Liu, M.; Qin, X.; Wu, Q.; Ding, H.; Zhao, Q. DZW-310, a novel phosphoinositide 3-kinase inhibitor, attenuates the angiogenesis and growth of hepatocellular carcinoma cells via PI3K/AKT/mTOR axis. *Biochem. Pharmacol.* **2022**, *201*, 115093. [CrossRef]
76. Liu, J.; Liu, Y.; Zhang, J.; Liu, D.; Bao, Y.; Chen, T.; Tang, T.; Lin, J.; Luo, Y.; Jin, Y.; et al. Indole hydrazide compound ZJQ-24 inhibits angiogenesis and induces apoptosis cell death through abrogation of AKT/mTOR pathway in hepatocellular carcinoma. *Cell Death Dis.* **2020**, *11*, 926. [CrossRef]
77. Huynh, H.; Chow, K.H.; Soo, K.C.; Toh, H.C.; Choo, S.P.; Foo, K.F.; Poon, D.; Ngo, V.C.; Tran, E. RAD001 (everolimus) inhibits tumour growth in xenograft models of human hepatocellular carcinoma. *J. Cell. Mol. Med.* **2009**, *13*, 1371–1380. [CrossRef]

78. Ong, L.C.; Song, I.C.; Jin, Y.; Kee, I.H.; Siew, E.; Yu, S.; Thng, C.H.; Huynh, H.; Chow, P.K. Effective inhibition of xenografts of hepatocellular carcinoma (HepG2) by rapamycin and bevacizumab in an intrahepatic model. *Mol. Imaging Biol.* **2009**, *11*, 334–342. [CrossRef]
79. Ling, S.; Song, L.; Fan, N.; Feng, T.; Liu, L.; Yang, X.; Wang, M.; Li, Y.; Tian, Y.; Zhao, F.; et al. Combination of metformin and sorafenib suppresses proliferation and induces autophagy of hepatocellular carcinoma via targeting the mTOR pathway. *Int. J. Oncol.* **2017**, *50*, 297–309. [CrossRef]
80. Varshney, A.; Panda, J.J.; Singh, A.K.; Yadav, N.; Bihari, C.; Biswas, S.; Sarin, S.K.; Chauhan, V.S. Targeted delivery of microRNA-199a-3p using self-assembled dipeptide nanoparticles efficiently reduces hepatocellular carcinoma in mice. *Hepatology* **2018**, *67*, 1392–1407. [CrossRef]
81. Li, D.; Liu, X.; Lin, L.; Hou, J.; Li, N.; Wang, C.; Wang, P.; Zhang, Q.; Zhang, P.; Zhou, W.; et al. MicroRNA-99a inhibits hepatocellular carcinoma growth and correlates with prognosis of patients with hepatocellular carcinoma. *J. Biol. Chem.* **2011**, *286*, 36677–36685. [CrossRef]
82. Hausch, F.; Kozany, C.; Theodoropoulou, M.; Fabian, A.K. FKBP and the Akt/mTOR pathway. *Cell Cycle* **2013**, *12*, 2366–2370. [CrossRef]
83. Yip, C.K.; Murata, K.; Walz, T.; Sabatini, D.M.; Kang, S.A. Structure of the human mTOR complex I and its implications for rapamycin inhibition. *Mol. Cell* **2010**, *38*, 768–774. [CrossRef]
84. Perrone, F.; Craparo, E.F.; Cemazar, M.; Kamensek, U.; Drago, S.E.; Dapas, B.; Scaggiante, B.; Zanconati, F.; Bonazza, D.; Grassi, M.; et al. Targeted delivery of siRNAs against hepatocellular carcinoma-related genes by a galactosylated polyaspartamide copolymer. *J. Control. Release* **2021**, *330*, 1132–1151. [CrossRef]
85. Scarabel, L.; Perrone, F.; Garziera, M.; Farra, R.; Grassi, M.; Musiani, F.; Russo Spena, C.; Salis, B.; De Stefano, L.; Toffoli, G.; et al. Strategies to optimize siRNA delivery to hepatocellular carcinoma cells. *Expert. Opin. Drug Deliv.* **2017**, *14*, 797–810. [CrossRef]
86. Farra, R.; Musiani, F.; Perrone, F.; Čemažar, M.; Kamensek, U.; Tonon, F.; Abrami, M.; Ručigaj, A.; Grassi, M.; Pozzato, G.; et al. Polymer-Mediated Delivery of siRNAs to Hepatocellular Carcinoma: Variables Affecting Specificity and Effectiveness. *Molecules* **2018**, *23*, 777. [CrossRef]
87. Ji, L.; Lin, Z.; Wan, Z.; Xia, S.; Jiang, S.; Cen, D.; Cai, L.; Xu, J.; Cai, X. miR-486-3p mediates hepatocellular carcinoma sorafenib resistance by targeting FGFR4 and EGFR. *Cell Death Dis.* **2020**, *11*, 250. [CrossRef]
88. Shi, T.; Fujita, K.; Gong, J.; Nakahara, M.; Iwama, H.; Liu, S.; Yoneyama, H.; Morishita, A.; Nomura, T.; Tani, J.; et al. Aspirin inhibits hepatocellular carcinoma cell proliferation in vitro and in vivo via inducing cell cycle arrest and apoptosis. *Oncol. Rep.* **2020**, *44*, 457–468. [CrossRef]
89. Wang, L.; Yao, J.; Shi, X.; Hu, L.; Li, Z.; Song, T.; Huang, C. MicroRNA-302b suppresses cell proliferation by targeting EGFR in human hepatocellular carcinoma SMMC-7721 cells. *BMC Cancer* **2013**, *13*, 448. [CrossRef]
90. Lang, Q.; Ling, C. MiR-124 suppresses cell proliferation in hepatocellular carcinoma by targeting PIK3CA. *Biochem. Biophys. Res. Commun.* **2012**, *426*, 247–252. [CrossRef]
91. Zhang, Y.; Guo, X.; Xiong, L.; Yu, L.; Li, Z.; Guo, Q.; Li, B.; Lin, N. Comprehensive analysis of microRNA-regulated protein interaction network reveals the tumor suppressive role of microRNA-149 in human hepatocellular carcinoma via targeting AKT-mTOR pathway. *Mol. Cancer* **2014**, *13*, 253. [CrossRef] [PubMed]
92. Damodaran, S.; Zhao, F.; Deming, D.A.; Mitchell, E.P.; Wright, J.J.; Gray, R.J.; Wang, V.; McShane, L.M.; Rubinstein, L.V.; Patton, D.R.; et al. Phase II Study of Copanlisib in Patients With PIK3CA Mutations: Results From the NCI-MATCH ECOG-ACRIN Trial (EAY131) Subprotocol Z1F. *J. Clin. Oncol.* **2022**, *40*, 1552–1561. [CrossRef] [PubMed]
93. Ahn, D.H.; Li, J.; Wei, L.; Doyle, A.; Marshall, J.L.; Schaaf, L.J.; Phelps, M.A.; Villalona-Calero, M.A.; Bekaii-Saab, T. Results of an abbreviated phase-II study with the Akt Inhibitor MK-2206 in Patients with Advanced Biliary Cancer. *Sci. Rep.* **2015**, *5*, 12122. [CrossRef]
94. Matter, M.S.; Decaens, T.; Andersen, J.B.; Thorgeirsson, S.S. Targeting the mTOR pathway in hepatocellular carcinoma: Current state and future trends. *J. Hepatol.* **2014**, *60*, 855–865. [CrossRef]
95. Lee, K.W.; Kim, S.H.; Yoon, K.C.; Lee, J.M.; Cho, J.H.; Hong, S.K.; Yi, N.J.; Han, S.S.; Park, S.J.; Suh, K.S. Sirolimus Prolongs Survival after Living Donor Liver Transplantation for Hepatocellular Carcinoma Beyond Milan Criteria: A Prospective, Randomised, Open-Label, Multicentre Phase 2 Trial. *J. Clin. Med.* **2020**, *9*, 3264. [CrossRef]
96. Tian, L.Y.; Smit, D.J.; Jücker, M. The Role of PI3K/AKT/mTOR Signaling in Hepatocellular Carcinoma Metabolism. *Int. J. Mol. Sci.* **2023**, *24*, 2652. [CrossRef]
97. Cervello, M.; McCubrey, J.A.; Cusimano, A.; Lampiasi, N.; Azzolina, A.; Montalto, G. Targeted therapy for hepatocellular carcinoma: Novel agents on the horizon. *Oncotarget* **2012**, *3*, 236–260. [CrossRef]
98. Thomas, M.B.; Garrett-Mayer, E.; Anis, M.; Anderton, K.; Bentz, T.; Edwards, A.; Brisendine, A.; Weiss, G.; Siegel, A.B.; Bendell, J.; et al. A Randomized Phase II Open-Label Multi-Institution Study of the Combination of Bevacizumab and Erlotinib Compared to Sorafenib in the First-Line Treatment of Patients with Advanced Hepatocellular Carcinoma. *Oncology* **2018**, *94*, 329–339. [CrossRef]
99. Kelley, R.K.; Joseph, N.M.; Nimeiri, H.S.; Hwang, J.; Kulik, L.M.; Ngo, Z.; Behr, S.C.; Onodera, C.; Zhang, K.; Bocobo, A.G.; et al. Phase II Trial of the Combination of Temozolomide and Sorafenib in Advanced Hepatocellular Carcinoma with Tumor Mutation Profiling. *Liver Cancer* **2021**, *10*, 561–571. [CrossRef]
100. Chan, S.L.; Yeo, W. Development of systemic therapy for hepatocellular carcinoma at 2013: Updates and insights. *World J. Gastroenterol.* **2014**, *20*, 3135–3145. [CrossRef]

101. Lu, X.; Paliogiannis, P.; Calvisi, D.F.; Chen, X. Role of the Mammalian Target of Rapamycin Pathway in Liver Cancer: From Molecular Genetics to Targeted Therapies. *Hepatology* **2021**, *73* (Suppl. S1), 49–61. [CrossRef]
102. Avramović, N.; Mandić, B.; Savić-Radojević, A.; Simić, T. Polymeric Nanocarriers of Drug Delivery Systems in Cancer Therapy. *Pharmaceutics* **2020**, *12*, 298. [CrossRef]
103. Mu, H.; Lin, K.X.; Zhao, H.; Xing, S.; Li, C.; Liu, F.; Lu, H.Z.; Zhang, Z.; Sun, Y.L.; Yan, X.Y.; et al. Identification of biomarkers for hepatocellular carcinoma by semiquantitative immunocytochemistry. *World J. Gastroenterol.* **2014**, *20*, 5826–5838. [CrossRef] [PubMed]
104. Baumhoer, D.; Tornillo, L.; Stadlmann, S.; Roncalli, M.; Diamantis, E.K.; Terracciano, L.M. Glypican 3 expression in human nonneoplastic, preneoplastic, and neoplastic tissues: A tissue microarray analysis of 4,387 tissue samples. *Am. J. Clin. Pathol.* **2008**, *129*, 899–906. [CrossRef] [PubMed]

**Disclaimer/Publisher’s Note:** The statements, opinions and data contained in all publications are solely those of the individual author(s) and contributor(s) and not of MDPI and/or the editor(s). MDPI and/or the editor(s) disclaim responsibility for any injury to people or property resulting from any ideas, methods, instructions or products referred to in the content.

## Article

# Synthesis and Anticancer Activity of Novel Dual Inhibitors of Human Protein Kinases CK2 and PIM-1 †

Patrycja Wińska <sup>1,\*</sup>, Monika Wielechowska <sup>1</sup>, Mirosława Koronkiewicz <sup>2</sup> and Paweł Borowiecki <sup>1,\*</sup>

<sup>1</sup> Faculty of Chemistry, Warsaw University of Technology, 00-664 Warsaw, Poland; mwielechowska@ch.pw.edu.pl

<sup>2</sup> Department of Biomedical Research, National Medicines Institute, 00-725 Warsaw, Poland; m.koronkiewicz@nil.gov.pl

\* Correspondence: patrycja.winska@pw.edu.pl (P.W.); pawel.borowiecki@pw.edu.pl (P.B.); Tel.: +48-222345573 (P.W.); +48-222347677 (P.B.)

† Tribute to Zygmunt Antoni Kazimierzczuk (1945–2021).

**Abstract:** CK2 and PIM-1 are serine/threonine kinases involved in the regulation of many essential processes, such as proliferation, differentiation, and apoptosis. Inhibition of CK2 and PIM-1 kinase activity has been shown to significantly reduce the viability of cancer cells by inducing apoptosis. A series of novel amino alcohol derivatives of parental DMAT were designed and synthesized as potent dual CK2/PIM-1 inhibitors. Concomitantly with the inhibition studies toward recombinant CK2 and PIM-1, the influence of the obtained compounds on the viability of three human carcinoma cell lines, i.e., acute lymphoblastic leukemia (CCRF-CEM), human chronic myelogenous leukemia (K-562), and breast cancer (MCF-7), as well as non-cancerous cells (Vero), was evaluated using an MTT assay. Induction of apoptosis and cell cycle progression after treatment with the most active compound and a lead compound were studied by flow-cytometry-based assay. Additionally, autophagy induction in K-562 cells and intracellular inhibition of CK2 and PIM-1 in all the tested cell lines were evaluated by qualitative/quantitative fluorescence-based assay and Western blot method, respectively. Among the newly developed inhibitors, 1,1,1-trifluoro-3-[(4,5,6,7-tetrabromo-1*H*-benzimidazol-2-yl)amino]propan-2-ol demonstrates the highest selectivity and the most prominent proapoptotic properties towards the studied cancer cells, especially towards acute lymphoblastic leukemia, in addition to inducing autophagy in K-562 cells.

**Keywords:** 4,5,6,7-tetrabromo-*N,N*-dimethyl-1*H*-benzimidazol-2-amine (DMAT) derivatives; protein kinase CK2; protein kinase PIM-1; dual protein kinase inhibitors; antitumor activity; apoptosis; autophagy

**Citation:** Wińska, P.; Wielechowska, M.; Koronkiewicz, M.; Borowiecki, P. Synthesis and Anticancer Activity of Novel Dual Inhibitors of Human Protein Kinases CK2 and PIM-1. *Pharmaceutics* **2023**, *15*, 1991. <https://doi.org/10.3390/pharmaceutics15071991>

Academic Editors: Francesca Musumeci and Anna Carbone

Received: 26 May 2023  
Revised: 5 July 2023  
Accepted: 17 July 2023  
Published: 20 July 2023



**Copyright:** © 2023 by the authors. Licensee MDPI, Basel, Switzerland. This article is an open access article distributed under the terms and conditions of the Creative Commons Attribution (CC BY) license (<https://creativecommons.org/licenses/by/4.0/>).

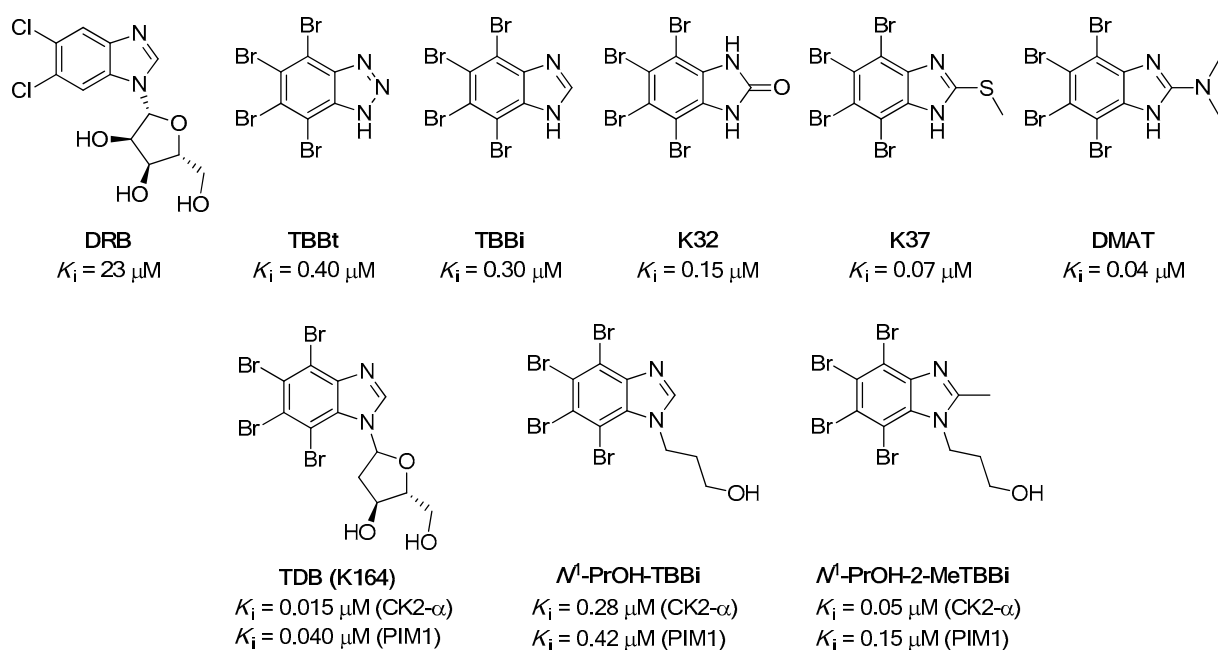
## 1. Introduction

Protein kinase CK2 (an acronym derived from the old misnomer “casein kinase 2”) and PIM-1 (proviral integration of Moloney virus-1) are protein serine/threonine kinases that have been implicated in cell growth and proliferation [1,2]. CK2 phosphorylates over 300 substrates and has multiple roles in the cell cycle, including in cell growth, proliferation, and survival [3,4]. The PIM kinase family contains three strongly evolutionary conservative isoforms: PIM-1, PIM-2, and PIM-3 [5]. Although CK2 and PIM kinases belong to different branches of the kinome [6], they exhibit structural and functional similarities. Unlike other eukaryotic kinases, both CK2 and PIM-1 demonstrate constitutive activity associated with a lack of phosphorylation sites in the activation loop [7,8]. Overexpression of these kinases occurs in many types of cancers, including leukemia, breast, and prostate cancer [9–12]. The increased catalytic activity of PIM-1 and CK2 kinases has been shown to enhance cell resistance to chemotherapy, inter alia, by inactivating BAD protein, a member of the Bcl-2 family [13], and interacting with the Myc factor [14]. It has been reported that the phosphorylation of BAD by CK2 and PIM kinases inhibits its proapoptotic functions in leukemia and prostate cancer, contributing to increased cell survival [13,15]. Moreover,

PIM-1 overexpression combined with Myc leads to the development of the advanced form of prostate carcinoma [16]. The data show that overexpression of CK2 and PIM-1 kinases is a poor predictor in many cancers, such as prostate cancer and breast cancer, among others [17–19], and the reduction in CK2 and PIM-1 activity by chemical or molecular methods induces apoptosis in tumor cells [20–22].

Recent studies have shown that the contribution of CK2 and PIM-1 kinases to the regulation of transcription, differentiation, or signaling of DNA damage/repair systems is achieved by regulating survival pathways and hypoxia [23]. The activity of both CK2 and PIM-1 has been demonstrated to be elevated in hypoxia, which increases HIF-1 transcriptional activity (hypoxia-induced factor), whereas under normoxia, this factor is degraded [24]. In contrast, in hypoxia, its active form impacts the expression of many genes, stimulating angiogenesis and tumor cell resistance to chemotherapy [25–27]. Moreover, both kinases activate the transcriptional factor NF- $\kappa$ B, which is observed in transformed cells [28]. Furthermore, tumor transformation of lymphocytes with PIM-2 involvement depends on the activation of NF- $\kappa$ B [29]. In addition, PIM-1 is essential in activating the NF- $\kappa$ B pathway, which allows for the survival of prostate cancer cells treated with docetaxel, whereas PIM-1 knockdown or expression of a dominant negative protein sensitizes cells to the cytotoxic effects of docetaxel [30].

Over the last three decades, a plethora of potent and cell-permeable ATP-competitive inhibitors for CK2 kinase has been developed [4]. Among the most prominent examples are the polyhalogenated compounds depicted in Figure 1.



**Figure 1.** Chemical structures of the representative examples of CK2 inhibitors (5,6-dichloro-1- $\beta$ -D-ribofuranosylbenzimidazole (DRB), 4,5,6,7-tetrabromo-1H-benzotriazole (TBBt), 4,5,6,7-tetrabromo-1H-benzimidazole (TBBi), 4,5,6,7-tetrabromo-2,3-dihydro-1H-1,3-benzodiazol-2-one (K32), 4,5,6,7-tetrabromo-2,3-dihydro-1H-1,3-benzodiazol-2-one (K37), and 4,5,6,7-tetrabromo-*N,N*-dimethyl-1H-benzimidazol-2-amine (DMAT)), and dual CK2/PIM-1 inhibitors (1-( $\beta$ -D-2'-deoxyribofuranosyl)-4,5,6,7-tetrabromo-1H-benzimidazole (TDB, also termed K164), 3-(4,5,6,7-tetrabromo-1H-1,3-benzodiazol-1-yl)propan-1-ol ( $N^1$ -PrOH-TBBi), and 3-(4,5,6,7-tetrabromo-2-methyl-1H-1,3-benzodiazol-1-yl)propan-1-ol ( $N^1$ -PrOH-TBBi)).

Essential chemical features necessary for efficient inhibitory activity toward CK2 have already been well-identified. Moreover, most of the structural characteristics of halogenated compounds were proven beneficial for the inhibition of the catalytic activity of PIM-1 [31,32].

Since complex signaling pathways and multiple targets are often involved in cancers, synergistically inhibiting multiple targets may be a more effective therapeutic strategy than a convenient single-target approach [33]. To date, quite a few multitarget CK2 inhibitors have been disclosed, which have the potential to become clinical candidates [31]. In this regard, the real breakthrough in the field of developing cell-permeable dual inhibitors of protein kinases CK2 and PIM-1 was achieved by discovering 1-( $\beta$ -D-2'-deoxyribofuranosyl)-4,5,6,7-tetrabromo-1*H*-benzimidazole (TDB, also termed K164) [34,35]. These studies have shown that the use of dual inhibitors of CK2 and PIM-1 is beneficial for the reduction in cell proliferation and induction of apoptosis in cancer cell lines, i.e., cervical cancer (HeLa) and chronic myeloid leukemia (CML) [35,36]. The most recent studies demonstrated that inhibitor K164 is a promising compound that can be considered a potential active agent in targeted therapy in selected types of breast cancer [37].

In our previous studies [38,39], we evaluated the influence of the structure of the TBBi-alkanol side chain. We found that introducing hydroxyl groups into the aliphatic substituent attached to the hydrophobic TBBi scaffold is critical for the efficient inhibition of CK2. Although this structural fragment is located towards the outer part of the CK2 ATP-binding site, it generates additional polar interactions with a catalytic cavity, which increase the affinity toward the kinase receptor. In view of these findings, we also obtained a novel potent dual CK2/PIM-1 inhibitor, namely 3-(4,5,6,7-tetrabromo-2-methyl-1*H*-1,3-benzodiazol-1-yl)propan-1-ol ( $N^1$ -PrOH-TBBi), which, after functionalization into its corresponding acetyl prodrug, turned out to be a very promising anticancer agent toward breast cancer cell lines [40]. Therefore, we expect that further structural modification of aliphatic substituents possessing efficient hydrogen bond-forming moieties installed at the appropriate distance from the TBBi core structure will enhance the affinity and selectivity of the designed 2-alkanol-TBBi derivatives toward titled kinases.

In this work, our ultimate goal was to design and synthesize novel amino alcohol derivatives of parental DMAT as potent dual CK2/PIM-1 inhibitors exhibiting promising anticancer activity. In this regard, intending to potentiate a DMAT-lead structure, we obtained a series of its model analogs differing in the structural topology of aliphatic amino alcohol substituents. Given that previous studies showed that breast cancer, as well as leukemic cells, is sensitive to dual CK2/PIM-1 inhibitor treatment [35–37], two leukemic cell lines, i.e., CCRF-CEM and K-562, and breast cancer cells, i.e., MCF-7, were used in the present study.

## 2. Materials and Methods

### 2.1. Chemistry

#### 2.1.1. General Procedure for the Synthesis of 2-Bromo-1*H*-benzimidazole (2)

Compound **2** was synthesized according to the procedure reported by Ellingboe et al. [41]. Br<sub>2</sub> (12 mL, 0.24 mol) was added dropwise to a cooled (water bath, 5–10 °C) and mechanically stirred mixture of 2-mercapto-1*H*-benzimidazole (**1**, 10.0 g, 66.58 mmol), 48% aqueous HBr (10 mL), and glacial AcOH (100 mL) over 25 min. The mixture warmed slightly (40–45 °C) during the addition, and additional glacial AcOH (50 mL) was added to aid in the stirring of the thick mixture. After the addition was complete, stirring was continued at room temperature for 4 h. Afterwards, H<sub>2</sub>O (200 mL) was added, and the resulting solution was cooled in an ice bath (0–5 °C). The pH was adjusted to 4 with solid NaOH (ca. 40 g), and the precipitate was collected by filtration to afford a crude product, which was further purified by recrystallization from acetone to afford 2-bromo-1*H*-benzimidazole (**2**, 6.93 g, 35.17 mmol, 53% yield) as a white solid. Mp 194–196 °C (acetone) [41] 190–192 °C (acetone); *R*<sub>f</sub> [CH<sub>2</sub>Cl<sub>2</sub>/MeOH (99:1, *v/v*)] 0.24; <sup>1</sup>H NMR (500 MHz, DMSO-*d*<sub>6</sub>):  $\delta$  13.18 (br. s, 1H), 7.51 (s, 2H), 7.19 (m, 2H), 2.07 (s, 1H); <sup>13</sup>C NMR (126 MHz, DMSO-*d*<sub>6</sub>):  $\delta$  139.7, 127.2, 122.2, 114.6; MS (ESI-TOF) *m/z*: [M + H]<sup>+</sup> Calcd for C<sub>7</sub>H<sub>6</sub>BrN<sub>2</sub><sup>+</sup> *m/z*: 196.9709, Found 196.9697; FTMS (ESI-TOF) *m/z*: [M + H]<sup>+</sup> Calcd for C<sub>7</sub>H<sub>6</sub>BrN<sub>2</sub><sup>+</sup> *m/z*: 196.97089 and 198.96884, Found 196.97125 and 198.96854; GC [200–260 (10 °C/min)]: *t*<sub>R</sub> = 3.16 min.



### 2.1.2. General Procedure for the Synthesis of 2,4,5,6,7-Pentabromo-1*H*-benzimidazole (**3**)

Compound **3** was synthesized according to the procedure reported by Andrzejewska et al. [42]. Br<sub>2</sub> (8 mL, 160 mmol) was added portionwise to a stirred and refluxed suspension of 2-bromo-1*H*-benzimidazole (**2**, 1.5 g, 7.6 mmol) in H<sub>2</sub>O (60 mL) within 6 h. The reflux was continued for 24 h under irradiation of purple LEDs (390 nm) (for details, see Figure S1 in the Supplementary Materials). Afterward, the reaction mixture was cooled, and the orange precipitate was filtered off under suction. The collected solid was dissolved in MeOH/25% NH<sub>3</sub>aq. (80 mL, 3:1, *v/v*) and treated with charcoal (1.3 g) and Celite® 545 (3.5 g). After filtering the solids under suction, the pale-yellow solution of the permeate was brought to pH 4–5 with conc. AcOH (150 mL), and the formed precipitate was recrystallized from a mixture of MeOH/H<sub>2</sub>O (50 mL, 1:1, *v/v*) to afford 2,4,5,6,7-pentabromo-1*H*-benzimidazole (**3**, 1.65 g, 3.22 mmol, 42%) as a yellowish solid.

Yield, 42% (1.65 g); yellowish solid; *R*<sub>f</sub> [hexane/AcOEt (50:50, *v/v*)] 0.15; <sup>1</sup>H NMR (500 MHz, DMSO-*d*<sub>6</sub>): δ Not found; <sup>13</sup>C NMR (126 MHz, DMSO-*d*<sub>6</sub> + 2 drops of 2M HCl<sub>aq</sub>, and registered for 16 h): δ 142.7, 138.9, 138.0, 131.3, 121.0, 120.9, 110.3; FTMS (ESI-TOF) *m/z*: [M + H]<sup>+</sup> Calcd for C<sub>7</sub>H<sub>2</sub>Br<sub>5</sub>N<sub>2</sub><sup>+</sup> *m/z*: 512.60884, Found 512.60913.

### 2.1.3. General Procedure for the Synthesis of Dual CK2/PIM-1 Inhibitors—TBBi Amino Alcohol Derivatives (**4–11**)

Compounds **4–11** were synthesized according to the procedure reported by Kazimierczuk and Pinna et al. [43].

*Method A*: A mixture of 2,4,5,6,7-pentabromo-1*H*-benzimidazole (**3**, 150 mg, 0.30 mmol) and the respective amino alcohol (4.9 equiv) in anhydrous EtOH (4.5 mL) was heated in an ace pressure tube (bushing type, back seal, *V* = 15 mL, *L* × O.D. 10.2 cm × 25.4 mm, Sigma Aldrich (Darmstadt, Germany): Z181064) at 110–115 °C for 72 h. Afterward, the reaction mixture was cooled to room temperature, and the volatiles were evaporated under reduced pressure using a rotavap. The oil residue was purified by a column chromatography using a sequential mixture of hexane/AcOEt (500 mL, 50:50 *v/v*) and CHCl<sub>3</sub>/MeOH (500 mL, 90:10 *v/v*) as an eluent to afford the desired solid-state products (**4**, *rac*-**6**, **8**, *rac*-**9**, **10**, and **11**).

*Method B*: A mixture of 2,4,5,6,7-pentabromo-1*H*-benzimidazole (**3**, 500 mg, 0.98 mmol) and racemic 2-hydroxypropylamine (1.10 g, 14.63 mmol, 1.13 mL) in anhydrous EtOH (7.5 mL) was heated in an ace pressure tube (bushing type, back seal, *V* = 15 mL, *L* × O.D. 10.2 cm × 25.4 mm, Sigma Aldrich (Darmstadt, Germany): Z181064) at 110–115 °C for 72 h. Afterward, the reaction mixture was cooled to room temperature, and the volatiles were evaporated under reduced pressure using a rotavap. The oil residue was purified by a column chromatography using a sequential mixture of hexane/AcOEt (500 mL, 50:50 *v/v*) and CHCl<sub>3</sub>/MeOH (500 mL, 90:10 *v/v*) as an eluent to afford the desired product, 1-[(4,5,6,7-tetrabromo-1*H*-benzimidazol-2-yl)amino]propan-2-ol (*rac*-**5**, 247 mg, 0.49 mmol, 50%), as a white solid.

*Method C*: A mixture of 2,4,5,6,7-pentabromo-1*H*-benzimidazole (**3**, 50 mg, 98 μmol) and optically active (*S*)- or (*R*)-1-aminopropan-2-ol (110 mg, 1.46 mmol, 113 μL) in dry PhCH<sub>3</sub> (1 mL) was heated in an ace pressure tube (bushing type, back seal, *V* = 15 mL, *L* × O.D. 10.2 cm × 25.4 mm, Sigma Aldrich (Darmstadt, Germany): Z181064) at 100 °C for 48 h. Afterward, the reaction mixture was cooled to room temperature, and the volatiles were evaporated under reduced pressure using a rotavap. The oil residue was purified by a column chromatography using CHCl<sub>3</sub>/MeOH (95:5 *v/v*) as an eluent to afford the desired enantiomerically pure (2*S*)-1-[(4,5,6,7-tetrabromo-1*H*-benzimidazol-2-yl)amino]propan-2-ol [(*S*)-**5**, 46 mg, 91 μmol, 93% yield, >99% ee] or (2*R*)-1-[(4,5,6,7-tetrabromo-1*H*-benzimidazol-2-yl)amino]propan-2-ol [(*R*)-**5**, 42 mg, 83 μmol, 85% yield, >99% ee] as a white solid.

4,5,6,7-Tetrabromo-*N,N*-dimethyl-1*H*-benzimidazol-2-amine (DMAT, **4**)

Synthesized according to *Method A* (Section 2.3). Yield, 29% (41 mg); white solid; *R*<sub>f</sub> [CHCl<sub>3</sub>/MeOH (95:5 *v/v*)] 0.82; <sup>1</sup>H NMR (500 MHz, DMSO-*d*<sub>6</sub>): δ 11.44 (br. s, 1H, NH), 3.13 (s, 6H, CH<sub>3</sub>); <sup>13</sup>C NMR (126 MHz, DMSO-*d*<sub>6</sub>): δ 158.1 (CNCH<sub>3</sub>), 38.3 (CH<sub>3</sub>), the rest of

the peaks were not detected; FTMS (ESI-TOF)  $m/z$ :  $[M + H]^+$  Calcd for  $C_9H_8Br_4N_3^+$   $m/z$ : 477.74053, Found 477.74015.

*1-[(4,5,6,7-Tetrabromo-1H-benzimidazol-2-yl)amino]propan-2-ol (rac-5)*

Synthesized according to *Method B* (Section 2.3). Yield, 50% (247 mg); white solid;  $R_f$  [hexane/AcOEt (50:50,  $v/v$ )] 0.22 or  $R_f$  [ $CHCl_3$ /MeOH (90:10,  $v/v$ )] 0.60 or  $R_f$  [ $CHCl_3$ /MeOH (95:5  $v/v$ )] 0.54;  $^1H$  NMR (500 MHz, acetone- $d_6$ ):  $\delta$  11.04 (br. s, 1H), 6.48 (br. s, 1H), 4.70 (br. s, 1H), 4.07–3.92 (m, 1H), 3.56 (ddd,  $J = 13.6, 6.5, 3.5$  Hz, 1H), 3.33 (ddd,  $J = 13.5, 7.3, 5.1$  Hz, 1H), 1.19 (d,  $J = 6.3$  Hz, 3H);  $^1H$  NMR (500 MHz, DMSO- $d_6$ ):  $\delta$  11.41 (br. s, 1H), 6.62 (br. s, 1H), 4.95 (br. s, 1H), 3.83 (d,  $J = 5.9$  Hz, 1H), 3.38 (ddd,  $J = 13.2, 6.5, 4.4$  Hz, 1H), 3.26–3.18 (m, 1H), 1.10 (d,  $J = 6.2$  Hz, 3H);  $^{13}C$  NMR (126 MHz, DMSO- $d_6$  + 2 drops of 2M  $HCl_{aq}$ . and registered for 16 h):  $\delta$  154.8, 153.2, 131.5, 130.5, 120.8, 118.0, 106.4, 103.7, 65.2, 50.1, 20.8; FTMS (ESI-TOF)  $m/z$ :  $[M + H]^+$  Calcd for  $C_{10}H_{10}Br_4N_3O^+$   $m/z$ : 507.75110, Found 507.75086; HPLC [*n*-hexane-2-PrOH (95:5,  $v/v$ );  $f = 0.8$  mL/min;  $\lambda = 225$  nm;  $T = 25$  °C (Chiralpak AD-H)]:  $t_R = 19.105$  (S-isomer) and 21.524 min (R-isomer).

*1,1,1-Trifluoro-3-[(4,5,6,7-tetrabromo-1H-benzimidazol-2-yl)amino]propan-2-ol (rac-6)*

Synthesized according to *Method A* (Section 2.3). Yield, 28% (46 mg); beige solid;  $R_f$  [ $CHCl_3$ /MeOH (95:5  $v/v$ )] 0.55;  $^1H$  NMR (500 MHz, DMSO- $d_6$ ):  $\delta$  11.69 (br. s, 1H), 6.76 (t,  $J = 5.9$  Hz, 1H), 6.66 (br. s, 1H), 4.39–4.27 (m, 1H), 3.70 (ddd,  $J = 13.8, 6.1, 4.0$  Hz, 1H), 3.49 (ddd,  $J = 13.9, 8.1, 5.8$  Hz, 1H);  $^{19}F$  NMR (470 MHz,  $CD_3CN$ ):  $\delta$  -77.26 (d,  $J = 7.4$  Hz, 3F); FTMS (ESI-TOF)  $m/z$ :  $[M + H]^+$  Calcd for  $C_{10}H_7Br_4F_3N_3O^+$   $m/z$ : 561.72283, Found 561.72251.

*3-[(4,5,6,7-Tetrabromo-1H-benzimidazol-2-yl)amino]propan-1-ol (7)*

Synthesized according to *Method A* (Section 2.3). Yield, 44% (67 mg); light green solid;  $R_f$  [ $CHCl_3$ /MeOH (95:5  $v/v$ )] 0.32;  $^1H$  NMR (500 MHz, DMSO- $d_6$ ):  $\delta$  11.59 (br. s, 1H), 6.77 (t,  $J = 5.4$  Hz, 1H), 3.50 (t,  $J = 6.1$  Hz, 4H), 3.43 (q,  $J = 6.6$  Hz, 2H), 1.71 (p,  $J = 6.5$  Hz, 2H); FTMS (ESI-TOF)  $m/z$ :  $[M + H]^+$  Calcd for  $C_{10}H_{10}Br_4N_3O^+$   $m/z$ : 507.75110, Found 507.75116.

*2-[Methyl(4,5,6,7-tetrabromo-1H-benzimidazol-2-yl)amino]ethanol (8)*

Synthesized according to *Method A* (Section 2.3). Yield, 37% (56 mg); white solid;  $R_f$  [ $CHCl_3$ /MeOH (95:5  $v/v$ )] 0.60;  $^1H$  NMR (500 MHz, DMSO- $d_6$ ):  $\delta$  11.44 (br. s, 1H), 4.89 (br. s, 1H), 3.67–3.59 (m, 4H), 3.17 (s, 3H); FTMS (ESI-TOF)  $m/z$ :  $[M + H]^+$  Calcd for  $C_{10}H_{10}Br_4N_3O^+$   $m/z$ : 507.75110, Found 507.75116.

*1-(Diethylamino)-3-[(4,5,6,7-tetrabromo-1H-benzimidazol-2-yl)amino]propan-2-ol (rac-9)*

Synthesized according to *Method A* (Section 2.3). Yield, 64% (112 mg); white solid;  $R_f$  [ $CHCl_3$ /MeOH (95:5  $v/v$ )] 0.48;  $^1H$  NMR (500 MHz, DMSO- $d_6$ ):  $\delta$  8.22 (br. s, 1H), 5.32 (dt,  $J = 11.1, 5.5$  Hz, 1H), 5.04 (ddd,  $J = 13.3, 5.8, 4.4$  Hz, 1H), 4.85–4.76 (m, 1H), 4.24–3.80 (m, 12H); FTMS (ESI-TOF)  $m/z$ :  $[M + H]^+$  Calcd for  $C_{14}H_{19}Br_4N_4O^+$   $m/z$ : 578.82459, Found 578.82454.

*2-[(4,5,6,7-Tetrabromo-1H-benzimidazol-2-yl)amino]propane-1,3-diol (10)*

Synthesized according to *Method A* (Section 2.3). Yield, 13% (20 mg); white solid;  $R_f$  [ $CHCl_3$ /MeOH (95:5  $v/v$ )] 0.10;  $^1H$  NMR (500 MHz, DMSO- $d_6$ ):  $\delta$  6.39 (d,  $J = 7.7$  Hz, 1H), 3.88–3.79 (m, 1H), 3.55 (qd,  $J = 10.7, 5.4$  Hz, 4H); FTMS (ESI-TOF)  $m/z$ :  $[M + H]^+$  Calcd for  $C_{10}H_{10}Br_4N_3O_2^+$   $m/z$ : 523.74601, Found 523.74597.

*3-[(4,5,6,7-Tetrabromo-1H-benzimidazol-2-yl)amino]propane-1,2-diol (rac-11)*

Synthesized according to *Method A* (Section 2.3). Yield, 38% (60 mg); white solid;  $R_f$  [ $CHCl_3$ /MeOH (95:5  $v/v$ )] 0.13;  $^1H$  NMR (500 MHz, DMSO- $d_6$ ):  $\delta$  6.61 (t,  $J = 5.3$  Hz, 1H), 4.09 (d,  $J = 4.7$  Hz, 1H), 3.70–3.60 (m, 1H), 3.51 (ddd,  $J = 13.4, 6.3, 4.6$  Hz, 1H), 3.43–3.36 (m, 1H), 3.17 (d,  $J = 2.6$  Hz, 2H); FTMS (ESI-TOF)  $m/z$ :  $[M + H]^+$  Calcd for  $C_{10}H_{10}Br_4N_3O_2^+$   $m/z$ : 523.74601, Found 523.74584.

## 2.2. Biological Evaluation

### 2.2.1. Reagents and Antibodies

Dimethyl sulfoxide (DMSO), a molecular-biology-grade solvent used for all stocks of the chemical agents, was obtained from Carl Roth (Karlsruhe, Germany). All reagents used in flow cytometry analysis were purchased from BD Biosciences Pharmingen (San Diego, CA, USA). Information about antibodies is provided in Supplementary Materials (Section S3.1).

### 2.2.2. Cloning, Expression, and Purification of Human CK2 $\alpha$ , holoCK2, and PIM-1

CK2 $\alpha$ , holoCK2, and PIM-1 were obtained according to Borowiecki [44] and Chojnacki [45]. The protein concentration in the final solution was 12.68 mg/mL for CK2 $\alpha$ , 1.61 mg/mL for holoCK2, and 3.0 mg/mL for PIM-1 (determined by the Bradford method using bovine serum albumin as a standard) [46].

### 2.2.3. Inhibition of Recombinant CK2 and PIM-1

The obtained compounds were tested for their inhibitory activity toward human CK2 $\alpha$ , human CK2 holoenzyme, and PIM-1 using a P81 filter isotopic assay as described previously [39]. IC<sub>50</sub> values were determined for the tested compounds at eight concentrations in the range of 0.005 to 400  $\mu$ M. The experimental data were fitted to the sigmoidal dose-response equation, i.e., (variable slope)  $Y = \text{Bottom} + (\text{Top} - \text{Bottom}) / (1 + 10^{((\text{LogIC}_{50} - X) * \text{HillSlope})})$ , in GraphPad Prism (Prism 9, v. 9.0.1).

### 2.2.4. Cell Culture and Agent Treatment

An acute lymphoblastic leukemia ALL cell line (named CCRF-CEM) was purchased from the European Collection of Authenticated Cell Cultures (ECACC), whereas MCF-7 (hormone-dependent breast adenocarcinoma), K-562 (human chronic myelogenous leukemia), and Vero cells (*Cercopithecus aethiops* kidney) were purchased from the American Type Culture Collection (ATCC, Manassas, VA, USA). For more details, see Supplementary Materials (Section S3.2).

### 2.2.5. 3-(4,5-Dimethylthiazol-2-yl)-2,5-diphenyltetrazolium Bromide (MTT)-Based Viability Assay

After incubation with the tested compounds, an MTT test was performed as described previously [39]. Optical densities were measured at 570 nm using a BioTek microplate reader (BioTek Instruments, Inc., Winooski, VT, USA). All measurements were carried out in a minimum of three biological replicates.

### 2.2.6. Detection of Apoptosis by Annexin V/propidium Iodide (PI) Labeling

MCF-7 cells were seeded in 6-well plates at  $1.2 \times 10^5$  cells/well, whereas CCRF-CEM and K-562 cells were seeded in 24-well plates at a density of  $2 \times 10^5$ /mL. Cells were treated with the tested compounds used in 5  $\mu$ M and 10  $\mu$ M concentrations. Then, the plates were incubated for 48 h. After exposure to the examined compounds, the cells were collected and centrifugated at  $200 \times g$  at 4  $^{\circ}$ C for 5 min, washed twice in cold phosphate-buffered saline (PBS), and subsequently suspended in binding buffer at  $1 \times 10^6$  cells/mL. Subsequently, 100- $\mu$ L aliquots of the cell suspension were labeled according to the instructions of the respective manufacturer's kit. Briefly, annexin V-fluorescein isothiocyanate and propidium iodide (BD Biosciences, Pharmingen, San Diego, CA, USA) were added to the cell suspension, and the mixture was vortexed, then incubated for 15 min at RT in the dark. A cold binding buffer (400  $\mu$ L) was then added, and the cells were vortexed again and kept on ice. Flow cytometric measurements were performed within 1 h after labeling. Viable, necrotic, early, and late apoptotic cells were detected by flow cytometry using a BD FACSCanto II flow cytometer and analyzed using BD FACSDiva operating software (BD Biosciences, San Jose, CA, USA).

### 2.2.7. Mitochondrial Membrane Potential ( $\Delta\Psi$ m) Assay

Mitochondrial membrane potential was assessed by flow cytometry using 5,5',6,6'-tetrachloro-1,1',3,3'-tetraethylbenzimidazolocarboyanine iodide (JC-1; Sigma-Aldrich, St. Louis, MO, USA). JC-1 undergoes potential-dependent accumulation in mitochondria. In healthy cells, the dye accumulates in mitochondria, forming aggregates with red fluorescence (FL-2 channel), whereas in dead and apoptotic cells, the dye remains in the cytoplasm in a monomeric form and emits green fluorescence (FL-1 channel). Cells were harvested by centrifugation 48 h post treatment, suspended in 1 mL of complete culture medium

at approximately  $1 \times 10^6$  cells/mL, and incubated with 2.5  $\mu$ L of JC-1 solution in DMSO (1 mg/mL) for 15 min at 37 °C in the dark. The stained cells were then washed with cold PBS, suspended in 400  $\mu$ L of PBS, and examined by flow cytometry.

#### 2.2.8. Microscopic Examination

K-562 cells were seeded in 6-well plates at  $2.5 \times 10^5$ /mL and subjected to the tested compounds. After 48 h of incubation, cells were centrifugated at  $200 \times g$  at 4 °C for 5 min, subsequently suspended in PBS containing 2  $\mu$ g/mL AO and Hoechst 33342, and incubated at 37 °C for 20 min in the dark. Subsequently, cells were centrifugated at  $200 \times g$  at 4 °C for 5 min. Then, 5  $\mu$ L of the sample was mounted on a glass slide and covered with a coverslip and examined under a Nikon ECLIPSE Y-TV55 fluorescent microscope.

#### 2.2.9. Fluorescence Intensity Assay

K-562 cells were seeded in 6-well plates at  $2.5 \times 10^5$ /mL and subjected to the tested compounds. After 48 h of incubation, cells were centrifugated at  $200 \times g$  at 4 °C for 5 min, subsequently suspended in PBS containing 2  $\mu$ g/mL AO and Hoechst 33342, and incubated at 37 °C for 20 min in the dark. Subsequently, cells were centrifugated at  $200 \times g$  at 4 °C for 5 min, and 150  $\mu$ L of the sample was measured on dark plates (Sarstedt). The fluorescence intensity of AO at Ex. 502 nm/Em. 520–524 nm (aggregated or DNA complexed form), Ex. 457 nm/Em. 630–644 nm (aggregated or RNA complexed form), Ex. 540 nm/Em. 640–660 nm (red-stained lysosomes), and Ex. 488 nm/Em. 540–550 nm (yellowish stained lysosomes) and that of Hoechst (nuclei, Ex. 361 nm/Em. 497 nm) in K-562 cells was measured with a Synergy H4 Hybrid Multi-Mode Microplate Reader (BioTek Instruments, Inc., Winooski, VT, USA). The data were normalized to the intensity of Hoechst (nuclei, Ex. 361 nm/Em. 497 nm) in comparison to control cells serving as the reference point, showing 100%.

#### 2.2.10. Detection of Cell Cycle Progression by Flow Cytometry

MCF-7, CCRF-CEM, and K-562 cells were cultured in 6-well plates and treated with the tested compounds for 48 h. After exposure to the compounds, the cells were collected and washed with cold PBS and fixed at  $-20$  °C in 70% ethanol for at least 24 h. Subsequently, cells were washed in PBS and stained with 50  $\mu$ g/mL PI (propidium iodide) and 100  $\mu$ g/mL RNase solution in PBS supplemented with 0.1% *v/v* Triton X-100 for 30 min in the dark at RT. Cellular DNA content was determined by flow cytometry employing a BD FACSCanto II flow cytometer (BD Biosciences, San Jose, CA, USA). The obtained DNA histograms were analyzed using MacCycle software (Phoenix Flow Systems, San Diego, CA, USA) for evaluation of the distribution of the cells in different phases of the cell cycle.

#### 2.2.11. Western Blotting

All the procedures are described in detail in Supplementary Materials (Section S3.3). The protein concentration was determined using a Bradford assay [46].

#### 2.2.12. Densitometry

For densitometry, immunoblots were scanned using G Box Chemi (Syngene, Cambridge, UK), and the density of each lane of phosphorylated and total protein was quantified using GeneSys software (Syngene, Cambridge, UK). Phosphorylated protein densities were normalized to GAPDH densities, assuming 1 for untreated cells; then, they were converted to a percentage of the appropriate control.

#### 2.2.13. Statistical Evaluation

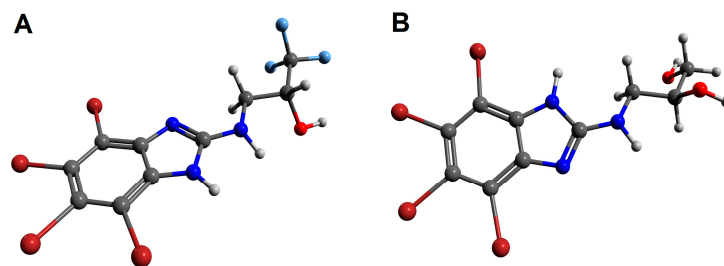
Results are represented as mean  $\pm$  s.e.m. of at least three independent experiments. Statistical analysis was performed using GraphPad Prism 5.0 software (GraphPad Software Inc., San Diego, CA, USA). Significance was determined using a one-way ANOVA analysis.

The statistical significance of differences is indicated in figures by asterisks as follows: \*  $p \leq 0.05$ , \*\*  $p \leq 0.01$ , and \*\*\*  $p \leq 0.001$ .

### 2.3. Molecular Docking

#### 2.3.1. Molecular Docking Preparation

Molecular docking studies to establish favorable ligand binding geometries for both studied inhibitors, namely 1,1,1-trifluoro-3-[(4,5,6,7-tetrabromo-1*H*-benzimidazol-2-yl)amino]propan-2-ol (*rac*-6) and 3-[(4,5,6,7-tetrabromo-1*H*-benzimidazol-2-yl)amino]propane-1,2-diol (*rac*-11), were performed using AutoDock Vina v. 1.1.2 (<http://autodock.scripps.edu/>; accessed on 21 October 2021) [47]. First, ligands *rac*-6 and *rac*-11 in non-ionizable form were prepared with ChemAxon MarvinSketch v. 14.9.1.0 (<http://www.chemaxon.com/marvin/>; accessed on 9 September 2014). The initial geometries of the ligands with the minimum energy conformation ( $E_{\text{calc.}} = -226.758$  kJ/mol for *rac*-6 and  $E_{\text{calc.}} = -171.375$  kJ/mol for *rac*-11) were optimized in Avogadro v. 1.2.0. (<http://avogadro.cc/>; accessed on 15 June 2016) using General Amber Force Field (GAFF) [48] and/or MMFF94 force field with 500 steps and the steepest descent algorithm. The visualization of the optimized geometries was performed using POV-Ray for Windows v. 3.7.0.msvc10.win64 licensed under the terms of the GNU Affero General Public License (AGPL3) (Figure 2). Afterward, the Gasteiger partial charges were calculated with AutoDock Tools v. 1.5.6 (ADT, S3 <http://mglttools.scripps.edu/>; accessed on 29 October 2022). In contrast, all torsion angles for each ligand were considered flexible, and all the possible rotatable bonds and non-polar hydrogens were determined. The final ‘ligand’ files were saved as PDBQT files (.pdbqt format) and were ready for the docking procedure disclosed below in Section 2.3.2. Molecular Docking Procedure.



**Figure 2.** The geometries of 1,1,1-trifluoro-3-[(4,5,6,7-tetrabromo-1*H*-benzimidazol-2-yl)amino]propan-2-ol (*rac*-6, (A)) and 3-[(4,5,6,7-tetrabromo-1*H*-benzimidazol-2-yl)amino]propane-1,2-diol (*rac*-11, (B)) optimized in Avogadro v. 1.2.0. The figures rendered using POV-Ray v. 3.7.0 molecular visualization software. Nitrogen atoms are presented with blue color, oxygen atoms with red color, bromine atoms with burgundy (maroon) color, and fluorine atoms with light blue color, whereas hydrogen atoms are expressed as light grey balls.

The crystal structures of human protein kinases, namely CK2- $\alpha$  (PDB code: 4KWP) [35] of the highest available resolution (1.25 Å) and PIM-1 (PDB code: 4DTK) [49] with a resolution of 1.86 Å, were downloaded from the PDB database (<http://www.rcsb.org/pdb/>). The crude target proteins were prepared using the UCSF Chimera v. 1.11.2 package (<http://www.cgl.ucsf.edu/chimera/>; accessed on 2 December 2016) [50] after removing all nonstandard molecules, including 4,5,6,7-tetrabromo-1-(2-deoxy-beta-*D*-erythro-pentofuranosyl)-1*H*-benzimidazole (EXX), sulfate ion (SO<sub>4</sub>), 1,2-ethanediol (EDO), triethylene glycol (PGE), di(hydroxyethyl)ether (PEG), and dimethyl sulfoxide (DMS) in the case of 4KWP, as well as (5*Z*)-5-{2-[(3*R*)-3-aminopiperidin-1-yl]-3-(propan-2-yloxy)benzylidene}-1,3-thiazolidine-2,4-dione (7LI), EDO, and SO<sub>4</sub> in the case of 4DTK. All the procedures are described in detail in Supplementary Materials (Section S5.1).

#### 2.3.2. Molecular Docking Procedure

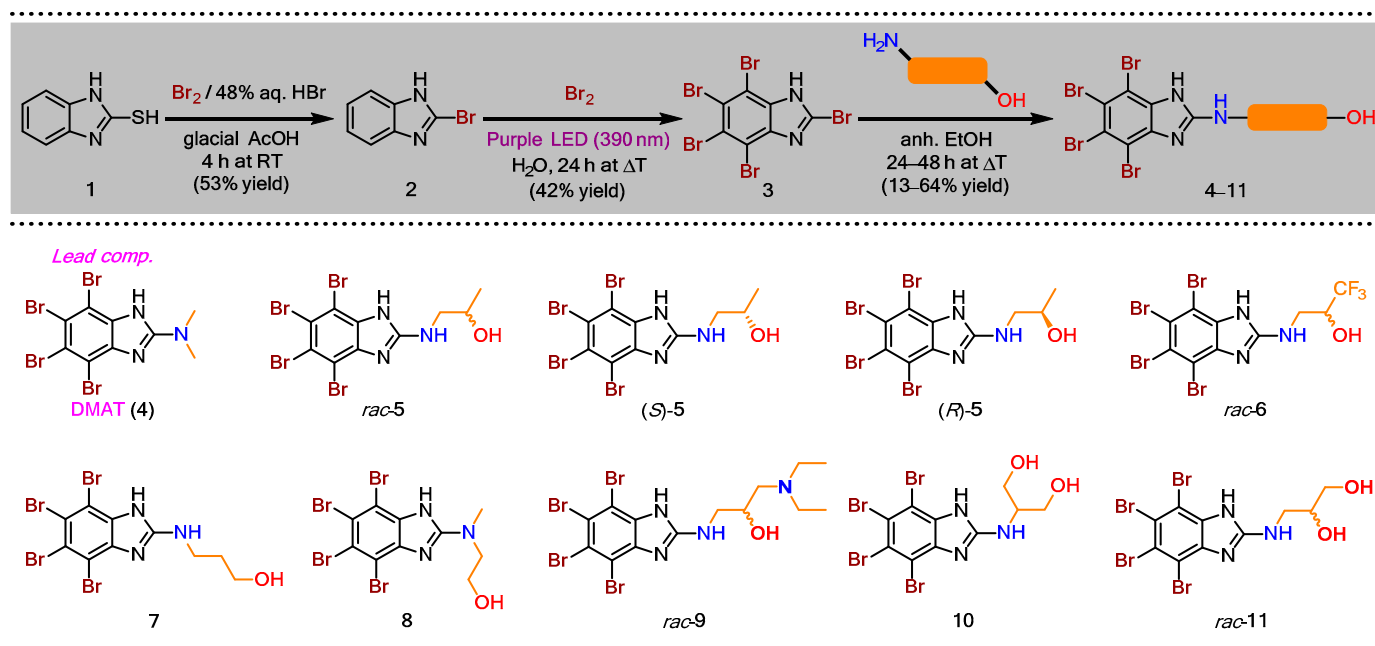
Docking was performed using standard protocols as described in Supplementary Materials (Section S5.2). For validation of the docking calculations, two prominent ki-

nase inhibitors crystallized with 4KWP and 4DTK, i.e., 4,5,6,7-tetrabromo-1-(2-deoxy-beta-*D*-erythro-pentofuranosyl)-1*H*-benzimidazole (EXX) for CK2- $\alpha$  and (5*Z*)-5-[2-[(3*R*)-3-aminopiperidin-1-yl]-3-(propan-2-yloxy)benzylidene]-1,3-thiazolidine-2,4-dione (7LI) for PIM-1, were docked as control ligands. The docking modes of each studied ligand (i.e., 1,1,1-trifluoro-3-[(4,5,6,7-tetrabromo-1*H*-benzimidazol-2-yl)amino]propan-2-ol (*rac*-6) and 3-[(4,5,6,7-tetrabromo-1*H*-benzimidazol-2-yl)amino]propane-1,2-diol (*rac*-11)) were clustered and ranked based on a mutual ligand–protein affinity expressed as absolute free binding energies ( $\Delta G_{\text{calc}}$  (kcal/mol)), as well as the values of root mean square deviation (rmsd) in both modes with respect to the rmsd lower bound (l.b.) and the rmsd upper bound (u.b.). The rmsd values were computed with reference to the input structure submitted to docking simulations. For CK2- $\alpha$  (PDB code: 4KWP), the used random seed amounted to +1342461868 for *rac*-6 and –2037069392 for *rac*-11, whereas for PIM-1 (PDB code: 4DTK), the used random seed amounted to +956047904 for *rac*-6 and –769683352 for *rac*-11. The results of docking are collected in Table S3. The optimized binding poses of *rac*-6 and *rac*-11 in hypothetical complexes with CK2- $\alpha$  and PIM-1 were visualized using PyMOL Molecular Graphics System software, v. 1.3, Schrödinger, LLC (<https://www.pymol.org/>; accessed on 13 October 2011).

### 3. Results

#### 3.1. Chemical Synthesis

Taking DMAT (4) as the lead compound, a series of dual CK2/PIM-1 inhibitors were designed and synthesized in analogy to the methods already reported in the literature [41,42]. The general synthetic route is described in Scheme 1. Briefly, in the first step, a commercially available 2-mercapto-1*H*-benzimidazole (1) was brominated with bromine (Br<sub>2</sub>) diluted in a mixture of 48% aqueous HBr and glacial acetic acid to afford 2-bromo-1*H*-benzimidazole (2) in 53% yield. Next, an exhaustive bromination of the resulting 2 with Br<sub>2</sub> in boiling water performed under irradiation of purple LEDs (390 nm) for 24 h afforded the desired 2,4,5,6,7-pentabromo-1*H*-benzimidazole (3) in 42% yield. Finally, the aminolysis of the key intermediate 3 was carried out using the appropriate amino alcohol in anhydrous ethanol in a pressure glass tube reactor at elevated temperatures (110–115 °C) to afford DMAT (4) and its derivatives (5–11) in the yield range of 13–64%.



**Scheme 1.** Synthesis of amino alcohol-like DMAT derivatives (5–11) as potential dual CK2/PIM-1 inhibitors.

Due to the strong impact of the stereochemistry of xenobiotics on their biological activity *in vivo*, there is an urgent need to evaluate the single enantiomers of designed inhibitors toward target proteins, as well as cancer cell lines. Such an evaluation is incredibly valid especially when one of the optical isomers from the pair acts as the eutomer, while its counterpart behaves as the distomer. We envisioned that if the eudismic ratio (ER) is high in the case of the developed chiral compounds (i.e., *rac-5*, *rac-6*, and *rac-11*), then the inhibitory activity of each enantiomer will significantly differ toward target kinases. Therefore, we found it pivotal for biological studies to elaborate on a highly efficient and stereoselective synthetic method for the preparation of both enantiomers of one of the chiral products (*rac-5*). This task was accomplished by employing commercially available, optically pure (*S*)- and/or (*R*)-1-aminopropan-2-ol (>99% ee) as chiral building blocks. Unfortunately, conducting the reaction with (*S*)-1-aminopropan-2-ol using a standard protocol afforded (*S*)-**5** with only 39% ee. To our delight, a detailed screening of the reaction conditions, including the selection of organic solvent, as well as the evaluation of the effect of the reaction time and temperature on the stereochemical outcome, led to obtaining enantiomerically pure antipodes (*S*)-**5** and (*R*)-**5** (>99% ee) in the 85–93% yield range (for details, see Table S1 in Supplementary Materials). Among the solvents used, only toluene (PhCH<sub>3</sub>) guaranteed that the enantiomers of **5** were isolated without undesired racemization. Other tested solvents (i.e., 1,4-dioxane, DMF, and CH<sub>3</sub>CN) achieved inferior results in terms of enantiomeric purity (26–83% ee). The considerable erosion in % ee-values with respect to the desired products ((*S*)-**5** and (*R*)-**5**) obtained from the reactions performed in aprotic polar solvents is interesting; however, the explanation for the racemization phenomenon is complex and definitely exceeds the scope of these studies.

All the resulting products (**4**–**11**) were characterized by single-proton nuclear magnetic resonance (<sup>1</sup>H-NMR) spectroscopy, high-resolution mass spectrometry (HR-MS), and high-performance liquid chromatography (HPLC). A lack of <sup>13</sup>C-NMR spectra is typical for polyhalogenobenzimidazoles, since recording the narrow signals corresponding to quaternary carbon atoms is highly challenging for these compounds due to the electronic features of the TBB-ring possessing a N-H tautomeric proton. On the other hand, this problem is not observed in all the cases when the tautomeric proton is replaced by any substituent [45]. A series of modifications of the NMR experimental conditions implemented to overcome this drawback, including the significant extension of the time of analysis, changes in the values of relaxation times, application of high magnetic fields, and the use of lower temperatures to achieve slow exchange conditions, failed to obtain spectra with all the predicted signals. Interestingly, only the treatment of the samples with hydrochloric acid to avoid the existence of 1,3-tautomeric equilibrium by the protonation of nitrogen atom present in the imidazole ring allowed the <sup>13</sup>C-NMR spectra to be recorded with the appropriate signals. Nevertheless, these results are subject to the risk of error, as no correction for the substituent effect was performed. For details, see copies of the recorded spectra appended in Supplementary Materials.

### 3.2. Biological Evaluation

#### 3.2.1. Inhibition of Recombinant CK2 and PIM-1

Inhibition of the human CK2 catalytic subunit (CK2 $\alpha$ ), CK2 holoenzyme (CK2 $\alpha$ 2 $\beta$ 2), and PIM-1 by the newly obtained compounds was evaluated using a radiometric assay (Table 1, Figure S2). The synthetic peptide RRRADDSDDDDDD was used as the substrate of CK2, and peptide ARKRRRHPSGPPTA was used as the substrate of PIM-1. The values of the inhibition constant ( $K_i$ ) were calculated using the Cheng–Prusoff equation:  $K_i = IC_{50}/(1 + [S]/K_m)$  [51].

**Table 1.** Inhibition of CK2 and PIM-1 by compounds 4–11.

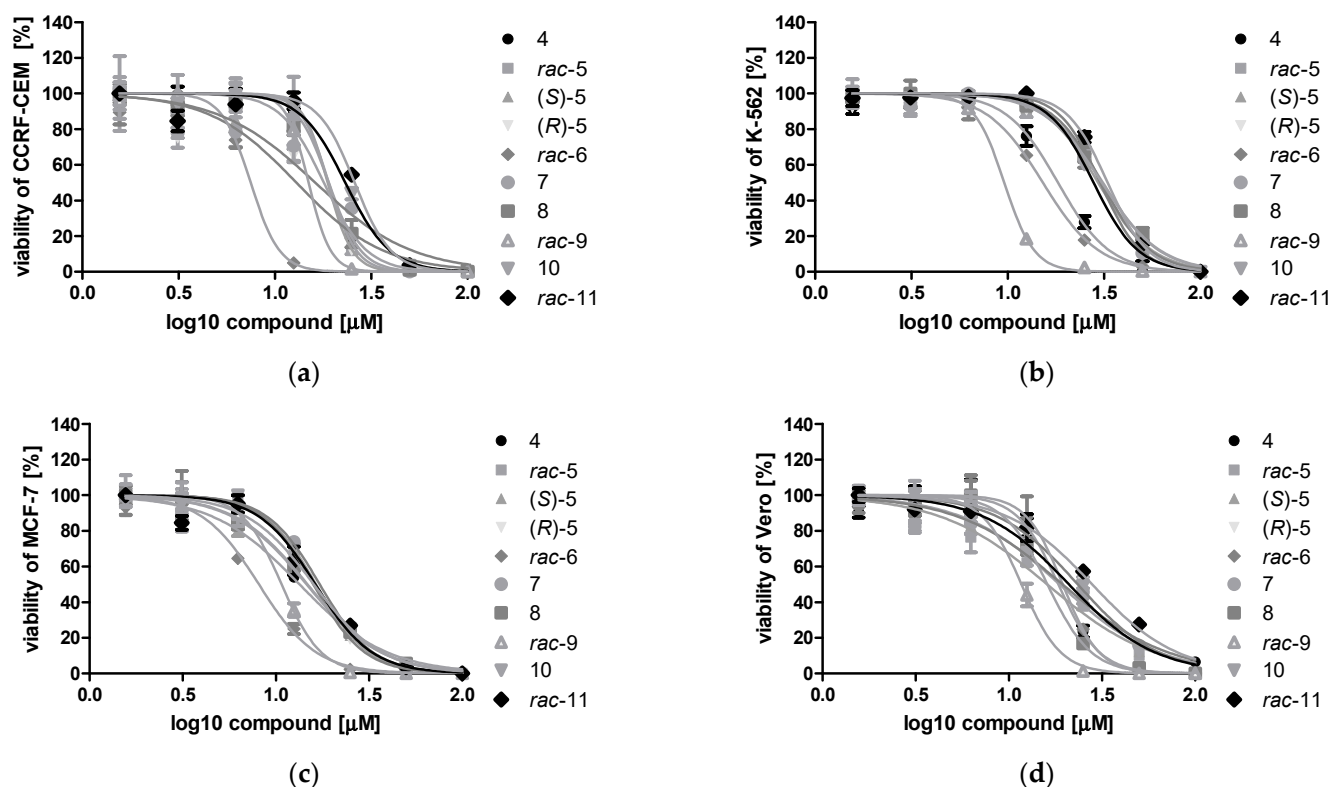
Cpd.	$K_i$ ( $\mu\text{M}$ )		
	CK2 $\alpha$	CK2 $\alpha_2\beta_2$	PIM-1
<b>4</b>	0.223	0.056	0.052
<i>rac</i> -5	0.296	0.127	0.064
( <i>S</i> )-5	0.271	0.167	0.099
( <i>R</i> )-5	0.394	0.104	0.089
<i>rac</i> -6	0.294	0.112	0.067
<b>7</b>	0.156	0.114	0.082
<b>8</b>	0.256	0.072	0.071
<i>rac</i> -9	1.671	0.605	0.267
<b>10</b>	0.139	0.124	0.093
<i>rac</i> -11	0.151	0.089	0.073

All the tested compounds were efficient inhibitors of both recombinant forms of CK2 and PIM-1, with  $K_i$  values in the range of 0.56–0.605  $\mu\text{M}$  for CK2 $\alpha_2\beta_2$  and 0.052–0.267  $\mu\text{M}$  for PIM-1. None of the newly obtained inhibitors inhibited CK2 $\alpha_2\beta_2$  or PIM-1 more strongly than the parent compound, DMAT (**4**); however, compounds **7**, **10**, and *rac*-**11** demonstrated lower  $K_i$  values for CK2 $\alpha$  than for DMAT (**4**), i.e., 0.156  $\mu\text{M}$ , 0.139  $\mu\text{M}$ , and 0.151  $\mu\text{M}$ , respectively. Among the newly obtained compounds, the *rac*-**11** derivative was the most efficient inhibitor of CK2 $\alpha_2\beta_2$ , with  $K_i$  values equal to 0.089  $\mu\text{M}$ , whereas *rac*-**5** was the most potent inhibitor of PIM-1, with  $K_i = 0.064$   $\mu\text{M}$ . The effectiveness of *rac*-**11** towards CK2 kinase can be attributed to the presence of two hydroxyl groups in its structure, which can additionally interact with structural water molecules accommodated in the enzyme's active site. On the contrary, the weakest inhibitor of CK2, compound *rac*-**9** ( $K_i = 0.605$   $\mu\text{M}$ ), has the largest substituent when compared to other studied inhibitors and can therefore potentially undergo clashes with amino acid residues present in the binding pocket of the enzyme.

### 3.2.2. Cytotoxic Effect of DMAT Derivatives 4–11 toward Cancer Cell Lines: CCRF-CEM, K-562, MCF-7, and Non-Cancerous Vero Cells

To test the cytotoxicity of the DMAT derivatives, we treated the CCRF-CEM, K-562, MCF-7, and Vero cells with the newly synthesized compounds in the concentration range of 1.575–100  $\mu\text{M}$  for 48 h. The representative plots demonstrating sigmoidal dose–response curves for compounds 4–11 are shown in Figure 3. The  $\text{IC}_{50}$  values describing the half-maximal effective concentration of each tested compound were calculated and are summarized in Table 2. Selectivity is an important feature of compounds demonstrating anticancer properties; therefore, the selectivity indices (SI) were calculated, as presented in Table 2. Using an MTT viability assay, we demonstrated that all tested compounds significantly decreased the viability of the studied cells, with  $\text{IC}_{50}$  values ranging from 9.66  $\mu\text{M}$  to 41.53  $\mu\text{M}$ . Among the newly obtained DMAT derivatives, *rac*-**6** and *rac*-**9** were the most cytotoxic toward the tested tumor cells (Table 2). The viability of CCRF-CEM and MCF-7 was most strongly reduced by *rac*-**6**, with  $\text{IC}_{50}$  values of 11.83  $\mu\text{M}$  (for CCRF-CEM) and 9.66  $\mu\text{M}$  (for MCF-7), whereas the viability of K-562 was the most strongly decreased by *rac*-**9**, with an  $\text{IC}_{50}$  value of 11.61  $\mu\text{M}$ . Interestingly, *rac*-**6** demonstrated higher SI values than *rac*-**9**, with the highest value of 2.11 obtained for MCF-7. Considering the obtained results in terms of the lowest  $\text{IC}_{50}$  and the highest SI values, subsequent biological studies were devoted to *rac*-**6** and **4** (DMAT) as lead compounds.





**Figure 3.** Sigmoidal dose–response curves for compounds 4–11 determined for CCRF-CEM (a), K-562 (b), MCF-7 (c), and Vero cells (d) after 48 h of treatment. Plots were generated by GraphPad Prism after fitting the MTT data to the sigmoidal dose–response equation:  $Y = 100 / (1 + 10^{((\text{LogIC}_{50} - X) * \text{HillSlope}))}$ .

**Table 2.** Viability of CCRF-CEM (acute lymphoblastic leukemia), K-562 (chronic myelogenous leukemia), MCF-7 (breast carcinoma), and non-cancerous Vero cells after treatment with the tested compounds. The  $\text{IC}_{50}$  values were calculated using an MTT-based assay and the following equation:  $Y = 100 / (1 + 10^{((\text{LogIC}_{50} - X) * \text{HillSlope}))}$ .

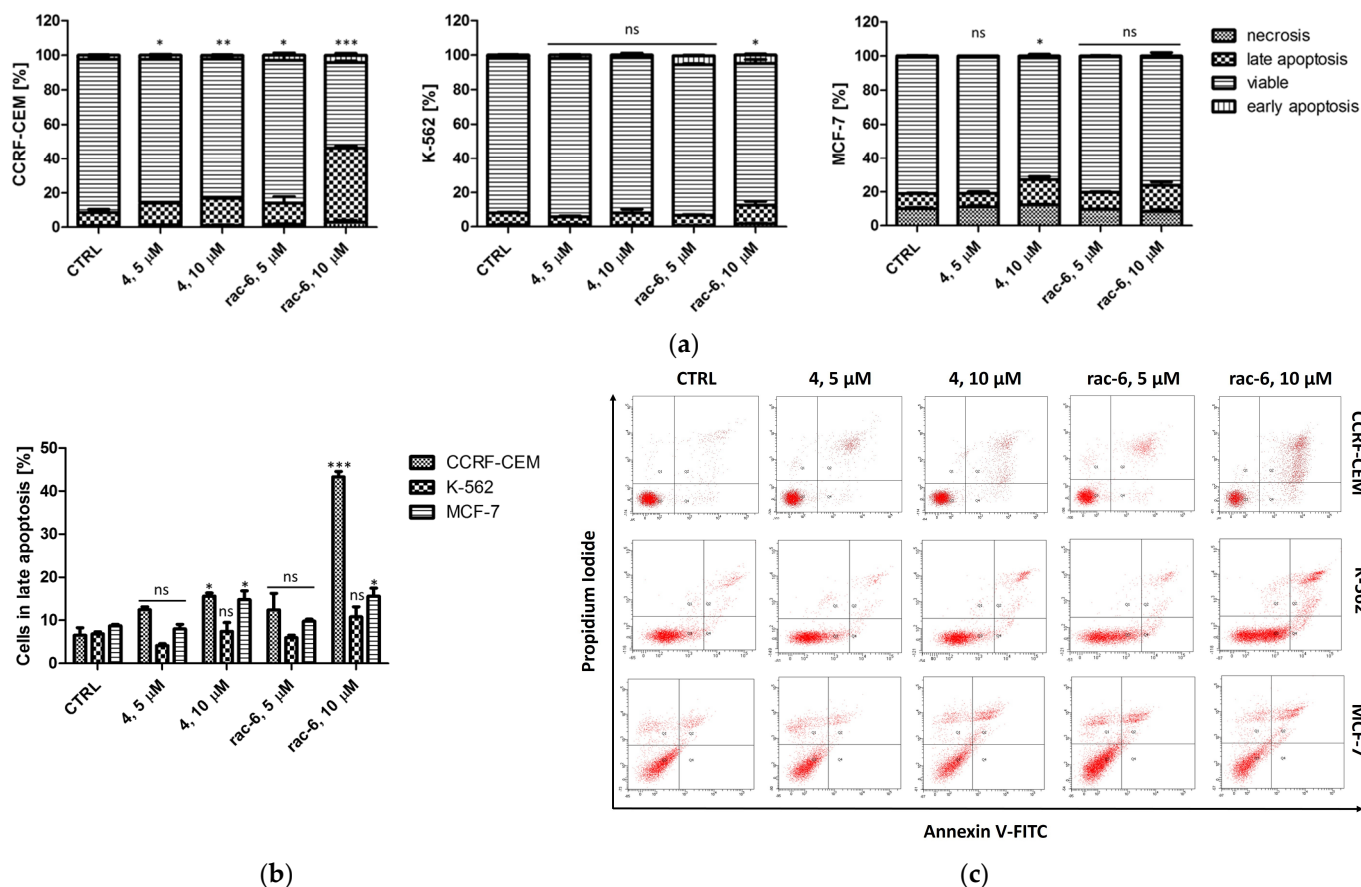
Cpd.	Cell Line				SI *			logP **
	CCRF-CEM	K-562	MCF-7	Vero	CCRF-CEM	K-562	MCF-7	
4	18.94 ± 0.88	22.54 ± 6.09	14.68 ± 0.27	18.72 ± 0.33	0.99	0.83	1.27	5.39
rac-5	21.70 ± 0.86	38.70 ± 8.08	16.86 ± 0.30	22.58 ± 0.13	1.04	0.58	1.34	4.41
(S)-5	23.21 ± 4.01	39.28 ± 9.05	16.55 ± 0.30	25.20 ± 0.54	1.11	0.64	1.52	4.41
(R)-5	22.31 ± 0.10	39.59 ± 8.11	16.09 ± 0.19	28.30 ± 0.43	1.27	0.71	1.76	4.41
rac-6	11.83 ± 0.40	17.74 ± 3.54	9.66 ± 0.31	20.38 ± 0.41	1.72	1.15	2.11	5.05
7	25.64 ± 0.54	33.70 ± 4.92	18.21 ± 0.30	29.46 ± 0.12	1.15	0.87	1.62	4.19
8	17.37 ± 0.27	40.02 ± 7.45	15.11 ± 0.39	16.07 ± 0.27	0.92	0.40	1.06	4.88
rac-9	13.59 ± 0.84	11.61 ± 2.85	10.80 ± 0.23	12.01 ± 0.21	0.88	1.03	1.11	4.74
10	24.47 ± 0.21	38.06 ± 5.56	16.65 ± 0.23	25.19 ± 0.10	1.03	0.66	1.51	3.55
rac-11	33.80 ± 0.26	41.49 ± 8.45	17.20 ± 0.39	41.53 ± 0.10	1.23	1.00	2.41	3.55

\* SI (selectivity index) was calculated with the following formula:  $x = \frac{\text{IC}_{50} \text{ Vero}}{\text{IC}_{50} \text{ cancer cells}}$ . \*\* Logarithm of the partition coefficient of a given inhibitor between n-octanol and water calculated using ChemBioDraw Ultra 13.0 software (PerkinElmer Informatics Indications, Waltham, MA, USA).

### 3.2.3. Induction of Apoptosis in CCRF-CEM, K-562, and MCF-7 Cells

In order to evaluate the proapoptotic properties of *rac-6*, we analyzed annexin V-binding to phosphatidylserine using flow cytometry. The results are shown in Figure 4 and Table S2. The obtained results indicate that *rac-6* induced apoptosis in CCRF-CEM at both concentrations, with the highest proportion of 47% of cells in early and late apoptosis after treatment

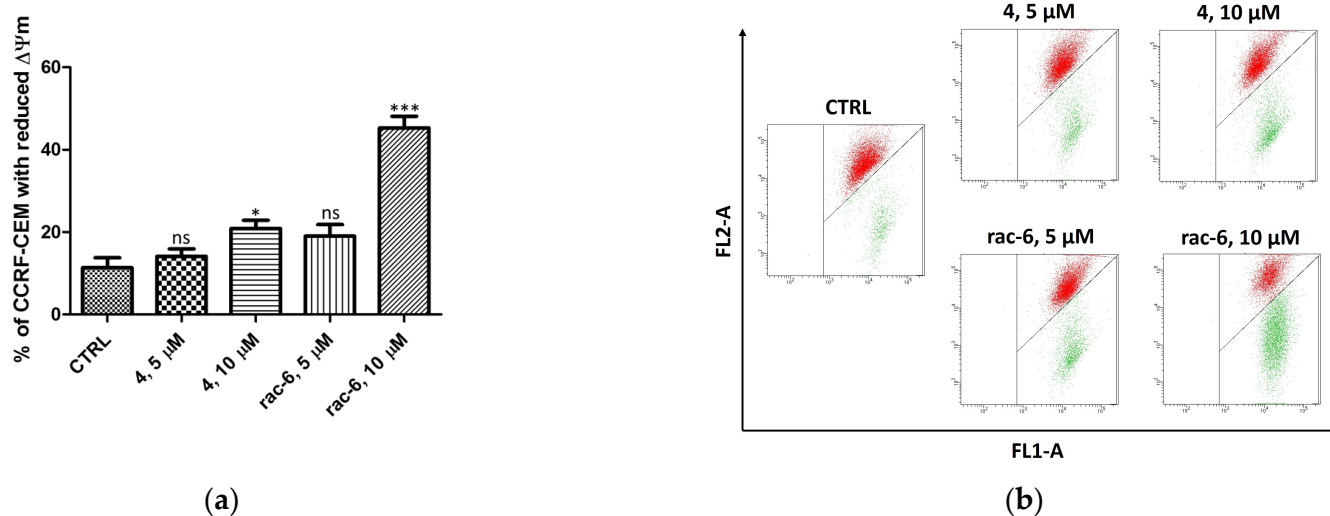
with 10  $\mu\text{M}$  conc. The examined racemate, *rac-6*, also induced apoptosis in MCF-7 cells at 10  $\mu\text{M}$  conc. (statistically significant result), whereas K-562 cells were the least sensitive to *rac-6* (no significant apoptosis observed). However, the percentage of total apoptotic K-562 cells was higher after treatment with 10  $\mu\text{M}$  conc. of *rac-6* than after treatment with parental compound 4 (DMAT), with values of 15.5% and 8.7%, respectively. We also observed the unusual presence of two different pools of unstained cells (considered alive) that were especially visible on cytograms obtained for K-562 cells treated with 10  $\mu\text{M}$  conc. of *rac-6* (Figure 4c). The results obtained for this line utilizing flow cytometry suggest a mechanism of death induction other than apoptosis for *rac-6*.



**Figure 4.** Induction of apoptosis in CCRF-CEM, K-562, and MCF-7 cells. The data were determined by a FACSCanto II flow cytometer after 48 h of treatment with compounds 4 and *rac-6*. Cells were stained with annexin V-FITC and PI (propidium iodide). (a) Mean and standard deviation (SD) of necrosis, as well as viable, early, and late apoptosis, as percent from three independent experiments each. (b) Percentage of late apoptosis in CCRF-CEM, K-562, and MCF-7 cells. (c) Representative cytograms. The data for viable cells (a) and in late apoptosis (b) were analyzed by Dunnett's multiple comparison test as follows: \*  $p < 0.05$ , \*\*  $p < 0.01$ , and \*\*\*  $p < 0.001$  relative to control; ns—not significant.

### 3.2.4. Mitochondrial Membrane Potential ( $\Delta\Psi\text{m}$ ) in CCRF-CEM

Regarding the significant proapoptotic effect of *rac-6* on CCRF-CEM cells, in the next step of our investigation, we measured mitochondrial membrane potential ( $\Delta\Psi\text{m}$ ) in leukemia cells treated with compounds 4 and *rac-6* for 48 h (Figure 5). Incubation with the tested compounds caused mitochondrial membrane depolarization in a dose-dependent manner (as evidenced by the shift from a red to green fluorescence ratio). The most significant effect, i.e., 45% of cells with reduced  $\Delta\Psi\text{m}$ , was obtained in cells treated with 10  $\mu\text{M}$  conc. of *rac-6*. The results correlate well with annexin binding studies of *rac-6*-treated CCRF-CEM cells, suggesting the intrinsic nature of the apoptotic pathway.

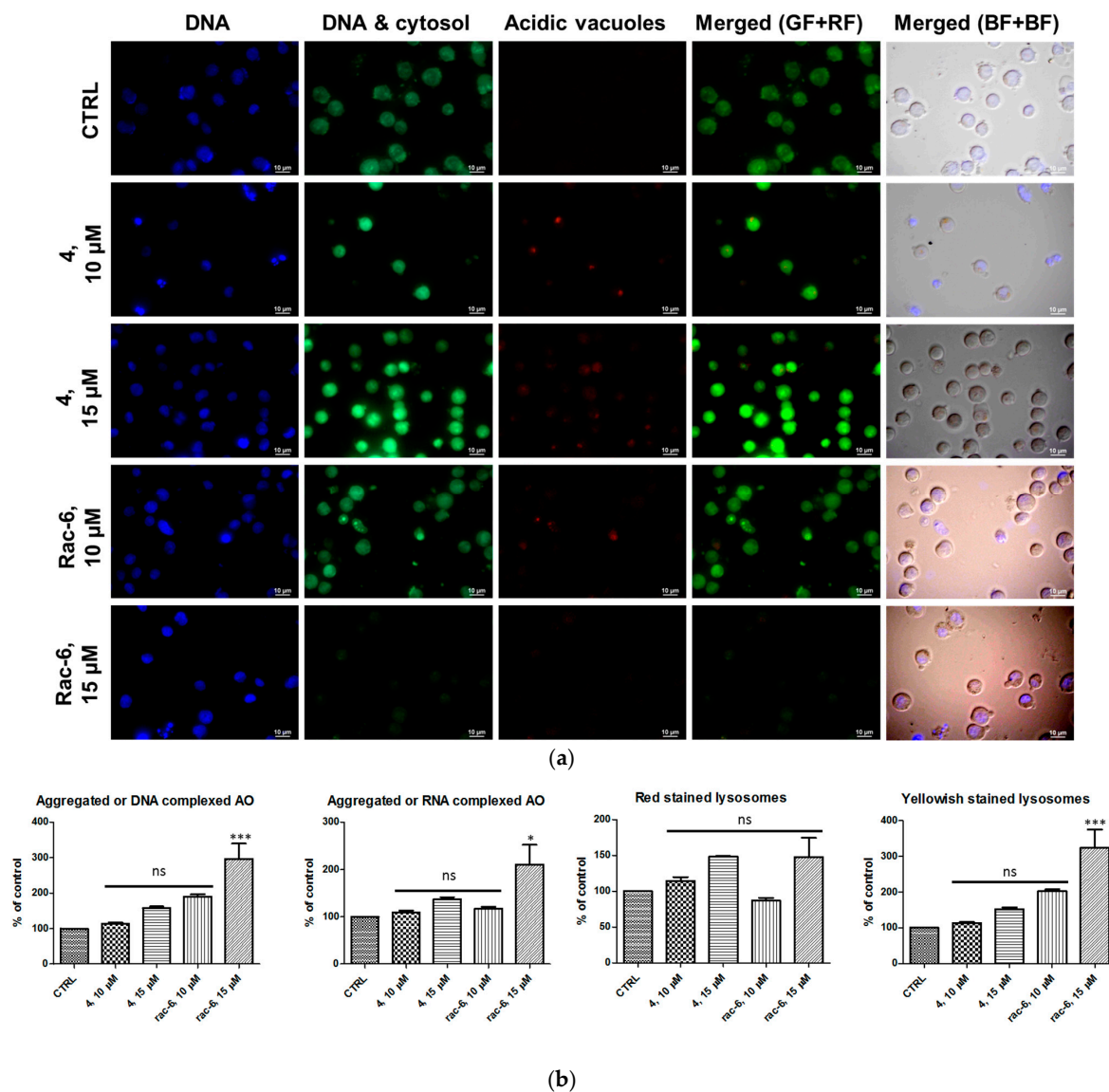


**Figure 5.** Mitochondrial membrane potential ( $\Delta\Psi_m$ ) in CCRF-CEM treated for 48 h with 4 and *rac-6*. **(a)** The percentage of CCRF-CEM cells with reduced  $\Delta\Psi_m$ . **(b)** Representative flow cytograms demonstrating changes in cells induced by 48 h of culturing with 4 or *rac-6*. The cells were stained with JC-1 dye. The cells in the lower-right region of panel **(b)** show increased green fluorescence (apoptotic cells). The data were analyzed by Dunnett's multiple comparison test as follows: \*  $p < 0.05$ , \*\*\*  $p < 0.001$  relative to control; ns—not significant.

### 3.2.5. Detection of Autophagy in K-562 Cells

In order to conclude the mechanism of death of K-562 cells treated with the tested active agents, microscopic observations and a fluorescence intensity assay were performed after staining the cells with an acridine orange (AO). The employed dye is a cell-permeable fluorophore that can be protonated and trapped in acidic vesicular organelles (AVOs). Its metachromatic shift to red fluorescence is concentration-dependent, and therefore, acridine orange fluoresces red in AVOs, such as autolysosomes, can be detected quantitatively [52]. In addition, OA has the ability to intercalate between the nitrogenous bases of the nucleic acids present in cells and their labeling. DNA or RNA is digested during the autophagy process, and the resulting damage makes it easier to bind with OA molecules [52].

After 48 h of treatment with 4 and *rac-6*, K-562 cells, were subjected to staining with Hoechst (nuclei staining) and AO, followed by fluorescent microscopy and a fluorescence intensity measurement. As shown in Figure 6, control cells primarily displayed green fluorescence, with minimal red fluorescence, indicating a lack of acidic vesicular organelles (AVOs). Both 4- and *rac-6*-treated cells showed yellowish-stained lysosomes and a fold-increase in red fluorescent AVOs compared to the controls (Figure 6). Interestingly, cells treated with *rac-6* demonstrated reduced green fluorescence (DNA and cytosol staining) in comparison to control cells (especially at higher concentrations of the compound). Since the obtained microscopic data were inconclusive, we additionally measured fluorescence intensity of AO at four different wavelengths, i.e., Ex. 502 nm/Em. 520–524 nm (aggregated or DNA complexed form), Ex. 457 nm/Em. 630–644 nm (aggregated or RNA complexed form), Ex. 540 nm/Em. 640–660 nm (red-stained lysosomes), and Ex. 488 nm/Em. 540–550 nm (yellowish stained lysosomes) (Figure 6b). The obtained quantitative data indicated that the fluorescence of K-562 cells treated with the tested compounds was increased in a dose-dependent manner for aggregated or DNA/RNA-complexed AO, as well as for yellowish-stained lysosomes, with the highest percentage of lysosomes reaching 324% of the control in a 15  $\mu\text{M}$  conc. of the *rac-6*-treated cells.



**Figure 6.** Induction of autophagy in K-562 cells. **(a)** Visualization of intracellular autophagic vacuoles in K-562 cells: fluorescence microscopy of Hoechst (blue-stained nuclei, BF) and AO-stained K-562 cells (green fluorescence (GF) and red fluorescence (RF)) treated for 48 h with 4 and *rac-6* (using a fluorescence microscope: ECLIPSE Y-TV55, Nikon,  $\times 600$ , magnification). **(b)** The fluorescence intensity of AO in K-562 cells measured with a Synergy H4 Hybrid Multi-Mode Microplate Reader (Biotek) as described in the Methods section. The data were normalized to the intensity of Hoechst (nuclei, Ex. 361 nm/Em. 497 nm). The data were analyzed by Dunnett's multiple comparison test as follows: \*  $p < 0.05$ , \*\*\*  $p < 0.001$  relative to control; ns—not significant.

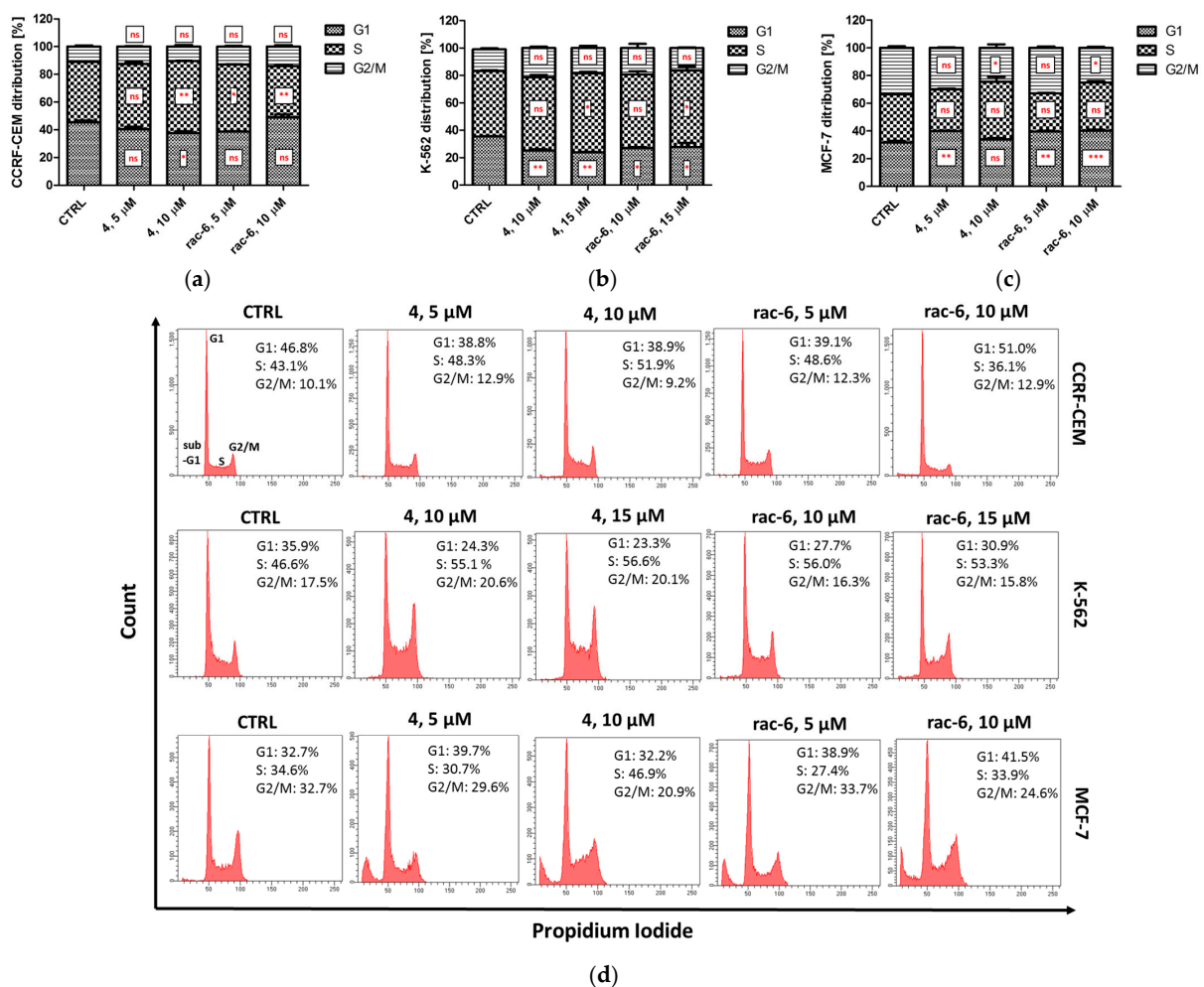
Furthermore, the only statistically significant results were obtained for 15  $\mu\text{M}$  conc. of the *rac-6*-treated cells. Moreover, the red fluorescence was reduced in the case of 10  $\mu\text{M}$  conc. of the *rac-6*-treated cells. On the contrary, the red fluorescence was increased in 4-treated cells (both concentrations) and 15  $\mu\text{M}$  conc. of the *rac-6*-treated cells up to 148% of the control, although the results in these cases were not statistically significant.

Because proton pump-driven lysosomal acidity generates a significant pH gradient, resulting in an efficient concentration of AO within the lysosome organelles and because the effectiveness of the AO concentration process is sufficient to create intralysosomal concentrations, leading to precipitation of the AO into aggregated granules, the obtained results indicate that some of the treated cells can, in fact, undergo autophagy, especially after treatment with *rac-6*. The results obtained for an aggregated form of AO correspond

to the increase in the yellowish-stained lysosomes and red-stained lysosomes, with the exception of 10  $\mu\text{M}$  conc. of the *rac-6*-treated cells.

### 3.2.6. The Effect of 4 and *rac-6* on Cell Cycle Progression in CCRF-CEM, K-562, and MCF-7 Cells

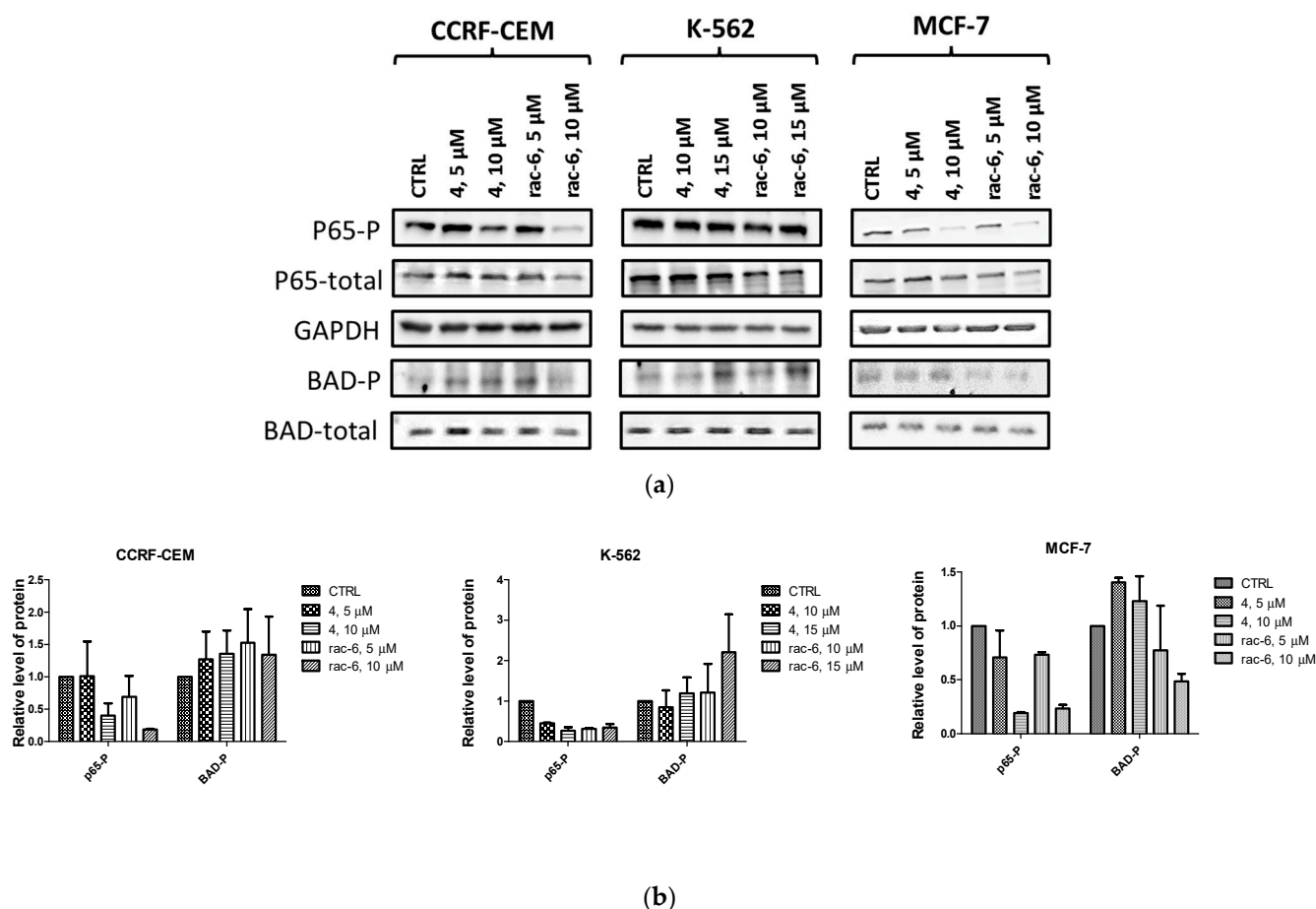
Since CK2 controls cell cycle progression and, consequently, its inhibition can affect the distribution of cells in the individual phases of the cell cycle, we tested the cell cycle progression in CCRF-CEM, K-562, and MCF-7 cells after treatment with 4 and *rac-6*. Representative plots DNA histograms with the calculations of cell percentages in each phase of the cell cycle are depicted in Figure 7. The results indicate differences in the mode of action of the two tested compounds, i.e., 4 led to S-phase arrest in all the tested cell lines, with a maximum of 57.7% of K-562 cells in that phase after treatment with 15  $\mu\text{M}$  conc., whereas *rac-6* induced G1-phase arrest in CCRF-CEM and MCF-7 cells, with a maximum accumulation of 49% of leukemia cells in that phase after using 10  $\mu\text{M}$  conc. of this compound. Interestingly, *rac-6* induced S-phase arrest only in K-562 cells, with a maximum of 56.1% of cells in that phase after 15  $\mu\text{M}$  conc. of this compound. Furthermore, MCF-7 cells were observed in the sub-G1 phase (Figure 7d). Accumulation of cells in sub-G1 indicates DNA degradation, as often seen in apoptotic cells, confirming the results obtained with annexin V and PI staining.



**Figure 7.** Cell cycle progression in CCRF-CEM, K-562, and MCF-7 cells. The data were determined by a FACSCanto II flow cytometer after 48 h of treatment with compounds 4 and *rac-6*. (a–c) The cell cycle distribution profiles determined by flow cytometry. (d) Representative DNA histograms of cell lines. The data were analyzed by Dunnett’s multiple comparison test as follows: \*  $p < 0.05$ , \*\*  $p < 0.01$ , and \*\*\*  $p < 0.001$  relative to control; ns—not significant.

### 3.2.7. Intracellular Inhibition of Protein Kinase CK2 and PIM-1 in CCRF-CEM, K-562, and MCF-7 Cells

To confirm the intracellular inhibition of CK2 and PIM-1 by compounds 4 and *rac-6* in the tested cell lines, we evaluated site-specific phosphorylation of Ser529 in NF- $\kappa$ Bp65 (nuclear factor kappa-light-chain-enhancer of activated B-cells) and Ser112 in BAD after 48 h of treatment (Figure 8). The data obtained for p65 confirmed the intracellular inhibition of CK2 by the tested compounds in all the studied cell lines in a dose-dependent manner. Both tested compounds inhibited CK2-mediated phosphorylation of p65 to a similar extent, with the relative level of p65-P in the range of 0.18–0.47  $\mu$ M in CCRF-CEM, 0.26–0.44  $\mu$ M in K-562, and 0.19–0.73  $\mu$ M in MCF-7. However, the most potent inhibition was observed in CCRF-CEM cells after treatment with 10  $\mu$ M conc. of *rac-6*. Otherwise, Western blot data for BAD (a marker of PIM-1 activity) indicated inhibition of PIM-1 only in MCF-7 cells, with the most significant reduction in phosphorylated BAD in cells treated with 10  $\mu$ M conc. of *rac-6* (0.49 of control) (Figure 8b). Unexpectedly, the relative level of BAD-P in the drug-treated CCRF-CEM and K-562 cells was even higher than in control cells.



**Figure 8.** Intracellular inhibition of protein kinases CK2 and PIM-1 in CCRF-CEM, K-562, and MCF-7 cell lines after 48 h treatment with compounds 4 and *rac-6*. (a) Representative Western blots of p65-P-Ser 529 (nuclear factor kappa-light-chain-enhancer of activated B-cells), p65 total, BAD-P-Ser112, BAD total, and GAPDH in the tested cells. (b) Densitometric quantifications for each tested protein were calculated with untreated cells (CTRL) serving as the reference point, showing relative protein levels. The preparation of cell extracts and protein detection is described in the Materials and Methods Section.

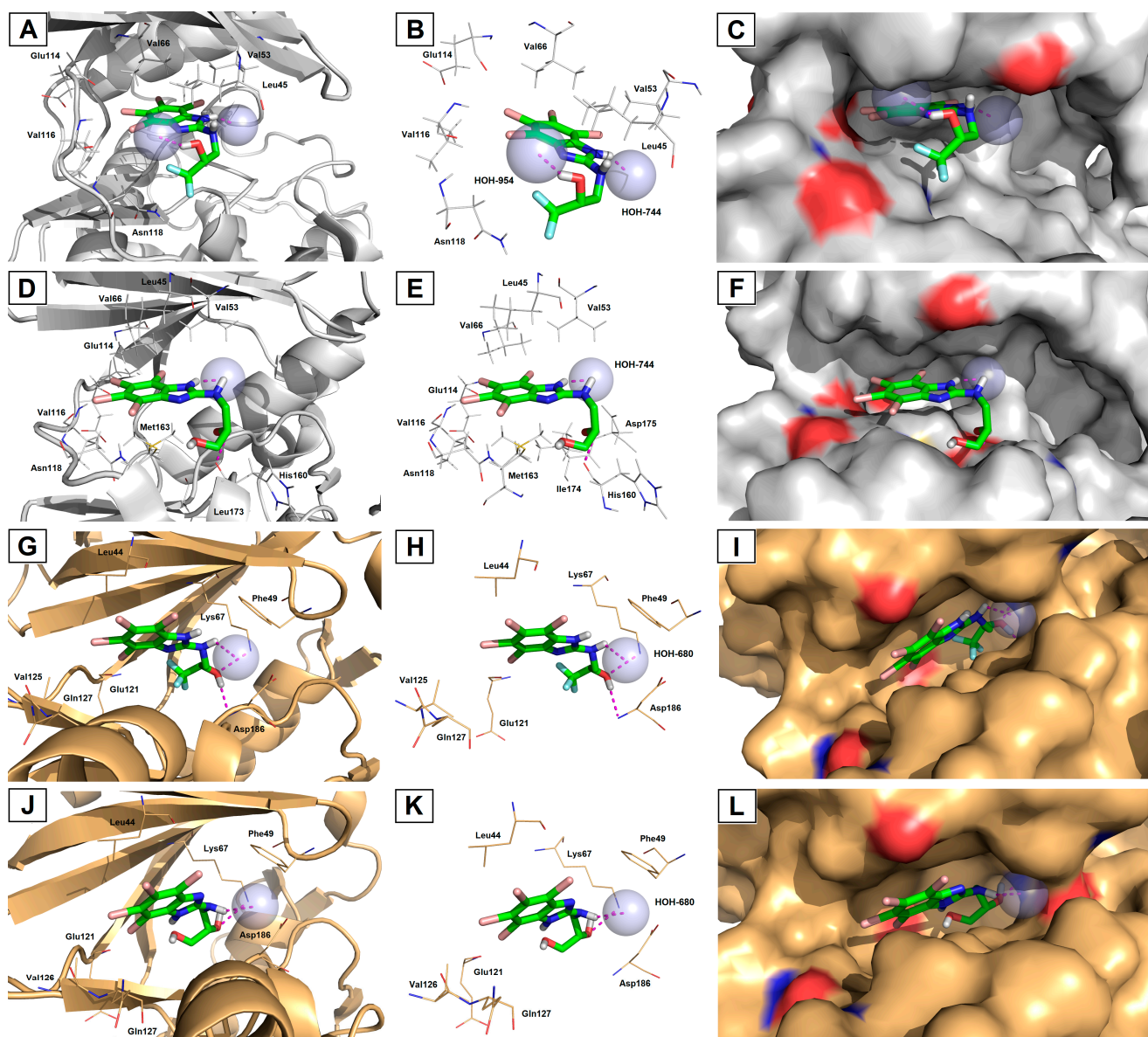
### 3.3. Molecular Docking

In order to rationalize the results of in vitro enzymatic assays and cellular activity in cancer cell lines of the most potent dual CK2- $\alpha$ /PIM-1 inhibitors with the highest

selectivity factor (SI), comprehensive in silico enzyme–substrate docking calculations were performed. For this purpose, the respective TBBi derivatives (*rac-6* and *rac-11*) were docked with receptor molecules prepared based on the crystal structures of both titled kinases, CK2- $\alpha$  (PDB code: 4KWP) [35] and PIM-1 (PDB code: 4DTK) [49], which were retrieved from the Protein Data Bank (PDB; <https://www.rcsb.org/>). As a result of molecular docking experiments, nine of the most energetically favorable binding modes for the ligand–protein complexes for ligands *rac-6* and *rac-11* and target CK2- $\alpha$  and PIM-1 proteins were generated. The results of their binding affinity energies expressed as  $\Delta G_{\text{calc}}$  (kcal/mol) are presented in Table S3 (Supplementary Materials). A visualization of the representative docking poses of *rac-6* and *rac-11* to CK2- $\alpha$  and PIM-1 with close contacts with amino acid residues located in the related ATP-binding sites of both studied kinases is presented in Figure 9.

Inspection of the productive pose of *rac-6* in CK2- $\alpha$  (Figure 9A–C) showed that this inhibitor forms strong 2.1–2.2 Å-long hydrogen bonds with crystal waters (HOH-744 and HOH-954) present in the catalytic cavity. At the same time, the 4,5,6,7-tetrabromobenzimidazole moiety of *rac-6* is located deep inside the ATP-binding pocket, thus exhibiting strong hydrophobic interactions with Val53, Val66, and Val116. In contrast, *rac-11* establishes hydrogen bonding between the backbone carbonyl oxygen of His160 residue and the hydrogen atom of the secondary hydroxyl moiety present in the propane-1,2-diol substituent (Figure 9D–F). Moreover, the CK2- $\alpha$ -*rac-11* complex is stabilized through an additional water-mediated hydrogen bond between the imidazole-NH moiety and the oxygen atom of the bridging conserved water molecule (HOH-744). In this case, the ATP-binding pocket, which is surrounded by hydrophobic amino acids, was also occupied by the TBBi scaffold, providing alkyl CH–CH van der Waals (vdW) and  $\pi$ –alkyl interactions with Val53, Leu45, Val66, Glu114, Val116, Met163, and Ile174 residues. It is worth noting that docking simulations revealed that both TBBi inhibitors bind to CK2 $\alpha$ , exploiting two different poses. In this context, *rac-6* is anchored to the hinge region through Br1 and Br2 closer to Leu45, Val53, and Val66 residues (1.9–2.7 Å-long distance), while *rac-11* is oriented through Br2 and Br3 closer to Glu114, Val116, Asn118, and Met163 residues (2.4–3.4 Å-long distance). As a consequence of the second orientation, ligand *rac-11* can avoid unfavorable repulsion and steric clashes of the tailed hydrophilic propane-1,2-diol chain and hydrophobic residues located more profoundly in the ATP-binding pocket. The second plausible explanation for this orientation is that the additional primary hydroxyl group present in the amino alcohol substituent introduces a steric hindrance due to the proximity of Met163, which pushes *rac-11* out of the hinge region. Interestingly, although *rac-11* slightly protrudes from the ATP-binding site as compared to *rac-6*, the drop in the inhibitory potency of this compound was not detected during in vitro kinase activity assays.

In turn, complexes of PIM-1 and the selected top-scoring binding modes of *rac-6* (Figure 9G–I) and *rac-11* (Figure 9J–L) revealed that both inhibitors are accommodated inside the ATP-binding cleft with similar poses, explaining the marginal differences in inhibitory potency towards target protein in vitro. The only difference among the studied PIM-1 complexes concerns the feature of the H-bonding network between the inhibitors' amino alcohol skeletons and interacting amino acid residues, as well as crystal water. The docking of *rac-6* with PIM-1 protein shows that the secondary hydroxyl group of the alkyl substituent formed H-bond interactions with PIM-1 via amine groups of Lys67 or Asp186, whereas the TBBi-NH moiety interacted via crystal water (HOH-680). On the other hand, the secondary hydroxyl functionality of *rac-11* interacted only with Lys67, while the TBBi-NH moiety was H-bonded with HOH-680. Interestingly, when comparing both inhibitors complexed with target kinases, one can see that in the case of CK2- $\alpha$ , it is the proton of imidazole-NH moiety that forms H-bonds with crystal water. In contrast, in the case of PIM-1, both inhibitors' TBBi-NH scaffolds are engaged in the formation of H-bonding interaction with the crystal water.



**Figure 9.** Representative three-dimensional (3D) binding modes of 1,1,1-trifluoro-3-[(4,5,6,7-tetrabromo-1*H*-benzimidazol-2-yl)amino]propan-2-ol (*rac*-6) (A–C,G–I) and 3-[(4,5,6,7-tetrabromo-1*H*-benzimidazol-2-yl)amino]propane-1,2-diol (*rac*-11) (D–F,J–L) with human protein kinases, CK2- $\alpha$  (PDB code: 4KWP; (A–F)) and PIM-1 (PDB code: 4DTK; (G–L)) with close contacts with residues in the ATP-binding site. All nine panels (A–L) show inhibition of protein kinases CK2- $\alpha$  and PIM-1 by blocking the substrate-binding site through direct interaction of the ligands with critical amino acids of the receptors in the catalytic cavity. Ligands are shown as *sticks*. The overall receptor structures are shown as a *cartoon* diagram (left column) or *surface* representation (right column), where CK2- $\alpha$  is light grey and PIM-1 is gold. The most significant amino acid residues contributing to the stabilization of the ligand molecules in the complex with CK2- $\alpha$  and PIM-1 by polar interactions and by CH–CH van der Waals (vdW) or  $\pi$ –alkyl interactions are shown as *lines*. Nitrogen atoms are presented with blue color, oxygen atoms with red color, fluorine atoms with light blue color, and bromine atoms with burgundy (maroon) color, whereas the hydrogen atoms (attached to nitrogen and/or oxygen atoms of the ligand molecules) are represented by grey color. Only polar hydrogens are shown for clarity. The bridging conserved water molecules (crystal waters) are presented as light blue *spheres*. The formation of intermolecular hydrogen bonds is represented by magenta dashed lines.



Notably, no halogen bonding was detected among the docked ligand *rac-6*, suggesting that the fluorine atoms of the  $-CF_3$  group are less detrimental for polar interactions within CK2- $\alpha$  and PIM-1 receptor molecules. Therefore, it is more likely that the organofluorine moiety in the studied lead compound *rac-6* is responsible for enhanced membrane permeation and higher bioavailability (due to the greater lipophilicity of bioisosteric fluorine compared to hydrogen), as well as improved metabolic stability (due to resistance of the C–F bond toward intracellular biotransformations compared to the C–H bond). Both aforementioned features can modulate the performance and pharmacokinetics of this compound in vivo but have no significant influence on the increased binding affinity of fluorinated derivatives to target kinases. Nevertheless, such a phenomenon concerning the physicochemical properties and pharmacological behavior of TBBi-based derivatives demands a deeper understanding.

#### 4. Discussion

A series of novel amino alcohol derivatives (5–11) of parental DMAT (4) were designed and synthesized as potent dual CK2/PIM-1 inhibitors. All the compounds were obtained in up to 14% total yield after a three-step synthetic procedure, following a well-known route elaborated by Andrzejewska et al. [42], which includes: (i) bromination of 2-mercapto-1H-benzimidazole (1) with  $Br_2$  and 48% aqueous HBr in glacial AcOH, (ii) an exhaustive bromination of 2-bromo-1H-benzimidazole (2) with  $Br_2$  in boiling water and modified using additional LED (390 nm) irradiation to intensify the process, and (iii) aminolysis of the resulting key intermediate, namely 2,4,5,6,7-pentabromo-1H-benzimidazole (3), with commercial amino alcohols different than those used in the literature. Because the designed compounds included chiral small molecules, we also extended our synthetic efforts toward the preparation of the corresponding (R)- and (S)-enantiomers using commercially available chiral building blocks as starting materials. This strategy was applied to evaluate the structure–activity relationship with respect to the absolute configuration of stereogenic centers present in one of the studied DMAT analogs: (2S)- or (2R)-1-[(4,5,6,7-tetrabromo-1H-benzimidazol-2-yl)amino]propan-2-ol [(S)-5 or (R)-5].

Although the results of in vitro kinetics studies revealed that all inhibitors decrease the catalytic activity of recombinant CK2- and PIM-1 enzymes to a similar extent as a parental DMAT, the cytotoxicity and selectivity of the tested compounds were even better than in the case of DMAT. Moreover, the cytotoxic activity of the tested compounds corresponds better with their lipophilicity than their inhibitory activity. This correlation is in agreement with our previous findings demonstrating that the most promising compound characterized by a higher  $\log P$  value can penetrate cell membranes more efficiently, therefore exhibiting improved intracellular inhibition of CK2 [40]. The present results were supported by molecular docking studies for the most selective compounds, i.e., *rac-6* and *rac-11*. The in silico results demonstrated that both compounds are accommodated inside the ATP-binding cleft with similar poses, explaining the marginal differences in inhibitory potency towards target protein in vitro. These findings confirm that efficient inhibitors of recombinant CK2 should possess (nearby hydrophobic TBBi scaffold) a polar carboxyl or hydroxyl moiety, which are prone to forming strong hydrogen bonds similar to the phosphate groups present in the ATP physiological substrate.

Because cytotoxicity against tumor cells and selectivity are important features of compounds demonstrating anticancer properties, further investigations of biological action of the most promising compounds, i.e., *rac-6* and 4, were performed. We observed that among tested cell lines, K-562, a Philadelphia (Ph) chromosome-positive (BCR-ABL-positive) leukemia cell line derived from chronic myeloid leukemia (CML) in blast crisis [53], was the most resistant toward the tested compounds. Previous studies demonstrated that CK2 expression was increased in leukemia cells from CML patients in blast crisis as compared to healthy peripheral blood mononuclear cells and showed that Bcr-Abl in K-562 cells physically interacts with CK2 $\alpha$ , affecting its activity [54]. The therapeutic resistance of K-562 cells can also be partially correlated with an increased metabolic flux towards the Warburg

phenotype, which promotes survival and proliferation [55]. It has been demonstrated that hexokinase-II (HK-II) is expressed predominantly in cancer cells, which promotes the Warburg metabolic phenotype and protects the cancer cells from drug-induced apoptosis. It was proven that K-562 cells have multifold higher levels of HK-II, glucose uptake, and endogenous ROS with respect to normal peripheral blood mononuclear cells [55].

The resistance of K-562 cells to the tested compounds correlates well with the lack of apoptosis in these cells after their treatment with *rac-6* and **4**. Moreover, the poor proapoptotic activity of the tested compounds towards K-562 cells also correlates with the lack of efficient intracellular inhibition of CK2 or PIM-1 protein kinases after **4**- and *rac-6*-treatment. Considering that CK2 has been demonstrated as an essential mediator of BCR-ABL oncogenic signals and the BCR-ABL/CK2 complex is responsible for mediating BCR-ABL-induced cell proliferation and survival [56], the lack of efficient intracellular inhibition of CK2 by the tested compounds is in agreement with the poor proapoptotic activity of this treatment. We also observed that the phospho-BAD (Ser112) level in K-562 cells increased significantly after treatment with both inhibitors, which supports cell survival and prevents the occurrence of apoptosis. Moreover, it was demonstrated that the inactivation of BAD by PIM-1-mediated phosphorylation of Ser112 can affect BCL-2, an apoptotic cell death suppressor, which consequently leads to cell survival [57]. A similarly increased level of phospho-BAD (Ser112) was observed in TNBC MDA-MB-231 cells after treatment with a dual CK2/PIM-1 inhibitor, 1-( $\beta$ -D-2'-deoxyribofuranosyl)-4,5,6,7-tetrabromo-1*H*-benzimidazole, named K164 (TDB) [37]. Interestingly, the same inhibitor reduced the catalytic activity of both CK2 and PIM-1 kinases, as manifested by decreased phosphorylated levels of Akt and BAD in K-562 cells, and induced apoptosis in this cell line [36].

Our present studies show that both tested compounds are prone to induce autophagy in the K-562 cell line. Although autophagy is a physiological cellular process that leads to the degradation and recycling of damaged cellular components [58], depending on the degree of activation, it can lead to death. In cancer, autophagy exhibits contradictory behavior, and depending on the cell type, it may be an important factor for the induction of cell death or tumor progression [59]. Previous studies have demonstrated that a well-established inhibitor of tyrosine kinase, imatinib, induces autophagy in the K-562 cell line and in primary cultures of patients with CML [60]. In turn, novel JAK inhibitor ruxolitinib (INCB018424) reported by Lin et al. [61] is able to notably decrease the expression of AKT, mTOR, and STAT autophagy inhibitor genes in K-562 cells relative to the control cell line.

Among the tested cell lines, apoptosis was induced by *rac-6* to the greatest extent in CCRF-CEM. Moreover, the proapoptotic activity of this compound was even better than the parental DMAT and corresponded to its strong ability to reduce  $\Delta\Psi_m$ , suggesting the intrinsic nature of the apoptotic pathway. The obtained results concerning CK2-mediated phosphorylation of NF- $\kappa$ B strongly correlate with the proapoptotic properties of *rac-6*, confirming the antiapoptotic role of this kinase. It was demonstrated that CK2 and its substrates protect cells from apoptosis by phosphorylating a wide range of proteins involved in the apoptotic response [62,63]. Interestingly, intracellular inhibition of CK2 in the *rac-6*-treated CCRF-CEM cells was not accompanied by inhibition of PIM-1 (increased level of phosphorylated BAD).

Among studied cell lines, the decreased level of (PIM-1)-mediated phosphorylation of BAD was observed only in MCF-7, and similarly to CCRF-CEM cells, CK2-mediated phosphorylation of p65 was reduced in MCF-7 cells treated with **4** and *rac-6*. The obtained results correlate with the ability of the tested compounds to induce apoptosis in breast cancer cells; however, its intensity is lower than in CCRF-CEM cells. The indicated differences in the proapoptotic efficacy of the tested inhibitors between CCRF-CEM and MCF-7 cell lines may be related to the caspase-3 deficiency in MCF-7 cells, which consequently undergo cell death due to a lack of typical apoptotic properties [64]. Interestingly, intracellular inhibition of CK2 after treatment with *rac-6* detected in CCRF-CEM and MCF-7 cells correlates with G1-phase arrest in these cells, and it is opposite to S-phase arrest in

K-562 cells. The G1-arrest that occurred in CCRF-CEM and MCF-7 cells after inhibition of CK2 is in agreement with the literature data, showing cell cycle regulation by CK2. It was demonstrated that treatment of cells with a selective inhibitor of CK2, i.e., CX-4945, resulted in reduced phosphorylation of a key cell cycle inhibitor protein [p21 (T145)] and increased the stability and levels of total p21 and p27 [65]. These cell cycle inhibitors are responsible for stopping the cell cycle in the G1 phase, activation of repair mechanisms, and apoptosis of cells with damaged DNA.

## 5. Conclusions

All the tested compounds were found to be efficient dual inhibitors of both recombinant forms of CK2 and PIM-1, with activity comparable to that of the parent compound. We concluded that the cytotoxic activity of the tested compounds corresponds better with their lipophilicity than their inhibitory activity. This correlation confirms our previous findings demonstrating that the most promising compound characterized by a higher  $\log P$  value can penetrate cell membranes more efficiently.

Among the newly developed amino alcohol derivatives of DMAT, 1,1,1-trifluoro-3-[(4,5,6,7-tetrabromo-1*H*-benzimidazol-2-yl)amino]propan-2-ol (*rac*-6) demonstrates the most promising anticancer properties. Its ability to induce apoptosis in breast cancer cells can be attributed to efficient intracellular inhibition of both CK2 and PIM-1 activity. Moreover, *rac*-6 demonstrates the best anticancer properties towards acute lymphoblastic leukemia cells, inducing apoptosis via an intrinsic apoptotic pathway. Interestingly, both studied inhibitors, i.e., DMAT and *rac*-6, are able to induce autophagy in the BCR-ABL-positive chronic myeloid leukemia (CML) cell line.

The obtained results also support the concept that CK2 kinase is a vital factor for breast cancer cell survival and an appealing molecular drug target in the development of novel antineoplastic agents. Taking into account the obtained data, as well as our previous results demonstrating a synergistic effect of TBBi derivatives and classical cytostatics [66–68], it may be valuable to test a combination of *rac*-6 with 5-fluorouracil or methotrexate against breast cancer and leukemic cells.

**Supplementary Materials:** The following supporting information can be downloaded at: <https://www.mdpi.com/xxx/s1>. Table S1: Screening conditions for the synthesis of (2*S*)-1-[(4,5,6,7-tetrabromo-1*H*-benzimidazol-2-yl)amino]propan-2-ol [(*S*)-5] using commercially available (*S*)-1-aminopropan-2-ol (>99% ee); Table S2: Induction of apoptosis in CCRF-CEM, K-562, and MCF-7 cells; Table S3: Docking scoring of the respective ligands (*rac*-6 and *rac*-11) complexed with human protein kinases. Next, the copies of HPLC chromatograms of inhibitors in their racemic and optically active form, as well as copies of NMR and FTMS spectra, can be found. Figure S1. Synthesis of 2,4,5,6,7-pentabromo-1*H*-benzimidazole (3) as a key precursor for novel dual CK2/PIM-1 inhibitors carried out under (A) convenient heating conditions, and (B–C) the influence of purple light (390 nm). Light-induced chemical reactions were conducted using self-prepared (made-in-home) device equipped with light-emitting diodes (LEDs). Figure S2. Sigmoidal dose-response curves. Inhibition of human CK2 catalytic subunit (CK2 $\alpha$ ), CK2 holoenzyme (CK2  $\alpha$ 2 $\beta$ 2), and PIM-1 kinases by the newly synthesized compounds were evaluated using the radiometric assay. The synthetic peptide RRRADDSDDDDD was used as the substrate of CK2, and peptide ARKRRRHPSGPPTA as the substrate of PIM-1. The experimental data were fitted to sigmoidal dose-response (variable slope)  $Y = \text{Bottom} + (\text{Top} - \text{Bottom}) / (1 + 10^{((\text{LogIC50} - X) * \text{HillSlope}))}$  equation in GraphPad Prism. Reference [69] is cited in the supplementary materials.

**Author Contributions:** Conceptualization, P.W. (biological studies) and P.B. (synthetic and computational studies); Methodology and Investigation, P.W. (biological studies with cells), M.W. (assays with recombinant enzymes), M.K. (flow cytometry analyses), and P.B. (synthesis and analysis of the organic compounds; molecular docking studies); Software, P.B.; Validation, P.W. and P.B.; Formal Analysis, P.W. and P.B.; Resources, P.W. and P.B.; Data Curation, P.W., M.K. and P.B.; Writing—Original Draft Preparation, P.W. and P.B.; Writing—Review and Editing, P.W. and P.B.; Visualization, P.W. and P.B.; Supervision, P.W. and P.B.; Project Administration, P.W. and P.B.; Funding Acquisition, P.W. and P.B. All authors have read and agreed to the published version of the manuscript.

**Funding:** This research was funded by the Warsaw University of Technology (WUT) and partially by the National Science Centre (NCN) of Poland within the framework of the SONATA 15 grant (No. 2019/35/D/ST4/01556). This work was also supported by Polish Ministry of Science and Higher Education (financial support for statutory activity of the National Medicines Institute).

**Institutional Review Board Statement:** Not applicable.

**Informed Consent Statement:** Not applicable.

**Data Availability Statement:** The data presented in this article are openly available.

**Acknowledgments:** The authors thank undergraduate students Kristina Fateyeva, Patrycja Puk, and Anna Gabor for assistance with the chemical and biological studies. P.B. is grateful to the IDUB project ('The Best of the Best' program) for providing individual support dedicated to young, talented WUT scientists.

**Conflicts of Interest:** All authors declare no financial/commercial conflict of interest.

## References

1. Trembley, J.H.; Kren, B.T.; Afzal, M.; Scaria, G.A.; Klein, M.A.; Ahmed, K. Protein kinase CK2—Diverse roles in cancer cell biology and therapeutic promise. *Mol. Cell. Biochem.* **2023**, *478*, 899–926. [CrossRef] [PubMed]
2. Walhekar, V.; Bagul, C.; Kumar, D.; Muthal, A.; Achaiah, G.; Kulkarni, R. Topical advances in PIM kinases and their inhibitors: Medicinal chemistry perspectives. *Biochim. Biophys. Acta Rev. Cancer* **2022**, *1877*, 188725. [CrossRef]
3. Borgo, C.; Ruzzene, M. Role of protein kinases in antitumor drug resistance. *J. Exp. Clin. Cancer Res.* **2019**, *38*, 287. [CrossRef]
4. Atkinson, E.L.; Iegre, J.; Brear, P.D.; Zhabina, E.Z.; Hyvönen, M.; Spring, D.R. Downfalls of Chemical Probes Acting at the Kinase ATP-Site: CK2 as a Case Study. *Molecules* **2021**, *26*, 1977. [CrossRef]
5. Narlik-Grassow, M.; Blanco-Aparicio, C.; Carnero, A. The PIM family of serine/threonine kinases in cancer. *Med. Res. Rev.* **2014**, *34*, 136–159. [CrossRef] [PubMed]
6. Manning, G.; Whyte, D.B.; Martinez, R.; Hunter, T.; Sudarsanam, S. The protein kinase complement of the human genome. *Science* **2002**, *298*, 1912–1934. [CrossRef] [PubMed]
7. Qian, K.C.; Wang, L.; Hickey, E.R.; Studts, J.; Barringer, K.; Peng, C.; Kronkaitis, A.; Li, J.; White, A.; Mische, S.; et al. Structural basis of constitutive activity and a unique nucleotide binding mode of human Pim-1 kinase. *Biol. Chem.* **2005**, *280*, 6130–6137. [CrossRef]
8. Niefind, K.; Guerra, B.; Pinna, L.A.; Issinger, O.G.; Schomburg, D. Crystal structure of the catalytic subunit of protein kinase CK2 from *Zea mays* at 2.1 Å resolution. *EMBO J.* **1998**, *17*, 2451–2462. [CrossRef]
9. Pucko, E.B.; Ostrowski, R.P. Inhibiting CK2 among Promising Therapeutic Strategies for Gliomas and Several Other Neoplasms Emanuela, B. *Pharmaceutics* **2022**, *14*, 331. [CrossRef]
10. Brault, L.; Gasser, C.; Bracher, F.; Huber, K.; Knapp, S.; Schwaller, J. PIM serine/threonine kinases in the pathogenesis and therapy of hematologic malignancies and solid cancers. *Haematologica* **2010**, *95*, 1004–1015. [CrossRef]
11. Valdman, A.; Fang, X.; Pang, S.T.; Ekman, P.; Egevad, L. Pim-1 expression in prostatic intraepithelial neoplasia and human prostate cancer. *Prostate* **2004**, *60*, 367–371. [CrossRef] [PubMed]
12. Tursynbay, Y.; Zhang, J.; Li, Z.; Tokay, T.; Zhumadilov, Z.; Wu, D.; Xie, Y. Pim-1 kinase as cancer drug target: An update (Review). *Biomed. Rep.* **2016**, *4*, 140–146. [CrossRef] [PubMed]
13. Yan, B.; Zemskova, M.; Holder, S.; Chin, V.; Kraft, A.; Koskinen, P.J.; Lilly, M.J. The PIM-2 kinase phosphorylates BAD on serine 112 and reverses BAD-induced cell death. *Biol. Chem.* **2003**, *278*, 45358–45367. [CrossRef] [PubMed]
14. Channavajhala, P.; Seldin, D.C. Functional interaction of protein kinase CK2 and c-Myc in lymphomagenesis. *Oncogene* **2002**, *21*, 5280–5288. [CrossRef] [PubMed]
15. Klumpp, S.; Maurer, A.; Zhu, Y.; Aichele, D.; Pinna, L.A.; Kriegstein, J. Protein kinase CK2 phosphorylates BAD at threonine-117. *J. Neurochem. Int.* **2004**, *45*, 747–752. [CrossRef]
16. Wang, J.; Kim, J.; Roh, M.; Franco, O.E.; Hayward, S.W.; Wills, M.L.; Abdulkadir, S.A. PIM-1 kinase synergizes with c-MYC to induce advanced prostate carcinoma. *Oncogene* **2010**, *29*, 2477–2487. [CrossRef]
17. Laramas, M.; Pasquier, D.; Filhol, O.; Ringeisen, F.; Descotes, J.L.; Cochet, C. Nuclear localization of protein kinase CK2 catalytic subunit (CK2 $\alpha$ ) is associated with poor prognostic factors in human prostate cancer. *Eur. J. Cancer* **2007**, *43*, 928–934. [CrossRef]
18. Cibull, T.L.; Jones, T.D.; Li, L.; Eble, J.N.; Baldrige, A.L.; Malott, S.R.; Luo, Y.; Cheng, L. Overexpression of Pim-1 during progression of prostatic adenocarcinoma. *J. Clin. Pathol.* **2006**, *59*, 285–288. [CrossRef]
19. Trembley, J.H.; Kren, B.T.; Abedin, M.J.; Vogel, R.I.; Cannon, C.M.; Unger, G.M.; Ahmed, K. CK2 Molecular Targeting-Tumor Cell-Specific Delivery of RNAi in Various Models of Cancer. *Pharmaceutics* **2017**, *10*, 25. [CrossRef]
20. Ahmad, K.A.; Wang, G.; Slaton, J.; Unger, G.; Ahmed, K. Targeting CK2 for cancer therapy. *Anticancer Drugs* **2005**, *16*, 1037–1043. [CrossRef]

21. Hu, X.F.; Li, J.; Vandervalk, S.; Wang, Z.; Magnuson, N.S.; Xing, P.X.J. PIM-1-specific mAb suppresses human and mouse tumor growth by decreasing PIM-1 levels, reducing Akt phosphorylation, and activating apoptosis. *Clin. Invest.* **2009**, *119*, 362–375. [CrossRef] [PubMed]
22. Gowda, C.; Sachdev, M.; Muthusami, S.; Kapadia, M.; Petrovic-Dovat, L.; Hartman, M.; Ding, Y.; Song, C.; Payne, J.L.; Tan, B.H.; et al. Casein Kinase II (CK2) as a Therapeutic Target for Hematological Malignancies. *Curr. Pharm. Des.* **2017**, *23*, 95–107. [CrossRef] [PubMed]
23. Milani, M.; Venturini, S.; Bonardi, S.; Allevi, G.; Strina, C.; Cappelletti, M.R.; Corona, S.P.; Aguggini, S.; Bottini, A.; Berruti, A.; et al. Hypoxia-related biological markers as predictors of epirubicin-based treatment responsiveness and resistance in locally advanced breast cancer. *Oncotarget* **2017**, *8*, 78870–78881. [CrossRef] [PubMed]
24. Garziera, M.; Scarabel, L.; Toffoli, G. Hypoxic Modulation of HLA-G Expression through the Metabolic Sensor HIF-1 in Human Cancer Cells. *J. Immunol. Res.* **2017**, *2017*, 4587520. [CrossRef]
25. Chen, J.; Kobayashi, M.; Darmanin, S.; Qiao, Y.; Gully, C.; Zhao, R.; Yeung, S.C.; Lee, M.H. Pim-1 plays a pivotal role in hypoxia-induced chemoresistance. *Oncogene* **2009**, *28*, 2581–2592. [CrossRef]
26. Mottet, D.; Ruys, S.P.; Demazy, C.; Raes, M.; Michiels, C. Role for casein kinase 2 in the regulation of HIF-1 activity. *Int. J. Cancer.* **2005**, *117*, 764–774. [CrossRef]
27. Casillas, A.L.; Toth, R.K.; Sainz, A.G.; Singh, N.; Desai, A.A.; Kraft, A.S.; Warfel, N.A. Hypoxia-inducible PIM kinase expression promotes resistance to anti-angiogenic agents. *Clin. Cancer Res.* **2018**, *24*, 169–180. [CrossRef]
28. Landesman-Bollag, E.; Song, D.H.; Romieu-Mourez, R.; Sussman, D.J.; Cardiff, R.D.; Sonenshein, G.E.; Seldin, D.C. Protein kinase CK2: Signaling and tumorigenesis in the mammary gland. *Mol. Cell. Biochem* **2001**, *227*, 153–165. [CrossRef]
29. Hammerman, P.S.; Fox, C.J.; Cinalli, R.M.; Xu, A.; Wagner, J.D.; Lindsten, T.; Thompson, C.B. Lymphocyte transformation by Pim-2 is dependent on nuclear factor-kappaB activation. *Cancer Res.* **2004**, *64*, 8341–8348. [CrossRef]
30. Zemskova, M.; Sahakian, E.; Bashkirova, S.; Lilly, M.J. The PIM-1 kinase is a critical component of a survival pathway activated by docetaxel and promotes survival of docetaxel-treated prostate cancer cells. *Biol. Chem.* **2008**, *283*, 20635–20644. [CrossRef]
31. Sarno, S.; Papinutto, E.; Franchin, C.; Bain, J.; Elliott, M.; Meggio, F.; Kazimierczuk, Z.; Orzeszko, A.; Zanotti, G.; Battistutta, R.; et al. ATP site-directed inhibitors of protein kinase CK2: An update. *Curr. Top. Med. Chem.* **2011**, *11*, 1340–1351. [CrossRef] [PubMed]
32. Gingipalli, L.; Block, M.H.; Bao, L.; Cooke, E.; Dakin, L.A.; Denz, C.R.; Ferguson, A.D.; Johannes, J.W.; Larsen, N.A.; Dowling, J.E.; et al. Discovery of 2,6-disubstituted pyrazine derivatives as inhibitors of CK2 and PIM kinases. *Bioorg. Med. Chem. Lett.* **2018**, *28*, 1336–1341. [CrossRef] [PubMed]
33. Chen, Y.; Wang, Y.; Wang, J.; Zhou, Z.; Cao, S.; Zhang, J. Strategies of Targeting CK2 in Drug Discovery: Challenges, Opportunities, and Emerging Prospects. *J. Med. Chem.* **2023**, *66*, 2257–2281. [CrossRef] [PubMed]
34. Cozza, G.; Sarno, S.; Ruzzene, M.; Girardi, C.; Orzeszko, A.; Kazimierczuk, Z.; Zagotto, G.; Bonaiuto, E.; Di Paolo, M.L.; Pinna, L. Exploiting the repertoire of CK2 inhibitors to target DYRK and PIM kinases. *Biochim. Biophys. Acta* **2013**, *1834*, 1402–1409. [CrossRef] [PubMed]
35. Cozza, G.; Girardi, C.; Ranchio, A.; Lolli, G.; Sarno, S.; Orzeszko, A.; Kazimierczuk, Z.; Battistutta, R.; Ruzzene, M.; Pinna, L.A. Cell-permeable dual inhibitors of protein kinases CK2 and PIM-1: Structural features and pharmacological potential. *Cell. Mol. Life Sci.* **2014**, *71*, 3173–3185. [CrossRef]
36. Koronkiewicz, M.; Chilmoneczyk, Z.; Kazimierczuk, Z.; Orzeszko, A. Deoxynucleosides with benzimidazoles as aglycone moiety are potent anticancer agents. *Eur. J. Pharmacol.* **2018**, *820*, 146–155. [CrossRef]
37. Koronkiewicz, M.; Kazimierczuk, Z.; Orzeszko, A. Antitumor activity of the protein kinase inhibitor 1-( $\beta$ -D-2'-deoxyribofuranosyl)-4,5,6,7-tetrabromo-1H-benzimidazole in breast cancer cell lines. *BMC Cancer* **2022**, *22*, 1069. [CrossRef]
38. Łukowska-Chojnacka, E.; Wińska, P.; Wielechowska, M.; Poprzeczko, M.; Bretner, M. Synthesis of novel polybrominated benzimidazole derivatives-potential CK2 inhibitors with anticancer and proapoptotic activity. *Bioorg. Med. Chem.* **2016**, *24*, 735–741. [CrossRef]
39. Chojnacki, K.; Wińska, P.; Skierka, K.; Wielechowska, M.; Bretner, M. Synthesis, in vitro antiproliferative activity and kinase profile of new benzimidazole and benzotriazole derivatives. *Bioorg. Chem.* **2017**, *72*, 1–10. [CrossRef]
40. Chojnacki, K.; Winska, P.; Karatsai, O.; Koronkiewicz, M.; Milner-Krawczyk, M.; Wielechowska, M.; Redowicz, M.J.; Bretner, M.; Borowiecki, P. Synthesis of Novel Acyl Derivatives of 3-(4,5,6,7-Tetrabromo-1H-benzimidazol-1-yl)propan-1-ols-Intracellular TBBi-Based CK2 Inhibitors with Proapoptotic Properties. *Int. J. Mol. Sci.* **2021**, *22*, 6261. [CrossRef]
41. Ellingboe, J.W.; Spinelli, W.; Winkley, M.W.; Nguyen, T.T.; Parsons, R.W.; Moubarak, I.F.; Kitzen, J.M.; Von Engen, D.; Bagli, J.F. Class III antiarrhythmic activity of novel substituted 4-[(methylsulfonyl)amino]benzamides and sulfonamides. *J. Med. Chem.* **1992**, *35*, 705–716. [CrossRef] [PubMed]
42. Andrzejewska, M.; Pagano, M.A.; Meggio, F.; Brunati, A.M.; Kazimierczuk, Z. Polyhalogenobenzimidazoles: Synthesis and their inhibitory activity against casein kinases. *Bioorg. Med. Chem.* **2003**, *11*, 3997–4002. [CrossRef] [PubMed]
43. Pagano, M.A.; Andrzejewska, M.; Ruzzene, M.; Sarno, S.; Cesaro, L.; Bain, J.; Elliott, M.; Meggio, F.; Kazimierczuk, Z.; Pinna, L.A. Optimization of protein kinase CK2 inhibitors derived from 4,5,6,7-tetrabromobenzimidazole. *J. Med. Chem.* **2004**, *47*, 6239–6247. [CrossRef] [PubMed]

44. Borowiecki, P.; Wawro, A.; Wińska, P.; Wielechowska, M.; Bretner, M. Synthesis of novel chiral TBBt derivatives with hydroxyl moiety. Studies on inhibition of human protein kinase CK2 $\alpha$  and cytotoxicity properties. *Eur. J. Med. Chem.* **2014**, *84*, 364–374. [CrossRef] [PubMed]
45. Chojnacki, K.; Wińska, P.; Wielechowska, M.; Łukowska-Chojnacka, E.; Tölzer, C.; Niefind, K.; Bretner, M. Biological properties and structural study of new aminoalkyl derivatives of benzimidazole and benzotriazole, dual inhibitors of CK2 and PIM1 kinases. *Bioorg. Chem.* **2018**, *80*, 266–275. [CrossRef]
46. Bradford, M.M. A rapid and sensitive method for the quantitation of microgram quantities of protein utilizing the principle of protein-dye binding. *Anal. Biochem.* **1976**, *72*, 248–254. [CrossRef]
47. Trott, O.; Olson, A.J. AutoDock Vina: Improving the speed and accuracy of docking with a new scoring function, efficient optimization, and multithreading. *J. Comput. Chem.* **2010**, *31*, 455–461. [CrossRef]
48. Wang, J.; Wolf, R.M.; Caldwell, J.W.; Kollman, P.A.; Case, D.A. Development and testing of a general amber force field. *J. Comput. Chem.* **2004**, *25*, 1157–1174. [CrossRef]
49. Dakin, L.A.; Block, M.H.; Chen, H.; Code, E.; Dowling, J.E.; Feng, X.; Ferguson, A.D.; Green, I.; Hird, A.W.; Howard, T.; et al. Discovery of novel benzylidene-1,3-thiazolidine-2,4-diones as potent and selective inhibitors of the PIM-1, PIM-2, and PIM-3 protein kinases. *Bioorg. Med. Chem. Lett.* **2012**, *22*, 4599–4604. [CrossRef]
50. Pettersen, E.F.; Goddard, T.D.; Huang, C.C.; Couch, G.S.; Greenblatt, D.M.; Meng, E.C.; Ferrin, T.E. UCSF Chimera—a visualization system for exploratory research and analysis. *J. Comput. Chem.* **2004**, *25*, 1605–1612. [CrossRef]
51. Yung-Chi, C.; Prusoff, W.H. Relationship between the inhibition constant (K<sub>i</sub>) and the concentration of inhibitor which causes 50 per cent inhibition (IC<sub>50</sub>) of an enzymatic reaction. *Biochem. Pharmacol.* **1973**, *22*, 3099–3108. [CrossRef] [PubMed]
52. Thomé, M.P.; Filippi-Chiela, E.C.; Villodre, E.V.; Migliavaca, C.B.; Onzi, G.R.; Felipe, K.F.; Lenz, G. Ratiometric analysis of Acridine Orange staining in the study of acidic organelles and autophagy. *J. Cell Sci.* **2016**, *129*, 4622–4632. [CrossRef] [PubMed]
53. Lozzio, C.B.; Lozzio, B.B. Human chronic myelogenous leukemia cell-line with positive Philadelphia-chromosome. *Blood* **1975**, *45*, 321–334. [CrossRef] [PubMed]
54. Heriche, J.K.; Chambaz, E.M. Protein kinase CK2 $\alpha$  is a target for the Abl and Bcr-Abl tyrosine kinases. *Oncogene* **1998**, *17*, 13–18. [CrossRef]
55. Rai, Y.; Yadav, P.; Kumari, N.; Kalra, N.; Bhatt, A.N. Hexokinase II inhibition by 3-bromopyruvate sensitizes myeloid leukemic cells K-562 to anti-leukemic drug, daunorubicin. *Biosci Rep.* **2019**, *39*, BSR20190880. [CrossRef]
56. Morotti, A.; Carrà, G.; Panuzzo, C.; Crivellaro, S.; Taulli, R.; Guerrasio, A.; Saglio, G. Protein Kinase CK2: A Targetable BCR-ABL Partner in Philadelphia Positive Leukemias. *Adv. Hematol.* **2015**, *2015*, 612567. [CrossRef]
57. Hori, M.; Nogami, T.; Itabashi, M.; Yoshim, F.; Ono, H.; Koizumi, S. Expression of Bcl-2 in human breast cancer: Correlation between hormone receptor status, p53 protein accumulation and DNA strand breaks associated with apoptosis. *Pathol. Int.* **1997**, *47*, 757–762. [CrossRef]
58. Galluzzi, L.; Vitale, I.; Aaronson, S.A.; Abrams, J.M.; Adam, D.; Agostinis, P.; Alnemri, E.S.; Altucci, L.; Amelio, I.; Andrews, D.W.; et al. Molecular mechanisms of cell death: Recommendations of the Nomenclature Committee on Cell Death 2018. *Cell Death Differ.* **2018**, *25*, 486–541. [CrossRef]
59. Denton, D.; Kumar, S. Autophagy-dependent cell death. *Cell Death Differ.* **2018**, *26*, 605–616. [CrossRef]
60. Bellodi, C.; Lidonnici, M.; Hamilton, A.; Helgason, V.; Soliera, A.R.; Ronchetti, M.; Galavotti, S.; Young, K.W.; Selmi, T.; Yacobi, R.; et al. Targeting autophagy. *J. Clin. Investig.* **2009**, *119*, 1109–1123. [CrossRef]
61. Lin, Q.; Meloni, D.; Pan, Y.; Xia, M.; Rodgers, J.; Shepard, S.; Li, M.; Galya, L.; Metcalf, B.; Yue, T.-Y.; et al. Enantioselective synthesis of Janus kinase inhibitor INCB018424 via an organocatalytic aza-Michael reaction. *Org. Lett.* **2009**, *11*, 1999–2002. [CrossRef] [PubMed]
62. Izeradjene, K.; Douglas, L.; Delaney, A.; Houghton, J.A. Casein kinase ii (CK2) enhances death-inducing signaling complex (disc) activity in trail-induced apoptosis in human colon carcinoma cell lines. *Oncogene* **2005**, *24*, 2050–2058. [CrossRef] [PubMed]
63. Trembley, J.H.; Chen, Z.; Unger, G.; Slaton, J.; Kren, B.T.; Van Waes, C.; Ahmed, K. Emergence of protein kinase ck2 as a key target in cancer therapy. *BioFactors* **2010**, *36*, 187–195. [CrossRef] [PubMed]
64. Wang, S.; He, M.; Li, L.; Liang, Z.; Zou, Z.; Tao, A. Cell-in-cell death is not restricted by caspase-3 deficiency in mcf-7 cells. *J. Breast Cancer* **2016**, *19*, 231–241. [CrossRef] [PubMed]
65. Li, Y.; Dowbenko, D.; Lasky, L.A. AKT/PKB phosphorylation of p21Cip/WAF1 enhances protein stability of p21Cip/WAF1 and promotes cell survival. *J. Biol. Chem.* **2002**, *277*, 11352–11361. [CrossRef] [PubMed]
66. Wińska, P.; Skierka, K.; Łukowska-Chojnacka, E.; Koronkiewicz, M.; Cieśla, J.; Bretner, M. Effect of Simultaneous Inhibition of Protein Kinase CK2 and Thymidylate Synthase in Leukemia and Breast Cancer Cells. *Anticancer Res.* **2018**, *38*, 4617–4627. [CrossRef]
67. Wińska, P.; Widło, L.; Skierka, K.; Krzyśko, A.; Koronkiewicz, M.; Cieśla, J.M.; Cieśla, J.; Bretner, M. Simultaneous Inhibition of Protein Kinase CK2 and Dihydrofolate Reductase Results in Synergistic Effect on Acute Lymphoblastic Leukemia Cells. *Anticancer Res.* **2019**, *39*, 3531–3542. [CrossRef]

68. Wińska, P.; Karatsai, O.; Staniszewska, M.; Koronkiewicz, M.; Chojnacki, K.; Rędownicz, M.J. Synergistic Interactions of 5-Fluorouracil with Inhibitors of Protein Kinase CK2 Correlate with p38 MAPK Activation and FAK Inhibition in the Triple-Negative Breast Cancer Cell Line. *Int. J. Mol. Sci.* **2020**, *21*, 6234. [CrossRef]
69. Daina, A.; Blatter, M.-C.; Baillie Gerritsen, V.; Palagi, P.M.; Marek, D.; Xenarios, I.; Schwede, T.; Michielin, O.; Zoete, V. Drug design workshop: A web-based educational tool to introduce computer-aided drug design to the general public. *J. Chem. Educ.* **2017**, *94*, 335–344. [CrossRef]

**Disclaimer/Publisher's Note:** The statements, opinions and data contained in all publications are solely those of the individual author(s) and contributor(s) and not of MDPI and/or the editor(s). MDPI and/or the editor(s) disclaim responsibility for any injury to people or property resulting from any ideas, methods, instructions or products referred to in the content.

## Article

# An Aptamer against MNK1 for Non-Small Cell Lung Cancer Treatment

Rebeca Carrión-Marchante <sup>1,†</sup>, Celia Pinto-Díez <sup>2,†</sup>, José Ignacio Klett-Mingo <sup>1</sup>, Esther Palacios <sup>1</sup>, Miriam Barragán-Usero <sup>1</sup>, M. Isabel Pérez-Morgado <sup>1</sup>, Manuel Pascual-Mellado <sup>1</sup>, Sonia Alcalá <sup>3,4</sup>, Laura Ruiz-Cañas <sup>3,4</sup>, Bruno Sainz, Jr. <sup>3,4,5</sup>, Víctor M. González <sup>1,\*</sup> and M. Elena Martín <sup>1,\*</sup>

<sup>1</sup> Aptamer Group, Department Biochemistry-Research, IRYCIS—Hospital Universitario Ramón y Cajal, 28034 Madrid, Spain

<sup>2</sup> Aptus Biotech SL, 28035 Madrid, Spain

<sup>3</sup> Department of Cancer, Instituto de Investigaciones-Biomédicas “Alberto Sols” (IIBM), CSIC-UAM, 28034 Madrid, Spain

<sup>4</sup> Chronic Diseases and Cancer Area 3—Instituto Ramón y Cajal de Investigación Sanitaria (IRYCIS), 28034 Madrid, Spain

<sup>5</sup> Centro de Investigación Biomédica en Red, Área Cáncer—CIBERONC, ISCIII, 28029 Madrid, Spain

\* Correspondence: victor.m.gonzalez@hrc.es (V.M.G.); m.elena.martin@hrc.es (M.E.M.); Tel.: +34-913-368-173 (V.M.G. & M.E.M.)

† These authors contributed equally to this work.

**Abstract:** Lung cancer is the leading cause of cancer-related death worldwide. Its late diagnosis and consequently poor survival make necessary the search for new therapeutic targets. The mitogen-activated protein kinase (MAPK)-interacting kinase 1 (MNK1) is overexpressed in lung cancer and correlates with poor overall survival in non-small cell lung cancer (NSCLC) patients. The previously identified and optimized aptamer from our laboratory against MNK1, apMNKQ2, showed promising results as an antitumor drug in breast cancer in vitro and in vivo. Thus, the present study shows the antitumor potential of apMNKQ2 in another type of cancer where MNK1 plays a significant role, such as NSCLC. The effect of apMNKQ2 in lung cancer was studied with viability, toxicity, clonogenic, migration, invasion, and in vivo efficacy assays. Our results show that apMNKQ2 arrests the cell cycle and reduces viability, colony formation, migration, invasion, and epithelial-mesenchymal transition (EMT) processes in NSCLC cells. In addition, apMNKQ2 reduces tumor growth in an A549-cell line NSCLC xenograft model. In summary, targeting MNK1 with a specific aptamer may provide an innovative strategy for lung cancer treatment.

**Keywords:** aptamer; MNK1; therapeutic target; non-small cell lung cancer; NSCLC; antitumor

**Citation:** Carrión-Marchante, R.; Pinto-Díez, C.; Klett-Mingo, J.I.; Palacios, E.; Barragán-Usero, M.; Pérez-Morgado, M.I.; Pascual-Mellado, M.; Alcalá, S.; Ruiz-Cañas, L.; Sainz, B., Jr.; et al. An Aptamer against MNK1 for Non-Small Cell Lung Cancer Treatment. *Pharmaceutics* **2023**, *15*, 1273. <https://doi.org/10.3390/pharmaceutics15041273>

Academic Editor: Francesca Musumeci

Received: 3 March 2023

Revised: 13 April 2023

Accepted: 14 April 2023

Published: 18 April 2023



**Copyright:** © 2023 by the authors. Licensee MDPI, Basel, Switzerland. This article is an open access article distributed under the terms and conditions of the Creative Commons Attribution (CC BY) license (<https://creativecommons.org/licenses/by/4.0/>).

## 1. Introduction

Lung cancer is the leading cause of cancer-related death worldwide and the second most commonly diagnosed tumor among all cancer types [1]. The 5-year survival rate is greater for early-stage lung cancer than for advanced-stage lung cancer. Lung cancer is usually diagnosed in advanced stages, or even when it metastasizes to other areas, which increases therapeutic failure, decreasing patient survival rates [2]. Therefore, the search for new therapies against lung cancer is a healthcare priority.

The mitogen-activated protein kinase (MAPK)-interacting kinases (MNKs) are serine/threonine kinases that are directly activated by an extracellular signal-regulated kinase (ERK) 1/2 or p38 MAP kinases [3,4]. In humans, MNKs comprise a group of four isoforms (MNK1a/b and MNK2a/b) from two genes by alternative splicing. The four isoforms are similar in their N-terminus but differ in their C-terminus. MNK1b was first described in our laboratory [5], and it lacks the MAPK binding site motif present in the C-terminal region of MNK1a. MNK1b has higher basal activity than MNK1a, being independent of



ERK1/2 and p38 MAPK activation [6]. MNKs phosphorylate several substrates including eukaryotic initiation factor 4E (eIF4E) [7] and 4G (eIF4G) [8], heterogeneous nuclear ribonucleoprotein A1 (hnRNPA1) [9], cPLA2 [10], Sprouty2 [11], and polypyrimidine-tract binding protein-associated splicing factor (PSF) [12], being eIF4E the best characterized.

The eIF4E improves the translation of proteins involved in proliferation, survival, invasion, and angiogenesis such as cyclin D1, c-Myc, Bcl-2, metalloproteases (MMPs), Snail, vascular endothelial growth factor (VEGF) and fibroblast growth factor (FGF) [13–17]. Phosphorylation of eIF4E on serine 209 by MNKs is associated with tumor progression and poor prognosis, with high levels of phosphorylated eIF4E (p-eIF4E) found in different types of cancer [18]. Similarly, overexpression of MNKs has been found in glioblastoma, lung cancer, hepatocellular carcinoma, ovarian cancer, and breast cancer [19–24], and high expression of MNK1 is correlated with poor prognosis in several types of cancers [25]. Of all MNK inhibitors developed thus far [25], some have been evaluated in clinical trials for cancer therapy such as BAY1143269 [26], eFT508 [27], or ETC-206 [28]. Likewise, in MNK1 and MNK2 knockout (KO) mice, while their development is normal, there is a delay in tumor progression in KO mice compared to wild-type mice [29]. Thus, since MNKs are not essential but overexpressed in many tumor types, they represent good therapeutic cancer targets, with theoretically no adverse effects in non-tumor cells.

Aptamers are single-strand nucleic acids (ssDNA or RNA) that bind to different targets by folding into a three-dimensional conformation. They are identified by the SELEX method [30,31], which represents an important tool for the discovery of novel biomarkers of both therapeutic and diagnostic interest. Aptamers offer several advantages over antibodies including their high stability, low immunogenicity, no batch-to-batch variability, small size, short generation time, and quick modification [32]. So far, Macugen<sup>®</sup> is the only aptamer approved by the FDA for the treatment of age-related macular degeneration [33]. However, several aptamers have entered into clinical trials [34]; some for cancer treatment such as the DNA aptamer AS1411 which targets nucleolin, inducing apoptosis [35], or NOX-A12, an RNA aptamer that inhibits tumor growth by binding to CXCL-12.

We selected an aptamer against MNK1 capable of inhibiting proliferation, migration, and colony formation in MDA-MB-231 breast cancer cells [36]. In order to decrease its size, we obtained four different sequences from the initial aptamer, where apMNKQ2 was the most efficient sequence at inhibiting the proliferation of breast cancer cell lines. Further studies showed that apMNKQ2 inhibits the tumorigenic and metastatic activity of breast cancer cells and reduces tumor growth and metastasis numbers in an in vivo model [37].

Thus, the objective of this work was to evaluate the potential of apMNKQ2 as an antitumor drug. For this purpose, we studied the effect of apMNKQ2 in another type of cancer where MNK1 is overexpressed, specifically lung cancer. Our results show that apMNKQ2 arrests the cell cycle and inhibits the proliferation, colony formation, migration, invasion, and adhesion of lung cancer cell lines, and reduces tumor growth in a mouse xenograft model of lung adenocarcinoma. These results highlight apMNKQ2 as a potential anticancer drug for lung cancer.

## 2. Materials and Methods

### 2.1. Materials

The ssDNA aptamers, apMNKQ2 (TGGGGTGGGCGGGCGGGGGTGGGGGTGGT) and p29 (GCGGTCTGACTTAAATGTCCATCTCAAAC) were purchased from Biospring, Frankfurt am Main, Germany. The apMNKQ2 aptamer used in this study does not have any modification. The origin of the rest of the material is indicated in the text.

### 2.2. Cell Culture and Transfection

A549 (human lung adenocarcinoma cell line) and SW900 (human lung squamous cell carcinoma cell line) cells were authenticated in May of 2019, and H460 cells (human lung large cell carcinoma cell line) were authenticated in September of 2022, through the GenePrint<sup>®</sup> 10 System. SW900 and H460 were cultured in RPMI medium (PAA, Pasching, Austria) containing 10% fetal

calf serum (Gibco, Grand Island, New York, NY, USA), 100 U/mL penicillin, 100 µg/mL streptomycin, and 25 µg/mL amphotericin (Sigma, St. Louis, MO, USA). A549 cells were cultured in Dulbecco's modified Eagle's medium (DMEM) (Biowest SAS, Nuaillé, France) with 10% fetal calf serum (Gibco, Grand Island, New York, NY, USA), 1% pyruvate, 100 U/mL penicillin, 100 µg/mL streptomycin, and 25 µg/mL amphotericin (Sigma, St. Louis, MO, USA). All cell lines were maintained at 37 °C in a humidified incubator with 5% CO<sub>2</sub>. For cell transfection with aptamers, cells were seeded at different concentrations according to the assay and after 24 h, aptamers were transfected into cells using Lipofectamine™ 2000 (Invitrogen, Carlsbad, CA, USA), according to the manufacturer's instructions. Cells were incubated at 37 °C in a humidified incubator with 5% CO<sub>2</sub> until the assay was carried out. Before transfection, aptamers were dissolved in selection buffer (20 mM Tris-HCl pH 7.4, 150 mM NaCl, 1 mM MgCl<sub>2</sub>, and 5 mM KCl), denatured at 90 °C for 10 min and then cooled on ice for 10 min.

### 2.3. Protein and RNA Extraction

For protein extraction, cells were mechanically dissociated and washed once with cold buffer A (20 mM Tris-HCl pH 7.6, 1 mM ethylenediaminetetraacetic acid (EDTA), 1 mM dithiothreitol (DTT), 1 mM benzamidine, 1 mM phenylmethylsulfonyl fluoride (PMSF), 10 mM sodium β-glycerophosphate, 10 mM sodium molybdate, 1 mM sodium orthovanadate, 120 mM potassium chloride (KCl), 10 µg/mL antipain, 1 µg/mL pepstatin A, and leupeptin). Then, cells were lysed in buffer A with 1% Triton X-100 (volume ratio 1:2) and centrifugated for 10 min at 12,000× g. Supernatants were used to determine protein concentrations using the BCA kit (ThermoFisher Scientific, Waltham, MA, USA) and then they were stored at −80 °C until use.

For total RNA extraction, cells were trypsinized and centrifugated at 400× g for 5 min. Pellets were lysed in NucleoZOL (Macherey-Nagel, Düren, Germany) according to the manufacturer's instructions. RNA pellets were resuspended in 50 µL of RNase-free water, quantified, and stored at −80 °C until use.

### 2.4. Western Blot

Cell lysates were resolved in 7.5%, 10%, or 12% sodium dodecyl sulphate-polyacrilamide gels (SDS-PAGE) by electrophoresis and transferred onto polyvinylidene difluoride (PVDF) membranes. Membranes were incubated for 1 h at room temperature with 5% non-fat milk in PBS and then overnight at 4 °C with monoclonal or polyclonal antibodies. After washing, membranes were incubated with the corresponding peroxidase-conjugated secondary antibodies for 1 h at room temperature and proteins were visualized using Clarity Western ECL Substrate (BioRad, Hercules, CA, USA) and a ChemiDoc™ (BioRad, Hercules, CA, USA). Bands were quantified using ImageLab 6.1 software (BioRad, Hercules, CA, USA). PageRuler Plus Prestained Protein Ladder (ThermoFisher Scientific, Waltham, MA, USA) was the molecular weight marker used in all the experiments. β-actin (Sigma, St. Louis, MO, USA) antibody was used to control the homogeneity of loading. Antibodies used in this work can be found in Supplementary Table S1.

### 2.5. Cell Viability (MTT) and Cell Toxicity (LDH) Assays

To study cell viability, 3-(4,5-dimethylthiazol-2-yl)-2,5-diphenyl-2H-tetrazolium bromide (MTT) assays were performed. A549 and H460 cells were plated at  $6 \times 10^3$  cells/well and SW900 at  $10^4$  cells/well in 96-well plates. After 16–24 h, cells were transfected with apMKNQ2 or the unspecific p29 aptamer as described above and incubated at 37 °C in a humidified incubator with 5% CO<sub>2</sub> for 48 h. Then, the medium was removed to add 100 µL/well of MTT (Sigma, St. Louis, MO, USA) at 1 mg/mL in culture medium. A549 and H460 cells were incubated for 1.5 h and the SW900 cell line for 3 h at 37 °C. Next, 100 µL/well of lysis buffer (10% SDS and 10 mM HCl) was added. After 24 h, absorbance was read at 540 nm in an Infinite F200 spectrophotometer (TECAN, Männedorf, Switzerland).

To determine cytotoxicity in cells, lactate dehydrogenase (LDH) assays were performed 48 h after cell transfection with aptamers. Supernatants were collected and the

Cytotoxicity Detection kit (LDH) (Roche, Madrid, Spain) reagent was added according to the manufacturer's instructions. After incubation for 30 min at room temperature, the reaction was stopped by adding 1M HCl and absorbance was read at 490 nm in an Infinite F200 spectrophotometer (TECAN, Männedorf, Switzerland). To calculate the percentage of cytotoxicity, two controls were used: the supernatant of untreated cells (LDH<sub>low</sub>) and of lysed cells (LDH<sub>high</sub>) with 0.2% Triton X-100. Results are expressed as:

$$\text{Cytotoxicity (\%)} = \frac{\text{LDH}_{\text{treated}} - \text{LDH}_{\text{low}}}{\text{LDH}_{\text{high}} - \text{LDH}_{\text{low}}} \times 100$$

#### 2.6. Trypan Blue Exclusion Test of Cell Viability

In order to determine the viable cells after transfection with apMKNQ2, cells were collected from the plates and 10  $\mu$ L of cells were mixed with 10  $\mu$ L of trypan blue and were counted on a TC20 counter (BioRad, Hercules, CA, USA). Those cells that excluded the dye were considered viable.

#### 2.7. Cell Cycle Assay

Cells were plated at  $5 \times 10^5$  cells/well in a 6-well plate and transfected with the aptamers. Cells were trypsinized 24 h post-transfection, and both attached and floating cells were collected, fixed with PFA 4%, washed twice with PBS, and stored at 4 °C. Next, cells were incubated with FxCycle Violet Ready Flow Reagent (Thermo Fisher Scientific, Waltham, MA, USA) for 30 min at 25 °C and DNA content was evaluated with a 4-laser Attune NxT Acoustic Cytometer (Thermo Fisher Scientific, Waltham, MA, USA). Results were analyzed using FCSalyzer 0.9.22 alpha Software.

#### 2.8. Apoptosis Assay

Cells were plated at  $5 \times 10^5$  cells/well in a 6-well plate, transfected with the aptamers during 24 h, resuspended, and stained with Annexin V Apoptosis detection kit (Canvax, Córdoba, Spain) as described previously [37] and analyzed with a 4-laser Attune NxT Acoustic Cytometer (Thermo Fisher Scientific, Waltham, MA, USA). Results were analyzed using FCSalyzer 0.9.22 alpha Software.

#### 2.9. Clonogenic Assays

Cells were seeded at  $5 \times 10^4$  cells/well in 24-well plates and 16–24 h later, they were transfected with aptamers. After 16–24 h, cells were collected and seeded at  $10^3$  cells/well in 6-well plates. Cells were incubated at 37 °C in a humidified incubator with 5% CO<sub>2</sub> during 5–8 days. Then, cells were fixed with 1 mL/well of ethanol for 10 min at room temperature and stained with Giemsa 0.2% (Sigma, St. Louis, MO, USA) for 30 min. Remains of Giemsa were removed with water, images of colonies were taken and colonies were counted using ImageJ Java 1.8.0\_172 software (National Institutes of Health, Bethesda, MD, USA).

#### 2.10. Migration Assays

Migration assays were performed using transwell insert chambers (Corning, New York, NY, USA). Cells were seeded at  $5 \times 10^4$  cells/well in 24-well plates and transfected with aptamers 16–24 h later. After 16 h of serum-deprivation, cells were collected and added at  $4 \times 10^4$  cells/well into the upper chamber in 300  $\mu$ L of serum-free medium. In the lower chamber, 500  $\mu$ L of complete medium (10% FSB) was added as a chemoattractant. After 24 h, both media were removed and cells in the insert were fixed for 2 min with 4% formaldehyde followed by 20 min with 100% methanol. Next, cells were stained with 30  $\mu$ M Hoechst 33342 for 15 min and washed twice with PBS. At least five photographs were taken for each sample using a fluorescence microscope Olympus IX70 (Olympus Iberia, Barcelona, Spain). Cells were counted using ImageJ Java 1.8.0\_172 software (National Institutes of Health, Bethesda, MD, USA).

### 2.11. Cell Adhesion Assays

Plates were coated with 10 µg/mg type I collagen (Sigma, St. Louis, MO, USA) or BSA (Sigma, St. Louis, MO, USA) as a control for 1 h at 37 °C. Cells were seeded at  $5 \times 10^4$  cells/well in 6-well plates and transfected with aptamers 16–24 h later. After 24 h, cells were collected, added to coated plates at  $3 \times 10^4$  cells/well in serum-free medium, and allowed to bind at 37 °C for 1 h. Wells were washed twice with PBS to remove non-adhered cells and an MTT assay was performed with 1 h of incubation between the addition of the MTT reagent and lysis buffer. After 24 h, absorbance was read at 540 nm in an Infinite F200 spectrophotometer (TECAN, Männedorf, Switzerland).

### 2.12. Zymography

The MMP activity of cells was analyzed through zymography. Cells were transfected and after 18 h of serum-deprivation, supernatants were collected and concentrated using Centricon tubes with a 3 kDa cutoff (Merck, Rahway, NJ, USA). Samples were mixed with loading buffer without mercaptoethanol and then separated in 7.5% polyacrylamide gels with 1 mg/mL gelatin. Gels were then incubated for 30 min in 2.5% Triton X-100 at room temperature and overnight at 37 °C in developing buffer (50 mM Tris-HCl pH 7.5, 200 mM NaCl, 5 mM CaCl<sub>2</sub>, and 0.02% Tween). Coomassie blue staining revealed the presence of MMP activity as clear bands against the blue background. Bands were quantified with ImageLab 6.1 software (BioRad, Hercules, CA, USA).

### 2.13. Aptamer Quantification

To quantify intracellular aptamers, cells were collected 4-, 24- and 48-h post-transfection, washed twice in PBS, lysed in 1 mL of H<sub>2</sub>O for 5 min, vortexed, and boiled at 90 °C for 10 min. Lysates were centrifuged at 12,000× *g* for 10 min and the aptamer in the supernatant was quantified by quantitative PCR. Pellets were resuspended in 10 µL of 0.1 M NaOH to determine protein concentration by BCA as described above. Results are expressed in fmol of aptamer/µg of protein. To quantify aptamer in tumors and organs, 50–100 mg of tissue were lysed and homogenized in NucleoZOL reagent (Macherey-Nagel, Düren, Germany) following the manufacturer's instructions to isolate small RNA fraction, in which the aptamer is found. Results are expressed in fmol of aptamer/µg of tissue. Since apMNKQ2 is only 29 nucleotides in length, we designed a method that allows us to amplify this small-size aptamer in which apMNKQ2 acts as a primer on a template oligo-nucleotide called QR short (see Supplementary Table S2). After this reaction, both apMNKQ2 and QR short are elongated generating a 76-nucleotide template that can then be amplified with the appropriate primers (R3 and QF) (see Supplementary Table S2). Thus, in the absence of apMNKQ2, no amplification occurs, being the amplification proportional to the amount of apMNKQ2 present in the sample. The qPCR was performed using the AceQ qPCR SYBR<sup>®</sup> Green Master Mix-Vazyme (Quimigen, Madrid, Spain) according to the manufacturer's instructions in a StepOne Plus Real-Time PCR system (Applied Biosystem, Waltham, MA, USA). The reaction mixture consisted of 1× Mix FastGene<sup>®</sup> IC Green, 1 pmol QR short, 100 nM QF and R3 primers, and 1 µL of samples in a 10 µL/tube final volume. Aptamers were quantified using a standard curve (100 fmol–100 amol).

### 2.14. Quantification of mRNA

Total RNA was obtained as described above and was used to synthesize first strand cDNA using the SensiFAST<sup>™</sup> cDNA Synthesis Kit (Bioline, Segovia, Spain) following the manufacturer's instructions. Products were used for qPCR amplification using the AceQ qPCR SYBR<sup>®</sup> Green Master Mix-Vazyme (Quimigen, Madrid, Spain) according to the manufacturer's protocol in a StepOne Plus Real-Time PCR system (Applied Biosystem, Waltham, MA, USA). Triplicate reactions of the targets and housekeeping genes were performed simultaneously for each cDNA template. Sequences of oligonucleotides are in Supplementary Table S2. To calculate the relative expression of each target gene, the  $2^{-\Delta\Delta Ct}$

method was performed, using  $\beta$ -actin as a housekeeping normalization gene, where  $\Delta Ct$  is  $C_{t\text{target}} - C_{t\text{housekeeping}}$ .

### 2.15. Tolerability Study

Non-tumor-bearing CD1 mice were used to determine the maximum tolerated dose (MTD) of apMNKQ2. The aptamer was administered once per day intraperitoneally (i.p.) for 7 consecutive days. We applied a modified “3 + 3” study design [38,39], using cohorts of 3 animals per dose and with the first cohort treated at a starting dose (1 mg/Kg). Subsequent cohorts were treated with increasing or decreasing doses according to the observed dose-limiting toxicities (DLTs) responses with guided subsequent doses, as described in [40]. DLT endpoints included weight loss (>20%), abnormal behavior, signs of physical discomfort, and/or death. Mice were evaluated daily and if any of the endpoints were met, animals were euthanized.

### 2.16. In Vivo Efficacy Assays

For in vivo experiments, mice were housed according to institutional guidelines, and all experimental procedures were performed in compliance with the institutional guidelines for the welfare of experimental animals approved by the Universidad Autónoma de Madrid Ethics Committee (CEI 60-1057-A068 and CEI 103-1958-A337) and La Comunidad de Madrid (PROEX 294/19) and in accordance with the guidelines for Ethical Conduct in the Care and Use of Animals as stated in The International Guiding Principles for Biomedical Research involving Animals, developed by the Council for International Organizations of Medical Sciences (CIOMS). Briefly, mice were housed according to the following guidelines: a 12-h light/12-h dark cycle, with no access during the dark cycle; temperatures of 65–75 °F (~18–23 °C) with 40–60% humidity; a standard diet with fat content ranging from 4–11%; sterilized water was accessible at all times; for handling, mice were manipulated gently and as little as possible; noises, vibrations, and odors were minimized to prevent stress and decreased breeding performance; and enrichment was always used per the facility’s guidelines to help alleviate stress.

Female 9-week-old Foxn1<sup>nu/nu\*</sup> (Janvier Labs, Le Genest-Saint-Isle, France) were injected subcutaneously in the dorsal flanks with  $8 \times 10^6$  A549 cells resuspended in 100  $\mu$ L Matrigel (Corning, New York, NY, USA) per injection. Once tumors were established, mice were randomized into 3 groups (5 mice per group) and injected intraperitoneally with vehicle control (selection buffer), 10 mg/kg apMNKQ2 or 25 mg/kg apMNKQ2. Aptamer injections were daily and tumor volumes were determined twice per week for 25 days using a manual caliper. At the time of sacrifice, tumors were excised and weighed. One half was frozen in liquid nitrogen for western blot and qPCR analysis and the other half was fixed in 4% PFA and processed for histologic analysis. At the end of the treatment, the TGI ratio (%) was calculated using the following formula:  $\text{TGI (\%)} = [1 - (\text{Volume of the treated group}) / (\text{volume of the control group})] \times 100 (\%)$ .

### 2.17. Statistical Analyses

Results are presented as means  $\pm$  standard error of the mean (SEM) unless stated otherwise. Pair-wise multiple comparisons were performed with one-way ANOVA (two-sided) with Turkey’s test adjustment, as indicated in the figure legends. A student’s *t*-test was used to determine differences between the means of groups. The *p*-values < 0.05 were considered statistically significant. All analyses were performed using GraphPad Prism version 8.0 (San Diego, CA, USA).

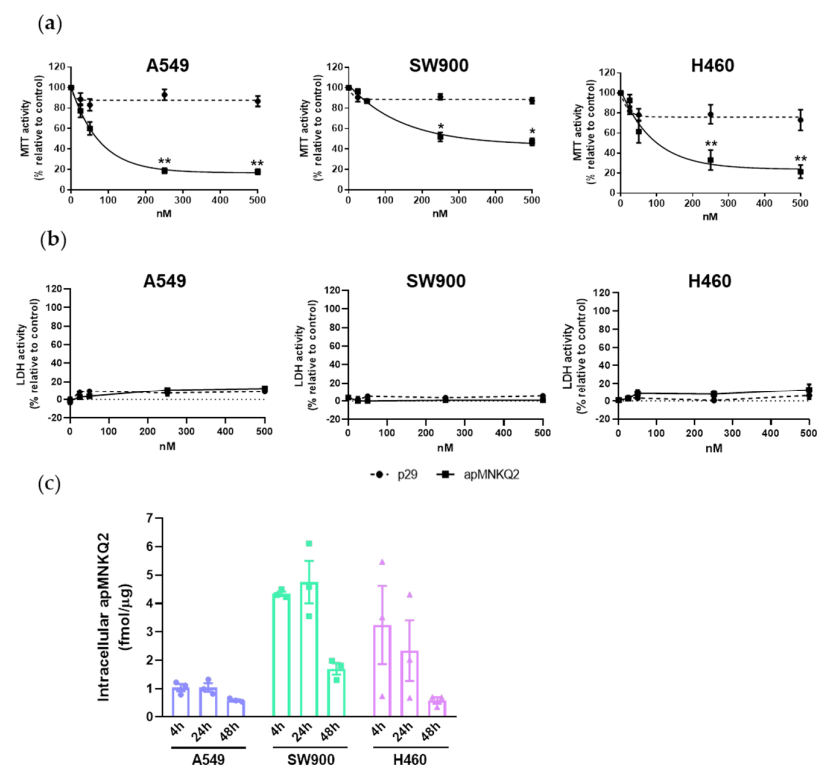
## 3. Results

### 3.1. apMNKQ2 Inhibits Cell Viability in NSCLC Cell Lines

In our previous work [37], four sequences were designed (apMNKQ1, apMNKQ2, apMNKQ3, and apMNKQ4) from the aptamer apMNK2F against MNK1b and tested in breast cancer cell lines. Here, to study the effect of the four sequences in the context of lung

cancer, A549 and SW900 cell lines were transfected with the four aptamers at 250 nM, and cell viability was assessed 48 h later by measuring MTT activity. The nonspecific aptamer (p29) was used as a control. Results (Supplementary Figure S1) showed that apMKNKQ2 had the greatest effect on MTT activity in both cell lines, producing a significant reduction in cell viability of 77% in A549 and 51% in SW900 cells.

Consequently, the effect of apMKNKQ2 on cell proliferation and toxicity was evaluated in three cell lines (A549, SW900, and H460) representing the main types of non-small cell lung cancer (adenocarcinoma, squamous cell carcinoma, and large cell carcinoma, respectively). Cells were transfected with increasing concentrations (0–500 nM) of apMKNKQ2 or the nonspecific control aptamer (p29). MTT activity was measured after 48 h and to study possible cell death by necrosis, LDH enzyme activity was simultaneously measured. Results showed that apMKNKQ2 decreased MTT activity in all three cell lines in a concentration-dependent manner, with A549 cells being the most sensitive (Figure 1a). The nonspecific p29 aptamer had a slight effect on the cell lines (less than 20%). The IC<sub>50</sub> values were 70 nM, 250 nM, and 100 nM for A549, SW900, and H460, respectively. This effect was not necrosis-mediated since there was little to no cytotoxicity (Figure 1b).



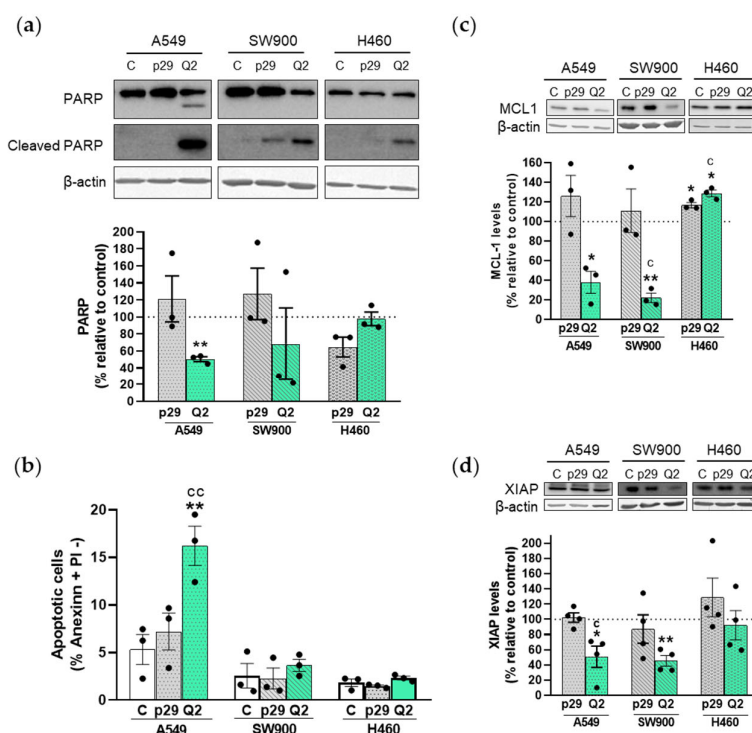
**Figure 1.** Aptamer effect on the viability of lung cancer cells. (a) Effect of apMKNKQ2 on MTT and (b) LDH activity. A549 and H460 cells were seeded at  $6 \times 10^3$  cells/well and SW900 cells were seeded at  $10^4$  cells/well in 96-well plates. After 48 h MTT and LDH assays were performed. Graphs represent the mean  $\pm$  SEM of 6 and 3 independent experiments. \*  $p < 0.05$  and \*\*  $p < 0.01$  relative to p29 control. (c) The half-life of apMKNKQ2 in lung cancer cells. Cells were seeded at  $5 \times 10^5$  cells/well in 6-well plates and transfected with the corresponding IC<sub>50</sub> of apMKNKQ2 16–24 h later. After 4, 24, and 48 h, cells were lysed and apMKNKQ2 was quantified through qPCR. Results are expressed as fmol of aptamer/ $\mu$ g of protein. Bars represent mean  $\pm$  SEM of 3 independent experiments. Solid blue circles (A549 cell line), green squares (SW900 cell line) and violet triangles (H460 cell line) represent one individual value.

When aptamers are used against intracellular targets it is important to determine their half-life inside the cell, which may be affected by their molecular nature or structure. To study the intracellular stability of apMKNKQ2, cells were transfected according to their IC<sub>50</sub>.

After 4, 24, and 48 h, cells were lysed and apMKNKQ2 was quantified by qPCR. As shown in Figure 1c, apMKNKQ2 is stable in all three cell lines for at least 48 h.

### 3.2. apMKNKQ2 Induces Apoptosis, Cell Cycle Arrest, and Inhibits Colony Formation in Lung Cancer Cells

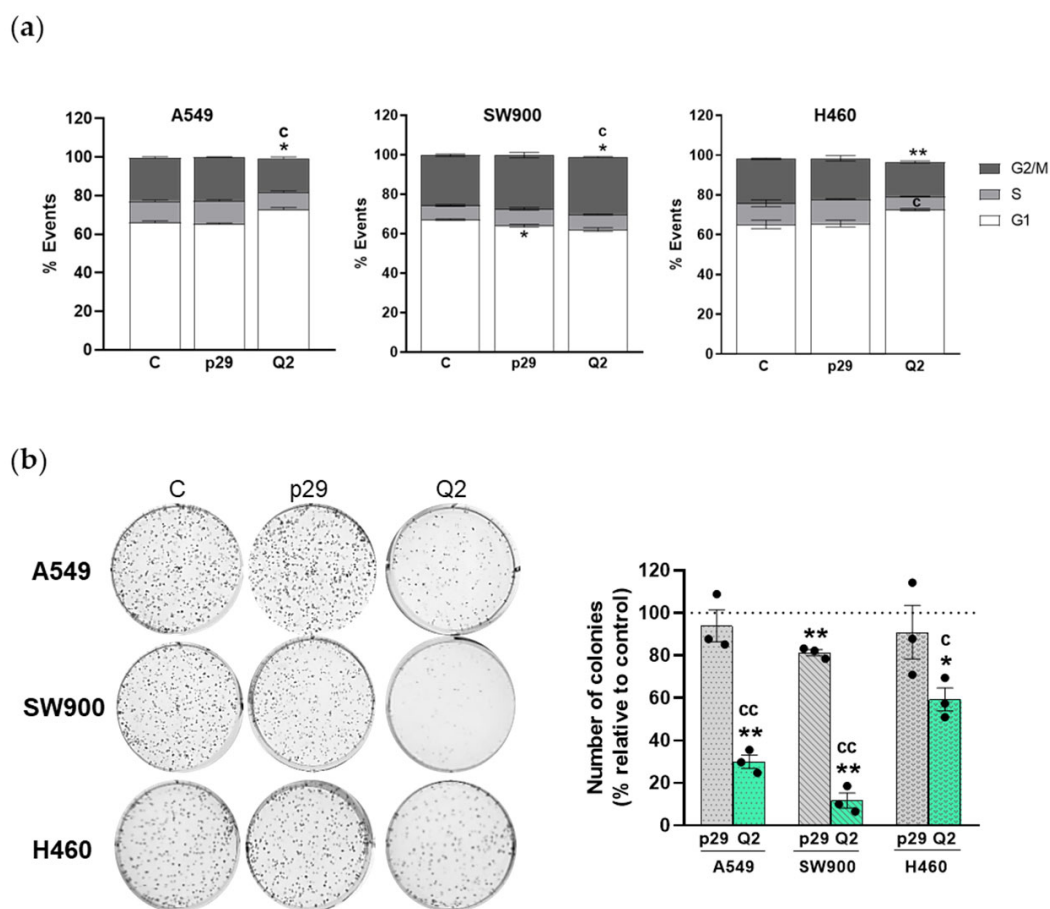
To determine whether the decrease in cell viability was a consequence of apMKNKQ2-induced apoptosis, we analyzed the apoptotic marker cleaved-PARP. Aptamer-transfected cells were lysed after 24 h of transfection (cell viability 24 h after transfection is shown in Supplementary Figure S2) and analyzed by western blot as described in the Material and Methods section (Section 2). Figure 2a shows that the cleavage of PARP by caspase 3 occurs in the three cell lines albeit to a different extent. A decrease in the uncleaved form of PARP was observed in A549 and SW900 cell lines, being statistically significant in A549 cells. In addition, we observed a significant increase in both the percentage of Annexin-V positive and propidium iodide (PI) negative cells (Figure 2b) and the percentage of the sub-G1 phase in the A549 cells (Supplementary Figure S2c), indicating that apMKNKQ2 induces apoptosis in this cell line.



**Figure 2.** Apoptotic activity of apMKNKQ2 on NSCLC cells. (a) On the top, lysates (20  $\mu$ g) were resolved in 10% SDS-PAGE gels for PARP and cleaved PARP. On the bottom, densitometry analyses of total PARP in the three cell lines. Data were normalized to respective  $\beta$ -actin bands and expressed as the percentage relative to control (C) cells. The graphs represent the mean  $\pm$  SEM of 3 independent experiments. (b) Quantification of early apoptotic cells by Annexin-V staining. The bars represent the mean percentage of Annexin-V positive and PI negative cells  $\pm$  SEM of 3 independent experiments. (c,d) Densitometry analyses of XIAP and MCL-1. Both were normalized to respective  $\beta$ -actin bands and expressed as the percentage relative to control (C) cells. The graphs represent the mean  $\pm$  SEM of 3–4 independent experiments. Lysates (20  $\mu$ g) were resolved in 12% gels for XIAP and MCL-1 and western blot analysis was carried out using specific antibodies (see Supplementary Table S1). A representative blot is shown on the top of each graph. \*  $p < 0.05$  and \*\*  $p < 0.01$  relative to control cells;  $^c p < 0.05$  and  $^{cc} p < 0.01$  relative to p29 control. Control is shown as C, p29 is the unspecific aptamer used as a negative control, and apMKNKQ2 is shown as Q2. Each solid black circle represents one individual value.

We also analyzed XIAP and MCL1 levels since both are antiapoptotic proteins regulated by MNK1 [23,41,42]. Results show that apMNKQ2 significantly decreased both XIAP and MCL1 levels in A549 and SW900 cell lines, again confirming the proapoptotic effect of apMNKQ2 (Figure 2c,d). However, apMNKQ2 seemed to significantly increase the levels of MCL1 in H460 cells (Figure 2c).

Next, we determined the effect of the aptamers on cell cycle distribution. Cells were transfected and 24 h later analyzed by flow cytometry. Figure 3a shows that apMNKQ2 increased the percentage of cells in the G1 phase in A549 (6.6%) and H460 (7.5%) cells compared with control cells, indicating that apMNKQ2 induces an arrest in the G1 phase of the cell cycle. Surprisingly, apMNKQ2 induced an increase in the percentage of cells in the G2/M phase (3.8%) in SW900 cells.



**Figure 3.** apMNKQ2 arrests cell cycle progression and colony formation in NSCLC cells. (a) Cells were transfected with apMNKQ2 at IC<sub>50</sub> concentrations. After 24 h, cells were stained with PI and analyzed by flow cytometry. The bars represent the mean percentage of cells gated in each phase, G1 (white), S (grey), and G2/M (dark grey)  $\pm$  SEM of 3 independent experiments. (b) Cells were transfected with aptamers at IC<sub>50</sub> and after 24 h reseeded at 10<sup>3</sup> cells/well in 6-well plates. After 7–8 days, colonies were fixed, stained, and counted. (Left) shown are representative images. (Right) The bars represent the mean percentage of the number of colonies obtained  $\pm$  SEM of 3 independent experiments relative to control (C). \*  $p < 0.05$  and \*\*  $p < 0.01$  relative to control cells; <sup>c</sup>  $p < 0.05$  and <sup>cc</sup>  $p < 0.01$  relative to p29 control. Control is shown as C, p29 is the unspecific aptamer used as a negative control, and apMNKQ2 is shown as Q2. Each solid black circle represents one individual value.

Moreover, we studied the effect of apMNKQ2 on colony formation and observed that apMNKQ2 significantly reduced the clonogenic capacity of the three cell lines (Figure 3b). The unspecific p29 aptamer had a slight but significantly less effect compared to apMNKQ2.



### 3.3. *apMNKQ2 Inhibits Migration, Invasion, Cell Adhesion, and Epithelial-Mesenchymal Transition (EMT) in Lung Cancer Cells*

Metastatic dissemination requires cancer cells to detach from the primary tumor and colonize distant organs through pivotal steps such as cell migration, invasion, and adhesion. We have studied how *apMNKQ2* affects all these cell features in order to determine its antimetastatic potential. We performed transwell migration assays to determine the migratory ability of lung cancer cells after being transfected with *apMNKQ2*. Results showed that the number of migrated cells was lower in the three cell lines following transfection with *apMNKQ2*, and statistically significant in both A549 and SW900 cells (Figure 4a).

The Invasiveness of cancer cell lines depends on the expression of proteins such as MMPs. Thus, we analyzed the invasive potential of the three cell lines by zymography in order to detect changes in the proteolytic activity of matrix metalloproteases MMP2 and MMP9 after transfection with *apMNKQ2*. As Figure 4b shows, *apMNKQ2* decreased MMP9 and MMP2 activity in both A549 and SW900 cells, although the effect was only statistically significant for MMP9 in A549 cells. In H460 cells, however, *apMNKQ2* seemed to increase MMP9 activity and did not produce changes in MMP2.

Next, we analyzed whether *apMNKQ2* affected the ability of cells to adhere to extracellular matrix components such as type I collagen. For these assays, 24 h after transfection with aptamers, cells were reseeded in plates previously coated with type I collagen in order to measure adherence. Subsequently, MTT assays were performed to quantify the number of adherent cells. Results demonstrated that *apMNKQ2* significantly reduced cell adhesion in A549 cells but did not have any effect on SW900 and H460 cells (Figure 4c).

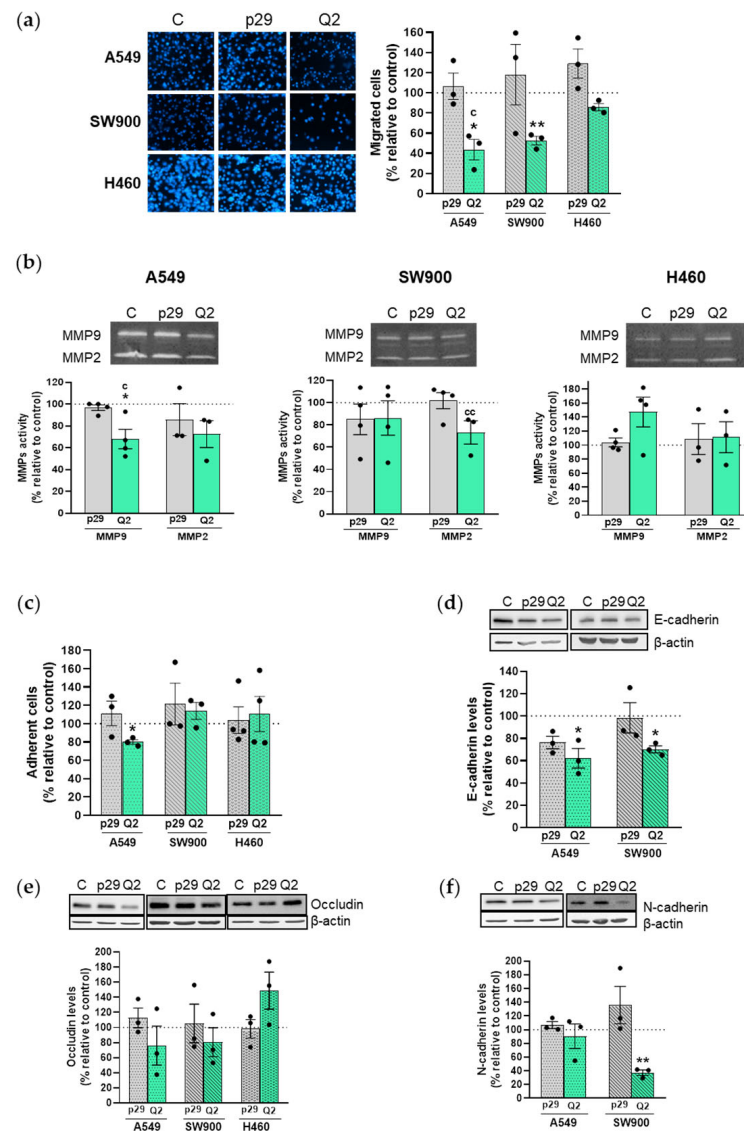
Finally, we studied the effect of *apMNKQ2* on epithelial-mesenchymal transition (EMT), in which cancer cells lose epithelial features and acquire a mesenchymal phenotype. For this purpose, cells were transfected with *apMNKQ2* and the expression of the epithelial markers E-cadherin and occludin and the mesenchymal marker N-cadherin were analyzed by western blotting. E-cadherin and N-cadherin were only detected in A549 and SW900 cells while occludin was detected in the three cell lines (Supplementary Figure S3). Results showed that *apMNKQ2* significantly reduced E-cadherin levels in both A549 and SW900 cells (Figure 4d) and increased occludin levels in H460 cells (Figure 4e). Moreover, *apMNKQ2* produced a significant reduction in N-cadherin expression levels in SW900 cells (Figure 4f).

### 3.4. *Effect of apMNKQ2 on MNK1 Isoforms*

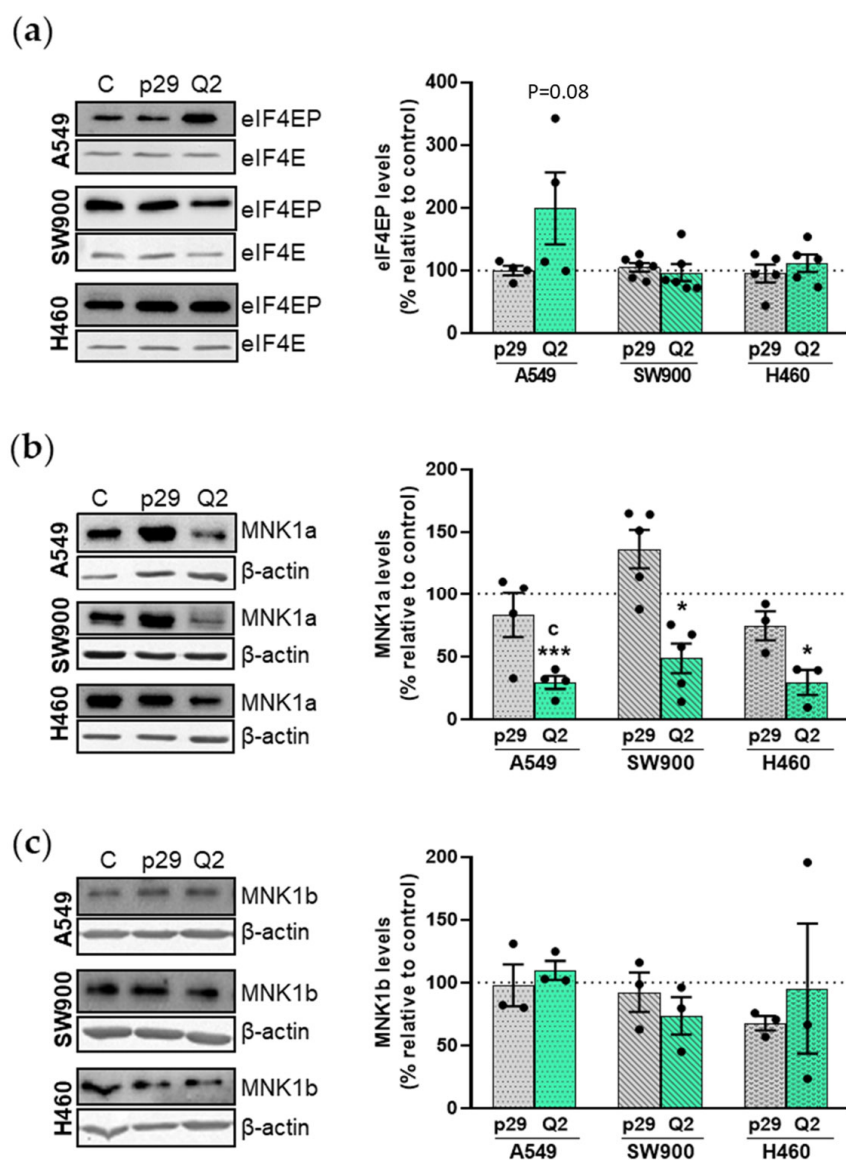
The expression levels of both MNK1 isoforms were analyzed as well as eIF4E phosphorylation after cell transfection with aptamers. Figure 5a shows that *apMNKQ2* increased eIF4E phosphorylation in A549 cells while no changes were observed in SW900 and H460 cells. MNK1a was significantly reduced in the three cell lines after *apMNKQ2* transfection (Figure 5b), but MNK1b did not change in any of the three cell lines (Figure 5c). The reduction of MNK1a observed in SW900 cells may be a consequence of a reduction in mRNA levels (Supplementary Figure S4).

### 3.5. *apMNKQ2 Reduces Tumor Growth In Vivo*

To investigate the antitumor efficacy of *apMNKQ2*, we first performed a tolerability study as described in the Materials and Methods section (Section 2). During the course of this experiment, no DLTs were observed at any of the doses tested, including the maximum feasible dose of 400 mg/kg. Thus, for practical purposes, doses of 10 and 25 mg/kg were used in the xenograft studies. Then, A549 cells were subcutaneously xenografted in athymic nude mice, and *apMNKQ2* was administered intraperitoneally at 10 mg/kg and 25 mg/kg. Our preliminary results showed that treatment with *apMNKQ2* produced a reduction in both tumor volume (Figure 6a) and weight (Figure 6b) reaching a tumor growth inhibition (TGI) of 18.2% and 28.5% for 10 mg/kg and 25 mg/kg of *apMNKQ2*, respectively. However, these results were not statistically significant, probably due to unexpectedly slow tumor growth and/or the necessity of a higher dose of the aptamer.



**Figure 4.** ApMNKQ2-mediated effects on migration, invasion, and EMT in NSCLC cells. (a) Cells were transfected with aptamers at IC50, maintained in serum-deprived medium for 16 h, and collected and reseeded at  $4 \times 10^4$  cells/well in the upper chamber of a transwell. Representative images are shown in the left panel. The graphs represent the mean percentage of migrated cells  $\pm$  SEM relative to the value of control (C) cells from 3 independent experiments. (b) Zymography was performed as described in Materials and Methods. The graphs represent the mean percentage of MMP activity  $\pm$  SEM relative to the value of control (C) cells from 3–4 independent experiments. (c) Cells were transfected with aptamers at IC50 and reseeded in plates previously coated with type I collagen. After binding, cells were quantified by MTT assay. The graphs represent the mean percentage of adherent cells  $\pm$  SEM relative to the value of control cells from 3 independent experiments. (d–f) Western blot and corresponding densitometry analyses of lysates (20  $\mu$ g) that were subjected to SDS-PAGE (10%). Specific antibodies are shown in Supplementary Table S1. Actin detection was used as a loading control. A representative blot is shown at the top of each graph. Densitometric quantification of E-cadherin, occludin, and N-cadherin was normalized to respective  $\beta$ -actin bands, and levels are expressed as a percentage relative to control cells. The graphs represent mean percentage levels  $\pm$  SEM of 3 independent experiments. \*  $p < 0.05$  and \*\*  $p < 0.01$  relative to control cells; <sup>c</sup>  $p < 0.05$  and <sup>cc</sup>  $p < 0.01$  relative to p29 control. Control is shown as C, p29 is the unspecific aptamer used as a negative control, and apMNKQ2 is shown as Q2. Each solid black circle represents one individual value.

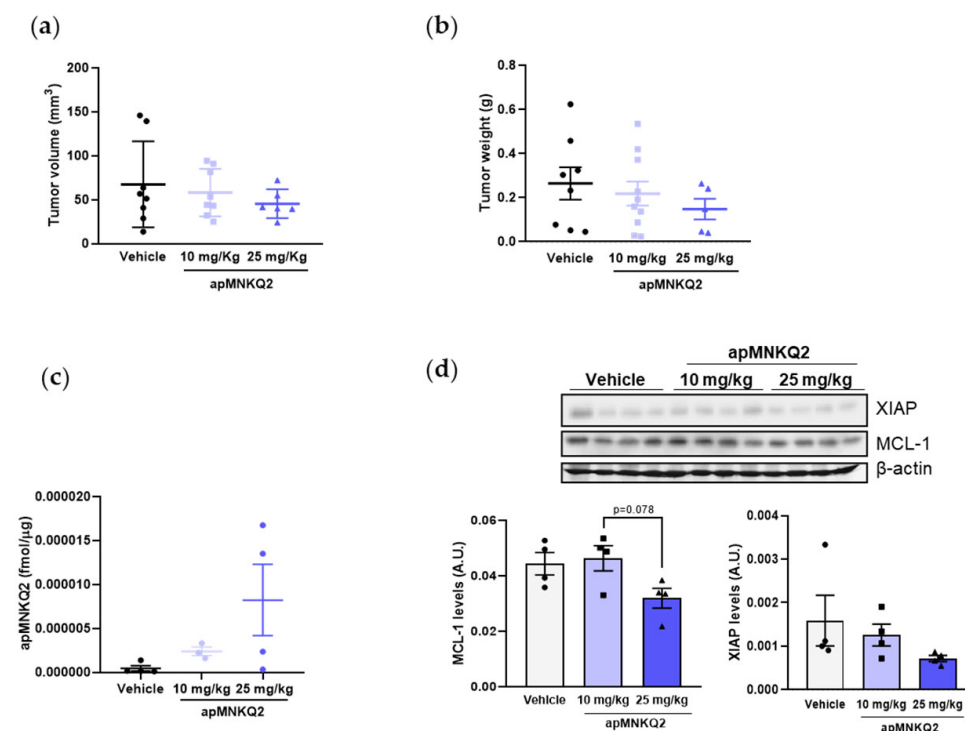


**Figure 5.** Effect of apMKNKQ2 on eIF4E phosphorylation and MNK1 isoforms. Lysates (20  $\mu$ g) were subjected to SDS-PAGE (12%) and western blotting was performed using specific antibodies (see Supplementary Table S1). Actin detection was used as a loading control. A representative blot and corresponding densitometry analyses are shown in each figure. (a) Quantification of eIF4EP was normalized to total eIF4E levels and expressed as a percentage relative to control (C) cells (b) and (c) quantification of MNK1a/b was normalized to  $\beta$ -actin levels and expressed as a percentage relative to control cells. The graphs represent mean values  $\pm$  SEM of 3–5 independent experiments. \*  $p < 0.05$  and \*\*\*  $p < 0.001$  relative to control cells; <sup>c</sup>  $p < 0.05$  relative to p29 control. Control is shown as C, p29 is the unspecific aptamer used as a negative control, and apMKNKQ2 is shown as Q2. Each solid black circle represents one individual value.

We analyzed aptamer uptake after intraperitoneal administration by qRT-PCR and demonstrate that apMKNKQ2 reaches different organs, such as the lung or pancreas but not the brain and is cleared by the kidney and liver (Supplementary Figure S5). In tumors, apMKNKQ2 reached the tumor in a dose-dependent manner (Figure 6c) and exerted a biological effect on the tumor, with no toxic macroscopic effects observed in other organs.

In order to determine the association between the anti-tumor effects observed in vivo and the inhibition of MNK1 downstream signaling, XIAP and MCL1 levels were analyzed from tumor samples by western blotting. Results showed a reduction of both proteins in

25 mg/kg apMNKQ2-treated tumor samples (Figure 6d). These results corroborate our *in vitro* findings of the apoptotic effect of apMNKQ2 in A549 cells.



**Figure 6.** apMNKQ2 efficacy in an adenocarcinoma xenograft model. **(a,b)** Reduction in **(a)** volume and **(b)** weight of A549 xenografts following treatment with apMNKQ2 at 10 and 25 mg/kg daily. Mice were treated intraperitoneally with apMNKQ2 or vehicle control (selection buffer) for 4 weeks. Scatter plots represent the mean  $\pm$  SEM from 6–8 tumors. Solid black circles (vehicle), blue squares (apMNKQ2 at 10 mg/Kg) or blue triangles (apMNKQ2 at 25 mg/Kg) represent one individual value. **(c)** Quantification of apMNKQ2 levels in tumors by qRT-PCR. RNA fraction, where apMNKQ2 is found, was obtained from tumor samples and used in qPCR analyses as described in Material and Methods. Results are expressed as pmol/ $\mu$ g of tissue. Scatter plot represents the mean  $\pm$  SEM from 3–4 tumors. Each solid circle represents one individual value. **(d)** Proteins were obtained from tumor samples as described in Material and Methods and lysates (20  $\mu$ g) were subjected to SDS-PAGE (12%). Western blotting was performed using specific antibodies (see Supplementary Table S1). Actin detection was used as a loading control. Blots are shown on the top of the graphs. The bars represent mean protein levels  $\pm$  SEM, expressed as arbitrary units (A.U.) for 4 tumors from each treatment arm. Each solid black symbol represents one individual value.

#### 4. Discussion

Lung cancer is considered one of the most invasive cancers and the fastest to metastasize, being the leading cause of cancer-related death worldwide and the third most frequently diagnosed in 2022 after colorectal and breast cancer [2]. To date, therapeutic strategies to treat lung cancer, such as chemotherapy, molecular targeted therapy, or immunotherapy, have been developed [43] and have improved the survival of lung cancer patients. Despite these advances, the prognosis for patients with lung cancer remains poor, highlighting the need for new therapeutic approaches.

MNKs are involved in several types of cancer [25] including NSCLC, where MNK1 overexpression correlates with poor overall patient survival [44]. This suggests that blocking the MNK/eIF4E pathway may be a good strategy to treat NSCLC.

Here we studied the antitumor potential of apMNKQ2 as an antitumor agent in NSCLC using *in vitro* and *in vivo* assays. The three cell lines used harbor KRAS mutations,

SW900 cells carry an inactivated mutation in the tumor suppressor gene TP53, and H460 cells also harbor PI3KCA mutations [45,46].

One of the most important characteristics of aptamers is their stability and half-life inside cells, and apMNKQ2 is stable inside lung cancer cells for at least 48 h, which may be an advantage for its clinical application in terms of decreasing the number of injections and improving patient comfort [47].

Inhibiting tumorigenic characteristics is an important aspect of the development of antitumor drugs. Consequently, we show that apMNKQ2 reduces the viability in A549 and SW900 cells via apoptosis induction, but to a less extent in the latter. While SW900 cells are not Annexin-V positive after transfection with apMNKQ2, PARP was cleaved. In addition, XIAP and MCL1 are antiapoptotic proteins that are overexpressed in several types of cancers and whose expression is regulated by MNK1 [23,41,42]. Moreover, MCL1 overexpression inhibits apoptosis and promotes cell survival in NSCLC [48]. The apMNKQ2 reduced both XIAP and MCL1 in A549 and SW900 cells both *in vitro* and *in vivo* (the latter only for A549) proving its effect through MNK1, and confirming the pro-apoptotic effect of the aptamer. However, despite the fact that other MNK inhibitors [26] promote the induction of apoptosis in H460 cells, apMNKQ2 did not induce it, which may explain the lack of effect on MCL1 and XIAP levels.

Some MNK inhibitors produce a cell cycle arrest in breast cancer cells [19,49]. For example, the MNK1 inhibitor BAY1143269 induces a G0/G1 arrest in NSCLC cells. This is consistent with our results in A549 and H460 cells in which a G1 phase arrest is produced when cells are transfected with apMNKQ2. Surprisingly, the aptamer induces a G2 phase arrest in SW900 cells. This difference among the three cell lines could be explained since both A549 and H460 cells contain a wild-type TP53, while SW900 cells carry an inactivated mutation in TP53.

MNKs also play an important role in metastasis [16], and several MNK inhibitors reduce cell migration and invasion [26,50–53]. Indeed, apMNKQ2 decreased migration and invasion of NSCLC cells. During metastasis, cells migrate and attach to extracellular matrix (ECM) components. apMNKQ2 was also able to reduce cell adhesion capacity in A549 cells.  $\beta$ 1 integrin is involved in the adhesion of cells to the surroundings ECM and its inhibition reduces the adhesion of A549 cells by inhibiting the ERK1/2 signaling pathway [54]. This suggests that apMNKQ2 may reduce cell adhesion through MNK1 inhibition. The catalytic subunit p110 $\alpha$  mediates  $\beta$ 1 integrin-regulated activation of AKT [55], which could contribute to the tumorigenic properties of cells expressing constitutively active p110  $\alpha$ , as in H460 cells.

Similarly, apMNKQ2 alters cell migration and MMP activity only in A549 and SW900 cells. The PI3K/AKT/mTOR pathway plays an important role in lung cancer cell migration and invasion, specifically in the regulation of MMP2 and MMP9 [56]. These data suggest that the increased activity in the PI3K pathway in H460 cells could compensate for the effects of apMNKQ2.

Therefore, apMNKQ2 seems to exert more potent effects in A549 and SW900 cells than in H460 cells probably due to the PI3KCA mutation in the latter. It would be interesting to use apMNKQ2 in combination with inhibitors of the PI3K pathway to increase the sensitivity of H460 cells to apMNKQ2.

apMNKQ2 significantly reduced N-cadherin levels in SW900 cells, which is in accordance with other MNK inhibitors such as VNLG-152 that reverse EMT in prostate cancer [57]. The aptamer also increased the epithelial marker occludin in H460 cells, recovering part of the epithelial characteristics in these cells. Since Snail is a direct repressor of E-cadherin [58], the overexpression of Snail in A549 cells (data not shown) may be associated with low E-cadherin expression in these cells.

Some MNK inhibitors such as MNK-I1, BAY1143269, MNK-7g, eFT508 or novel retinamides inhibits eIF4E phosphorylation [26,51,59–61]. apMNKQ2 also inhibits eIF4E phosphorylation in breast cancer cells [37]; however, in NSCLC cells, apMNKQ2 did not affect eIF4E phosphorylation, which is in accordance with other MNK inhibitors such as

apMNK2F and apMNK3R aptamers [36] or ferrocene analogs [62]. Since eIF4E phosphorylation is mainly mediated by MNK2 in breast cancer cells MDA-MB-231 [36], this could also occur in lung cancer cells. Moreover, MNK2b acts as a proto-oncogene increasing eIF4E phosphorylation [63] and in NSCLC, MNK2 is involved in tumorigenesis through eIF4E phosphorylation [21]. To answer this unknown, we propose to use of CRISPR/Cas, which is currently being developed in the laboratory.

Even though eIF4E is the best characterized substrate of MNK1, it is possible that eIF4E-independent effects, through other MNK substrates, may contribute to the observed MNK-mediated effects of apMNKQ2. Here we show that apMNKQ2 exerts its effects through proteins regulated by MNK1 such as XIAP and MCL1, but in the last few years, other proteins regulated by MNK1 have been described such as NODAL [64], NDRG1 [65] or ANGPTL-4 [66], which may be involved in the antitumoral mechanism of apMNKQ2.

We have studied different administration routes of apMNKQ2 in preliminary assays in mice, such as oral, intravenous, and intraperitoneal routes. The latter was the most effective in breast and pancreatic cancer tumor models and was therefore chosen for the *in vivo* experiments presented herein. We have shown that there is a downward trend in tumor growth after treatment with apMNKQ2. Although tumor growth with xenografted A549 cells was slower than expected, we have obtained promising results that can be improved by increasing the dose of the aptamer. It must be emphasized that in previous studies [37] we used a transfectant as a vehicle to administer apMNKQ2 into animals, while in this study apMNKQ2 was injected without the transfectant, which is an advantage since it allowed us to increase the aptamer dose. Importantly, in the absence of the transfectant, the aptamer still reached the tumor and was easily detectable by qRT-PCR and increased as a function of the dose. Indeed, further studies are still necessary to determine the antitumor mechanism and the full antitumor potential of apMNKQ2. Thus, apMNKQ2 is currently being tested in a patient-derived xenograft (PDX) of NSCLC. This will allow us to learn more about the therapeutic potential of the aptamer in a more physiologically relevant tumor model.

One of the most important points to take into account is the toxicity commonly observed with antitumor chemotherapeutics [67] or immunotherapy and molecular targeted therapy, even though the latter two are better tolerated, side effects can occur [68,69]. Toxicity regarding aptamers is very limited. For example, the aptamers NOX-A12 or ApTOLL have been administered to patients with no signs of toxicity [70]. Moreover, treatment with apMNKQ2 was well tolerated in breast cancer *in vivo* assays as indicated by no difference in body weight [37] indicating the low toxicity of apMNKQ2. Likewise, daily administration of apMNKQ2 in this study showed no obvious signs of toxicity in mice. Moreover, we performed a maximum tolerated dose (MTD) assay in CD1 mice and no toxicity was observed at any dose, including the highest dose tested (400 mg/kg, maximum feasible dose), indicating that the data obtained so far demonstrates low toxicity for apMNKQ2. However, future ADME Tox are still necessary and are currently planned.

In summary, we show that apMNKQ2 inhibits the tumorigenic and metastatic processes of lung cancer cells, and preliminary *in vivo* experiments indicate that apMNKQ2 can reduce tumor growth and induce apoptosis in an adenocarcinoma xenograft model. Further studies are still needed in order to elucidate the mechanism of action of apMNKQ2 as well as its pharmacokinetics and pharmacological security to expedite its possible use as a therapeutic tool in the different types of cancers where MNK1 plays an important biological role.

## 5. Patents

C.P-D, V.M.G. and M.E.M. declare that a patent application has been filed relating to this work.

**Supplementary Materials:** The following supporting information can be downloaded at: <https://www.mdpi.com/article/10.3390/pharmaceutics15041273/s1>, Figure S1: Effect of the four aptamers on MTT activity in A549 and SW900 cells; Figure S2: Aptamer effect on the viability of lung cancer cells 24 h after transfection; Figure S3: E-cadherin, N-cadherin, and occludin levels in NSCLC cells; Figure S4: ApMNKQ2 effect in MNK1a/b expression in NSCLC cells; Figure S5. Quantification of apMNKQ2 levels in several organs by qRT-PCR. Table S1: Antibodies used in this study; Table S2: Oligonucleotides used in this study.

**Author Contributions:** Conceptualization, V.M.G. and M.E.M.; investigation, R.C.-M., C.P.-D., J.I.K.-M., E.P., M.B.-U., M.I.P.-M., M.P.-M., L.R.-C. and S.A.; writing—original draft preparation, R.C.-M.; writing—review and editing, R.C.-M., C.P.-D., B.S.J., V.M.G. and M.E.M., Funding Acquisition, V.M.G. and M.E.M. All authors have read and agreed to the published version of the manuscript.

**Funding:** R.C.-M. was supported for predoctoral contracts (PEJD 2016-BMD-2145 and 2018-BMD-9201) from the Community of Madrid and grant RTC2019-07227-1. M.E.M. and V.M.G. are researchers from FIBio-HRC supported by Consejería de Sanidad (CAM). This work was supported by grants RTC2019-07227-1 and PID2019-105417RB-I00, funded by MCIN/AEI/10.13039/501100011033 (Ministry of Economy and Competitiveness, Spain).

**Institutional Review Board Statement:** Not applicable.

**Informed Consent Statement:** Not applicable.

**Data Availability Statement:** Not applicable.

**Acknowledgments:** We thank Eloisa Jantus and Silvia Calabuig from Fundación para la Investigación del Hospital General Universitario de Valencia (FIHGUV) for kindly providing lung cancer cell lines used in this study.

**Conflicts of Interest:** The authors declare no conflict of interest.

## References

1. Sung, H.; Ferlay, J.; Siegel, R.L.; Laversanne, M.; Soerjomataram, I.; Jemal, A.; Bray, F. Global Cancer Statistics 2020: GLOBOCAN Estimates of Incidence and Mortality Worldwide for 36 Cancers in 185 Countries. *CA Cancer J. Clin.* **2021**, *71*, 209–249. [CrossRef]
2. Li, C.; Wang, H.; Jiang, Y.; Fu, W.; Liu, X.; Zhong, R.; Cheng, B.; Zhu, F.; Xiang, Y.; He, J.; et al. Advances in lung cancer screening and early detection. *Cancer Biol. Med.* **2022**, *19*, 591–608. [CrossRef] [PubMed]
3. Fukunaga, R.; Hunter, T. MNK1, a new MAP kinase-activated protein kinase, isolated by a novel expression screening method for identifying protein kinase substrates. *EMBO J.* **1997**, *16*, 1921–1933. [CrossRef]
4. Waskiewicz, A.J.; Flynn, A.; Proud, C.G.; Cooper, J.A. Mitogen-activated protein kinases activate the serine/threonine kinases Mnk1 and Mnk2. *EMBO J.* **1997**, *16*, 1909–1920. [CrossRef]
5. O’Loughlen, A.; Gonzalez, V.M.; Pineiro, D.; Perez-Morgado, M.I.; Salinas, M.; Martín, M.E. Identification and molecular characterization of Mnk1b, a splice variant of human MAP kinase-interacting kinase Mnk1. *Exp. Cell Res.* **2004**, *299*, 343–355. [CrossRef]
6. O’Loughlen, A.; González, V.M.; Jurado, T.; Salinas, M.; Martín, M.E. Characterization of the activity of human MAP kinase-interacting kinase Mnk1b. *Biochim. Biophys. Acta* **2007**, *1773*, 1416–1427. [CrossRef]
7. Waskiewicz, A.J.; Johnson, J.C.; Penn, B.; Mahalingam, M.; Kimball, S.R.; Cooper, J.A. Phosphorylation of the cap-binding protein eukaryotic translation initiation factor 4E by protein kinase Mnk1 in vivo. *Mol. Cell Biol.* **1999**, *19*, 1871–1880. [CrossRef]
8. Shveygert, M.; Kaiser, C.; Bradrick, S.S.; Gromeier, M. Regulation of eukaryotic initiation factor 4E (eIF4E) phosphorylation by mitogen-activated protein kinase occurs through modulation of Mnk1-eIF4G interaction. *Mol. Cell Biol.* **2010**, *30*, 5160–5167. [CrossRef] [PubMed]
9. Buxade, M.; Parra, J.L.; Rousseau, S.; Shpiro, N.; Marquez, R.; Morrice, N.; Bain, J.; Espel, E.; Proud, C.G. The Mnk1s are novel components in the control of TNF alpha biosynthesis and phosphorylate and regulate hnRNP A1. *Immunity* **2005**, *23*, 177–189. [CrossRef]
10. Hefner, Y.; Borsch-Haubold, A.G.; Murakami, M.; Wilde, J.I.; Pasquet, S.; Schieltz, D.; Ghomashchi, F.; Yates, J.R., 3rd; Armstrong, C.G.; Paterson, A.; et al. Serine 727 phosphorylation and activation of cytosolic phospholipase A2 by MNK1-related protein kinases. *J. Biol. Chem.* **2000**, *275*, 37542–37551. [CrossRef] [PubMed]

11. DaSilva, J.; Xu, L.; Kim, H.J.; Miller, W.T.; Bar-Sagi, D. Regulation of sprouty stability by Mnk1-dependent phosphorylation. *Mol. Cell Biol.* **2006**, *26*, 1898–1907. [CrossRef] [PubMed]
12. Buxadé, M.; Morrice, N.; Krebs, D.L.; Proud, C.G. The PSF.p54nrb complex is a novel Mnk substrate that binds the mRNA for tumor necrosis factor alpha. *J. Biol. Chem.* **2008**, *283*, 57–65. [CrossRef] [PubMed]
13. Rousseau, D.; Kaspar, R.; Rosenwald, I.; Gehrke, L.; Sonenberg, N. Translation initiation of ornithine decarboxylase and nucleocytoplasmic transport of cyclin D1 mRNA are increased in cells overexpressing eukaryotic initiation factor 4E. *Proc. Natl. Acad. Sci. USA* **1996**, *93*, 1065–1070. [CrossRef]
14. Culjkovic, B.; Topisirovic, I.; Borden, K.L. Controlling gene expression through RNA regulons: The role of the eukaryotic translation initiation factor eIF4E. *Cell Cycle* **2007**, *6*, 65–69. [CrossRef]
15. Furic, L.; Rong, L.; Larsson, O.; Koumakpayi, I.H.; Yoshida, K.; Brueschke, A.; Petroulakis, E.; Robichaud, N.; Pollak, M.; Gaboury, L.A.; et al. eIF4E phosphorylation promotes tumorigenesis and is associated with prostate cancer progression. *Proc. Natl. Acad. Sci. USA* **2010**, *107*, 14134–14139. [CrossRef]
16. Robichaud, N.; del Rincon, S.V.; Huor, B.; Alain, T.; Petrucci, L.A.; Hearnden, J.; Goncalves, C.; Grotegut, S.; Spruck, C.H.; Furic, L.; et al. Phosphorylation of eIF4E promotes EMT and metastasis via translational control of SNAIL and MMP-3. *Oncogene* **2015**, *34*, 2032–2042. [CrossRef]
17. Robichaud, N.; Hsu, B.E.; Istomine, R.; Alvarez, F.; Blagih, J.; Ma, E.H.; Morales, S.V.; Dai, D.L.; Li, G.; Souleimanova, M.; et al. Translational control in the tumor microenvironment promotes lung metastasis: Phosphorylation of eIF4E in neutrophils. *Proc. Natl. Acad. Sci. USA* **2018**, *115*, E2202–E2209. [CrossRef]
18. Yang, X.; Zhong, W.; Cao, R. Phosphorylation of the mRNA cap-binding protein eIF4E and cancer. *Cell Signal.* **2020**, *73*, 109689. [CrossRef] [PubMed]
19. Wheeler, M.J.; Johnson, P.W.; Blaydes, J.P. The role of MNK proteins and eIF4E phosphorylation in breast cancer cell proliferation and survival. *Cancer Biol.* **2010**, *10*, 728–735. [CrossRef]
20. Grzmil, M.; Morin, P., Jr.; Lino, M.M.; Merlo, A.; Frank, S.; Wang, Y.; Moncayo, G.; Hemmings, B.A. MAP kinase-interacting kinase 1 regulates SMAD2-dependent TGF- $\beta$  signaling pathway in human glioblastoma. *Cancer Res.* **2011**, *71*, 2392–2402. [CrossRef] [PubMed]
21. Guo, Z.; Peng, G.; Li, E.; Xi, S.; Zhang, Y.; Li, Y.; Lin, X.; Li, G.; Wu, Q.; He, J. MAP kinase-interacting serine/threonine kinase 2 promotes proliferation, metastasis, and predicts poor prognosis in non-small cell lung cancer. *Sci. Rep.* **2017**, *7*, 10612. [CrossRef] [PubMed]
22. Hou, S.; Du, P.; Wang, P.; Wang, C.; Liu, P.; Liu, H. Significance of MNK1 in prognostic prediction and chemotherapy development of epithelial ovarian cancer. *Clin. Transl. Oncol.* **2017**, *19*, 1107–1116. [CrossRef]
23. Pinto-Díez, C.; García-Recio, E.M.; Pérez-Morgado, M.I.; García-Hernández, M.; Sanz-Criado, L.; Sacristán, S.; Toledo-Lobo, M.V.; Pérez-Mies, B.; Esteban-Rodríguez, I.; Pascual, A.; et al. Increased expression of MNK1b, the spliced isoform of MNK1, predicts poor prognosis and is associated with triple-negative breast cancer. *Oncotarget* **2018**, *9*, 13501–13516. [CrossRef]
24. Wang, X.; Wang, Y.; Zhang, Q.; Zhuang, H.; Chen, B. MAP Kinase-Interacting Kinase 1 Promotes Proliferation and Invasion of Hepatocellular Carcinoma and Is an Unfavorable Prognostic Biomarker. *Med. Sci. Monit.* **2018**, *24*, 1759–1767. [CrossRef] [PubMed]
25. Pinto-Díez, C.; Ferreras-Martín, R.; Carrión-Marchante, R.; González, V.M.; Martín, M.E. Deepening in the Role of the MAP-Kinases Interacting Kinases (MNKs) in Cancer. *Int. J. Mol. Sci.* **2020**, *21*, 2967. [CrossRef]
26. Santag, S.; Siegel, F.; Wengner, A.M.; Lange, C.; Bömer, U.; Eis, K.; Pühler, F.; Lienau, P.; Bergemann, L.; Michels, M.; et al. BAY 1143269, a novel MNK1 inhibitor, targets oncogenic protein expression and shows potent anti-tumor activity. *Cancer Lett.* **2017**, *390*, 21–29. [CrossRef]
27. Reich, S.H.; Sprengeler, P.A.; Chiang, G.G.; Appleman, J.R.; Chen, J.; Clarine, J.; Eam, B.; Ernst, J.T.; Han, Q.; Goel, V.K.; et al. Structure-Based Design of Pyridone-Aminal eFT508 Targeting Dysregulated Translation by Selective Mitogen-Activated Protein Kinase Interacting Kinases 1 and 2 (MNK1/2) Inhibition. *J. Med. Chem.* **2018**, *61*, 3516–3540. [CrossRef]
28. Xu, W.; Kannan, S.; Verma, C.S.; Nacro, K. Update on the Development of MNK Inhibitors as Therapeutic Agents. *J. Med. Chem.* **2022**, *65*, 983–1007. [CrossRef]
29. Ueda, T.; Watanabe-Fukunaga, R.; Fukuyama, H.; Nagata, S.; Fukunaga, R. Mnk2 and Mnk1 are essential for constitutive and inducible phosphorylation of eukaryotic initiation factor 4E but not for cell growth or development. *Mol. Cell Biol.* **2004**, *24*, 6539–6549. [CrossRef] [PubMed]
30. Ellington, A.D.; Szostak, J.W. In vitro selection of RNA molecules that bind specific ligands. *Nature* **1990**, *346*, 818–822. [CrossRef]
31. Tuerk, C.; Gold, L. Systematic evolution of ligands by exponential enrichment: RNA ligands to bacteriophage T4 DNA polymerase. *Science* **1990**, *249*, 505–510. [CrossRef] [PubMed]
32. Zhou, J.; Rossi, J. Aptamers as targeted therapeutics: Current potential and challenges. *Nat. Rev. Drug Discov.* **2017**, *16*, 181–202. [CrossRef]
33. Ng, E.W.; Shima, D.T.; Calias, P.; Cunningham, E.T., Jr.; Guyer, D.R.; Adamis, A.P. Pegaptanib, a targeted anti-VEGF aptamer for ocular vascular disease. *Nat. Rev. Drug Discov.* **2006**, *5*, 123–132. [CrossRef]
34. Zhang, N.; Chen, Z.; Liu, D.; Jiang, H.; Zhang, Z.K.; Lu, A.; Zhang, B.T.; Yu, Y.; Zhang, G. Structural Biology for the Molecular Insight between Aptamers and Target Proteins. *Int. J. Mol. Sci.* **2021**, *22*, 4093. [CrossRef]
35. Fu, Z.; Xiang, J. Aptamers, the Nucleic Acid Antibodies, in Cancer Therapy. *Int. J. Mol. Sci.* **2020**, *21*, 2793. [CrossRef] [PubMed]



36. García-Recio, E.M.; Pinto-Díez, C.; Pérez-Morgado, M.I.; García-Hernández, M.; Fernández, G.; Martín, M.E.; González, V.M. Characterization of MNK1b DNA Aptamers That Inhibit Proliferation in MDA-MB231 Breast Cancer Cells. *Mol. Nucleic Acids* **2016**, *5*, e275. [CrossRef]
37. Pinto-Díez, C.; Ferreras-Martín, R.; Carrión-Marchante, R.; Klett-Mingo, J.I.; García-Hernández, M.; Pérez-Morgado, M.I.; Sacristán, S.; Barragán, M.; Seijo-Vila, M.; Tundidor, I.; et al. An optimized MNK1b aptamer, apMNKQ2, and its potential use as a therapeutic agent in breast cancer. *Mol. Ther. Nucleic Acids* **2022**, *30*, 553–568. [CrossRef]
38. Huang, X.; Biswas, S.; Oki, Y.; Issa, J.P.; Berry, D.A. A parallel phase I/II clinical trial design for combination therapies. *Biometrics* **2007**, *63*, 429–436. [CrossRef]
39. Le Tourneau, C.; Lee, J.J.; Siu, L.L. Dose escalation methods in phase I cancer clinical trials. *J. Natl. Cancer Inst.* **2009**, *101*, 708–720. [CrossRef]
40. Frank, K.J.; Mulero-Sanchez, A.; Berninger, A.; Ruiz-Canas, L.; Bosma, A.; Gorgulu, K.; Wu, N.; Diakopoulos, K.N.; Kaya-Aksoy, E.; Ruess, D.A.; et al. Extensive preclinical validation of combined RMC-4550 and LY3214996 supports clinical investigation for KRAS mutant pancreatic cancer. *Cell Rep. Med.* **2022**, *3*, 100815. [CrossRef] [PubMed]
41. Wendel, H.G.; Silva, R.L.; Malina, A.; Mills, J.R.; Zhu, H.; Ueda, T.; Watanabe-Fukunaga, R.; Fukunaga, R.; Teruya-Feldstein, J.; Pelletier, J.; et al. Dissecting eIF4E action in tumorigenesis. *Genes Dev.* **2007**, *21*, 3232–3237. [CrossRef] [PubMed]
42. Evans, M.K.; Brown, M.C.; Geradts, J.; Bao, X.; Robinson, T.J.; Jolly, M.K.; Vermeulen, P.B.; Palmer, G.M.; Gromeier, M.; Levine, H.; et al. XIAP Regulation by MNK Links MAPK and NFκB Signaling to Determine an Aggressive Breast Cancer Phenotype. *Cancer Res.* **2018**, *78*, 1726–1738. [CrossRef]
43. Alexander, M.; Kim, S.Y.; Cheng, H. Update 2020: Management of Non-Small Cell Lung Cancer. *Lung* **2020**, *198*, 897–907. [CrossRef] [PubMed]
44. Wen, Q.; Wang, W.; Luo, J.; Chu, S.; Chen, L.; Xu, L.; Zang, H.; Alnemah, M.M.; Ma, J.; Fan, S. CGP57380 enhances efficacy of RAD001 in non-small cell lung cancer through abrogating mTOR inhibition-induced phosphorylation of eIF4E and activating mitochondrial apoptotic pathway. *Oncotarget* **2016**, *7*, 27787–27801. [CrossRef]
45. Blanco, R.; Iwakawa, R.; Tang, M.; Kohno, T.; Angulo, B.; Pio, R.; Montuenga, L.M.; Minna, J.D.; Yokota, J.; Sanchez-Cespedes, M. A gene-alteration profile of human lung cancer cell lines. *Hum. Mutat.* **2009**, *30*, 1199–1206. [CrossRef] [PubMed]
46. Korrodi-Gregório, L.; Soto-Cerrato, V.; Vitorino, R.; Fardilha, M.; Pérez-Tomás, R. From Proteomic Analysis to Potential Therapeutic Targets: Functional Profile of Two Lung Cancer Cell Lines, A549 and SW900, Widely Studied in Pre-Clinical Research. *PLoS ONE* **2016**, *11*, e0165973. [CrossRef]
47. Zhang, Y.; Zhang, H.; Chan, D.W.H.; Ma, Y.; Lu, A.; Yu, S.; Zhang, B.; Zhang, G. Strategies for developing long-lasting therapeutic nucleic acid aptamer targeting circulating protein: The present and the future. *Front. Cell Dev. Biol.* **2022**, *10*, 1048148. [CrossRef]
48. Zhang, H.; Guttikonda, S.; Roberts, L.; Uziel, T.; Semizarov, D.; Elmore, S.W.; Levenson, J.D.; Lam, L.T. Mcl-1 is critical for survival in a subgroup of non-small-cell lung cancer cell lines. *Oncogene* **2011**, *30*, 1963–1968. [CrossRef] [PubMed]
49. Abdelaziz, A.M.; Basnet, S.K.C.; Islam, S.; Li, M.; Tadesse, S.; Albrecht, H.; Gerber, C.; Yu, M.; Wang, S. Synthesis and evaluation of 2′H-spiro[cyclohexane-1,3′-imidazo[1,5-a]pyridine]-1′,5′-dione derivatives as Mnk inhibitors. *Bioorg. Med. Chem. Lett.* **2019**, *29*, 2650–2654. [CrossRef] [PubMed]
50. Ramalingam, S.; Gediya, L.; Kwegyir-Afful, A.K.; Ramamurthy, V.P.; Purushottamachar, P.; Mbatia, H.; Njar, V.C. First MNKs degrading agents block phosphorylation of eIF4E, induce apoptosis, inhibit cell growth, migration and invasion in triple negative and Her2-overexpressing breast cancer cell lines. *Oncotarget* **2014**, *5*, 530–543. [CrossRef]
51. Beggs, J.E.; Tian, S.; Jones, G.G.; Xie, J.; Iadevaia, V.; Jenei, V.; Thomas, G.; Proud, C.G. The MAP kinase-interacting kinases regulate cell migration, vimentin expression and eIF4E/CYFIP1 binding. *Biochem. J.* **2015**, *467*, 63–76. [CrossRef]
52. Kwegyir-Afful, A.K.; Bruno, R.D.; Purushottamachar, P.; Murigi, F.N.; Njar, V.C. Galeterone and VNPT55 disrupt Mnk-eIF4E to inhibit prostate cancer cell migration and invasion. *FEBS J.* **2016**, *283*, 3898–3918. [CrossRef] [PubMed]
53. Zhan, Y.; Guo, J.; Yang, W.; Goncalves, C.; Rzymiski, T.; Dreas, A.; Żyłkiewicz, E.; Mikulski, M.; Brzózka, K.; Golas, A.; et al. MNK1/2 inhibition limits oncogenicity and metastasis of KIT-mutant melanoma. *J. Clin. Investig.* **2017**, *127*, 4179–4192. [CrossRef] [PubMed]
54. Guo, L.; Zhang, F.; Cai, Y.; Liu, T. Expression profiling of integrins in lung cancer cells. *Pathol. Res. Pr.* **2009**, *205*, 847–853. [CrossRef]
55. Zeller, K.S.; Idevall-Hagren, O.; Stefansson, A.; Velling, T.; Jackson, S.P.; Downward, J.; Tengholm, A.; Johansson, S. PI3-kinase p110α mediates β1 integrin-induced Akt activation and membrane protrusion during cell attachment and initial spreading. *Cell Signal.* **2010**, *22*, 1838–1848. [CrossRef] [PubMed]
56. Iksen; Pothongrisit, S.; Pongrakhananon, V. Targeting the PI3K/AKT/mTOR Signaling Pathway in Lung Cancer: An Update Regarding Potential Drugs and Natural Products. *Molecules* **2021**, *26*, 4100. [CrossRef]
57. Ramamurthy, V.P.; Ramalingam, S.; Gediya, L.K.; Njar, V.C.O. The retinamide VNLG-152 inhibits f-AR/AR-V7 and MNK-eIF4E signaling pathways to suppress EMT and castration-resistant prostate cancer xenograft growth. *FEBS J.* **2018**, *285*, 1051–1063. [CrossRef] [PubMed]
58. Puisieux, A.; Brabletz, T.; Caramel, J. Oncogenic roles of EMT-inducing transcription factors. *Nat. Cell Biol.* **2014**, *16*, 488–494. [CrossRef]

59. Ramalingam, S.; Ramamurthy, V.P.; Gediya, L.K.; Murigi, F.N.; Purushottamachar, P.; Huang, W.; Choi, E.Y.; Zhang, Y.; Vasaitis, T.S.; Kane, M.A.; et al. The Novel Mnk1/2 Degradator and Apoptosis Inducer VNLG-152 Potently Inhibits TNBC Tumor Growth and Metastasis. *Cancers* **2019**, *11*, 299. [CrossRef] [PubMed]
60. Jin, X.; Merrett, J.; Tong, S.; Flower, B.; Xie, J.; Yu, R.; Tian, S.; Gao, L.; Zhao, J.; Wang, X.; et al. Design, synthesis and activity of Mnk1 and Mnk2 selective inhibitors containing thieno[2,3-d]pyrimidine scaffold. *Eur. J. Med. Chem.* **2019**, *162*, 735–751. [CrossRef]
61. Suarez, M.; Blyth, G.T.; Mina, A.A.; Kosciuczuk, E.M.; Dolniak, B.; Dinner, S.; Altman, J.K.; Eklund, E.A.; Saleiro, D.; Beauchamp, E.M.; et al. Inhibitory effects of Tomivosertib in acute myeloid leukemia. *Oncotarget* **2021**, *12*, 955–966. [CrossRef] [PubMed]
62. Sansook, S.; Lineham, E.; Hassell-Hart, S.; Tizzard, G.J.; Coles, S.J.; Spencer, J.; Morley, S.J. Probing the Anticancer Action of Novel Ferrocene Analogues of MNK Inhibitors. *Molecules* **2018**, *23*, 2126. [CrossRef]
63. Maimon, A.; Mogilevsky, M.; Shilo, A.; Golan-Gerstl, R.; Obiedat, A.; Ben-Hur, V.; Lebenthal-Loinger, I.; Stein, I.; Reich, R.; Beenstock, J.; et al. Mnk2 alternative splicing modulates the p38-MAPK pathway and impacts Ras-induced transformation. *Cell Rep.* **2014**, *7*, 501–513. [CrossRef]
64. Guo, Q.; Li, V.Z.; Nichol, J.N.; Huang, F.; Yang, W.; Preston, S.E.J.; Talat, Z.; Lefrère, H.; Yu, H.; Zhang, G.; et al. MNK1/NODAL Signaling Promotes Invasive Progression of Breast Ductal Carcinoma In Situ. *Cancer Res.* **2019**, *79*, 1646–1657. [CrossRef]
65. Tian, S.; Wang, X.; Proud, C.G. Oncogenic MNK signalling regulates the metastasis suppressor NDRG1. *Oncotarget* **2017**, *8*, 46121–46135. [CrossRef] [PubMed]
66. Yang, W.; Khoury, E.; Guo, Q.; Prabhu, S.A.; Emond, A.; Huang, F.; Gonçalves, C.; Zhan, Y.; Plourde, D.; Nichol, J.N.; et al. MNK1 signaling induces an ANGPTL4-mediated gene signature to drive melanoma progression. *Oncogene* **2020**, *39*, 3650–3665. [CrossRef]
67. Rossi, A.; Di Maio, M. Platinum-based chemotherapy in advanced non-small-cell lung cancer: Optimal number of treatment cycles. *Expert Rev. Anticancer* **2016**, *16*, 653–660. [CrossRef] [PubMed]
68. Barquín-García, A.; Molina-Cerrillo, J.; Garrido, P.; Garcia-Palos, D.; Carrato, A.; Alonso-Gordoa, T. New oncologic emergencies: What is there to know about immunotherapy and its potential side effects? *Eur. J. Intern. Med.* **2019**, *66*, 1–8. [CrossRef]
69. Hsu, W.H.; Yang, J.C.; Mok, T.S.; Loong, H.H. Overview of current systemic management of EGFR-mutant NSCLC. *Ann. Oncol.* **2018**, *29*, i3–i9. [CrossRef]
70. Steurer, M.; Montillo, M.; Scarfò, L.; Mauro, F.R.; Andel, J.; Wildner, S.; Trentin, L.; Janssens, A.; Burgstaller, S.; Frömming, A.; et al. Olaptosed pegol (NOX-A12) with bendamustine and rituximab: A phase IIa study in patients with relapsed/refractory chronic lymphocytic leukemia. *Haematologica* **2019**, *104*, 2053–2060. [CrossRef]

**Disclaimer/Publisher’s Note:** The statements, opinions and data contained in all publications are solely those of the individual author(s) and contributor(s) and not of MDPI and/or the editor(s). MDPI and/or the editor(s) disclaim responsibility for any injury to people or property resulting from any ideas, methods, instructions or products referred to in the content.

Review

# Lights and Shadows on the Cancer Multi-Target Inhibitor Rigosertib (ON-01910.Na)

Ana Monfort-Vengut and Guillermo de Cárcer \*

Cell Cycle and Cancer Biomarkers Group, Instituto de Investigaciones Biomédicas Alberto Sols (IIBM) CSIC-UAM, 28029 Madrid, Spain

\* Correspondence: gdecarcer@iib.uam.es; Tel.: +34-91-585-4426

**Abstract:** Rigosertib (ON-01910.Na) is a small-molecule member of the novel synthetic benzyl-styryl-sulfonate family. It is currently in phase III clinical trials for several myelodysplastic syndromes and leukemias and is therefore close to clinical translation. The clinical progress of rigosertib has been hampered by a lack of understanding of its mechanism of action, as it is currently considered a multi-target inhibitor. Rigosertib was first described as an inhibitor of the mitotic master regulator Polo-like kinase 1 (Plk1). However, in recent years, some studies have shown that rigosertib may also interact with the PI3K/Akt pathway, act as a Ras–Raf binding mimetic (altering the Ras signaling pathway), as a microtubule destabilizing agent, or as an activator of a stress-induced phospho-regulatory circuit that ultimately hyperphosphorylates and inactivates Ras signaling effectors. Understanding the mechanism of action of rigosertib has potential clinical implications worth exploring, as it may help to tailor cancer therapies and improve patient outcomes.

**Keywords:** rigosertib; ON-01910.Na; cancer therapy; kinase allosteric inhibition; Plk1; Ras; JNK; PI3K/Akt; microtubule-destabilizing agents; stress-signaling pathways

## 1. Introduction

Rigosertib (ON-01910.Na) is a non-cyclooxygenase inhibitor sulfone metabolite with the ability to act as a non-ATP competitor kinase inhibitor. Originally described as an inhibitor for the master mitotic kinase Polo-like kinase (Plk1) [1], rigosertib has been reported to have broad activity against a number of different targets, including kinases such as PI3K/Akt or NF- $\kappa$ B complex proteins [2,3]. Interestingly, rigosertib has also been described as a Ras mimetic molecule, inhibiting Ras–Raf binding and, therefore, hampering Ras mitogenic signaling [4]. Recent data from CRISPR genome-wide screens describe rigosertib as a microtubule-depolymerizing agent that leads to cell-cycle alterations that are typical of other microtubule dynamic poisons [5]. It has also been proposed that the induced mitotic stress, upon rigosertib treatment, leads to oxidative stress resulting in a JNK-mediated inhibition of the Ras–MAPK pathway [6]. Overall, rigosertib is highly effective in killing tumoral cells in vitro and in vivo, with cells arrested in mitosis being the most prominent phenotype, although there is abundant data showing that rigosertib effectively stops cell proliferation through various combined effects.

Based on the promising in vitro data, rigosertib was subjected to clinical trials and showed good tolerability in patients with low levels of toxicity. As a result, rigosertib reached phase III trials for second-line treatment of patients with high-risk myelodysplastic syndrome (MDS) [7] and, in combination with gemcitabine, for patients with metastatic pancreatic cancer [8]. Unfortunately, these clinical trials were not successful, as the patients did not show a significant benefit over the standard of care, suggesting a need to find the right sensitivity biomarkers to achieve a therapeutic benefit. In summary, the multi-target activity of rigosertib, which is controversial, makes this drug an interesting molecule to study in order to deeply understand its mechanism of action and, subsequently, to find the biomarkers that can make rigosertib a profitable drug in the treatment of diseases.

**Citation:** Monfort-Vengut, A.; de Cárcer, G. Lights and Shadows on the Cancer Multi-Target Inhibitor Rigosertib (ON-01910.Na). *Pharmaceutics* **2023**, *15*, 1232. <https://doi.org/10.3390/pharmaceutics15041232>

Academic Editor: Francesca Musumeci

Received: 27 February 2023

Revised: 11 April 2023

Accepted: 11 April 2023

Published: 13 April 2023



**Copyright:** © 2023 by the authors. Licensee MDPI, Basel, Switzerland. This article is an open access article distributed under the terms and conditions of the Creative Commons Attribution (CC BY) license (<https://creativecommons.org/licenses/by/4.0/>).

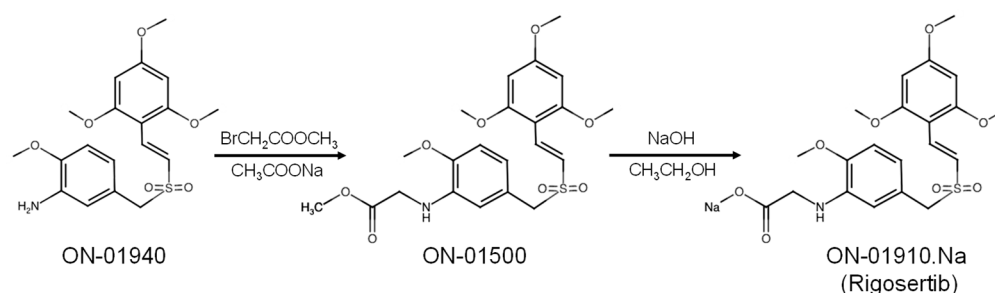
This review collects data on the different targets and cell phenotypes associated with rigosertib response and attempts to clarify the targeting controversy raised in recent years. We also discuss some of the previously described mechanisms of resistance to rigosertib and, finally, summarize all the rigosertib clinical trials conducted to date. Overall, our aim is to help the growing number of researchers working with this small compound.

## 2. Development of Rigosertib (ON-01910.Na)

One of the main problems associated with kinase-inhibition-based strategies is the development of drug resistance due to the accumulation of mutations in the ATP binding site of the kinase [9]. The scientific community has focused its efforts on developing inhibitors that target regions outside the ATP binding site of the target kinases and may act as better drug candidates in cancer therapy.

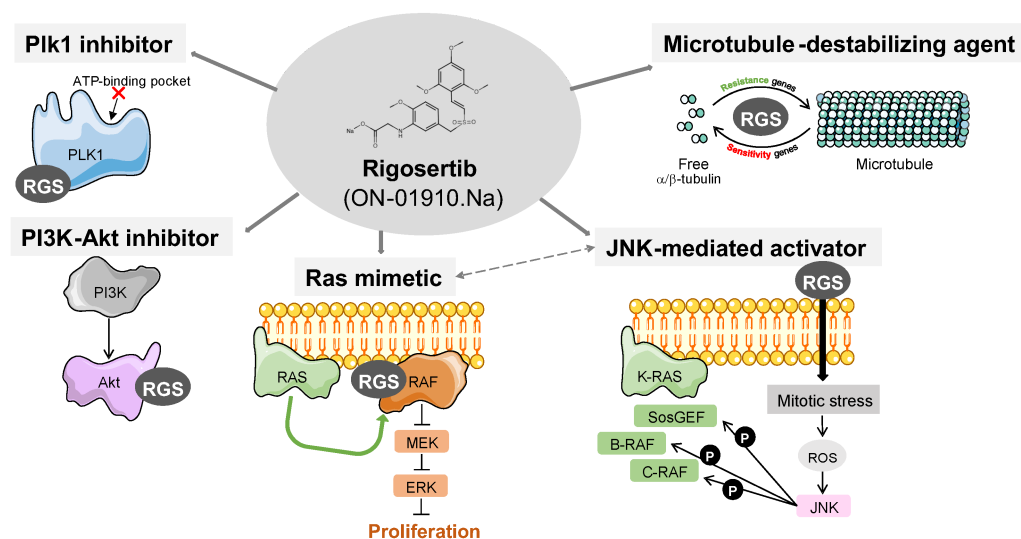
Between 2002 and 2003, Reddy et al. described the synthesis of several small-molecule kinase inhibitors, based on styryl-benzyl-sulfones, that exhibited high antitumor activity and were not ATP-competitors, but allosterically inhibited substrate binding [10–12]. Since the cytotoxic activity depends on the nature and position of the styryl aromatic ring, the group synthesized a collection of molecules capable of targeting cancer cells while leaving non-malignant cells unaffected, thus lacking many side effects associated with commonly used chemotherapeutic agents. This advantage opened a therapeutic opportunity window for this collection of new small molecules against cancer.

One of the most analyzed styryl-benzyl-sulfones is rigosertib (ON-01910), commercially known as Estybon<sup>®</sup>. Rigosertib was derived from ON-01940 ((E)-2',4',6'-trimethoxystyryl-4-methoxy-3-aminobenzylsulfone) in a two-step synthetic reaction (Figure 1): first, ON-01940 is reacted with a methyl 2-bromo acetate in a mild basic sodium acetate media to generate ON-01500 ((E)-2-methoxy-5-(((2,4,6-trimethoxystyryl)sulfonyl)methyl)aniline). Second, ON-01500 is hydrolyzed with sodium hydroxide in ethanol and dichloromethane, followed by washing with methyl ethyl ketone to obtain ON-01910 (rigosertib, sodium (E)-2-{2-methoxy-5-[(2',4',6'-trimethoxystyrylsulfonyl)methyl]phenylamino}acetate [13]. After screening these compounds for activity against tumoral cell lines, the researchers found ON-01910 to be a potent inhibitor of the mitotic kinase Plk1, inducing mitotic arrest of tumor cells. It is worth noting that rigosertib also showed certain affinity to other kinases, such as PDGFR, Abl, Flt-1, CDK1, Plk2, Src, and Fyn, which share common features in their binding sites [1].



**Figure 1.** Scheme of development of the rigosertib molecule. Images generated using (chemaxon.com/marvin (accessed on 25 January 2023)).

After rigosertib was first described, research began to flourish and many studies have provided new insights into this small molecule, describing new mechanisms and putative targets such as the PI3K–Akt pathway [14] the Ras–Raf signaling cascade [4], and microtubule dynamics [5] (Figure 2).



**Figure 2.** Diagram showing the described rigosertib targets and mechanisms of action. Rigosertib was first described as an allosteric Plk1 inhibitor [1]. Other data show that rigosertib can inhibit the PI3K–Akt signaling axis [2,3]. Rigosertib is also defined as a Ras–Raf binding competitor, altering the Ras–MAPK signaling cascade [4]. This Ras–Raf signaling impairment might be due to altering the response of stress kinases such as JNK [6]. Finally, using CRISPR genome-wide screens, rigosertib is also identified as a microtubule destabilizing agent [5].

### 3. Described Targets for Rigosertib

Over the years, many studies have been published in attempts to unravel the mechanism of action of rigosertib, to the point where it is now considered a multi-kinase inhibitor. In recent years, rigosertib has also been described as a non-kinase drug, further complicating the understanding of its mechanism of action. The main targets described are the following:

#### 3.1. Rigosertib as a Plk1 Inhibitor

Rigosertib has been generally considered a Plk1 inhibitor. Pioneering phosphorylation experiments performed immediately after rigosertib synthesis, combining recombinant Plk1 and CDC25 or Casein as substrates, showed a very efficient rigosertib-mediated Plk1 inhibition with an  $IC_{50}$  of 9–10 nM [1]. In parallel, the chemical mechanism of action of rigosertib was defined as allosteric, since increasing concentrations of ATP in the kinase reaction did not alter the inhibition constant. Notably, the allosteric binding of rigosertib to Plk1 has not yet been demonstrated [15].

To further evaluate the specificity of rigosertib for Plk1, the authors evaluated the activity of a panel of 29 recombinant kinases and showed that rigosertib was most active against Plk1 and, therefore, likely to be its primary target. However, rigosertib also showed some activity against other kinases, such as PDGF receptor (PDGFR), Abl, Flt-1, CDK1, Plk2, and Src, when tested in recombinant kinase assays. Similarly, when the authors performed cell synchronization assays and tested for Plk1 activation, they showed that rigosertib inhibited Plk1 activity, although total levels of the kinase were not affected. This effect of rigosertib seemed to be specific for Plk1, since there is almost no alteration in CDK1 activity, although other kinases were not tested in these experiments. Since Plk1 is required for tumor cell proliferation, the authors showed that rigosertib induced apoptotic activity against 94 tumor cell lines with a  $GI_{50}$  between 50–200 nM, resulting in tumor cell death by mitotic arrest, demonstrating its potential efficacy. Notably, this cytotoxic effect was not observed in non-tumoral cells. More recently, in an effort to evaluate the efficacy of rigosertib in retinoblastoma-derived cells, Ma et al. showed suppression of Cdc25C phosphorylation as a readout for Plk1 activity and concomitant accumulation of CDK1 phosphorylation [16]. They also performed flow cytometry cell-cycle analysis and

demonstrated that upon rigosertib treatment there was an arrest in the G2/M phase of the cell cycle, although it was not as strong as that identified in other reports.

Polo-like kinase 1 is a master regulator of cell division, controlling several important processes throughout the cell cycle, including centrosome maturation, spindle assembly, chromosome segregation, and, ultimately, cytokinesis [17]. The chemical inhibition or genetic depletion of Plk1 results in strong mitotic arrest and efficient cell death, making it a bona fide cancer target [18]. Importantly, Plk1 inhibition produces a highly recognizable phenotype, which is the presence of monopolar mitotic spindles [19,20] leading to impaired mitotic progression and subsequent mitotic arrest.

To confirm Plk1 as a substrate for rigosertib, confocal microscopy experiments were performed to examine the cell fate of treated cells. Rigosertib-treated HeLa cells exhibit mitotic spindle aberrations, such as multipolar spindles, chromosome mislocalization in metaphase cells, and centrosome fragmentation [1]. Although, as mentioned above, the chemical inhibition of Plk1 is known to induce mitotic arrest, the observed phenotypes in the HeLa-treated cells did not accurately reflect the classical Plk1 inhibition phenotype, which consists of monopolar spindle organization due to impaired centrosome duplication [21]. Indeed, other studies have shown that rigosertib-treated U2OS do not show alterations in centrosome maturation, a well-known function for Plk1, and present increased levels of gamma-tubulin loading at the centrosomes [22].

As the Plk1 inhibition phenotype is controversial, there are other possible explanations for the mitotic arrest observed with rigosertib treatment. Oussenko et al. described how rigosertib induces a prolonged phosphorylation of RanGAP1-SUMO1, thereby arresting cells in mitosis and ultimately inducing apoptosis in acute lymphoblastic leukemia (MOLT-3), prostate cancer (DU-145), and lymphoma cells (U937) [23]. As it is well known that RanGAP1 is phosphorylated at the onset of mitosis [24], it is difficult to determine whether RanGAP1-SUMO1 phosphorylation is directly due to rigosertib function or, on the other hand, a secondary effect of the mitotic arrest mediated by rigosertib. The authors claimed that RanGAP1-SUMO1 phosphorylation happens in short time after adding rigosertib, thus not having enough time to arrest in mitosis.

In summary, although there is still a tendency to use rigosertib as a Plk1 inhibitor [16,25–27], the Plk1 inhibition mechanism for rigosertib is controversial, as there is strong evidence that this may not be the real mechanism and some alternative mechanisms have been described for the mitotic arrest phenotype.

### *3.2. Rigosertib as a PI3K–Akt Pathway Inhibitor*

Although most of the initial studies pointed to rigosertib as a Plk1 inhibitor, or more generally as a mitotic inhibitor [14,28–33], some reports additionally demonstrated that it disrupted other non-cell-cycle-related signaling pathways. Xu et al. hypothesized that since rigosertib was being used as a kinase inhibitor, it was worth studying the dysregulation of signaling transduction pathways after rigosertib treatment; they tested samples from myelodysplastic syndrome (MDS) patients and found 31 significant upregulated pathways and 14 downregulated pathways. The PI3K–Akt, MAPK, Jak-STAT, Wnt, and Notch signaling pathways were among the most dysregulated in MDS patients, which could point to apoptotic cell death regulation [14].

These phenotypes were also observed in cell lines derived from head and neck squamous cell carcinoma (HNSCC), where PI3K dysregulation is a common event. Authors demonstrated that rigosertib induced toxicity in HNSCC cell lines, inhibiting PI3K/Akt/mTOR pathways in a dose-dependent manner, which ultimately led to the inhibition of cell-cycle progression. It also induced oxidative stress that generated reactive oxygen species (ROS) and activated extracellular-regulated kinases (ERK1/2) and c-Jun NH2-terminal kinase (JNK). They demonstrated that rigosertib triggered the mitochondria translocation of the stress kinase ATF-2, which is also related to apoptosis induction [3]. In contrast, another study done in HNSCC found rigosertib to be an effective treatment, but by a completely different mechanism than PI3K–Akt inhibition [2]. Here, the authors did not observe any

alterations in the PI3K pathway, such as the phosphorylation on Akt Ser-473 residue, or Ser-240/244 of the S6 ribosomal protein. On the contrary, a complete G2 arrest is observed, which fits with rigosertib being a mitotic inhibitor.

Overall, the possible inhibition of the PI3K–Akt axis by rigosertib seems to be cell-dependent and often accompanied by mitotic arrest. Therefore, it is difficult to interpret if both mechanisms are autonomous.

### 3.3. Rigosertib as a Ras Mimetic and Ras–Raf–MEK Axis Inhibitor

Up to this point, observations suggested that rigosertib's mechanism of action involved several alternatives and appeared to be dependent on cell type and genetic background. In 2016, the laboratory of E. Premkumar Reddy described rigosertib as the first Ras–RBD inhibitor, binding to the RBD (Ras-binding domain) of the Ras effectors and impeding Ras binding, therefore blocking the activation of Raf kinase activity and inhibiting Ras–Raf–MEK signaling [4]. The binding of rigosertib to the Raf–RBD domain was elegantly demonstrated by NMR studies, further showing that rigosertib does indeed impede Raf heterodimerization. Notably, the authors claimed that rigosertib specifically inhibits the Ser-388 residue phosphorylation of c-Raf that associates with Plk1 [34], and this may explain the relationship between rigosertib and Plk1 inhibition. Likewise, other studies showed that rigosertib treatment induces cell-cycle arrest and disrupts Ras signaling [35,36]. Finally, the authors also found that rigosertib can bind to the RBDs of Ral-GDS and PI3Ks, which might explain the inhibitory mechanism on PI3K and, therefore, its multi-target capacity.

On the other hand, Ritt et al. demonstrated that rigosertib leads to an inhibition of the Ras/Raf/MEK/ERK signaling axis, but in an indirect way. Rigosertib-induced mitotic arrest generates an oxidative stress that activates the stress cascade mediated by the cJun N-terminal kinases 1/2 (JNK1/2). This stress signaling hyperphosphorylates RasGEF, Sos1, and the Raf proteins, rendering them unresponsive to upstream signals [6]. Notably, this effect of rigosertib can be mimicked by other microtubule poisons such as taxol, suggesting that mitotic arrest is the main inducer of such a stress response, rather than a specific targeting of Ras–MEK signaling by rigosertib. In the same trend, Günther et al. provided more detail on the JNK-mediated mechanism of rigosertib, showing that rigosertib treatment activates p66Shc [37], which is a known effector of the JNK1/2 kinases [38]. Subsequently, p66Shc translocates to the mitochondria, where it induces ROS production [39].

Following the description of the Ras–Raf inhibitory activity of rigosertib, there has been a growing collection of articles exploiting this evidence. Rahmani et al. investigated the mechanism of rigosertib in colorectal cancer and confirmed that it inhibited cell proliferation and the cell cycle and that it was dependent on mutations in K-Ras [40], which also elevates ROS. More interestingly, they showed that rigosertib regulates the expression of CD31, an angiogenic marker, which opens an alternative for rigosertib as an antiangiogenic drug.

Rigosertib was also used as a canonical Ras–Raf signaling inhibitor with the intention to evaluate the impact of Ras signaling during the immune checkpoint blockade (ICB) in metastatic melanoma. The efficacy of rigosertib in melanoma is dependent on the activity of CD40, a receptor molecule of the TNF receptor family that is normally expressed on antigen-presenting cells [41]. Rigosertib Ras/Raf/PI3K inhibition promotes CD40 expression that induces immunogenic cell death and enhances the response to immune checkpoint inhibitors, thus conferring immunogenicity to rigosertib [42]. Whether this effect on CD40 is due to Ras–Raf signaling or to the dependence of CD40 function upon ROS induction [43,44] is not yet clear. Finally, in a non-cancer related study, Wang et al. studied lipopolysaccharide-induced sepsis, using rigosertib as a MEK1-ERK signaling inhibitor, concluding that it prevented the production of proinflammatory cytokines induced by LPS by disrupting the activation of the MEK1-ERK signaling axis [45].

Overall, although strong data show that rigosertib interferes with Ras–Raf–MEK signaling, the precise mechanism by which this effect is mediated is still unclear, and it

is also unclear whether it is a direct molecular impact on Ras–Raf molecules or indirectly induced by cytotoxic stress mediated by ROS induction and stress kinase (JNK) signaling.

#### 3.4. Rigosertib as a Tubulin Polymerization Destabilizer

A common cellular phenotype upon rigosertib treatment, observed by many different groups, is the G2/M arrest accompanied by mitotic aberrations. As mentioned above, this was originally assumed to be dependent on the Plk1 inhibition. However, there are examples providing evidence that rigosertib might be a microtubule dynamics inhibitor and this might be also responsible for the mentioned G2/M arrest.

Hyoda et al. showed that rigosertib induced the phosphorylation of histone H2AX and led to a DNA damage-induced G2/M arrest in HL-60, Jurkat, Ramos, and MDS-L cell lines. Rigosertib caused an abnormal localization of Aurora A kinase (AurKA), suggesting that it disrupts the spindle assembly machinery, and they finally concluded that the rigosertib effect had a possible involvement with genes related to microtubule kinetics [28]. More recently, the efficacy and mechanism of rigosertib have been tested in rhabdomyosarcoma (RMS) and neuroblastoma (NBs) cell lines. Here, the authors showed that the main cytotoxic effect is due to an efficient cell arrest in mitosis, mainly by interfering with mitotic spindle assembly, which leads to cell death [46,47]. In fact, the authors have shown a similar behavior of rigosertib with respect to other Vinca alkaloids, although it is better tolerated. Interestingly, these studies also provided evidence that rigosertib does not induce cell death by inhibiting the Ras pathway in either RMS or NB cells, demonstrating that the mechanism of action of rigosertib may be cell-type dependent.

An explanation for the rigosertib-mediated mitotic arrest was recently described by Jost et al., who claimed that rigosertib is indeed a microtubule-destabilizing agent [5]. Their study aimed to identify novel rigosertib response-associated biomarkers by performing a combined CRISPRi/a (inactivation/activation) genome-wide screen using the myeloid leukemia cell line K562. The authors demonstrated that rigosertib causes spindle and mitotic defects because it binds to  $\alpha\beta$ -tubulin heterodimers, in a region similar to that of other microtubule destabilizers, such as colchicine. This binding of rigosertib to tubulin alters microtubule dynamics both in vitro and in vivo. Moreover, the authors used structural analysis to depict the residues involved in the binding of rigosertib to  $\beta$ -tubulin, with Lys-240 being critical for this interaction. Interestingly, the mutation of this Lys-240 to phenylalanine (L240F) confers resistance to rigosertib in K562 cells, confirming that the rigosertib effect is mainly mediated by altering microtubule dynamics and, subsequently, mitotic alterations.

An important aspect to consider in these results is that rigosertib is synthesized from ON-01500 (Figure 1), which is a microtubule poison. In fact, this feature opened a dispute when the Reddy group published a contrary article stating that the microtubule-destabilizing effect is most likely due to the presence of the late intermediate impurity ON-01500 in commercial rigosertib formulations, which has a potent tubulin depolymerizing activity [48]. NMR and mass spectrometry analysis determined that the commercial grade rigosertib contained at least 5% of ON-01500. This ON-01500 impurity may result from the degradation of rigosertib due to poor storage conditions, including elevated temperature, acidic pH, and exposure to intense light. In contrast, pharmaceutical-grade rigosertib directly supplied from Onconova Therapeutics (Onconova Therapeutics, Inc., Newtown, PA 18940, USA), which is free of the ON-01500 contaminant, does not exhibit in vitro tubulin-binding activity. More importantly, they also showed that different cell lines harboring the L240F mutations were sensitive to the pharmaceutical-grade rigosertib and failed to proliferate. The disagreement does not end here, as Jost et al. reevaluated the effect of commercial and clinical-grade rigosertib, showing indistinguishable phenotypes and agreeing with their previous findings [49]. Both rigosertib versions destabilize microtubules either in vivo or in vitro, and both show significantly reduced toxicity in cell lines expressing the L240F tubulin mutant. Interestingly, a very recent screen for identifying



tubulin polymerization inhibitors pinpointed rigosertib as a major hit and demonstrated the capacity of rigosertib binding to tubulin by *in silico* docking analysis [50].

On the other hand, earlier studies made these conclusions even more controversial by showing that rigosertib-mediated effects do not depend on altered microtubule dynamics. Oussenko et al. not only described rigosertib-induced mitotic arrest as mentioned above, but also shed light on the microtubule destabilizer hypothesis by testing the ability of rigosertib and the inactive analog molecule ON-01911 to modify the tubulin polymerization. They revealed that clinical-grade rigosertib directly obtained from Onconova Therapeutics and control ON-01911 had a minor inhibition effect on tubulin polymerization, whereas nocodazole (another well-known microtubule poison) completely inhibited the process. This is indeed in agreement with the original article describing rigosertib as a Plk1 inhibitor, in which; they also established that rigosertib does not alter microtubule polymerization [1].

In summary, it is clear that rigosertib induces mitotic arrest and this appears to be a major cause of cell death. Whether this mitotic arrest is a direct effect of rigosertib due to changes in microtubule dynamics or other targets, such as Plk1, is still under debate. The source of the drug also appears to determine the outcome. While the clinical-grade rigosertib supplied by the proprietary pharmaceutical company Onconova Therapeutics appears to be more reliable than the commercial stocks, it is probably more important that the storage and handling conditions are precise to avoid degradation to synthesis intermediates, such as ON-01500, which has a strong affinity for microtubule heterodimers.

#### 4. Rigosertib Clinical Trials for Cancer Therapy

Successful preclinical *in vivo* studies performed with rigosertib confirmed its safety profile with no evidence of myelotoxicity, neuropathy, or cardiotoxicity in xenograft mouse models, while successfully inhibiting liver, breast, and pancreatic cancers [1,51]. Rigosertib was, therefore, immediately included in a series of clinical trials to test its efficacy in a wide range of different cancers, including both solid tumors and hematological malignancies (Table 1).

Phase I trials suggested a maximum tolerated drug dose of 1800 mg/24 h in a three-day constant intravenous infusion rate, delivered every other week, with an acceptable toxicity profile [52–54]. The most common adverse events (AEs) included fatigue, gastrointestinal, and urinary symptoms. More severe grade 3 to 4 AEs were uncommon. Thrombocytopenia AE was also observed, yet to a lesser extent. Interestingly, drug-induced myelosuppression was also infrequent, thus providing a therapeutic advantage for myelodysplastic syndrome patients, given their compromised bone marrow function.

Rigosertib can be also administrated orally with a positive clinical activity [55]. Dose-limiting toxicity was established at 700 mg twice daily (b.i.d) upon severe grade 3 AE appearance, and the recommended dose was identified as 560 mg b.i.d. Overall, oral rigosertib was well tolerated. The most significant grade 2–3 toxicities included mainly urinary symptoms, abdominal pain and diarrhea, fatigue, hypotension, and anorexia. These positive toxicity and tolerability data encouraged clinicians to move forward into more advanced clinical trial phases.

Although some phase II tests were performed on some solid tumors, such as non-small cell lung cancer adenocarcinoma, and a wide variety of squamous cell carcinomas, they were predominately focused on hematological malignancies and, more concretely, on myelodysplastic syndromes (MDS) and myeloid leukemias. Similarly, phase III trials were mainly done in myelodysplastic syndromes, and only a recent phase III trial was performed on pancreatic adenocarcinoma patients (Table 1). It is also important to note that although most trials with rigosertib have been conducted as a monotherapy strategy (mainly phase I), advanced phase II and III studies have also been undertaken in combination with other chemotherapeutic agents in an effort to achieve a better response for those patients. Gemcitabine (DNA synthesis inhibitor) was combined with rigosertib in the phase III trial for pancreatic adenocarcinoma [8,56]. Azacitidine or decitabine (DNA methyltransferase inhibitors) were combined with rigosertib for MDS trials. Some solid

tumor trials also combined rigosertib with either oxaliplatin (DNA synthesis inhibitor) or irinotecan (topoisomerase I inhibitor).

Despite the motivating number of clinical trials annotated in the U.S. National Library of Medicine website (ClinicalTrials.gov, accessed on 20 February 2023), very few of them provide results that indicate the efficacy of the drug. Data from phase I and II trials in MDS and myeloid leukemias were promising, with some patients showing a positive response to the treatment, with either a partial or complete bone marrow blast response and subsequent hematological improvement. This encouraged the initiation of a large-scale phase III trial comparing rigosertib administration to the standard best supportive care (BSC) for MDS (low dose cytarabine). Unfortunately, the results of the large trial were not positive [7]. The median overall survival (OS) in the rigosertib arm was 8.2 months and the median OS in the BSC arm was 5.9 months. In addition, no patients had a complete or partial response, although there is a modest increase in the bone marrow blast response with rigosertib, which was previously associated with improved survival.

In summary, rigosertib did not reach its primary objective of providing a survival benefit compared to the BSC-treated cohort, although certain subgroups appeared to benefit from treatment. Another interesting phase III trial is the combination of rigosertib with gemcitabine in a cohort of metastatic pancreatic adenocarcinoma, with 160 enrolled patients [8,56]. Unfortunately, despite the good data from preclinical studies using PDX models of pancreatic tumors [51], the combination treatment did not show an improvement in survival or response in pancreatic cancer patients and the authors stated that further studies with rigosertib in this type of cancer would not be performed.

In an attempt to understand the variability in sensitivity to rigosertib, and to shed light on what may be the best tumoral context for a rigosertib therapeutic strategy, we took advantage of the DepMap portal (depmap.org), which provides chemical and genetic cancer dependency information, allowing data visualization from a large scale of viability screens across hundreds of cell lines. We selected data generated by the Broad Institute CTD<sup>2</sup> Center originally published via the Cancer Therapeutics Response Portal (CTRP) [57,58] to plot rigosertib sensitivity (AUC, area under the curve) against different cancer lineages. We observed a specific sensitivity against rigosertib of hematological cancers cells (leukemias, myeloid and lymphoid) in comparison with solid cancer-derived cell lines (Figure 3). This probably explains why clinical trials have focused primarily on myeloid and lymphoid tumors, although in vitro data have never really translated into the clinical trials for these cancers.

Interestingly, and according to DepMap portal data, the most sensitive cell populations are those derived from neuroblastoma tumors. Indeed, the sensitivity of rigosertib to neuroblastoma models, both in vitro and in vivo, has been reported by others [46,47,59], demonstrating that rigosertib may be a good therapeutic alternative for this tumoral type. Perhaps the fact that neuroblastoma is a pediatric tumor is one of the reasons why its testing in clinical trials has been negatively affected. The data from the DepMap portal also confirm why the clinical trial that was focused on pancreatic cancer was completely unsuccessful. The cell lines derived from pancreatic adenocarcinoma are the most refractive to rigosertib treatment, among the 20 cohorts tested, with values equivalent to those for biliary tract and kidney tumors.

**Table 1.** Summary of rigosertib clinical trials.

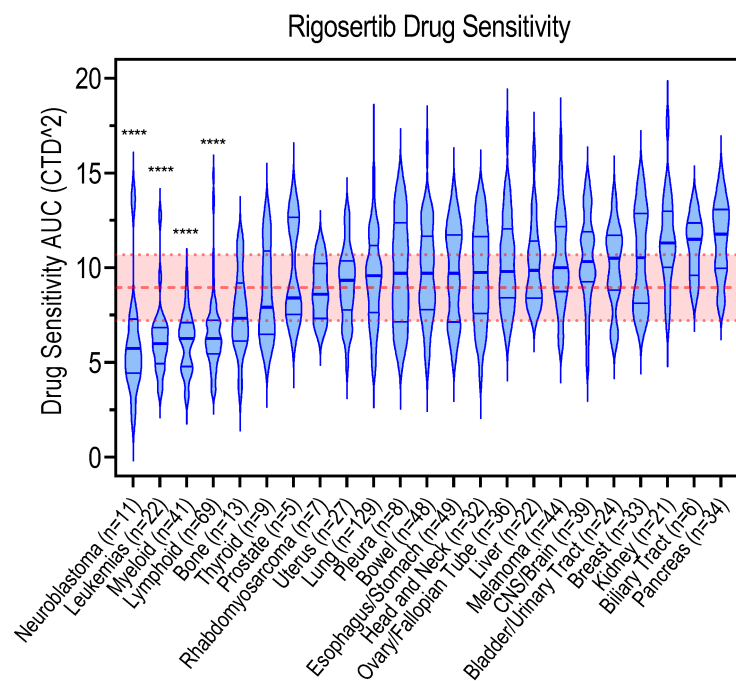
Phase	NCT Number	Treatment	Disease	Participants	References
Phase I	NCT01048619	ON-01910.Na	Myelodysplastic Syndrome	36	[55]
	NCT01168011	ON-01910.Na	Solid Tumor	68	
	NCT01125891	Gemcitabine or ON-01910.Na	Malignant Neoplasms Solid Tumors	39	[60]

Table 1. Cont.

Phase	NCT Number	Treatment	Disease	Participants	References
Phase I	NCT00854646	ON-01910.Na	Acute Myelocytic Leukemia Acute Lymphocytic Leukemia Chronic Myelocytic Leukemia Chronic Lymphocytic Leukemia Myelodysplastic Syndromes	22	[61]
	NCT01538537	ON-01910.Na	Advanced Cancer Solid Tumors Cancer Neoplasms	29	[53]
	NCT01538563	ON-01910.Na	Solid Tumors Advanced Cancer Neoplasms	42	-
	NCT01165905	Gemcitabine or ON-01910.Na	Solid Tumor	10	-
	NCT00861783	Irinotecan + ON-01910.Na Oxaliplatin + ON-01910.Na	Hepatoma Advanced Solid Tumor	16	-
	NCT00861328	Irinotecan + ON-01910.Na Oxaliplatin + ON-01910.Na	Advanced Solid Tumors	18	-
	NCT00861510	ON-01910.Na	Lymphoma Mantle-cell Leukemia Lymphocytic Chronic B-Cell Leukemia Hairy Cell Waldenstrom Macroglobulinemia Multiple Myeloma	16	[62]
NCT00533416	ON-01910.Na	Myelodysplastic Syndrome (MDS)	14	[63]	
Phase I/II	NCT01167166	ON-01910.Na	Acute Myelocytic Leukemia Acute Lymphocytic Leukemia Myeloproliferative Disease Chronic Myeloid Leukemia	30	-
	NCT00854945	ON-01910.Na	Myelodysplastic Syndromes Acute Myeloid Leukemia	36	-
	NCT01926587	Azacitidine + ON-01910.Na	Myelodysplastic Syndromes Acute Myeloid Leukemia Chronic Myelomonocytic Leukemia	45	[64]
	NCT04263090	Nivolumab + ON-01910.Na	Non-small Cell Lung Cancer Adenocarcinoma Stage IV	20	-
	NCT03786237	ON-01910.Na	Epidermolysis Bullosa Dystrophica Squamous Cell Carcinoma	12	-
Phase II	NCT01807546	ON-01910.Na	Head and Neck Squamous Cell Carcinoma Anal Squamous Cell Carcinoma Lung Squamous Cell Carcinoma Cervical Squamous Cell Carcinoma Esophageal Squamous Cell Carcinoma Skin Squamous Cell Carcinoma Penile Squamous Cell Carcinoma	64	-
	NCT01904682	ON-01910.Na	Myelodysplastic Syndromes	45	-
	NCT01584531	ON-01910.Na	Myelodysplastic Syndromes MDS Trisomy 8	82	-
	NCT00906334	ON-01910.Na	Myelodysplastic Syndromes	14	[65]

Table 1. Cont.

Phase	NCT Number	Treatment	Disease	Participants	References
Phase III	NCT01241500	ON-01910.Na	Myelodysplastic Syndromes MDS RAEB Chronic Myelomonocytic Leukemia	299	-
	NCT01928537	ON-01910.Na	Myelodysplastic Syndromes Refractory Anemia with Excess Blasts Chronic Myelomonocytic Leukemia Cytopenia	67	-
	NCT02562443	Best supportive care (BSC) + ON-01910.Na Vs. Physician's choice (PC) + ON-01910.Na	Myelodysplastic Syndromes MDS Refractory Anemia with Excess Blasts RAEB	372	[7]
	NCT01360853	Gemcitabine + ON-01910.Na	Metastatic Pancreatic Adenocarcinoma	160	[8,56,66]



**Figure 3.** Data adapted from the DepMap Portal, retrieved from the Cancer Therapeutics Response Portal (CTRP), showing the sensitivity of cancer-cell lines of multiple origins to rigosertib. AUC reflects the area under the concentration-response curve. The lower the AUC, the more sensitive the cell line. Violin plots show median rigosertib sensitivity values (thick blue line). The thick dashed red line shows the average of all median AUCs. The shaded red area is defined by the standard deviation of the average median values. An unpaired t-test was performed, comparing the neuroblastoma, leukemias, myeloid, or lymphoid cohorts with the rest of all cohorts together and significance is indicated by  $p < 0.0001$  (\*\*\*\*). The number of cell lines (n) in each cohort is indicated in the X axis. Statistics were calculated using GraphPad Software version 9.5.1.

### 5. Genetic Biomarkers Associated with Rigosertib Response

In an effort to elucidate the mechanism of action of rigosertib and to identify therapeutic biomarkers, some researchers have recently begun to identify the genetic alteration that may determine the efficacy of the response to rigosertib.

Oussenko et al. performed cross-resistance experiments and showed that rigosertib did not induce an MDR1 (multi-drug resistance 1) or an MRP1 (multi-drug resistance-associated protein 1) response. Moreover, cells resistant to other drugs did not show

cross-resistance to rigosertib, making it a favorable anticancer agent [23]; hence, rigosertib appears to escape the general resistance mechanisms described for other drugs. On the contrary, Sánchez-Burgos et al. described how deficiency of the FBXW7 gene leads to resistance to rigosertib treatment. Interestingly, FBXW7 deficiency also confers resistance to a wide range of other chemotherapeutic agents, making it a general drug-resistance mechanism, rather than rigosertib-specific [67].

Another described biomarker of rigosertib efficacy is the deubiquitinating enzyme USP28 [68]. USP28 destabilizes the Raf family proteins by a feedback-loop-mediated mechanism. When USP28 is downregulated, B-Raf is hyper stabilized and, therefore, enhances downstream MAPK signaling, promoting resistance to Raf inhibitor therapy strategies. As USP28 is frequently deleted in a proportion of melanoma patients, the authors suggested rigosertib as a potential therapeutic strategy for USP28-depleted cells, demonstrating an increased sensitivity of USP28-depleted cells to rigosertib. Surprisingly, rigosertib appears to kill USP28 null cells in an ERK independent manner, and with a strong mitotic arrest phenotype. Hence, there is still doubt as to whether this USP28-null synthetic lethality is due to an amplification of the Ras–Raf signaling pathway, or simply to an increase in the proliferation ratio and a strong dependence on mitosis. Indeed, the same authors observed that USP28-depleted cells are more sensitive to small molecules such as microtubule poisons (taxol, vincristine, nocodazole) or even Plk1 inhibitors such as BI-2536.

Focusing on myelodysplastic syndromes (MDS), a possible biomarker for rigosertib response is the presence of trisomy 8. Trisomy of chromosome 8 and monosomy of chromosome 7 are common alterations observed in MDS patients [69] and these cytogenetic features correlate with the upregulation of the oncogenes *c-myc*, Wilms Tumor 1 (*WT1*), and Cyclin D1, thus increasing the proliferation capacity of these cells [70]. Interestingly, rigosertib has a selective inhibitory effect in trisomy-8 MDS cells and, to a lesser extent, in monosomy-7. This was also seen in patients enrolled in the MDS clinical trial (NCT00533416) and occurred even when these chromosomal abnormalities were part of a more complex karyotype. [63]. Thus, trisomy-8/monosomy-7 and elevated Cyclin D1, can behave as bona fide biomarkers for rigosertib treatment, at least in MDS.

Seeking to identify relevant cellular biomarkers following rigosertib treatment, Jost et al. performed a chemical screen for rigosertib using a CRISPRi (inactivation) and a CRISPRa (activation) strategy and identified a signature of microtubule-related genes that antagonized or synergized with the drug [5]. Specifically, the authors determined that the overexpression of the *KIF2C* gene, which encodes the microtubule depolymerizing enzyme MCAK [71], sensitizes cells to rigosertib. At the same time, the knockdown of *TACC3*, a microtubule-binding protein involved in microtubule stability [72], sensitizes cells to rigosertib. Thus, genetic manipulations that destabilize microtubules lead to increased sensitivity to rigosertib, whereas genetic alterations that induce microtubule stabilization lead to a protective effect against rigosertib [5]. To validate this hypothesis, the authors knocked-down both genes involved in microtubule stability with CRISPR-Cas9 technology and confirmed in different tumoral cell lines that the downregulation of *KIF2C* and *TACC3* dictate resistance or sensitivity to rigosertib, respectively. In addition, they confirmed that rigosertib destabilizes microtubules by docking into the colchicine-binding site of tubulin. These results, although requiring further validation, identify specific genes whose expression predicts response to rigosertib and may serve as biomarkers for rigosertib treatment in a clinical context.

Despite these initial efforts to identify biomarkers of response to rigosertib, there is still very little known, and further efforts are needed in order to find genetic signatures that might help to better stratify patients in future clinical trials.

## 6. Conclusions, Current Challenges, and Prospects

Rigosertib is considered a promising therapeutic strategy for cancer for several reasons. It is defined as a non-ATP competitor multi-kinase inhibitor, which makes it an attractive molecule, as it avoids the associated drug-resistance mechanisms that can arise with ATP-

competitor molecules [9]. Data suggest that rigosertib does not present cross-resistance to other drugs and is not an MDR1 or MPR1 substrate, making rigosertib a good choice of treatment for multi-drug resistant cancers. Preclinical studies prompted rigosertib as a promising molecule for the treatment of cancer therapy because *in vivo* studies demonstrated its efficacy in killing cancer cells with little associated toxicity. This tolerable toxicity was also seen in many clinical trials performed; therefore, rigosertib was considered a promising therapeutic strategy. Unfortunately, advanced clinical trials turned out to not be as efficient as initially thought and there was very little improvement when compared to the standard therapies for several types of cancer. This indicates that we still lack the right biomarkers to better stratify the patients for a rigosertib-mediated therapy. In this regard, all efforts trying to define the drug target have been confusing and controversial.

Rigosertib's mechanism of action was originally suggested to be an allosteric inhibitor of the mitotic master regulator Plk1 [1]. Over the years, Plk1 specificity has been debated [22] and, in parallel, there was increasing evidence showing that rigosertib might alter other pathways. Indeed, it was described as a the PI3K–Akt axis inhibitor [2,3] or acting as a Ras–Raf binding mimetic leading to MEK signaling inhibition [4]. In the same vein, the inhibition of MEK signaling was attributed to the generation of mitotic stress [6], thus altering stress-signaling pathways. Finally, the mitotic arrest phenotype was recently explained by demonstrating that rigosertib is a microtubule-destabilizing drug [6]. This raised a strong controversy about the source quality of the drug, its stability, and its storage accuracy [48,49].

Because of the multiple mechanisms of action described, the scientific community has followed waves of studies, often viewing rigosertib as a unique inhibitor for Plk1, Ras, or PI3K/Akt, overlooking all other possible targets and side effects. Although some research groups have begun efforts to define the mechanisms of rigosertib, these studies are still at an early stage, and only a few genetic determinants have been described, with little clinical impact.

Therefore, a strong effort to elucidate rigosertib's mechanism of action and understand how rigosertib inhibits cancer cell growth is critical to better define the potential patients who could benefit from this inhibitor and, thus, advance clinical trials.

**Author Contributions:** Conceptualization, G.d.C.; data curation from DepMap portal and ClinicalTrials.gov web pages, A.M.-V. and G.d.C.; manuscript writing, A.M.-V. and G.d.C.; funding acquisition, G.d.C. All authors have read and agreed to the published version of the manuscript.

**Funding:** This research was funded by the Spanish Ministry of Science and Innovation MCIN/AEI/FEDER (doi:10.13039/501100011033), grants RTI2018-095496-B-I00 and PID2021-125705OB-I00, and by the Spanish Association Against Cancer (AECC) Scientific Foundation, grant LABAE16017DECA.

**Institutional Review Board Statement:** Not applicable.

**Informed Consent Statement:** Not applicable.

**Data Availability Statement:** Table 1 was generated retrieving data from the Clinical Trial web page (<https://clinicaltrials.gov/ct2/home>, accessed on 20 February 2023) of the U.S. National Library of Medicine. Figure 1 was generated using the chemical drawing tool Marvin JS (<https://chemaxon.com/marvin>, accessed on 25 January 2023). Figure 2 was drawn using templates from Servier Medical Art. Servier Medical Art by Servier is licensed under a Creative Commons Attribution 3.0 Unported License (<https://creativecommons.org/licenses/by/3.0/>, accessed on 15 January 2023). Figure 3 was generated using data from the DepMap Portal (<https://depmap.org/portal/>, accessed on 15 February 2023), retrieved from the Cancer Therapeutics Response Portal (CTRP).

**Acknowledgments:** G.d.C belongs to the Spanish National Research Council (CSIC)'s Cancer Hub (<https://conexion-cancer.csic.es/>).

**Conflicts of Interest:** The authors declare no conflict of interest.

## References

- Gumireddy, K.; Reddy, M.V.R.; Cosenza, S.C.; Nathan, R.B.; Baker, S.J.; Papathi, N.; Jiang, J.; Holland, J.; Reddy, E.P. ON01910, a Non-ATP-Competitive Small Molecule Inhibitor of Plk1, Is a Potent Anticancer Agent. *Cancer Cell* **2005**, *7*, 275–286. [CrossRef] [PubMed]
- Anderson, R.T.; Keysar, S.B.; Bowles, D.W.; Glogowska, M.J.; Astling, D.P.; Morton, J.J.; Le, P.; Umpierrez, A.; Eagles-Soukup, J.; Gan, G.N.; et al. The Dual Pathway Inhibitor Rigosertib Is Effective in Direct Patient Tumor Xenografts of Head and Neck Squamous Cell Carcinomas. *Mol. Cancer Ther.* **2013**, *12*, 1994–2005. [CrossRef] [PubMed]
- Prasad, A.; Khudaynazar, N.; Tantravahi, R.V.; Gillum, A.M.; Hoffman, B.S. ON 01910.Na (Rigosertib) Inhibits PI3K/Akt Pathway and Activates Oxidative Stress Signals in Head and Neck Cancer Cell Lines. *Oncotarget* **2016**, *7*, 79388–79400. [CrossRef] [PubMed]
- Athuluri-Divakar, S.K.; Vasquez-Del Carpio, R.; Dutta, K.; Baker, S.J.; Cosenza, S.C.; Basu, I.; Gupta, Y.K.; Reddy, M.V.R.; Ueno, L.; Hart, J.R.; et al. A Small Molecule RAS-Mimetic Disrupts RAS Association with Effector Proteins to Block Signaling. *Cell* **2016**, *165*, 643–655. [CrossRef] [PubMed]
- Jost, M.; Chen, Y.; Gilbert, L.A.; Horlbeck, M.A.; Krenning, L.; Menchon, G.; Rai, A.; Cho, M.Y.; Stern, J.J.; Protá, A.E.; et al. Combined CRISPR/a-Based Chemical Genetic Screens Reveal That Rigosertib Is a Microtubule-Destabilizing Agent. *Mol. Cell* **2017**, *68*, 210–223.e6. [CrossRef] [PubMed]
- Ritt, D.A.; Abreu-Blanco, M.T.; Bindu, L.; Durrant, D.E.; Zhou, M.; Specht, S.I.; Stephen, A.G.; Holderfield, M.; Morrison, D.K. Inhibition of Ras/Raf/MEK/ERK Pathway Signaling by a Stress-Induced Phospho-Regulatory Circuit. *Mol. Cell* **2016**, *64*, 875–887. [CrossRef] [PubMed]
- Garcia-Manero, G.; Fenaux, P.; Al-Kali, A.; Baer, M.R.; Sekeres, M.A.; Roboz, G.J.; Gaidano, G.; Scott, B.L.; Greenberg, P.; Platzbecker, U.; et al. Rigosertib versus Best Supportive Care for Patients with High-Risk Myelodysplastic Syndromes after Failure of Hypomethylating Drugs (ONTIME): A Randomised, Controlled, Phase 3 Trial. *Lancet Oncol.* **2016**, *17*, 496–508. [CrossRef]
- O’Neil, B.H.; Scott, A.J.; Ma, W.W.; Cohen, S.J.; Aisner, D.L.; Menter, A.R.; Tejani, M.A.; Cho, J.K.; Granfortuna, J.; Coveler, L.; et al. A Phase II/III Randomized Study to Compare the Efficacy and Safety of Rigosertib plus Gemcitabine versus Gemcitabine Alone in Patients with Previously Untreated Metastatic Pancreatic Cancer. *Ann. Oncol.* **2015**, *26*, 1923–1929. [CrossRef]
- Sawyers, C.L. Opportunities and Challenges in the Development of Kinase Inhibitor Therapy for Cancer. *Genes Dev.* **2003**, *17*, 2998–3010. [CrossRef]
- Reddy, E.; Reddy, M. Substituted Styryl Benzylsulfones for Treating Proliferative Disorders. U.S. Patent No. 6486210 B2, 22 November 2002.
- Reddy, E.; Reddy, M. Preparation of  $\alpha,\beta$ -Unsaturated Sulfones for Treating Proliferative Disorders. U.S. Patent No. 6541475, 7 March 2002.
- Reddy, E.; Reddy, M.  $\alpha,\beta$ -Unsaturated Sulfones for Treating Proliferative Disorders. U.S. Patent No. 6599932 B1, 29 July 2003.
- Reddy, M.V.R.; Venkatapuram, P.; Mallireddigari, M.R.; Pallela, V.R.; Cosenza, S.C.; Robell, K.A.; Akula, B.; Hoffman, B.S.; Reddy, E.P. Discovery of a Clinical Stage Multi-Kinase Inhibitor Sodium (*E*)-2-[(2',4',6'-Trimethoxystyrylsulfonyl)methyl]phenylaminoacetate (ON 01910.Na): Synthesis, Structure–Activity Relationship, and Biological Activity. *J. Med. Chem.* **2011**, *54*, 6254–6276. [CrossRef]
- Xu, F.; He, Q.; Li, X.; Chang, C.-K.; Wu, L.-Y.; Zhang, Z.; Liu, L.; Shi, W.-H.; Zhu, Y.; Zhao, Y.-S.; et al. Rigosertib as a Selective Anti-Tumor Agent Can Ameliorate Multiple Dysregulated Signaling Transduction Pathways in High-Grade Myelodysplastic Syndrome. *Sci. Rep.* **2014**, *4*, 7310. [CrossRef] [PubMed]
- Archambault, V.; Normandin, K. Several Inhibitors of the Plk1 Polo-Box Domain Turn out to Be Non-Specific Protein Alkylators. *Cell Cycle* **2017**, *16*, 1220–1224. [CrossRef] [PubMed]
- Ma, H.; Nie, C.; Chen, Y.; Li, J.; Xie, Y.; Tang, Z.; Gao, Y.; Ai, S.; Mao, Y.; Sun, Q.; et al. Therapeutic Targeting PLK1 by ON-01910.Na Is Effective in Local Treatment of Retinoblastoma. *Oncol. Res. Featur. Preclin. Clin. Cancer Ther.* **2021**, *28*, 745–761. [CrossRef] [PubMed]
- de Cárcer, G.; Manning, G.; Malumbres, M. From Plk1 to Plk5. *Cell Cycle* **2011**, *10*, 2255–2262. [CrossRef] [PubMed]
- Chiappa, M.; Petrella, S.; Damia, G.; Broggin, M.; Guffanti, F.; Ricci, F. Present and Future Perspective on PLK1 Inhibition in Cancer Treatment. *Front. Oncol.* **2022**, *12*, 903016. [CrossRef]
- Wachowicz, P.; Fernández-Miranda, G.; Marugán, C.; Escobar, B.; de Cárcer, G. Genetic Depletion of Polo-like Kinase 1 Leads to Embryonic Lethality Due to Mitotic Aberrancies. *BioEssays* **2016**, *38*, S96–S106. [CrossRef] [PubMed]
- Lénárt, P.; Petronczki, M.; Steegmaier, M.; Di Fiore, B.; Lipp, J.J.; Hoffmann, M.; Rettig, W.J.; Kraut, N.; Peters, J.-M. The Small-Molecule Inhibitor BI 2536 Reveals Novel Insights into Mitotic Roles of Polo-like Kinase 1. *Curr. Biol.* **2007**, *17*, 304–315. [CrossRef] [PubMed]
- Haren, L.; Stearns, T.; Lüders, J. Plk1-Dependent Recruitment of  $\gamma$ -Tubulin Complexes to Mitotic Centrosomes Involves Multiple PCM Components. *PLoS ONE* **2009**, *4*, e5976. [CrossRef]
- Peters, U.; Cherian, J.; Kim, J.H.; Kwok, B.H.; Kapoor, T.M. Probing Cell-Division Phenotype Space and Polo-like Kinase Function Using Small Molecules. *Nat. Chem. Biol.* **2006**, *2*, 618–626. [CrossRef]
- Oussenko, I.A.; Holland, J.F.; Reddy, E.P.; Ohnuma, T. Effect of ON 01910.Na, an Anticancer Mitotic Inhibitor, on Cell-Cycle Progression Correlates with RanGAP1 Hyperphosphorylation. *Cancer Res.* **2011**, *71*, 4968–4976. [CrossRef]

24. Swaminathan, S.; Kiendl, F.; Körner, R.; Lupetti, R.; Hengst, L.; Melchior, F. RanGAP1\*SUMO1 Is Phosphorylated at the Onset of Mitosis and Remains Associated with RanBP2 upon NPC Disassembly. *J. Cell Biol.* **2004**, *164*, 965–971. [CrossRef] [PubMed]
25. Atanasova, V.S.; Pourreyron, C.; Farshchian, M.; Lawler, M.; Brown, C.A.; Watt, S.A.; Wright, S.; Warkala, M.; Guttmann-Gruber, C.; Hofbauer, J.P.; et al. Identification of Rigosertib for the Treatment of Recessive Dystrophic Epidermolysis Bullosa-Associated Squamous Cell Carcinoma. *Clin. Cancer Res.* **2019**, *25*, 3384–3391. [CrossRef] [PubMed]
26. Seo, Y.; Kang, Y.; Ham, Y.; Kim, M.-H.; Kim, S.-J.; Yoon, S.K.; Jang, S.K.; Park, J.B.; Cho, S.; Kim, J.H. PLK1-ELAVL1/HuR-MiR-122 Signaling Facilitates Hepatitis C Virus Proliferation. *Proc. Natl. Acad. Sci. USA* **2022**, *119*, e2214911119. [CrossRef] [PubMed]
27. Vulin, M.; Jehanno, C.; Sethi, A.; Correia, A.L.; Obradović, M.M.S.; Couto, J.P.; Coissieux, M.-M.; Diepenbruck, M.; Preca, B.-T.; Volkmann, K.; et al. A High-Throughput Drug Screen Reveals Means to Differentiate Triple-Negative Breast Cancer. *Oncogene* **2022**, *41*, 4459–4473. [CrossRef] [PubMed]
28. Hyoda, T.; Tsujioka, T.; Nakahara, T.; Suemori, S.; Okamoto, S.; Kataoka, M.; Tohyama, K. Rigosertib Induces Cell Death of a Myelodysplastic Syndrome-derived Cell Line by DNA Damage-induced G2/M Arrest. *Cancer Sci.* **2015**, *106*, 287–293. [CrossRef]
29. Lin, Y.G.; Shen, J.; Yoo, E.; Liu, R.; Yen, H.-Y.; Mehta, A.; Rajaei, A.; Yang, W.; Mhawech-Fauceglia, P.; DeMayo, F.J.; et al. Targeting the Glucose-Regulated Protein-78 Abrogates Pten-Null Driven AKT Activation and Endometrioid Tumorigenesis. *Oncogene* **2015**, *34*, 5418–5426. [CrossRef]
30. Liu, Z.; Wang, M.; Wang, H.; Fang, L.; Gou, S. Targeting RAS-RAF Pathway Significantly Improves Antitumor Activity of Rigosertib-Derived Platinum(IV) Complexes and Overcomes Cisplatin Resistance. *Eur. J. Med. Chem.* **2020**, *194*, 112269. [CrossRef]
31. Lu, T.; Laughton, C.A.; Wang, S.; Bradshaw, T.D. In Vitro Antitumor Mechanism of (*E*)-*N*-(2-Methoxy-5-((2,4,6-Trimethoxystyryl)Sulfonyl)Methyl)Pyridin-3-Yl)Methanesulfonamide. *Mol. Pharmacol.* **2015**, *87*, 18–30. [CrossRef]
32. Malacrida, A.; Rigolio, R.; Celio, L.; Damian, S.; Cavaletti, G.; Mazzaferro, V.; Miloso, M. In Vitro Evaluation of Rigosertib Antitumoral and Radiosensitizing Effects against Human Cholangiocarcinoma Cells. *Int. J. Mol. Sci.* **2021**, *22*, 8230. [CrossRef]
33. Ruppenthal, S.; Kleiner, H.; Nolte, F.; Fabarius, A.; Hofmann, W.-K.; Nowak, D.; Seifarth, W. Increased Separase Activity and Occurrence of Centrosome Aberrations Concur with Transformation of MDS. *PLoS ONE* **2018**, *13*, e0191734. [CrossRef]
34. Mielgo, A.; Seguin, L.; Huang, M.; Camargo, M.F.; Anand, S.; Franovic, A.; Weis, S.M.; Advani, S.J.; Murphy, E.A.; Cheresch, D.A. A MEK-Independent Role for CRAF in Mitosis and Tumor Progression. *Nat. Med.* **2011**, *17*, 1641–1645. [CrossRef] [PubMed]
35. Dietrich, P.; Freese, K.; Mahli, A.; Thasler, W.E.; Hellerbrand, C.; Bosserhoff, A.K. Combined Effects of PLK1 and RAS in Hepatocellular Carcinoma Reveal Rigosertib as Promising Novel Therapeutic “Dual-Hit” Option. *Oncotarget* **2018**, *9*, 3605–3618. [CrossRef] [PubMed]
36. Urasaki, Y.; Fiscus, R.R.; Le, T.T. Detection of the Cell Cycle-Regulated Negative Feedback Phosphorylation of Mitogen-Activated Protein Kinases in Breast Carcinoma Using Nanofluidic Proteomics. *Sci. Rep.* **2018**, *8*, 9991. [CrossRef] [PubMed]
37. Galimov, E.R. The Role of P66shc in Oxidative Stress and Apoptosis. *Acta Nat.* **2010**, *2*, 44–51. [CrossRef]
38. Günther, J.K.; Nikolajevic, A.; Ebner, S.; Troppmair, J.; Khalid, S. Rigosertib-Activated JNK1/2 Eliminate Tumor Cells through P66Shc Activation. *Biology* **2020**, *9*, 99. [CrossRef]
39. Giorgio, M.; Migliaccio, E.; Orsini, F.; Paolucci, D.; Moroni, M.; Contursi, C.; Pelliccia, G.; Luzi, L.; Minucci, S.; Marcaccio, M.; et al. Electron Transfer between Cytochrome c and P66Shc Generates Reactive Oxygen Species That Trigger Mitochondrial Apoptosis. *Cell* **2005**, *122*, 221–233. [CrossRef]
40. Rahmani, F.; Hashemzahi, M.; Avan, A.; Barneh, F.; Asgharzadeh, F.; Moradi Marjaneh, R.; Soleimani, A.; Parizadeh, M.; Ferns, G.A.; Ghayour Mobarhan, M.; et al. Rigosertib Elicits Potent Anti-Tumor Responses in Colorectal Cancer by Inhibiting Ras Signaling Pathway. *Cell. Signal.* **2021**, *85*, 110069. [CrossRef]
41. Tong, A.W.; Stone, M.J. Prospects for CD40-Directed Experimental Therapy of Human Cancer. *Cancer Gene Ther.* **2003**, *10*, 1–13. [CrossRef] [PubMed]
42. Yan, C.; Saleh, N.; Yang, J.; Nebhan, C.A.; Vilgelm, A.E.; Reddy, E.P.; Roland, J.T.; Johnson, D.B.; Chen, S.-C.; Shattuck-Brandt, R.L.; et al. Novel Induction of CD40 Expression by Tumor Cells with RAS/RAF/PI3K Pathway Inhibition Augments Response to Checkpoint Blockade. *Mol. Cancer* **2021**, *20*, 85. [CrossRef]
43. Lee, J.R.; Koretzky, G.A. Production of Reactive Oxygen Intermediates Following CD40 Ligation Correlates with C-Jun N-Terminal Kinase Activation and IL-6 Secretion in Murine B Lymphocytes. *Eur. J. Immunol.* **1998**, *28*, 4188–4197. [CrossRef]
44. Liu, J.; Yoshida, Y.; Yamashita, U. Suppressive Effect of Reactive Oxygen Species on CD40-Induced B Cell Activation. *FEBS Lett.* **2007**, *581*, 5043–5049. [CrossRef] [PubMed]
45. Wang, Y.; Du, P.; Jiang, D. Rigosertib Inhibits MEK1–ERK Pathway and Alleviates Lipopolysaccharide-induced Sepsis. *Immun. Inflamm. Dis.* **2021**, *9*, 991–999. [CrossRef] [PubMed]
46. Kowalczyk, J.T.; Wan, X.; Hernandez, E.R.; Luo, R.; Lyons, G.C.; Wilson, K.M.; Gallardo, D.C.; Isanogle, K.A.; Robinson, C.M.; Mendoza, A.; et al. Rigosertib Induces Mitotic Arrest and Apoptosis in RAS-Mutated Rhabdomyosarcoma and Neuroblastoma. *Mol. Cancer Ther.* **2021**, *20*, 307–319. [CrossRef] [PubMed]
47. Radke, K.; Hansson, K.; Sjölund, J.; Wolska, M.; Karlsson, J.; Esfandyari, J.; Pietras, K.; Aaltonen, K.; Gisselsson, D.; Bexell, D. Anti-Tumor Effects of Rigosertib in High-Risk Neuroblastoma. *Transl. Oncol.* **2021**, *14*, 101149. [CrossRef] [PubMed]
48. Baker, S.J.; Cosenza, S.C.; Athuluri-Divakar, S.; Reddy, M.V.R.; Vasquez-Del Carpio, R.; Jain, R.; Aggarwal, A.K.; Reddy, E.P. A Contaminant Impurity, Not Rigosertib, Is a Tubulin Binding Agent. *Mol. Cell* **2020**, *79*, 180–190.e4. [CrossRef] [PubMed]



49. Jost, M.; Chen, Y.; Gilbert, L.A.; Horlbeck, M.A.; Krenning, L.; Menchon, G.; Rai, A.; Cho, M.Y.; Stern, J.J.; Prota, A.E.; et al. Pharmaceutical-Grade Rigosertib Is a Microtubule-Destabilizing Agent. *Mol. Cell* **2020**, *79*, 191–198.e3. [CrossRef] [PubMed]
50. Khachatryan, H.; Olszowy, B.; Barrero, C.A.; Gordon, J.; Perez-Leal, O. Identification of Inhibitors of Tubulin Polymerization Using a CRISPR-Edited Cell Line with Endogenous Fluorescent Tagging of  $\beta$ -Tubulin and Histone H1. *Biomolecules* **2023**, *13*, 249. [CrossRef]
51. Jimeno, A.; Chan, A.; Cusatis, G.; Zhang, X.; Wheelhouse, J.; Solomon, A.; Chan, F.; Zhao, M.; Cosenza, S.C.; Reddy, M.R.; et al. Evaluation of the Novel Mitotic Modulator ON 01910.Na in Pancreatic Cancer and Preclinical Development of an Ex Vivo Predictive Assay. *Oncogene* **2009**, *28*, 610–618. [CrossRef]
52. Navada, S.C.; Silverman, L.R. The Safety and Efficacy of Rigosertib in the Treatment of Myelodysplastic Syndromes. *Expert Rev. Anticancer Ther.* **2016**, *16*, 805–810. [CrossRef]
53. Ohnuma, T.; Lehrer, D.; Ren, C.; Cho, S.Y.; Maniar, M.; Silverman, L.; Sung, M.; Gretz, H.F.; Benisovich, V.; Navada, S.; et al. Phase 1 Study of Intravenous Rigosertib (ON 01910.Na), a Novel Benzyl Styryl Sulfone Structure Producing G2/M Arrest and Apoptosis, in Adult Patients with Advanced Cancer. *Am. J. Cancer Res.* **2013**, *3*, 323–338.
54. Silverman, L.R.; Greenberg, P.; Raza, A.; Olnes, M.J.; Holland, J.F.; Reddy, P.; Maniar, M.; Wilhelm, F. Clinical Activity and Safety of the Dual Pathway Inhibitor Rigosertib for Higher Risk Myelodysplastic Syndromes Following DNA Methyltransferase Inhibitor Therapy. *Hematol. Oncol.* **2015**, *33*, 57–66. [CrossRef] [PubMed]
55. Komrokji, R.S.; Raza, A.; Lancet, J.E.; Ren, C.; Taft, D.; Maniar, M.; Wilhelm, F.; List, A.F. Phase I Clinical Trial of Oral Rigosertib in Patients with Myelodysplastic Syndromes. *Br. J. Haematol.* **2013**, *162*, 517–524. [CrossRef] [PubMed]
56. Ottaiano, A.; Capozzi, M.; De Divitiis, C.; De Stefano, A.; Botti, G.; Avallone, A.; Tafuto, S. Gemcitabine Mono-Therapy versus Gemcitabine plus Targeted Therapy in Advanced Pancreatic Cancer: A Meta-Analysis of Randomized Phase III Trials. *Acta Oncol.* **2017**, *56*, 377–383. [CrossRef]
57. Rees, M.G.; Seashore-Ludlow, B.; Cheah, J.H.; Adams, D.J.; Price, E.V.; Gill, S.; Javaid, S.; Coletti, M.E.; Jones, V.L.; Bodycombe, N.E.; et al. Correlating Chemical Sensitivity and Basal Gene Expression Reveals Mechanism of Action. *Nat. Chem. Biol.* **2016**, *12*, 109–116. [CrossRef] [PubMed]
58. Seashore-Ludlow, B.; Rees, M.G.; Cheah, J.H.; Cokol, M.; Price, E.V.; Coletti, M.E.; Jones, V.; Bodycombe, N.E.; Soule, C.K.; Gould, J.; et al. Harnessing Connectivity in a Large-Scale Small-Molecule Sensitivity Dataset. *Cancer Discov.* **2015**, *5*, 1210–1223. [CrossRef] [PubMed]
59. Hansson, K.; Radke, K.; Aaltonen, K.; Saarela, J.; Mañas, A.; Sjölund, J.; Smith, E.M.; Pietras, K.; Pählman, S.; Wennerberg, K.; et al. Therapeutic Targeting of KSP in Preclinical Models of High-Risk Neuroblastoma. *Sci. Transl. Med.* **2020**, *12*, eaba4434. [CrossRef] [PubMed]
60. Ma, W.W.; Messersmith, W.A.; Dy, G.K.; Weekes, C.D.; Whitworth, A.; Ren, C.; Maniar, M.; Wilhelm, F.; Eckhardt, S.G.; Adjei, A.A.; et al. Phase I Study of Rigosertib, an Inhibitor of the Phosphatidylinositol 3-Kinase and Polo-like Kinase 1 Pathways, Combined with Gemcitabine in Patients with Solid Tumors and Pancreatic Cancer. *Clin. Cancer Res.* **2012**, *18*, 2048–2055. [CrossRef] [PubMed]
61. Navada, S.C.; Fruchtman, S.M.; Odchimar-Reissig, R.; Demakos, E.P.; Petrone, M.E.; Zbyszewski, P.S.; Holland, J.F.; Silverman, L.R. A Phase 1/2 Study of Rigosertib in Patients with Myelodysplastic Syndromes (MDS) and MDS Progressed to Acute Myeloid Leukemia. *Leuk. Res.* **2018**, *64*, 10–16. [CrossRef]
62. Roschewski, M.; Farooqui, M.; Aue, G.; Wilhelm, F.; Wiestner, A. Phase I Study of ON 01910.Na (Rigosertib), a Multikinase PI3K Inhibitor in Relapsed/Refractory B-Cell Malignancies. *Leukemia* **2013**, *27*, 1920–1923. [CrossRef]
63. Olnes, M.J.; Shenoy, A.; Weinstein, B.; Pfannes, L.; Loeliger, K.; Tucker, Z.; Tian, X.; Kwak, M.; Wilhelm, F.; Yong, A.S.M.; et al. Directed Therapy for Patients with Myelodysplastic Syndromes (MDS) by Suppression of Cyclin D1 with ON 01910.Na. *Leuk. Res.* **2012**, *36*, 982–989. [CrossRef]
64. Navada, S.C.; Garcia-Manero, G.; Odchimar-Reissig, R.; Pemmaraju, N.; Alvarado, Y.; Ohanian, M.N.; John, R.B.; Demakos, E.P.; Zbyszewski, P.S.; Maniar, M.; et al. Rigosertib in Combination with Azacitidine in Patients with Myelodysplastic Syndromes or Acute Myeloid Leukemia: Results of a Phase 1 Study. *Leuk. Res.* **2020**, *94*, 106369. [CrossRef] [PubMed]
65. Seetharam, M.; Fan, A.C.; Tran, M.; Xu, L.; Renschler, J.P.; Felsher, D.W.; Sridhar, K.; Wilhelm, F.; Greenberg, P.L. Treatment of Higher Risk Myelodysplastic Syndrome Patients Unresponsive to Hypomethylating Agents with ON 01910.Na. *Leuk. Res.* **2012**, *36*, 98–103. [CrossRef] [PubMed]
66. Nazha, A.; Sekeres, M.A.; Komrokji, R.; Steensma, D.P.; Kantarjian, H.; Roboz, G.; Fenaux, P.; Prebet, T.; Azarnia, N.; Zbyszewski, P.S.; et al. Validation of a Post-Hypomethylating Agent Failure Prognostic Model in Myelodysplastic Syndromes Patients Treated in a Randomized Controlled Phase III Trial of Rigosertib vs. Best Supportive Care. *Blood Cancer J.* **2017**, *7*, 644. [CrossRef] [PubMed]
67. Sanchez-Burgos, L.; Navarro-González, B.; García-Martín, S.; Sirozh, O.; Mota-Pino, J.; Fueyo-Marcos, E.; Tejero, H.; Antón, M.E.; Murga, M.; Al-Shahrour, F.; et al. Activation of the Integrated Stress Response Is a Vulnerability for Multidrug-resistant FBXW7-deficient Cells. *EMBO Mol. Med.* **2022**, *14*, e15855. [CrossRef] [PubMed]
68. Saei, A.; Palafox, M.; Benoukraf, T.; Kumari, N.; Jaynes, P.W.; Iyengar, P.V.; Muñoz-Couselo, E.; Nuciforo, P.; Cortés, J.; Nötzel, C.; et al. Loss of USP28-Mediated BRAF Degradation Drives Resistance to RAF Cancer Therapies. *J. Exp. Med.* **2018**, *215*, 1913–1928. [CrossRef] [PubMed]

69. Haase, D.; Germing, U.; Schanz, J.; Pfeilstöcker, M.; Nösslinger, T.; Hildebrandt, B.; Kundgen, A.; Lübbert, M.; Kunzmann, R.; Giagounidis, A.A.N.; et al. New Insights into the Prognostic Impact of the Karyotype in MDS and Correlation with Subtypes: Evidence from a Core Dataset of 2124 Patients. *Blood* **2007**, *110*, 4385–4395. [CrossRef] [PubMed]
70. Schoch, C.; Kohlmann, A.; Dugas, M.; Kern, W.; Hiddemann, W.; Schnittger, S.; Haferlach, T. Genomic Gains and Losses Influence Expression Levels of Genes Located within the Affected Regions: A Study on Acute Myeloid Leukemias with Trisomy 8, 11, or 13, Monosomy 7, or Deletion 5q. *Leukemia* **2005**, *19*, 1224–1228. [CrossRef]
71. Tanenbaum, M.E.; Medema, R.; Akhmanova, A. Regulation of Localization and Activity of the Microtubule Depolymerase MCAK. *Bioarchitecture* **2011**, *1*, 80–87. [CrossRef] [PubMed]
72. Hood, F.E.; Royle, S.J. Pulling It Together. *Bioarchitecture* **2011**, *1*, 105–109. [CrossRef]

**Disclaimer/Publisher’s Note:** The statements, opinions and data contained in all publications are solely those of the individual author(s) and contributor(s) and not of MDPI and/or the editor(s). MDPI and/or the editor(s) disclaim responsibility for any injury to people or property resulting from any ideas, methods, instructions or products referred to in the content.

## Article

# A Small Molecule Targeting the Intracellular Tyrosine Kinase Domain of ROR1 (KAN0441571C) Induced Significant Apoptosis of Non-Small Cell Lung Cancer (NSCLC) Cells

Amineh Ghaderi <sup>1</sup>, Mohammad-Ali Okhovat <sup>1,†</sup>, Jemina Lehto <sup>2,†</sup>, Luigi De Petris <sup>1,3</sup>, Ehsan Manouchehri Doulabi <sup>1</sup>, Parviz Kokhaei <sup>1,4</sup>, Wen Zhong <sup>1</sup>, Georgios Z. Rassidakis <sup>1</sup>, Elias Drakos <sup>1,5</sup>, Ali Moshfegh <sup>1,2</sup>, Johan Schultz <sup>2</sup>, Thomas Olin <sup>2</sup>, Anders Österborg <sup>1,6</sup>, Håkan Mellstedt <sup>1,\*</sup> and Mohammad Hojjat-Farsangi <sup>1,\*</sup>

<sup>1</sup> Department of Oncology-Pathology, BioClinicum, Karolinska University Hospital Solna, Karolinska Institutet, 171 64 Stockholm, Sweden

<sup>2</sup> Kancera AB, Nanna Svartz Väg 4, 171 65 Solna, Sweden

<sup>3</sup> Thoracic Oncology Center, Karolinska Comprehensive Cancer Center, 171 76 Solna, Sweden

<sup>4</sup> Department of Immunology, Arak University of Medical Sciences, Arak 3848170001, Iran

<sup>5</sup> Department of Pathology, Medical School, University of Crete, 700 13 Heraklion, Greece

<sup>6</sup> Department of Hematology, Karolinska University Hospital Solna, 171 64 Solna, Sweden

\* Correspondence: hakan.mellstedt@ki.se (H.M.); mohammad.hojat-farsangi@ki.se (M.H.-F.); Tel.: +46-735234706 (H.M.); +46-706589809 (M.H.-F.)

† These authors contributed equally to this work.

**Citation:** Ghaderi, A.; Okhovat, M.-A.; Lehto, J.; De Petris, L.; Manouchehri Doulabi, E.; Kokhaei, P.; Zhong, W.; Rassidakis, G.Z.; Drakos, E.; Moshfegh, A.; et al. A Small Molecule Targeting the Intracellular Tyrosine Kinase Domain of ROR1 (KAN0441571C) Induced Significant Apoptosis of Non-Small Cell Lung Cancer (NSCLC) Cells. *Pharmaceutics* **2023**, *15*, 1148. <https://doi.org/10.3390/pharmaceutics15041148>

Academic Editor: Gabriele Grassi

Received: 27 February 2023

Revised: 28 March 2023

Accepted: 31 March 2023

Published: 5 April 2023



**Copyright:** © 2023 by the authors. Licensee MDPI, Basel, Switzerland. This article is an open access article distributed under the terms and conditions of the Creative Commons Attribution (CC BY) license (<https://creativecommons.org/licenses/by/4.0/>).

**Abstract:** The ROR1 receptor tyrosine kinase is expressed in embryonic tissues but is absent in normal adult tissues. ROR1 is of importance in oncogenesis and is overexpressed in several cancers, such as NSCLC. In this study, we evaluated ROR1 expression in NSCLC patients (N = 287) and the cytotoxic effects of a small molecule ROR1 inhibitor (KAN0441571C) in NSCLC cell lines. ROR1 expression in tumor cells was more frequent in non-squamous (87%) than in squamous (57%) carcinomas patients, while 21% of neuroendocrine tumors expressed ROR1 ( $p = 0.0001$ ). A significantly higher proportion of p53 negative patients in the ROR1<sup>+</sup> group than in the p53 positive non-squamous NSCLC patients ( $p = 0.03$ ) was noted. KAN0441571C dephosphorylated ROR1 and induced apoptosis (Annexin V/PI) in a time- and dose-dependent manner in five ROR1<sup>+</sup> NSCLC cell lines and was superior compared to erlotinib (EGFR inhibitor). Apoptosis was confirmed by the downregulation of MCL-1 and BCL-2, as well as PARP and caspase 3 cleavage. The non-canonical Wnt pathway was involved. The combination of KAN0441571C and erlotinib showed a synergistic apoptotic effect. KAN0441571C also inhibited proliferative (cell cycle analyses, colony formation assay) and migratory (scratch wound healing assay) functions. Targeting NSCLC cells by a combination of ROR1 and EGFR inhibitors may represent a novel promising approach for the treatment of NSCLC patients.

**Keywords:** ROR1; NSCLC; small molecules; KAN0441571C; erlotinib; ibrutinib; TTP

## 1. Introduction

Lung cancer is one of the main causes of death in cancer patients [1], and non-small cell lung cancer (NSCLC) accounts for around 85% of lung cancer cases. Current treatments for NSCLC are not sufficiently effective and there is an urgent need for new precision medicines [2].

Receptor tyrosine kinases (RTKs) are phosphotransferase enzymes that are essential for intracellular signal transduction and that are important targets for cancer treatment [3]. ROR1 (receptor tyrosine kinase-like orphan receptor 1), also known as neurotrophic tyrosine kinase receptor-related 1 (NTRKR1), is a transmembrane tyrosine-kinase enzyme encoded by a gene on chromosome 1. ROR1 belongs to the ROR family (ROR1 and ROR2) and was discovered based on amino acid sequence homology to the Trk family of neurotrophin receptors [4]. ROR1 is highly expressed during embryonic development in central

neurons, and respiratory, cardiac, and skeletal tissues, and is essential for the proliferation, differentiation, polarity, and migration of neurons [5]. ROR1 is downregulated after birth but maintains a low expression in a few normal tissues, such as adipocytes, stomach and duodenum, pancreatic islets, parathyroid glands, and early B-cells [6–8]. Wnt5a is a ligand for ROR receptor proteins [9].

ROR1 is, however, expressed in hematologic malignancies and solid tumors, such as chronic lymphocytic leukemia (CLL) [10,11], mantle cell lymphoma (MCL) [12], diffuse large B-cell lymphoma (DLBCL) [13–15], melanoma [16–22], and NSCLC [17,23]. ROR1 is essential for the expansion, survival, epithelial-to-mesenchymal transition (EMT), migration, and metastasis of malignant cells [15,16,24–26]. ROR1 is involved in sustaining the self-renewal of cancer stem cells, and is related to disease activity and resistance to chemotherapy [27–29]. Several key signaling pathways such as PI3K/AKT/mTOR and the canonical/non-canonical Wnt pathways, as well as transcription factors such as CREB and C-Jun, have been proposed to be associated with ROR1 activation [30–35]. In various tumors, such as CLL, breast, and gastric cancers, high expression of ROR1 was associated with advanced disease and short survival [31,36–40].

ROR1 targeting agents, such as siRNA, monoclonal antibodies (mAbs), chimeric antigen receptor-modified T cells (CAR-T), and small molecule inhibitors (SMI), induced significant tumor cell death in hematological malignancies and cancers of epithelial origin [31,36,37,41–45]. The first-in-class ROR1 inhibitor (KAN0439834), which binds to the intracellular tyrosine kinase (TK) domain of ROR1, induced apoptosis of CLL cells and inhibited tumor cell growth in NOD/SCID mice xenotransplanted with human CLL cells [46]. KAN0439834 dephosphorylated ROR1 and inhibited the PI3K/AKT/mTOR pathway [20]. The combination of the ROR1 inhibitor with ibrutinib or erlotinib showed additive effects on pancreatic tumor cell death, compared to treatment with either agent alone [20]. KAN0441571C is the second generation of a ROR1 tyrosine kinase inhibitor (TKI) that induced apoptosis and death of DLBCL cells and small cell carcinoma of the lung, and that acted synergistically with venetoclax on tumor cell apoptosis [13,47].

In this study, ROR1 expression was analyzed in NSCLC tumors from patients as well as in cell lines. The anti-tumor effects of KAN0441571C alone were evaluated *in vitro* and in combination with erlotinib (EGFR inhibitor) and ibrutinib (BTK inhibitor). Erlotinib is a standard drug for the treatment of lung cancer [48] and ibrutinib has been suggested to be evaluated in lung cancer treatment [49,50]. These three drug molecules represent compounds with different mechanisms of action (MOA). Our data indicate that KAN0441571C in combination with EGFR or BTK inhibitors had synergistic apoptotic effects on lung cancer cells.

## 2. Materials and Methods

### 2.1. Patients

In total, 287 surgically resected NSCLC tumor specimens were analyzed for ROR1 expression. The use of patient samples was in accordance with the Declaration of Helsinki and ethically approved by the national ethics committee ([www.etikprovningensmyndigheten.se](http://www.etikprovningensmyndigheten.se)) (accessed on 3 August 2015). Diagnosis was based on the WHO classification [51–53]. Patients were diagnosed, registered, and treated at the Oncology Department of Karolinska University Hospital Solna, Stockholm, Sweden, according to Swedish national guidelines. Based on histology, patients were divided in 3 groups including non-squamous adenocarcinoma ( $n = 157$ ), squamous ( $n = 106$ ), and neuroendocrine (mainly carcinoids) ( $n = 24$ ) tumors (Table S1). Of these, 118, 89, 40, and 9 patients were at stages IA, IB, II, and III-IV, respectively (Table S2).

### 2.2. Immunohistochemical (IHC) Assays

Immunohistochemistry (IHC) staining of ROR1 was performed as previously described [54], using an anti-ROR1 polyclonal antibody (Proteintech, Manchester, UK). ROR1

expression was scored as negative (0), weak (1), or strong (2) according to staining intensity [6]. Slides were blindly scored by 3 independent pathologists.

### 2.3. Lung Cancer Cell Lines

Five ROR1<sup>+</sup> NSCLC cell lines were used for in vitro experiments and obtained from ATCC: NCI-H1975 (EGFR mutated L858R/T790M), NCI-H23 (EGFR wild type (WT)), NCI-HCC827 (EGFR mutated E746-A750 del19), A549 (EGFR WT), and NCI-H1299 (EGFR WT) (Table S3).

### 2.4. ROR1, BTK and EGFR Inhibitors

KAN0441571C, an SMI targeting ROR1, was produced and developed by Kancera AB (Stockholm, Sweden) [13,46]. Erlotinib (EGFR inhibitor) and ibrutinib (BTK inhibitor) were purchased from Selleckchem (Rungsted, Denmark).

### 2.5. Flow Cytometry

Surface ROR1 expression was evaluated by flow cytometry, as previously described [46]. Briefly, cell lines (single-cell suspension) were harvested and washed in 100 µL phosphate buffered saline (PBS) and re-suspended in 100 µL cell staining buffer (BD Biosciences, San Jose, CA, USA). Next, 10<sup>6</sup> cells were incubated with an APC (allophycocyanin)-conjugated anti-ROR1 monoclonal antibody (Miltenyi Biotec, Bergisch Gladbach, Germany) and an isotype-matched antibody (Miltenyi Biotec) for twenty minutes at room temperature (RT). Cells were then washed with cell staining buffer (BD Biosciences) and were prepared for analysis by flow cytometry (Canto II, BD Biosciences). To analyze the data, the FlowJo program was used (Tree Star Inc., Ashland, OR, USA) [13].

### 2.6. Western Blot Analysis

Western blot was used to analyze the expression of proteins, as previously described [46]. Cells were lysed on ice for 1 h by lysis buffer [46]. Supernatants were collected, and a BCA Kit (ThermoFisher Scientific, Bartlett, IL, USA) was used to measure the protein concentration. Next, 10 to 20 µg of the protein lysate was mixed with loading dye and reducing agent, and then loaded onto 8 or 10% polyacrylamide gel (ThermoFisher Scientific). Proteins were separated by electrophoresis and transferred to a polyvinylidene fluoride membrane (Millipore Corporation, Bedford, MA, USA). Membranes were then blocked in 5% bovine serum albumin (BSA) (Santa Cruz Biotechnology, Heidelberg, Germany) or skimmed milk (Sigma-Aldrich, St. Louis, MO, USA). After blocking, membranes were incubated with the primary antibodies at 4 °C for overnight, washed and probed with a peroxidase (HRP)-conjugated mAb (Dako Cytomation, Glostrup, Denmark). Finally, membranes were washed and a chemiluminescence detection system (GE Healthcare, Uppsala, Sweden) was used for protein visualization. The following primary antibodies were used for protein staining: phospho (p) ROR1 (against amino acid residues Ser 652, Tyr 641, 646) [46], anti-ROR1 antibody (R&D Systems, Minneapolis, MN, USA), anti-EGFR and anti-pEGFR (Y1173) antibodies, anti-SRC and anti-p-SRC (Tyr 416) antibodies, anti-AKT and anti-p-AKT (Ser 473) antibodies, anti-mTOR and anti-p-mTOR (Ser 2448) antibodies, anti-cAMP response element-binding protein (CREB) and anti-p-CREB (Ser 133) antibodies, anti-cleaved poly ADP ribose polymerase (PARP) antibody, anti-B-cell lymphoma (BCL)-2 antibody, anti-BAX antibody, anti-myeloid cell leukemia (MCL)-1 antibody, anti-cleaved caspases 3, 8, 9 antibodies (Cell Signaling Technology, Danvers, MA, USA), anti-phosphoinositide 3-kinase (PI3K) p110δ and anti-p-PI3Kp110δ (Tyr 485) antibodies (Santa Cruz), and anti-β-actin antibody (Sigma-Aldrich). Image J 1.44p software (National Institute of Health, Bethesda, MD, USA) was used for the densitometric measurement of proteins. Ratios of phosphorylated protein/total protein were calculated.

### 2.7. MTT Cytotoxicity Assay

The MTT [3-(4,5-Dimethylthiazol-2-yl)-2,5-Diphenyltetrazolium Bromide] assay (Sigma-Aldrich) was applied to evaluate the cytotoxicity of KAN0441571C, ibrutinib, and erlotinib.

Briefly, 20,000 lung cancer cells were cultured in 96 well plates in 200  $\mu$ L of RPMI-1640 (ThermoFisher Scientific) (triplicates) containing 10% FBS and the drugs (diluted in DMSO). The maximum concentration of DMSO in the medium was 1%. Cells were then incubated at 37 °C for several time points (24, 48, and 72 h), followed by adding 20  $\mu$ L of 5 mg/mL of the MTT solution to each well, and then further incubated for 4 h at 37 °C. Next, 100 microliters of MTT stop solution (10% SDS in 0.01 M HCL) was then added to wells and incubated for 2–4 h at 37 °C. Cells treated with DMSO alone were used as the control. Optical density (OD) was defined using a plate reader at 570 nm. The effects of the drugs in vitro on the apoptosis (additive, synergistic, or antagonist effects) of the combined treatment of KAN0441571C with erlotinib or ibrutinib was evaluated by the Chou–Talalay method using the CompuSyn software (Combosyn Inc., New York, NY, USA) [55].

### 2.8. Apoptosis Assay (Flow Cytometry)

Lung cancer cells were incubated with the drugs and cultured in 6-well plates ( $10^6$ /well) at 37 °C for 24 h. After incubation, cells were prepared and stained for apoptosis assay as previously described [13,46].

### 2.9. Immunofluorescence (IF) Assay

The immunofluorescent (IF) assay was completed as previously described [46]. Briefly, cell lines were cultured on a sterile 8-well glass slide (BD Biosciences) for 24 hours to form a monolayer. Next, 4% formaldehyde was used to fix cells (15 min), which were then washed with PBS and blocked for 2 h in buffer containing 0.01% sodium azide, 2% bovine serum albumin, and 1% Tween 20 in PBS buffer. Cells were incubated with an anti-ROR1 antibody (2  $\mu$ g/mL) (Sigma-Aldrich) and a non-specific antibody (mouse IgG) (eBioscience, San Diego, CA, USA) for 24 h at 4 °C, washed with PBS, and then treated with Alexa Flour 488-conjugated goat anti-mouse IgG (1:200) (ThermoFisher Scientific) for 1 h. After washing, the cell nuclei were stained with mounting media (VectaShield H-1000) containing 4',6-diamidino-2-phenylindole (DAPI) (Vector Laboratories, Burlingame, CA, USA). A Zeiss Axioplan2 fluorescence microscope (Oberkochen, Germany) with a 63 X objective lens and the ZEN software (Carl Zeiss Microscopy, Munich, Germany) was used to take pictures.

### 2.10. Colony Formation Assay

Two-hundred cells per well were seeded in 6 well plates (BD Biosciences) and incubated at 37 °C overnight. KAN0441571C and DMSO alone (control) were added and the cells were incubated for 72 h at 37 °C. The medium was removed and the cells were washed with PBS. Fresh medium was added and cell colonies were maintained in culture until control cultures were confluent. The medium was then removed and the colonies were stained with 4% methylene blue/MeOH (Sigma-Aldrich) for 30 min. Finally, the cells were washed with water and the plates were left to dry. Colonies were counted and the relative colony count to DMSO control was calculated using the following formula: plating efficiency (%) = number of colonies (treated)/average number of colonies (DMSO)  $\times$  100. For each cell line, the assay was repeated 2–4 times.

### 2.11. Scratch Wound Healing Assay (Migration Assay)

Lung cancer cells were seeded in 96-well plates ( $6 \times 10^4$  cells/well) and incubated overnight at 37 °C. When cells reached >90% confluence, the IncuCyte<sup>®</sup> wound maker tool (Sartorius AG, Gottingen, Germany) was used to scratch all wells uniformly. Cell migration in the presence of KAN0441571C was assessed by measuring the migration of cells into the scraped wound area. The wound-healing process was captured after 0, 24, and 48 h by IncuCyte<sup>®</sup> S3 Live-Cell Analysis System (Sartorius). Three different parameters, namely wound width ( $\mu$ M), wound confluence (%), and relative wound density (%), were determined by scratch wound cell migration analysis using IncuCyte<sup>™</sup> Software. For each cell line, the test was done in quadruplicate.

### 2.12. Cell Cycle Analysis

For cell cycle analysis, 100,000 A549 cells/well were seeded in 6-well plates and incubated at 37 °C overnight. KAN0441571C was added (500–5000 nM) in medium with 10% FBS and incubated for a further 24 h. DMSO 1% was used as the control. After incubation, the medium was removed and the wells were washed once with PBS. Adherent cells were detached by trypsin, transferred to tubes, and washed twice with PBS. Next, 700 µL of ice-cold 100% ethanol was added drop-wise while vortexing the tube. The tubes were incubated for 30 min to 1 h on ice and kept at 4 °C for 24 h. For propidium iodide (PI) staining, the cells were centrifuged at 1000 g at 4 °C for 10 min. The supernatant was discarded and the cells were washed with 250 µL cold PBS with 2% BSA. The samples were then centrifuged at 1000 g, at 4 °C for 10 min. The cells were re-suspended in 300 µL of staining buffer containing 40 µg/mL PI, 100 µg/mL RNase A, and 0.1% Triton X 100/PBS. The cells were transferred to FACS tubes, incubated for 20 min in RT in the dark, and then analyzed by flow cytometry (Navios, Beckman Coulter, Indianapolis, IN, USA). Data was analyzed with the Kaluza software (Navios, Beckman Coulter).

### 2.13. Statistical Methods

For comparison of ROR1 expression in the patient groups, the Kruskal–Wallis test was applied. The Mann–Whitney U test was used to check the association of variables among various groups (R version 3.3.2, The R Foundation for Statistical Computing, Vienna, Austria). The Chi-square test was utilized to find differences in the expression of ROR1. Time to progression (TTP) from diagnosis was demonstrated by the Kaplan–Meier method. Overall survival (OS) was determined from the time of diagnosis to death or last follow-up. Statistical significance was assessed by the log-rank test. For multivariable analyses, Cox regression models were used. Student's t-test and Mann–Whitney U test were utilized for comparison of EC<sub>50</sub> values (GraphPad Software, Inc., La Jolla, CA, USA). *p*-values < 0.05 were considered significant. Asterisks represent *p* values of: \*: 0.01 to 0.05, \*\*: 0.001 to 0.01, \*\*\*: <0.001.

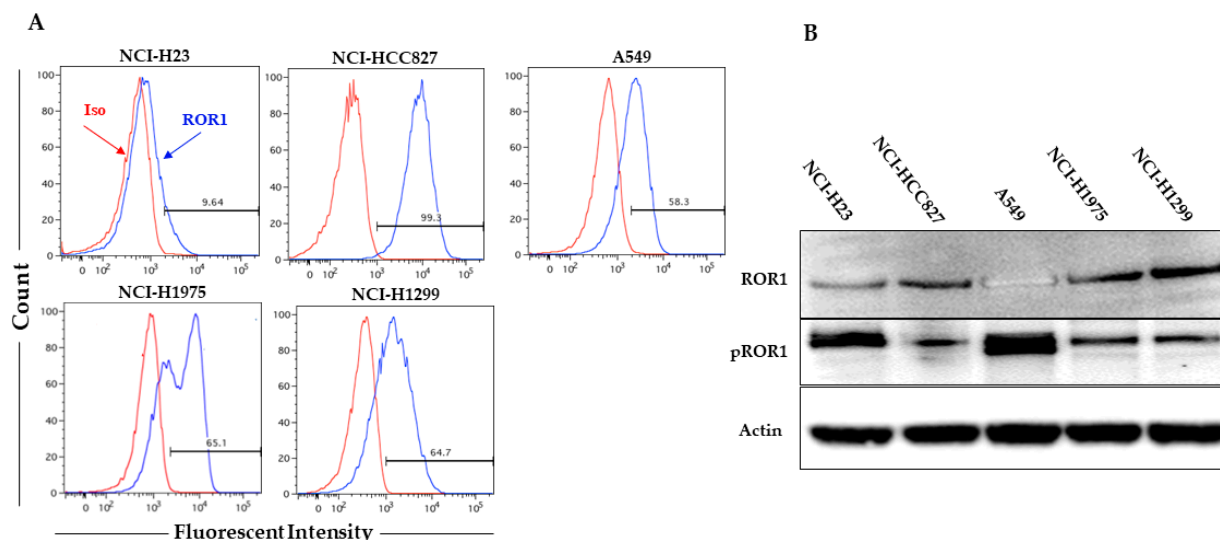
## 3. Results

### 3.1. ROR1 Expression in Subtypes of Lung Cancer and Cell Lines

ROR1 expression was significantly higher in non-squamous (136/157, 86%) and squamous (60/106, 57%) lung cancer patients compared to 5/24 (21%) patients with neuroendocrine tumors (*p* = 0.0001) (Table S1). No association between ROR1 expression and pathological disease stage was noted, irrespective of the histopathological subtype (Table S2). In adenocarcinoma, no statistical association between ROR1 expression and age, grading, smoking status, and overall survival was seen (Table S4). However, a trend to shorter TTP in ROR1<sup>+</sup> vs ROR1<sup>-</sup> patients was found (*p* = 0.09) (Figure S1). In addition, a significant higher proportion of p53 negative cases (63%) was seen in the ROR1<sup>+</sup> group as compared to p53 positive patients (25%) (*p* = 0.03) (Table S4).

In patients with squamous NSCLC, no statistically significant association was observed between ROR1 expression and age, stage, grading, smoking status, p53 expression, and overall survival.

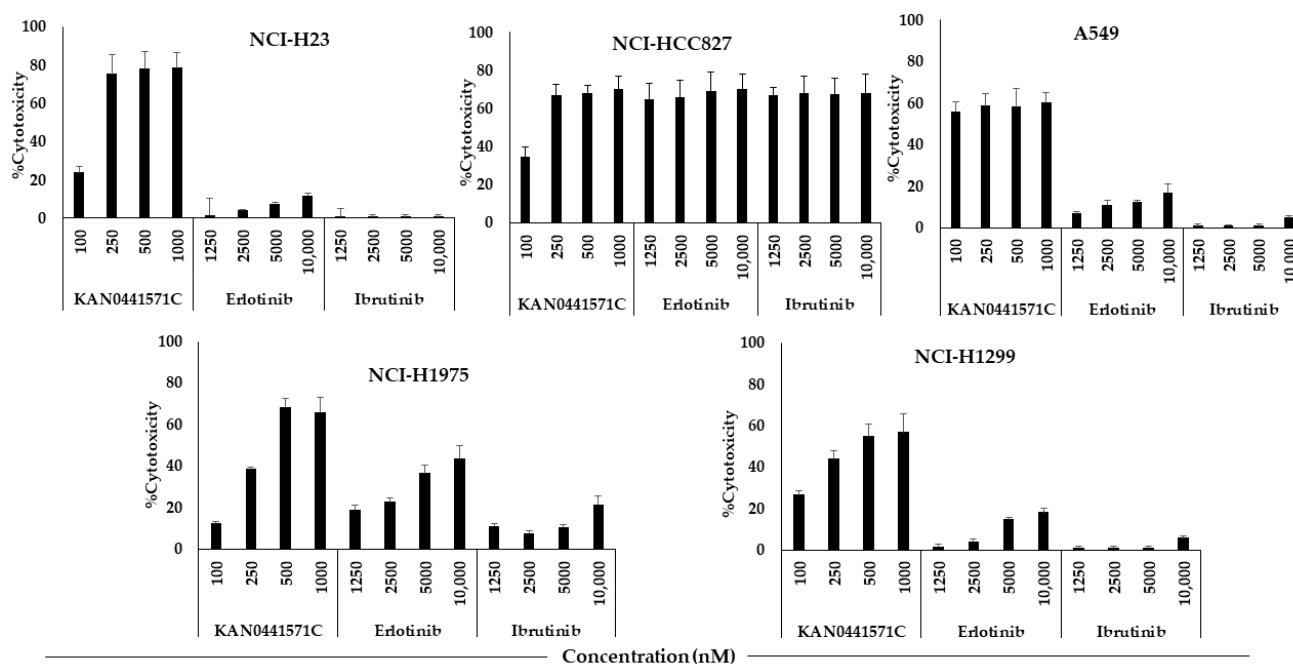
Surface ROR1 expression was detected in all cell lines with the exception for NCI-H23 (Figure 1A). However, using Western blot and IF, ROR1 was shown to be expressed in all cell lines (Figure 1B and Figure S2). ROR1 was phosphorylated in all cell lines (Figure 1B).



**Figure 1.** (A) Surface staining for ROR1 (flow cytometry) (red line: isotype control; blue line: anti-ROR1 antibody); (B) Western blot for ROR1 and pROR1 expression (130 KDa) in 5 lung cancer cell lines. Actin was used as internal control.

### 3.2. Cytotoxicity of KAN0441571C, Ibrutinib and Erlotinib in Lung Cancer Cell Lines

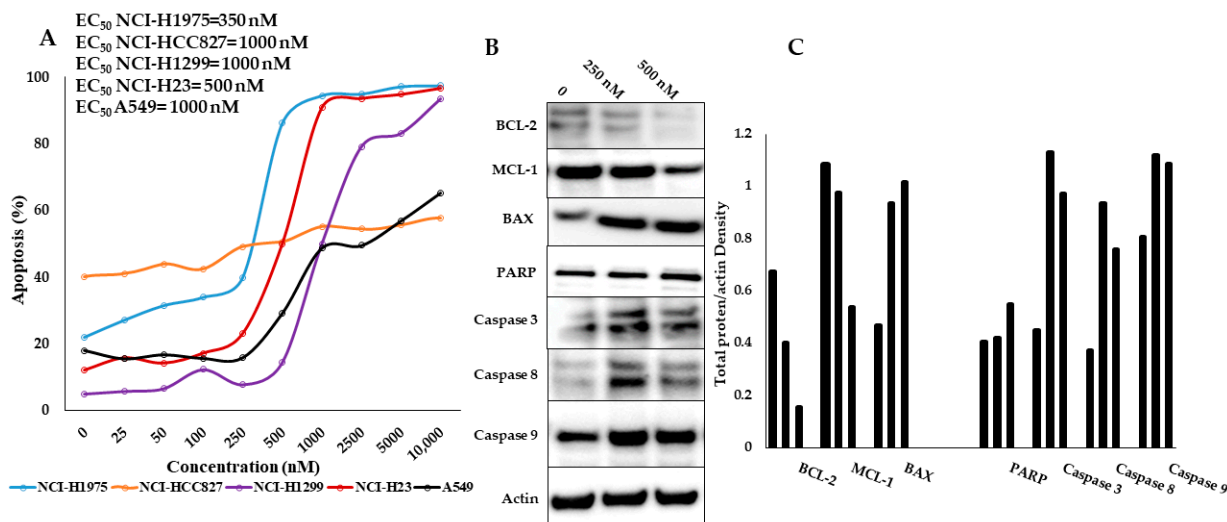
KAN0441571C induced a dose-dependent cytotoxicity (MTT) in all cell lines with the exception for A549. The cytotoxic effect of KAN0441571C varied between cell lines. In comparison to ibrutinib and erlotinib, the cytotoxic effect of KAN0441571C was similar or significantly better. Both erlotinib and ibrutinib induced the highest cytotoxic effect in HCC827 with EGFR Del19 (mutated E746-A750) compared to cell lines without EGFR Del19 or of the EGFR wild-type. However, in the HCC827 cell line, a dose-dependency within the used concentrations of erlotinib and ibrutinib could not be seen (compared to KAN0441571C in A549) (Figure 2). EC<sub>50</sub> values for erlotinib and ibrutinib were >10,000 nM for all cell lines with the exception for NCI-HCC827, where EC<sub>50</sub> was <1250 nM for both erlotinib and ibrutinib (Figure 2).



**Figure 2.** Cytotoxicity (MTT) (72 h) in 5 lung cancer cell lines incubated with various concentrations of KAN0441571C, erlotinib, or ibrutinib.



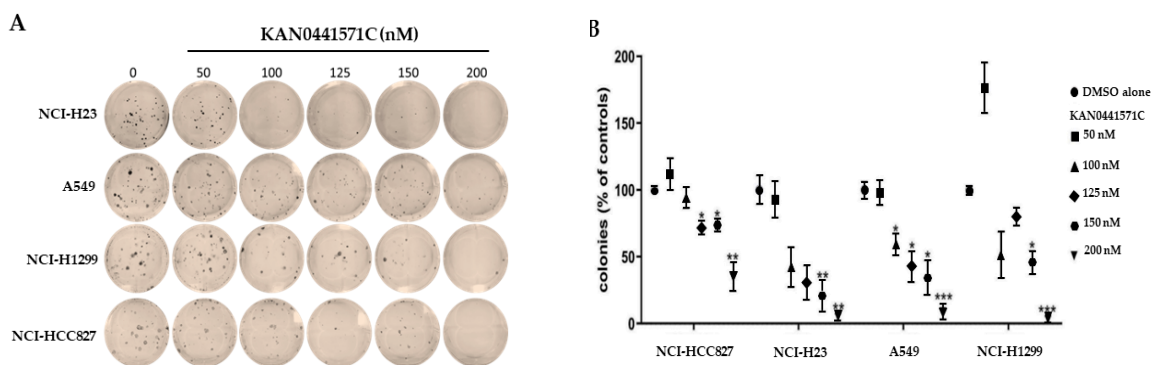
Apoptosis was confirmed by Annexin V/PI staining (Figure 3A). A dose-response relationship was noted for all cell lines with the exception for NCI-HCC827 (compared with MTT for KAN0441571C, which seemed to be the most resistant in the Annexin V/PI assay). EC<sub>50</sub> values are also shown in Figure 3A. Apoptosis was accompanied by downregulation of BCL-2, and MCL-1, as well as by cleavage of PARP and caspases 3, 8, and 9, while the BAX protein was upregulated (Figure 3B,C). Caspase 8 and 9 cleavage indicates activation of both the extrinsic and intrinsic apoptotic pathways.



**Figure 3.** (A) Apoptosis (Annexin V/PI) of KAN0441571C in 5 lung cancer cell lines (EC<sub>50</sub> values are shown to the upper left). (B) Western blots of apoptotic proteins BCL-2, MCL-1, BAX, PARP, and caspases-3, 8, and 9 after 24 h of incubation with KAN0441571C in NCI-H23 cells. One representative data of three individual experiments are shown. (C) Densitometric measurements of protein bands in Figure 3B expressed as total protein/actin intensity.

### 3.3. Colony Formation Assay

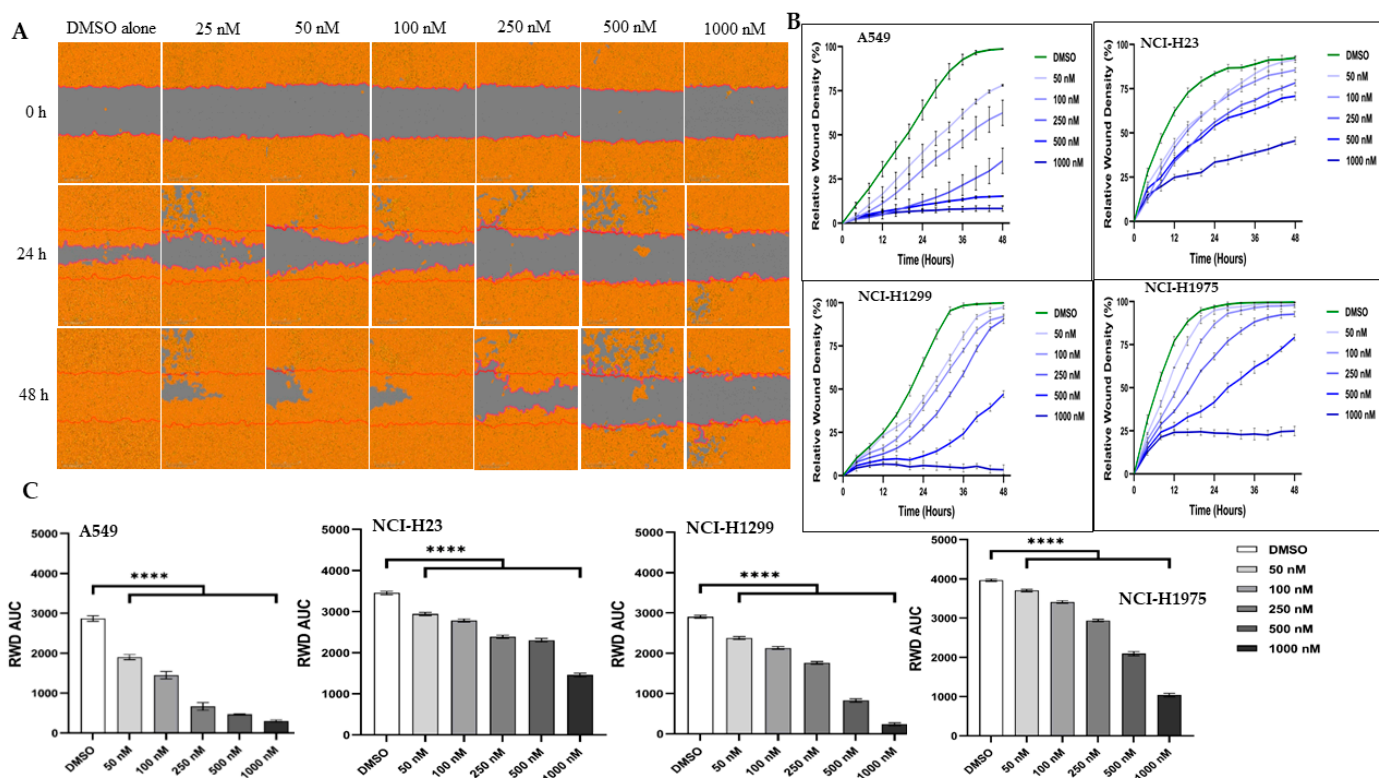
In a colony tumor cell formation assay (72 h), KAN0441571C reduced the ability of A549, NCI-HCC827, NCI-H23, and NCI-H1299 cells at concentrations ranging from 100 to 200 nM to form colonies, indicating that the drug compromised the clonogenic capacity of the cells (Figure 4) (NCI-H1975 was not included in this assay). Colonies were completely abolished at 200 nM of KAN0441571C in all cell lines. In H1299, only few colonies were seen at 125 nM. These findings indicate that inhibition of ROR1 may irreversible prevent NSCLC cells to recover after exposure to ROR1 inhibition.



**Figure 4.** (A) Lung cancer cell lines (NCI-H23, A549, NCI-H1299, and NCI-HCC827) incubated with KAN0441571C (72 h) prevented formation of cell colonies in a dose-dependent manner (representative images). (B) Relative quantification of colonies (mean ± SEM) at various concentrations of KAN0441571C. \*  $p < 0.05$ , \*\*  $p < 0.01$ , \*\*\*  $p < 0.001$  (one-way ANOVA).

### 3.4. Migration of Lung Cancer Cells

The migratory ability of lung cancer cells was analyzed by the scratch wound healing assay (Figure 5 and Figure S3). After 48 h of incubation with KAN0441571C, untreated (DMSO alone) cells proliferated and migrated as expected. KAN0441571C inhibited migration in a dose- and time-dependent manner. At 1  $\mu\text{M}$ , tumor cell mobility was completely abrogated.



**Figure 5.** KAN0441571C inhibited migration of lung cancer cell lines in the scratch wound healing assay. (A) Migration of A549 was inhibited as shown by images acquired after 0, 24, and 48 h of incubation with different concentrations of KAN0441571C. Images of 1 representative experiment out of 4 for each cell line is shown. (B) Rate of wound closure (relative wound density) of lung cancer cells. The Incucyte Zoom Imager Software Analyzer was used to count the number of lung cancer cells during 48 h of incubation with of KAN0441571C (25–1000 nM). DMSO used as control. (C) Reduction (mean  $\pm$  SEM) of cell migration (RWD AUC) after treatment with KAN0441571C (0–1000 nM) in 4 cell lines. \*\*\*\*  $p < 0.0001$ .

### 3.5. Cell Cycle Analysis

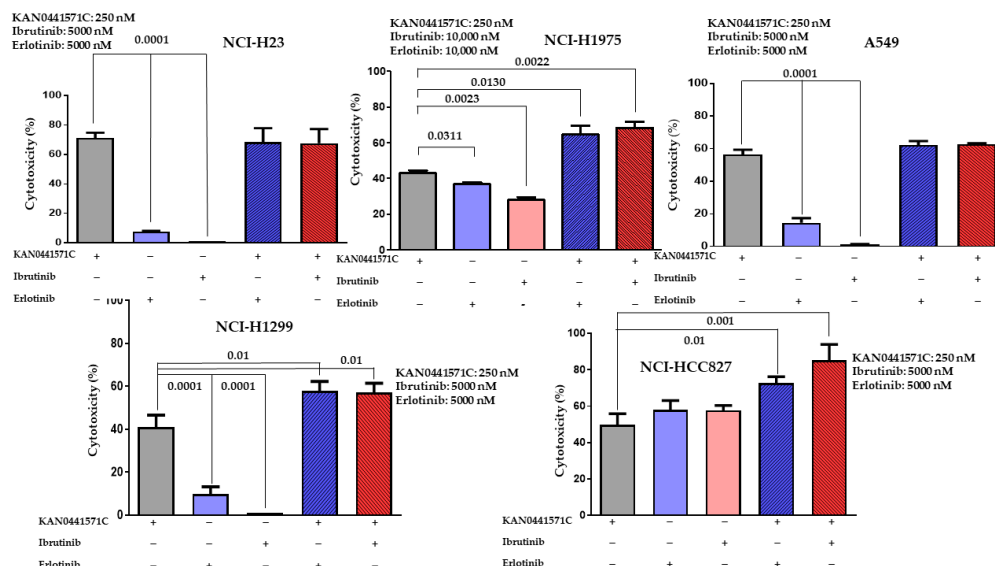
The cell cycle profile of the lung cancer cell line A549 cell was analyzed after treatment with KAN0441571C. A decrease in S phase cells, including the accumulation of G2/M phase cells and augmented cell death (sub-G1 cells), was noted with increasing concentrations of KAN0441571C in 24 h cell culture. A decrease in G1 cells was also seen at the highest concentration of KAN0441571C. Data indicate that replicating cells might be vulnerable to cell death at exposure to the ROR1 inhibitor KAN0441571C and/or that KAN0441571C induced a cytostatic effect in lung cancer cells preventing exit from G2/M phase and cell proliferation (Figure S4).

### 3.6. Effect of KAN0441571C on Signaling Molecules

As expected [56], KAN0441571C induced dephosphorylation of ROR1 in a dose-dependent manner, as well as EGFR, SRC, PI3K110 $\delta$ /AKT/mTOR (non-canonical Wnt pathway), and CREB in the NCI-H23 lung cancer cell line (Figure S5).

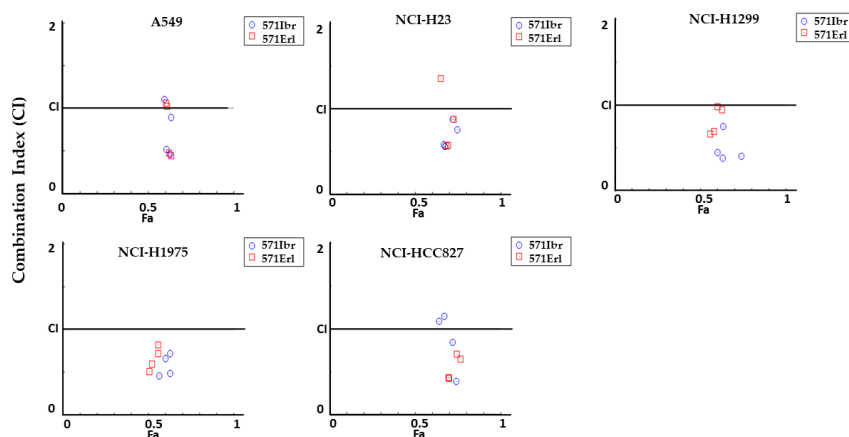
### 3.7. Effects on Tumor Cell Death of KAN0441571C Alone and in Combination with Ibrutinib or Erlotinib

KAN0441571C induced a significant cell death (MTT) in all cell lines, at a concentration of 250 nM. For erlotinib and ibrutinib, significantly higher concentrations were required) 5000–10,000 nM) (Figure 6). The cytotoxic effect of KAN0441571C was significantly higher than that of erlotinib and ibrutinib with the exception of NCI-HCC827 (EGFR mutated E746-A750, Del19). When KAN0441571C was combined with ibrutinib or erlotinib, cytotoxicity increased significantly in 3 out of 5 cell lines.



**Figure 6.** Cytotoxicity (MTT) (mean ± SEM) of five lung cancer cell lines incubated with KAN0441571C in combination with ibrutinib or erlotinib. Results of 3 independent experiments are shown. The concentration of the respective drug are shown for each cell line (–: No inhibitor added, +: inhibitor added).

To further assess the efficacy (antagonism, addition, or synergism) of the combinations of KAN0441571C/erlotinib and KAN0441571C/ibrutinib on apoptosis, the Chou–Talalay method was applied. The combinations had synergistic or additive apoptotic effect in all tested lung cancer cell lines (Figure 7 and Figure S6A,B).



**Figure 7.** Combination index (CI) plots for apoptosis (Annexin V/PI) in lung cancer cell lines incubated (24 h) with a combination of KAN0441571C (250 nM) with ibrutinib (571Ibr) (blue symbols) or erlotinib (571Erl) (red symbols) (5000–10,000 nM, see Figure 6). Values across Fa in lung cancer cells are shown, where Fa is the % of cell death. CI < 1 synergistic effect; CI = 1 additive effect; CI > 1 antagonistic effect (Chou–Talalay method).

#### 4. Discussion

In the present study, we analyzed ROR1 expression in primary tumors of patients with surgically resected NSCLC. In non-squamous and squamous carcinomas, 86% and 56%, respectively, expressed ROR1, while in neuroendocrine tumors only about 20% exhibited ROR1. No relationship between ROR1 expression and age, stage, tumor grading, smoking status, and overall survival was observed in adenocarcinoma or squamous NSCLC patients. However, an inverse relationship to p53 expression in non-squamous NSCLC ( $p = 0.03$ ) was seen. Such a finding might be expected as low or no p53 expression is associated with a poor outcome in malignancies [57]. There was also a trend towards shorter TTP in ROR1<sup>+</sup> adenocarcinoma NSCLC patients compared to ROR1<sup>-</sup> patients.

KAN0441571C prevented ROR1 phosphorylation and inactivated both Wnt non-canonical pathway molecules and the transcription factor CREB. Apoptosis was induced in NSCLC cell lines both through the extrinsic and intrinsic pathways, including downregulation of pro-survival molecules (BCL-2 and MCL-1) and upregulation of the pro-apoptotic BAX protein. The ROR1 inhibitor was more effective than an EGFR inhibitor in inducing apoptosis. There seemed to be no relation between the response to KAN0441571C and mutations of EGFR, K-Ras, or p53. The combination of KAN0441571C with erlotinib or ibrutinib had synergistic apoptotic effects.

ROR1 is dysregulated during tumorigenesis and is constitutively expressed and phosphorylated in various tumors [13,29,31,39,58]. ROR1 has been shown to be a prognostic marker in several tumors [59]. A high level of ROR1 expression was noted to be associated with an aggressive and poor prognosis disease in, for example, CLL, DLBCL, MCL, ALL, as well as in ovarian, breast, pancreatic, gastric, colorectal, and lung cancers [15,18,21,32,59–63]. In meta-analyses, high ROR1 expression was found to relate to worse overall survival in hematologic malignancies and solid tumors [59,64]. The data may support an important role of ROR1 in cancer.

ROR1 is involved in a lot of functions in tumor cells, such as proliferation, survival, migration, stemness, epithelial to mesenchymal transition (EMT), chemotaxis, and drug resistance, through the planar cell polarity (PCP) activation and Ca<sup>2+</sup> dependent pathways of non-canonical Wnt signaling [25,26,65,66]. Binding of Wnt5a to ROR1 stimulates several signaling pathways, such as PI3K/AKT and RhoA/Rac1 GTPases, activating the transcriptional coactivator YAP/TAZ or polycomb complex protein BMI-1 to sustain stemness, metastatic ability, and drug resistance [66].

ROR1 has been described as an oncogenic molecule of interest for the development of targeted therapy for antibody-drug conjugates [67], chimeric antigen receptor T-cells (CAR-T) [68,69], mAbs [27], and bi-specific T-cell engager (BiTE) [70], as well as SMIs targeting the intracellular [20,56] or extracellular parts of ROR1 [42,43].

Targeting ROR1 by small molecules and mAbs has been shown to be an effective therapeutic approach in pre-clinical and clinical studies in various malignancies, such as CLL, MCL, lung, breast cancers, etc. [27,43,46,67,71]. The silencing of ROR1 significantly inhibited the proliferation of tumor cells in lung adenocarcinoma via the PI3K/AKT/mTOR signaling pathway [72,73]. NSCLC is still a major therapeutic challenge and there is a great need for new treatment alternatives.

In previous reports, we have described the effects of two small-molecule ROR1 inhibitors (KAN0439834 and KAN0441571C) targeting the cytoplasmic tyrosine kinase domain that dephosphorylated ROR1 and induced tumor cell apoptosis [13,20,46,74]. In the current study, we analyzed the effects of KAN0441571C in lung cancer cells. We also compared its tumor cell killing effect with erlotinib, which is one of the current drug options for the treatment of NSCLC patients with EGFR exon 19 deletions or exon 21 L858R substitution mutational status [75]. KAN0441571C was more effective than erlotinib in inducing apoptosis of lung cancer cells, irrespective of EGFR mutations. The combination of the two inhibitors had significantly improved the synergistic apoptotic effects, in the NCI-H1299, NCI-H1975, and NCI-HCC827 cell lines.

NKX2-1, a lineage-specific transcription factor, has been noted to be essential for the development of peripheral parts of the lung and in morphogenesis, and it is overexpressed in lung adenocarcinomas [24,76,77]. NKX2-1 induced ROR1 transcription and was critically involved in the maintenance of a balance between the pro-apoptotic p38 pathway and the pro-survival PI3K/AKT signaling pathway [16]. Furthermore, activated ROR1 binds to SRC and activates it. SRC activation inhibits PTEN activity and results in AKT activation. An association between EGFR mutations and NKX2-1 expression has been described in lung adenocarcinoma [78]. ROR1 has also been shown to form heterodimers with EGFR, promoting the maintenance of lung cancer cell survival [16,79]. High ROR1 expression in EGFR T790M NSCLC patients was related to an inferior progression-free survival in erlotinib-treated patients compared to those with low ROR1 expression, substantiating a role of ROR1 in the disease pathobiology and supporting that the inhibition of ROR1 might add to the therapeutic effect [79]. Overall, the data indicate a role of ROR1 expression in lung adenocarcinoma, which may be independent of ROR1 kinase activity [16].

ROR1 inhibition by KAN0441571C blocked the phosphorylation of ROR1 and EGFR. Dephosphorylation of EGFR may be due to the inhibition of the phosphorylation of ROR1, resulting in the inactivation of the ROR1-EGFR dimer and the suppression of survival signals [16,80].

In addition, to target the TK domain of ROR1 by KAN0441571C, ROR1 targeting SMIs against other extracellular and intracellular regions of ROR1 have been produced [42,43,46]. ARI-1 ((R)-5,7-bis (methoxymethoxy)-2-(4-methoxyphenyl) chroman-4-one) is a novel ROR1 inhibitor targeting the external CRD domain of ROR1, preventing NSCLC cell proliferation, migration, as well as inactivating the PI3K/AKT/mTOR signaling pathway [42]. ARI-1 decreased the growth of ROR1-expressing NSCLC in vitro and in vivo with no significant side effects in mice [42]. This inhibitor seemed to interrupt Wnt5a binding to ROR1 via CRD domain blockage.

Strictinin, isolated from *Myrothamnus flabellifolius*, targeted the intracellular region of ROR1 and induced apoptosis of triple-negative breast cancer cells (TNBC) through the intrinsic apoptotic pathway. Therefore, this inhibitor prevented ROR1 activation via inhibiting the binding to Wnt5a, dephosphorylating AKT and GSK3 $\beta$ , and blocking ROR1 signaling in a  $\beta$ -catenin-independent PI3K/AKT/GSK3 $\beta$  signaling pathway [43].

In contrast to AR-1 and strictinin, KAN0441571C may not directly inhibit the binding of Wnt5a to ROR1, but instead might change the conformational structure of ROR1 [42,43], which thus prevents ROR1 from binding with Wnt5a. The treatment of human cells with KAN0441571C has also been shown to dephosphorylate SRC, which binds to phosphorylated intracellular regions of ROR1 [81].

In conclusion, ROR1 is expressed in NSCLC and seems to be of importance in the pathobiology of the disease. A ROR1 small molecule inhibitor (KAN0441571C) was highly effective in inducing apoptosis of NSCLC cells, and was superior to erlotinib and ibrutinib. The combination of KAN0441571C with erlotinib had significant synergistic cytotoxic effects. The development of new targeted drugs with other MOAs than those clinically available is warranted to improve the prognosis in NSCLC patients. A ROR1 inhibitor may be a new promising drug candidate.

**Supplementary Materials:** The following supporting information can be downloaded at: <https://www.mdpi.com/article/10.3390/pharmaceutics15041148/s1>, Figure S1: Time to progression (TTP) in non-squamous NSCLC patients with no ROR1 expression (red line) ( $n = 16$ ) compared to those positive for ROR1 (green line) ( $n = 123$ ) ( $p = 0.09$ ). Figure S2: Immunofluorescent staining of lung cancer cell lines using anti-ROR1 antibodies (20 $\times$ ). Lung cancer cells were cultured on a sterile 8-well glass slide for 24 h, fixed, blocked in PBS containing BSA, and then incubated with an anti-ROR1 antibody for 24 h at 4  $^{\circ}$ C, and finally treated with Alexa Flour 488-conjugated goat anti-mouse IgG for 1 h. After washing, the cell nuclei were stained with mounting media containing DAPI. A Zeiss Axioplan2 fluorescence microscope was used. Figure S3: Migration of lung cancer cell lines (NCI-H1299 and NCI-H1975) in the wound scratch healing assay. Migration of lung cancer cell lines was inhibited by treatment with 50–1000 nM of KAN0441571C for 0, 24, and 72 h.

Figure S4: Cell cycle profiles of A549 lung cancer cells treated with KAN0441571C. KAN0441571C induced reduction of S phase cells and accumulation in the G2 phase with a simultaneous increased cell death. Representative histograms (A) and quantifications (B) of 3 independent experiments. Figure S5: Effect of KAN0441571C on ROR1-associated signaling molecules (Western blot) in the lung cancer cell line NCI-H23 (4 h). ROR1, EGFR, SRC, AKT, PI3K110 $\delta$ , mTOR, and CREB were dephosphorylated. One of three representative experiments is shown. Figure S6A: Apoptosis (Annexin V/PI) in 5 lung cancer cell lines incubated with a combination of KAN0441571C (250 nM) with erlotinib (5000–10,000 nM). For each combination, data are shown as combination index plot (CI), isobologram, and dose reduction index (DRI). Combination index (CI) plot (Fa-CI plot): values across Fa in lung cancer cells, where Fa is the % of cell death. CI < 1 synergistic effect; CI = 1 additive effect; CI > 1 antagonistic effect. (Chou–Talalay) method). Figure S6B: Apoptosis (Annexin V/PI) in 5 lung cancer cell lines incubated with a combination of KAN0441571C (250 nM) with ibrutinib (5000–10,000 nM). For each combination, data are shown as combination index plot (CI), isobologram, and does reduction index (DRI). Combination index (CI) plot (Fa-CI-plot): values across Fa in lung cancer cell lines, where Fa is the % of cell death. CI < 1 synergistic effect; CI = 1 additive effect; CI > 1 antagonistic effect. (Chou–Talalay method). Table S1: Relation between ROR1 expression and subgroups of lung cancer patients. Table S2: ROR1 expression by pathological stage (7th TNM). Table S3: Characteristics of the ROR1 positive lung cancer cell lines. Table S4: Clinical characteristics of adenocarcinoma NSCLC patients ( $n = 139$ ) in relation to ROR1 expression.

**Author Contributions:** A.G., M.-A.O., J.L., E.M.D., P.K. and W.Z. performed experiments, analyzed data and finalized the manuscript. J.S. and T.O. produced the small molecule and finalized the manuscript. L.D.P. and G.Z.R. provided clinical material, analyzed data and finalized the manuscript. E.D. and A.M. provided clinical material, analyzed data and finalized the manuscript. A.Ö., H.M. and M.H.-F. designed the study, performed experiments, supervised the study and wrote the manuscript. All authors have read and agreed to the published version of the manuscript.

**Funding:** This research was funded by Åke Olsson Foundation for hematology research, grant numbers 2017-00436; 2019-00396 (M.H.-F.). The Cancer and Allergy Foundation, grant numbers 2016/5, 2017/63, 2018/63, 2019/189, 2020/258 (A.Ö.); 2017/64, 2018/140, 2019/194, 2020/260 (H.M.). The Cancer Society in Stockholm, grant numbers 151313, 184203 (A.Ö.); 144142, 164122 (H.M.). The Swedish Cancer Society, grant numbers CAN 2015/408, CAN 2018/499 (A.Ö.). AFA Insurance, grant number 130054 (A.Ö.). The Karolinska Institutet Foundation (A.Ö., H.M.) and Region Stockholm, grant numbers 20150070, 20180030 (A.Ö.).

**Institutional Review Board Statement:** The study was conducted in accordance with Good Clinical Practice guidelines and the Declaration of Helsinki. All patients or their legally acceptable representative, or both (if possible), provided written informed consent. The study was authorized by the National Ethics Authority of Sweden ([www.etikprovningmyndigheten.se](http://www.etikprovningmyndigheten.se)) (accessed on 3 August 2015) (approval code: 2016/2506-32 and date of approval: 20 December 2016).

**Informed Consent Statement:** Informed consent was obtained from all subjects involved in the study.

**Data Availability Statement:** Not applicable.

**Acknowledgments:** For excellent secretarial assistance we thank Leila Relander.

**Conflicts of Interest:** J.L. was employed by Kancera AB at the time of the project experiments and manuscript preparation, J.S. is employee and shareholder of Kancera AB. T.O. is founder, employee, and shareholder of Kancera AB. P.K. and M.H.F. are shareholders of Kancera AB. H.M. is founder and shareholder of Kancera AB and received research grant and honorarium from Kancera AB. The remaining authors declare no conflict of interest.

## References

1. Sung, H.; Ferlay, J.; Siegel, R.L.; Laversanne, M.; Soerjomataram, I.; Jemal, A.; Bray, F. Global Cancer Statistics 2020: GLOBOCAN Estimates of Incidence and Mortality Worldwide for 36 Cancers in 185 Countries. *CA Cancer J. Clin.* **2021**, *71*, 209–249. [CrossRef] [PubMed]
2. Siegel, R.; DeSantis, C.; Virgo, K.; Stein, K.; Mariotto, A.; Smith, T.; Cooper, D.; Gansler, T.; Lerro, C.; Fedewa, S.; et al. Cancer treatment and survivorship statistics, 2012. *CA Cancer J. Clin.* **2012**, *62*, 220–241. [CrossRef] [PubMed]
3. Hojjat-Farsangi, M. Small-Molecule inhibitors of the receptor tyrosine kinases: Promising tools for targeted cancer therapies. *Int. J. Mol. Sci.* **2014**, *15*, 13768–13801. [CrossRef]

4. Masiakowski, P.; Carroll, R.D. A novel family of cell surface receptors with tyrosine kinase-like domain. *J. Biol. Chem.* **1992**, *267*, 26181–26190. [CrossRef] [PubMed]
5. Stricker, S.; Rauschenberger, V.; Schambony, A. ROR-Family Receptor Tyrosine Kinases. *Curr. Top. Dev. Biol.* **2017**, *123*, 105–142.
6. Balakrishnan, A.; Goodpaster, T.; Randolph-Habecker, J.; Hoffstrom, B.G.; Jalikis, F.G.; Koch, L.K.; Berger, C.; Kosasih, P.L.; Rajan, A.; Sommermeyer, D.; et al. Analysis of ROR1 Protein Expression in Human Cancer and Normal Tissues. *Clin. Cancer Res.* **2017**, *23*, 3061–3071. [CrossRef]
7. Hudecek, M.; Schmitt, T.M.; Baskar, S.; Lupo-Stanghellini, M.T.; Nishida, T.; Yamamoto, T.N.; Bleakley, M.; Turtle, C.J.; Chang, W.C.; Greisman, H.A.; et al. The B-cell tumor-associated antigen ROR1 can be targeted with T cells modified to express a ROR1-specific chimeric antigen receptor. *Blood* **2010**, *116*, 4532–4541. [CrossRef]
8. Yoda, A.; Oishi, I.; Minami, Y. Expression and function of the Ror-family receptor tyrosine kinases during development: Lessons from genetic analyses of nematodes, mice, and humans. *J. Recept. Signal. Transduct. Res.* **2003**, *23*, 1–15. [CrossRef]
9. Billiard, J.; Way, D.S.; Seestaller-Wehr, L.M.; Moran, R.A.; Mangine, A.; Bodine, P.V. The orphan receptor tyrosine kinase Ror2 modulates canonical Wnt signaling in osteoblastic cells. *Mol. Endocrinol.* **2005**, *19*, 90–101. [CrossRef]
10. Daneshmanesh, A.H.; Mikaelsson, E.; Jeddi-Tehrani, M.; Bayat, A.A.; Ghods, R.; Ostadkarampour, M.; Akhondi, M.; Lagercrantz, S.; Larsson, C.; Osterborg, A.; et al. Ror1, a cell surface receptor tyrosine kinase is expressed in chronic lymphocytic leukemia and may serve as a putative target for therapy. *Int. J. Cancer* **2008**, *123*, 1190–1195. [CrossRef]
11. Baskar, S.; Kwong, K.Y.; Hofer, T.; Levy, J.M.; Kennedy, M.G.; Lee, E.; Staudt, L.M.; Wilson, W.H.; Wiestner, A.; Rader, C. Unique cell surface expression of receptor tyrosine kinase ROR1 in human B-cell chronic lymphocytic leukemia. *Clin. Cancer Res.* **2008**, *14*, 396–404. [CrossRef]
12. Karvonen, H.; Chiron, D.; Niininen, W.; Ek, S.; Jerkeman, M.; Moradi, E.; Nykter, M.; Heckman, C.A.; Kallioniemi, O.; Murumagi, A.; et al. Crosstalk between ROR1 and BCR pathways defines novel treatment strategies in mantle cell lymphoma. *Blood Adv.* **2017**, *1*, 2257–2268. [CrossRef]
13. Ghaderi, A.; Daneshmanesh, A.H.; Moshfegh, A.; Kokhaei, P.; Vagberg, J.; Schultz, J.; Olin, T.; Harrysson, S.; Smedby, K.E.; Drakos, E.; et al. ROR1 Is Expressed in Diffuse Large B-Cell Lymphoma (DLBCL) and a Small Molecule Inhibitor of ROR1 (KAN0441571C) Induced Apoptosis of Lymphoma Cells. *Biomedicines* **2020**, *8*, 170. [CrossRef]
14. Lovat, F.; Gasparini, P.; Nigita, G.; Larkin, K.; Byrd, J.C.; Minden, M.D.; Andreeff, M.; Carter, B.Z.; Croce, C.M. Loss of expression of both miR-15/16 loci in CML transition to blast crisis. *Proc. Natl. Acad. Sci. USA* **2021**, *118*, e2101566118. [CrossRef] [PubMed]
15. Bicocca, V.T.; Chang, B.H.; Masouleh, B.K.; Muschen, M.; Loriaux, M.M.; Druker, B.J.; Tyner, J.W. Crosstalk between ROR1 and the Pre-B cell receptor promotes survival of t(1;19) acute lymphoblastic leukemia. *Cancer Cell* **2012**, *22*, 656–667. [CrossRef] [PubMed]
16. Yamaguchi, T.; Yanagisawa, K.; Sugiyama, R.; Hosono, Y.; Shimada, Y.; Arima, C.; Kato, S.; Tomida, S.; Suzuki, M.; Osada, H.; et al. NKX2-1/TTF1/TTF-1-Induced ROR1 is required to sustain EGFR survival signaling in lung adenocarcinoma. *Cancer Cell* **2012**, *21*, 348–361. [CrossRef] [PubMed]
17. Gentile, A.; Lazzari, L.; Benvenuti, S.; Trusolino, L.; Comoglio, P.M. Ror1 is a pseudokinase that is crucial for Met-driven tumorigenesis. *Cancer Res.* **2011**, *71*, 3132–3141. [CrossRef]
18. Avasarala, S.; Bikkavilli, R.K.; Van Scoyk, M.; Zhang, W.; Lapite, A.; Hostetter, L.; Byers, J.T.; Heasley, L.E.; Sohn, J.W.; Winn, R.A. Heterotrimeric G-protein, Galpha16, is a critical downstream effector of non-canonical Wnt signaling and a potent inhibitor of transformed cell growth in non small cell lung cancer. *PLoS ONE* **2013**, *8*, e76895. [CrossRef] [PubMed]
19. Zhang, R.; Wang, Z.; Yu, Q.; Shen, J.; He, W.; Zhou, D.; Yu, Q.; Fan, J.; Gao, S.; Duan, L. Atractylenolide II reverses the influence of lncRNA XIST/miR-30a-5p/ROR1 axis on chemo-resistance of colorectal cancer cells. *J. Cell. Mol. Med.* **2019**, *23*, 3151–3165. [CrossRef]
20. Daneshmanesh, A.H.; Hojjat-Farsangi, M.; Ghaderi, A.; Moshfegh, A.; Hansson, L.; Schultz, J.; Vagberg, J.; Bystrom, S.; Olsson, E.; Olin, T.; et al. A receptor tyrosine kinase ROR1 inhibitor (KAN0439834) induced significant apoptosis of pancreatic cells which was enhanced by erlotinib and ibrutinib. *PLoS ONE* **2018**, *13*, e0198038. [CrossRef] [PubMed]
21. Zhang, H.; Qiu, J.; Ye, C.; Yang, D.; Gao, L.; Su, Y.; Tang, X.; Xu, N.; Zhang, D.; Xiong, L.; et al. ROR1 expression correlated with poor clinical outcome in human ovarian cancer. *Sci. Rep.* **2014**, *4*, 5811. [CrossRef] [PubMed]
22. Fernandez, N.B.; Lorenzo, D.; Picco, M.E.; Barbero, G.; Dergan-Dylon, L.S.; Marks, M.P.; Garcia-Rivello, H.; Gimenez, L.; Labovsky, V.; Grumolato, L.; et al. ROR1 contributes to melanoma cell growth and migration by regulating N-cadherin via the PI3K/Akt pathway. *Mol. Carcinog.* **2016**, *55*, 1772–1785. [CrossRef] [PubMed]
23. Schiavone, G.; Epistolio, S.; Martin, V.; Molinari, F.; Barizzi, J.; Mazzucchelli, L.; Frattini, M.; Wannesson, L. Functional and clinical significance of ROR1 in lung adenocarcinoma. *BMC Cancer* **2020**, *20*, 1085.
24. Ida, L.; Yamaguchi, T.; Yanagisawa, K.; Kajino, T.; Shimada, Y.; Suzuki, M.; Takahashi, T. Receptor tyrosine kinase-like orphan receptor 1, a target of NKX2-1/TTF-1 lineage-survival oncogene, inhibits apoptosis signal-regulating kinase 1-mediated proapoptotic signaling in lung adenocarcinoma. *Cancer Sci.* **2016**, *107*, 155–161. [CrossRef] [PubMed]
25. Cui, B.; Zhang, S.; Chen, L.; Yu, J.; Widhopf, G.F., 2nd; Fecteau, J.F.; Rassenti, L.Z.; Kipps, T.J. Targeting ROR1 inhibits epithelial-mesenchymal transition and metastasis. *Cancer Res.* **2013**, *73*, 3649–3660. [CrossRef] [PubMed]
26. Long, M.P.; Wang, H.L.; Luo, Y.B.; Yang, J.H. Targeting ROR1 inhibits epithelial to mesenchymal transition in human lung adenocarcinoma via mTOR signaling pathway. *Int. J. Clin. Exp. Pathol.* **2018**, *11*, 4759–4770.

27. Choi, M.Y.; Widhopf, G.F., 2nd; Ghia, E.M.; Kidwell, R.L.; Hasan, M.K.; Yu, J.; Rassenti, L.Z.; Chen, L.; Chen, Y.; Pittman, E.; et al. Phase I Trial: Cirmtuzumab Inhibits ROR1 Signaling and Stemness Signatures in Patients with Chronic Lymphocytic Leukemia. *Cell Stem Cell* **2018**, *22*, 951–959.e3. [CrossRef]
28. Jung, E.H.; Lee, H.N.; Han, G.Y.; Kim, M.J.; Kim, C.W. Targeting ROR1 inhibits the self-renewal and invasive ability of glioblastoma stem cells. *Cell. Biochem. Funct.* **2016**, *34*, 149–157. [CrossRef]
29. Zhang, S.; Cui, B.; Lai, H.; Liu, G.; Ghia, E.M.; Widhopf, G.F., 2nd; Rassenti, L.Z.; Chen, L.; Chen, Y.; Pittman, E.; et al. Ovarian cancer stem cells express ROR1, which can be targeted for anti-cancer-stem-cell therapy. *Proc. Natl. Acad. Sci. USA* **2014**, *111*, 17266–17271. [CrossRef]
30. Fukuda, T.; Chen, L.; Endo, T.; Tang, L.; Lu, D.; Castro, J.E.; Widhopf, G.F., 2nd; Rassenti, L.Z.; Cantwell, M.J.; Prussak, C.E.; et al. Antisera induced by infusions of autologous Ad-CD154-leukemia B cells identify ROR1 as an oncofetal antigen and receptor for Wnt5a. *Proc. Natl. Acad. Sci. USA* **2008**, *105*, 3047–3052. [CrossRef]
31. Zhang, S.; Chen, L.; Cui, B.; Chuang, H.Y.; Yu, J.; Wang-Rodriguez, J.; Tang, L.; Chen, G.; Basak, G.W.; Kipps, T.J. ROR1 is expressed in human breast cancer and associated with enhanced tumor-cell growth. *PLoS ONE* **2012**, *7*, e31127. [CrossRef]
32. Hojjat-Farsangi, M.; Khan, A.S.; Daneshmanesh, A.H.; Moshfegh, A.; Sandin, A.; Mansouri, L.; Palma, M.; Lundin, J.; Osterborg, A.; Mellstedt, H. The tyrosine kinase receptor ROR1 is constitutively phosphorylated in chronic lymphocytic leukemia (CLL) cells. *PLoS ONE* **2013**, *8*, e78339. [CrossRef] [PubMed]
33. Mikels, A.J.; Nusse, R. Purified Wnt5a protein activates or inhibits beta-catenin-TCF signaling depending on receptor context. *PLoS Biol.* **2006**, *4*, e115. [CrossRef] [PubMed]
34. Nomachi, A.; Nishita, M.; Inaba, D.; Enomoto, M.; Hamasaki, M.; Minami, Y. Receptor tyrosine kinase Ror2 mediates Wnt5a-induced polarized cell migration by activating c-Jun N-terminal kinase via actin-binding protein filamin A. *J. Biol. Chem.* **2008**, *283*, 27973–27981. [CrossRef] [PubMed]
35. Zhuo, W.; Kang, Y. Lnc-ing ROR1-HER3 and Hippo signalling in metastasis. *Nat. Cell. Biol.* **2017**, *19*, 81–83. [CrossRef]
36. Hojjat-Farsangi, M.; Moshfegh, A.; Daneshmanesh, A.H.; Khan, A.S.; Mikaelsson, E.; Osterborg, A.; Mellstedt, H. The receptor tyrosine kinase ROR1—an oncofetal antigen for targeted cancer therapy. *Semin. Cancer Biol.* **2014**, *29*, 21–31. [CrossRef] [PubMed]
37. Mao, Y.; Xu, L.; Wang, J.; Zhang, L.; Hou, N.; Xu, J.; Wang, L.; Yang, S.; Chen, Y.; Xiong, L.; et al. ROR1 associates unfavorable prognosis and promotes lymphoma growth in DLBCL by affecting PI3K/Akt/mTOR signaling pathway. *Biofactors* **2019**, *45*, 416–426. [CrossRef]
38. Cui, B.; Ghia, E.M.; Chen, L.; Rassenti, L.Z.; DeBoever, C.; Widhopf, G.F., 2nd; Yu, J.; Neuberger, D.S.; Wierda, W.G.; Rai, K.R.; et al. High-Level ROR1 associates with accelerated disease progression in chronic lymphocytic leukemia. *Blood* **2016**, *128*, 2931–2940. [CrossRef]
39. Daneshmanesh, A.H.; Porwit, A.; Hojjat-Farsangi, M.; Jeddi-Tehrani, M.; Tamm, K.P.; Grander, D.; Lehmann, S.; Norin, S.; Shokri, F.; Rabbani, H.; et al. Orphan receptor tyrosine kinases ROR1 and ROR2 in hematological malignancies. *Leuk. Lymphoma* **2013**, *54*, 843–850. [CrossRef]
40. Ikeda, T.; Nishita, M.; Hoshi, K.; Honda, T.; Kakeji, Y.; Minami, Y. Mesenchymal stem cell-derived CXCL16 promotes progression of gastric cancer cells by STAT3-mediated expression of Ror1. *Cancer Sci.* **2020**, *111*, 1254–1265. [CrossRef]
41. Choudhury, A.; Derkow, K.; Daneshmanesh, A.H.; Mikaelsson, E.; Kiaii, S.; Kokhaei, P.; Osterborg, A.; Mellstedt, H. Silencing of ROR1 and FMOD with siRNA results in apoptosis of CLL cells. *Br. J. Haematol.* **2010**, *151*, 327–335. [CrossRef]
42. Liu, X.; Pu, W.; He, H.; Fan, X.; Zheng, Y.; Zhou, J.K.; Ma, R.; He, J.; Zheng, Y.; Wu, K.; et al. Novel ROR1 inhibitor ARI-1 suppresses the development of non-small cell lung cancer. *Cancer Lett.* **2019**, *458*, 76–85. [CrossRef] [PubMed]
43. Fultang, N.; Illendula, A.; Chen, B.; Wu, C.; Jonnalagadda, S.; Baird, N.; Klase, Z.; Peethambaran, B. Strictinin, a novel ROR1-inhibitor, represses triple negative breast cancer survival and migration via modulation of PI3K/AKT/GSK3ss activity. *PLoS ONE* **2019**, *14*, e0217789. [CrossRef] [PubMed]
44. Srivastava, S.; Furlan, S.N.; Jaeger-Ruckstuhl, C.A.; Sarvothama, M.; Berger, C.; Smythe, K.S.; Garrison, S.M.; Specht, J.M.; Lee, S.M.; Amezquita, R.A.; et al. Immunogenic Chemotherapy Enhances Recruitment of CAR-T Cells to Lung Tumors and Improves Antitumor Efficacy when Combined with Checkpoint Blockade. *Cancer Cell.* **2021**, *39*, 193–208.e10. [CrossRef]
45. Khaledian, B.; Taguchi, A.; Shin-Ya, K.; Kondo-Ida, L.; Kagaya, N.; Suzuki, M.; Kajino, T.; Yamaguchi, T.; Shimada, Y.; Takahashi, T. Inhibition of heat shock protein 90 destabilizes receptor tyrosine kinase ROR1 in lung adenocarcinoma. *Cancer Sci.* **2021**, *112*, 1225–1234. [CrossRef] [PubMed]
46. Hojjat-Farsangi, M.; Daneshmanesh, A.H.; Khan, A.S.; Shetye, J.; Mozaffari, F.; Kharaziha, P.; Rathje, L.S.; Kokhaei, P.; Hansson, L.; Vagberg, J.; et al. First-in-Class oral small molecule inhibitor of the tyrosine kinase ROR1 (KAN0439834) induced significant apoptosis of chronic lymphocytic leukemia cells. *Leukemia* **2018**, *32*, 2291–2295. [CrossRef]
47. Wang, W.Z.; Shilo, K.; Amann, J.M.; Shulman, A.; Hojjat-Farsangi, M.; Mellstedt, H.; Schultz, J.; Croce, C.M.; Carbone, D.P. Predicting ROR1/BCL2 combination targeted therapy of small cell carcinoma of the lung. *Cell Death Dis.* **2021**, *12*, 577. [CrossRef] [PubMed]
48. Kumar, A.; Wakelee, H. Second- and third-line treatments in non-small cell lung cancer. *Curr. Treat. Options Oncol.* **2006**, *7*, 37–49. [CrossRef]
49. Hong, D.; Rasco, D.; Veeder, M.; Luke, J.J.; Chandler, J.; Balmanoukian, A.; George, T.J.; Munster, P.; Berlin, J.D.; Gutierrez, M.; et al. A Phase 1b/2 Study of the Bruton Tyrosine Kinase Inhibitor Ibrutinib and the PD-L1 Inhibitor Durvalumab in Patients with Pretreated Solid Tumors. *Oncology* **2019**, *97*, 102–111. [CrossRef]



50. Wang, A.; Yan, X.E.; Wu, H.; Wang, W.; Hu, C.; Chen, C.; Zhao, Z.; Zhao, P.; Li, X.; Wang, L.; et al. Ibrutinib targets mutant-EGFR kinase with a distinct binding conformation. *Oncotarget* **2016**, *7*, 69760–69769. [CrossRef]
51. Travis, W.D.; Brambilla, E.; Nicholson, A.G.; Yatabe, Y.; Austin, J.H.M.; Beasley, M.B.; Chirieac, L.R.; Dacic, S.; Duhig, E.; Flieder, D.B.; et al. The 2015 World Health Organization Classification of Lung Tumors: Impact of Genetic, Clinical and Radiologic Advances Since the 2004 Classification. *J. Thorac. Oncol.* **2015**, *10*, 1243–1260. [CrossRef]
52. Mengoli, M.C.; Longo, F.R.; Fraggetta, F.; Cavazza, A.; Dubini, A.; Ali, G.; Guddo, F.; Gilioli, E.; Bogina, G.; Nannini, N.; et al. The 2015 World Health Organization Classification of lung tumors: New entities since the 2004 Classification. *Pathologica* **2018**, *110*, 39–67.
53. Micke, P.; Mattsson, J.S.; Djureinovic, D.; Nodin, B.; Jirstrom, K.; Tran, L.; Jonsson, P.; Planck, M.; Botling, J.; Brunnstrom, H. The Impact of the Fourth Edition of the WHO Classification of Lung Tumours on Histological Classification of Resected Pulmonary NSCCs. *J. Thorac. Oncol.* **2016**, *11*, 862–872. [CrossRef]
54. Akyurek, N.; Drakos, E.; Giaslaktiotis, K.; Knoblock, R.J.; Abruzzo, L.V.; Ning, Y.; Rassidakis, G.Z.; Medeiros, L.J. Differential expression of CKS-1B in typical and blastoid variants of mantle cell lymphoma. *Hum. Pathol.* **2010**, *41*, 1448–1455. [CrossRef]
55. Chou, T.C. Drug combination studies and their synergy quantification using the Chou-Talalay method. *Cancer Res.* **2010**, *70*, 440–446. [CrossRef]
56. Hojjat-Farsangi, M.; Moshfegh, A.; Schultz, J.; Norin, M.; Olin, T.; Osterborg, A.; Mellstedt, H. Targeting the Receptor Tyrosine Kinase ROR1 by Small Molecules. *Handb. Exp. Pharmacol.* **2021**, *269*, 75–99.
57. Kwan, K.; Castro-Sandoval, O.; Gaiddon, C.; Storr, T. Inhibition of p53 protein aggregation as a cancer treatment strategy. *Curr. Opin. Chem. Biol.* **2022**, *72*, 102230. [CrossRef] [PubMed]
58. Zhang, S.; Chen, L.; Wang-Rodriguez, J.; Zhang, L.; Cui, B.; Frankel, W.; Wu, R.; Kipps, T.J. The onco-embryonic antigen ROR1 is expressed by a variety of human cancers. *Am. J. Pathol.* **2012**, *181*, 1903–1910. [CrossRef] [PubMed]
59. Saleh, R.R.; Antras, J.F.; Peinado, P.; Perez-Segura, P.; Pandiella, A.; Amir, E.; Ocana, A. Prognostic value of receptor tyrosine kinase-like orphan receptor (ROR) family in cancer: A meta-analysis. *Cancer Treat. Rev.* **2019**, *77*, 11–19. [CrossRef] [PubMed]
60. Chien, H.P.; Ueng, S.H.; Chen, S.C.; Chang, Y.S.; Lin, Y.C.; Lo, Y.F.; Chang, H.K.; Chuang, W.Y.; Huang, Y.T.; Cheung, Y.C.; et al. Expression of ROR1 has prognostic significance in triple negative breast cancer. *Virchows Arch.* **2016**, *468*, 589–595. [CrossRef]
61. Zhou, J.K.; Zheng, Y.Z.; Liu, X.S.; Gou, Q.; Ma, R.; Guo, C.L.; Croce, C.M.; Liu, L.; Peng, Y. ROR1 expression as a biomarker for predicting prognosis in patients with colorectal cancer. *Oncotarget* **2017**, *8*, 32864–32872. [CrossRef] [PubMed]
62. Cetin, M.; Odabas, G.; Douglas, L.R.; Duriez, P.J.; Balcik-Ercin, P.; Yalim-Camci, I.; Sayan, A.E.; Yagci, T. ROR1 Expression and Its Functional Significance in Hepatocellular Carcinoma Cells. *Cells* **2019**, *8*, 210. [CrossRef]
63. Zheng, Y.Z.; Ma, R.; Zhou, J.K.; Guo, C.L.; Wang, Y.S.; Li, Z.G.; Liu, L.X.; Peng, Y. ROR1 is a novel prognostic biomarker in patients with lung adenocarcinoma. *Sci. Rep.* **2016**, *6*, 36447. [CrossRef]
64. Jeong, S.Y.; Lee, K.J.; Cha, J.; Park, S.Y.; Kim, H.S.; Kim, J.H.; Lee, J.J.; Kim, N.; Park, S.T. Meta-Analysis of Survival Effects of Receptor Tyrosine Kinase-like Orphan Receptor 1 (ROR1). *Medicina* **2022**, *58*, 1867. [CrossRef] [PubMed]
65. Katoh, M. Canonical and non-canonical WNT signaling in cancer stem cells and their niches: Cellular heterogeneity, omics reprogramming, targeted therapy and tumor plasticity (Review). *Int. J. Oncol.* **2017**, *51*, 1357–1369. [CrossRef]
66. Karvonen, H.; Barker, H.; Kaleva, L.; Niininen, W.; Ungureanu, D. Molecular Mechanisms Associated with ROR1-Mediated Drug Resistance: Crosstalk with Hippo-YAP/TAZ and BMI-1 Pathways. *Cells* **2019**, *8*, 812. [CrossRef]
67. Islam, S.S.; Uddin, M.; Noman, A.S.M.; Akter, H.; Dity, N.J.; Basiruzzman, M.; Uddin, F.; Ahsan, J.; Annoor, S.; Alaiya, A.A.; et al. Antibody-drug conjugate T-DM1 treatment for HER2+ breast cancer induces ROR1 and confers resistance through activation of Hippo transcriptional coactivator YAP1. *EBioMedicine* **2019**, *43*, 211–224. [CrossRef]
68. Huang, X.; Park, H.; Greene, J.; Pao, J.; Mulvey, E.; Zhou, S.X.; Albert, C.M.; Moy, F.; Sachdev, D.; Yee, D.; et al. IGF1R- and ROR1-Specific CAR T Cells as a Potential Therapy for High Risk Sarcomas. *PLoS ONE* **2015**, *10*, e0133152. [CrossRef] [PubMed]
69. Wallstabe, L.; Gottlich, C.; Nelke, L.C.; Kuhnemundt, J.; Schwarz, T.; Nerreter, T.; Einsele, H.; Walles, H.; Dandekar, G.; Nietzer, S.L.; et al. ROR1-CAR T cells are effective against lung and breast cancer in advanced microphysiologic 3D tumor models. *JCI Insight* **2019**, *4*, e126345. [CrossRef]
70. Gohil, S.H.; Paredes-Moscossa, S.R.; Harrasser, M.; Vezzalini, M.; Scarpa, A.; Morris, E.; Davidoff, A.M.; Sorio, C.; Nathwani, A.C.; Della Peruta, M. An ROR1 bi-specific T-cell engager provides effective targeting and cytotoxicity against a range of solid tumors. *Oncoimmunology* **2017**, *6*, e1326437. [CrossRef]
71. Daneshmanesh, A.H.; Hojjat-Farsangi, M.; Khan, A.S.; Jeddi-Tehrani, M.; Akhondi, M.M.; Bayat, A.A.; Ghods, R.; Mahmoudi, A.R.; Hadavi, R.; Osterborg, A.; et al. Monoclonal antibodies against ROR1 induce apoptosis of chronic lymphocytic leukemia (CLL) cells. *Leukemia* **2012**, *26*, 1348–1355. [CrossRef]
72. Liu, Y.; Yang, H.; Chen, T.; Luo, Y.; Xu, Z.; Li, Y.; Yang, J. Silencing of Receptor Tyrosine Kinase ROR1 Inhibits Tumor-Cell Proliferation via PI3K/AKT/mTOR Signaling Pathway in Lung Adenocarcinoma. *PLoS ONE* **2015**, *10*, e0127092. [CrossRef] [PubMed]
73. Zhou, Q.; Zhou, S.; Wang, H.; Li, Y.; Xiao, X.; Yang, J. Stable silencing of ROR1 regulates cell cycle, apoptosis, and autophagy in a lung adenocarcinoma cell line. *Int. J. Clin. Exp. Pathol.* **2020**, *13*, 1108–1120. [PubMed]
74. Ghaderi, A.; Zhong, W.; Okhovat, M.A.; Aschan, J.; Svensson, A.; Sander, B.; Schultz, J.; Olin, T.; Osterborg, A.; Hojjat-Farsangi, M.; et al. A ROR1 Small Molecule Inhibitor (KAN0441571C) Induced Significant Apoptosis of Mantle Cell Lymphoma (MCL) Cells. *Pharmaceutics* **2022**, *14*, 2238. [CrossRef]

75. Zhang, Y.X.; He, D.C.; Fang, W.F.; Kang, S.Y.; Chen, G.; Hong, S.D.; Sheng, J.; Zhan, J.H.; Chen, N.; Hu, Z.H.; et al. The Difference of Clinical Characteristics Between Patients With Exon 19 Deletion and Those With L858R Mutation in Nonsmall Cell Lung Cancer. *Medicine* **2015**, *94*, e1949. [CrossRef] [PubMed]
76. Yatabe, Y.; Mitsudomi, T.; Takahashi, T. TTF-1 expression in pulmonary adenocarcinomas. *Am. J. Surg. Pathol.* **2002**, *26*, 767–773. [CrossRef]
77. Liu, Z.; Yanagisawa, K.; Griesing, S.; Iwai, M.; Kano, K.; Hotta, N.; Kajino, T.; Suzuki, M.; Takahashi, T. TTF-1/NKX2-1 binds to DDB1 and confers replication stress resistance to lung adenocarcinomas. *Oncogene* **2017**, *36*, 3740–3748. [CrossRef]
78. Yatabe, Y.; Kosaka, T.; Takahashi, T.; Mitsudomi, T. EGFR mutation is specific for terminal respiratory unit type adenocarcinoma. *Am. J. Surg. Pathol.* **2005**, *29*, 633–639. [CrossRef]
79. Karachaliou, N.; Gimenez-Capitan, A.; Drozdowskyj, A.; Viteri, S.; Moran, T.; Carcereny, E.; Massuti, B.; Vergnenegre, A.; de Marinis, F.; Molina, M.A.; et al. ROR1 as a novel therapeutic target for EGFR-mutant non-small-cell lung cancer patients with the EGFR T790M mutation. *Transl. Lung Cancer Res.* **2014**, *3*, 122–130.
80. Wang, H.L.; Liu, Y.C.; Long, M.P.; Zheng, C.; Yang, J.H. Blocking ROR1 enhances the roles of erlotinib in lung adenocarcinoma cell lines. *Oncol. Lett.* **2019**, *18*, 2977–2984. [CrossRef]
81. Villarreal, A.; Del Valle-Perez, B.; Fuertes, G.; Curto, J.; Ontiveros, N.; Garcia de Herreros, A.; Dunach, M. Src and Fyn define a new signaling cascade activated by canonical and non-canonical Wnt ligands and required for gene transcription and cell invasion. *Cell. Mol. Life Sci.* **2019**, *77*, 919–935. [CrossRef] [PubMed]

**Disclaimer/Publisher’s Note:** The statements, opinions and data contained in all publications are solely those of the individual author(s) and contributor(s) and not of MDPI and/or the editor(s). MDPI and/or the editor(s) disclaim responsibility for any injury to people or property resulting from any ideas, methods, instructions or products referred to in the content.

Review

# Immunomodulatory Activity of the Tyrosine Kinase Inhibitor Dasatinib to Elicit NK Cytotoxicity against Cancer, HIV Infection and Aging

Andrea Rodríguez-Agustín <sup>1,†</sup>, Víctor Casanova <sup>1,†</sup>, Judith Grau-Expósito <sup>1</sup>, Sonsoles Sánchez-Palomino <sup>1,2</sup>, José Alcamí <sup>2,3</sup> and Núria Climent <sup>1,2,\*</sup>

<sup>1</sup> HIV Unit, Hospital Clínic-IDIBAPS, University of Barcelona, 08036 Barcelona, Spain

<sup>2</sup> CIBER of Infectious Diseases (CIBERINFEC), 28029 Madrid, Spain

<sup>3</sup> AIDS Immunopathogenesis Unit, Instituto de Salud Carlos III (ISCIII), 28029 Madrid, Spain

\* Correspondence: ncliment@recerca.clinic.cat; Tel.: +34-93-2275400 (ext. 3144); Fax: +34-93-2271775

† These authors contributed equally to this work.

**Abstract:** Tyrosine kinase inhibitors (TKIs) have been extensively used as a treatment for chronic myeloid leukemia (CML). Dasatinib is a broad-spectrum TKI with off-target effects that give it an immunomodulatory capacity resulting in increased innate immune responses against cancerous cells and viral infected cells. Several studies reported that dasatinib expanded memory-like natural killer (NK) cells and  $\gamma\delta$  T cells that have been related with increased control of CML after treatment withdrawal. In the HIV infection setting, these innate cells are associated with virus control and protection, suggesting that dasatinib could have a potential role in improving both the CML and HIV outcomes. Moreover, dasatinib could also directly induce apoptosis of senescence cells, being a new potential senolytic drug. Here, we review in depth the current knowledge of virological and immunogenetic factors associated with the development of powerful cytotoxic responses associated with this drug. Besides, we will discuss the potential therapeutic role against CML, HIV infection and aging.

**Keywords:** dasatinib; tyrosine kinase inhibitors; CML; cancer; HIV-1; CMV; HIV functional cure; memory-like NK cells;  $\gamma\delta$  T cells; anti-aging; senolytic

**Citation:** Rodríguez-Agustín, A.; Casanova, V.; Grau-Expósito, J.; Sánchez-Palomino, S.; Alcamí, J.; Climent, N. Immunomodulatory Activity of the Tyrosine Kinase Inhibitor Dasatinib to Elicit NK Cytotoxicity against Cancer, HIV Infection and Aging. *Pharmaceutics* **2023**, *15*, 917. <https://doi.org/10.3390/pharmaceutics15030917>

Academic Editor: Francesca Musumeci

Received: 18 February 2023

Revised: 7 March 2023

Accepted: 9 March 2023

Published: 11 March 2023



**Copyright:** © 2023 by the authors. Licensee MDPI, Basel, Switzerland. This article is an open access article distributed under the terms and conditions of the Creative Commons Attribution (CC BY) license (<https://creativecommons.org/licenses/by/4.0/>).

## 1. Introduction

### 1.1. Dasatinib

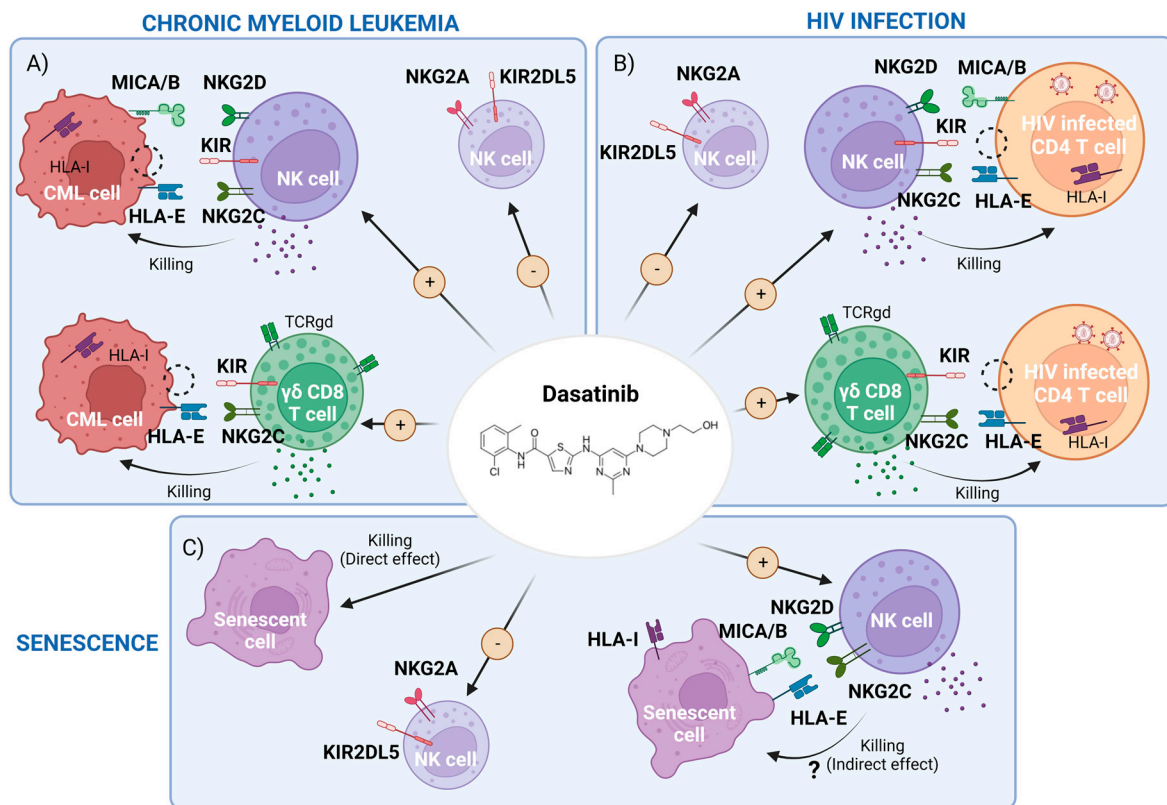
Dasatinib is a broad-spectrum tyrosine kinase inhibitor originally developed to treat chronic myeloid leukemia (CML) [1]. CML is a hematopoietic progenitor cell leukemia, in which overgrown myeloid cells accumulate in bone marrow and peripheral blood [2]. A translocation between chromosomes 9 and 22 results in an aberrant chromosome 22 (or Philadelphia (Ph) chromosome), generating the BCR-ABL oncogene. BCR-ABL constitutively activates tyrosine kinases (TK) that drives both Ph<sup>+</sup> CML and Ph<sup>+</sup> acute lymphoblastic leukemia (ALL) [3]. Treatment for CML was drastically improved with imatinib, one of the first TK Inhibitors (TKI) targeting BCR-ABL TK [4]. Furthermore, development of these small molecules led to the development of alternative inhibitors such as the second-generation drug dasatinib, which yield up to 20–300 times higher activity and has faster and deep molecular response (DMR) than imatinib [1].

Dasatinib has other off-target effects inhibiting other TK (Table 1) [5] with potential side effects such as hematological, pulmonary and gastrointestinal toxicity that could limit its clinical use [6]. Interestingly, off-target effects have been related to potential benefits such as an increased natural killer cell (NK)-mediated cytotoxic capacity against cancerous cells and viral infected cells [7] and an anti-aging capacity. In this review, we will discuss

the potential immunomodulatory effects of dasatinib on NK cells and other innate cells and its therapeutic role against CML, HIV infection and aging (Figure 1).

**Table 1.** Tyrosine kinases (TKs) targeted by dasatinib and the cellular processes in which they are involved. Adapted from Araujo et al., 2010 [5]. Abbreviations: PDGFR $\beta$ , platelet-derived growth factor receptor beta; EPHA2, ephrin type-A receptor 2; EFNB, ephrin-B; M-CSF, macrophage colony-stimulating factor.

Tyrosine Kinase Target (s)	Pathways and Processes
SRC family (SRC, LCK, YES, FYN)	Oncogenic, invasive and bone-metastatic processes
BCR-ABL	Promotion of growth advantage of leukemic cells
c-KIT	Cell growth
PDGFR $\beta$	Tumor growth capacity and cell survival
c-FMS	Macrophage behavior regulation by M-CSF
EPHA2 receptor	Interference with EFNB-dependent suppression of apoptosis/Cell behavior

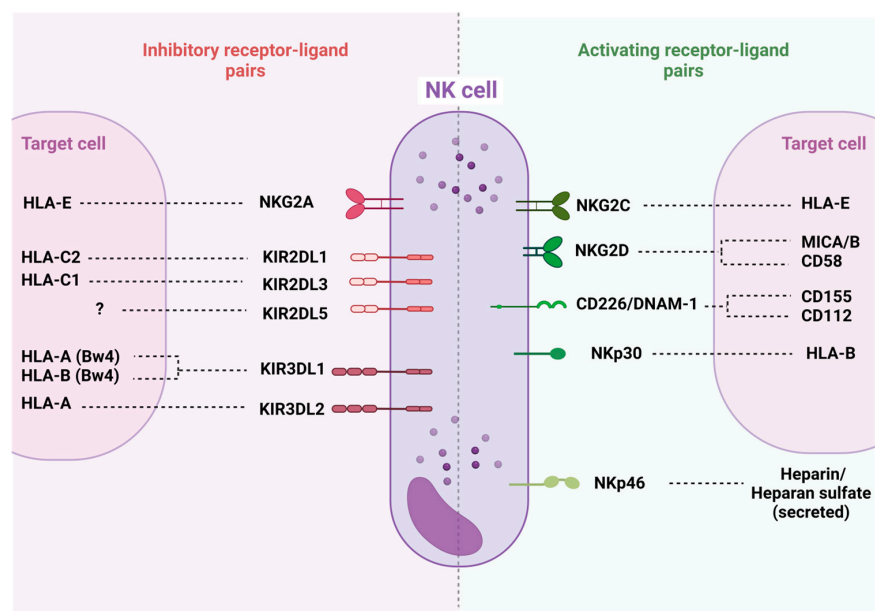


**Figure 1.** Scheme of dasatinib-mediated effects that may interfere with chronic myeloid leukemia (CML), HIV-1 infection and cellular senescence. (A) CML cell killing by the enhancement of memory natural killer (NK) cells and cytotoxic CD8<sup>+</sup> T cells expressing  $\gamma\delta$ TCR and a reduction of inhibitory receptors driven by dasatinib. (B) HIV infected cells' clearance, carrying pro-viral DNA, by dasatinib activity through the potentiation of the above cell subpopulations. (C) Representation of both direct killing and a potential indirect effect by boosting NK and CD8<sup>+</sup> cells of senescent cells with dasatinib. Figure made with BioRender.com (accessed on 7 March 2023).

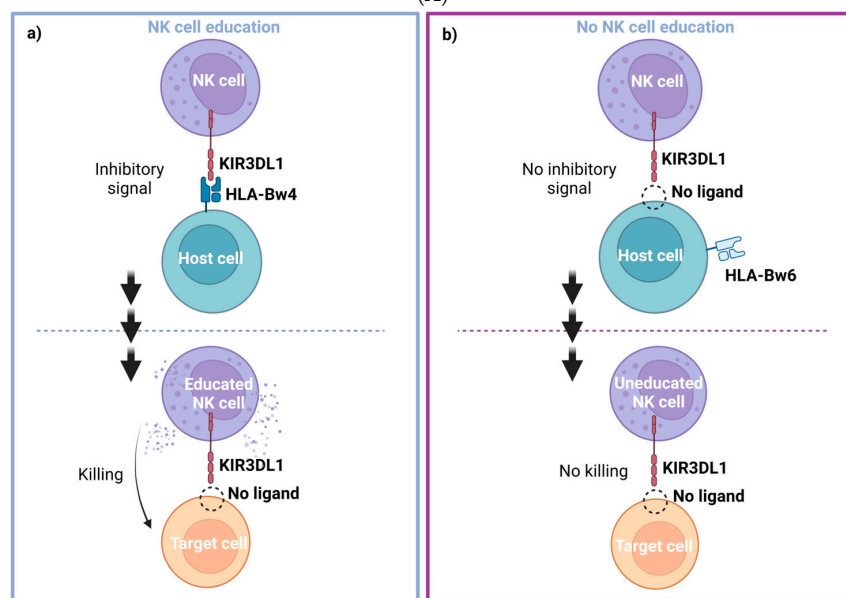
### 1.2. Natural Killer Cell Biology

Natural killer cells (NK cells), are cells from the innate immune system that show strong cytolytic function against stressed cells such as tumoral cells and virus-infected

cells. NK activation state is determined by a balance of multiple activation and inhibition signals mediated by NK inhibitory and activating receptors that bind to NK ligands from other neighboring cells (Figure 2A). Most of these ligands are HLA class I molecules, such as HLA-A, B, C and HLA-E. Depending on the balance between these NK receptors (NKR) and their HLA ligands, NK cells will either be activated to kill the target cell or inhibited, allowing the target cell to survive. NK cells are a heterogeneous population harboring multiple subsets that differentially expressed NK receptors such as: killer cell immunoglobulin-like receptors (KIRs), natural killer group 2 such as NKG2A, NKG2C and NKG2D, and natural cytotoxicity receptors (NCRs), for example NKp30, NKp40 or NKp46 [8,9]. The main activating and inhibiting NK receptors and their respective target cell ligands are shown in Figure 2A. The NKG2C and NKG2D receptors are activating NK receptors that could detect abnormal or malignant cells by binding with HLA-E and the MIC A/B ligands, respectively. These interactions potentiate NK cell killing [10,11] (Figure 2A).

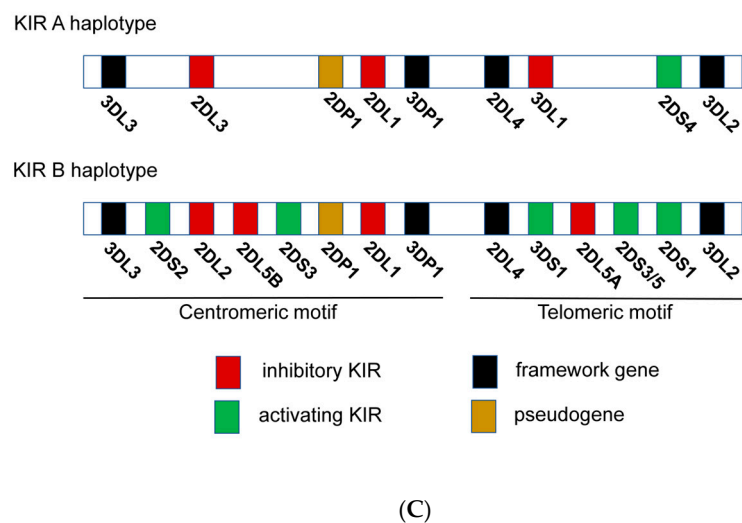


(A)



(B)

Figure 2. Cont.



**Figure 2.** (A) Representation of NK cell inhibitory and activating receptor-ligand pairs. Adapted from [9]. Figure made with BioRender.com. (B) NK cell education process and “missing self” killing of target cells. (a) NK cells are recognized through KIR3DL1 receptor host cells expressing HLA-Bw4 and become educated to recognize its absence then in target cells. This process leads to an efficient target cell killing. (b) Absence of recognition of HLA-Bw4 by KIR3DL1 drives a deficient cell killing of target cells with “missing self” by miseducation of the NK cell. Adapted from [12]. Figure made with BioRender.com. (C) Genomic organization of KIR A and B haplotypes. Adapted from [12].

NK cells are activated by target cells that down regulate “self” HLA. This NK activation mechanism appears by a phenomenon known as education or licensing. Education requires the interaction between inhibitory NK cell receptors and their own HLA ligands [13,14]. Educated NK cells remain inactive by the interaction of NKRs inhibitor with autologous HLA-expressing neighboring cells. However, NK cells can also be activated by viral infected cells and abnormal or injured cells that usually have a lower HLA class I expression to evade cytotoxicity driven by conventional CD8+ T cells. NK cells can detect these anomalous target cells by the lack of inhibiting interaction (low or non-inhibitory HLA interactions). This phenomenon is called “missing self” detection and generally results in NK cell activation, degranulation and target cell death (Figure 2B). For NK cell activation, additional activating signals are necessary [15]. NK cells are activated when the ratio of inhibitory and activator NKR signaling favors activation [9] (Figure 2B). Many inhibitory KIRs from NK cells interact with HLA alleles. KIR and HLA proteins are both encoded by highly polymorphic alleles, enabling a wide diversity of receptor/ligand interactions. Education through inhibitory receptors sensitizes NK cells to detect “missing self” cells, while education through activating receptors inhibited NK cell cytotoxicity [16] (Figure 2B).

Despite the high level of KIR gene content variability, there are two main groups of KIR haplotypes, termed “A” and “B” (Figure 2C). The A haplotypes include inhibitory KIR genes coding for receptors such as KIR3DL1, which recognize HLA-A and HLA-B molecules that contain Bw4 epitopes. The B haplotypes include several activating KIR genes such as KIR3DS1 (Figure 2C). Then, the KIR genetic combination can be AA, AB or BB genotype. There are two possible established epitopes for HLA-B: Bw4 or Bw6. KIR3DL1 is highly polymorphic and, depending on the haplotype, NK cells can express: high, low, or null levels of KIR3DL1 [17]. In fact, KIR3DL1 and HLA-B genetic polymorphisms regulate NK cell function. Their stronger ligand affinity correlates with enhanced NK cell inhibition but also with increased education and, consequently, potentiates “missing self” NK capacity to detect and kill anomalous cells [18] (Figure 2B).

The inhibitory NKG2A receptor binds to HLA-E molecules. Signal peptides from the leader sequence of HLA-A, -B and -C proteins, which are codified by the first exon of the MHC gene, must bind to HLA-E in order to fold properly and reach the cell membrane and to become a ligand for the inhibitory NKG2A receptor. In addition, the anchor residue of

the nonamer peptides that bind to HLA-E corresponds to residue -21 of the classical HLA class I leader sequence. There are two amino acid variations at position -21, a methionine (-21M) or a threonine (-21T) [19,20]. HLA-B antigens can have both -21M and -21T variants, depending on the HLA-B haplotypes that are associated with two NK cell education profiles. On the one hand, HLA-B -21M alleles contribute more effectively to NKG2A-mediated education, which suppresses NK cell activation when the target cell expresses stabilized levels of HLA-E. HLA-B -21T alleles mainly contribute to education through inhibitory KIRs, especially KIR3DL1 [15], as HLA-B -21T and HLA-Bw4 are genetically linked. Then, the HLA-Bw4 alleles are, in fact, HLA antigens encoded by -21T, able to interact and educate through KIR3DL1/HLA-Bw4, allowing the NK cell cytotoxicity upon “missing self” recognition [9,20] (Figure 2B).

## 2. Dasatinib-Mediated Immunomodulatory Effects in CML

### 2.1. Dasatinib Effect on NK Cells and Innate T Cells

Besides its direct impact on leukemic cells through inhibition of constitutive tyrosine kinase activity, dasatinib's off-target effects include: inhibition of proliferation and activation of T cells, and in vitro suppression of cytotoxic activity of NK cells [21,22]. This is due to the potent inhibition of several off-target kinases of the Src family, such as Lck and Fyn in T cells [23]. TKI treatments can restore an anti-leukemic effector function, such as specific cytotoxic T lymphocytes' (CTL) responses against leukemia-associated antigen (LAA). Overall, this results in a reduction in leukemic cell load major molecular remission (MMR) and a better recovery [24,25]. Dasatinib has the potential to reduce Tregs and derived factors (sCTLA-4), especially in patients developing large granular lymphocytes (LGLs), lymphocytosis [26] and NK cell differentiation, promoting immune stimulation [27]. This is relevant because the proportion of Treg cells is abnormally elevated in CML individuals at diagnosis, compared to healthy controls. Furthermore, dasatinib also reduces myeloid-derived suppressor cells (MDSC) in CML patients [28].

Up to half of the patients receiving dasatinib treatment develop an LGL lymphocytosis, mainly composed of cytotoxic cells (NK cells and CD8<sup>+</sup>  $\gamma\delta$  T cells) [29,30] but this also includes CD57<sup>+</sup> cytotoxic CD4<sup>+</sup> T cells with anti-leukemic properties [31]. This LGL expansion is associated with an improved anti-leukemic response in both CML and Ph+ ALL patients [29,32–35]. The CD8<sup>+</sup> T cell response in dasatinib-mediated LGL response includes TCR-V $\beta$ <sup>+</sup> expansion of either oligoclonal or polyclonal origin with cells resembling healthy memory CD8<sup>+</sup> T cells [36]. Importantly, dasatinib may have an immunomodulatory role in non-conventional or innate T cells by increasing cell number, activation status and Th-1 polarization of innate  $\alpha\beta$  iNKT-cells in treated CML patients [37]. In addition, it has been reported that dasatinib increased a novel innate subset termed innate CD8<sup>+</sup> T-cell-expressing IFN $\gamma$  [37].

CML patients treated with dasatinib presented more classical NK cells (CD3<sup>-</sup>CD56<sup>+</sup>) and matured NK cells (CD56<sup>+</sup>CD57<sup>+</sup>) compared to imatinib- or nilotinib-treated patients [38]. These patients also presented lower expression of NK-inhibitory markers (KIR2DL5A, KIR2DL5B and KIR2DL5), which was associated with an MMR [39] and an increase in KIR2DL1 expression [8].

Dasatinib promoted NK-cell cytokine expression and cytotoxic activity towards the CML-derived cell line K562 [18,40], especially when KIR3DL1/HLA-Bw4 interactions were null, low or weak. Of note, Izumi et al. showed that blocking KIR3DL1/HLA-Bw4 binding with an anti-KIR3DL1 antibody potentiated NK cytotoxicity [18]. Furthermore, Shen et al. reported that this increased NK cytotoxic activity can be emulated in vitro using dasatinib treatment after IL-2/IL-15-mediated expansion of NK cells. In this setting, dasatinib also increases the percentage of NKG2A<sup>-</sup>CD57<sup>+</sup> NK cells and the expression of activating receptors CD226 (DNAM-1), NKp46 and NKG2D [41], promoting their capacity to kill by degranulation of the CML cell line K562, not expressing HLA class I. Finally, dasatinib-mediated reduction of NKG2A also may boost NK cytotoxicity and improve MMR [18,42].

### 2.2. Dasatinib Increases Memory-like Natural Killer (NK) Subsets Displaying Activity against Both Leukemic and Cytomegalovirus (CMV) Infected Cells

There is discussion on whether development of LGLs with dasatinib is associated with previous immunity to CMV [32,43] or related to CMV viral load (VL) [7,43]. Ishiyama et al. reported that NK cells are the main component of LGLs in patients with CML treated with dasatinib, and NK cell expansion was highly associated with CMV-serostatus [7]. The authors performed a principal component analysis (PCA) with multiple markers on NK cells after dasatinib treatment and determined that NK cells from CMV<sup>+</sup> individuals had a CMV-associate phenotype, named memory-like NK cells, with highly differentiated NK phenotypes (NKG2C<sup>high</sup>NKG2A<sup>low</sup>CD57<sup>high</sup>LIR-1<sup>high</sup>NKp30<sup>low</sup>NKp46<sup>low</sup>). NK cells from CMV-uninfected individuals were negative for this CMV-related signature [7,44]. Remarkably, a higher grade of NK cell differentiation at CML diagnosis predicts both a greater expansion of CMV-related memory-like NK cells and a lower leukemic-cell load after dasatinib treatment in CMV<sup>+</sup>CML patients [7,44]. Kadowaki et al. reported that a persistent, low-level CMV replication, often subclinical, triggered memory-like NK cell expansion. This suggests that CMV may trigger NK-cell expansion and both leukemia and dasatinib are enhancing factors that expand this NK subpopulation [45]. This hypothesis was reviewed by Climent et al. [46]. Importantly, this NKG2C<sup>+</sup>CD57<sup>+</sup> subset of memory-like NK cells may represent NK cells with unique adaptive and editing properties [44]. Thus, the expansion of this subset could promote long-term memory and high cytotoxic activity against CML, even after dasatinib treatment interruption [45]. Recent studies have also observed an expansion of CD56<sup>neg</sup> NK cell populations exclusively in CMV<sup>+</sup> patients treated with dasatinib, and this increase parallels memory NKG2C<sup>+</sup>CD57<sup>+</sup> NK cells [47]. These authors propose that CD56<sup>-</sup> NK cells may be an exhausted population induced by chronic activation through CMV reactivation but, paradoxically, are proposed as a hallmark of CML control because it predicts a better clinical outcome. Overall, these results suggest that dasatinib immunomodulatory effects on NK cell responses against CMV could also be relevant against malignancies or other viral infections [48], such as HIV infection [46].

### 2.3. CML Control and Therapeutic Treatment Interruption: Immunological Factors Involved in a Successful Treatment-Free Remission (TFR)

Once a DMR is observed, TKI treatment can be interrupted in selected patients with the aim of achieving a TFR [49]. Dasatinib and nilotinib treatments are associated with a stronger DMR, increasing the chances of longer TFR [49]. A better understanding of the factors that could predict longer TFR is of paramount importance [50–52]. Moreover, half of the individuals who stopped treatment were able to keep TFR during at least one year and developed high levels of NK cells [53–55] and neutrophils [56] but not T cells [53,57] indicating that these populations are key to keeping CML under control.

Regarding the implication of NK cells in TFR, individuals who controlled CML after imatinib therapy cessation showed higher NK cytotoxic function towards the target K562 cell line, lacking HLA class I. Furthermore, NKG2D gene polymorphisms [58] and the IFN- $\gamma$  and TNF- $\alpha$  cytokine secretion by NK (CD56<sup>dim</sup>CD16<sup>-</sup>) cells correlated with the successful drug discontinuation and control of CML [57,59]. Increased mature (CD57<sup>+</sup>) and cytotoxic (CD16<sup>+</sup> and CD57<sup>+</sup>) NK cells, together with IFN therapy prior to TKI cessation, have been also shown to produce better CML outcomes after treatment interruption [60]. IFN $\alpha$  treatment also increased differentiated NKG2C<sup>+</sup> NK cells, increased NKp46 expression on the CD56<sup>bright</sup>/CD16<sup>-</sup> NK cell subpopulation and modulated NK cell cytotoxicity [61].

TFR has also been evaluated in dasatinib stopping TKI trials [62]. The DADI study [53,63] demonstrated that high levels of NK cells (CD56<sup>+</sup>), LGL NK cells (CD56<sup>+</sup>CD57<sup>+</sup>) and low levels of Treg (CD25<sup>+</sup>CD127<sup>low</sup>) preceding the dasatinib interruption were associated with longer TFR periods. Furthermore, a critical role of Treg inhibition by dasatinib, potentiating NK cell function, promotes a DMR [64]. Likely expanded NK cell functionality and lower Treg frequencies may decrease the probability of a worse outcome after dasatinib interruption and result in longer TFR [65].



Recent studies suggest that the features most consistently linked to longer TFR, independently of the type of TKI treatment stopped, are: (1) a high frequency of cytotoxic subsets such as NK, NKT and CD8<sup>+</sup>  $\gamma\delta$  T cells [66,67]; (2) high level of NK-activating receptors such as NKG2D, NKp30 or NKG2C on NK [11,67,68] and NKT cells [67]; (3) enhanced expression of activation cytokines or granzyme B in NK cells after stimulating with HSP70; and (4) KIR homozygosity at haplotype AA, which includes KIR3DL1. These hallmarks may be useful as prognostic biomarkers of longer TFR [67]. Further clinical trials are needed to test these predicting biomarkers for TFR [69]. Moreover, the memory-like NK cells, characterized as CD3<sup>-</sup> CD56<sup>dim</sup> CD57<sup>+</sup> NKG2A<sup>-</sup> NKG2C<sup>+</sup>, were increased in patients with TFR success [70].

Results concerning NKG2A expression on NK cells are controversial [11]. Several studies suggested that low levels of NKG2A expression in NK cells is associated with longer TFR [70] and better CML prognostic [42]. In stark contrast, Xu et al. reported that an elevated expression of NKG2A in NK cells, especially in the CD56<sup>bright</sup> subset, was a good prognostic biomarker for TFR [11], as also reported by Vigón et al. [67]. The inhibitor receptor NKG2A has a dual function on NK cells: firstly, it has a key function in the NK education process; second, after inhibition of NK cell activation it could send other signals to NK cells [71]. In fact, we recently found that high expression of NKG2A is present in NK cells able to kill cancerous cells such as reprogrammed cells or those that downregulate HLA-E. Reprogrammed cells express Yamanaka factors and this gives them the capacity of being pluripotent embryonic stem cells (e.g., teratoma-like cells). These educated NK cells are able to kill by the missing self-recognition [72]. NKG2A expression could not be per se detrimental to the function of all NK cell subsets. Altogether, the increased expression of NKG2A in the CD56<sup>bright</sup> subset could be interpreted as an increased killing capacity against target cells with lower expression of HLA-E, such as cancerous cells or CML cells [11].

#### 2.4. NK Immunogenetics Associated with CML Control or TFR

The diversity of allotypes of KIR3DL1 and HLA-Bw4 is associated with the receptor/ligand avidity and the NK cytotoxic capacity [12,17,73,74]. KIR genotypes have high genomic variations or allotypes that are associated with NK cell cytotoxic activity against CML and extended TFR periods [75,76]. Some reports suggested that CML patients with KIR2DL5B and KIR2DL2 alleles reached higher DMR after TKIs, implying that some KIR alleles or a specific combination of KIR genes can modify NK cell activity against CML cells [77,78]. In fact, KIR AA haplotypes, which include many KIR inhibitors such as KIR3DL1, are associated with better outcomes in TKI-treated CML patients [77] and are also linked to patients with sustained TFR [8,75]. It is interesting that the A haplotype including KIR3DL1 is highly associated with NK education (Figure 2B,C). Interaction of KIR3DL1 and HLA-Bw4 could affect NK cell education and cytotoxicity. In fact, the KIR3DL1\*005 allele was highly linked with DMR, suggesting the relevance of this specific KIR3DL1. Consistently, DMR was coupled with higher NK cell killing in vitro in a NK cell cytotoxic assay against the CML cell line K562 without HLA class I, indicating that these educated NK cells could contribute to eliminating CML cells in vivo (Figure 2B). However, verification is needed, and the specific A haplotype KIR gene with the greatest impact needs to be identified [12] (Figure 2B). It has been shown that haplotypes of KIRs and HLAs were linked to a better outcome in a Japanese cohort [18,76]; specifically, Ureshino et al. reported that TFR in patients with HLA-Bw4 was higher than in patients with HLA-Bw6 alleles [79]. Similarly, HLA-Bw4 has been related to HIV control [80]. Altogether these genetic associations suggest that NK cells from patients achieving DMR or TFR could be better educated by interaction between the inhibitor receptor KIR3DL1 and HLA-Bw4, allowing activation of NK cells against cancerous cells that downregulate HLA expression, triggering “missing-self activation” (Figure 2B). Clinical trials with large cohorts are needed in order to explore deeply the NK immunogenetic factors associated with CML control [12].

### 2.5. Dasatinib as an Immunomodulator in Other Therapeutic Strategies against Cancer

The immunomodulatory activity of dasatinib has also been evaluated in combination with other therapeutic strategies against advanced malignancies such (1) immunotherapy with immune checkpoint inhibitors, where dasatinib immunomodulatory capacity has been investigated in increased programmed cell death protein 1 (PD-1) and programmed cell death ligand 1 (PD-L1) (PD1-PDL1) immunotherapy [81,82]; or (2) with chimeric antigen receptor (CAR)-engineered T cells (CAR-T). In CAR-T therapies, T cells are ex vivo modified by adding a gene for a receptor that helps the T cells to target specific myeloid antigens. A combined CAR-T and TKI approach has also been evaluated in some studies to enhance antitumor immunity and demonstrated that dasatinib limits CAR-T cells' therapy side effects, such as the cytokine release syndrome (CRS) [83], and increases the anti-leukemia activity of CAR-T cells by decreasing cell exhaustion [84].

### 2.6. Summary of the CML Section

In brief, these findings support the idea that dasatinib contributes to better treatment response in CML patients through enhancement of the immune system, particularly via NK cell differentiation. CML patients with better outcomes could have done better due to genetic factors, such as AA alleles (homozygosis at KIR3DL1) and HLA-Bw4 associated with educated and highly cytotoxic NK cells able to detect malignant cells. Consequently, dasatinib could be useful, especially in the patients that do not have these protective features, to enhance cytotoxic activity of NK cells against CML cells by increasing memory-like NKG2C<sup>+</sup>CD57<sup>+</sup> NK cells [70],  $\gamma\delta$  T cells and other innate CD8<sup>+</sup> T cells [7,30,37,44]. In addition, these innate cells could express high levels of the activation receptor NKG2C, NKG2D, NKp46 or DNAM-1 and downregulate some inhibitory receptors such as NKG2A and KIR2DL5 [7,39,41,44] (Figure 1A).

## 3. Potential Use of Dasatinib in the Setting of HIV-1 Infection

Current antiretroviral therapy (ART) can prevent progression to AIDS, blocking new infections by interfering with the virus life cycle. ART efficiently decreases the plasma VL under the limit of detection of conventional techniques (50 copies/mL) but is unable to fully eliminate HIV from the body. Latently infected cells, established during the early stages of infection, harbor integrated forms of the virus that are responsible for viral rebound when ART is stopped. These viral reservoirs represent the major barrier to the complete eradication of HIV, because it is invisible to the immune system and inaccessible to treatment [85]. In recent years, several strategies have been proposed to eliminate these reservoirs, including the 'shock and kill' strategy, but none of them have demonstrated a significant decrease of the reservoir size [86]. Therefore, new strategies are needed to avoid the formation of the reservoir, but also its replenishment and maintenance, by additional mechanisms including immunotherapy and new immunomodulatory compounds [87].

### 3.1. Effect of Dasatinib on HIV Infection and Reservoir: Direct Effect

Dasatinib directly interferes with CD4<sup>+</sup> T-cell activation, which is the main HIV-1 cell target, by inhibiting the Src TK implicated in T cell receptor (TCR) signaling and the phosphorylation of SAM domain and HD domain-containing protein 1 (SAMHD1), a cell restriction factor. Here, we discuss the potential use of dasatinib as an adjuvant of the ART during HIV-1 infection. This strategy might reduce the viral reservoir and control infection [87–89]. Quite unexpectedly, CD4<sup>+</sup> T cells from CML individuals under dasatinib therapy were shown to be resistant to ex vivo HIV-1 infection [88,90]. Results from our own work showed that dasatinib preserved SAMHD1 activity, by maintaining its active conformation, which restricts HIV-1 replication [46,87–89]. This enzyme controls homeostatic balance of dNTPs. When active (unphosphorylated), SAMHD1 restricts HIV-1 replication by lowering dNTP to levels that do not allow an effective viral replication. In contrast, when SAMHD1 is inactive (phosphorylated), it increases intracellular dNTPs' availability, facilitating HIV-1 replication [46,87–89]. Moreover, Williams et al. described

how the inhibition of cyclin-dependent kinases (CDKs) 1, 2, 4 and 6 in macrophages by dasatinib leads to blockade of HIV-1 infection by dephosphorylation of SAMHD1. This confers protection from the virus not only in the CD4<sup>+</sup> T cells but also in monocyte-derived macrophages [91].

Dasatinib targets multiple host non-receptor tyrosine kinases, in particular the ABL family of kinases such as ABL1 or ARG. It has been demonstrated that siRNA knockdown of ABL1 and ARG kinases inhibits HIV-1 at a step after reverse transcription during early infection of activated CD4<sup>+</sup> T cells, increasing the unintegrated two-long terminal repeat DNA circles (2-LTRCs) generated through the ligation of the cDNA ends by the host cell non-homologous DNA end-joining system. These results suggest preliminary efficacy of dasatinib treatment during acute HIV-1 infection [92]. Meanwhile, Bermejo et al. and Vigón et al. found that the frequency of proviral integration was strongly reduced in activated CD4<sup>+</sup> T cells from CML patients treated with dasatinib compared with those from untreated healthy donors [88,93]. Importantly, we collaborated to find that peripheral blood lymphocytes obtained from CML patients treated for at least 6 months with dasatinib and individuals that were in TFR for more than one year were resistant to HIV-1 infection [46,93]. This indicates that mechanisms other than SAMHD1 phosphorylation are implicated and suggests an immunomodulatory role of dasatinib.

Despite CML and HIV-1 infection not being commonly associated, several cases of people living with HIV (PLWH) who developed CML have been described. Studies performed on this special subset of HIV<sup>+</sup> individuals treated with ART and dasatinib showed that the frequency of latently infected cells was reduced more than 5-fold compared with PLWH only on ART. In addition, reactivation of proviruses in CD4<sup>+</sup> T cells isolated from PLWH with CML on ART and dasatinib was reduced 7-fold compared with individuals only on ART. Importantly, dasatinib treatment dramatically impaired SAMHD1 phosphorylation *both in vitro and in vivo* (30-fold and 21-fold, respectively) [94]. Dasatinib also blocks CD4<sup>+</sup> T cell proliferation induced by homeostatic cytokines such as IL-7 and IL-15, which are crucial for the stability of the viral reservoir. Innis et al. described the restriction of both homeostatic and antigen-driven proliferation in memory CD4<sup>+</sup> T cells from PLWH by dasatinib, consistent with promoting a smaller reservoir size [95]. In addition, the antimetabolic properties associated with dasatinib can reduce the clonal expansion of infected cells, limiting the permanent filling of viral reservoirs [87].

### 3.2. Dasatinib's Indirect Effect in HIV-1 Infection: Potentiation of NK and $\gamma\delta$ CD8<sup>+</sup>T Cell Responses

Vigón et al. suggested that potentiation of memory-like NK cells and a  $\gamma\delta$  CD8<sup>+</sup> T cell responses in dasatinib-treated CML patients may contribute to the observed resistance of these individuals' PBMCs to HIV-1 infection. This mechanism would operate in parallel to the previously described phosphorylation of SAMHD1 [93]. Interestingly, this increased cytotoxic activity of memory-like NK cells and a  $\gamma\delta$  CD8<sup>+</sup> T cell subsets might be effective both against HIV infection and CML. A similar cytotoxic cell signature has recently been described in a case of exceptional HIV long-term post-treatment control (>15 years, Barcelona patient). This control has been linked to a strong memory-like NK cell response, with NKG2C<sup>+</sup>CD57<sup>+</sup> phenotype and  $\gamma\delta$  cytotoxic CD8<sup>+</sup> T cells [96]. This NK cell phenotype (NKG2C<sup>+</sup>CD57<sup>+</sup>) was also found in long-term HIV elite controllers [97] and in individuals during primary infection who showed lower HIV RNA expression and more quickly reached an undetectable VL [98–100]. The above phenotype has been described together with a reduction of KIR2DL5, NKG2A (inhibitory receptors) and Nkp30 in NK cells [93,97].

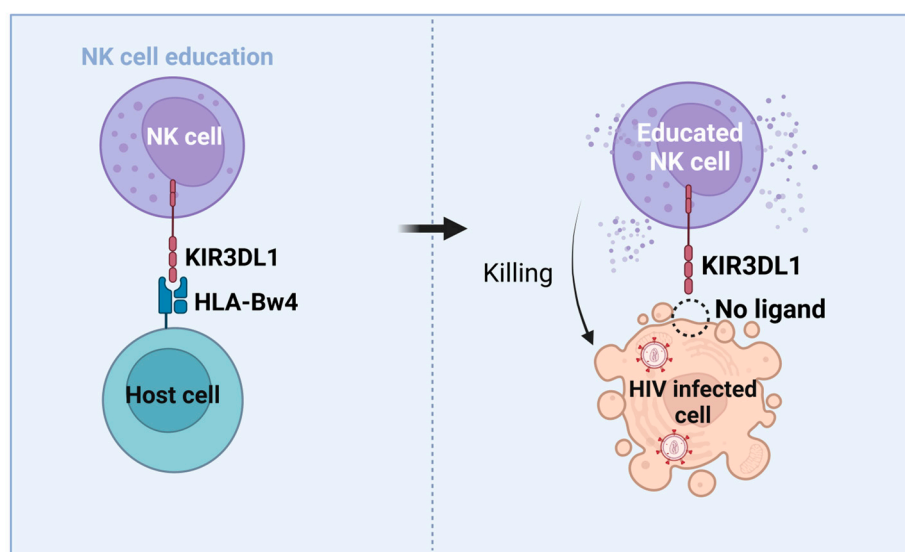
Taking all this into account, it could be considered that, despite immune exhaustion in PLWH, dasatinib is able to increase NK memory-like (CD56<sup>+</sup>CD57<sup>+</sup>) and  $\gamma\delta$  CD8<sup>+</sup> T cells subsets and to reduce NKG2A expression in NK cells [42], contributing to HIV-1 infection control.

### 3.3. NK Cells' Role in HIV-Mediated Control and Functional Cure

Functional HIV cure, defined as control of viral replication in the absence of treatment, has been described in two scenarios: in those PLWH who maintain undetectable HIV VL (<50 copies/mL) in the absence of ART, known as “elite controllers” (EC), and those individuals who demonstrate sustained virologic suppression for months or years after treatment cessation, called “post-treatment controllers” (PTC). The definitions of these patients vary depending on the time elapsed without treatment, since in many of them a “loss of control” occurs over time, defined by an increase in VL, which makes it necessary to restart ART. The patients of greatest medical and biological interest are those who have controlled the infection for at least ten years in the absence of ART and will be called long-term or exceptional elite controllers (LTEC or EEC) and long-term post-treatment controllers (LTPTC). This rare subset of patients may serve as a realistic model of a functional cure for HIV-1. LTPTC have a NK-mediated HIV control [96]. Most LTPTC are patients treated in the acute infection phase in whom spontaneous control of the viral load is observed when the treatment is discontinued months or years later [101,102]. The percentage of LTPTC patients is difficult to estimate and although some authors put it at 10%, it is probably lower [101].

### 3.4. Immunogenetic Factors of HIV Control and Functional Cure

The most relevant genetic alleles that are associated with HIV control are the HLA-B allotypes, such as HLA-B\*57 and HLA-B\*27, both being members of the HLA-Bw4 epitope [103]. Interestingly, HLA-Bw4 homozygosity is associated with HIV control and protection [80,104–106]. HLA-A expression levels change from one allotype to another [107]. Decreased HLA-A expression correlates with HIV control, being seen in the EC patients that have reduced HLA-A levels [107]. In addition, -21T amino acid variation at the signal peptide HLA-B has been associated with being HLA-Bw4 [9,20]. For that reason, homozygosity at HLA-B -21T, likely associated with Bw4 homozygosity, contributes to HIV control [80]. Some KIR3DL1/Bw4 combinations also are associated with HIV control [9]. In this context, HLA alleles carrying HLA-B -21T, such as Bw4 and low-expression HLA-A allotypes, codify HLA molecules that reduce HLA-E levels in HIV-infected CD4<sup>+</sup> T cells. Once KIR3DL1/HLA-Bw4-educated NK cells interact with HIV-infected target cells expressing low levels of HLA-E, activation of NK cells by lack of inhibitory signaling could be able to enhance cytotoxic function against HIV-infected cells, thus promoting HIV control [9,107] (Figure 3).



**Figure 3.** NK cell education outline in HIV context by KIR3DL1/HLA-Bw4, associated with HIV infection control. Adapted from [9]. Figure made with BioRender.com.

Consistently, *in vitro* experiments have suggested that KIR3DL1/HLA-Bw4 genotype combinations have higher educated NK cytotoxic responses than NK cells from Bw6 homozygotes against HLA-downregulated target CML cell lines (K562) [9,108–110] or HIV-infected CD4<sup>+</sup> T cells that decreased the levels of HLA-A, -B and -C by Nef and Vpu HIV proteins [111–114] emulating the missing-self NK cytotoxic activity (Figure 3) [4,114,115]. Moreover, a higher number of educated NK cells by KIR2DL1/HLA-C2 and KIR2DL3/HLA-C1 interactions can mediate the killing of K562 cell lines and HIV-infected CD4<sup>+</sup> T cells compared with uneducated NK cells [9,116,117].

HIV control in children Bw4 has been linked to reduced levels of HLA-A. In fact, levels of HLA-A in cells depends on the specific HLA-A alleles [105,107,118]. HLA-Bw4 mediates education of NK cells by its NK ligand, KIR3DL1. In fact, controller children reportedly had enriched Bw4 and co-expressed KIR3DL1, which educates these NK cells [9]. A deletion in the NKG2C gene is also associated with enhanced HIV infection, suggesting that this NK-activating receptor is a clue in the context of HIV protection [119].

Recently communicated data from several international congresses published by our group reported that LTPTC are enriched in alleles implicated in educated NK cells. Sáez-Ciri3n et al. found that LTPTC had certain education-related alleles such as homozygosity at HLA-Bw4 and its ligand, KIR3DL1, and also at HLAB\*35, which is also an HLA-B -21 T allotype [120,121]. In fact, the HLA-B\*35 allele is not a Bw4 epitope, but exceptionally is an HLA-B -21T [20,107]. These results suggest that HLA -21T (HLA B\*35), Bw4 (also HLA -21T) and KIR3DL1 alleles have been associated with HIV LTPTC, suggesting an important role of NK cell education in NK-mediated HIV control [96,121]. These recent data point to a possible role of NK cells and, possibly, other innate T cells such as  $\gamma\delta$  T cells, in LTPTC HIV control process [96,122].

Moreover, a recent communication indicated that EEC have a high content of homozygous Bw4 alleles. In fact, 75% of EEC have two Bw4 alleles, suggesting that a high amount Bw4 homozygosity could be related to HIV functional cure [123–129]. Consistently, another recent communication suggests that LTEC have a high percentage of NKG2C<sup>+</sup>CD57<sup>+</sup> NK cells [97]. Due to similar features in EEC and LTEC, such as persistent HIV control for more than 10 years, we could hypothesize that the high frequency of memory-like NK cells found in LTEC could be related to favorable NK immunogenetic characteristics. Thus, these features could be linked to HIV long-term control and functional cure. Consistent with these data and as Sáez-Ciri3n communicated [120], our recently published results concerning the case report of the “Barcelona patient”, reveal that this patient is a homozygote not only for the HLA haplotypes KIR3DL1/HLA-Bw4, but also for KIR2DL3/HLA-C1 (C\*16) alleles. In fact, both genotypes are compatible with highly educated NK cells. Moreover, we found that this genotype is linked to an increased expansion of memory-like NK cells and  $\gamma\delta$  CD8<sup>+</sup> T cell subpopulations associated with persistent HIV control and a low viral reservoir. These factors might be contributing to the observed HIV functional cure [96].

In summary, homozygosity at Bw4, and homozygosity at -21T and at KIR3DL1 genes is highly associated with persistent HIV control. These results may suggest that PLWH with these genetic features could educate NK cells by the KIR3DL1/HLA-Bw4 interaction having an enhanced capacity to mediate killing of HIV-infected CD4<sup>+</sup> T cells (Figure 3) than the ones with uneducated NK cells. This fact suggests that not only CTL but also NK cells could have an important role in HIV control and protection. Genetic studies of NK cell education alleles related to both NKG2A/HLA-E, KIR/HLA-B interactions and HLA-A and HLA-B -21 alleles could increase the knowledge of the NK immunogenetics associated with HIV functional cure. Larger clinical trials with cohorts of LTPTC, LTEC or EEC will be necessary to explore more deeply whether protective HLA and KIR allotypes are able to potentiate NK cells against HIV infected cells by KIR3DL1/HLA-Bw4 NK education [9].

### 3.5. Summary of the HIV Section

In conclusion, due to the fact that dasatinib is able to induce these innate NK and  $\gamma\delta$  T cell subsets highly associated with long-term HIV control, the use of this drug could

be a new strategy in the HIV functional cure field. Dasatinib could activate NK cells by up-regulation of activating receptors such as NKG2C, NKG2D, NKP46 and reducing the NKG2A/HLA-E interaction by reducing NKG2A expression in NK cells mediating HIV- infected cells killing (Figure 1B). Dasatinib could act against HIV-1 by maintaining the antiviral effect of SAMHD1 and by inhibiting CD4<sup>+</sup> T-cell activation and proliferation, reducing the establishment of viral reservoirs and limiting the replenishment and maintenance of infected cells. Additionally, the potentiation of subpopulations such as memory-like NK cells and  $\gamma\delta$  CD8<sup>+</sup> T cells associated with low reservoirs, persistent HIV control and having high cytotoxic potential against HIV infected cells could be key against HIV-1 infection.

Clinical trials using dasatinib as a new immunomodulatory drug that potentiates innate cytotoxic cells could be relevant to increase the knowledge on the role of dasatinib as an NK-activating drug against HIV infection. In fact, our group has a recently approved pilot clinical trial (DASAHIVCURE NCT05527418) that will test the safety, tolerability, and antiretroviral activity of dasatinib in a cohort of recently asymptomatic HIV-infected individuals. This study will evaluate the capacity of dasatinib to inhibit HIV replication and to potentiate cytotoxic responses against HIV mediated by NK and  $\gamma\delta$  T cells.

#### 4. Dasatinib as a Senolytic Drug

##### 4.1. Cellular Senescence Results in Increased Immune Surveillance

Cellular senescence is activated in response to a myriad of stressors or insults. Senescent cells display a series of features that result in the recruitment and activation of immune cells with the ultimate goal of removing damaged cells and restoring tissue homeostasis. Thus, activation of cellular senescence has beneficial effects in wound healing, tissue regeneration and blocking tumor progression [130–132]. However, accumulation of senescent cells during aging or due to different pathologies has deleterious consequences [133].

To target senescent cells, it is key to define characteristic biomarkers, taking into consideration that these will vary depending on cell type and the type of stress [134]. The upregulation of cell cycle inhibitors such as p16<sup>INK4a</sup>, p21<sup>CIP1</sup> and p53, or the increased expression of BCL-2, an anti-apoptotic marker, define most senescent cell types. In addition, these cells present some metabolic changes, such as an augmented activity of lysosomal senescence-associated  $\beta$ -galactosidase (SA- $\beta$ -gal) due to a mitochondrial expansion, and also secrete specific inflammatory factors named senescence-associated secretory phenotype or SASP [133].

Immunosurveillance mechanisms are key to detect and eliminate senescent cells. A growing body of evidence points towards NK cells and their activating receptors as key cells in removing senescent cells. Gasser et al. first reported that NKG2D ligands ULBP1, ULBP2 and ULBP3 were upregulated in human fibroblasts after ionizing radiation or inhibitors of DNA replication, stimuli that activate the ATM/ATR DNA damage response and are now known to induce cellular senescence [135].

Krizhanovsky's group [136] found that senescent cells accumulate in the liver of mice treated with CCl<sub>4</sub>, a chemical known to induce liver fibrosis. Livers from p53 and INK4a/ARF double knockout animals showed up to a 50% increase in liver fibrosis markers after CCL4 treatment compared to WT animals, with little to no accumulation of senescent cells. While WT animals fully resolved liver fibrosis and eliminated senescent cells in 20 days after treatment, double KO animals were severely impaired in doing so, underscoring that inducing cell senescence is important for liver fibrosis resolution [136]. Through gene profiling of senescent hepatic stellate cells (HSCs), authors show that many genes upregulated in those cells mediate an increased NK cell function, including CD58, IL-8 and NKG2D ligands such as MICA, ULBP2. Depletion of NK cells in these mice models resulted in delayed fibrosis resolution and incomplete senescent cells' removal. Conversely, boosting NK cell function with Poly I:C (TL3-agonist) resulted in decreased fibrosis and reduced senescent cell persistence. Several studies have expanded this knowledge, showing that a wide variety of senescent cells express increased levels of NKG2D ligands, such as

MICA, ULBP1 and ULBP2, in response to DNA damage (etoposide), telomere shortening (replicative renaissance) or H-RAS<sup>V12</sup> overexpression (oncogene-induced senescence) [137]. Further, pharmacological blockade or gene knockdown (siRNA) of NKG2D interaction with MICA or ULBP2 ligands reduces NK-mediated cytotoxicity towards senescent cells by 80–90% in vitro [137], confirming the important role of NKG2D and NK cells in removing senescent cells.

Interestingly, a recent study shows that activated invariant natural killer T cells (iNKT) are able to target and eliminate senescent cells both in a human in vitro setting and in two different mouse in vivo models [138]. Authors report that beta-2-microglobulin (B2M) and CD1d are upregulated in senescent cells, forming a complex that activates iNKT cells [138].

It is widely known that senescent cells accumulate with chronological age and that immune function also declines over time. Recent studies show that perforin release and binding (a key effector mechanism of NK and other cytotoxic cells) in the immunological synapse declines with age [139]. This is further modeled in *prf<sup>-/-</sup>* KO mice, which lack perforin. These mice show an up to 2- to 4-fold increase in senescent cells across a variety of tissues, resulting in chronic inflammation and increased age-related disorders, showing that cytotoxic activity has an important role to avoid excessive senescent cell accumulation.

All of this body of evidence suggests that NK cells could be harnessed as a therapeutic option to remove senescent cells. To this end, [140] has already shown that infusion of autologous, in vitro expanded and activated NK cells ( $1 \times 10^9$ ) can reduce p16<sup>INK4a</sup> and SA- $\beta$ -gal in PBMCs up to 90 days after infusion.

#### 4.2. NK Cells Can Remove Senescent Tumor Cells

In the cancer research setting, the contribution of cellular senescence to immune surveillance is demonstrated by reactivation of endogenous p53 in p53-deficient tumors [141]. Briefly, reactivating p53 in such tumors causes cell senescence, in vitro cell cycle arrest, and triggers an NK-mediated immune response that targets tumor cells in vivo, resulting in tumor regression. Further studies using the same p53 reactivation model in mice showed that the elimination of senescent tumor cells depend on NKG2D expression. In addition, p53 is key for senescent cells to secrete pro-inflammatory chemokines such as CCL2 that recruit NK cells to senescent cells [142]. A blocking antibody against CCL2 prevented NK cell recruitment to senescent tumors, reducing their elimination. This contribution of the SASP for an optimal NK cell function was also revealed in a model of therapy-induced tumor senescence, where targeting the p65 subunit of NF- $\kappa$ B reduced senescent SASP secretion and proper NK-cytotoxic function [143].

The fact that senescent cells are prone to be detected and cleared by the immune system prompted researchers to test inducing cell senescence in tumors to address whether malignant cells can be then eliminated by the immune system. New therapeutic avenues are being studied to sensitize cancer cells to NK-mediated killing. In this regard, the chemotherapeutic drug doxorubicin, which is also a senescence-inducing drug, is able to improve NK-mediated killing of the MCF7 breast cancer cell line, through upregulation of death receptors FASR [144].

#### 4.3. Senescent Cells Can Avoid NK-Cell Recognition, Thwarting Immune Clearance

While activating NK ligands are clearly upregulated in senescent cells, these cells may also upregulate inhibitory signals, resulting in the inhibition of NK-cell function. In this regard, Pereira et al. elegantly showed that primary human dermal fibroblasts were made senescent by ionizing radiation upregulating HLA-E [145]. This results in NK cell and T CD8<sup>+</sup> cell inhibition as a result of NKG2A ligation in those cells. HLA-E upregulation seems greatly dependent on SASP mediators such as IL-6 and the activation of the P38 signaling pathway. Authors confirm that NKG2D is key for NK-mediated killing of senescent cells, as blocking NKG2D with a monoclonal antibody abrogates NK-mediated killing of senescent fibroblasts. Conversely, authors showed for the first time that blocking or inhibiting NKG2A with siRNA actually boosted NK-mediated senescent killing.

This underscores the key role of these receptors in senescent or tumor cell removal [146]. Additional mechanisms of NK-cell resistance include the SASP-mediated recruitment of CCR2<sup>+</sup> immature myeloid cells (iMC), which inhibit NK-cell inhibition in established tumors, thus further contributing to tumor growth [147,148].

#### 4.4. Dasatinib as a Senolytic Therapy in Animal Models and Human Models

The senolytic effect of dasatinib was first reported by Zhu et al., after a transcript analysis of preadipocytes made senescent by ionizing radiation (10 Gy) [149]. Further analysis showed increased negative regulators of apoptosis and anti-apoptotic gene sets in senescent cells such as ephrin receptors, the BCL-2/BCL-XL family, P13K/AKT, HIF-1a and others. Out of a panel of 46 drug candidates targeting these pathways, dasatinib and quercetin (D+Q) showed promise in selectively eliminating senescent preadipocytes, although with much reduced effect in other senescent cell types [149]. Importantly, the broad-spectrum tyrosine kinase inhibition mediated by dasatinib interferes with the ephrin receptor family (EFNB), which are the most extended tyrosine kinase receptor family and mediate key antiapoptotic signals [149].

In Zhu et al.'s work, in vivo administration of D+Q reduced the senescent cell burden in chronologically aged, radiation-exposed, and progeroid *Erc1*<sup>-</sup>/D mice, delaying age-related symptoms and pathologies [149]. A similar effect was observed by Xu et al., when they found a healthier, longer mouse lifespan as a result of a senolytic therapy with dasatinib [140]. Since this first observation, D or D+Q senolytic strategies have been successfully used in a wide range of mouse models of diseases such as lung fibrosis [150], renal fibrosis [151], T2 diabetes [152] vascular pathology and atherosclerosis [153]. In all these models, D+Q reduced the senescent cell burden and improved organ function and physical health of treated animals. In the mouse setting, intestinal inflammation was reduced after D+Q intervention [154]. These D+Q effects have also been addressed in zebrafish models of skin inflammation and fatty liver disease, also resulting in reduced inflammation after therapy [155].

There are two early phase clinical trials with published results on D+Q senolytic therapy. The first in-human open-label pilot study (NCT02874989) showed that intermittent D+Q treatment (100 mg D + 1250 mg Q over three consecutive days in three consecutive weeks) is feasible, well tolerated and can alleviate physical dysfunction in idiopathic pulmonary fibrosis [156]. The second study (NCT02848131) showed that a single, 3-day dose of D+Q significantly reduced senescent cell burden (p16<sup>INK4a</sup>, P21<sup>CIP</sup> and SA-β-gal positive cells) and plasma pro-inflammatory SASP mediators in diabetic kidney disease [157].

Different clinical trials are currently ongoing comparing the D + Q senolytic strategy to other drugs such as Fisetin in a variety of conditions, ranging from Alzheimer disease (NCT04063124) to hematopoietic stem cell transplant survivors (who are at risk of premature aging) (NCT02652052) and skeletal muscle health in older individuals (NCT04313634). More clinical trials are under way [158], which will shed light on whether senolytic D+Q treatments can improve a number of conditions.

In addition to its senolytic effects, D+Q therapy has also been shown to reduce the secretion of pro-inflammatory molecules and SASP mediators. In this regard, D+Q reduced the secretion of pro-inflammatory cytokines in human adipose tissue explants from obese individuals [153]. In the HIV context, our own work shows that D+Q senolytic therapy is able to reduce senescence biomarkers in PBMCs derived from PLWH [159].

While NK function is key to remove senescent cells both in vitro and in vivo, we are not aware of studies addressing whether senolytic treatment (dasatinib or others) may impact NK cell-mediated senescent cell clearance. This would be valuable to better understand the beneficial effects of dasatinib senolytic treatments. Furthermore, while promising, D+Q senolytic therapy may not be effective in all in vitro models, underscoring the importance of the experimental setting and cell type chosen when evaluating D+Q effects [149,160,161].



Results of ongoing studies and clinical trials will give clues to demonstrate if D+Q remains effective against aging related pathologies and could be translated towards new effective and safe anti-aging therapies.

#### 4.5. Summary of the Senescence Section

Dasatinib treatment is effective in removing senescent cells in a wide variety of conditions, as shown in human clinical models. In addition, more evidence points to NK cells being key in senescent cell clearance and immunosurveillance. Dasatinib has the potential to activate NK cells by downregulating inhibitory receptors such as NKG2A and increasing activating receptors such as NKG2C and NKG2D. Thus, dasatinib may potentiate the NK cytotoxic effect against senescent cells. More research is needed in the aging field to attempt to elucidate this open question and the interesting therapeutic avenue (Figure 1C).

### 5. Concluding Remarks and Perspectives

Dasatinib treatment in CML induced populations of NK memory-like cells,  $\gamma\delta$  T cells and other innate T cells, which are associated with better prognosis of CML, a possible indefinite TFR and good cellular response. Knowledge on the precise mechanisms by which dasatinib treatment yields these immunomodulatory effects is important, as this may improve treatment interruption parameters in CML, but also help to fight against other malignancies (Figure 1A).

A future goal is to explore whether dasatinib could safely prevent HIV-1 replication in patients both directly inhibiting SAMHD1-phosphorylation and also indirectly promoting the expansion of NK (NKG2C<sup>+</sup>CD57<sup>+</sup>) cells,  $\gamma\delta$  T cells and other innate T cells. These cell subsets show a highly effective anti-HIV response and seem to be expanded in CMV<sup>+</sup> individuals. Recently, our published data concerning the case of a functionally cured HIV patient suggest that there are genetic features associated with the expansion of these innate NK and  $\gamma\delta$  T cell subsets that allow HIV persistent control. Consequently, strategies able to expand these subpopulations are important to potentiate NK cytotoxicity against HIV. This would be extremely valuable in PLWH without these genetic characteristics and may pave the way to achieve a possible functional cure. The use of dasatinib in combination with ART or new combined immunotherapies could protect CD4<sup>+</sup> T cells and macrophages from HIV infection and activate a powerful cytotoxic response that could promote the elimination of the viral reservoirs (Figure 1B) and also reduce HIV-associated inflammation and senescence.

Finally, dasatinib shows potential against inflammation and cellular senescence or aging (Figure 1C). While most senolytic effects are reported in synergy with quercetin, dasatinib on its own downregulates NKG2A and increases NKG2C and -D in NK cells. Thus, dasatinib could potentiate the already important role of NK cells in removing senescent cells, which may be an important contributor to the overall senolytic effects. More research is needed in the field to attempt to elucidate this open question.

**Author Contributions:** N.C., A.R.-A., V.C., J.G.-E., S.S.-P. and J.A. conceived and wrote the review manuscript. All authors have read and agreed to the published version of the manuscript.

**Funding:** This review was partially supported by grants from the “Programa de becas Gilead a la investigación Biomédica GLD21\_00111”; “Fondo Europeo para el Desarrollo Regional” (FEDER); the SPANISH AIDS Research Network RD12/0017/0001, RD16/0025/0002 and RD16/0025/0014-ISCIII-FEDER (RIS); the “Fondo de Investigación Sanitaria” (FIS) PI04/0363, PI20/00676; HIVACAT Programme and the CERCA Programme/“Generalitat de Catalunya” SGR 615 and SGR 653. Our group received funding from “la Caixa” Foundation under agreement, as well as from CIBERINFEC from the “Instituto de Salud Carlos III”, Madrid, Spain.

**Acknowledgments:** We would like to acknowledge all PLWH participants who made research possible. We would especially like to thank María José Maleno, Cristina Rovira and Carmen Hurtado for their technical support and advice.

**Conflicts of Interest:** The authors declare that the research was conducted in the absence of any commercial or financial relationships that could be construed as a potential conflict of interest.

## References

1. Simoneau, C.-A. Treating Chronic Myeloid Leukemia: Improving Management through Understanding of the Patient Experience. *Clin. J. Oncol. Nurs.* **2013**, *17*, E13–E20. [CrossRef]
2. D’Antonio, J. Chronic Myelogenous Leukemia. *Clin. J. Oncol. Nurs.* **2007**, *9*, 535–538. [CrossRef]
3. Quintás-Cardama, A.; Kantarjian, H.; Cortes, J. Imatinib and Beyond—Exploring the Full Potential of Targeted Therapy for CML. *Nat. Rev. Clin. Oncol.* **2009**, *6*, 535–543. [CrossRef]
4. Thompson, P.A.; Kantarjian, H.M.; Cortes, J.E. Diagnosis and Treatment of Chronic Myeloid Leukemia in 2015. *Mayo Clin. Proc.* **2015**, *90*, 1440–1454. [CrossRef]
5. Araujo, J.; Logothetis, C. Dasatinib: A Potent SRC Inhibitor in Clinical Development for the Treatment of Solid Tumors. *Cancer Treat Rev* **2010**, *36*, 492–500. [CrossRef]
6. Cheng, F.; Xu, Q.; Li, Q.; Cui, Z.; Li, W.; Zeng, F. Adverse Reactions after Treatment with Dasatinib in Chronic Myeloid Leukemia: Characteristics, Potential Mechanisms, and Clinical Management Strategies. *Front Oncol* **2023**, *13*, 1113462. [CrossRef]
7. Ishiyama, K.; Kitawaki, T.; Sugimoto, N.; Sozu, T.; Anzai, N.; Okada, M.; Nohgawa, M.; Hatanaka, K.; Arima, N.; Ishikawa, T.; et al. Principal Component Analysis Uncovers Cytomegalovirus-Associated NK Cell Activation in Ph<sup>+</sup> Leukemia Patients Treated with Dasatinib. *Leukemia* **2017**, *31*, 268. [CrossRef]
8. Hsieh, Y.-C.; Kirschner, K.; Copland, M. Improving Outcomes in Chronic Myeloid Leukemia through Harnessing the Immunological Landscape. *Leukemia* **2021**, *35*, 1229–1242. [CrossRef] [PubMed]
9. Bernard, N.F.; Kant, S.; Kiani, Z.; Tremblay, C.; Dupuy, F.P. Natural Killer Cells in Antibody Independent and Antibody Dependent HIV Control. *Front. Immunol.* **2022**, *13*, 879124. [CrossRef] [PubMed]
10. Liu, H.; Wang, S.; Xin, J.; Wang, J.; Yao, C.; Zhang, Z. Role of NKG2D and Its Ligands in Cancer Immunotherapy. *Am. J. Cancer Res.* **2019**, *9*, 2064–2078. [PubMed]
11. Xu, Z.; Yin, J.; Sun, Q.; Hu, J.; Hong, M.; Qian, S.; Liu, W. The Prognostic Role of NKG2A Expression for Patients with Chronic Myeloid Leukemia after Treatment Discontinuation. *Leuk. Lymphoma* **2022**, *63*, 2616–2626. [CrossRef] [PubMed]
12. Shindo, T.; Ureshino, H.; Kojima, H.; Tanaka, H.; Kimura, S. Allelic Polymorphisms of KIRs and Antitumor Immunity against Chronic Myeloid Leukemia. *Immunol. Med.* **2021**, *44*, 61–68. [CrossRef] [PubMed]
13. Kim, S.; Poursine-Laurent, J.; Truscott, S.M.; Lybarger, L.; Song, Y.-J.; Yang, L.; French, A.R.; Sunwoo, J.B.; Lemieux, S.; Hansen, T.H.; et al. Licensing of Natural Killer Cells by Host Major Histocompatibility Complex Class I Molecules. *Nature* **2005**, *436*, 709–713. [CrossRef]
14. Boudreau, J.E.; Hsu, K.C. Natural Killer Cell Education and the Response to Infection and Cancer Therapy: Stay Tuned. *Trends Immunol.* **2018**, *39*, 222–239. [CrossRef]
15. Long, E.O.; Kim, H.S.; Liu, D.; Peterson, M.E.; Rajagopalan, S. Controlling Natural Killer Cell Responses: Integration of Signals for Activation and Inhibition. *Annu. Rev. Immunol.* **2013**, *31*, 227–258. [CrossRef] [PubMed]
16. Fauriat, C.; Ivarsson, M.A.; Ljunggren, H.-G.; Malmberg, K.-J.; Michaëlsson, J. Education of Human Natural Killer Cells by Activating Killer Cell Immunoglobulin-like Receptors. *Blood* **2010**, *115*, 1166–1174. [CrossRef]
17. Gardiner, C.M.; Guethlein, L.A.; Shilling, H.G.; Pando, M.; Carr, W.H.; Rajalingam, R.; Vilches, C.; Parham, P. Different NK Cell Surface Phenotypes Defined by the DX9 Antibody Are Due to KIR3DL1 Gene Polymorphism. *J. Immunol.* **2001**, *166*, 2992–3001. [CrossRef]
18. Izumi, K.; Shindo, T.; Ngo, H.T.; Nakayama-Hosoya, K.; Akahane, K.; Tamai, M.; Nguyen, T.T.T.; Kawana-Tachikawa, A.; Inukai, T.; Takaori-Kondo, A. KIR3DL1 Allotype-Dependent Modulation of NK Cell Immunity against Chronic Myeloid Leukemia. *Immunohorizons* **2021**, *5*, 687–702. [CrossRef]
19. Lee, N.; Goodlett, D.R.; Ishitani, A.; Marquardt, H.; Geraghty, D.E. HLA-E Surface Expression Depends on Binding of TAP-Dependent Peptides Derived from Certain HLA Class I Signal Sequences. *J. Immunol.* **1998**, *160*, 4951–4960. [CrossRef]
20. Horowitz, A.; Djaoud, Z.; Nemat-Gorgani, N.; Blokhuis, J.; Hilton, H.G.; Béziat, V.; Malmberg, K.-J.; Norman, P.J.; Guethlein, L.A.; Parham, P. Class I HLA Haplotypes Form Two Schools That Educate NK Cells in Different Ways. *Sci. Immunol.* **2016**, *1*, eaag1672. [CrossRef]
21. Marinelli Busilacchi, E.; Costantini, A.; Viola, N.; Costantini, B.; Olivieri, J.; Butini, L.; Mancini, G.; Scortechini, I.; Chiarucci, M.; Poiani, M.; et al. Immunomodulatory Effects of Tyrosine Kinase Inhibitor In Vitro and In Vivo Study. *Biol. Blood Marrow Transplant.* **2018**, *24*, 267–275. [CrossRef] [PubMed]
22. Damele, L.; Montaldo, E.; Moretta, L.; Vitale, C.; Mingari, M.C. Effect of Tyrosin Kinase Inhibitors on NK Cell and ILC3 Development and Function. *Front. Immunol.* **2018**, *9*, 2433. [CrossRef] [PubMed]
23. Giansanti, P.; Preisinger, C.; Huber, K.V.M.; Gridling, M.; Superti-Furga, G.; Bennett, K.L.; Heck, A.J.R. Evaluating the Promiscuous Nature of Tyrosine Kinase Inhibitors Assessed in A431 Epidermoid Carcinoma Cells by Both Chemical- and Phosphoproteomics. *ACS Chem. Biol.* **2014**, *9*, 1490–1498. [CrossRef] [PubMed]
24. Hughes, A.; Clarkson, J.; Tang, C.; Vidovic, L.; White, D.L.; Hughes, T.P.; Yong, A.S.M. CML Patients with Deep Molecular Responses to TKI Have Restored Immune Effectors and Decreased PD-1 and Immune Suppressors. *Blood* **2017**, *129*, 1166–1176. [CrossRef] [PubMed]

25. Hughes, A.; Yong, A.S.M. Immune Effector Recovery in Chronic Myeloid Leukemia and Treatment-Free Remission. *Front. Immunol.* **2017**, *8*, 469. [CrossRef] [PubMed]
26. Nomura, S.; Ito, T.; Satake, A.; Ishii, K. Assessment of Soluble Cytotoxic T Lymphocyte-Associated Antigen-4, Transforming Growth Factor B1, and Platelet-Derived Microparticles during Dasatinib Therapy for Patients with Chronic Myelogenous Leukemia. *J. Blood Med.* **2019**, *10*, 1–8. [CrossRef]
27. Najima, Y.; Yoshida, C.; Iriyama, N.; Fujisawa, S.; Wakita, H.; Chiba, S.; Okamoto, S.; Kawakami, K.; Takezako, N.; Kumagai, T.; et al. Regulatory T Cell Inhibition by Dasatinib Is Associated with Natural Killer Cell Differentiation and a Favorable Molecular Response—The Final Results of the D-First Study. *Leuk. Res.* **2018**, *66*, 66–72. [CrossRef]
28. Christiansson, L.; Söderlund, S.; Mangsbo, S.; Hjorth-Hansen, H.; Höglund, M.; Markevörn, B.; Richter, J.; Stenke, L.; Mustjoki, S.; Loskog, A.; et al. The Tyrosine Kinase Inhibitors Imatinib and Dasatinib Reduce Myeloid Suppressor Cells and Release Effector Lymphocyte Responses. *Mol. Cancer Ther.* **2015**, *14*, 1181–1191. [CrossRef] [PubMed]
29. Mustjoki, S.; Ekblom, M.; Arstila, T.P.; Dybedal, I.; Epling-Burnette, P.K.; Guilhot, F.; Hjorth-Hansen, H.; Höglund, M.; Kovanen, P.; Laurinoli, T.; et al. Clonal Expansion of T/NK-Cells during Tyrosine Kinase Inhibitor Dasatinib Therapy. *Leukemia* **2009**, *23*, 1398–1405. [CrossRef] [PubMed]
30. Qiu, Z.-Y.; Xu, W.; Li, J.-Y. Large Granular Lymphocytosis during Dasatinib Therapy. *Cancer Biol. Ther.* **2014**, *15*, 247–255. [CrossRef]
31. Watanabe, N.; Takaku, T.; Takeda, K.; Shirane, S.; Toyota, T.; Koike, M.; Noguchi, M.; Hirano, T.; Fujiwara, H.; Komatsu, N. Dasatinib-Induced Anti-Leukemia Cellular Immunity through a Novel Subset of CD57 Positive Helper/Cytotoxic CD4 T Cells in Chronic Myelogenous Leukemia Patients. *Int. J. Hematol.* **2018**, *108*, 588–597. [CrossRef]
32. Kreutzman, A.; Juvonen, V.; Kairisto, V.; Ekblom, M.; Stenke, L.; Seggewiss, R.; Porkka, K.; Mustjoki, S. Mono/Oligoclonal T and NK Cells Are Common in Chronic Myeloid Leukemia Patients at Diagnosis and Expand during Dasatinib Therapy. *Blood* **2010**, *116*, 772–782. [CrossRef]
33. Mustjoki, S.; Auvinen, K.; Kreutzman, A.; Rousselot, P.; Hernesniemi, S.; Melo, T.; Lahesmaa-Korpinen, A.-M.; Hautaniemi, S.; Bouchet, S.; Molimard, M.; et al. Rapid Mobilization of Cytotoxic Lymphocytes Induced by Dasatinib Therapy. *Leukemia* **2013**, *27*, 914–924. [CrossRef]
34. Schiffer, C.A.; Cortes, J.E.; Hochhaus, A.; Saglio, G.; le Coutre, P.; Porkka, K.; Mustjoki, S.; Mohamed, H.; Shah, N.P. Lymphocytosis after Treatment with Dasatinib in Chronic Myeloid Leukemia: Effects on Response and Toxicity. *Cancer* **2016**, *122*, 1398–1407. [CrossRef]
35. Kim, D.H.; Kamel-Reid, S.; Chang, H.; Sutherland, R.; Jung, C.W.; Kim, H.-J.; Lee, J.-J.; Lipton, J.H. Natural Killer or Natural Killer/T Cell Lineage Large Granular Lymphocytosis Associated with Dasatinib Therapy for Philadelphia Chromosome Positive Leukemia. *Haematologica* **2009**, *94*, 135–139. [CrossRef]
36. Lissina, A.; McLaren, J.E.; Ilander, M.; Andersson, E.I.; Lewis, C.S.; Clement, M.; Herman, A.; Ladell, K.; Llewellyn-Lacey, S.; Miners, K.L.; et al. Divergent Roles for Antigenic Drive in the Aetiology of Primary versus Dasatinib-Associated CD8+ TCR-V $\beta$ + Expansions. *Sci. Rep.* **2018**, *8*, 2534. [CrossRef] [PubMed]
37. Barbarin, A.; Abdallah, M.; Lefèvre, L.; Piccirilli, N.; Cayssials, E.; Roy, L.; Gombert, J.-M.; Herbelin, A. Innate T-A $\beta$  Lymphocytes as New Immunological Components of Anti-Tumoral “off-Target” Effects of the Tyrosine Kinase Inhibitor Dasatinib. *Sci. Rep.* **2020**, *10*, 3245. [CrossRef] [PubMed]
38. Hayashi, Y.; Nakamae, H.; Katayama, T.; Nakane, T.; Koh, H.; Nakamae, M.; Hirose, A.; Hagihara, K.; Terada, Y.; Nakao, Y.; et al. Different Immunoprofiles in Patients with Chronic Myeloid Leukemia Treated with Imatinib, Nilotinib or Dasatinib. *Leuk. Lymphoma* **2012**, *53*, 1084–1089. [CrossRef] [PubMed]
39. Kreutzman, A.; Jaatinen, T.; Greco, D.; Vakkila, E.; Richter, J.; Ekblom, M.; Hjorth-Hansen, H.; Stenke, L.; Melo, T.; Paquette, R.; et al. Killer-Cell Immunoglobulin-like Receptor Gene Profile Predicts Good Molecular Response to Dasatinib Therapy in Chronic Myeloid Leukemia. *Exp. Hematol.* **2012**, *40*, 906–913.e1. [CrossRef] [PubMed]
40. Hassold, N.; Seystahl, K.; Kempf, K.; Urlaub, D.; Zekl, M.; Einsele, H.; Watzl, C.; Wischhusen, J.; Seggewiss-Bernhardt, R. Enhancement of Natural Killer Cell Effector Functions against Selected Lymphoma and Leukemia Cell Lines by Dasatinib. *Int. J. Cancer* **2012**, *131*, E916–E927. [CrossRef]
41. Sheng, L.-X.; Wang, J.-P.; Lai, Y.-L.; Wu, H.; Sun, Y.-C.; Zhou, M.; Ouyang, G.-F.; Huang, H. Effects of Dasatinib on the Expansion, Subsets, Receptor Expression and Cytotoxic Function of NK Cells in Vitro. *Zhongguo Shi Yan Xue Ye Xue Za Zhi* **2020**, *28*, 1762–1768. [CrossRef] [PubMed]
42. Chang, M.-C.; Cheng, H.-I.; Hsu, K.; Hsu, Y.-N.; Kao, C.-W.; Chang, Y.-F.; Lim, K.-H.; Chen, C.G. NKG2A Down-Regulation by Dasatinib Enhances Natural Killer Cytotoxicity and Accelerates Effective Treatment Responses in Patients With Chronic Myeloid Leukemia. *Front. Immunol.* **2018**, *9*, 3152. [CrossRef] [PubMed]
43. Kreutzman, A.; Ladell, K.; Koehel, C.; Gostick, E.; Ekblom, M.; Stenke, L.; Melo, T.; Einsele, H.; Porkka, K.; Price, D.A.; et al. Expansion of Highly Differentiated CD8+ T-Cells or NK-Cells in Patients Treated with Dasatinib Is Associated with Cytomegalovirus Reactivation. *Leukemia* **2011**, *25*, 1587–1597. [CrossRef]
44. Rölle, A.; Brodin, P. Immune Adaptation to Environmental Influence: The Case of NK Cells and HCMV. *Trends Immunol.* **2016**, *37*, 233–243. [CrossRef]
45. Kadowaki, N.; Ishiyama, K.; Kitawaki, T. Cytomegalovirus Pulls Strings behind NK Cells. *Oncotarget* **2017**, *8*, 93297–93298. [CrossRef] [PubMed]

46. Climent, N.; Plana, M. Immunomodulatory Activity of Tyrosine Kinase Inhibitors to Elicit Cytotoxicity Against Cancer and Viral Infection. *Front. Pharmacol.* **2019**, *10*, 1232. [CrossRef] [PubMed]
47. Ishiyama, K.-I.; Kitawaki, T.; Otsuka, Y.; Takaori-Kondo, A.; Kadowaki, N. Programmed Cell Death 1-Expressing CD56-Negative Natural Killer (NK) Cell Expansion Is a Hallmark of Chronic NK Cell Activation during Dasatinib Treatment. *Cancer Sci.* **2021**, *112*, 523–536. [CrossRef] [PubMed]
48. Duerkop, B.A.; Hooper, L.V. Resident Viruses and Their Interactions with the Immune System. *Nat. Immunol.* **2013**, *14*, 654–659. [CrossRef]
49. Cortes, J.E.; Saglio, G.; Kantarjian, H.M.; Baccarani, M.; Mayer, J.; Boqué, C.; Shah, N.P.; Chuah, C.; Casanova, L.; Bradley-Garelik, B.; et al. Final 5-Year Study Results of DASISION: The Dasatinib Versus Imatinib Study in Treatment-Naïve Chronic Myeloid Leukemia Patients Trial. *J. Clin. Oncol.* **2016**, *34*, 2333–2340. [CrossRef] [PubMed]
50. Sauße, S.; Richter, J.; Hochhaus, A.; Mahon, F.-X. The Concept of Treatment-Free Remission in Chronic Myeloid Leukemia. *Leukemia* **2016**, *30*, 1638–1647. [CrossRef] [PubMed]
51. Cortes, J.; Rea, D.; Lipton, J.H. Treatment-Free Remission with First- and Second-Generation Tyrosine Kinase Inhibitors. *Am. J. Hematol.* **2019**, *94*, 346–357. [CrossRef] [PubMed]
52. Guru Murthy, G.S.; Atallah, E. Treatment-Free Remission in CML: The US Perspective. *Curr. Hematol. Malign. Rep.* **2019**, *14*, 56–61. [CrossRef]
53. Imagawa, J.; Tanaka, H.; Okada, M.; Nakamae, H.; Hino, M.; Murai, K.; Ishida, Y.; Kumagai, T.; Sato, S.; Ohashi, K.; et al. Discontinuation of Dasatinib in Patients with Chronic Myeloid Leukemia Who Have Maintained Deep Molecular Response for Longer than 1 Year (DADI Trial): A Multicentre Phase 2 Trial. *Lancet Haematol.* **2015**, *2*, e528–e535. [CrossRef] [PubMed]
54. Mizoguchi, I.; Yoshimoto, T.; Katagiri, S.; Mizuguchi, J.; Tauchi, T.; Kimura, Y.; Inokuchi, K.; Ohyashiki, J.H.; Ohyashiki, K. Sustained Upregulation of Effector Natural Killer Cells in Chronic Myeloid Leukemia after Discontinuation of Imatinib. *Cancer Sci.* **2013**, *104*, 1146–1153. [CrossRef]
55. Rea, D.; Henry, G.; Khaznadar, Z.; Etienne, G.; Guilhot, F.; Nicolini, F.; Guilhot, J.; Rouselot, P.; Huguet, F.; Legros, L.; et al. Natural Killer-Cell Counts Are Associated with Molecular Relapse-Free Survival after Imatinib Discontinuation in Chronic Myeloid Leukemia: The IMMUNOSTIM Study. *Haematologica* **2017**, *102*, 1368–1377. [CrossRef] [PubMed]
56. Ureshino, H.; Kamachi, K.; Sano, H.; Okamoto, S.; Itamura, H.; Yoshimura, M.; Katsuya, H.; Ando, T.; Kimura, S. Higher Neutrophil Counts Are Associated with Successful Tyrosine Kinase Inhibitor Discontinuation in Patients with Chronic Myeloid Leukemia. *Hematology* **2022**, *27*, 1171–1175. [CrossRef] [PubMed]
57. Ilander, M.; Olsson-Strömberg, U.; Schlums, H.; Guilhot, J.; Brück, O.; Lähteenmäki, H.; Kasanen, T.; Koskenvesa, P.; Söderlund, S.; Höglund, M.; et al. Increased Proportion of Mature NK Cells Is Associated with Successful Imatinib Discontinuation in Chronic Myeloid Leukemia. *Leukemia* **2017**, *31*, 1108–1116. [CrossRef]
58. Hara, R.; Onizuka, M.; Matsusita, E.; Kikkawa, E.; Nakamura, Y.; Matsushita, H.; Ohgiya, D.; Murayama, H.; Machida, S.; Ohmachi, K.; et al. NKG2D Gene Polymorphisms Are Associated with Disease Control of Chronic Myeloid Leukemia by Dasatinib. *Int. J. Hematol.* **2017**, *106*, 666–674. [CrossRef] [PubMed]
59. Hughes, A.; Clarkson, J.; White, D.L.; Ross, D.M.; Hughes, T.P.; Yong, A.S. Enhanced Natural Killer and Cytotoxic T Lymphocyte Responses, with Decreased Monocytic Myeloid Derived Suppressor Cells May Promote Treatment Free Remission in Chronic Myeloid Leukemia Patients Following Tyrosine Kinase Inhibitor Cessation. *Blood* **2016**, *128*, 1122. [CrossRef]
60. Burchert, A.; Saussele, S.; Eigendorff, E.; Müller, M.C.; Sohlbach, K.; Inselmann, S.; Schütz, C.; Metzelder, S.K.; Ziermann, J.; Kostrewa, P.; et al. Interferon Alpha 2 Maintenance Therapy May Enable High Rates of Treatment Discontinuation in Chronic Myeloid Leukemia. *Leukemia* **2015**, *29*, 1331–1335. [CrossRef]
61. Puzzolo, M.C.; Breccia, M.; Mariglia, P.; Colafigli, G.; Pepe, S.; Scalzulli, E.; Mariggio, E.; Latagliata, R.; Guarini, A.; Foà, R. Immunomodulatory Effects of IFN $\alpha$  on T and NK Cells in Chronic Myeloid Leukemia Patients in Deep Molecular Response Preparing for Treatment Discontinuation. *J. Clin. Med.* **2022**, *11*, 5594. [CrossRef]
62. Rea, D.; Nicolini, F.E.; Tulliez, M.; Guilhot, F.; Guilhot, J.; Guerci-Bresler, A.; Gardembas, M.; Coiteux, V.; Guillerm, G.; Legros, L.; et al. Discontinuation of Dasatinib or Nilotinib in Chronic Myeloid Leukemia: Interim Analysis of the STOP 2G-TKI Study. *Blood* **2017**, *129*, 846–854. [CrossRef] [PubMed]
63. Okada, M.; Imagawa, J.; Tanaka, H.; Nakamae, H.; Hino, M.; Murai, K.; Ishida, Y.; Kumagai, T.; Sato, S.; Ohashi, K.; et al. Final 3-Year Results of the Dasatinib Discontinuation Trial in Patients With Chronic Myeloid Leukemia Who Received Dasatinib as a Second-Line Treatment. *Clin. Lymphoma Myeloma Leuk.* **2018**, *18*, 353–360.e1. [CrossRef]
64. Yoshida, C.; Iriyama, N.; Najima, Y.; Fujisawa, S.; Wakita, H.; Chiba, S.; Okamoto, S.; Kawakami, K.; Takezako, N.; Kumagai, T.; et al. Association of Peripheral Regulatory T Cells with Achievement of Deep Molecular Response in Newly Diagnosed Chronic Phase Chronic Myeloid Leukemia Treated with Dasatinib - the Final Results of D-First Study. *Blood* **2016**, *128*, 1916. [CrossRef]
65. Takaku, T.; Iriyama, N.; Mitsumori, T.; Sato, E.; Gotoh, A.; Kirito, K.; Noguchi, M.; Koike, M.; Sakamoto, J.; Oba, K.; et al. Clinical Efficacy and Safety of First-Line Dasatinib Therapy and the Relevance of Velocity of BCR-ABL1 Transcript Decline for Achievement of Molecular Responses in Newly Diagnosed Chronic-Phase Chronic Myeloid Leukemia: Report from the Juntendo Yamanashi Cooperative Study Group. *Oncology* **2018**, *94*, 85–91. [CrossRef]
66. Cayssials, E.; Jacomet, F.; Piccirilli, N.; Lefèvre, L.; Roy, L.; Guilhot, F.; Chomel, J.-C.; Leleu, X.; Gombert, J.-M.; Herbelin, A.; et al. Sustained Treatment-Free Remission in Chronic Myeloid Leukemia Is Associated with an Increased Frequency of Innate CD8(+) T-Cells. *Br. J. Haematol.* **2019**, *186*, 54–59. [CrossRef]

67. Vigón, L.; Luna, A.; Galán, M.; Rodríguez-Mora, S.; Fuertes, D.; Mateos, E.; Piris-Villaespesa, M.; Bautista, G.; San José, E.; Rivera-Torres, J.; et al. Identification of Immunological Parameters as Predictive Biomarkers of Relapse in Patients with Chronic Myeloid Leukemia on Treatment-Free Remission. *J. Clin. Med.* **2020**, *10*, 42. [CrossRef]
68. Irani, Y.D.; Hughes, A.; Clarkson, J.; Kok, C.H.; Shanmuganathan, N.; White, D.L.; Yeung, D.T.; Ross, D.M.; Hughes, T.P.; Yong, A.S.M. Successful Treatment-Free Remission in Chronic Myeloid Leukaemia and Its Association with Reduced Immune Suppressors and Increased Natural Killer Cells. *Br. J. Haematol.* **2020**, *191*, 433–441. [CrossRef] [PubMed]
69. Stuckey, R.; López Rodríguez, J.F.; Gómez-Casares, M.T. Discontinuation of Tyrosine Kinase Inhibitors in Patients with Chronic Myeloid Leukemia: A Review of the Biological Factors Associated with Treatment-Free Remission. *Curr. Oncol. Rep.* **2022**, *24*, 415–426. [CrossRef] [PubMed]
70. Schlums, H.; Cichocki, F.; Tesi, B.; Theorell, J.; Beziat, V.; Holmes, T.D.; Han, H.; Chiang, S.C.C.; Foley, B.; Mattsson, K.; et al. Cytomegalovirus Infection Drives Adaptive Epigenetic Diversification of NK Cells with Altered Signaling and Effector Function. *Immunity* **2015**, *42*, 443–456. [CrossRef]
71. He, Y.; Tian, Z. NK Cell Education via Nonclassical MHC and Non-MHC Ligands. *Cell Mol. Immunol.* **2017**, *14*, 321–330. [CrossRef]
72. Melendez, E.; Chondronasiou, D.; Mosteiro, L.; Martínez de Villarreal, J.; Fernández-Alfara, M.; Lynch, C.J.; Grimm, D.; Real, F.X.; Alcami, J.; Climent, N.; et al. Natural Killer Cells Act as an Extrinsic Barrier for in Vivo Reprogramming. *Development* **2022**, *149*, dev200361. [CrossRef] [PubMed]
73. Yawata, M.; Yawata, N.; Draghi, M.; Little, A.-M.; Partheniou, F.; Parham, P. Roles for HLA and KIR Polymorphisms in Natural Killer Cell Repertoire Selection and Modulation of Effector Function. *J. Exp. Med.* **2006**, *203*, 633–645. [CrossRef]
74. O'Connor, G.M.; Guinan, K.J.; Cunningham, R.T.; Middleton, D.; Parham, P.; Gardiner, C.M. Functional Polymorphism of the KIR3DL1/S1 Receptor on Human NK Cells. *J. Immunol.* **2007**, *178*, 235–241. [CrossRef] [PubMed]
75. Caocci, G.; Martino, B.; Greco, M.; Abruzzese, E.; Trawinska, M.M.; Lai, S.; Ragatzu, P.; Galimberti, S.; Baratè, C.; Mulas, O.; et al. Killer Immunoglobulin-like Receptors Can Predict TKI Treatment-Free Remission in Chronic Myeloid Leukemia Patients. *Exp. Hematol.* **2015**, *43*, 1015–1018.e1. [CrossRef]
76. Ureshino, H.; Shindo, T.; Kojima, H.; Kusunoki, Y.; Miyazaki, Y.; Tanaka, H.; Saji, H.; Kawaguchi, A.; Kimura, S. Allelic Polymorphisms of KIRs and HLAs Predict Favorable Responses to Tyrosine Kinase Inhibitors in CML. *Cancer Immunol. Res.* **2018**, *6*, 745–754. [CrossRef]
77. La Nasa, G.; Caocci, G.; Littera, R.; Atzeni, S.; Vacca, A.; Mulas, O.; Langiu, M.; Greco, M.; Orrù, S.; Orrù, N.; et al. Homozygosity for Killer Immunoglobulin-like Receptor Haplotype A Predicts Complete Molecular Response to Treatment with Tyrosine Kinase Inhibitors in Chronic Myeloid Leukemia Patients. *Exp. Hematol.* **2013**, *41*, 424–431. [CrossRef]
78. Yeung, D.T.; Tang, C.; Vidovic, L.; White, D.L.; Branford, S.; Hughes, T.P.; Yong, A.S. KIR2DL5B Genotype Predicts Outcomes in CML Patients Treated with Response-Directed Sequential Imatinib/Nilotinib Strategy. *Blood* **2015**, *126*, 2720–2723. [CrossRef]
79. Ureshino, H.; Shindo, T.; Tanaka, H.; Saji, H.; Kimura, S. HLA Polymorphisms Are Associated with Treatment-Free Remission Following Discontinuation of Tyrosine Kinase Inhibitors in Chronic Myeloid Leukemia. *Mol. Cancer Ther.* **2021**, *20*, 142–149. [CrossRef]
80. Flores-Villanueva, P.O.; Yunis, E.J.; Delgado, J.C.; Vittinghoff, E.; Buchbinder, S.; Leung, J.Y.; Ugialoro, A.M.; Clavijo, O.P.; Rosenberg, E.S.; Kalams, S.A.; et al. Control of HIV-1 Viremia and Protection from AIDS Are Associated with HLA-Bw4 Homozygosity. *Proc. Natl. Acad. Sci. USA* **2001**, *98*, 5140–5145. [CrossRef] [PubMed]
81. Yu, G.-T.; Mao, L.; Wu, L.; Deng, W.-W.; Bu, L.-L.; Liu, J.-F.; Chen, L.; Yang, L.-L.; Wu, H.; Zhang, W.-F.; et al. Inhibition of SRC Family Kinases Facilitates Anti-CTLA4 Immunotherapy in Head and Neck Squamous Cell Carcinoma. *Cell Mol. Life Sci.* **2018**, *75*, 4223–4234. [CrossRef]
82. Tu, M.M.; Lee, F.Y.F.; Jones, R.T.; Kimball, A.K.; Saravia, E.; Graziano, R.F.; Coleman, B.; Menard, K.; Yan, J.; Michaud, E.; et al. Targeting DDR2 Enhances Tumor Response to Anti-PD-1 Immunotherapy. *Sci. Adv.* **2019**, *5*, eaav2437. [CrossRef]
83. Mestermann, K.; Giavridis, T.; Weber, J.; Rydzek, J.; Frenz, S.; Nerretter, T.; Mades, A.; Sadelain, M.; Einsele, H.; Hudecek, M. The Tyrosine Kinase Inhibitor Dasatinib Acts as a Pharmacologic on/off Switch for CAR T Cells. *Sci. Transl. Med.* **2019**, *11*, eaau5907. [CrossRef]
84. Zhang, H.; Hu, Y.; Shao, M.; Teng, X.; Jiang, P.; Wang, X.; Wang, H.; Cui, J.; Yu, J.; Liang, Z.; et al. Dasatinib Enhances Anti-Leukemia Efficacy of Chimeric Antigen Receptor T Cells by Inhibiting Cell Differentiation and Exhaustion. *J. Hematol. Oncol.* **2021**, *14*, 113. [CrossRef]
85. Board, N.L.; Moskovljevic, M.; Wu, F.; Siliciano, R.F.; Siliciano, J.D. Engaging Innate Immunity in HIV-1 Cure Strategies. *Nat. Rev. Immunol.* **2022**, *22*, 499–512. [CrossRef] [PubMed]
86. Rasmussen, T.A.; Tolstrup, M.; Søgaaard, O.S. Reversal of Latency as Part of a Cure for HIV-1. *Trends Microbiol.* **2016**, *24*, 90–97. [CrossRef]
87. Coiras, M.; Ambrosioni, J.; Cervantes, F.; Miró, J.M.; Alcami, J. Tyrosine Kinase Inhibitors: Potential Use and Safety Considerations in HIV-1 Infection. *Expert. Opin. Drug Saf.* **2017**, *16*, 547–559. [CrossRef] [PubMed]
88. Bermejo, M.; López-Huertas, M.R.; García-Pérez, J.; Climent, N.; Descours, B.; Ambrosioni, J.; Mateos, E.; Rodríguez-Mora, S.; Rus-Bercial, L.; Benkirane, M.; et al. Dasatinib Inhibits HIV-1 Replication through the Interference of SAMHD1 Phosphorylation in CD4+ T Cells. *Biochem. Pharmacol.* **2016**, *106*, 30–45. [CrossRef] [PubMed]

89. Coiras, M.; Bermejo, M.; Descours, B.; Mateos, E.; García-Pérez, J.; López-Huertas, M.-R.; Lederman, M.M.; Benkirane, M.; Alcamí, J. IL-7 Induces SAMHD1 Phosphorylation in CD4+ T Lymphocytes, Improving Early Steps of HIV-1 Life Cycle. *Cell Rep.* **2016**, *14*, 2100–2107. [CrossRef] [PubMed]
90. Bermejo, M.; Ambrosioni, J.; Bautista, G.; Climent, N.; Mateos, E.; Rovira, C.; Rodríguez-Mora, S.; López-Huertas, M.R.; García-Gutiérrez, V.; Steegmann, J.L.; et al. Evaluation of Resistance to HIV-1 Infection Ex Vivo of PBMCs Isolated from Patients with Chronic Myeloid Leukemia Treated with Different Tyrosine Kinase Inhibitors. *Biochem. Pharmacol.* **2018**, *156*, 248–264. [CrossRef]
91. Williams, E.S.C.P.; Szaniawski, M.A.; Martins, L.J.; Innis, E.A.; Alcamí, J.; Hanley, T.M.; Spivak, A.M.; Coiras, M.; Planelles, V. Dasatinib: Effects on the Macrophage Phospho Proteome with a Focus on SAMHD1 and HIV-1 Infection. *Clin. Res. HIV AIDS* **2022**, *8*, 1053.
92. McCarthy, S.D.S.; Leontyev, D.; Nicoletti, P.; Binnington, B.; Kozłowski, H.N.; Ostrowski, M.; Cochrane, A.; Branch, D.R.; Wong, R.W. Targeting ABL1 or ARG Tyrosine Kinases to Restrict HIV-1 Infection in Primary CD4+ T-Cells or in Humanized NSG Mice. *J. Acquir. Immune Defic. Syndr.* **2019**, *82*, 407–415. [CrossRef] [PubMed]
93. Vigón, L.; Rodríguez-Mora, S.; Luna, A.; Sandonís, V.; Mateos, E.; Bautista, G.; Steegmann, J.L.; Climent, N.; Plana, M.; Pérez-Romero, P.; et al. Cytotoxic Cell Populations Developed during Treatment with Tyrosine Kinase Inhibitors Protect Autologous CD4+ T Cells from HIV-1 Infection. *Biochem. Pharmacol.* **2020**, *182*, 114203. [CrossRef] [PubMed]
94. Vigón, L.; Martínez-Román, P.; Rodríguez-Mora, S.; Torres, M.; Puertas, M.C.; Mateos, E.; Salgado, M.; Navarro, A.; Sánchez-Conde, M.; Ambrosioni, J.; et al. Provirus Reactivation Is Impaired in HIV-1 Infected Individuals on Treatment with Dasatinib and Antiretroviral Therapy. *Biochem. Pharmacol.* **2021**, *192*, 114666. [CrossRef]
95. Innis, E.A.; Levinger, C.; Szaniawski, M.A.; Williams, E.S.C.P.; Alcamí, J.; Bosque, A.; Schiffer, J.T.; Coiras, M.; Spivak, A.M.; Planelles, V. Pharmacologic Control of Homeostatic and Antigen-Driven Proliferation to Target HIV-1 Persistence. *Biochem. Pharmacol.* **2021**, *194*, 114816. [CrossRef]
96. Climent, N.; Ambrosioni, J.; González, T.; Xufré, C.; Casadellà, M.; Noguera-Julian, M.; Paredes, R.; Plana, M.; Grau-Expósito, J.; Mallolas, J.; et al. Immunological and Virological Findings in a Patient with Exceptional Post-Treatment Control: A Case Report. *Lancet HIV* **2023**, *10*, e42–e51. [CrossRef]
97. Sánchez-Gaona, N.; Gallego, A.; Astorga, A.; Rallón, N.; Benito, J.M.; Falcó, V.; Genescà, M.; Buzón, M.J. Characterization of NK Cells in Elite Controllers Losig HIV Control. [CROI Abstract 307]. In Proceedings of the CROI 2022 Conference on Retroviruses and Opportunistic Infections, Virtual, 12–16 February 2022; p. 118.
98. Gondois-Rey, F.; Chéret, A.; Granjeaud, S.; Mallet, F.; Bidaut, G.; Lécuroux, C.; Ploquin, M.; Müller-Trutwin, M.; Rouzioux, C.; Avettand-Fenoël, V.; et al. NKG2C+ Memory-like NK Cells Contribute to the Control of HIV Viremia during Primary Infection: Optiprim-ANRS 147. *Clin. Transl. Immunol.* **2017**, *6*, e150. [CrossRef]
99. Flórez-Álvarez, L.; Hernandez, J.C.; Zapata, W. NK Cells in HIV-1 Infection: From Basic Science to Vaccine Strategies. *Front. Immunol.* **2018**, *9*, 2290. [CrossRef] [PubMed]
100. Peppas, D.; Pedroza-Pacheco, I.; Pellegrino, P.; Williams, I.; Maini, M.K.; Borrow, P. Adaptive Reconfiguration of Natural Killer Cells in HIV-1 Infection. *Front. Immunol.* **2018**, *9*, 474. [CrossRef]
101. Sáez-Cirión, A.; Bacchus, C.; Hocqueloux, L.; Avettand-Fenoel, V.; Girault, I.; Lecuroux, C.; Potard, V.; Versmisse, P.; Melard, A.; Prazuck, T.; et al. Post-Treatment HIV-1 Controllers with a Long-Term Virological Remission after the Interruption of Early Initiated Antiretroviral Therapy ANRS VISCONTI Study. *PLoS Pathog.* **2013**, *9*, e1003211. [CrossRef]
102. Namazi, G.; Fajnzylber, J.M.; Aga, E.; Bosch, R.J.; Acosta, E.P.; Sharaf, R.; Hartogensis, W.; Jacobson, J.M.; Connick, E.; Volberding, P.; et al. The Control of HIV After Antiretroviral Medication Pause (CHAMP) Study: Posttreatment Controllers Identified From 14 Clinical Studies. *J. Infect. Dis.* **2018**, *218*, 1954–1963. [CrossRef]
103. Carlson, J.M.; Listgarten, J.; Pfeifer, N.; Tan, V.; Kadie, C.; Walker, B.D.; Ndung'u, T.; Shapiro, R.; Frater, J.; Brumme, Z.L.; et al. Widespread Impact of HLA Restriction on Immune Control and Escape Pathways of HIV-1. *J. Virol.* **2012**, *86*, 5230–5243. [CrossRef] [PubMed]
104. Zhang, X.; Huang, X.; Xia, W.; Li, W.; Zhang, T.; Wu, H.; Xu, X.; Yan, H. HLA-B\*44 Is Associated with a Lower Viral Set Point and Slow CD4 Decline in a Cohort of Chinese Homosexual Men Acutely Infected with HIV-1. *Clin. Vaccine Immunol.* **2013**, *20*, 1048–1054. [CrossRef]
105. Singh, K.K.; Qin, M.; Brummel, S.S.; Angelidou, K.; Trout, R.N.; Fenton, T.; Spector, S.A. Killer Cell Immunoglobulin-Like Receptor Alleles Alter HIV Disease in Children. *PLoS ONE* **2016**, *11*, e0151364. [CrossRef]
106. Maruthamuthu, S.; Rajalingam, R.; Pandian, K.; Madasamy, S.; Manoharan, M.; Pitchai, L.; Murugesan, A.; Mariakuttikan, J. Inhibitory Natural Killer Cell Receptor KIR3DL1 with Its Ligand Bw4 Constraints HIV-1 Disease among South Indians. *AIDS* **2018**, *32*, 2679–2688. [CrossRef]
107. Ramsuran, V.; Naranbhai, V.; Horowitz, A.; Qi, Y.; Martin, M.P.; Yuki, Y.; Gao, X.; Walker-Sperling, V.; Del Prete, G.Q.; Schneider, D.K.; et al. Elevated HLA-A Expression Impairs HIV Control through Inhibition of NKG2A-Expressing Cells. *Science* **2018**, *359*, 86–90. [CrossRef] [PubMed]
108. Boulet, S.; Song, R.; Kanya, P.; Bruneau, J.; Shoukry, N.H.; Tsoukas, C.M.; Bernard, N.F. HIV Protective KIR3DL1 and HLA-B Genotypes Influence NK Cell Function Following Stimulation with HLA-Devoid Cells. *J. Immunol.* **2010**, *184*, 2057–2064. [CrossRef]

109. Parsons, M.S.; Boulet, S.; Song, R.; Bruneau, J.; Shoukry, N.H.; Routy, J.-P.; Tsoukas, C.M.; Bernard, N.F. Mind the Gap: Lack of Association between KIR3DL1\*004/HLA-Bw4-Induced Natural Killer Cell Function and Protection from HIV Infection. *J. Infect. Dis.* **2010**, *202* (Suppl. S3), S356–S360. [CrossRef] [PubMed]
110. Kamy, P.; Boulet, S.; Tsoukas, C.M.; Routy, J.-P.; Thomas, R.; Côté, P.; Boulassel, M.-R.; Baril, J.-G.; Kovacs, C.; Migueles, S.A.; et al. Receptor-Ligand Requirements for Increased NK Cell Polyfunctional Potential in Slow Progressors Infected with HIV-1 Coexpressing KIR3DL1\*h/\*y and HLA-B\*57. *J. Virol.* **2011**, *85*, 5949–5960. [CrossRef]
111. Schwartz, O.; Maréchal, V.; Le Gall, S.; Lemonnier, F.; Heard, J.M. Endocytosis of Major Histocompatibility Complex Class I Molecules Is Induced by the HIV-1 Nef Protein. *Nat. Med.* **1996**, *2*, 338–342. [CrossRef]
112. Cohen, G.B.; Gandhi, R.T.; Davis, D.M.; Mandelboim, O.; Chen, B.K.; Strominger, J.L.; Baltimore, D. The Selective Downregulation of Class I Major Histocompatibility Complex Proteins by HIV-1 Protects HIV-Infected Cells from NK Cells. *Immunity* **1999**, *10*, 661–671. [CrossRef] [PubMed]
113. Bonaparte, M.I.; Barker, E. Killing of Human Immunodeficiency Virus-Infected Primary T-Cell Blasts by Autologous Natural Killer Cells Is Dependent on the Ability of the Virus to Alter the Expression of Major Histocompatibility Complex Class I Molecules. *Blood* **2004**, *104*, 2087–2094. [CrossRef]
114. Apps, R.; Del Prete, G.Q.; Chatterjee, P.; Lara, A.; Brumme, Z.L.; Brockman, M.A.; Neil, S.; Pickering, S.; Schneider, D.K.; Piechocka-Trocha, A.; et al. HIV-1 Vpu Mediates HLA-C Downregulation. *Cell Host Microbe* **2016**, *19*, 686–695. [CrossRef] [PubMed]
115. Song, R.; Lisovsky, I.; Lebouché, B.; Routy, J.-P.; Bruneau, J.; Bernard, N.F. HIV Protective KIR3DL1/S1-HLA-B Genotypes Influence NK Cell-Mediated Inhibition of HIV Replication in Autologous CD4 Targets. *PLoS Pathog* **2014**, *10*, e1003867. [CrossRef]
116. Kiani, Z.; Dupuy, F.P.; Bruneau, J.; Lebouché, B.; Retière, C.; Geraghty, D.E.; Bernard, N.F. The Education of NK Cells Determines Their Responsiveness to Autologous HIV-Infected CD4 T Cells. *J. Virol.* **2019**, *93*, e01185-19. [CrossRef]
117. Körner, C.; Simoneau, C.R.; Schommers, P.; Granoff, M.; Ziegler, M.; Hölzemer, A.; Lunemann, S.; Chukwukelu, J.; Corleis, B.; Naranbhai, V.; et al. HIV-1-Mediated Downmodulation of HLA-C Impacts Target Cell Recognition and Antiviral Activity of NK Cells. *Cell Host Microbe* **2017**, *22*, 111–119.e4. [CrossRef] [PubMed]
118. Vieira, V.A.; Adland, E.; Malone, D.F.G.; Martin, M.P.; Groll, A.; Ansari, M.A.; Garcia-Guerrero, M.C.; Puertas, M.C.; Muenchhoff, M.; Guash, C.F.; et al. An HLA-I Signature Favouring KIR-Educated Natural Killer Cells Mediates Immune Control of HIV in Children and Contrasts with the HLA-B-Restricted CD8+ T-Cell-Mediated Immune Control in Adults. *PLoS Pathog.* **2021**, *17*, e1010090. [CrossRef] [PubMed]
119. Thomas, R.; Low, H.Z.; Kniesch, K.; Jacobs, R.; Schmidt, R.E.; Witte, T. NKG2C Deletion Is a Risk Factor of HIV Infection. *AIDS Res. Hum. Retrovir.* **2012**, *28*, 844–851. [CrossRef]
120. Essat, A.; Scott-Algara, D.; Monceaux, V.; Avettand-Fenoel, V.; Didier, C.; Caillat-Zucman, S.; Orr, S.; Theodorou, I.; Goujard, C.; Boufassa, F.; et al. Association between Immunogenetic Factors and Post-Treatment Control of HIV-1 Infection. ANRS VISCONTI and PRIMO Studies. In Proceedings of the 22nd International AIDS Conference (AIDS 2018), Amsterdam, Netherlands, 23–27 July 2018. [CrossRef]
121. Sáez-Cirión, A. Mechanisms of Post-Treatment HIV Control: ANRS VISCONTI Study. In Proceedings of the IAS 2019, 10th International Conference on HIV Science, Mexico City, Mexico, 21 July 2019. [CrossRef]
122. Juno, J.A.; Kent, S.J. What Can Gamma Delta T Cells Contribute to an HIV Cure? *Front. Cell Infect. Microbiol.* **2020**, *10*, 233. [CrossRef] [PubMed]
123. Lambotte, O.; Boufassa, F.; Madec, Y.; Nguyen, A.; Goujard, C.; Meyer, L.; Rouzioux, C.; Venet, A.; Delfraissy, J.-F. SEROCO-HEMOCO Study Group HIV Controllers: A Homogeneous Group of HIV-1-Infected Patients with Spontaneous Control of Viral Replication. *Clin. Infect. Dis.* **2005**, *41*, 1053–1056. [CrossRef]
124. McLaren, P.J.; Ripke, S.; Pelak, K.; Weintrob, A.C.; Patsopoulos, N.A.; Jia, X.; Erlich, R.L.; Lennon, N.J.; Kadie, C.M.; Heckerman, D.; et al. Fine-Mapping Classical HLA Variation Associated with Durable Host Control of HIV-1 Infection in African Americans. *Hum. Mol. Genet.* **2012**, *21*, 4334–4347. [CrossRef]
125. Mendoza, D.; Johnson, S.A.; Peterson, B.A.; Natarajan, V.; Salgado, M.; Dewar, R.L.; Burbelo, P.D.; Doria-Rose, N.A.; Graf, E.H.; Greenwald, J.H.; et al. Comprehensive Analysis of Unique Cases with Extraordinary Control over HIV Replication. *Blood* **2012**, *119*, 4645–4655. [CrossRef] [PubMed]
126. Casado, C.; Galvez, C.; Pernas, M.; Tarancon-Diez, L.; Rodriguez, C.; Sanchez-Merino, V.; Vera, M.; Olivares, I.; De Pablo-Bernal, R.; Merino-Mansilla, A.; et al. Permanent Control of HIV-1 Pathogenesis in Exceptional Elite Controllers: A Model of Spontaneous Cure. *Sci. Rep.* **2020**, *10*, 1902. [CrossRef]
127. Jiang, C.; Lian, X.; Gao, C.; Sun, X.; Einkauf, K.B.; Chevalier, J.M.; Chen, S.M.Y.; Hua, S.; Rhee, B.; Chang, K.; et al. Distinct Viral Reservoirs in Individuals with Spontaneous Control of HIV-1. *Nature* **2020**, *585*, 261–267. [CrossRef]
128. Martinez-Picado, J. Exceptional HIV Elite Controllers. Towards an HIV Cure. In Proceedings of the AIDS 2022 Congress, Montreal, Canada, 28 July 2022; Abstract Supplement Abstracts from AIDS 2022—the 24th International AIDS Conference, Virtual, 29 July–2 August 2022. [CrossRef]
129. Turk, G.; Seiger, K.; Lian, X.; Sun, W.; Parsons, E.M.; Gao, C.; Rassadkina, Y.; Polo, M.L.; Czernikier, A.; Ghiglione, Y.; et al. A Possible Sterilizing Cure of HIV-1 Infection Without Stem Cell Transplantation. *Ann. Intern. Med.* **2022**, *175*, 95–100. [CrossRef] [PubMed]
130. Campisi, J. Aging, Cellular Senescence, and Cancer. *Annu. Rev. Physiol.* **2013**, *75*, 685–705. [CrossRef] [PubMed]

131. Demaria, M.; Ohtani, N.; Youssef, S.A.; Rodier, F.; Toussaint, W.; Mitchell, J.R.; Laberge, R.-M.; Vijg, J.; Van Steeg, H.; Dollé, M.E.T.; et al. An Essential Role for Senescent Cells in Optimal Wound Healing through Secretion of PDGF-AA. *Dev. Cell* **2014**, *31*, 722–733. [CrossRef]
132. Ritschka, B.; Storer, M.; Mas, A.; Heinzmann, F.; Ortells, M.C.; Morton, J.P.; Sansom, O.J.; Zender, L.; Keyes, W.M. The Senescence-Associated Secretory Phenotype Induces Cellular Plasticity and Tissue Regeneration. *Genes Dev.* **2017**, *31*, 172–183. [CrossRef]
133. Paramos-de-Carvalho, D.; Martins, I.; Cristóvão, A.M.; Dias, A.F.; Neves-Silva, D.; Pereira, T.; Chapela, D.; Farinho, A.; Jacinto, A.; Saúde, L. Targeting Senescent Cells Improves Functional Recovery after Spinal Cord Injury. *Cell Rep.* **2021**, *36*, 109334. [CrossRef]
134. Calcinotto, A.; Kohli, J.; Zagato, E.; Pellegrini, L.; Demaria, M.; Alimonti, A. Cellular Senescence: Aging, Cancer, and Injury. *Physiol. Rev.* **2019**, *99*, 1047–1078. [CrossRef] [PubMed]
135. Gasser, S.; Orsulic, S.; Brown, E.J.; Raulet, D.H. The DNA Damage Pathway Regulates Innate Immune System Ligands of the NKG2D Receptor. *Nature* **2005**, *436*, 1186–1190. [CrossRef]
136. Krizhanovsky, V.; Yon, M.; Dickins, R.A.; Hearn, S.; Simon, J.; Miething, C.; Yee, H.; Zender, L.; Lowe, S.W. Senescence of Activated Stellate Cells Limits Liver Fibrosis. *Cell* **2008**, *134*, 657–667. [CrossRef]
137. Sagiv, A.; Burton, D.G.A.; Moshayev, Z.; Vadai, E.; Wensveen, F.; Ben-Dor, S.; Golani, O.; Polic, B.; Krizhanovsky, V. NKG2D Ligands Mediate Immunosurveillance of Senescent Cells. *Aging* **2016**, *8*, 328–344. [CrossRef] [PubMed]
138. Arora, S.; Thompson, P.J.; Wang, Y.; Bhattacharyya, A.; Apostolopoulou, H.; Hatano, R.; Naikawadi, R.P.; Shah, A.; Wolters, P.J.; Koliwad, S.; et al. Invariant Natural Killer T Cells Coordinate Removal of Senescent Cells. *Med* **2021**, *2*, 938–950. [CrossRef]
139. Hazeldine, J.; Hampson, P.; Lord, J.M. Reduced Release and Binding of Perforin at the Immunological Synapse Underlies the Age-Related Decline in Natural Killer Cell Cytotoxicity. *Aging Cell* **2012**, *11*, 751–759. [CrossRef] [PubMed]
140. Chelyapov, N.; Nguyen, T.T.; Gonzalez, R. Autologous NK Cells Propagated and Activated Ex Vivo Decrease Senescence Markers in Human PBMCs. *Biochem. Biophys. Rep.* **2022**, *32*, 101380. [CrossRef] [PubMed]
141. Xue, W.; Zender, L.; Miething, C.; Dickins, R.A.; Hernandez, E.; Krizhanovsky, V.; Cordon-Cardo, C.; Lowe, S.W. Senescence and Tumour Clearance Is Triggered by P53 Restoration in Murine Liver Carcinomas. *Nature* **2007**, *445*, 656–660. [CrossRef]
142. Iannello, A.; Raulet, D.H. Immune Surveillance of Unhealthy Cells by Natural Killer Cells. *Cold Spring Harb. Symp. Quant. Biol.* **2013**, *78*, 249–257. [CrossRef]
143. Ruscetti, M.; Leibold, J.; Bott, M.J.; Fennell, M.; Kulick, A.; Salgado, N.R.; Chen, C.-C.; Ho, Y.-J.; Sanchez-Rivera, F.J.; Feucht, J.; et al. NK Cell-Mediated Cytotoxicity Contributes to Tumor Control by a Cytostatic Drug Combination. *Science* **2018**, *362*, 1416–1422. [CrossRef] [PubMed]
144. Sawasdee, N.; Wattanapanitch, M.; Thongsin, N.; Phanthaphol, N.; Chiawpanit, C.; Thuwajit, C.; Yenchitsomanus, P.-T.; Panya, A. Doxorubicin Sensitizes Breast Cancer Cells to Natural Killer Cells in Connection with Increased Fas Receptors. *Int. J. Mol. Med.* **2022**, *49*, 40. [CrossRef]
145. Pereira, B.I.; Devine, O.P.; Vukmanovic-Stejic, M.; Chambers, E.S.; Subramanian, P.; Patel, N.; Virasami, A.; Sebire, N.J.; Kinsler, V.; Valdovinos, A.; et al. Senescent Cells Evade Immune Clearance via HLA-E-Mediated NK and CD8+ T Cell Inhibition. *Nat. Commun.* **2019**, *10*, 2387. [CrossRef]
146. Yang, H.; Rei, M.; Brackenridge, S.; Brenna, E.; Sun, H.; Abdulhaqq, S.; Liu, M.K.P.; Ma, W.; Kurupati, P.; Xu, X.; et al. HLA-E-Restricted, Gag-Specific CD8+ T Cells Can Suppress HIV-1 Infection, Offering Vaccine Opportunities. *Sci. Immunol.* **2021**, *6*, eabg1703. [CrossRef] [PubMed]
147. Di Mitri, D.; Toso, A.; Chen, J.J.; Sarti, M.; Pinton, S.; Jost, T.R.; D’Antuono, R.; Montani, E.; Garcia-Escudero, R.; Guccini, I.; et al. Tumour-Infiltrating Gr-1+ Myeloid Cells Antagonize Senescence in Cancer. *Nature* **2014**, *515*, 134–137. [CrossRef]
148. Eggert, T.; Wolter, K.; Ji, J.; Ma, C.; Yevsa, T.; Klotz, S.; Medina-Echeverez, J.; Longerich, T.; Forgues, M.; Reisinger, F.; et al. Distinct Functions of Senescence-Associated Immune Responses in Liver Tumor Surveillance and Tumor Progression. *Cancer Cell* **2016**, *30*, 533–547. [CrossRef] [PubMed]
149. Zhu, Y.; Tchkonja, T.; Pirtskhalava, T.; Gower, A.C.; Ding, H.; Giorgadze, N.; Palmer, A.K.; Ikeno, Y.; Hubbard, G.B.; Lenburg, M.; et al. The Achilles’ Heel of Senescent Cells: From Transcriptome to Senolytic Drugs. *Aging Cell* **2015**, *14*, 644–658. [CrossRef]
150. Schafer, M.J.; White, T.A.; Iijima, K.; Haak, A.J.; Ligresti, G.; Atkinson, E.J.; Oberg, A.L.; Birch, J.; Salmonowicz, H.; Zhu, Y.; et al. Cellular Senescence Mediates Fibrotic Pulmonary Disease. *Nat. Commun.* **2017**, *8*, 14532. [CrossRef]
151. Li, C.; Shen, Y.; Huang, L.; Liu, C.; Wang, J. Senolytic Therapy Ameliorates Renal Fibrosis Postacute Kidney Injury by Alleviating Renal Senescence. *FASEB J.* **2021**, *35*, e21229. [CrossRef]
152. Aguayo-Mazzucato, C.; Andle, J.; Lee, T.B.; Midha, A.; Talemal, L.; Chipashvili, V.; Hollister-Lock, J.; van Deursen, J.; Weir, G.; Bonner-Weir, S. Acceleration of  $\beta$  Cell Aging Determines Diabetes and Senolysis Improves Disease Outcomes. *Cell Metab.* **2019**, *30*, 129–142.e4. [CrossRef]
153. Roos, C.M.; Zhang, B.; Palmer, A.K.; Ogrodnik, M.B.; Pirtskhalava, T.; Thalji, N.M.; Hagler, M.; Jurk, D.; Smith, L.A.; Casaclang-Verzosa, G.; et al. Chronic Senolytic Treatment Alleviates Established Vasomotor Dysfunction in Aged or Atherosclerotic Mice. *Aging Cell* **2016**, *15*, 973–977. [CrossRef] [PubMed]
154. Saccon, T.D.; Nagpal, R.; Yadav, H.; Cavalcante, M.B.; Nunes, A.D.d.C.; Schneider, A.; Gesing, A.; Hughes, B.; Yousefzadeh, M.; Tchkonja, T.; et al. Senolytic Combination of Dasatinib and Quercetin Alleviates Intestinal Senescence and Inflammation and Modulates the Gut Microbiome in Aged Mice. *J. Gerontol. A Biol. Sci. Med. Sci.* **2021**, *76*, 1895–1905. [CrossRef]



155. Hernández-Silva, D.; Cantón-Sandoval, J.; Martínez-Navarro, F.J.; Pérez-Sánchez, H.; de Oliveira, S.; Mulero, V.; Alcaraz-Pérez, F.; Cayuela, M.L. Senescence-Independent Anti-Inflammatory Activity of the Senolytic Drugs Dasatinib, Navitoclax, and Venetoclax in Zebrafish Models of Chronic Inflammation. *Int. J. Mol. Sci.* **2022**, *23*, 10468. [CrossRef] [PubMed]
156. Justice, J.N.; Nambiar, A.M.; Tchkonja, T.; LeBrasseur, N.K.; Pascual, R.; Hashmi, S.K.; Prata, L.; Masternak, M.M.; Kritchevsky, S.B.; Musi, N.; et al. Senolytics in Idiopathic Pulmonary Fibrosis: Results from a First-in-Human, Open-Label, Pilot Study. *EBioMedicine* **2019**, *40*, 554–563. [CrossRef] [PubMed]
157. Hickson, L.J.; Langhi Prata, L.G.P.; Bobart, S.A.; Evans, T.K.; Giorgadze, N.; Hashmi, S.K.; Herrmann, S.M.; Jensen, M.D.; Jia, Q.; Jordan, K.L.; et al. Senolytics Decrease Senescent Cells in Humans: Preliminary Report from a Clinical Trial of Dasatinib plus Quercetin in Individuals with Diabetic Kidney Disease. *EBioMedicine* **2019**, *47*, 446–456. [CrossRef] [PubMed]
158. Chaib, S.; Tchkonja, T.; Kirkland, J.L. Cellular Senescence and Senolytics: The Path to the Clinic. *Nat. Med.* **2022**, *28*, 1556–1568. [CrossRef]
159. Climent, N.; Casanova, V.; Maleno, M.J.; Rodríguez-Agustín, A.; Sánche-Palomino, S.; González, T.; Hurtado, C.; Martínez, E.; Mallolas, J.; Ambrosioni, J.; et al. HIV-Induced Cellular Senescence in PLWH Is Decreased by D+Q Senolytic Drugs. [CROI Abstract 223]. In Proceedings of the CROI 2022 Conference on Retroviruses and Opportunistic Infections, Virtual, 12–16 February 2022; p. 222.
160. Baar, M.P.; Brandt, R.M.C.; Putavet, D.A.; Klein, J.D.D.; Derks, K.W.J.; Bourgeois, B.R.M.; Stryeck, S.; Rijksen, Y.; van Willigenburg, H.; Feijtel, D.A.; et al. Targeted Apoptosis of Senescent Cells Restores Tissue Homeostasis in Response to Chemotoxicity and Aging. *Cell* **2017**, *169*, 132–147.e16. [CrossRef]
161. Kovacovicova, K.; Skolnaja, M.; Heinmaa, M.; Mistrik, M.; Pata, P.; Pata, I.; Bartek, J.; Vinciguerra, M. Senolytic Cocktail Dasatinib+Quercetin (D+Q) Does Not Enhance the Efficacy of Senescence-Inducing Chemotherapy in Liver Cancer. *Front. Oncol.* **2018**, *8*, 459. [CrossRef] [PubMed]

**Disclaimer/Publisher's Note:** The statements, opinions and data contained in all publications are solely those of the individual author(s) and contributor(s) and not of MDPI and/or the editor(s). MDPI and/or the editor(s) disclaim responsibility for any injury to people or property resulting from any ideas, methods, instructions or products referred to in the content.

Review

# Drugging Hijacked Kinase Pathways in Pediatric Oncology: Opportunities and Current Scenario

Marina Ferreira Candido <sup>1</sup>, Mariana Medeiros <sup>2</sup>, Luciana Chain Veronez <sup>3</sup>, David Bastos <sup>4</sup>, Karla Laissa Oliveira <sup>4</sup>, Julia Alejandra Pezuk <sup>5</sup>, Elvis Terce Valera <sup>3</sup> and María Sol Brassesco <sup>5,\*</sup>

<sup>1</sup> Department of Cell Biology, Ribeirão Preto Medical School, University of São Paulo, Ribeirão Preto 14049-900, SP, Brazil

<sup>2</sup> Regional Blood Center, University of São Paulo, Ribeirão Preto 14049-900, SP, Brazil

<sup>3</sup> Department of Pediatrics, Ribeirão Preto Medical School, University of São Paulo, Ribeirão Preto 14049-900, SP, Brazil

<sup>4</sup> Department of Biology, Faculty of Philosophy, Sciences and Letters at Ribeirão Preto, University of São Paulo, Ribeirão Preto 14040-901, SP, Brazil

<sup>5</sup> Department of Biotechnology and Innovation, Anhanguera University of São Paulo, UNIAN/SP, São Paulo 04119-001, SP, Brazil

\* Correspondence: solbrassesco@usp.br; Tel.: +55-16-3315-9144; Fax: +55-16-3315-4886

**Abstract:** Childhood cancer is considered rare, corresponding to ~3% of all malignant neoplasms in the human population. The World Health Organization (WHO) reports a universal occurrence of more than 15 cases per 100,000 inhabitants around the globe, and despite improvements in diagnosis, treatment and supportive care, one child dies of cancer every 3 min. Consequently, more efficient, selective and affordable therapeutics are still needed in order to improve outcomes and avoid long-term sequelae. Alterations in kinases' functionality is a trademark of cancer and the concept of exploiting them as drug targets has burgeoned in academia and in the pharmaceutical industry of the 21st century. Consequently, an increasing plethora of inhibitors has emerged. In the present study, the expression patterns of a selected group of kinases (including tyrosine receptors, members of the PI3K/AKT/mTOR and MAPK pathways, coordinators of cell cycle progression, and chromosome segregation) and their correlation with clinical outcomes in pediatric solid tumors were accessed through the R2: Genomics Analysis and Visualization Platform and by a thorough search of published literature. To further illustrate the importance of kinase dysregulation in the pathophysiology of pediatric cancer, we analyzed the vulnerability of different cancer cell lines against their inhibition through the Cancer Dependency Map portal, and performed a search for kinase-targeted compounds with approval and clinical applicability through the CanSAR knowledgebase. Finally, we provide a detailed literature review of a considerable set of small molecules that mitigate kinase activity under experimental testing and clinical trials for the treatment of pediatric tumors, while discuss critical challenges that must be overcome before translation into clinical options, including the absence of compounds designed specifically for childhood tumors which often show differential mutational burdens, intrinsic and acquired resistance, lack of selectivity and adverse effects on a growing organism.

**Keywords:** childhood cancer; kinases; chemical inhibitors; clinical trials

**Citation:** Candido, M.F.; Medeiros, M.; Veronez, L.C.; Bastos, D.; Oliveira, K.L.; Pezuk, J.A.; Valera, E.T.; Brassesco, M.S. Drugging Hijacked Kinase Pathways in Pediatric Oncology: Opportunities and Current Scenario. *Pharmaceutics* **2023**, *15*, 664. <https://doi.org/10.3390/pharmaceutics15020664>

Academic Editor: Francesca Musumeci

Received: 15 December 2022

Revised: 9 February 2023

Accepted: 10 February 2023

Published: 16 February 2023



**Copyright:** © 2023 by the authors. Licensee MDPI, Basel, Switzerland. This article is an open access article distributed under the terms and conditions of the Creative Commons Attribution (CC BY) license (<https://creativecommons.org/licenses/by/4.0/>).

## 1. Pediatric Cancer

The past two decades have witnessed tremendous advances in our understanding of cancer pathogenesis, with most neoplasms resulting from the accumulation of gains in function in proto-oncogenes and losses of tumor suppressors.

In the pediatric setting (between 0 and 19 years of age), cancer is defined as a group of several diseases that have in common the uncontrolled proliferation of abnormal cells that can occur in any region of the body. However, unlike adult tumors that are classified

according to the primary site, the International Classification of Childhood Cancer (CICI) categorizes pediatric tumors into 12 main groups based on histological findings [1].

Of these, leukemias are the most frequent, representing 35% of all tumors that affect children and adolescents [2]. The second most common group is represented by lymphomas (20%), followed in descending order by tumors of the central (15%) and sympathetic (7%) nervous system, soft tissue sarcomas (6%), bone tumors (5%), kidney tumors (3%), germ cell tumors (3%), retinoblastoma (2%), carcinomas (2%), liver tumors (1%) and other rare pediatric neoplasms.

Several specific characteristics converge on the premise that childhood and adult cancer should be studied separately. First of all, most pediatric tumors have histological findings that resemble fetal tissues at different stages of development, being considered embryonic and carrying different levels of cell differentiation. Furthermore, the spectrum of tumors in the pediatric age group differs from that in adult patients. Medulloblastoma (MB), neuroblastoma (NB), rhabdomyosarcoma (RMS), Ewing's sarcoma (EWS), osteosarcoma (OS), retinoblastoma (RB) and Wilms' tumor (WT), which are the most frequent pediatric solid tumors, are rarely found in adulthood [3].

Moreover, latency periods are shorter in pediatric cancer, with several histologies presenting even shortly after birth. Such rapid proliferation in embryonic tissues relies mainly on genomic errors with lesser contribution of environmental factors [4]. Similarly, unlike what happens in adults, pediatric tumors are usually more aggressive with nonspecific signs and symptoms, confusing them with common childhood illnesses and making early diagnosis difficult.

Additionally, tumors in this age group show clear differences in their presentation, clinical course and response to treatment when compared to adult counterparts. Tumors of the EWS family, for example, in adults, in addition to presenting a more differentiated histology (PNET—primitive neuroectodermal tumor), manifest preferentially with greater volume at diagnosis, affecting soft tissues and with distant metastases, resulting in poorer survival. In children, EWS preferentially affects the bones of the extremities, have a smaller volume, and respond better to chemotherapy. Still, in this population, the chance of survival after 5 years (without metastasis at diagnosis) is 75%, significantly higher than that calculated for adults (50%) [5]. Similar observations have been reported for RMS. In a cohort of 1071 adults and 1529 children, for example, the survival rate in the first group was considerably lower (27% versus 61%), with tumors occurring in unfavorable locations and with rare histologies [6].

Another peculiarity of childhood cancer lies in the fact that specific histological subtypes and clinical behavior are also age-dependent, suggesting differential pathogenic mechanisms and underlying molecular alterations for tumor initiation and progression. The general incidence of acute lymphoblastic leukemia (ALL), for example, is highest in the 1–4-year-old age group, while the highest frequency of lymphomas occurs among adolescents (between 15 and 19 years old). Embryonic tumors (NB, WT, RB, etc.), on the other hand, share a descending incidence, which is highest early in life and almost dissipates after 5 years of age, while the incidence of bone sarcomas reaches a sharp peak at the time of the pubertal growth spurt [7].

Finally, with the methodologic refinements in the identification of genomic alterations, it has become increasingly evident that the spectra of mutations and the subsequent dysregulation of signaling pathways in pediatric neoplasms differ from those that occur predominantly in adult cancer. In fact, it has been stipulated that most pediatric tumors carry between 5 and 10 mutations; however, the average number of mutations in adult tumors varies between 33 and 66 (i.e., colon, breast or pancreas carcinomas) and increases up to 200 in tumors caused by mutagens (such as melanoma/ultraviolet radiation (UV) and lung cancer/smoking) and up to 1000 in tumors with defects in mismatch repair genes, as is the case of nonpolyposis colorectal cancer, among others [8]. In this regard, a recent integrative study based on whole-genome sequencing data from 24 tumor types (914 patients) showed that even though mutation frequencies (SNV and indels) vary

between pediatric tumor types (from 0.02 to 0.49 per Mb), these were 14 times lower than in adult cancers [9]. Of note, a high prevalence of mutations affecting genes related to cancer predisposition syndrome are seen in children affected by different tumor types [10]. In addition, pediatric cancers are usually enriched by gene fusions, driving tumorigenesis and showing impact on both diagnostic and targeted-treatments [11].

In fact, this work identified 52 genes significantly mutated for childhood and juvenile tumors and 102 genes for adult tumors, 25 of which were shared by both groups. *TP53* was the most commonly mutated gene (4% of childhood tumors), followed by *KRAS*, *ATRX*, *NF1* and *RB1* (1–2% of tumors). In adult tumors, *TP53* was also the gene most affected by mutations, albeit tenfold more frequently. Furthermore, the burden of mutations increased with patient age except for tumors characterized by *kataegis* or *chromothripsis* events [9].

Moreover, the mutational identity may also vary. Glioblastoma (GBM) (grade IV astrocytoma), for example, is characterized by mutations in *PTEN* and epidermal growth factor receptor (*EGFR*) amplification in adults [12]; the pediatric counterpart more frequently presents mutations in the N-terminal tail of the histone variant 3.3 [13], in platelet-derived growth factor (*PDGF*) and its receptor (*PDGFR*) [14]. As previously described, gene fusions that are rare in adult tumors appear recurrently in pediatric tumors such as *BRAF/KIAA1549* in pilocytic astrocytoma (PA) [15], *C11orf95/RELA* [16] in supratentorial ependymoma (EPN), *PAX3/FOXO1* and *PAX7/FOXO1* in alveolar RMS [17], and variants involving the *EWS* gene (*EWS/FLI1*, *EWS/ERG* and others less frequent) in EWS [18]; the majority of these fusions involve transcription factors associated with the development/differentiation of the affected tissue.

More recently, with the establishment of cooperative study groups and progress in imaging associated with more accurate anatomopathological and molecular diagnosis, the mortality of children affected by cancer, especially those with leukemia and some types of solid tumors, has shown an important decline. Five-year overall survival rates increased from 56% in the 1970s to 77% in the following vicennial [19].

In accordance, today ALL represents the paradigm of curable cancer in children, with current overall survival rates exceeding 85% in most modern treatment protocols [20]. However, for some aggressive leukemia subtypes and certain solid tumor histologies, the persisting advances in biological characterization combined with new technologies in radiotherapy (RT), chemotherapy (CT) and supportive/rehabilitation care have resulted in marginal survival advantages, and cure rates have stagnated at around 70% [21]. Yet, in underdeveloped areas such as Eastern Europe, Africa and South America, these reductions in mortality have been less expressive, and a considerable portion of children with cancer fail to respond to traditional chemotherapy.

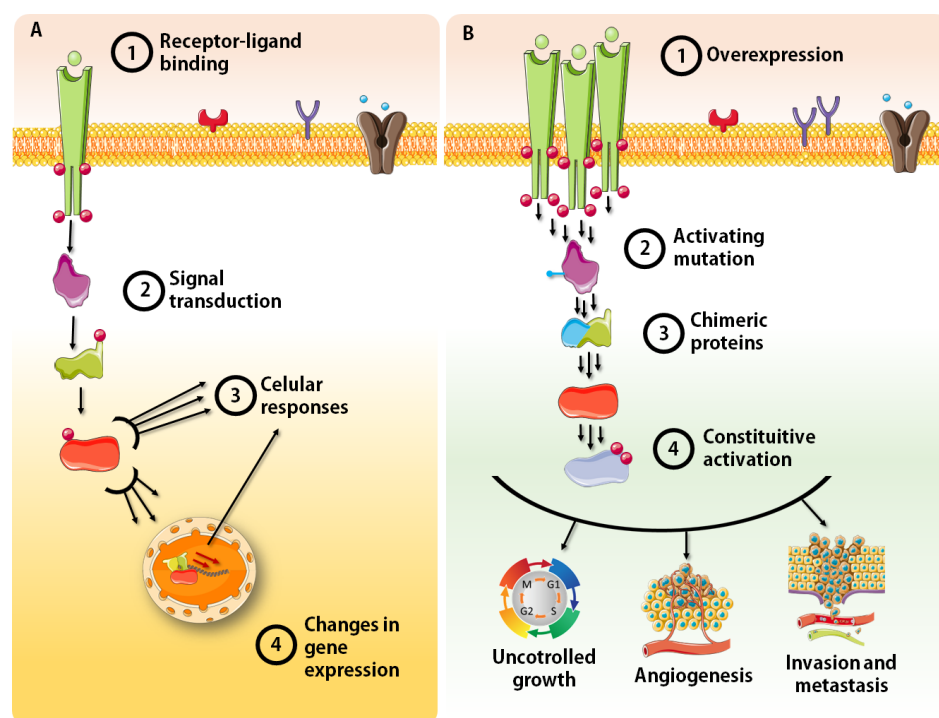
In this scenario, alternative rationally targeted pharmacological options are still needed to overcome clinical resistance, tumor progression, and prevent the adverse side effects of standard therapy.

## 2. Kinases as Cancer Drivers

The human genome encodes more than 500 protein kinases, enzymes responsible for turning protein functions “on” through the transference of  $\gamma$ -phosphate groups from ATP to one of their three amino acids with free hydroxyl groups: serine, threonine or tyrosine. Human protein kinases have been divided into nine classes which are further subdivided into families, and often subfamilies whose actions can alter up to 30% of all cell proteins [22]. The molecular shifts exerted by them through phosphorylation not only can affect the function of a given protein, but it can also stabilize it, localize it in a particular cellular compartment and modulate its association with other proteins [23].

Protein kinases may be triggered or deactivated in many ways, including cis- or autophosphorylation, binding with substrates or activator/inhibitor proteins. Once activated, they act as crucial regulators of many features of cell behavior and specialized functions by coupling reception of extracellular signals, intracellular signaling transduction and cellular responses [24].

Playing fundamental roles in cell division, survival and migration, their dysregulation is commonly associated with human malignancies and contributes to tumor initiation and all stages of cancer progression. In fact, innumerable mutations, translocations, and amplifications that result in constitutively overexpressed or active kinases have been demonstrated in many human cancers [23]. Mutations within the catalytic domain serve to stabilize the kinase in an active conformation and to destabilize cis-inhibitory interactions. Other domains can also be affected and elicit constitutive activity and hyperactive pathways as well. DNA translocations, on the other hand, predominantly create in frame gene fusions leading to chimeric proteins with novel/increased activity, leading to continued cancer cell growth and survival (Figure 1) [25,26]. Moreover, the dysregulation of different kinases has been repeatedly associated with tumor prognosis and categorized as a determinant of patient survival [27,28].



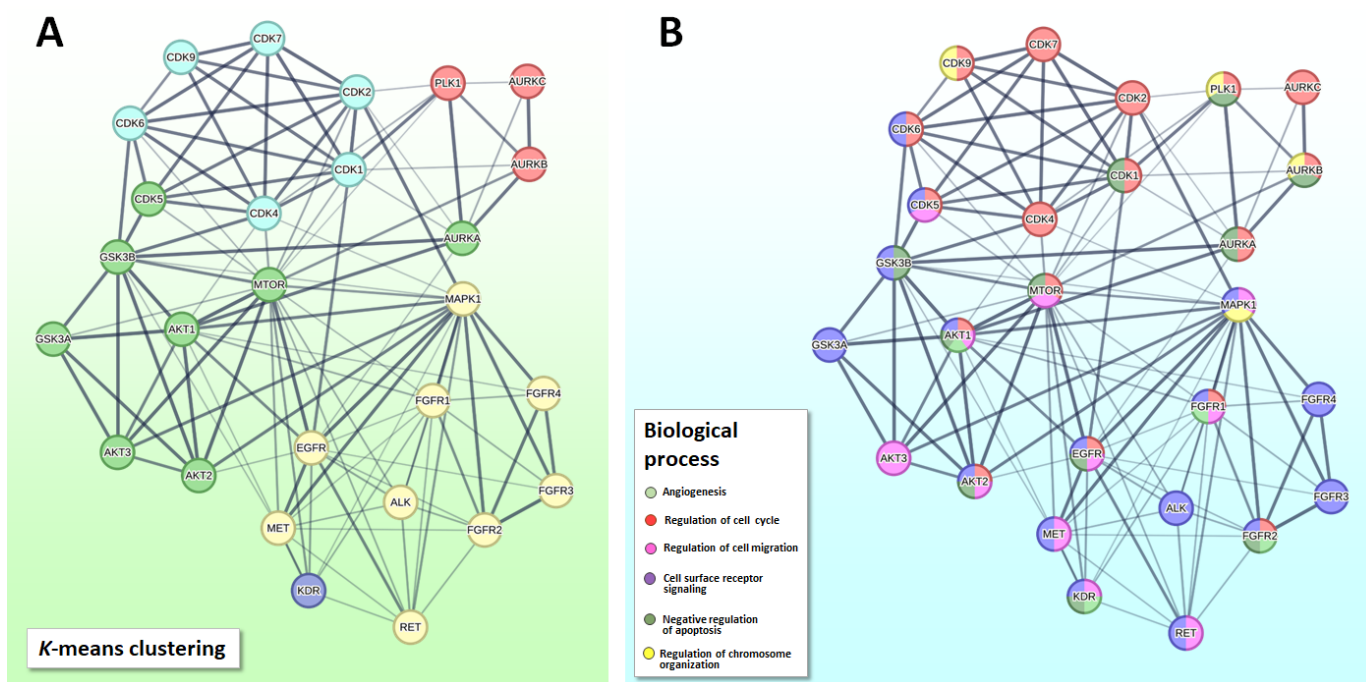
**Figure 1.** (A) Protein kinases may be triggered or deactivated in many ways, acting as key regulators of many features of cell behavior and specialized functions by coupling (1) reception of extracellular signals and (2) intracellular signaling transduction, leading to (3) direct cellular responses or (4) changes in gene expression. (B) In cancer, increased kinase activity may result from gene amplification (1,4), mutations that stabilize the kinase in an active conformation and destabilize cis-inhibitory interactions (2) and translocations that encode chimeric proteins with novel/increased activity (3). This figure was created using Servier Medical Art templates, which are licensed under a Creative Commons Attribution 3.0 Unported License; <https://smart.servier.com> (accessed on 14 December 2022).

Hence, the so-called “Kinome” (the complete set of protein kinases encoded in the human genome—about 2% of all genes) has become an attractive target for the treatment of a variety of tumors. Even so, despite the great diversity, over the years, it has become more apparent that only certain kinases are among the most frequently occurring drivers of human cancer, including tyrosine receptors (RTK) (i.e., FGFR, EGFR, VEGFR, RET, MET, ALK), members of the PI3K/AKT/mTOR and Mitogen-Activated Protein Kinase (MAPK) pathways, along with central coordinators of cell cycle progression (i.e., cyclin-dependent kinases) and chromosome segregation such as polo-like and aurora kinases [25].

In this way, the present study aimed to present evidence of the involvement of these kinases' dysregulation in the pathophysiology of pediatric tumors, their correlation with clinical outcomes and prospects of their inhibition through *in silico* analysis, along with an up-to-date revision of compound development and testing.

### 3. Protein Kinases in Pediatric Oncology and Their Association with Tumor Prognosis

As stated above, substrate reversible phosphorylation by protein kinases is nature's main molecular system for organizing cellular signal transduction and regulating cell metabolism, growth and differentiation. The phosphorylation state of a protein determines not only its function, subcellular distribution and stability, but also its interaction with other proteins or cellular components. Intrinsically, signaling pathways are remarkably complex and as our knowledge increases, it has become progressively evident that such molecular networks are not linear but contain modules of multi-protein complexes, many feedbacks, feedforwards and competing protein mechanisms that not only assemble at various intracellular compartments to process, integrate and transmit information that will ultimately specify a particular biological response, but also crosstalk with many other signaling pathways [29]. Thus, even though the kinases that were selected for this review will be treated separately, many, if not all, are directly or indirectly interconnected (Figure 2).



**Figure 2.** (A) Protein–protein interactions accessed through the software STRING v11.5 (available at <https://string-db.org/> (accessed on 2 November 2022)). The parameters evaluated were text mining, experiments and databases. Network edges denote confidence and the minimum required interaction score was 0.700, considered high. (A) K-means clustering; (B) enrichment analysis for biological processes.

In this section, the different roles of protein kinases in oncogenic transformation and tumor prognosis in the pediatric setting were assessed by two different approaches: by a thorough search of published literature, and by a systematic search in publicly available data retrieved from expression arrays accessed through the R2: Genomics Analysis and Visualization Platform (<http://r2.amc.nl> (accessed on 15 October 2022)). For this, datasets were included if they met the following criteria: inclusion of pediatric samples (exclusively or in which adult variants could be omitted), normal counterparts and having information

about clinical features of prognosis (Supplementary Figure S1). Datasets and probes are detailed in Supplementary Tables S1 and S2.

### 3.1. Published Evidence of Kinase Dysregulation in Pediatric Oncology

#### 3.1.1. Receptor Tyrosine Kinases (RTK)

Humans express 58 receptor tyrosine kinases (RTK) which function as entry points for many extracellular signals and the recruitment of the intracellular signaling networks that orchestrate a particular response [30].

These cell surface receptors possess multi-domain identical architectures that are made up of an extracellular ligand-binding domain (which differs between subfamilies), a single transmembrane helix and an intracellular region that contains a juxtamembrane regulatory region (composed of 40–80 amino acids), a tyrosine kinase domain (TKD) and a carboxyl (C-) terminal tail [31].

Generally, RTK activation occurs upon binding of ligands (i.e., growth factors or cytokines) to their extracellular domains. This interaction results in RTK non-covalent dimerization/oligomerization, which juxtaposes the cytoplasmic TKDs and facilitates autophosphorylation in trans of tyrosine residues in the juxtamembrane regulatory region, inducing conformational changes that serve to stabilize the active state of the kinase. Then, a second phase of tyrosine autophosphorylation occurs on phosphotyrosines that recruit downstream signaling proteins that typically contain Src homology 2 (SH2) or phosphotyrosine-binding (PTB) domains. The recruitment of these adapter molecules then initiates a cascade of RTK-specific pathways that determine cell fate [22,31,32].

About 20 different RTKs classes or subfamilies have been described [33]. Their activity is tightly regulated in normal cells; however, constitutive kinase activity acquired through mutation, overexpression and/or autocrine/paracrine stimulation has been strongly associated with pathological disorders, neoplastic transformation and metastasis [34]. Dysregulation of the epidermal growth factor receptor (EGFR/ErbB), the receptor for insulin (IR), the platelet-derived growth factor receptor (PDGFR), the fibroblast growth factor receptor (FGFR), the vascular endothelial growth factor receptor (VEGFR) and the hepatocyte growth factor receptor (HGFR/MET), for example, results in uncontrolled activation of multiple downstream signal transduction pathways and provides a strong drive toward malignancy [35]. Some of these oncogenes are paradigms of certain tumor types, as is the case of the amplification of EGFR/ErbB in breast cancer or MET overexpression in non-small cell lung cancer (NSCLC) [36,37]. Nevertheless, information about RTKs' involvement in the pathophysiology of childhood cancer is less discernible, as illustrated below.

**FGFR.** The signaling cascades of fibroblast growth factor receptors (FGFR1, FGFR2, FGFR3 and FGFR4) play pivotal roles in the regulation of development and tissue repair and regeneration. These receptors are highly conserved and widely distributed and their dysregulation promotes tumor growth, survival and development of drug resistance, as well as the development of angiogenesis and immune evasion [38]. A recent pan-cancer next-generation sequencing profiling demonstrated that ~7% of cancers harbor gain-of-function FGFR aberrations, with varying frequencies between family members (FGFR1 > FGFR3 > FGFR2 > FGFR4) [39]. Gene amplifications or activating mutations have been observed in multiple cancer types, although they are most commonly detected in breast, lung, liver, stomach, uterus and bladder cancer [40]. In fact, most of the aberrations detected in the survey performed by Helsten et al. (2016) involved adult carcinomas, while the percentage of cases positive for *FGFR* aberrations in childhood tumors (NB and OS) was around 3% [39]. Additionally, *FGFR1* fusions (i.e., FGFR1-TACC1), TKD duplications and hotspot mutations (i.e., N5465K and K656E) are frequently observed in certain types of pediatric brain cancer, particularly dysembryoplastic neuroepithelial tumors (DNET) and PA [41]. Moreover, germline mutations in *FGFR1*, either complete or in mosaicism, may predispose low-grade central nervous system (CNS) tumors in children and adolescents [42,43].

Other research groups have also found correlations between altered expression of FGFRs and poor prognosis. *FGFR1* amplification, for example, was correlated with worse prognosis and poor response to chemotherapy in a large cohort of patients with OS [44]. Moreover, *FGFR1* has been correlated with tumor development and lung metastasis in xenographic models, whereas its activation improved survival and radiation resistance, a phenotype which was reversed when *FGFR1* was inhibited [45]. Similar to OS, *FGFR1* copy number gains are frequent in EWS, where patients with activating *FGFR1* mutations present higher incidence of metastatic disease [46]. In vitro, *FGFR1* suppression through interference RNA (RNAi) significantly reduced cell proliferation. Decreased xenograft tumor growth and 18F-fluorodeoxyglucose activity were also observed [47].

*FGFR1* amplification and gene fusions have also been described in RMS with an active role cancer cell proliferation [48,49]. However, opposite expression patterns have been reported [50,51]. Nevertheless, it has already been shown that embryonal (ERMS) histologies present higher *FGFR1* expression levels compared to the alveolar forms (ARMS) [51].

Considering CNS tumors, upregulation of *FGFR1* has been associated with worse prognosis and shorter overall and recurrence-free survival in EPN and NB [52–55]. The analysis of *FGFR1* protein abundance in human MB tissues, through an anonymized, validated MB, and cerebellum tissue microarray (TMA) and immunohistochemistry (IHC) found high levels of *FGFR1* expression in 18% of the tumor tissues. In the case of gliomas, many mutations involving the *FGFR1* gene were described, one of which was associated with radioresistance [56–60]. Otherwise, in WT and MB, there is no published evidence.

Regarding *FGFR2*, information in the literature about its relevance in pediatric tumors is scarce. Besides correlations with higher tumor grade, radioresistance and poorer survival in gliomas [61–63], its phosphorylation (indicative of activation) was seen increased in NB samples (compared to normal tissues) and correlated with cisplatin resistance [62]. Alternatively, low expression of this kinase was observed MB [63] and in RMS when compared to normal myeloblasts [64]. Downregulation or undetectable expression of *FGFR3* was also reported in RMS with no evidence of correlation with the clinical outcome [64]. However, a more recent study described a small population of *FGFR3*-positive cells as strongly tumorigenic with a stem cell-like phenotype [65].

*FGFR3* is also downregulated in WT [66]; however, in pediatric CNS tumors, opposite *FGFR3* expression profiles are observed. In NB, high expression levels are associated with worse overall survival and event-free survival (EFS) [67]. In glioma, its upregulation was associated with increased patient age [52], a feature that denotes a more invasive phenotype in adult counterparts [59]. Moreover, *FGFR3* amplification [68] and fusions (*FGFR3-TACC3*) seem to play a role in tumor metabolism and tumor growth promotion in low-grade gliomas (LGG) [69–71]. Such correlation with poor prognosis was also observed in EPN in which *FGFR3* was associated with shorter overall survival and shorter time to tumor recurrence [52].

Moderate-to-high expression of *FGFR3* mRNA was also observed in 80% of samples from EWS family tumors [71]. Mutations in this gene were also reported in circulating tumor cell samples [72]. However, neither of these studies presented information about correlations with clinical outcomes. Of note, when *FGFR3* is downregulated in OS cell lines (by long noncoding, microRNA or iRNA), there is a reduction in tumor growth and angiogenesis, reinforcing its relevance to this disease [73–76].

Regarding *FGFR4*, little information about its prognostic value has been published in the pediatric setting, with a few reports on glioma, MB, RMS and NB. The prognostic value of this kinase in the first group was initially evaluated by in 2019 by Jimenez-Pascual and Siebzehnrb1, who did not find any correlations between *FGFR4* expression and clinical outcomes [59]. Nevertheless, a recent evaluation of transcriptomic glioma datasets from The Cancer Genome Atlas (TCGA) revealed a direct association of high *FGFR4* expression and dismal prognosis, progressively upregulated in recurrent tumors. In addition, the contribution of *FGFR4* to the malignant phenotype of a highly aggressive GBM subgroup was further validated by increased viability, adhesion, migration and



clonogenicity in vitro, along with abolished xenograft formation in mice and reduced invasiveness in zebrafish xenotransplantation models [76].

In MB, high *FGFR4* expression levels were observed in HD-MBO3 cells and in a small cohort ( $n = 12$ ) of primary MB tissues, even though there was no validation upon TMA [63]. Of note, a pilot study based on an independent blinded set of 112 samples showed that protein levels of *FGFR4* in urine, together with cadherin-1 (*CADH1*) and fibrinogen beta chain (*FIBB*), could be used to discriminate MB patients from healthy control patients with acceptable accuracy. Moreover, the authors reported a positive correlation of urine *FGFR4* detection with the age of affected patients [77].

Additionally, *FGFR4* overexpression in RMS contributes to the failure of cells to complete normal skeletal muscle development, leading to constitutive signaling and unregulated growth in correlation with poor differentiation [78–81]. *FGFR4* mutations in childhood RMS (7–8% of tumors) are more frequently observed within the kinase domain. From those, N535K and V550E increase autophosphorylation of the receptor and promote proliferation and metastatic potential when expressed in vitro [79]. High expression levels of *FGFR4* have also been associated with advanced stage and poor survival in RMS [82,83]. Furthermore, *FGFR4* has been reported as a downstream target of *PAX3* and *PAX3-FOXO1* [81] and thus is commonly altered in fusion-positive RMS [83] and a key contributor to RMS invasion and metastasis [84].

Last but not least, a germline polymorphism in the *FGFR4* gene (rs351855) which results in the expression of an arginine at codon 388 (Arg388), rather than the more common glycine (Gly388), is frequently associated with decreased survival rates, treatment resistance and more aggressive disease in a variety of malignancies, and is associated with an increased prevalence of NB in children [85], and this association may be linked to differences in *FGFR4* degradation rates [86]. It was also observed that cases with the *FGFR4* AA genotype were 2.5 times more likely to have tumors with *MYCN* amplification compared with those with AG and GG genotypes, although such association was not statistically significant [85].

**EGFR.** The epidermal growth factor receptor (EGFR) (also recognized as HER-1 or ERBB-1) is a transmembrane glycoprotein of the ERBB receptor tyrosine kinase superfamily. Overexpression and/or enhanced activity of EGFR activate the downstream pro-oncogenic signaling, including the RAS-RAF-MEK-ERK and AKT-PI3K-mTOR pathways. These consequently activate several biologic expressions that proceed human cancer progression [87].

Overexpression of EGFR has been reproducibly detected in a large number of tumor samples and found to act as a strong prognostic indicator in head and neck, ovarian, cervical, bladder and esophageal cancers, correlating to poorer survival rates [88,89]. In the pediatric setting, however, there are few reports about its prognostic relevance. In gliomas, for example, fewer molecular alterations in the EGFR gene (mutations and amplifications) are observed in children when compared to adult counterparts [90–95]. *EGFR* gene amplification/overexpression is a genetic hallmark in adult GBM (observed ~40% of tumors) [95], whereas this feature is only observed in 25% of pediatric cases; nevertheless, it is associated in a similar manner with higher proliferation and increased tumor grade [96–98].

Likewise, high-level amplification and EGFR overexpression correlate with shorter event-free survival and relapse in high-grade EPN, being considered an independent prognostic marker for intracranial forms [99–101]. In MB patients, high expression of HER-2, another member of the EGFR gene family, was also associated with limited survival and metastasis [102,103]. Moreover, this RTK often co-expresses with HER-4 (more than 50% of samples), suggesting that HER-2/HER-4 heterodimerization may be of particular biological significance in this disease [101].

HER-2 expression was also reported to be associated with the aggressive behavior of NB and to significantly reduce survival [103]. However, a later study demonstrated that EGFR and HER-2 positivity are more frequently found in favorable histological risk groups, including younger age ( $\leq 18$  months), localized disease, and favorable histological group [104]. Similar results were obtained by Izycka-Swieszewska et al. (2010), where

HER-2-negative cases were more often found in the metastatic tumor group, associated with increased mitotic index and higher KI67 expression. *MYCN* non-amplified tumors were more often HER-2-positive than amplified tumors [105]. In contrast, higher expression levels of HER-4 are more often found in patients with metastatic disease [104].

For other pediatric tumors, the biological relevance of EGFR family members remains to be clarified. In EWS, for example, while HER-2 is not considered an important prognostic factor, an association of HER-4 and metastasis was found [106]. In OS, *EGFR* expression is common [107], but correlations between EGFR or HER-2 expression and clinical prognosis have been controversial, as no treatment improvements are achieved when EGFR is inhibited in pre-clinical and clinical trials [106].

In RMS, RB and WT, no strong associations of EGFR expression with clinical data have been found [108–111], although the ERBB family seems to be important for the malignant phenotype of RMS: ERBB1 sustains cell proliferation and growth, ERBB2 regulates myoblast cell transformation and survival and ERBB3 induces myogenic differentiation. Additionally, activation of ERBB2 coupled with inactivation of p53 induces RMS in animal models [106].

**VEGFR (KDR—kinase insert domain receptor).** The vascular endothelial growth factor receptor (VEGFR) family consists of three members: VEGFR1, VEGFR2 and VEGFR3 [112]. These receptors are established players in the formation of new blood vessels and the maintenance and remodeling of existing ones, during development and in adult tissues [113]. As such, in neoplastic growth, VEGFRs play an essential role in tumor neovascularization, providing oxygen and nutrition, and they facilitate tumor cells to metastasize and spread to distant organs [114]. Regarding pediatric cancer, VEGFRs have already been quantitatively evaluated in various types of refractory brain tumors [115]. Both VEGFR1 and VEGFR2 were detected in anaplastic astrocytoma tumor cells, MB and EPN samples [116–120]. Moreover, these receptors are frequently mutated and highly expressed in gliomas, NB and OS; in all cases, there is a negative correlation with unfavorable prognosis, advanced tumor stage, metastasis and shorter overall survival [121–127].

**RET.** Under normal conditions, the RET (“rearranged during transfection”) TKR pathway is activated by glial cell line-derived neurotrophic factor (GDNF) ligands that bind to coreceptors from the GDNF family receptor alphas (GFR $\alpha$ s), playing a major role during sympathetic and enteric nervous system development, where it signals toward proliferation, migration and differentiation. Apart from amplification, the constitutive activation of RET is caused by point mutations and gene rearrangements that drive malignancy in multiple tissues (i.e., papillary and medullary thyroid carcinomas and non-small cell lung carcinomas) [128–131].

RET rearrangements are also found in a high proportion of childhood papillary thyroid cancers [132–134]. Recently, it was observed that pediatric tumors (soft tissue sarcomas or medullary thyroid cancer) harboring either an RET-fused or RET-mutated pathogenic somatic alteration show clinical response to the RET inhibitor Selpercatinib [134].

RET mutations leading to dysfunctional ligand binding have also been described as the second most significant cancer-predisposing gene in the germline of patients with OS [135,136]. Moreover, RET is activated and can promote motility and colony formation in metastatic OS cells, contributing to the higher resistance of this tumor type to different chemotherapeutic agents [137–140]. Furthermore, NB cells and tumor samples demonstrated high RET expression levels [140], and its activation induces invasive spread NB in animal models [141].

**c-MET.** The mesenchymal–epithelial transition factor (c-MET), which is also known as hepatocyte growth factor receptor (HGFR), is an essential molecule for the survival and function of normal cells that promotes tissue remodeling and organ homeostasis [142]. MET’s gain of function either via overexpression, amplification, aberrant splicing or mutations is associated with the constant activation of downstream classic signaling pathways that sustain rapid proliferation, promote cell migration, angiogenesis and survival of cancer cells [143]. Moreover, recent evidence indicates that MET signaling participates in the acquirement of mesenchymal phenotype, tumor plasticity and adaptive responses to

metabolic stress, contributing to the recurrence and metastatic dissemination of cancer cells [144,145].

The c-MET gene was first identified in the human OS cell line (HOS) that had been treated with N-methyl-N'-nitro-N-nitrosoguanidine (MNNG) as a gene able to transform normal fibroblasts [146]. Since then, its involvement in cancer establishment and progression has been repeatedly described in a variety of common and high-risk pediatric solid tumors, including not only sarcomas, but also gliomas, MB, NB, WT and hepatoblastomas, among others [147]. Of note, infantile hemispheric gliomas were recently recognized to be driven by different RTKs, including somatic fusions and alterations involving ALK, ROS1, NTRK and c-MET [148]. Especially in anaplastic, diffuse and PA, c-MET levels often correlate with tumor grade [149].

Cytoplasmic c-MET immunoreactivity is also associated with poor clinical outcome, and tissues with overexpression often exhibit higher vascular proliferation and proliferative index [150–152]. Similar phenotypes have been observed in NB, where overexpression of this receptor promotes invasion and is associated with advanced metastatic stage [153,154].

Likewise, high levels of MET protein are associated with increased proliferative activity invasion and metastasis in WT [155,156], and represent a risk factor for invasion in RB [156].

In childhood sarcomas, several studies have pointed out c-MET as a promising biomarker capable of predicting poor prognosis. Forced expression of MET in primary osteoblasts induces transformation and is essential for the maintenance of the cancer phenotype [157], while loss-of-function approaches in OS cell lines (143B and U2OS) demonstrated that this oncogene promotes cell proliferation, migration and invasion, and inhibits cell apoptosis [158]. However, the study of genomic status of MET and other genes implied in ossification processes in a cohort of 91 children and teenagers showed that *MET* is mainly deleted, although the clinical subgroup with MET amplification presents worse outcomes [159].

In EWS, modest to high MET cytoplasmic/membranous expression is detected in the majority of tumor samples and is significantly correlated with a poor overall survival. However, there were no significant correlations between MET expression and clinical characteristics, including tumor stage, tumor location and age at diagnosis. The same group also detected genetic alterations that result in the formation of truncated MET proteins in 5% of patients and in two cell lines (ES-2 and ES-7) [160].

Finally, this RTK is overexpressed in RMS tumor samples [161–163] and cell lines, contributing to the metastatic and invasive features of this tumor type [163,164].

**ALK.** This RTK was first described in 1994, as a fusion partner in the t(2;5)(p23;q35) chromosomal translocation characteristic of anaplastic lymphoma from which takes its name [165]. In general, ALK activates multiple signaling cascades, such as the PI3K-AKT, CRKL-C3G, MEKK2/3-MEK5-ERK5, JAK-STAT and MAPK pathways, and its role in cancer may vary due to many factors, including not only its fusion partners (more than 30 described so far), but also the tumor type or its genetic background (its effects on NB, for example, are dependent on *MYCN* status) [166].

Next-generation sequencing has revealed the presence of several *ALK* mutations in pediatric cases with RMS, EWS, WT and OS [161,167–170]. Most mutations are located within the kinase domain and can be divided into three groups: ligand-independent mutations (F1174I, F1174S, F1174L and R1275Q), ligand-dependent mutations (D1091N, T1151M and A1234T) and a kinase-dead mutation (I1250T) [167].

Germline gain-of-function point mutations are observed in half of hereditary NB and in 9% of the sporadic forms [170], and correlate with high risk and poor prognosis [171,172], mainly because both the wildtype and mutant forms of ALK induce *MYCN* transcription and potentiate its oncogenic activity in this tumor type [173]. Other ALK-driven pediatric tumors include infantile hemispheric gliomas [149,174], inflammatory myofibroblastic tumors, renal cell carcinomas [167] and pediatric mesotheliomas [175].

ALK in-frame translocations have been described in EPN and EWS as detected by fluorescent in situ hybridization with the break-apart of 5' and 3' probes [160,176]. Finally,

ALK expression is strongly associated with the WNT-activated MB subtype in which, differently from other pediatric tumors, it represents an independent indicator of good prognosis for medulloblastoma patients [177].

### 3.1.2. PI3K/AKT/mTOR Pathway

The phosphatidylinositol 3-kinase (PI3K)/Akt/mammalian target of rapamycin (mTOR) signaling pathway is among the best investigated in human biology, and is considered a key player in both physiological and pathological conditions [178].

The first step of activation of this pathway consists of the recognition of various growth factors and cytokines by RTKs localized at the cytoplasmic membrane. Then, these receptors dimerize and undergo autophosphorylation, activating GRB2 (Growth Factor Receptor Bound Protein 2) and SOS (Ras/Rac Guanine Nucleotide Exchange Factor). These activate Ras through the exchange of GDP with GTP, which then phosphorylates and activates the PI3K [179]. Active PI3K catalyzes the conversion of PIP2 (phosphatidylinositol 4,5-bisphosphate) to phosphatidylinositol-3,4,5-trisphosphate (PIP3), a second messenger that binds and recruits AKT to the cell membrane, which causes a conformational change in AKT and makes it more accessible to the PDK1-mediated phosphorylation of Thr308, followed by the phosphorylation at serine-473 by the mTOR2 complex [180]. This activation then induces a detachment of AKT from the inner surface of the plasma membrane, and the relocation to the nucleus where AKT isoforms phosphorylate and modulate the activity of several transcription factors. More than 100 different effectors have been described, including cyclin-dependent kinase inhibitor kip1 (p27kip1) through the FOXO family of Forkhead transcription factors, glycogen synthase kinase 3 (GSK3) and cell cycle stimulators, including cyclin D1 and c-Myc. AKT can regulate apoptosis by the inhibition of Fas ligand (FasL), BCL2-associated death promoter (BAD), BCL-2-interacting mediator of cell death (BIM) or BCL-2-associated X-protein (BAX), and by the degradation of p53 [181].

AKT also activates mTOR1, which has many different targets, including translation transcription factors that initiate transcription of genes associated with cell survival and growth and factors associated with hypoxia and angiogenesis (Figure 2) [182].

In cancer, this pathway can be dysregulated as a result of the activation of upstream oncoproteins including RTKs, by the loss or decreased level of its negative regulators such as the phosphatase PTEN (phosphate and tensin homolog deleted on chromosome 10), or directly through mutation and overexpression [183].

Undeniably, this pathway is activated in a wide variety of tumors (i.e., prostate, breast, lung and leukemia, among many others), leading to a profound disturbance of cell growth control, metabolic reprogramming and invasion/metastasis, as well as the suppression of autophagy and senescence [179,184–189]. Moreover, increasing evidence points to its critical participation in the maintenance of stemness in a variety of cancers, contributing directly to recurrence and chemoresistance [189].

In the pediatric setting, the PI3K/AKT/mTOR signaling axis has been described as abnormally activated in both hematologic and solid tumors, mainly as a consequence of chromosomal gains amplifying the AKT1 gene (described in rare cases of leukemia) [190–192] or the aberrant expression of PI3K isoforms [193]. Below, the involvement of this pathway's individual members in childhood tumors is explored.

**PI3K.** PI3K is a group of plasma membrane-associated lipid kinases, consisting of three subunits: p85 regulatory subunit, p55 regulatory subunit and p110 catalytic subunit. According to their structure and substrate specificity, these kinases are grouped into three categories (classes I, II and III) [194,195]. PIK3CA (phosphatidylinositol 3-kinase, catalytic,  $\alpha$ -polypeptide), the gene encoding the p110 $\alpha$  subunit, is frequently mutated in ~30% of common human cancers and has been studied most thoroughly [196,197]. Although numerous mutations in this gene have been described, most gain-of-function mutations cluster around two hotspots at exons 9 and 20 [197]; however, contrasting roles for mutations at each exon have been described depending on the tumor type [198,199]. PI3K amplifi-

cations have also been frequently described and correlated with aggressive phenotypes, chemoresistance and poor prognosis [200–203].

The prognostic power of PI3K alterations in childhood cancer has been less explored. In MB, however, although no mutations have been detected [196], the p110 $\alpha$  isoform is typically overexpressed, promoting cell proliferation, chemoresistance and migration [204–206].

Dysregulation of PI3K signaling is also considered an important player in gliomagenesis, with key roles in regulating cell movement and thus contributing to the highly invasive phenotype of GBM. Compared with normal human astrocytes, overexpression of PI3K p110 catalytic subunits, p85 regulatory subunits and phosphorylated Akt (Ser473) was also detected in two pediatric GBM cell lines (GBM6840 and GBM2603) [206]. Likewise, overexpression of the catalytic p110 $\delta$  and regulatory p85 $\alpha$  isoforms was also detected in a panel of primary NB samples and cell lines with active roles in cell growth and survival. Especially, p110 $\delta$  was correlated with *MYCN* amplification [207]. However, this gene is significantly lower in NB samples with loss of heterozygosity at 1p36 and associated with poor clinical outcome [208–210].

The regulatory domain of PI3K, p55, is upregulated in sarcoma stem-like cells and promotes invasion, migration and chemotherapy resistance [210]. In EWS, despite variable expression levels between samples, this positive regulator has an oncogenic role [211]. Moreover, p55 analysis on a human sarcoma TMA (that includes two EWS samples) performed by Yoon et al. demonstrated a 4.1-fold increase compared with normal tissues [210].

**AKT (PKB).** AKT or PKB (protein kinase B) is a serine/threonine kinase that functions as an important regulator of cell growth, survival and glucose metabolism. There are three isoforms of mammalian AKT which are encoded by different genes [212]. AKT1 and AKT2 are ubiquitously expressed and are mostly involved in regulating cellular survival and protein synthesis, involved in glucose transport through the insulin signaling pathway, respectively. The function of AKT3 is not yet fully understood and its expression is almost entirely limited to the nervous system tissue [213–215]. Nevertheless, it has been reported that despite the high similarity, AKT isoforms exert non-redundant specific effects under physiological and pathological conditions [215].

Gain-of-function mutations in all three AKT genes have been identified in ~40% of breast, colon, melanoma and ovarian cancers [216,217]. G49A mutations affecting the pleckstrin homology domain of AKT1, for instance, were identified in ~5% of breast, colorectal and ovarian cancers [217]; however, this mutation was not detected in any of the 100 cases of GBM or 75 cases of MB analyzed by Schüller et al. in 2008 [218]. In the pediatric population, MB samples show p-AKT, and cell lines have shown to be crucially dependent on PI3K/AKT pathway activation; however, the phenotype was attributed to PTEN inactivation as a result of the loss of heterozygosity of chromosome 10q or promoter [219].

In pediatric sarcomas, Akt1 has been shown to contribute to the maintenance of the undifferentiated state of myoblasts pointing towards Akt signaling as a critical RMS nodal point [220]. The AKT pathway is also considered to be an important mediating survival signal in EWS [221]. Likewise, an increasing body of evidence has shown that this pathway is frequently hyperactivated in OS and contributes to disease initiation and development, including tumorigenesis, proliferation, invasion, cell cycle progression, inhibition of apoptosis, angiogenesis, metastasis and chemoresistance [222–224]. The AKT2 gene is significantly upregulated in chemoresistant OS cell lines [224] and tumor samples, being significantly associated with positive recurrence, the presence of metastasis, poor response to chemotherapy and shorter EFS and overall survival [224]. Moreover, the AKT3 isoform was evidently upregulated in OS tissues and positively associated with tumor size [225].

AKT2 also plays an important role in NB by regulating N-myc expression. Of note, attenuation of this AKT isoform impaired proliferation and anchorage-independent cell growth, and decreased the secretion of angiogenic factor VEGF and decreased the potential

to metastasize to the liver in vivo, thus implicating AKT2 in multiple aspects of NB initiation and progression [226].

**mTOR.** mTOR is a serine/threonine protein kinase that forms the catalytic subunit of two structurally and functionally distinct protein complexes, known as mTOR Complex 1 (mTORC1) and 2 (mTORC2) [227]. mTORC1 consists of mTOR, Raptor, G $\beta$ L (mammalian lethal with SEC13 protein 8) and domain-containing mTOR-interacting protein (DEPTOR), and plays active roles in integrating various signals that specify the availability of growth factors, nutrients and energy in order to endorse ribosomal biogenesis, protein translation during cell growth and the expression of metabolism-related genes, while inhibiting apoptosis and autophagy [228]. mTORC2, on the other hand, is composed of mTOR, Rictor, G $\beta$ L, Sin1, PRR5/Protor-1 and DEPTOR, and regulates cytoskeletal dynamics, ion transport and promotes cell proliferation and survival through the activation of Akt [229–231].

mTOR is frequently improperly activated in human cancers and results in alteration of both mTORC1 and mTORC2 signaling pathways, leading to increased cell proliferation and decreased apoptosis. However, among 33 mTOR activating mutations identified in 2014 by Grabiner et al. [231], those that were functionally tested in vitro conferred varying degrees of pathway activation, and, most importantly, a few displayed some substrate preference towards the eukaryotic translation initiation factor 4E binding protein 1 (4EBP1) and ribosomal protein S6 kinase (S6K1), or towards AKT1, implying that such mutations had distinct effects on mTORC1 or mTORC2. Specifically, 4EBP1 activation by mTOR1 is a major contributor to accelerated cell proliferation or increased cell survival; the so-called eIF4E-sensitive mRNAs code for various cell cycle and apoptosis regulators, including cyclins D1 and D3, CDK2, MYC, PIM1, Bcl-2, Bcl-xL and VEGF, among others [232–234].

mTOR overactivation is observed in many childhood tumors, including EPN, MB and PA, high-risk NB, WT and RB, leading to worse prognosis and survival [105,235–241].

Constitutive activation of the mTOR pathway, predominantly through mTORC2, is observed in EWS, with active roles in metastasis formation [241–244]. The metastatic behavior of OS is also dependent on the PI3K/Akt/mTOR cascade, in which mTOR contributes to cellular transformation and poor cancer prognosis via its downstream effectors S6K1, 4EBP1 and eIF4E [245,246]. In RMS, lower disease-free or overall survival is also associated with the activation (phosphorylation) of multiple interconnected Akt/mTOR pathways [246]. Of note, rapamycin treatment can greatly reduce the growth of cell lines derived from these three sarcoma types [242].

**GSK-3.** The glycogen synthase kinase is a ubiquitously expressed serine/threonine kinase existing as GSK-3 $\alpha$  and GSK-3 $\beta$  isoforms (encoded by separate genes), both of which are downstream effectors of AKT [247]. Differentially from other kinases, GSK3 is one of the few whose activity tends to be high in resting cells, and exposure of cells to growth factors, serum or insulin results in its catalytic inactivation [248].

The GSK3 kinases are pleiotropic, phosphorylate many proteins, and interact with multiple signaling pathways [249]. These kinases can modify the activity of transcription factors that have profound regulatory roles in cellular proliferation (such as p53 and NF- $\kappa$ B), transcription factors important for epithelial–mesenchymal transition (EMT) (i.e., Snail) and pro-apoptotic molecules including BCL2 and BAX [250]. Therefore, aberrant activity of GSK3s can result in many diseases and disorders and influence oncogenesis and metastasis [251]. However, since GSK3s are involved in a wide range of signal transduction cascades and a plethora of cellular functions [252,253], their roles in cancer establishment and maintenance can deviate from their chief tumor suppressor effects and also promote neoplastic transformation [254–257]. This dichotomy is also observed in the pediatric setting. Strong evidence provided by Wang et al. (2008) [257], for example, demonstrated that GSK-3 activity is essential for the maintenance of MLL-positive leukemias. MLL rearrangements are in >70% of infant leukemia, and irrespective of the translocation partner, they are associated with poor clinical outcomes [258–260]. Alternatively, as a key suppressor of the Wnt, Hedgehog and Notch pathways GSK3 has attracted much scrutiny. Within these pathways, this kinase is critical in regulating the turnover of the effectors  $\beta$ -catenin, c-Myc

and c-Jun, targeting them for degradation/inactivation, and this inhibits proliferation and stem cell maintenance [250].

The literature about the prognostic value of GSK3A in pediatric cancer is scarce. No evidence was found in the literature about its involvement in EWS, OS, RMS, WT, RB, NB and EPN. However, its role in MB has been explored *in vitro* and *in vivo*, showing to be important for cell proliferation and tumor growth [260], a phenotype that seems to be similar in pediatric glioma [261].

On the other hand, the role of GSK3B is more extensively studied. In EWS, this gene can either promote or impair tumor growth and is associated with good prognosis [262–265]. Interestingly, in OS, the same gene acts as an oncogene [265], and is associated with worse response to neoadjuvant chemotherapy [266].

The oncogene status also occurs in alveolar RMS, where GSK3B is directly involved in regulating the transcriptional activity of PAX3/FKHR [267] at the same time that the chimeric protein enhances GSK3B activity, which in turn represses MYOGENIN, a member of the muscle regulatory factor family that orchestrates the terminal differentiation step of skeletal muscle cells [268]. GSK3B is also involved in the maintenance of undifferentiated phenotypes in ERMS [269].

GSK-3B is highly expressed in high-risk NB; however, its expression is not associated with clinical stage, survival or other clinicopathological parameters [270]. GSK-3B has also been involved in the protection of NB cells against chemotherapy by regulating NF- $\kappa$ B signaling [271]. In this regard, several authors have shown that GSK3 inhibitors are able to regulate MYCN mRNA levels and reduce NB cell viability through multiple mechanisms, including p53 and Wnt signaling, BDNF/TrkB/PI3K/Akt, suggesting that targeting this kinase might potentiate chemotherapy [271–274].

Alternatively, a predominantly tumor-suppressive role for GSK3B is observed in MB, in which its accumulation leads to the downregulation of GLI, the most important activator and driver of the SHH medulloblastoma subtype [274]. Constitutive phosphorylation leading to GSK3 $\beta$  activation improves cell survival and contributes to malignant transformation [275]. Dysregulated GSK3B also sustains the survival, immortalization, migration, invasion and maintenance of stem cells in glioma [276–278].

### 3.1.3. MAPK Pathway

The mitogen-activated protein kinases (MAPKs) comprise a group of serine–threonine protein kinases that control numerous cellular processes, including proliferation, differentiation, apoptosis, survival, inflammation and innate immunity [278]. In mammals, MAPKs include three main signaling axes, namely c-Jun NH<sub>2</sub>-terminal kinase (JNK), p38 MAPK and extracellular signal-regulated kinase (ERK), each of which exists in several isoforms [279].

This pathway mediates intracellular signaling triggered by extracellular stimuli such as growth factors and cytokines (ERK), or by intracellular stimuli such as genotoxic, osmotic, hypoxic, oxidative or endoplasmic reticulum (ER) stress (JNK and p38), for example [280,281].

The general cascade pattern includes initial activation of MAP4Ks (membrane-bound GTPases such as RAS, RHO, RAN, RAB and ARF) by RTKs, which phosphorylate intermediate MAP3Ks (i.e., RAF, MEKK). These then mediate phosphorylation and activation of MAP2Ks (MEK1/2—mitogen-activated protein/extracellular signal-regulated kinases, MKK4/7), followed by the positive phosphorylation of MAPKs (ERK1/2, p38 or JNK). Once activated, MAPKs phosphorylate diverse substrates, including transcription factors such as c-Jun, c-Myc, P53 and ATF2, thereby giving rise to the various cellular responses [282,283]. p38 MAPKs have also emerged as important modulators of gene expression by regulating chromatin modifiers and remodelers [281].

Thus, compromised MAPK signaling contributes to the pathology of a wide spectrum of human malignancies [282]. However, while the roles of JNK and p38 pathways are

elusive [284–290], dysregulation of the RAS/RAF/MAPK(MEK)/ERK pathway explicitly drives the oncogenic process [291].

In fact, many of the cancer-associated mutations of components of MAPK signaling pathways have been found in RAS. Missense gain-of-function mutations in all three RAS genes (HRAS, KRAS and NRAS) are found in ~30% of all human cancers [292–294]. Other perturbations in GDP–GTP regulation, persistent receptor tyrosine kinase-mediated activation of GEFs, and miRNA deregulation are additional mechanisms of RAS activation in cancer and result in constant input signals with downstream kinases [291,295].

In this regard, the frequency of genomic alterations in the MAPK pathway as a whole parallels the direction of the signaling cascade: RAS > BRAF > MEK, and ERK mutations are exceptionally rare [296,297].

**RAF.** RAF has three isoforms (ARAF, BRAF and CRAF/RAF1), sharing a high similarity of domain organization. These cytoplasmic serine/threonine-specific protein kinases are essential effectors of the MAPK pathway through the association with activated RAS. This binding leads to their homo- or heterodimerization and activation with the phosphorylation of ERK.

Altered activation of RAF members results in increased proliferation in a broad range of human tumors [298,299]. The most common gain-of-function mutation in the members of the family occurs in BRAF codon 600, in which a valine is substituted for glutamic acid (BRAF-V600E). This point mutation is notably widespread in pilocytic astrocytoma (15%), melanomas (63%) and papillary thyroid carcinomas (more than 50%) [300,301]. Overexpression of full-length RAF or the truncated catalytic domain also leads to hyperactivated ERK signaling, resulting in increased malignant behavior [302].

**ERK1/2.** ERK1 and ERK2 are the prototypes of the eight isoforms of ERK and are activated by MAPK/ERK kinase (MEK) 1 or 2. Upon activation, ERK detaches from cytoplasmic anchoring proteins and translocates to the nucleus to exert its transcriptional regulation. Despite the well-recognized importance of ERK activation in cancer malignancy, mutations in these genes have rarely been reported as drivers in human cancers. Nonetheless, The Human Protein Atlas classifies them with enhanced expression compared to normal tissues.

The most compelling evidence of MAPK activity in cellular processes contributing to the development and progression of childhood tumors is represented by the duplication/rearrangement of *BRAF* at 7q34 leading to *KIAA1549:BRAF* fusion product, which is the most common molecular alteration in sporadic PA, occurring at the highest frequency in tumors of the posterior fossa [303–305]. ERK2 was identified as differentially expressed in tumor samples compared to normal tissues [306]. RAS/MAPK activation was associated with metastatic disease in MB [307,308]. Associations of ERK hyperexpression with distant metastasis and poor overall survival were also reported for childhood sarcomas, including RMS and OS [309–312]. For other pediatric tumors, activation of this pathway results from their interaction with dysregulated microRNAs [313,314].

#### 3.1.4. Cell Cycle Kinases

The cell cycle is a complex and well-ordered series of irreversible events through which a cell duplicates its DNA and grows to produce two daughter cells with identical genomes [315,316]. Transitions from one state to the next are driven by many oscillating regulators that determine whether cells proceed through G1 into the S phase, and from G2 to M, each of which are characterized by distinct molecular features and functional outputs [317]. Central to this process are the cyclin-dependent kinases and other key regulators such as kinases from the Polo and Aurora families.

##### Cyclin-Dependent Kinases

Cyclin-dependent kinases (CDKs) comprise 13 key regulatory enzymes involved in cell proliferation through the regulation of cell cycle checkpoints and transcriptional events in response to extracellular and intracellular signals. These intracellular serine/threonine



kinases, whose catalytic activities are regulated by interactions with the adaptor molecules cyclins and CDK inhibitors (CKIs), orchestrate the evolution through the sequential phases, including entry into the cell cycle from quiescence, the G1/S phase transition, DNA replication in the S phase, nuclear breakdown, chromosome condensation and segregation, and cytokinesis [318].

CDKs coordinate cell cycle regulation at different stages to ensure the coherence, integrity and maintenance of every step in a sequential manner. CDK1 and CDK2, for instance, are necessary to direct the transition from S to G2, but only CDK1 governs the G2/M transition and mitotic progression [319]. Other CDKs regulate the cell cycle indirectly by activating other members of the family (CDK7, CDK20) or transcription (CDK7, CDK8, CDK9, CDK12, CDK19) [320,321].

Changes in the expression and regulation of CDKs induce unscheduled proliferation and chromosomal instability, well-known hallmarks of cancer and tumor aggressiveness [322–327]. Amplification or mutation of genes encoding CDKs, cyclins or endogenous inhibitors of CDKs have been described in many solid cancer types, and are recurrent events in the development of breast cancer [328] and GBM [329], for example. Such alterations are also described as molecular drivers in childhood tumors [330–334].

**CDK1.** Cyclin-dependent kinase 1 (CDK1) is vital in governing cell division and transition from G2 to the M phase [335]. Its dysregulation is common in many tumors of diverse origins, leading to chromosomal instability via replication stress and enhanced proliferation of cells. A recent pan-cancer integrative analysis based on TCGA and GTEx databases performed by Liu et al. (2022) showed that CDK1 expression levels are increased in many tumor types when compared to normal tissues and are generally associated with poor clinical prognosis [336]. For example, CDK1 expression is positively and highly associated with advanced cancer stages in lung and endometrial cancer [337,338]. Similar results were reported for other tumors, such as breast [339–341]. Moreover, CDK1 expression is positively correlated with the expression of the stemness marker SOX2, indicating a direct action on tumor maintenance and chemoresistance [342,343].

Regarding pediatric tumors, this kinase is associated with lower overall survival and EFS rates in EPN [344,345], RMS [346,347] and NB [348]. *In silico* analyses have also demonstrated that CDK1 is differentially expressed in RB [349] and plays a key role in the development of OS, since its negative regulation or depletion leads to significant decreases in proliferation while inducing apoptosis [350–353].

Furthermore, according to the literature, a well-described relationship exists between CDK1 and EWS, WT and high-grade gliomas (HGG). Specifically, this kinase expression has been directly associated with tumor progression [354], being considered a hub gene for GBM [355].

**CDK2.** Cyclin-dependent kinase 2 (CDK2) drives the entry of cells into the S and M phases of the cell cycle. Except for a few exceptions (i.e., testis), the majority of normal tissues have low expression of this serine/threonine kinase [356], and its activity is not essential for normal development [357]. However, CDK2 has been associated with cancer progression and aggressiveness across several malignancies [339,358], contributing not only with genomic instability and under-replication of DNA in the late S phase [359] but also through interactions with other proteins in a wide range of biological processes such as DNA damage response, intracellular transport, protein degradation and signal transduction, among others. Differentially from other kinases, several investigations have demonstrated that CDK2 is not upregulated or amplified; instead, its dysregulation results from altered binding partners or alterations due to post-translational modifications [360]. In tumors with MYCN overexpression, as is the case of NB, interaction with CDK2 appears to be critical for senescence avoidance and immortalization [361], being associated with worse prognosis and considered a suitable therapeutic target in this tumor type [362,363]. CDK2 inhibitors effectively induced cell cycle arrest or apoptosis in MYC-driven MB [364].

The literature also shows overexpression of CDK2 in HGG compared to normal tissue and low-grade forms, with a direct association with worse prognosis due to immune cell

infiltration [365]. Moreover, this kinase plays a central role in the development of NB. Even though there is no well-established relationship between this kinase and the development of this tumor type, Zhang et al. (2016) [366] demonstrated that the inactivation of TAZ (a biomarker of aggressiveness in RB through miR-125a-5p) inhibited proliferation and tumor formation by decreasing cyclin E and CDK2 expression [367]. Similarly, although there is no clear and explicit description in the literature about the relationship of this kinase with RMS, Knudsen et al. also discussed the relationship between sustained CDK2 levels in RD cells irrespective of the exposure of cells to differentiating culture media, explaining the inability of those cells to arrest growth and thus contributing to oncogenesis [368]. Moreover, there are reports of apoptosis induction in several sarcoma cells after CDK1 and CDK2 co-depletion [369,370]. Of note, in a microarray-based study, CDK2 was found to be overexpressed and associated with poor prognosis in EWS [371].

**CDK4/6.** Cyclin-dependent kinases 4 and 6 are highly homologous key components of the cell cycle to drive the passage from G1 to S phase. Upon interaction with any D-type cyclin (CCND1, CCND2 or CCND3), these interphase kinases phosphorylate Rb to release E2F from Rb and initiate the transcription of genes required for cell cycle progression. Besides proliferation, other roles of cyclin-D/CDK4/6 have been confirmed, including the regulation of senescence, apoptosis, migration/invasion and angiogenesis [372].

Consequently, the complex CCND/CDK4/6 shortens G1, and hence, its constitutive activation represents a driving force of tumorigenesis. These proteins are generally concurrently studied and, in many cases, they present themselves with similar patterns, being simultaneously dysregulated [373,374].

CDK4 was identified as a major risk factor for disease progression in Paget's disease [375] and its overexpression and/or hyperactivation is implicated in many types of human cancers [376–381]. Point mutations at the CDK4 locus (CDK4R24C) have also been reported [382].

Co-overexpression of both CCND1 and CDK4 is common in hepatoblastoma, a rare malignant liver tumor of childhood, and usually positively correlated with tumor recurrence [383]. In parallel, enhanced kinase activity of CDK6 has been associated with other childhood tumors [384]. This kinase plays an important role during hematopoiesis and is frequently altered in hematological malignancies of different immunophenotypes [385,386]. MLL-AF9 oncofusions in myeloid leukemia, for example, induce high CDK6 levels, acting as a blocker of myeloid differentiation and contributing to the maintenance of an immature phenotype [387]. This MLL fusion-driven activation of CDK6 (through MLL-AF4 and MLL-ENL) has also been described in infant leukemia [388].

Likewise, CDK4 and CDK6 have been described with similar frequencies in WT compared to normal mature kidneys, even though only CDK4 showed correlation with relapse [389]. However, a more recent study by Haruta et al. (2019) showed that WT samples with chromosome 12 trisomy does indeed show upregulation of this kinase, but that stronger expression is associated with better overall survival [390].

Activation of the CDK4/6 pathway is also a powerful driver of sarcomagenesis [391]. Amplification of 12q13-15 also occurs in OS, and a recent copy number analysis of pediatric high-grade OS detected a recurrent gain of chromosome 12q14.1 in ~25% of samples, which resulted in CDK4 overexpression. In vitro, higher expression of CDK4 was considered a predictive biomarker for resistance to cisplatin [392]. Indeed, elevated CDK4 expression is correlated with metastasis potential and poor prognosis in this tumor type [393–395]. Consistent with these findings, a recent study demonstrated that about 50% of OS samples present CDK4 somatic variants, 9.5% of which were identified as gain-of-function CNVs correlated with metastasis and death [396].

The inhibition of CDK4/6 also represents a promising precision medicine-guided therapy for other childhood sarcomas. A parcel of PAX3/PAX7-FOXO1-positive RMS tumors with amplification of the chromosomal region 12q13-q14, for example, also presents elevated CDK4 levels relative to non-amplified, fusion-negative forms [397,398]. In addition, in Brazilian cohorts, amplification or overrepresentation of CDK4 was evinced

through qRT-PCR and immunoreactivity in both forms of RMS (ERMS and ARMS), along with several leiomyosarcoma samples [399,400]. Similarly, using a human TMA, Saab et al. (2007) demonstrated CDK4 expression in 82% of ARMS and 63% of ERMS tumors [401]. CDK6 was detected at high levels in six RMS-derived cell lines, reinforcing the prospects of its inhibition as a therapeutic opportunity [402]. In a similar manner, a shRNA-based screening demonstrated that CDK4 (together with CCND1) is required for survival and anchorage-independent growth in EWS [403].

More recently, a systematic evaluation of CDK4/6 as targets in a series 16 pediatric cancer types indicated that further preclinical evaluations are still needed to affirm the dependence of tumors on CDK4/6. Nevertheless, the results provided evidence for benefits in EWS, malignant peripheral nerve sheath tumors and MB [391]. Of note, within MB subgroups, CDK6 and CDK14 co-amplifications were identified in 20% samples from patients with relapsed group-4 MB [330].

Shubert et al. (2022) also pointed out that patients with atypical rhabdoid tumor/malignant rhabdoid tumor, NB or HGG may also benefit from anti-CDK4/6 therapy [391].

CDK4 and CDK6 are both highly expressed in NB compared to normal tissues [404]. Moreover, like CDK2, CDK4/CDK6 exert oncogenic roles in this tumor type, especially in MYC-amplified forms [405]. Additionally, when co-amplified with MDM2/FRS2, CDK4 and CDK6 are associated with poor prognosis and atypical clinical features, including poorly differentiated or undifferentiated histology and metastasis at diagnosis and at relapse [406].

In line with Schubert et al. (2022) [391], CDK4/6 upregulation also plays an important role in the pathogenesis and progression of high-grade gliomas with potential actionability [407–409]. However, the use of CDK4/6 inhibitors alone did not show satisfactory results, suggesting the use of combinatorial intervention [410].

CDK4 was likewise found overexpressed in EPN and associated with adverse outcomes [411]; accordingly, its inhibition restricted cell proliferation and reduced the expression of genes associated with the cell cycle and DNA repair (*CCNB1*, *TOP2A*, *CDK2*, *BRCA1* and *RAD51*), and induced morphological changes that culminated in cell death [412]. Considering EPN subgroups, De Almeida Magalhaes et al. (2020) showed that *CDK6* is overexpressed in ST-EPN-RELA tumors compared to other ST-EPN subgroups [413], even though others have suggested that the dysregulations of the p16-CDK4/6-pRB-E2F pathway might also compose the genetic background underlying the aggressive biology of posterior fossa EPN in infants less than 1 year old [414].

**CDK5.** The cyclin-dependent kinase 5 (CDK5) represents an unusual member of the family of cyclin-dependent kinases, which is activated upon binding to p35 and p39 proteins, which are not cyclins. Conversely, interactions with CCND1 or CCND can attenuate CDK5 activity [415]. CDK5 is expressed ubiquitously, but with higher activity in the nervous system, participating in neuron migration, neurite outgrowth and synaptogenesis. Nevertheless, increasing evidence points to a diverse array of functions in other tissues, ranging from cell proliferation to cytoskeleton remodeling and cell motility by regulating actin dynamics [416–418].

Apart from neurodegenerative disorders, amplification and increased expression of CDK5 have been described in multiple tumor types and are associated with worse prognosis and stemness [419–431]. Mutations located in key domains of CDK5 that influence its structure and post-translational modifications have also been described as contributors to tumorigenesis [432].

The participation of CDK5 in pediatric tumors is purported; however, the stimulation of cancer-related signaling pathways by this kinase remains obscure, and reports are scarce. CDK5 was found to be hyperactivated in NB and its inhibition resulted in cell cycle arrest and morphological differentiation [433,434]. Moreover, as a crucial regulator of neuronal signal transduction, CDK5 can be found differentially expressed in gliomas, progressively

augmenting with tumor grade, suggesting an active role not only in tumorigenesis but in aggressiveness as well [424,435,436].

CDK5 also appears to be a central regulator of OS tumorigenesis, with high levels of expression being associated with low survival and increased angiogenesis [437,438]. Interestingly, CDK5 also plays a role in osteoblastic differentiation. Fu et al., for example, demonstrated that CDK5 inhibition promotes the expression of *Runx2*, *ALP*, *OCN* and *OPN* in mesenchymal stem cells, the mineralization of MC-3T3E1 cells and suppresses the migration of the OS cell line MG-63 [439]. Additionally, the CDK5/p35 complex strongly inhibits the Wnt/beta-catenin signaling pathway, also able to stimulate osteoblastic differentiation [440].

The WNT pathway defines a molecular subgroup of MB [441]; thus, it may be assumed that CDK5 might also contribute to this tumor malignancy. In fact, *Cdk5* expression has been demonstrated in different MB cell lines and in a reduced cohort of patients; however, its deletion did not alter proliferation, reflecting the more favorable prognosis of MB with WNT activation [441]. Nevertheless, a role for CDK5 in tumor immune evasion through the regulation of PD-L1 was suggested [442].

**CDK7/9.** Cyclin-dependent kinase 7 (CDK7) and 9 (CDK9), apart from directing cell cycle progression, have critical roles in transcription initiation and elongation as regulators of the phosphorylation of the carboxy-terminal domain (CTD) of RNA polymerase II (CDK7 is a component of TFIIF, and CDK9, a subunit of pTEFb) [443–445]. CDK7/9 also controls many transcription factors, functioning to either promote their activity and/or regulate their turnover [445]. Recently, other uncovered transcription-associated functions have been revealed, including epigenetic modifications and mRNA-3' termination [446–448].

CDK7/9 levels are elevated in several cancer types and are associated with clinical outcomes [449–455]. In many cases, they can indirectly impact gene expression profiles by aberrantly controlling the functioning of transcription factors that are critical in specific tumor types, as is the case of estrogen- or androgen receptor-mediated transcription in breast and prostate cancer, respectively [449,456,457]. MYCN-dependent transcription can also be affected, as demonstrated in NB cells, or contribute to histone-3 methylation in diffuse intrinsic pontine glioma (DIPG) [445,458].

With regard to other pediatric tumors, CDK7 has been shown to be upregulated in a panel of OS cell lines and tumor samples, being associated with worse prognosis and higher metastasis rates [459]. Accordingly, CDK7 knockdown in SJSA-1 cells reduced phosphorylation of the RNAPII CTD and reduced tumor volume and weight in xenograft models compared with tumors derived from wild-type cells [460]. Similarly, higher levels of expression of CDK9 have been associated with lower Huvos grade and lower survival rates, characterizing this kinase as a suitable therapeutic target, as determined through siRNA assays [461,462].

Descriptions about the relationship between CDK7 expression and EPN, RMS, EWS, WT, RB and NB are rare. Nevertheless, the use of THZ1 (CDK7 inhibitor) has exposed positive scenarios, considering that EWS cells are sensitive to this compound and that reduced EMT capacity of RB cells is observed after treatment [463,464]. In contrast, CDK9 kinase is widely expressed in RMS, where it impedes the physiological cellular differentiation [448,465–467]. Additionally, inhibition of CDK9 demonstrated a general disruption of transcription [465]. Similarly, this kinase is widely expressed in pediatric sarcomas, such as EWS, and its pharmacological inhibition (PHA-767491) enhanced the mithramycin-mediated suppression of the EWS-FLI1 transcriptional program, leading to a shift in the IC<sub>50</sub> and striking regressions of mouse xenografts. Furthermore, this kinase is upregulated in NB, increasing with the degree of differentiation of the tumor [468]. Of note, Poon et al. (2020) demonstrated that CDK9 inhibitors are able to downregulate MYCN to varying degrees and to induce apoptosis, as detected by induction of poly (ADP-ribose) polymerase (PARP) cleavage [469].

### Polo-Like Kinases

Polo-like kinases (PLKs) comprise a highly conserved multifunctional family of kinases of five members: PLK1, PLK2, PLK3, PLK4 and PLK5 [470–472]. These serine/threonine kinases are traditional controllers of cell cycle progression, with major roles in the formation of the mitotic spindle, chromatid separation, regulation of the anaphase-promoting complex, DNA damage response and cytokinesis [472,473]. Structurally, these proteins share an N-terminal highly conserved catalytic domain and a regulatory domain fundamental to the functionality and localization of PLKs, called Polo-Box (PBD) and located at the C-terminus [474].

PLKs are differentially expressed depending on the tissue and cell cycle phase [475]. Alterations in the expression of PLK genes have already been described in different types of cancer (breast, OS, leukemia, gliomas, among others) and have generally been correlated with dismal prognosis [476].

**PLK1.** PLK1 is the most studied member of the family. This protein plays key roles at different points of the cell cycle, especially during the progression of mitosis [477]. Nevertheless, other non-mitotic functions such as cell survival, genomic maintenance, cell fate and DNA damage control are also regulated by PLK1 through the interaction of with effector pathway components, including the oncogenes AKT, MYC, MDM2, B-catenin and the tumor suppressors P53, PRB, BRCA2 and PTEN [478,479].

A plethora of studies have firmly established the active role of this kinase in oncogenesis and its prognostic value along with its potentiality as a therapeutic target [480–486]. Childhood cancer is not an exception. Higher levels of PLK1 have been observed in a variety of cell lines, including EWS, OS, NB and RMS [483,484]. Moreover, this protein has been described as overexpressed in MB samples, where it is associated with higher recurrence and lower survival rates [487,488]. Furthermore, other studies have validated this positive correlation between PLK1 expression and higher cell proliferation in, mainly in undifferentiated tumors with the presence of massive choroidal invasion [205,476,489–491]. PLK1 overexpression is also present in unfavorable NB and associated with poor prognostic markers such as lower age at diagnosis and MYC amplification [492]. This interaction between PLK1 and MYC has also been observed in OS, in which the kinase contributes to MYC stabilization [493].

### Aurora Kinases

Three members of the Aurora family of serine/threonine kinases have been identified in humans: Aurora kinase A (AURKA), Aurora kinase B (AURKB) and Aurora kinase C (AURKC). These kinases (named after the resemblance or their localization to the poles of the mitotic spindle to the way aurora borealis are observed at one of the poles of the earth) have pivotal parts in the execution of mitosis (AURKA and AURKB) and meiosis (AURKC), and even exerting conserved function, they cannot fully compensate for the loss of one another [494,495].

**AURKA.** Aurora kinase A is involved in the centrosome maturation process and promotes the transition from G2 to mitosis. AURKA levels increase along late S and G2 phases and reach a higher peak in mitosis, followed by proteasome-dependent degradation [496,497]. This kinase is early localized at the centrosome and regulates the progression of mitosis by phosphorylation of multiple substrates, promoting mitotic entry through the activation of Cyclin-B/CDK1 [498]. Moreover, AURKA progressively associates with the mitotic poles and the adjacent spindle microtubules, contributing to chromosome separation and bipolar spindle [499,500].

Among the three human aurora kinases, AURKA has been the family member most consistently associated with cancer. Amplification of the chromosomal region 20q13 where the AURKA gene is located is commonly observed in cancer cells [501–503]. Nevertheless, according to Mou et al., almost 90% of tumors present in the TCGA database show AURKA overexpression [504]. Indeed, high levels of AURKA expression can endorse abnormal cell cycle progression, resulting in genomic and chromosomal instabilities, which are hallmarks

of highly proliferative tumors [505,506]. Thus, AURKA expression not only enhances proliferation, but may also influence other processes, including apoptosis evasion, EMT, drug resistance and metastasis [507–517].

Besides AURKA mitotic functions, other non-canonical and kinase-independent activities have been gradually discovered in cancer cells. After mitosis, most AURKA proteins degraded, but a remnant population may be still detected inside the nucleus, pointing to the possibility that the kinase could work as a transcriptional regulator [518]. In this regard, AURKA overexpression has been associated with the upregulation of stem cell markers such as SOX2 and NANOG, imposing participation in the maintenance of the self-renewal capacity of cancer stem cells (CSCs) [519].

In pediatric tumors, AURKA polymorphism rs8173 G > C has shown to decrease WT risk [520]. Conversely, AURKA plays an active role protecting MYCN from ubiquitinylation and proteolysis in NB, thus contributing to more aggressive phenotypes and poor survival probability [521,522]. Moreover, this role has also been described in RMS, where AURKA not only stabilizes MYC but also PAX3-FOXO1 [523]. Moreover, in this tumor type, AURK is overexpressed and considered a key factor in the observed aneuploidy and chromosomal instability [524]. AURKA is also closely related to the oncogenic process of EWS and is considered a chemotherapy resistance and may act as a potential biomarker for prognosis [525,526].

AURKA overexpression has also been associated with OS, as many cell lines are highly sensitive to its inhibition [527,528]. Similar patterns have been seen for WT, where AURKA inhibition impaired tumor growth and induced apoptosis both *in vitro* and *in vivo*; however, such effects were improved in RB1-deficient cell lines compared to those with MYC amplification [529].

Moreover, expression profiling of pediatric brain tumors has shown that AURKA was consistently and highly overexpressed (up to 106-fold) in tumor samples from all glioma grades and from patients varying from 4 months to 82 years old; however, mRNA expression showed only weak correlation with the Ki-67 labeling index, and significant associations with poor patient survival were only observed for GBM [530]. Overexpression of AURKA is also linked with survival in MB patients [531].

**AURKB.** The second member of the family, Aurora kinase B (AURKB) is one of the most intensively studied kinases because it provides catalytic activity to the chromosome passenger complex (CPC), formed by AURKB, INCEP (inner centromere protein), survivin and borealin (Cell 2002;13:3064–77). The CPC governs highly different processes, such as chromosome alignment, histone modification and cytokinesis [532–535]. Additionally, AURKB kinase activity is essential for faithful chromosome segregation and functions to correct any improper kinetochore attachment to the spindle [532,536–538]. Finally, Aurora kinase B (AURKB) is also essential in mitotic DNA damage response, protecting against DNA damage-induced chromosome segregation errors, including the control of abscission checkpoint and prevention of micronuclei formation [539]. Consequently, AURKB dysregulation results in aneuploidy and genomic instability and in turn promotes cell cycle progression and survival of cancer cells [540–543]. Indeed, expanding evidence at the gene, mRNA and protein levels supports a carcinogenic role of AURKB. Overexpression has been reported in clear cell renal cell carcinoma (RCC) and cervical carcinoma, among many others, with clear associations with clinicopathological parameters such as stage and tumor volume, chemoresistance, tumor progression and poorer survival [544–553].

In the pediatric setting, overexpression of AURKB was closely correlated with poor prognosis and carboplatin resistance in NB patients [552,554]. Similar profiles were observed for pediatric ALL and AML patients, especially in T-cell and E2A-PBX1-translocated ALL cases. Further *in vitro* assays demonstrated that AURKB is an essential protein for the proliferation and survival of acute leukemia cells [555].

The importance of Aurora kinases as potential therapeutic targets for childhood brain malignancies is highlighted by AURKB being highly and consistently overexpressed in the majority of high-grade gliomas, but despite reflecting the presence of aneuploidy,

at least in EPN, it did not emerge as a prognostic factor [556,557]. For other tumor types, however, data about the prognostic value of AURKB are less explored and primarily rely on experimental assays using pharmacological inhibitors. In this context, OS, EWS and RB are included [558–560].

**AURKC.** Differentially from AURKA and AURKB, Aurora kinase C (AURKC) is limited to cells that undergo meiosis (sperm and oocyte). This kinase is located on human chromosome 19q13.43, regulated by promoter methylation and when expressed in germ cells, can undergo alternative splicing resulting in three protein variants [561–563]. As the major enzymatic component of the CPC during meiosis, it plays a specific role during human female meiosis and preimplantation embryo development [564].

A body of evidence shows that overexpression of AURKC in mitotic cells leads to centrosome amplification and multinucleation [565]. Its upregulation and other CPC components occur in cancer cells and may correlate with clinical characteristics [566,567]. In line with this, AURKC is overexpressed in tumors of the reproductive system and in breast and prostate cancer cell lines [568,569]. Nevertheless, varying degrees of CpG islands hypermethylation leading to lower AURKC mRNA levels have been described in WT, suggesting that this kinase might not be of importance in this childhood tumor [570]. Likewise, AURKC expression was not associated with survival or risk status in neuroblastoma patients [571]. In OS, knockout of AURKC displayed no changes in cell proliferation, migrated less and formed fewer colonies in soft agar compared to wild-type cells. Moreover, whole-transcriptome sequencing revealed over 400 differentially expressed genes which included genes encoding proteinaceous extracellular matrix components, suggesting that therapeutics targeting this aurora kinase isoform could decrease cancer cell metastasis and disease progression, the most limiting characteristic of survival [572].

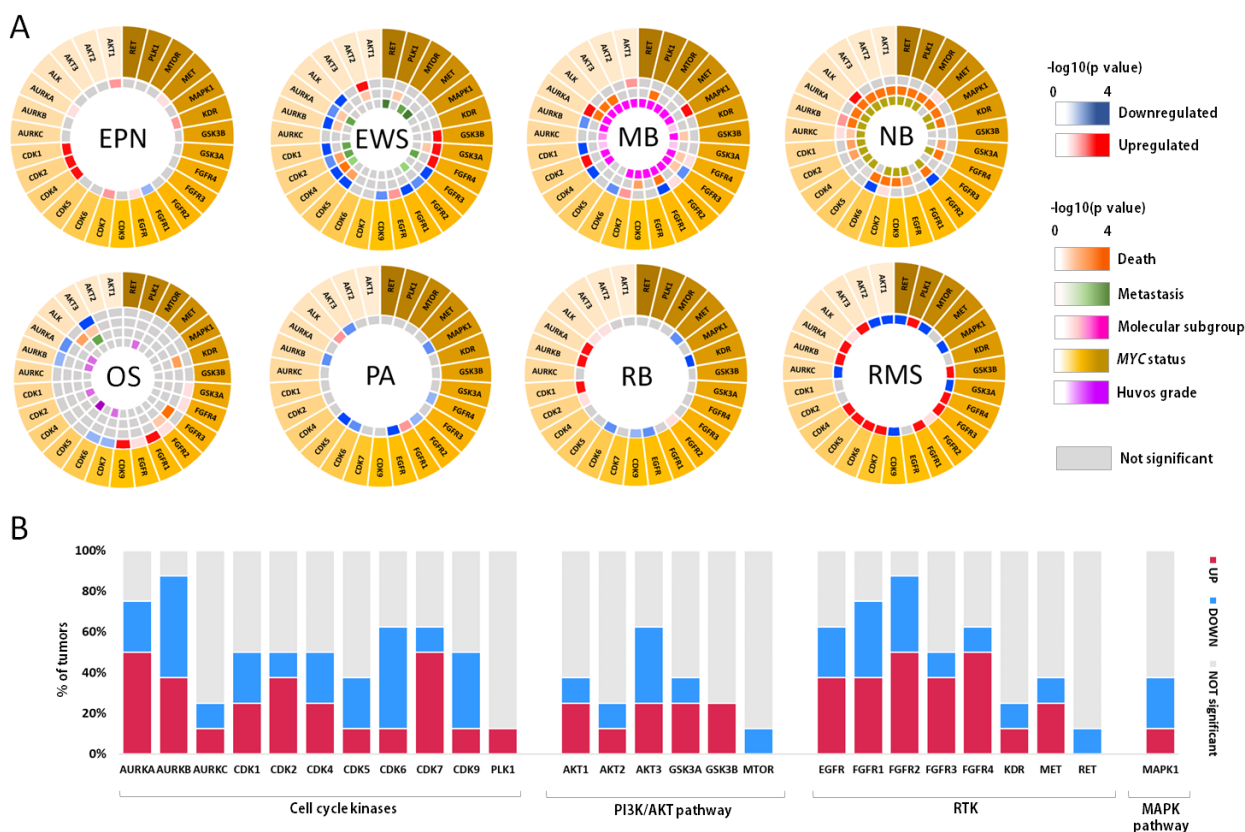
### 3.2. *In Silico* Analysis of Different Kinases Expression and Their Association with Clinical Prognosis

According to our systematic *in silico* analysis of the selected group of kinases, comparisons of expression patterns between pediatric tumors and normal samples showed varying results, and despite what was expected from the data already published, few commonalities were found (Figure 3A,B, Supplementary Table S1). Considering CNS tumors, overexpression of *AKT1*, *AURKA*, *CDK2* and *CDK7* was observed in EPN and MB, but not in PA. Similarly, EPN showed higher levels of *CDK1*, *CDK4*, *EGFR*, *KDR* and *MET*, while for MB, the upregulation of *FGFR2*, *FGFR4* and *MAPK1* was highlighted. Conversely, EPN samples demonstrated low levels *AKT3* and *FGFR1*, while *CDK1/4/6*, *FGFR1/3* and *AURKB* were downregulated in MB tissues. PA, on the other hand, exhibited high levels of only *ALK* and *FGFR1*, and downregulated genes included *AKT3*, *AURKB*, *CDK5*, *EGFR*, *FGFR2*, *FGFR4* and *MAPK1*.

Neuroblastoma was the tumor type with the more reduced number of hub genes. In this tumor type, *CDK6* and *FGFR2* were less expressed than in normal tissue, whereas *CDK7*, *MET*, *ALK* and *AURKB* stood out as upregulated in tumor samples. Concomitantly, RB showed high levels of *AKT3*, *ALK*, *AURKA*, *AURKB*, *CDK1*, *CDK2* and *FGFR2* genes and low levels of *CDK6*, *CDK9*, *EGFR*, *KDR* and *MET*.

Among sarcomas, RMS was the tumor type with the most altered kinase profile, including high levels of *AKT3*, *ALK*, *AURKA*, *AURKB*, *CDK4*, *CDK5*, *CDK6*, *CDK7*, *GSK3B*, *PLK1* and all *FGFR*. Then, *AKT2*, *EGFR*, *FGFR4* and *GSK3s* (A and B) showed higher expression in EWS, contrasting the low levels of *ALK*, *AURKs* (A and B), *CDKs* (1, 2, 4, 5 and 9) and *FGFRs* (1, 2 and 3). Finally, our analysis of OS samples demonstrated upregulation of the receptor genes *EGFR* and *FGFR* (1, 2 and 4), as well as *CDK9* and *GSK3A*. Alternatively, *CDK6/7*, *AURKA/B* and *AKT3* had low expression profiles.

Notwithstanding, further analysis showed that, in the same line as reported in the literature, the expression of most of the selected kinases is indeed associated with clinical features of worse prognosis, including associations with *MYC* amplification in NB and molecular subtypes in MB, and metastases in bone sarcomas (Supplementary Table S2).



**Figure 3.** (A) Polar plots of differentially expressed kinases in pediatric tumors obtained through the analysis of available data on the R2: Genomics Analysis and Visualization Platform (<http://r2.amc.nl> (accessed on 15 October 2022)). Tumor abbreviations: EPN—ependymoma; EWS—Ewing sarcoma; MB—medulloblastoma; NB—neuroblastoma; OS—osteosarcoma; PA—pilocytic astrocytoma; RB—retinoblastoma; RMS—rhabdomyosarcoma. *p*-values are represented by differential coloring gradients. The external inner circle corresponds with “tumor versus normal tissue” results. The other concentric layers represent data related to associations with clinical features: metastasis, death, molecular subgroup (MB), MYC status (NB) and Huvos grade (OS). For actual *p*-values, refer to Supplementary Table S2. (B) Percentage of tumors with altered expression of each kinase. Few commonalities were found.

#### 4. Kinases as Druggable Targets—Evidence and Limitations

The gradual advancements in genetics and biochemistry during the second half of the last century not only contributed to the better understanding of molecular events underneath signaling pathways in both natural and pathological settings, but also laid the foundation for the development of modern targeted agents. Perhaps the most expressive example of that trajectory involves chronic myeloid leukemia and the “Philadelphia chromosome”. After its simple description (250 words) by Nowell and Hungerford, it took a decade to properly identify the chromosome pairs involved in the translocation [573]. It was only after the introduction of the G-bands by Marina Seabright that Janet D. Rowley from the University of Chicago that it was possible to identify the little chromosome as a result of the reciprocal translocation between chromosomes 9 and 22, specifically, t(9;22)(q34;q11) [574,575]. However, its molecular characterization only came to light between 1982 and 1984 [576–578], demonstrating the in-frame juxtaposition of the *ABL* oncogene (on chromosome 9) with the *BCR* gene (on chromosome 22), resulting in the hybrid *BCR/ABL* gene that gives rise to a chimeric protein with high tyrosine kinase activity and with a critical role in the development of leukemia [579]. Later, the discovery of this tumor-specific protein led to development of imatinib mesylate, providing an incredibly



successful treatment that converted a fatal cancer into a manageable chronic condition, and pioneered an era of target-directed therapy [580].

More recently, the emergence of integrative laboratorial methods such as kinome-wide siRNA screens, next-generation sequencing (NGS) and phosphoproteomics have dramatically intensified the assortment of kinase inhibitors for the treatment of human cancers, currently accounting for about a quarter of all drug discovery research and development efforts.

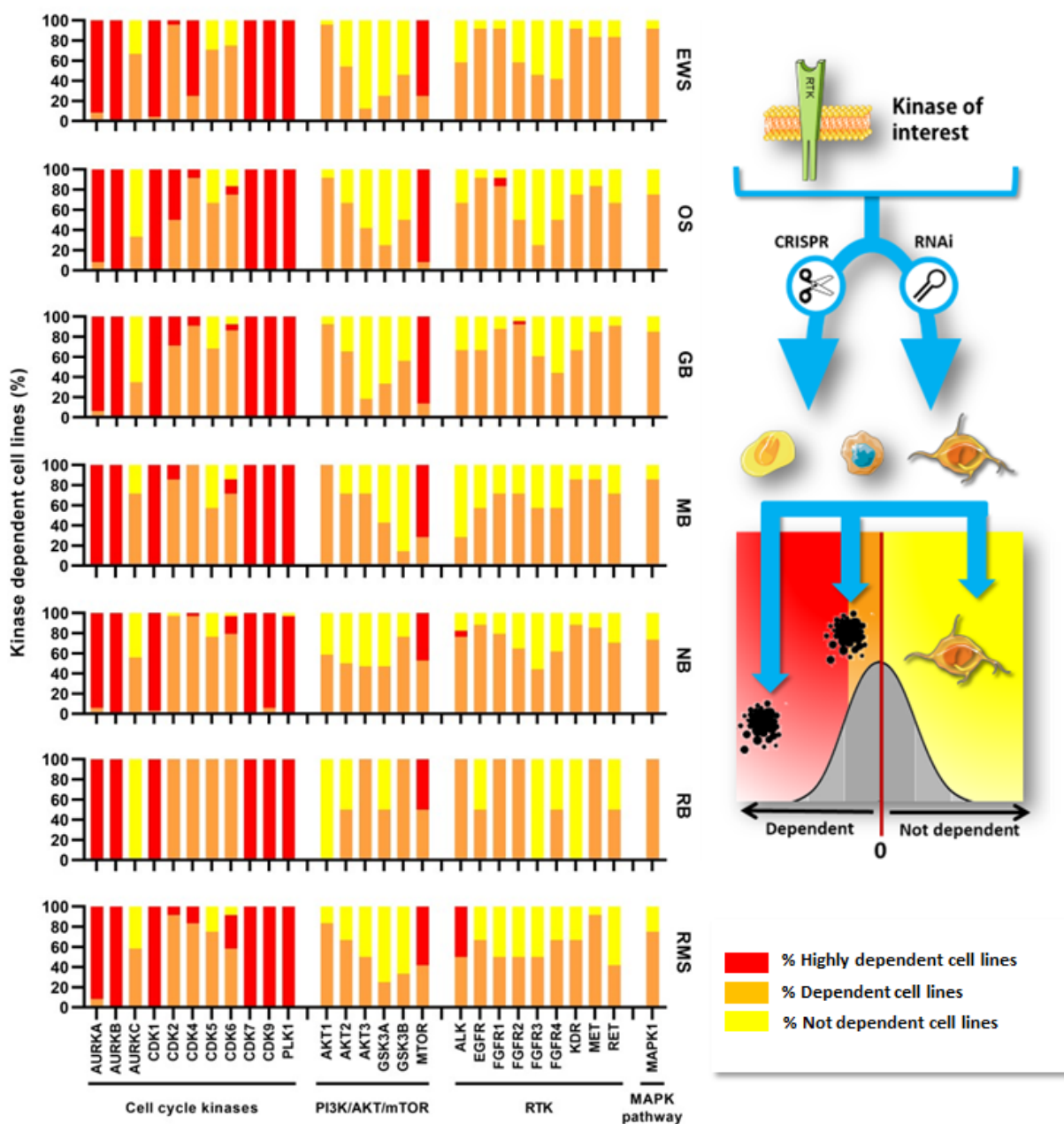
Moreover, the increasing number of databases and analytical and visualization tools has facilitated advanced drug discovery not only by gathering information about the prognostic value of specific genes in oncology, but also it is now possible to access chemical structures and docking, affinities and structural features of approved small-molecule inhibitors in more easily, accessible and systematic ways, thus accelerating the discovery and optimizing screening to more direct translational assays.

In this regard, to further illustrate the importance of the selected kinases' dysregulation in the pathophysiology of pediatric cancer, other bioinformatic tools were used (Supplementary Figure S2). As a first step, we analyzed the vulnerability of different cancer cell lines against their inhibition through the Cancer Dependency Map portal (<http://depmap.org> accessed on 14 December 2022), a platform that provides information about how dependent different cell lines are on a specific gene depletion based on CRISPR and RNAi knockout experiments. The results are presented as a score generated by the platform itself: greater than zero ( $>0$ ) indicates that the cell line is not dependent, less than zero ( $<0$ ) indicates that the lineage is dependent and scores below  $-1$  indicate that the analyzed gene is essential for the survival of the cell lineage.

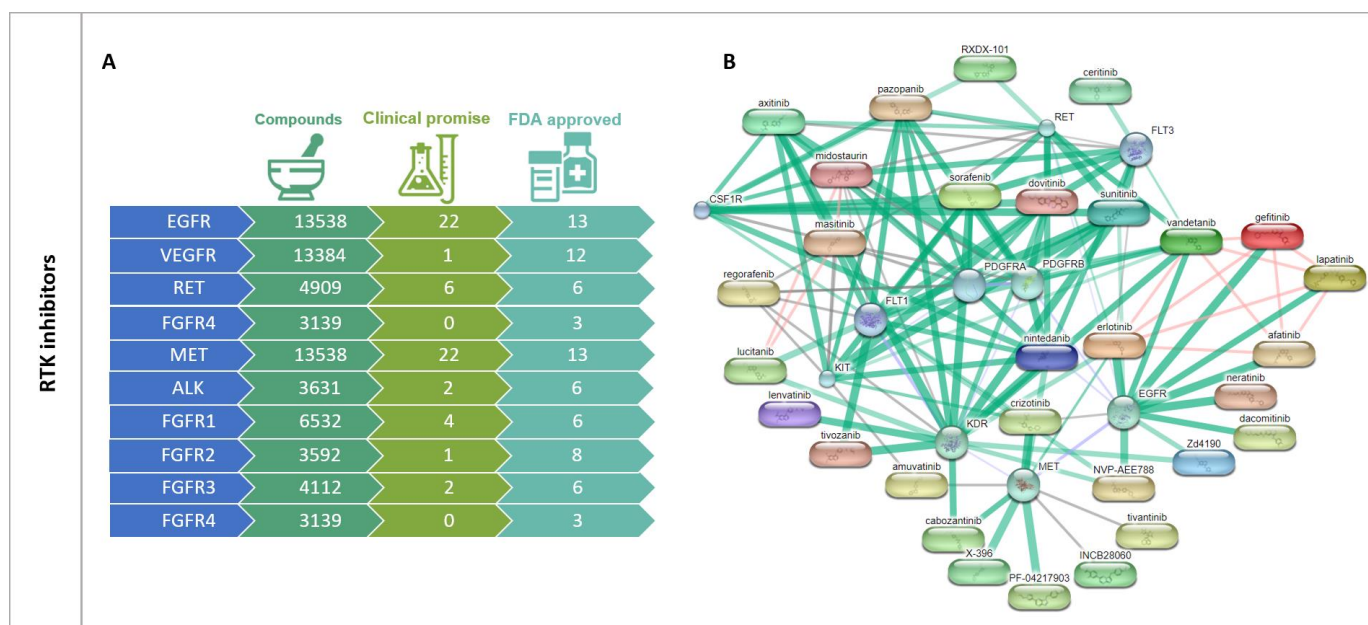
Initial screening showed that all or most cell lines are dependent on the kinases analyzed, with comparable scores between adult or pediatric origins (Figure 4; Supplementary Table S3). Interestingly, a similar pattern occurs across the different tumors, irrespective of histology. Almost 100% of the cell lines are highly dependent on cell cycle kinases, especially AURKA/B AURKB, cyclin-dependent kinases CDK1 and CDK7/9, and PLK1. Cell lines were also highly dependent on mTOR. Conversely, cell lines were less vulnerable to the depletion of AURKC, AKT3, GSK3A and FGFR3, with more than 50% of cell lines presenting scores above 1 (in line with published data reviewed above).

Then, aiming to further exemplify information on individual kinase-targeted compounds and their analogs, we performed a search through the CanSAR knowledgebase (<http://cansar.icr.ac.uk> accessed on 14 December 2022), an integrative platform that compiles multidisciplinary data and provides useful drug discovery predictions. The analysis of predicted compounds for our selected group of kinases showed more than 55,000 potential compounds that are able to target RTK, with EGFR and VEGFR representing the most druggable ones. As shown in Figure 5, FDA-approved drugs are already identified for all the RTKs, and more than 20 additional drugs are being studied as novel clinical candidates.

For PI3K, although the CanSAR analysis revealed more than 20,000 potential compounds, only the mTOR inhibitors perhexiline and everolimus are described as FDA-approved drugs. Nonetheless, 15, 4 and 2 clinical candidates are being investigated as specific inhibitors for mTOR, AKT1 and GSK3B, respectively (Supplementary Figure S3). Approved drugs for MAPK are also scarce, including only sorafenib, regorafenib, dabrafenib and encorafenib, all of which target RAF1. For this specific kinase, CanSAR identified 4764 promising compounds and three clinical candidates (Supplementary Figure S3). Among the cell cycle kinases, CanSAR identified only approved drugs targeting CDK4 and CDK6. However, many clinical candidates (more than 15) targeting the other kinases of this group are being studied. According to the platform, cell cycle kinases are the second druggable category of kinases with the highest number of compounds described as potential specific drugs, totaling more than 48,000 (Supplementary Figure S3).



**Figure 4.** Percentage of pediatric cell lines dependent on the selected group of kinases. Dependency data were imported from the DepMap consortium (CRISPR (DepMap 22Q2 Public + Score, Chronos; <https://depmap.org/portal/> (accessed on 30 October 2022)) and classified as highly dependent, dependent or not dependent. The data were plotted on a histogram where it is possible to see the vulnerability of pediatric cell lines mainly to cell cycle kinases and PI3K/AKT/mTOR families. Cell lines selected included Ewing sarcoma (EWS), osteosarcoma (OS), glioma (GB), medulloblastoma (MB), neuroblastoma (NB), neuroblastoma (NB), retinoblastoma (RB) and rhabdomyosarcoma (RMS). Dependency scores for each cell line are shown in Supplementary Table S3.



**Figure 5.** (A) Schematic illustrations of RTK druggability identified by the CanSAR database, including the total number of compounds with predicted interaction capacity with each kinase, as well as FDA-approved drugs and clinical candidates. (B) Interaction networks of RTK inhibitors and associated binding proteins according to STITCH (search tool for known and predicted interactions between chemicals and proteins available at <http://stitch.embl.de> (accessed on 1 November 2022)). Compounds are represented as pill-shaped nodes, while proteins are shown as spheres. Small nodes represent proteins of unknown 3D structures, while large nodes show proteins with known or predicted structures. Nodes that are associated with each other are linked by an edge: thicker lines represent stronger binding affinities. Networks were constructed considering a minimum required interaction score of 0.700, and based on associations reported in curated databases (gray lines), or on both databases and experimental/biochemical data (green lines). Purple lines represent functional links between proteins.

Further, for compilation of the preclinical results on kinase inhibitors, and considering that information in the literature often appears scattered and fragmented, the following section shows published evidence for (1) solid tumors that showed differential gene expression through in silico analysis (refer to Figure 3), (2) compounds considered “FDA approved” or with “clinical promise” and (3) compounds that have been assessed in vitro or in vivo before entering clinical trials. Thus, in the following subsections, experimental data on individual kinase inhibitors are detailed within each category. For further information, see Supplementary Table S4.

#### 4.1. RTK Inhibitors

**Erlotinib (Tarceva®).** This compound is a quinazoline derivative that selectively and reversibly inhibits EGFR [581]. Erlotinib is an FDA-approved drug for the treatment of NSCLC and pancreatic cancer in combination with gemcitabine chemotherapy [582]. In the pediatric setting, this inhibitor has shown contrasting results. As monotherapy, Erlotinib was not efficient in reducing cell growth in a panel of NB cell lines, albeit effective indirect responses were obtained in xenograft tumors [583]. Similar results were obtained in sarcomas. This compound alone was ineffective in OS cells, in which the STAT3 cascade pathway has been pointed as the molecular mediator of both intrinsic and acquired resistance. In EWS, this compound alone or in combination did not inhibit growth of tumor xenografts and even led to a decrease in the therapeutic activity of cyclophosphamide when compared to single-agent activity [584,585]. Erlotinib had no effect on tumor progression in genetically engineered ARMS mouse models [586].

In contrast, satisfactory results were obtained in CNS tumors, where erlotinib therapy inhibited MB migration *in vitro* and successfully diminished the levels of phosphorylated EGFR in EPN models [587,588]. Treatment with this drug was also cytotoxic in Y79 and WERI RB cells in a dose-dependent manner, leading to cell cycle arrest and reduced migration, while oral administration dramatically reduced the growth of Y79 tumor grafts [589]. Regarding patients, phase I clinical studies have been developed in order to evaluate the acceptable tolerability profile in cases of brain and refractory solid tumors including RMS, soft tissue sarcomas, NB or germ cell tumor. Children appeared to tolerate erlotinib similarly to adult patients, and drug disposition was similar between these populations. The combination of temozolomide and erlotinib was well tolerated and it was also suggested in combination with radiotherapy [590,591].

**Vandetanib (Caprelsa®).** This is a multitargeted tyrosine kinase inhibitor with potent effects against VEGFR2/3, EGFR and RET [592,593]. This compound is approved to treat medullary thyroid cancer that cannot be removed by surgery and is locally advanced or has metastasized, and has demonstrated modest efficacy in patients with metastatic breast cancer [594,595]. Regarding pediatric tumors, vandetanib has been shown to inhibit the proliferation of NB cells mediated by the induction of G1-phase cell cycle arrest at lower concentrations and by apoptosis at higher concentrations. Migration and invasion were also markedly decreased compared with the control group [596,597]. Treatment also decreased (p)RET expression in five other NB cell lines and strongly impaired tumor growth *in vivo* in both MYCN/KI AlkR1279Q and MYCN/KI AlkF1178L mice, and was able to sensitize cisplatin-resistant NB subcutaneous tumor growth with less severe liver toxicity compared with high-dose cisplatin [598–600]. Moreover, vandetanib, in combination with 13-cis-retinoic acid, reduced tumor vascularity and induced apoptosis in NB xenografts [601]. Indeed, according to Craveiro et al. (2017), the narrow target spectrum of Vandetanib along with a favorable toxicity profile makes this drug ideal for multimodal treatment approaches. These authors tested this compound against SHH-TP53-mutated and MYC-amplified MB cell lines and found that it leads to a dose-dependent reduction in cell viability, interferes with clonogenicity and has pro-apoptotic effects after 48 h. Of note, combinations with GDC-0941 (clinically available PI3K inhibitor) and etoposide resulted in complete loss of cell viability [602]. The combination of vandetanib and celecoxib displayed a synergistic or additive antitumor effect on OS *in vitro* and *in vivo* [603]. However, combinations of gefitinib and vandetanib only inhibited the proliferation of EWS cell lines at very high concentrations (>1  $\mu\text{M}$  vandetanib, >5  $\mu\text{M}$  gefitinib), indicating the action on off-target effects [604].

**Gefitinib (Iressa®).** This drug, also known as ZD1839, is a member of the 4-anilinoquinazoline class of compounds that specifically and selectively inhibits EGFR [605]. In preclinical studies, gefitinib treatment was associated with growth inhibition and increased apoptosis in human cancer cell lines, and antitumor effects against xenografts of human tumors [606,607]. Gefitinib was shown to inhibit proliferation in juvenile PA primary cell cultures with an  $\text{IC}_{50}$  determined between 1.6 and 9.6  $\mu\text{M}$  [608]. In addition, this compound was shown to inhibit invasion and metastasis of intratibial OS xenografts via inhibition of macrophage receptor interacting serine-threonine kinase 2 (RIPK2) [609]. Moreover, in children, Gefitinib has been tested for refractory solid tumors and CNS malignancies, showing similar pharmacokinetics as in adults [610].

**Regorafenib (Stivarga®).** This drug is an oral multikinase inhibitor that targets VEGFR1/3, FGFR and other receptor kinases [611]. This compound is already approved to treat metastatic cases of colorectal cancer and advanced hepatocellular carcinoma (HCC) previously treated with Sorafenib [610]. *In vitro*, regorafenib exhibits antiproliferative effects against a panel of 33 pediatric tumor cell lines, including MB (D341 Med, Med-Meb-8A), OS (IOR-OS-18), EWS (EW7, ORS, POE, SIM, STA-ET-1) NB and (SJ-NB-8, SK-N-BE(2), SH-SY5Y), with a mean half maximal growth inhibition of 12.5  $\mu\text{mol/L}$  [612]. Particularly in the last, Regorafenib has shown to be effective against through the inhibition of RAS/MAPK, PI3K/Akt/mTOR and Fos/Jun pathways [612]. Similarly, regorafenib

demonstrated antitumor activity in animals bearing subcutaneous RMS, EWS (STA-ET-1 and EW7) and NB (SJ-N-B8 and SK-N-AS) xenografts with tumor growth inhibition ranging from 73% to 93%. Moreover, when associated with radiation and irinotecan, it induced 100% regression in an MB patient-derived xenografts (PDX) model [610].

**Dacomitinib (Vizimpro<sup>®</sup>).** Also known as PF-00299804, this drug is an orally administered, second-generation, irreversible inhibitor of EGFR, HER2 and HER4, which has shown positive anticancer activities in some preclinical and clinical trials, being approved by the FDA for the treatment of metastatic NSCLC [613,614]. Besides its ATP-competitive action, dacomitinib covalently binds to Cys773 located in the ATP-binding cleft of EGFR, which irreversibly blocks ATP binding and inactivates the receptor [615]. For pediatric MB, dacomitinib has shown to block EGFR/HER signaling in DAOY cells and in orthotopic xenografts, extending median survival as a single agent; however, it was antagonistic when used in combination with standard frontline chemotherapy (4HPC, vincristine or cisplatin) [616].

**Lapatinib (Tykerb<sup>®</sup>).** This compound is an oral dual tyrosine kinase inhibitor that inhibits human EGFR and blocks the EGF receptor 2 (HER2) [617]. It was FDA-approved to treat HER2-positive advanced or metastatic breast cancer as monotherapy or in combination with other drugs [618]. Lapatinib has been tested in childhood solid tumors (including RMS, EWS and NB) and leukemia cells by the NCI-supported Pediatric Preclinical Testing Program (PPTP) [619]. In this study, among 23 cell lines, fifteen achieved at least 50% growth inhibition, and the median IC<sub>50</sub> value for lapatinib against the entire cell line panel was 6.84  $\mu$ M (range 2.08  $\mu$ M to >10.0  $\mu$ M). In vivo, however, lapatinib presented little activity against the 41 xenograft models of pediatric tumors [619,620].

**Cetuximab (Erbix<sup>®</sup>).** This compound, available as Erbitux<sup>®</sup> (Merck Sereno), is a human–murine chimeric monoclonal antibody that competes to bind to the extracellular domain of EGFR and has been approved for the treatment of colorectal and head and neck cancer [620]. Information about preclinical use of this compound is scarce. However, a report showed that the proliferation of RMS cell lines was not influenced by this EGFR inhibitor [621]. However, later, it was shown that the combination of cetuximab and actinomycin D was highly effective in EGFR-positive RMS cells (RD and Rh30, of embryonal and alveolar origin, respectively), synergistically inhibiting cell growth and inducing apoptosis [622].

**Sunitinib:** Sold under the brand name Sutent<sup>®</sup>, this drug is a small-molecule multitarget inhibitor functioning on PDGFR, VEGFR, KIT, Flt-3 and RET [623–625]. In a preclinical study, this drug demonstrated limited growth inhibitory effects in a panel of 23 pediatric cell lines that included OS, ALL, EWS, RMS, MB, EPN, NR, GBM, WT and others [625]. However, in vivo, it presented growth inhibitory activity against pediatric solid xenograft models of EWS, RMS and NB [625]. A later study showed decreased cell proliferation and phosphorylation of VEGFRs NB cells after treatment with sunitinib, and tumor growth, angiogenesis and metastasis in tumor xenograft models [624]. Moreover, in combination with an mTOR inhibitor (rapamycin), it showed a synergic cytotoxic effect, which was more effective than the traditional chemotherapeutic agent cyclophosphamide [624].

**Lenvatinib (Lenvima<sup>®</sup>).** This drug is a synthetic, orally available type I tyrosine kinase inhibitor exhibiting powerful antiangiogenic activity currently used to treat certain types of thyroid cancer and potentially other tumor types [626]. Lenvatinib was initially reported in 2008 as a multitargeted RTK inhibitor of VEGFR1/2/3, but it also inhibits FGFR1–4, PDGFR-alpha and KIT [627–629]. Preclinical findings in sarcomas indicated that lenvatinib was able to inhibit tumor growth in xenografts obtained through direct implantation of patient tumor specimens in nude mice. The experiment showed positive results in 7 out of 10 xenografts accompanied by marked decrease in microvessel densities. However, in vitro, Lenvatinib did not show potent effects on tumor viability in OS-derived cell lines [629]. Others showed that the drug was able to inhibit tumor cell migration and invasion in U2OS cells [630]. Further, in a phase I/II study, lenvatinib as a single-agent reported a response rate of 7% and a median progression-free survival of 3 months in a

cohort of 31 children and young adults with OS, although many patients had treatment-related adverse events of grade  $\geq 3$  [631]. In other pediatric tumors, the effects of lenvatinib remain to be investigated.

**Pazopanib (Votrient®).** This compound is an FDA-approved pan-VGFR inhibitor, even though it also targets PDGFR- $\alpha$  and - $\beta$ , FGFR1/3, KIT as well as BRAF proteins [632]. In a pan-cancer study, pazopanib was unable to affect the viability of any of the treated cell lines, which included SK-N-BE(2) (N-Myc amplified) and SH-SY5Y (non-N-Myc amplified) NB cell lines, the KHOS OS cell line, and the RMS cell lines RH30 and RD. However, in combination with topotecan, this compound showed significant antitumor activity in vitro and halted tumor growth in NB xenograft-bearing mice, but after 50 days, gradual growth was observed [633,634]. The combination of pazopanib with trametinib showed antitumor effects in vitro and in vivo against a panel of seven OS cell lines, in which treatment reduced proliferation and colony-forming capacity and increased the percentage of apoptotic and dead cells. In MNNG/HOS and KHOS xenograft models, both drugs induced a significant inhibition of tumor growth compared to the untreated controls [635]. The in vivo antitumor activity of pazopanib was also tested by the PPTP Program in a subset of sarcoma models that also included EWS and RMS. Although objective responses were not observed for any of the sarcoma xenografts studied, treatment prolonged survival [636]. Even with modest benefits, pazopanib has been approved for line treatment of metastatic non-adipocytic soft tissue sarcomas after the failure of standard chemotherapy. Its efficacy in patients with OS is limited to case reports [637]. One metastatic extraosseous EWS was also reported as successful after treatment with pazopanib [638].

Regarding CNS tumors, EPN cells showed to be sensitive to Pazopanib with a viability reduction of around 35% at 1  $\mu\text{mol/L}$  [639]. Additionally, treatment with Pazopanib reduced the mobility of MB cell lines, inducing clumping of the actin microfilaments (which facilitated cell detachment), as detected by wound healing assays and Fluor-555-coupled phalloidin [640]. Further in vivo tests demonstrated delayed growth of group-3-MB cells transplanted into the cerebellum of mice and prolonged survival (by 10 days) of mice treated once daily by gavage with 60 mg/kg compared to untreated controls [641]. Alternatively, for patients with recurrent high-grade gliomas as part of phase I or II clinical trials, this drug has not been beneficial [642].

**Cabozantinib (Cometriq®).** This compound is an orally available multitarget tyrosine kinase inhibitor that inhibits VEGFR1/2/3, MET, KIT, RET, AXL and FLT3. FDA-approved since 2012, it is currently used to treat metastatic medullary thyroid cancer, RCC, HCC and differentiated thyroid cancer [643,644]. In preclinical studies, reports of its anticancer effects include the inhibition of metastasis, angiogenesis and tumor growth [645–647]. In vitro, cabozantinib has been shown to diminish the cell viability of EWS and OS cells in a dose-dependent manner [160]. Moreover, it also interferes with migration and the microenvironment by inducing the production of osteoprotegerin and causing a decrease in the synthesis of the RANK ligand by osteoblasts [648]. Positive effects on decreasing proliferation were also observed in MB with no differences between cell lines corresponding to different molecular subgroups [649]. Cabozantinib also exhibited anti-proliferative effects in NB cells and reduced cell migration in vitro and significantly inhibited tumor growth of orthotopic xenografts on a daily basis [650].

**Nintedanib (Ofev®).** This drug, commercially available under the brand names Ofev and Vargatefi, is an indolinone-derived inhibitor of multiple kinases including VEGFR, FGFR and PDGFR. Recently approved for the treatment of idiopathic pulmonary fibrosis and advanced non-small cell cancer of adenocarcinoma tumor histology, it exerts its antitumor activity by reducing proliferation, migration and angiogenesis [651–653]. Considering pediatric tumors, nintedanib has been shown to inhibit growth in EWS (A673, CHP100) and OS (SaOS2) cell lines, with a key role in controlling OS lung metastatic growth by blocking the fibrogenic reprogramming of OS stem cells (OSCs) [654,655]. Growth inhibition was also observed in a panel of 13 RMS cells, with the PAX3-FOXO1 fusion-gene-positive ones more sensitive to treatment [656]. Moreover, there are reports of EPN cells being sensitive

to nintedanib treatment, while this drug is able to extend the survival of mice bearing ST-RELA xenografts [657,658].

**Midostaurin** (Rydapt/Tauritmo<sup>®</sup>). Also known as PKC412 and CGP 41251, this small molecule acts as a multikinase inhibitor targeting PKC $\alpha/\beta/\gamma$ , Syk, Flk-1, Akt, PKA, c-Kit, c-Fgr, c-Src, FLT3, PDGFR $\beta$  and VEGFR1/2. Presenting anticancer roles in vitro and in vivo, it is currently approved for the treatment of acute myeloid leukemia and advanced systemic mastocytosis [659,660]. Midostaurin has been shown to be an efficient anti-sarcoma agent. Indeed, it inhibited EWS cell proliferation in a dose- and time-dependent manner and decreased tumor growth in vivo [661,662]. Moreover, the combination of midostaurin with the cytokine oncostatin M has been shown to be efficient in reducing in vivo tumors, pointing to this combination as a potential adjuvant treatment for OS [663].

**Axitinib (Inlyta<sup>®</sup>)**. Also known as AG-013736 this is an oral VEGFR1/3 and PDGFR inhibitor explored to control angiogenesis [664]. Currently, this compound is approved for treatment as monotherapy or in combination with other drugs for renal carcinoma, and is under phase I, II and III clinical trials for many other tumor types [664]. Pre-clinical studies in EPN showed that this drug inhibited PDGFR $\alpha$  and PDGFR $\beta$ , and reduced the expression of mitosis-related genes including *ASF1B*, *MKI67*, *HMGA1*, *BRCA2*, *ESPL1*, *TACC3*, *CDC25A*, *RAD51AP1*, *AURKA*, *BUB1B*, *CENPE* and *HELLS*. It also decreased proliferation resulting from cellular senescence [639]. Similar antiproliferative effects were observed in MB 2D and 3D cell cultures, without affecting normal brain cells. Of note, the compound efficiently crossed the blood–brain barrier (BBB), reducing growth rates of experimental brain tumors without acute toxicity in juvenile rats [649]. In GBM, the cytotoxic activity of Axitinib was also reported in vitro and in vivo, characterized by an anti-angiogenic effect and survival prolongation [665]. Moreover, combinations of axitinib and other therapeutic targets have been explored with satisfactory results [666]. Indeed, the combinatorial treatment of Axitinib and PLK4 inhibitor has shown to be beneficial in MB and RMS [667]. Combinations with etoposide or gemcitabine also showed favorable effects on preventing tumor progression in an orthotopic group-3-MB xenograft models [649,668]. Furthermore, in immunodeficient and immunocompetent orthotopic GBM models, axitinib + G47 $\Delta$ -mIL12 resulted in an extensive decrease in vascularity, increased macrophage infiltration and significant tumor necrosis [669]. Such a antimetastatic effect was also observed in NB [670].

**Ramucirumab (Cyramza<sup>®</sup>)**. This is a humanized monoclonal antibody that acts by binding to VEGFR-2, thus limiting angiogenesis and the proliferation and migration of human endothelial cells [671]. Preclinical studies in NB, RB, OS, RMS and EWS have also shown that ramucirumab enhances anti-tumor activity by abrogating endothelial cord formation, while in vivo, it has also induced tumor growth delay. However, modest or no response was observed in OS [672]. This compound was approved by the FDA in 2014 and indicated for the treatment of gastric cancer, NSCLC, colorectal cancer and HCC [673–675]. As a well-tolerated drug, its combinatorial use was also approved, even though its use in clinics is limited due to a lack of specific markers and high costs [676].

**Alectinib (Alecensa<sup>®</sup>)**. Also known as CH5424802, this is an orally available selective ALK inhibitor already approved by the FDA for lung cancer treatment [677]. The compound is able to bind wild-type ALK and its fusions and its anticancer effects have been widely described. Noteworthy, it has shown acceptable results after treatment of intracranial EML4-ALK-positive tumors in rats with a high brain-to-plasma ratio, and permeability independent of P-glycoprotein transport [678]. Moreover, despite heterogeneous intratumoral distribution, alectinib delayed tumor growth in an NB mouse model, leading to increased survival, providing an option for future clinical treatment [679–681]. An interesting point in this regard is that Alectinib may improve sensitivity to chemotherapeutic since it increases the intracellular accumulation of ABCB1/ABCG2 substrates such as doxorubicin (DOX) and rhodamine [682]. Moreover, it has also shown effectiveness in combination with the histone deacetylase inhibitor vorinostat in NB harboring the ALK R1275Q mutation and

after intensive radiotherapy for the treatment of a rare intraosseous RMS with FUS-TFPC2 fusion, evidencing the potential of this drug to treat extremely aggressive tumors [683,684].

**AEE-788.** This drug is an orally bioavailable bispecific EGFR/HER2 inhibitor that exerts significant anti-tumoral activities and radio-sensitizes EGFR-overexpressing cells [685]. By targeting this receptor, the compound efficiently reduced clonogenicity, proliferation and survival of EPN cells and prolonged the survival of tumor-bearing mice, probably due to the increase in apoptosis of endothelial cells (as shown by others in cutaneous cancer xenografts) [686,687]. AEE788 also inhibited cell proliferation and prevented epidermal growth factor- and neuregulin-induced HER1, HER2 and HER3 activation in chemosensitive and chemoresistant (cisplatin selected) MB cells in vitro and in vivo [688].

**Crizotinib (Xalkori®).** This drug is an orally available aminopyridine-based ATP-competitive inhibitor of ALK that has shown positive results against NSCLC [689]. In turn, in pediatric tumors, growth-suppressive activities have been reported in some tumor types, such as PA, EPN, EWS and MB [160,690,691]. This drug was also able to induce apoptosis and autophagy in a dose-dependent manner in RMS cells, reducing cell migration and invasion, as well [692]. However, despite these promising results, this compound lacks clinical significance in patients with FOXO1-rearranged ARMS [693]. Similarly, crizotinib responses in NB are variable and mostly dependent on the mutation variants present in the tumor, considerably limiting its applicability [694–696]. Moreover, the literature widely illustrates that despite initial effectiveness, the vast majority of tumors treated with this compound will develop resistance within a few years [697].

**Capmatinib (Tabrecta®).** This compound is an orally bioavailable inhibitor of c-MET [597]. The information about the effects of this compound in pediatric oncology is limited. There are reports of its action in pediatric HGG in which this compound appeared to be more efficient than crizotinib in terms of specificity, potency and brain availability, resulting in a higher cellular response compared to crizotinib treatment in vitro and in vivo [698]. Nevertheless, in a phase I dose escalation study that included EWS and OS patients, only mild responses were observed [699].

**Tepotinib (Tepmetko®).** This compound is a phenylmethyl-pyrimidine derivative developed to disrupt MET phosphorylation that received approval from the FDA and the Japanese Ministry of Health, Labour and Welfare for the treatment of patients with metastatic NSCLC harboring METex14 skipping alterations who progressed following platinum-based cancer therapy [700]. According to PubChem (CID 25171648), this compound has been investigated in the treatment of neuroblastoma.

**PF-04217903.** This compound is an ATP-competitive small-molecule inhibitor with 1000-fold selectivity for c-MET compared with more than 150 kinases, making it one of the most selective c-MET inhibitors described to date. In vitro, it inhibited tumor cell proliferation, survival and migration/invasion in cell lines where c-MET is activated by different mechanisms, including c-MET gene amplification, HGF/c-MET autocrine loop formation and c-MET overexpression [701]. In vivo, oral administration or subcutaneous minipump infusions led to a robust tumor growth inhibition at doses of 30 mg/kg with suitable tolerability. Reductions in microvessel density were also observed [701]. Considering pediatric tumors, similar results were obtained when two highly metastatic OS cell lines were injected by tail vein into immunodeficient mice. In this experiment, mice were treated with PF-04217903 (30 mg/kg) or vehicle control by gavage 5 days on and 2 days off for 30 days. Mice injected with MNNG-HOS cells (which has constitutively activated MET) treated with PF-04217903 had a tenfold reduction in the number of metastatic nodules, while those with injected MG63.2-derived tumors (which have high levels of total and phospho-MET) had a 37% reduction in nodules compared to control mice [702]. This compound has also shown potential for the treatment of malignant peripheral nerve sheath tumors in NF1 patients [703].

**Tivantinib.** This compound, also known as ARQ 197, was described as an orally bioavailable small-molecule c-MET inhibitor with antitumor activity. Tivantinib inhibited cell viability with similar potency in both c-MET-addicted and nonaddicted adult carci-



noma cells, pointing to alternative mechanisms of action [704]. Despite this, the failure of a pioneer phase I clinical trial in pediatric tumors was attributed to the lack of selection for MET amplification during patient enrollment. In the study, which comprised 36 patients, including 4 glioma, 4 MB, 4 EPN, 4 EWS, 4 OS, 3 RMS, 2 WT and 2 NB, sub-optimal responses were achieved when tivantinib was given with food to children with refractory solid tumors is 240 mg/m<sup>2</sup>/dose. Moreover, while the drug was well tolerated, its pharmacokinetic profile was also variable, discouraging further investigation in this setting [705]. However, two of those patients (alveolar soft part sarcoma) who responded to tivantinib administration and were transitioned to a follow-up protocol experienced extended progression-free survival receiving 360 mg twice every day without adverse events [706].

**Lorlatinib (Lorbrena®).** This small molecule represents an orally available, ATP-competitive inhibitor developed by Johnson et al., and further investigated for the treatment of ALK-positive NSCLC [707]. Also named PF-06463922, the drug has shown minimal toxicity in adults and there has been much interest in its prospective use in NB treatment. In this regard, Infarnato et al. described higher potency of PF-06463922 across ALK variants in a panel of 10 NB cell lines, with IC<sub>50</sub> values for inhibition of F1174L- and F1245C-mutated ALK significantly lower than those seen for its predecessor, crizotinib (0.2–10 nmol/L) [708]. Moreover, this compound at 10 mg/kg/day induced complete tumor regression in xenograft mouse models of NB, and in (PDX) harboring the crizotinib-resistant F1174L or F1245C mutations within 3 weeks [708]. Similar 10-fold lower IC<sub>50</sub> values were obtained by Guan et al. (2016). In another group of cell lines, PF-06463922 inhibited growth, reduced levels of tyrosine 1278 (Y1278) phosphorylation on ALK, and induced apoptosis. Comparatively, treatment reduced tumor volume in subcutaneous and orthotopic xenograft models of NB, as well as in the Th-ALKF1174L/MYCN-driven transgenic NB mouse model [709]. PF-06463922 has also been tested sporadically in patients affected with NB. Two recent articles portray favorable responses in a 3-year-old boy with ALK-fusion-positive HGG and an adolescent with relapsed, refractory, metastatic ALK F1174L-mutated NB. The first, considering that the compound is able to cross the BBB, was treated through a nasogastric tube at a dose of 95 mg per square meter of body surface area once daily [710]. Histology after tumor resection showed a marked decrease in the proliferative index of the tumor and since the tumor was not seen on postsurgical MRI, therapy stopped. After 6 months, metastatic lesions were identified on cranial nerve VII and treatment was restarted at a dose of 95 mg per square meter administered by mouth once daily, achieving a near-complete response after 1 month [711]. In the second case, the patient had already shown no response to the first-generation ALK inhibitor crizotinib (240 mg/m<sup>2</sup>/dose given twice daily combined with the standard cytotoxic chemotherapy regimen). The tumor was reduced with continuous 95 mg/m<sup>2</sup>/dose lorlatinib and the only significant side effect observed was grade 2 hypercholesterolemia. However, differentially from the infant, she relapsed after 13 months of treatment and died from progressive disease 3 months later [712].

**Ceritinib (Zykadia™).** Formerly known as LDK378, it is an oral ALK inhibitor that also targets insulin-like growth factor receptor IGFR, insulin receptor and ROS1. This compound was approved by the FDA through an accelerated process to treat ALK-positive metastatic NSCLC [713]. Preclinical studies in the pediatric setting have indicated antiproliferative effects and improved inhibition (11-fold) compared to crizotinib [714]. However, in an exploratory study with a panel of NB cell lines, it was noted that inhibition occurs irrespective of ALK mutational status, and cell lines that carry other driver mutations (i.e., MYC amplification) are sensitive to treatment as well. The same authors further treated a child with ALK-I1171T high-risk NB that was not responding to conventional treatment due to an underlying congenital genetic condition, Fanconi anemia. Monotherapy with ceritinib was well tolerated and resulted in tumor shrinkage and complete clinical remission including all metastatic sites [715]. This compound can be given with food and penetrates the human brain, and thus presents itself as an option for the treatment of CNS tumors with ALK alter-

ations such as EPN and MB [715–718]. However, in orthotopic PDX (from a 10-year-old boy with a multiple recurrent GBM), it was observed that even though ceritinib-treated mice lived longer, the drug had only a moderate effect [719]. Monotherapy was also inefficient in treating a 16-year-old patient with a long history of OS lung metastases, despite acceptable results in primary tumor cells of six other patients and the HOS cell line [720]. Similarly, Ceritinib treatment led to decreased cell proliferation, cell cycle arrest and apoptosis in a dose-dependent manner in a panel of RMS cell lines, all of which lack intrinsic ALK phosphorylation (PAX3-FOXO1-positive Rh30, Rh41 and -negative Rh18 and RD cell lines). The work showed that the compound affects the IGF1R signaling pathway without effects on the migratory ability of cells. Moreover, in subcutaneous Rh41 xenografts, a reduction in tumor growth was observed after approximately 2 weeks, albeit subsequent evaluation of tumor characteristics showed no difference in proliferation or vascularization between the treatment groups and controls [721]. Others also showed that even though LDK378 reduces cell viability and induces cell death in RMS cell lines at low micromolar concentrations irrespective of ALK expression levels or phosphorylation status, cells are far less sensitive compared with Karpas 299 non-Hodgkin's lymphoma cells carrying the NPM-ALK fusion gene [722].

**Brigatinib (Alunbrig®).** Originally named AP26113, this next-generation ALK inhibitor was first described in 2016 and is considered highly CNS-penetrant [723,724]. This compound was granted approval for the treatment of patients with metastatic ALK+ NSCLC and intolerance to crizotinib [725]. In an NB setting, preliminary indication of efficacy was observed after exposure of several NB cell lines, including CLB-BAR (MYCN amplification, ALK ( $\Delta$ 4-11) and amplified, ALK addicted), CLB-GE (MYCN amplification, ALK (F1174V) amplification, ALK addicted), IMR32 (MYCN amplification, WT ALK) and CLB-PE (MYCN amplified, WT ALK), in which treatment inhibited cell growth and ALK phosphorylation in a dose-dependent manner. However, while  $IC_{50}$  values varied between 75 and 100 nM in ALK-addicted cell lines, the compound was unable to inhibit growth of both non-ALK addicted NB cell lines, IMR32 and CLB-PE. The effects of brigatinib were further validated in vivo through two complementary models. The first used transgenic *Drosophila melanogaster* flies expressing two gain-of-function variants, F1174L and R1275Q, which disrupt the eye morphology, giving a “rough phenotype”. The authors showed that larvae grown on food containing Brigatinib displayed a concentration-dependent improvement of the rough eye phenotype. Then, brigatinib was used as a single agent to treat BalbC/NUDE mice bearing ALK-addicted CLB-BAR xenografts. In this model, the compound also showed to be effective, with robust and potent anti-tumor activity [726].

**Entrectinib (Rozlytrek®).** This compound (also called RXDX-101, NMS-E628, NMS-01191372, Rozlytrek) is a selective, oral tyrosine pan-TRK, ALK and ROS1 inhibitor that has demonstrated preclinical efficacy in tumors with NTRK1/2/3, ALK and ROS1 alterations [727]. This inhibitor can pass through the BBB and has clinically proven to be effective against primary and metastatic brain diseases, with no adverse off-target activity [728].

Entrectinib also displays promising anti-tumor activity in NB, evinced by diminished Ki-67 and activation of caspase-3 in ALK wild-type, amplified or mutated cell lines [729]. In vivo growth inhibition and substantially reduced phosphorylation in TrkB-expressing NB xenografts were also observed after treatment as a single agent or in combination with irinotecan or temozolomide (TMZ), eliciting increased EFS when compared to controls [730]. Moreover, the ability of entrectinib to inhibit p-TrkB, p-PLC $\gamma$ , p-Akt and p-Erk suggested that this compound may have improved efficacy compared to other targeted inhibitors previously evaluated in NB [172]. However, despite durable responses in pediatric patients with intracranial tumors or NB harboring NTRK1/2/3 or ROS1 fusions, its utility may be hampered by the appearance of acquired resistance in this tumor type [730,731].

**X-396.** This compound, also known as Ensartinib, is an aminopyridazine-based second-generation ALK/MET inhibitor that holds much clinical promise with increased potency as compared with crizotinib and other second-generation ALK inhibitors such as alectinib and ceritinib [732]. X-396 significantly reduced growth (by 40% at a 3 nM concentration)

and ALK phosphorylation in SY5Y NB cells that harbor ALK-F1174L. Biochemical IC<sub>50</sub> values for MET inhibition were 2-fold higher [733]. Ensartinib was significantly more effective than crizotinib at inhibiting the intracranial growth of the SH-SY5Y NB model harboring the F1174L mutation [732]. Furthermore, the activity of X-396 administered alone or in combination with liposomes carrying ALK-siRNAs (that are active irrespective of ALK gene mutational status) was later tested in a mouse model by Di Paolo et al. (2011). These authors corroborated previous *in vitro* data with a second NB cell line (LAN-5) and showed that in subcutaneous NB models, the compound acted in a dose-dependent manner, with adequate bioavailability, moderate half-life, high mean plasma and tumor concentrations. Moreover, against human NB orthotopic xenografts obtained by implanting of Luciferase stably transduced NB cells, SH-SY5Y-Luc and LAN-5-Luc, into the adrenal gland of nu/nu mice, significant dose-dependent anti-tumor activity was also observed, with even more reduced tumors and prolonged survival with the combination with the liposomal formulation [734].

**Erdafitinib (Balversa™).** This compound is an oral pan-FGFR inhibitor with quinoline structure [735]. Known as JNJ-42756493, this compound is already approved by the FDA for the treatment of advanced or metastatic urothelial carcinoma, and is now under clinical trials that also include childhood CNS tumors [736]. It inhibits FGFR1/2/3/4 with increasing IC<sub>50</sub> values of 1.2, 2.5, 3.0 and 5.7 nM, respectively [737]. This compound inhibited proliferation on five different NB cell lines (SK-N-AS, SK-N-BE(2)-C, SK-N-DZ, SK-N-FI and SK-N-SH) as monotherapy, but showed variable synergistic, additive and antagonistic effects when combined with commonly used cytotoxic agents such as cisplatin, vincristine and doxorubicin [738]. Additionally, IC<sub>50</sub> for FGFR4 inhibition by this compound on the A-204 RMS cell line was determined as 4.5 nM, while treatment of mice xenografts resulted in a 58% volume reduction after 21 days of treatment with daily doses of 30 mg/kg [735].

Erdafitinib has also been tested alone and in combination with cisplatin, vincristine and radiotherapy on the SHH-MB cell lines DAOY and UW228-3. Under all conditions, the cell lines showed dose-dependent decreases in viability and proliferation after 48 and 72 h [739].

**Dovitinib.** Also known as TKI258, this is a multi-targeted tyrosine kinase inhibitor with potent activity against FGFR1/3, VEGFR1/2/3 and to different extents, PDGFR-β, Flt3, c-Kit and CSF-1R, that showed promising results as an antitumoral and antiangiogenic compound [658]. This compound is already in clinical trials in adult patients [740]. However, in pediatric neoplasms, information about preclinical studies is limited. Preliminary results of Dovitinib in NB cells, which express high levels of FGFR, indicated anticancer-activity in this tumor type [741]. Similar results were reported for RMS, albeit it was demonstrated that this inhibitor is not as potent as other FGFR inhibitors (i.e., ponatinib) [656,742]. In addition, due to its ability to cross the BBB, this compound has been indicated as a suitable candidate for the treatment of CNS tumors. In this regard, *in vitro*, it reduced the capacity of EPN cells to re-adhere and proliferate in a dose-dependent manner [658]. In DIPG and GBM, however, true effects on viability were observed at high dovitinib concentrations (>400 nM) [743]. Of note, others showed that despite killing glioma cells *in vitro* (up to 55% of cells at the assay end point), the drug exerted minimal anti-tumoral effects *in vivo*, suggesting a microenvironment-mediated therapeutic resistance mechanism [744].

**Masitinib (Masivet®).** This compound, also known as AB1010, is an orally administered, novel, potent and selective phenyl aminothiazole-type tyrosine kinase inhibitor of KIT, used in the treatment of canine mast cell tumors acting as a blocker of mast cell degranulation, cytokine production and migration of bone marrow cells [745,746]. Masitinib is under clinical investigation in several human malignancies that harbor similar canine KIT mutations (i.e., gastro-intestinal stromal tumors, ovarian and prostate cancer). In fact, this inhibitor acts on several mutated forms of KIT, and other receptors, including PDGFR, FGFR3 and focal adhesion kinase (FAK) [747,748]. Noteworthy, a brain tumor xenograft

model using pediatric GBM cells suggested that masitinib may potentiate the effects of TMZ, providing decreased tumor growth relative to either drug used as a monotherapy [749].

#### 4.2. PI3K/AKT/mTOR Pathway Inhibitors

**Everolimus (Afinitor®).** Everolimus (Afinitor, Novartis) is an orally administered rapamycin derivative approved by the FDA and the European Medicines Agency for the treatment of RCC [749]. This compound reduces tumor cell proliferation and induces apoptosis and autophagy through the phosphorylation inhibition of mTOR [750,751]. Pre-clinically, the combination of everolimus with sorafenib yielded enhanced antiproliferative and proapoptotic effects, potentiated antiangiogenesis and reduced the metastatic potential of OS [751]. Prolonged exposure to everolimus also improved the CNS retention of dasatinib and extended the survival of mice bearing pediatric high-grade glioma tumors [752]. Comparatively, everolimus is synergistic with carboplatin in low-grade glioma models [753]. However, in the literature, there is significantly more information about clinical experience because, since its approval, everolimus has become widely accepted by the medical community where treatment options may be limited. One major clinical example involves subependymal giant cell astrocytomas (SEGA), tumors that are frequently diagnosed in patients with tuberous sclerosis complex (TSC) [754]. Loss of function of either TSC1 or TSC2 leads to downstream constitutional activation of the mTOR complex [755]. Besides surgical excision, patients with large or recurring SEGAs did not have robust treatment options, and Everolimus has been shown to induce tumor shrinkage and presents additional clinical benefits including seizure control [756,757].

**Palomid-529.** Also known as RES-529, this compound is a small-molecule drug dual novel inhibitor of mTOR complex 1 (mTORC1) and mTOR complex 2 (mTORC2). Palomid 529 likewise inhibits both VEGF-driven and bFGF-driven endothelial cell proliferation [758]. Due to its potential to penetrate the BBB without restriction by the ABCB1 and ABCG2 efflux transporters, the anti-glioma effects of this drug have been investigated [759–761]. In childhood cancer, a single report proved a potent inhibition of viability, cell cycle progression and proliferation of the OS cell line U2OS [762].

**OSI-027.** This compound is an orally bioavailable selective ATP competitive inhibitor of mTOR and off-targeted PI3K $\alpha$  (100-fold selectivity for mTOR relative to PI3K $\alpha$ ) that has been studied in the treatment of many tumors [763]. OSI-027 is active in vitro against cell lines and primary cells of pediatric pre-T-ALL, with superior efficacy to rapalogs and in vitro synergy with a number of conventional cytotoxic agents [181]. Preliminary studies combining OSI-027 treatment with alpelisib demonstrate similar antineoplastic results inhibiting PI3K/mTOR signaling MB, EWS and RMS cell lines [764–767].

**VS-5584.** This dual inhibitor of mTORC1/2 and class I PI3-kinases has shown anti-tumor potential in a broad spectrum of tumor types in vitro and in vivo [768–770]. Noteworthy, evidence supports that this compound has an active role in reducing stem cell viability in multiple mouse xenograft models of human cancer (30-fold more potent compared to non-stem cells) [769]. Thus, the activity of VS-5584 was recently explored in OS, in which treatment dramatically suppressed growth and cell migration and synergized with CCT128930, an AKT2 inhibitor [771–773]. In the same way, this drug is cytotoxic, showing apoptosis induction and a robust limitation of the colony-forming ability in NB cell lines. Delay of tumor growth was also observed in mice subcutaneously inoculated with BE(2)-M17 cells and treated with VS-5584 (25 mg/kg, three times per week) for 2 weeks [773].

**Dactolisib (BEZ235).** This drug, also called BEZ235 or NVP-BEZ235, is a reversible PI3K/mTOR inhibitor belonging to the imidazoquinoline class already tested in a variety of cancers in preclinical studies. In sarcomas (EWS, OS and RMS), dactolisib showed promising results in vitro, such as a reduction in cell proliferation, G1 cell cycle arrest and decreased in cell migration [774,775]. Interestingly, it was also shown that BEZ235 elicits strong cytostatic effects in EWS cells and results in a global modulation of the transcriptome affecting other pathways related to splicing and metabolism. This drug also reduced

the expression of EWS/FLI1 by 50%, reinforcing its potential for EWS treatment [773]. However, its capacity to induce apoptosis is uncertain. Mild results were obtained by Giorgi et al. (2018), and when OS cells were treated with a similar inhibitor range, U2-OS and MG63 presented no significant differences in apoptosis induction, although the drug was efficacious with either doxorubicin or vincristine [774–776]. In RB, GBM, and MB, decreased viability and proliferation in a dose-dependent pattern was observed in most cell lines [777–780]. When tested *in vivo*, dactolisib could reduce tumor volume, vascularity and metastasis and improve animal survival, especially when combined with other drugs, such as topotecan, carboplatin, vincristine or the SMO inhibitor LDE225 [773,781–783].

**SF-1126.** This is a pan and dual first-in-class soluble PI3K/mTORC inhibitor that exhibits antitumor and antiangiogenic activity against several malignancies [784,785]. In the literature, there are few reports of this inhibitor in pediatric preclinical models. SF-1126 promoted a decrease in cell viability of a panel of EWS cell lines and CD15+ stem cell population in SHH-driven MB [786,787]. Moreover, SF1126 has been shown to enhance the cytotoxicity of doxorubicin in NB cells, leading to p53-mediated activation of apoptosis [788]. Treatment of NB tumors with SF1126 also reduced MYC expression and inhibited growth *in vivo*, leading to tumor shrinkage and reduced neovascularization [789].

**Triciribine.** Triciribine is a pan-AKT 1 inhibitor with anticancer effects in various tumor types [790]. This compound has been shown to decrease the survival of SH-SY5Y NB cells in both 2D and 3D culture models, affecting the migratory abilities of their sphere-forming units [791]. Triciribine demonstrated activity in EWS cell lines as well, with a mean IC<sub>50</sub> of 24  $\mu$ M, with robust synergy when combined with dasatinib; however, it did not affect tumor growth *in vivo* [792]. Moreover, Smeester and colleagues (2020) tested this drug in OS and showed that ATK inhibition in HOS and SJS-1 cell lines leads to decreased cell proliferation, migration and colony capacity, and increased apoptosis. Further assessment in an orthotopic OS model also demonstrated reduced tumor growth (volume and weight) and metastasis after triciribine 40 mg/kg three times weekly [793].

**Sapanisertib.** Also called MLN0128, INK-128 or TAK-228, this is an ATP-competitive mTOR inhibitor already tested for safety in an adult cohort [794]. In studies including pediatric models, this inhibitor has shown promising results *in vitro*, reducing cell viability and colony formation and inducing apoptosis in sarcoma cells (EWS, OS and RMS) without affecting human osteoblast and osteocyte cells (normal bone cells); effects were improved by combination with MK2206, an AKT-specific inhibitor [795,796]. Similarly, the inhibition of mTOR (oral gavage for 21 days-3 mg/kg twice daily 3  $\times$ /week in EWS and RMS, or 2.5 mg/kg, daily) in OS resulted in tumor volume reduction, without observable side effects [795,796]. Comparable results were obtained for brain tumors (MB, NB and GB), with reduced cell invasion at low concentrations [797,798]. Interestingly, it was also observed that sapanisertib promotes metabolic alterations, such as disrupting glutathione synthesis and reducing glucose and lactate (a common feature of cancer cells) [797,798]. When tested in murine models, it reduced tumor weight and size, improving animal survival [797–799]. However, in combination with trametinib (1 mg/kg; 3  $\times$ /week; p.o. + MAPK inhibitor; 1.5 mg/kg; 5  $\times$ /week; p.o.), despite showing antitumor effects (reduction in angiogenesis and improvement in animal survival), some adverse effects were observed, including weight loss and skin redness [800]. Finally, in RB models, sapanisertib inhibited growth and increased apoptosis, whereas it inhibited cell migration and angiogenesis [801].

**LY-2090314.** This drug belongs to the ATP-competitive class of GSK-3 inhibitors with limited activity against additional kinases. Preclinical data suggested partial anticancer activity as a single agent against solid-tumor-derived cancer cell lines *in vitro* and in xenograft models, although it seemed to potentiate platinum-based chemotherapy [802]. Only a single report of its activity against pediatric tumors was found in the literature. Kunnimalaiyaan et al. (2018) tested LY2090314 in a panel of NB cell lines with different genetic backgrounds: SH-SY-5Y (non-amplified MYCN or single-copy, wild-type TP53, F1174L ALK mutation), NGP (1p alteration, MYCN-amplified, wild-type ALK, TP53 mutated, MDM2-amplified) and SK-N-AS (1p deletion, MYCN single-copy, H168R TP53 mutation, wild-type ALK),

and found that this GSK-3 inhibitor at nanomolar range promoted growth inhibition in a time- and dose-dependent manner irrespective of the cell line markers. Reduced growth resulted mainly due to apoptosis induction, evinced by a 2-fold increase in the expression of cleaved PARP and caspase-3/7 activity. Downregulation of survivin and cyclin 1 was also observed [803].

**Tideglusib.** This compound represents another GSK-3 inhibitor, although it acts in a non-ATP competitive manner. Evidence of its antineoplastic effects with a pediatric scope includes in vitro experiments in OS and NB cell lines. In both models, treatment showed a significant reduction in cell proliferation in a dose-dependent manner, cell cycle arrest, and apoptosis induction, even though micromolar concentrations are required to achieve comparable results to LY2090314 [804–806]. Nevertheless, inhibition of GSK-3 by Tideglusib importantly compromises stem cell characteristics of both cell types. In the OS, treatment decreases stem cell markers, including OCT4, CD133 and SOX2, while in NB, it decreases neurosphere self-renewal. In mice models, tideglusib treatment (10 or 20 mg/kg in OS- and NB-derived tumors, respectively) promoted a reduction in tumor growth with few side effects [804,806]. Of note, PDX-derived cell cultures of both variants of RMS (embryonal and alveolar) treatment with tideglusib substantially reduced  $\beta$ -catenin phosphorylation at 60 nM; however, tumor-bearing mice treated with 200 mg/kg of tideglusib daily by oral gavage did not benefit in terms of survival or myodifferentiation [807].

**MK-2206.** This compound is an orally bioavailable allosteric and non-ATP-competitive AKT inhibitor tested in several tumors [808]. In OS, for instance, this drug was able to induce cytotoxic effects both in vitro and in vivo [223,796,809,810]. Similarly, in NB cells, MK-2206 diminished cell viability and increased apoptosis in cells with high expression of FOXO3a [810,811]. In vivo, the drug promoted inhibition of tumor growth and increased animal survival, effects that were even improved by combination with etoposide [812]. Of note, EWS and RMS cells were not sensitive or had less sensitivity to AKT inhibition [809].

**Ipatasertib.** Also known as GDC-0068, this compound is an ATP-competitive pan-AKT inhibitor developed by Array BioPharma/Genentech Inc. Having similar activity against Akt-1 and Akt-3, it is effective against several tumor types [813]. So far, Choo and colleagues are the only group that has tested this compound in childhood sarcomas. The drug induced a reduction in cell viability; however, RMS cells were more sensitive to PI3K/AKT pathway inhibition than OS cells [814].

#### 4.3. MAPK Pathway Inhibitors

**Sorafenib (Nexavar®).** Sorafenib is an inhibitor of VEGFR2/3, PDGFR, KIT, FGFR-1, RAF and RET, approved by the U.S. FDA for the treatment of unresectable HCC and advanced RCC [815]. In preclinical models of MB, this compound reduced cell viability and increased apoptosis in established cell lines and primary tumor cultures. Moreover, it induced cytoskeletal alterations that ended in impaired cell migration [640]. In vivo, sorafenib (100  $\mu$ L of 10  $\mu$ mol/L administered three times a week for five weeks) was able to reduce the volume of subcutaneous tumors [816]. Similar results were obtained NB, in vitro and in vivo. Of note, in this model, sorafenib also impaired angiogenesis and G1 cell cycle arrest [817,818]. Conversely, despite reducing initial viability in EPN and PA, growth-factor-driven rescue was also seen, reducing the potential of using sorafenib for treatment of these tumors [691]. Indeed, in pediatric patients with PA, sorafenib induced progressive tumor growth acceleration as a result of ERK upregulation, which resulted in premature termination of the study [819]. In bone sarcomas, dubious results were also observed. In OS, sorafenib treatment blocked cell proliferation and was able to reduce tumor growth in murine models [820–822]. However, other studies showed that sorafenib was only able to reduce tumor growth when combined with everolimus, or palbociclib, probably due to the capacity of sorafenib to induce mTORC activation [821,823]. At the same time, in EWS and RMS, sorafenib only showed efficacy when combined with doxorubicin or with ceritinib, respectively [823,824].

**Regorafenib.** Also called BAY 73–4506, this is a new-generation multi-tyrosine kinase inhibitor that already showed antitumor and antiangiogenic effects. This inhibitor diminished cell proliferation in a cell line panel from the Innovative Therapies for Children with Cancer (ITCC), which includes 5 MB, 7 EWS, 7 NB, 7 OS and 7 RMS cell lines [610]. Regorafenib also induced cell cycle arrest and promoted apoptosis in NB cells [612]. In vivo, 10 mg/kg/d or 30 mg/kg/d treatment resulted in tumor growth inhibition in RMS, EWS and NB orthotopic models and improved EFS in EWS, NB, OS and RMS [610,825,826].

#### 4.4. Cyclin-Dependent Kinases Inhibitors

**Milciclib.** This is a second-generation ATP competitive pan-CDK inhibitor, developed by Tiziana Life Sciences, that also acts on TRKs (from tropomyosin receptor kinase A) [827,828]. In preclinical trials performed in different tumors, such as MB and gliomas, it showed promise given its ability to cross the BBB, even though there are reports of MDR transporters limiting the penetration into the brain [829–831]. Moreover, MYCN-amplified the Grp3-MB cell lines MB002, Sd425 and D283 and the MYCN-amplified NB cell line Kelly are particularly sensitive to MILCICLIB treatment, evinced by cell cycle arrest and massive apoptosis [829].

**Terameprocol (CINelim™).** This is a semi-synthetic inhibitor developed by Erimos Pharmaceuticals LLC from a plant lignan, showing antiviral and anti-cancer potential [829,832]. The drug is considered a global inhibitor of the transcription process, which in turn acts by preventing, for example, the synthesis and activation of survivin, by competing with the transcription factor Sp1 for specific Sp1 DNA-binding domains within gene-promoter regions during DNA synthesis [833]. To date, only a single in vitro study (that included the childhood GBM cell line SF188) showed that this inhibitor was able to reduce the proliferation capacity of the cells in a dose-dependent manner, and showed synergism with TMZ under simultaneous exposure for 48 h. Increased effects were also observed when combined with ionizing radiation. Moreover, as expected, this compound induced significant arrest in the G0/G1 phase, decreasing the mitotic index and almost killing all cells at 30  $\mu$ M [833].

**UCN.** UCN-01, or 7-Hydroxystaurosporine, is a synthetic derivative of staurosporine with antineoplastic activity that acts on AKT, CDKs and calcium-dependent protein kinase C (in an ATP-competitive manner), and is able to act synergistically with others [834]. In experimental models described in the literature, UCN-01 showed promising results by inducing apoptosis in leukemic and colon cancer cells; moreover, according to the pediatric tumors included in this work, this inhibitor also showed potential against OS tumor cells, reducing viability, proliferation and migration [835,836]. Similar results were observed in a panel of NB cell lines (with genetic backgrounds differing in MYC, p53 and BCL2 statuses), where this inhibitor was the most effective compound in reducing cell proliferation (compared to BiCNU, docetaxel, flavopiridol, staurosporine) and induced apoptosis measured through both caspase activation and caspase-3 and PARP cleavage [837].

**BMS-387032.** Also called SNS-032, this is a small aminothiazole molecule that acts as an ATP-competitive cyclin CDK inhibitor, especially for CDK2/7/9. Preclinical studies have shown that as a cell cycle blocker, it causes cytotoxicity and prevents tumor cell growth in several models [838–840]. Regarding pediatric tumors, this inhibitor showed positive results in the OS cell line U2-OS, evoking downregulation of RNA polymerase II Ser2 phosphorylation and some degree of caspase activation at all doses tested [839]. Similarly, this CDK inhibitor showed encouraging results in a panel of 109 NB cell lines, consisting of 19 parental cell lines and 90 sublines with acquired resistance to 14 different anticancer drugs. Doses between 58.3 and 14,615 nM were able to reduce viability in a great proportion of cell lines and impaired the growth of the multidrug-resistant cisplatin-adapted UKF-NB-3 subline UKF-NB-3(r)CDDP(1000) injected into the right flank of NMRI:nu/nu mice. Of note, p53 status did not affect the response of NB cells; however, ABCB1 expression conferred resistance to this drug [841–843]. Other interesting results, albeit not in child-derived cell lines, were also published, including the inhibition of hypoxia-mediated GBM

cell invasion and cell-mediated capillary formation of HUVEC cells when co-cultured with U87MG cells in the presence of the drug [844,845]. Nevertheless, further studies with this inhibitor were stopped due to its high toxicity and low selectivity [846–848].

**Seliciclib (Roscovitine®).** Formerly known as Roscovitine, CYC202 or R-roscovitine, this is a selective ATP-competitive pan-CDK inhibitor that blocks cell proliferation in almost all phases of the cell cycle. Seliciclib is a potent inhibitor of CDK9/cyclin T, CDK7/cyclin H, CDK2/cyclin E and CDK1/cyclin B. The negative influence of seliciclib on CDK7 and CDK9 also portrays a role for this inhibitor in modulating RNA polymerase II CTD phosphorylation [848]. Its antitumor activity has been explored in a wide spectrum of hematological and solid malignancies as a single agent and in combination with other cytotoxic agents [848–850]. Among pediatric tumors, Roscovitine showed promising results, in EWS, where it was able to reduce cell proliferation and induce caspase-dependent activation (half minimal dose 10  $\mu\text{mol/L}$ ) in a panel of six cell lines, while it slowed A4573-derived tumor growth in mice after intraperitoneal injection [851]. Similar results were found in OS, with reduced proliferation and migration at doses up to 90  $\mu\text{M}$  [437,851]. Moreover, in NB, the drug resulted concentration-dependent cytotoxicity, both in vitro and in vivo, with doses between 10 and 200  $\mu\text{M}$  [851–855]. Roscovitine also reduced MB viability, with IC<sub>50</sub> values of around 25  $\mu\text{M}$  [856]. Moreover, treatment of Pzp53med cells (derived from a mouse Ptc+/-/p53-/- tumor) with 10 nM roscovitine resulted in reduced levels of E2F1, FASN, Bmi1, cyclin D2, cdk2 and cdk4. Synergistic effects were also observed when combined with C75, an inhibitor of FASN [857].

**Ribociclib (Kisqali®).** Also known as Kisqali® (Novartis, Basel, Switzerland), this compound is a highly specific inhibitor of CDKs 4/6 that received FDA approval for use in the upfront treatment of hormone receptor-positive (HR<sup>+</sup>), HER2-negative breast cancer in 2017 [858]. With respect to the pediatric tumors, this compound demonstrated adequate results in EWS, causing cell cycle arrest mainly in combination with IGF1R inhibitors [859]. Moreover, in NB, this drug was able to reduce proliferation in vitro and in vivo, with doses between 0 and 10,000 nmol/L [331,860,861]. Most importantly, ribociclib showed high CNS penetration (>10 nM) in vivo, suggesting prospects for its use in the treatment of brain tumors. In this regard, oral doses of ribociclib inhibited RB phosphorylation, downregulated E2F target genes (CNE2, CCNA2, MKI67, TOP2A and PLK1) and decreased proliferation in group-3-MB mouse and human orthotopic PDX. Additionally, the combination of ribociclib and gemcitabine slowed tumor progression and metastatic spread and increased survival, warranting further investigation [862].

**Palbociclib (Ibrance®).** Also known as PD-0332991 (Ibrance®, Pfizer, New York, USA), this compound represents an ATP-competitor with selective potency against CDK4/6, approved by the FDA in 2015 [859]. The effects of this inhibitor have been assessed in several childhood tumors. In primary EPN cells, for example, it was able to reduce proliferation at 0.5  $\mu\text{M}$ , with G1 arrest and reduced expression of CDC6, MCM2, MAD2L1, CDK2, BRCA2 and RAD51 [863]. Similar results were observed in NB, where this inhibitor reduced proliferation, inhibited colony formation in a dose-dependent manner and affected cell differentiation, tumor progression and metastasis in a preclinical chick embryo model [863–866]. Palbociclib has also been shown to be a new option for targeted therapy in childhood sarcomas. Perez et al. (2015), by treating a panel of 10 low-passaged sarcoma cell lines generated directly from patient samples and two commercial cell lines of heterogeneous origin and different molecular karyotypes (including liposarcoma, leiomyosarcoma, EWS, RMS and myxofibrosarcoma), determined IC<sub>50</sub> values ranging from 8 to 26  $\mu\text{M}$  depending on their levels of CDK4 expression. Moreover, palbociclib was active in vivo against subcutaneously engrafted CDK4-expressing sarcomas, although responses were negative in tumors displaying low levels of CDK4 and high levels of p16ink4a [867]. Strong decreased cell proliferation and G0/G1-phase arrest with decreased S/G2 fractions were also observed in leiomyosarcomas by another group [868]. Most interestingly, this compound is capable of inhibiting growth in sarcomas with different translocation backgrounds. For example, Palbociclib (100 mg/kg) was able to reduce the volume of tumors originated



from an EWS sample with CDKN2A/B loss and FUS-ERG fusion implanted in the right chest wall of nude mice [869]. Additionally, satisfactory results were obtained after the treatment of a child with a refractory pediatric sarcoma harboring paracentric inversion on the short arm of chromosome X, resulting in the fusion of the BCOR and CCNB3 genes [870]. Regarding assays in OS, this inhibitor reduced proliferation and migration with doses of 0.04, 0.16, 0.625, 2.5 and 10  $\mu$ M [393]. Migration and invasion have also been hampered by palbociclib in glioma cell lines, both in vitro and in vivo, with doses ranging between 10 nM and 10  $\mu$ M [871–873]. Moreover, this inhibitor showed significant therapeutic benefit in mice after intracranial transplant of genetically relevant murine or human astrocytoma cells expressing BRAFV600E, and extended survival of animals when combined with PLX4720 (PubChem CID24180719) [874]. Similar results were also obtained in a DIPG with PDGF-B overexpression and Ink4a-ARF loss. Palbociclib induced cell cycle arrest in vitro and in vivo. However, in models engineered for PDGF-B expression with p53 deletion, the results were disappointing. Regarding survival, Palbociclib treatment prolonged animal survival by 12%, which was further increased by combinations with a previous single dose of 10 Gy radiation therapy [875].

**Abemaciclib (Verzenio®)**. This compound, under the name Verzenios® (Eli Lilly, Indianapolis, USA), is a highly selective CDKs 4/6 inhibitor that acts by competing for the ATP binding site. This inhibitor is the most different from its peers (palbociclib and ribociclib), being more lipophilic and able to cross the BBB and penetrate breast tissue [859]. In addition, this inhibitor has potent activity against recurrent ER+/HER2- breast cancers [876,877]. However, its clinical adverse effects are not well described [878–880]. Preclinical studies in pediatric tumors indicate effectiveness against EP, NB, EWS and OS [412,880–882]. Moreover, in gliomas, this inhibitor has been shown to be efficient in reducing cell migration and invasion, as well [883,884]. Finally, combining abemaciclib with other inhibitors, one of them being trametinib (MEK inhibitor), synergistically reduced the survival of the RAS-mutant RMS cell line RD. However, when PDX-bearing mice were treated with that combination, they exhibited progressive disease compared to the RMS standard-of-care regimen (irinotecan + vincristine) [885].

**AT-7519**. This is a potent pan-CDK inhibitor, acting on CDK1/2/4/6/9. Preclinical studies have shown a reduction in cell proliferation and induction of cell death in many cell lines, regardless of tumor origin [886–888]. In addition, this inhibitor showed promise for the treatment of MYC-amplified NB, evinced by apoptosis induction in vitro and dose-dependent growth inhibition in PDX, with improved survival and tumor regression in 86% of patients 7 days of treatment initiation [889].

#### 4.5. Polo-Like and Aurora Kinases Inhibitors

**BI-2536**. This is an ATP-competitor dihydropteridinone that has proved to be more than 1000 times more specific for PLK1 than for other kinases [471,890]. This compound has been tested in several tumor cells, although reports for pediatric tumors are more uncommon. Our group showed that this compound reduces proliferation in up to 64% of cases, causes G2/M arrest and induces apoptosis after 24 h of treatment in the SF188 cell line, and it exerts the strongest radiosensitizing effect among all the cell lines tested [891,892]. Anti-mitotic and sensitizing to ionizing radiation effects were also demonstrated by us in MB cells, even though the results were comparable to other PLK1 inhibitors [893]. Others also showed that this compound suppresses self-renewal of patient-derived primary cells with high PLK1 but not low PLK1 expression, and it did not affect the growth of normal neural stem cells. Finally, BI2536 extended survival in MB-bearing mice [487,488]. Sensitizing effects were also observed for hyperthermia in the RB cell lines Y79 and WERI-Rb-1 [894].

With IC<sub>50</sub> lower than 100 nM, BI 3526 was also able to induce cell cycle arrest at the G2/M phase and cell apoptosis in NB cells [492,895,896]. It has recently been proposed that this drug induces cell death by regulating the expression of the minichromosome

maintenance complex components 2 and 10, which are involved in DNA replication and have been associated with poor outcome in other tumors [897].

Perturbation of normal mitotic progression by BI 2536 nanomolar concentrations (10, 50 and 100 nmol/L) also significantly decreased cell proliferation and clonogenic capacity, inducing mitotic arrest and aneuploidy in OS cell lines, resulting in caspase-independent mitotic catastrophe followed by necrosis [898]. Conversely, in another set of OS cell lines, apoptosis induction was validated through PARP cleavage and caspase activation. Irrespective of this, BI 2536-treated xenograft mouse models presented significantly smaller tumors compared with controls [899]. Moreover, in RMS, PLK1 inhibition by BI 2536 led to elevated ubiquitination and rapid proteasomal degradation of the PAX3-FOXO1 chimeric oncoprotein in vitro, whereas it reduced PAX3-FOXO1-mediated gene expression and elicited tumor regression in a xenograft mouse model [900]. Moreover, in this tumor type, this drug presented high antiproliferative activity when combined with Eribulin, a microtubule-interfering drug [901].

**NMS-1286937.** Also known as Onvansertib or NMS-P937, this novel PLK1-specific inhibitor has shown high potency at low nanomolar concentrations on a large number of cell lines, both from solid and hematologic tumors; in addition, differentially from other PLK1 inhibitors that compulsorily need intravenous administration, this small molecule can be administered orally [902]. Considering pediatric tumors, onvansertib has shown promising results in OS and MB. In the former, this drug proved to be highly active in both drug-sensitive and drug-resistant cell lines, except for cell lines overexpressing the multiple-drug-resistant transporter ABCB1 [903]. Results were also very promising in group-3 MB, which is characterized by PLK1 overexpression. In the study, treatment of D341, D425 and D458 cell lines resulted in reduced colony formation, cell proliferation, stem cell renewal and G2/M arrest. The half-maximal inhibitory concentrations varied from 4.9 to 6 nM. Other cell lines within the SHH subgroup needed 27.94 nM for comparable results. Moreover, onvansertib acted as a radiosensitizer, and showed marked time- and dose-dependent growth arrest of neurospheres and patient-derived short-term cultures. Most notably, onvansertib dramatically improved the median survival of orthotopic PDX models from 68 to 95 days [904].

**GSK-461364.** This compound is a second-generation and potent ATP-competitive thiophene amide PLK1 inhibitor. The anti-mitotic effects of this compound have been demonstrated in several tumors; however, it has been observed that its activity can be hampered by the overexpression of the multidrug resistance pump ABCB1 [905]. Preclinical findings in the pediatric setting include reduced viability after treatment in NB, MB and OS, in all of which it diminished growth and caused cell cycle arrest with massive apoptosis at a low-dose nanomolar range [906,907]. This compound also demonstrated a synergistic cytotoxic effect with paclitaxel, even though combination with methotrexate, cisplatin, vinblastine or doxorubicin was not that effective [907]. Conversely, this PLK1 inhibitor has been shown to be an effective radiosensitizer [908]. In vivo, GSK461364 treatment (50 mg/kg body weight intraperitoneally administered) strongly delayed the establishment of high-risk NB tumors in nude mice (by 22 days) irrespective of MYC status of the cell lines used, and significantly increased survival time in the treated group [906].

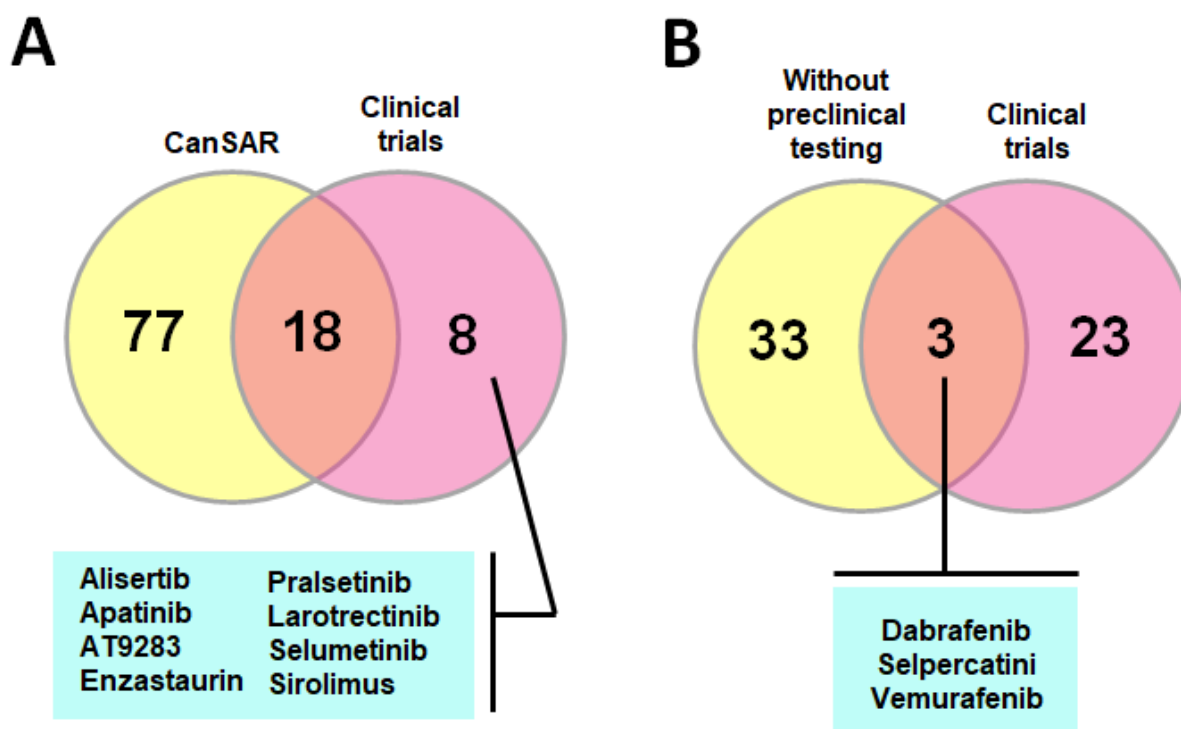
**Volasertib.** This drug, also known as BI 6727, is also a dihydropteridinone derivative that induces a distinct prometaphase arrest phenotype (polo-arrest) and subsequent apoptosis. Regarding pediatric tumors, in 2014, the NCI-supported PPTP Program published initial results about the use of BI 6727 in pediatric tumors. The systematic work presented in vitro results on 24 cell lines that included 4 RMS, 4 EWS, 1 GBM, 4 NB and several leukemias, concluding that the compound was effective without histotype selectivity. Then, the responsiveness of solid tumor xenografts (that also included OS and WT) using a dose of 30 mg/kg for 3 weeks was also tested. Volasertib was able to induce regression in only a minority of the models tested; however, significant differences in EFS distribution compared to control in 59% of the evaluable xenografts were observed, with better results for OS, WT and NB (the only one that showed objective responses) [909]. The results for OS

were later validated in vitro by our research group, where treatment with BI 6727 not only led to growth arrest, triggered apoptosis and radiosensitized cells, but also it seemed to be more efficient in sensitizing OS cells to standard cytotoxics compared with GSK461364 [908]. Anti-mitotic effects were also observed in MB cells [893].

**Aurora kinase inhibitors.** Over the past two decades, several small-molecule inhibitors of Aurora kinases have been developed, most of which primarily target Aurora B. Despite not being approved or with clinical promise by the CanSAR platform, some of these inhibitors have shown promising results. MLN8237, for instance, was evaluated against a panel of EWS ( $n = 11$ ) and NB ( $n = 17$ ) cell lines with acceptable results in vivo [910]. The drug also inhibited growth uniformly in the majority of the cell lines from the PPTP in vitro panel, with  $IC_{50}$  values ranging from 49 nM to 61 nM. In vivo, EFS was 80% higher in treated animals compared to controls, showing even more auspicious results than those obtained for Volasertib [911]. More recently another AURK inhibitor, designated as PHA-680626, disrupted the AURKA/N-Myc, presenting a new alternative for the treatment of high-risk NB [912,913]. Additionally, AMG-900 (pan-aurora inhibitor) blocked MB cell proliferation and increased apoptosis and acted synergistically with the histone deacetylase inhibitor SaHa [914].

### 5. Kinase Inhibitors in Clinical Trials

Clinical trials including children and using kinase inhibitors have been increasingly reported in recent decades. Among the 95 predicted compounds for our selected group of kinases retrieved through the CanSAR platform, for instance, 18 have already entered clinical trials (Figure 6A), most of which have focused on measuring cytotoxic effects on high-risk, refractory and recurrent tumors.



**Figure 6.** (A) Venn diagram showing the number of kinase inhibitors retrieved from the CanSAR platform versus those already tested in clinical trials. Around 30% of the compounds have been tested in patients. Of note, eight kinase inhibitors tested in clinical trials were not found in the CanSAR platform. (B) Venn diagram comparing kinase inhibitors found in the CanSAR platform without evidence of preclinical tests in pediatric cancer versus clinical trials. Three of the drugs are already tested in pediatric patients, without in vitro or in vivo evidence.

In order to gather an updated and comprehensive review on clinical data and outcome of pediatric tumors treated by these new TKIs compounds and already published to date, a PubMed search was performed (as per Oct 2022) using the following uniterms: ((cancer AND (pediatric)) AND (kinase inhibitor)). The following additional filters were set: clinical trial, meta-analysis, randomized controlled trial. In total, 233 articles were retrieved. Abstracts of the whole set of results were carefully read to exclude duplicated data/patients from the same clinical trial, articles where children and/or adolescents (<21 years of age) were not included or where clinical trials not testing kinase inhibitors were retrieved. A total of 53 articles met these inclusion/exclusion criteria, and were read and analyzed in full. Data on study design, study population, main clinical information and outcomes are summarized in Supplementary Table S5. The next part of this section does not review all studies on this subject, and also does not include clinical trials under development or in recruitment with unpublished data. Our main purpose was to gather and to discuss major sedimented data of clinical value and of clinical interest and applicability in this setting.

### 5.1. TRK—Tyrosine Receptor Kinases

#### 5.1.1. EGFR and VEGFR

Abnormal or disrupted angiogenesis is considered to be one of the hallmarks of cancer, and an increasing interest in targeting EGFR and VEGFR pathways has been observed in clinical oncology [915]. Unfortunately, most of these studies are focused on the adult population, and experience with these drugs in pediatric cancer is less robust. Yet, many of these compounds were tested in clinical trials that included children and/or adolescents with cancer, with variable results.

Regarding VEGFR inhibitors, at least three major molecule subtypes have been described. Type I VEGFR inhibitors exert their action as competing molecules to ATP [916]. Some examples of type I VEGFR inhibitors include pazopanib, axitinib, sunitinib, ponatinib and others. Type II inhibitors bind to the inactive “DFG-out” conformation adjacent to the ATP-binding site. Some examples of type II inhibitors include sorafenib and lenvatinib. Type III inhibitors lead to an irreversible binding of kinases at specific sites [917]. In addition, many of these VEGFR inhibitor molecules are under clinical evaluation in association with different inhibitors, particularly immunotherapy [918]. In addition, VEGFR2 inhibitors of dual action against other tumor-associated biomarkers are gaining much attention lately [919].

Inaba et al. (2011) evaluated the combination of sorafenib, a potent multikinase inhibitor, in association with cytarabine and clofarabine to treat relapsed or refractory childhood leukemia [916]. A total of 12 patients (<21 years of age; 11 with acute myeloid leukemia (AML) and one with early T-cell precursor leukemia) entered this phase I study. Of note, complete remission (CR) was obtained in 6 out of 12 patients, CR without complete blood recovery in 2 cases and partial remission (PR) in 1 case. Dermatologic, gastrointestinal (GI), metabolic and infectious adverse events were observed, and were more pronounced in the sorafenib higher-dose stratum. Grade 3 hand–foot skin reactions and/or rash were dose-limiting toxicities (DLTs). Sorafenib was also evaluated in a phase II trial, in association with everolimus to treat patients with progressive and unresectable high-grade osteosarcoma who failed standard treatment [920]. Although some encouraging initial results with sorafenib were observed earlier in this setting, a larger phase II study by Grignani et al. has shown some minor activity for selected cases, and the trial did not reach the 6-month progression-free survival target in at least 50% of patients [920]. Sorafenib was also evaluated in a phase I study that included refractory or relapsed hepatic tumors (hepatoblastoma or HCC) in children. The drug was used in association with irinotecan [921]. Six patients were evaluable for tumor response: two patients survived with no evidence of disease (NOD), one patient was alive with disease (AWD) and two patients DOD upon publication date. Radiation therapy and/or metastasectomies were offered after study protocol based on individual clinical needs. Increased grade 3 or 4 transaminase levels or neutropenia were reported.

Axitinib, a VEGFR1, 2 and 3 inhibitor, was also evaluated in a phase I study that included refractory solid tumors, as part of a Children's Oncology Group (COG) trial and a pilot consortium trial ADVL1315. Nineteen patients were evaluated, with ages ranging from 9 to 17 years. Five patients achieved stable disease (SD), and a PR was observed in one case (an alveolar soft tissue sarcoma). The maximum tolerated dose (MTD) of axitinib was set at 2.4 mg/m<sup>2</sup>/dose [922]. Lenvatinib, a multiple oral tyrosine-kinase inhibitor against VEGFRs 1 to 3, RET, KIT, FGFRs and PDGFR-alpha were evaluated in a phase I/II pediatric and young adult trial for osteosarcomas [631]. The phase I study observed SD (some lasting for 23 weeks) as the best response obtained with Lenvatinib; the phase II study depicted two patients with partial response and thirteen children with SD. Although this single agent showed some activity in osteosarcoma, future studies will focus on the association of Lenvatinib with chemotherapy, or different molecules. Recently (September 2021), the FDA approved the use of cabozantinib for the treatment of patients (>12 years of age) with metastatic or locally advanced differentiated thyroid cancer (DTC), not amenable to receive iodine therapy, and who have failed different TKIs therapies. This approval was mainly achieved as a result of clinical findings of the COSMIC-311 study that observed prolonged progression-free survival in the group receiving the drug compared to the control (placebo) group.

Anti-EGFR therapy to treat pediatric malignancies has been less frequently evaluated in clinical trials. The Children's Oncology Group (COG) evaluated gefitinib, an oral EGFR tyrosine kinase inhibitor, in children with refractory solid tumors [923]. Twenty-five patients were enrolled, and although the drug was well tolerated, only one patient showed partial tumor response in this study cohort. Gefitinib was also evaluated in concomitance to radiotherapy in newly diagnosed children with brainstem gliomas (DIPGs). Forty-three eligible patients entered this study. Although the vast majority of patients experienced rapid and fatal tumor progression, three patients remained free of tumor progression for more than 36 months, pointing to a possible benefit of this approach for a small subset of DIPGs [924].

#### 5.1.2. RET Inhibitors

Recently, RET-altered tumors were considered amenable to receive targeted therapy with RET inhibitors in a tissue-agnostic manner [925]. Vandetanib, a multi-TKI including RET inhibition, was evaluated in association with bortezomib in 22 patients (17 evaluable cases) with medullary thyroid cancer, with 27% showing partial responses [926]. Additionally, selpercatinib was evaluated in 42 patients with RET-fused tumors of different histologies other than lung and thyroid; durable antitumor activity across different tumor subtypes was observed, with only minor adverse effects [927]. Tissue-agnostic benefits of the use of RET inhibitors in patients with RET-fused tumors of different histologies were also confirmed with different drugs, such as Pralsetinib [928].

#### 5.1.3. ALK Inhibitors

A consortium phase I study coordinated by the COG evaluated the use of crizotinib for childhood cancer with refractory solid tumors or anaplastic large-cell lymphomas (ALCL). Seventy-nine children (aged 6 years or older) and adolescents were enrolled; tumor responses were more pronounced among patients with tumors with activating ALK aberrations [929]. In addition, Fukano et al. investigated the role of alectinib in primary refractory ALCL, or after relapsing, in a phase II study that included both children and adults. Eight out of ten enrolled patients responded to alectinib, with minor adverse effects described [930].

Moreover, Entrectinib, a potent CNS-penetrant inhibitor of TRKA/B/C, ROS1 and ALK, was also evaluated to treat children and young adults with solid or primary CNS tumors harboring NTRK, ROS1 or ALK aberrations [730]. In this phase I/II trial, the objective response rate (ORR) was 57.7% among 43 response-evaluable patients. Entrectinib

shows a suitable safety profile and is effective as an option to treat pediatric patients with solid tumors harboring NTRK1/2/3 or ROS1 fusions.

### 5.2. PI3K/AKT/mTOR Pathway

The use of mTOR inhibitors, particularly everolimus, may be considered an important hallmark to treat children (>3 years old) with subependymal giant cell astrocytomas (SEGAs) associated with tuberous sclerosis complex (TSC) and not amenable to surgical treatment. This indication is largely derived from a phase III study (EXIST-1) that evaluated 117 patients in a double-blind placebo controlled trial, showing 50% tumor reduction exclusively in the treatment arm. The most frequent adverse events were oral ulcer and pyrexia; however, there was no treatment discontinuation due to adverse events [931].

### 5.3. MAPK Pathway

Abnormal, disrupted or constitutively activated MAPK pathways are involved in many pediatric cancers, particularly in low-grade gliomas (LGG). Recently, BRAF V600E-mutated tumors in children were eligible for agnostic treatment with BRAF plus MEK inhibitors [932]. Patients were randomized to receive either dabrafenib plus trametinib or standard chemotherapy. Among 110 treated children, complete and partial responses were reached in 47% of patients receiving the targeted therapy versus 11% for patients receiving chemotherapy alone. Of note, the clinical benefit rate, defined as complete, partial and stable disease lasting for more than 24 weeks, was 86% for trametinib plus dabrafenib versus 46% for standard chemotherapy [933]. Monotherapy with the BRAF inhibitor Dabrafenib was also previously evaluated in refractory or relapsed BRAF V600-mutated LGGs in children in a phase I/II study [934]. Among 32 enrolled patients (aged 1 to <18 years), the ORR was 44% and the 1-year PFS was 85%. In addition, adverse events (AE) were described in 91% of the participants; the most frequent AEs were fatigue, skin rash, dry skin and fever.

Disrupted MAPK pathways are also observed in patients with NF-1, where germline pathogenic neurofibromin mutations lead to the abrogation of the repressive function of this protein, with consequent activation of the PI3-K/AKT and RAS/MAPK cell signaling [935]. Besides the augmented frequency of LGG in patients with NF-1, plexiform neurofibromas are also frequently diagnosed in these patients, sometimes with life-threatening clinical consequences. Selumetinib, an MEK inhibitor, was evaluated in patients with symptomatic and inoperable plexiform neurofibromas [936]. Fifty children were enrolled in this phase II study that showed sustained tumor reduction, associated with clinical benefits. Improvements were observed in reducing pain and recovering motor function. However, 5 out of 50 patients discontinued treatment due to adverse effects possibly related to selumetinib, and 6 patients experienced disease progression while receiving the medication.

### 5.4. Cell Cycle Kinases

Ribociclib, an oral CDK4/6 inhibitor with pre-clinical evidence of action in different types of pediatric cancer, was tested either alone or in combination with chemotherapy in phase I and I/II studies, respectively [331,937]. Stable disease was the best response observed for both trials. The most common AEs were hematologic, including neutropenia, anemia and lymphopenia. More recently, palbociclib, a different oral CDK4/6 inhibitor, was evaluated in a phase I study directed at children and adolescents with progressive brain tumors. MTD of palbociclib was set at 75 mg/m<sup>2</sup> (as monotherapy) for 21 days, followed by 7 days without medication. Neutropenia and thrombocytopenia were common AEs; no objective responses were observed among 35 enrolled patients [938].

In addition, different aurora-kinase inhibitors (AKIs) have undergone clinical trials in pediatric cancer. Thirty-seven patients were enrolled in a phase I COG study evaluating MLN8237, a selective AKI-A [939]. Myelosuppression, mucositis and hand-foot skin syndrome were common side effects. One PR and six prolonged SD were observed. AT9283, a different multitarget of AKIs A and B, was evaluated to treat pediatric patients with

different types of solid tumors [940]. Of twenty-three evaluable patients, the authors described one confirmed PR and nine cases of disease stabilization after two courses of AT9283. More recently, Alisertib, a potent AKI-A, was evaluated in the pediatric population with both recurred/refractory solid tumors or leukemia (phase I). Five objective responses were reported, including two complete responses out of one-hundred and thirty-seven evaluable participants [941].

## 6. Final Remarks

Despite improvements, cancer is still responsible for 8% of all disease-related deaths in the pediatric setting [942]. Conventional chemotherapy not only is often ineffective but can also cause long-term complications that hamper the patient's quality of life.

Over the past two decades, precision oncology and the advent of innovator small-molecule drugs or immunotherapy have revolutionized the treatment of many adult cancers, such as CML, GBM and certain types of breast carcinomas [12,943–947]. The tidal increase in genomic, epigenomic, transcriptomic, proteomic and biochemical data has enormously improved our understanding of the specific molecular signatures of pediatric solid tumors, as well as allowing the sub-classification of some tumor types, as is the case of MB and EPN [948], and the application of corresponding specific therapies. Indeed, we are currently in a transition state where the broadly applied decades-old and not always conclusively curative cytotoxic drugs are being gradually substituted by targeted ones, and in the near future, molecular technology will steer diagnosis and personalized treatment [949].

With over 500 kinases in the human genome regulating key biological processes, many members of this molecular family have gained scientific limelight in oncology and academic pharma. Herein, we provided an in-depth review of published data on the roles of the dysregulation of a selected group of kinases in tumor pathophysiology and corroborated their importance as therapeutic candidates in the context of pediatric solid tumors.

By 2020, the FDA had approved 52 small-molecule therapeutics that target nearly 20 different protein kinases (half of them are multikinase inhibitors and the majority target RTKs) [950]. Other drugs targeting an additional 15–20 protein kinases remain in clinical trials worldwide. Nevertheless, a total of 40 target kinases represents only 10% of the kinase superfamily, and most of those kinase-directed drugs have not been tested in pediatric patients. Still, critical challenges must be overcome in experimental oncology and the translation into clinical options. These challenges include the following:

- (1) **Selectivity:** Most inhibitors developed so far target the ATP-binding site, meaning that they may act on multiple targets simultaneously and open new opportunities for the treatment of different tumor histologies [951,952]. Imatinib, for example, which has led to a significant increase in CML survival rates by selectively targeting the tumor-specific protein BCR/ABL, was included for the treatment of gastrointestinal stromal tumors (GIST), which are characterized by KIT-activating mutations [953]. Nevertheless, most inhibitors discovered to date have faced several adversities limiting their clinical use. First of all, the high sequence similarity in the ATP-binding sites frequently results in poor selectivity (refer to Figure 5 and Supplementary Figure S3) that may lead to undesired side effects. Moreover, these small molecules must compete with high intracellular ATP levels, leading to differences in potency when measured *in vivo* by biochemical versus cellular assays. In fact, many compounds inhibit their enzymes at nanomolar concentrations when measured biochemically, but only inhibit tumor cell growth under 3-fold higher concentrations [954]. Nevertheless, the increasing number of recognized kinase-specific structural features has allowed the emergence of superior non-ATP competitive kinase inhibitors that target other allosteric sites, which mostly act by inducing a conformational shift in the target enzyme, depleting its function [951,955–957].
- (2) **Adverse effects:** Imatinib and dasatinib, for instance, are both licensed for the treatment of children with CML. Despite its undeniable benefits, and with the spectrum of

side effects being comparable to what has been reported in adults (i.e., gastrointestinal toxicity, skin rash and muscle cramps), in a growing organism, imatinib treatment impairs longitudinal growth through the disturbance of osseous remodeling and inhibition of growth hormone secretion, which raises concerns about its lifelong use [958]. Moreover, despite the wealth of compounds that emerge on a daily basis, showing selectivity, potency and favorable pharmacological profiles, the probabilities for the translation into effective patient treatment for the great majority of them are extremely low. In this regard, less than 30% of the compounds approved or with clinical promise retrieved from the CanSAR platform have entered clinical trials in the pediatric setting (refer to Figure 6A). PLK1 inhibitors, for instance, despite the robust results obtained *in vitro* and *in vivo*, have demonstrated poor applicability due to severe hematological toxicity [959].

- (3) **Mutational burden and lack of predictive biomarkers:** As stated before, the mutational identity may vary between adult and pediatric cancer, a feature that reflects in treatment response. Current treatments targeting ALK mutations in other cancers, for example, have not shown significant efficacy against NB. In this tumor, two hotspot mutations, at positions R1275Q and F1174L, occur in a high proportion of patients; tumors harboring the first are highly sensitive to crizotinib, while tumors bearing the second are resistant [960–962]. Moreover, as suggested by Bellantoni and Wagner (2021), childhood solid tumors may have fewer potentially targetable mutations, evinced by the inhibition of RTK for the treatment of OS, where it is necessary to target several relevant RTKs simultaneously to achieve desirable results [821]. Therefore, ground-breaking drugs for adult cancer may not be effective in the pediatric setting. In parallel, inhibitors are not effective if the target is not essential to drive tumor growth or does not represent a prognostic factor, as is the case of ROCK kinases. Even though these proteins have gained popularity and progressively been researched as targets for the development of novel anti-cancer drugs due to their association with metastasis and poorer patient survival in adult tumors, the influence of both isoforms on the prognosis of childhood cancer remains controversial [963].
- (4) **Intrinsic and acquired resistance:** Resistance to targeted therapies is considered a largely inevitable hurdle that has a substantial impact on patients. Refractoriness to chemotherapy due to acquired F1174S ALK mutation in NB has been reported [964]. Likewise, the location of EGFR mutations significantly changes the effectiveness of EGFR; several mutations conferring resistance to EGFR tyrosine kinase inhibitors (such as T790M, L833V, A839T, V851I, A871T and G873E) have been reported [938]. Other examples include inadequate response to imatinib due to BCR-ABL1 kinase domain mutations that impart varying degrees of drug insensitivity, observed as underlying mechanism in 5–10% of adults and children with CML, bypassing pathway activation [965,966]. Moreover, despite an initial benefit of the targeted drug in molecularly well-defined tumors, patients inevitably experience tumor progression due to the development of resistance (i.e., Crizotinib in ALK-rearranged NSCLC population and CNS relapses) [967].
- (5) **Lack of compounds designed specifically for childhood tumors:** In general, few pediatric patients with cancer are enrolled in clinical trials. The perception that adult studies can be generalized to children with similar diseases is a major obstacle. Consequently, most treatments are based on modifications of previously approved regimes for the adult population, and many compounds enter clinical trials without preclinical testing in pediatric oncology (refer to Figure 6B), which is mandatory to obtain a more accurate interpretation of its possible therapeutic potential in a certain cancer entity [968]. Moreover, pediatric cancer is rare, and even among patients with the same cancer type, there is often broad heterogeneity in terms of prognosis, molecular features or pathology. Therefore, few institutions have sufficient patients and the chances of every potential agent or combination being tested are reduced. Even so, priorities for funding are typically assessed according to the “burden of



illness” for diseases, which is traditionally determined by disease frequency and mortality rate, leading to reluctance to distribute limited research funding to pediatric trials [969–971].

Regardless of the above challenges, kinase-based drug discovery has attained dramatic growth in the past 20 years. Although kinase inhibition represents a young therapeutic strategy compared with other traditional tactics, the FDA has approved a median of almost two small-molecule kinase inhibitors per year [952]. Thus, increasing numbers of targeted therapies are being tested for pediatric cancers, and many have shown undeniable success. Besides, the inhibition of kinases in normal cells can be clinically tolerated, presenting a therapeutic window that allows the softening of the acute side effects that generally lead to refusal and abandonment of treatment [972].

Moreover, as research advances, it has become clear that kinase inhibitors do not have to be absolutely selective. Crizotinib, for instance, was initially developed as an MET inhibitor, but later it was found to be even more efficient in cancers with ALK rearrangements. Additionally, molecularly targeted therapies are proving to be more effective in combination regimes to completely shut down the dysregulated pathway. As an example, it has been shown that everolimus improves CNS retention of vandetanib, dasatinib and sorafenib, which may have a great impact on the treatment of CNS tumors or brain metastases [751,752]. In the same vein, third- or fourth-generation inhibitors are being developed to avoid resistance and improve other biopharmaceutical properties such as brain penetration. These inhibitors, coupled with the increased ability to characterize tumors on molecular and genomic levels, will not only enable treatment refinement by identifying which patients may benefit most, but in the near future may conquer many diseases that are currently incurable.

**Supplementary Materials:** The following supporting information can be downloaded at: <https://www.mdpi.com/article/10.3390/pharmaceutics15020664/s1>, Figure S1: Flowchart depicting the identification of databases used in the present study, describing the number originally identified, included and excluded, and the reasons for exclusions; Figure S2: Flowchart representing kinases of interest analysis in cell line dependency score and the identification of inhibitors, preclinical studies and clinical test describing the number originally identified, included and excluded, and the reasons for exclusions; Figure S3: Schematic illustrations of kinases druggability identified by the CanSAR database in the other kinase families, including the total number of compounds with predicted interaction capacity with each kinase, as well as FDA-approved drugs, and clinical candidates. Interaction networks of kinase inhibitors and associated binding proteins according to STITCH (‘search tool for interactions of chemicals’). Compounds are represented as pill-shaped nodes, while proteins are shown as spheres. Small nodes represent proteins of unknown 3D structures, while large nodes show proteins with known or predicted structures. Nodes that are associated to each other are linked by an edge: thicker lines represent stronger binding affinities. Networks were constructed considering a minimum required interaction score of 0.700, and based on associations reported in Curated Databases (gray lines), or on both Databases and Experimental/Biochemical Data (green lines). Purple lines represent functional links between proteins; Table S1: Differential expression of kinases (pediatric tumors vs normal tissue); Table S2: Kinase expression and clinical features; Table S3: DepMap scores; Table S4: preclinical data; Table S5: Clinical trials.

**Author Contributions:** Conceptualization, funding acquisition, figures design, review and editing, M.S.B.; project administration M.F.C.; formal analysis, investigation, data curation, writing—original draft preparation M.F.C., M.M., L.C.V., D.B., K.L.O., J.A.P., E.T.V. and M.S.B. All authors have read and agreed to the published version of the manuscript.

**Funding:** This research was in part supported by Coordenação de Aperfeiçoamento de Pessoal de Nível Superior (CAPES—001) and CNPq—Bolsas de Produtividade em Pesquisa.

**Institutional Review Board Statement:** Not applicable.

**Informed Consent Statement:** Patient consent does not apply to this study.

**Data Availability Statement:** Not applicable.

**Conflicts of Interest:** The authors declare no conflict of interests.

## References

1. Steliarova-Foucher, E.; Stiller, C.; Lacour, B.; Kaatsch, P. International Classification of Childhood Cancer, third edition. *Cancer* **2005**, *103*, 1457–1467. [CrossRef] [PubMed]
2. Instituto Nacional de Câncer (Brazil). *Coordenação de Prevenção e Vigilância and Sociedade Brasileira de Oncologia Pediátrica, Câncer na Criança e no Adolescente no Brasil: Dados dos Registros de Base Populacional e de Mortalidade*; Ministério da Saúde, Instituto Nacional de Câncer–INCA: Brasília, Brazil, 2008.
3. Downing, J.R.; Wilson, R.K.; Zhang, J.; Mardis, E.R.; Pui, C.-H.; Ding, L.; Ley, T.J.; E Evans, W. The Pediatric Cancer Genome Project. *Nat. Genet.* **2012**, *44*, 619–622. [CrossRef] [PubMed]
4. Toren, A.; Rechavi, G.; Ramot, B. Pediatric Cancer: Environmental and Genetic Aspects. *Pediatr. Hematol. Oncol.* **1996**, *13*, 319–331. [CrossRef] [PubMed]
5. Verma, V.; Denniston, K.A.; Lin, C.; Lin, C. A Comparison of Pediatric vs. Adult Patients with the Ewing Sarcoma Family of Tumors. *Front. Oncol.* **2017**, *7*, 82. [CrossRef]
6. Sultan, I.; Qaddoumi, I.; Yaser, S.; Rodriguez-Galindo, C.; Ferrari, A. Comparing Adult and Pediatric Rhabdomyosarcoma in the Surveillance, Epidemiology and End Results Program, 1973 to 2005: An Analysis of 2,600 Patients. *J. Clin. Oncol.* **2009**, *27*, 3391–3397. [CrossRef]
7. Spector, L.; Brown, M.B.; Wantman, E.; Letterie, G.S.; Toner, J.P.; Doody, K.; Ginsburg, E.; Williams, M.; Koch, L.; Schymura, M.J.; et al. Association of In Vitro Fertilization With Childhood Cancer in the United States. *JAMA Pediatr.* **2019**, *173*, e190392. [CrossRef]
8. Rahal, Z.; Abdulhai, F.; Kadara, H.; Saab, R. Genomics of adult and pediatric solid tumors. *Am. J. Cancer Res.* **2018**, *8*, 1356–1386.
9. Gröbner, S.N.; Worst, B.C.; Weischenfeldt, J.; Buchhalter, I.; Kleinheinz, K.; Rudneva, V.A.; Johann, P.D.; Balasubramanian, G.P.; Segura-Wang, M.; Brabetz, S.; et al. The landscape of genomic alterations across childhood cancers. *Nature* **2018**, *555*, 321–327. [CrossRef]
10. Sweet-Cordero, E.A.; Biegel, J.A. The genomic landscape of pediatric cancers: Implications for diagnosis and treatment. *Science* **2019**, *363*, 1170–1175. [CrossRef]
11. Vellichirammal, N.N.; Chaturvedi, N.K.; Joshi, S.S.; Coulter, D.W.; Guda, C. Fusion genes as biomarkers in pediatric cancers: A review of the current state and applicability in diagnostics and personalized therapy. *Cancer Lett.* **2020**, *499*, 24–38. [CrossRef]
12. The Cancer Genome Atlas Research Network. Comprehensive genomic characterization defines human glioblastoma genes and core pathways. *Nature* **2008**, *455*, 1061–1068. [CrossRef]
13. Schwartzentruber, J.; Korshunov, A.; Liu, X.-Y.; Jones, D.T.W.; Pfaff, E.; Jacob, K.; Sturm, D.; Fontebasso, A.M.; Khuong-Quang, D.-A.; Tönjes, M.; et al. Driver mutations in histone H3.3 and chromatin remodelling genes in paediatric glioblastoma. *Nature* **2012**, *482*, 226–231. [CrossRef]
14. Paugh, B.S.; Qu, C.; Jones, C.; Liu, Z.; Adamowicz-Brice, M.; Zhang, J.; Bax, D.A.; Coyle, B.; Barrow, J.; Hargrave, D.; et al. Integrated Molecular Genetic Profiling of Pediatric High-Grade Gliomas Reveals Key Differences With the Adult Disease. *J. Clin. Oncol.* **2010**, *28*, 3061–3068. [CrossRef]
15. Appay, R.; Fina, F.; Macagno, N.; Padovani, L.; Colin, C.; Baretts, D.; Ordioni, J.; Scavarda, D.; Giangaspero, F.; Badiali, M.; et al. Duplications of KIAA1549 and BRAF screening by Droplet Digital PCR from formalin-fixed paraffin-embedded DNA is an accurate alternative for KIAA1549-BRAF fusion detection in pilocytic astrocytomas. *Mod. Pathol.* **2018**, *31*, 1490–1501. [CrossRef]
16. Fukuoka, K.; on behalf of the Japan Pediatric Molecular Neuro-Oncology Group (JPMNG); Kanemura, Y.; Shofuda, T.; Fukushima, S.; Yamashita, S.; Narushima, D.; Kato, M.; Honda-Kitahara, M.; Ichikawa, H.; et al. Significance of molecular classification of ependymomas: C11orf95-RELA fusion-negative supratentorial ependymomas are a heterogeneous group of tumors. *Acta Neuropathol. Commun.* **2018**, *6*, 134. [CrossRef]
17. Wachtel, M.; Schäfer, B.W. PAX3-FOXO1: Zooming in on an “undruggable” target. *Semin. Cancer Biol.* **2018**, *50*, 115–123. [CrossRef]
18. Giovannini, M.; Biegel, J.A.; Serra, M.; Wang, J.Y.; Wei, Y.H.; Nycum, L.; Emanuel, B.S.; Evans, G.A. EWS-erg and EWS-Fli1 fusion transcripts in Ewing’s sarcoma and primitive neuroectodermal tumors with variant translocations. *J. Clin. Investig.* **1994**, *94*, 489–496. [CrossRef]
19. Jemal, A.; Murray, T.; Samuels, A.; Ghafoor, A.; Ward, E.; Thun, M.J. Cancer Statistics, 2003. *CA A Cancer J. Clin.* **2003**, *53*, 5–26. [CrossRef]
20. Pui, C.-H. Recent Research Advances in Childhood Acute Lymphoblastic Leukemia. *J. Formos. Med. Assoc.* **2010**, *109*, 777–787. [CrossRef]
21. Pezuk, J.A.; Valera, E.T.; Brassesco, M.S. PLK1 Inhibition: Prospective Role for the Treatment of Pediatric Tumors. *Curr. Drug Targets* **2016**, *17*, 1661–1672. [CrossRef]
22. Manning, G.; Whyte, D.B.; Martinez, R.; Hunter, T.; Sudarsanam, S. The Protein Kinase Complement of the Human Genome. *Science* **2002**, *298*, 1912–1934. [CrossRef] [PubMed]
23. Theivendren, P.; Kunjiappan, S.; Hegde, Y.M.; Vellaichamy, S.; Gopal, M.; Dhramalingam, S.R.; Kumar, S. Importance of Protein Kinase and Its Inhibitor: A Review. *Protein Kinases-Promis Targets Anticance. Drug Res. IntechOpen Ser. Biochem.* **2021**, *24*, 75–100. [CrossRef]

24. Alberts, B.; Johnson, A.; Lewis, J.; Raff, M.; Roberts, K.; Walter, P. *Bruce Alberts, Molecular Biology of the Cell*, 4th ed.; Garland Science: New York, NY, USA, 2002.
25. Turdo, A.; D'Accardo, C.; Glaviano, A.; Porcelli, G.; Colarossi, C.; Colarossi, L.; Mare, M.; Faldetta, N.; Modica, C.; Pistone, G.; et al. Targeting Phosphatases and Kinases: How to Checkmate Cancer. *Front. Cell Dev. Biol.* **2021**, *9*, 690306. [CrossRef] [PubMed]
26. Giamas, G.; Man, Y.L.; Hirner, H.; Bischof, J.; Kramer, K.; Khan, K.; Ahmed, S.S.L.; Stebbing, J.; Knippschild, U. Kinases as targets in the treatment of solid tumors. *Cell Signal.* **2010**, *22*, 984–1002. [CrossRef]
27. Armstrong, H.; Bording-Jorgensen, M.; Dijk, S.; Wine, E. The Complex Interplay between Chronic Inflammation, the Microbiome, and Cancer: Understanding Disease Progression and What We Can Do to Prevent It. *Cancers* **2018**, *10*, 83. [CrossRef]
28. Das, S.; Bhattacharya, B.; Das, B.; Sinha, B.; Jamatia, T.; Paul, K. Etiologic Role of Kinases in the Progression of Human Cancers and Its Targeting Strategies. *Indian J. Surg. Oncol.* **2019**, *12*, 34–45. [CrossRef]
29. McKay, M.M.; Morrison, D.K. Integrating signals from RTKs to ERK/MAPK. *Oncogene* **2007**, *26*, 3113–3121. [CrossRef]
30. Hubbard, S.R.; Miller, W.T. Receptor tyrosine kinases: Mechanisms of activation and signaling. *Curr. Opin. Cell Biol.* **2007**, *19*, 117–123. [CrossRef]
31. Lemmon, M.A.; Schlessinger, J. Cell Signaling by Receptor Tyrosine Kinases. *Cell* **2010**, *141*, 1117–1134. [CrossRef]
32. Ullrich, A.; Schlessinger, J. Signal transduction by receptors with tyrosine kinase activity. *Cell* **1990**, *61*, 203–212. [CrossRef]
33. Popovic, N.; Wilson, E. Cell Surface Receptors. In *Comprehensive Toxicology*; Elsevier: Amsterdam, The Netherlands, 2010; pp. 81–91. [CrossRef]
34. Paul, M.K.; Mukhopadhyay, A.K. Tyrosine kinase—Role and significance in Cancer. *Int. J. Med. Sci.* **2004**, *1*, 101–115. [CrossRef]
35. Schmidt-Arras, D.; Böhmer, F.-D. Mislocalisation of Activated Receptor Tyrosine Kinases—Challenges for Cancer Therapy. *Trends Mol. Med.* **2020**, *26*, 833–847. [CrossRef]
36. Bhargava, R.; Gerald, W.L.; Li, A.R.; Pan, Q.; Lal, P.; Ladanyi, M.; Chen, B. EGFR gene amplification in breast cancer: Correlation with epidermal growth factor receptor mRNA and protein expression and HER-2 status and absence of EGFR-activating mutations. *Mod. Pathol.* **2005**, *18*, 1027–1033. [CrossRef]
37. Drilon, A.; Cappuzzo, F.; Ou, S.-H.I.; Camidge, D.R. Targeting MET in Lung Cancer: Will Expectations Finally Be MET? *J. Thorac. Oncol.* **2017**, *12*, 15–26. [CrossRef]
38. Katoh, M. Fibroblast growth factor receptors as treatment targets in clinical oncology. *Nat. Rev. Clin. Oncol.* **2018**, *16*, 105–122. [CrossRef]
39. Helsten, T.; Elkin, S.; Arthur, E.; Tomson, B.N.; Carter, J.; Kurzrock, R. The FGFR Landscape in Cancer: Analysis of 4,853 Tumors by Next-Generation Sequencing. *Clin. Cancer Res.* **2016**, *22*, 259–267. [CrossRef]
40. Liu, G.; Chen, T.; Ding, Z.; Wang, Y.; Wei, Y.; Wei, X. Inhibition of FGF-FGFR and VEGF-VEGFR signalling in cancer treatment. *Cell Prolif.* **2021**, *54*, e13009. [CrossRef]
41. Ryall, S.; Tabori, U.; Hawkins, C. Pediatric low-grade glioma in the era of molecular diagnostics. *Acta Neuropathol. Commun.* **2020**, *8*, 30. [CrossRef]
42. Rivera, B.; Gayden, T.; Carrot-Zhang, J.; Nadaf, J.; Boshari, T.; Faury, D.; Zeinieh, M.; Blanc, R.; Burk, D.L.; Fahiminiya, S.; et al. Germline and somatic FGFR1 abnormalities in dysembryoplastic neuroepithelial tumors. *Acta Neuropathol.* **2016**, *131*, 847–863. [CrossRef]
43. Valera, E.T.; McConechy, M.K.; Gayden, T.; Rivera, B.; Jones, D.T.W.; Wittmann, A.; Han, H.; Bareke, E.; Nikbakht, H.; Mikael, L.; et al. Methylation analysis and whole-exome sequencing reveal that brain tumors associated with encephalocraniocutaneous lipomatoses are midline pilocytic astrocytomas. *Acta Neuropathol.* **2018**, *136*, 657–660. [CrossRef]
44. Amary, M.F.; Ye, H.; Berisha, F.; Khatri, B.; Forbes, G.; Lehovsky, K.; Frezza, A.M.; Behjati, S.; Tarpey, P.; Pillay, N.; et al. Fibroblastic growth factor receptor 1 amplification in osteosarcoma is associated with poor response to neo-adjuvant chemotherapy. *Cancer Med.* **2014**, *3*, 980–987. [CrossRef] [PubMed]
45. Kim, J.-A.; Berlow, N.E.; Lathara, M.; Bharathy, N.; Martin, L.R.; Purohit, R.; Cleary, M.M.; Liu, Q.; Michalek, J.E.; Srinivasa, G.; et al. Sensitization of osteosarcoma to irradiation by targeting nuclear FGFR1. *Biochem. Biophys. Res. Commun.* **2022**, *621*, 101–108. [CrossRef] [PubMed]
46. Ogura, K.; Elkrif, A.; Bowman, A.S.; Koche, R.P.; de Stanchina, E.; Benayed, R.; Mauguen, A.; Mattar, M.S.; Khodos, I.; Meyers, P.A.; et al. Prospective Clinical Genomic Profiling of Ewing Sarcoma: *ERF* and *FGFR1* Mutations as Recurrent Secondary Alterations of Potential Biologic and Therapeutic Relevance. *JCO Precis. Oncol.* **2022**, *6*, e2200048. [CrossRef] [PubMed]
47. Agelopoulos, K.; Richter, G.H.; Schmidt, E.; Dirksen, U.; von Heyking, K.; Moser, B.; Klein, H.-U.; Kontny, U.; Dugas, M.; Poos, K.; et al. Deep Sequencing in Conjunction with Expression and Functional Analyses Reveals Activation of FGFR1 in Ewing Sarcoma. *Clin. Cancer Res.* **2015**, *21*, 4935–4946. [CrossRef]
48. Rakheja, D.; Park, J.Y.; Yang, M.S.; Martinez, D.P.; Koduru, P.; Wilson, K.S.; Garcia, R.; Uddin, N. Rhabdomyosarcoma With Epithelioid Features And *NSD3::FOXO1* Fusion: Evidence For Reconsideration Of Previously Reported *FOXO1::FGFR1* Fusion. *Int. J. Surg. Pathol.* **2022**. [CrossRef]
49. Goldstein, M.; Meller, I.; Orr-Urtreger, A. FGFR1 over-expression in primary rhabdomyosarcoma tumors is associated with hypomethylation of a 5' CpG Island and abnormal expression of the AKT1, NOG, and BMP4 genes. *Genes Chromosom. Cancer* **2007**, *46*, 1028–1038. [CrossRef]

50. Gasparini, P.; Fortunato, O.; De Cecco, L.; Casanova, M.; Iannó, M.F.; Carenzo, A.; Centonze, G.; Milione, M.; Collini, P.; Boeri, M.; et al. Age-Related Alterations in Immune Contexture Are Associated with Aggressiveness in Rhabdomyosarcoma. *Cancers* **2019**, *11*, 1380. [CrossRef]
51. Missiaglia, E.; Selfe, J.; Pritchard-Jones, K.; Kool, M.; Shipley, J.; Hamdi, M.; Williamson, D.; Schaaf, G.; Fang, C.; Koster, J.; et al. Genomic imbalances in rhabdomyosarcoma cell lines affect expression of genes frequently altered in primary tumors: An approach to identify candidate genes involved in tumor development. *Genes Chromosom. Cancer* **2009**, *48*, 455–467. [CrossRef]
52. Lehtinen, B.; Raita, A.; Kesseli, J.; Annala, M.; Nordfors, K.; Yli-Harja, O.; Zhang, W.; Visakorpi, T.; Nykter, M.; Haapasalo, H.; et al. Clinical association analysis of ependymomas and pilocytic astrocytomas reveals elevated FGFR3 and FGFR1 expression in aggressive ependymomas. *BMC Cancer* **2017**, *17*, 310. [CrossRef]
53. Cimmino, F.; Montella, A.; Tirelli, M.; Avitabile, M.; Lasorsa, V.A.; Visconte, F.; Cantalupo, S.; Maiorino, T.; De Angelis, B.; Morini, M.; et al. FGFR1 is a potential therapeutic target in neuroblastoma. *Cancer Cell Int.* **2022**, *22*, 174. [CrossRef]
54. Schmelz, K.; Toedling, J.; Huska, M.; Cwikla, M.C.; Kruetzfeldt, L.-M.; Proba, J.; Ambros, P.F.; Ambros, I.M.; Boral, S.; Lodrini, M.; et al. Spatial and temporal intratumour heterogeneity has potential consequences for single biopsy-based neuroblastoma treatment decisions. *Nat. Commun.* **2021**, *12*, 6804. [CrossRef] [PubMed]
55. Nobusawa, S.; Hirato, J.; Yokoo, H. Molecular genetics of ependymomas and pediatric diffuse gliomas: A short review. *Brain Tumor Pathol.* **2014**, *31*, 229–233. [CrossRef] [PubMed]
56. Park, S.-H.; Won, J.; Kim, S.-I.; Lee, Y.; Park, C.-K.; Kim, S.-K.; Choi, S.-H. Molecular Testing of Brain Tumor. *J. Pathol. Transl. Med.* **2017**, *51*, 205–223. [CrossRef] [PubMed]
57. Georgiou, V.; Gkretsi, V. The role of fibroblast growth factors and their receptors in gliomas: The mutations involved. *Rev. Neurosci.* **2018**, *30*, 543–554. [CrossRef]
58. Vega, J.E.V.; Brat, D.J. Incorporating Advances in Molecular Pathology Into Brain Tumor Diagnostics. *Adv. Anat. Pathol.* **2018**, *25*, 143–171. [CrossRef]
59. Jimenez-Pascual, A.; Siebzehnruhl, F.A. Fibroblast Growth Factor Receptor Functions in Glioblastoma. *Cells* **2019**, *8*, 715. [CrossRef]
60. Ohashi, R.; Matsuda, Y.; Ishiwata, T.; Naito, Z. Downregulation of fibroblast growth factor receptor 2 and its isoforms correlates with a high proliferation rate and poor prognosis in high-grade glioma. *Oncol. Rep.* **2014**, *32*, 1163–1169. [CrossRef]
61. Yan, Y.; Li, Z.; Zeng, S.; Wang, X.; Gong, Z.; Xu, Z. FGFR2-mediated phosphorylation of PTEN at tyrosine 240 contributes to the radioresistance of glioma. *J. Cell Commun. Signal.* **2019**, *13*, 279–280. [CrossRef]
62. Salm, F.; Cwiek, P.; Ghosal, A.; Buccarello, A.L.; Largey, F.; Wotzkow, C.; Höland, K.; Styp-Rekowska, B.; Djonov, V.; Zlobec, I.; et al. RNA interference screening identifies a novel role for autocrine fibroblast growth factor signaling in neuroblastoma chemoresistance. *Oncogene* **2012**, *32*, 3944–3953. [CrossRef]
63. Kumar, K.S.; Neve, A.; Stucklin, A.S.G.; Kuzan-Fischer, C.M.; Rushing, E.J.; Taylor, M.D.; Tripolitsioti, D.; Behrmann, L.; Kirschenbaum, D.; Grotzer, M.; et al. TGF- $\beta$  Determines the Pro-migratory Potential of bFGF Signaling in Medulloblastoma. *Cell Rep.* **2018**, *23*, 3798–3812.e8. [CrossRef]
64. Vignovich, J.; Becker, D. Expression of BFGF and differential expression of FGF receptors in normal human myoblasts and rhabdomyosarcomas. *Int. J. Oncol.* **1993**, *2*, 637–642. [CrossRef]
65. Hirotsu, M.; Setoguchi, T.; Matsunoshita, Y.; Sasaki, H.; Nagao, H.; Gao, H.; Sugimura, K.; Komiya, S. Tumour formation by single fibroblast growth factor receptor 3-positive rhabdomyosarcoma-initiating cells. *Br. J. Cancer* **2009**, *101*, 2030–2037. [CrossRef]
66. Sahu, D.K.; Singh, N.; Das, M.; Rawat, J.; Gupta, D.K. Differential expression profiling of onco and tumor-suppressor genes from major-signaling pathways in Wilms' tumor. *Pediatr. Surg. Int.* **2022**, *38*, 1601–1617. [CrossRef]
67. Kostopoulou, O.N.; Holzhauser, S.; Lange, B.; Ohmayer, A.; Andonova, T.; Bersani, C.; Dalianis, T. Analyses of FGFR3 and PIK3CA mutations in neuroblastomas and the effects of the corresponding inhibitors on neuroblastoma cell lines. *Int. J. Oncol.* **2019**, *55*, 1372–1384. [CrossRef]
68. Ahrendsen, J.T.; Sinai, C.; Meredith, D.M.; Malinowski, S.W.; Cooney, T.M.; Bandopadhyay, P.; Ligon, K.L.; Alexandrescu, S. Molecular Alterations in Pediatric Low-Grade Gliomas That Led to Death. *J. Neuropathol. Exp. Neurol.* **2021**, *80*, 1052–1059. [CrossRef]
69. Johnson, A.; Severson, E.; Gay, L.; Vergilio, J.-A.; Elvin, J.; Suh, J.; Daniel, S.; Covert, M.; Frampton, G.M.; Hsu, S.; et al. Comprehensive Genomic Profiling of 282 Pediatric Low- and High-Grade Gliomas Reveals Genomic Drivers, Tumor Mutational Burden, and Hypermutation Signatures. *Oncologist* **2017**, *22*, 1478–1490. [CrossRef]
70. Frattini, V.; Pagnotta, S.M.; Tala, J.J.; Russo, M.V.; Lee, S.B.; Garofano, L.; Zhang, J.; Shi, P.; Lewis, G.; et al. A metabolic function of FGFR3-TACC3 gene fusions in cancer. *Nature* **2018**, *553*, 222–227. [CrossRef]
71. Kamura, S.; Matsumoto, Y.; Fukushi, J.-I.; Fujiwara, T.; Iida, K.; Okada, Y.; Iwamoto, Y. Basic fibroblast growth factor in the bone microenvironment enhances cell motility and invasion of Ewing's sarcoma family of tumours by activating the FGFR1-PI3K-Rac1 pathway. *Br. J. Cancer* **2010**, *103*, 370–381. [CrossRef]
72. Lee, S.; Lim, S.; Cho, D. Personalized genomic analysis based on circulating tumor cells of extra-skeletal Ewing sarcoma of the uterus: A case report of a 16-year-old Korean female. *Exp. Ther. Med.* **2018**, *16*, 1343–1349. [CrossRef]
73. Li, Z.; Dou, P.; Liu, T.; He, S. Application of Long Noncoding RNAs in Osteosarcoma: Biomarkers and Therapeutic Targets. *Cell. Physiol. Biochem.* **2017**, *42*, 1407–1419. [CrossRef]

74. Ren, T.; Qing, Y.; Dai, N.; Li, M.; Qian, C.; Yang, Y.; Cheng, Y.; Li, Z.; Zhang, S.; Zhong, Z.; et al. Apurinic/aprimidinic endonuclease 1 induced upregulation of fibroblast growth factor 2 and its receptor 3 induces angiogenesis in human osteosarcoma cells. *Cancer Sci.* **2014**, *105*, 186–194. [CrossRef] [PubMed]
75. Bi, Y.; Jing, Y.; Cao, Y. Overexpression of miR-100 inhibits growth of osteosarcoma through FGFR3. *Tumor Biol.* **2015**, *36*, 8405–8411. [CrossRef]
76. Gabler, L.; Jaunecker, C.N.; Katz, S.; van Schoonhoven, S.; Englinger, B.; Pirker, C.; Mohr, T.; Vician, P.; Stojanovic, M.; Woitzuck, V.; et al. Fibroblast growth factor receptor 4 promotes glioblastoma progression: A central role of integrin-mediated cell invasiveness. *Acta Neuropathol. Commun.* **2022**, *10*, 65. [CrossRef] [PubMed]
77. Hao, X.; Guo, Z.; Sun, H.; Liu, X.; Zhang, Y.; Zhang, L.; Sun, W.; Tian, Y. Urinary protein biomarkers for pediatric medulloblastoma. *J. Proteom.* **2020**, *225*, 103832. [CrossRef] [PubMed]
78. El Demellawy, D.; McGowan-Jordan, J.; de Nanassy, J.; Chernetsova, E.; Nasr, A. Update on molecular findings in rhabdomyosarcoma. *Pathology* **2017**, *49*, 238–246. [CrossRef] [PubMed]
79. Taylor Vi, J.G.T.; Cheuk, A.T.; Tsang, P.S.; Chung, J.-Y.; Song, Y.K.; Desai, K.; Yu, Y.; Chen, Q.-R.; Shah, K.; Youngblood, V.; et al. Identification of FGFR4-activating mutations in human rhabdomyosarcomas that promote metastasis in xenotransplanted models. *J. Clin. Investig.* **2009**, *119*, 3395–3407. [CrossRef]
80. Wesche, J.; Haglund, K.; Haugsten, E.M. Fibroblast growth factors and their receptors in cancer. *Biochem. J.* **2011**, *437*, 199–213. [CrossRef]
81. Baird, K.; Davis, S.; Antonescu, C.R.; Harper, U.L.; Walker, R.L.; Chen, Y.; Glatfelter, A.A.; Duray, P.H.; Meltzer, P.S. Gene Expression Profiling of Human Sarcomas: Insights into Sarcoma Biology. *Cancer Res* **2005**, *65*, 9226–9235. [CrossRef]
82. Cao, L.; Yu, Y.; Bilke, S.; Walker, R.L.; Mayeenuddin, L.H.; Azorsa, D.O.; Yang, F.; Pineda, M.; Helman, L.J.; Meltzer, P.S. Genome-Wide Identification of PAX3-FKHR Binding Sites in Rhabdomyosarcoma Reveals Candidate Target Genes Important for Development and Cancer. *Cancer Res* **2010**, *70*, 6497–6508. [CrossRef]
83. Shern, J.F.; Chen, L.; Chmielecki, J.; Wei, J.S.; Patidar, R.; Rosenberg, M.; Ambrogio, L.; Auclair, D.; Wang, J.; Song, Y.K.; et al. Comprehensive genomic analysis of rhabdomyosarcoma reveals a landscape of alterations affecting a common genetic axis in fusion-positive and fusion-negative tumors. *Cancer Discov.* **2014**, *4*, 216–231. [CrossRef]
84. Ramadan, F.; Fahs, A.; Ghayad, S.E.; Saab, R. Signaling pathways in Rhabdomyosarcoma invasion and metastasis. *Cancer Metastasis Rev.* **2020**, *39*, 287–301. [CrossRef]
85. Whittle, S.B.; Reyes, S.; Du, M.; Gireud-Goss, M.; Zhang, L.; Woodfield, S.E.; Ittmann, M.; Scheurer, M.; Bean, A.J.; Zage, P.E. A Polymorphism in the FGFR4 Gene Is Associated With Risk of Neuroblastoma and Altered Receptor Degradation. *J. Pediatr. Hematol.* **2016**, *38*, 131–138. [CrossRef]
86. Sugiyama, N.; Varjosalo, M.; Meller, P.; Lohi, J.; Chan, K.M.; Zhou, Z.; Alitalo, K.; Taipale, J.; Keski-Oja, J.; Lehti, K. FGF receptor-4 (FGFR4) polymorphism acts as an activity switch of a membrane type 1 matrix metalloproteinase–FGFR4 complex. *Proc. Natl. Acad. Sci. USA* **2010**, *107*, 15786–15791. [CrossRef]
87. Hajjo, R.; Sweidan, K. Review on Epidermal Growth Factor Receptor (EGFR) Structure, Signaling Pathways, Interactions, and Recent Updates of EGFR Inhibitors. *Curr. Top. Med. Chem.* **2020**, *20*, 815–834. [CrossRef]
88. Nicholson, R.; Gee, J.; Harper, M. EGFR and cancer prognosis. *Eur. J. Cancer* **2001**, *37*, 9–15. [CrossRef]
89. Spano, J.-P.; Lagorce, C.; Atlan, D.; Milano, G.; Domont, J.; Benamouzig, R.; Attar, A.; Benichou, J.; Martin, A.; Morere, J.-F.; et al. Impact of EGFR expression on colorectal cancer patient prognosis and survival. *Ann. Oncol.* **2005**, *16*, 102–108. [CrossRef]
90. Zarghooni, M.; Bartels, U.; Lee, E.; Buczkowicz, P.; Morrison, A.; Huang, A.; Bouffet, E.; Hawkins, C. Whole-Genome Profiling of Pediatric Diffuse Intrinsic Pontine Gliomas Highlights Platelet-Derived Growth Factor Receptor  $\alpha$  and Poly (ADP-ribose) Polymerase As Potential Therapeutic Targets. *J. Clin. Oncol.* **2010**, *28*, 1337–1344. [CrossRef]
91. Suri, V.; Das, P.; Jain, A.; Sharma, M.C.; Borkar, S.A.; Suri, A.; Gupta, D.; Sarkar, C. Pediatric glioblastomas: A histopathological and molecular genetic study. *Neuro-Oncology* **2009**, *11*, 274–280. [CrossRef]
92. Wong, A.J.; Bigner, S.H.; Bigner, D.D.; Kinzler, K.W.; Hamilton, S.R.; Vogelstein, B. Increased expression of the epidermal growth factor receptor gene in malignant gliomas is invariably associated with gene amplification. *Proc. Natl. Acad. Sci. USA* **1987**, *84*, 6899–6903. [CrossRef]
93. Kraus, J.A.; Felsberg, J.; Tonn, J.C.; Reifenberger, G.; Pietsch, T. Molecular genetic analysis of the TP53, PTEN, CDKN2A, EGFR, CDK4 and MDM2 tumour-associated genes in supratentorial primitive neuroectodermal tumours and glioblastomas of childhood. *Neuropathol. Appl. Neurobiol.* **2002**, *28*, 325–333. [CrossRef]
94. Pollack, I.F.; Hamilton, R.L.; James, C.D.; Finkelstein, S.D.; Burnham, J.; Yates, A.J.; Holmes, E.J.; Zhou, T.; Finlay, J.L. Rarity of PTEN deletions and EGFR amplification in malignant gliomas of childhood: Results from the Children’s Cancer Group 945 cohort. *J. Neurosurgery Pediatr.* **2006**, *105*, 418–424. [CrossRef] [PubMed]
95. Hatanpaa, K.J.; Burma, S.; Zhao, D.; Habib, A.A. Epidermal Growth Factor Receptor in Glioma: Signal Transduction, Neuropathology, Imaging, and Radioresistance. *Neoplasia* **2010**, *12*, 675–684. [CrossRef] [PubMed]
96. Ganigi, P.; Santosh, V.; Anandh, B.; Chandramouli, B.; Kolluri, V.S. Expression of p53, EGFR, pRb and bcl-2 Proteins in Pediatric Glioblastoma Multiforme: A Study of 54 Patients. *Pediatr. Neurosurg.* **2005**, *41*, 292–299. [CrossRef] [PubMed]
97. Gilbertson, R.J.; Hill, D.A. ERBB1 is amplified and overexpressed in high-grade diffusely infiltrative pediatric brain stem glioma. *Clin. Cancer Res.* **2003**, *9 Pt 1*, 3620–3624. [PubMed]

98. Korshunov, A.; Golanov, A.; Timirgaz, V. Immunohistochemical markers for intracranial ependymoma recurrence: An analysis of 88 cases. *J. Neurol. Sci.* **2000**, *177*, 72–82. [CrossRef] [PubMed]
99. Mendrzyk, F.; Korshunov, A.; Benner, A.; Toedt, G.; Pfister, S.; Radlwimmer, B.; Lichter, P. Identification of Gains on 1q and Epidermal Growth Factor Receptor Overexpression as Independent Prognostic Markers in Intracranial Ependymoma. *Clin. Cancer Res.* **2006**, *12*, 2070–2079. [CrossRef]
100. Massimino, M.; Buttarelli, F.R.; Antonelli, M.; Gandola, L.; Modena, P.; Giangaspero, F. Intracranial ependymoma: Factors affecting outcome. *Futur. Oncol.* **2009**, *5*, 207–216. [CrossRef]
101. Gilbertson, R.J.; Perry, R.H.; Kelly, P.J.; Pearson, A.D.; Lunec, J. Prognostic significance of HER2 and HER4 coexpression in childhood medulloblastoma. *Cancer Res.* **1997**, *57*, 3272–3280.
102. Bodey, B.; E Kaiser, H.; E Siegel, S. Epidermal growth factor receptor (EGFR) expression in childhood brain tumors. *Vivo* **2005**, *19*, 931–941.
103. Layfield, L.J.; Thompson, J.K.; Ms, R.K.D.; Kerns, B.-J. Prognostic indicators for neuroblastoma: Stage, grade, DNA ploidy, MIB-1-proliferation index, p53, HER-2/neu and EGFR—a survival study. *J. Surg. Oncol.* **1995**, *59*, 21–27. [CrossRef]
104. Izycka-Swieszewska, E.; Wozniak, A.; Drozyska, E.; Kot, J.; Grajkowska, W.; Klepacka, T.; Perek, D.; Koltan, S.; Bien, E.; Limon, J. Expression and significance of HER family receptors in neuroblastic tumors. *Clin. Exp. Metastasis* **2011**, *28*, 271–282. [CrossRef]
105. Izycka-Swieszewska, E.; Wozniak, A.; Kot, J.; Grajkowska, W.; Balcerska, A.; Perek, D.; Dembowska-Baginska, B.; Klepacka, T.; Drozyska, E. Prognostic significance of HER2 expression in neuroblastic tumors. *Mod. Pathol.* **2010**, *23*, 1261–1268. [CrossRef]
106. Wang, H.; Yang, Q.; Fu, Z.; Zuo, D.; Hua, Y.; Cai, Z. ErbB Receptors as Prognostic and Therapeutic Drug Targets in Bone and Soft Tissue Sarcomas. *Cancer Investig.* **2014**, *32*, 533–542. [CrossRef]
107. Wen, Y.H.; Koeppen, H.; Garcia, R.; Chiriboga, L.; Tarlow, B.D.; Peters, B.A.; Eigenbrot, C.; Yee, H.; Steiner, G.; Greco, M.A. Epidermal growth factor receptor in osteosarcoma: Expression and mutational analysis. *Hum. Pathol.* **2007**, *38*, 1184–1191. [CrossRef]
108. Liu, L.; Xiao, C.; Sun, Q. MiRNA-375 inhibits retinoblastoma progression through targeting ERBB2 and inhibiting MAPK1/MAPK3 signalling pathway. *Cutan. Ocul. Toxicol.* **2021**, *41*, 1–10. [CrossRef]
109. Vasei, M.; Modjtahedi, H.; Ale-Booyeh, O.; Mosallaei, A.; Kajbafzadeh, A.M.; Shahriari, M.; Ghaderi, A.A.; Soleymampour, H.; Kosari, F.; Moch, H.; et al. Amplification and expression of EGFR and ERBB2 in Wilms tumor. *Cancer Genet. Cytogenet.* **2009**, *194*, 88–95. [CrossRef]
110. Little, S.E.; Bax, D.A.; Rodriguez-Pinilla, M.; Natrajan, R.; Messahel, B.; Pritchard-Jones, K.; Vujanic, G.M.; Reis-Filho, J.S.; Jones, C. Multifaceted Dysregulation of the Epidermal Growth Factor Receptor Pathway in Clear Cell Sarcoma of the Kidney. *Clin. Cancer Res.* **2007**, *13*, 4360–4364. [CrossRef]
111. Armistead, P.M.; Salganick, J.; Roh, J.S.; Steinert, D.M.; Patel, S.; Munsell, M.; El-Naggar, A.K.; Benjamin, R.S.; Zhang, W.; Trent, J.C. Expression of receptor tyrosine kinases and apoptotic molecules in rhabdomyosarcoma: Correlation with overall survival in 105 patients. *Cancer* **2007**, *110*, 2293–2303. [CrossRef]
112. Shibuya, M. Vascular endothelial growth factor and its receptor system: Physiological functions in angiogenesis and pathological roles in various diseases. *J. Biochem.* **2012**, *153*, 13–19. [CrossRef]
113. Risau, W. Mechanisms of angiogenesis. *Nature* **1997**, *386*, 671–674. [CrossRef]
114. Simons, M.; Gordon, E.; Claesson-Welsh, L. Mechanisms and regulation of endothelial VEGF receptor signalling. *Nat. Rev. Mol. Cell Biol.* **2016**, *17*, 611–625. [CrossRef] [PubMed]
115. Tamura, R.; Sato, M.; Morimoto, Y.; Ohara, K.; Kosugi, K.; Oishi, Y.; Kuranari, Y.; Murase, M.; Yoshida, K.; Toda, M. Quantitative assessment and clinical relevance of VEGFRs-positive tumor cells in refractory brain tumors. *Exp. Mol. Pathol.* **2020**, *114*, 104408. [CrossRef] [PubMed]
116. Slongo, M.L.; Molena, B.; Brunati, A.M.; Frasson, M.; Gardiman, M.; Carli, M.; Perilongo, G.; Rosolen, A.; Onisto, M. Functional VEGF and VEGF receptors are expressed in human medulloblastomas. *Neuro-Oncology* **2007**, *9*, 384–392. [CrossRef] [PubMed]
117. Gesundheit, B.; Klement, G.; Senger, C.; Kerbel, R.; Kieran, M.; Baruchel, S.; Becker, L. Differences in vasculature between pilocytic and anaplastic astrocytomas of childhood. *Med. Pediatr. Oncol.* **2003**, *41*, 516–526. [CrossRef]
118. Farschtschi, S.; Merker, V.L.; Wolf, D.; Schuhmann, M.; Blakeley, J.; Plotkin, S.R.; Hagel, C.; Mautner, V.F. Bevacizumab treatment for symptomatic spinal ependymomas in neurofibromatosis type 2. *Acta Neurol. Scand.* **2015**, *133*, 475–480. [CrossRef]
119. Virág, J.; Kenessey, I.; Haberler, C.; Piurko, V.; Bálint, K.; Döme, B.; Tímár, J.; Garami, M.; Hegedűs, B. Angiogenesis and Angiogenic Tyrosine Kinase Receptor Expression in Pediatric Brain Tumors. *Pathol. Oncol. Res.* **2013**, *20*, 417–426. [CrossRef]
120. Zhou, Q.; Yan, X.; Zhu, H.; Xin, Z.; Zhao, J.; Shen, W.; Yin, W.; Guo, Y.; Xu, H.; Zhao, M.; et al. Identification of three tumor antigens and immune subtypes for mRNA vaccine development in diffuse glioma. *Theranostics* **2021**, *11*, 9775–9790. [CrossRef]
121. Fakhari, M.; Pullirsch, D.; Abraham, D.; Paya, K.; Hofbauer, R.; Holzfeind, P.; Hofmann, M.; Aharinejad, S. Selective upregulation of vascular endothelial growth factor receptors neuropilin-1 and -2 in human neuroblastoma. *Cancer* **2001**, *94*, 258–263. [CrossRef]
122. Czapiewski, P.; Kunc, M.; Haybaeck, J. Genetic and molecular alterations in olfactory neuroblastoma: Implications for pathogenesis, prognosis and treatment. *Oncotarget* **2016**, *7*, 52584–52596. [CrossRef]
123. Behjati, S.; Tarpey, P.S.; Haase, K.; Ye, H.; Young, M.D.; Alexandrov, L.B.; Farnon, S.J.; Collord, G.; Wedge, D.C.; Martincorena, I.; et al. Recurrent mutation of IGF signalling genes and distinct patterns of genomic rearrangement in osteosarcoma. *Nat. Commun.* **2017**, *8*, 15936. [CrossRef]

124. Joseph, C.G.; Hwang, H.; Jiao, Y.; Wood, L.D.; Kinde, I.; Wu, J.; Mandahl, N.; Luo, J.; Hruban, R.H.; Diaz, L.; et al. Exomic analysis of myxoid liposarcomas, synovial sarcomas, and osteosarcomas. *Genes Chromosom. Cancer* **2013**, *53*, 15–24. [CrossRef]
125. Perry, J.A.; Kiezun, A.; Tonzi, P.; Van Allen, E.M.; Carter, S.L.; Baca, S.C.; Cowley, G.S.; Bhatt, A.S.; Rheinbay, E.; Pedamallu, C.S.; et al. Complementary genomic approaches highlight the PI3K/mTOR pathway as a common vulnerability in osteosarcoma. *Proc. Natl. Acad. Sci. USA* **2014**, *111*, E5564–E5573. [CrossRef]
126. Negri, G.L.; Grande, B.M.; Delaidelli, A.; El-Naggar, A.; Cochrane, D.; Lau, C.C.; Triche, T.J.; Moore, R.A.; Jones, S.J.M.; Montpetit, A.; et al. Integrative genomic analysis of matched primary and metastatic pediatric osteosarcoma. *J. Pathol.* **2019**, *249*, 319–331. [CrossRef]
127. Subbiah, V.; Cote, G.J. Advances in Targeting RET-Dependent Cancers. *Cancer Discov.* **2020**, *10*, 498–505. [CrossRef]
128. Takahashi, M.; Kawai, K.; Asai, N. Roles of the *RET* Proto-oncogene in Cancer and Development. *JMA J.* **2020**, *3*, 175–181. [CrossRef]
129. Li, A.Y.; McCusker, M.G.; Russo, A.; Scilla, K.A.; Gittens, A.; Arensmeyer, K.; Mehra, R.; Adamo, V.; Rolfo, C. RET fusions in solid tumors. *Cancer Treat. Rev.* **2019**, *81*, 101911. [CrossRef]
130. Adashek, J.J.; Desai, A.P.; Andreev-Drakhlina, A.Y.; Roszik, J.; Cote, G.J.; Subbiah, V. Hallmarks of RET and Co-occurring Genomic Alterations in RET-aberrant Cancers. *Mol. Cancer Ther.* **2021**, *20*, 1769–1776. [CrossRef]
131. Elisei, R.; Romei, C.; Vorontsova, T.; Cosci, B.; Veremeychik, V.; Kuchinskaya, E.; Basolo, F.; Demidchik, E.P.; Miccoli, P.; Pinchera, A.; et al. RET/PTC Rearrangements in Thyroid Nodules: Studies in Irradiated and Not Irradiated, Malignant and Benign Thyroid Lesions in Children and Adults. *J. Clin. Endocrinol. Metab.* **2001**, *86*, 3211–3216. [CrossRef]
132. Rabes, H.M.; Klugbauer, S. Molecular genetics of childhood papillary thyroid carcinomas after irradiation: High prevalence of RET rearrangement. *Genes Environ. Cancer* **1998**, *154*, 248–264. [CrossRef]
133. Zimmerman, D. Thyroid neoplasia in children. *Curr. Opin. Pediatr.* **1997**, *9*, 413–418. [CrossRef]
134. Ortiz, M.V.; Gerdemann, U.; Raju, S.G.; Henry, D.; Smith, S.; Rothenberg, S.M.; Cox, M.C.; Proust, S.; Bender, J.G.; Frazier, A.L.; et al. Activity of the Highly Specific RET Inhibitor Selpercatinib (LOXO-292) in Pediatric Patients With Tumors Harboring RET Gene Alterations. *JCO Precis. Oncol.* **2020**, *4*, 341–347. [CrossRef] [PubMed]
135. Kovac, M.; Woolley, C.; Ribic, S.; Blattmann, C.; Roth, E.; Morini, M.; Kovacova, M.; Ameline, B.; Kulozik, A.; Bielack, S.; et al. Germline RET variants underlie a subset of paediatric osteosarcoma. *J. Med. Genet.* **2020**, *58*, 20–24. [CrossRef] [PubMed]
136. Greenfield, E.M.; Collier, C.D.; Getty, P.J. Receptor Tyrosine Kinases in Osteosarcoma: 2019 Update. *Adv. Exp. Med. Biol.* **2020**, *1258*, 141–155. [CrossRef] [PubMed]
137. Luo, J.; Xia, Y.; Yin, Y.; Luo, J.; Liu, M.; Zhang, C.; Zhao, Y.; Yang, L.; Kong, L. ATF4 destabilizes RET through nonclassical GRP78 inhibition to enhance chemosensitivity to bortezomib in human osteosarcoma. *Theranostics* **2019**, *9*, 6334–6353. [CrossRef] [PubMed]
138. Rettew, A.N.; Young, E.D.; Lev, D.C.; Kleinerman, E.S.; Abdulkarim, F.W.; Getty, P.J.; Greenfield, E.M. Multiple receptor tyrosine kinases promote the in vitro phenotype of metastatic human osteosarcoma cell lines. *Oncogenesis* **2012**, *1*, e34. [CrossRef]
139. Rettew, A.N.; Getty, P.J.; Greenfield, E.M. Receptor Tyrosine Kinases in Osteosarcoma: Not Just the Usual Suspects. *Curr. Adv. Osteosarcoma* **2014**, *804*, 47–66. [CrossRef]
140. Dabir, S.; Babakoohi, S.; Kluge, A.; Morrow, J.J.; Kresak, A.; Yang, M.; MacPherson, D.; Wildey, G.; Dowlati, A. RET Mutation and Expression in Small-Cell Lung Cancer. *J. Thorac. Oncol.* **2014**, *9*, 1316–1323. [CrossRef]
141. Cockburn, J.G.; Richardson, D.S.; Gujral, T.S.; Mulligan, L.M. RET-Mediated Cell Adhesion and Migration Require Multiple Integrin Subunits. *J. Clin. Endocrinol. Metab.* **2010**, *95*, E342–E346. [CrossRef]
142. Trusolino, L.; Bertotti, A.; Comoglio, P.M. MET signalling: Principles and functions in development, organ regeneration and cancer. *Nat. Rev. Mol. Cell Biol.* **2010**, *11*, 834–848. [CrossRef]
143. Park, K.C.; Richardson, D.R. The c-MET oncoprotein: Function, mechanisms of degradation and its targeting by novel anti-cancer agents. *Biochim. Biophys. Acta (BBA)-Gen. Subj.* **2020**, *1864*, 129650. [CrossRef]
144. Marona, P.; Górka, J.; Kotlinowski, J.; Majka, M.; Jura, J.; Miekus, K. C-Met as a Key Factor Responsible for Sustaining Undifferentiated Phenotype and Therapy Resistance in Renal Carcinomas. *Cells* **2019**, *8*, 272. [CrossRef]
145. Zambelli, A.; Biamonti, G.; Amato, A. HGF/c-Met Signalling in the Tumor Microenvironment. *TumorMicroenviron. Signal. Pathw. Part B* **2020**, *1270*, 31–44. [CrossRef]
146. Cooper, C.S.; Park, M.; Blair, D.G.; Tainsky, M.A.; Huebner, K.; Croce, C.M.; Vande Woude, G.F. Molecular cloning of a new transforming gene from a chemically transformed human cell line. *Nature* **1984**, *311*, 29–33. [CrossRef]
147. Grundy, M.; Narendran, A. The hepatocyte growth factor/mesenchymal epithelial transition factor axis in high-risk pediatric solid tumors and the anti-tumor activity of targeted therapeutic agents. *Front. Pediatr.* **2022**, *10*, 910268. [CrossRef]
148. Stucklin, A.S.G.; Ryall, S.; Fukuoka, K.; Zapotocky, M.; Lassaletta, A.; Li, C.; Bridge, T.; Kim, B.; Arnoldo, A.; Kowalski, P.E.; et al. Alterations in ALK/ROS1/NTRK/MET drive a group of infantile hemispheric gliomas. *Nat. Commun.* **2019**, *10*, 4343. [CrossRef]
149. Kunkel, P.; Müller, S.; Schirmacher, P.; Stavrou, D.; Fillbrandt, R.; Westphal, M.; Lamszus, K. Expression and localization of scatter factor/hepatocyte growth factor in human astrocytomas. *Neuro-Oncology* **2001**, *3*, 82–88. [CrossRef]
150. Li, Y.; Lal, B.; Kwon, S.; Fan, X.; Saldanha, U.; Reznik, T.E.; Kuchner, E.B.; Eberhart, C.; Laterra, J.; Abounader, R. The Scatter Factor/Hepatocyte Growth Factor: C-Met Pathway in Human Embryonal Central Nervous System Tumor Malignancy. *Cancer Res* **2005**, *65*, 9355–9362. [CrossRef]

151. Provençal, M.; Labbé, D.; Veitch, R.; Boivin, D.; Rivard, G.; Sartelet, H.; Robitaille, Y.; Gingras, D.; Béliveau, R. c-Met activation in medulloblastoma induces tissue factor expression and activity: Effects on cell migration. *Carcinog.* **2009**, *30*, 1089–1096. [CrossRef]
152. E Crosswell, H.; Dasgupta, A.; Alvarado, C.S.; Watt, T.; Christensen, J.G.; De, P.; Durden, D.L.; Findley, H.W. PHA665752, a small-molecule inhibitor of c-Met, inhibits hepatocyte growth factor-stimulated migration and proliferation of c-Met-positive neuroblastoma cells. *BMC Cancer* **2009**, *9*, 411. [CrossRef]
153. Hecht, M.; Papoutsi, M.; Tran, H.D.; Wilting, J.; Schweigerer, L. Hepatocyte Growth Factor/c-Met Signaling Promotes the Progression of Experimental Human Neuroblastomas. *Cancer Res* **2004**, *64*, 6109–6118. [CrossRef]
154. Alami, J.; Williams, B.R.G.; Yeager, H. Expression and localization of HGF and met in Wilms' tumours. *J. Pathol.* **2001**, *196*, 76–84. [CrossRef]
155. Cao, X.; Liu, D.-H.; Zhou, Y.; Yan, X.-M.; Yuan, L.-Q.; Pan, J.; Fu, M.-C.; Zhang, T.; Wang, J. Histone deacetylase 5 promotes Wilms' tumor cell proliferation through the upregulation of c-Met. *Mol. Med. Rep.* **2016**, *13*, 2745–2750. [CrossRef]
156. Nair, R.M.; Prabhu, V.; Manukonda, R.; Mishra, D.K.; Kaliki, S.; Vemuganti, G.K. Overexpression of metastasis-associated in colon cancer 1 in retinoblastoma. *Tumor Biol.* **2020**, *42*, 1010428320975973. [CrossRef]
157. Patanè, S.; Avnet, S.; Coltella, N.; Costa, B.; Sponza, S.; Olivero, M.; Vigna, E.; Naldini, L.; Baldini, N.; Ferracini, R.; et al. *MET* Overexpression Turns Human Primary Osteoblasts into Osteosarcomas. *Cancer Res* **2006**, *66*, 4750–4757. [CrossRef]
158. Chen, W.; Wu, S.; Huang, Y.; Zhang, T.; Dong, H.; Zheng, X.; Chen, T.; Gong, X.; Liu, G.; Zhao, X. A c-Met Inhibitor Suppresses Osteosarcoma Progression via the ERK1/2 Pathway in Human Osteosarcoma Cells. *Oncotargets Ther.* **2021**, *14*, 4791–4804. [CrossRef]
159. Entz-Werle, N.; Lavaux, T.; Metzger, N.; Stoetzel, C.; Lasthaus, C.; Marec, P.; Kalita, C.; Brugieres, L.; Pacquement, H.; Schmitt, C.; et al. Involvement of MET/TWIST/APC Combination or the Potential Role of Ossification Factors in Pediatric High-Grade Osteosarcoma Oncogenesis. *Neoplasia* **2007**, *9*, 678–688. [CrossRef]
160. Fleuren, E.D.; Roeffen, M.H.; Leenders, W.P.; Flucke, U.E.; Vletterie, M.; Schreuder, H.W.; Boerman, O.C.; van der Graaf, W.T.; Versleijen-Jonkers, Y.M. Expression and clinical relevance of MET and ALK in Ewing sarcomas. *Int. J. Cancer* **2013**, *133*, 427–436. [CrossRef]
161. Yan, D.; Da Dong, X.; Chen, X.; Wang, L.; Lu, C.; Wang, J.; Qu, J.; Tu, L. MicroRNA-1/206 Targets c-Met and Inhibits Rhabdomyosarcoma Development. *J. Biol. Chem.* **2009**, *284*, 29596–29604. [CrossRef]
162. Du, J.; Wang, Y.; Meng, L.; Liu, Y.; Pang, Y.; Cui, W.; Zhang, L.; Li, Z.; Liu, Q.; Shang, H.; et al. c-MET expression potentially contributes to the poor prognosis of rhabdomyosarcoma. *Int. J. Clin. Exp. Pathol.* **2018**, *11*, 4083–4092.
163. Otabe, O.; Kikuchi, K.; Tsuchiya, K.; Katsumi, Y.; Yagyū, S.; Miyachi, M.; Iehara, T.; Hosoi, H. MET/ERK2 pathway regulates the motility of human alveolar rhabdomyosarcoma cells. *Oncol. Rep.* **2016**, *37*, 98–104. [CrossRef]
164. Taulli, R.; Scuoppo, C.; Bersani, F.; Accornero, P.; Forni, P.E.; Miretti, S.; Grinza, A.; Allegra, P.; Schmitt-Ney, M.; Crepaldi, T.; et al. Validation of Met as a Therapeutic Target in Alveolar and Embryonal Rhabdomyosarcoma. *Cancer Res* **2006**, *66*, 4742–4749. [CrossRef]
165. Morris, S.W.; Kirstein, M.N.; Valentine, M.B.; Dittmer, K.G.; Shapiro, D.N.; Saltman, D.L.; Look, A.T. Fusion of a Kinase Gene, *ALK*, to a Nucleolar Protein Gene, *NPM*, in Non-Hodgkin's Lymphoma. *Science* **1994**, *263*, 1281–1284. [CrossRef]
166. Hallberg, B.; Palmer, R. The role of the ALK receptor in cancer biology. *Ann. Oncol.* **2016**, *27*, iii4–iii15. [CrossRef]
167. Takita, J. The role of anaplastic lymphoma kinase in pediatric cancers. *Cancer Sci.* **2017**, *108*, 1913–1920. [CrossRef]
168. Peron, M.; Lovisa, F.; Poli, E.; Basso, G.; Bonvini, P. Understanding the Interplay between Expression, Mutation and Activity of ALK Receptor in Rhabdomyosarcoma Cells for Clinical Application of Small-Molecule Inhibitors. *PLoS ONE* **2015**, *10*, e0132330. [CrossRef]
169. Felkai, L.; Bánusz, R.; Kovalszky, I.; Sápi, Z.; Garami, M.; Papp, G.; Karászi, K.; Varga, E.; Csóka, M. The Presence of ALK Alterations and Clinical Relevance of Crizotinib Treatment in Pediatric Solid Tumors. *Pathol. Oncol. Res.* **2017**, *25*, 217–224. [CrossRef]
170. Aygun, N. Biological and Genetic Features of Neuroblastoma and Their Clinical Importance. *Curr. Pediatr. Rev.* **2018**, *14*, 73–90. [CrossRef]
171. Pastor, E.R.; Mousa, S.A. Current management of neuroblastoma and future direction. *Crit. Rev. Oncol.* **2019**, *138*, 38–43. [CrossRef]
172. Pacenta, H.L.; E Macy, M. Entrectinib and other ALK/TRK inhibitors for the treatment of neuroblastoma. *Drug Des. Dev. Ther.* **2018**, *12*, 3549–3561. [CrossRef]
173. Berry, T.; Luther, W.; Bhatnagar, N.; Jamin, Y.; Poon, E.; Sanda, T.; Pei, D.; Sharma, B.; Vetharoy, W.R.; Hallsworth, A.; et al. The ALKF1174L Mutation Potentiates the Oncogenic Activity of MYCN in Neuroblastoma. *Cancer Cell* **2012**, *22*, 117–130. [CrossRef]
174. Valera, E.T.; Neder, L.; Queiroz, R.G.; Santos, A.C.; Sousa, G.R.; Oliveira, R.S.; Santos, M.V.; Machado, H.R.; Tone, L.G. Perinatal complex low- and high-grade glial tumor harboring a novel *GIGYF2-ALK* fusion. *Pediatr. Blood Cancer* **2019**, *67*, e28015. [CrossRef]
175. Argani, P.; Lian, D.W.; Agaimy, A.; Metzler, M.; Wobker, S.E.; Matoso, A.; Epstein, J.I.; Sung, Y.-S.; Zhang, L.; Antonescu, C.R. Pediatric Mesothelioma With ALK Fusions. *Am. J. Surg. Pathol.* **2021**, *45*, 653–661. [CrossRef] [PubMed]
176. Olsen, T.K.; Panagopoulos, I.; Meling, T.R.; Micci, F.; Gorunova, L.; Thorsen, J.; Due-Tønnessen, B.; Scheie, D.; Lund-Iversen, M.; Krossnes, B.; et al. Fusion genes with *ALK* as recurrent partner in ependymoma-like gliomas: A new brain tumor entity? *Neuro-Oncology* **2015**, *17*, 1365–1373. [CrossRef] [PubMed]



177. Łastowska, M.; Trubicka, J.; Niemira, M.; Paczkowska-Abdulsalam, M.; Karkucińska-Więckowska, A.; Kaleta, M.; Drogosiewicz, M.; Tarasińska, M.; Perek-Polnik, M.; Krętowski, A.; et al. ALK Expression Is a Novel Marker for the WNT-activated Type of Pediatric Medulloblastoma and an Indicator of Good Prognosis for Patients. *Am. J. Surg. Pathol.* **2017**, *41*, 781–787. [CrossRef] [PubMed]
178. Porta, C.; Paglino, C.; Mosca, A. Targeting PI3K/Akt/mTOR Signaling in Cancer. *Front. Oncol.* **2014**, *4*, 64. [CrossRef]
179. Castellano, E.; Downward, J. RAS Interaction with PI3K: More than Just another Effector Pathway. *Genes Cancer* **2011**, *2*, 261–274. [CrossRef]
180. Revathidevi, S.; Munirajan, A.K. Akt in cancer: Mediator and more. *Semin. Cancer Biol.* **2019**, *59*, 80–91. [CrossRef]
181. Barrett, D.; Brown, V.I.; Grupp, S.A.; Teachey, D.T. Targeting the PI3K/AKT/mTOR Signaling Axis in Children with Hematologic Malignancies. *Pediatr. Drugs* **2012**, *14*, 299–316. [CrossRef]
182. Zoncu, R.; Efeyan, A.; Sabatini, D.M. mTOR: From growth signal integration to cancer, diabetes and ageing. *Nat. Rev. Mol. Cell Biol.* **2011**, *12*, 21–35. [CrossRef]
183. Aoki, M.; Fujishita, T. Oncogenic Roles of the PI3K/AKT/mTOR Axis. *Curr. Top. Microbiol. Immunol.* **2017**, *407*, 153–189. [CrossRef]
184. Shorning, B.; Dass, M.; Smalley, M.; Pearson, H. The PI3K-AKT-mTOR Pathway and Prostate Cancer: At the Crossroads of AR, MAPK, and WNT Signaling. *Int. J. Mol. Sci.* **2020**, *21*, 4507. [CrossRef]
185. Narayanankutty, A. PI3K/ Akt/ mTOR Pathway as a Therapeutic Target for Colorectal Cancer: A Review of Preclinical and Clinical Evidence. *Curr. Drug Targets* **2019**, *20*, 1217–1226. [CrossRef]
186. Fattahi, S.; Amjadi-Moheb, F.; Tabaripour, R.; Ashrafi, G.H.; Akhavan-Niaki, H. PI3K/AKT/mTOR signaling in gastric cancer: Epigenetics and beyond. *Life Sci.* **2020**, *262*, 118513. [CrossRef]
187. Bertacchini, J.; Heidari, N.; Mediani, L.; Capitani, S.; Shahjahani, M.; Ahmadzadeh, A.; Saki, N. Targeting PI3K/AKT/mTOR network for treatment of leukemia. *Cell. Mol. Life Sci.* **2015**, *72*, 2337–2347. [CrossRef]
188. Miricescu, D.; Totan, A.; Stanescu-Spinu, I.-I.; Badoiu, S.; Stefani, C.; Greabu, M. PI3K/AKT/mTOR Signaling Pathway in Breast Cancer: From Molecular Landscape to Clinical Aspects. *Int. J. Mol. Sci.* **2020**, *22*, 173. [CrossRef]
189. Gann, C.-N.; Morsli, N.; Chen, X.; Barrueco, J. Response to ‘Dai W et al. Am J Cancer Res 2015;5(10):3270-3275’ from the makers of nintedanib. *Am. J. Cancer Res.* **2016**, *6*, 1547–1548.
190. Remke, M.; Pfister, S.; Kox, C.; Toedt, G.; Becker, N.; Benner, A.; Werft, W.; Breit, S.; Liu, S.; Engel, F.; et al. High-resolution genomic profiling of childhood T-ALL reveals frequent copy-number alterations affecting the TGF- $\beta$  and PI3K-AKT pathways and deletions at 6q15-16.1 as a genomic marker for unfavorable early treatment response. *Blood* **2009**, *114*, 1053–1062. [CrossRef]
191. Armengol, G.; Canellas, A.; Álvarez, Y.; Bastida, P.; De Toledo, J.S.; Pérez-Iribarne, M.D.M.; Camós, M.; Tuset, E.; Estella, J.; Coll, M.D.; et al. Genetic changes including gene copy number alterations and their relation to prognosis in childhood acute myeloid leukemia. *Leuk. Lymphoma* **2009**, *51*, 114–124. [CrossRef]
192. Knobbe, C.B.; Reifenberger, G. Genetic Alterations and Aberrant Expression of Genes Related to the Phosphatidylinositol-3'-Kinase/Protein Kinase B (Akt) Signal Transduction Pathway in Glioblastomas. *Brain Pathol.* **2006**, *13*, 507–518. [CrossRef]
193. Engelman, J.A.; Luo, J.; Cantley, L.C. The evolution of phosphatidylinositol 3-kinases as regulators of growth and metabolism. *Nat. Rev. Genet.* **2006**, *7*, 606–619. [CrossRef]
194. Okkenhaug, K.; Ahmadi, K.; White, S.; Timms, J.; Waterfield, M.D. Cellular Function of Phosphoinositide 3-Kinases: Implications for Development, Immunity, Homeostasis, and Cancer. *Annu. Rev. Cell Dev. Biol.* **2001**, *17*, 615–675. [CrossRef]
195. Zhao, L.; Vogt, P.K. Helical domain and kinase domain mutations in p110 of phosphatidylinositol 3-kinase induce gain of function by different mechanisms. *Proc. Natl. Acad. Sci. USA* **2008**, *105*, 2652–2657. [CrossRef]
196. Samuels, Y.; Wang, Z.; Bardelli, A.; Silliman, N.; Ptak, J.; Szabo, S.; Yan, H.; Gazdar, A.; Powell, S.M.; Riggins, G.J.; et al. High Frequency of Mutations of the *PIK3CA* Gene in Human Cancers. *Science* **2004**, *304*, 554. [CrossRef] [PubMed]
197. Jiang, W.; He, T.; Liu, S.; Zheng, Y.; Xiang, L.; Pei, X.; Wang, Z.; Yang, H. The *PIK3CA* E542K and E545K mutations promote glycolysis and proliferation via induction of the  $\beta$ -catenin/SIRT3 signaling pathway in cervical cancer. *J. Hematol. Oncol.* **2018**, *11*, 139. [CrossRef] [PubMed]
198. Ikenoue, T.; Kanai, F.; Hikiba, Y.; Obata, T.; Tanaka, Y.; Imamura, J.; Ohta, M.; Jazag, A.; Guleng, B.; Tateishi, K.; et al. Functional Analysis of *PIK3CA* Gene Mutations in Human Colorectal Cancer. *Cancer Res* **2005**, *65*, 4562–4567. [CrossRef] [PubMed]
199. Murat, C.; Braga, P.; Fortes, M.; Bronstein, M.; Correa-Giannella, M.L.; Giorgi, R. Mutation and genomic amplification of the *PIK3CA* proto-oncogene in pituitary adenomas. *Braz. J. Med. Biol. Res.* **2012**, *45*, 851–855. [CrossRef]
200. Shi, J.; Yao, D.; Liu, W.; Wang, N.; Lv, H.; Zhang, G.; Ji, M.; Xu, L.; He, N.; Shi, B.; et al. Highly frequent *PIK3CA* amplification is associated with poor prognosis in gastric cancer. *BMC Cancer* **2012**, *12*, 50. [CrossRef]
201. Holst, F.; Werner, H.M.; Mjøs, S.; Hoivik, E.A.; Kusonmano, K.; Wik, E.; Berg, A.; Birkeland, E.; Gibson, W.J.; Halle, M.K.; et al. *PIK3CA* Amplification Associates with Aggressive Phenotype but Not Markers of AKT-MTOR Signaling in Endometrial Carcinoma. *Clin. Cancer Res.* **2019**, *25*, 334–345. [CrossRef]
202. Huw, L.-Y.; O'Brien, C.; Pandita, A.; Mohan, S.; Spoerke, J.M.; Lu, S.; Wang, Y.; Hampton, G.M.; Wilson, T.R.; Lackner, M.R. Acquired *PIK3CA* amplification causes resistance to selective phosphoinositide 3-kinase inhibitors in breast cancer. *Oncogenesis* **2013**, *2*, e83. [CrossRef]

203. Salm, F.; Dimitrova, V.; Von Bueren, A.O.; Ćwiek, P.; Rehrauer, H.; Djonov, V.; Anderle, P.; Arcaro, A. The Phosphoinositide 3-Kinase p110 $\alpha$  Isoform Regulates Leukemia Inhibitory Factor Receptor Expression via c-Myc and miR-125b to Promote Cell Proliferation in Medulloblastoma. *PLoS ONE* **2015**, *10*, e0123958. [CrossRef]
204. Guerreiro, A.S.; Fattet, S.; Fischer, B.; Shalaby, T.; Jackson, S.P.; Schoenwaelder, S.M.; Grotzer, M.A.; Delattre, O.; Arcaro, A. Targeting the PI3K p110 $\alpha$  Isoform Inhibits Medulloblastoma Proliferation, Chemoresistance, and Migration. *Clin. Cancer Res.* **2008**, *14*, 6761–6769. [CrossRef]
205. Guerreiro, A.S.; Fattet, S.; Kulesza, D.W.; Atamer, A.; Elsing, A.N.; Shalaby, T.; Jackson, S.P.; Schoenwaelder, S.M.; Grotzer, M.A.; Delattre, O.; et al. A Sensitized RNA Interference Screen Identifies a Novel Role for the PI3K p110 $\gamma$  Isoform in Medulloblastoma Cell Proliferation and Chemoresistance. *Mol. Cancer Res.* **2011**, *9*, 925–935. [CrossRef]
206. Luk, S.K.; Piekorz, R.P.; Nürnberg, B.; To, S.-S.T. The catalytic phosphoinositid 3-kinase isoform p110 $\delta$  is required for glioma cell migration and invasion. *Eur. J. Cancer* **2012**, *48*, 149–157. [CrossRef]
207. Boller, D.; Schramm, A.; Doepfner, K.T.; Shalaby, T.; von Bueren, A.O.; Eggert, A.; Grotzer, M.A.; Arcaro, A. Targeting the Phosphoinositide 3-Kinase Isoform p110 $\delta$  Impairs Growth and Survival in Neuroblastoma Cells. *Clin. Cancer Res.* **2008**, *14*, 1172–1181. [CrossRef]
208. Fransson, S.; Martinsson, T.; Ejeskär, K. Neuroblastoma tumors with favorable and unfavorable outcomes: Significant differences in mRNA expression of genes mapped at 1p36.2. *Genes Chromosom. Cancer* **2006**, *46*, 45–52. [CrossRef]
209. Wang, Q.; Diskin, S.; Rappaport, E.; Attiyeh, E.; Mosse, Y.; Shue, D.; Seiser, E.; Jagannathan, J.; Shusterman, S.; Bansal, M.; et al. Integrative Genomics Identifies Distinct Molecular Classes of Neuroblastoma and Shows That Multiple Genes Are Targeted by Regional Alterations in DNA Copy Number. *Cancer Res* **2006**, *66*, 6050–6062. [CrossRef]
210. Yoon, C.; Lu, J.; Ryeom, S.W.; Simon, M.C.; Yoon, S.S. PIK3R3, part of the regulatory domain of PI3K, is upregulated in sarcoma stem-like cells and promotes invasion, migration, and chemotherapy resistance. *Cell Death Dis.* **2021**, *12*, 749. [CrossRef]
211. Staff, T.P.O. Correction: Variable expression of PIK3R3 and PTEN in Ewing sarcoma impacts oncogenic phenotypes. *PLoS ONE* **2015**, *10*, e0120830. [CrossRef]
212. Bellacosa, A.; Franke, T.F.; E Gonzalez-Portal, M.; Datta, K.; Taguchi, T.; Gardner, J.; Cheng, J.Q.; Testa, J.R.; Tsichlis, P.N. Structure, expression and chromosomal mapping of c-akt: Relationship to v-akt and its implications. *Oncogene* **1993**, *8*, 745–754.
213. Basu, A.; Lambring, C. Akt Isoforms: A Family Affair in Breast Cancer. *Cancers* **2021**, *13*, 3445. [CrossRef]
214. Meier, R.; Alessi, D.R.; Cron, P.; Andjelković, M.; Hemmings, B.A. Mitogenic Activation, Phosphorylation, and Nuclear Translocation of Protein Kinase B $\beta$ . *J. Biol. Chem.* **1997**, *272*, 30491–30497. [CrossRef]
215. Hinz, N.; Jücker, M. Distinct functions of AKT isoforms in breast cancer: A comprehensive review. *Cell Commun. Signal.* **2019**, *17*, 1–29. [CrossRef]
216. Chen, H.; Zhou, L.; Wu, X.; Li, R.; Wen, J.; Sha, J.; Wen, X. The PI3K AKT pathway in the pathogenesis of prostate cancer. *Front. Biosci.* **2016**, *21*, 1084–1091. [CrossRef]
217. Carpten, J.D.; Faber, A.L.; Horn, C.; Donoho, G.P.; Briggs, S.L.; Robbins, C.M.; Hostetter, G.; Boguslawski, S.; Moses, T.Y.; Savage, S.; et al. A transforming mutation in the pleckstrin homology domain of AKT1 in cancer. *Nature* **2007**, *448*, 439–444. [CrossRef]
218. Schüller, U.; Rüter, M.; Herms, J.; Kretzschmar, H.A.; Grasbon-Frodl, E. Absence of mutations in the AKT1 oncogene in glioblastomas and medulloblastomas. *Acta Neuropathol.* **2008**, *115*, 367–368. [CrossRef]
219. Hartmann, W.; Digon-Söntgerath, B.; Koch, A.; Waha, A.; Endl, E.; Dani, I.; Denkhäus, D.; Goodyer, C.G.; Sörensen, N.; Wiestler, O.D.; et al. Phosphatidylinositol 3'-Kinase/AKT Signaling Is Activated in Medulloblastoma Cell Proliferation and Is Associated with Reduced Expression of PTEN. *Clin. Cancer Res.* **2006**, *12*, 3019–3027. [CrossRef]
220. Granados, V.A.; Avirmeni-Vadlamudi, U.; Dalal, P.; Scarborough, S.R.; Galindo, K.A.; Mahajan, P.; Galindo, R.L. Selective Targeting of Myoblast Fusogenic Signaling and Differentiation-Arrest Antagonizes Rhabdomyosarcoma Cells. *Cancer Res* **2019**, *79*, 4585–4591. [CrossRef] [PubMed]
221. Hotfilder, M.; Sondermann, P.; Senß, A.; van Valen, F.; Jürgens, H.; Vormoor, J. PI3K/AKT is involved in mediating survival signals that rescue Ewing tumour cells from fibroblast growth factor 2-induced cell death. *Br. J. Cancer* **2005**, *92*, 705–710. [CrossRef]
222. Ren, C.; Pan, R.; Hou, L.; Wu, H.; Sun, J.; Zhang, W.; Tian, X.; Chen, H. Suppression of CLEC3A inhibits osteosarcoma cell proliferation and promotes their chemosensitivity through the AKT1/mTOR/HIF1 $\alpha$  signaling pathway. *Mol. Med. Rep.* **2020**, *21*, 1739–1748. [CrossRef]
223. Kuijjer, M.L.; Akker, B.E.W.M.V.D.; Hilhorst, R.; Mommersteeg, M.; Buddingh, E.; Serra, M.; Bürger, H.; Hogendoorn, P.C.W.; Cleton-Jansen, A.-M. Kinome and mRNA expression profiling of high-grade osteosarcoma cell lines implies Akt signaling as possible target for therapy. *BMC Med. Genom.* **2014**, *7*, 4. [CrossRef]
224. Zhu, Y.; Zhou, J.; Ji, Y.; Yu, B. Elevated expression of AKT2 correlates with disease severity and poor prognosis in human osteosarcoma. *Mol. Med. Rep.* **2014**, *10*, 737–742. [CrossRef] [PubMed]
225. Liu, W.; Zhou, Z.; Zhang, Q.; Rong, Y.; Li, L.; Luo, Y.; Wang, J.; Yin, G.; Lv, C.; Cai, W. Overexpression of miR-1258 inhibits cell proliferation by targeting AKT3 in osteosarcoma. *Biochem. Biophys. Res. Commun.* **2019**, *510*, 479–486. [CrossRef] [PubMed]
226. Qiao, J.; Lee, S.; Paul, P.; Qiao, L.; Taylor, C.J.; Schlegel, C.; Colon, N.C.; Chung, D.H. Akt2 Regulates Metastatic Potential in Neuroblastoma. *PLoS ONE* **2013**, *8*, e56382. [CrossRef] [PubMed]
227. Saxton, R.A.; Sabatini, D.M. mTOR Signaling in Growth, Metabolism, and Disease. *Cell* **2017**, *168*, 960–976, Erratum in *Cell* **2017**, *169*, 361–371. [CrossRef] [PubMed]
228. Hemmings, B.A.; Restuccia, D.F. PI3K-PKB/Akt Pathway. *Cold Spring Harb. Perspect. Biol.* **2012**, *4*, a011189. [CrossRef]

229. Zarogoulidis, P.; Lampaki, S.; Turner, J.F.; Huang, H.; Kakolyris, S.; Syrigos, K.; Zarogoulidis, K. mTOR pathway: A current, up-to-date mini-review (Review). *Oncol. Lett.* **2014**, *8*, 2367–2370. [CrossRef]
230. Zou, Z.; Tao, T.; Li, H.; Zhu, X. mTOR signaling pathway and mTOR inhibitors in cancer: Progress and challenges. *Cell Biosci.* **2020**, *10*, 31. [CrossRef]
231. Grabiner, B.C.; Nardi, V.; Birsoy, K.; Possemato, R.; Shen, K.; Sinha, S.; Jordan, A.; Beck, A.H.; Sabatini, D.M. A Diverse Array of Cancer-Associated MTOR Mutations Are Hyperactivating and Can Predict Rapamycin Sensitivity. *Cancer Discov.* **2014**, *4*, 554–563. [CrossRef]
232. Culjkovic, B.; Topisirovic, I.; Skrabanek, L.; Ruiz-Gutierrez, M.; Borden, K.L. eIF4E is a central node of an RNA regulon that governs cellular proliferation. *J. Cell Biol.* **2006**, *175*, 415–426. [CrossRef]
233. Mamane, Y.; Petroulakis, E.; Rong, L.; Yoshida, K.; Ler, L.W.; Sonenberg, N. eIF4E—From translation to transformation. *Oncogene* **2004**, *23*, 3172–3179. [CrossRef]
234. Wang, G.; Jia, Y.; Ye, Y.; Kang, E.; Chen, H.; Wang, J.; He, X. Identification of key methylation differentially expressed genes in posterior fossa ependymoma based on epigenomic and transcriptome analysis. *J. Transl. Med.* **2021**, *19*, 1–14. [CrossRef] [PubMed]
235. Machado, L.E.; Alvarenga, A.W.; Da Silva, F.F.; Roffé, M.; Begnami, M.D.; Torres, L.F.B.; Da Cunha, I.W.; Martins, V.R.; Hajj, G.N.M. Overexpression of mTOR and p(240–244)S6 in IDH1 Wild-Type Human Glioblastomas Is Predictive of Low Survival. *J. Histochem. Cytochem.* **2018**, *66*, 403–414. [CrossRef]
236. Shi, J.; Zhang, P.; Su, H.; Cai, L.; Zhao, L.; Zhou, H. Bioinformatics Analysis of Neuroblastoma miRNA Based on GEO Data. *Pharmacogenomics Pers. Med.* **2021**, *14*, 849–858. [CrossRef]
237. Pócza, T.; Sebestyén, A.; Turányi, E.; Krénacs, T.; Márk, A.; Sticz, T.B.; Jakab, Z.; Hauser, P. mTOR Pathway As a Potential Target In a Subset of Human Medulloblastoma. *Pathol. Oncol. Res.* **2014**, *20*, 893–900. [CrossRef]
238. Kaid, C.; Assoni, A.; Marçola, M.; Semedo-Kuriki, P.; Bortolin, R.H.; Carvalho, V.M.; Okamoto, O.K. Proteome and miRNome profiling of microvesicles derived from medulloblastoma cell lines with stem-like properties reveals biomarkers of poor prognosis. *Brain Res.* **2020**, *1730*, 146646. [CrossRef]
239. Chakraborty, S.; Khare, S.; Dorairaj, S.K.; Prabhakaran, V.C.; Prakash, D.R.; Kumar, A. Identification of genes associated with tumorigenesis of retinoblastoma by microarray analysis. *Genomics* **2007**, *90*, 344–353. [CrossRef]
240. Subbiah, V.; Brown, R.E.; Jiang, Y.; Buryanek, J.; Hayes-Jordan, A.; Kurzrock, R.; Anderson, P.M. Morphoproteomic Profiling of the Mammalian Target of Rapamycin (mTOR) Signaling Pathway in Desmoplastic Small Round Cell Tumor (EWS/WT1), Ewing's Sarcoma (EWS/FLI1) and Wilms' Tumor (WT1). *PLoS ONE* **2013**, *8*, e68985. [CrossRef]
241. Ahmed, A.A.; Sherman, A.K.; Pawel, B.R. Expression of therapeutic targets in Ewing sarcoma family tumors. *Hum. Pathol.* **2012**, *43*, 1077–1083. [CrossRef]
242. Dobashi, Y.; Suzuki, S.; Sato, E.; Hamada, Y.; Yanagawa, T.; Ooi, A. EGFR-dependent and independent activation of Akt/mTOR cascade in bone and soft tissue tumors. *Mod. Pathol.* **2009**, *22*, 1328–1340. [CrossRef]
243. Krishnan, K.; Bruce, B.; Hewitt, S.; Thomas, D.; Khanna, C.; Helman, L.J. Ezrin mediates growth and survival in Ewing's sarcoma through the AKT/mTOR, but not the MAPK, signaling pathway. *Clin. Exp. Metastasis* **2006**, *23*, 227–236. [CrossRef]
244. Hu, K.; Dai, H.-B.; Qiu, Z.-L. mTOR signaling in osteosarcoma: Oncogenesis and therapeutic aspects (Review). *Oncol. Rep.* **2016**, *36*, 1219–1225. [CrossRef] [PubMed]
245. Egas-Bejar, D.; Anderson, P.M.; Agarwal, R.; Corrales-Medina, F.; Devarajan, E.; Huh, W.W.; Brown, R.E.; Subbiah, V. Theranostic profiling for actionable aberrations in advanced high risk osteosarcoma with aggressive biology reveals high molecular diversity: The human fingerprint hypothesis. *Oncoscience* **2014**, *1*, 167–179. [CrossRef] [PubMed]
246. Petricoin, E.F.; Espina, V.; Araujo, R.P.; Midura, B.; Yeung, C.; Wan, X.; Eichler, G.S.; Johann, D.J.; Qualman, S.; Tsokos, M.; et al. Phosphoprotein Pathway Mapping: Akt/Mammalian Target of Rapamycin Activation Is Negatively Associated with Childhood Rhabdomyosarcoma Survival. *Cancer Res* **2007**, *67*, 3431–3440. [CrossRef]
247. Doble, B.W.; Woodgett, J.R. GSK-3: Tricks of the trade for a multi-tasking kinase. *J. Cell Sci.* **2003**, *116*, 1175–1186. [CrossRef]
248. Kockeritz, L.; Doble, B.; Patel, S.; Woodgett, J. Glycogen Synthase Kinase-3—An Overview of An Over-Achieving Protein Kinase. *Curr. Drug Targets* **2006**, *7*, 1377–1388. [CrossRef]
249. Sutherland, C. What Are the bona fide GSK3 Substrates? *Int. J. Alzheimer's Dis.* **2011**, *2011*, 505607. [CrossRef]
250. McCubrey, J.A.; Davis, N.M.; Abrams, S.L.; Montalto, G.; Cervello, M.; Basecke, J.; Libra, M.; Nicoletti, F.; Cocco, L.; Martelli, A.M.; et al. Diverse roles of GSK-3: Tumor promoter–tumor suppressor, target in cancer therapy. *Adv. Biol. Regul.* **2014**, *54*, 176–196. [CrossRef]
251. Patel, S.; Woodgett, J. Glycogen Synthase Kinase-3 and Cancer: Good Cop, Bad Cop? *Cancer Cell* **2008**, *14*, 351–353. [CrossRef]
252. Mancinelli, R.; Carpino, G.; Petrunaro, S.; Mammola, C.L.; Tomaipitina, L.; Filippini, A.; Facchiano, A.; Ziparo, E.; Giampietri, C. Multifaceted Roles of GSK-3 in Cancer and Autophagy-Related Diseases. *Oxidative Med. Cell. Longev.* **2017**, *2017*, 1–14. [CrossRef]
253. Luo, J. Glycogen synthase kinase 3 $\beta$  (GSK3 $\beta$ ) in tumorigenesis and cancer chemotherapy. *Cancer Lett.* **2008**, *273*, 194–200. [CrossRef]
254. Banerji, V.; Frumm, S.M.; Ross, K.N.; Li, L.S.; Schinzel, A.C.; Hahn, C.K.; Kakoza, R.M.; Chow, K.T.; Ross, L.; Alexe, G.; et al. The intersection of genetic and chemical genomic screens identifies GSK-3 $\alpha$  as a target in human acute myeloid leukemia. *J. Clin. Investig.* **2012**, *122*, 935–947. [CrossRef] [PubMed]

255. Farago, M.; Dominguez, I.; Landesman-Bollag, E.; Xu, X.; Rosner, A.; Cardiff, R.D.; Seldin, D.C. Kinase-Inactive Glycogen Synthase Kinase 3 $\beta$  Promotes Wnt Signaling and Mammary Tumorigenesis. *Cancer Res* **2005**, *65*, 5792–5801. [CrossRef]
256. Ougolkov, A.V.; Fernandez-Zapico, M.E.; Savoy, D.N.; Urrutia, R.A.; Billadeau, D.D. Glycogen Synthase Kinase-3 $\beta$  Participates in Nuclear Factor  $\kappa$ B-Mediated Gene Transcription and Cell Survival in Pancreatic Cancer Cells. *Cancer Res* **2005**, *65*, 2076–2081. [CrossRef] [PubMed]
257. Wang, Z.; Smith, K.S.; Murphy, M.; Piloto, O.; Somervaille, T.C.P.; Cleary, M.L. Glycogen synthase kinase 3 in MLL leukaemia maintenance and targeted therapy. *Nature* **2008**, *455*, 1205–1209. [CrossRef] [PubMed]
258. Brassesco, M.S.; Valera, E.T.; Meyer, C.; Marschalek, R.; Lopes, B.A.; Queiroz, R.G.D.P.; Calado, R.D.T.; Scrideli, C.; Tone, L.G. A new complex rearrangement in infant ALL: T(X;11;17)(p11.2;q23;q12). *Cancer Genet.* **2018**, *228–229*, 110–114. [CrossRef]
259. Meyer, C.; Burmeister, T.; Gröger, D.; Tsaur, G.; Fehina, L.; Renneville, A.; Sutton, R.; Venn, N.C.; Emerenciano, M.; Pombo-De-Oliveira, M.S.; et al. The MLL recombinome of acute leukemias in 2017. *Leukemia* **2018**, *32*, 273–284. [CrossRef]
260. Ocasio, J.K.; Bates, R.D.P.; Rapp, C.D.; Gershon, T.R. GSK-3 modulates SHH-driven proliferation in postnatal cerebellar neurogenesis and medulloblastoma. *Development* **2019**, *146*, dev177550. [CrossRef]
261. Silva-Evangelista, C.; Barret, E.; Ménez, V.; Merlevede, J.; Kergrohen, T.; Saccasyn, A.; Oberlin, E.; Puget, S.; Beccaria, K.; Grill, J.; et al. A kinome-wide shRNA screen uncovers vaccinia-related kinase 3 (VRK3) as an essential gene for diffuse intrinsic pontine glioma survival. *Oncogene* **2019**, *38*, 6479–6490. [CrossRef]
262. Lenz, J.E.; Riester, R.; Schleicher, S.B.; Handgretinger, R.; Boehme, K.A.; Traub, F. Interaction of arsenic trioxide and etoposide in Ewing sarcoma cell lines. *Oncol. Rep.* **2019**, *43*, 337–345. [CrossRef]
263. Machado, I.; López-Guerrero, J.A.; Navarro, S.; Alberghini, M.; Scotlandi, K.; Picci, P.; Llombart-Bosch, A. Epithelial cell adhesion molecules and epithelial mesenchymal transition (EMT) markers in Ewing’s sarcoma family of tumors (ESFTs). Do they offer any prognostic significance? *Virchows Arch.* **2012**, *461*, 333–337. [CrossRef]
264. Ma, C.; Bower, K.A.; Chen, G.; Shi, X.; Ke, Z.-J.; Luo, J. Interaction between ERK and GSK3 $\beta$  Mediates Basic Fibroblast Growth Factor-induced Apoptosis in SK-N-MC Neuroblastoma Cells. *J. Biol. Chem.* **2008**, *283*, 9248–9256. [CrossRef]
265. Woodgett, J.R. Can a two-faced kinase be exploited for osteosarcoma? *Gynecol. Oncol.* **2012**, *104*, 722–723. [CrossRef]
266. Le Guellec, S.; Moyal, E.C.-J.; Filleron, T.; Delisle, M.-B.; Chevreau, C.; Rubie, H.; Castex, M.-P.; De Gauzy, J.S.; Bonneville, P.; Gomez-Brouchet, A. The  $\beta$ 5/focal adhesion kinase/glycogen synthase kinase 3 $\beta$  integrin pathway in high-grade osteosarcoma: A protein expression profile predictive of response to neoadjuvant chemotherapy. *Hum. Pathol.* **2013**, *44*, 2149–2158. [CrossRef]
267. Zeng, F.-Y.; Dong, H.; Cui, J.; Liu, L.; Chen, T. Glycogen synthase kinase 3 regulates PAX3-FKHR-mediated cell proliferation in human alveolar rhabdomyosarcoma cells. *Biochem. Biophys. Res. Commun.* **2010**, *391*, 1049–1055. [CrossRef]
268. Dionyssiou, M.G.; Ehyai, S.; Avrutin, E.; Connor, M.K.; McDermott, J.C. Glycogen synthase kinase 3 $\beta$  represses MYOGENIN function in alveolar rhabdomyosarcoma. *Cell Death Dis.* **2014**, *5*, e1094. [CrossRef]
269. Belyea, B.; Kephart, J.G.; Blum, J.; Kirsch, D.G.; Linaudic, C.M. Embryonic Signaling Pathways and Rhabdomyosarcoma: Contributions to Cancer Development and Opportunities for Therapeutic Targeting. *Sarcoma* **2012**, *2012*, 1–13. [CrossRef]
270. Ugolokov, A.V.; Bondarenko, G.I.; Dubrovskiy, O.; Berbegall, A.P.; Navarro, S.; Noguera, R.; O’Halloran, T.V.; Hendrix, M.J.; Giles, F.J.; Mazar, A.P. 9-ING-41, a small-molecule glycogen synthase kinase-3 inhibitor, is active in neuroblastoma. *Anti-Cancer Drugs* **2018**, *29*, 717–724. [CrossRef]
271. Li, Z.; Tan, F.; Thiele, C.J. Inactivation of glycogen synthase kinase-3 $\beta$  contributes to brain-derived neurotrophic factor/TrkB-induced resistance to chemotherapy in neuroblastoma cells. *Mol. Cancer Ther.* **2007**, *6*, 3113–3121. [CrossRef]
272. Duffy, D.J.; Krstic, A.; Schwarzl, T.; Higgins, D.G.; Kolch, W. GSK3 Inhibitors Regulate MYCN mRNA Levels and Reduce Neuroblastoma Cell Viability through Multiple Mechanisms, Including p53 and Wnt Signaling. *Mol. Cancer Ther.* **2014**, *13*, 454–467. [CrossRef]
273. Dickey, A.; Schleicher, S.; Leahy, K.; Hu, R.; Hallahan, D.; Thotala, D.K. GSK-3 $\beta$  inhibition promotes cell death, apoptosis, and in vivo tumor growth delay in neuroblastoma Neuro-2A cell line. *J. Neuro-Oncology* **2010**, *104*, 145–153. [CrossRef]
274. Katoh, Y.; Katoh, M. Hedgehog Target Genes: Mechanisms of Carcinogenesis Induced by Aberrant Hedgehog Signaling Activation. *Curr. Mol. Med.* **2009**, *9*, 873–886. [CrossRef] [PubMed]
275. Urbanska, K.; Trojanek, J.; Del Valle, L.; Eldeen, M.B.; Hofmann, F.; Garcia-Echeverria, C.; Khalili, K.; Reiss, K. Inhibition of IGF-I receptor in anchorage-independence attenuates GSK-3 $\beta$  constitutive phosphorylation and compromises growth and survival of medulloblastoma cell lines. *Oncogene* **2006**, *26*, 2308–2317. [CrossRef] [PubMed]
276. Atkins, R.; Stylli, S.; Luwor, R.; Kaye, A.; Hovens, C. Glycogen synthase kinase-3 $\beta$  (GSK-3 $\beta$ ) and its dysregulation in glioblastoma multiforme. *J. Clin. Neurosci.* **2013**, *20*, 1185–1192. [CrossRef] [PubMed]
277. Domoto, T.; Pyko, I.V.; Furuta, T.; Miyashita, K.; Uehara, M.; Shimasaki, T.; Nakada, M.; Minamoto, T. Glycogen synthase kinase-3 $\beta$  is a pivotal mediator of cancer invasion and resistance to therapy. *Cancer Sci.* **2016**, *107*, 1363–1372. [CrossRef] [PubMed]
278. Peti, W.; Page, R. Molecular basis of MAP kinase regulation. *Protein Sci.* **2013**, *22*, 1698–1710. [CrossRef]
279. Schaeffer, H.J.; Weber, M.J. Mitogen-Activated Protein Kinases: Specific Messages from Ubiquitous Messengers. *Mol. Cell. Biol.* **1999**, *19*, 2435–2444. [CrossRef]
280. Kim, E.K.; Choi, E.-J. Compromised MAPK signaling in human diseases: An update. *Arch. Toxicol.* **2015**, *89*, 867–882. [CrossRef]
281. Cuadrado, A.; Nebreda, A.R. Mechanisms and functions of p38 MAPK signalling. *Biochem. J.* **2010**, *429*, 403–417. [CrossRef]

282. Kim, E.K.; Choi, E.-J. Pathological roles of MAPK signaling pathways in human diseases. *Biochim. Biophys. Acta (BBA)-Mol. Basis Dis.* **2010**, *1802*, 396–405. [CrossRef]
283. Cicenás, J.; Zalyte, E.; Rimkus, A.; Dapkus, D.; Noreika, R.; Urbonavicius, S. JNK, p38, ERK, and SGK1 Inhibitors in Cancer. *Cancers* **2017**, *10*, 1. [CrossRef]
284. Mishima, K.; Inoue, K.; Hayashi, Y. Overexpression of extracellular-signal regulated kinases on oral squamous cell carcinoma. *Oral Oncol.* **2002**, *38*, 468–474. [CrossRef]
285. Kudaravalli, S.; Hollander, P.D.; Mani, S.A. Role of p38 MAP kinase in cancer stem cells and metastasis. *Oncogene* **2022**, *41*, 3177–3185. [CrossRef]
286. Tournier, C. The 2 Faces of JNK Signaling in Cancer. *Genes Cancer* **2013**, *4*, 397–400. [CrossRef]
287. Martínez-Limón, A.; Joaquin, M.; Caballero, M.; Posas, F.; de Nadal, E. The p38 Pathway: From Biology to Cancer Therapy. *Int. J. Mol. Sci.* **2020**, *21*, 1913. [CrossRef]
288. Pandey, P.; Raingeaud, J.; Kaneki, M.; Weichselbaum, R.; Davis, R.J.; Kufe, D.; Kharbanda, S. Activation of p38 Mitogen-activated Protein Kinase by c-Abl-dependent and -independent Mechanisms. *J. Biol. Chem.* **1996**, *271*, 23775–23779. [CrossRef]
289. Sui, X.; Kong, N.; Ye, L.; Han, W.; Zhou, J.; Zhang, Q.; He, C.; Pan, H. p38 and JNK MAPK pathways control the balance of apoptosis and autophagy in response to chemotherapeutic agents. *Cancer Lett.* **2014**, *344*, 174–179. [CrossRef]
290. Grossi, V.; Peserico, A.; Tezil, T.; Simone, C. p38 $\alpha$  MAPK pathway: A key factor in colorectal cancer therapy and chemoresistance. *World J. Gastroenterol.* **2014**, *20*, 9744–9758. [CrossRef]
291. Masliah-Planchon, J.; Garinet, S.; Pasmant, E. RAS-MAPK pathway epigenetic activation in cancer: miRNAs in action. *Oncotarget* **2015**, *7*, 38892–38907. [CrossRef]
292. Schubbert, S.; Shannon, K.; Bollag, G. Hyperactive Ras in developmental disorders and cancer. *Nat. Rev. Cancer* **2007**, *7*, 295–308. [CrossRef]
293. Liu, F.; Yang, X.; Geng, M.; Huang, M. Targeting ERK, an Achilles' Heel of the MAPK pathway, in cancer therapy. *Acta Pharm. Sin. B* **2018**, *8*, 552–562. [CrossRef]
294. Malumbres, M.; Barbacid, M. RAS oncogenes: The first 30 years. *Nat. Rev. Cancer* **2003**, *3*, 459–465. [CrossRef] [PubMed]
295. Hobbs, G.A.; Der, C.J.; Rossman, K.L. RAS isoforms and mutations in cancer at a glance. *J. Cell Sci.* **2016**, *129*, 1287–1292. [CrossRef]
296. Yaeger, R.; Corcoran, R.B. Targeting Alterations in the RAF–MEK Pathway. *Cancer Discov.* **2019**, *9*, 329–341. [CrossRef] [PubMed]
297. Burotto, M.; Chiou, V.L.; Lee, J.-M.; Kohn, E.C. The MAPK pathway across different malignancies: A new perspective. *Cancer* **2014**, *120*, 3446–3456. [CrossRef] [PubMed]
298. Stefan, E.; Bister, K. MYC and RAF: Key Effectors in Cellular Signaling and Major Drivers in Human Cancer. *Poxviruses* **2017**, *407*, 117–151. [CrossRef]
299. Maurer, G.; Tarkowski, B.; Baccharini, M. Raf kinases in cancer—roles and therapeutic opportunities. *Oncogene* **2011**, *30*, 3477–3488. [CrossRef]
300. Lito, P.; Rosen, N.; Solit, D.B. Tumor adaptation and resistance to RAF inhibitors. *Nat. Med.* **2013**, *19*, 1401–1409. [CrossRef]
301. The Cancer Genome Atlas Network. Genomic Classification of Cutaneous Melanoma. *Cell* **2015**, *161*, 1681–1696. [CrossRef]
302. Samatar, A.A.; Poulikakos, P.I. Targeting RAS–ERK signalling in cancer: Promises and challenges. *Nat. Rev. Drug Discov.* **2014**, *13*, 928–942. [CrossRef]
303. Pfister, S.; Janzarik, W.G.; Remke, M.; Ernst, A.; Werft, W.; Becker, N.; Toedt, G.; Wittmann, A.; Kratz, C.; Olbrich, H.; et al. BRAF gene duplication constitutes a mechanism of MAPK pathway activation in low-grade astrocytomas. *J. Clin. Investig.* **2008**, *118*, 1739–1749. [CrossRef]
304. Bar, E.E.; Lin, A.; Tihan, T.; Burger, P.C.; Eberhart, C.G. Frequent Gains at Chromosome 7q34 Involving BRAF in Pilocytic Astrocytoma. *J. Neuropathol. Exp. Neurol.* **2008**, *67*, 878–887. [CrossRef]
305. Reis, G.F.; Bloomer, M.M.; Perry, A.; Phillips, J.J.; Grenert, J.P.; Karnezis, A.N.; Tihan, T. Pilocytic astrocytomas of the optic nerve and their relation to pilocytic astrocytomas elsewhere in the central nervous system. *Mod. Pathol.* **2013**, *26*, 1279–1287. [CrossRef]
306. Anagnostopoulos, A.K.; Dimas, K.S.; Papathanassiou, C.; Braoudaki, M.; Anastasiadou, E.; Vougas, K.; Karamolegou, K.; Kontos, H.; Prodromou, N.; Tzortzatou-Stathopoulou, F.; et al. Proteomics Studies of Childhood Pilocytic Astrocytoma. *J. Proteome Res.* **2011**, *10*, 2555–2565. [CrossRef]
307. MacDonald, T.J.; Brown, K.M.; LaFleur, B.; Peterson, K.; Lawlor, C.; Chen, Y.; Packer, R.J.; Cogen, P.; Stephan, D.A. Expression profiling of medulloblastoma: PDGFRA and the RAS/MAPK pathway as therapeutic targets for metastatic disease. *Nat. Genet.* **2001**, *29*, 143–152. [CrossRef]
308. Badodi, S.; Pomella, N.; Lim, Y.M.; Brandner, S.; Morrison, G.; Pollard, S.M.; Zhang, X.; Zabet, N.R.; Marino, S. Combination of BMI1 and MAPK/ERK inhibitors is effective in medulloblastoma. *Neuro-Oncology* **2022**, *24*, 1273–1285. [CrossRef]
309. Tsumura, H.; Yoshida, T.; Saito, H.; Imanaka-Yoshida, K.; Suzuki, N. Cooperation of oncogenic K-ras and p53 deficiency in pleomorphic rhabdomyosarcoma development in adult mice. *Oncogene* **2006**, *25*, 7673–7679. [CrossRef]
310. Na, K.Y.; Kim, Y.W.; Park, Y.-K. Mitogen-activated protein kinase pathway in osteosarcoma. *Pathology* **2012**, *44*, 540–546. [CrossRef]
311. Wu, J.; Zhang, C.; Chen, L. MiR-511 mimic transfection inhibits the proliferation, invasion of osteosarcoma cells and reduces metastatic osteosarcoma tumor burden in nude mice via targeting MAPK1. *Cancer Biomarkers* **2019**, *26*, 343–351. [CrossRef]
312. Guo, H.; Zhang, H.-Y.; Wang, S.-L.; Ye, L.; Yang, G.-H.; Bu, H. Smad4 and ERK2 stimulated by transforming growth factor beta1 in rhabdomyosarcoma. *Chin. Med. J.* **2007**, *120*, 515–521. [CrossRef]

313. Lynch, J.; Fay, J.; Meehan, M.; Bryan, K.; Watters, K.M.; Murphy, D.M.; Stallings, R.L. MiRNA-335 suppresses neuroblastoma cell invasiveness by direct targeting of multiple genes from the non-canonical TGF- $\beta$  signalling pathway. *Carcinog.* **2012**, *33*, 976–985. [CrossRef]
314. Tabatabaei, S.N.; Derbali, R.M.; Yang, C.; Superstein, R.; Hamel, P.; Chain, J.L.; Hardy, P. Co-delivery of miR-181a and melphalan by lipid nanoparticles for treatment of seeded retinoblastoma. *J. Control. Release* **2019**, *298*, 177–185. [CrossRef] [PubMed]
315. Poon, R.Y.C. Cell cycle control: A system of interlinking oscillators. *Methods Mol. Biol.* **2016**, *1342*, 3–19. [PubMed]
316. Saka, Y.; Giuraniuc, C.V.; Ohkura, H. Accurate chromosome segregation by probabilistic self-organisation. *BMC Biol.* **2015**, *13*, 1–10. [CrossRef] [PubMed]
317. Gao, S.-W.; Liu, F. Novel insights into cell cycle regulation of cell fate determination. *J. Zhejiang Univ. B* **2019**, *20*, 467–475. [CrossRef]
318. Ding, L.; Cao, J.; Lin, W.; Chen, H.; Xiong, X.; Ao, H.; Yu, M.; Lin, J.; Cui, Q. The Roles of Cyclin-Dependent Kinases in Cell-Cycle Progression and Therapeutic Strategies in Human Breast Cancer. *Int. J. Mol. Sci.* **2020**, *21*, 1960. [CrossRef]
319. Pines, J. The cell cycle kinases. *Semin. Cancer Biol.* **1994**, *5*, 305–313.
320. Bruyère, C.; Meijer, L. Targeting cyclin-dependent kinases in anti-neoplastic therapy. *Curr. Opin. Cell Biol.* **2013**, *25*, 772–779. [CrossRef]
321. Chilà, R.; Guffanti, F.; Damia, G. Role and therapeutic potential of CDK12 in human cancers. *Cancer Treat. Rev.* **2016**, *50*, 83–88. [CrossRef]
322. Sherr, C.J. Cancer Cell Cycles. *Science* **1996**, *274*, 1672–1677. [CrossRef]
323. Hall, M.; Peters, G. Genetic Alterations of Cyclins, Cyclin-Dependent Kinases, and Cdk Inhibitors in Human Cancer. *Adv. Cancer Res.* **1996**, *68*, 67–108. [CrossRef]
324. Malumbres, M. Cyclins and related kinases in cancer cells. *J. BUON.* **2007**, *12* (Suppl. S1), S45–S52.
325. Malumbres, M.; Barbacid, M. Cell cycle, CDKs and cancer: A changing paradigm. *Nat. Rev. Cancer* **2009**, *9*, 153–166. [CrossRef]
326. Niwa, T.; Akaike, Y.; Watanabe, K.; Chibazakura, T. Hyperactivation of cyclin A-CDK induces centrosome overduplication and chromosome tetraploidization in mouse cells. *Biochem. Biophys. Res. Commun.* **2021**, *549*, 91–97. [CrossRef]
327. Viotto, D.; Russo, F.; Anania, I.; Segatto, I.; Vinciguerra, G.L.R.; Dall’Acqua, A.; Bomben, R.; Perin, T.; Cusan, M.; Schiappacassi, M.; et al. *CDKN1B* mutation and copy number variation are associated with tumor aggressiveness in luminal breast cancer. *J. Pathol.* **2020**, *253*, 234–245. [CrossRef]
328. Lu, Y.; Leow, A.; O Madu, C. The Role of Cyclin-Dependent Kinases on the Metastasis of Breast Cancer. *Nov. Approaches Cancer Study* **2020**, *4*, 377–385. [CrossRef]
329. Lam, Y.; E. di Tomaso, H.-K.; Ng, J.C.S.; Pang, M.F.; Roussel, N.M.; Hjelm, P. Expression of p19 INK4d, CDK4, CDK6 in glioblastoma multiforme. *Br. J. Neurosurg.* **2000**, *14*, 28–32. [CrossRef]
330. Richardson, S.; Hill, R.M.; Kui, C.; Lindsey, J.C.; Grabovksa, Y.; Keeling, C.; Pease, L.; Bashton, M.; Crosier, S.; Vinci, M.; et al. Emergence and maintenance of actionable genetic drivers at medulloblastoma relapse. *Neuro-Oncology* **2021**, *24*, 153–165. [CrossRef]
331. Wood, A.C.; Krytska, K.; Ryles, H.T.; Infarinato, N.R.; Sano, R.; Hansel, T.D.; Hart, L.S.; King, F.J.; Smith, T.R.; Ainscow, E.; et al. Dual *ALK* and *CDK4/6* Inhibition Demonstrates Synergy against Neuroblastoma. *Clin. Cancer Res.* **2017**, *23*, 2856–2868. [CrossRef]
332. Iolascon, A.; Faienza, M.F.; Coppola, B.; Rosolen, A.; Basso, G.; Ragione, F.D.; Schettini, F. Analysis of cyclin-dependent kinase inhibitor genes (*CDKN2A*, *CDKN2B*, and *CDKN2C*) in childhood rhabdomyosarcoma. *Genes Chromosomes Cancer* **1996**, *15*, 217–222. [CrossRef]
333. Komuro, H.; Valentine, M.B.; Rubnitz, J.E.; Saito, M.; Raimondi, S.C.; Carroll, A.J.; Yi, T.; Sherr, C.J.; Look, A.T. p27KIP1 Deletions in Childhood Acute Lymphoblastic Leukemia. *Neoplasia* **1999**, *1*, 253–261. [CrossRef]
334. Martinez-Soria, N.; McKenzie, L.; Draper, J.; Ptasinska, A.; Issa, H.; Potluri, S.; Blair, H.J.; Pickin, A.; Isa, A.; Chin, P.S.; et al. The Oncogenic Transcription Factor *RUNX1/ETO* Corrupts Cell Cycle Regulation to Drive Leukemic Transformation. *Cancer Cell* **2018**, *34*, 626–642.e8, Erratum in **2019**, *35*, P705. [CrossRef] [PubMed]
335. Diril, M.K.; Ratnacaram, C.K.; Padmakumar, V.C.; Du, T.; Wasser, M.; Coppola, V.; Tessarollo, L.; Kaldis, P. Cyclin-dependent kinase 1 (Cdk1) is essential for cell division and suppression of DNA re-replication but not for liver regeneration. *Proc. Natl. Acad. Sci. USA* **2012**, *109*, 3826–3831. [CrossRef] [PubMed]
336. Liu, X.; Wu, H.; Liu, Z. An Integrative Human Pan-Cancer Analysis of Cyclin-Dependent Kinase 1 (CDK1). *Cancers* **2022**, *14*, 2658. [CrossRef] [PubMed]
337. Ying, X.; Che, X.; Wang, J.; Zou, G.; Yu, Q.; Zhang, X. CDK1 serves as a novel therapeutic target for endometrioid endometrial cancer. *J. Cancer* **2021**, *12*, 2206–2215. [CrossRef]
338. Li, M.; He, F.; Zhang, Z.; Xiang, Z.; Hu, D. CDK1 serves as a potential prognostic biomarker and target for lung cancer. *J. Int. Med. Res.* **2020**, *48*. [CrossRef]
339. Kim, S.J.; Nakayama, S.; Miyoshi, Y.; Taguchi, T.; Tamaki, Y.; Matsushima, T.; Torikoshi, Y.; Tanaka, S.; Yoshida, T.; Ishihara, H.; et al. Determination of the specific activity of CDK1 and CDK2 as a novel prognostic indicator for early breast cancer. *Ann. Oncol.* **2007**, *19*, 68–72. [CrossRef]
340. Wang, C.; Xie, X.; Li, W.; Jiang, D. Expression of *KIF2A*, *NDC80*, *CDK1*, and *CCNB1* in breast cancer patients: Their interaction and linkage with tumor features and prognosis. *J. Clin. Lab. Anal.* **2022**, *36*, e24647. [CrossRef]

341. Xing, Z.; Wang, X.; Liu, J.; Zhang, M.; Feng, K.; Wang, X. Expression and prognostic value of CDK1, CCNA2, and CCNB1 gene clusters in human breast cancer. *J. Int. Med. Res.* **2021**, *49*. [CrossRef]
342. Huang, Z.; Shen, G.; Gao, J. CDK1 promotes the stemness of lung cancer cells through interacting with Sox2. *Clin. Transl. Oncol.* **2021**, *23*, 1743–1751. [CrossRef]
343. Ravindran Menon, D.; Luo, Y.; Arcaroli, J.J.; Liu, S.; Krishnankutty, L.N.; Osborne, D.G.; Li, Y.; Samson, J.M.; Bagby, S.; Tan, A.C.; et al. CDK1 Interacts with Sox2 and Promotes Tumor Initiation in Human Melanoma. *Cancer Res.* **2018**, *78*, 6561–6574. [CrossRef]
344. Zhong, S.; Yan, Q.; Ge, J.; Dou, G.; Zhao, G. Identification of driver genes and key pathways of ependymoma. *Turk. Neurosurg.* **2018**. [CrossRef]
345. Pérez-Ramírez, M.; Hernández-Jiménez, A.J.; Guerrero-Guerrero, A.; Benadón-Darszon, E.; Pérezpeña-Díazconti, M.; Siordia-Reyes, A.G.; García-Méndez, A.; de León, F.C.-P.; Salamanca-Gómez, F.A.; García-Hernández, N. Genomics and epigenetics: A study of ependymomas in pediatric patients. *Clin. Neurol. Neurosurg.* **2016**, *144*, 53–58. [CrossRef]
346. Li, Q.; Zhang, L.; Jiang, J.; Zhang, Y.; Wang, X.; Zhang, Q.; Wang, Y.; Liu, C.; Li, F. CDK1 and CCNB1 as potential diagnostic markers of rhabdomyosarcoma: Validation following bioinformatics analysis. *BMC Med. Genom.* **2019**, *12*, 198. [CrossRef]
347. Lu, S.; Sun, C.; Chen, H.; Zhang, C.; Li, W.; Wu, L.; Zhu, J.; Sun, F.; Huang, J.; Wang, J.; et al. Bioinformatics Analysis and Validation Identify CDK1 and MAD2L1 as Prognostic Markers of Rhabdomyosarcoma. *Cancer Manag. Res.* **2020**, *12*, 12123–12136. [CrossRef]
348. Schwermer, M.; Lee, S.; Köster, J.; van Maerken, T.; Stephan, H.; Eggert, A.; Morik, K.; Schulte, J.H.; Schramm, A. Sensitivity to cdk1-inhibition is modulated by p53 status in preclinical models of embryonal tumors. *Oncotarget* **2015**, *6*, 15425–15435. [CrossRef]
349. Shi, K.; Zhu, X.; Wu, J.; Chen, Y.; Zhang, J.; Sun, X. Centromere protein E as a novel biomarker and potential therapeutic target for retinoblastoma. *Bioengineered* **2021**, *12*, 5950–5970. [CrossRef]
350. Liu, J.; Wu, S.; Xie, X.; Wang, Z.; Lei, Q. Identification of potential crucial genes and key pathways in osteosarcoma. *Hereditas* **2020**, *157*, 29. [CrossRef]
351. Liu, L.; Xu, Y.; Reiter, R.J. Melatonin inhibits the proliferation of human osteosarcoma cell line MG-63. *Bone* **2013**, *55*, 432–438. [CrossRef]
352. Zhang, J.; Zhu, X.; Li, H.; Li, B.; Sun, L.; Xie, T.; Zhu, T.; Zhou, H.; Ye, Z. Piperine inhibits proliferation of human osteosarcoma cells via G2/M phase arrest and metastasis by suppressing MMP-2/-9 expression. *Int. Immunopharmacol.* **2015**, *24*, 50–58. [CrossRef]
353. Cai, D.; Latham, V.M.; Zhang, X.; Shapiro, G.I. Combined Depletion of Cell Cycle and Transcriptional Cyclin-Dependent Kinase Activities Induces Apoptosis in Cancer Cells. *Cancer Res* **2006**, *66*, 9270–9280. [CrossRef]
354. Chen, H.; Huang, Q.; Zhai, D.; Dong, J.; Wang, A.; Lan, Q. CDK1 expression and effects of CDK1 silencing on the malignant phenotype of glioma cells. *Zhonghua Zhong Liu Za Zhi* **2007**, *29*, 484–488.
355. Zhou, Y.; Yang, L.; Zhang, X.; Chen, R.; Chen, X.; Tang, W.; Zhang, M. Identification of Potential Biomarkers in Glioblastoma through Bioinformatic Analysis and Evaluating Their Prognostic Value. *BioMed Res. Int.* **2019**, *2019*, 1–13. [CrossRef] [PubMed]
356. McCurdy, S.R.; Pacal, M.; Ahmad, M.; Bremner, R. A CDK2 activity signature predicts outcome in CDK2-low cancers. *Oncogene* **2016**, *36*, 2491–2502. [CrossRef] [PubMed]
357. Santamaría, D.; Barrière, C.; Cerqueira, A.; Hunt, S.; Tardy, C.; Newton, K.; Cáceres, J.F.; Dubus, P.; Malumbres, M.; Barbacid, M. Cdk1 is sufficient to drive the mammalian cell cycle. *Nature* **2007**, *448*, 811–815. [CrossRef] [PubMed]
358. Tadesse, S.; Caldon, E.C.; Tilley, W.; Wang, S. Cyclin-Dependent Kinase 2 Inhibitors in Cancer Therapy: An Update. *J. Med. Chem.* **2018**, *62*, 4233–4251. [CrossRef]
359. Teixeira, L.K.; Wang, X.; Li, Y.; Ekholm-Reed, S.; Wu, X.; Wang, P.; Reed, S.I. Cyclin E Deregulation Promotes Loss of Specific Genomic Regions. *Curr. Biol.* **2015**, *25*, 1327–1333. [CrossRef]
360. Tadesse, S.; Anshabo, A.T.; Portman, N.; Lim, E.; Tilley, W.; Caldon, C.E.; Wang, S. Targeting CDK2 in cancer: Challenges and opportunities for therapy. *Drug Discov. Today* **2019**, *25*, 406–413. [CrossRef]
361. Campaner, S.; Doni, M.; Hydrbring, P.; Verrecchia, A.; Bianchi, L.; Sardella, D.; Schleker, T.; Perna, D.; Tronnorsjö, S.; Murga, M.; et al. Cdk2 suppresses cellular senescence induced by the c-myc oncogene. *Nature* **2009**, *12*, 54–59. [CrossRef]
362. Chen, Z.; Wang, Z.; Pang, J.; Yu, Y.; Bieerkehazhi, S.; Lu, J.; Hu, T.; Zhao, Y.; Xu, X.; Zhang, H.; et al. Multiple CDK inhibitor dinaciclib suppresses neuroblastoma growth via inhibiting CDK2 and CDK9 activity. *Sci. Rep.* **2016**, *6*, 29090. [CrossRef]
363. Bo, L.; Wei, B.; Wang, Z.; Kong, D.; Gao, Z.; Miao, Z. Bioinformatics analysis of the CDK2 functions in neuroblastoma. *Mol. Med. Rep.* **2017**, *17*, 3951–3959. [CrossRef]
364. Bolin, S.; Borgenvik, A.; Persson, C.; Rosén, G.; Sundström, A.; Qi, J.; Bradner, J.E.; Weiss, W.A.; Cho, Y.-J.; Weishaupt, H.; et al. Abstract 2473: Combined BET-bromodomain and CDK2 inhibition in MYC-driven medulloblastoma. *Cancer Res* **2016**, *76*, 2473. [CrossRef]
365. Liu, H.; Weng, J. A comprehensive bioinformatic analysis of cyclin-dependent kinase 2 (CDK2) in glioma. *Gene* **2022**, *822*, 146325. [CrossRef]
366. Zhang, Y.; Xue, C.; Zhu, X.; Xian, H.; Huang, Z. Suppression of microRNA-125a-5p upregulates the TAZ-EGFR signaling pathway and promotes retinoblastoma proliferation. *Cell Signal.* **2016**, *28*, 850–860. [CrossRef]
367. Zhang, Y.; Xue, C.; Cui, H.; Huang, Z. High expression of TAZ indicates a poor prognosis in retinoblastoma. *Diagn. Pathol.* **2015**, *10*, 187. [CrossRef]
368. Knudsen, E.S.; Pazzagli, C.; Born, T.L.; Bertolaet, B.L.; Knudsen, K.; Arden, K.C.; Henry, R.R.; Feramisco, J.R. Elevated cyclins and cyclin-dependent kinase activity in the rhabdomyosarcoma cell line RD. *Cancer Res* **1998**, *58*, 2042–2049.

369. Fu, W.; Ma, L.; Chu, B.; Wang, X.; Bagui, T.K.; Bui, M.M.; Gemmer, J.; Altiok, S.; Letson, D.G.; Pledger, W.J. Abstract 3596: SCH727965, a cyclin-dependent kinases inhibitor, induces apoptosis in sarcoma cells through caspase 3- dependent pathway. *Cancer Res* **2011**, *71*, 3596. [CrossRef]
370. Musa, J.; Cidre-Aranaz, F.; Aynaud, M.-M.; Orth, M.F.; Knott, M.M.L.; Mirabeau, O.; Mazor, G.; Varon, M.; Hölting, T.L.B.; Grossetête, S.; et al. Cooperation of cancer drivers with regulatory germline variants shapes clinical outcomes. *Nat. Commun.* **2019**, *10*, 4128. [CrossRef]
371. Ohali, A.; Avigad, S.; Zaizov, R.; Ophir, R.; Horn-Saban, S.; Cohen, I.J.; Meller, I.; Kollender, Y.; Issakov, J.; Yaniv, I. Prediction of high risk Ewing's sarcoma by gene expression profiling. *Oncogene* **2004**, *23*, 8997–9006. [CrossRef]
372. Gao, X.; Leone, G.W.; Wang, H. Cyclin D-CDK4/6 functions in cancer. *Adv. Cancer Res.* **2020**, *148*, 147–169.
373. Dobashi, Y.; Goto, A.; Fukayama, M.; Abe, A.; Ooi, A. Overexpression of cdk4/cyclin D1, a possible mediator of apoptosis and an indicator of prognosis in human primary lung carcinoma. *Int. J. Cancer* **2004**, *110*, 532–541. [CrossRef]
374. Nadal, A.; Jares, P.; Pinyol, M.; Conde, L.; Romeu, C.; Fernández, P.L.; Campo, E.; Cardesa, A. Association of CDK4 and CCND1 mRNA overexpression in laryngeal squamous cell carcinomas occurs without CDK4 amplification. *Virchows Arch.* **2006**, *450*, 161–167. [CrossRef] [PubMed]
375. Hashimoto, H.; Kaku-Ito, Y.; Oda, Y.; Ito, T. CDK4: A Novel Therapeutic Target for Extramammary Paget's Disease. *Front. Oncol.* **2021**, *11*, 710378. [CrossRef] [PubMed]
376. Dong, Y.; Sui, L.; Sugimoto, K.; Tai, Y.; Tokuda, M. Cyclin D1-CDK4 complex, a possible critical factor for cell proliferation and prognosis in laryngeal squamous cell carcinomas. *Int. J. Cancer* **2001**, *95*, 209–215. [CrossRef] [PubMed]
377. Chen, T.-J.; Lee, S.-W.; Lin, L.-C.; Lin, C.-Y.; Chang, K.-Y.; Li, C.-F. Cyclin-dependent kinase 4 overexpression is mostly independent of gene amplification and constitutes an independent prognosticator for nasopharyngeal carcinoma. *Tumor Biol.* **2014**, *35*, 7209–7216. [CrossRef]
378. Wu, A.; Wu, B.; Guo, J.; Luo, W.; Wu, D.; Yang, H.; Zhen, Y.; Yu, X.; Wang, H.; Zhou, Y.; et al. Elevated expression of CDK4 in lung cancer. *J. Transl. Med.* **2011**, *9*, 38. [CrossRef]
379. Lu, J.-W.; Lin, Y.-M.; Chang, J.-G.; Yeh, K.-T.; Chen, R.-M.; Tsai, J.J.P.; Su, W.-W.; Hu, R.-M. Clinical implications of deregulated CDK4 and Cyclin D1 expression in patients with human hepatocellular carcinoma. *Med. Oncol.* **2013**, *30*, 379. [CrossRef]
380. An, H.-X.; Beckmann, M.W.; Reifenberger, G.; Bender, H.G.; Niederacher, D. Gene Amplification and Overexpression of CDK4 in Sporadic Breast Carcinomas Is Associated with High Tumor Cell Proliferation. *Am. J. Pathol.* **1999**, *154*, 113–118. [CrossRef]
381. Yang, C.; Li, Z.; Bhatt, T.; Dickler, M.; Giri, D.; Scaltriti, M.; Baselga, J.; Rosen, N.; Chandralapaty, S. Acquired CDK6 amplification promotes breast cancer resistance to CDK4/6 inhibitors and loss of ER signaling and dependence. *Oncogene* **2016**, *36*, 2255–2264. [CrossRef]
382. Wölfel, T.; Hauer, M.; Schneider, J.; Serrano, M.; Wölfel, C.; Klehmann-Hieb, E.; De Plaen, E.; Hankeln, T.; Büschenfelde, K.-H.M.Z.; Beach, D. A p16<sup>INK4a</sup>-Insensitve CDK4 Mutant Targeted by Cytolytic T Lymphocytes in a Human Melanoma. *Science* **1995**, *269*, 1281–1284. [CrossRef]
383. Kim, H.; Ham, E.K.; Kim, Y.I.; Chi, J.G.; Lee, H.S.; Park, S.H.; Jung, Y.M.; Myung, N.K.; Lee, M.J.; Jang, J.-J. Overexpression of cyclin D1 and cdk4 in tumorigenesis of sporadic hepatoblastomas. *Cancer Lett.* **1998**, *131*, 177–183. [CrossRef]
384. Nebenfuehr, S.; Kollmann, K.; Sexl, V. The role of CDK6 in cancer. *Int. J. Cancer* **2020**, *147*, 2988–2995. [CrossRef]
385. Jena, N.; Sheng, J.; Hu, J.K.; Li, W.; Zhou, W.; Lee, G.; Tschlis, N.; A Pathak, A.; Brown, N.; A Deshpande, A.; et al. CDK6-mediated repression of CD25 is required for induction and maintenance of Notch1-induced T-cell acute lymphoblastic leukemia. *Leukemia* **2015**, *30*, 1033–1043. [CrossRef]
386. Kollmann, K.; Sexl, V. CDK6 and p16INK4A in lymphoid malignancies. *Oncotarget* **2013**, *4*, 1858–1859. [CrossRef]
387. Placke, T.; Faber, K.; Nonami, A.; Putwain, S.L.; Salih, H.R.; Heidel, F.H.; Krämer, A.; Root, D.E.; Barbie, D.A.; Krivtsov, A.V.; et al. Requirement for CDK6 in MLL-rearranged acute myeloid leukemia. *Blood* **2014**, *124*, 13–23. [CrossRef]
388. Van der Linden, M.; Willekes, M.; van Roon, E.; Seslija, L.; Schneider, P.; Pieters, R.; Stam, R. MLL fusion-driven activation of CDK6 potentiates proliferation in MLL-rearranged infant ALL. *Cell Cycle* **2014**, *13*, 834–844. [CrossRef]
389. Faussillon, M.; Monnier, L.; Junien, C.; Jeanpierre, C. Frequent overexpression of cyclin D2/cyclin-dependent kinase 4 in Wilms' tumor. *Cancer Lett.* **2005**, *221*, 67–75. [CrossRef]
390. Haruta, M.; Arai, Y.; Okita, H.; Tanaka, Y.; Takimoto, T.; Sugino, R.P.; Yamada, Y.; Kamijo, T.; Oue, T.; Fukuzawa, M.; et al. Combined Genetic and Chromosomal Characterization of Wilms Tumors Identifies Chromosome 12 Gain as a Potential New Marker Predicting a Favorable Outcome. *Neoplasia* **2018**, *21*, 117–131. [CrossRef]
391. Schubert, N.A.; Chen, C.Y.; Rodriguez, A.; Koster, J.; Dowless, M.; Pfister, S.M.; Shields, D.J.; Stancato, L.F.; Vassal, G.; Caron, H.N.; et al. Target actionability review to evaluate CDK4/6 as a therapeutic target in paediatric solid and brain tumours. *Eur. J. Cancer* **2022**, *170*, 196–208. [CrossRef]
392. Iwata, S.; Tatsumi, Y.; Yonemoto, T.; Araki, A.; Itami, M.; Kamoda, H.; Tsukanishi, T.; Hagiwara, Y.; Kinoshita, H.; Ishii, T.; et al. CDK4 overexpression is a predictive biomarker for resistance to conventional chemotherapy in patients with osteosarcoma. *Oncol. Rep.* **2021**, *46*, 1–11. [CrossRef]
393. Zhou, Y.; Shen, J.K.; Yu, Z.; Hornicek, F.J.; Kan, Q.; Duan, Z. Expression and therapeutic implications of cyclin-dependent kinase 4 (CDK4) in osteosarcoma. *Biochim. Biophys. Acta (BBA)-Mol. Basis Dis.* **2018**, *1864*, 1573–1582. [CrossRef]
394. Wunder, J.S.; Eppert, K.; Burrow, S.R.; Gogkoz, N.; Bell, R.S.; Andrulis, I.L. Co-amplification and overexpression of CDK4, SAS and MDM2 occurs frequently in human parosteal osteosarcomas. *Oncogene* **1999**, *18*, 783–788. [CrossRef] [PubMed]



395. Suehara, Y.; Alex, D.; Bowman, A.; Middha, S.; Zehir, A.; Chakravarty, D.; Wang, L.; Jour, G.; Nafa, K.; Hayashi, T.; et al. Clinical Genomic Sequencing of Pediatric and Adult Osteosarcoma Reveals Distinct Molecular Subsets with Potentially Targetable Alterations. *Clin. Cancer Res.* **2019**, *25*, 6346–6356. [CrossRef] [PubMed]
396. Guimarães, G.; Tesser-Gamba, F.; Petrilli, A.; Donato-Macedo, C.; Alves, M.; de Lima, F.; Garcia-Filho, R.; Oliveira, R.; Toledo, S. Molecular profiling of osteosarcoma in children and adolescents from different age groups using a next-generation sequencing panel. *Cancer Genet.* **2021**, *258–259*, 85–92. [CrossRef] [PubMed]
397. Hettmer, S.; Linardic, C.M.; Kelsey, A.; Rudzinski, E.R.; Vokuhl, C.; Selfe, J.; Ruhen, O.; Shern, J.F.; Khan, J.; Kovach, A.R.; et al. Molecular testing of rhabdomyosarcoma in clinical trials to improve risk stratification and outcome: A consensus view from European paediatric Soft tissue sarcoma Study Group, Children’s Oncology Group and Cooperative Weichteilsarkom-Studiengruppe. *Eur. J. Cancer* **2022**, *172*, 367–386. [CrossRef]
398. Barr, F.G.; Duan, F.; Smith, L.M.; Gustafson, D.; Pitts, M.; Hammond, S.; Gastier-Foster, J.M. Genomic and clinical analyses of 2p24 and 12q13-q14 amplification in alveolar rhabdomyosarcoma: A report from the Children’s Oncology Group. *Genes Chromosom. Cancer* **2009**, *48*, 661–672. [CrossRef]
399. de Andrade, C.R.; Jr, A.T.; Nishimoto, I.N.; Kowalski, L.P.; Lopes, M.A. Rhabdomyosarcoma of the head and neck: A clinicopathological and immunohistochemical analysis of 29 cases. *Braz. Dent. J.* **2010**, *21*, 68–73. [CrossRef]
400. Ragazzini, P.; Gamberi, G.; Pazzaglia, L.; Serra, M.; Magagnoli, G. Amplification of CDK4, MDM2, SAS and GLI genes in leiomyosarcoma, alveolar and embryonal rhabdomyosarcoma. *Histol. Histopathol.* **2004**, 401–411. [CrossRef]
401. Saab, R.; Bills, J.L.; Miceli, A.P.; Anderson, C.M.; Khoury, J.D.; Fry, D.W.; Navid, F.; Houghton, P.J.; Skapek, S.X. Pharmacologic inhibition of cyclin-dependent kinase 4/6 activity arrests proliferation in myoblasts and rhabdomyosarcoma-derived cells. *Mol. Cancer Ther.* **2006**, *5*, 1299–1308. [CrossRef]
402. Barghi, F.; Shannon, H.E.; Saadatzaheh, M.R.; Bailey, B.J.; Riyahi, N.; Bijangi-Vishehsaraei, K.; Just, M.; Ferguson, M.J.; Pandya, P.H.; Pollok, K.E. Precision Medicine Highlights Dysregulation of the CDK4/6 Cell Cycle Regulatory Pathway in Pediatric, Adolescents and Young Adult Sarcomas. *Cancers* **2022**, *14*, 3611. [CrossRef]
403. Kennedy, A.L.; Vallurupalli, M.; Chen, L.; Crompton, B.; Cowley, G.; Vazquez, F.; Weir, B.A.; Tsherniak, A.; Parasuraman, S.; Kim, S.; et al. Functional, chemical genomic, and super-enhancer screening identify sensitivity to cyclin D1/CDK4 pathway inhibition in Ewing sarcoma. *Oncotarget* **2015**, *6*, 30178–30193. [CrossRef]
404. Molenaar, J.J.; Ebus, M.E.; Koster, J.; van Sluis, P.; van Noesel, C.J.; Versteeg, R.; Caron, H.N. Cyclin D1 and CDK4 Activity Contribute to the Undifferentiated Phenotype in Neuroblastoma. *Cancer Res* **2008**, *68*, 2599–2609. [CrossRef]
405. Rader, J.; Russell, M.R.; Hart, L.S.; Nakazawa, M.S.; Belcastro, L.T.; Martinez, D.; Li, Y.; Carpenter, E.L.; Attiyeh, E.F.; Diskin, S.J.; et al. Dual CDK4/CDK6 Inhibition Induces Cell-Cycle Arrest and Senescence in Neuroblastoma. *Clin. Cancer Res.* **2013**, *19*, 6173–6182. [CrossRef]
406. Amoroso, L.; Ognibene, M.; Morini, M.; Conte, M.; Di Cataldo, A.; Tondo, A.; D’Angelo, P.; Castellano, A.; Garaventa, A.; Lasorsa, V.A.; et al. Genomic coamplification of CDK4/MDM2/FRS2 is associated with very poor prognosis and atypical clinical features in neuroblastoma patients. *Genes Chromosom. Cancer* **2019**, *59*, 277–285. [CrossRef]
407. Huang, W.; Hao, Z.; Mao, F.; Guo, D. Small Molecule Inhibitors in Adult High-Grade Glioma: From the Past to the Future. *Front. Oncol.* **2022**, *12*, 911876. [CrossRef]
408. Liu, A.; Zhao, H.; Sun, B.; Han, X.; Zhou, D.; Cui, Z.; Ma, X.; Zhang, J.; Yuan, L. A predictive analysis approach for paediatric and adult high-grade glioma: miRNAs and network insight. *Ann. Transl. Med.* **2020**, *8*, 242. [CrossRef]
409. Rallis, K.S.; George, A.M.; Wozniak, A.M.; Bigogno, C.M.; Chow, B.; Hanrahan, J.G.; Sideris, M. Molecular Genetics and Targeted Therapies for Paediatric High-grade Glioma. *Cancer Genom.-Proteom.* **2022**, *19*, 390–414. [CrossRef]
410. Sepúlveda-Sánchez, J.M.; Gil-Gil, M.; Alonso-García, M.; Salgado, M.V.; Vicente, E.; Barroso, C.M.; Sánchez, R.; Durán, G.; Peñas, R.D.L.; Muñoz-Langa, J.; et al. Phase II Trial of Palbociclib in Recurrent Retinoblastoma-Positive Anaplastic Oligodendroglioma: A Study from the Spanish Group for Research in Neuro-Oncology (GEINO). *Target. Oncol.* **2020**, *15*, 613–622. [CrossRef]
411. Zangen, I.L.; Kneitz, S.; Monoranu, C.-M.; Rutkowski, S.; Hinkes, B.; Vince, G.H.; Huang, B.; Roggendorf, W. Ependymoma gene expression profiles associated with histological subtype, proliferation, and patient survival. *Acta Neuropathol.* **2007**, *113*, 325–337. [CrossRef]
412. Liang, M.-L.; Chen, C.-H.; Liu, Y.-R.; Huang, M.-H.; Lin, Y.-C.; Wong, T.-T.; Lin, S.-E.; Chu, S.-S.; Ding, Y.-H.; Hsieh, T.-H. Abemaciclib, A Selective CDK4/6 Inhibitor, Restricts the Growth of Pediatric Ependymomas. *Cancers* **2020**, *12*, 3597. [CrossRef]
413. Magalhães, T.D.A.; Cruzeiro, G.A.V.; de Sousa, G.R.; da Silva, K.R.; Lira, R.C.P.; Scrideli, C.A.; Tone, L.G.; Valera, E.T.; Borges, K.S. Notch pathway in ependymoma RELA-fused subgroup: Upregulation and association with cancer stem cells markers expression. *Cancer Gene Ther.* **2019**, *27*, 509–512. [CrossRef]
414. Lummus, S.C.; Donson, A.M.; Gowan, K.; Jones, K.L.; Vibhakar, R.; Foreman, N.K.; Kleinschmidt-DeMasters, B.K. p16Loss and E2F/cell cycle deregulation in infant posterior fossa ependymoma. *Pediatr. Blood Cancer* **2017**, *64*, e26656. [CrossRef] [PubMed]
415. Shupp, A.; Casimiro, M.C.; Pestell, R.G. Biological functions of CDK5 and potential CDK5 targeted clinical treatments. *Oncotarget* **2017**, *8*, 17373–17382. [CrossRef] [PubMed]
416. Sharma, S.; Sicinski, P. A kinase of many talents: Non-neuronal functions of CDK5 in development and disease. *Open Biol.* **2020**, *10*, 190287. [CrossRef] [PubMed]
417. Shah, K.; Rossie, S. Tale of the Good and the Bad Cdk5: Remodeling of the Actin Cytoskeleton in the Brain. *Mol. Neurobiol.* **2017**, *55*, 3426–3438. [CrossRef]

418. Liu, W.; Li, J.; Song, Y.-S.; Li, Y.; Jia, Y.-H.; Zhao, H.-D. Cdk5 links with DNA damage response and cancer. *Mol. Cancer* **2017**, *16*, 60. [CrossRef]
419. Liu, S.-L.; Wang, C.; Jiang, T.; Tan, L.; Xing, A.; Yu, J.-T. The Role of Cdk5 in Alzheimer's Disease. *Mol. Neurobiol.* **2015**, *53*, 4328–4342. [CrossRef]
420. Liang, Q.; Li, L.; Zhang, J.; Lei, Y.; Wang, L.; Liu, D.-X.; Feng, J.; Hou, P.; Yao, R.; Zhang, Y.; et al. CDK5 is essential for TGF- $\beta$ 1-induced epithelial-mesenchymal transition and breast cancer progression. *Sci. Rep.* **2013**, *3*, 2932. [CrossRef]
421. Zeng, J.; Xie, S.; Liu, Y.; Shen, C.; Song, X.; Zhou, G.-L.; Wang, C. CDK5 Functions as a Tumor Promoter in Human Lung Cancer. *J. Cancer* **2018**, *9*, 3950–3961. [CrossRef]
422. Lin, H.; Lin, T.-Y.; Juang, J.-L. Abl deregulates Cdk5 kinase activity and subcellular localization in *Drosophila* neurodegeneration. *Cell Death Differ.* **2006**, *14*, 607–615. [CrossRef]
423. de Porras, V.R.; Bystrup, S.; Heras, S.C.-D.L.; Musulén, E.; Palomero, L.; Alonso, M.H.; Nieto, R.; Arango, D.; Moreno, V.; Queralt, C.; et al. Tumor Expression of Cyclin-Dependent Kinase 5 (Cdk5) Is a Prognostic Biomarker and Predicts Outcome of Oxaliplatin-Treated Metastatic Colorectal Cancer Patients. *Cancers* **2019**, *11*, 1540. [CrossRef]
424. Zhou, Y.; Wang, X.; Lv, P.; Yu, H.; Jiang, X. CDK5 Knockdown inhibits proliferation and induces apoptosis and Cell Cycle Arrest in Human Glioblastoma. *J. Cancer* **2021**, *12*, 3958–3966. [CrossRef]
425. Lin, H.; Chen, M.-C.; Chiu, C.-Y.; Song, Y.-M.; Lin, S.-Y. Cdk5 Regulates STAT3 Activation and Cell Proliferation in Medullary Thyroid Carcinoma Cells. *J. Biol. Chem.* **2007**, *282*, 2776–2784. [CrossRef]
426. Oner, M.; Lin, E.; Chen, M.-C.; Hsu, F.-N.; Prince, G.M.S.H.; Chiu, K.-Y.; Teng, C.-L.J.; Yang, T.-Y.; Wang, H.-Y.; Yue, C.-H.; et al. Future Aspects of CDK5 in Prostate Cancer: From Pathogenesis to Therapeutic Implications. *Int. J. Mol. Sci.* **2019**, *20*, 3881. [CrossRef]
427. Huang, P.-H.; Chen, M.-C.; Peng, Y.-T.; Kao, W.-H.; Chang, C.-H.; Wang, Y.-C.; Lai, C.-H.; Hsieh, J.-T.; Wang, J.-H.; Lee, Y.-T.; et al. Cdk5 Directly Targets Nuclear p21CIP1 and Promotes Cancer Cell Growth. *Cancer Res* **2016**, *76*, 6888–6900. [CrossRef]
428. Sun, Y.-Q.; Xie, J.-W.; Xie, H.-T.; Chen, P.-C.; Zhang, X.-L.; Zheng, C.-H.; Li, P.; Wang, J.-B.; Lin, J.-X.; Cao, L.-L.; et al. Expression of CRM1 and CDK5 shows high prognostic accuracy for gastric cancer. *World J. Gastroenterol.* **2017**, *23*, 2012–2022. [CrossRef]
429. Kour, S.; Rana, S.; Contreras, J.I.; King, H.M.; Robb, C.M.; Sonawane, Y.A.; Bendjennat, M.; Crawford, A.J.; Barger, C.J.; Kizhake, S.; et al. CDK5 Inhibitor Downregulates Mcl-1 and Sensitizes Pancreatic Cancer Cell Lines to Navitoclax. *Mol. Pharmacol.* **2019**, *96*, 419–429. [CrossRef]
430. Mukherjee, S.; Tucker-Burden, C.; Kaissi, E.; Newsam, A.; Duggireddy, H.; Chau, M.; Zhang, C.; Diwedi, B.; Rupji, M.; Seby, S.; et al. CDK5 Inhibition Resolves PKA/cAMP-Independent Activation of CREB1 Signaling in Glioma Stem Cells. *Cell Rep.* **2018**, *23*, 1651–1664. [CrossRef]
431. Do, P.A.; Lee, C.H. The Role of CDK5 in Tumours and Tumour Microenvironments. *Cancers* **2020**, *13*, 101. [CrossRef]
432. Gao, G.-B.; Sun, Y.; Fang, R.-D.; Wang, Y.; Wang, Y.; He, Q.-Y. Post-translational modifications of CDK5 and their biological roles in cancer. *Mol. Biomed.* **2021**, *2*, 1–15. [CrossRef]
433. Peyressatre, M.; Laure, A.; Pellerano, M.; Boukhaddaoui, H.; Soussi, I.; Morris, M.C. Fluorescent Biosensor of CDK5 Kinase Activity in Glioblastoma Cell Extracts and Living Cells. *Biotechnol. J.* **2020**, *15*, e1900474. [CrossRef]
434. Binlath, T.; Reudhabadh, R.; Prommeenat, P.; Hutamekalin, P. Investigation of mechanisms underlying the inhibitory effects of metformin against proliferation and growth of neuroblastoma SH-SY5Y cells. *Toxicol. Vitro.* **2022**, *83*, 105410. [CrossRef] [PubMed]
435. Yushan, R.; Wenjie, C.; Suning, H.; Yiwu, D.; Tengfei, Z.; Madushi, W.M.; Feifei, L.; Changwen, Z.; Xin, W.; Roodrajeetsing, G.; et al. Insights into the clinical value of cyclin-dependent kinase 5 in glioma: A retrospective study. *World J. Surg. Oncol.* **2015**, *13*, 223. [CrossRef] [PubMed]
436. Catania, A.; Urban, S.; Yan, E.; Hao, C.; Barron, G.; Allalunis-Turner, J. Expression and localization of cyclin-dependent kinase 5 in apoptotic human glioma cells. *Neuro-Oncology* **2001**, *3*, 89–98. [CrossRef] [PubMed]
437. de Nigris, F.; Mancini, F.P.; Schiano, C.; Infante, T.; Zullo, A.; Minucci, P.B.; Al-Omran, M.; Giordano, A.; Napoli, C. Osteosarcoma cells induce endothelial cell proliferation during neo-angiogenesis. *J. Cell. Physiol.* **2012**, *228*, 846–852. [CrossRef] [PubMed]
438. Bao, H.-X.; Bi, Q.; Han, Y.; Zhao, C.; Zou, H. Potential mechanisms underlying CDK5 related Osteosarcoma progression. *Expert Opin. Ther. Targets* **2017**, *21*, 455–460. [CrossRef]
439. Fu, H.; Zhao, H.; Yang, Y.; Duan, K.; Guo, T. CDK5 Inhibitor Seliciclib Promotes Osteoblastic Differentiation of MSCs and Suppresses the Migration of MG-63 Osteosarcoma Cells. *BioRxiv* **2020**. [CrossRef]
440. Saidak, Z.; Le Henaff, C.; Azzi, S.; Marty, C.; Da Nascimento, S.; Sonnet, P.; Marie, P.J. Wnt/ $\beta$ -Catenin Signaling Mediates Osteoblast Differentiation Triggered by Peptide-induced  $\alpha$ 5 $\beta$ 1 Integrin Priming in Mesenchymal Skeletal Cells. *J. Biol. Chem.* **2015**, *290*, 6903–6912. [CrossRef]
441. Schwalbe, E.C.; Lindsey, J.C.; Nakjang, S.; Crosier, S.; Smith, A.J.; Hicks, D.; Rafiee, G.; Hill, R.M.; Iliasova, A.; Stone, T.; et al. Novel molecular subgroups for clinical classification and outcome prediction in childhood medulloblastoma: A cohort study. *Lancet Oncol.* **2017**, *18*, 958–971. [CrossRef]
442. Dorand, R.D.; Nthale, J.; Myers, J.T.; Barkauskas, D.S.; Avril, S.; Chirieleison, S.M.; Pareek, T.K.; Abbott, D.W.; Stearns, D.S.; Letterio, J.J.; et al. Cdk5 disruption attenuates tumor PD-L1 expression and promotes antitumor immunity. *Science* **2016**, *353*, 399–403. [CrossRef]
443. Sava, G.P.; Fan, H.; Coombes, R.C.; Buluwela, L.; Ali, S. CDK7 inhibitors as anticancer drugs. *Cancer Metastasis Rev.* **2020**, *39*, 805–823. [CrossRef]

444. Schachter, M.M.; Fisher, R.P. The CDK-activating kinase Cdk7: Taking yes for an answer. *Cell Cycle* **2013**, *12*, 3239–3240. [CrossRef]
445. Chipumuro, E.; Marco, E.; Christensen, C.L.; Kwiatkowski, N.; Zhang, T.; Hatheway, C.M.; Abraham, B.J.; Sharma, B.; Yeung, C.; Altabef, A.; et al. CDK7 Inhibition Suppresses Super-Enhancer-Linked Oncogenic Transcription in MYCN-Driven Cancer. *Cell* **2014**, *159*, 1126–1139. [CrossRef]
446. Fisher, R.P. Cdk7: A kinase at the core of transcription and in the crosshairs of cancer drug discovery. *Transcription* **2018**, *10*, 47–56. [CrossRef]
447. Bacon, C.W.; D’Orso, I. CDK9: A signaling hub for transcriptional control. *Transcription* **2018**, *10*, 57–75. [CrossRef]
448. Zhang, H.; Pandey, S.; Travers, M.; Sun, H.; Morton, G.; Madzo, J.; Chung, W.; Khowsathit, J.; Perez-Leal, O.; Barrero, C.A.; et al. Targeting CDK9 Reactivates Epigenetically Silenced Genes in Cancer. *Cell* **2018**, *175*, 1244–1258.e26. [CrossRef]
449. Patel, H.; Abduljabbar, R.; Lai, C.-F.; Periyasamy, M.; Harrod, A.; Gemma, C.; Steel, J.H.; Patel, N.; Busonero, C.; Jerjees, D.; et al. Expression of CDK7, Cyclin H, and MAT1 Is Elevated in Breast Cancer and Is Prognostic in Estrogen Receptor-Positive Breast Cancer. *Clin. Cancer Res.* **2016**, *22*, 5929–5938. [CrossRef]
450. Naseh, G.; Mohammadifard, M. Upregulation of cyclin-dependent kinase 7 and matrix metalloproteinase-14 expression contribute to metastatic properties of gastric cancer. *IUBMB Life* **2016**, *68*, 799–805. [CrossRef]
451. Jagomast, T.; Idel, C.; Klapper, L.; Kuppler, P.; Offermann, A.; Dreyer, E.; Bruchhage, K.-L.; Ribbat-Idel, J.; Perner, S. CDK7 Predicts Worse Outcome in Head and Neck Squamous-Cell Cancer. *Cancers* **2022**, *14*, 492. [CrossRef]
452. Kim, J.; Cho, Y.-J.; Ryu, J.-Y.; Hwang, I.; Han, H.D.; Ahn, H.J.; Kim, W.Y.; Cho, H.; Chung, J.-Y.; Hewitt, S.M.; et al. CDK7 is a reliable prognostic factor and novel therapeutic target in epithelial ovarian cancer. *Gynecol. Oncol.* **2020**, *156*, 211–221. [CrossRef]
453. Tang, L.; Zhu, C.; Jin, J.; Wang, X.; Yu, L.; Guan, X. Expression of CDK7 correlates with molecular subtypes and predicts clinical outcomes in breast cancer. *Transl. Cancer Res.* **2021**, *10*, 669–680. [CrossRef]
454. Kretz, A.-L.; Schaum, M.; Richter, J.; Kitzig, E.F.; Engler, C.C.; Leithäuser, F.; Henne-Bruns, D.; Knippschild, U.; Lemke, J. CDK9 is a prognostic marker and therapeutic target in pancreatic cancer. *Tumor Biol.* **2017**, *39*. [CrossRef] [PubMed]
455. Yang, W.; Liu, S.; Luo, Q.; Tan, X. Expression of CDK9 in endometrial cancer tissues and its effect on the proliferation of HEC-1B. *Open Life Sci.* **2021**, *16*, 1341–1346. [CrossRef] [PubMed]
456. Rasool, R.U.; Natesan, R.; Deng, Q.; Aras, S.; Lal, P.; Effron, S.S.; Mitchell-Velasquez, E.; Posimo, J.M.; Carskadon, S.; Baca, S.C.; et al. CDK7 Inhibition Suppresses Castration-Resistant Prostate Cancer through MED1 Inactivation. *Cancer Discov.* **2019**, *9*, 1538–1555. [CrossRef] [PubMed]
457. Gao, X.; Liang, J.; Wang, L.; Zhang, Z.; Yuan, P.; Wang, J.; Gao, Y.; Ma, F.; Calagua, C.; Ye, H.; et al. Phosphorylation of the androgen receptor at Ser81 is co-sustained by CDK1 and CDK9 and leads to AR-mediated transactivation in prostate cancer. *Mol. Oncol.* **2021**, *15*, 1901–1920. [CrossRef] [PubMed]
458. Nagaraja, S.; Vitanza, N.A.; Woo, P.J.; Taylor, K.R.; Liu, F.; Zhang, L.; Li, M.; Meng, W.; Ponnuswami, A.; Sun, W.; et al. Transcriptional Dependencies in Diffuse Intrinsic Pontine Glioma. *Cancer Cell* **2017**, *31*, 635–652.e6. [CrossRef]
459. Ma, H.; Dean, D.C.; Wei, R.; Hornicek, F.J.; Duan, Z. Cyclin-dependent kinase 7 (CDK7) is an emerging prognostic biomarker and therapeutic target in osteosarcoma. *Ther. Adv. Musculoskelet. Dis.* **2021**, *13*. [CrossRef]
460. Zhang, J.; Liu, W.; Zou, C.; Zhao, Z.; Lai, Y.; Shi, Z.; Xie, X.; Huang, G.; Wang, Y.; Zhang, X.; et al. Targeting Super-Enhancer-Associated Oncogenes in Osteosarcoma with THZ2, a Covalent CDK7 Inhibitor. *Clin. Cancer Res.* **2020**, *26*, 2681–2692. [CrossRef]
461. Ma, H.; Seebacher, N.A.; Hornicek, F.J.; Duan, Z. Cyclin-dependent kinase 9 (CDK9) is a novel prognostic marker and therapeutic target in osteosarcoma. *Ebiomedicine* **2018**, *39*, 182–193. [CrossRef]
462. Qin, J.-J. Is CDK9 a promising target for both primary and metastatic osteosarcoma? *Ebiomedicine* **2019**, *40*, 27–28. [CrossRef]
463. Iniguez, A.B.; Stolte, B.; Wang, E.J.; Conway, A.S.; Alexe, G.; Dharia, N.V.; Kwiatkowski, N.; Zhang, T.; Abraham, B.J.; Mora, J.; et al. EWS/FLI Confers Tumor Cell Synthetic Lethality to CDK12 Inhibition in Ewing Sarcoma. *Cancer Cell* **2018**, *33*, 202–216.e6. [CrossRef]
464. Ning, J.; Ma, X.; Long, C.; Mao, Y.; Kuang, X.; Huang, Z.; Fan, Y.; Zhang, H.; Xia, Q.; Wang, R.; et al. Anti-tumor Drug THZ1 Suppresses TGFβ2-mediated EMT in Lens Epithelial Cells via Notch and TGFβ/Smad Signaling Pathway. *J. Cancer* **2019**, *10*, 3778–3788. [CrossRef]
465. Cassandri, M.; Fioravanti, R.; Pomella, S.; Valente, S.; Rotili, D.; Del Baldo, G.; De Angelis, B.; Rota, R.; Mai, A. CDK9 as a Valuable Target in Cancer: From Natural Compounds Inhibitors to Current Treatment in Pediatric Soft Tissue Sarcomas. *Front. Pharmacol.* **2020**, *11*, 1230. [CrossRef]
466. Simone, C.; Giordano, A. Abrogation of signal-dependent activation of the cdk9/cyclin T2a complex in human RD rhabdomyosarcoma cells. *Cell Death Differ.* **2006**, *14*, 192–195. [CrossRef]
467. Richter, G.H.; Hensel, T.; Schmidt, O.; Saratov, V.; von Heyking, K.; Becker-Dettling, F.; Prexler, C.; Yen, H.-Y.; Steiger, K.; Fulda, S.; et al. Combined Inhibition of Epigenetic Readers and Transcription Initiation Targets the EWS-ETS Transcriptional Program in Ewing Sarcoma. *Cancers* **2020**, *12*, 304. [CrossRef]
468. De Falco, G.; Bellan, C.; D’Amuri, A.; Angeloni, G.; Leucci, E.; Giordano, A.; Leoncini, L. Cdk9 regulates neural differentiation and its expression correlates with the differentiation grade of neuroblastoma and PNET tumors. *Cancer Biol. Ther.* **2005**, *4*, 277–281. [CrossRef]
469. Poon, E.; Liang, T.; Jamin, Y.; Walz, S.; Kwok, C.; Hakkert, A.; Barker, K.; Urban, Z.; Thway, K.; Zeid, R.; et al. Orally bioavailable CDK9/2 inhibitor shows mechanism-based therapeutic potential in MYCN-driven neuroblastoma. *J. Clin. Investig.* **2020**, *130*, 5875–5892. [CrossRef]

470. Hamanaka, R.; Maloid, S.; Smith, M.R.; O'Connell, C.D.; Longo, D.L.; Ferris, D.K. Cloning and characterization of human and murine homologues of the Drosophila polo serine-threonine kinase. *Cell Growth Differ.* **1994**, *5*, 249–257.
471. Johnson, E.F.; Stewart, K.; Woods, K.W.; Giranda, V.L.; Luo, Y. Pharmacological and Functional Comparison of the Polo-like Kinase Family: Insight into Inhibitor and Substrate Specificity. *Biochemistry* **2007**, *46*, 9551–9563. [CrossRef]
472. Cizmecioglu, O.; Warnke, S.; Arnold, M.; Duensing, S.; Hoffmann, I. Plk2 regulated centriole duplication is dependent on its localization to the centrosome and a functional polo-box domain. *Cell Cycle* **2008**, *7*, 3548–3555. [CrossRef]
473. Archambault, V.; Glover, D. Polo-like kinases: Conservation and divergence in their functions and regulation. *Nat. Rev. Mol. Cell Biol.* **2009**, *10*, 265–275. [CrossRef]
474. Glover, D.M.; Hagan, I.M.; Tavares, A. Polo-like kinases: A team that plays throughout mitosis. *Genes Dev.* **1998**, *12*, 3777–3787. [CrossRef]
475. Barr, F.; Silljé, H.H.W.; Nigg, E. Polo-like kinases and the orchestration of cell division. *Nat. Rev. Mol. Cell Biol.* **2004**, *5*, 429–441. [CrossRef] [PubMed]
476. A Winkles, J.; Alberts, G.F. Differential regulation of polo-like kinase 1, 2, 3, and 4 gene expression in mammalian cells and tissues. *Oncogene* **2005**, *24*, 260–266. [CrossRef] [PubMed]
477. Iliaki, S.; Beyaert, R.; Afonina, I.S. Polo-like kinase 1 (PLK1) signaling in cancer and beyond. *Biochem. Pharmacol.* **2021**, *193*, 114747. [CrossRef] [PubMed]
478. Raab, C.A.; Raab, M.; Becker, S.; Strebhardt, K. Non-mitotic functions of polo-like kinases in cancer cells. *Biochim. Biophys. Acta (BBA)-Rev. Cancer* **2020**, *1875*, 188467. [CrossRef]
479. Cholewa, B.D.; Liu, X.; Ahmad, N. The Role of Polo-like Kinase 1 in Carcinogenesis: Cause or Consequence? *Cancer Res* **2013**, *73*, 6848–6855. [CrossRef]
480. Strebhardt, K. Multifaceted polo-like kinases: Drug targets and antitargets for cancer therapy. *Nat. Rev. Drug Discov.* **2010**, *9*, 643–660. [CrossRef]
481. Pellegrino, R.; Calvisi, D.F.; Ladu, S.; Ehemann, V.; Staniscia, T.; Evert, M.; Dombrowski, F.; Schirmacher, P.; Longerich, T. Oncogenic and tumor suppressive roles of polo-like kinases in human hepatocellular carcinoma. *Hepatology* **2009**, *51*, 857–868. [CrossRef]
482. Degenhardt, Y.; Lampkin, T. Targeting Polo-like kinase in cancer therapy. *Clin. Cancer Res. Off. J. Am. Assoc. Cancer Res.* **2010**, *16*, 384–389. [CrossRef]
483. Ando, K.; Ozaki, T.; Yamamoto, H.; Furuya, K.; Hosoda, M.; Hayashi, S.; Fukuzawa, M.; Nakagawara, A. Polo-like Kinase 1 (Plk1) Inhibits p53 Function by Physical Interaction and Phosphorylation. *J. Biol. Chem.* **2004**, *279*, 25549–25561. [CrossRef]
484. Li, S.; Li, H.; Cao, Y.; Geng, H.; Ren, F.; Li, K.; Dai, C.; Li, N. Integrated bioinformatics analysis reveals CDK1 and PLK1 as potential therapeutic targets of lung adenocarcinoma. *Medicine* **2021**, *100*, e26474. [CrossRef]
485. Li, H.; Wang, H.; Sun, Z.; Guo, Q.; Shi, H.; Jia, Y. The clinical and prognostic value of polo-like kinase 1 in lung squamous cell carcinoma patients: Immunohistochemical analysis. *Biosci. Rep.* **2017**, *37*. [CrossRef]
486. Ramani, P.; Nash, R.; Sowa-Avugrah, E.; A Rogers, C. High levels of polo-like kinase 1 and phosphorylated translationally controlled tumor protein indicate poor prognosis in neuroblastomas. *J. Neuro-Oncology* **2015**, *125*, 103–111. [CrossRef]
487. Harris, P.S.; Venkataraman, S.; Alimova, I.; Birks, D.K.; Donson, A.M.; Knipstein, J.; Dubuc, A.; Taylor, M.D.; Handler, M.H.; Foreman, N.K.; et al. Polo-like kinase 1 (PLK1) inhibition suppresses cell growth and enhances radiation sensitivity in medulloblastoma cells. *BMC Cancer* **2012**, *12*, 80. [CrossRef]
488. Triscott, J.; Lee, C.; Foster, C.; Manoranjan, B.; Pambid, M.R.; Berns, R.; Fotovati, A.; Venugopal, C.; O'Halloran, K.; Narendran, A.; et al. Personalizing the Treatment of Pediatric Medulloblastoma: Polo-like Kinase 1 as a Molecular Target in High-Risk Children. *Cancer Res* **2013**, *73*, 6734–6744. [CrossRef]
489. Pezuk, J.A.; Brassescio, M.S.; de Oliveira, R.S.; Machado, H.R.; Neder, L.; Scrideli, C.A.; Tone, L.G. PLK1-associated microRNAs are correlated with pediatric medulloblastoma prognosis. *Child's Nerv. Syst.* **2017**, *33*, 609–615. [CrossRef]
490. Ma, H.; Nie, C.; Chen, Y.; Li, J.; Xie, Y.; Tang, Z.; Gao, Y.; Ai, S.; Mao, Y.; Sun, Q.; et al. Therapeutic Targeting PLK1 by ON-01910.Na Is Effective in Local Treatment of Retinoblastoma. *Oncol. Res. Featur. Preclin. Clin. Cancer Ther.* **2021**, *28*, 745–761. [CrossRef]
491. Singh, L.; Pushker, N.; Sen, S.; Singh, M.K.; A Chauhan, F.; Kashyap, S. Prognostic significance of polo-like kinases in retinoblastoma: Correlation with patient outcome, clinical and histopathological parameters. *Clin. Exp. Ophthalmol.* **2015**, *43*, 550–557. [CrossRef]
492. Ackermann, S.; Goeser, F.; Schulte, J.H.; Schramm, A.; Ehemann, V.; Hero, B.; Eggert, A.; Berthold, F.; Fischer, M. Polo-Like Kinase 1 is a Therapeutic Target in High-Risk Neuroblastoma. *Clin. Cancer Res.* **2011**, *17*, 731–741. [CrossRef]
493. Mo, H.; He, J.; Yuan, Z.; Wu, Z.; Liu, B.; Lin, X.; Guan, J. PLK1 contributes to autophagy by regulating MYC stabilization in osteosarcoma cells. *Oncotargets Ther.* **2019**, *12*, 7527–7536. [CrossRef]
494. Mountzios, G.; Terpos, E.; Dimopoulos, M. Aurora kinases as targets for cancer therapy. *Cancer Treat. Rev.* **2008**, *34*, 175–182. [CrossRef] [PubMed]
495. Goldenson, B.; Crispino, J.D. The aurora kinases in cell cycle and leukemia. *Oncogene* **2014**, *34*, 537–545. [CrossRef] [PubMed]
496. Toji, S.; Yabuta, N.; Hosomi, T.; Nishihara, S.; Kobayashi, T.; Suzuki, S.; Tamai, K.; Nojima, H. The centrosomal protein Lats2 is a phosphorylation target of Aurora-A kinase. *Genes Cells* **2004**, *9*, 383–397. [CrossRef]
497. Naso, F.D.; Boi, D.; Ascanelli, C.; Pamfil, G.; Lindon, C.; Paiardini, A.; Guarguaglini, G. Nuclear localisation of Aurora-A: Its regulation and significance for Aurora-A functions in cancer. *Oncogene* **2021**, *40*, 3917–3928. [CrossRef] [PubMed]

498. Marumoto, T.; Honda, S.; Hara, T.; Nitta, M.; Hirota, T.; Kohmura, E.; Saya, H. Aurora-A Kinase Maintains the Fidelity of Early and Late Mitotic Events in HeLa Cells. *J. Biol. Chem.* **2003**, *278*, 51786–51795. [CrossRef]
499. Crane, R.; Gadea, B.; Littlepage, L.; Wu, H.; Ruderman, J.V. Aurora A, Meiosis and Mitosis. *Biol. Cell* **2004**, *96*, 215–229. [CrossRef]
500. Musacchio, A.; Hardwick, K.G. The spindle checkpoint: Structural insights into dynamic signalling. *Nat. Rev. Mol. Cell Biol.* **2002**, *3*, 731–741. [CrossRef]
501. Werner, M.; Mattis, A.; Aubele, M.; Cummings, M.; Zitzelsberger, H.; Hutzler, P.; Höfler, H. 20q13.2 Amplification in intraductal hyperplasia adjacent to in situ and invasive ductal carcinoma of the breast. *Virchows Arch.* **1999**, *435*, 469–472. [CrossRef]
502. Bui, V.-M.; Mettling, C.; Jou, J.; Sun, H.S. Genomic amplification of chromosome 20q13.33 is the early biomarker for the development of sporadic colorectal carcinoma. *BMC Med. Genom.* **2020**, *13*, 149. [CrossRef]
503. Tanner, M.M.; Tirkkonen, M.; Kallioniemi, A.; Holli, K.; Collins, C.; Kowbel, D.; Gray, J.W.; Kallioniemi, O.; Isola, J. Amplification of chromosomal region 20q13 in invasive breast cancer: Prognostic implications. *Clin. Cancer Res.* **1995**, *1*, 1455–1461.
504. Mou, P.K.; Yang, E.J.; Shi, C.; Ren, G.; Tao, S.; Shim, J.S. Aurora kinase A, a synthetic lethal target for precision cancer medicine. *Exp. Mol. Med.* **2021**, *53*, 835–847. [CrossRef]
505. Murga-Zamalloa, C.; Inamdar, K.V.; Wilcox, R.A. The role of aurora A and polo-like kinases in high-risk lymphomas. *Blood Adv.* **2019**, *3*, 1778–1787. [CrossRef]
506. Bast, R.C., Jr.; Hennessy, B.; Mills, G.B. The biology of ovarian cancer: New opportunities for translation. *Nat. Rev. Cancer* **2009**, *9*, 415–428. [CrossRef]
507. Sun, H.; Wang, H.; Wang, X.; Aoki, Y.; Wang, X.; Yang, Y.; Cheng, X.; Wang, Z.; Wang, X. Aurora-A/SOX8/FOXK1 signaling axis promotes chemoresistance via suppression of cell senescence and induction of glucose metabolism in ovarian cancer organoids and cells. *Theranostics* **2020**, *10*, 6928–6945. [CrossRef]
508. Wan, X.-B.; Long, Z.-J.; Yan, M.; Xu, J.; Xia, L.-P.; Liu, L.; Zhao, Y.; Huang, X.-F.; Wang, X.-R.; Zhu, X.-F.; et al. Inhibition of Aurora-A suppresses epithelial–mesenchymal transition and invasion by downregulating MAPK in nasopharyngeal carcinoma cells. *Carcinog.* **2008**, *29*, 1930–1937. [CrossRef]
509. Nguyen, T.T.B.; Silva, F.N.M.; Golemis, E.A. Aurora Kinases as Therapeutic Targets in Head and Neck Cancer. *Cancer J.* **2022**, *28*, 387–400. [CrossRef]
510. Do, T.-V.; Xiao, F.; E Bickel, L.; Klein-Szanto, A.J.; Pathak, H.B.; Hua, X.; Howe, C.; O'Brien, S.W.; Maglaty, M.; A Ecsedy, J.; et al. Aurora kinase A mediates epithelial ovarian cancer cell migration and adhesion. *Oncogene* **2013**, *33*, 539–549. [CrossRef]
511. Katayama, H.; Wang, J.; Treekitkarnmongkol, W.; Kawai, H.; Sasai, K.; Zhang, H.; Wang, H.; Adams, H.P.; Jiang, S.; Chakraborty, S.N.; et al. Aurora Kinase-A Inactivates DNA Damage-Induced Apoptosis and Spindle Assembly Checkpoint Response Functions of p73. *Cancer Cell* **2012**, *21*, 196–211. [CrossRef]
512. Anand, S.; Penrhyn-Lowe, S.; Venkitaraman, A.R. AURORA-A amplification overrides the mitotic spindle assembly checkpoint, inducing resistance to Taxol. *Cancer Cell* **2003**, *3*, 51–62. [CrossRef]
513. Cirak, Y.; Furuncuoglu, Y.; Yapicier, O.; Aksu, A.; Cubukcu, E. Aurora A overexpression in breast cancer patients induces taxane resistance and results in worse prognosis. *J. BUON.* **2016**, *20*, 1414–1419.
514. Reiter, R.; Gais, P.; Jütting, U.; Steuer-Vogt, M.K.; Pickhard, A.; Bink, K.; Rauser, S.; Lassmann, S.; Höfler, H.; Werner, M.; et al. Aurora Kinase A Messenger RNA Overexpression Is Correlated with Tumor Progression and Shortened Survival in Head and Neck Squamous Cell Carcinoma. *Clin. Cancer Res.* **2006**, *12*, 5136–5141. [CrossRef] [PubMed]
515. Noh, E.-M.; Lee, Y.-R.; Hong, O.-Y.; Jung, S.H.; Youn, H.J.; Kim, J.-S. Aurora kinases are essential for PKC-induced invasion and matrix metalloproteinase-9 expression in MCF-7 breast cancer cells. *Oncol. Rep.* **2015**, *34*, 803–810. [CrossRef] [PubMed]
516. Landen, C.N.; Lin, Y.G.; Immaneni, A.; Deavers, M.T.; Merritt, W.M.; Spanuth, W.A.; Bodurka, D.C.; Gershenson, D.M.; Brinkley, W.R.; Sood, A.K. Overexpression of the Centrosomal Protein Aurora-A Kinase is Associated with Poor Prognosis in Epithelial Ovarian Cancer Patients. *Clin. Cancer Res.* **2007**, *13*, 4098–4104. [CrossRef] [PubMed]
517. Tuncel, H.; Shimamoto, F.; Qi, H.K.; Aoki, E.; Jikihara, H.; Nakai, S.; Takata, T.; Tatsuka, M. Nuclear Aurora B and cytoplasmic Survivin expression is involved in lymph node metastasis of colorectal cancer. *Oncol. Lett.* **2012**, *3*, 1109–1114. [CrossRef]
518. Rannou, Y.; Troadec, M.-B.; Petretti, C.; Hans, F.; Dutertre, S.; Dimitrov, S.; Prigent, C. Localization of aurora A and aurora B kinases during interphase: Role of the N-terminal domain. *Cell Cycle* **2008**, *7*, 3012–3020. [CrossRef]
519. Xia, Z.; Wei, P.; Zhang, H.; Ding, Z.; Yang, L.; Huang, Z.; Zhang, N. AURKA Governs Self-Renewal Capacity in Glioma-Initiating Cells via Stabilization/Activation of  $\beta$ -catenin/Wnt Signaling. *Mol. Cancer Res.* **2013**, *11*, 1101–1111. [CrossRef]
520. Lu, T.; Li, L.; Zhu, J.; Liu, J.; Lin, A.; Fu, W.; Liu, G.; Xia, H.; Zhang, T.; He, J. AURKA rs8173 G>C Polymorphism Decreases Wilms Tumor Risk in Chinese Children. *J. Oncol.* **2019**, *2019*, 9074908–7. [CrossRef]
521. Otto, T.; Horn, S.; Brockmann, M.; Eilers, U.; Schüttrumpf, L.; Popov, N.; Kenney, A.M.; Schulte, J.H.; Beijersbergen, R.; Christiansen, H.; et al. Stabilization of N-Myc Is a Critical Function of Aurora A in Human Neuroblastoma. *Cancer Cell* **2009**, *15*, 67–78. [CrossRef]
522. Maris, J.M. Unholy Matrimony: Aurora A and N-Myc as Malignant Partners in Neuroblastoma. *Cancer Cell* **2009**, *15*, 5–6. [CrossRef]
523. Ommer, J.; Selfe, J.L.; Wachtel, M.; O'Brien, E.M.; Laubscher, D.; Roemmele, M.; Kasper, S.; Delattre, O.; Surdez, D.; Petts, G.; et al. Aurora A Kinase Inhibition Destabilizes PAX3-FOXO1 and MYCN and Synergizes with Navitoclax to Induce Rhabdomyosarcoma Cell Death. *Cancer Res* **2020**, *80*, 832–842. [CrossRef]

524. Goldstein, M.; Meller, I.; Issakov, J.; Orr-Urtreger, A. Novel Genes Implicated in Embryonal, Alveolar, and Pleomorphic Rhabdomyosarcoma: A Cytogenetic and Molecular Analysis of Primary Tumors. *Neoplasia* **2006**, *8*, 332–343. [CrossRef]
525. Zhao, R.; Li, Z.; Huang, Y.; Xiong, C.; Zhang, C.; Liang, H.; Xu, J.; Luo, X. A Novel Ferroptosis-Related Gene Signature for Prognosis Prediction in Ewing Sarcoma. *Anal. Cell Pathol.* **2022**, *2022*, 1–22. [CrossRef]
526. Liao, H.; Xie, X.; Xu, Y.; Huang, G. Identification of driver genes associated with chemotherapy resistance of Ewing's sarcoma. *OncoTargets Ther.* **2018**, *11*, 6947–6956. [CrossRef]
527. Huang, W.-T.; Liu, A.-G.; Cai, K.-T.; He, R.-Q.; Li, Z.; Wei, Q.-J.; Chen, M.-Y.; Huang, J.-Y.; Yan, W.-Y.; Zhou, H.; et al. Exploration and validation of downregulated microRNA-199a-3p, downstream messenger RNA targets and transcriptional regulation in osteosarcoma. *Am. J. Transl. Res.* **2019**, *11*, 7538–7554.
528. Zhu, X.; Mei, J.; Wang, Z. Aurora-A kinase: Potential tumor marker of osteosarcoma. *J. Cancer Res. Ther.* **2014**, *10*, 102–107. [CrossRef]
529. Yang, W.; Jiang, X.; Zhao, X.; Mao, P. Treatment of RB -deficient retinoblastoma with Aurora-A kinase inhibitor. *Kaohsiung J. Med. Sci.* **2021**, *38*, 244–252. [CrossRef]
530. Lehman, N.L.; O'Donnell, J.P.; Whiteley, L.J.; Stapp, R.T.; Lehman, T.D.; Roszka, K.M.; Schultz, L.R.; Williams, C.J.; Mikkelsen, T.; Brown, S.L.; et al. Aurora A is differentially expressed in gliomas, is associated with patient survival in glioblastoma and is a potential chemotherapeutic target in gliomas. *Cell Cycle* **2012**, *11*, 489–502. [CrossRef]
531. Liang, B.; Zhou, Y.; Jiao, J.; Xu, L.; Yan, Y.; Wu, Q.; Tong, X.; Yan, H. Integrated Analysis of Transcriptome Data Revealed AURKA and KIF20A as Critical Genes in Medulloblastoma Progression. *Front. Oncol.* **2022**, *12*. [CrossRef]
532. Vader, G.; Medema, R.; Lens, S.M. The chromosomal passenger complex: Guiding Aurora-B through mitosis. *J. Cell Biol.* **2006**, *173*, 833–837. [CrossRef]
533. Vagnarelli, P.; Earnshaw, W.C. Chromosomal passengers: The four-dimensional regulation of mitotic events. *Chromosoma* **2004**, *113*, 211–222. [CrossRef]
534. Adams, R.R.; Carmena, M.; Earnshaw, W.C. Chromosomal passengers and the (aurora) ABCs of mitosis. *Trends Cell Biol.* **2001**, *11*, 49–54. [CrossRef] [PubMed]
535. Minoshima, Y.; Kawashima, T.; Hirose, K.; Tonozuka, Y.; Kawajiri, A.; Bao, Y.C.; Deng, X.; Tatsuka, M.; Narumiya, S.; May, W.; et al. Phosphorylation by Aurora B Converts MgcRacGAP to a RhoGAP during Cytokinesis. *Dev. Cell* **2003**, *4*, 549–560. [CrossRef] [PubMed]
536. Hsu, J.-Y.; Sun, Z.-W.; Li, X.; Reuben, M.; Tatchell, K.; Bishop, D.K.; Grushcow, J.M.; Brame, C.J.; A Caldwell, J.; Hunt, D.F.; et al. Mitotic Phosphorylation of Histone H3 Is Governed by Ipl1/aurora Kinase and Glc7/PP1 Phosphatase in Budding Yeast and Nematodes. *Cell* **2000**, *102*, 279–291. [CrossRef] [PubMed]
537. Murnion, M.E.; Adams, R.R.; Callister, D.M.; Allis, C.D.; Earnshaw, W.C.; Swedlow, J.R. Chromatin-associated Protein Phosphatase 1 Regulates Aurora-B and Histone H3 Phosphorylation. *J. Biol. Chem.* **2001**, *276*, 26656–26665. [CrossRef] [PubMed]
538. Lan, W.; Zhang, X.; Kline-Smith, S.L.; E Rosasco, S.; A Barrett-Wilt, G.; Shabanowitz, J.; Hunt, D.F.; E Walczak, C.; Stukenberg, T. Aurora B Phosphorylates Centromeric MCAK and Regulates Its Localization and Microtubule Depolymerization Activity. *Curr. Biol.* **2004**, *14*, 273–286. [CrossRef]
539. Ma, H.T.; Poon, R.Y. Aurora kinases and DNA damage response. *Mutat. Res. Mol. Mech. Mutagen.* **2020**, *821*, 111716. [CrossRef]
540. González-Loyola, A.; Fernández-Miranda, G.; Trakala, M.; Partida, D.; Samejima, K.; Ogawa, H.; Cañamero, M.; de Martino, A.; Martínez-Ramírez, A.; de Cárcer, G.; et al. Aurora B Overexpression Causes Aneuploidy and p21<sup>Cip1</sup> Repression during Tumor Development. *Mol. Cell. Biol.* **2015**, *35*, 3566–3578. [CrossRef]
541. Takeshita, M.; Koga, T.; Takayama, K.; Ijichi, K.; Yano, T.; Maehara, Y.; Nakanishi, Y.; Sueishi, K. Aurora-B overexpression is correlated with aneuploidy and poor prognosis in non-small cell lung cancer. *Lung Cancer* **2013**, *80*, 85–90. [CrossRef]
542. Porcelli, L.; Guida, G.; E Quatrala, A.; Cocco, T.; Sidella, L.; Maida, I.; Iacobazzi, R.M.; Ferretta, A.; A Stolfa, D.; Strippoli, S.; et al. Aurora kinase B inhibition reduces the proliferation of metastatic melanoma cells and enhances the response to chemotherapy. *J. Transl. Med.* **2015**, *13*, 26. [CrossRef]
543. Wang, C.; Chen, J.; Cao, W.; Sun, L.; Sun, H.; Liu, Y. Aurora-B and HDAC synergistically regulate survival and proliferation of lymphoma cell via AKT, mTOR and Notch pathways. *Eur. J. Pharmacol.* **2016**, *779*, 1–7. [CrossRef]
544. Wan, B.; Huang, Y.; Liu, B.; Lu, L.; Lv, C. AURKB: A promising biomarker in clear cell renal cell carcinoma. *PeerJ* **2019**, *7*, e7718. [CrossRef]
545. Twu, N.-F.; Yuan, C.-C.; Yen, M.-S.; Lai, C.-R.; Chao, K.-C.; Wang, P.-H.; Wu, H.-H.; Chen, Y.-J. Expression of Aurora kinase A and B in normal and malignant cervical tissue: High Aurora A kinase expression in squamous cervical cancer. *Eur. J. Obstet. Gynecol. Reprod. Biol.* **2009**, *142*, 57–63. [CrossRef]
546. Pannone, G.; Hindi, S.; Santoro, A.; Sanguedolce, F.; Rubini, C.; Cincione, R.; De Maria, S.; Tortorella, S.; Rocchetti, R.; Cagiano, S.; et al. Aurora B Expression as a Prognostic Indicator and Possible Therapeutic Target in Oral Squamous Cell Carcinoma. *Int. J. Immunopathol. Pharmacol.* **2011**, *24*, 79–88. [CrossRef]
547. Alafate, W.; Zuo, J.; Deng, Z.; Guo, X.; Wu, W.; Zhang, W.; Xie, W.; Wang, M.; Wang, J. Combined elevation of AURKB and UBE2C predicts severe outcomes and therapy resistance in glioma. *Pathol.-Res. Pract.* **2019**, *215*, 152557. [CrossRef] [PubMed]
548. Liu, M.; Li, Y.; Zhang, C.; Zhang, Q. Role of aurora kinase B in regulating resistance to paclitaxel in breast cancer cells. *Hum. Cell* **2022**, *35*, 678–693. [CrossRef]

549. Wang, Z.; Yu, Z.; Wang, G.-H.; Zhou, Y.-M.; Deng, J.-P.; Feng, Y.; Chen, J.-Q.; Tian, L. AURKB Promotes the Metastasis of Gastric Cancer, Possibly by Inducing EMT. *Cancer Manag. Res.* **2020**, *12*, 6947–6958. [CrossRef]
550. Nie, M.; Wang, Y.; Yu, Z.; Li, X.; Deng, Y.; Wang, Y.; Yang, D.; Li, Q.; Zeng, X.; Ju, J.; et al. AURKB promotes gastric cancer progression via activation of CCND1 expression. *Aging* **2020**, *12*, 1304–1321. [CrossRef]
551. Yuan, K.; Wu, M.; Lyu, S.; Li, Y. Identification of prognostic genes for early basal-like breast cancer with weighted gene co-expression network analysis. *Medicine* **2022**, *101*, e30581. [CrossRef]
552. Gao, X.; Jiang, A.; Shen, Y.; Lu, H.M.; Chen, R. Expression and clinical significance of AURKB gene in lung adenocarcinoma. *Medicine* **2021**, *100*, e26439. [CrossRef]
553. Yang, Y.; Sheng, Y.; Sun, D.; Sun, J.; Li, L.; Sun, L. AURKB promotes tumorigenesis and carboplatin resistance by regulating the ERK pathway in neuroblastoma cells. *Int. J. Neurosci.* **2021**, 1–11. [CrossRef]
554. Bogen, D.; Wei, J.S.; Azorsa, D.O.; Ormanoglu, P.; Buehler, E.; Guha, R.; Keller, J.M.; Griner, L.A.M.; Ferrer, M.; Song, Y.K.; et al. Aurora B kinase is a potent and selective target in MYCN-driven neuroblastoma. *Oncotarget* **2015**, *6*, 35247–35262. [CrossRef] [PubMed]
555. Hartsink-Segers, S.; Zwaan, C.; Exalto, C.; Luijendijk, M.W.J.; Calvert, V.; Petricoin, E.F.; Evans, W.; Reinhardt, D.; De Haas, V.; Hedtjörn, M.; et al. Aurora kinases in childhood acute leukemia: The promise of aurora B as therapeutic target. *Leukemia* **2012**, *27*, 560–568. [CrossRef] [PubMed]
556. Saletta, F.; Wadham, C.; Ziegler, D.; Marshall, G.M.; Haber, M.; McCowage, G.; Norris, M.D.; Byrne, J.A. Molecular profiling of childhood cancer: Biomarkers and novel therapies. *BBA Clin.* **2014**, *1*, 59–77. [CrossRef]
557. Gibson, S.E.; Zeng, W.F.; Weil, R.J.; Prayson, R.A. Aurora B Kinase Expression in Ependymal Neoplasms. *Appl. Immunohistochem. Mol. Morphol.* **2008**, *16*, 274–278. [CrossRef]
558. Wang, S.; Hwang, E.E.; Guha, R.; O'Neill, A.F.; Melong, N.; Veinotte, C.J.; Saur, A.C.; Wuerthele, K.; Shen, M.; McKnight, C.; et al. High-throughput Chemical Screening Identifies Focal Adhesion Kinase and Aurora Kinase B Inhibition as a Synergistic Treatment Combination in Ewing Sarcoma. *Clin. Cancer Res.* **2019**, *25*, 4552–4566. [CrossRef] [PubMed]
559. Zhao, Z.; Jin, G.; Yao, K.; Liu, K.; Liu, F.; Chen, H.; Wang, K.; Gorja, D.R.; Reddy, K.; Bode, A.M.; et al. Aurora B kinase as a novel molecular target for inhibition the growth of osteosarcoma. *Mol. Carcinog.* **2019**, *58*, 1056–1067. [CrossRef]
560. Borah, N.A.; Sradhanjali, S.; Barik, M.R.; Jha, A.; Tripathy, D.; Kaliki, S.; Rath, S.; Raghav, S.K.; Patnaik, S.; Mittal, R.; et al. Aurora Kinase B Expression, Its Regulation and Therapeutic Targeting in Human Retinoblastoma. *Investig. Ophthalmology Vis. Sci.* **2021**, *62*, 16. [CrossRef]
561. Kimura, M.; Matsuda, Y.; Yoshioka, T.; Okano, Y. Cell Cycle-dependent Expression and Centrosome Localization of a Third Human Aurora/Ipl1-related Protein Kinase, AIK3. *J. Biol. Chem.* **1999**, *274*, 7334–7340. [CrossRef]
562. Fujii, S.; Srivastava, V.; Hegde, A.; Kondo, Y.; Shen, L.; Hoshino, K.; Gonzalez, Y.; Wang, J.; Sasai, K.; Ma, X.; et al. Regulation of AURKC expression by CpG island methylation in human cancer cells. *Tumor Biol.* **2015**, *36*, 8147–8158. [CrossRef]
563. Tseng, T.-C.; Chen, S.-H.; Hsu, Y.-P.P.; Tang, T.K. Protein Kinase Profile of Sperm and Eggs: Cloning and Characterization of Two Novel Testis-Specific Protein Kinases (AIE1, AIE2) Related to Yeast and Fly Chromosome Segregation Regulators. *DNA Cell Biol.* **1998**, *17*, 823–833. [CrossRef]
564. Santos, M.A.; van de Werken, C.; de Vries, M.; Jahr, H.; Vromans, M.J.; Laven, J.S.; Fauser, B.C.; Kops, G.J.; Lens, S.M.; Baart, E.B. A role for Aurora C in the chromosomal passenger complex during human preimplantation embryo development. *Hum. Reprod.* **2011**, *26*, 1868–1881. [CrossRef]
565. Khan, J.; Ezan, F.; Crémet, J.-Y.; Fautrel, A.; Gilot, D.; Lambert, M.; Benaud, C.; Troadec, M.-B.; Prigent, C. Overexpression of Active Aurora-C Kinase Results in Cell Transformation and Tumour Formation. *PLoS ONE* **2011**, *6*, e26512. [CrossRef]
566. Yan, X.; Cao, L.; Li, Q.; Wu, Y.; Zhang, H.; Saiyin, H.; Liu, X.; Zhang, X.; Shi, Q.; Yu, L. Aurora C is directly associated with Survivin and required for cytokinesis. *Genes Cells* **2005**, *10*, 617–626. [CrossRef]
567. Kobayashi, K.; Kiyomura, H. The theoretical analysis on the tooth movement (II). *Nihon Kyosei Shika Gakkai zasshi = J. Jpn. Orthod. Soc.* **1982**, *41*, 716–722.
568. Tsou, J.-H.; Chang, K.-C.; Chang-Liao, P.-Y.; Yang, S.-T.; Lee, C.-T.; Chen, Y.-P.; Lee, Y.-C.; Lin, B.-W.; Lee, J.-C.; Shen, M.-R.; et al. Aberrantly expressed AURKC enhances the transformation and tumourigenicity of epithelial cells. *J. Pathol.* **2011**, *225*, 243–254. [CrossRef]
569. Zekri, A.; Lesan, V.; Ghaffari, S.H.; Tabrizi, M.H.; Modarressi, M.H. Gene Amplification and Overexpression of Aurora-C in Breast and Prostate Cancer Cell Lines. *Oncol. Res. Featur. Preclin. Clin. Cancer Ther.* **2012**, *20*, 241–250. [CrossRef]
570. Seuánez, H.N.; Pereira, H.S.; Lima, S.C.S.; de Faria, P.S.; Cardoso, L.C.D.A. i RPS6KA4 i i MIR1237 i and i AURKC i promoter regions are differentially methylated in Wilms tumor. *Front. Biosci.* **2018**, *10*, 143–154. [CrossRef]
571. Hsieh, C.-H.; Cheung, C.H.Y.; Liu, Y.-L.; Hou, C.-L.; Hsu, C.-L.; Huang, C.-T.; Yang, T.-S.; Chen, S.-F.; Chen, C.-N.; Hsu, W.-M.; et al. Quantitative Proteomics of Th-MYCN Transgenic Mice Reveals Aurora Kinase Inhibitor Altered Metabolic Pathways and Enhanced ACADM To Suppress Neuroblastoma Progression. *J. Proteome Res.* **2019**, *18*, 3850–3866. [CrossRef]
572. Bejar, J.F.; DiSanza, Z.; Quartuccio, S.M. The oncogenic role of meiosis-specific Aurora kinase C in mitotic cells. *Exp. Cell Res.* **2021**, *407*, 112803. [CrossRef]
573. Nowell, P.C.; Hungerford, D.A. Chromosome studies on normal and leukemic human leukocytes. *J. Natl. Cancer Inst.* **1960**, *25*, 85–109.
574. Seabright, M. A rapid banding technique for human chromosomes. *Lancet* **1971**, *298*, 971–972. [CrossRef] [PubMed]

575. Rowley, J.D. A New Consistent Chromosomal Abnormality in Chronic Myelogenous Leukaemia identified by Quinacrine Fluorescence and Giemsa Staining. *Nature* **1973**, *243*, 290–293. [CrossRef] [PubMed]
576. Heisterkamp, N.; Stephenson, J.R.; Groffen, J.; Hansen, P.F.; de Klein, A.; Bartram, C.R.; Grosveld, G. Localization of the c-abl oncogene adjacent to a translocation break point in chronic myelocytic leukaemia. *Nature* **1983**, *306*, 239–242. [CrossRef] [PubMed]
577. de Klein, A.; van Kessel, A.G.; Grosveld, G.; Bartram, C.R.; Hagemeijer, A.; Bootsma, D.; Spurr, N.K.; Heisterkamp, N.; Groffen, J.; Stephenson, J.R. A cellular oncogene is translocated to the Philadelphia chromosome in chronic myelocytic leukaemia. *Nature* **1982**, *300*, 765–767. [CrossRef] [PubMed]
578. Groffen, J.; Stephenson, J.R.; Heisterkamp, N.; De Klein, A.; Bartram, C.R.; Grosveld, G. Philadelphia chromosomal breakpoints are clustered within a limited region, bcr, on chromosome 22. *Cell* **1984**, *36*, 93–99. [CrossRef]
579. Koschmieder, S.; Göttgens, B.; Zhang, P. Inducible chronic phase of myeloid leukemia with expansion of hematopoietic stem cells in a trans-genic model of BCR-ABL leukemogenesis. *Blood* **2005**, *105*, 324–334. [CrossRef]
580. Druker, B.J.; Talpaz, M.; Resta, D.J.; Peng, B.; Buchdunger, E.; Ford, J.M.; Lydon, N.B.; Kantarjian, H.; Capdeville, R.; Ohno-Jones, S.; et al. Efficacy and Safety of a Specific Inhibitor of the BCR-ABL Tyrosine Kinase in Chronic Myeloid Leukemia. *N. Engl. J. Med.* **2001**, *344*, 1031–1037. [CrossRef]
581. Festuccia, C.; Gravina, G.L.; Biordi, L.; D’Ascenzo, S.; Dolo, V.; Ficorella, C.; Ricevuto, E.; Tombolini, V. Effects of EGFR tyrosine kinase inhibitor erlotinib in prostate cancer cells in vitro. *Prostate* **2009**, *69*, 1529–1537. [CrossRef]
582. Abdelgalil, A.A.; Al-Kahtani, H.M.; Al-Jenoobi, F.I. Erlotinib. *Profiles DrugSubst. Excip. Relat. Methodol.* **2019**, *45*, 93–117. [CrossRef]
583. Ms, K.N.R.; Zweidler-McKay, P.A.; Van Roy, N.; Speleman, F.; Trevino, J.; Zage, P.E.; Hughes, D.P.M. Signaling of ERBB receptor tyrosine kinases promotes neuroblastoma growth in vitro and in vivo. *Cancer* **2010**, *116*, 3233–3243. [CrossRef]
584. Ji, X.L.; He, M. Sodium cantharidate targets STAT3 and abrogates EGFR inhibitor resistance in osteosarcoma. *Aging* **2019**, *11*, 5848–5863. [CrossRef]
585. Bandyopadhyay, A.; Favours, E.; Phelps, D.A.; Del Pozo, V.; Ghilu, S.; Kurmashev, D.; Michalek, J.; Trevino, A.; Guttridge, D.; London, C.; et al. Evaluation of patritumab with or without erlotinib in combination with standard cytotoxic agents against pediatric sarcoma xenograft models. *Pediatr. Blood Cancer* **2017**, *65*, e26870. [CrossRef]
586. Abraham, J.; Nelon, L.D.; Kubicek, C.B.; Kilcoyne, A.; Hampton, S.T.; Zarzabal, L.A.; Giles, F.J.; Michalek, J.E.; Rubin, B.P.; Keller, C. Preclinical Testing of Erlotinib in a Transgenic Alveolar Rhabdomyosarcoma Mouse Model. *Sarcoma* **2011**, *2011*, 1–5. [CrossRef]
587. Hernan, R.; Fasheh, R.; Calabrese, C.; Frank, A.J.; MacLean, K.H.; Allard, D.; Barraclough, R.; Gilbertson, R.J. ERBB2 up-regulates S100A4 and several other prometastatic genes in medulloblastoma. *Cancer Res* **2003**, *63*, 140–148.
588. Guan, S.; Shen, R.; Lafortune, T.; Tiao, N.; Houghton, P.; Yung, W.A.; Koul, D. Establishment and characterization of clinically relevant models of ependymoma: A true challenge for targeted therapy. *Neuro-Oncology* **2011**, *13*, 748–758. [CrossRef]
589. Shao, Y.; Yu, Y.; Zong, R.; Quyang, L.; He, H.; Zhou, Q.; Pei, C. Erlotinib has tumor inhibitory effect in human retinoblastoma cells. *Biomed. Pharmacother.* **2017**, *85*, 479–485. [CrossRef]
590. Jakacki, R.I.; Hamilton, M.; Gilbertson, R.J.; Blaney, S.M.; Tersak, J.; Krailo, M.D.; Ingle, A.M.; Voss, S.D.; Dancey, J.E.; Adamson, P.C. Pediatric Phase I and Pharmacokinetic Study of Erlotinib Followed by the Combination of Erlotinib and Temozolomide: A Children’s Oncology Group Phase I Consortium Study. *J. Clin. Oncol.* **2008**, *26*, 4921–4927. [CrossRef]
591. Georger, B.; Hargrave, D.; Thomas, F.; Ndiaye, A.; Frappaz, D.; Andreiuolo, F.; Varlet, P.; Aerts, I.; Riccardi, R.; Jaspan, T.; et al. Innovative Therapies for Children with Cancer pediatric phase I study of erlotinib in brainstem glioma and relapsing/refractory brain tumors. *Neuro-Oncology* **2010**, *13*, 109–118. [CrossRef]
592. Frampton, J.E. Vandetanib. *Drugs* **2012**, *72*, 1423–1436. [CrossRef]
593. Karras, S.; Anagnostis, P.; E Krassas, G. Vandetanib for the treatment of thyroid cancer: An update. *Expert Opin. Drug Metab. Toxicol.* **2014**, *10*, 469–481. [CrossRef]
594. Hatem, R.; Labiod, D.; Château-Joubert, S.; de Plater, L.; El Botty, R.; Vacher, S.; Bonin, F.; Servely, J.-L.; Dieras, V.; Bièche, I.; et al. Vandetanib as a potential new treatment for estrogen receptor-negative breast cancers. *Int. J. Cancer* **2016**, *138*, 2510–2521. [CrossRef] [PubMed]
595. Valerio, L.; Bottici, V.; Matrone, A.; Piaggi, P.; Viola, D.; Cappagli, V.; Agate, L.; Molinaro, E.; Ciampi, R.; Tacito, A.; et al. Medullary thyroid cancer treated with vandetanib: Predictors of a longer and durable response. *Endocrine-Related Cancer* **2020**, *27*, 97–110. [CrossRef] [PubMed]
596. Ding, X.; Xiang, L.; Wang, N.; Zhao, Z.; Jin, X.; Sun, Y.; Duan, W.; Wang, S.; Jin, X. Vandetanib-induced inhibition of neuroblastoma cell migration and invasion is associated with downregulation of the SDF-1/CXCR4 axis and matrix metalloproteinase 14. *Oncol. Rep.* **2013**, *31*, 1165–1174. [CrossRef] [PubMed]
597. Li, H.; Li, C.-W.; Li, X.; Ding, Q.; Guo, L.; Liu, S.; Liu, C.; Lai, C.-C.; Hsu, J.-M.; Dong, Q.; et al. MET Inhibitors Promote Liver Tumor Evasion of the Immune Response by Stabilizing PDL1. *Gastroenterology* **2019**, *156*, 1849–1861.e7. [CrossRef]
598. Beaudry, P.; Nilsson, M.; Rioth, M.; Prox, D.; Poon, D.; Xu, L.; Zweidler-Mckay, P.; Ryan, A.; Folkman, J.; Ryeom, S.; et al. Potent antitumor effects of ZD6474 on neuroblastoma via dual targeting of tumor cells and tumor endothelium. *Mol. Cancer Ther.* **2008**, *7*, 418–424. [CrossRef]
599. Cazes, A.; Lopez-Delisle, L.; Tsarovina, K.; Pierre-Eugène, C.; De Preter, K.; Peuchmaur, M.; Nicolas, A.; Provost, C.; Louis-Brennetot, C.; Daveau, R.; et al. Activated Alk triggers prolonged neurogenesis and Ret upregulation providing a therapeutic target in ALK-mutated neuroblastoma. *Oncotarget* **2014**, *5*, 2688–2702. [CrossRef]



600. Li, C.; Yang, C.; Wei, G. Vandetanib inhibits cisplatin-resistant neuroblastoma tumor growth and invasion. *Oncol. Rep.* **2018**, *39*, 1757–1764. [CrossRef]
601. Zage, P.E.; Zeng, L.; Palla, S.; Fang, W.; Nilsson, M.B.; Heymach, J.V.; Zweidler-McKay, P.A. A novel therapeutic combination for neuroblastoma. *Cancer* **2010**, *116*, 2465–2475. [CrossRef]
602. Craveiro, R.B.; Ehrhardt, M.; Velz, J.; Olschewski, M.; Goetz, B.; Pietsch, T.; Dilloo, D. The anti-neoplastic activity of Vandetanib against high-risk medulloblastoma variants is profoundly enhanced by additional PI3K inhibition. *Oncotarget* **2017**, *8*, 46915–46927. [CrossRef]
603. Liu, J.; Wu, J.; Zhou, L.; Pan, C.; Zhou, Y.; Du, W.; Chen, J.-M.; Zhu, X.; Shen, J.; Chen, S.; et al. ZD6474, a new treatment strategy for human osteosarcoma, and its potential synergistic effect with celecoxib. *Oncotarget* **2015**, *6*, 21341–21352. [CrossRef]
604. Andersson, M.K.; Åman, P. Proliferation of Ewing sarcoma cell lines is suppressed by the receptor tyrosine kinase inhibitors gefitinib and vandetanib. *Cancer Cell Int.* **2008**, *8*, 1–6. [CrossRef]
605. Maloney, C.; Kallis, M.P.; Edelman, M.; Tzanavaris, C.; Lesser, M.; Soffer, S.Z.; Symons, M.; Steinberg, B.M. Gefitinib Inhibits Invasion and Metastasis of Osteosarcoma via Inhibition of Macrophage Receptor Interacting Serine-Threonine Kinase 2. *Mol. Cancer Ther.* **2020**, *19*, 1340–1350. [CrossRef]
606. Wakeling, A.E.; Guy, S.P.; Woodburn, J.R.; Ashton, S.E.; Curry, B.J.; Barker, A.J.; Gibson, K.H. ZD1839 (Iressa): An orally active inhibitor of epidermal growth factor signaling with potential for cancer therapy. *Cancer Res.* **2002**, *62*, 5749–5754.
607. Ciardiello, F.; Caputo, R.; Bianco, R.; Damiano, V.; Pomato, G. Antitumor effect and potentiation of cytotoxic drugs activity in human cancer cells by ZD-1839 (Iressa), an epidermal growth factor receptor-selective tyrosine kinase inhibitor. *Clin Cancer Res* **2000**, *6*, 2053–2063.
608. Foreman, N.K.; Gore, L.; Wells, D.; Bs, J.S.; Heideman, R.; Donson, A.M. Gefitinib is effective against juvenile pilocytic astrocytoma in vitro. *Pediatr. Blood Cancer* **2005**, *47*, 293–298. [CrossRef]
609. Schaiquevich, P.; Panetta, J.C.; Throm, S.; Daw, N.C.; Geyer, J.R.; Furman, W.L.; Stewart, C.F. Population pharmacokinetic (PK) analysis of gefitinib in pediatric cancer patients. *J. Clin. Oncol.* **2008**, *26*, 2523. [CrossRef]
610. Daudigeos-Dubus, E.; Le Dret, L.; Lanvers-Kaminsky, C.; Bawa, O.; Opolon, P.; Vievard, A.; Villa, I.; Pagès, M.; Bosq, J.; Vassal, G.; et al. Regorafenib: Antitumor Activity upon Mono and Combination Therapy in Preclinical Pediatric Malignancy Models. *PLoS ONE* **2015**, *10*, e0142612. [CrossRef]
611. Ettrich, T.J.; Seufferlein, T. Regorafenib. In *Recent Results in Cancer Research*; Springer LLC: New York, NY, USA, 2018; Volume 211, pp. 45–56. [CrossRef]
612. Subramonian, D.; Phanthilath, N.; Rinehardt, H.; Flynn, S.; Huo, Y.; Zhang, J.; Messer, K.; Mo, Q.; Huang, S.; Lesperance, J.; et al. Regorafenib is effective against neuroblastoma in vitro and in vivo and inhibits the RAS/MAPK, PI3K/Akt/mTOR and Fos/Jun pathways. *Br. J. Cancer* **2020**, *123*, 568–579. [CrossRef]
613. Carpenter, R.L.; Lo, H.-W. Dacomitinib, an emerging HER-targeted therapy for non-small cell lung cancer. *J. Thorac. Dis.* **2012**, *4*, 639–642. [CrossRef]
614. Shirley, M. Dacomitinib: First Global Approval. *Drugs* **2018**, *78*, 1947–1953. [CrossRef]
615. Popat, S.; Yap, T. Toward precision medicine with next-generation EGFR inhibitors in non-small-cell lung cancer. *Pharmacogenomics Pers. Med.* **2014**, *7*, 285–295. [CrossRef] [PubMed]
616. Endersby, R.; Whitehouse, J.; Hii, H.; Greenall, S.A.; Johns, T.G.; Gottardo, N.G. A Pre-Clinical Assessment of the Pan-ERBB Inhibitor Dacomitinib in Pediatric and Adult Brain Tumors. *Neoplasia* **2018**, *20*, 432–442. [CrossRef] [PubMed]
617. Moreira, C.; Kaklamani, V. Lapatinib and breast cancer: Current indications and outlook for the future. *Expert Rev. Anticancer Ther.* **2010**, *10*, 1171–1182. [CrossRef] [PubMed]
618. Bouchalova, K.; Cizkova, M.; Cwierka, K.; Trojanec, R.; Friedecký, D.; Hajdich, M. Lapatinib in breast cancer—the predictive significance of her1 (egfr), her2, pten and pik3ca genes and lapatinib plasma level assessment. *Biomed. Pap.* **2010**, *154*, 281–288. [CrossRef]
619. Gorlick, R.; Kolb, E.A.; Houghton, P.J.; Morton, C.L.; Phelps, D.; Schaiquevich, P.; Stewart, C.; Keir, S.T.; Lock, R.; Carol, H.; et al. Initial testing (stage 1) of lapatinib by the pediatric preclinical testing program. *Pediatr. Blood Cancer* **2009**, *53*, 594–598. [CrossRef]
620. Tebbutt, N.; Pedersen, M.W.; Johns, T.G. Targeting the ERBB family in cancer: Couples therapy. *Nat. Rev. Cancer* **2013**, *13*, 663–673. [CrossRef]
621. Herrmann, D.; Seitz, G.; Warmann, S.W.; Bonin, M.; Fuchs, J.; Armeanu-Ebinger, S. Cetuximab Promotes Immunotoxicity Against Rhabdomyosarcoma In Vitro. *J. Immunother.* **2010**, *33*, 279–286. [CrossRef]
622. Yamamoto, Y.; Fukuda, K.; Fuchimoto, Y.; Matsuzaki, Y.; Saikawa, Y.; Kitagawa, Y.; Morikawa, Y.; Kuroda, T. Cetuximab promotes anticancer drug toxicity in rhabdomyosarcomas with EGFR amplification in vitro. *Oncol. Rep.* **2013**, *30*, 1081–1086. [CrossRef]
623. O’Farrell, A.-M.; Abrams, T.J.; Yuen, H.A.; Ngai, T.J.; Louie, S.G.; Yee, K.W.H.; Wong, L.M.; Hong, W.; Lee, L.B.; Town, A.; et al. SU11248 is a novel FLT3 tyrosine kinase inhibitor with potent activity in vitro and in vivo. *Blood* **2003**, *101*, 3597–3605. [CrossRef]
624. Zhang, L.; Smith, K.M.; Chong, A.L.; Stempak, D.; Yeger, H.; Marrano, P.; Thorner, P.S.; Irwin, M.S.; Kaplan, D.R.; Baruchel, S. In Vivo Antitumor and Antimetastatic Activity of Sunitinib in Preclinical Neuroblastoma Mouse Model. *Neoplasia* **2009**, *11*, 426–435. [CrossRef]
625. Maris, J.M.; Bs, J.C.; Houghton, P.J.; Bs, C.L.M.; Kolb, E.A.; Lock, R.; Bs, M.T.; Reynolds, C.P.; Keir, S.T.; Wu, J.; et al. Initial testing (stage 1) of sunitinib by the pediatric preclinical testing program. *Pediatr. Blood Cancer* **2008**, *51*, 42–48. [CrossRef]
626. Hao, Z.; Wang, P. Lenvatinib in Management of Solid Tumors. *Oncologist* **2020**, *25*, e30. [CrossRef]

627. Matsui, J.; Yamamoto, Y.; Funahashi, Y.; Tsuruoka, A.; Watanabe, T.; Wakabayashi, T.; Uenaka, T.; Asada, M. E7080, a novel inhibitor that targets multiple kinases, has potent antitumor activities against stem cell factor producing human small cell lung cancer H146, based on angiogenesis inhibition. *Int. J. Cancer* **2007**, *122*, 664–671. [CrossRef]
628. Capozzi, M.; De Divitiis, C.; Ottaiano, A.; von Arx, C.; Scala, S.; Tatangelo, F.; Delrio, P.; Tafuto, S. Lenvatinib, a molecule with versatile application: From preclinical evidence to future development in anti-cancer treatment. *Cancer Manag. Res.* **2019**, *11*, 3847–3860. [CrossRef]
629. Bruheim, S.; Kristian, A.; Uenaka, T.; Suo, Z.; Tsuruoka, A.; Nesland, J.M.; Fodstad, A. Antitumour activity of oral E7080, a novel inhibitor of multiple tyrosine kinases, in human sarcoma xenografts. *Int. J. Cancer* **2011**, *129*, 742–750. [CrossRef]
630. Glen, H.; Mason, S.; Patel, H.; MacLeod, K.; Brunton, V.G. E7080, a multi-targeted tyrosine kinase inhibitor suppresses tumor cell migration and invasion. *BMC Cancer* **2011**, *11*, 309. [CrossRef]
631. Gaspar, N.; Campbell-Hewson, Q.; Melcon, S.G.; Locatelli, F.; Venkatramani, R.; Hecker-Nolting, S.; Gambart, M.; Bautista, F.; Thebaud, E.; Aerts, I.; et al. Phase I/II study of single-agent lenvatinib in children and adolescents with refractory or relapsed solid malignancies and young adults with osteosarcoma (ITCC-050). *ESMO Open* **2021**, *6*, 100250. [CrossRef]
632. Wilky, B.A.; Meyer, C.F.; Trent, J.C. Pazopanib in sarcomas. *Curr. Opin. Oncol.* **2013**, *25*, 373–378. [CrossRef]
633. Kumar, S.; Mokhtari, R.B.; Oliveira, I.D.; Islam, S.; Toledo, S.R.C.; Yeager, H.; Baruchel, S. Tumor Dynamics in Response to Antiangiogenic Therapy with Oral Metronomic Topotecan and Pazopanib in Neuroblastoma Xenografts. *Transl. Oncol.* **2013**, *6*, 493–503. [CrossRef]
634. Kumar, S.; Mokhtari, R.B.; Sheikh, R.; Wu, B.; Zhang, L.; Xu, P.; Man, S.; Oliveira, I.D.; Yeager, H.; Kerbel, R.S.; et al. Metronomic Oral Topotecan with Pazopanib Is an Active Antiangiogenic Regimen in Mouse Models of Aggressive Pediatric Solid Tumor. *Clin. Cancer Res.* **2011**, *17*, 5656–5667. [CrossRef]
635. Chiabotto, G.; Grignani, G.; Todorovic, M.; Martin, V.; Centomo, M.L.; Prola, E.; Giordano, G.; Merlini, A.; Miglio, U.; Berrino, E.; et al. Pazopanib and Trametinib as a Synergistic Strategy against Osteosarcoma: Preclinical Activity and Molecular Insights. *Cancers* **2020**, *12*, 1519. [CrossRef] [PubMed]
636. Keir, S.T.; Bs, C.L.M.; Wu, J.; Kurmasheva, R.T.; Houghton, P.J.; Smith, M.A. Initial testing of the multitargeted kinase inhibitor pazopanib by the pediatric preclinical testing program. *Pediatr. Blood Cancer* **2011**, *59*, 586–588. [CrossRef] [PubMed]
637. Aggerholm-Pedersen, N.; Rossen, P.; Rose, H.; Safwat, A. Pazopanib in the Treatment of Bone Sarcomas: Clinical Experience. *Transl. Oncol.* **2020**, *13*, 295–299. [CrossRef] [PubMed]
638. Mori, Y.; Kinoshita, S.; Kanamori, T.; Kataoka, H.; Joh, T.; Iida, S.; Takemoto, M.; Kondo, M.; Kuroda, J.; Komatsu, H. The Successful Treatment of Metastatic Extraosseous Ewing Sarcoma with Pazopanib. *Intern. Med.* **2018**, *57*, 2753–2757. [CrossRef] [PubMed]
639. Donson, A.M.; Amani, V.; Warner, E.A.; Griesinger, A.M.; Witt, D.A.; Levy, J.M.M.; Hoffman, L.M.; Hankinson, T.C.; Handler, M.H.; Vibhakar, R.; et al. Identification of FDA-Approved Oncology Drugs with Selective Potency in High-Risk Childhood Ependymoma. *Mol. Cancer Ther.* **2018**, *17*, 1984–1994. [CrossRef]
640. Schoen, L.F.; Craveiro, R.B.; Pietsch, T.; Moritz, T.; Troeger, A.; Jordans, S.; Dilloo, D. The PI3K inhibitor pictilisib and the multikinase inhibitors pazopanib and sorafenib have an impact on Rac1 level and migration of medulloblastoma in vitro. *J. Cell. Mol. Med.* **2022**, *26*, 5832–5845. [CrossRef]
641. Craveiro, R.B.; Ehrhardt, M.; Holst, M.I.; Pietsch, T.; Dilloo, D. In Comparative Analysis of Multi-Kinase Inhibitors for Targeted Medulloblastoma Therapy Pazopanib Exhibits Promising In Vitro and In Vivo Efficacy, 2014. Available online: [www.impactjournals.com/oncotarget](http://www.impactjournals.com/oncotarget) (accessed on 22 October 2022).
642. Scott, B.J.; Quant, E.C.; McNamara, M.B.; Ryg, P.A.; Batchelor, T.T.; Wen, P.Y. Bevacizumab salvage therapy following progression in high-grade glioma patients treated with VEGF receptor tyrosine kinase inhibitors. *Neuro-Oncology* **2010**, *12*, 603–607. [CrossRef]
643. Duke, E.S.; Barone, A.K.; Chatterjee, S.; Mishra-Kalyani, P.S.; Shen, Y.-L.; Isikwei, E.; Zhao, H.; Bi, Y.; Liu, J.; Rahman, N.A.; et al. FDA Approval Summary: Cabozantinib for Differentiated Thyroid Cancer. *Clin. Cancer Res.* **2022**, *28*, 4173–4177. [CrossRef]
644. Leavitt, J.; Copur, M.S. FDA Approved Uses of Cabozantinib. *Oncology* **2019**, *33*, 685004.
645. Yakes, F.M.; Chen, J.; Tan, J.; Yamaguchi, K.; Shi, Y.; Yu, P.; Qian, F.; Chu, F.; Bentzien, F.; Cancilla, B.; et al. Cabozantinib (XL184), a Novel MET and VEGFR2 Inhibitor, Simultaneously Suppresses Metastasis, Angiogenesis, and Tumor Growth. *Mol. Cancer Ther.* **2011**, *10*, 2298–2308. [CrossRef]
646. Bentzien, F.; Zuzow, M.; Heald, N.; Gibson, A.; Shi, Y.; Goon, L.; Yu, P.; Engst, S.; Zhang, W.; Huang, D.; et al. In Vitro and In Vivo Activity of Cabozantinib (XL184), an Inhibitor of RET, MET, and VEGFR2, in a Model of Medullary Thyroid Cancer. *Thyroid* **2013**, *23*, 1569–1577. [CrossRef]
647. Santoni, M.; Iacovelli, R.; Colonna, V.; Klinz, S.; Mauri, G.; Nuti, M. Antitumor effects of the multi-target tyrosine kinase inhibitor cabozantinib: A comprehensive review of the preclinical evidence. *Expert Rev. Anticancer. Ther.* **2021**, *21*, 1029–1054. [CrossRef]
648. Fioramonti, M.; Fausti, V.; Pantano, F.; Iuliani, M.; Ribelli, G.; Lotti, F.; Pignochino, Y.; Grignani, G.; Santini, D.; Tonini, G.; et al. Cabozantinib Affects Osteosarcoma Growth Through A Direct Effect On Tumor Cells and Modifications In Bone Microenvironment. *Sci. Rep.* **2018**, *8*, 4177. [CrossRef]
649. Pagnuzzi-Boncompagni, M.; Picco, V.; Vial, V.; Planas-Bielsa, V.; Vandenberghe, A.; Daubon, T.; Derieppe, M.-A.; Montemagno, C.; Durivault, J.; Grépin, R.; et al. Antiangiogenic Compound Axitinib Demonstrates Low Toxicity and Antitumoral Effects against Medulloblastoma. *Cancers* **2021**, *14*, 70. [CrossRef]

650. Daudigeos-Dubus, E.; Le Dret, L.; Bawa, O.; Opolon, P.; Vievard, A.; Villa, I.; Bosq, J.; Vassal, G.; Geoerger, B. Dual inhibition using cabozantinib overcomes HGF/MET signaling mediated resistance to pan-VEGFR inhibition in orthotopic and metastatic neuroblastoma tumors. *Int. J. Oncol.* **2016**, *50*, 203–211. [CrossRef]
651. Wind, S.; Schmid, U.; Freiwald, M.; Marzin, K.; Lotz, R.; Ebner, T.; Stopfer, P.; Dallinger, C. Clinical Pharmacokinetics and Pharmacodynamics of Nintedanib. *Clin. Pharmacokinet.* **2019**, *58*, 1131–1147. [CrossRef]
652. A Kharlamova, L. Study of the radiobiological reactions of Amoeba proteus. 2. The effect of the binuclear state on the radiosensitivity of amebae. *Radiobiologia* **1972**, *12*, 934–937.
653. Lin, T.; Gong, L. Inhibition of lymphangiogenesis in vitro and in vivo by the multikinase inhibitor nintedanib. *Drug Des. Dev. Ther.* **2017**, *11*, 1147–1158. [CrossRef]
654. Patwardhan, P.P.; Musi, E.; Schwartz, G.K. Preclinical Evaluation of Nintedanib, a Triple Angiokinase Inhibitor, in Soft-tissue Sarcoma: Potential Therapeutic Implication for Synovial Sarcoma. *Mol. Cancer Ther.* **2018**, *17*, 2329–2340. [CrossRef]
655. Zhang, W.; Zhao, J.-M.; Lin, J.; Hu, C.-Z.; Zhang, W.-B.; Yang, W.-L.; Zhang, J.; Zhu, J. Adaptive Fibrogenic Reprogramming of Osteosarcoma Stem Cells Promotes Metastatic Growth. *Cell Rep.* **2018**, *24*, 1266–1277.e5. [CrossRef]
656. Milton, C.I.; Selfe, J.; Aladowicz, E.; Man, S.Y.K.; Bernauer, C.; Missiaglia, E.; Walters, Z.S.; Gatz, S.A.; Kelsey, A.; Generali, M.; et al. FGF7–FGFR2 autocrine signaling increases growth and chemoresistance of fusion-positive rhabdomyosarcomas. *Mol. Oncol.* **2021**, *16*, 1272–1289. [CrossRef]
657. Loetsch, D.; Gojo, J.; Kirchhofer, D.; Van Schoonhoven, S.; Pajtlar, K.; Kool, M.; Haberler, C.; Czech, T.; Slavic, I.; Berger, W. OS5.2 FGFR a novel target in malignant pediatric ependymoma. *Neuro-Oncology* **2018**, *20*, iii224. [CrossRef]
658. Lötsch, D.; Kirchhofer, D.; Englinger, B.; Jiang, L.; Okonechnikov, K.; Senfter, D.; Laemmerer, A.; Gabler, L.; Pirker, C.; Donson, A.M.; et al. Targeting fibroblast growth factor receptors to combat aggressive ependymoma. *Acta Neuropathol.* **2021**, *142*, 339–360. [CrossRef] [PubMed]
659. Kasamon, Y.L.; Ko, C.-W.; Subramaniam, S.; Ma, L.; Yang, Y.; Nie, L.; Shord, S.; Przepiorka, D.; Farrell, A.T.; McKee, A.E.; et al. FDA Approval Summary: Midostaurin for the Treatment of Advanced Systemic Mastocytosis. *Oncologist* **2018**, *23*, 1511–1519. [CrossRef] [PubMed]
660. Midostaurin Gets FDA Nod for AML. *Cancer Discov.* **2017**, *7*, OF5. [CrossRef]
661. Kawamoto, T.; Akisue, T.; Kishimoto, K.; Hara, H.; Imabori, M.; Fujimoto, T.; Kurosaka, M.; Hitora, T.; Kawaguchi, Y.; Yamamoto, T. Inhibition of PKC $\alpha$  activation in human bone and soft tissue sarcoma cells by the selective PKC inhibitor PKC412. *Anticancer Res.* **2008**, *28*, 825–832.
662. Boro, A.; Prêtre, K.; Rechfeld, F.; Thalhammer, V.; Oesch, S.; Wachtel, M.; Schäfer, B.W.; Niggli, F.K. Small-molecule screen identifies modulators of EWS/FLI1 target gene expression and cell survival in Ewing’s sarcoma. *Int. J. Cancer* **2012**, *131*, 2153–2164. [CrossRef]
663. Brounais, B.; Chipoy, C.; Mori, K.; Charrier, C.; Battaglia, S.; Pilet, P.; Richards, C.D.; Heymann, D.; Rédini, F.; Blanchard, F. Oncostatin M Induces Bone Loss and Sensitizes Rat Osteosarcoma to the Antitumor Effect of Midostaurin *In vivo*. *Clin. Cancer Res.* **2008**, *14*, 5400–5409. [CrossRef]
664. Kelly, R.J.; Rixe, O. Axitinib (AG-013736). *Small Mol. Oncol.* **2009**, *184*, 33–44. [CrossRef]
665. Lu, L.; Saha, D.; Martuza, R.L.; Rabkin, S.; Wakimoto, H. Single agent efficacy of the VEGFR kinase inhibitor axitinib in preclinical models of glioblastoma. *J. Neuro-Oncology* **2014**, *121*, 91–100. [CrossRef]
666. Ehrhardt, M.; Craveiro, R.B.; Velz, J.; Olschewski, M.; Casati, A.; Schönberger, S.; Pietsch, T.; Dilloo, D. The FDA approved PI 3K inhibitor GDC -0941 enhances in vitro the anti-neoplastic efficacy of Axitinib against c-myc-amplified high-risk medulloblastoma. *J. Cell. Mol. Med.* **2018**, *22*, 2153–2161. [CrossRef]
667. Suri, A.; Bailey, A.W.; Tavares, M.T.; Gunosewoyo, H.; Dyer, C.P.; Grupenmacher, A.T.; Piper, D.R.; Horton, R.A.; Tomita, T.; Kozikowski, A.P.; et al. Evaluation of Protein Kinase Inhibitors with PLK4 Cross-Over Potential in a Pre-Clinical Model of Cancer. *Int. J. Mol. Sci.* **2019**, *20*, 2112. [CrossRef]
668. Schwinn, S.; Mokhtari, Z.; Thusek, S.; Schneider, T.; Sirén, A.-L.; Tiemeyer, N.; Caruana, I.; Miele, E.; Schlegel, P.G.; Beilhack, A.; et al. Cytotoxic effects and tolerability of gemcitabine and axitinib in a xenograft model for c-myc amplified medulloblastoma. *Sci. Rep.* **2021**, *11*, 1–15. [CrossRef]
669. Saha, D.; Wakimoto, H.; Peters, C.W.; Antoszczyk, S.J.; Rabkin, S.D.; Martuza, R.L. Combinatorial Effects of VEGFR Kinase Inhibitor Axitinib and Oncolytic Virotherapy in Mouse and Human Glioblastoma Stem-Like Cell Models. *Clin. Cancer Res.* **2018**, *24*, 3409–3422. [CrossRef]
670. Rössler, J.; Monnet, Y.; Farace, F.; Opolon, P.; Daudigeos-Dubus, E.; Bourredjem, A.; Vassal, G.; Geoerger, B. The selective VEGFR1-3 inhibitor axitinib (AG-013736) shows antitumor activity in human neuroblastoma xenografts. *Int. J. Cancer* **2010**, *128*, 2748–2758. [CrossRef]
671. Lu, D.; Jimenez, X.; Zhang, H.; Bohlen, P.; Witte, L.; Zhu, Z. Selection of high affinity human neutralizing antibodies to VEGFR2 from a large antibody phage display library for antiangiogenesis therapy. *Int. J. Cancer* **2001**, *97*, 393–399. [CrossRef]
672. Lowery, C.D.; Blosser, W.; Dowless, M.; Renschler, M.; Perez, L.V.; Stephens, J.; Pytowski, B.; Wasserstrom, H.; Stancato, L.F.; Falcon, B. Anti-VEGFR2 therapy delays growth of preclinical pediatric tumor models and enhances anti-tumor activity of chemotherapy. *Oncotarget* **2019**, *10*, 5523–5533. [CrossRef]
673. Casak, S.J.; Fashoyin-Aje, I.; Lemery, S.J.; Zhang, L.; Jin, R.; Li, H.; Zhao, L.; Zhao, H.; Zhang, H.; Chen, H.; et al. FDA Approval Summary: Ramucirumab for Gastric Cancer. *Clin. Cancer Res.* **2015**, *21*, 3372–3376. [CrossRef]

674. Syed, Y.Y. Ramucirumab: A Review in Hepatocellular Carcinoma. *Drugs* **2020**, *80*, 315–322. [CrossRef]
675. Tiwari, P. Ramucirumab: Boon or bane. *J. Egypt. Natl. Cancer Inst.* **2016**, *28*, 133–140. [CrossRef]
676. Debeuckelaere, C.; Murgioni, S.; Lonardi, S.; Girardi, N.; Alberti, G.; Fano, C.; Gallimberti, S.; Magro, C.; Ahcene-Djaballah, S.; Daniel, F.; et al. Ramucirumab: The long and winding road toward being an option for mCRC treatment. *Expert Opin. Biol. Ther.* **2019**, *19*, 399–409. [CrossRef] [PubMed]
677. Larkins, E.; Blumenthal, G.M.; Chen, H.; He, K.; Agarwal, R.; Gieser, G.; Stephens, O.; Zahalka, E.; Ringgold, K.; Helms, W.; et al. FDA Approval: Alectinib for the Treatment of Metastatic, ALK-Positive Non-Small Cell Lung Cancer Following Crizotinib. *Clin. Cancer Res.* **2016**, *22*, 5171–5176. [CrossRef] [PubMed]
678. Kodama, T.; Hasegawa, M.; Takanashi, K.; Sakurai, Y.; Kondoh, O.; Sakamoto, H. Antitumor activity of the selective ALK inhibitor alectinib in models of intracranial metastases. *Cancer Chemother. Pharmacol.* **2014**, *74*, 1023–1028. [CrossRef] [PubMed]
679. Ryu, S.; Hayashi, M.; Aikawa, H.; Okamoto, I.; Fujiwara, Y.; Hamada, A. Heterogeneous distribution of alectinib in neuroblastoma xenografts revealed by matrix-assisted laser desorption ionization mass spectrometry imaging: A pilot study. *Br. J. Pharmacol.* **2017**, *175*, 29–37. [CrossRef]
680. Chen, L.; Humphreys, A.; Turnbull, L.; Bellini, A.; Schleiermacher, G.; Salwen, H.; Cohn, S.L.; Bown, N.; Tweddle, D.A. Identification of different ALK mutations in a pair of neuroblastoma cell lines established at diagnosis and relapse. *Oncotarget* **2016**, *7*, 87301–87311. [CrossRef]
681. Lu, J.; Guan, S.; Zhao, Y.; Yu, Y.; Woodfield, S.E.; Zhang, H.; Yang, K.L.; Bieerkehazhi, S.; Qi, L.; Li, X.; et al. The second-generation ALK inhibitor alectinib effectively induces apoptosis in human neuroblastoma cells and inhibits tumor growth in a TH-MYCN transgenic neuroblastoma mouse model. *Cancer Lett.* **2017**, *400*, 61–68. [CrossRef]
682. Yang, K.; Chen, Y.; Wang, F. Correction: Alectinib (CH5424802) antagonizes ABCB1- and ABCG2-mediated multidrug resistance in vitro, in vivo and ex vivo. *Exp. Mol. Med.* **2020**, *52*, 989–990. [CrossRef]
683. Brunac, A.; Laprie, A.; Castex, M.; Laurent, C.; Le Loarer, F.; Karanian, M.; Le Guellec, S.; Guillemot, D.; Pierron, G.; Gomez-Brouchet, A. The combination of radiotherapy and ALK inhibitors is effective in the treatment of intraosseous rhabdomyosarcoma with *FUS-TFCP2* fusion transcript. *Pediatr. Blood Cancer* **2020**, *67*, e28185. [CrossRef]
684. Hagiwara, K.; Tokunaga, T.; Iida, H.; Nagai, H. Combined Inhibition of ALK and HDAC Induces Synergistic Cytotoxicity in Neuroblastoma Cell Lines. *Anticancer. Res.* **2019**, *39*, 3579–3584. [CrossRef]
685. Berezowska, S.; Diermeier-Daucher, S.; Brockhoff, G.; Busch, R.; Duyster, J.; Grosu, A.-L.; Schlegel, J. Effect of additional inhibition of human epidermal growth factor receptor 2 with the bispecific tyrosine kinase inhibitor AEE788 on the resistance to specific EGFR inhibition in glioma cells. *Int. J. Mol. Med.* **2010**, *26*, 713–721. [CrossRef]
686. Servidei, T.; Meco, D.; Trivieri, N.; Patriarca, V.; Vellone, V.G.; Zannoni, G.F.; Lamorte, G.; Pallini, R.; Riccardi, R. Effects of epidermal growth factor receptor blockade on ependymoma stem cells in vitro and in orthotopic mouse models. *Int. J. Cancer* **2012**, *131*, E791–E803. [CrossRef]
687. Park, Y.W.; Younes, M.N.; Jasser, S.A.; Yigitbasi, O.G.; Zhou, G.; Bucana, C.D.; Bekele, B.N.; Myers, J.N. AEE788, a Dual Tyrosine Kinase Receptor Inhibitor, Induces Endothelial Cell Apoptosis in Human Cutaneous Squamous Cell Carcinoma Xenografts in Nude Mice. *Clin. Cancer Res.* **2005**, *11*, 1963–1973. [CrossRef]
688. Meco, D.; Servidei, T.; Zannoni, G.F.; Martinelli, E.; Prisco, M.G.; de Waure, C.; Riccardi, R. Dual Inhibitor AEE78 Reduces Tumor Growth in Preclinical Models of Medulloblastoma. *Transl. Oncol.* **2010**, *3*, 326–335. [CrossRef]
689. Heigener, D.F.; Reck, M. Crizotinib. In *Recent Results in Cancer Research*; Springer LLC: New York, NY, USA, 2018; Volume 211, pp. 57–65. [CrossRef]
690. Zomeran, W.W.; Plasschaert, S.L.A.; Diks, S.H.; Lourens, H.-J.; Boer, T.M.-D.; Hoving, E.W.; Dunnen, W.F.A.D.; De Bont, E.S.J.M. Exogenous HGF Bypasses the Effects of ErbB Inhibition on Tumor Cell Viability in Medulloblastoma Cell Lines. *PLoS ONE* **2015**, *10*, e0141381. [CrossRef]
691. Sie, M.; Dunnen, W.F.A.D.; Lourens, H.J.; Boer, T.G.J.M.-D.; Scherpen, F.J.G.; Zomeran, W.W.; Kampen, K.; Hoving, E.W.; De Bont, E.S.J.M. Growth-Factor-Driven Rescue to Receptor Tyrosine Kinase (RTK) Inhibitors through Akt and Erk Phosphorylation in Pediatric Low Grade Astrocytoma and Ependymoma. *PLoS ONE* **2015**, *10*, e0122555. [CrossRef]
692. Megiorni, F.; McDowell, H.P.; Camero, S.; Mannarino, O.; Ceccarelli, S.; Paiano, M.; Losty, P.D.; Pizer, B.; Shukla, R.; Pizzuti, A.; et al. Crizotinib-induced antitumour activity in human alveolar rhabdomyosarcoma cells is not solely dependent on ALK and MET inhibition. *J. Exp. Clin. Cancer Res.* **2015**, *34*, 1–16. [CrossRef]
693. Schöffski, P.; Wozniak, A.; Leahy, M.G.; Aamdal, S.; Rutkowski, P.; Bauer, S.; Richter, S.; Grünwald, V.; Debiec-Rychter, M.; Sciort, R.; et al. The tyrosine kinase inhibitor crizotinib does not have clinically meaningful activity in heavily pre-treated patients with advanced alveolar rhabdomyosarcoma with FOXO rearrangement: European Organisation for Research and Treatment of Cancer phase 2 trial 90101 'CREATE'. *Eur. J. Cancer* **2018**, *94*, 156–167. [CrossRef]
694. Heuckmann, J.M.; Hölzel, M.; Sos, M.L.; Heynck, S.; Balke-Want, H.; Koker, M.; Peifer, M.; Weiss, J.; Lovly, C.M.; Grütter, C.; et al. ALK Mutations Conferring Differential Resistance to Structurally Diverse ALK Inhibitors. *Clin. Cancer Res.* **2011**, *17*, 7394–7401. [CrossRef]
695. George, R.E.; Sanda, T.; Hanna, M.; Fröhling, S.; Luther, W., II; Zhang, J.; Ahn, Y.; Zhou, W.; London, W.B.; McGrady, P.; et al. Activating mutations in ALK provide a therapeutic target in neuroblastoma. *Nature* **2008**, *455*, 975–978. [CrossRef]

696. Bresler, S.C.; Weiser, D.A.; Huwe, P.J.; Park, J.H.; Krytska, K.; Ryles, H.; Laudenslager, M.; Rappaport, E.F.; Wood, A.C.; McGrady, P.W.; et al. ALK Mutations Confer Differential Oncogenic Activation and Sensitivity to ALK Inhibition Therapy in Neuroblastoma. *Cancer Cell* **2014**, *26*, 682–694. [CrossRef]
697. Dagogo-Jack, I.; Shaw, A.T. Crizotinib resistance: Implications for therapeutic strategies. *Ann. Oncol.* **2016**, *27* (Suppl. S3), iii42–iii50. [CrossRef] [PubMed]
698. Zuckermann, M.; He, C.; Andrews, J.; Sloan-Henry, R.; Bianski, B.; Xie, J.; Wang, Y.; Twarog, N.; Onar-Thomas, A.; Ernst, K.; et al. MODL-06. Targeting c-MET in combination with radiation is effective in MET-fusion driven high-grade glioma. *Neuro-Oncology* **2022**, *24*, i169. [CrossRef]
699. Esaki, T.; Hirai, F.; Makiyama, A.; Seto, T.; Bando, H.; Naito, Y.; Yoh, K.; Ishihara, K.; Kakizume, T.; Natsume, K.; et al. Phase I dose-escalation study of capmatinib (INC 280) in Japanese patients with advanced solid tumors. *Cancer Sci.* **2019**, *110*, 1340–1351. [CrossRef] [PubMed]
700. Markham, A. Tepotinib: First Approval. *Drugs* **2020**, *80*, 829–833. [CrossRef]
701. Zou, H.Y.; Li, Q.; Lee, J.H.; Arango, M.E.; Burgess, K.; Qiu, M.; Engstrom, L.D.; Yamazaki, S.; Parker, M.; Timofeevski, S.; et al. Sensitivity of Selected Human Tumor Models to PF-04217903, a Novel Selective c-Met Kinase Inhibitor. *Mol. Cancer Ther.* **2012**, *11*, 1036–1047. [CrossRef]
702. Niswander, L.M.; Guenther, L.M.; Mendoza, A.; Khanna, C.; Christensen, J.G.; Helman, L.J.; Kim, S. Effect of modulation of MET with the small molecule inhibitor PF-04217903 on osteosarcoma metastasis in vivo. *J. Clin. Oncol.* **2010**, *28*, 9567. [CrossRef]
703. Lock, R.; Ingraham, R.; Maertens, O.; Miller, A.L.; Weledji, N.; Legius, E.; Konicek, B.M.; Yan, S.-C.B.; Graff, J.R.; Cichowski, K. Cotargeting MNK and MEK kinases induces the regression of NF1-mutant cancers. *J. Clin. Investig.* **2016**, *126*, 2181–2190. [CrossRef]
704. Katayama, R.; Aoyama, A.; Yamori, T.; Qi, J.; Oh-Hara, T.; Song, Y.; Engelman, J.A.; Fujita, N. Cytotoxic Activity of Tivantinib (ARQ 197) Is Not Due Solely to c-MET Inhibition. *Cancer Res* **2013**, *73*, 3087–3096. [CrossRef]
705. Geller, J.I.; Perentesis, J.P.; Liu, X.; Minard, C.G.; Kudgus, R.A.; Reid, J.M.; Fox, E.; Blaney, S.M.; Weigel, B.J. A phase 1 study of the c-Met inhibitor, tivantinib (ARQ197) in children with relapsed or refractory solid tumors: A Children’s Oncology Group study phase 1 and pilot consortium trial (ADVL1111). *Pediatr. Blood Cancer* **2017**, *64*, e26565. [CrossRef]
706. Goldberg, J.M.; Gavcovich, T.; Saigal, G.; Goldman, J.W.; Rosen, L.S. Extended Progression-Free Survival in Two Patients With Alveolar Soft Part Sarcoma Exposed to Tivantinib. *J. Clin. Oncol.* **2014**, *32*, e114–e116. [CrossRef]
707. Johnson, T.W.; Richardson, P.F.; Bailey, S.; Brooun, A.; Burke, B.J.; Collins, M.R.; Cui, J.J.; Deal, J.G.; Deng, Y.-L.; Dinh, D.; et al. Discovery of (10R)-7-Amino-12-fluoro-2,10,16-trimethyl-15-oxo-10,15,16,17-tetrahydro-2H-8,4-(metheno)pyrazolo[4,3-h][[2,5,11]-benzoxadiazacyclotetradecine-3-carbonitrile (PF-06463922), a Macrocyclic Inhibitor of Anaplastic Lymphoma Kinase (ALK) and c-ros Oncogene 1 (ROS1) with Preclinical Brain Exposure and Broad-Spectrum Potency against ALK-Resistant Mutations. *J. Med. Chem.* **2014**, *57*, 4720–4744. [CrossRef]
708. Infarinato, N.R.; Park, J.H.; Krytska, K.; Ryles, H.T.; Sano, R.; Szigety, K.M.; Li, Y.; Zou, H.Y.; Lee, N.V.; Smeal, T.; et al. The ALK/ROS1 Inhibitor PF-06463922 Overcomes Primary Resistance to Crizotinib in ALK-Driven Neuroblastoma. *Cancer Discov.* **2016**, *6*, 96–107. [CrossRef]
709. Guan, J.; Tucker, E.R.; Wan, H.; Chand, D.; Danielson, L.S.; Ruuth, K.; El Wakil, A.; Witek, B.; Jamin, Y.; Umaphathy, G.; et al. The ALK inhibitor PF-06463922 is effective as a single agent in neuroblastoma driven by expression of ALK and MYCN. *Dis. Model. Mech.* **2016**, *9*, 941–952. [CrossRef]
710. Collier, T.L.; Maresca, K.P.; Normandin, M.D.; Richardson, P.; McCarthy, T.J.; Liang, S.H.; Waterhouse, R.N.; Vasdev, N. Brain Penetration of the ROS1/ALK Inhibitor Lorlatinib Confirmed by PET. *Mol. Imaging* **2017**, *16*. [CrossRef] [PubMed]
711. Bagchi, A.; Orr, B.A.; Campagne, O.; Dhanda, S.; Nair, S.; Tran, Q.; Christensen, A.M.; Gajjar, A.; Furtado, L.V.; Vasilyeva, A.; et al. Lorlatinib in a Child with ALK-Fusion-Positive High-Grade Glioma. *New Engl. J. Med.* **2021**, *385*, 761–763. [CrossRef] [PubMed]
712. Liu, T.; Merguerian, M.D.; Rowe, S.P.; Pratilas, C.A.; Chen, A.R.; Ladle, B.H. Exceptional response to the ALK and ROS1 inhibitor lorlatinib and subsequent mechanism of resistance in relapsed ALK F1174L-mutated neuroblastoma. *Mol. Case Stud.* **2021**, *7*, a006064. [CrossRef] [PubMed]
713. Khozin, S.; Blumenthal, G.M.; Zhang, L.; Tang, S.; Brower, M.; Fox, E.; Helms, W.; Leong, R.; Song, P.; Pan, Y.; et al. FDA Approval: Ceritinib for the Treatment of Metastatic Anaplastic Lymphoma Kinase-Positive Non-Small Cell Lung Cancer. *Clin. Cancer Res.* **2015**, *21*, 2436–2439. [CrossRef] [PubMed]
714. Guan, J.; Fransson, S.; Siaw, J.T. Clinical response of the novel activating ALK-I1171T mutation in neuroblastoma to the ALK inhibitor ceritinib Running title: Clinical response to ceritinib in ALK-positive neuroblastoma. *Cold Spring Harb. Mol. Case Stud.* **2018**, *4*, a002550. [CrossRef]
715. Mittal, A.; Gupta, A.; Rastogi, S.; Barwad, A.; Sharma, S. Near-complete response to low-dose ceritinib in recurrent infantile inflammatory myofibroblastic tumour. *Ecancermedalscience* **2021**, *15*. [CrossRef]
716. Russo, A.; Paret, C.; Lehmann, N.; Bender, H.; Wingerter, A.; Neu, M.A.; Alt, F.; Backes, N.; Roth, L.; Seidmann, L.; et al. Epen-29. individualized therapy of an anaplastic ependymoma pediatric patient with a notch1 germline mutation. *Neuro-Oncology* **2018**, *20*, i79. [CrossRef]
717. Russo, A.; Paret, C.; Alt, F.; Burhenne, J.; Fresnais, M.; Wagner, W.; Glaser, M.; Bender, H.; Huprich, S.; Harter, P.N.; et al. Ceritinib-Induced Regression of an Insulin-Like Growth Factor-Driven Neuroepithelial Brain Tumor. *Int. J. Mol. Sci.* **2019**, *20*, 4267. [CrossRef] [PubMed]

718. Lin, C.Y.; Erkek, S.; Tong, Y.; Yin, L.; Federation, A.J.; Zapatka, M.; Haldipur, P.; Kawauchi, D.; Risch, T.; Warnatz, H.-J.; et al. Active medulloblastoma enhancers reveal subgroup-specific cellular origins. *Nature* **2016**, *530*, 57–62. [CrossRef] [PubMed]
719. Tsoli, M.; Wadham, C.; Pinese, M.; Failes, T.; Joshi, S.; Mould, E.; Yin, J.X.; Gayevskiy, V.; Kumar, A.; Kaplan, W.; et al. Integration of genomics, high throughput drug screening, and personalized xenograft models as a novel precision medicine paradigm for high risk pediatric cancer. *Cancer Biol. Ther.* **2018**, *19*, 1078–1087. [CrossRef] [PubMed]
720. Beck, O.; Paret, C.; Russo, A.; Burhenne, J.; Fresnais, M.; Steimel, K.; Seidmann, L.; Wagner, D.-C.; Vewinger, N.; Lehmann, N.; et al. Safety and Activity of the Combination of Ceritinib and Dasatinib in Osteosarcoma. *Cancers* **2020**, *12*, 793. [CrossRef] [PubMed]
721. van Erp, A.E.M.; Hillebrandt-Roeffen, M.H.S.; van Houdt, L.; Fleuren, E.D.G.; van der Graaf, W.T.A.; Versleijen-Jonkers, Y.M.H. Targeting Anaplastic Lymphoma Kinase (ALK) in Rhabdomyosarcoma (RMS) with the Second-Generation ALK Inhibitor Ceritinib. *Target. Oncol.* **2017**, *12*, 815–826. [CrossRef] [PubMed]
722. Dolgikh, N.; Fulda, S. Rhabdomyosarcoma cells are susceptible to cell death by LDK378 alone or in combination with sorafenib independently of anaplastic lymphoma kinase status. *Anti-Cancer Drugs* **2017**, *28*, 1118–1125. [CrossRef]
723. Huang, W.-S.; Liu, S.; Zou, D.; Thomas, M.; Wang, Y.; Zhou, T.; Romero, J.; Kohlmann, A.; Li, F.; Qi, J.; et al. Discovery of Brigatinib (AP26113), a Phosphine Oxide-Containing, Potent, Orally Active Inhibitor of Anaplastic Lymphoma Kinase. *J. Med. Chem.* **2016**, *59*, 4948–4964. [CrossRef]
724. Mo, F.; Pellerino, A.; Soffietti, R.; Rudà, R. Blood–Brain Barrier in Brain Tumors: Biology and Clinical Relevance. *Int. J. Mol. Sci.* **2021**, *22*, 12654. [CrossRef]
725. Spencer, S.A.; Riley, A.C.; Matthew, A.; Di Pasqua, A.J. Brigatinib: Novel ALK Inhibitor for Non–Small-Cell Lung Cancer. *Ann. Pharmacother.* **2019**, *53*, 621–626. [CrossRef]
726. Siaw, J.T.; Wan, H.; Pfeifer, K.; Rivera, V.M.; Guan, J.; Palmer, R.H.; Hallberg, B. Brigatinib, an anaplastic lymphoma kinase inhibitor, abrogates activity and growth in ALK-positive neuroblastoma cells, *Drosophila* and mice. *Oncotarget* **2016**, *7*, 29011–29022. [CrossRef]
727. Drilon, A.; De Braud, F.G.; Siena, S.; Ou, S.-H.I.; Patel, M.; Ahn, M.-J.; Lee, J.; Bauer, T.M.; Farago, A.F.; Liu, S.V.; et al. Abstract CT007: Entrectinib, an oral pan-Trk, ROS1, and ALK inhibitor in TKI-naïve patients with advanced solid tumors harboring gene rearrangements: Updated phase I results. *Cancer Res* **2016**, *76*, CT007. [CrossRef]
728. Jiang, Q.; Li, M.; Li, H.; Chen, L. Entrectinib, a new multi-target inhibitor for cancer therapy. *Biomed. Pharmacother.* **2022**, *150*, 112974. [CrossRef]
729. Iyer, R.; Wehrmann, L.; Golden, R.L.; Naraparaju, K.; Croucher, J.L.; MacFarland, S.P.; Guan, P.; Kolla, V.; Wei, G.; Cam, N.; et al. Entrectinib is a potent inhibitor of Trk-driven neuroblastomas in a xenograft mouse model. *Cancer Lett.* **2016**, *372*, 179–186. [CrossRef]
730. Desai, A.V.; Robinson, G.W.; Gauvain, K.; Basu, E.M.; E Macy, M.; Maese, L.; Whipple, N.S.; Sabnis, A.J.; Foster, J.H.; Shusterman, S.; et al. Entrectinib in children and young adults with solid or primary CNS tumors harboring *NTRK*, *ROS1*, or *ALK* aberrations (STARTRK-NG). *Neuro-Oncology* **2022**, *24*, 1776–1789. [CrossRef]
731. MacFarland, S.P.; Naraparaju, K.; Iyer, R.; Guan, P.; Kolla, V.; Hu, Y.; Tan, K.; Brodeur, G.M. Mechanisms of Entrectinib Resistance in a Neuroblastoma Xenograft Model. *Mol. Cancer Ther.* **2020**, *19*, 920–926. [CrossRef]
732. Spitaleri, G.; Passaro, A.; de Marinis, F. Ensartinib (X-396) a novel drug for anaplastic lymphoma kinase-positive non-small cell lung cancer patients: We need smart trials to avoid wasting good bullets. *Chin. Clin. Oncol.* **2019**, *8*, S1. [CrossRef]
733. Lovly, C.M.; Heuckmann, J.M.; de Stanchina, E.; Chen, H.; Thomas, R.K.; Liang, C.; Pao, W. Insights into ALK-Driven Cancers Revealed through Development of Novel ALK Tyrosine Kinase Inhibitors. *Cancer Res* **2011**, *71*, 4920–4931. [CrossRef]
734. Di Paolo, D.; Yang, D.; Pastorino, F.; Emionite, L.; Cilli, M.; Daga, A.; Destafanis, E.; Di Fiore, A.; Piaggio, F.; Brignole, C.; et al. New therapeutic strategies in neuroblastoma: Combined targeting of a novel tyrosine kinase inhibitor and liposomal siRNAs against *ALK*. *Oncotarget* **2015**, *6*, 28774–28789. [CrossRef]
735. Perera, T.P.; Jovcheva, E.; Mevellec, L.; Vialard, J.; De Lange, D.; Verhulst, T.; Paulussen, C.; Van De Ven, K.; King, P.; Freyne, E.; et al. Discovery and Pharmacological Characterization of JNJ-42756493 (Erdafitinib), a Functionally Selective Small-Molecule FGFR Family Inhibitor. *Mol. Cancer Ther.* **2017**, *16*, 1010–1020. [CrossRef]
736. Luzzi, S.; Brambilla, I.; Mantelli, S.S.; Mosconi, M.; Foadelli, T.; Savasta, S. Targeting the medulloblastoma: A molecular-based approach. *Acta Biomed.* **2020**, *91*, 79–100. [CrossRef]
737. Musumeci, F.; Cianciusi, A.; D’Agostino, I.; Grossi, G.; Carbone, A.; Schenone, S. Synthetic Heterocyclic Derivatives as Kinase Inhibitors Tested for the Treatment of Neuroblastoma. *Molecules* **2021**, *26*, 7069. [CrossRef] [PubMed]
738. Holzhauser, S.; Lukoseviciute, M.; Papachristofi, C.; Vasilopoulou, C.; Herold, N.; Wickström, M.; Kostopoulou, O.N.; Dalianis, T. Effects of PI3K and FGFR inhibitors alone and in combination, and with/without cytostatics in childhood neuroblastoma cell lines. *Int. J. Oncol.* **2021**, *58*, 211–225. [CrossRef] [PubMed]
739. Lukoseviciute, M.; Maier, H.; Poulou-Sidiropoulou, E.; Rosendahl, E.; Holzhauser, S.; Dalianis, T.; Kostopoulou, O.N. Targeting PI3K, FGFR, CDK4/6 Signaling Pathways Together With Cytostatics and Radiotherapy in Two Medulloblastoma Cell Lines. *Front. Oncol.* **2021**, *11*, 748657. [CrossRef] [PubMed]
740. Angevin, E.; Lopez-Martin, J.A.; Lin, C.-C.; Gschwend, J.E.; Harzstark, A.; Castellano, D.; Soria, J.-C.; Sen, P.; Chang, J.; Shi, M.; et al. Phase I Study of Dovitinib (TKI258), an Oral FGFR, VEGFR, and PDGFR Inhibitor, in Advanced or Metastatic Renal Cell Carcinoma. *Clin. Cancer Res.* **2013**, *19*, 1257–1268. [CrossRef]

741. Arnz, E.; Hertwig, F.; Krämer, A.; Ikram, F.; Roels, F.; Kocak, H.; Engesser, A.; Thomas, R.; Peifer, M.; Ackermann, S.; et al. Fibroblast growth factor receptors as therapeutic targets in neuroblastoma. *Klin. Pädiatrie* **2014**, *226*, A22. [CrossRef]
742. Li, S.Q.; Cheuk, A.T.; Shern, J.F.; Song, Y.K.; Hurd, L.; Liao, H.; Wei, J.S.; Khan, J. Targeting Wild-Type and Mutationally Activated FGFR4 in Rhabdomyosarcoma with the Inhibitor Ponatinib (AP24534). *PLoS ONE* **2013**, *8*, e76551. [CrossRef]
743. Schramm, K.; Iskar, M.; Statz, B.; Jäger, N.; Haag, D.; Slabicki, M.; Pfister, S.M.; Zapatka, M.; Gronych, J.; Jones, D.T.W.; et al. DECIPHER pooled shRNA library screen identifies PP2A and FGFR signaling as potential therapeutic targets for diffuse intrinsic pontine gliomas. *Neuro-Oncology* **2019**, *21*, 867–877. [CrossRef]
744. Yan, D.; Kowal, J.; Akkari, L.; Schuhmacher, A.J.; Huse, J.T.; West, B.L.; Joyce, J. Inhibition of colony stimulating factor-1 receptor abrogates microenvironment-mediated therapeutic resistance in gliomas. *Oncogene* **2017**, *36*, 6049–6058. [CrossRef]
745. Georjin-Lavialle, S.; Lhermitte, L.; Suarez, F.; Yang, Y.; Létard, S.; Hanssens, K.; Feger, F.; Renand, A.; Brouze, C.; Canioni, D.; et al. Mast cell leukemia: Identification of a new c-Kit mutation, dup(501-502), and response to masitinib, a c-Kit tyrosine kinase inhibitor. *Eur. J. Haematol.* **2012**, *89*, 47–52. [CrossRef]
746. Dubreuil, P.; Letard, S.; Ciufolini, M.; Gros, L.; Humbert, M.; Castéran, N.; Borge, L.; Hajem, B.; Lermet, A.; Sippl, W.; et al. Masitinib (AB1010), a Potent and Selective Tyrosine Kinase Inhibitor Targeting KIT. *PLoS ONE* **2009**, *4*, e7258. [CrossRef]
747. Marech, I.; Patruno, R.; Zizzo, N.; Gadaleta, C.; Introna, M.; Zito, A.F.; Gadaleta, C.D.; Ranieri, G. Masitinib (AB1010), from canine tumor model to human clinical development: Where we are? *Crit. Rev. Oncol.* **2014**, *91*, 98–111. [CrossRef]
748. Fleming, T.; Cunningham, C.; Keir, S. *The Effect of Masitinib on Pediatric Glioblastoma*; Duke University: Durham, NC, USA, 2014.
749. Buti, S.; Leonetti, A.; Dallatomasina, A.; Bersanelli, M. Everolimus in the management of metastatic renal cell carcinoma: An evidence-based review of its place in therapy. *Core Evid.* **2016**, *11*, 23–36. [CrossRef]
750. Nashan, B. Review of the proliferation inhibitor everolimus. *Expert Opin. Investig. Drugs* **2002**, *11*, 1845–1857. [CrossRef]
751. Pignochino, Y.; Dell’Aglia, C.; Basiricò, M.; Capozzi, F.; Soster, M.; Marchiò, S.; Bruno, S.; Gammaitoni, L.; Sangiolo, D.; Torchiario, E.; et al. The Combination of Sorafenib and Everolimus Abrogates mTORC1 and mTORC2 Upregulation in Osteosarcoma Preclinical Models. *Clin. Cancer Res.* **2013**, *19*, 2117–2131. [CrossRef]
752. Miklja, Z.; Yadav, V.N.; Cartaxo, R.T.; Siada, R.; Thomas, C.C.; Cummings, J.R.; Mullan, B.; Stallard, S.; Paul, A.; Bruzek, A.K.; et al. Everolimus improves the efficacy of dasatinib in PDGFR $\alpha$ -driven glioma. *J. Clin. Investig.* **2020**, *130*, 5313–5325. [CrossRef]
753. Poore, B.; Yuan, M.; Arnold, A.; Price, A.; Alt, J.; A Rubens, J.; Slusher, B.S.; Eberhart, C.G.; Raabe, E.H. Inhibition of mTORC1 in pediatric low-grade glioma depletes glutathione and therapeutically synergizes with carboplatin. *Neuro-Oncology* **2018**, *21*, 252–263. [CrossRef]
754. Salussolia, C.L.; Klonowska, K.; Kwiatkowski, D.J.; Sahin, M. Genetic Etiologies, Diagnosis, and Treatment of Tuberous Sclerosis Complex. *Annu. Rev. Genom. Hum. Genet.* **2019**, *20*, 217–240. [CrossRef]
755. Rosset, C.; Netto, C.B.O.; Ashton-Prolla, P. TSC1 and TSC2 gene mutations and their implications for treatment in Tuberous Sclerosis Complex: A review. *Genet. Mol. Biol.* **2017**, *40*, 69–79. [CrossRef]
756. Krueger, D.A.; Care, M.M.; Holland, K.; Agricola, K.; Tudor, C.; Mangeshkar, P.; Wilson, K.A.; Byars, A.; Sahnoud, T.; Franz, D.N. Everolimus for Subependymal Giant-Cell Astrocytomas in Tuberous Sclerosis. *N. Engl. J. Med.* **2010**, *363*, 1801–1811. [CrossRef]
757. Franz, D.N.; Lawson, J.A.; Yapici, Z.; Ikeda, H.; Polster, T.; Nabbout, R.; Curatolo, P.; de Vries, P.J.; Dlugos, D.J.; Voi, M.; et al. Everolimus for treatment-refractory seizures in TSC. *Neurol. Clin. Pract.* **2018**, *8*, 412–420. [CrossRef]
758. Xue, Q.; Hopkins, B.; Perruzzi, C.; Udayakumar, D.; Sherris, D.; Benjamin, L.E. Palomid 529, a Novel Small-Molecule Drug, Is a TORC1/TORC2 Inhibitor That Reduces Tumor Growth, Tumor Angiogenesis, and Vascular Permeability. *Cancer Res* **2008**, *68*, 9551–9557. [CrossRef] [PubMed]
759. Lin, F.; Buil, L.; Sherris, D.; Beijnen, J.H.; van Tellingen, O. Dual mTORC1 and mTORC2 inhibitor Palomid 529 penetrates the Blood-Brain Barrier without restriction by ABCB1 and ABCG2. *Int. J. Cancer* **2013**, *133*, 1222–1233. [CrossRef] [PubMed]
760. Gravina, G.L.; Mancini, A.; Colapietro, A.; Monache, S.D.; Sferra, R.; Pompili, S.; Vitale, F.; Martellucci, S.; Marampon, F.; Mattei, V.; et al. The Brain Penetrating and Dual TORC1/TORC2 Inhibitor, RES529, Elicits Anti-Glioma Activity and Enhances the Therapeutic Effects of Anti-Angiogenic Compounds in Preclinical Murine Models. *Cancers* **2019**, *11*, 1604. [CrossRef] [PubMed]
761. Cerna, D.; Carter, D.; Flaherty, S.; Cao, L.; Sherris, D.; Yoo, S.S. Abstract 2506: Palomid 529, a PI3K/Akt/mTOR dual TORC1/2 inhibitor, is a radiosensitizer with effect in both subcutaneous and orthotopic U251 glioblastoma tumor xenograft models. *Cancer Res.* **2010**, *70*, 2506. [CrossRef]
762. Hu, X.; Wang, Z.; Chen, M.; Chen, X.; Liang, W. The anti-osteosarcoma cell activity by a mTORC1/2 dual inhibitor RES-529. *Biochem. Biophys. Res. Commun.* **2018**, *497*, 499–505. [CrossRef]
763. Bhagwat, S.V.; Gokhale, P.C.; Crew, A.P.; Cooke, A.; Yao, Y.; Mantis, C.; Kahler, J.; Workman, J.; Bittner, M.; Dudkin, L.; et al. Preclinical Characterization of OSI-027, a Potent and Selective Inhibitor of mTORC1 and mTORC2: Distinct from Rapamycin. *Mol. Cancer Ther.* **2011**, *10*, 1394–1406. [CrossRef]
764. Eckerdt, F.; Clymer, J.; Bell, J.B.; Beauchamp, E.M.; Blyth, G.T.; Goldman, S.; Plataniias, L.C. Pharmacological mTOR targeting enhances the antineoplastic effects of selective PI3K $\alpha$  inhibition in medulloblastoma. *Sci. Rep.* **2019**, *9*, 12822. [CrossRef]
765. Srivastava, R.K.; Guroji, P.; Jin, L.; Mukhtar, M.S.; Athar, M. Combined inhibition of BET bromodomain and mTORC1/2 provides therapeutic advantage for rhabdomyosarcoma by switching cell death mechanism. *Mol. Carcinog.* **2022**, *61*, 737–751. [CrossRef]
766. Eckerdt, F.; Beauchamp, E.; Bell, J.; Iqbal, A.; Su, B.; Fukunaga, R.; Lulla, R.R.; Goldman, S.; Plataniias, L.C. Regulatory effects of a Mnk2-eIF4E feedback loop during mTORC1 targeting of human medulloblastoma cells. *Oncotarget* **2014**, *5*, 8442–8451. [CrossRef]

767. Clymer, J.; Eckerd, F.; Bell, J.; Lulla, R.; Goldman, S.; Platanius, L. MEDU-44. TARGETING SHH SIGNALING VIA PI3K/MTOR INHIBITION IN MEDULLOBLASTOMA AND EWING SARCOMA. *Neuro-Oncology* **2017**, *19*, iv47. [CrossRef]
768. Calimeri, T.; Ferreri, A.J.M. m-TOR inhibitors and their potential role in haematological malignancies. *Br. J. Haematol.* **2017**, *177*, 684–702. [CrossRef]
769. Kolev, V.N.; Wright, Q.G.; Vidal, C.M.; Ring, J.E.; Shapiro, I.M.; Ricono, J.; Weaver, D.T.; Padval, M.V.; Pachter, J.A.; Xu, Q. PI3K/mTOR Dual Inhibitor VS-5584 Preferentially Targets Cancer Stem Cells. *Cancer Res* **2015**, *75*, 446–455. [CrossRef]
770. Sun, J.-Y.; Hou, Y.-J.; Cui, H.-J.; Zhang, C.; Yang, M.-F.; Wang, F.-Z.; Sun, Z.; Fan, C.-D.; Sun, B.-L.; Oh, J.R. VS-5584 Inhibits Human Osteosarcoma Cells Growth by Induction of G1- phase Arrest through Regulating PI3K/mTOR and MAPK Pathways. *Curr. Cancer Drug Targets* **2020**, *20*, 616–623. [CrossRef]
771. Sun, J.-Y.; Hou, Y.-J.; Yin, Y.-B.; Wang, F.-Z.; Yang, M.-F.; Zhang, Y.-Y.; Fan, C.-D.; Sun, B.-L. CCT128930 induces G1-phase arrest and apoptosis and synergistically enhances the anticancer efficiency of VS5584 in human osteosarcoma cells. *Biomed. Pharmacother.* **2020**, *130*, 110544. [CrossRef] [PubMed]
772. Maira, S.-M.; Stauffer, F.; Brueggen, J.; Furet, P.; Schnell, C.; Fritsch, C.; Brachmann, S.; Chène, P.; De Pover, A.; Schoemaker, K.; et al. Identification and characterization of NVP-BEZ235, a new orally available dual phosphatidylinositol 3-kinase/mammalian target of rapamycin inhibitor with potent in vivo antitumor activity. *Mol. Cancer Ther.* **2008**, *7*, 1851–1863. [CrossRef]
773. Manara, M.C.; Nicoletti, G.; Zambelli, D.; Ventura, S.; Guerzoni, C.; Landuzzi, L.; Lollini, P.-L.; Maira, S.-M.; García-Echeverría, C.; Mercuri, M.; et al. NVP-BEZ235 as a New Therapeutic Option for Sarcomas. *Clin. Cancer Res.* **2010**, *16*, 530–540. [CrossRef]
774. Giorgi, C.; Boro, A.; Rechfeld, F.; Lopez-Garcia, L.A.; Gierisch, M.E.; Schäfer, B.W.; Niggli, F.K. PI3K/AKT signaling modulates transcriptional expression of EWS/FLI1 through specificity protein 1. *Oncotarget* **2015**, *6*, 28895–28910. [CrossRef]
775. Zhu, Y.-R.; Min, H.; Fang, J.-F.; Zhou, F.; Deng, X.-W.; Zhang, Y.-Q. Activity of the novel dual phosphatidylinositol 3-kinase/mammalian target of rapamycin inhibitor NVP-BEZ235 against osteosarcoma. *Cancer Biol. Ther.* **2015**, *16*, 602–609. [CrossRef]
776. Meng, W.; Wang, B.; Mao, W.; Wang, J.; Zhao, Y.; Li, Q.; Zhang, C.; Ma, J. Enhanced efficacy of histone deacetylase inhibitor panobinostat combined with dual PI3K/mTOR inhibitor BEZ235 against glioblastoma. *Nagoya J. Med. Sci.* **2019**, *81*, 93–102. [CrossRef]
777. Vazquez, N.; Lopez, A.; Cuello, V.; Persans, M.; Schuenzel, E.; Innis-Whitehouse, W.; Keniry, M. NVP-BEZ235 or JAKi Treatment leads to decreased survival of examined GBM and BBC cells. *Cancer Treat. Res. Commun.* **2021**, *27*, 100340. [CrossRef]
778. Xie, C.; Freeman, M.J.; Lu, H.; Wang, X.; Forster, C.L.; Sarver, A.L.; Hallstrom, T.C. Retinoblastoma cells activate the AKT pathway and are vulnerable to the PI3K/mTOR inhibitor NVP-BEZ235. *Oncotarget* **2017**, *8*, 38084–38098. [CrossRef] [PubMed]
779. Holzhauser, S.; Lukoseviciute, M.; Andonova, T.; Ursu, R.G.; Dalianis, T.; Wickström, M.; Kostopoulou, O.N. Targeting Fibroblast Growth Factor Receptor (FGFR) and Phosphoinositide 3-kinase (PI3K) Signaling Pathways in Medulloblastoma Cell Lines. *Anticancer. Res.* **2019**, *40*, 53–66. [CrossRef] [PubMed]
780. Gobin, B.; Battaglia, S.; Lanel, R.; Chesneau, J.; Amiaud, J.; Rédini, F.; Ory, B.; Heymann, D. NVP-BEZ235, a dual PI3K/mTOR inhibitor, inhibits osteosarcoma cell proliferation and tumor development in vivo with an improved survival rate. *Cancer Lett.* **2014**, *344*, 291–298. [CrossRef] [PubMed]
781. Chaturvedi, N.K.; Kling, M.J.; Griggs, C.N.; Kesharwani, V.; Shukla, M.; McIntyre, E.M.; Ray, S.; Liu, Y.; McGuire, T.R.; Sharp, J.G.; et al. A Novel Combination Approach Targeting an Enhanced Protein Synthesis Pathway in MYC-driven (Group 3) Medulloblastoma. *Mol. Cancer Ther.* **2020**, *19*, 1351–1362. [CrossRef] [PubMed]
782. Buonamici, S.; Williams, J.; Morrissey, M.; Wang, A.; Guo, R.; Vattay, A.; Hsiao, K.; Yuan, J.; Green, J.; Ospina, B.; et al. Interfering with Resistance to Smoothed Antagonists by Inhibition of the PI3K Pathway in Medulloblastoma. *Sci. Transl. Med.* **2010**, *2*, 51ra70. [CrossRef]
783. Garlich, J.R.; De, P.; Dey, N.; Su, J.D.; Peng, X.; Miller, A.; Murali, R.; Lu, Y.; Mills, G.B.; Kundra, V.; et al. A Vascular Targeted Pan Phosphoinositide 3-Kinase Inhibitor Prodrug, SF1126, with Antitumor and Antiangiogenic Activity. *Cancer Res* **2008**, *68*, 206–215. [CrossRef]
784. Mahadevan, D.; Chiorean, E.; Harris, W.; Von Hoff, D.; Stejskal-Barnett, A.; Qi, W.; Anthony, S.; Younger, A.; Rensvold, D.; Cordova, F.; et al. Phase I pharmacokinetic and pharmacodynamic study of the pan-PI3K/mTORC vascular targeted pro-drug SF1126 in patients with advanced solid tumours and B-cell malignancies. *Eur. J. Cancer* **2012**, *48*, 3319–3327. [CrossRef]
785. Singh, A.R.; Joshi, S.; Zulcic, M.; Alcaraz, M.; Garlich, J.R.; Morales, G.A.; Cho, Y.J.; Bao, L.; Levy, M.L.; Newbury, R.; et al. PI-3K Inhibitors Preferentially Target CD15+ Cancer Stem Cell Population in SHH Driven Medulloblastoma. *PLoS ONE* **2016**, *11*, e0150836. [CrossRef]
786. Goldin, A.N.; Singh, A.; Joshi, S.; Jamieson, C.; Durden, D.L.M. Augmented Antitumor Activity for Novel Dual PI3K/BDR4 Inhibitors, SF2523 and SF1126 in Ewing Sarcoma. *J. Pediatr. Hematol.* **2021**, *43*, e304–e311. [CrossRef]
787. Peirce, S.; Durden, D.; Garlich, J.; Findley, H. SF1126, a novel pan-PI3K inhibitor, inhibits activation of Mdm2 and in-crases sensitivity to doxorubicin in wild type p53 neuroblastoma cell lines. *Cancer Res.* **2007**, *67*, LB-294.
788. Erdreich-Epstein, A.; Singh, A.R.; Joshi, S.; Vega, F.M.; Guo, P.; Xu, J.; Groshen, S.; Ye, W.; Millard, M.; Campan, M.; et al. Association of high microvessel  $\alpha\beta 3$  and low PTEN with poor outcome in stage 3 neuroblastoma: Rationale for using first in class dual PI3K/BRD4 inhibitor, SF1126. *Oncotarget* **2016**, *8*, 52193–52210. [CrossRef]
789. Beljanski, V. Triciribine. In *xPharm: The Comprehensive Pharmacology Reference*; Elsevier: Amsterdam, The Netherlands, 2009; pp. 1–5. [CrossRef]



790. Bahmad, H.F.; Mouhieddine, T.H.; Chalhoub, R.M.; Assi, S.; Araji, T.; Chamaa, F.; Itani, M.M.; Nokkari, A.; Kobeissy, F.; Daoud, G.; et al. The Akt/mTOR pathway in cancer stem/progenitor cells is a potential therapeutic target for glioblastoma and neuroblastoma. *Oncotarget* **2018**, *9*, 33549–33561. [CrossRef]
791. Cubitt, C.L.; Menth, J.; Dawson, J.; Martinez, G.V.; Foroutan, P.; Morse, D.L.; Bui, M.M.; Letson, G.D.; Sullivan, D.M.; Reed, D.R. Rapid Screening of Novel Agents for Combination Therapy in Sarcomas. *Sarcoma* **2013**, *2013*, 1–12. [CrossRef]
792. Smeester, B.A.; Draper, G.M.; Slipek, N.J.; Larsson, A.T.; Stratton, N.; Pomeroy, E.J.; Becklin, K.L.; Yamamoto, K.; Williams, K.B.; Laoharawee, K.; et al. Implication of ZNF217 in Accelerating Tumor Development and Therapeutically Targeting ZNF217-Induced PI3K–AKT Signaling for the Treatment of Metastatic Osteosarcoma. *Mol. Cancer Ther.* **2020**, *19*, 2528–2541. [CrossRef]
793. Voss, M.H.; Gordon, M.S.; Mita, M.; Rini, B.; Makker, V.; Macarulla, T.; Smith, D.C.; Cervantes, A.; Puzanov, I.; Pili, R.; et al. Phase 1 study of mTORC1/2 inhibitor sapanisertib (TAK-228) in advanced solid tumours, with an expansion phase in renal, endometrial or bladder cancer. *Br. J. Cancer* **2020**, *123*, 1590–1598. [CrossRef]
794. Slotkin, E.K.; Patwardhan, P.P.; Vasudeva, S.D.; de Stanchina, E.; Tap, W.D.; Schwartz, G.K. MLN0128, an ATP-Competitive mTOR Kinase Inhibitor with Potent In Vitro and In Vivo Antitumor Activity, as Potential Therapy for Bone and Soft-Tissue Sarcoma. *Mol. Cancer Ther.* **2015**, *14*, 395–406. [CrossRef]
795. Jiang, H.; Zeng, Z. Dual mTORC1/2 inhibition by INK-128 results in antitumor activity in preclinical models of osteosarcoma. *Biochem. Biophys. Res. Commun.* **2015**, *468*, 255–261. [CrossRef]
796. Maynard, R.E.; Poore, B.; Hanaford, A.R.; Pham, K.; James, M.; Alt, J.; Park, Y.; Slusher, B.S.; Tamayo, P.; Mesirov, J.; et al. TORC1/2 kinase inhibition depletes glutathione and synergizes with carboplatin to suppress the growth of MYC-driven medulloblastoma. *Cancer Lett.* **2021**, *504*, 137–145. [CrossRef]
797. Zhang, H.; Dou, J.; Yu, Y.; Zhao, Y.; Fan, Y.; Cheng, J.; Xu, X.; Liu, W.; Guan, S.; Chen, Z.; et al. mTOR ATP-competitive inhibitor INK128 inhibits neuroblastoma growth via blocking mTORC signaling. *Apoptosis* **2014**, *20*, 50–62. [CrossRef]
798. Miyahara, H.; Yadavilli, S.; Natsumeda, M.; Rubens, J.A.; Rodgers, L.; Kambhampati, M.; Taylor, I.C.; Kaur, H.; Asnaghi, L.; Eberhart, C.G.; et al. The dual mTOR kinase inhibitor TAK228 inhibits tumorigenicity and enhances radiosensitization in diffuse intrinsic pontine glioma. *Cancer Lett.* **2017**, *400*, 110–116. [CrossRef]
799. Arnold, A.; Yuan, M.; Price, A.; Harris, L.; Eberhart, C.G.; Raabe, E.H. Synergistic activity of mTORC1/2 kinase and MEK inhibitors suppresses pediatric low-grade glioma tumorigenicity and vascularity. *Neuro-Oncology* **2019**, *22*, 563–574. [CrossRef]
800. Tang, L.; Fu, Y.; Song, J.; Hu, T.; Li, K.; Li, Z. mTOR inhibition by TAK-228 is effective against growth, survival and angiogenesis in preclinical retinoblastoma models. *Pharmacol. Res. Perspect.* **2022**, *10*, e00930. [CrossRef] [PubMed]
801. Gray, J.E.; Infante, J.R.; Brail, L.H.; Simon, G.R.; Cooksey, J.F.; Jones, S.F.; Farrington, D.L.; Yeo, A.; Jackson, K.A.; Chow, K.H.; et al. A first-in-human phase I dose-escalation, pharmacokinetic, and pharmacodynamic evaluation of intravenous LY2090314, a glycogen synthase kinase 3 inhibitor, administered in combination with pemetrexed and carboplatin. *Investig. New Drugs* **2015**, *33*, 1187–1196. [CrossRef] [PubMed]
802. Kunnimalaiyaan, S.; Schwartz, V.K.; Jackson, I.A.; Gamblin, T.C.; Kunnimalaiyaan, M. Antiproliferative and apoptotic effect of LY2090314, a GSK-3 inhibitor, in neuroblastoma in vitro. *BMC Cancer* **2018**, *18*, 560. [CrossRef]
803. Wei, D.; Zhu, X.; Li, S.; Liu, G.; Wang, Y.; Wang, W.; Zhang, Q.; Jiang, S. Tideglusib suppresses stem-cell-like features and progression of osteosarcoma by inhibiting GSK-3 $\beta$ /NOTCH1 signaling. *Biochem. Biophys. Res. Commun.* **2021**, *554*, 206–213. [CrossRef]
804. Bahmad, H.F.; Chalhoub, R.M.; Harati, H.; Bou-Gharios, J.; Assi, S.; Ballout, F.; Monzer, A.; Msheik, H.; Araji, T.; Elajami, M.K.; et al. Tideglusib attenuates growth of neuroblastoma cancer stem/progenitor cells in vitro and in vivo by specifically targeting GSK-3 $\beta$ . *Pharmacol. Rep.* **2020**, *73*, 211–226. [CrossRef]
805. Mathuram, T.L.; Ravikumar, V.; Reece, L.M.; Karthik, S.; Sasikumar, C.S.; Cherian, K.M. Tideglusib induces apoptosis in human neuroblastoma IMR32 cells, provoking sub-G 0 /G 1 accumulation and ROS generation. *Environ. Toxicol. Pharmacol.* **2016**, *46*, 194–205. [CrossRef]
806. Bharathy, N.; Svalina, M.N.; Settelmeier, T.P.; Cleary, M.M.; Berlow, N.E.; Airhart, S.D.; Xiang, S.; Keck, J.; Hayden, J.B.; Shern, J.F.; et al. Preclinical testing of the glycogen synthase kinase-3 $\beta$  inhibitor tideglusib for rhabdomyosarcoma. *Oncotarget* **2017**, *8*, 62976–62983. [CrossRef]
807. Hirai, H.; Sootome, H.; Nakatsuru, Y.; Miyama, K.; Taguchi, S.; Tsujioka, K.; Ueno, Y.; Hatch, H.; Majumder, P.K.; Pan, B.-S.; et al. MK-2206, an Allosteric Akt Inhibitor, Enhances Antitumor Efficacy by Standard Chemotherapeutic Agents or Molecular Targeted Drugs In vitro and In vivo. *Mol. Cancer Ther.* **2010**, *9*, 1956–1967. [CrossRef]
808. Gorlick, R.; Maris, J.M.; Houghton, P.J.; Lock, R.; Carol, H.; Kurmasheva, R.T.; Kolb, E.A.; Keir, S.T.; Reynolds, C.P.; Kang, M.H.; et al. Testing of the Akt/PKB inhibitor MK-2206 by the pediatric preclinical testing program. *Pediatr. Blood Cancer* **2011**, *59*, 518–524. [CrossRef]
809. Duan, L.; E Perez, R.; Hansen, M.; Gitelis, S.; Maki, C.G. Increasing cisplatin sensitivity by schedule-dependent inhibition of AKT and Chk1. *Cancer Biol. Ther.* **2014**, *15*, 1600–1612. [CrossRef]
810. Santo, E.E.; Stroeken, P.; Sluis, P.V.; Koster, J.; Versteeg, R.; Westerhout, E.M. FOXO3a Is a Major Target of Inactivation by PI3K/AKT Signaling in Aggressive Neuroblastoma. *Cancer Res* **2013**, *73*, 2189–2198. [CrossRef]
811. Qi, L.; Toyoda, H.; Xu, D.-Q.; Zhou, Y.; Sakurai, N.; Amano, K.; Kihira, K.; Hori, H.; Azuma, E.; Komada, Y. PDK1-mTOR signaling pathway inhibitors reduce cell proliferation in MK2206 resistant neuroblastoma cells. *Cancer Cell Int.* **2015**, *15*, 1–14. [CrossRef]

812. Li, Z.; Yan, S.; Attayan, N.; Ramalingam, S.; Thiele, C.J. Combination of an Allosteric Akt Inhibitor MK-2206 with Etoposide or Rapamycin Enhances the Antitumor Growth Effect in Neuroblastoma. *Clin. Cancer Res.* **2012**, *18*, 3603–3615. [CrossRef]
813. Kang, B.W.; Chau, I. Molecular target: Pan-AKT in gastric cancer. *ESMO Open* **2020**, *5*, e000728. [CrossRef]
814. Choo, F.; Odintsov, I.; Nusser, K.; Nicholson, K.S.; Davis, L.; Corless, C.L.; Stork, L.; Somwar, R.; Ladanyi, M.; Davis, J.L.; et al. Functional impact and targetability of *PI3KCA*, *GNAS*, and *PTEN* mutations in a spindle cell rhabdomyosarcoma with MYOD1 L122R mutation. *Mol. Case Stud.* **2022**, *8*, a006140. [CrossRef]
815. Abdelgalil, A.A.; Alkahtani, H.M.; Al-Jenoobi, F.I. Sorafenib. *Profiles Drug Subst. Excip. Relat. Methodol.* **2019**, *44*, 239–266. [CrossRef]
816. Yang, F.; Van Meter, T.E.; Buettner, R.; Hedvat, M.; Liang, W.; Kowolik, C.M.; Mepani, N.; Mirosevich, J.; Nam, S.; Chen, M.Y.; et al. Sorafenib inhibits signal transducer and activator of transcription 3 signaling associated with growth arrest and apoptosis of medulloblastomas. *Mol. Cancer Ther.* **2008**, *7*, 3519–3526. [CrossRef]
817. Chai, H.; Luo, A.Z.; Weerasinghe, P.; E Brown, R. Sorafenib downregulates ERK/Akt and STAT3 survival pathways and induces apoptosis in a human neuroblastoma cell line. *Int. J. Clin. Exp. Pathol.* **2010**, *3*, 408–415.
818. Kakodkar, N.C.; Peddinti, R.R.; Tian, Y.; Guerrero, L.J.; Chlenski, A.; Yang, Q.; Salwen, H.R.; Maitland, M.L.; Cohn, S.L. Sorafenib inhibits neuroblastoma cell proliferation and signaling, blocks angiogenesis, and impairs tumor growth. *Pediatr. Blood Cancer* **2011**, *59*, 642–647. [CrossRef]
819. Karajannis, M.A.; Legault, G.; Fisher, M.J.; Milla, S.S.; Cohen, K.J.; Wisoff, J.H.; Harter, D.H.; Goldberg, J.D.; Hochman, T.; Merkelson, A.; et al. Phase II study of sorafenib in children with recurrent or progressive low-grade astrocytomas. *Neuro-Oncology* **2014**, *16*, 1408–1416. [CrossRef] [PubMed]
820. Albarrán, V.; Villamayor, M.L.; Chamorro, J.; Rosero, D.I.; Pozas, J.; Román, M.S.; Calvo, J.C.; de Aguado, P.P.; Moreno, J.; Guerrero, P.; et al. Receptor Tyrosine Kinase Inhibitors for the Treatment of Recurrent and Unresectable Bone Sarcomas. *Int. J. Mol. Sci.* **2022**, *23*, 13784. [CrossRef] [PubMed]
821. Tian, Z.; Niu, X.; Yao, W. Receptor Tyrosine Kinases in Osteosarcoma Treatment: Which Is the Key Target? *Front. Oncol.* **2020**, *10*, 1642. [CrossRef] [PubMed]
822. Wu, C.-H.; Lin, K.-H.; Fu, B.-S.; Hsu, F.-T.; Tsai, J.-J.; Weng, M.-C.; Pan, P.-J. Sorafenib Induces Apoptosis and Inhibits NF- $\kappa$ B-mediated Anti-apoptotic and Metastatic Potential in Osteosarcoma Cells. *Anticancer. Res.* **2021**, *41*, 1251–1259. [CrossRef]
823. Dumont, S.; Yang, D.; Dumont, A.; Reynoso, D.; Blay, J.-Y.; Trent, J. Targeted polytherapy in small cell sarcoma and its association with doxorubicin. *Mol. Oncol.* **2014**, *8*, 1458–1468. [CrossRef]
824. Higuchi, T.; Igarashi, K.; Yamamoto, N.; Hayashi, K.; Kimura, H.; Miwa, S.; Bouvet, M.; Tsuchiya, H.; Hoffman, R.M. Osteosarcoma Patient-derived Orthotopic Xenograft (PDOX) Models Used to Identify Novel and Effective Therapeutics: A Review. *Anticancer. Res.* **2021**, *41*, 5865–5871. [CrossRef]
825. Chen, Z.; Zhao, Y.; Yu, Y.; Pang, J.C.; Woodfield, S.E.; Tao, L.; Guan, S.; Zhang, H.; Bieerkehazhi, S.; Shi, Y.; et al. Small molecule inhibitor regorafenib inhibits RET signaling in neuroblastoma cells and effectively suppresses tumor growth in vivo. *Oncotarget* **2017**, *8*, 104090–104103. [CrossRef]
826. Harrison, D.J.; Gill, J.D.; Roth, M.E.; Zhang, W.; Teicher, B.; Erickson, S.; Gatto, G.; Kurmasheva, R.T.; Houghton, P.J.; Smith, M.A.; et al. Initial in vivo testing of a multitarget kinase inhibitor, regorafenib, by the Pediatric Preclinical Testing Consortium. *Pediatr. Blood Cancer* **2020**, *67*, e28222. [CrossRef]
827. Jindal, A.; Thadi, A.; Shailubhai, K. Hepatocellular Carcinoma: Etiology and Current and Future Drugs. *J. Clin. Exp. Hepatol.* **2019**, *9*, 221–232. [CrossRef]
828. Aspeslagh, S.; Shailubhai, K.; Bahleda, R.; Gazzah, A.; Varga, A.; Hollebecque, A.; Massard, C.; Spreafico, A.; Reni, M.; Soria, J.-C. Phase I dose-escalation study of miliclib in combination with gemcitabine in patients with refractory solid tumors. *Cancer Chemother. Pharmacol.* **2017**, *79*, 1257–1265. [CrossRef]
829. Bolin, S.; Borgenvik, A.; Persson, C.U.; Sundström, A.; Qi, J.; Bradner, J.E.; Weiss, W.A.; Cho, Y.-J.; Weishaupt, H.; Swartling, F.J. Combined BET bromodomain and CDK2 inhibition in MYC-driven medulloblastoma. *Oncogene* **2018**, *37*, 2850–2862. [CrossRef]
830. Albanese, C.; Alzani, R.; Amboldi, N.; Degrassi, A.; Festuccia, C.; Fiorentini, F.; Gravina, G.L.; Mercurio, C.; Pastori, W.; Brasca, M.; et al. Anti-tumour efficacy on glioma models of PHA-848125, a multi-kinase inhibitor able to cross the blood-brain barrier. *Br. J. Pharmacol.* **2013**, *169*, 156–166. [CrossRef]
831. Martínez-Chávez, A.; Broeders, J.; Lebre, M.C.; Tibben, M.T.; Rosing, H.; Beijnen, J.H.; Schinkel, A.H. The role of drug efflux and uptake transporters ABCB1 (P-gp), ABCG2 (BCRP) and OATP1A/1B and of CYP3A4 in the pharmacokinetics of the CDK inhibitor miliclib. *Eur. J. Pharm. Sci.* **2021**, *159*, 105740. [CrossRef]
832. Smolewski, P. Terameprocol, a novel site-specific transcription inhibitor with anticancer activity. *IDrugs.* **2008**, *11*, 204–214.
833. Castro-Gamero, A.M.; Borges, K.S.; Moreno, D.A.; Suazo, V.K.; Fujinami, M.M.; Queiroz, R.D.P.G.; de Oliveira, H.F.; Carlotti, C.G.; Scrideli, C.; Tone, L.G. Tetra-O-methyl nordihydroguaiaretic acid, an inhibitor of Sp1-mediated survivin transcription, induces apoptosis and acts synergistically with chemo-radiotherapy in glioblastoma cells. *Investig. New Drugs* **2013**, *31*, 858–870. [CrossRef]
834. Akinaga, S.; Sugiyama, K.; Akiyama, T. UCN-01 (7-hydroxystaurosporine) and other indolocarbazole compounds: A new generation of anti-cancer agents for the new century? *Anti-Cancer Drug Des.* **2000**, *15*, 43–52.
835. Shao, R.-G.; Shimizu, T.; Pommier, Y. 7-Hydroxystaurosporine (UCN-01) Induces Apoptosis in Human Colon Carcinoma and Leukemia Cells Independently of p53. *Exp. Cell Res.* **1997**, *234*, 388–397. [CrossRef]

836. Lien, W.C.; Chen, T.Y.; Sheu, S.Y.; Lin, T.C.; Kang, F.C.; Yu, C.H.; Kuan, T.S.; Huang, B.M.; Wang, C.Y. 7-hydroxy-staurosporine, UCN-01, induces DNA damage response, and autophagy in human osteosarcoma U2-OS cells. *J. Cell. Biochem.* **2018**, *119*, 4729–4741. [CrossRef]
837. Shankar, S.L.; Krupski, M.; Parashar, B.; Okwuaka, C.; O'Guin, K.; Mani, S.; Shafit-Zagardo, B. UCN-01 alters phosphorylation of Akt and GSK3beta and induces apoptosis in six independent human neuroblastoma cell lines. *J. Neurochem.* **2004**, *90*, 702–711. [CrossRef]
838. Zhang, J.; Liu, S.; Ye, Q.; Pan, J. Transcriptional inhibition by CDK7/9 inhibitor SNS-032 abrogates oncogene addiction and reduces liver metastasis in uveal melanoma. *Mol. Cancer* **2019**, *18*, 1–17. [CrossRef]
839. Wu, Y.; Chen, C.; Sun, X.; Shi, X.; Jin, B.; Ding, K.; Yeung, S.-C.J.; Pan, J. Cyclin-Dependent Kinase 7/9 Inhibitor SNS-032 Abrogates FIP1-like-1 Platelet-Derived Growth Factor Receptor  $\alpha$  and Bcr-Abl Oncogene Addiction in Malignant Hematologic Cells. *Clin. Cancer Res.* **2012**, *18*, 1966–1978. [CrossRef] [PubMed]
840. Xie, G.; Tang, H.; Wu, S.; Chen, J.; Liu, J.; Liao, C. The cyclin-dependent kinase inhibitor SNS-032 induces apoptosis in breast cancer cells via depletion of Mcl-1 and X-linked inhibitor of apoptosis protein and displays antitumor activity in vivo. *Int. J. Oncol.* **2014**, *45*, 804–812. [CrossRef] [PubMed]
841. Scrae, S.F.; Kierstan, P.; Borgognoni, J.; Denny, S.; Wayne, J.; Bentley, C.; Cansfield, A.D.; Jackson, P.S.; Lockie, A.M.; Curtin, N.J.; et al. Transient treatment with CDK inhibitors eliminates proliferative potential even when their abilities to evoke apoptosis and DNA damage are blocked. *Cell Cycle* **2008**, *7*, 3898–3907. [CrossRef] [PubMed]
842. Löschmann, N.; Michaelis, M.; Rothweiler, F.; Voges, Y.; Balónová, B.; Blight, B.A.; Jr, J.C. ABCB1 as predominant resistance mechanism in cells with acquired SNS-032 resistance. *Oncotarget* **2016**, *7*, 58051–58064. [CrossRef] [PubMed]
843. Löschmann, N.; Michaelis, M.; Rothweiler, F.; Zehner, R.; Cinatl, J.; Voges, Y.; Sharifi, M.; Riecken, K.; Meyer, J.; von Deimling, A.; et al. Testing of SNS-032 in a Panel of Human Neuroblastoma Cell Lines with Acquired Resistance to a Broad Range of Drugs. *Transl. Oncol.* **2013**, *6*, 685–IN18. [CrossRef]
844. Saha, D.; Ali, M.A.; Reis, A.; Ding, L.-H.; Story, M.D.; Habib, A.A.; Chattopadhyay, A. SNS-032 prevents hypoxia-mediated glioblastoma cell invasion by inhibiting hypoxia inducible factor-1 $\alpha$  expression. *Int. J. Oncol.* **2009**, *34*, 1051–1060. [CrossRef]
845. Ali, M.A.; Choy, H.; Habib, A.A.; Saha, D. SNS-032 Prevents Tumor Cell-Induced Angiogenesis By Inhibiting Vascular Endothelial Growth Factor. *Neoplasia* **2007**, *9*, 370–381. [CrossRef]
846. Gaevyí, M.D.; Seif, M.N. Cerebral blood circulation during angiotensin-converting enzyme inhibition. *Fiziol Zh Im I M Sechenova* **1993**, *79*, 74–78.
847. Zhang, M.; Zhang, L.; Hei, R.; Li, X.; Cai, H.; Wu, X.; Zheng, Q.; Cai, C. CDK inhibitors in cancer therapy, an overview of recent development. *Am. J. Cancer Res.* **2021**, *11*, 1913–1935.
848. Aldoss, I.T.; Tashi, T.; Ganti, A.K. Seliciclib in malignancies. *Expert Opin. Investig. Drugs* **2009**, *18*, 1957–1965. [CrossRef]
849. Wu, T.; Qin, Z.; Tian, Y.; Wang, J.; Xu, C.; Li, Z.; Bian, J. Recent Developments in the Biology and Medicinal Chemistry of CDK9 Inhibitors: An Update. *J. Med. Chem.* **2020**, *63*, 13228–13257. [CrossRef]
850. Khalil, H.S.; Mitev, V.; Vlaykova, T.; Cavicchi, L.; Zhelev, N. Discovery and development of Seliciclib. How systems biology approaches can lead to better drug performance. *J. Biotechnol.* **2015**, *202*, 40–49. [CrossRef]
851. Tirado, O.M.; Mateo-Lozano, S.; Notario, V. Roscovitine Is an Effective Inducer of Apoptosis of Ewing's Sarcoma Family Tumor Cells In vitro and In vivo. *Cancer Res* **2005**, *65*, 9320–9327. [CrossRef]
852. Iurisci, I.; Filipski, E.; Reinhardt, J.; Bach, S.; Gianella-Borradori, A.; Iacobelli, S.; Meijer, L.; Lévi, F. Improved Tumor Control through Circadian Clock Induction by Seliciclib, a Cyclin-Dependent Kinase Inhibitor. *Cancer Res* **2006**, *66*, 10720–10728. [CrossRef]
853. Pizarro, J.G.; Folch, J.; Junyent, F.; Verdager, E.; Auladell, C.; Beas-Zarate, C.; Pallàs, M.; Camins, A. Antiapoptotic effects of roscovitine on camptothecin-induced DNA damage in neuroblastoma cells. *Apoptosis* **2011**, *16*, 536–550. [CrossRef]
854. Garrofé-Ochoa, X.; Cosiáls, A.M.; Ribas, J.; Gil, J.; Boix, J. Transcriptional modulation of apoptosis regulators by roscovitine and related compounds. *Apoptosis* **2011**, *16*, 660–670. [CrossRef]
855. Chen, Y.; Tsai, Y.-H.; Tseng, S.-H. Inhibition of cyclin-dependent kinase 1-induced cell death in neuroblastoma cells through the microRNA-34a–MYCN–survivin pathway. *Surgery* **2012**, *153*, 4–16. [CrossRef]
856. Ribas, J.; Boix, J.; Meijer, L. (R)-Roscovitine (CYC202, Seliciclib) sensitizes SH-SY5Y neuroblastoma cells to nutlin-3-induced apoptosis. *Exp. Cell Res.* **2006**, *312*, 2394–2400. [CrossRef]
857. Krüger, K.; Geist, K.; Stuhldreier, F.; Schumacher, L.; Blümel, L.; Remke, M.; Wesselborg, S.; Stork, B.; Klöcker, N.; Bormann, S.; et al. Multiple DNA damage-dependent and DNA damage-independent stress responses define the outcome of ATR/Chk1 targeting in medulloblastoma cells. *Cancer Lett.* **2018**, *430*, 34–46. [CrossRef]
858. Bhatia, B.; Hsieh, M.; Kenney, A.M.; Nahlé, Z. Mitogenic Sonic hedgehog signaling drives E2F1-dependent lipogenesis in progenitor cells and medulloblastoma. *Oncogene* **2010**, *30*, 410–422. [CrossRef]
859. Braal, C.L.; Jongbloed, E.M.; Wilting, S.M.; Mathijssen, R.H.J.; Koolen, S.L.W.; Jager, A. Inhibiting CDK4/6 in Breast Cancer with Palbociclib, Ribociclib, and Abemaciclib: Similarities and Differences. *Drugs* **2020**, *81*, 317–331. [CrossRef] [PubMed]
860. Guenther, L.M.; Dharia, N.V.; Ross, L.; Conway, A.; Robichaud, A.L.; Catlett, J.L., II; Wechsler, C.S.; Frank, E.S.; Goodale, A.; Church, A.J.; et al. A Combination CDK4/6 and IGF1R Inhibitor Strategy for Ewing Sarcoma. *Clin. Cancer Res.* **2019**, *25*, 1343–1357. [CrossRef]

861. Martinez-Monleon, A.; Öberg, H.K.; Gaarder, J.; Berbegall, A.P.; Javanmardi, N.; Djos, A.; Ussowicz, M.; Taschner-Mandl, S.; Ambros, I.M.; Øra, I.; et al. Amplification of CDK4 and MDM2: A detailed study of a high-risk neuroblastoma subgroup. *Sci. Rep.* **2022**, *12*, 1–17. [CrossRef] [PubMed]
862. Guntner, A.S.; Peyrl, A.; Mayr, L.; Englinger, B.; Berger, W.; Slavc, I.; Buchberger, W.; Gojo, J. Cerebrospinal fluid penetration of targeted therapeutics in pediatric brain tumor patients. *Acta Neuropathol. Commun.* **2020**, *8*, 78. [CrossRef] [PubMed]
863. Liang, M.-L.; Hsieh, T.-H.; Liu, Y.-R.; Chen, Y.-W.; Lee, Y.-Y.; Chang, F.-C.; Lin, S.-C.; Huang, M.-C.; Ho, D.M.-T.; Wong, T.-T.; et al. Significance of cyclin D1 overexpression in progression and radio-resistance of pediatric ependymomas. *Oncotarget* **2017**, *9*, 2527–2542. [CrossRef]
864. D’Oto, A.; Fang, J.; Jin, H.; Xu, B.; Singh, S.; Mullasseril, A.; Jones, V.; Abu-Zaid, A.; von Buttlar, X.; Cooke, B.; et al. KDM6B promotes activation of the oncogenic CDK4/6-pRB-E2F pathway by maintaining enhancer activity in MYCN-amplified neuroblastoma. *Nat. Commun.* **2021**, *12*, 7204. [CrossRef]
865. Swadi, R.R.; Sampat, K.; Herrmann, A.; Losty, P.D.; See, V.; Moss, D.J. CDK inhibitors reduce cell proliferation and reverse hypoxia-induced metastasis of neuroblastoma tumours in a chick embryo model. *Sci. Rep.* **2019**, *9*, 9136. [CrossRef]
866. Rihani, A.; Vandesompele, J.; Speleman, F.; Van Maerken, T. Inhibition of CDK4/6 as a novel therapeutic option for neuroblastoma. *Cancer Cell Int.* **2015**, *15*, 76. [CrossRef]
867. Perez, M.; Muñoz-Galván, S.; Jiménez-García, M.P.; Marín, J.J.; Carnero, A. Efficacy of CDK4 inhibition against sarcomas depends on their levels of CDK4 and p16ink4 mRNA. *Oncotarget* **2015**, *6*, 40557–40574. [CrossRef]
868. Böhm, M.J.; Marienfeld, R.; Jäger, D.; Mellert, K.; von Witzleben, A.; Brüderlein, S.; Wittau, M.; von Baer, A.; Schultheiss, M.; Mayer-Steinacker, R.; et al. Analysis of the CDK4/6 Cell Cycle Pathway in Leiomyosarcomas as a Potential Target for Inhibition by Palbociclib. *Sarcoma* **2019**, *2019*, 1–10. [CrossRef]
869. Murakami, T.; Singh, A.S.; Kiyuna, T.; Dry, S.M.; Li, Y.; James, A.W.; Igarashi, K.; Kawaguchi, K.; DeLong, J.C.; Zhang, Y.; et al. Effective molecular targeting of CDK4/6 and IGF-1R in a rare *FUS-ERG* fusion *CDKN2A*-deletion doxorubicin-resistant Ewing’s sarcoma patient-derived orthotopic xenograft (PDOX) nude-mouse model. *Oncotarget* **2016**, *7*, 47556–47564. [CrossRef]
870. Tramontana, T.F.; Marshall, M.S.; Helvie, A.E.; Schmitt, M.R.; Ivanovich, J.; Carter, J.L.; Renbarger, J.L.; Ferguson, M.J. Sustained Complete Response to Palbociclib in a Refractory Pediatric Sarcoma With *BCOR-CCNB3* Fusion and Germline *CDKN2B* Variant. *JCO Precis. Oncol.* **2020**, 466–471. [CrossRef]
871. Riess, C.; Koczan, D.; Schneider, B.; Linke, C.; del Moral, K.; Classen, C.F.; Maletzki, C. Cyclin-dependent kinase inhibitors exert distinct effects on patient-derived 2D and 3D glioblastoma cell culture models. *Cell Death Discov.* **2021**, *7*, 1–15. [CrossRef]
872. Sun, Y.; Sun, Y.; Yan, K.; Li, Z.; Xu, C.; Geng, Y.; Pan, C.; Chen, X.; Zhang, L.; Xi, Q. Potent anti-tumor efficacy of palbociclib in treatment-naïve H3.3K27M-mutant diffuse intrinsic pontine glioma. *Ebiomedicine* **2019**, *43*, 171–179. [CrossRef]
873. Morris-Hanon, O.; Marazita, M.C.; Romorini, L.; Isaja, L.; Fernandez-Espinosa, D.D.; Sevlever, G.E.; Scassa, M.E.; Videla-Richardson, G.A. Palbociclib Effectively Halts Proliferation but Fails to Induce Senescence in Patient-Derived Glioma Stem Cells. *Mol. Neurobiol.* **2019**, *56*, 7810–7821. [CrossRef]
874. Huillard, E.; Hashizume, R.; Phillips, J.J.; Griveau, A.; Ihrle, R.A.; Aoki, Y.; Nicolaidis, T.; Perry, A.; Waldman, T.; McMahon, M.; et al. Cooperative interactions of BRAF<sup>V600E</sup> kinase and *CDKN2A* locus deficiency in pediatric malignant astrocytoma as a basis for rational therapy. *Proc. Natl. Acad. Sci. USA* **2012**, *109*, 8710–8715. [CrossRef]
875. Barton, K.L.; Misuraca, K.; Cordero, F.; Dobrikova, E.; Min, H.D.; Gromeier, M.; Kirsch, D.G.; Becher, O.J. PD-0332991, a CDK4/6 Inhibitor, Significantly Prolongs Survival in a Genetically Engineered Mouse Model of Brainstem Glioma. *PLoS ONE* **2013**, *8*, e77639. [CrossRef]
876. Lallena, M.J.; Boehnke, K.; Torres, R.; Hermoso, A.; Amat, J.; Calsina, B.; De Dios, A.; Buchanan, S.; Du, J.; Beckmann, R.P.; et al. Abstract 3101: In-vitro characterization of Abemaciclib pharmacology in ER+ breast cancer cell lines. *Cancer Res* **2015**, *75*, 3101. [CrossRef]
877. Torres-Guzmán, R.; Calsina, B.; Hermoso, A.; Baquero, C.; Alvarez, B.; Amat, J.; McNulty, A.M.; Gong, X.; Boehnke, K.; Du, J.; et al. Preclinical characterization of abemaciclib in hormone receptor positive breast cancer. *Oncotarget* **2017**, *8*, 69493–69507. [CrossRef]
878. Chong, Q.-Y.; Kok, Z.-H.; Bui, N.-L.; Xiang, X.; Wong, A.L.-A.; Yong, W.-P.; Sethi, G.; Lobie, P.E.; Wang, L.; Goh, B.-C. A unique CDK4/6 inhibitor: Current and future therapeutic strategies of abemaciclib. *Pharmacol. Res.* **2020**, *156*, 104686. [CrossRef]
879. Goetz, M.P.; Toi, M.; Campone, M.; Sohn, J.; Paluch-Shimon, S.; Huober, J.; Park, I.H.; Trédan, O.; Chen, S.-C.; Manso, L.; et al. MONARCH 3: Abemaciclib As Initial Therapy for Advanced Breast Cancer. *J. Clin. Oncol.* **2017**, *35*, 3638–3646. [CrossRef] [PubMed]
880. Dowless, M.S.; Lowery, C.D.; Shackelford, T.J.; Renschler, M.; Stephens, J.R.; Flack, R.; Blosser, W.; Gupta, S.; Stewart, J.; Webster, Y.; et al. Abemaciclib Is Active in Preclinical Models of Ewing Sarcoma via Multipronged Regulation of Cell Cycle, DNA Methylation, and Interferon Pathway Signaling. *Clin. Cancer Res.* **2018**, *24*, 6028–6039. [CrossRef] [PubMed]
881. Wang, D.; Bao, H. Abemaciclib is synergistic with doxorubicin in osteosarcoma pre-clinical models via inhibition of CDK4/6–Cyclin D–Rb pathway. *Cancer Chemother. Pharmacol.* **2021**, *89*, 31–40. [CrossRef] [PubMed]
882. Schubert, N.A.; Schild, L.; van Oirschot, S.; Keller, K.M.; Alles, L.K.; Vernooij, L.; Nulle, M.E.; Dolman, M.E.M.; van den Boogaard, M.L.; Molenaar, J.J. Combined targeting of the p53 and pRb pathway in neuroblastoma does not lead to synergistic responses. *Eur. J. Cancer* **2020**, *142*, 1–9. [CrossRef] [PubMed]
883. Cao, Y.; Li, X.; Kong, S.; Shang, S.; Qi, Y. CDK4/6 inhibition suppresses tumour growth and enhances the effect of temozolomide in glioma cells. *J. Cell. Mol. Med.* **2020**, *24*, 5135–5145. [CrossRef]

884. Mayr, L.; Guntner, A.S.; Madlener, S.; Schmook, M.T.; Peyrl, A.; Azizi, A.A.; Dieckmann, K.; Reisinger, D.; Stepien, N.M.; Schramm, K.; et al. Cerebrospinal Fluid Penetration and Combination Therapy of Entrectinib for Disseminated *ROS1/NTRK*-Fusion Positive Pediatric High-Grade Glioma. *J. Pers. Med.* **2020**, *10*, 290. [CrossRef]
885. Stewart, E.; McEvoy, J.; Wang, H.; Chen, X.; Honnell, V.; Ocarz, M.; Gordon, B.; Dapper, J.; Blankenship, K.; Yang, Y.; et al. Identification of Therapeutic Targets in Rhabdomyosarcoma through Integrated Genomic, Epigenomic, and Proteomic Analyses. *Cancer Cell* **2018**, *34*, 411–426.e19. [CrossRef]
886. Rana, S.; Kour, S.; Sonawane, Y.A.; Robb, C.M.; Contreras, J.I.; Kizhake, S.; Zahid, M.; Karpf, A.R.; Natarajan, A. Symbiotic prodrugs (SymProDs) dual targeting of NFkappaB and CDK. *Chem. Biol. Drug Des.* **2020**, *96*, 773–784. [CrossRef]
887. Squires, M.S.; Feltell, R.E.; Wallis, N.G.; Lewis, E.J.; Smith, D.-M.; Cross, D.M.; Lyons, J.F.; Thompson, N.T. Biological characterization of AT7519, a small-molecule inhibitor of cyclin-dependent kinases, in human tumor cell lines. *Mol. Cancer Ther.* **2009**, *8*, 324–332. [CrossRef]
888. Oghabi, M.; Safaroghli-Azar, A.; Pourbagheri-Sigaroodi, A.; Sayyadi, M.; Hamidpour, M.; Mohammadi, M.H.; Bashash, D. Anti-proliferative effects of a small molecule inhibitor of CDK AT7519 on chronic myeloid leukemia (CML) cells through halting the transition of cells from G2/M phase of the cell cycle. *Biocell* **2020**, *44*, 183–192. [CrossRef]
889. Dolman, M.E.M.; Poon, E.; Ebus, M.E.; Hartog, I.J.D.; van Noesel, C.J.; Jamin, Y.; Hallsworth, A.; Robinson, S.P.; Petrie, K.; Sparidans, R.W.; et al. Cyclin-Dependent Kinase Inhibitor AT7519 as a Potential Drug for MYCN-Dependent Neuroblastoma. *Clin. Cancer Res.* **2015**, *21*, 5100–5109. [CrossRef]
890. Steegmaier, M.; Hoffmann, M.; Baum, A.; Lénárt, P.; Petronczki, M.; Krššák, M.; Gürtler, U.; Garin-Chesa, P.; Lieb, S.; Quant, J.; et al. BI 2536, a Potent and Selective Inhibitor of Polo-like Kinase 1, Inhibits Tumor Growth In Vivo. *Curr. Biol.* **2007**, *17*, 316–322. [CrossRef]
891. Pezuk, J.A.; Brassesco, M.S.; Morales, A.G.; de Oliveira, J.C.; de Oliveira, H.F.; Scrideli, C.A.; Tone, L.G. Inhibition of Polo-Like Kinase 1 Induces Cell Cycle Arrest and Sensitizes Glioblastoma Cells to Ionizing Radiation. *Cancer Biotherapy Radiopharm.* **2013**, *28*, 516–522. [CrossRef]
892. A Pezuk, J.; Brassesco, M.S.; Morales, A.G.; de Oliveira, J.C.; Queiroz, R.G.D.P.; Machado, H.R.; Carlotti, C.G.; Neder, L.; A Scrideli, C.; Tone, L.G. Polo-like kinase 1 inhibition causes decreased proliferation by cell cycle arrest, leading to cell death in glioblastoma. *Cancer Gene Ther.* **2013**, *20*, 499–506. [CrossRef]
893. Pezuk, J.A.; Brassesco, M.S.; Ramos, P.M.M.; Scrideli, C.A.; Tone, L.G.; Pezuk, M.S.B.J.A. Polo-Like Kinase 1 Pharmacological Inhibition as Monotherapy or in Combination: Comparative Effects of Polo-Like Kinase 1 Inhibition in Medulloblastoma Cells. *Anti-Cancer Agents Med. Chem.* **2017**, *17*, 1278–1291. [CrossRef]
894. Yunoki, T.; Tabuchi, Y.; Hayashi, A.; Kondo, T. Inhibition of Polo-Like Kinase 1 Promotes Hyperthermia Sensitivity via Inactivation of Heat Shock Transcription Factor 1 in Human Retinoblastoma Cells. *Investig. Ophthalmology Vis. Sci.* **2013**, *54*, 8353–8363. [CrossRef]
895. Li, Z.; Yang, C.; Li, X.; Du, X.; Tao, Y.; Ren, J.; Fang, F.; Xie, Y.; Li, M.; Qian, G.; et al. The dual role of BI 2536, a small-molecule inhibitor that targets PLK1, in induction of apoptosis and attenuation of autophagy in neuroblastoma cells. *J. Cancer* **2020**, *11*, 3274–3287. [CrossRef]
896. Grinshtein, N.; Datti, A.; Fujitani, M.; Uehling, D.; Prakesch, M.; Isaac, M.; Irwin, M.S.; Wrana, J.L.; Al-Awar, R.; Kaplan, D.R. Small Molecule Kinase Inhibitor Screen Identifies Polo-Like Kinase 1 as a Target for Neuroblastoma Tumor-Initiating Cells. *Cancer Res* **2011**, *71*, 1385–1395. [CrossRef]
897. Hsieh, C.-H.; Yeh, H.-N.; Huang, C.-T.; Wang, W.-H.; Hsu, W.-M.; Huang, H.-C.; Juan, H.-F. BI-2536 Promotes Neuroblastoma Cell Death via Minichromosome Maintenance Complex Components 2 and 10. *Pharmaceutics* **2021**, *15*, 37. [CrossRef]
898. Morales, A.G.; Brassesco, M.S.; Pezuk, J.A.; Oliveira, J.C.; Montaldi, A.P.; Sakamoto-Hojo, E.T.; Scrideli, C.A.; Tone, L.G. BI 2536-mediated PLK1 inhibition suppresses HOS and MG-63 osteosarcoma cell line growth and clonogenicity. *Anti-Cancer Drugs* **2011**, *22*, 995–1001. [CrossRef]
899. Liu, X.; Choy, E.; Harmon, D.; Yang, S.; Yang, C.; Mankin, H.; Hornicek, F.J.; Duan, Z. Inhibition of polo-like kinase 1 leads to the suppression of osteosarcoma cell growth in vitro and in vivo. *Anti-Cancer Drugs* **2011**, *22*, 444–453. [CrossRef] [PubMed]
900. Thalhammer, V.; Lopez-Garcia, L.A.; Herrero-Martin, D.; Hecker, R.; Laubscher, D.; Gierisch, M.E.; Wachtel, M.; Bode, P.; Nanni, P.; Blank, B.; et al. PLK1 Phosphorylates PAX3-FOXO1, the Inhibition of Which Triggers Regression of Alveolar Rhabdomyosarcoma. *Cancer Res* **2015**, *75*, 98–110. [CrossRef] [PubMed]
901. Stehle, A.; Hügler, M.; Fulda, S. Eribulin synergizes with Polo-like kinase 1 inhibitors to induce apoptosis in rhabdomyosarcoma. *Cancer Lett.* **2015**, *365*, 37–46. [CrossRef] [PubMed]
902. Valsasina, B.; Beria, I.; Alli, C.; Alzani, R.; Avanzi, N.; Ballinari, D.; Cappella, P.; Caruso, M.; Casolaro, A.; Ciavolella, A.; et al. NMS-P937, an Orally Available, Specific Small-Molecule Polo-like Kinase 1 Inhibitor with Antitumor Activity in Solid and Hematologic Malignancies. *Mol. Cancer Ther.* **2012**, *11*, 1006–1016. [CrossRef]
903. Sero, V.; Tavanti, E.; Vella, S.; Hattinger, C.M.; Fanelli, M.; Michelacci, F.; Versteeg, R.; Valsasina, B.; Gudeman, B.; Picci, P.; et al. Targeting polo-like kinase 1 by NMS-P937 in osteosarcoma cell lines inhibits tumor cell growth and partially overcomes drug resistance. *Investig. New Drugs* **2014**, *32*, 1167–1180. [CrossRef]
904. Wang, D.; Veo, B.; Pierce, A.; Fosmire, S.; Madhavan, K.; Balakrishnan, I.; Donson, A.; Alimova, I.; Sullivan, K.D.; Joshi, M.; et al. A novel PLK1 inhibitor onvansertib effectively sensitizes MYC-driven medulloblastoma to radiotherapy. *Neuro-Oncology* **2021**, *24*, 414–426. [CrossRef]

905. Wu, C.-P.; Hsiao, S.-H.; Luo, S.-Y.; Tuo, W.-C.; Su, C.-Y.; Li, Y.-Q.; Huang, Y.-H.; Hsieh, C.-H. Overexpression of Human ABCB1 in Cancer Cells Leads to Reduced Activity of GSK461364, a Specific Inhibitor of Polo-like Kinase 1. *Mol. Pharm.* **2014**, *11*, 3727–3736. [CrossRef]
906. Pajtlér, K.W.; Sadowski, N.; Ackermann, S.; Althoff, K.; Schönbeck, K.; Batzke, K.; Schäfers, S.; Odersky, A.; Heukamp, L.; Astrahantseff, K.; et al. The GSK461364 PLK1 inhibitor exhibits strong antitumoral activity in preclinical neuroblastoma models. *Oncotarget* **2016**, *8*, 6730–6741. [CrossRef]
907. Chou, Y.-S.; Yen, C.-C.; Chen, W.-M.; Lin, Y.-C.; Wen, Y.-S.; Ke, W.-T.; Wang, J.-Y.; Liu, C.-Y.; Yang, M.-H.; Chen, T.-H.; et al. Cytotoxic mechanism of PLK1 inhibitor GSK461364 against osteosarcoma: Mitotic arrest, apoptosis, cellular senescence, and synergistic effect with paclitaxel. *Int. J. Oncol.* **2016**, *48*, 1187–1194. [CrossRef]
908. Bogado, R.F.; Pezuk, J.A.; de Oliveira, H.F.; Tone, L.G.; Brassesco, M.S. BI 6727 and GSK461364 suppress growth and radiosensitize osteosarcoma cells, but show limited cytotoxic effects when combined with conventional treatments. *Anti-Cancer Drugs* **2015**, *26*, 56–63. [CrossRef]
909. Gorlick, R.; Kolb, E.A.; Keir, S.T.; Maris, J.M.; Reynolds, C.P.; Kang, M.H.; Carol, H.; Lock, R.; Billups, C.A.; Kurmasheva, R.T.; et al. Initial testing (stage 1) of the polo-like kinase inhibitor volasertib (BI 6727), by the Pediatric Preclinical Testing Program. *Pediatr. Blood Cancer* **2013**, *61*, 158–164. [CrossRef]
910. Carol, H.; Boehm, I.; Reynolds, C.P.; Kang, M.H.; Maris, J.M.; Morton, C.L.; Gorlick, R.; Kolb, E.A.; Keir, S.T.; Wu, J.; et al. Efficacy and pharmacokinetic/pharmacodynamic evaluation of the Aurora kinase A inhibitor MLN8237 against preclinical models of pediatric cancer. *Cancer Chemother. Pharmacol.* **2011**, *68*, 1291–1304. [CrossRef]
911. Maris, J.M.; Bs, C.L.M.; Gorlick, R.; Kolb, E.A.; Lock, R.; Carol, H.; Keir, S.T.; Reynolds, C.P.; Kang, M.H.; Wu, J.; et al. Initial testing of the aurora kinase a inhibitor MLN8237 by the Pediatric Preclinical Testing Program (PPTP). *Pediatr. Blood Cancer* **2010**, *55*, 26–34. [CrossRef]
912. Boi, D.; Souvalidou, F.; Capelli, D.; Polverino, F.; Marini, G.; Montanari, R.; Pochetti, G.; Tramonti, A.; Contestabile, R.; Trisciuglio, D.; et al. PHA-680626 Is an Effective Inhibitor of the Interaction between Aurora-A and N-Myc. *Int. J. Mol. Sci.* **2021**, *22*, 13122. [CrossRef]
913. Brockmann, M.; Poon, E.; Berry, T.; Carstensen, A.; Deubzer, H.E.; Rycak, L.; Jamin, Y.; Thway, K.; Robinson, S.P.; Roels, F.; et al. Small Molecule Inhibitors of Aurora-A Induce Proteasomal Degradation of N-Myc in Childhood Neuroblastoma. *Cancer Cell* **2013**, *24*, 75–89. [CrossRef]
914. Geron, L.; Borges, K.S.; Andrade, A.F.; Suazo, V.K.; Scrideli, C.A.; Tone, L.G. Antitumour activity of AMG 900 alone or in combination with histone deacetylase inhibitor SaHa on medulloblastoma cell lines. *Neurol. Res.* **2015**, *37*, 703–711. [CrossRef]
915. Hanahan, D. Hallmarks of Cancer: New Dimensions. *Cancer Discov.* **2022**, *12*, 31–46. [CrossRef]
916. Grignani, G.; Palmerini, E.; Ferraresi, V.; D’Ambrosio, L.; Bertulli, R.; Asaftei, S.D.; Tamburini, A.; Pignochino, Y.; Sangiolo, D.; Marchesi, E.; et al. Sorafenib and everolimus for patients with unresectable high-grade osteosarcoma progressing after standard treatment: A non-randomised phase 2 clinical trial. *Lancet Oncol.* **2015**, *16*, 98–107. [CrossRef]
917. Liu, Y.; Li, Y.; Wang, Y.; Lin, C.; Zhang, D.; Chen, J.; Ouyang, L.; Wu, F.; Zhang, J.; Chen, L. Recent progress on vascular endothelial growth factor receptor inhibitors with dual targeting capabilities for tumor therapy. *J. Hematol. Oncol.* **2022**, *15*, 1–28. [CrossRef]
918. Chambers, A.; Kundranda, M.; Rao, S.; Niu, J. Anti-angiogenesis Revisited: Combination with Immunotherapy in Solid Tumors. *Lung Cancer* **1912**, *23*, 100. [CrossRef]
919. Inaba, H.; Rubnitz, J.E.; Coustan-Smith, E.; Li, L.; Furmanski, B.D.; Mascara, G.P.; Heym, K.M.; Christensen, R.; Onciu, M.; Shurtleff, S.A.; et al. Phase I Pharmacokinetic and Pharmacodynamic Study of the Multikinase Inhibitor Sorafenib in Combination With Clofarabine and Cytarabine in Pediatric Relapsed/Refractory Leukemia. *J. Clin. Oncol.* **2011**, *29*, 3293–3300. [CrossRef] [PubMed]
920. Grignani, G.; Palmerini, E.; Dileo, P.; Asaftei, S.D.; D’Ambrosio, L.; Pignochino, Y.; Mercuri, M.; Picci, P.; Fagioli, F.; Casali, P.G.; et al. A phase II trial of sorafenib in relapsed and unresectable high-grade osteosarcoma after failure of standard multimodal therapy: An Italian Sarcoma Group study. *Ann. Oncol.* **2011**, *23*, 508–516. [CrossRef] [PubMed]
921. Keino, D.; Yokosuka, T.; Hirose, A.; Sakurai, Y.; Nakamura, W.; Fujita, S.; Hayashi, A.; Miyagawa, N.; Iwasaki, F.; Hamanoue, S.; et al. Pilot study of the combination of sorafenib and fractionated irinotecan in pediatric relapse/refractory hepatic cancer (FINEX pilot study). *Pediatr. Blood Cancer* **2020**, *67*, e28655. [CrossRef] [PubMed]
922. Geller, J.I.; Fox, E.; Turpin, B.K.; Goldstein, S.L.; Liu, X.; Minard, C.G.; Kudgus, R.A.; Reid, J.M.; Berg, S.L.; Weigel, B.J. A study of axitinib, a VEGF receptor tyrosine kinase inhibitor, in children and adolescents with recurrent or refractory solid tumors: A Children’s Oncology Group phase 1 and pilot consortium trial (ADVL1315). *Cancer* **2018**, *124*, 4548–4555. [CrossRef] [PubMed]
923. Daw, N.C.; Furman, W.L.; Stewart, C.F.; Iacono, L.C.; Krailo, M.; Bernstein, M.L.; Dancey, J.E.; Speights, R.A.; Blaney, S.M.; Croop, J.M.; et al. Phase I and Pharmacokinetic Study of Gefitinib in Children With Refractory Solid Tumors: A Children’s Oncology Group Study. *J. Clin. Oncol.* **2005**, *23*, 6172–6180. [CrossRef]
924. Pollack, I.F.; Stewart, C.F.; Kocak, M.; Poussaint, T.Y.; Broniscer, A.; Banerjee, A.; Douglas, J.G.; Kun, L.E.; Boyett, J.M.; Geyer, J.R. A phase II study of gefitinib and irradiation in children with newly diagnosed brainstem gliomas: A report from the Pediatric Brain Tumor Consortium. *Neuro-Oncology* **2011**, *13*, 290–297. [CrossRef]
925. Subbiah, V.; Wolf, J.; Konda, B.; Kang, H.; Spira, A.; Weiss, J.; Takeda, M.; Ohe, Y.; Khan, S.; Ohashi, K.; et al. Tumour-agnostic efficacy and safety of selpercatinib in patients with RET fusion-positive solid tumours other than lung or thyroid tumours (LIBRETTO-001): A phase 1/2, open-label, basket trial. *Lancet Oncol.* **2022**, *23*, 1261–1273. [CrossRef]

926. Del Rivero, J.; Edgerly, M.; Ward, J.; Madan, R.A.; Balasubramaniam, S.; Fojo, T.; Gramza, A.W. Phase I/II Trial of Vandetanib and Bortezomib in Adults with Locally Advanced or Metastatic Medullary Thyroid Cancer. *Oncol.* **2018**, *24*, 16–e14. [CrossRef]
927. Subbiah, V.; Wolf, J.; Konda, B.; Kang, H.; Spira, A.I.; Weiss, J.; Takeda, M.; Ohe, Y.; Khan, S.A.; Ohashi, K.; et al. Tumor agnostic efficacy of selpercatinib in patients with *RET* fusion+ solid tumors: A global, multicenter, registrational trial update (LIBRETTO-001). *J. Clin. Oncol.* **2022**, *40*, 3094. [CrossRef]
928. Subbiah, V.; Cassier, P.A.; Siena, S.; Garralda, E.; Paz-Ares, L.; Garrido, P.; Nadal, E.; Vuky, J.; Lopes, G.; Kalemkerian, G.P.; et al. Pan-cancer efficacy of pralsetinib in patients with *RET* fusion-positive solid tumors from the phase 1/2 ARROW trial. *Nat. Med.* **2022**, *28*, 1640–1645. [CrossRef]
929. Mossé, Y.P.; Lim, M.S.; Voss, S.D.; Wilner, K.; Ruffner, K.; Laliberte, J.; Rolland, D.; Balis, F.M.; Maris, J.M.; Weigel, B.J.; et al. Safety and activity of crizotinib for paediatric patients with refractory solid tumours or anaplastic large-cell lymphoma: A Children's Oncology Group phase 1 consortium study. *Lancet Oncol.* **2013**, *14*, 472–480. [CrossRef]
930. Fukano, R.; Mori, T.; Sekimizu, M.; Choi, I.; Kada, A.; Saito, A.M.; Asada, R.; Takeuchi, K.; Terauchi, T.; Tateishi, U.; et al. Alectinib for relapsed or refractory anaplastic lymphoma kinase-positive anaplastic large cell lymphoma: An open-label phase II trial. *Cancer Sci.* **2020**, *111*, 4540–4547. [CrossRef]
931. Franz, D.N.; Belousova, E.; Sparagana, S.; Bebin, E.M.; Frost, M.; Kuperman, R.; Witt, O.; Kohrman, M.H.; Flamini, J.R.; Wu, J.Y.; et al. Efficacy and safety of everolimus for subependymal giant cell astrocytomas associated with tuberous sclerosis complex (EXIST-1): A multicentre, randomised, placebo-controlled phase 3 trial. *Lancet* **2013**, *381*, 125–132. [CrossRef]
932. Adashek, J.J.; Menta, A.K.; Reddy, N.K.; Desai, A.P.; Roszik, J.; Subbiah, V. Tissue-Agnostic Activity of BRAF plus MEK Inhibitor in BRAF V600-Mutant Tumors. *Mol. Cancer Ther.* **2022**, *21*, 871–878. [CrossRef]
933. Bouffet, E.; Hansford, J.; Garré, M.L.; Hara, J.; Plant-Fox, A.; Aerts, I.; Locatelli, F.; Van der Lugt, J.; Papusha, L.; Sahm, F.; et al. Primary analysis of a phase II trial of dabrafenib plus trametinib (dab + tram) in *BRAF* V600-mutant pediatric low-grade glioma (pLGG). *J. Clin. Oncol.* **2022**, *40*, LBA2002. [CrossRef]
934. Hargrave, D.R.; Bouffet, E.; Tabori, U.; Broniscer, A.; Cohen, K.J.; Hansford, J.R.; Geoerger, B.; Hingorani, P.; Dunkel, I.J.; Russo, M.W.; et al. Efficacy and Safety of Dabrafenib in Pediatric Patients with *BRAF* V600 Mutation-Positive Relapsed or Refractory Low-Grade Glioma: Results from a Phase I/IIa Study. *Clin. Cancer Res.* **2019**, *25*, 7303–7311. [CrossRef]
935. Lau, N.; Feldkamp, M.M.; Roncari, L.; Loehr, A.H.; Shannon, P.; Gutmann, D.H.; Guha, A. Loss of Neurofibromin Is Associated with Activation of RAS/MAPK and PI3-K/AKT Signaling in a Neurofibromatosis 1 Astrocytoma. *J. Neuropathol. Exp. Neurol.* **2000**, *59*, 759–767. [CrossRef]
936. Gross, A.M.; Wolters, P.L.; Dombi, E.; Baldwin, A.; Whitcomb, P.; Fisher, M.J.; Weiss, B.; Kim, A.; Bornhorst, M.; Shah, A.C.; et al. Selumetinib in Children with Inoperable Plexiform Neurofibromas. *N. Engl. J. Med.* **2020**, *382*, 1430–1442. [CrossRef]
937. Bautista, F.; Paoletti, X.; Rubino, J.; Brard, C.; Rezai, K.; Nebchi, S.; Andre, N.; Aerts, I.; De Carli, E.; van Eijkelenburg, N.; et al. Phase I or II Study of Ribociclib in Combination With Topotecan-Temozolomide or Everolimus in Children With Advanced Malignancies: Arms A and B of the AcSé-ESMART Trial. *J. Clin. Oncol.* **2021**, *39*, 3546–3560. [CrossRef]
938. Yang, Y.; Li, S.; Wang, Y.; Zhao, Y.; Li, Q. Protein tyrosine kinase inhibitor resistance in malignant tumors: Molecular mechanisms and future perspective. *Signal Transduct. Target. Ther.* **2022**, *7*, 1–36. [CrossRef]
939. Van Mater, D.; Gururangan, S.; Becher, O.; Campagne, O.; Leary, S.; Phillips, J.J.; Huang, J.; Lin, T.; Poussaint, T.Y.; Goldman, S.; et al. A phase I trial of the CDK 4/6 inhibitor palbociclib in pediatric patients with progressive brain tumors: A Pediatric Brain Tumor Consortium study (PBTC-042). *Pediatr. Blood Cancer* **2021**, *68*, e28879. [CrossRef] [PubMed]
940. Mossé, Y.P.; Lipsitz, E.; Fox, E.; Teachey, D.T.; Maris, J.M.; Weigel, B.; Adamson, P.C.; Ingle, M.A.; Ahern, C.H.; Blaney, S.M. Pediatric Phase I Trial and Pharmacokinetic Study of MLN8237, an Investigational Oral Selective Small-Molecule Inhibitor of Aurora Kinase A: A Children's Oncology Group Phase I Consortium Study. *Clin. Cancer Res.* **2012**, *18*, 6058–6064. [CrossRef] [PubMed]
941. Moreno, L.; Marshall, L.V.; Pearson, A.D.; Morland, B.; Elliott, M.; Campbell-Hewson, Q.; Makin, G.; Halford, S.E.; Acton, G.; Ross, P.; et al. A Phase I Trial of AT9283 (a Selective Inhibitor of Aurora Kinases) in Children and Adolescents with Solid Tumors: A Cancer Research UK Study. *Clin. Cancer Res.* **2015**, *21*, 267–273. [CrossRef] [PubMed]
942. Mossé, Y.P.; Fox, E.; Teachey, D.T.; Reid, J.M.; Safgren, S.L.; Carol, H.; Lock, R.B.; Houghton, P.J.; Smith, M.A.; Hall, D.; et al. A Phase II Study of Alisertib in Children with Recurrent/Refractory Solid Tumors or Leukemia: Children's Oncology Group Phase I and Pilot Consortium (ADV0921). *Clin. Cancer Res.* **2019**, *25*, 3229–3238. [CrossRef] [PubMed]
943. Feliciano, S.V.M.; Santos, M.D.O.; Pombo-De-Oliveira, M.S. Incidência e Mortalidade por Câncer entre Crianças e Adolescentes: Uma Revisão Narrativa. *Rev. Bras. Cancerol.* **2019**, *64*, 389–396. [CrossRef]
944. Verhaak, R.G.W.; Hoadley, K.A.; Purdom, E.; Wang, V.; Wilkerson, M.D.; Miller, C.R.; Ding, L.; Golub, T.; Jill, P.; Alexe, G.; et al. Integrated Genomic Analysis Identifies Clinically Relevant Subtypes of Glioblastoma Characterized by Abnormalities in PDGFRA, IDH1, EGFR, and NF1. *Cancer Cell* **2010**, *17*, 98–110. [CrossRef]
945. Maximiano, S.; Magalhães, P.; Guerreiro, M.P.; Morgado, M. Trastuzumab in the Treatment of Breast Cancer. *Biodrugs* **2016**, *30*, 75–86. [CrossRef]
946. Lee, J.; Park, Y.H. Trastuzumab deruxtecan for HER2+ advanced breast cancer. *Futur. Oncol.* **2022**, *18*, 7–19. [CrossRef]
947. Hochhaus, A.; Baccarani, M.; Silver, R.T.; Schiffer, C.; Apperley, J.F.; Cervantes, F.; Clark, R.E.; Cortes, J.E.; Deininger, M.W.; Guilhot, F.; et al. European LeukemiaNet 2020 recommendations for treating chronic myeloid leukemia. *Leukemia* **2020**, *34*, 966–984. [CrossRef]

948. Louis, D.N.; Perry, A.; Wesseling, P.; Brat, D.J.; Cree, I.A.; Figarella-Branger, D.; Hawkins, C.; Ng, H.K.; Pfister, S.M.; Reifenberger, G.; et al. The 2021 WHO Classification of Tumors of the Central Nervous System: A summary. *Neuro-Oncology* **2021**, *23*, 1231–1251. [CrossRef]
949. Nørøxe, D.S.; Poulsen, H.S.; Lassen, U. Hallmarks of glioblastoma: A systematic review. *ESMO Open* **2016**, *1*, e000144. [CrossRef]
950. Roskoski, R., Jr. Properties of FDA-approved small molecule protein kinase inhibitors: A 2020 update. *Pharmacol. Res.* **2020**, *152*, 104609. [CrossRef]
951. Roskoski, R., Jr. Classification of small molecule protein kinase inhibitors based upon the structures of their drug-enzyme complexes. *Pharmacol. Res.* **2016**, *103*, 26–48. [CrossRef]
952. Wu, P.; Nielsen, T.E.; Clausen, M.H. FDA-approved small-molecule kinase inhibitors. *Trends Pharmacol. Sci.* **2015**, *36*, 422–439. [CrossRef]
953. Lopes, L.F.; Bacchi, C.E. Imatinib treatment for gastrointestinal stromal tumour (GIST). *J. Cell. Mol. Med.* **2009**, *14*, 42–50. [CrossRef]
954. Fischer, P.M. The Design of Drug Candidate Molecules as Selective Inhibitors of Therapeutically Relevant Protein Kinases. *Curr. Med. Chem.* **2004**, *11*, 1563–1583. [CrossRef]
955. A Bogoyevitch, M.; Fairlie, D. A new paradigm for protein kinase inhibition: Blocking phosphorylation without directly targeting ATP binding. *Drug Discov. Today* **2007**, *12*, 622–633. [CrossRef]
956. Gaumann, A.K.; Kiefer, F.; Alfer, J.; Lang, S.A.; Geissler, E.K.; Breier, G. Receptor tyrosine kinase inhibitors: Are they real tumor killers? *Int. J. Cancer* **2015**, *138*, 540–554. [CrossRef]
957. Roberti, M.; Bottegoni, G. Non-ATP Competitive Protein Kinase Inhibitors. *Curr. Med. Chem.* **2010**, *17*, 2804–2821. [CrossRef]
958. Suttorp, M.; Bornhäuser, M.; Metzler, M.; Millot, F.; Schleyer, E. Pharmacology and pharmacokinetics of imatinib in pediatric patients. *Expert Rev. Clin. Pharmacol.* **2017**, *11*, 219–231. [CrossRef]
959. Angel, M.C.-G.; Julia, A.P.; María, S.B.; Luiz, G.T. G2/M inhibitors as pharmacotherapeutic opportunities for glioblastoma: The old, the new, and the future. *Cancer Biol. Med.* **2018**, *15*, 354–374. [CrossRef] [PubMed]
960. Kwak, E.L.; Bang, Y.-J.; Camidge, D.R.; Shaw, A.T.; Solomon, B.; Maki, R.G.; Ou, S.-H.I.; Dezube, B.J.; Jänne, P.A.; Costa, D.B.; et al. Anaplastic Lymphoma Kinase Inhibition in Non-Small-Cell Lung Cancer. *N. Engl. J. Med.* **2010**, *363*, 1693–1703. [CrossRef] [PubMed]
961. De Brouwer, S.; De Preter, K.; Kumps, C.; Zabrocki, P.; Porcu, M.; Westerhout, E.M.; Lakeman, A.; Vandesompele, J.; Hoebeek, J.; Van Maerken, T.; et al. Meta-analysis of Neuroblastomas Reveals a Skewed *ALK* Mutation Spectrum in Tumors with *MYCN* Amplification. *Clin. Cancer Res.* **2010**, *16*, 4353–4362. [CrossRef] [PubMed]
962. Bresler, S.C.; Wood, A.C.; Haglund, E.A.; Courtright, J.; Belcastro, L.T.; Plegaria, J.S.; Cole, K.; Toporovskaya, Y.; Zhao, H.; Carpenter, E.L.; et al. Differential Inhibitor Sensitivity of Anaplastic Lymphoma Kinase Variants Found in Neuroblastoma. *Sci. Transl. Med.* **2011**, *3*, 108ra114. [CrossRef]
963. de Sousa, G.R.; Vieira, G.M.; das Chagas, P.F.; Pezuk, J.A.; Brassesco, M.S. Should we keep rocking? Portraits from targeting Rho kinases in cancer. *Pharmacol. Res.* **2020**, *160*, 105093. [CrossRef]
964. Martinsson, T.; Eriksson, T.; Abrahamsson, J.; Caren, H.; Hansson, M.; Kogner, P.; Kamaraj, S.; Schönherr, C.; Weinmar, J.; Ruuth, K.; et al. Appearance of the Novel Activating F1174S *ALK* Mutation in Neuroblastoma Correlates with Aggressive Tumor Progression and Unresponsiveness to Therapy. *Cancer Res* **2011**, *71*, 98–105. [CrossRef]
965. Braun, T.P.; Eide, C.A.; Druker, B.J. Response and Resistance to BCR-ABL1-Targeted Therapies. *Cancer Cell* **2020**, *37*, 530–542. [CrossRef]
966. Katayama, R. Drug resistance in anaplastic lymphoma kinase-rearranged lung cancer. *Cancer Sci.* **2018**, *109*, 572–580. [CrossRef]
967. Rolfo, C.; Passiglia, F.; Castiglia, M.; E Raez, L.; Germonpre, P.; Gil-Bazo, I.; Zwaenepoel, K.; De Wilde, A.; Bronte, G.; Russo, A.; et al. *ALK* and crizotinib: After the honeymoon . . . what else? Resistance mechanisms and new therapies to overcome it. *Transl. Lung Cancer Res.* **2014**, *3*, 250–261. [CrossRef]
968. Sharma, S.V.; Haber, D.A.; Settleman, J. Cell line-based platforms to evaluate the therapeutic efficacy of candidate anticancer agents. *Nat. Rev. Cancer* **2010**, *10*, 241–253. [CrossRef]
969. Massicotte, M.P.; Sofronas, M.; Deveber, G. Difficulties in performing clinical trials of antithrombotic therapy in neonates and children. *Thromb. Res.* **2006**, *118*, 153–163. [CrossRef]
970. Bond, M.C.; Pritchard, S. Understanding clinical trials in childhood cancer. *Paediatr. Child Health* **2006**, *11*, 148–150. [CrossRef]
971. Renfro, L.A.; Ji, L.; Piao, J.; Onar-Thomas, A.; Kairalla, J.A.; Alonzo, T.A. Trial Design Challenges and Approaches for Precision Oncology in Rare Tumors: Experiences of the Children’s Oncology Group. *JCO Precis. Oncol.* **2019**, *1*, 1–13. [CrossRef]
972. Bavcar, S.; Argyle, D.J. Receptor tyrosine kinase inhibitors: Molecularly targeted drugs for veterinary cancer therapy. *Veter- Comp. Oncol.* **2012**, *10*, 163–173. [CrossRef]

**Disclaimer/Publisher’s Note:** The statements, opinions and data contained in all publications are solely those of the individual author(s) and contributor(s) and not of MDPI and/or the editor(s). MDPI and/or the editor(s) disclaim responsibility for any injury to people or property resulting from any ideas, methods, instructions or products referred to in the content.



## Article

# Biological Evaluation and In Vitro Characterization of ADME Profile of In-House Pyrazolo[3,4-*d*]pyrimidines as Dual Tyrosine Kinase Inhibitors Active against Glioblastoma Multiforme

Federica Poggialini <sup>1</sup>, Chiara Vagaggini <sup>1</sup>, Annalaura Brai <sup>1</sup>, Claudia Pasqualini <sup>1</sup>, Emmanuele Crespan <sup>2</sup>, Giovanni Maga <sup>2</sup>, Cecilia Perini <sup>2</sup>, Noemi Cabella <sup>2</sup>, Lorenzo Botta <sup>3</sup>, Francesca Musumeci <sup>4</sup>, Maria Frosini <sup>5</sup>, Silvia Schenone <sup>4</sup> and Elena Dreassi <sup>1,\*</sup>

<sup>1</sup> Department of Biotechnology, Chemistry and Pharmacy (DBCF), University of Siena, 53100 Siena, Italy

<sup>2</sup> Institute of Molecular Genetics (IGM), CNR “Luigi Luca Cavalli-Sforza”, 27100 Pavia, Italy

<sup>3</sup> Department of Ecological and Biological Sciences, University of Tuscia, Via S.C. De Lellis s.n.c., 01100 Viterbo, Italy

<sup>4</sup> Department of Pharmacy, University of Genoa, 16132 Genoa, Italy

<sup>5</sup> Department of Life Sciences, University of Siena, 53100 Siena, Italy

\* Correspondence: elena.dreassi@unisi.it; Tel.: +39-0577-234321

**Abstract:** The therapeutic use of tyrosine kinase inhibitors (TKIs) represents one of the successful strategies for the treatment of glioblastoma (GBM). Pyrazolo[3,4-*d*]pyrimidines have already been reported as promising small molecules active as c-Src/Abl dual inhibitors. Herein, we present a series of pyrazolo[3,4-*d*]pyrimidine derivatives, selected from our in-house library, to identify a promising candidate active against GBM. The inhibitory activity against c-Src and Abl was investigated, and the antiproliferative profile against four GBM cell lines was studied. For the most active compounds endowed with antiproliferative efficacy in the low-micromolar range, the effects toward nontumoral, healthy cell lines (fibroblasts FIBRO 2-93 and keratinocytes HaCaT) was investigated. Lastly, the *in silico* and *in vitro* ADME properties of all compounds were also assessed. Among the tested compounds, the promising inhibitory activity against c-Src and Abl ( $K_i$  3.14  $\mu$ M and 0.44  $\mu$ M, respectively), the irreversible, apoptotic-mediated death toward U-87, LN18, LN229, and DBTRG GBM cell lines ( $IC_{50}$  6.8  $\mu$ M, 10.8  $\mu$ M, 6.9  $\mu$ M, and 8.5  $\mu$ M, respectively), the significant reduction in GBM cell migration, the safe profile toward FIBRO 2-93 and HaCaT healthy cell lines ( $CC_{50}$  91.7  $\mu$ M and 126.5  $\mu$ M, respectively), the high metabolic stability, and the excellent passive permeability across gastrointestinal and blood–brain barriers led us to select compound 5 for further *in vivo* assays.

**Keywords:** glioblastoma; tyrosine kinase; c-Src/Abl dual inhibitors; pyrazolo[3,4-*d*]pyrimidines; ADME; antiproliferative activity

**Citation:** Poggialini, F.; Vagaggini, C.; Brai, A.; Pasqualini, C.; Crespan, E.; Maga, G.; Perini, C.; Cabella, N.; Botta, L.; Musumeci, F.; et al. Biological Evaluation and In Vitro Characterization of ADME Profile of In-House Pyrazolo[3,4-*d*]pyrimidines as Dual Tyrosine Kinase Inhibitors Active against Glioblastoma Multiforme. *Pharmaceutics* **2023**, *15*, 453. <https://doi.org/10.3390/pharmaceutics15020453>

Academic Editor: Yu-Fen Huang

Received: 28 October 2022

Revised: 19 January 2023

Accepted: 27 January 2023

Published: 30 January 2023



**Copyright:** © 2023 by the authors. Licensee MDPI, Basel, Switzerland. This article is an open access article distributed under the terms and conditions of the Creative Commons Attribution (CC BY) license (<https://creativecommons.org/licenses/by/4.0/>).

## 1. Introduction

According to the World Health Organization (WHO), glioblastoma multiforme (GBM) is classified as the most aggressive form of primary brain cancer (grade IV), associated with poor prognosis, high morbidity, and mortality [1]. Among GBM patients, the median survival time is typically no longer than 1 year from the diagnosis, and <3% of cases have a 5-year survival rate. Responsible for 18% of brain tumors, GBM is one of the most common primary tumors of the central nervous system in adults [2]. Histologically, GBM is typed by high microvasculature and necrotic areas, typical signs of the high proliferation, invasiveness, and angiogenesis of the tumor, demanding nutrients and oxygen for its development. The current standard treatments of GBM are represented by surgical resection, followed by a combination of radiotherapy and chemotherapy; despite these massive and intense

treatments, the prognosis remains inauspicious [3]. Failure in GBM therapy is mostly represented by the lack of drugs able to hit effective molecular targets, overcome the blood–brain barrier, and escape from multidrug resistance mechanisms occurring during the therapy. Therefore, novel and more effective pharmacological approaches are urgently needed to improve the prognosis of GBM patients [4]. Genomic studies highlighted the aberrant activation of receptor tyrosine kinases (RTKs) over different types of cancers, including GBM. A common feature of GBM has been identified by transcriptional analyses in the downregulation of TP53, RB1, and RTKs/Ras/PI3K pathways, recognizing these as fundamental requirements for the pathogenesis of GBM. Moreover, the massive activation of RTKs leads to the downregulation of the downstream signaling cascade resulting in the activation of both ERK and MAPK pathways and non-receptor tyrosine kinases (TKs), such as Src and Abl. Src family kinases regulate cell proliferation, survival, and angiogenesis and play an essential role in cancer progression and diffusion [5]. Additionally, the upregulation of the Abelson (Abl) family members is a trademark of GBM, involved in tumorigenesis, proliferation, and migration [6,7]. Thus, targeted therapy toward activated Src and Abl might represent a favorable strategy to counteract the high proliferation rate and invasion of GBM. In the last few decades, great attention has been paid to the implication of TKs in glioma biology and development of novel small-molecule compounds able to target and inhibit these molecular targets. Although monotherapy with Src inhibitors, such as dasatinib and bosutinib, resulted unsatisfactory for recurrent GBM, TKs remain one of the most promising targets to arrest cancer invasion [4]. In this context, several pyrazolo[3,4-*d*]pyrimidines have been studied and developed by our research group as ATP-competitive TKIs. Several compounds showed potent antitumor activities, inducing apoptosis and downregulating cell proliferation, in several cancer cell lines, including solid tumors such as osteosarcoma [8], neuroblastoma [9], GBM [1,5,10], and mesothelioma [11], as well as hematological tumors such as leukemia and Burkitt lymphoma [12,13]. In vivo data, obtained from xenograft mouse models, supported the antitumor activity of these small molecules against neuroblastoma, leukemia, and GBM [14]. Compound **1** was previously reported by us as a potent c-Src/Abl dual inhibitor with favorable  $K_i$  values and micromolar efficacy against the U-87 GBM cell line [10]. The ADME profile was characterized by suboptimal aqueous solubility and good passive permeability across the gastrointestinal (GI) and blood–brain barrier (BBB) membranes, but metabolic stability was lower than 80%. With the purpose of identifying molecules with the right balance between efficacy against GBM and suitable pharmacokinetic properties, we selected a series of pyrazolo[3,4-*d*]pyrimidines from our internal library. We performed structure–activity relationship (SAR) studies along with biological and ADME evaluations to select a promising molecule active as a TKI against GBM. The compounds were characterized by heterogeneous chemical features at the N1, C4, and C6 positions. First, a cell-free assay was set up to determine the  $K_i$  values against c-Src and Abl, followed by the assessment of the antiproliferative activity against four GBM cell lines (U-87, LN18, LN229, and DBTRG). Furthermore, the cytotoxic profile was established on two nontumoral, healthy cell lines (fibroblasts FIBRO 2-93 and keratinocytes HaCaT) for the most active compounds of the series. Lastly, the in silico and in vitro ADME profile was investigated for all derivatives. On the basis of the biological and ADME studies, compound **5** resulted as the most promising pyrazolo[3,4-*d*]pyrimidine derivative of the panel. Its favorable inhibitory activity against c-Src/Abl, its promising antitumor efficacy against all GBM cell lines tested, and its safe cytotoxic profile led us to select compound **5** for further in vitro assays. Its ability to elicit an irreversible cytotoxic effect, arrest cellular migration, and induce apoptotic-mediated cell death was assessed. Moreover, the high metabolic stability and satisfactory passive permeability across the GI and BBB membranes suggest that compound **5**, with appropriate formulation studies to overcome solubility issues, could represent a strong candidate for future in vivo PK studies.

## 2. Materials and Methods

### 2.1. Drugs and Materials

Compounds herein reported were previously synthesized and reported by us [12,15–19]. The NMR characterizations, chemical names, and structures are presented in the Supplementary Materials (Chemistry chapter and Scheme S1). All reagents, solvents, and materials were purchased from Sigma Aldrich S.r.l. (Milan, Italy) and Carlo Erba Reagents S.r.l. (Milan, Italy). Cell culture mediums, fetal bovine serum (FBS), L-glutamine, and penicillin–streptomycin were purchased from Euroclone S.p.A. (Milan, Italy). Human glioblastoma multiforme cell lines (U-87, LN18, LN229, and DBTRG) and the normal human dermal fibroblast (FIBRO 2-93) cell line were purchased from American Type Culture Collection (ATCC) (Manassas, VA, USA). Human keratinocytes (HaCaT) were kindly donated by Professor Federica Pessina from the Department of Molecular and Developmental Medicine (University of Siena, Italy). All the compounds were dissolved in dimethyl sulfoxide (DMSO) as a 20 mM stock solution immediately before use and diluted to final desired concentration with appropriate cell culture medium (see below).

### 2.2. Enzymatic Assay

Active recombinant kinases and specific peptide substrates were purchased from Promega (Madison, WI, USA). The reactions were carried out in accordance with the manufacturer's instructions, with minor modifications. The experiments were run using all substrates at least twice the concentration of apparent  $K_m$ . Src reactions were carried out with 500  $\mu$ M Src-peptide (KVEKIGEGTYGVVYK), 100  $\mu$ M ATP, and 0.00087% NP-40; Abl reactions were performed with 50  $\mu$ M Abltide (EAI-YAAPFAKKK), 30  $\mu$ M ATP, and 0.00087% NP-40, and T315I reactions were carried out with 100  $\mu$ M Abltide, 60  $\mu$ M ATP, and 0.0013% NP-40. All reactions were run out at 30 °C for 10 min with 10–50 ng of enzyme and 10  $\mu$ L of 10% DMSO. Protein low-binding tubes were used to prevent peptide adsorption onto the plastic surface. To detect kinase activity, the ADP-Glo Kinase Assay (Promega, Madison, WI, USA) was used according to the manufacturer's protocol. Into white 384-well plates, reactions were stopped for 50 min at RT by adding 10  $\mu$ L of ADP-Glo Reagent (Promega, Madison, WI, USA). After 30 min, 20  $\mu$ L of Detection Reagent (Promega, Madison, WI, USA) was added, and the reaction was read using a GloMax Discover microplate reader (Promega, Madison, WI, USA). Data were plotted using GraphPad Prism 5.04 (GraphPad Software Inc., San Diego, CA, USA), and  $ID_{50}$  values were calculated according to Equation (1).

$$v = V/(1 + (I/ID_{50})), \quad (1)$$

where  $v$  represents the measured reaction velocity,  $V$  is the apparent maximal velocity without the inhibitor,  $I$  is the inhibitor concentration, and  $ID_{50}$  is the 50% inhibitory dose. Compounds analyzed were considered to act as ATP-competitive inhibitors. Thus,  $K_i$  values were calculated using Equation (2).

$$K_i = (ID_{50}/(1 + K_{mATP}/[SATP]))/(1 + K_{mpep}/[Spep]), \quad (2)$$

where  $K_i$  represents the affinity of the inhibitor for the enzyme,  $S$  is the ATP concentration, and  $K_m$  is the affinity of ATP calculated according to Michaelis–Menten equation.

### 2.3. Cell Culture, Antiproliferative Effects, and Cytotoxicity on Cell-Based Assays

Cell-based assays were performed using four GBM cell lines, i.e., U-87, LN18, LN229, and DBTRG, cultured in Dulbecco's modified Eagle medium (DMEM) (U-87, LN18, and LN229) or Roswell Park Memorial Institute medium (RPMI 1640) (DBTRG). Both media were implemented with 10% fetal bovine serum (FBS), 2 mM L-glutamine, and 10,000 units/mL penicillin/streptomycin at 37 °C in a 5% CO<sub>2</sub> atmosphere. To evaluate the antiproliferative activity of the compounds reported as  $IC_{50}$  (i.e., drug concentration that caused 50% of cell growth inhibition), cells were seeded at a density of  $1 \times 10^4$  in 96-well plates and, after 24 h of incubation, treated with increasing concentrations of com-

pounds for an additional 72 h. The final concentration of DMSO used never exceeded 0.5% *v/v*, and appropriate controls were always performed in each assay. To assess the potential cytotoxic profile of the three most promising and active compounds toward nontumoral cells, reported as CC<sub>50</sub> (i.e., concentration that reduced the proliferation of cells by 50%), further investigations were conducted using healthy fibroblasts FIBRO 2-93 and keratinocytes HaCaT. These were cultured in DMEM supplemented with 10% FBS, 2 mM L-glutamine, and 10,000 units/mL penicillin/streptomycin at 37 °C in a 5% CO<sub>2</sub> atmosphere. The protocol used to assess the cytotoxic effect on both healthy cell lines was the same described above for the antiproliferative assay. For both the antiproliferative and the cytotoxic assays, 3-(4,5-dimethylthiazol-2-yl)-2,5-diphenyltetrazolium bromide (MTT) was used to assess cell viability as previously described [20]. Briefly, 150 µL of MTT (5 mg/mL in FBS-free culture medium) was added to each well, and the plates incubated for 4 h in a 5% CO<sub>2</sub> atmosphere at 37 °C. Afterward, formazan violet crystals were solubilized in 150 µL of isopropanol, and the absorbance was quantified at 570 nm using a Multiskan SkyHigh Microplate Spectrophotometer (ThermoFisher, Waltham, MA, USA). Cell viability was expressed as a percentage of DMSO-treated cells (controls), taken as 100%. IC<sub>50</sub> and CC<sub>50</sub> values were calculated by fitting data to a nonlinear regression analysis (sigmoidal log concentration vs. normalized response curve; GraphPad Prism 5.04 software, GraphPad Software Inc., San Diego, CA, USA) using at least six points in a concentration range from 0% to 100% of the studied effects (total widest range 0.01–1000 µM). To support MTT data, cytotoxicity assays was always paralleled by a careful observation of cells under a phase-contrast light microscope, as described in USP 28 (United States Pharmacopeia edition 2005) as an alternative method [21–23]. This analysis was performed by an expert operator blind to the treatment, and exemplificative photos representing the effects of compound 5 on LN229 and DBTRG cells are reported in Figures S2 and S3 (Supplementary Materials).

#### 2.4. *In Vitro* ADME Assays

##### 2.4.1. HPLC/UV–MS Method

UV/LC–MS chromatographic analyses were carried out using an Agilent 1100 LC/MSD VL system (G1946C) purchased from Agilent Technologies (Palo Alto, CA, USA). Chromatographic separations were achieved at room temperature (RT) using a Phenomenex Kinetex C18-100 column (150 mm × 4.6 mm, 5 µm) and gradient elution consisting of a solution of solvent A (H<sub>2</sub>O) and solvent B (ACN), both acidified with 0.1% *v/v* formic acid (FA). The analysis began with 5% B (t = 0–1 min), increased to 95% (t = 1–10 min), maintained at 95% (t = 10–19 min), and finally returned to 5% solvent A. The analyses were performed at a flow rate of 0.6 mL/min, UV detection was monitored at 254 nm, and spectra were acquired over the scan range of *m/z* 100–1000 in both positive and negative modes.

##### 2.4.2. Parallel Artificial Membrane Permeability Assay (PAMPA)

The DMSO stock of each compound was diluted with phosphate buffer (PBS 25 mM, pH 7.4) to a final concentration of 500 µM in order to obtain the “donor”. For GI and BBB permeability, filters were coated with 10 µL of 1% *w/v* dodecane phosphatidylcholine solution or 5 µL of 10% *w/v* CHCl<sub>3</sub>/dodecane brain polar lipid solution. The donor (150 µL) was poured over the artificial membranes on the filter plate. DMSO/PBS (300 µL, 1:1 *v/v*) was then added to the acceptor wells. After assembling the sandwich plates, the experiments were run for 5 h at room temperature (RT). Lastly, the amount of compound passed through the artificial membranes was determined using the UV/LC–MS method described above. Apparent permeability (P<sub>app</sub>) and membrane retention (MR%) were determined as previously described [24,25].

##### 2.4.3. Metabolic Stability Assay

Each DMSO compound solution was incubated for 1 h at 37 °C in the presence of 500 µL of PBS (25 mM, pH 7.4), human liver microsomal (HLM) proteins (0.2 mg/mL), and 10 mM NADPH solution in MgCl<sub>2</sub> (48 mM). The reactions were stopped with 1.0 mL

of cold ACN. The samples were centrifuged (4000 rpm for 10 min), and the supernatants were collected, dried under N<sub>2</sub> flow, and suspended in 100 µL of methanol (MeOH). Parent drugs and metabolites were determined using the previously described HPLC/UV–MS method. The percentage metabolic stability was calculated by comparing the metabolized and unmetabolized compounds.

### 2.5. Reversible/Irreversible Effect on LN229 Cell Death

To check if cytotoxic effects of compound 5 were reversible or irreversible, LN229 cells were seeded and treated as previously described. After 24 h of incubation with increasing concentration of compound 5 (0.1–1–10–100 µM), plates were washed with PBS and cultured in drug-free DMEM with 10% FBS for a further period of 48 h [20]. Afterward, the MTT assay was performed to assess cell viability as previously described.

### 2.6. Cell-Cycle Analysis

Flow cytometry was used to investigate the apoptotic effect of compound 5 on LN229 and DBTRG cells. These were seeded in a six-well plate ( $5 \times 10^5$  cells/well) and treated with compound 5 at the respective IC<sub>50</sub> values concentrations for 72 h. Afterward, the cells were treated as previously reported [26]. Red fluorescence (DNA) was detected through a 563–607 nm bandpass filter (FL2 channel,  $10^4$  cells/sample) using an FACScan flow cytometer coupled with Cell Quest software v.3.0, (both purchase from BD Biosciences, San Jose, CA, USA), and the latter was used to calculate the percentage of cells in the different phases of the cell cycle.

### 2.7. T-Scratch Assay

To investigate the inhibitory effect of compound 5 on cell migration, LN229 cells ( $8 \times 10^4$  cells/well) were seeded in 24 well-plate such that they were at 90% confluence the following day, at which point a scratch was made in the cell layer using a sterile p200 pipet tip. After washing the cells with warm PBS to remove the detached cells, 500 µL of fresh DMEM containing 1% FBS and increasing concentrations (0.25–0.5–2.5–5 µM) of compound 5 were added to each well. The scratched area was observed and photographed at 10× magnification after 0–24–48–72 h (see Figure S5, Supplementary Materials). Finally, the size of the area covered by cells at selected timepoints was obtained using ImageJ software (National Institute of Health, Bethesda, MD, USA, 1.37v), and the percentage cellular migration was plotted as percentage wound closure using GraphPad Prism version 5.04 (GraphPad Software Inc., San Diego, CA, USA).

### 2.8. Data Analysis

Data are reported as the mean ± standard deviation (SD) of at least three independent experiments. Statistical analysis was performed using two-way ANOVA followed by Tukey's multiple comparison test (reversible/irreversible effect on LN229 cell death, T-scratch assay) and Student's *t*-test for unpaired samples (cell-cycle analysis) as appropriate.

## 3. Results and Discussion

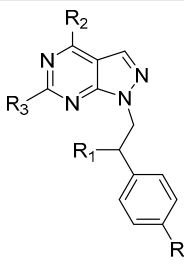
### 3.1. In Vitro Biological Evaluation

#### 3.1.1. Enzymatic Assay

GBM is a highly aggressive tumor with low expectations of recovery. Today, the standard treatment for GBM is surgical ablation, combined with and/or followed by radiotherapy and chemotherapy. The Src and Abl families play a crucial role in carcinogenesis, angiogenesis, and metastasis, and contribute to the development of the mechanisms of resistance, particularly in GBM, in which they are highly upregulated [5–7]. On the basis of these factors, the development of small molecules that act as dual Src/Abl inhibitors with improved pharmacokinetic properties, especially the ability to reach the target beyond the BBB, represents one successful strategy to attack GBM on several fronts while targeting the molecular mechanisms implicated in resistance. Thus, to investigate the

structure–activity relationship (SAR) of the selected compounds, a cell-free enzymatic assay was used to assess the affinity toward c-Src and Abl, as shown in Table 1. As already reported [10], compound **1** inhibited both enzymes with  $K_i$  values in the micromolar and low-micromolar range (3  $\mu\text{M}$  and 0.37  $\mu\text{M}$  against c-Src and Abl, respectively). A wide-ranging SAR study on this class of derivatives suggested that the presence of a benzylamine moiety (**3**, **4**, **5**, **6**, **7**, **9**, and **11**) in the  $R_2$  position resulted in more active derivatives than cyclopropylamine (**2**), aniline (**12**), or phenethylamine ones (**8** and **10**). Among the first group of compounds, with respect to parent compound **1**, an improvement in the inhibitory efficacy against c-Src was achieved thanks to the introduction of a fluorine atom in the ortho (**3**), para (**4**) [16], or meta (**11**) [19] position of the benzylamine group. These modifications led to a significant reduction in the inhibitory efficacy against Abl when compared to that of reference compound **1**. The introduction of a fluorine (**6**) [16] or a chlorine atom (**7**) [17] in the R position resulted in promising derivatives with  $K_i$  values in the low-micromolar range. Compound **5** did not show substantial changes in c-Src/Abl inhibition, despite having one more fluorine atom than **1**. Lastly, the introduction of a morpholine ethanethiol moiety (**9**) in  $R_3$  provoked a favorable improvement in the inhibition of Abl, but no significant differences against c-Src [17].

**Table 1.** Chemical structures and enzymatic activity ( $\mu\text{M}$ ) against c-Src and Abl of compounds **1**–**12**.



Enzymatic Data

Compounds	R	R <sub>1</sub>	R <sub>2</sub>	R <sub>3</sub>	c-Src $K_i$ <sup>a</sup>	Abl $K_i$ <sup>a</sup>
<b>1</b> <sup>b</sup>	H	Cl	NHCH <sub>2</sub> C <sub>6</sub> H <sub>5</sub>	H	3 *	0.37 *
<b>2</b>	H	Cl	NH-cyclopropyl	H	11.57 ± 1.08	8.01 ± 0.73
<b>3</b> <sup>c</sup>	H	Cl	NHCH <sub>2</sub> C <sub>6</sub> H <sub>4</sub> -oF	H	0.15 ± 0.02	0.73 ± 0.05 *
<b>4</b> <sup>c</sup>	H	Cl	NHCH <sub>2</sub> C <sub>6</sub> H <sub>4</sub> -pF	H	0.51 ± 0.08	2.00 ± 0.10 *
<b>5</b> <sup>c</sup>	F	Cl	NHCH <sub>2</sub> C <sub>6</sub> H <sub>5</sub>	H	3.14 ± 0.38	0.44 ± 0.06 *
<b>6</b> <sup>c</sup>	F	Cl	NHCH <sub>2</sub> C <sub>6</sub> H <sub>4</sub> -oF	H	0.07 ± 0.01	0.02 ± 0.01 *
<b>7</b> <sup>d</sup>	Cl	Cl	NHCH <sub>2</sub> C <sub>6</sub> H <sub>4</sub> -pF	H	0.80 ± 0.09	0.08 *
<b>8</b> <sup>e</sup>	H	Cl	NHCH <sub>2</sub> CH <sub>2</sub> C <sub>6</sub> H <sub>5</sub>	SCH <sub>3</sub>	0.70 *	7.30 *
<b>9</b> <sup>f</sup>	H	Cl	NHCH <sub>2</sub> C <sub>6</sub> H <sub>5</sub>	SCH <sub>2</sub> CH <sub>2</sub> -4-morpholino	2.90 ± 0.30 *	0.09 ± 0.01 *
<b>10</b>	Cl	Cl	NHCH <sub>2</sub> CH <sub>2</sub> C <sub>6</sub> H <sub>5</sub>	H	0.22 ± 0.03	0.31 ± 0.02
<b>11</b> <sup>e</sup>	H	H	NHCH <sub>2</sub> C <sub>6</sub> H <sub>4</sub> -mF	H	0.51 *	4.92 *
<b>12</b> <sup>b</sup>	Br	Cl	NHC <sub>6</sub> H <sub>5</sub>	H	0.06 *	0.61 *

<sup>a</sup> Values are the means ± SD of three different experiments run in triplicate. \* Compounds previously published.

<sup>b</sup> Ref. [10]. <sup>c</sup> Ref. [16]. <sup>d</sup> Ref. [12]. <sup>e</sup> Ref. [19]. <sup>f</sup> Ref. [17].

While the cyclopropylamino derivative **2** showed  $K_i$  values approximately 10  $\mu\text{M}$  against both enzymes, the anilino-substituted compound **12**, typed also by the presence of a bromine in R [10], was characterized by a relevant improvement in the inhibitory efficacy against c-Src. Among the phenethylamine derivatives, compound **8** possessed a promising activity against c-Src, but a lower activity against Abl, probably due to the presence of methanethiol group in  $R_3$  position [19], while compound **10** substituted with a chlorine in R, showed a better profile, acting as a low-micromolar dual inhibitor ( $K_i$  values of 0.22 and

0.31  $\mu\text{M}$  against c-Src and Abl, respectively). The present enzymatic studies revealed a general improvement in the inhibitory efficacy against c-Src, with  $K_i$  values usually lower than the reference compound **1**. The low-micromolar inhibitory activity against Abl was confirmed and sometimes also improved; only a few exceptions resulted in potential TKI inhibition worse than compound **1**.

### 3.1.2. Cell Viability Assay

In light of the previous results, further SAR studies were conducted to investigate the antiproliferative activity of the pyrazolo[3,4-*d*]pyrimidine derivatives against four GBM cell lines (U-87, LN18, LN229, and DBTRG) (Table 2).

**Table 2.** Antiproliferative activity ( $\mu\text{M}$ ) of compounds **1–12** against four GBM cell lines and cytotoxicity ( $\mu\text{M}$ ) of the most promising ones on nontumoral, healthy FIBRO 2-93 and HaCaT cell lines.

Compounds	IC <sub>50</sub> <sup>a</sup>				CC <sub>50</sub> <sup>b</sup>	
	U-87	LN18	LN229	DBTRG	FIBRO 2-93	HaCaT
<b>1</b> <sup>c</sup>	2.9 ± 1.1 *	3.6 ± 0.5	3.4 ± 0.8	4.3 ± 0.8	86.9 ± 4.2	88.7 ± 5.7
<b>2</b>	NA	49.4 ± 2.8	NA	NA	-	-
<b>3</b>	40.2 ± 3.6	27.5 ± 2.1	29.2 ± 2.6	15.1 ± 2.1	-	-
<b>4</b>	29.8 ± 2.5	9.0 ± 1.2	NA	68.5 ± 3.8	-	-
<b>5</b>	6.8 ± 0.3	10.8 ± 1.4	6.9 ± 0.5	8.5 ± 1.4	91.7 ± 5.3	126.5 ± 6.4
<b>6</b>	32.4 ± 2.7	11.7 ± 1.5	33.8 ± 2.3	20.1 ± 1.8	-	-
<b>7</b>	22.7 ± 2.3	3.9 ± 0.6	7.1 ± 1.1	14.6 ± 0.9	28.6 ± 3.7	37.8 ± 4.9
<b>8</b>	37.9 ± 3.9	5.9 ± 1.1	26.1 ± 2.8	31.2 ± 2.5	-	-
<b>9</b>	NA	2.9 ± 0.5	58.2 ± 3.4	59.4 ± 3.7	-	-
<b>10</b>	33.9 ± 2.9	6.2 ± 1.0	27.9 ± 2.1	46.5 ± 4.1	-	-
<b>11</b>	56.9 ± 3.3	34.1 ± 2.9	58.4 ± 3.0	69.2 ± 3.9	-	-
<b>12</b> <sup>c</sup>	14.0 ± 1.9 *	NA	NA	NA	-	-

<sup>a</sup> IC<sub>50</sub> = drug concentration that caused 50% of cell growth inhibition, <sup>b</sup> CC<sub>50</sub> = concentration that reduced the proliferation of cells by 50%, both determined by measuring the cell viability with the colorimetric MTT assay. Values are the means ± SD of at least three different experiments run in triplicate. \* Compounds previously published. <sup>c</sup> Ref. [10]. NA means not active (IC<sub>50</sub> > 100  $\mu\text{M}$ ). Empty cells were not determined.

Compound **1**, previously reported to be active against U-87 cells in the low-micromolar range [10], confirmed its potent antitumor activity against the other GBM cell lines (LN18, LN229, and DBTRG). As shown in Table 2, the cyclopropylamine derivative **2** resulted the least active of the series with only a slight activity against LN18 cells, while compounds **3** and **4**, with a fluorine atom in the ortho and para positions of the benzylamine group, displayed promising IC<sub>50</sub> values. Interestingly, the best results were obtained with compound **5** (characterized by an additional fluorine atom in the R position with respect to reference compound **1**), which showed low-micromolar activity against all GBM cells tested (concentration vs. cytotoxic effect curves relative to each cell line are reported in Figure S1, Supplementary Materials). Ortho and para fluorobenzylamino derivatives bearing a fluorine (**6**) or chlorine (**7**) atom in the R position presented a slight or significant improvement in anticancer efficacy compared to the corresponding unsubstituted compounds (**3** and **4**) on the N1 side-chain. To further investigate the SAR around the scaffold, substituents such as methanethiol and 4-morpholinoethanethiol moieties were introduced in R<sub>3</sub> position leading to compounds **8** and **9**, respectively. The phenethylamine derivative **8** demonstrated a mild ability to act as an antiproliferative agent, especially against LN18 cells, while the efficacy of compound **9** was reduced in the other GBM cell lines. Compound **10** followed the same trend as compound **8**, proving to be a valuable antiproliferative agent with encouraging IC<sub>50</sub> values. Lastly, if compound **11** was a weak cytotoxic agent, the

introduction of the aniline moiety in R<sub>2</sub> (**12**) produced a potent compound active against U-87 cells [10], but was ineffective against the other GBM cell lines. Taken together, the present results strongly suggest that our compounds are promising anticancer candidates toward GBM. Compound **1** and the two most encouraging derivatives (**5** and **7**), endowed with antiproliferative activity comparable to that of reference one, were further investigated for their safety profile by assessing their activity in two different nontumoral, immortalized healthy cells (FIBRO 2-93 and HaCaT). Except for compound **7** which affected the viability of both healthy cell lines (CC<sub>50</sub> values of 28.6 and 37.8 μM on FIBRO 2-93 and HaCaT, respectively), compounds **1** and **5** were characterized by an optimal safety profile (CC<sub>50</sub> ~87 μM for compound **1** and >90 μM for compound **5**, i.e., 10 times higher than their IC<sub>50</sub>), thus suggesting a reassuring ability to distinguish between tumoral and healthy cells.

### 3.2. In Vitro ADME Evaluation

To assess the capability of the selected pyrazolo[3,4-*d*]pyrimidine derivatives to reach their target in vivo, the in silico and in vitro ADME properties were assessed for all compounds (Table 3). Our research group was efficiently involved in the attempt to overtake the suboptimal solubility of these compounds with prodrugs [10] or formulations such as albumin nanoparticles [27], cyclodextrins [28], and liposomes [27]. For this reason, we decided to analyze this property using a computational approach followed by proper in vitro investigations. The QikProp software confirmed the hydrophobicity of the derivatives. All compounds were characterized by suboptimal LogS values which could limit their in vivo bioavailability depending on the solvation rate. Nevertheless, the entire series of pyrazolo[3,4-*d*]pyrimidines had the optimal ability to cross the GI membrane and, most importantly, the BBB, as demonstrated by PAMPA assays. Similar to the reference compound **1**, previously reported to show high passive permeability across membranes, compounds **3**, **4**, **5**, **6**, **7**, **10**, and **11** were characterized by high apparent permeability values, never lower than 10 cm/s × 10<sup>-6</sup>, and limited percentages of membrane retention.

**Table 3.** In silico and in vitro ADME properties of compounds 1–12.

Compounds	QP LogS	GI Papp <sup>a,b</sup> (MR%) <sup>c</sup>	BBB Papp <sup>a,b</sup> (MR%) <sup>c</sup>	Metabolic Stability <sup>a</sup> (%)	Metabolite Formation (%) <sup>d</sup>
<b>1</b> <sup>e</sup>	−5.715	11.08 *	16.5 *	78.3 *	M <sub>1</sub> = 14.5 * M <sub>2</sub> < 0.1 * M <sub>3</sub> = 2.6 * M <sub>4</sub> = 4.5 *
<b>2</b>	−4.862	6.46 (34.7)	4.96 (55.0)	96.3	M <sub>1</sub> = 2.1 M <sub>2</sub> = 1.6
<b>3</b>	−6.358	12.4 (7.3)	12.2 (4.8)	80.4	M <sub>1</sub> = 14.5 M <sub>3</sub> = 5.1
<b>4</b>	−6.784	11.2 (7.8)	10.6 (2.1)	92.2	M <sub>1</sub> = 5.9 M <sub>2</sub> = 1.0 M <sub>3</sub> = 0.9
<b>5</b>	−6.511	10.7 (9.2)	11.2 (5.6)	84.2	M <sub>1</sub> = 10.8 M <sub>2</sub> = 1.7 M <sub>3</sub> = 3.3
<b>6</b>	−6.955	11.4 (10.1)	12.4 (4.4)	69.9	M <sub>1</sub> = 21.9 M <sub>2</sub> = 3.0 M <sub>3</sub> = 5.2
<b>7</b> <sup>f</sup>	−7.533	16.6 *	9.6 (4.4)	94.0 *	M <sub>1</sub> = 4 * M <sub>3</sub> = 2 *
<b>8</b>	−6.207	3.2 (42.7)	5.96 (18.3)	96.6	M <sub>1</sub> = 1.9 M <sub>2</sub> = 1.5



Table 3. Cont.

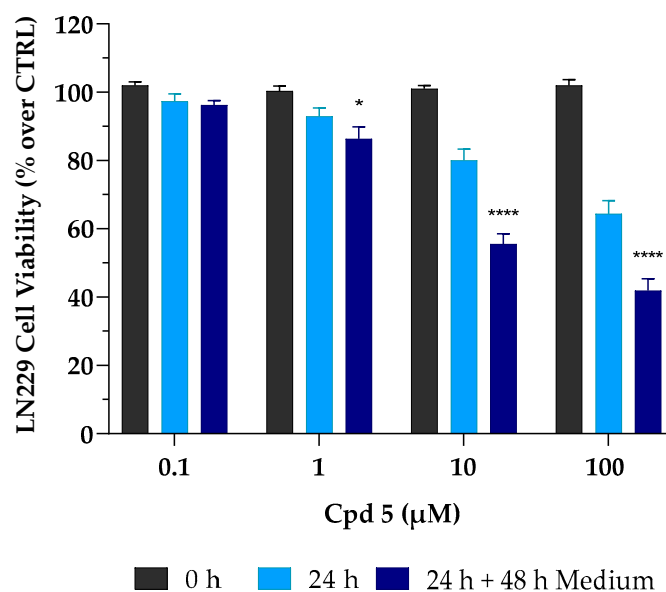
Compounds	QP LogS	GI Papp <sup>a,b</sup> (MR%) <sup>c</sup>	BBB Papp <sup>a,b</sup> (MR%) <sup>c</sup>	Metabolic Stability <sup>a</sup> (%)	Metabolite Formation (%) <sup>d</sup>
9 <sup>g</sup>	−5.6 <sup>*</sup>	9.1 <sup>*</sup>	2.6 (6.3)	95 <sup>*</sup>	M <sub>1</sub> = 5 <sup>*</sup>
10	−7.589	10.8 (17.2)	11.3 (4.8)	85.9	M <sub>1</sub> = 10.3 M <sub>3</sub> = 3.8
11	−5.973	10.1 (6.7)	10.8 (5.2)	93.0	M <sub>1</sub> = 0.4 M <sub>2</sub> = 6.7
12 <sup>e</sup>	−6.576	6.64 <sup>*</sup>	13.1 <sup>*</sup>	96.4 <sup>*</sup>	-

<sup>a</sup> Values represent the mean values of three independent experiments run in triplicate. <sup>b</sup> Apparent permeability (Papp) reported in cm/s × 10<sup>−6</sup>. <sup>c</sup> Membrane retention %. <sup>d</sup> M<sub>1</sub> = M − HCl + O (−36 + 16); M<sub>2</sub> = M + OH (−16); M<sub>3</sub> = M—group bearing NH moiety in R<sub>2</sub>; M<sub>4</sub> = M − Cl + OH (−35 + 17). <sup>\*</sup> Compounds previously published. <sup>e</sup> Refs. [10,18]. <sup>f</sup> Ref. [12]. <sup>g</sup> Ref. [17]. Empty cells were not determined or not found.

The *in silico* and *in vitro* results confirmed the well-known suboptimal aqueous solubility characterizing the pyrazolo[3,4-*d*]pyrimidine derivatives, as well as the satisfactory ability to efficiently overcome membranes (especially the BBB) without remaining entrapped in the phospholipidic bilayer. Regarding the metabolic stability in the presence of HLMs, the principal metabolites were identified because of dechlorination (M<sub>1</sub> and M<sub>4</sub>), oxidation (M<sub>2</sub>), and the loss of the groups bearing the amine moiety in R<sub>2</sub> (M<sub>3</sub>). The percentage of metabolite formation was calculated as previously reported [18]. With respect to reference compound **1**, most of the derivatives resulted in higher metabolic stability, around 90% or more (**2**, **4**, **7**, **8**, **9**, **11**, and **12**), when incubated in presence of HLMs. Compound **6** underwent massive metabolization with the formation of more than 20% of metabolite M<sub>1</sub>, resulting definitively worse than the reference compound **1**. Lastly, compounds **3**, **5**, and **10** were characterized by improved metabolic stability of approximately 80–85%. As a general conclusion, metabolic stability studies highlighted the tendency of selected compounds to lead to the massive formation of metabolite M<sub>1</sub> (M − HCl + O), followed by the loss of the group bearing the NH moiety in R<sub>2</sub> (M<sub>3</sub>).

### 3.3. Irreversible Cytotoxic Effect on LN229 Cell Death

Results so far obtained highlighted that compound **5** is a dual inhibitor, endowed with low-micromolar activity against four different GBM cell lines, an optimal safety profile toward healthy cells, and promising ADME properties, particularly a high BBB permeability that represents the Achilles heel of many GBM candidates. These characteristics strongly led us to further investigate its anticancer activity. In the case of cancer cells, it is mandatory to investigate whether a cell line may (or may not) be able to restart its proliferative activity upon drug treatment. It is crucial to demonstrate the presence of the so-called “point of no return”, a limit line between cell injury and cell death, whereby surpassing this point drives irreversible damage. Thus, to better elucidate the biological effect and the mechanism of compound **5**-mediated cell death, further investigations were performed on the LN229 cell line. To check whether the growth inhibitory effect was reversible or irreversible, LN229 cells were initially treated with compound **5** for 24 h; after that, cells were carefully washed to remove the treatment and were cultured for a further 48 h in a complete drug-free medium. At the timepoint of 72 h, as described above, the MTT assay was used to assess cell viability. As reported in Figure 1, compound **5** caused an irreversible cytotoxic effect. This trend was emphasized at the concentrations of 10 and 100 μM with a further decrease in cell viability (~30% for both concentrations) after 24 h of treatment, followed by 48 h of incubation without compound **5**.

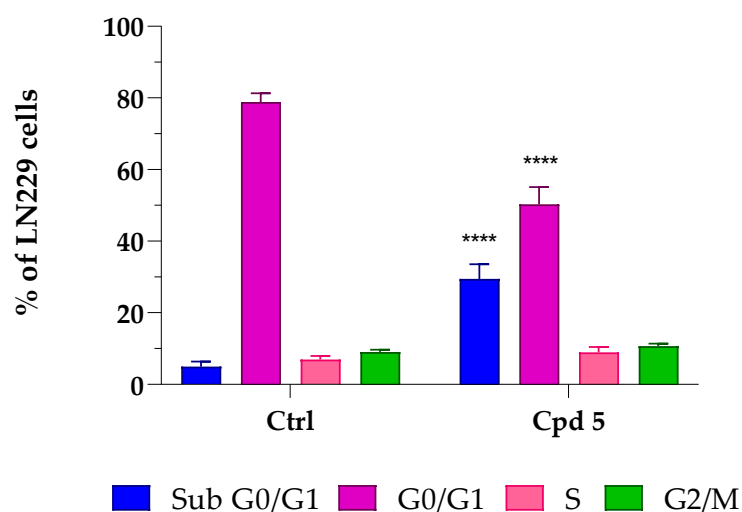


**Figure 1.** Irreversible cytotoxic effect of compound 5 (Cpd 5) on LN229 GBM cell line. These were treated with the compound for 24 h (24 h, light-blue column) and then incubated for 48 h with fresh, drug-free medium (24 h + 48 h medium, dark-blue column). Afterward, cell viability was assessed using the MTT assay. Values are the means  $\pm$  SD of  $n = 3$  independent experiments run in triplicate. \*  $p < 0.05$ , \*\*\*\*  $p < 0.001$  vs. 24 h at the same concentration (ANOVA followed by Tukey's multiple comparison test).

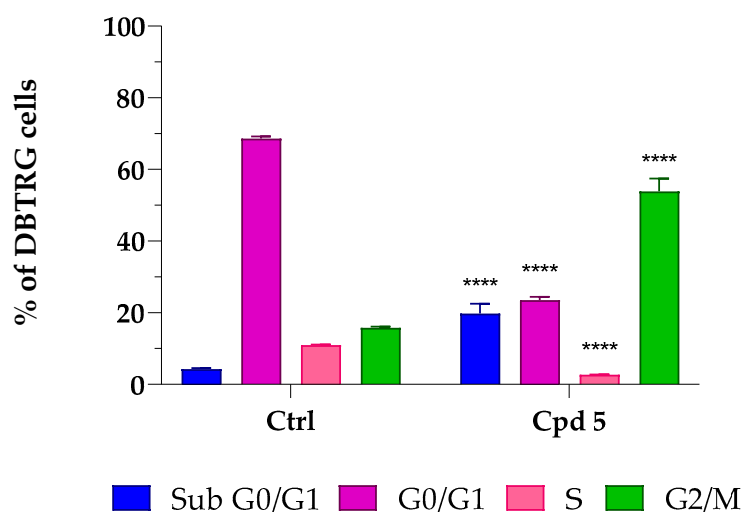
Interestingly, it is important to note that, after 24 h of treatment, cytotoxic effects occurring at both 1 and 10  $\mu\text{M}$ , although moderate ( $\sim -10\%$  and  $-20\%$ , respectively), were immediately irreversible, as cell viability was not restored after withdrawal of the drug. This might prove to be very useful to support a full cytotoxic effect achieved in the low  $\mu\text{M}$  range after 72 h of treatment.

### 3.4. Cell-Cycle Analysis

To further investigate whether compound 5-mediated cell death involved some characteristics of apoptosis such as loss of DNA due to DNA fragmentation, as well as effects on cell-cycle progression, flow cytometry-mediated cell-cycle analyses were conducted by treating LN229 and DBTRG cells for 72 h with compound 5 at its  $\text{IC}_{50}$  concentrations. As reported in Figure 2a, a relevant accumulation of LN229 hypodiploid cells in the sub G0/G1 phase was observed ( $+32.1\%$ ,  $p < 0.0001$  vs. control), which was accompanied by a proportional reduction in those in the G0/G1 phase ( $-32.4\%$ ,  $p < 0.0001$  vs. control), suggesting that compound 5 induced apoptotic-mediated cell death. No significant differences were detected in the percentage of cells in the S and G2/M phases. As reported in Figure 2b, a significant accumulation of hypodiploid cells was also found in the sub G0/G1 area in DBTRG cells ( $+15.6\%$ ,  $p < 0.0001$  vs. control) (see exemplificative histograms of cell-cycle analysis reported in Figure S4, Supplementary Materials), thus suggesting that, in the presence of compound 5, both LN229 and DBTRG cells respond by initiating programmed cell death. This hypothesis was also supported by the analysis at phase-contrast microscopy, which highlighted significant morphological alterations, including a tendency to round up and detach from the culture plate, shrinkage, loss of contact with adjacent cells, membrane blebbing, and formation of apoptotic bodies (see Figures S2 and S3, Supplementary Materials). The increased number of cells with DNA fragmentation was accompanied by an arrest of DBTRG cells in the G2/M phase ( $+38.1\%$ ,  $p < 0.0001$  vs. control).



(a)



(b)

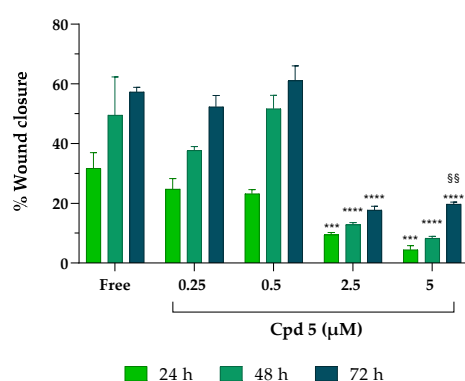
**Figure 2.** Compound 5-mediated effects on the glioblastoma LN229 (a) and DBTRG (b) cell cycle. Cells were treated for 72 h at the compound 5 IC<sub>50</sub> concentrations, i.e., 6.9  $\mu$ M for LN229 and 8.5  $\mu$ M for DBTRG. Percentages of cells in sub G0/G1 (Blue), G0/G1 (Purple), S (Pink), and G2/M (Green) phases are reported as the means  $\pm$  SD of at least three independent experiments run in triplicate. \*\*\*\*  $p < 0.0001$  vs. ctrl, same cell-cycle phase (unpaired Student *t*-test).

A cell-cycle completion is essential for proliferation, and cell apoptosis often results from cell-cycle arrest [29]. To complete the cell cycle, a successful G2/M phase is crucial, and uncontrolled cell proliferation might result from imbalanced cell-cycle regulation, which is a hallmark of cancer cells, including GBM [30,31]. Several anticancer drugs have been found to induce G2/M cell-cycle arrest and apoptosis in different GBM cell lines, effectively suppressing proliferation [32,33]. Moreover, the observation that, upon compound 5 treatment, G2/M phase arrest was observed in DBTRG, but not in LN229 cells can be explained by considering that these GBM cell lines possess a diverse genetic background and, in turn, possibly different mechanisms leading to tumor development [34], which might impact the cells' capacity to respond to drugs. Taken together, results from cell-cycle analysis, showing an increased population in cells with a reduced DNA content

(LN299 and DBTRG) and G2/M arrest (DBTRG), suggest the possibility of an apoptotic-mediated cell death caused by compound 5. As types of cell death other than apoptosis might result in loss of DNA appearing in the sub G0/G1 region, the possibility that other mechanisms may drive compound 5 effects cannot be ruled out.

### 3.5. T-Scratch Assay

Glioblastoma is a malignant primary brain tumor strongly characterized by aggressive invasion of the surrounding cerebral tissues that obstacles surgery and target therapies. Although gliomas rarely metastasize out of the brain tissue, the massive infiltration of tumor cells along blood vessels, with matter tracts and the subarachnoid space is a common hallmark of this type of cancer [35,36]. Therefore, studying the effect of drugs on cell migration is of primary importance; to fulfill this task, we decided to use an easy, low-cost, and reproducible T-scratch assay. The overall ability of compound 5 to influence GBM cell migration was assessed in LN229 cells (Figure 3).



**Figure 3.** Effect of compound 5 on cancer cell migration. After scratching, LN229 cells were treated with increasing concentrations of compound 5 for 24–48–72 h. Results were obtained from  $n = 3$  independent experiments run in triplicate; values are reported as the means  $\pm$  SD. Two-way ANOVA followed by Tukey's multiple comparison test was performed to determine statistical significance. 2.5  $\mu$ M and 5  $\mu$ M: \*\*\*  $p < 0.001$ , \*\*\*\*  $p < 0.0001$  vs. free at the same timepoints; 5  $\mu$ M at 72 h: §§  $p < 0.01$  vs. the same concentration at 24 h.

While, in free samples and in the presence of the lowest concentrations of the inhibitor (0.25 and 0.5  $\mu$ M), the closure of the monolayer significantly increased after 72 h (getting close to 60% of wound closure), at 2.5 and 5  $\mu$ M, compound 5 suppressed healing, leaving more than 80% of the wound opened at all the timepoints analyzed, suggesting that compound 5 can inhibit the horizontal migration ability of LN229 cells already at the early stage (24 h) of drug stimulation and is sustained over time (72 h), albeit with decreased inhibition rates.

## 4. Conclusions

GBM continues to be a highly aggressive tumor with low expectations of recovery. Today, the standard treatment for GBM is surgical ablation, combined with and/or followed by radiotherapy and chemotherapy. However, such methods are not curative, and patients affected by GBM still have poor prognoses, primarily due to the onset of resistance, often caused by the presence of cancer stem cells [6]. Progressive and increasing interest in developing small-molecule kinase inhibitors has been recorded since the 1980s, with more than 30 new drugs approved by the FDA for the treatment of tumors [37]. In recent years, our research team has created a large library of pyrazolo[3,4-*d*]pyrimidines, capable of inhibiting tyrosine kinases, identified as potent antitumor agents, demonstrating a powerful action both in vitro and in vivo. Thus, moving from our in-house library, a panel of compounds characterized by the pyrazolo[3,4-*d*]pyrimidine scaffold and heterogeneously decorated at N1, C4, and C6 was selected for this study. Compounds were tested against

c-Src and Abl, showing promising  $K_i$  values in the micromolar and low-micromolar range. Then, the antiproliferative activity of the compounds was assessed on four GBM cell lines (U-87, LN229, LN18, and DBTRG); for the most active derivatives, a safety profile was established with the healthy fibroblasts FIBRO 2-93 and keratinocytes HaCaT. The ability of the compounds to cross both GI and BBB membranes was assessed in vitro. The optimal passive permeability values suggest that several compounds could efficiently cross the BBB. Moreover, a complete ADME profile was studied for all compounds, revealing comparable solubility but higher metabolic stability with respect to parent compound 1. Lastly, considering the in vitro biological and pharmacokinetic data, compound 5 was chosen to further characterize its biological effect on LN229 and DBTRG GBM cells. Compound 5 induced irreversible cytotoxicity, significantly reduced cell migration, and increased the number of cells with DNA fragmentation, possibly because of an apoptotic-mediated cell death. Overall, this study led to the identification of a new promising pyrazolo[3,4-*d*]pyrimidine derivative for GBM treatment. Although further investigations are needed to characterize its mechanism of action, as well as to evaluate the in vivo pharmacokinetic profile and efficacy, our present findings demonstrate that compound 5 could represent a new excellent approach to GBM treatment.

**Supplementary Materials:** The following supporting information can be downloaded at <https://www.mdpi.com/article/10.3390/pharmaceutics15020453/s1>, Chemistry; Scheme S1: Chemical Structures of tested compound; Figure S1: Effects of compound 5 on viability of four different GBM cell lines (U-87, LN18, LN229, DBTRG), as well as on two non-tumoral, healthy cells (the fibroblast FIBRO 2-93 cells and the keratinocytes HaCaT cells). Cell viability was expressed as percentage of that of DMSO-treated cells (controls), taken as 100%.  $IC_{50}$  and  $CC_{50}$  values were calculated by fitting data according to a non-linear regression analysis (sigmoidal log concentration vs. normalized response curve) and reported in Table 2. Each point represents mean  $\pm$  SD (if not visible, SD was covered by the point); Figure S2: Morphological comparison performed at contrast phase microscopy (scale bar 180  $\mu$ m) between controls, untreated LN229 cells (panel (a)) and those treated with compound 5 (6.9  $\mu$ M, 72 h, panel (b)) in which significant morphological alterations, including tendency to round-up, shrinkage, loss of contact with adjacent cells, membrane blebbing and formation of apoptotic bodies are evident. Each photograph was representative of three independent observations; Figure S3: Morphological comparison performed at contrast phase microscopy (scale bar 180  $\mu$ m) between controls, untreated DBTRG cells (panel (a)) and those treated with compound 5 (8.5  $\mu$ M, 72h, panel (b)) in which significant morphological changes caused by the drug are evident. Compound 5 caused the cells to lose contact with adjacent cells, cell membrane blebbing and a general tendency to round-up. Each photograph was representative of three independent observations; Figure S4: Exemplificative cell cycle distribution histograms of the LN229 and DBTRG cell lines in control condition (CTRL) and after 72 h of treatment with compound 5 (6.9  $\mu$ M and 8.5  $\mu$ M, respectively). Following incubation, the DNA of the cells was stained with propidium iodide and its content was analysed by flow cytometry. The cells were normally distributed in the population of sub G0/G1, G0/G1, S, and G2/M of cell cycle phases in CTRL samples. After 72 h of treatment with compound 5, an increase in sub G0/G1 cells in both cells lines was observed, while the same compound also caused an arrest the cell cycle in G2/M phase in DBTRG cells; Figure S5: Time-lapse images of a representative T-scratch assay to investigate the effect of compound 5 on GBM cancer cell migration. LN229 cells were seeded, scratched, and finally incubated with increasing concentrations of compound 5 (0.25–0.5–2.5–5  $\mu$ M) for 24–48–72 h. Scale bar 100  $\mu$ m.

**Author Contributions:** Conceptualization, F.P., C.V., A.B. and E.D.; methodology, F.P., C.V., A.B., C.P. (Claudia Pasqualini), G.M., M.F., S.S. and E.D.; formal analysis, F.P., C.V., A.B., E.C., F.M. and M.F.; investigation, F.P., C.V., A.B., C.P. (Claudia Pasqualini), E.C., F.M., L.B., C.P. (Cecilia Perini), N.C. and M.F.; resources, G.M., S.S., L.B., M.F. and E.D.; data curation, F.P., C.V., A.B., E.C., F.M. and M.F.; writing—original draft preparation, F.P.; writing—review and editing, C.V., A.B., C.P. (Claudia Pasqualini), E.C., G.M., L.B., F.M., M.F., S.S. and E.D.; visualization, F.P., C.V., A.B. and M.F.; supervision, G.M., E.C., L.B., M.F., S.S. and E.D.; project administration, E.D.; funding acquisition, E.D. All authors have read and agreed to the published version of the manuscript.

**Funding:** This research was funded by the TUSCAVIR.NET Bando Ricerca Salute 2018 CUP: B64I18013740002 funded by Tuscany Region, PI Elena Dreassi, the AIRC Foundation for Cancer Research in Italy (Fondazione AIRC per la Ricerca sul Cancro, AIRC): (i) Grant IG-2019, project code 23725, PI Silvia Schenone, (ii) Grant IG-2017, project code 20762, PI Giovanni Maga, (iii) Grant IG-2020, project code 24448, PI Emmanuele Crespan, and the Italian MIUR Project PRIN 2017 2017SA5837\_004 (C.P. (Cecilia Perini) and G.M.).

**Institutional Review Board Statement:** Not applicable.

**Informed Consent Statement:** Not applicable.

**Data Availability Statement:** Data are reported in this article and the Supplementary Materials.

**Acknowledgments:** E.C. wishes to thank the Cariplo Foundation, project 2019-1836.

**Conflicts of Interest:** The authors declare no conflict of interest.

## References

1. Fallacara, A.L.; Zamperini, C.; Podolski-Renić, A.; Dinić, J.; Stanković, T.; Stepanović, M.; Mancini, A.; Rango, E.; Iovenitti, G.; Molinari, A.; et al. A New Strategy for Glioblastoma Treatment: In Vitro and In Vivo Preclinical Characterization of Si306,a Pyrazolo [3,4-d]Pyrimidine DualSrc/P-Glycoprotein Inhibitor. *Cancers* **2019**, *11*, 848. [CrossRef]
2. Tamimi, A.F.; Juweid, M. Epidemiology and Outcome of Glioblastoma. *Glioblastoma* **2017**, 143–153. [CrossRef]
3. Ceccherini, E.; Indovina, P.; Zamperini, C.; Dreassi, E.; Casini, N.; Cutaia, O.; Forte, I.M.; Pentimalli, F.; Esposito, L.; Polito, M.S.; et al. SRC Family Kinase Inhibition through a New Pyrazolo[3,4-d]Pyrimidine Derivative as a Feasible Approach for Glioblastoma Treatment. *J. Cell. Biochem.* **2015**, *116*, 856–863. [CrossRef]
4. Molinari, A.; Iovenitti, G.; Mancini, A.; Gravina, G.L.; Chebbi, M.; Caruana, M.; Vignaroli, G.; Orofino, F.; Rango, E.; Angelucci, A.; et al. AuNP Pyrazolo[3,4-d]Pyrimidine Nanosystem in Combination with Radiotherapy against Glioblastoma. *ACS Med. Chem. Lett.* **2020**, *11*, 664–670. [CrossRef]
5. Cirotti, C.; Contadini, C.; Barilà, D. SRC Kinase in Glioblastoma: News from an Old Acquaintance. *Cancers* **2020**, *12*, 1558. [CrossRef]
6. Lamballe, F.; Toscano, S.; Conti, F.; Arechederra, M.; Baeza, N.; Figarella-Branger, D.; Helmbacher, F.; Maina, F. Coordination of Signalling Networks and Tumorigenic Properties by ABL in Glioblastoma Cells. *Oncotarget* **2016**, *7*, 74747–74767. [CrossRef]
7. Luttmann, J.H.; Colemon, A.; Mayro, B.; Pendergast, A.M. Role of the ABL Tyrosine Kinases in the Epithelial–Mesenchymal Transition and the Metastatic Cascade. *Cell Commun. Signal.* **2021**, *19*, 59. [CrossRef]
8. Spreafico, A.; Schenone, S.; Serchi, T.; Orlandini, M.; Angelucci, A.; Magrini, D.; Bernardini, G.; Collodel, G.; Di Stefano, A.; Tintori, C.; et al. Antiproliferative and Proapoptotic Activities of New Pyrazolo[3,4-d]Pyrimidine Derivative Src Kinase Inhibitors in Human Osteosarcoma Cells. *FASEB J.* **2008**, *22*, 1560–1571. [CrossRef]
9. Molinari, A.; Fallacara, A.L.; Di Maria, S.; Zamperini, C.; Poggialini, F.; Musumeci, F.; Schenone, S.; Angelucci, A.; Colapietro, A.; Crespan, E.; et al. Efficient Optimization of Pyrazolo[3,4-d]Pyrimidines Derivatives as c-Src Kinase Inhibitors in Neuroblastoma Treatment. *Bioorg. Med. Chem. Lett.* **2018**, *28*, 3454–3457. [CrossRef]
10. Vignaroli, G.; Iovenitti, G.; Zamperini, C.; Coniglio, F.; Calandro, P.; Molinari, A.; Fallacara, A.L.; Sartucci, A.; Calgani, A.; Colechia, D.; et al. Prodrugs of Pyrazolo[3,4-d]Pyrimidines: From Library Synthesis to Evaluation as Potential Anticancer Agents in an Orthotopic Glioblastoma Model. *J. Med. Chem.* **2017**, *60*, 6305–6320. [CrossRef]
11. Indovina, P.; Giorgi, F.; Rizzo, V.; Khadang, B.; Schenone, S.; Di Marzo, D.; Forte, I.M.; Tomei, V.; Mattioli, E.; D’urso, V.; et al. New Pyrazolo[3,4-d]Pyrimidine SRC Inhibitors Induce Apoptosis in Mesothelioma Cell Lines through P27 Nuclear Stabilization. *Oncogene* **2012**, *31*, 929–938. [CrossRef] [PubMed]
12. Radi, M.; Tintori, C.; Musumeci, F.; Brullo, C.; Zamperini, C.; Dreassi, E.; Fallacara, A.L.; Vignaroli, G.; Crespan, E.; Zanolì, S.; et al. Design, Synthesis, and Biological Evaluation of Pyrazolo[3,4-d]Pyrimidines Active in Vivo on the Bcr-Abl T315I Mutant. *J. Med. Chem.* **2013**, *56*, 5382–5394. [CrossRef] [PubMed]
13. Cozzi, M.; Giorgi, F.; Marcelli, E.; Pentimalli, F.; Forte, I.M.; Schenone, S.; D’urso, V.; De Falco, G.; Botta, M.; Giordano, A.; et al. Antitumor Activity of New Pyrazolo[3,4-d]Pyrimidine SRC Kinase Inhibitors in Burkitt Lymphoma Cell Lines and Its Enhancement by WEE1 Inhibition. *Cell Cycle* **2012**, *11*, 1029–1039. [CrossRef]
14. Schenone, S.; Bruno, O.; Bondavalli, F.; Ranise, A.; Mosti, L.; Menozzi, G.; Fossa, P.; Manetti, F.; Morbidelli, L.; Trincavelli, L.; et al. Synthesis of 1-(2-Chloro-2-Phenylethyl)-6-Methylthio-1H-Pyrazolo[3,4-d]Pyrimidines 4-Amino Substituted and Their Biological Evaluation. *Eur. J. Med. Chem.* **2004**, *39*, 153–160. [CrossRef] [PubMed]
15. Schenone, S.; Bruno, O.; Bondavalli, F.; Ranise, A.; Mosti, L.; Menozzi, G.; Fossa, P.; Donnini, S.; Santoro, A.; Ziche, M.; et al. Antiproliferative Activity of New 1-Aryl-4-Amino-1H-Pyrazolo[3,4-d]Pyrimidine Derivatives toward the Human Epidermoid Carcinoma A431 Cell Line. *Eur. J. Med. Chem.* **2004**, *39*, 939–946. [CrossRef] [PubMed]
16. Manetti, F.; Brullo, C.; Magnani, M.; Mosci, F.; Chelli, B.; Crespan, E.; Schenone, S.; Naldini, A.; Bruno, O.; Trincavelli, M.L.; et al. Structure-Based Optimization of Pyrazolo[3,4-d]Pyrimidines as Abl Inhibitors and Antiproliferative Agents toward Human Leukemia Cell Lines. *J. Med. Chem.* **2008**, *51*, 1252–1259. [CrossRef] [PubMed]

17. Radi, M.; Dreassi, E.; Brullo, C.; Crespan, E.; Tintori, C.; Bernardo, V.; Valoti, M.; Zamperini, C.; Daigl, H.; Musumeci, F.; et al. Design, Synthesis, Biological Activity, and ADME Properties of Pyrazolo[3,4-d]Pyrimidines Active in Hypoxic Human Leukemia Cells: A Lead Optimization Study. *J. Med. Chem.* **2011**, *54*, 2610–2626. [CrossRef] [PubMed]
18. Zamperini, C.; Dreassi, E.; Vignaroli, G.; Radi, M.; Dragoni, S.; Schenone, S.; Musumeci, F.; Valoti, M.; Antiochia, R.; Botta, M. CYP-Dependent Metabolism of Antitumor Pyrazolo[3,4-d]Pyrimidine Derivatives Is Characterized by an Oxidative Dechlorination Reaction. *Drug Metab. Pharmacokinet.* **2014**, *29*, 433–440. [CrossRef]
19. Radi, M.; Brullo, C.; Crespan, E.; Tintori, C.; Musumeci, F.; Biava, M.; Schenone, S.; Dreassi, E.; Zamperini, C.; Maga, G.; et al. Identification of Potent C-Src Inhibitors Strongly Affecting the Proliferation of Human Neuroblastoma Cells. *Bioorg. Med. Chem. Lett.* **2011**, *21*, 5928–5933. [CrossRef]
20. Chiaino, E.; Micucci, M.; Durante, M.; Budriesi, R.; Gotti, R.; Marzetti, C.; Chiarini, A.; Frosini, M. Apoptotic-Induced Effects of Acacia Catechu Willd. Extract in Human Colon Cancer Cells. *Int. J. Mol. Sci.* **2020**, *21*, 2102. [CrossRef]
21. Santulli, C.; Brizi, C.; Micucci, M.; del Genio, A.; de Cristofaro, A.; Bracco, F.; Pepe, G.L.; di Perna, I.; Budriesi, R.; Chiarini, A.; et al. Castanea Sativa Mill. Bark Extract Protects U-373 MG Cells and Rat Brain Slices Against Ischemia and Reperfusion Injury. *J. Cell. Biochem.* **2017**, *118*, 839–850. [CrossRef] [PubMed]
22. Durante, M.; Frosini, M.; Fusi, F.; Neri, A.; Sticozzi, C.; Saponara, S. In Vitro Vascular Toxicity of Tariquidar, a Potential Tool for in Vivo PET Studies. *Toxicol. Vitro.* **2017**, *44*, 241–247. [CrossRef] [PubMed]
23. Chiaino, E.; Micucci, M.; Budriesi, R.; Mattioli, L.B.; Marzetti, C.; Corsini, M.; Frosini, M. Hibiscus Flower and Olive Leaf Extracts Activate Apoptosis in SH-SY5Y Cells. *Antioxidants* **2021**, *10*, 1962. [CrossRef] [PubMed]
24. Tintori, C.; Brai, A.; Dasso Lang, M.C.; Deodato, D.; Greco, A.M.; Bizzarri, B.M.; Cascone, L.; Casian, A.; Zamperini, C.; Dreassi, E.; et al. Development and in Vitro Evaluation of a Microbicide Gel Formulation for a Novel Non-Nucleoside Reverse Transcriptase Inhibitor Belonging to the N-Dihydroalkoxybenzoxypyrimidines (N-DABOs) Family. *J. Med. Chem.* **2016**, *59*, 2747–2759. [CrossRef] [PubMed]
25. Brai, A.; Riva, V.; Saladini, F.; Zamperini, C.; Trivisani, C.I.; Garbelli, A.; Pennisi, C.; Giannini, A.; Boccutto, A.; Bugli, F.; et al. DDX3X Inhibitors, an Effective Way to Overcome HIV-1 Resistance Targeting Host Proteins. *Eur. J. Med. Chem.* **2020**, *200*, 112319. [CrossRef]
26. Chiaino, E.; Stella, R.; Peggion, C.; Micucci, M.; Budriesi, R.; Mattioli, L.B.; Marzetti, C.; Pessina, F.; Valoti, M.; Frosini, M. *Acacia catechu* Willd. Extract Protects Neuronal Cells from Oxidative Stress-Induced Damage. *Antioxidants* **2021**, *11*, 81. [CrossRef]
27. Vignaroli, G.; Calandro, P.; Zamperini, C.; Coniglio, F.; Iovenitti, G.; Tavanti, M.; Colecchia, D.; Dreassi, E.; Valoti, M.; Schenone, S.; et al. Improvement of Pyrazolo[3,4-d]Pyrimidines Pharmacokinetic Properties: Nanosystem Approaches for Drug Delivery. *Sci. Rep.* **2016**, *6*, 21509. [CrossRef]
28. Dreassi, E.; Zizzari, A.T.; Mori, M.; Filippi, I.; Belfiore, A.; Naldini, A.; Carraro, F.; Santucci, A.; Schenone, S.; Botta, M. 2-Hydroxypropyl- $\beta$ -Cyclodextrin Strongly Improves Water Solubility and Anti-Proliferative Activity of Pyrazolo[3,4-d]Pyrimidines Src-Abl Dual Inhibitors. *Eur. J. Med. Chem.* **2010**, *45*, 5958–5964. [CrossRef]
29. Schwartz, G.K.; Shah, M.A. Targeting the Cell Cycle: A New Approach to Cancer Therapy. *J. Clin. Oncol.* **2005**, *23*, 9408–9421. [CrossRef]
30. Stewart, Z.A.; Westfall, M.D.; Pietenpol, J.A. Cell-Cycle Dysregulation and Anticancer Therapy. *Trends Pharmacol. Sci.* **2003**, *24*, 139–145. [CrossRef]
31. Hanahan, D.; Weinberg, R.A. Hallmarks of Cancer: The next Generation. *Cell* **2011**, *144*, 646–674. [CrossRef] [PubMed]
32. Xu, J.; Sun, S.; Zhang, W.; Dong, J.; Huang, C.; Wang, X.; Jia, M.; Yang, H.; Wang, Y.; Jiang, Y.; et al. Iridenin Inhibits Glioblastoma Progression through Suppressing YAP/ $\beta$ -Catenin Signaling. *Front. Pharmacol.* **2022**, *13*, 1027577. [CrossRef]
33. Othman, N.S.; Mohd Azman, D.K. Andrographolide Induces G2/M Cell Cycle Arrest and Apoptosis in Human Glioblastoma DBTRG-05MG Cell Line via ERK1/2 /c-Myc/P53 Signaling Pathway. *Molecules* **2022**, *27*, 6686. [CrossRef] [PubMed]
34. Demircan, T.; Yavuz, M.; Kaya, E.; Akgül, S.; Altuntaş, E. Cellular and Molecular Comparison of Glioblastoma Multiform Cell Lines. *Cureus* **2021**, *13*, 43. [CrossRef]
35. Hatoum, A.; Mohammed, R.; Zakieh, O. The Unique Invasiveness of Glioblastoma and Possible Drug Targets on Extracellular Matrix. *Cancer Manag. Res.* **2019**, *11*, 1843. [CrossRef] [PubMed]
36. Vollmann-Zwerenz, A.; Leidgens, V.; Feliciello, G.; Klein, C.A.; Hau, P. Tumor Cell Invasion in Glioblastoma. *Int. J. Mol. Sci.* **2020**, *21*, 1932. [CrossRef] [PubMed]
37. Bhullar, K.S.; Lagarón, N.O.; McGowan, E.M.; Parmar, I.; Jha, A.; Hubbard, B.P.; Rupasinghe, H.P.V. Kinase-Targeted Cancer Therapies: Progress, Challenges and Future Directions. *Mol. Cancer* **2018**, *17*, 48. [CrossRef]

**Disclaimer/Publisher’s Note:** The statements, opinions and data contained in all publications are solely those of the individual author(s) and contributor(s) and not of MDPI and/or the editor(s). MDPI and/or the editor(s) disclaim responsibility for any injury to people or property resulting from any ideas, methods, instructions or products referred to in the content.

## Article

# Influence of Lenvatinib on the Functional Reprogramming of Peripheral Myeloid Cells in the Context of Non-Medullary Thyroid Carcinoma

Chunying Peng<sup>1</sup>, Katrin Rabold<sup>1</sup>, Mihai G. Netea<sup>2,3</sup>, Martin Jaeger<sup>2</sup> and Romana T. Netea-Maier<sup>1,\*</sup>

<sup>1</sup> Department of Internal Medicine, Division of Endocrinology, Radboud University Medical Center, 6525 GA Nijmegen, The Netherlands

<sup>2</sup> Department of Internal Medicine and Radboud Center for Infectious Diseases, Radboud University Medical Center, 6525 GA Nijmegen, The Netherlands

<sup>3</sup> Department of Immunology and Metabolism, Life and Medical Sciences Institute, University of Bonn, 53115 Bonn, Germany

\* Correspondence: romana.netea-maier@radboudumc.nl; Tel.: +31-24-3614599

**Abstract:** Lenvatinib is a multitarget tyrosine kinase inhibitor (TKI) approved for the treatment of several types of cancers, including metastatic differentiated thyroid cancer (DTC). The intended targets include VEGFR 1–3, FGFR 1–4, PDGFR $\alpha$ , RET, and KIT signaling pathways, but drug resistance inevitably develops and a complete cure is very rare. Recent data has revealed that most of the TKIs have additional ‘off-target’ immunological effects, which might contribute to a protective antitumor immune response; however, human cellular data are lacking regarding Lenvatinib-mediated immunomodulation in DTC. Here, we investigated in ex vivo models the impact of Lenvatinib on the function of immune cells in healthy volunteers. We found that monocytes and macrophages were particularly susceptible to Lenvatinib, while neutrophils and lymphocytes were less affected. In tumor-immune cell co-culture experiments, Lenvatinib exerted a broad inhibitory effect on the proinflammatory response in TC-induced macrophages. Interestingly, Lenvatinib-treated cells had decreased cellular M2 membrane markers, whereas they secreted a significantly higher level of the anti-inflammatory cytokine IL-10 upon LPS stimulation. In addition, prolonged exposure to Lenvatinib impaired macrophages survival and phenotypical differentiation, which was accompanied by remarkable morphological changes and suppressed cellular metabolic activity. These effects were mediated by myeloid cell-intrinsic mechanisms which are independent of Lenvatinib’s on-target activity. Finally, using specific inhibitors, we argue that dual effects on p38 MAPK and Syk pathways are likely the underlying mechanism of the off-target immunological effects we observed in this study. Collectively, our data show the immunomodulatory properties of Lenvatinib on human monocytes. These insights could be harnessed for the future design of novel treatment strategies involving a combination of Lenvatinib with other immunotherapeutic agents.

**Citation:** Peng, C.; Rabold, K.; Netea, M.G.; Jaeger, M.; Netea-Maier, R.T. Influence of Lenvatinib on the Functional Reprogramming of Peripheral Myeloid Cells in the Context of Non-Medullary Thyroid Carcinoma. *Pharmaceutics* **2023**, *15*, 412. <https://doi.org/10.3390/pharmaceutics15020412>

Academic Editor:  
Francesca Musumeci

Received: 15 December 2022  
Revised: 21 January 2023  
Accepted: 24 January 2023  
Published: 26 January 2023

**Keywords:** tyrosine kinase inhibitors; innate immunity; thyroid cancer; tumor-associated macrophages; cytokines



**Copyright:** © 2023 by the authors. Licensee MDPI, Basel, Switzerland. This article is an open access article distributed under the terms and conditions of the Creative Commons Attribution (CC BY) license (<https://creativecommons.org/licenses/by/4.0/>).

## 1. Introduction

Differentiated thyroid cancer (DTC) constitutes the majority of thyroid carcinomas (TC) worldwide. Generally, treatment with surgery and radioactive iodine are effective for most cases. However, up to 15% of patients develop radioiodine-refractory metastatic disease (RAI-refractory-DTC) and have poor long-term prognosis [1]. Currently, the only therapeutic option available for these patients is systemic molecular targeted therapy, which is represented by tyrosine kinase inhibitors (TKIs). Lenvatinib, a multitargeted TKI against VEGFR 1–3, FGFR 1–4, PDGFR $\alpha$ , RET, and KIT signaling networks, has been approved for the treatment of metastatic DTC since 2015. Despite positive results from a



SELECT trial, in a real-world setting, response to treatment differs among patients [2,3]. Oncological drug development is a time- and cost-consuming task, yet a high frequency of secondary mutations and paradoxical activation of alternative pathways often leads to drug resistance [3–5]. Therefore, innovative strategies to fully assess the antitumor activity of Lenvatinib are urgently needed.

Beyond targeting oncogenesis and angiogenesis processes, tumor immunotherapy remains a highly attractive yet not fully operational approach to treatment. Recent advances in immune checkpoint inhibitors (ICIs) offer a promising approach to achieve durable improvement by remobilizing the immune system against tumor proliferation and metastasis. However, the efficacy of ICIs is largely dependent on an immunogenic tumor microenvironment (TME), and, to date, ICI monotherapy has been proved effective only in a minority of solid cancers, as it largely blunted by the immunosuppressive factors with TME [6–8]. Myeloid cells constitute a highly plastic and heterogenous cell population in the tumor milieu and are often hijacked and reprogrammed by malignant cells to facilitate disease progression [9]. Notably, tumor-associated macrophages (TAMs) identified in advanced DTC display an immunosuppressive and tumor-promoting phenotype, and increased TAMs infiltration is correlated with poor prognosis [10–12]. This, in turn, makes them suitable targets for therapeutic intervention [13]. Interestingly, there has been emerging evidence indicating that most TKI therapies exert additional immunological effects via tumor intrinsic or extrinsic mechanisms [14–18]. Part of the immunomodulatory properties could be explained by their anti-angiogenesis effects via direct binding to the primary targets VEGFRs, which is also known as on-target activity. It should be noted that many FDA-approved TKIs interact with undesigned kinases/proteins expressed by healthy cells, termed as off-target effects. Interestingly, these off-target effects could lead to beneficial drug repurposing if the underlying mechanism could be characterized [19].

Recent results from different murine models revealed that an intact immune system was an essential prerequisite for the Lenvatinib-mediated tumor killing activity, and the combination with anti-PD-1 therapy significantly improved animal survival [20–22]. This is indicative of possible Lenvatinib-mediated immunomodulation, mainly involving the adaptive immune system. However, thus far, little has been known about the role of myeloid cells in these effects and how such a mechanism can be leveraged to improve clinical outcomes. Therefore, in this study, we set out to study whether Lenvatinib modulates the immune system in the context of TC and the potential mechanisms mediating these effects. This knowledge could contribute to the development of combination treatment strategies to enhance its effectivity and reduce toxicity. Our data show that *ex vivo* Lenvatinib treatment induced functional and metabolic reprogramming in circulating monocytes obtained from healthy volunteers, and this was mediated via dual inhibition of the p38 MAPK and Syk pathways.

## 2. Materials and Methods

### 2.1. Monocyte Isolation

Peripheral blood mononuclear cells (PBMCs) were isolated by density gradient centrifugation with Ficoll-Paque (GE healthcare, Diegem, Belgium) from buffy coats obtained from the Sanquin bloodbank, Nijmegen, The Netherlands. Percoll-monocyte enrichment was performed as previously described [23]. Briefly, PBMCs were layered on top of a hyper-osmotic Percoll solution, and the interphase layer was collected after centrifugation. Cells were resuspended in RPMI culture medium (Life Technologies, Carlsbad, CA, USA) supplemented with pyruvate (1 mM), glutamine (2 mM), gentamicin (50 µg/mL), HEPES (10 mM), glucose (5 mM), and 10% human pooled serum (HPS). In selected experiments, highly purified monocytes were obtained from PBMCs through negative selection using a human pan monocyte isolation kit, following the manufacturer's instruction (Miltenyi Biotec, Bergisch Gladbach, Germany).

## 2.2. Neutrophil Isolation and ROS Production Analysis

Neutrophil isolation and functional analysis were performed as previously described [24]. EDTA-anticoagulated peripheral blood was collected from healthy donors with informed consent. After density-gradient centrifugation, red blood cells were lysed with hypotonic buffer, and the purity of the remaining neutrophils was measured on a Sysmex XN-450 Hematology Analyzer (Sysmex Corporation, Kobe, Japan). Reactive oxygen species (ROS) assays were performed with freshly isolated neutrophils using a luminescence assay in quadruplicates. A total of 200,000 neutrophils per well were added into a 96-well white assay plate (Corning, Corning, NY, USA). Due to the relatively brief lifespan of neutrophils, ROS production was measured after 1 h preincubation of Lenvatinib. Cells were stimulated with 0.5 µg/mL of phorbol myristate acetate (PMA) or plasma-opsonized Zymosan A (Sigma-Aldrich, St. Louis, MO, USA) at a concentration of 1 mg/mL. Luminol (Sigma-Aldrich) was added with a final concentration of 0.1 mM, and chemiluminescence was measured at a wavelength of 425 nm every 142 s for 1 h.

## 2.3. Cell Culture, Viability Test, and Stimulation

Several Lenvatinib concentrations within the clinically achievable dose range (100 nM to 1 µM) were tested in our experimental setup with both PBMCs and monocytes. Cell viability was determined by flowcytometry using fixable viability dye (FVD) eFlour 780 (Invitrogen, Carlsbad, CA, USA). After 24 h of incubation with Lenvatinib, the cells were labelled with FVD for 30 min and stained with surface marker. CD14<sup>+</sup> viable cells were gated for analysis.

Cells stimulation was performed with  $5 \times 10^5$  PBMCs/well in 96-well round-bottom plates or  $1 \times 10^5$  Percoll-enriched monocytes/well in 96-well flat-bottom plates. After 24 h of preincubation with Lenvatinib/DMSO, the cells were stimulated with  $1 \times 10^6$  mL of heat-killed *Candida albicans* for 7 days or 10 ng/mL of LPS for 24 h. Supernatant was collected and stored at  $-20$  °C until measurement.

Three TC cell lines were used for co-culture assay; these were characterized by different pathological types and mutation status, namely, TPC-1 (RET/PTC rearrangement), BCPAP (BRAF V600E mutation), and FTC-133 (PTEN deficient). All cancer cell lines were grown in RPMI 1640 Dutch modification culture medium supplemented with 10% Fetal Bovine Serum. ThinCert™ cell culture inserts were placed in the 24-well plate to create the co-culture setting (Greiner Bio-One GmbH, Kremsmünster, Austria). Cell counts were determined with a Coulter particle counter (Beckman Coulter Inc., Brea, CA, USA). A total of 50,000 TPC-1 cells (or the other TC cell lines, as indicated) were added to the trans-well inserts (the upper chamber). The same number of monocytes were added into trans-well inserts as the control. After overnight attachment, TC cell lines were co-incubated with  $5 \times 10^5$  monocytes in the lower chamber in 500 µL of medium containing 1 µM of Lenvatinib or DMSO vehicle control. In some experiments, tumor cells were pre-treated with Lenvatinib in serum-free medium for 6 h. Prior to co-culture, medium containing Lenvatinib was removed, cells were washed with PBS, and fresh medium without Lenvatinib was added into the upper and lower chambers; this was termed as the pre-treatment group. After 24 h of co-culture, the trans-well inserts were discarded, and monocytes were stimulated as previously described.

GM-CSF/M-CSF differentiated macrophages were generated by culturing Percoll-enriched monocytes in 10% HPS RPMI medium containing GM-CSF (10 ng/mL, Miltenyi) or M-CSF (50 ng/mL, Miltenyi) for 6 days. Cells were seeded with  $2.5 \times 10^6$  per well in a 6-well plate for RNA, Western blot, and seahorse experiments;  $5 \times 10^5$  cells per well in a 24-well plate for flowcytometry analysis. The cells were detached by gentle scraping and the concentration was adjusted based on the results of flowcytometry (Beckman Coulter Inc.).

## 2.4. Flow Cytometry Analysis

Adherent monocytes/macrophages were harvested by gentle scraping, followed by viability staining. The cells were preincubated at 4 °C for 10 min with staining buffer

containing 2% HPS prior to mAb labelling to CD14, CD163, CD206, CD64, CD86, HLA-DR. Intracellular TNF- $\alpha$  was measured in macrophages stimulated for 6 h with LPS (10 ng/mL) in the presence of Golgi plug (BD Bioscience, Franklin Lakes, CA, USA). The cells were fixed and permeabilized (Invitrogen, Carlsbad, CA, USA) followed by incubation with mAb to TNF- $\alpha$ . For the T cell proliferation assay, PBMCs were loaded with CellTrace violet (Invitrogen, Carlsbad, CA, USA) per the manufacturer's instructions and cultured for 7 days. The CellTrace dilution signal was analyzed on gated CD3<sup>+</sup> cells. Data were acquired using Cytotflex (Beckman Coulter Inc.) and analyzed with FlowJo V10 software (Tree Star, Inc., Ashland, OR, USA). The results were presented as geometric mean fluorescence intensity (gMFI) or as the percentage of positive cell populations.

### 2.5. Cytokine Measurements

Cytokine (TNF- $\alpha$ , IL-6, IL-10, IL-17, IFN- $\gamma$ , IL-22) concentrations in supernatant were determined using a commercial ELISA kit (R&D System, Minneapolis, MN, USA), following the instructions of the manufacturer.

### 2.6. Metabolic Measurements

GM-CSF differentiated macrophages were cultured as described above and detached on Day 6. A total of 50,000 cells/well were seeded onto overnight-calibrated cartridges in assay medium (DMEM supplemented with 1 mM of pyruvate, 2 mM of L-Glutamine, and 1 mM of glucose for the Mito Stress Test; DMEM supplemented with 1 mM of L-Glutamine for the Glyco Stress Test, pH = 7.4) and incubated for 1 h in a non-CO<sub>2</sub> corrected incubator at 37 °C. The oxygen consumption rate (OCR) and extracellular acidification rate (ECAR) were analyzed using the Mito Stress and Glyco Stress Test kit in an XFp analyzer (Seahorse bioscience, Copenhagen, Denmark). The Mito Stress Test was performed with sequential injections of mitochondrial respiration inhibitors at final concentrations of 1  $\mu$ M of oligomycin, 1  $\mu$ M of FCCP, 0.5  $\mu$ M of Rotenone/Antimycin A. The Glyco Stress Test was performed with 2-DG (50 mM) in the presence of glucose (10 mM). Each condition was tested in 5 replicates. Lactate concentration was measured in serum-free medium using Amplex Red Lactate oxidase assay (Sigma-Aldrich).

### 2.7. RT-qPCR

Total RNA was extracted with the RNeasy Mini kit (Qiagen, Hilden, Germany) and reverse-transcribed into cDNA with the iScript™ kit (Bio-Rad, Hercules, CA, USA). A real-time PCR was performed with the SYBR Green assay (Applied Biosystems, Foster City, CA, USA). Relative quantification was performed using the 2<sup>- $\Delta\Delta$ Ct</sup> method, and RPL37A was used as the housekeeping gene.

### 2.8. Western Blotting

Monocytes or GM-CSF differentiated macrophages were cultured in 6-well plates and lysed with RIPA buffer for Western blot. Protein concentration was determined by a BCA assay. An amount of 20  $\mu$ g of proteins was loaded onto 10-well pre-casted gradient gels (4–15%) (Bio-Rad). Protein was transferred using the Trans-Blot Turbo Transfer system (Bio-Rad), after which PVDF membrane was incubated overnight at 4 °C with monoclonal antibodies against VEGFR1 and FGFR1.  $\beta$ -actin were used to normalize the protein expression.

### 2.9. Kinase Inhibition Experiments

Kinase inhibitors SB 202190 (p38 MAPK inhibitor), U0126 (ERK1/2 inhibitor), SP 600125 (JNK inhibitor), and R406 (Syk inhibitor) (Sigma-Aldrich) were dissolved in sterile DMSO and stored at -20 °C. Monocytes were treated with kinase inhibitors (0, 1  $\mu$ M, 10  $\mu$ M) with or without Lenvatinib (1  $\mu$ M) for 4 h or 24 h before LPS stimulation. Cytokine production was determined as previously described.

### 2.10. Statistical Analysis

The statistical analysis was performed with Prism 9 (GraphPad Software Inc., La Jolla, CA, USA). Nonparametric Wilcoxon matched-pair tests were used to compare means. Data are shown as means  $\pm$  SEM. \*  $p < 0.05$ , \*\*  $p < 0.01$ , \*\*\*  $p < 0.001$ .

## 3. Results

### 3.1. Lenvatinib Modulates the Function of Monocytes

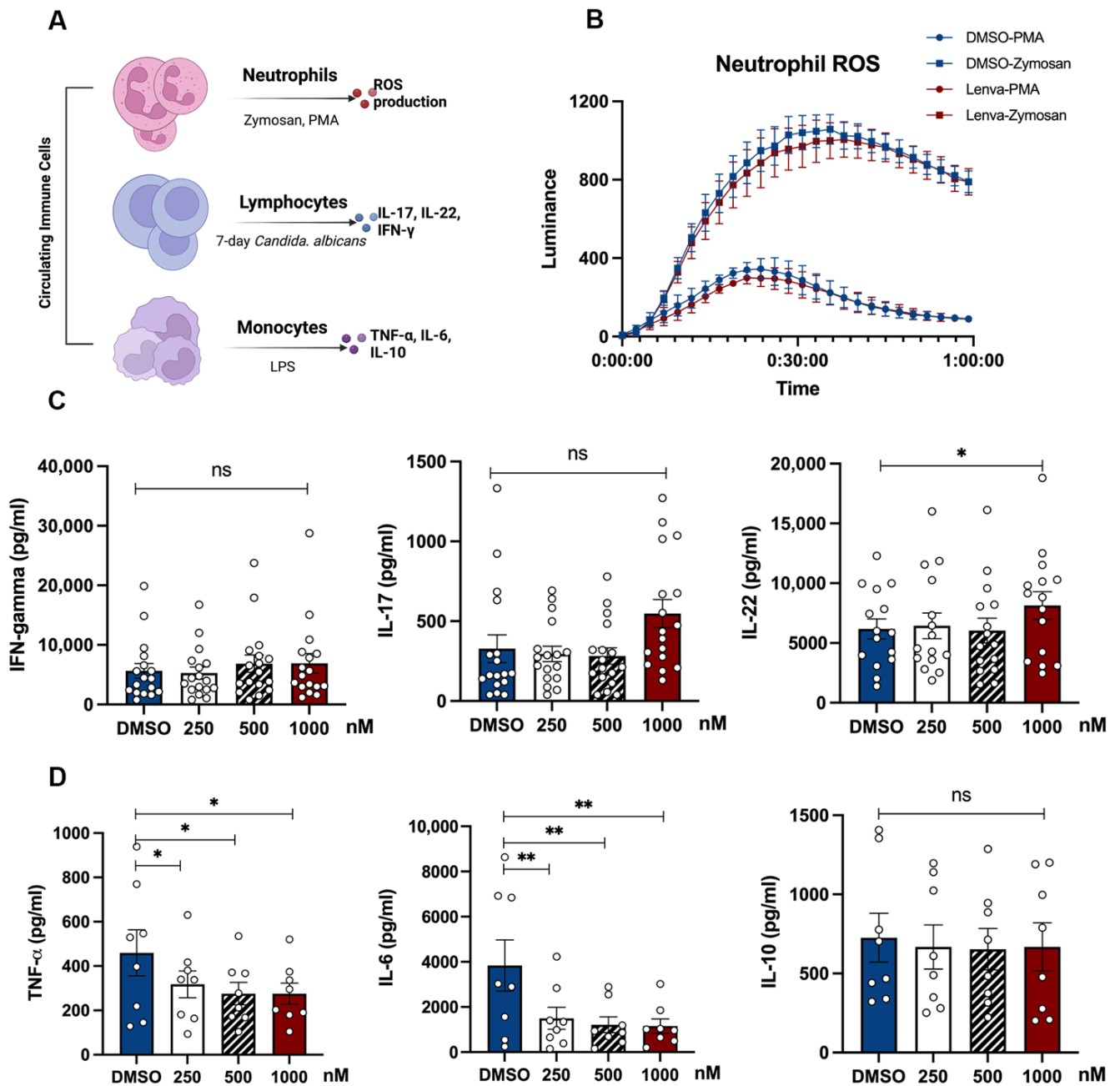
As a first step to evaluate whether Lenvatinib interferes with immune cell function, we performed a dose–response test on human circulating immune cells in vitro. The physiologically relevant dose range was determined based on pharmacokinetic data from Phase I/II clinical trials. Plasma maximum and trough concentrations were reported as 598.0 ng/mL (1401 nM) and 33.9 ng/mL (79.4 nM), respectively [25,26]; hence, 100 nM to 1  $\mu$ M was deemed as a clinically meaningful dose range in our study. The immune response was determined by measuring the ROS production from neutrophils, and the secretion of monocyte-derived (TNF- $\alpha$ , IL-6) and lymphocyte-derived (IL-17, INF- $\gamma$ , IL-22) cytokines upon stimulation (Figure 1A).

No significant changes in neutrophil ROS production were observed, either by pathogen-specific (zymosan) or non-specific (PMA) stimulation (Figure 1B). Moreover, no spontaneous cytokine secretion was detected in monocytes or PBMCs incubated with Lenvatinib for 24 h or 7 days. Interestingly, the production of TNF- $\alpha$  and IL-6 elicited by LPS was largely attenuated by Lenvatinib in a dose-dependent manner (Figure 1C). In contrast, no detectable effect on Lenvatinib on either T cell proliferation (Supplementary Figure S1) or IL-17 and INF- $\gamma$  production was observed after a 7-day *Candida* stimulation, except a slight increase in IL-22 at the highest Lenvatinib concentration (Figure 1D). Taken together, these data suggest that monocytes are particularly susceptible to Lenvatinib treatment, whereas lymphocytes and neutrophils are less affected.

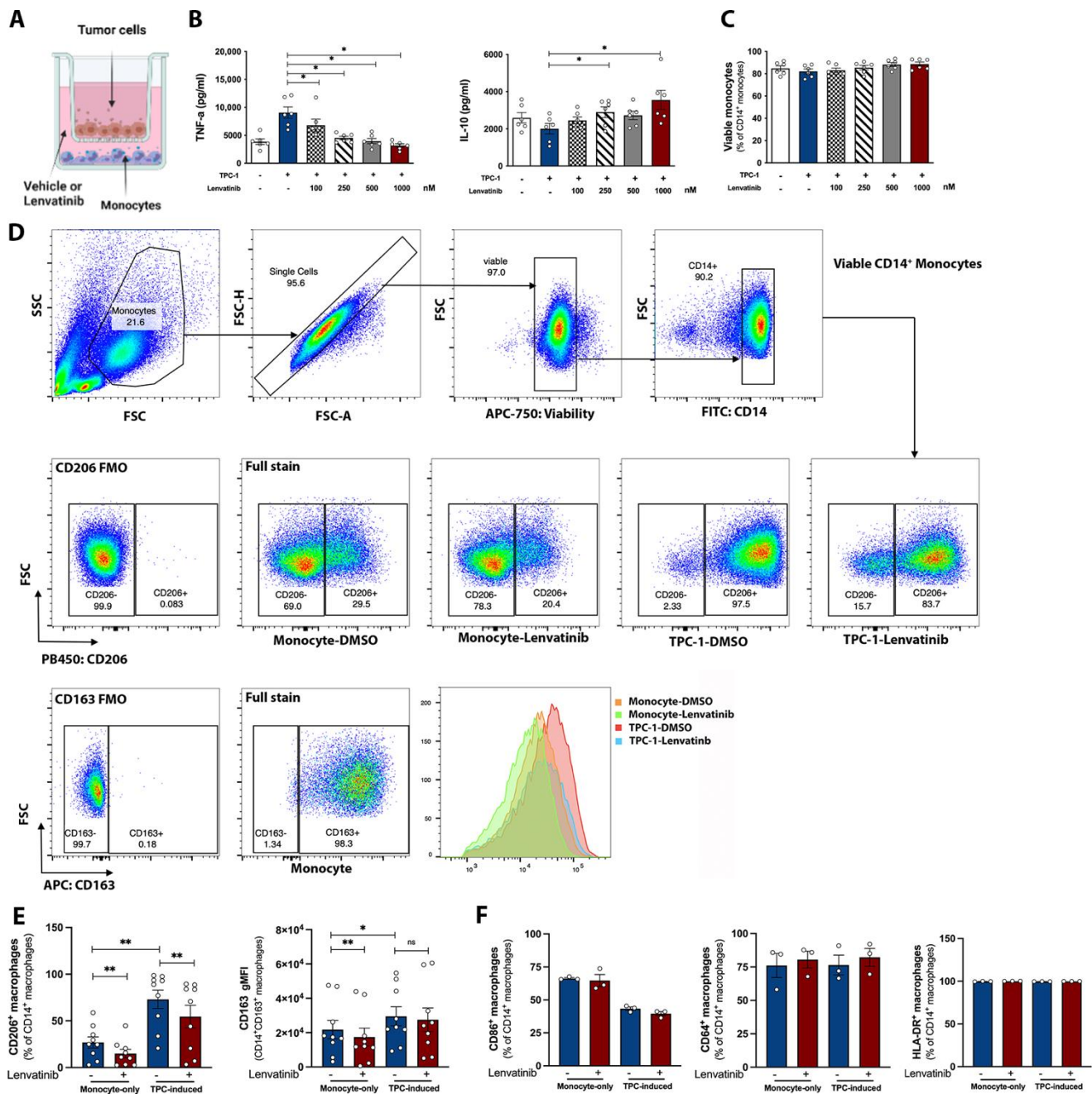
### 3.2. Lenvatinib Partially Reverses the TC-Induced Monocyte Phenotype

Noting that Lenvatinib affects monocytes stimulated with exogenous ligands, we further investigated whether the functional rewiring of monocytes in the context of TC is also affected by Lenvatinib treatment. Therapeutic perturbation of the TC secretome by Lenvatinib might interfere with the functional and phenotypic differentiation of TAMs [27]. To test this hypothesis, Lenvatinib was added into the trans-well co-culture system, which aims to mimic the cell-to-cell communication within TME.

In these sets of experiments, we observed the spontaneous production of IL-6 and IL-8 from the TPC-1 cell line, whereas TNF- $\alpha$  and IL-10 were below the detection limit (data not shown). To exclude the possibility of any influence of tumor-derived cytokines on the interpretation of monocytes' immune response, TNF- $\alpha$  and IL-10 were used as the major readout of cytokine response. In agreement with previously published data [28], after 24 h of co-culture with TPC-1 cells, monocytes showed a higher expression of immunosuppressive surface markers, CD163 and CD206. Concomitantly, a pro-inflammatory cytokine response was observed, which was demonstrated as an elevated TNF- $\alpha$  and downregulated IL-10 level (Figure 2B). This points towards a mixed M1/M2 phenotype which resembles TAMs [29]. Having validated the efficacy of the co-culture model, we applied this method to evaluate the role of Lenvatinib in regulating TAMs induction. Interestingly, Lenvatinib significantly attenuated TNF- $\alpha$  production, while it increased IL-10 release. Furthermore, the expression of the M2 surface marker, CD206, was diminished by Lenvatinib, which was shown as a lowered percentage of CD206<sup>+</sup> CD14<sup>+</sup> cells. CD163 is generally expressed on almost all the CD14<sup>+</sup> monocytes at baseline; however, the signal intensity was attenuated by Lenvatinib (Figure 2D). In the meantime, the M1 markers (CD64, CD86, and HLA-DR) remained unchanged (Figure 2E). Flowcytometric cell discrimination and viability measurements revealed that cell viability was not affected after 24 h exposure to Lenvatinib within the clinically relevant dose range (100 nM to 1  $\mu$ M) (Figure 2C).

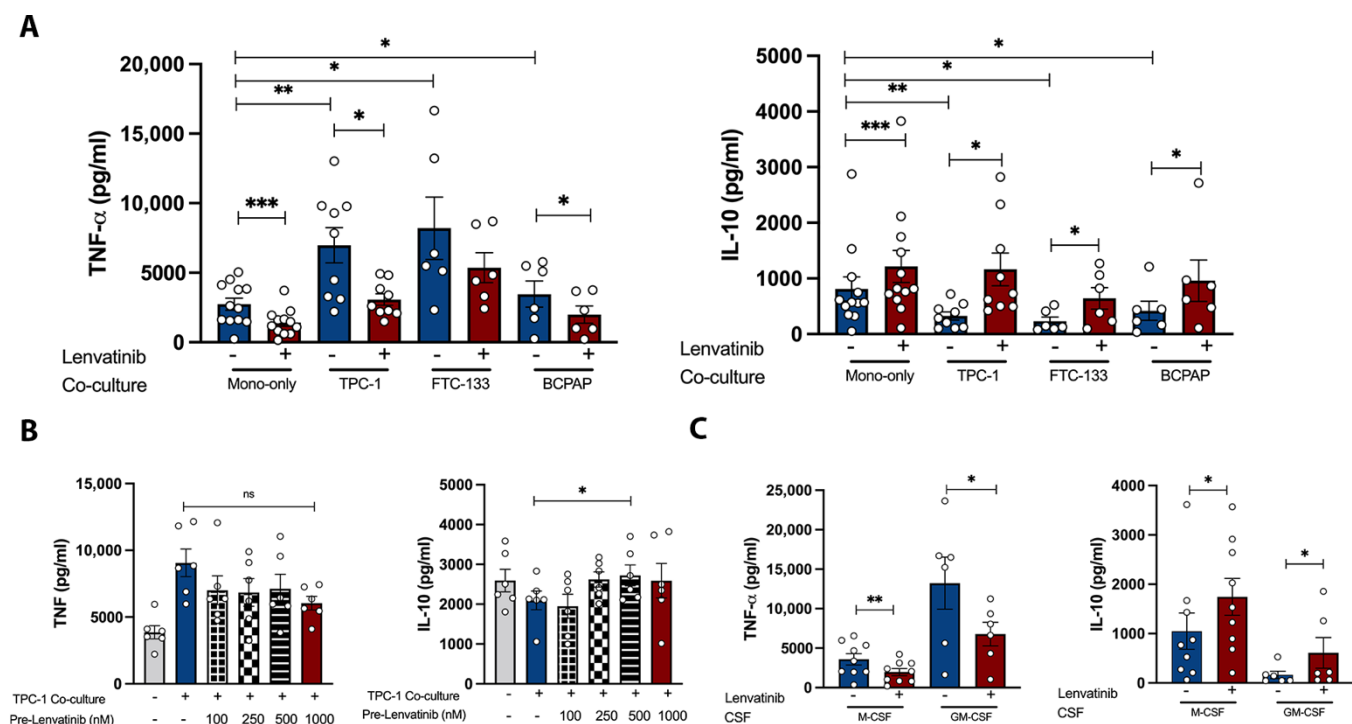


**Figure 1.** Lenvatinib modulates in vitro monocyte-derived cytokine secretion in dose-response experiments. (A) Schematic diagram of the dose-response test. Freshly isolated neutrophils were stimulated with opsonized zymosan or PMA for the measurement of ROS production, after brief exposure to Lenvatinib (1  $\mu$ M) for 1 h. PBMCs from healthy donors were incubated with Lenvatinib with indicated concentrations for 24 h, after which cells were stimulated with LPS or *Candida albicans*. Cytokines levels in supernatants were determined by ELISA. (B) ROS production from neutrophils; data represent mean  $\pm$  SME at each time point, n = 6. (C) Lymphocyte-derived cytokines (IFN- $\gamma$ , IL-17, and IL-22) after 7-day *Candida albicans* stimulation, n = 15. (D) Monocyte-derived cytokines (IL-6, TNF- $\alpha$ , IL-10) after 24 h of LPS stimulation, n = 8. The bar graphs indicate mean  $\pm$  SME; each dot represents one healthy donor. \* p < 0.05, \*\* p < 0.01 by nonparametric Wilcoxon matched-pair tests; ns, not significant; PMA, phorbol myristate acetate; ROS, reactive oxygen species.



**Figure 2.** Lenvatinib interferes with monocytes' functional rewiring in co-culture experiments. (A) Schematic diagram of the co-culture experiments. (B) Cytokine secretion from TPC-1 induced monocytes treated with indicated concentrations of Lenvatinib; monocytes cultured in RPMI were included as the baseline control,  $n = 6$ . (C) Viability of monocytes after 24 h exposure to Lenvatinib; percentage of viable CD14<sup>+</sup> cells were gated for statistical analysis,  $n = 6$ . (D) Expression of M2 markers in TPC-1-induced monocytes. The upper panel shows the gating strategy to identify the viable CD14<sup>+</sup> monocytes. Identification of CD206<sup>+</sup> and CD163<sup>+</sup> subsets within viable CD14<sup>+</sup> monocytes was based on FMO controls. The lower panel shows the representative dot plot and histogram from one donor. (E) Quantification of the percentage of CD206<sup>+</sup> subsets within CD14<sup>+</sup> monocytes and fluorescence intensity of CD163 signal on CD14<sup>+</sup>CD163<sup>+</sup> monocytes,  $n = 6$ . (F) Expression of M1 markers (CD86, CD64, and HLA-DR),  $n = 3$ . The bar graphs indicate mean  $\pm$  SME; each dot represents one healthy donor. \*  $p < 0.05$ , \*\*  $p < 0.01$  by nonparametric Wilcoxon matched-pair tests. FMO, fluorescence minus one control; gMFI, geometric mean fluorescence intensity.

The fact that Lenvatinib concomitantly affected monocyte function raised the question regarding to what extent the alteration in TPC-1 secretome could explain the immunological effects we observed. To address this, we tested two additional TC cell lines, FTC-133 and BCPAP, in the co-culture setting. Previous reports have shown that the growth rate of TPC-1, which bears a Lenvatinib-targeted RTK mutation-RET rearrangement, is strongly inhibited by Lenvatinib, whereas FTC-133 and BCPAP, negative for Lenvatinib-targeted mutations, are not sensitive to the drug treatment [30]. Strikingly, similar changes in cytokine production caused by Lenvatinib were observed across all three co-cultures (Figure 3A). On the other hand, a TC-pre-treatment group was included as the control, where only TPC-1 cells had been pre-exposed to Lenvatinib for 6 h before starting the co-culture. Interestingly, incubation with Lenvatinib-pre-treated TC cells resulted in a similar (albeit less strong) effect on cytokine production, suggesting that Lenvatinib partially abolished the pro-inflammatory and tumor-promoting phenotype induced by TPC-1 (Figure 3B). These data demonstrated that the tumor cell-mediated mechanism alone was insufficient to explain the immunomodulatory nature of Lenvatinib in the co-culture experiments, arguing for the direct immunological effects of Lenvatinib on immune cells. These results were further supported by the similar results from GM-CSF- or M-CSF-primed monocytes in the absence of tumor cells (Figure 3C), which is suggestive of a more critical role of the monocyte-intrinsic mechanism underlying this effect.

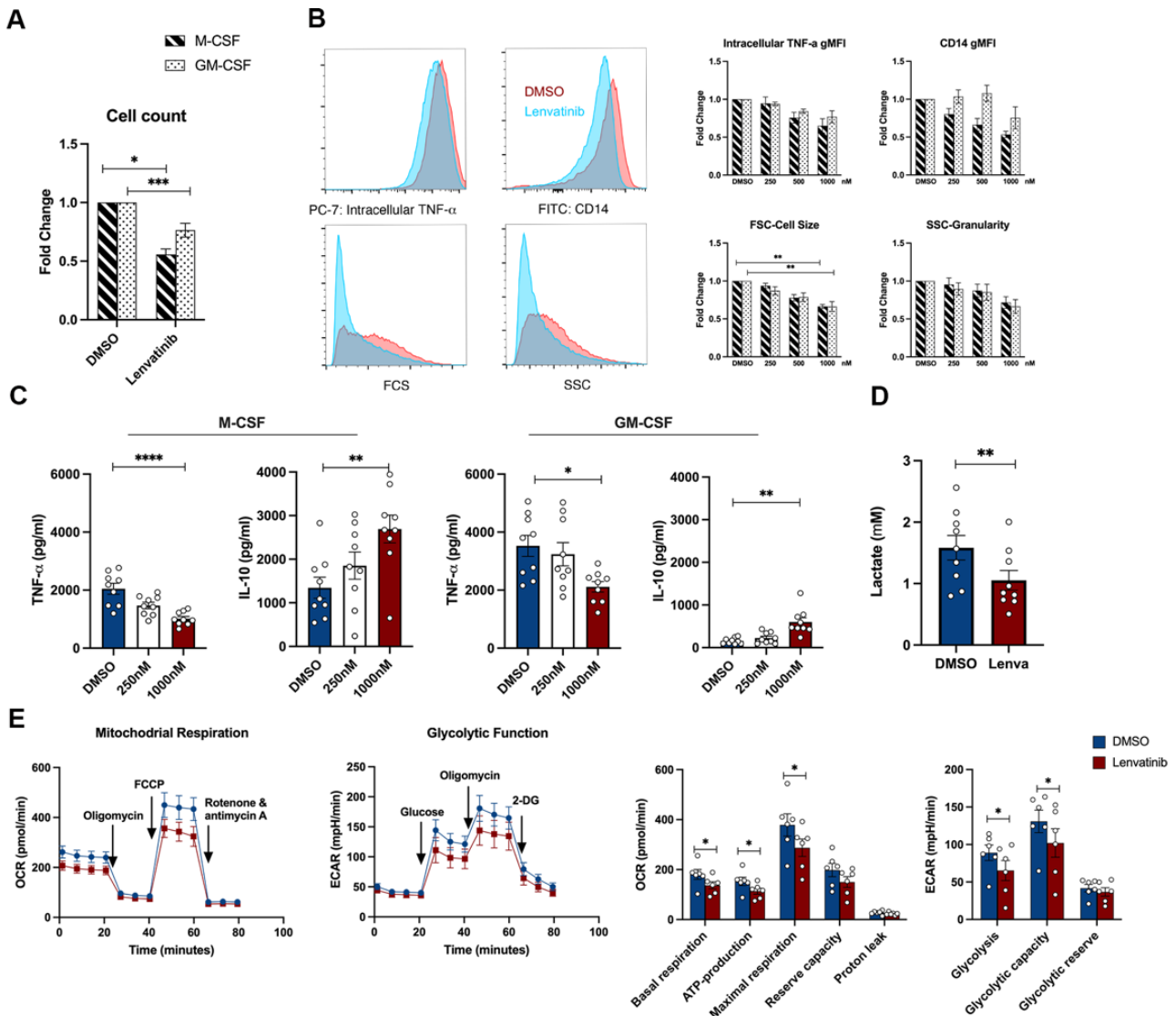


**Figure 3.** Similar patterns of cytokine production caused by Lenvatinib in different experimental settings. (A) In vitro generation of tumor-associated macrophages with 3 TC cell lines. (B) Co-culture experiments with TPC-1 cell line pretreated by Lenvatinib for 6 h. (C) Monocytes primed by GM-CSF and M-CSF for 24 h,  $n = 6$ . The bar graphs indicate mean  $\pm$  SME; each dot represents one healthy donor. \*  $p < 0.05$ , \*\*  $p < 0.01$ , \*\*\*  $p < 0.001$  by nonparametric Wilcoxon matched-pair tests.

### 3.3. Prolonged Exposure to Lenvatinib Affects Macrophage Survival and Differentiation

We next investigated whether Lenvatinib could affect the survival and phenotypic differentiation of macrophages. To address this, monocytes were cultured with either GM-CSF (M1 differentiation) or M-CSF (M2 differentiation) for 6 days in the presence of Lenvatinib or a DMSO control. We found that long-term exposure to Lenvatinib impaired macrophage survival, with M-CSF-induced macrophages being more vulnerable to

Lenvatinib, resulting in approximately half of the cells being lost during the differentiation process (Figure 4A). More importantly, we observed drastic morphological changes in Lenvatinib-treated macrophages. As indicated in the flowcytometry FSC channel, the cells were significantly smaller (Figure 4B), suggesting the potential impairment of macrophage differentiation.



**Figure 4.** Morphological, functional, and metabolic changes in Lenvatinib-treated macrophages. (A) Overall macrophage survival determined by flowcytometry; the cell counts of macrophages were gated on FCS-A and SSC-A (n = 11). (B) Left panel indicates representative histogram of the parameters, including intracellular TNF, CD14 expression, cell size (FSC), and granularity (SSC), analyzed by flowcytometry from one donor. The right panel shows the corresponding quantification of gMFI, n = 6. (C) Cytokine production from GM-CSF/M-CSF primed macrophages, n = 9. (D) Lactate production from GM-CSF-induced macrophages after 24 h of stimulation with LPS, n = 6. (E) Analysis of ECAR and OCR from GM-CSF-polarized macrophages was performed with a seahorse XF analyzer. The left figure shows the OCR and ECAR profiles for macrophages exposed to Lenvatinib or DMSO vehicle control. The right figure shows mitochondrial bioenergetic and glycolytic parameters calculated from OCR and ECAR (n = 6). The bar graphs indicate mean ± SME; each dot represents one healthy donor. \* p < 0.05, \*\* p < 0.01, \*\*\* p < 0.001, \*\*\*\* p < 0.0001 by nonparametric Wilcoxon matched-pair tests. FSC, forward scatter; ECAR, extracellular acidification rate; OCR, oxygen consumption rate; SSC, side scatter.



Cytokine production was determined after the adjustment of cell concentration, despite a prototypical anti- and pro-inflammatory cytokine production pattern upon LPS stimulation from GM-CSF/M-CSF primed macrophages. The modulation of TNF- $\alpha$  and IL-10 production induced by Lenvatinib was similar in both groups (Figure 4C). This was further supported by intracellular TNF- $\alpha$  level measurement (Figure 4B), recapitulating our observations from monocytes.

Metabolic reprogramming shapes a distinct immune response to stimulus [31]. To explore the cellular metabolic mechanisms that might contribute to the cytokine production pattern, we quantified the indicators of mitochondrial respiration and glycolytic capacity by oxygen consumption rate (OCR) and extracellular acidification rate (ECAR) using Seahorse. Lenvatinib-treated macrophages displayed a trend towards suppressed metabolic activities, which is shown as lower basal and maximal respiration, lower glycolysis activity and glycolytic capacity, while the glycolytic reserve remains unchanged (Figure 4E). Consistent with these findings, the Lenvatinib-treated group produced lower amounts of lactate upon 24 h of LPS challenge (Figure 4D), which was indicative of general defects in both oxidative phosphorylation and glycolytic activities [32].

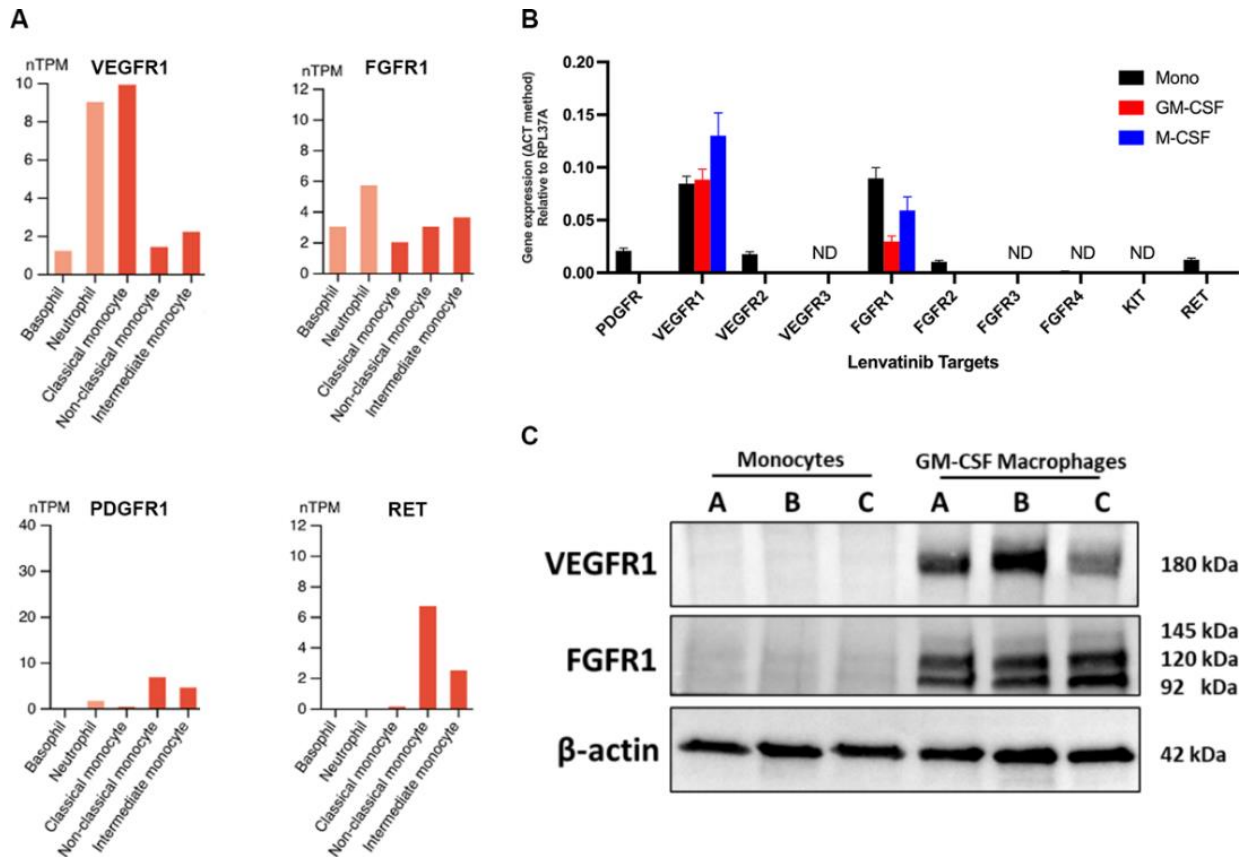
Taken together, these data demonstrate that Lenvatinib exerts multifaceted inhibitory effects on macrophage survival and maturation.

#### 3.4. The Immunological Effects on Monocytes Are Independent of the Lenvatinib-Targeted Receptor Tyrosine Kinase (RTK) Pathways

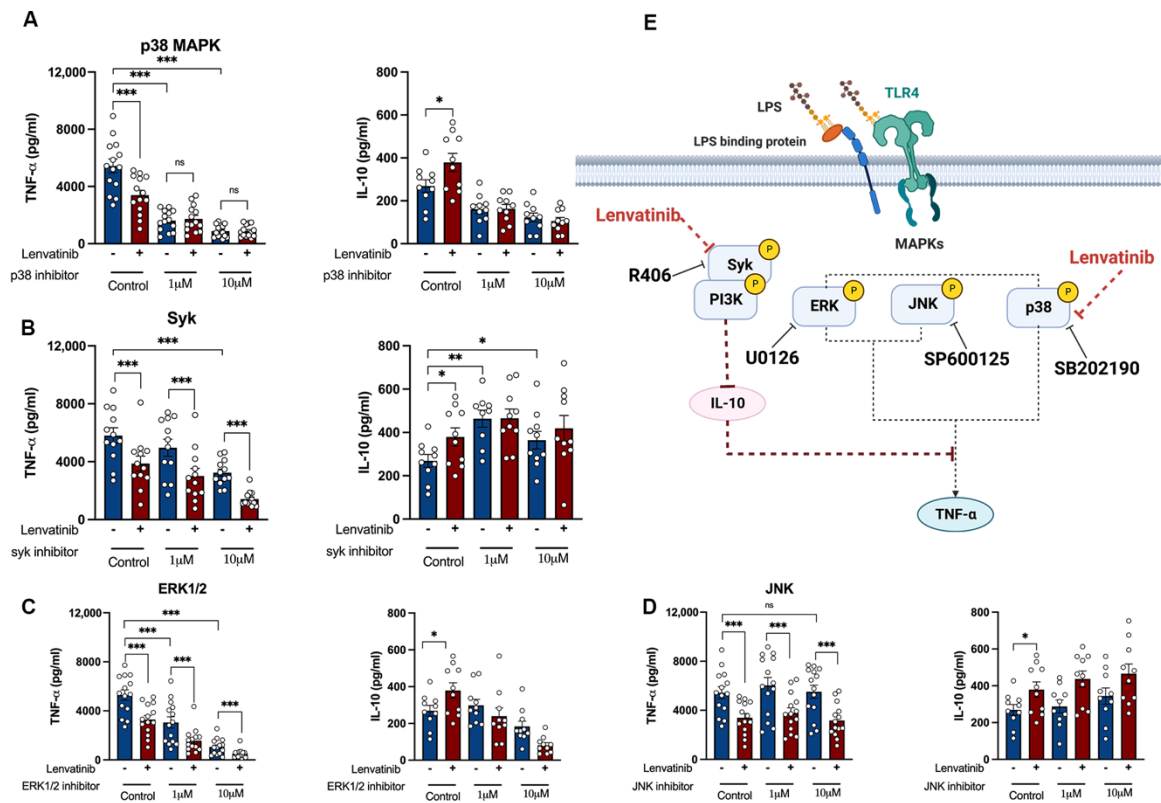
To explore the underlying mechanism of Lenvatinib-mediated immunological effects, we evaluated the expression of Lenvatinib-targeted RTKs on myeloid cells. Mining into the publicly available transcriptomic database Human Protein Atlas [33], we found that most of the Lenvatinib targets were not detected in circulating myeloid cells, except VEGFR1 and FGFR1, with a relatively low level of mRNA expression in classical monocytes, shown as normalized transcript per million (nTPM) (Figure 5A). To further validate the expression of VEGFR1 and FGFR1, we performed RT-qPCR and Western blotting using samples harvested from buffy coat monocytes and 6-day differentiated macrophages. Despite comparatively consistent mRNA expression in both monocytes and macrophages (Figure 5B), the Western blots did not show any detectable VEGFR1 and FGFR1 expression on monocytes (Figure 5C). Therefore, it is hard to explain the Lenvatinib-mediated immunomodulation by its on-target activity, pointing instead to potential off-target mechanisms.

To elucidate the potential alternative mechanisms of the action of Lenvatinib, we explored the ProteomeXchange database (dataset PXD005336), a public resource containing the target landscape of 243 clinically tested kinase drugs. The data were obtained via systemic kinase assays using four cancer cell lines [34]. Surprisingly, we found that Lenvatinib interacts with multiple unanticipated kinases (Supplementary Figure S2). Among all the additional targets, several mitogen-activated protein kinases (MAPKs) were of particular interest. The sequential induction of pro- and anti-inflammatory cytokine by LPS requires fine-tuned control via MAPKs, consisting of extracellular signal-regulated kinases 1/2 (ERK1/2), JUN N-terminal kinase (JNK), and p38 MAPKs [35–37]. In addition to the MAPK family, the tyrosine kinase Syk regulates LPS-mediated TLR4 endocytosis [38]. If the TLR4 downstream kinases are responsible for Lenvatinib-induced immunomodulation, then the blockage of a certain kinase pathway with highly selective inhibitors could potentially abolish Lenvatinib's influence on monocytes. To test this hypothesis, we combined Lenvatinib with different inhibitors against p38 MAPK, ERK1/2, JNK, and Syk, respectively [39]. As expected, the inhibition of p38 MAPK, ERK1/2, and Syk alone was able to attenuate TNF- $\alpha$  release. More interestingly, the reduction in TNF- $\alpha$  production caused by Lenvatinib was completely abrogated by concomitant p38 MAPK inhibition, whereas Lenvatinib's effect persisted in the presence of the ERK1/2, JNK, and Syk inhibitors (Figure 6A–D). Despite this, p38 MAPK blockage alone was not able to recapitulate the IL-10 response induced by Lenvatinib. Strikingly, the Syk inhibitor, R406, resulted in enhanced IL-10 production by itself, and the dual treatment of R406 plus Lenvatinib did not further increase the IL-10

level [40]. Furthermore, we observed similar effects in GM-CSF/M-CSF primed monocytes ( Supplementary Figure S3). Therefore, Lenvatinib’s ability to block p38 MAPK and Syk appears to be the possible mechanism underlying its opposing effect on TNF- $\alpha$  and IL-10 production.



**Figure 5.** The expression of Lenvatinib-targeted RTKs on monocytes. (A) Normalized transcript expression levels of 4 detectable Lenvatinib-targeted RTKs (VEGFR1, FGFR1, PDGFR, RET) from the transcriptome signatures are visualized for different peripheral myeloid cell types from Monaco et al. The panels are screenshots from the Human Protein Atlas resource. (B) Quantified Lenvatinib-targeted RTKs mRNA expression by RT-qPCR. Transcript copy number was normalized to cellular control (RPL37A). n = 6. (C) Levels of VEGFR1 and FGFR1 in the cell lysate from buffy coat monocytes and GM-CSF polarized macrophages were analyzed by Western blot, and  $\beta$ -actin was used as the loading control. Three isoforms of FGFR1 were detected with molecular weights of 92, 120, and 145 kDa. n = 3. ND, not determined; nTPM, normalized transcripts per million.



**Figure 6.** Effects of TLR4 downstream kinase inhibitors on Lenvatinib-mediated immunomodulation. (A–D) Monocytes were treated with selective inhibitors against kinases within the TLR4 signaling networks: SB 201019 as p38 MAPK inhibitor, R406 as Syk inhibitor, U0126 as ERK1/2 inhibitor, SP 600125 as JNK inhibitor. All the inhibitors were tested at two concentrations (1 μM and 10 μM), either used alone or in combination with Lenvatinib. Cytokine response was determined by ELISA after 24 h LPS stimulation. Kinase inhibitor single agent versus DMSO control was compared, and kinase inhibitor plus Lenvatinib versus kinase inhibitor alone was compared, n = 10 to 14. (E) Schematic diagram of the possible mechanism behind Lenvatinib’s off-target effect on monocytes via dual inhibition of p38 and Syk pathways. The bar graphs indicate mean ± SME; each dot represents one healthy donor. \* *p* < 0.05, \*\* *p* < 0.01, \*\*\* *p* < 0.001 by nonparametric Wilcoxon matched-pair tests. ERK, extracellular signal-regulated kinases; JNK, c-Jun N-terminal kinases; ns, not significant; p38 MAPK, p38 mitogen-activated protein kinases; Syk, spleen tyrosine kinase; TLR4, toll-like receptor 4.

**4. Discussion**

In the present study, we show that circulating monocytes are particularly vulnerable to ex vivo Lenvatinib treatment at the concentrations equivalent to pharmacological concentrations achievable during treatment, with the function of neutrophils and lymphocytes being less affected. Specifically, the induction of pro-inflammatory monocytic cytokine response was largely attenuated in the presence of Lenvatinib. Furthermore, the drug also interferes with the proinflammatory potential of TC-induced TAMs. Critically, these effects could not be explained by the drug impact on the TPC-1 tumor cells, but rather through direct effects on immune cells. The direct drug impact on monocytes is further supported by in vitro experiments of macrophage differentiation, showing effects of Lenvatinib on cell survival, morphology, cytokine response, and metabolism. Strikingly, we observed no detectable expression in the monocytes of Lenvatinib’s classical targets. On the other hand, blockage of the p38 MAPK and Syk pathways partially diminished Lenvatinib’s immunological effects. Thus, we propose that Lenvatinib directly impacts the functional status of human monocytes via non-canonical mechanisms.

Due to the importance of tumor-immune cell interaction, we initially hypothesized that Lenvatinib might interfere with TAMs-induction by an indirect tumor-instructed mechanism. Previous reports using murine models have shown that TKIs prompt tumor cells to release chemotactic factors (CXCL12 and HMGB-1) or induce immunogenic cell death, resulting in robust immune cell infiltration and tumor clearance [16,41]. Contrary to this, in our co-culture experiments, we did not observe significant differences between the settings with or without the presence of tumor cells. One of the possible explanations is that the tumor-killing capacity of Lenvatinib *in vivo* relies more on its anti-angiogenic effects, which require the presence of TME. Supporting this, clinical trials revealed that tumor response to Lenvatinib was not correlated with targeted RTK mutation status [7,42]. Therefore, we were unable to fully recapitulate the tumor response to Lenvatinib with simple two-factor co-culture experiments. Future *in vivo* studies will be required to elucidate the possible tumor-mediated mechanism.

The direct influence of Lenvatinib on monocytes was interesting and unexpected. Recent advances in drug-target interaction led to the realization that the majority of previously established TKIs bind to additional kinases, including serine-threonine kinases that are not closely related to the function and sequence of the intended targets [34,43]. However, their immunological implications remain largely unexplored, and preclinical results reflect that the immunologic effects of individual TKIs are largely drug-specific and context-dependent [19,44,45].

Lenvatinib is a multitargeted kinase inhibitor with a particularly potent activity against the VEGFR2 via type V binding model [46]. The side effects of Lenvatinib, such as hypertension, are predominantly caused by its anti-angiogenic activity [4], while no major immune-related side effects have been reported. It might be reasonable to postulate that Lenvatinib-mediated immunological effects are well tolerated by patients, yet they have been largely overlooked since the early stage of drug development [2]. No data on intratumoral Lenvatinib concentrations have been reported; thus, the working concentration in this study was based on plasma pharmacokinetic data. We selected 1  $\mu\text{M}$  as the highest non-cytotoxic concentration and observed that monocyte activation status was significantly influenced at this concentration. In line with this, a recent study also demonstrated that, compared to other immune cells, monocytes were less resistant to *in vitro* TKIs treatment [47]. Similarly, a clinical observational study also reported decreased levels of circulating TNF- $\alpha$  and IL-6 in hepatocellular carcinoma (HCC) patients after Lenvatinib treatment [48].

As for the mode of action, it appears plausible that Lenvatinib might exert inhibitory activity through p38 MAPK and Syk kinase in monocytes. We found that the inhibition of p38 by SB202190 completely abolished the effect of Lenvatinib on TNF- $\alpha$  production. In line with our findings, it has been previously described that, in tumor cells, Lenvatinib directly binds with several components within the MAPK signaling pathway, including MAP4K2, MAP4K5, MAPK14, and MAPKAPK2 [49,50]. p38 MAPK plays a pivotal role in governing macrophage alternative activation and preventing apoptosis [51,52]. Indeed, we observed the selective downregulation of M2 cell surface markers on TC-induced monocytes and significant cell loss caused by Lenvatinib during macrophage differentiation. Additionally, a recent study investigating the immunological effects of Regorafenib, another TKI used for HCC, revealed that its synergizing efficacy with anti-PD1 therapy was associated with the suppression of p38 kinase phosphorylation, which reversed the M2-like polarization of murine bone marrow-derived macrophages (BMDMs) [45], thus supporting the off-target effects via p38MAPK blockage seen in our study.

A striking aspect of the Lenvatinib-treated monocyte is the persistent elevation of IL-10 production across all the experimental settings. The high production of IL-10 and TGF- $\beta$  is a hallmark of TAMs [53]. However, seemingly counterintuitively, we did not observe the concomitant upregulation of other immunosuppressive markers in Lenvatinib-treated TC-induced monocytes, such as CD163 and CD206. The elevation of IL-10 seemed to be independent of the general immunosuppressive traits. As part of the host defense

mechanism, the induction of IL-10 occurs simultaneously with proinflammatory cytokines via shared p38 MAPK and ERK pathways [54]. The opposing effects on IL-10 and TNF- $\alpha$  production indicate additional pathways influenced by Lenvatinib treatment.

Syk is a non-receptor tyrosine kinase transmitting signals of immunoreceptors, regulating the activation of innate immunity [55,56]. We found that Syk inhibitor, R406, was the only agent that could enhance IL-10 production upon LPS stimulation, and no synergizing effect with Lenvatinib was observed. It is tempting to speculate that the Syk pathway is also involved in Lenvatinib's off-target effects. Consistent with our findings, others have shown that R406 selectively blocks the induction of IL-6 and TNF- $\alpha$ , while restoring the IL-10 production in human monocytes [40]. However, this is at odds with previous reports showing that Syk functions as a negative-feedback mechanism to limit inflammation by promoting IL-10 production [56]. Nevertheless, the Syk inhibitor we used, R406, was proposed to be potent and selective against Syk, but it also binds to several other kinases, including Salt-inducible kinase 2 (SIK2) [34]. SIK2 is one of the most common additional targets of TKIs, as revealed by large-scale drug screening [34]. Due to its restriction on the formation of regulatory macrophages, the inhibition of SIK2 stimulates the production of IL-10 [57]. Importantly, drugs with an SIK2 affinity of greater than 500nM are capable of suppressing TNF- $\alpha$  and upregulating IL-10 in BMDM, recapitulating the cytokine response to Lenvatinib [34]. However, due to the complex crosstalk among signaling pathways and the model we used, it is not possible to make a definitive statement about the off-target effect of Lenvatinib on the p38 MAPK, Syk, or SIK2 pathways. Future work will be required to define the comprehensive drug-kinase activity in immune cells using high-throughput profiling techniques [58].

Clinical evidence highlights the beneficial role of Lenvatinib in combination with immunotherapy in metastatic renal cell carcinoma and endometrial cancer, mirrored by an increased objective response rate and prolonged progression-free survival [59,60]. Recently, clinical trials investigating the safety and efficacy of Lenvatinib plus Pembrolizumab (anti-PD-1 antibody) in advanced DTC (NCT02973997) and HCC (NCT03713593) have also been initiated. However, combination regimens generally lead to more severe side-effects than monotherapies. Therefore, attempts to incorporate TKIs into immunotherapy have been largely limited by an increased incidence of high-grade toxicities [61,62]. Thus, a deeper understanding of the neglected immune-cell intrinsic off-target effect is of great clinical significance. Our study provided preclinical evidence that Lenvatinib has a direct impact on the myeloid compartment of the immune system. Recent studies have demonstrated the deleterious role of inflammation in cancer survival, with proinflammatory mediators playing an important role in angiogenesis, as well as acting as survival factors for cancer cells [63]. Our data, demonstrating the anti-inflammatory effects of Lenvatinib, argue that this effect is likely to contribute to the therapeutic effect of this class of drugs, extending their potential therapeutic applicability in tumors characterized by a prominent inflammatory profile. Future work should characterize the immune landscape in patients receiving Lenvatinib and identify predictive biomarkers for sensitivity to immunotherapies.

**Supplementary Materials:** The following supporting information can be downloaded at: <https://www.mdpi.com/article/10.3390/pharmaceutics15020412/s1>, Figure S1: T cell proliferation in the presence of Lenvatinib; Figure S2: Target landscape of Lenvatinib in 4 cell lines; Figure S3. The impact of TLR4 downstream kinase inhibitors on Lenvatinib-mediated immunomodulation in GM-CSF/M-CSF-primed monocytes.

**Author Contributions:** Conceptualization, R.T.N.-M. and M.G.N.; methodology, C.P., K.R., and M.J.; validation, C.P.; formal analysis, C.P.; investigation, C.P., M.J., and K.R.; resources, R.T.N.-M., M.J., and M.G.N.; writing—original draft preparation, C.P.; writing—review and editing, R.T.N.-M., M.J., and M.G.N.; visualization, C.P.; supervision, R.T.N.-M.; project administration, R.T.N.-M.; funding acquisition, R.T.N.-M. All authors have read and agreed to the published version of the manuscript.

**Funding:** This investigator-initiated research was funded by an unrestricted research grant from EISAI Co. C.P. was supported by the China Scholarship Council, grant number 202006100049.

**Institutional Review Board Statement:** Not applicable.

**Informed Consent Statement:** Informed consent was obtained from all subjects involved in the study.

**Data Availability Statement:** The data presented in this study are available on request from the corresponding author. The data are not publicly available due to privacy issues.

**Acknowledgments:** The authors would like to thank Julia Brake for technical support in the ex vivo neutrophil experiments.

**Conflicts of Interest:** The authors declare no conflict of interest.

## References

1. Cabanillas, M.E.; McFadden, D.G.; Durante, C. Thyroid cancer. *Lancet* **2016**, *388*, 2783–2795. [CrossRef] [PubMed]
2. Locati, L.D.; Piovesan, A.; Durante, C.; Bregni, M.; Castagna, M.G.; Zovato, S.; Giusti, M.; Ibrahim, T.; Puxeddu, E.; Fedele, G.; et al. Real-world efficacy and safety of lenvatinib: Data from a compassionate use in the treatment of radioactive iodine-refractory differentiated thyroid cancer patients in Italy. *Eur. J. Cancer* **2019**, *118*, 35–40. [CrossRef] [PubMed]
3. Schlumberger, M.; Tahara, M.; Wirth, L.J.; Robinson, B.; Brose, M.S.; Elisei, R.; Habra, M.A.; Newbold, K.; Shah, M.H.; Hoff, A.O.; et al. Lenvatinib versus Placebo in Radioiodine-Refractory Thyroid Cancer. *N. Engl. J. Med.* **2015**, *372*, 621–630. [CrossRef] [PubMed]
4. Capozzi, M.; De Divitiis, C.; Ottaiano, A.; von Arx, C.; Scala, S.; Tatangelo, F.; Delrio, P.; Tafuto, S. Lenvatinib, a molecule with versatile application: From preclinical evidence to future development in anti-cancer treatment. *Cancer Manag. Res.* **2019**, *11*, 3847–3860. [CrossRef]
5. Brose, M.S.; Robinson, B.; Sherman, S.I.; Krajewska, J.; Lin, C.-C.; Vaisman, F.; Hoff, A.O.; Hitre, E.; Bowles, D.W.; Hernando, J.; et al. Cabozantinib for radioiodine-refractory differentiated thyroid cancer (COSMIC-311): A randomised, double-blind, placebo-controlled, phase 3 trial. *Lancet Oncol.* **2021**, *22*, 1126–1138. [CrossRef]
6. Sharma, P.; Allison, J.P. The future of immune checkpoint therapy. *Science* **2015**, *348*, 56–61. [CrossRef]
7. French, J.D.; Bible, K.; Spitzweg, C.; Haugen, B.R.; Ryder, M. Leveraging the immune system to treat advanced thyroid cancers. *Lancet Diabetes Endocrinol.* **2017**, *5*, 469–481. [CrossRef]
8. O'Donnell, J.S.; Teng, M.W.L.; Smyth, M.J. Cancer immunoediting and resistance to T cell-based immunotherapy. *Nat. Rev. Clin. Oncol.* **2019**, *16*, 151–167. [CrossRef]
9. Cassetta, L.; Fragiogianni, S.; Sims, A.H.; Swierczak, A.; Forrester, L.M.; Zhang, H.; Soong, D.Y.H.; Cotechini, T.; Anur, P.; Lin, E.Y.; et al. Human Tumor-Associated Macrophage and Monocyte Transcriptional Landscapes Reveal Cancer-Specific Reprogramming, Biomarkers, and Therapeutic Targets. *Cancer Cell* **2019**, *35*, 588–602.e510. [CrossRef]
10. DeNardo, D.G.; Ruffell, B. Macrophages as regulators of tumour immunity and immunotherapy. *Nat. Rev. Immunol.* **2019**, *19*, 369–382. [CrossRef]
11. Ryder, M.; Ghossein, R.A.; Ricarte-Filho, J.C.M.; Knauf, J.A.; Fagin, J.A. Increased density of tumor-associated macrophages is associated with decreased survival in advanced thyroid cancer. *Endocr.-Relat. Cancer* **2008**, *15*, 1069–1074. [CrossRef]
12. Qing, W.; Fang, W.Y.; Ye, L.; Shen, L.Y.; Zhang, X.F.; Fei, X.C.; Chen, X.; Wang, W.Q.; Li, X.Y.; Xiao, J.C.; et al. Density of tumor-associated macrophages correlates with lymph node metastasis in papillary thyroid carcinoma. *Thyroid* **2012**, *22*, 905–910. [CrossRef]
13. Weber, R.; Fleming, V.; Hu, X.Y.; Nagibin, V.; Groth, C.; Altevogt, P.; Utikal, J.; Umansky, V. Myeloid-Derived Suppressor Cells Hinder the Anti-Cancer Activity of Immune Checkpoint Inhibitors. *Front. Immunol.* **2018**, *9*, 9. [CrossRef]
14. Hage, C.; Hoves, S.; Strauss, L.; Bissinger, S.; Prinz, Y.; Pöschinger, T.; Kiessling, F.; Ries, C.H. Sorafenib Induces Pyroptosis in Macrophages and Triggers Natural Killer Cell-Mediated Cytotoxicity Against Hepatocellular Carcinoma. *Hepatology* **2019**, *70*, 1280–1297. [CrossRef]
15. Petroni, G.; Buque, A.; Zitvogel, L.; Kroemer, G.; Galluzzi, L. Immunomodulation by targeted anticancer agents. *Cancer Cell* **2021**, *39*, 310–345. [CrossRef]
16. Liu, P.; Zhao, L.; Pol, J.; Levesque, S.; Petrazzuolo, A.; Pfirschke, C.; Engblom, C.; Rickelt, S.; Yamazaki, T.; Iribarren, K.; et al. Crizotinib-induced immunogenic cell death in non-small cell lung cancer. *Nat. Commun.* **2019**, *10*, 1486. [CrossRef]
17. Yi, C.; Chen, L.; Lin, Z.; Liu, L.; Shao, W.; Zhang, R.; Lin, J.; Zhang, J.; Zhu, W.; Jia, H.; et al. Lenvatinib Targets FGF Receptor 4 to Enhance Antitumor Immune Response of Anti-Programmed Cell Death-1 in HCC. *Hepatology* **2021**, *74*, 2544–2560. [CrossRef]
18. Peng, C.; Rabold, K.; Mulder, W.J.M.; Jaeger, M.; Netea-Maier, R.T. Kinase Inhibitors' Effects on Innate Immunity in Solid Cancers. *Cancers* **2021**, *13*, 5695. [CrossRef]
19. Zitvogel, L.; Rusakiewicz, S.; Routy, B.; Ayyoub, M.; Kroemer, G. Immunological off-target effects of imatinib. *Nat. Rev. Clin. Oncol.* **2016**, *13*, 431–446. [CrossRef]
20. Torrens, L.; Montironi, C.; Puigvehí, M.; Mesropian, A.; Leslie, J.; Haber, P.K.; Maeda, M.; Balaseviciute, U.; Willoughby, C.E.; Abril-Fornaguera, J.; et al. Immunomodulatory Effects of Lenvatinib Plus Anti-Programmed Cell Death Protein 1 in Mice and Rationale for Patient Enrichment in Hepatocellular Carcinoma. *Hepatology* **2021**, *74*, 2652–2669. [CrossRef]

21. Kimura, T.; Kato, Y.; Ozawa, Y.; Kodama, K.; Ito, J.; Ichikawa, K.; Yamada, K.; Hori, Y.; Tabata, K.; Takase, K.; et al. Immunomodulatory activity of lenvatinib contributes to antitumor activity in the Hepa1-6 hepatocellular carcinoma model. *Cancer Sci.* **2018**, *109*, 3993–4002. [CrossRef] [PubMed]
22. Kato, Y.; Tabata, K.; Kimura, T.; Yachie-Kinoshita, A.; Ozawa, Y.; Yamada, K.; Ito, J.; Tachino, S.; Hori, Y.; Matsuki, M.; et al. Lenvatinib plus anti-PD-1 antibody combination treatment activates CD8+ T cells through reduction of tumor-associated macrophage and activation of the interferon pathway. *PLoS ONE* **2019**, *14*, e0212513. [CrossRef] [PubMed]
23. Repnik, U.; Knezevic, M.; Jeras, M. Simple and cost-effective isolation of monocytes from buffy coats. *J. Immunol. Methods* **2003**, *278*, 283–292. [CrossRef] [PubMed]
24. Kuhns, D.B.; Priel, D.A.L.; Chu, J.; Zarembek, K.A. Isolation and Functional Analysis of Human Neutrophils. *Curr. Protoc. Immunol.* **2015**, *111*, 7.23.21–27.23.16. [CrossRef]
25. Ikeda, K.; Kudo, M.; Kawazoe, S.; Osaki, Y.; Ikeda, M.; Okusaka, T.; Tamai, T.; Suzuki, T.; Hisai, T.; Hayato, S.; et al. Phase 2 study of lenvatinib in patients with advanced hepatocellular carcinoma. *J. Gastroenterol.* **2017**, *52*, 512–519. [CrossRef]
26. Boss, D.S.; Glen, H.; Beijnen, J.H.; Keesen, M.; Morrison, R.; Tait, B.; Copalu, W.; Mazur, A.; Wanders, J.; O'Brien, J.P.; et al. A phase I study of E7080, a multitargeted tyrosine kinase inhibitor, in patients with advanced solid tumours. *Br. J. Cancer* **2012**, *106*, 1598–1604. [CrossRef]
27. Bejarano, L.; Jordão, M.J.C.; Joyce, J.A. Therapeutic Targeting of the Tumor Microenvironment. *Cancer Discov.* **2021**, *11*, 933–959. [CrossRef]
28. Arts, R.J.; Plantinga, T.S.; Tuit, S.; Ulas, T.; Heinhuis, B.; Tesselaar, M.; Sloot, Y.; Adema, G.J.; Joosten, L.A.; Smit, J.W.; et al. Transcriptional and metabolic reprogramming induce an inflammatory phenotype in non-medullary thyroid carcinoma-induced macrophages. *Oncoimmunology* **2016**, *5*, e1229725. [CrossRef]
29. Christofides, A.; Strauss, L.; Yeo, A.; Cao, C.; Charest, A.; Boussiotis, V.A. The complex role of tumor-infiltrating macrophages. *Nat. Immunol.* **2022**, *23*, 1148–1156. [CrossRef]
30. Okamoto, K.; Kodama, K.; Takase, K.; Sugi, N.H.; Yamamoto, Y.; Iwata, M.; Tsuruoka, A. Antitumor activities of the targeted multi-tyrosine kinase inhibitor lenvatinib (E7080) against RET gene fusion-driven tumor models. *Cancer Lett.* **2013**, *340*, 97–103. [CrossRef]
31. Netea-Maier, R.T.; Smit, J.W.A.; Netea, M.G. Metabolic changes in tumor cells and tumor-associated macrophages: A mutual relationship. *Cancer Lett.* **2018**, *413*, 102–109. [CrossRef]
32. O'Neill, L.A.; Kishton, R.J.; Rathmell, J. A guide to immunometabolism for immunologists. *Nat. Rev. Immunol.* **2016**, *16*, 553–565. [CrossRef]
33. Monaco, G.; Lee, B.; Xu, W.; Mustafah, S.; Hwang, Y.Y.; Carré, C.; Burdin, N.; Visan, L.; Ceccarelli, M.; Poidinger, M.; et al. RNA-Seq Signatures Normalized by mRNA Abundance Allow Absolute Deconvolution of Human Immune Cell Types. *Cell Rep.* **2019**, *26*, 1627–1640.e1627. [CrossRef]
34. Klaeger, S.; Heinzlmeier, S.; Wilhelm, M.; Polzer, H.; Vick, B.; Koenig, P.-A.; Reinecke, M.; Ruprecht, B.; Petzoldt, S.; Meng, C.; et al. The target landscape of clinical kinase drugs. *Science* **2017**, *358*, eaan4368. [CrossRef]
35. Guha, M.; Mackman, N. LPS induction of gene expression in human monocytes. *Cell. Signal.* **2001**, *13*, 85–94. [CrossRef]
36. O'Neill, L.A.J.; Golenbock, D.; Bowie, A.G. The history of Toll-like receptors—redefining innate immunity. *Nat. Rev. Immunol.* **2013**, *13*, 453–460. [CrossRef]
37. Aksoy, E.; Taboubi, S.; Torres, D.; Delbauve, S.; Hachani, A.; Whitehead, M.A.; Pearce, W.P.; Berenjeno, I.M.; Nock, G.; Filloux, A.; et al. The p110 $\delta$  isoform of the kinase PI(3)K controls the subcellular compartmentalization of TLR4 signaling and protects from endotoxin shock. *Nat. Immunol.* **2012**, *13*, 1045–1054. [CrossRef]
38. Zaroni, I.; Ostuni, R.; Marek, L.R.; Barresi, S.; Barbalat, R.; Barton, G.M.; Granucci, F.; Kagan, J.C. CD14 Controls the LPS-Induced Endocytosis of Toll-like Receptor 4. *Cell* **2011**, *147*, 868–880. [CrossRef]
39. Voss, O.H.; Murakami, Y.; Pena, M.Y.; Lee, H.N.; Tian, L.J.; Margulies, D.H.; Street, J.M.; Yuen, P.S.T.; Qi, C.F.; Krzewski, K.; et al. Lipopolysaccharide-Induced CD300b Receptor Binding to Toll-like Receptor 4 Alters Signaling to Drive Cytokine Responses that Enhance Septic Shock. *Immunity* **2016**, *44*, 1365–1378. [CrossRef]
40. Vogelpoel, L.T.C.; Hansen, I.S.; Rispens, T.; Muller, F.J.M.; van Capel, T.M.M.; Turina, M.C.; Vos, J.B.; Baeten, D.L.P.; Kapsenberg, M.L.; de Jong, E.C.; et al. Fc gamma receptor-TLR cross-talk elicits pro-inflammatory cytokine production by human M2 macrophages. *Nat. Commun.* **2014**, *5*, 5444. [CrossRef]
41. Patnaik, A.; Swanson, K.D.; Csizmadia, E.; Solanki, A.; Landon-Brace, N.; Gehring, M.P.; Helenius, K.; Olson, B.M.; Pyzer, A.R.; Wang, L.C.; et al. Cabozantinib Eradicates Advanced Murine Prostate Cancer by Activating Antitumor Innate Immunity. *Cancer Discov.* **2017**, *7*, 750–765. [CrossRef] [PubMed]
42. Schlumberger, M.; Jarzab, B.; Cabanillas, M.E.; Robinson, B.; Pacini, F.; Ball, D.W.; McCaffrey, J.; Newbold, K.; Allison, R.; Martins, R.G.; et al. A Phase II Trial of the Multitargeted Tyrosine Kinase Inhibitor Lenvatinib (E7080) in Advanced Medullary Thyroid Cancer. *Clin. Cancer Res.* **2016**, *22*, 44–53. [CrossRef] [PubMed]
43. Fabian, M.A.; Biggs, W.H.; Treiber, D.K.; Atteridge, C.E.; Azimioara, M.D.; Benedetti, M.G.; Carter, T.A.; Ciceri, P.; Edeen, P.T.; Floyd, M.; et al. A small molecule–kinase interaction map for clinical kinase inhibitors. *Nat. Biotechnol.* **2005**, *23*, 329–336. [CrossRef] [PubMed]

44. Heine, A.; Schilling, J.; Grünwald, B.; Krüger, A.; Gevensleben, H.; Held, S.A.E.; Garbi, N.; Kurts, C.; Brossart, P.; Knolle, P.; et al. The induction of human myeloid derived suppressor cells through hepatic stellate cells is dose-dependently inhibited by the tyrosine kinase inhibitors nilotinib, dasatinib and sorafenib, but not sunitinib. *Cancer Immunol. Immunother.* **2016**, *65*, 273–282. [CrossRef]
45. Ou, D.L.; Chen, C.W.; Hsu, C.L.; Chung, C.H.; Feng, Z.R.; Lee, B.S.; Cheng, A.L.; Yang, M.H.; Hsu, C. Regorafenib enhances antitumor immunity via inhibition of p38 kinase/Creb1/Klf4 axis in tumor-associated macrophages. *J. Immunother. Cancer* **2021**, *9*, 14. [CrossRef]
46. Okamoto, K.; Ikemori-Kawada, M.; Jestel, A.; von König, K.; Funahashi, Y.; Matsushima, T.; Tsuruoka, A.; Inoue, A.; Matsui, J. Distinct binding mode of multikinase inhibitor lenvatinib revealed by biochemical characterization. *ACS. Med. Chem. Lett.* **2015**, *6*, 89–94. [CrossRef]
47. Bellora, F.; Dondero, A.; Corrias, M.V.; Casu, B.; Regis, S.; Caliendo, F.; Moretta, A.; Cazzola, M.; Elena, C.; Vinti, L.; et al. Imatinib and Nilotinib Off-Target Effects on Human NK Cells, Monocytes, and M2 Macrophages. *J. Immunol.* **2017**, *199*, 1516–1525. [CrossRef]
48. Zhu, J.; Fang, P.; Wang, C.; Gu, M.; Pan, B.; Guo, W.; Yang, X.; Wang, B. The immunomodulatory activity of lenvatinib prompts the survival of patients with advanced hepatocellular carcinoma. *Cancer Med.* **2021**, *10*, 7977–7987. [CrossRef]
49. Foey, A.D.; Parry, S.L.; Williams, L.M.; Feldmann, M.; Foxwell, B.M.J.; Brennan, F.M. Regulation of Monocyte IL-10 Synthesis by Endogenous IL-1 and TNF- $\alpha$ : Role of the p38 and p42/44 Mitogen-Activated Protein Kinases. *J. Immunol.* **1998**, *160*, 920–928. [CrossRef]
50. Wu, C.H.; Hsu, F.T.; Chao, T.L.; Lee, Y.H.; Kuo, Y.C. Revealing the suppressive role of protein kinase C delta and p38 mitogen-activated protein kinase (MAPK)/NF- $\kappa$ B axis associates with lenvatinib-inhibited progression in hepatocellular carcinoma in vitro and in vivo. *Biomed Pharm.* **2022**, *145*, 112437. [CrossRef]
51. Jiménez-García, L.; Herránz, S.; Luque, A.; Hortelano, S. Critical role of p38 MAPK in IL-4-induced alternative activation of peritoneal macrophages. *Eur. J. Immunol.* **2015**, *45*, 273–286. [CrossRef]
52. Seimon, T.A.; Wang, Y.; Han, S.; Senokuchi, T.; Schrijvers, D.M.; Kuriakose, G.; Tall, A.R.; Tabas, I.A. Macrophage deficiency of p38 $\alpha$  MAPK promotes apoptosis and plaque necrosis in advanced atherosclerotic lesions in mice. *J. Clin. Investig.* **2009**, *119*, 886–898. [CrossRef]
53. Zhang, H.Y.; Li, R.C.; Cao, Y.F.; Gu, Y.; Lin, C.; Liu, X.; Lv, K.P.; He, X.D.; Fang, H.J.; Jin, K.F.; et al. Poor Clinical Outcomes and Immuno-evasive Contexture in Intratumoral IL-10-Producing Macrophages Enriched Gastric Cancer Patients. *Ann. Surg.* **2022**, *275*, E626–E635. [CrossRef]
54. Saraiva, M.; O’Garra, A. The regulation of IL-10 production by immune cells. *Nat. Rev. Immunol.* **2010**, *10*, 170–181. [CrossRef]
55. Mocsai, A.; Ruland, J.; Tybulewicz, V.L.J. The SYK tyrosine kinase: A crucial player in diverse biological functions. *Nat. Rev. Immunol.* **2010**, *10*, 387–402. [CrossRef]
56. Lowell, C.A. Src-family and Syk Kinases in Activating and Inhibitory Pathways in Innate Immune Cells: Signaling Cross Talk. *Cold Spring Harb. Perspect. Biol.* **2011**, *3*, a002352. [CrossRef]
57. Clark, K.; MacKenzie, K.F.; Petkevicius, K.; Kristariyanto, Y.; Zhang, J.; Choi, H.G.; Pegg, M.; Plater, L.; Pedrioli, P.G.A.; McIver, E.; et al. Phosphorylation of CRT3 by the salt-inducible kinases controls the interconversion of classically activated and regulatory macrophages. *Proc. Natl. Acad. Sci. USA* **2012**, *109*, 16986–16991. [CrossRef]
58. Ferguson, F.M.; Gray, N.S. Kinase inhibitors: The road ahead. *Nat. Rev. Drug Discov.* **2018**, *17*, 353–377. [CrossRef]
59. Makker, V.; Colombo, N.; Casado Herráez, A.; Santin, A.D.; Colomba, E.; Miller, D.S.; Fujiwara, K.; Pignata, S.; Baron-Hay, S.; Ray-Coquard, I.; et al. Lenvatinib plus Pembrolizumab for Advanced Endometrial Cancer. *N. Engl. J. Med.* **2022**, *386*, 437–448. [CrossRef]
60. Motzer, R.; Alekseev, B.; Rha, S.-Y.; Porta, C.; Eto, M.; Powles, T.; Grünwald, V.; Hutson, T.E.; Kopyltsov, E.; Méndez-Vidal, M.J.; et al. Lenvatinib plus Pembrolizumab or Everolimus for Advanced Renal Cell Carcinoma. *N. Engl. J. Med.* **2021**, *384*, 1289–1300. [CrossRef]
61. European Medicines Agency: EMA/621567/2021-Assessment report. Available online: [https://www.ema.europa.eu/en/documents/variation-report/keytruda-h-c-003820-ii-0104-epar-assessment-report-variation\\_en.pdf](https://www.ema.europa.eu/en/documents/variation-report/keytruda-h-c-003820-ii-0104-epar-assessment-report-variation_en.pdf) (accessed on 21 January 2022).
62. European Medicines Agency: EMA/CHMP/618201/2021-Assessment report. Available online: [https://www.ema.europa.eu/en/documents/variation-report/lenvima-h-c-003727-ii-0042-epar-assessment-report-variation\\_en.pdf](https://www.ema.europa.eu/en/documents/variation-report/lenvima-h-c-003727-ii-0042-epar-assessment-report-variation_en.pdf) (accessed on 21 January 2022).
63. Bottazzi, B.; Riboli, E.; Mantovani, A. Aging, inflammation and cancer. *Semin. Immunol.* **2018**, *40*, 74–82. [CrossRef] [PubMed]

**Disclaimer/Publisher’s Note:** The statements, opinions and data contained in all publications are solely those of the individual author(s) and contributor(s) and not of MDPI and/or the editor(s). MDPI and/or the editor(s) disclaim responsibility for any injury to people or property resulting from any ideas, methods, instructions or products referred to in the content.



Article

# Comparative Analysis of Dasatinib Effect between 2D and 3D Tumor Cell Cultures

Samantha Sabetta, Davide Vecchiotti, Letizia Clementi, Mauro Di Vito Nolfi, Francesca Zazzeroni and Adriano Angelucci \*

Department of Biotechnological and Applied Clinical Science, University of L'Aquila, 67100 L'Aquila, Italy  
\* Correspondence: [adriano.angelucci@univaq.it](mailto:adriano.angelucci@univaq.it)

**Abstract:** Three-dimensional cell culture methods are able to confer new predictive relevance to in vitro tumor models. In particular, the 3D multicellular tumor spheroids model is considered to better resemble tumor complexity associated with drug resistance compared to the 2D monolayer model. Recent advances in 3D printing techniques and suitable biomaterials have offered new promises in developing 3D tissue cultures at increased reproducibility and with high-throughput characteristics. In our study, we compared the sensitivity to dasatinib treatment in two different cancer cell lines, prostate cancer cells DU145 and glioblastoma cells U87, cultured in the 3D spheroids model and in the 3D bioprinting model. DU145 and U87 cells were able to proliferate in 3D alginate/gelatin bioprinted structures for two weeks, forming spheroid aggregates. The treatment with dasatinib demonstrated that bioprinted cells were considerably more resistant to drug toxicity than corresponding cells cultured in monolayer, in a way that was comparable to behavior observed in the 3D spheroids model. Recovery and analysis of cells from 3D bioprinted structures led us to hypothesize that dasatinib resistance was dependent on a scarce penetrance of the drug, a phenomenon commonly reported also in spheroids. In conclusion, the 3D bioprinted model utilizing alginate/gelatin hydrogel was demonstrated to be a suitable model in drug screening when spheroid growth is required, offering advantages in feasibility, reproducibility, and scalability compared to the classical 3D spheroids model.

**Citation:** Sabetta, S.; Vecchiotti, D.; Clementi, L.; Di Vito Nolfi, M.; Zazzeroni, F.; Angelucci, A. Comparative Analysis of Dasatinib Effect between 2D and 3D Tumor Cell Cultures. *Pharmaceutics* **2023**, *15*, 372. <https://doi.org/10.3390/pharmaceutics15020372>

Academic Editor: Sudip K. Das

Received: 15 December 2022

Revised: 14 January 2023

Accepted: 18 January 2023

Published: 21 January 2023

**Keywords:** 3D tissue culture; 3D tumor model; tumor spheroids; drug resistance; drug screening; preclinical study

## 1. Introduction

Inhibition of key molecules in signaling pathways that regulate cancer cell proliferation and dissemination is one of the most promising strategies in modern cancer therapy. Specifically, tyrosine kinases represent a particularly important target because they mediate several biological processes, including cell growth and differentiation, metabolism, and apoptosis. Constitutive activation gives these enzymes an oncogene status, which directs the cell toward neoplastic transformation [1].

Src, a 60-kDa protein, is the most widely studied member of the Src family tyrosine kinases (SFKs), being frequently overexpressed in many tumors. SFKs are a large class of non-receptor kinases that control multiple signaling pathways in animal cells, the activation of which is necessary for mitogenic signaling of many growth factors, but also for the acquisition of the migratory and invasive phenotype. Indeed, oncogenic activation of SFKs has been shown to play an important role in solid tumors, promoting tumor growth and distant metastasis formation, and that is why they represent the most representative class of targeted proteins in cancer therapy [2]. This family consists of 11 highly homologous members: c-Src, Blk, Fgr, Fyn, Frk, Hck, Lck, Lyn, Yes, Yrk, and Srms [3,4]. Of the 11 members of SFKs, Src, Fyn, and Yes are implicated in tumorigenesis and metastasis formation [5]. In fact, Src, Fyn, and Yes, but also Frk, are widely expressed in a variety of



**Copyright:** © 2023 by the authors. Licensee MDPI, Basel, Switzerland. This article is an open access article distributed under the terms and conditions of the Creative Commons Attribution (CC BY) license (<https://creativecommons.org/licenses/by/4.0/>).

tissues, while for the other members, protein expression is more restricted in tissues, with a prevalence in cells of hematopoietic origin [6].

Src activity is regulated, at the cellular level, by the phosphorylation state of two key tyrosine residues and by interactions with ligands mediated by its regulatory domains, which stabilize the kinase in active or inactive configuration. In the inactive configuration, the SH2 domain binds phosphorylated Tyr527 in the C-terminal domain, while the SH3 domain interacts with the linker domain on the backside of the catalytic domain, thus promoting a closed conformation that prevents interaction with substrates. In the active configuration, Tyr527 is dephosphorylated, and the SH2 and SH3 domains are released by intramolecular interactions and thus available for binding of heterologous molecular partners; this open conformation also allows Tyr416 to be self-phosphorylated.

In cancer cells, Src transmits signals that promote cell survival and mitogenesis; in addition, Src exerts a profound effect on cytoskeleton reorganization and adhesion systems that underlie cell migration and invasion. Src, therefore, not only promotes cancer cell growth but is also involved in the control of adhesiveness and migration, functioning as a key molecule that regulates signal transduction pathways triggered by various surface molecules, such as growth factor receptors and integrins [2,7]. Indeed, most evidence suggests that Src has a predominant role in the maintenance of the neoplastic phenotype and tumor progression, rather than tumor initiation or growth [8]. During tumor progression, Src activity becomes abnormally elevated, and because mutation activation or amplification of Src is very rare in human tumors, altered extrinsic control of Src phosphorylation by kinase or phosphatase may represent an important mechanism of Src upregulation.

Dasatinib (BMS-354825, Sprycel) is an orally available small molecule that in 2006 received FDA approval for the treatment of chronic myelogenous leukemia and Philadelphia-positive acute lymphoblastic leukemia. Dasatinib has a low inhibition specificity and its potential targets comprise Src in addition to BCR-Abl, c-kit, PDGFR, and other SFKs, including Lck, Fyn, and Yes, with IC<sub>50</sub> < 1.0 nmol/L [9]. Preclinical data suggest that dasatinib could be effective also in solid cancer, and numerous results from phase I/II trials conducted in different cancer types have been published since 2009 [10]. Despite the encouraging preclinical results, the clinical validation of these data has been largely unproductive. In fact, although *in vitro* studies have demonstrated several gene signatures predictive of dasatinib response, these signatures have not yet permitted the definition of cohorts clinically sensitive to dasatinib [11]. In addition, available preclinical models have been shown to be largely inadequate in their predictive capacity, and new experimental strategies implementing microenvironment condition are needed. In fact, SFK activity is tightly dependent on ECM composition, and a changeable microenvironment could heavily impact SFK functions and thus treatment efficacy.

The tumor microenvironment is known to be complex, both in its content and dynamic nature, which is difficult to study using two-dimensional (2D) cell culture models. In contrast, three-dimensional (3D) cell models, such as spheroids, show peculiar molecular features that differ from monolayer cultures but are closer to the structural architecture of the tumor *in vivo*. Such models, in fact, can more accurately mimic both the structure of the malignant tissue and its microenvironment (physiological responses, secretion of soluble mediators, gene expression, patterns and mechanisms of drug resistance). Tumor cells within the spheroid reproduce the same concentric arrangement as tumors; in fact, they have a proliferative outer layer, a quiescent middle layer, and a hypoxic and necrotic core and have a growth pattern like solid tumors in the early non-vascularized stage. The use of 3D cell assays adds value to research and screening studies to identify potential anticancer compounds, bridging existing limitations between 2D cell cultures and animal models.

The theoretic superiority of 3D vs. 2D cultures has prompted the development of several protocols with the purpose to overcome the main weaknesses of 3D tissue cultures: technical complexity in performing and analyzing, high costs, reproducibility, and scalability. In particular, different approaches have been described to realize 3D sphere culture. Hanging drop protocol is a suspension culture method and it is one of the most

popular approaches used for culture of 3D spheres, because it does not need particular or expensive instruments [12]. There are other suspension culture approaches for large-scale formation of spheres, each with their distinct advantages and disadvantages [13]. They include device-assisted culture, in order to force cell aggregation by movement or magnetic levitation, and gel embedding culture, able to mimic ECM microenvironment. In particular, the use of gels or scaffolds may guarantee a higher predictivity of the tissue models because cells organize a complex dynamic 3D architecture making contact also with ECM [14].

Three-dimensional bioprinting is an emerging technology that, using dedicated software and hardware to design 3D patterns and structures, aims to precisely produce an engineered structure or tissue that can be used for biological and pharmacological studies or directly in humans for regenerative medicine. It represents a relatively new approach that provides high reproducibility and precise control over automated fabricated constructs, potentially enabling high-throughput production of the desired 3D model. Bioprinting modalities include extrusion-based bioprinting [15], inkjet-based bioprinting [16], and laser-based bioprinting. Extrusion-based bioprinting is the most common and reliable system for 3D printing of biological tissues and is characterized by robotic delivery of a continuous stream of bioink, under pneumatic or motorized forces.

During the bioprinting process, a solution of a biomaterial or a mixture of several biomaterials in the form of a hydrogel, which usually encapsulates the desired cell types, called a bioink, is used to create tissue scaffolds with the final shape resembling the designed construct. Bioinks can be made alone from natural or synthetic biomaterials or from a combination of the two as hybrid materials. Hydrogel is the most widely used bioink, as it has properties like those of extracellular matrices and also allows the encapsulation of cells in a 3D environment that is both highly hydrated and mechanically stable. Sodium alginate is frequently used as hydrogel in 3D tissue culture thanks to its favorable physio-chemical characteristics, including gelling, viscous, and stabilizing properties, and the ability to retain water. Although sodium alginate is biocompatible and biodegradable, it is frequently mixed with other polymers of animal origin in order to enhance its gelling properties and the viability of encapsulated cells. The combination of sodium alginate and gelatin provides an excellent hydrogel for use as a substrate in 3D printing technology due to its biological properties, such as its biocompatibility, biodegradability, and non-toxicity. The easily modified mechanical properties of these materials can be adapted to living tissue, making them ideal environments for cell culture development. However, the chemical and mechanical cues provided by the specific hydrogel formulation as well as protocol used when performing 3D culture can affect the behavior of spheres and their resistance to drugs, requesting more confirmatory data [17,18].

In our study, we aimed to investigate the preclinical potentiality of 3D bioprinting technology in the field of experimental oncology. In particular, we verified the effect of dasatinib in 3D bioprinting models based on alginate/gelatin matrix utilizing two different tumor cell models, prostate cancer and glioblastoma, in comparison with the corresponding 3D spheroids models and 2D monolayer cultures.

## 2. Material and Methods

### 2.1. Cell Lines and 2D Monolayer Culture

Experiments were performed using U87 MG cell line (U87) human glioblastoma astrocytoma derived from a malignant glioma from a female patient by the explant technique, able to produce a malignant tumor consistent with glioblastoma in nude mice, and DU145 cell line human prostate adenocarcinoma isolated from the brain of a 69-year-old male. The U87 cells were cultured in DMEM high-glucose growth medium and DU145 cells in RPMI 1640 medium. For all cell lines, the growth medium was supplemented with 10% fetal bovine serum, 2 mM glutamine 100 IU/mL penicillin, and 100 µg/mL streptomycin. Cell lines were supplied by ECACC and underwent regular testing for mycoplasma by Hoechst DNA staining and PCR. Authentication procedures included species verification by DNA barcoding and identity verification by DNA profiling. U87 and DU145 cells when passed

were initially plated at a density of  $10^4$  cells/cm<sup>2</sup>, and incubated in 5% CO<sub>2</sub> at 37 °C. For protein extraction, we initially recovered the cells with the scraper and then centrifuged at  $300\times g$  for 10 min and then at  $100\times g$  for 5 min. Cells were processed for protein extraction with cell lysis buffer containing 0.1% Triton X-100, 10 mM Tris-HCl (pH 7.5), 150 mM NaCl, 5 mM EDTA, and supplemented with 1 mM Na<sub>3</sub>VO<sub>4</sub> and 75 U of aprotinin (Sigma-Aldrich, St. Louis, MI, USA), and incubated for 20 min at 4 °C. Protein extracts were stored at  $-80$  °C until use.

### 2.2. Preparation of Hydrogel and Bioprinting

The hydrogel used for bioprinting is composed of 2% alginate and 8% gelatin (bioink). The powders were initially exposed to UV light for 15 min and then dissolved in sterile DPBS on a magnetic stirrer at 50 °C under laminar flow. Once prepared, bioink was placed in sterile syringes and stored at 4 °C until use. Prior to the bioprinting procedure, bioink was equilibrated at 37 °C. Next,  $20 \times 10^6$  cells were suspended in 400  $\mu$ L of culture medium and then mixed with 3.7 mL of bioink to reach a final concentration of  $5 \times 10^6$  cell/mL. Finally, a disposable cartridge was filled with cell-laden hydrogel and equilibrated at 29 °C for 30 min in a temperature-controlled printhead. Printing was carried out using BIO X<sup>TM</sup> bioprinter (Cellink, Gothenburg, Sweden) in a 12-well plate with a dispensing pressure of 50 kPa at a speed of 5 mm/s and setting the printbed temperature at 18 °C. The 3D structures were finally cross-linked with CaCl<sub>2</sub> for 10 min and for an additional 3 min with BaCl<sub>2</sub> before adding culture medium. For protein extraction, the 3D structures were quickly dissolved in a solution of EDTA 250 mM in PBS and cells were collected by centrifugation at  $400\times g$  for 10 min. The pellet was resuspended in PBS and centrifuged at  $400\times g$  for 5 min. The resulting pellet was dissolved in RIPA buffer for protein extraction.

### 2.3. Cell Viability and IC<sub>50</sub> Analysis

DU145 and U87 cell lines were seeded at a density of  $5 \times 10^4$  cells/mL in a 24 multiwell. After 24 h, the cells were treated with dasatinib by the serial dilution method for 72 h. At the end of 72 h, the growth medium was removed and substituted with fresh medium. Cell viability in both 2D and 3D cultures was assessed using PrestoBlue<sup>®</sup> (Thermo Fisher, Waltham, MA, USA) colorimetric viability assay, based on a ready-to-use, non-toxic, cell-permeable resazurin-based solution. It functions as a cell viability indicator by using the reducing power of living cells and quantitatively measuring the proliferation of cells. Cells were incubated with reagent in a 1:10 ratio for 2 h, in the dark. Then, a spectrophotometer reading was taken at wavelengths of 570 and 600 nm. For IC<sub>50</sub> analysis, data collected in triplicate were elaborated with DRFit software (<http://www.structuralchemistry.org/pcsb/drfit.php>, accessed on 2 November 2022).

### 2.4. Western Blot

Protein extracts were centrifuged for 10 min at  $300\times g$  to eliminate nuclei and large debris. After protein dosage by Bradford Dye Reagent assay (Bio-Rad, Hercules, CA, USA), the same protein quantity for each sample was subjected to 10% sodium-dodecyl sulphate polyacrilamide gel electrophoresis (SDS-PAGE). Prestained protein molecular markers sharpmass VII (Euroclone, Milan, Italy) were loaded on a separate well for each gel. Then, at the end of the run, proteins were electrophoretically transferred from gel onto nitrocellulose membranes Amersham protran 0.2  $\mu$ m (Cytiva Europe, Freiburg, Germany) for 90 min at 350 mA. Membranes were incubated for 1 h at RT with 10% nonfat dry milk in Tris-buffered saline (Bio-Rad) at pH 7.4 containing 20 mM Tris, 500 mM NaCl, and supplemented with 0.05% Tween 20 (Bio-Rad), and then probed for 1 h at RT with primary antibodies according to dilution suggested by the manufacturer: anti-Src (36D10), anti-Phospho-Src (Thr416) (E6G4R), and anti-GAPDH (0411) (all from Cell Signaling Technology, Danvers, MA, USA). Protein bands were visualized after 1 h of incubation with horseradish peroxidase (HRP)-conjugated anti-rabbit IgG or anti-mouse IgG (Cell Signaling Technology) at RT, and then with chemiluminescence reagents (Amersham, Buckinghamshire, UK).

Chemiluminescent signals were acquired by the Chemidoc XRS system and digitally analyzed for the determination of band molecular weight and density by Imagemag software (Bio-Rad).

### 2.5. 3D Multicellular Spheroid Model

For the formation of U87 and DU145 spheroids, we used the “hanging drops” method. The density chosen was 500,000 cells/mL, which were resuspended in 10  $\mu$ L of growth medium with 25% FBS and 25  $\mu$ L of collagen (10  $\mu$ g/mL). This method involves the deposition of 1  $\mu$ L of cells on the bottom of the lid of a Petri dish; inverting the dish forms a “hanging” drop, and the cells, by gravity, accumulate in the bottom of the drop, promoting cell aggregation into spheroids. The spheroids were kept in an incubator at 37 °C and 5% CO<sub>2</sub>. After 30 min, on each drop, growth medium was added to prevent evaporation of the drop. Then, 6 mL of PBS was added to the bottom of the plate, with the purpose of keeping the moisture level high. After 24 h, the formed spheroids were transferred to a 96 round-bottom multiwell with 200  $\mu$ L of DMEM growth medium for U87 and RPMI for DU145.

### 2.6. Spheroid Dissemination Assay

The dissemination assay was performed plating spheroids on collagen matrix. Briefly, a 24 multiwell was coated with 30  $\mu$ L of collagen (4 mg/mL) for 24 h before transferring the spheroids. Once transferred, the spheroids were treated with dasatinib at selected concentrations and monitored by phase contrast microscopy up to 24 h. Digital images were taken at T0 (newly transferred spheroid), T8, and T24, and were analyzed by the public domain software ImageJ (<https://imagej.nih.gov/ij/> accessed on 15 September 2022) for the semiquantitative evaluation of the invaded area.

### 2.7. Cell Migration Assay

For the migration assay, cells were first seeded at a density of  $5 \times 10^4$  cells/mL in a 6-well multiwell and the next day were treated with dasatinib at selected concentrations for 24 h. Then, cells were detached from the culture plate by trypsin–EDTA and centrifuged at  $300 \times g$  for 10 min. Alternatively, cells were recovered from 3D bioprinted structures with a solution of EDTA 250 mM in PBS. Cells were first counted and then seeded in serum-free medium at a density of  $3 \times 10^4$  cells/mL on top of the filter membrane of inserts that were placed in the 24-well multiwell. In each well was added 800  $\mu$ L of complete growth medium (DMEM for U87 and RPMI for DU145), which serves as a chemoattractant. The planned incubation time was 2 h. The insert was removed from the multiwell plate, and was cleaned of the remaining cells that did not migrate from the top of the membrane. Then, 200  $\mu$ L of filtered formalin was added to each insert for 10 min at room temperature, and then 200  $\mu$ L of crystal violet (12 mM in a 20% solution of methanol in water) was added to each insert for 10 min at room temperature. Crystal violet was then removed, and washing with tap water was performed to remove excess dye. The cells were counted by phase contrast microscopy at  $400 \times$  magnification, in at least 5 fields per membrane, to obtain the mean number of migrated cells per field.

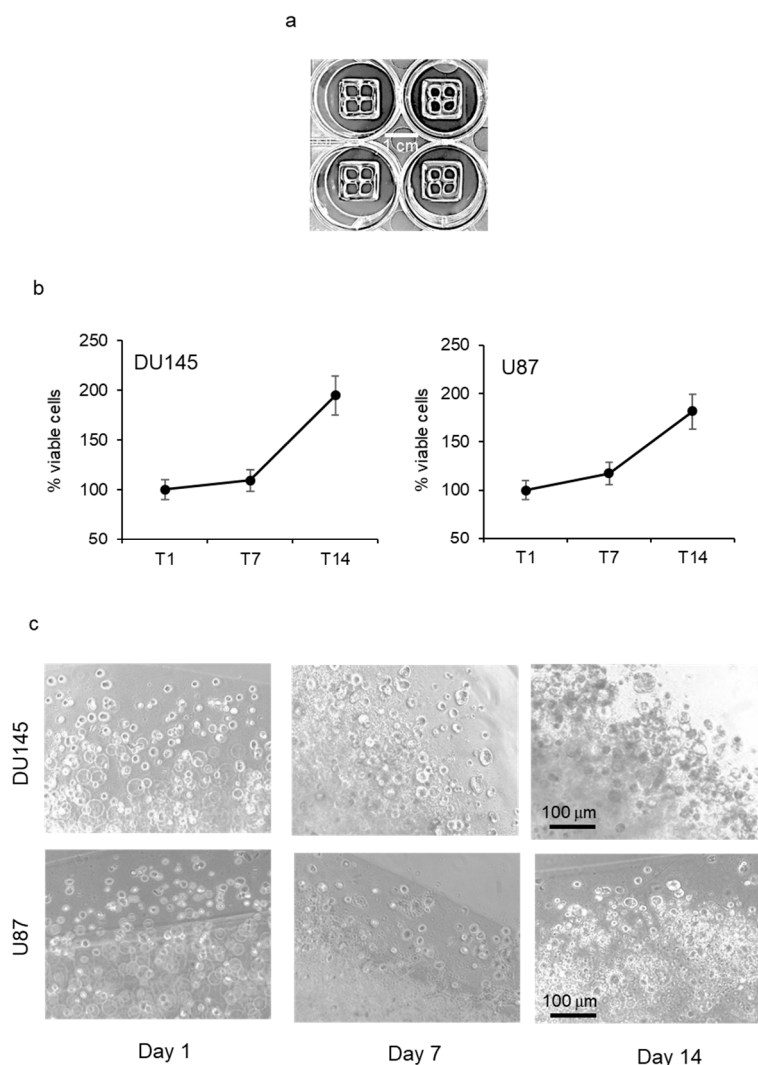
### 2.8. Statistical Analysis

All the statistical procedures were performed by GraphPad Prism Software Inc. (San Diego, CA, USA). Data are expressed as mean  $\pm$  standard deviations (SD) of at least three independent experiments. The statistical significance between measure series was calculated with parametric Student t test and *p* values of less than 0.01.

## 3. Results

*Tumor cell growth in bioprinted scaffold.* Prostate cancer (DU145) and glioblastoma (U87) cells were resuspended in alginate/gelatin hydrogel at a density of  $2 \times 10^6$  cells/mL. Cell suspension was bioprinted in a controlled environment onto each well of a 12-well plate

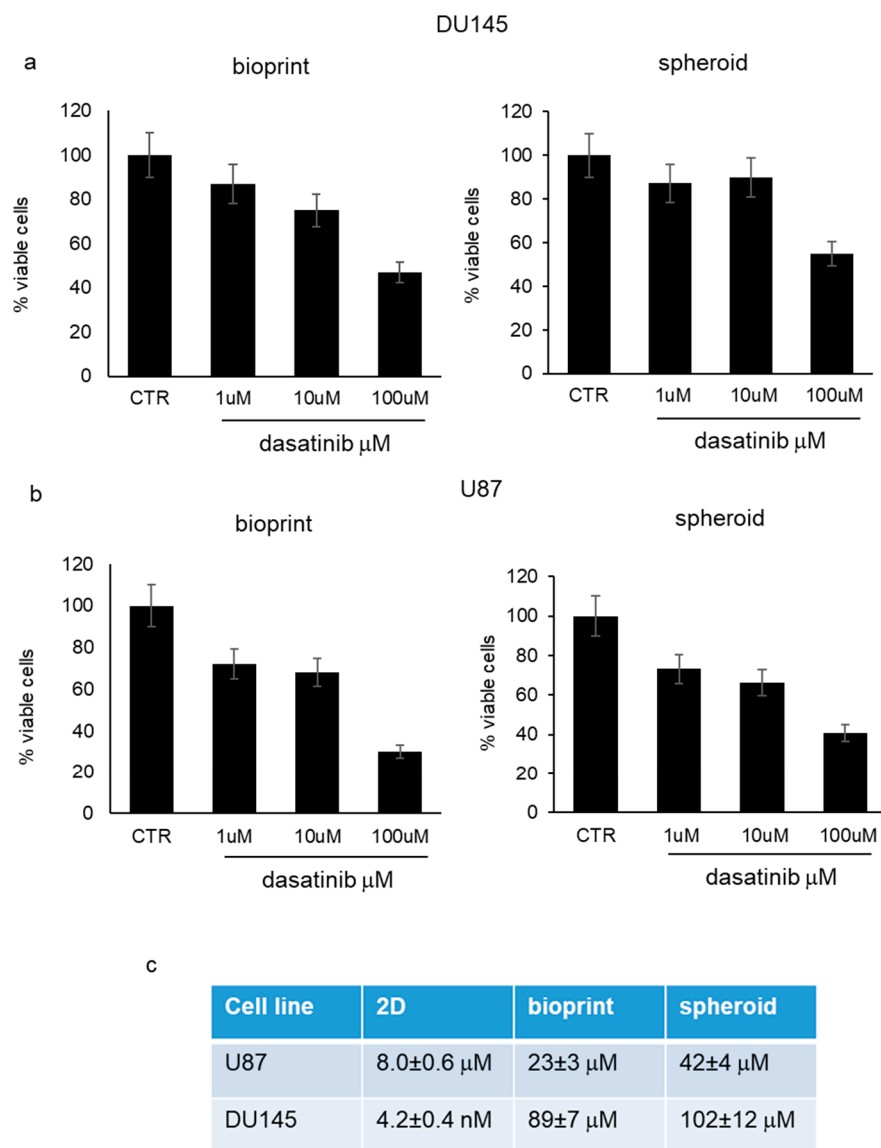
following the digital model of a cuboid shape with four internal empty spaces (structure size: L 12 mm  $\times$  W 12 mm  $\times$  H 1.2 mm) (Figure 1a). Tumor cell growth was monitored by PrestoBlue<sup>®</sup> cell viability reagent and revealed a progressive increase in the number of viable cells that was similar in the two cell lines, with a doubling time of about 14 days (Figure 1b). When bioprinted structures were observed by phase contrast microscopy, it was evident that tumor cells tended to form spheroid aggregates with increasing diameter over time (Figure 1c).



**Figure 1.** Tumor cell growth in bioprinted scaffold. (a) Exemplificative image of bioprinted al-gine/gelatin constructs printed in 12-well multiwell plate. (b) Mean percentage of viable DU145 and U87 cells grown in bioprinted scaffold and evaluated 1, 7, and 14 days (T1, T7, T14) after bioprinting. The mean values measured at T1 were adjusted at 100%. Each value represents the mean of five different bioprints ( $\pm$ standard deviation). (c) Representative images acquired by phase contrast microscopy (100 $\times$  magnification) of bioprints containing DU145 (upper images) and U87 cells at days 1, 7, and 14 after printing.

*Antiproliferative effect of dasatinib in 3D cell models.* Bioprinted tumor cells and tumor spheroids, utilizing both DU145 and U87 cells, were subjected to increasing concentrations of dasatinib (1  $\mu$ M, 10  $\mu$ M, and 100  $\mu$ M) for 72 h and tumor growth was monitored by PrestoBlue<sup>®</sup> cell viability reagent. Dasatinib determined a significant reduction in cell viability that was evident starting from 1  $\mu$ M with similar trends in the two different cell models (Figure 2a,b). Dasatinib cytotoxicity was more marked in U87 cells compared to

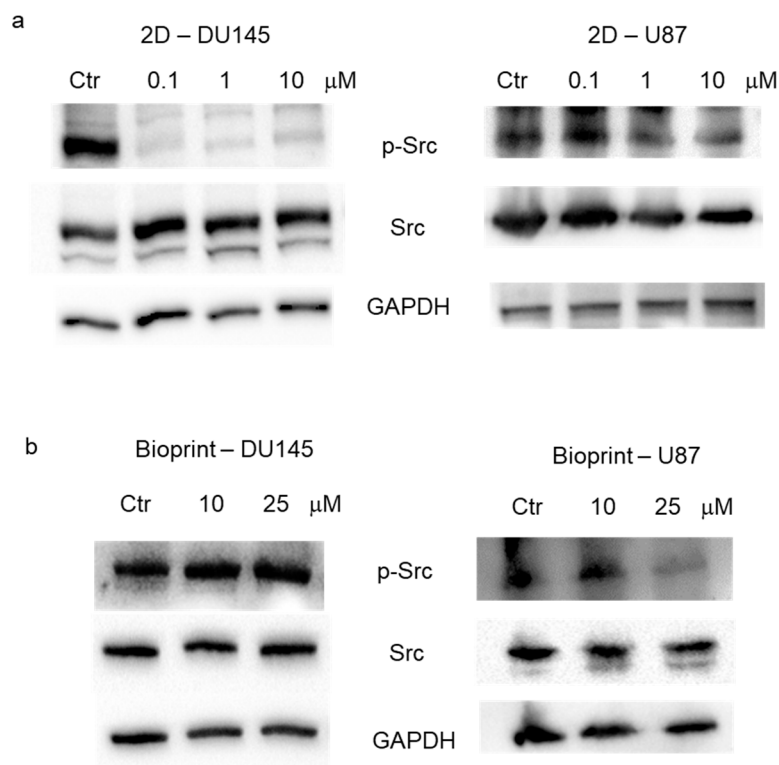
DU145 cells. In addition, according to IC<sub>50</sub> value, bioprinted cells demonstrated a higher sensitivity to dasatinib compared to spheroids, but both spheroids and bioprints were far less susceptible to dasatinib action compared to 2D cell culture treated in the same experimental conditions (Figure 2c).



**Figure 2.** Antiproliferative effect of dasatinib in 3D cell models. **(a)** Percentage of viable DU145 cells in bioprints (**left**) and in spheroids (**right**) 72 h after treatment with increasing concentrations of dasatinib (1, 10, and 100  $\mu\text{M}$ ). The mean values measured in untreated cells were adjusted at 100%. Each value represents the mean of five different measurements ( $\pm$ standard deviation). **(b)** Percentage of viable U87 cells in bioprints (**left**) and in spheroids (**right**) 72 h after treatment with increasing concentrations of dasatinib (1, 10, and 100  $\mu\text{M}$ ). The mean values measured in untreated cells were adjusted at 100%. Each value represents the mean of five different measurements ( $\pm$ standard deviation). **(c)** Mean IC<sub>50</sub> values calculated for U87 and DU145 cells treated with dasatinib for 72 h. The IC<sub>50</sub>s were calculated in standard culture conditions (2D), in 3D bioprint model (bioprint), and in spheroids and were the result of three different experiments ( $\pm$ standard deviation).

*Evaluation of Src activation.* The expression of Src and of its active form, pSrc (Tyr416), was evaluated in 2D culture and in bioprints realized with DU145 and U87 cells. Expression levels of total Src, pSrc (Tyr416), and GAPDH were evaluated in total cell lysates by Western

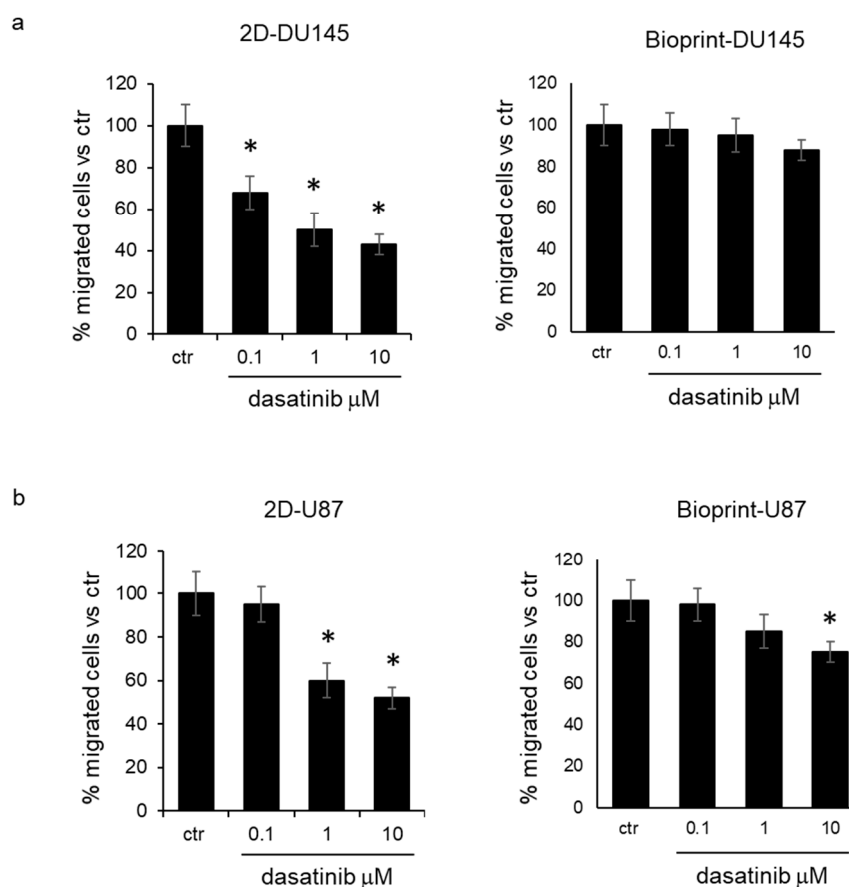
blot analysis in 2D cell cultures treated with increasing concentrations of dasatinib (0.1, 1, and 10  $\mu\text{M}$ ) for 24 h. In DU145 cells, a reduction in the active form of Src, but not in the total Src, was evident already from 0.1  $\mu\text{M}$  dasatinib, while in U87 cells, the first effective concentration was 1  $\mu\text{M}$  (Figure 3a). Expression levels of total Src, pSrc (Tyr416), and GAPDH were also evaluated in total cell lysates by Western blot analysis in bioprint models treated with 10 and 25  $\mu\text{M}$  of dasatinib for 24 h. The results did not show an appreciable reduction in the active form of Src in the DU145 model, while the first effective concentration of dasatinib in U87 cells was 25  $\mu\text{M}$  (Figure 2b).



**Figure 3.** Evaluation of Src activation. (a) Western blot analysis of total cell lysates from DU145 (left) and U87 (right) cells cultured in standard conditions (2D). Cell lysates were recovered 24 h after dasatinib treatment with increasing concentrations (0.1, 1, and 10  $\mu\text{M}$ ) and analyzed for the expression of pSrc (Tyr416), total Src, and GAPDH (loading reference). (b) Western blot analysis of total cell lysates from DU145 (left) and U87 (right) cells cultured alginate/gelatin bioprinted scaffold (bioprint). Bioprints were treated for 24 h with 10 or 25  $\mu\text{M}$  dasatinib and analyzed for the expression of pSrc (Tyr416), total Src, and GAPDH (loading reference).

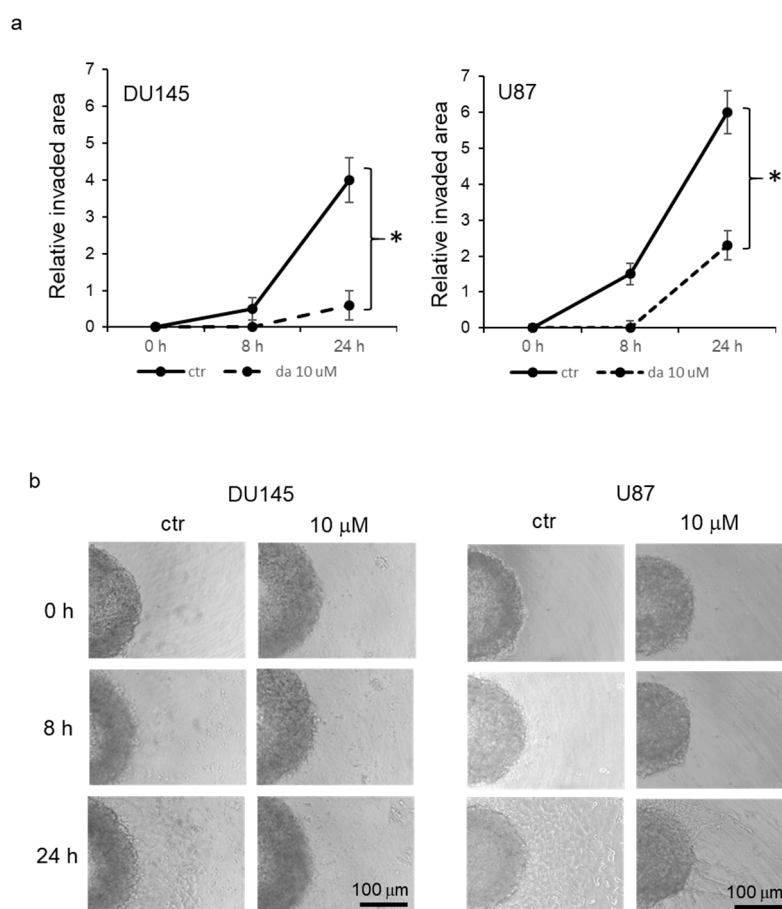
*Inhibition of cell migration by dasatinib.* Two-dimensional cell culture and bioprint models were treated for 24 h with increasing concentrations of dasatinib (0.1, 1, and 10  $\mu\text{M}$ ), and then cells were recovered to evaluate their migration ability. The analysis of the number of cells able to cross the membrane of the transwell system demonstrated that in DU145 and U87 cells treated in standard culture conditions, dasatinib was effective in reducing cell migration at a concentration of 0.1  $\mu\text{M}$  and 1  $\mu\text{M}$ , respectively (Figure 4a,b). On the contrary, cells recovered from bioprints did not show a significant reduction in cell migration with respect to control cells for DU145 cells, and only at the concentration of 10  $\mu\text{M}$  for U87 cells (Figure 4b).





**Figure 4.** Inhibition of cell migration by dasatinib. (a) Percentage of migrated DU145 cells evaluated in transwell system utilizing cells from standard cell culture (2D, left) or from bioprint model (right) and treated for 24 h with increasing concentrations of dasatinib (0.1, 1, and 10 μM). The mean values measured in untreated cells were adjusted at 100%. Each value represents the mean of five different measurements ( $\pm$ standard deviation). \*  $p < 0.01$  vs. ctr, according to Student's  $t$  test. (b) Percentage of migrated U87 cells evaluated in transwell system utilizing cells from standard cell culture (2D, left) or from bioprint model (right) and treated for 24 h with increasing concentrations of dasatinib (0.1, 1, and 10 μM). The mean values measured in untreated cells were adjusted at 100%. Each value represents the mean of five different measurements ( $\pm$ standard deviation). \*  $p < 0.01$  vs. ctr, according to Student's  $t$  test.

*Inhibition of cell dissemination in spheroids.* In order to verify the effect of dasatinib on migration of cells grown in spheroids, DU145 and U87 cells were used to form spheroids for 48 h and then spheroids were transferred to collagen-coated plates, where half of them were treated with 10 μM dasatinib. Then, spheroids were monitored by phase contrast microscopy, and time-course digital images were taken. The evaluation of dissemination was performed by measuring the area occupied by cells adhered to collagen, subtracting the area of the spheroid. The analysis of the mean relative values of the covered area revealed that cells in the control spheroids were able to disseminate progressively onto collagen from the surface of the spheroid, and this phenomenon was significantly evident starting from 8 h after cell plating (Figure 5a,b). On the other hand, dasatinib-treated spheroid demonstrated a reduced capacity to disseminate, and a significant increase in mean disseminated area was visible only after 24 h but to a smaller extent with respect to the mean control area.



**Figure 5.** Inhibition of cell dissemination in spheroid. (a) Mean relative invaded area in DU145 and U87 spheroids evaluated 8 and 24 days after plating onto collagen-coated surface. The values represent the mean of five different measurements ( $\pm$ standard deviation) of spheroids treated or not with 10  $\mu$ M dasatinib. \*  $p < 0.01$  between indicated points according to Student's  $t$  test. (b) Representative images acquired by phase contrast microscopy (100 $\times$  magnification) of DU145 and U87 cells at 0, 8, and 24 h after plating in the presence or not of 10  $\mu$ M dasatinib.

#### 4. Discussion

Cancer 3D tissue cultures represent an experimental model able to potentially mimic *in vivo* growth more closely. In particular, they show distinct characteristics in terms of cellular phenotype, mass transport, and cell–cell interactions as compared with conventional 2D cell cultures [19]. These specific characteristics can significantly affect the sensitivity to antitumoral drugs, and for this reason, it is fundamental to acquire detailed knowledge about their response in order to plan their effective utilization in preclinical drug testing. Spheroids are considered an ideal model in order to mimic some important tumor features, such as structural organization and the gradients of oxygen, pH, and nutrients [20]. Indeed, cancer spheroids have been frequently considered in preclinical studies to evaluate tumor response to chemotherapy. Although different techniques have been tested for spheroid formation, several issues with applying this model at a preclinical level still remain, particularly reproducibility and high-throughput application [21]. Recently, 3D bioprinting has been recognized as a promising technology for creating a tissue-based platform with high reproducibility and scalability. A key feature in developing a 3D bioprint model useful in pharmaceutical applications is the choice of an appropriate printable biomaterial, commonly referred to as bioink, essential for determining cancer cell phenotypes and biophysical properties of the tissue. Among the natural polymers, sodium alginate plays a significant role in tissue engineering applications owing to its biocompatibility, bioavailability, low cost, and thixotropic property [22]. Gelatin is frequently added to

alginate in order to enhance cytocompatibility and printability. In our study, we confirmed that DU145 and U87 cells survive in alginate/gelatin scaffold, showing a proliferation trend for at least 14 days. Cancer cells cultured in these conditions tended to grow as cell aggregates, resembling spheroids, and this is because the bioink does not represent an adhesive substrate for cells. When we compared 3D bioprinted tissue culture with 2D culture and spheroids in their susceptibility to dasatinib treatment, we ascertained that 3D bioprinted cells behaved more similarly to the spheroid model. In fact, both 3D bioprints and spheroids demonstrated higher resistance to dasatinib toxicity than 2D cell culture. The resistance was particularly evident in DU145 cells (about 20-fold higher IC<sub>50</sub> than 2D) and slightly higher in spheroids than in bioprinted tissue cultures (about 2-fold higher IC<sub>50</sub> in U87).

Spheroids frequently showed in the literature high resistance to most therapies, including chemotherapies and radiotherapies [23]. The acquisition of resistance in 3D models could be explained by different mechanisms. Besides biological features, including different interactions with surrounding cells or with the extracellular matrix and higher phenotypic heterogeneity, an important element to consider is the penetration of the drug into the spheroid. Large spheroids show higher drug resistance than small ones, and the penetration of drug is restricted to the outer layer. In our experiments, we utilized spheroids of >500 µm in diameter, in which drug resistance could be attributable just to their dimensions, as mentioned before [20]. Cells in bioprinted structures formed spheroids that after 12 days are heterogeneous in diameter and <500 µm; however, as indicated by the IC<sub>50</sub>, they express a drug resistance similar to that of the spheroids. However, also in this case, the reason could be attributable to a scarce penetrance of the drug. The analysis of the activation status of Src, the main target of dasatinib, showed a reduced ability of the drug to inhibit the formation of the phosphorylated Src. Thus, it is plausible that alginate/gelatin hydrogel generates a hurdle to the diffusion of dasatinib within the bioprinted structures. Resistance to dasatinib was also evident when cells were recovered from the bioprinted structure and subjected to migration assay. In fact, with respect to the expected reduction in migration demonstrated by cells treated in 2D culture, cells from bioprinted structures maintained a higher migration ability. The drug resistance was not apparently associated with a change in phenotype. In fact, the permanence of the susceptibility to dasatinib in 3D tissue culture was confirmed by the dissemination test performed with spheroids. In this test, dasatinib was effective in reducing the ability of cells to invade the surrounding microenvironment. Because the cells involved in the dissemination are mainly those present on the surface of the spheroid, this supports the hypothesis of the scarce penetrance of the drug within the 3D structure.

The application of bioprinting to drug screening in our experimental procedures offers different advantages with respect to spheroid formation by the hanging drop method that is performed manually. In fact, the hanging drop method requires a skilled operator, and its technical complications compromise its reproducibility and make it unsuitable for high-throughput screening. However, novel 3D tissue techniques emerge constantly. These include new multi-microwell platforms able to assure higher sphere formation yield, uniform sphere size, and scalability [24]. However, in these procedures, as in all suspension cell culture methods, a reliable non-adherent coating is critical to assure reproducibility in sphere formation and in their behavior during the prolonged culture. The use of hydrogel as embedding material may guarantee that cells can organize in a stable, complex, dynamic 3D architecture making contact also with extracellular matrices. Three-dimensional bioprinting does not require particular expertise and permits obtaining several uniform structures in a short time. Alginate/gelatin hydrogel supports 3D growth of cancer cells, and as we observed also in our experimental models, cells spontaneously formed spheroids without the need for a further repulsive procedure. In addition, the bioprinted structures, for their chemical and physical stability permitting a regular change in medium without affecting cell behavior, offer the possibility to perform frequent viability tests. At the same time, alginate/gelatin hydrogel can be dissolved with ion-chelating solution, freeing spheroids

that once in suspension could be utilized for further analyses. With this study, we have verified that bioprinting offers an abundant cellular material that could be easily used to analyze protein expression.

**Author Contributions:** L.C. and S.S. performed experiments with 2D cell cultures and 3D spheroids, wrote the Materials and Methods section, and performed the bibliographic search; M.D.V.N. and S.S. performed experiments with 3D bioprinting models; D.V. supervised and developed protocols for 3D models; F.Z. critically revised the manuscript; A.A. and S.S. collected data for the preparation of figures and wrote the main manuscript text. All authors have read and agreed to the published version of the manuscript.

**Funding:** The study was funded by the Department of Biotechnological and Applied Clinical Sciences, University of L'Aquila, with intramural research programs.

**Institutional Review Board Statement:** Not applicable.

**Informed Consent Statement:** Not applicable.

**Data Availability Statement:** Most data generated or analyzed during this study are included in this article. The datasets and materials used and/or analyzed during the current study are available from the corresponding author on reasonable request.

**Acknowledgments:** Samantha Sabetta is supported by MIUR with a doctoral fellowship within the National Operational Program for Research and Innovation (Programma Operativo Nazionale Ricerca e Innovazione 2014-2020, ref: DOT13SR6G7).

**Conflicts of Interest:** The authors declare that they have no conflict of interest.

## References

1. Angelucci, A. Targeting Tyrosine Kinases in Cancer: Lessons for an Effective Targeted Therapy in the Clinic. *Cancers* **2019**, *11*, 490. [CrossRef] [PubMed]
2. Yeatman, T.J. A renaissance for SRC. *Nat. Rev. Cancer* **2004**, *4*, 470–480. [CrossRef] [PubMed]
3. Kim, L.C.; Song, L.; Haura, E.B. Src kinases as therapeutic targets for cancer. *Nat. Rev. Clin. Oncol.* **2009**, *6*, 587–595. [CrossRef] [PubMed]
4. Rai, K. Personalized Cancer Therapy: YES1 Is the New Kid on the Block. *Cancer Res.* **2019**, *79*, 5702–5703. [CrossRef] [PubMed]
5. Stein, P.L.; Vogel, H.; Soriano, P. Combined deficiencies of Src, Fyn, and Yes tyrosine kinases in mutant mice. *Genes Dev.* **1994**, *8*, 1999–2007. [CrossRef] [PubMed]
6. Manning, G.; Whyte, D.B.; Martinez, R.; Hunter, T.; Sudarsanam, S. The protein kinase complement of the human genome. *Science* **2002**, *298*, 1912–1934. [CrossRef]
7. Frame, M.C. Src in cancer: Deregulation and consequences for cell behaviour. *Biochim. Biophys. Acta* **2002**, *1602*, 114–130. [CrossRef]
8. Summy, J.M.; Gallick, G.E. Src family kinases in tumor progression and metastasis. *Cancer Metastasis Rev.* **2003**, *22*, 337–358. [CrossRef]
9. Lombardo, L.J.; Lee, F.Y.; Chen, P.; Norris, D.; Barrish, J.C.; Behnia, K.; Castaneda, S.; Cornelius, L.A.; Das, J.; Doweyko, A.M.; et al. Discovery of N-(2-chloro-6-methyl-phenyl)-2-(6-(4-(2-hydroxyethyl)-piperazin-1-yl)-2-methylpyrimidin-4-ylamino)thiazole-5-carboxamide (BMS-354825), a dual Src/Abl kinase inhibitor with potent antitumor activity in preclinical assays. *J. Med. Chem.* **2004**, *47*, 6658–6661. [CrossRef]
10. Martellucci, S.; Clementi, L.; Sabetta, S.; Mattei, V.; Botta, L.; Angelucci, A. Src Family Kinases as Therapeutic Targets in Advanced Solid Tumors: What We Have Learned so Far. *Cancers* **2020**, *12*, 1448. [CrossRef]
11. Puzstai, L.; Moulder, S.; Altan, M.; Kwiatkowski, D.; Valero, V.; Ueno, N.; Esteva, F.; Avritscher, R.; Qi, Y.; Strauss, L.; et al. Gene signature-guided dasatinib therapy in metastatic breast cancer. *Clin. Cancer Res.* **2014**, *20*, 5265–5271. [CrossRef] [PubMed]
12. Kelm, J.; Timmins, N.; Brown, C.; Fussenegger, M.; Nielsen, L. Method for generation of homogeneous multicellular tumor spheroids applicable to a wide variety of cell types. *Biotechnol. Bioeng.* **2003**, *83*, 173–180. [CrossRef] [PubMed]
13. Lv, D.; Hu, Z.; Lu, L.; Lu, H.; Xu, X. Three-dimensional cell culture: A powerful tool in tumor research and drug discovery. *Oncol. Lett.* **2017**, *14*, 6999–7010. [CrossRef] [PubMed]
14. Loessner, D.; Stok, K.; Lutolf, M.; Huttmacher, D.; Clements, J.; Rizzi, S. Bioengineered 3D platform to explore cell-ECM interactions and drug resistance of epithelial ovarian cancer cells. *Biomaterials* **2010**, *31*, 8494–8506. [CrossRef] [PubMed]
15. Ozbolat, I.T.; Hospodiuk, M. Current advances and future perspectives in extrusion-based bioprinting. *Biomaterials* **2016**, *76*, 321–343. [CrossRef] [PubMed]
16. Gudapati, H.; Dey, M.; Ozbolat, I. A comprehensive review on droplet-based bioprinting: Past, present and future. *Biomaterials* **2016**, *102*, 20–42. [CrossRef]

17. Lan, S.; Starly, B. Alginate based 3D hydrogels as an in vitro co-culture model platform for the toxicity screening of new chemical entities. *Toxicol. Appl. Pharmacol.* **2011**, *256*, 62–72. [CrossRef]
18. Kimlin, L.C.; Casagrande, G.; Virador, V.M. In vitro three-dimensional (3D) models in cancer research: An update. *Mol. Carcinog.* **2013**, *52*, 167–182. [CrossRef]
19. Yamada, K.M.; Cukierman, E. Modeling tissue morphogenesis and cancer in 3D. *Cell* **2007**, *130*, 601–610. [CrossRef]
20. Thakuri, P.S.; Gupta, M.; Plaster, M.; Tavana, H. Quantitative Size-Based Analysis of Tumor Spheroids and Responses to Therapeutics. *Assay Drug Dev. Technol.* **2019**, *17*, 140–149. [CrossRef]
21. Han, S.J.; Kwon, S.; Kim, K.S. Challenges of applying multicellular tumor spheroids in preclinical phase. *Cancer Cell Int.* **2021**, *21*, 152. [CrossRef] [PubMed]
22. Fatimi, A.; Okoro, O.V.; Podstawczyk, D.; Siminska-Stanny, J.; Shavandi, A. Natural Hydrogel-Based Bio-Inks for 3D Bioprinting in Tissue Engineering: A Review. *Gels* **2022**, *8*, 179. [CrossRef] [PubMed]
23. Gong, X.; Lin, C.; Cheng, J.; Su, J.; Zhao, H.; Liu, T.; Wen, X.; Zhao, P. Generation of Multicellular Tumor Spheroids with Microwell-Based Agarose Scaffolds for Drug Testing. *PLoS ONE* **2015**, *10*, e0130348. [CrossRef] [PubMed]
24. Chen, Y.; Lou, X.; Zhang, Z.; Ingram, P.; Yoon, E. High-Throughput Cancer Cell Sphere Formation for Characterizing the Efficacy of Photo Dynamic Therapy in 3D Cell Cultures. *Sci. Rep.* **2015**, *5*, 12175. [CrossRef] [PubMed]

**Disclaimer/Publisher’s Note:** The statements, opinions and data contained in all publications are solely those of the individual author(s) and contributor(s) and not of MDPI and/or the editor(s). MDPI and/or the editor(s) disclaim responsibility for any injury to people or property resulting from any ideas, methods, instructions or products referred to in the content.

## Article

# Micellar Curcumin Substantially Increases the Antineoplastic Activity of the Alkylphosphocholine Erufosine against TWIST1 Positive Cutaneous T Cell Lymphoma Cell Lines

Antonios G. X. Trochopoulos <sup>1,†</sup>, Yana Ilieva <sup>2,†</sup>, Alexander D. Kroumov <sup>3</sup>, Lyudmila L. Dimitrova <sup>2</sup>, Ivanka Pencheva-El Tibi <sup>4</sup>, Stanislav Philipov <sup>5</sup>, Martin R. Berger <sup>6</sup>, Hristo M. Najdenski <sup>2</sup>, Krassimira Yoncheva <sup>7,\*</sup>, Spiro M. Konstantinov <sup>1</sup> and Maya M. Zaharieva <sup>2,\*</sup>

<sup>1</sup> Department of Pharmacology, Pharmacotherapy and Toxicology, Faculty of Pharmacy, Medical University of Sofia, 2 Dunav Str., 1000 Sofia, Bulgaria

<sup>2</sup> Department of Infectious Microbiology, The Stephan Angeloff Institute of Microbiology, Bulgarian Academy of Sciences, 26 Acad. G. Bonchev Str., 1113 Sofia, Bulgaria

<sup>3</sup> Department of Applied Microbiology, The Stephan Angeloff Institute of Microbiology, Bulgarian Academy of Sciences, 26 Acad. G. Bonchev Str., 1113 Sofia, Bulgaria

<sup>4</sup> Department of Pharmaceutical Chemistry, Faculty of Pharmacy, Medical University of Sofia, 2 Dunav Str., 1000 Sofia, Bulgaria

<sup>5</sup> Department of Human Anatomy, Histology, General and Clinical Pathology and Forensic Medicine, Faculty of Medicine, University Hospital Lozenetz, Sofia University "St. Kliment Ohridski", 2 Kozyak Str, 1421 Sofia, Bulgaria

<sup>6</sup> Unit of Toxicology and Chemotherapy, German Cancer Research Center, D-69120 Heidelberg, Germany

<sup>7</sup> Department of Pharmaceutical Technology and Biopharmaceutics, Faculty of Pharmacy, Medical University of Sofia, 2 Dunav Str., 1000 Sofia, Bulgaria

\* Correspondence: kyoncheva@pharmfac.mu-sofia.bg (K.Y.); zaharieva26@yahoo.com (M.M.Z.)

† These authors contributed equally to this work.

**Citation:** Trochopoulos, A.G.X.; Ilieva, Y.; Kroumov, A.D.; Dimitrova, L.L.; Pencheva-El Tibi, I.; Philipov, S.; Berger, M.R.; Najdenski, H.M.; Yoncheva, K.; Konstantinov, S.M.;

et al. Micellar Curcumin Substantially Increases the Antineoplastic Activity of the Alkylphosphocholine Erufosine against TWIST1 Positive Cutaneous T Cell Lymphoma Cell Lines.

*Pharmaceutics* **2022**, *14*, 2688.

<https://doi.org/10.3390/pharmaceutics14122688>

Academic Editor: Tomáš Etrych

Received: 31 October 2022

Accepted: 27 November 2022

Published: 1 December 2022

**Publisher's Note:** MDPI stays neutral with regard to jurisdictional claims in published maps and institutional affiliations.



**Copyright:** © 2022 by the authors. Licensee MDPI, Basel, Switzerland. This article is an open access article distributed under the terms and conditions of the Creative Commons Attribution (CC BY) license (<https://creativecommons.org/licenses/by/4.0/>).

**Abstract:** Cutaneous T-cell lymphoma (CTCL) is a rare form of cancer with local as well as systemic manifestations. Concomitant bacterial infections increase morbidity and mortality rates due to impaired skin barrier and immune deficiency. In the current study, we demonstrated that the in vitro anti-lymphoma potential of erufofosine is diminished by TWIST1 expression and micellar curcumin substantially increases its antineoplastic activity. Pharmacokinetic analysis showed that the micellar curcumin (MCRM) used in our study was characterized by low zeta potential, slow release of curcumin, and fast cell membrane penetration. The combination ratio 1:4 [erufofosine:MCRM] achieved strong synergism by inhibiting cell proliferation and clonogenicity. The combined antiproliferative effects were calculated using the symbolic mathematical software MAPLE 15. The synergistic combination strongly decreased the expression of TWIST1 and protein kinase B/Akt as proven by western blotting. Significant reductions in NF- $\kappa$ B activation, induction of apoptosis, and altered glutathione levels were demonstrated by corresponding assays. In addition, the synergistic combination enhanced the anti-staphylococcal activity and prevented biofilm formation, as shown by crystal violet staining. Taken together, the above results show that the development of nanotechnological treatment modalities for CTCL, based on rational drug combinations exhibiting parallel antineoplastic and antibacterial effects, may prove efficacious.

**Keywords:** cutaneous T-cell lymphoma; TWIST1; erufofosine; curcumin; synergy; nanotechnology

## 1. Introduction

Cutaneous T-cell lymphomas (CTCL) represent a heterogeneous group of rare extranodal T-cell lymphoproliferative disorders (non-Hodgkin's lymphomas, NHLs) which primarily affect the skin by a clonal accumulation of skin-homing CD4+CD45RO+ helper/memory neoplastic T-lymphocytes [1,2]. CTCL progresses by involving the lymph nodes, blood, and visceral organs [3,4], and many patients develop relapsed/refractory disease with

a potentially fatal prognosis [5]. Two of the most important subtypes of CTCL are the cutaneous mycosis fungoides (MF) [6] and the leukemic Sézary syndrome (SS) [7]. Both are characterized by a poor quality of life and may lead to seriously shortened overall survival, especially if an extracutaneous involvement is present. An additional important clinical problem associated with major morbidity and mortality rates is the high frequency of concomitant bacterial infections due to impaired barrier function of the skin and progressive immune deficiency [8]. Axelrod et al. found out that 396 of 478 documented microbial infections in CTCL patients were of bacterial origin, e.g., *Staphylococcus aureus*, and were intimately associated with the disease stage [9]. Other published data indicate that staphylococcal enterotoxins may promote the expansion of malignant T-cells [8].

The current therapy of CTCL is challenging, often empiric, and not typically based on specific molecular alterations due to limited insight into the genetic basis of the disease [10]. Recent research based on next-generation sequencing revealed potentially targetable oncogenic mutations in the nuclear factor  $\kappa$  B (NF- $\kappa$ B) and the Janus Kinase and Signal Transducer and Activator of Transcription (JAK-STAT) signaling pathways whose abnormal activation causes apoptosis resistance [11–13]. These cancer-promoting somatic mutations affect transcription factors such as TWIST1 (Twist-related protein 1), thereby altering the T-cell effector function and driving lymphomagenesis into proliferation [14,15]. The TWIST1 transcription regulator plays an essential role in cancer metastasis and is activated by a variety of signal transduction pathways, including protein kinase B (PKB/Akt), STAT3, mitogen-activated protein kinase (MAPK), Ras, and Wnt signaling. TWIST1 is thought to promote tumor progression in MF and SS via the p53 axes for cell G1/S cycle arrest with subsequent inhibition of the c-myc-induced apoptosis [16,17], which makes it an attractive molecular target in the personalized treatment approach.

The current therapeutic modalities of CTCL include skin-directed treatments (for patients with limited skin disease and favorable overall survival), retinoids and histone deacetylase inhibitors for advanced-stage disease, and classical cytoreductive chemotherapeutics for relapsed/refractory CTCL forms [7,18,19]. Extracorporeal photopheresis, which is characterized by an excellent side effect profile and moderate efficacy, is considered the first-line therapy for erythrodermic MF and SS [20,21]. Patients with significant nodal, visceral, or blood involvement are generally treated with biologic-response modifiers before escalating to systemic, single-agent chemotherapy. In highly-selected patients, allogeneic stem-cell transplantation may be considered, as this may be curative in some patients [22]. Systemic treatment for relapsed/refractory CTCL has historically relied on traditional chemotherapeutics, retinoids interferons, interleukins, phosphorylase inhibitors, histone deacetylase or proteasome inhibitors; however, responses are often short-lived [23]. Response rates of the clinically approved histone deacetylase inhibitors romidepsin and vorinostat are typically <35%. They can induce some durable responses in heavily pre-treated patients and alleviate bothersome symptoms, such as pruritus. Failure to cure advanced SS and MF with large cell transformation peripheral T-cell lymphoma has resulted in a search for novel targeted agents, including antibodies and gene modulators [7], such as anti-CD30 antibody-drug conjugate brentuximab vedotin, anti-CCR4 antibody mogamulizumab, and the fusion protein immunotoxin A-dmDT390-bisFv(UCHT1) [5,18]. Nevertheless, none of these drugs were related to distinguished advances in CTCL therapy.

The drug erufosine (ERF) is a third-generation alkylphosphocholine (APC) with favorable pharmacokinetics and a broad spectrum of in vitro and in vivo antineoplastic activities [24–28], as well as antibacterial activity against pathogenic *Staphylococcus aureus* strains in clinically applicable concentrations [29]. In contrast to other APCs [30], ERF exhibits less pronounced cholinomimetic side effects [31] and can be given intravenously due to a lack of hemolytic properties [32]. The comprehensive mode of action of erufosine includes apoptotic and/or autophagy-mediated cell death in a dose-dependent manner, inhibition of the PKB/Akt-Rb and mTOR axes, and induction of G2/M cell cycle arrest through modulation of the cyclin-dependent kinase inhibitor p27Kip1 [28,33–43]. One of the most important advantages of ERF is the absence of bone marrow toxicity [38,44,45],

which makes it an attractive candidate for combined chemotherapies. The progenitor of ERF, miltefosine, was tested in phase I-II studies for topical treatment (6% ointment) of cutaneous lymphomas and led to an overall response rate between 58 and 71% and response duration of 12 months without causing myelotoxicity [46–50]. However, more than 50% of the patients developed strong side effects such as erythema, scaling, skin atrophy, local desquamation, and pruritus [46–48], and the clinical trials were discontinued. These results raise the issue and give hope that erufosine could be a more suitable option for CTCL treatment, especially in rational synergistic combinations with anti-inflammatory compounds that could ameliorate possible adverse events without compromising the antineoplastic effect.

Curcumin (CRM) is the major active component of the spice turmeric (*Curcuma longa*, Zingiberaceae) [51] with pleiotropic pharmacological effects which has been used for centuries in the Indian traditional medicine as an anti-inflammatory and antimicrobial remedy [52]. The most important cellular target of curcumin is the pro-inflammatory mediator NF- $\kappa$ B which explains the chemoprotective, antiproliferative, anti-apoptotic, and anti-carcinogenic effects of the compound [53,54]. Curcumin is a potent inhibitor of lymphoblasts' proliferation in CTCL cell lines through modulation of the JAK/STAT and NF- $\kappa$ B signaling and induction of oxidative stress [55,56]. It is also a suitable candidate for combination therapies because of the low cytotoxicity on normal tissues. The cellular uptake of curcumin is higher in malignant cells than in normal; therefore, it is well tolerated in humans [57]. However, curcumin's clinical application is limited by the low water solubility and fast metabolism after absorption from the gastrointestinal tract leading to low bioavailability. As a consequence, only small amounts of curcumin are detectable in target tissues which can be overcome through incorporation into polymeric micellar systems suitable for cutaneous application [58–61].

Having in mind the published scientific data on the therapeutic approaches for CTCL and the gaps in this research area, we set ourselves the goal to evaluate in detail the in vitro pharmacological potential of basically new therapeutic modalities for targeted inhibition of signal transduction pathways involved in the carcinogenesis of CTCL such as TWIST1, PKB/Akt and NF- $\kappa$ B. The focus of the investigations falls on the antineoplastic activity and mode of action of rationally selected synergistic combinations between ERF and micellar curcumin (MCRM) in a panel of CTCL cell lines and the potential of such combinations to inhibit the growth and biofilm formation of pathogenic *Staphylococcus aureus* strains. Our specific aim was to demonstrate that (1) ERF is a suitable drug candidate for the treatment of CTCL, but the transcription factor TWIST 1 reduces the efficacy of ERF in TWIST1 expressing CTCL cell lines, and (2) combining ERF with MCRM will increase the antineoplastic effect of both substances, thus leading to a significant TWIST1 inhibition, deactivation of PKB/Akt and NF- $\kappa$ B, and suppression of *Staphylococcus aureus* biofilm formation.

## 2. Materials and Methods

### 2.1. Drugs and Chemicals

Curcumin (#C1386, Mw = 368.385 g/mol), absolute ethanol (#46139), methanol (#322415), methoxy poly(ethylene glycol)-block-poly( $\epsilon$ -caprolactone) (#900649), glacial acetic acid (#1005706 USP), crystal Violet (#C0775), Tris-HCl (#T5941), Sodium Dodecyl Sulfate (#L3771), glycerol (#G5516), DL-Dithiothreitol (#43815), skimmed milk powder (#70166), Tween 20<sup>®</sup> (#P1379), 5,5'-Dithiobis(2-nitrobenzoic acid) (#D8130), Hoechst 33342 (#14533) and 3-(4,5-dimethylthiazolyl-2)-2,5-diphenyltetrazolium bromide (#M2128, MTT dye) were purchased from Sigma<sup>®</sup> Life Science (Roedermark, Germany). Working solution of Gentamycin (40 mg/L) was prepared through dilution of commercially available stock (amp. 40 mg/mL, 1 mL, Sopharma<sup>®</sup>, Sofia, Bulgaria) in HPLC purified water. Erufosine (Mw = 503.74 g/mol) was kindly provided by Prof. Hans-Jörg Eibl [62] in the form of 20 mM stock solution in 0.9% NaCl and was stored at 4 °C.



## 2.2. Cell Lines and Cultivation Procedure

All three cell lines originated from the American Type Culture Collection (ATCC): HuT-78 (lymphoblasts, Sezary Syndrome, ATCC<sup>®</sup>TIB-161<sup>™</sup>), MJ (lymphoblasts, Mycosis fungoides, ATCC<sup>®</sup>CRL-8294<sup>™</sup>), HH (lymphoblasts, cutaneous T cell lymphoma; ATCC<sup>®</sup>CRL-2105<sup>™</sup>). Cell cultures were maintained at cell density  $5 \times 10^4$ – $8 \times 10^5$  viable cells/mL under standard conditions (37 °C, 5% CO<sub>2</sub>, humidified atmosphere, Panasonic CO<sub>2</sub> incubator, #MCO-18AC-PE, Osaka, Japan) according to the recommendations of ATCC for growth media and subculturing rate. The following buffers and media were used in the cell culturing procedures: (1) RPMI-1640 without Phenol Red (#RPMI-XXXA, Capricorn<sup>®</sup>, Düsseldorf, Germany), supplemented with 4 mM L-Glutamine (#G7513, Sigma<sup>®</sup> Life Science, Germany), 20% fetal bovine serum (#FBS-HI-12A, Capricorn<sup>®</sup>, Germany), 25 mM HEPES buffer solution (#HEP-B, Capricorn<sup>®</sup>, Germany) and 4.5 g/l D-(+)-glucose (#G8769, Sigma<sup>®</sup> Life Science, Germany); (2) IMDM (#IMDM-A, Capricorn<sup>®</sup>, Germany), supplemented with 4 mM L-Glutamine and 20% fetal bovine serum and (3) Dulbecco's Phosphate Buffered Saline (PBS, #D8537, Sigma<sup>®</sup> Life Science, Germany). For all experiments, cells were plated at cell density  $3 \times 10^5$  viable cells/mL.

## 2.3. Bacterial Strains and Growth Conditions

The methicillin-resistant *Staphylococcus aureus* strain NBIMCC 8327 (MRSA, Bulgarian National Bank for Industrial Microorganisms and Cell Cultures, Sofia, Bulgaria) was used for the testing of combination effects and biofilm assay. The bacterial cultures were maintained at 37 °C under aerobic conditions using Trypticase Soy Broth (TSB, #LQ508) and Agar (TSA, #M1968) purchased from HiMedia<sup>®</sup>, Mumbai, India. For the biofilm inhibition assay Brain Heart Infusion Broth (BHI, # GM210, HiMedia<sup>®</sup>, India), supplemented with 2% D-Glucose (#G8769, Sigma<sup>®</sup> Life Science, Germany) was used.

## 2.4. Preparation and Characterization of Curcumin Loaded Micelles

The mPEG-PCL copolymer and CRM were dissolved in dioxane at a ratio 10:1 (*wt/wt*). The organic solution was gently stirred for 30 min (700 rpm), and after that purified water was added drop by drop. The resulting micellar dispersion was introduced into a dialysis membrane (MW = 6000–8000), which was further immersed in purified water. The outer aqueous medium was replaced 4 times. The size and zeta potential were determined by photon correlation spectroscopy and electrophoretic laser doppler velocimetry (Zetamaster analyzer, Malvern Instruments, Malvern, UK). Freshly prepared micellar dispersions were measured at 25 °C with a scattering angle of 90°. In vitro release of CRM from the micelles was examined by dialysis. Briefly, the micellar dispersion was poured into a dialysis membrane bag (MW = 6000–8000) that was further placed into 100 mL of phosphate buffer (pH = 7) containing 10% ethanol. Samples were withdrawn from the medium outside the dialysis bag, and the concentration of the released CRM was determined by UV-Vis spectrophotometry at  $\lambda = 425$  nm.

## 2.5. Cell Viability Test

The cell viability was evaluated according to ISO10993-5, Annex C [63] (MTT dye reduction assay). Briefly, prior treatment cells were seeded in 96-well plates ( $3 \times 10^5$  cells/mL) under sterile conditions (Laminar Air Flow Telstar Bio II Advance, Terrassa, Spain), incubated for 24 h until entering the *log*-phase of the growth curve, and treated with erufosine (0–200  $\mu$ M in serial twofold dilutions) for 24, 48 and 72 h. The schema for the combinations between erufosine and micellar curcumin followed the recommendations of Chou and Talalay for constant drug ratios [64]. All experiments were performed in triplicate, wherein every sample was repeated 4 times. The formazan intensity was measured on an Absorbance Microplate Reader EL-800 (Bio-Tek Instruments Inc., Winooski, VT, USA) at  $\lambda = 550$  nm ( $\lambda_{\text{ref}} = 690$  nm) against a blank solution (culture medium, MTT, and solvent).

## 2.6. Mathematical Modeling of Cytotoxic Effects after Single Drug Treatment

The calculation of the median single drug effects (median inhibitory concentrations,  $IC_{50}$ ) was performed as published before [65]. Briefly, we coded a nonlinear regression procedure in MAPLE<sup>®</sup> software of symbolic mathematics based on weighted least squares statistical criterion as an objective function of the search. A numerical optimization algorithm was used to minimize the sum of weighted squares and to find the estimates of best-fitting parameter values. The median-dose model was applied to obtain the “ $IC_{50}$ ” and “ $m$ ”, as presented in Equation (1):

$$\frac{F_a}{F_u} = \left( \frac{Dose}{D_m} \right)^m, \quad (1)$$

where  $F_a$  represents the affected fraction;  $F_u$ —the unaffected fraction ( $1 - F_a = F_u$ );  $Dose$ —the applied drug concentration;  $D_m$ —the median-effect dose (in our case  $D_m = IC_{50}$ ), and  $m$ —a slope of median-effect plot (for  $m = 1$  the curve is hyperbolic; for  $m > 1$ —sigmoidal; for  $m < 1$ —negative (flat) sigmoidal). In addition, we performed response surface analysis (RSA) methodology in order to reveal the predictive power of the model as a function of the parameters “ $IC_{50}$ ” and “ $m$ ”. The range of the value changes in the RSA 3D plot was determined based on the standard deviation of the “ $IC_{50}$ ” and “ $m$ ” values obtained during the statistical evaluation of the experimental data with the GraphPad Prism software.

## 2.7. Mathematical Modelling of Drug-Drug Interactions in Cell Lines

A computer program in the platform of the symbolic mathematical software MAPLE<sup>®</sup> was applied for calculation of the combination effects, and the simulation results were compared with calculations of CompuSyn (Paramus, NJ, USA) [64]. The simulations quantitatively evaluated the effects of action of two applied drugs MCRM and ERF (Dose A:Dose B). The combinations schema followed the recommendations of Chou and Martin [64]. Combination ratios 1:2 and 1:4 [ERF:MCRM] were applied. The mathematical equation of CI (combination index) was written as follows for earlier determined  $IC_{50}$  values of drugs A, B, and the combination AB:

$$CI_{(\alpha = 0)} = D_1/D_{x1} + D_2/D_{x2} \quad (2)$$

$$CI_{(\alpha = 1)} = D_1/D_{x1} + D_2/D_{x2} + \alpha \times (D_1/D_{x1}) \times (D_2/D_{x2}), \quad (3)$$

where  $D_{x1}$  = dose of drug 1 only to obtain 50% cell inhibition;  $D_1$  = dose of drug 1 to obtain 50% cell inhibition in combination with  $D_2$ ;  $D_{x2}$  = dose of drug 2 only to obtain 50% cell killing;  $(D) 2$  = dose of drug 2 to obtain 50% cell killing in combination with  $D_1$ ; and the values of  $\alpha = 0$  for mutually exclusive or  $\alpha = 1$  for non-mutually exclusive actions of drugs. Only the results for mutually exclusive actions of drugs are presented in this study. The step-by-step, fully automated simulation procedure resulted in isobolograms for HuT-78 and MJ cell lines.

According to the theory included in the manuals of the software program CompuSyn [64], the meanings of CI can be classified in more detail as follows:  $CI > 1.3$  shows antagonism;  $CI = 1.1$  to  $1.3$  moderate antagonism;  $CI = 0.9$  to  $1.1$  additive effect;  $CI = 0.8$  to  $0.9$  slight synergism;  $CI = 0.6$  to  $0.8$  moderate synergism;  $CI = 0.4$  to  $0.6$  synergism;  $CI = 0.2$  to  $0.4$  strong synergism. It should be noted that in Equations (2) and (3) the value of  $D_x$  (dose of a single drug) can be determined from the following equation:

$$D_x = D_m [F_a / (1 - F_a)]^{1/m}, \quad (4)$$

where  $F_a$ —stands for the affected fraction (has inhibition);  $F_u$ —means the unaffected fraction “u”,  $F_u = (1 - F_a)$  (no inhibition, control);  $D_x$  is the single dose of the drug;  $D_m$  means the dose giving the mean effect; hence,  $D_m = IC_{50}$  (in our case) 50% inhibition; “ $m$ ”—is the slope of the dose-effect curve.

### 2.8. Determination of Extracellular Curcumin Levels

The extracellular levels of micellar curcumin were determined in comparison to pure reference substance curcumin with a UV-spectrophotometric method using the following system: UV/VIS Spectrometer HP; Diode array detector; Analytical wavelength  $426 \text{ nm} \pm 2 \text{ nm}$  and operating software. The analytical calculations are based on Multicomponent analysis calculations. The following method options were used: multicomponent analysis (MCA), Beer's law calibration curve type, least squares fit (LSQ) algorithm, derivative order 0, polynomial degree 0, 1 smoothing point, 2 nm data interval, 426 nm analytical wavelength and temperature of  $25 \text{ }^\circ\text{C}$ . The test was prepared in the following way: for reference solutions (a): accurately weighed masses curcumin RS were dissolved in ethanol to obtain a solution with the following concentrations:  $C_1 = 1.00 \times 10^{-5} \text{ g/mL}$ ,  $C_2 = 0.75 \times 10^{-5} \text{ g/mL}$ ,  $C_3 = 0.65 \times 10^{-5} \text{ g/mL}$ ,  $C_4 = 0.55 \times 10^{-5} \text{ g/mL}$ ,  $C_5 = 0.50 \times 10^{-5} \text{ g/mL}$ ,  $C_6 = 0.45 \times 10^{-5} \text{ g/mL}$ ,  $C_7 = 0.30 \times 10^{-5} \text{ g/mL}$  and  $C_8 = 0.20 \times 10^{-5} \text{ g/mL}$ ; For the bioanalytical assay, test solution (b) was prepared as follows: to each sample aliquot containing curcumin were added 4.5 mL solvent mixture from acetonitrile and methanol (1:1, *v/v*), the samples were sonicated at  $20 \text{ }^\circ\text{C}$  for 5 min and centrifuged ( $<5000 \text{ rpm}$ , 5 min) for separating of the precipitates, the supernatant mixtures were filtered additionally and subjected to spectrophotometric determination against blanks prepared respectively.

### 2.9. Colony Forming Units (CFU) Assay

The clonogenicity survival assay was performed as published before [40]. Briefly, cells were treated as for MTT assay with selected combinations between ERF and MCRM and the responding single drug concentrations and incubated for 48 h. After that period of time, the cells in all treated groups were counted, and 3000 cells/mL from each group were seeded in semisolid medium (0.8% RPMI-methylcellulose, 40% fetal bovine serum), plated in 12-well plates (600  $\mu\text{L}$ /well) in triplicate and cultured for 10 days. Colonies ( $\geq 20$  cells in clusters) were counted using an inverted microscope (Boeco BIB-100, Hamburg, Germany).

### 2.10. Determination of Reduced Glutathione (GSH) Content

The spectrophotometric assay of Sedlak and Lindsay based on Ellman's reagent was used to determine the GSH levels after single and combined treatment [66]. Briefly, HuT-78 and MJ cells were seeded at a density of  $0.3 \times 10^6 \text{ cells/mL}$ , incubated for 24 h, and treated with 20  $\mu\text{M}$  ERF, 80  $\mu\text{M}$  MCRM or the combination of both. After 48 h incubation,  $5 \times 10^5 \text{ cells/sample}$  were washed with PBR, centrifuged (6000 rpm, 5 min), and lysed in 100  $\mu\text{L}$  lysis buffer (0.5% triton-100 in 0.2 M EDTA) at  $4^\circ\text{C}$  (5 min). The proteins were precipitated with 20  $\mu\text{L}$  20% (*v/w*) trichloroacetic acid. The volume of each sample was adjusted to 200  $\mu\text{L}$  with distilled water, followed by centrifugation at 14 5000 rpm (10 min). Supernatant aliquots were transferred in a 96-well plate (100  $\mu\text{L}$ /well) and mixed with 160  $\mu\text{L}$  Tris buffer (0.4 M, pH 8.9) and 4  $\mu\text{L}$  Ellman's reagent (3.4 mg/mL in methanol). The resulting yellow product was measured at 405 nm on an Absorbance Microplate Reader EL-800 (Bio-Tek Instruments Inc., USA). The GSH levels were presented as a percentage of the untreated control.

### 2.11. Determination of Cytosolic Mono- and Oligonucleosomes

A photometric enzyme immunoassay (Cell Death ELISA kit, #11 544 675 001, Roche Applied Science, Penzberg, Germany) was used for quantitative in vitro determination of cytoplasmic histone-associated DNA fragments (mono- and oligonucleosomes). Briefly, HuT-78 and MJ cell lines were seeded at density of  $0.3 \times 10^6 \text{ cells/mL}$ , cultivated for 24 h until entering the exponential growth phase, and exposed to 80  $\mu\text{M}$  MCRM or 20  $\mu\text{M}$  ERF or the combination thereof. After 72 h incubation period, cells were counted, and the immunoassay was performed according to the manufacturer's manual. The absorbance of the reaction product was measured at  $\lambda = 405 \text{ nm}$  (490 reference wavelength) against a substrate solution blank.

### 2.12. Caspase-3 Activity Assay

HuT-78 and MJ cells were seeded in 6-well plates at a density of  $0.3 \times 10^6$  cells/mL, incubated for 24 h, and treated thereafter with 20  $\mu$ M ERF, 80  $\mu$ M MCRM, or the combination of both for further 48 h. Cells were counted and  $1 \times 10^6$  cells/sample were washed three times with PBS and frozen at  $-80^\circ\text{C}$ . The measurement of caspase-3 activation was performed with the Caspase-3 DEVD-R110 Fluorometric and Colorimetric Assay Kit (#30008, Biotium, Fremont, CA, USA) following the experimental protocol of the manufacturer. The absorbance was measured at  $\lambda = 490$  nm on an Absorbance Microplate Reader EL-800 (Bio-Tek Instruments Inc., USA). As positive control, HL-60 cells ( $5 \times 10^4$ ) were used and incubated in hypertonic buffer (10 mM Tris, pH 7.4, 400 mM NaCl, 5 mM  $\text{CaCl}_2$  and 10 mM  $\text{MgCl}_2$ ) for 2 h at  $37^\circ\text{C}$ .

### 2.13. Detection of Apoptosis with Hoechst Staining

HuT-78 and MJ cells were seeded and treated for the caspase-3 activity assay. Nuclear fragmentation was imaged by staining the cells with Hoechst 33342 (0.1 mg/mL final concentration) for 30 min according to the protocol of Chazotte [67]. Samples were examined under a Nikon TiU fluorescent microscope (UV filter,  $200\times$  magnification), and the images were acquired and processed using EZC1 software.

### 2.14. Western Blot Analysis for Protein Expression

The modulation of TWIST1 and related signal molecules, except for NF- $\kappa$ B, after treatment with erufosine or combinations between erufosine and micellar curcumin was tested by immunoblot analysis as published before [36]. Briefly, all three cell lines were seeded in 6-well plates at a density of  $0.3 \times 10^6$  cells/mL and treated with 12.5, 25, or 50  $\mu$ M of erufosine for 24 h or as for the caspase-3 assay. Thereafter, cells were washed in PBS and centrifuged for 5 min at 2000 rpm (Eppendorf<sup>®</sup> microcentrifuge, Hamburg, Germany). Cell pellets ( $2 \times 10^6$  cells) were lysed in a buffer containing 100 mM Tris-HCl with pH 8.0, 4% SDS, 20% Glycerol, 200 mM DTT, and complete protease inhibitor cocktail (#A7779 Applichem, Darmstadt, Germany). Lysates were boiled 10 min and centrifuged at 13,000 rpm for 10 min at  $4^\circ\text{C}$ . Aliquots of 10  $\mu$ L were taken from the lysates before adding DTT, diluted five-fold in distilled water and quantified for protein concentration with the Pierce BCA Protein Assay Kit (#23225, ThermoFisher Scientific, Waltham, MA, USA). The total protein lysates (50 mg) were subjected to electrophoresis (8% polyacrylamide SDS gels), and proteins were transferred onto PVDF membranes (#IPFL00005 Sigma-Aldrich). The specific antibody labeling was performed in Tris buffer saline supplemented with 0.1% Tween and 1% skimmed milk. The TWIST1 (sc-81417) and  $\beta$ -Actin antibodies (C-2, sc-8432) were purchased from Santa Cruz Biotechnology<sup>®</sup>, Inc. (Dallas, TX, USA), whereas p-Akt<sup>Ser473</sup> (#4060) and p-Akt<sup>Thr308</sup> (#13038) originated from Cell Signaling Technology<sup>®</sup> (Danvers, MA, USA). The antibodies were diluted according to the manufacturer's instructions. Immunoblots were developed using an HRP-conjugated anti-mouse m-IgG $\kappa$  BP-HRP (sc-516102, Santa Cruz Biotechnology) or anti-rabbit IgG (#7074, Cell Signaling Technologies, USA) on a C-DiGit Blot Scanner (Li-Cor Biotechnology, Lincoln, NE, USA). The protein expression was normalized based on  $\beta$ -Actin levels by densitometric analysis of the digitized autographic images using the Quantity One 1-D Analysis software 4.6.6. (Bio-Rad, Hercules, CA, USA).

### 2.15. NF- $\kappa$ B p65 ELISA

HuT-78 and MJ cells were plated and treated for the caspase-3 activity assay. The NF- $\kappa$ B p65 activation after single and combined treatment was evaluated using the NF- $\kappa$ B p65 ELISA (#ADI-EKS-446, Enzo Life Sciences (ELS) AG, Lausen, Switzerland). The protocol was performed following the manufacturer's instructions.

### 2.16. Biofilm Formation Assay

The biofilm formation assay was performed according to the protocol of Stepanovic et al. [68]. Two-fold serial dilutions of the combinations between ERF and MCRM in concentrations ranging from 1.25/5 to 20/80  $\mu\text{M}$  ERF/MCRM were prepared using BHI broth supplemented with 2% glucose (*w/v*). The samples were placed in 96-well polystyrene tissue culture plates at a final volume of 100  $\mu\text{L}$ /well. An equivalent volume of MRSA bacterial inoculum ( $5 \times 10^5$  CFU/mL) was added to each well. Cells were incubated aerobically for 24 h at 37 °C under static conditions. The supernatant was discarded, and planktonic cells were removed three times by washing with PBS (250  $\mu\text{L}$ /well). Cells attached in biofilm were fixed with methanol (200  $\mu\text{L}$ /well, 15 min), air dried, and stained with 0.1% crystal violet (200  $\mu\text{L}$ /well, 5 min). Excess stain was rinsed off with tap water and air dried. The biofilm formation was documented microscopically (40 $\times$  magnification). Thereafter, the stained biofilm was re-solubilized in 160  $\mu\text{L}$  of 33% acetic acid, and the OD was measured at  $\lambda = 550$  nm. The biofilm inhibitory concentrations (BIC) were calculated with the GraphPad Prism software and presented in graphs by using a nonlinear regression model (dose-response inhibition, variable slope after normalization, and logarithmic transformation of the applied concentrations). The minimum biofilm inhibition concentration (MBIC<sub>50</sub>) was defined as the concentration of the tested drug that led to 50% inhibition of the biofilm formation.

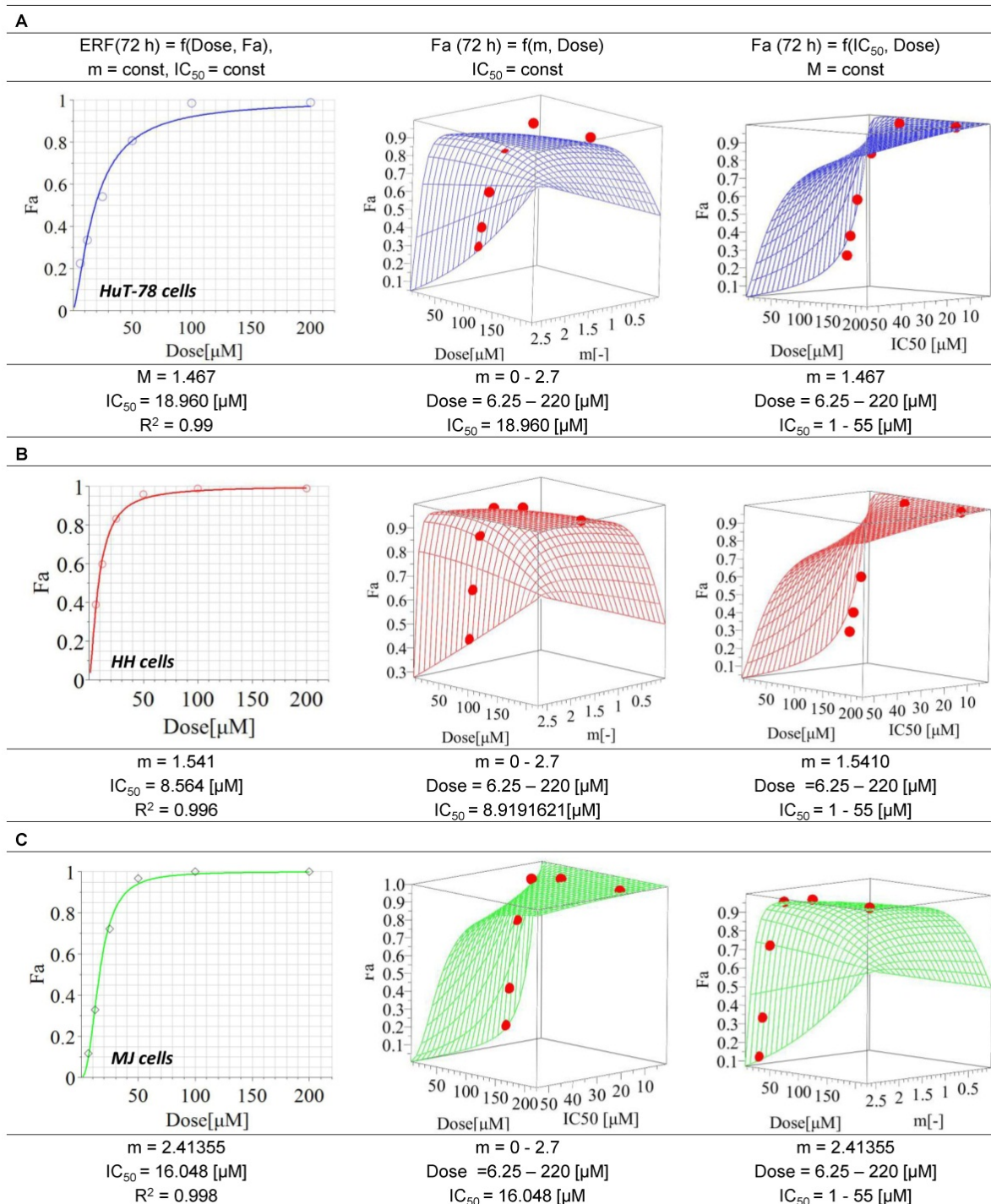
### 2.17. Statistical Evaluation

The experimental data were analyzed statistically with the GraphPad Prism software (Version 5.00, for Windows, GraphPad Software, La Jolla California, San Diego, CA, USA). Each experiment was performed in triplicate. Minimum of three samples for each concentration, the positive, negative, and untreated controls, were prepared. Data were presented as the mean  $\pm$  SD. One-way and two-way analysis of variance and the two-independent sample Student's *t*-tests were applied to compare two or more groups. A value of  $p < 0.05$  was considered statistically significant.

## 3. Results

### 3.1. Cytotoxic Effects of Erufosine on CTCL Cell Lines

The IC<sub>50</sub> value of ERF for HH cells (8.6  $\mu\text{M}$ ) was nearly twofold lower than that for MJ cells (16  $\mu\text{M}$ ) and twice and a half lower than that determined for HuT-78 cells (approx. 19  $\mu\text{M}$ ). All coefficients of determination were higher than 0.95, which ensures the best curve fit. The response surface analysis (RSA) confirmed the reliability of the model (Figure 1). No cytotoxic effect (cell viability > 70%) was found for MCRM.

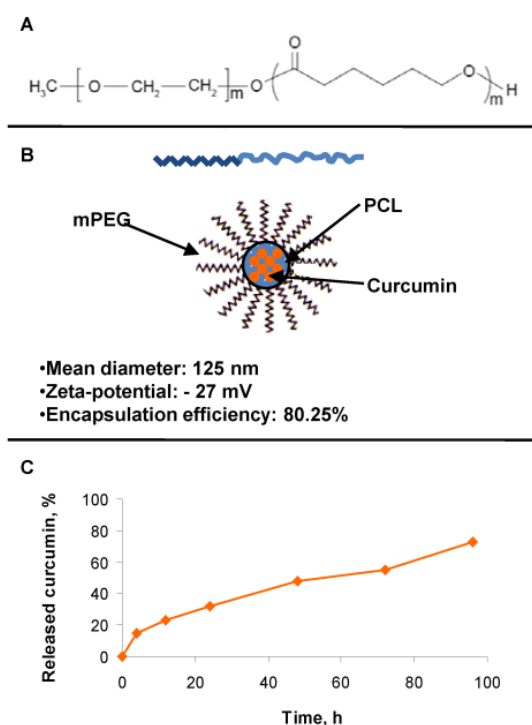


**Figure 1.** Median inhibitory concentrations of erufosine on the cell lines HuT-78, HH and MJ. **Legend:** ERF—erufosine; m—hillslope; R<sup>2</sup>—coefficient of determination; IC<sub>50</sub>—inhibitory concentration 50% (median inhibitory concentration); Fa—drug effect; (A)—Cell line HuT78 (Sézary Syndrome); (B)—Cell line HH (cutaneous T-cell lymphoma); (C)—Cell line MJ (Mycosis fungoides).

### 3.2. Production and Internalization Rate of MCRM

Due to the poor water solubility of curcumin, it was formulated in nano-sized micelles based on methoxy poly(ethylene glycol)-block-poly( $\epsilon$ -caprolactone) (mPEG-PCL) copolymer (Figure 2A). The mean diameter of the micelles loaded with curcumin was approximately 125 nm, and the zeta-potential was negative (−27 mV), providing colloidal

stability of the resulting nanosystem. The encapsulation efficiency reached 80%, probably due to a high affinity between curcumin and the hydrophobic block of the selected copolymer (Figure 2B). This fact was related to the achievement of sustained release of curcumin (Figure 2C). In order to quantify the cell internalization of MCRM in comparison to CRM dissolved in ethanol (ECRM), spectrophotometric estimation of the curcumin content was performed in the cultivation medium up to 3 h after the start of treatment (Table 1). Rest concentrations for MCRM were substantially lower than that for ECRM, thus confirming the enhanced internalization of MCRM.



**Figure 2.** Structure of the micelles and achievement of sustained release with slightly pronounced burst release of curcumin. **Legend:** (A)—Copolymer carrier mPEG-PCL; (B)—curcumin loaded mPEG-PCL micelles and their physicochemical properties; (C)—curcumin release from the loaded mPEG-PCL micelles.

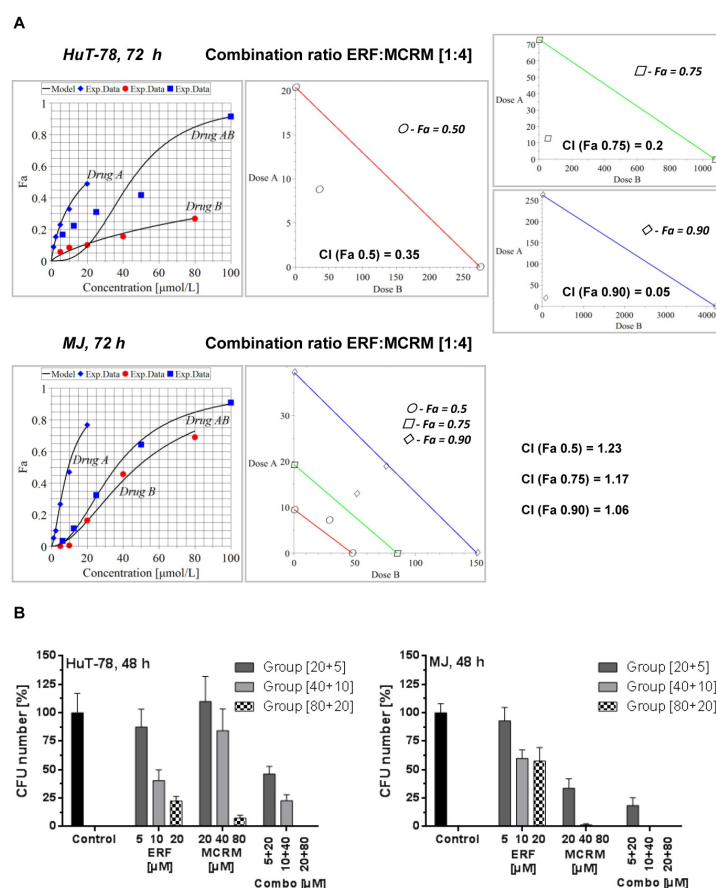
**Table 1.** Extracellular concentration of MCRM in comparison to pure curcumin after treatment of HuT-78 cells.

Drug	Incubation Time [h]	Absorption (AU) +/- SD	$A_{\text{sample}} - A_{\text{blank}}$ (AU)	Quantity of the Substance (mmol)
Control	0	0.05748 +/- 0.01	-	-
CRM		0.47531 +/- 0.01	0.41783	$8.0290 \times 10^{-5}$
MCRM		0.25410 +/- 0.01	0.19662	$3.3212 \times 10^{-5}$
Control	1	0.12833 +/- 0.02	-	-
CRM		0.38940 +/- 0.02	0.26107	$4.4100 \times 10^{-5}$
MCRM		0.27864 +/- 0.02	0.15033	$2.5394 \times 10^{-5}$
Control	2	0.10574 +/- 0.02	-	-
CRM		0.37878 +/- 0.02	0.27304	$4.612 \times 10^{-5}$
MCRM		0.23807 +/- 0.02	0.13233	$2.2354 \times 10^{-5}$
Control	3	0.15630 +/- 0.01	-	-
CRM		0.43492 +/- 0.01	0.27862	$4.7064 \times 10^{-5}$
MCRM		0.23947 +/- 0.01	0.08317	$1.4050 \times 10^{-5}$

**Legend:** AU—absorption units; CRM—pure curcumin dissolved in ethanol; MCRM—micellar curcumin.

### 3.3. Micellar Curcumin Potentiates the Antiproliferative and Anticlonogenic Effect of Erufosine in TWIST1 Expressing CTCL Cell Lines

Based on the calculated median inhibitory concentrations of ERF, we planned the combination treatment following the recommendations and the schema for constant combination ratio in the manual of Chou and Talalay [Manual of CompuSyn. Inc., Paramus, NJ, USA]. The following two combination ratios were investigated: 1:2 and 1:4 [ERF:MCRM]. The highest concentration of ERF used was near the  $IC_{50}$  value, and only the concentrations of MCRM were increased up to 80  $\mu\text{M}$  as far as curcumin is less toxic than ERF to normal cells. Only the combination ratio of 1:4 led to synergistic (HuT-78) or additive (MJ) interactions. The results are presented in Figure 3A. The CI values of the combination 80  $\mu\text{M}$  MCRM and 20  $\mu\text{M}$  ERF for HuT-78 cells were lower than 0.9 for all three Fa observed (50, 75, and 90% inhibition of the cell viability), which is indicative of synergism ( $CI_{Fa(0.5)} = 0.35$ ,  $CI_{Fa(0.75)} = 0.2$ ,  $CI_{Fa(0.9)} = 0.17$ ). For MJ cells, an additive effect was achieved by Fa0.9. The data from the CFU test (Figure 3B) revealed 100% CFU inhibition in HuT-78 cells for the combination [20  $\mu\text{M}$  ERF/80  $\mu\text{M}$  MCRM]. In MJ cells, treatment with 40 and 80  $\mu\text{M}$  MCRM and the respective combinations with ERF led to complete CFU inhibition.



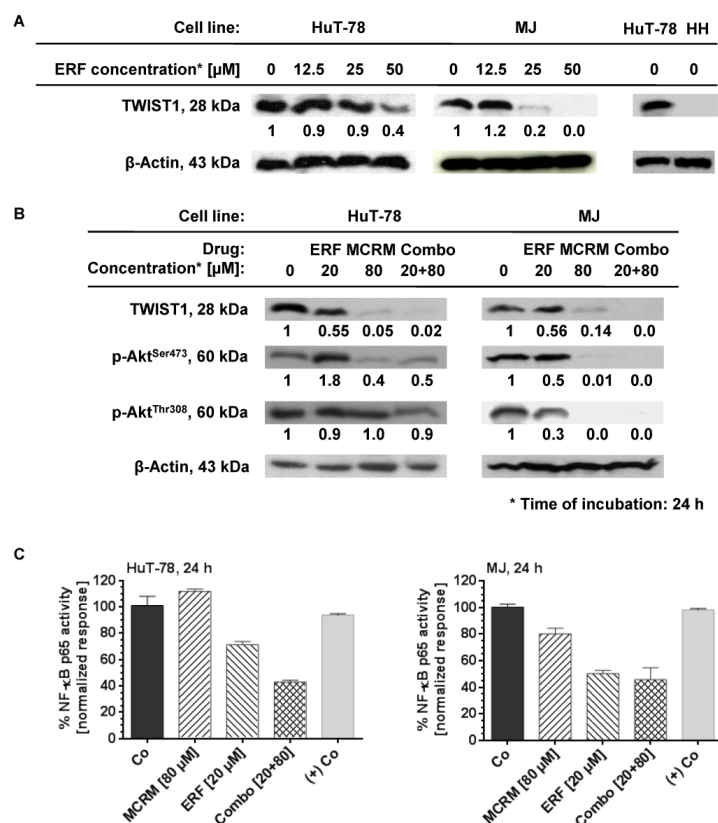
**Figure 3.** Synergistic and additive combinations between erufosine and micellar curcumin with an inhibitory effect on cell proliferation and clonogenicity of the cell lines HuT-78 and MJ. **Legend:** (A)—isobolograms for HuT-78 and MJ cells, calculated by MAPLE software from a MTT assay, where CI stands for Combination Index, Fa 0.5 is the median cytotoxic effect (denoted with points), Fa 0.75 is the effect killing 75% of the cells (denoted with squares) and Fa 0.9 is equal to 90% dead cells (denoted with rhombuses); (B)—clonogenic survival (CFU assay) of lymphoblasts from the TWIST1 expressing cell lines HuT-78 and MJ after treatment with combinations achieving Fa 0.9, including the single drug effects of the respective concentrations. Drug A stands for ERF, Drug B stands for MCRM and Drug AB stands for combination between ERF and MCRM.



The combination indexes for the combination ratio 1:2 from the MTT assay are as follows: (1) HuT-78— $CI_{Fa(0.5)} = 1.34$ ,  $CI_{Fa(0.75)} = 2.28$ ,  $CI_{Fa(0.9)} = 3.87$ ; (2) MJ— $CI_{Fa(0.5)} = 1.57$ ,  $CI_{Fa(0.75)} = 1.25$ ,  $CI_{Fa(0.9)} = 1.01$ . An additive effect was achieved in MJ cells at Fa(0.9). All other variants led to an antagonistic effect.

### 3.4. MCRM Increases the Inhibitory Effect of ERF on TWIST1, PKB/Akt and NF-κB in TWIST1 Expressing CTCL Cell Lines

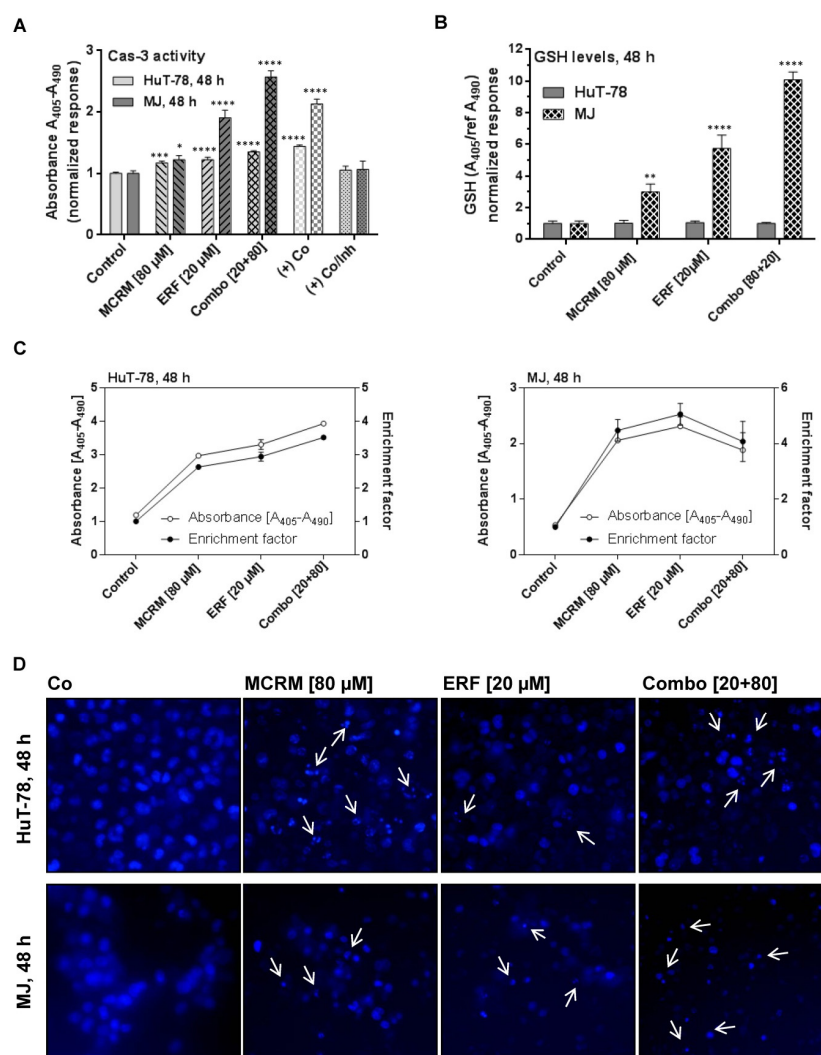
No expression of TWIST1 was detected in the cell line HH. HuT-78 and MJ cell lines express TWIST1 and ERF inhibited it in a dose-dependent manner (Figure 4A). ERF alone suppressed the expression of TWIST1 by 60% only at a concentration of 50 μM. In the presence of curcumin, a full TWIST1 inhibition was achieved by using more than a twofold lower concentration of ERF. The same effect was observed in the MJ cell line for single administration of ERF and the additive combination. A single administration of ERF (20 μM) on the MJ cell line inhibited both active forms of the protein kinase B. In the HuT-78 cell line, the dephosphorylation of PKB/Akt at Ser<sup>473</sup> was not significant against the untreated control, while its dephosphorylation at Thr<sup>308</sup> was more strongly expressed than the untreated control after treatment with 20 μM erufosine (value close to IC<sub>50</sub>). The combination achieved complete inhibition of protein phosphorylation at both amino acid residues in the MJ cell line, whereas, for HuT-78, this effect was poorly expressed and was the same as after a single treatment with ERF. The NF-κB p65 activity was significantly inhibited (up to 60%) in both cell lines 24 h after administrating the combination.



**Figure 4.** Micellar curcumin potentiates the inhibition effect of erufosine on NF-κB and TWIST1 in the CTCL cell lines HuT-78 and MJ. **Legend:** MCRM—micellar curcumin; ERF—erufosine; (+) Co—nuclear extract of TNFα-activated HeLa cells; Co—untreated control; Combo—combination between erufosine and micellar curcumin with the same concentrations as by the single treatment; (A)—expression of TWIST1 by western blot after exposure of the cell lines to erufosine; (B)—expression of TWIST1, p-Akt<sup>Ser472</sup> and p-Akt<sup>Thr308</sup> by western blot after exposure of the cell lines to the combinations; (C)—NF-κB p65 activity assay of ERF, MCRM and the combinations combination.

### 3.5. MCRM Potentiates the Anti-Apoptotic Effect of ERF in TWIST1 Expressing CTCL Cell Lines

In both cell lines, the combinations between MCRM and ERF induced apoptosis and resulted in significant nuclear fragmentation in the treated cells to a greater degree than after single administration of the corresponding concentrations. The caspase-3 activity induced in MJ cells by the combinations was twice as strong as compared to that induced by MCRM or ERF separately (Figure 5A). The effect of the combination in HuT-78 resulted in a fourfold higher accumulation of mono- and oligonucleotides in the cytosol of the treated cells as compared to the untreated control (Figure 5C). The Hoechst microscope images (Figure 5D) revealed nuclear fragmentation at preserved nuclear membrane in HuT-78. In MJ cells, a breakdown of cellular structures and extracellular condensed nuclear fragments were observed.



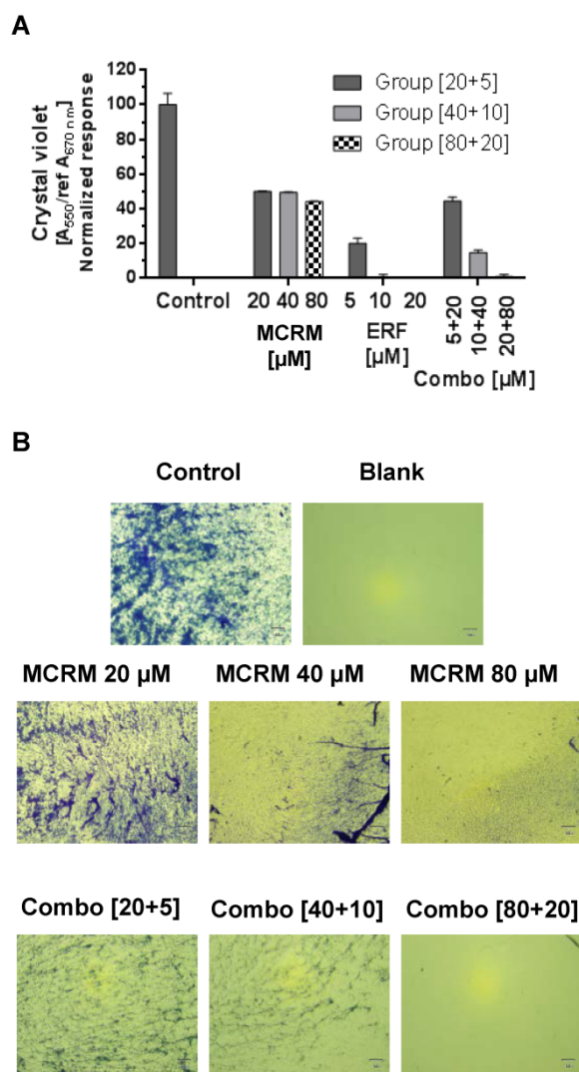
**Figure 5.** Synergistic interactions between micellar curcumin and erufosine in ratio 4:1 lead to apoptotic cell death in HuT-78 and MJ cells. **Legend:** (+) Co—cells incubated with hypertonic buffer; (+) Co/Inh—cells incubated with hypertonic buffer in the presence of caspase 3 inhibitor; (A)—caspase 3 activity of samples treated with ERF, MCRM or combinations; (B)—GSH levels in the same samples, presented in part A; (C)—accumulation of mono- and oligonucleotides in the cellular cytosol in the same samples presented in parts A and B; (D)—nuclear fragmentation after Hoechst staining in the cells in the same samples presented in parts A, B and C (depicted with white arrows). Significant differences between groups in (A,B) are marked with asterisks: \*— $p \leq 0.05$ ; \*\*— $p \leq 0.01$ ; \*\*\*— $p \leq 0.001$ , \*\*\*\*— $p \leq 0.0001$ .

### 3.6. Effects of the Combinations between ERF and MCRM on Total GSH Levels in TWIST1 Expressing CTCL Cell Lines

Glutathione levels did not change at the 48th hour of the treatment in any of the HuT-78 samples, unlike the other cell line MJ, which showed a strong enhancement of total GSH after treatment with MCRM and the combination (Figure 5B). The result correlates with increased levels of caspase-3 in the same samples. Obviously, in MJ cells, glutathione levels were significantly enhanced—up to 10-fold higher than in the untreated control. A concentration-dependent manner of the effect was detected.

### 3.7. The Combination Ratio of 4:1 between MCRM and ERF Inhibits Biofilm Formation of MRSA

The synergistic concentration MCRM:ERF [4:1] significantly inhibited the biofilm formation of MRSA. The effect of the combination of concentrations 80  $\mu\text{M}$  MCRM and 20  $\mu\text{M}$  ERF is equal to that of ERF after a single application, demonstrating full biofilm eradication (Figure 6). In lower concentrations of both drugs, the effect on biofilm formation was antagonistic.



**Figure 6.** Effect of the synergistic combination [ratio 4:1] between micellar curcumin and erufosine on the biofilm formation of MRSA. **Legend:** ERF—erufosine; MCRM—micellar curcumin; (A)—crystal violet absorbance of MRSA biofilm; (B)—Morphological evaluation of MRSA biofilm (40 $\times$  microscope magnification).

#### 4. Discussion

In the present study, we compared and evaluated in detail for the first time, to our knowledge, the in vitro efficacy of the alkylphosphocholine ERF in combination with curcumin incorporated in micellar formulation with a prolonged release on T-cell lymphoma cell lines with and without expression of the oncogene TWIST1. The transcription factor TWIST1 is not detected in normal peripheral blood mononuclear cells. Any increase in its expression levels is abnormal and has been identified as a marker of metastasis and poor prognosis in patients with MF and SS [69]. Furthermore, it has been found that its expression increases in advanced MF/SS lesions and triggers chemotherapy resistance [16,70]. The underlying mechanisms are related to the inhibition of both p53 and Rb tumor-suppressor pathways and the up-regulation of protein kinase B (PKB/Akt) in malignant cells with increased TWIST1 levels [70,71]. In cancer cells, TWIST1 targets several enzymes from the DNA damage response pathway, thus neutralizing senescence and cell death [72]. Based on the accumulated knowledge about the mode of action of the APCs [40,73] and our previous studies on the effects of ERF on CTCL cell lines demonstrating clear inhibition of PKB/Akt [41], increase in the Rb expression levels in T-cells, modulation of the Rb-protein signaling pathway [40] and induction of apoptosis, we presumed that the expression levels of TWIST1 might affect the activity of ERF or vice versa. In our study, ERF showed different activity in the tested cell lines, with HuT-78 being the most resistant and HH being the most sensitive (Figure 1), as evidenced by the estimated IC<sub>50</sub> values. The behavior of the RSA simulations, along with the dose-effect curves, confirmed the reliability of the chosen mathematical model in the MAPLE software. The deviation of the model from the experimental data (see points) for the selected 95% confidence interval was not very high, meaning that the values of all constants in the selected ranges of *m* and the IC<sub>50</sub> parameters can be considered reliable and stable. Determination of the TWIST1 expression levels in all three cell lines through western blot analysis revealed that the protein was expressed in HuT-78 and MJ but not in the most sensitive cell line HH (Figure 4). Moreover, inhibition of TWIST1 occurred in MJ at a lower ERF concentration (25 μM) than in HuT-78 (50 μM). This finding could explain the differences in the sensitivity of the cell lines toward the drug.

According to published data, there is cross-talk between TWIST1 and PKB/Akt in the promotion of metastasis via the TGF-β signaling axes [71]. On the one hand, TWIST1 mediates the phosphorylation of PKB/Akt, thus contributing to uncontrolled cell proliferation and invasion. On the other hand, TWIST1 associates directly with the subunit RELA of the pro-inflammatory factor NF-κB to activate the transcriptional activity of the latter and to promote cell invasion through IL8 production [74]. ERF is a potent inhibitor of the PKB/Akt signaling pathway in leukemic and lymphoma cell lines [35–37,39,41], whereas the natural product curcumin is a well-known proteasome inhibitor of NF-κB [75–78]. Based on these facts, we built our hypothesis on the presumption that a combination between ERF and MCRM will achieve simultaneous down-regulation of PKB/Akt and NF-κB with subsequent inhibition of cell proliferation and induction of apoptosis. In addition, ERF and CRM possess in vitro antimicrobial activity against the pathogenic bacterial species *Staphylococcus aureus* [29], which was shown to accelerate the pathogenesis of CTCL [79,80]. That is why; we set the additional goal to study the MRSA anti-biofilm activity of the selected combinations, as far as it is a highly important mechanism providing survival of the microorganisms in conditions of external stress and chemotherapy. Taking into account both the poor curcumin solubility and its hydrolytic instability in a slightly alkaline medium, we assumed that polymeric micelles would be appropriate nano-carriers for cutaneous application. The hydrophobic nature of their micellar core enables the loading of active substances with poor water solubility. Moreover, the loading of unstable drugs into micelles would increase their stability against different degradation processes such as hydrolysis or oxidation [58–61]. Despite the advantages of the micelles, the studies of polymeric micelles intended for the cutaneous application of curcumin are limited to a few reports [81,82]. Therefore, in the present study, we developed curcumin-loaded nano-sized micelles based on the methoxy poly (ethylene glycol)-block-poly (ε-caprolactone) (mPEG-PCL) copolymer

carrier, selected for its biocompatibility, biodegradation and suitable properties for loading of hydrophobic drugs (Figure 2). The nanoparticles were internalized into the treated cells significantly faster than pure CRM (Table 1), which is a prerequisite for the successful cytopenetration and the subsequent intracellular release of curcumin.

The tested interactions between ERF and MCRM in combination ratio 1:4 [ERF:MCRM] were proven to be synergistic for HuT-78 cells and additive for MJ cells (Figure 3A) in difference to the combination ratio 1:2, which led only to additive effects. As a final result, all CI values regarding the cell line HuT-78 were lower than 0.4 for the combination ratio 1:4, which indicates a strong synergism. The results clearly demonstrated that the applied strategy for experimental design and algorithms for calculation of isobolograms under particularly chosen combination ratios was robust and very reliable. The synergistic and additive effects were confirmed by the CFU assay (Figure 3B). The effect of the combination 1:4 [ERF:MCRM] in HuT-78 cells led to complete inhibition of cell clonogenicity, and therefore, this combination was subjected to a series of tests to study its effect on the expression of the transcription factor TWIST1, PKB/Akt phosphorylation, NF- $\kappa$ B activity, apoptosis induction, and glutathione reduction.

Undoubtedly, an important outcome was the complete suppression of the TWIST1 expression after the application of the synergistic combination [20  $\mu$ M ERF:80  $\mu$ M MCRM] on HuT-78 cells (Figure 4A) compared to the single application of erufosine that, although at a concentration of 50  $\mu$ M, suppressed the TWIST1 expression by only 60% (Figure 4B). The achieved effect makes it feasible to reduce the effective dose of ERF and thus minimize the occurrence of adverse effects. The same effect was observed with the MJ cell line, except that ERF alone inhibited TWIST1 by 80% at a twofold lower concentration than in HuT-78 cells (25  $\mu$ M vs. 50  $\mu$ M), which may explain why the effect of the combination [20  $\mu$ M ERF:80  $\mu$ M MCRM] is additive and not synergistic (as in HuT-78 cells). Regarding PKB/Akt dephosphorylation, the combination inhibited almost fully the protein phosphorylation at Ser473 in both cell lines, which correlates with the results from the MTT and CFU assay, suggesting that proliferation inhibition occurs via inhibition of PKB/Akt. It also confirms that the lower sensitivity of HuT-78 cells to ERF is due to the weaker inhibition of this protein than in MJ cells. A single administration of ERF (20  $\mu$ M) or MCRM (80  $\mu$ M) achieved this effect to a greater extent in MJ cells than in HuT-78. In MJ cells, dephosphorylation at Thr308 was more pronounced than at Ser473, which is in line with previously published data [36]. In HuT-78, there was no significant difference in the levels of p-AktThr308 between the treated samples, whereas the levels of p-AktSer473 decreased significantly and to the same extent after exposure to MCRM or the combination. The activity of NF- $\kappa$ B p65 was also inhibited by up to 60% in both cell lines after administration of the combination (Figure 4C). The differences between the effects of the combination and the self-administered drugs were significant. The lack of effect of MCRM on NF- $\kappa$ B expression can be explained by the slow, gradual release of curcumin from the particular micelles during the incubation period—35% (28  $\mu$ M) of the whole loaded dose, which is 80  $\mu$ M. The released amount of CRM is obviously not sufficient to achieve the desired effect for this incubation period (24 h). In contrast, according to published data, 80  $\mu$ M of pure CRM or CRM loaded in nanoparticles with rapid release significantly inhibits the activity of NF- $\kappa$ B [41,76,82,83]. In this regard, we could assume that not the gradual administration of low CRM doses over time but the fast release of higher doses in the first hours after treatment is crucial for the NF- $\kappa$ B inhibition. However, in combination with ERF, the low concentrations of CRM released from the micelles were sufficient to potentiate the effect of the inhibitory effect of the alkylphosphocholine on NF- $\kappa$ B, suggesting the unlocking of other mechanisms that deserve further investigation in a separate study. In the MJ cell line, the effect of ERF was the same as in the combination, which correlates with the determined additive effect.

The inhibition of NF- $\kappa$ B and PKB/Akt logically led to the induction of apoptosis in the treated cell lines. As visible in Figure 5, the combination 1:4 [ERF:MCRM] activated caspase-3, increased the fraction of mono- and oligonucleosomes in the cytosol of HuT-78

and MJ and led to nuclear fragmentation in both cell lines, indicating apoptosis (Figure 5C). Activation of caspase-3 and elevation of the reduced glutathione levels were more pronounced in MJ cells after treatment with the combination (Figure 5A,B). One possible explanation for this difference could be an earlier induction of apoptosis in HuT-78 cells, which could be proven in detail in a further study. As far as excess GSH in malignant cells correlates with increased metastasis and tumor progression [84,85], it could be speculated that the elevated GSH levels in the MJ cell line in our study could be one of the reasons why the best effect of the combination 1:4 [ERF:MCRM] on MJ cells is not synergistic but additive only.

Last but not least, the synergistic combination fully inhibited the formation of MRSA biofilm, which can bring additional benefits for patients with concomitant staphylococcal infections as this will further help reduce inflammation and limit the appearance of infected skin lesions. ERF alone is also a potent inhibitor of the MRSA biofilm, as published before [29], and the combination with MCRM did not reduce this effect.

## 5. Conclusions

The anti-lymphoma effect of ERF in CTCL cell lines was dependent on the TWIST1 expression. The combination between ERF and MCRM in a ratio of 1:4 achieves a synergistic or additive effect depending on the cell line, which was due to inhibition of TWIST1, dephosphorylation of PKB/AKT at Ser<sup>473</sup> and/or Thr<sup>308</sup>, and deactivation of the p65 subunit of NF- $\kappa$ B. Taken together, our experimental findings indicate that it is feasible to develop and investigate new micellar CRM formulations in rational combinations with the alkylphosphocholine ERF for future local and/or intravenous CTCL treatment perspectives. The low toxic profile of the two substances allows their combination to be used in a broader pharmacological regimen, with the combined antineoplastic, anti-inflammatory, and antibacterial activity assisting in overcoming primary and secondary drug resistance of CTCL-derived cells.

**Author Contributions:** Conceptualization, S.M.K., M.M.Z., K.Y., A.D.K., M.R.B. and H.M.N.; methodology, A.G.X.T., Y.I., I.P.-E.T., K.Y., M.M.Z. and A.D.K.; software, A.D.K.; formal analysis, A.G.X.T., Y.I., A.D.K., L.L.D., I.P.-E.T., K.Y. and M.M.Z.; investigation, A.G.X.T., Y.I., L.L.D., S.P., I.P.-E.T., K.Y. and M.M.Z.; resources, M.M.Z., H.M.N. and S.M.K.; writing—original draft preparation, M.M.Z., A.G.X.T., Y.I., A.D.K., I.P.-E.T. and K.Y.; writing—review and editing, S.M.K., M.R.B. and H.M.N.; visualization, M.M.Z. and S.M.K.; supervision, M.M.Z., H.M.N. and S.M.K.; project administration, M.M.Z. and S.M.K.; funding acquisition, S.M.K., M.M.Z., K.Y. and H.M.N. All authors have read and agreed to the published version of the manuscript.

**Funding:** This research was funded by the Bulgarian National Science Fund; grant number DN03/3 (16 December 2016).

**Institutional Review Board Statement:** Not applicable.

**Informed Consent Statement:** Not applicable.

**Data Availability Statement:** All raw data from the experiments are available from the authors.

**Acknowledgments:** Antonios G.X. Trochopoulos, was granted a research grant for ‘Doctoral candidates and young academics and scientists’ by the German Academic Exchange Service (DAAD), during the course of his doctoral studies. We would like to express our special gratitude to the Alexander von Humboldt Foundation for the Grant ‘Equipment subsidies’ to Maya M. Zaharieva, used for conducting the cell cytotoxicity and clonogenicity tests and the biofilm assay. The authors are also thankful to Ts. Paunova-Krasteva for her help with the imaging of the Hoechst-stained preparations. Vasiliki Tsorbatzian, ESL/EFL teacher, proofread the article.

**Conflicts of Interest:** The authors declare no conflict of interest.

## References

1. CheckOrphan. 2016. Available online: <http://www.checkorphan.org/diseases/cutaneous-t-cell-lymphoma> (accessed on 15 May 2021).
2. Rare Disease Registries in Europe. Orphanet Report Series: Rare Diseases Collection. 2016. Available online: [www.orpha.net](http://www.orpha.net) (accessed on 15 May 2021).
3. Bagherani, N.; Smoller, B.R. An overview of cutaneous T cell lymphomas. *F1000Research* **2016**, *5*, 1882. [CrossRef] [PubMed]
4. Cieza-Díaz, D.E.; Conde-Montero, E.; Menarguez-Palanca, J.; Longo-Imedio, I. Epidemiological and clinical features of patients diagnosed with cutaneous T-cell lymphomas in a spanish tertiary care hospital. *J. Eur. Acad. Dermatol. Venereol.* **2016**, *31*, e150–e153. [CrossRef] [PubMed]
5. Zinzani, P.L.; Bonthapally, V.; Huebner, D.; Lutes, R.; Chi, A.; Pileri, S. Panoptic clinical review of the current and future treatment of relapsed/refractory T-cell lymphomas: Cutaneous T-cell lymphomas. *Crit. Rev. Oncol.* **2016**, *99*, 228–240. [CrossRef] [PubMed]
6. Thestrup-Pedersen, K. Cutaneous T-Cell Lymphoma. A hypothesis on disease pathophysiology involving deficiency in DNA repair. *J. Eur. Acad. Dermatol. Venereol.* **2016**, *30*, 1682–1685. [CrossRef]
7. Duvic, M. Histone Deacetylase Inhibitors for Cutaneous T-Cell Lymphoma. *Dermatol. Clin.* **2015**, *33*, 757–764. [CrossRef]
8. Willerslev-Olsen, A.; Krejsgaard, T.; Lindahl, L.M.; Bonefeld, C.M.; Wasik, M.A.; Koralov, S.B.; Geisler, C.; Kilian, M.; Iversen, L.; Woetmann, A.; et al. Bacterial toxins fuel disease progression in cutaneous T-cell lymphoma. *Toxins* **2013**, *5*, 1402–1421. [CrossRef]
9. Axelrod, P.I.; Lorber, B.; Vonderheid, E.C. Infections complicating mycosis fungoides and Sézary syndrome. *JAMA* **1992**, *267*, 1354–1358. [CrossRef]
10. Brunner, P.M.; Jonak, C.; Knobler, R. Recent advances in understanding and managing cutaneous T-cell lymphomas. *F1000Research* **2020**, *9*, 331. [CrossRef]
11. Damsky, W.E.; Choi, J. Genetics of Cutaneous T Cell Lymphoma: From Bench to Bedside. *Curr. Treat. Options Oncol.* **2016**, *17*, 33. [CrossRef]
12. Nicolay, J.P.; Felcht, M.; Schledzewski, K.; Goerdts, S.; Geraud, C. Sezary syndrome: Old enigmas, new targets. *J. Dtsch. Dermatol. Ges.* **2016**, *14*, 256–264. [CrossRef]
13. Phyo, Z.; Shanbhag, S.; Rozati, S. Update on Biology of Cutaneous T-Cell Lymphoma. *Front. Oncol.* **2020**, *10*, 765. [CrossRef]
14. Khan, M.A.; Chen, H.-c.; Zhang, D.; Fu, J. Twist: A molecular target in cancer therapeutics. *Tumor Biol.* **2013**, *34*, 2497–2506. [CrossRef] [PubMed]
15. van Doorn, R.; Dijkman, R.; Vermeer, M.H.; Out-Luiting, J.J.; van der Raaij-Helmer, E.M.H.; Willemze, R.; Tensen, T.P. Aberrant Expression of the Tyrosine Kinase Receptor EphA4 and the Transcription Factor Twist in Sézary Syndrome Identified by Gene Expression Analysis. *Cancer Res.* **2004**, *64*, 5578–5586. [CrossRef] [PubMed]
16. Goswami, M.; Duvic, M.; Dougherty, A.; Ni, X. Increased Twist expression in advanced stage of mycosis fungoides and Sézary syndrome. *J. Cutan. Pathol.* **2012**, *39*, 500–507. [CrossRef]
17. Kempf, W.; Kazakov, D.V.; Kerl, K. Cutaneous lymphomas: An update. Part 1: T-cell and natural killer/t-cell lymphomas and related conditions. *Am. J. Dermatopathol.* **2014**, *36*, 105–123. [CrossRef]
18. Spaccarelli, N.; Rook, A.H. The Use of Interferons in the Treatment of Cutaneous T-Cell Lymphoma. *Dermatol. Clin.* **2015**, *33*, 731–745. [CrossRef]
19. Bobrowicz, M.; Fassnacht, C.; Ignatova, D.; Chang, Y.-T.; Dimitriou, F.; Guenova, E. Pathogenesis and Therapy of Primary Cutaneous T-Cell Lymphoma: Collegium Internationale Allergologicum (CIA) Update 2020. *Int. Arch. Allergy Immunol.* **2020**, *181*, 733–745. [CrossRef] [PubMed]
20. Zic, J.A. Extracorporeal Photopheresis in the Treatment of Mycosis Fungoides and Sézary Syndrome. *Dermatol. Clin.* **2015**, *33*, 765–776. [CrossRef]
21. Vieyra-Garcia, P.A.; Wolf, P. Extracorporeal Photopheresis: A Case of Immunotherapy Ahead of Its Time. *Transfus. Med. Hemotherapy* **2020**, *47*, 226–235. [CrossRef]
22. Wilcox, R.A. Cutaneous T-cell lymphoma: 2016 update on diagnosis, risk-stratification, and management. *Am. J. Hematol.* **2016**, *91*, 151–165. [CrossRef]
23. Chung, C.G.; Poligone, B. Other Chemotherapeutic Agents in Cutaneous T-Cell Lymphoma. *Dermatol. Clin.* **2016**, *33*, 787–805. [CrossRef] [PubMed]
24. Eibl, H.; Kaufmann-Kolle, P. Medical Application of Synthetic Phospholipids as Liposomes and Drugs. *J. Liposome Res.* **1995**, *5*, 131–148. [CrossRef]
25. Kaufmann-Kolle, P.; Koetting, J.; Drevs, J.; Berger, M.; Unger, C.; Eibl, H. Intravenous application of alkylphosphocholines: Comparison of different homologues in lamellar structures. *J. Cancer Res. Clin. Oncol.* **1992**, *120*, R14.
26. Konstantinov, S.M.; Eibl, H.; Berger, M.R. BCR-ABL influences the antileukaemic efficacy of alkylphosphocholines. *Br. J. Haematol.* **1999**, *107*, 365–374. [CrossRef] [PubMed]
27. Georgieva, M.C.; Konstantinov, S.M.; Topashka-Ancheva, M.; Berger, M.R. Combination effects of alkylphosphocholines and gemcitabine in malignant and normal hematopoietic cells. *Cancer Lett.* **2002**, *182*, 163–174. [CrossRef] [PubMed]
28. Martelli, A.M.; Papa, V.; Tazzari, P.L.; Ricci, F.; Evangelisti, C.; Chiarini, F.; Grimaldi, C.; Cappellini, A.; Martinelli, G.; Ottaviani, E.; et al. Erucylphosphocholine, the first intravenously applicable alkylphosphocholine, is cytotoxic to acute myelogenous leukemia cells through JNK- and PP2A-dependent mechanisms. *Leukemia* **2010**, *24*, 687–698. [CrossRef] [PubMed]

29. Zaharieva, M.M.; Kroumov, A.D.; Dimitrova, L.; Tsvetkova, I.; Trochopoulos, A.; Konstantinov, S.M.; Berger, M.R.; Momchilova, M.; Yoncheva, K.; Najdenski, H.M. Micellar curcumin improves the antibacterial activity of the alkylphosphocholines erufosine and miltefosine against pathogenic *Staphylococcus aureus* strains. *Biotechnol. Biotechnol. Equip.* **2019**, *33*, 38–53. [CrossRef]
30. Fleer, E.A.; Unger, C.; Kim, D.J.; Eibl, H. Metabolism of ether phospholipids and analogs in neoplastic cells. *Lipids* **1987**, *22*, 856–861. [CrossRef]
31. Fiegl, M.; Lindner, L.H.; Juergens, M.; Eibl, H.; Hiddemann, W.; Braess, J. Erufosine, a novel alkylphosphocholine, in acute myeloid leukemia: Single activity and combination with other antileukemic drugs. *Cancer Chemother. Pharmacol.* **2007**, *62*, 321–329. [CrossRef]
32. Berger, M.R.; Sobottka, S.B.; Konstantinov, S.; Eibl, H. Erucylphosphocholine is the prototype of i.v. injectable alkylphosphocholines. *Drugs Today* **1998**, *34*, 73–81.
33. Königs, S.K.; Pallasch, C.P.; Lindner, L.H.; Schwamb, J.; Schulz, A.; Brinker, R.; Claasen, J.; Veldurthy, A.; Eibl, H.; Hallek, M.; et al. Erufosine, a novel alkylphosphocholine, induces apoptosis in CLL through a caspase-dependent pathway. *Leuk. Res.* **2010**, *34*, 1064–1069. [CrossRef] [PubMed]
34. Yosifov, D.Y.; Konstantinov, S.M.; Berger, M.R. Erucylphospho-N,N,N-trimethylpropylammonium Shows Substantial Cytotoxicity in Multiple Myeloma Cells. *Ann. N.Y. Acad. Sci.* **2009**, *1171*, 350–358. [CrossRef] [PubMed]
35. Zaharieva, M.; Konstantinov, S.; Pilicheva, B.; Karaivanova, M.; Berger, M. Erufosine: A Membrane Targeting Antineoplastic Agent with Signal Transduction Modulating Effects. *Ann. N.Y. Acad. Sci.* **2007**, *1095*, 182–192. [CrossRef] [PubMed]
36. Kapoor, V.; Zaharieva, M.M.; Das, S.N.; Berger, M.R. Erufosine simultaneously induces apoptosis and autophagy by modulating the Akt-mTOR signaling pathway in oral squamous cell carcinoma. *Cancer Lett.* **2012**, *319*, 39–48. [CrossRef] [PubMed]
37. Dineva, I.K.; Zaharieva, M.M.; Konstantinov, S.M.; Eibl, H.; Berger, M.R. Erufosine suppresses breast cancer in vitro and in vivo for its activity on PI3K, c-Raf and Akt proteins. *J. Cancer Res. Clin. Oncol.* **2012**, *138*, 1909–1917. [CrossRef]
38. Yosifov, D.Y.; Todorov, P.T.; Zaharieva, M.; Georgiev, K.D.; Pilicheva, B.A.; Konstantinov, S.M.; Berger, M.R. Erucylphospho-N,N,N-trimethylpropylammonium (erufosine) is a potential antimyeloma drug devoid of myelotoxicity. *Cancer Chemother. Pharmacol.* **2010**, *67*, 13–25. [CrossRef]
39. Rudner, J.; Ruiner, C.-E.; Handrick, R.; Eibl, H.-J.; Belka, C.; Jendrossek, V. The Akt-inhibitor Erufosine induces apoptotic cell death in prostate cancer cells and increases the short term effects of ionizing radiation. *Radiat. Oncol.* **2010**, *5*, 108. [CrossRef]
40. Zaharieva, M.; Kirilov, M.; Chai, M.; Berger, S.M.; Konstantinov, S.; Berger, M.R. Reduced Expression of the Retinoblastoma Protein Shows That the Related Signaling Pathway Is Essential for Mediating the Antineoplastic Activity of Erufosine. *PLoS ONE* **2014**, *9*, e100950. [CrossRef]
41. Yosifov, D.Y.; Kaloyanov, K.A.; Guenova, M.L.; Prasadashka, K.; Balabanova, M.B.; Berger, M.R.; Konstantinov, S.M. Alkylphosphocholines and curcumin induce programmed cell death in cutaneous T-cell lymphoma cell lines. *Leuk. Res.* **2014**, *38*, 49–56. [CrossRef]
42. Chometon, G.; Cappuccini, F.; Raducanu, A.; Aumailley, M.; Jendrossek, V. The Membrane-targeted Alkylphosphocholine Erufosine Interferes with Survival Signals from the Extracellular Matrix. *Anti-Cancer Agents Med. Chem.* **2014**, *14*, 578–591. [CrossRef]
43. Ruiter, G.A.; Zerp, S.F.; Bartelink, H.; van Blitterswijk, W.J.; Verheij, M. Anti-cancer alkyl-lysophospholipids inhibit the phosphatidylinositol 3-kinase–Akt/PKB survival pathway. *Anti-Cancer Drugs* **2003**, *14*, 167–173. [CrossRef] [PubMed]
44. Konstantinov, S.M.; Topashka-Ancheva, M.; Benner, A.; Berger, M.R. Alkylphosphocholines: Effects on human leukemic cell lines and normal bone marrow cells. *Int. J. Cancer* **1998**, *77*, 778–786. [CrossRef]
45. Bagley, R.G.; Kurtzberg, L.; Rouleau, C.; Yao, M.; Teicher, B.A. Erufosine, an alkylphosphocholine, with differential toxicity to human cancer cells and bone marrow cells. *Cancer Chemother. Pharmacol.* **2011**, *68*, 1537–1546. [CrossRef] [PubMed]
46. Dummer, R.; Krasovec, M.; Röger, J.; Sindermann, H.; Burg, G. Topical administration of hexadecylphosphocholine in patients with cutaneous lymphomas: Results of a phase I/II study. *J. Am. Acad. Dermatol.* **1993**, *29*, 963–970. [CrossRef] [PubMed]
47. Dummer, R.; Vogt, T.; Hefner, H.; Sindermann, H.; Burg, G. Topical Application of Hexadecylphosphocholine in Patients with Cutaneous Lymphomas. *Prog. Exp. Tumor Res.* **1992**, *34*, 160–169. [CrossRef]
48. Dumontet, C.; Thomas, L.; Berard, F.; Gimonet, J.F.; Coiffier, B. A phase II trial of miltefosine in patients with cutaneous T-cell lymphoma. *Bull. Cancer* **2006**, *93*, E115–E118. [PubMed]
49. Pronk, L.; Planting, A.; Oosterom, R.; Drogendijk, T.; Stoter, G.; Verweij, J. Increases in leucocyte and platelet counts induced by the alkyl phospholipid hexadecylphosphocholine. *Eur. J. Cancer* **1994**, *30*, 1019–1022. [CrossRef] [PubMed]
50. Berkovic, D.; Bensch, M.; Bertram, J.; Wille, T.; Haase, D.; Binder, C.; Fleer, E. Effects of hexadecylphosphocholine on thrombocytopoiesis. *Eur. J. Cancer* **2001**, *37*, 503–511. [CrossRef]
51. Aggarwal, B.B.; Sung, B. Pharmacological basis for the role of curcumin in chronic diseases: An age-old spice with modern targets. *Trends Pharmacol. Sci.* **2009**, *30*, 85–94. [CrossRef]
52. Gupta, S.C.; Patchva, S.; Koh, W.; Aggarwal, B.B. Discovery of curcumin, a component of golden spice, and its miraculous biological activities. *Clin. Exp. Pharmacol. Physiol.* **2012**, *39*, 283–299. [CrossRef]
53. Duvoix, A.; Blasius, R.; Delhalle, S.; Schnekenburger, M.; Morceau, F.; Henry, E.; Dicato, M.; Diederich, M. Chemopreventive and therapeutic effects of curcumin. *Cancer Lett.* **2005**, *223*, 181–190. [CrossRef] [PubMed]



54. Syng-Ai, C.; Kumari, A.L.; Khar, A. Effect of curcumin on normal and tumor cells: Role of glutathione and bcl-2. *Mol. Cancer Ther.* **2004**, *3*, 1101–1108. [CrossRef] [PubMed]
55. Zhang, C.; Li, B.; Zhang, X.; Hazarika, P.; Aggarwal, B.B.; Duvic, M. Curcumin selectively induces apoptosis in cutaneous T-cell lymphoma cell lines and patients' PBMCs: Potential role for STAT-3 and NF-kappaB signaling. *J. Invest. Dermatol.* **2010**, *130*, 2110–2119. [CrossRef] [PubMed]
56. Khan, M.A.; Gahlot, S.; Majumdar, S. Oxidative Stress Induced by Curcumin Promotes the Death of Cutaneous T-cell Lymphoma (HuT-78) by Disrupting the Function of Several Molecular Targets. *Mol. Cancer Ther.* **2012**, *11*, 1873–1883. [CrossRef] [PubMed]
57. Kunwar, A.; Barik, A.; Mishra, B.; Rathinasamy, K.I.; Pandey, R.; Priyadarsini, K. Quantitative cellular uptake, localization and cytotoxicity of curcumin in normal and tumor cells. *Biochim. Biophys. Acta* **2008**, *1780*, 673–679. [CrossRef] [PubMed]
58. Anand, P.; Kunnumakkara, A.B.; Newman, R.A.; Aggarwal, B.B. Bioavailability of curcumin: Problems and promises. *Mol. Pharm.* **2007**, *4*, 807–818. [CrossRef]
59. Lapteva, M.; Mondon, K.; Möller, M.; Gurny, R.; Kalia, Y.N. Polymeric Micelle Nanocarriers for the Cutaneous Delivery of Tacrolimus: A Targeted Approach for the Treatment of Psoriasis. *Mol. Pharm.* **2014**, *11*, 2989–3001. [CrossRef]
60. Xue, B.; Wang, Y.; Tang, X.; Xie, P.; Wang, Y.; Luo, F.; Wu, C.; Qian, Z. Biodegradable Self-Assembled MPEG-PCL Micelles for Hydrophobic Oridonin Delivery In Vitro. *J. Biomed. Nanotechnol.* **2012**, *8*, 80–89. [CrossRef]
61. Lapteva, M.; Möller, M.; Gurny, R.; Kalia, Y.N. Self-assembled polymeric nanocarriers for the targeted delivery of retinoic acid to the hair follicle. *Nanoscale* **2015**, *7*, 18651–18662. [CrossRef]
62. Eibl, H.; Hilgard, C.; Unger, C. *Alkylphosphocholines: New Drugs in Cancer Therapy*; Eibl, H., Hilgard, C., Unger, C., Eds.; Karger: Basel, Switzerland, 1992; 173p.
63. ISO 10993-5:2009; Biological Evaluation of Medical Devices—Part 5: Tests for In Vitro Cytotoxicity. ISO: Geneva, Switzerland, 2017.
64. Chou, T.C.; Martin, N. (Eds.) *CompuSyn for Drug Combinations: PC Software and User's Guide: A Computer Program for Quantitation of Synergism and Antagonism in Drug Combinations, and the Determination of IC50 and ED50 and LD50 Values*; ComboSyn Inc: Paramus, NJ, USA, 2005.
65. Zaharieva, M.; Trochopoulos, A.; Dimitrova, L.; Berger, M.; Najdenski, H.; Konstantinov, S.; Kroumov, A. New Insights in Routine Procedure for Mathematical Evaluation of in vitro Cytotoxicity Data from Cancer Cell Lines. *Int. J. Bioautomation* **2018**, *22*, 87–106. [CrossRef]
66. Sedlak, J.; Lindsay, R.H. Estimation of total, protein-bound, and nonprotein sulfhydryl groups in tissue with Ellman's reagent. *Anal. Biochem.* **1968**, *25*, 192–205. [CrossRef]
67. Chazotte, B. Labeling Nuclear DNA with Hoechst 33342. *Cold Spring Harb. Protoc.* **2011**, *2011*, pdb.prot5557. [CrossRef] [PubMed]
68. Stepanović, S.; Vuković, D.; Hola, V.; DI Bonaventura, G.D.; Djukić, S.; Ćirković, I.; Ruzicka, F. Quantification of biofilm in microtiter plates: Overview of testing conditions and practical recommendations for assessment of biofilm production by staphylococci. *APMIS* **2007**, *115*, 891–899. [CrossRef]
69. Wong, H.K. STAT Assays with a TWIST: Differentiating Sézary Syndrome from Erythrodermic Inflammatory Dermatitis. *J. Invest. Dermatol.* **2016**, *136*, 1313–1315. [CrossRef]
70. Merindol, N.; Riquet, A.; Szablewski, V.; Eliaou, J.-F.; Puisieux, A.; Bonnefoy, N. The emerging role of Twist proteins in hematopoietic cells and hematological malignancies. *Blood Cancer J.* **2014**, *4*, e206. [CrossRef] [PubMed]
71. Xue, G.; Restuccia, D.F.; Lan, Q.; Hynx, D.; Dirnhofer, S.; Hess, D.; Rüegg, C.; Hemmings, B.A. Akt/PKB-Mediated Phosphorylation of Twist1 Promotes Tumor Metastasis via Mediating Cross-Talk between PI3K/Akt and TGF- $\alpha$  Signaling Axes. *Cancer Discov.* **2012**, *2*, 248–259. [CrossRef] [PubMed]
72. Zhao, Z.; Rahman, M.A.; Chen, Z.G.; Shin, D.M. Multiple biological functions of Twist1 in various cancers. *Oncotarget* **2017**, *8*, 20380–20393. [CrossRef] [PubMed]
73. Kaleağasıoğlu, F.; Zaharieva, M.; Konstantinov, S.M.; Berger, M.R. Alkylphospholipids are Signal Transduction Modulators with Potential for Anticancer Therapy. *Anti-Cancer Agents Med. Chem.* **2019**, *19*, 66–91. [CrossRef] [PubMed]
74. Li, S.; Kendall, S.E.; Raices, R.; Finlay, J.; Covarrubias, M.; Liu, Z.; Lowe, G.; Lin, Y.; Teh, Y.H.; Leigh, V.; et al. TWIST1 associates with NF- $\kappa$ B subunit RELA via carboxyl-terminal WR domain to promote cell autonomous invasion through IL8 production. *BMC Biol.* **2012**, *10*, 73. [CrossRef]
75. Ilieva, Y.; Kaloyanov, K.; Yosifov, D.; Robev, B.; Zhelezova, I.; Genova, M.; Mihova, A.; Balatzenko, G.; Zaharieva, M.; Berger, M.R.; et al. Antineoplastic potential of curcumin (cooperative study in Bulgaria and Germany). *Phytochem. Rev.* **2014**, *13*, 459–469. [CrossRef]
76. Aggarwal, B.B.; Kumar, A.; Bharti, A.C. Anticancer potential of curcumin: Preclinical and clinical studies. *Anticancer Res.* **2003**, *23*, 363–398. [PubMed]
77. Shishodia, S.; Amin, H.M.; Lai, R.; Aggarwal, B.B. Curcumin (diferuloylmethane) inhibits constitutive NF-kappaB activation, induces G1/S arrest, suppresses proliferation, and induces apoptosis in mantle cell lymphoma. *Biochem. Pharmacol.* **2005**, *70*, 700–713. [CrossRef] [PubMed]
78. Kunwar, A.; Kunwar, A.; Narang, H.; Priyadarsini, K.I.; Krishna, M.; Pandey, R.; Sainis, K.B. Delayed activation of PKCdelta and NFkappaB and higher radioprotection in splenic lymphocytes by copper (II)-Curcumin (1) complex as compared to curcumin. *J. Cell. Biochem.* **2007**, *102*, 1214–1224. [CrossRef] [PubMed]

79. Prasad, S.; Gupta, S.C.; Tyagi, A.K.; Aggarwal, B.B. Curcumin, a component of golden spice: From bedside to bench and back. *Biotechnol. Adv.* **2014**, *32*, 1053–1064. [CrossRef]
80. Obando, D.; Widmer, F.; Wright, L.C.; Sorrell, T.C.; Jolliffe, K.A. Synthesis, antifungal and antimicrobial activity of alkylphospholipids. *Bioorg. Med. Chem.* **2007**, *15*, 5158–5165. [CrossRef]
81. Gong, C.; Wu, Q.; Wang, Y.; Zhang, D.; Luo, F.; Zhao, X.; Wei, Y.; Qian, Z. A biodegradable hydrogel system containing curcumin encapsulated in micelles for cutaneous wound healing. *Biomaterials* **2013**, *34*, 6377–6387. [CrossRef]
82. Caon, T.; Mazzarino, L.; Simões, C.M.O.; Senna, E.L.; Silva, M.A.S. Lipid- and Polymer-Based Nanostructures for Cutaneous Delivery of Curcumin. *AAPS PharmSciTech* **2016**, *18*, 920–925. [CrossRef]
83. Trochopoulos, A.G.; Zaharieva, M.M.; Marinova, M.H.; Yoncheva, K.; Tibi, I.P.; Berger, M.R.; Konstantinov, S.M. Antineoplastic effect of a novel nanosized curcumin on cutaneous T cell lymphoma. *Oncol. Lett.* **2020**, *20*, 304. [CrossRef]
84. Kennedy, L.; Sandhu, J.K.; Harper, M.-E.; Cuperlovic-Culf, M. Role of Glutathione in Cancer: From Mechanisms to Therapies. *Biomolecules* **2020**, *10*, 1429. [CrossRef]
85. Bansal, A.; Celeste Simon, M. Glutathione metabolism in cancer progression and treatment resistance. *J. Cell Biol.* **2018**, *217*, 2291–2298. [CrossRef]

## Article

# From Serendipity to Rational Identification of the 5,6,7,8-Tetrahydrobenzo[4,5]thieno[2,3-*d*]pyrimidin-4(3*H*)-one Core as a New Chemotype of AKT1 Inhibitors for Acute Myeloid Leukemia

Andrea Astolfi <sup>1,†</sup>, Francesca Milano <sup>2,†</sup>, Deborah Palazzotti <sup>1,†</sup>, Jose Brea <sup>3</sup>, Maria Chiara Pismataro <sup>1</sup>, Mariangela Morlando <sup>1</sup>, Oriana Tabarrini <sup>1</sup>, Maria Isabel Loza <sup>3</sup>, Serena Massari <sup>1</sup>, Maria Paola Martelli <sup>2</sup> and Maria Letizia Barreca <sup>1,\*</sup>

<sup>1</sup> Department of Pharmaceutical Sciences, “Department of Excellence 2018–2022”, University of Perugia, 06123 Perugia, Italy

<sup>2</sup> Hematology and Clinical Immunology, Department of Medicine and Surgery, University of Perugia, 06132 Perugia, Italy

<sup>3</sup> CIMUS Research Center, University of Santiago de Compostela, 15782 Santiago de Compostela, Spain

\* Correspondence: maria.barreca@unipg.it

† These authors contributed equally to this work.

**Citation:** Astolfi, A.; Milano, F.; Palazzotti, D.; Brea, J.; Pismataro, M.C.; Morlando, M.; Tabarrini, O.; Loza, M.I.; Massari, S.; Martelli, M.P.; et al. From Serendipity to Rational Identification of the 5,6,7,8-Tetrahydrobenzo[4,5]thieno[2,3-*d*]pyrimidin-4(3*H*)-one Core as a New Chemotype of AKT1 Inhibitors for Acute Myeloid Leukemia. *Pharmaceutics* **2022**, *14*, 2295. <https://doi.org/10.3390/pharmaceutics14112295>

Academic Editor: Francesca Musumeci

Received: 30 August 2022

Accepted: 22 October 2022

Published: 26 October 2022

**Publisher’s Note:** MDPI stays neutral with regard to jurisdictional claims in published maps and institutional affiliations.



**Copyright:** © 2022 by the authors. Licensee MDPI, Basel, Switzerland. This article is an open access article distributed under the terms and conditions of the Creative Commons Attribution (CC BY) license (<https://creativecommons.org/licenses/by/4.0/>).

**Abstract:** Acute myeloid leukemia (AML) is a heterogeneous hematopoietic malignancy whose prognosis is globally poor. In more than 60% of AML patients, the PI3K/AKTs/mTOR signaling pathway is aberrantly activated because of oncogenic driver alterations and further enhanced by chemotherapy as a mechanism of drug resistance. Against this backdrop, very recently we have started a multidisciplinary research project focused on AKT1 as a pharmacological target to identify novel anti-AML agents. Indeed, the serendipitous finding of the in-house compound **T187** as an AKT1 inhibitor has paved the way to the rational identification of new active small molecules, among which **T126** has emerged as the most interesting compound with  $IC_{50} = 1.99 \pm 0.11 \mu\text{M}$ , ligand efficiency of 0.35, and a clear effect at low micromolar concentrations on growth inhibition and induction of apoptosis in AML cells. The collected results together with preliminary SAR data strongly indicate that the 5,6,7,8-tetrahydrobenzo[4,5]thieno[2,3-*d*]pyrimidin-4(3*H*)-one derivative **T126** is worthy of future biological experiments and medicinal chemistry efforts aimed at developing a novel chemical class of AKT1 inhibitors as anti-AML agents.

**Keywords:** AKT1; kinase inhibitors; cancer; acute myeloid leukemia; rare disease; molecular modeling; molecular docking; similarity search; MD simulation; computer-aided drug discovery

## 1. Introduction

The AGC kinases AKT1–3 are key mediators of the PI3K/AKT/mTOR signaling pathway, which plays a crucial role in major cellular functions such as proliferation, migration, and antiapoptotic survival [1]. The main downstream targets of AKT include the mammalian target of rapamycin (mTOR) of the mTOR complex 1 (mTORC1), that through phosphorylation activates the p70 ribosomal S6 kinase (p70S6K) and inactivates the 4E-BP1 (an inhibitor of the elongation initiating factor 4E, eIF4E) ultimately promoting protein translation and cell growth [2]. Among the three AKT isoforms, AKT1 is expressed ubiquitously and a high rate of AKT1 amplification occurs in a wide range of human cancers [3] including acute myeloid leukemia (AML) [4,5], a rare but often fatal blood cancer. The major activators of the PI3K/AKT/mTOR pathways are upstream kinases, such as tyrosine kinase receptors (e.g., fms-like tyrosine kinase 3, FLT3) or K/NRAS frequently involved in gain-of-function gene mutations in AML [6]. Indeed, a constitutive activation of the AKT pathway and the phosphorylation of its targets such as mTOR, p70S6K, and 4E-BP1

are detected in about 60% of AML patients [7–9], and are mostly described as connected with a poorer prognosis [10–14]. The level of AKT1 expression and kinase activity is often associated with the degree of differentiation, hormone dependency, and aggressive behavior of cancer cells and/or with a less favorable prognosis [12–14]. Additionally, accumulating evidence indicates that the acquisition of resistance to chemotherapeutic drugs involves the activation of the PI3K/AKT/mTOR pathway [15], suggesting that AKT1 inhibitors could be useful for overcoming drug resistance and improving response [16,17]. Recently, AKT activation in AML has also been implicated as a resistance mechanism to the targeted therapy **selinexor**, a newly FDA-approved small molecule inhibitor of exportin 1 (XPO1) [18].

In the era of precision oncology, AKT1 thus represents an attractive target for the development of targeted therapies selectively hitting cancer cells characterized by an aberrant activation of the PI3K/AKT/mTOR signaling pathway. To date, no drugs against AKT1 are on the market, although some AKT1 inhibitors are currently in clinical trials for solid cancers [19,20], but not for AML, which remains an urgent medical need. Against this backdrop, we have very recently started a multidisciplinary research program aimed at rationally identifying new AKT1 inhibitors as anti-AML agents.

## 2. Materials and Methods

### 2.1. Computational Studies

#### 2.1.1. Ligand Preparation

All compounds explored in molecular modelling studies (i.e., **T187**, the clinical candidates, and the selected UNIPG-lib compounds) were prepared using the LigPrep [21] to produce low energy 3D structures taking into account the ionization states, stereochemistry, the tautomerism, and ring conformations at the desired pH ( $7.5 \pm 0.5$ ).

#### 2.1.2. Similarity Search

The BioSolveIT Feature Tree (FTrees) [22] software tool was used to perform fast 2D-similarity assessments. The similarity searches were performed using the following command line:

```
ftrees -i T187.sdf -l $library --minSimilarityThreshold X -o output.csv
```

where the `-i` option defines the query molecule, the `-l` option states the screened library, the `--minSimilarityThreshold` defines the similarity threshold below which molecules are discarded, and the `-o` option states the output file.

To compute the similarity between **T187** and the known AKT1 inhibitor clinical candidates, the compounds reported in Table S2 were used as the `$library` file and the `--minSimilarityThreshold` was set to 0.

To build the **T187**-like compounds' library, the prepared UNIPG-lib was used as the `$library` file and the `--minSimilarityThreshold` was set to 0.65.

#### 2.1.3. Protein Preparation

The only two crystal structures of AKT1 co-crystallized with clinical candidates (i.e., **capivasertib** and **ipatasertib**) available from RCSB PDB [23] were PDB ID 4GV1 [24] and 4EKL [25], respectively. Considering the best resolution of the 4GV1 structure (1.49 Å vs. 2.00 Å for 4EKL), this protein conformation was used for further modeling studies. Firstly, the complex was prepared using Schrödinger's Protein Preparation Wizard (Schrödinger Release 2019-2) [26] in order to obtain satisfactory starting structures for the docking studies. The complex was pre-processed as follows: (i) hydrogen atoms were added and bond orders were assigned to amino acid residues and ligands, (ii) the missing side chains were filled, (iii) the protein was capped with acetyl (ACE) and N-methylamine (NMA) groups, (iv) all water molecules beyond 3 Å from heteroatoms were deleted, and (v) Epik (Schrödinger Release 2019-2) [27] was used to predict the ionization and tautomeric states for the ligands ( $\text{pH} = 7.0 \pm 2$ ). In addition, the structure presented some missed residues (loop 451–457) that were filled by using the homology modelling tool function implemented in the Prime

package (Schrödinger Release 2019-2) [28]. Then, the H-bond network of the complex was optimized using PROPKA for the assignment of the residue protonation states (pH = 7.0). Finally, the complex was submitted to a restrained minimization (OPLS3 force field), which was stopped when the RMSD of heavy atoms reached 0.30 Å.

#### 2.1.4. Molecular Docking

Docking studies were performed using Schrödinger's Glide software (Schrödinger Release 2019-2) [29]. In our protocol, the crystallographic position of **capivasertib** (PDB ID 4GV1) was used as reference to center the grid on the ATP-site. The docking space was defined as a cubic box (28 Å outerbox), with an inner cubic box (14 Å) defining the region where the centroid of the ligand had to be located. The centroid for the 4GV1 protein had coordinates of −20.00, 4.33, and 11.27 to the *x*-, *y*-, and *z*-axis, respectively. After grid preparation with the "receptor grid generation" tool, docking experiments were performed using the Glide XP (Extra Precision) protocol (Schrödinger Release 2019-2) [30], by generating three poses for each ligand. The generated poses were submitted to the MMGBSA minimization step using the "Refine Protein-Ligand Complex" tool in Prime (default settings—residues at 5 Å within the ligand considered as flexible) and only the pose with the lower MM-GBSA  $\Delta G$  of binding (MM-GBSA dG Bind) was retained.

The collected binding poses were then filtered for the presence of H-bond interaction(s) with the hinge residues Ala230 and/or Glu 228.

By using the above-described protocol, the initial hit, **T187**, was predicted to bind the catalytic site with a MM-GBSA dG Bind of −39.42 Kcal/mol. Based on this result, the **T187**-like compounds were docked and later filtered using a threshold of −40 Kcal/mol on the MM-GBSA dG Bind and then submitted to visual inspection.

The two co-crystallized advanced inhibitors were added to the ligand set for comparison. The best docking poses of **ipatasertib** (MM-GBSA dG Bind = −67.72 Kcal/mol) and **capivasertib** (MM-GBSA dG Bind = −62.42 Kcal/mol) agreed well with their experimental binding conformations (Figure S2).

#### 2.1.5. Molecular Dynamics Simulations

Explicit solvent Molecular Dynamics (MD) simulations were performed by using the Desmond package v5.8 (Schrödinger Release 2019-2) [31] to investigate the stability of the MMGBGA binding modes generated for **T126** and **T125** in complex with the 4GV1 protein conformation. The OPLS3e forcefield was selected and the systems were solvated in an orthorhombic box (size = 20.0 × 20.0 × 20.0) exploiting the TIP3P water molecule mode. Na<sup>+</sup> and Cl<sup>−</sup> counter ions at a concentration of 0.15 M were added to neutralize the system charge by means of the System Builder tool. The system setup step enabled the generation of the 4GV1-**T126** and 4GV1-**T125** complex systems consisting of 83,768 and 83,767 atoms, respectively. MD simulations were set up through the Molecular dynamics tool. The systems were relaxed before the simulation by using the protocol implemented in Desmond which comprises 5 equilibration steps. The system minimization was followed by a production step of 200 ns that was simulated by the NTP ensemble at 310 K and 1 atm. For each system, three replicas with different random seeds were performed. MD simulation results were analyzed through the Simulation interaction diagram (SID) tool provided by Schrödinger.

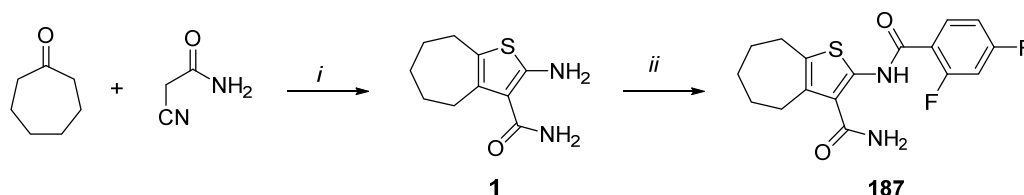
## 2.2. Chemistry

### 2.2.1. Synthetic Procedures

All the compounds evaluated in the biological assays (Table S2) were synthesized as previously reported by us, with the exception of compound **T187** which has never been reported so far and, therefore, is described in this paper, and compounds **T124**, **T126**, and **T128** that were synthesized as reported in the literature [32–35].

Compound **T187** was synthesized as reported in Scheme 1, starting from a one-pot Gewald reaction entailing the reaction of cycloheptanone with cyanoacetamide in the

presence of sulphur and morpholine in EtOH at reflux, to give the intermediate **1** [36]. Successive amidation of compound **1** [36] with 2,4-difluorobenzoic acid was performed in CH<sub>2</sub>Cl<sub>2</sub> at 50 °C, in the presence of the Mukaiyama reagent (2-chloro-1-methylpyridinium iodide, CMPI), 4-dimethylaminopyridine (DMAP), and triethylamine (TEA), furnishing compound **T187**.



**Scheme 1.** Reagents and conditions: (i) S8, morpholine, EtOH, reflux; (ii) 2,4-difluorobenzoic acid, CMPI, DMAP, TEA, CH<sub>2</sub>Cl<sub>2</sub>, 50 °C.

### 2.2.2. Experimental Section

The commercially available starting materials, reagents, and solvents were used as supplied. All reactions were routinely monitored by TLC on silica gel 60F254 (Merck) and visualized by using UV or iodine. Flash column chromatography was performed on Merck silica gel 60 (mesh 230–400). After extraction, the organic solutions were dried over anhydrous Na<sub>2</sub>SO<sub>4</sub>, filtered, and concentrated with a Büchi rotary evaporator at reduced pressure. Yields are of the purified product and were not optimized. The purities of compounds **T124**, **T126**, and **T128** (96.5%, 100%, and 100%, respectively) were determined by HPLC analysis using a Jasco LC-4000 instrument equipped with a DAD Jasco MD-4015 detector from 200 to 600 nm. The purity was revealed at 344 nm using an XTerra MS C18 Column, 5 µm, 4.6 mm × 150 mm with a flow rate: 0.4 mL/min; an acquisition time: 10 min; an isocratic: acetonitrile containing 0.1% of formic acid (85%) and water (15%); a column temperature: 25 °C; and an injection volume: 20 µL. The peak retention time is given in minutes and the Chromatograms were analyzed by Chromatography Data System software ChromNAV version number 2.03.06 [Build 4] (2003 JASCO Corporation, Tokyo, Japan). The purity of compound **T187** (95.09%) was determined by LC/MS using an Agilent 1290 Infinity System machine equipped with a DAD detector from 190 to 640 nm. The purity was revealed at 254 nm using a Phenomenex AERIS Widepore C4, 4.6 mm, 100 mm (6.6 lm) with a flow rate: 0.6 mL/min; an acquisition time: 10 min; a gradient: acetonitrile in water containing 0.1% of formic acid (0 100% in 10 min); a column temperature: 40 °C; and an injection volume: 2 µL. The peak retention time is given in minutes. Accurate mass measurements were performed with HRMS (Agilent Q-TOF 6540) and the monitored *m/z* values ranged from 100 *m/z* to 3000 *m/z* in positive polarity. The Mass spectrometry was equipped with an ESI source. The gas temperature, gas flow, nebulizer, sheath gas, and sheath gas flow were set at 350 °C, 9 L/min, 35 psig, 400 °C, and 9 L/min, respectively. The capillary voltage was set at 4000 V and the fragmentor at 120 V. The <sup>1</sup>H NMR and <sup>13</sup>C NMR spectra were recorded on a Bruker Avance DRX-400 MHz using a residual solvent such as dimethylsulfoxide (δ = 2.48) as an internal standard. The chemical shifts were recorded in ppm (δ) and the spectral data are consistent with the assigned structures. The spin multiplicities are indicated by the: d (doublet), t (triplet), and m (multiplet).

2-(2,4-Difluorobenzamido)-5,6,7,8-tetrahydro-4H-cyclohepta[b]thiophene-3-carboxamide (**T187**). 2,4-Difluorobenzoic acid (0.09 g, 0.61 mmol), CMPI (0.14 g, 0.57 mmol), DMAP (0.03 g, 0.24 mmol), and TEA (0.14 g, 1.4 mmol) were added to a solution of compound **1** [36] (0.10 g, 0.47 mmol) in dry CH<sub>2</sub>Cl<sub>2</sub> (5 mL). The reaction mixture was maintained at 40 °C overnight and then, after colling, it was evaporated to dryness. The obtained residue was suspended in a 1 M HCl solution, stirred for 10 min, and then filtered. The solid was purified by flash chromatography eluting with CHCl<sub>3</sub>/MeOH (98:2), to give **T187** (0.07 g, 42%). <sup>1</sup>H-NMR (400 MHz, DMSO-*d*<sub>6</sub>) δ 1.55–1.65 (m, 4H, cycloheptane CH<sub>2</sub>), 1.76–1.80, 2.70–2.75, 2.78–2.80 (m, each 2H, cycloheptane CH<sub>2</sub>), 7.28–7.32 (m, 1H, aromatic CH),

7.47–7.70 (m, 3H, aromatic CH and NH<sub>2</sub>), 8.00–8.10 (m, 1H, aromatic CH), 11.66–11.68 (d,  $J = 8.5$  Hz, 1H, NH); <sup>13</sup>C-NMR (101 MHz, DMSO-*d*<sub>6</sub>)  $\delta$  27.7, 28.1, 28.7, 28.8, 32.1, 105.6 (t,  $J_{C-F} = 27.3$  Hz), 113.3 (d,  $J_{C-F} = 20.2$  Hz), 117.6 (d,  $J_{C-F} = 9.1$  Hz), 122.1, 131.6, 133.8 (d,  $J_{C-F} = 11.1$  Hz), 135.6, 137.2, 158.7, 159.6, 160.8 (dd,  $J_{C-F} = 14.1$  and 253.5 Hz), 165.0 (dd,  $J_{C-F} = 13.1$  and 266.6 Hz), 167.9. HRMS:  $m/z$  calcd for C<sub>17</sub>H<sub>16</sub>F<sub>2</sub>N<sub>2</sub>O<sub>2</sub>S 351.0089 (M + H)<sup>+</sup>, found 351.0978 (M + H)<sup>+</sup>. HPLC, ret. time: 5.633 min, peak area: 95.09%.

### 2.3. Enzymatic Assays

The studied compounds, including the standard inhibitor Staurosporine (ThermoFisher, Madrid, Spain, Invitrogen BP2541), were incubated with 3 nM AKT1 (#Aps 01-101; Kinase Logistics, Meyn, Germany) and 1.5  $\mu$ M Profiler Pro peptide 6 (#760350; Perkin Elmer, Tres Cantos, Madrid, Spain) in the presence of different concentrations of Adenosine 5'triphosphate disodium salt, ATP (#A2383; Sigma Aldrich, Madrid, Spain) in a 384-well Microplate (#781076; Greiner, San Sebastián de los Reyes, Madrid, Spain). The reaction rate was calculated from kinetic measurements carried out measured in a Caliper EzReader LabChip 3000 (Caliper, Hopkinton, MA, USA) reader with samples taken each 10 min for a total time of 60 min. The percentage of substrate conversion rate was plotted versus the ATP concentration. The data was analyzed by non-linear fitting with GraphPad Prism by employing the Michaelis–Menten equation. The buffer assay used in the inhibition hAKT1 assay is: Hepes 100 mM, DMSO 4%, Brij 0.003%, Tween 20 0.004%, MgCl<sub>2</sub> 10 mM, with a pH = 7.5.

The K<sub>i</sub> values were calculated by employing the GraphPad Prism equations.

### 2.4. Cell-Based Assays

#### 2.4.1. Cells and Compound Treatments

The human AML cell lines, OCI-AML3 (carrying the *NPM1* gene mutation A and the *DNMT3A*<sup>R882C</sup> mutation), IMS-M2 (carrying the *NPM1* gene mutation A), OCI-AML2 (with the wild-type *NPM1* and *DNMT3A*<sup>R635W</sup> mutation), and SKM-1 and MOLM-13 (with the wild-type *NPM1*) were previously reported [37,38]. The cell lines were purchased from the Deutsche Sammlung von Mikroorganismen und Zellkulturen (DSMZ) (Braunschweig, Germany) cell bank and maintained according to the vendors' instructions. Briefly, cultured cells were split every 3 days and maintained in an exponential growth phase. The cell lines were tested for mycoplasma using the Universal Mycoplasma Detection Kit (ATCC). The OCI-AML3 were grown in  $\alpha$ -MEM supplemented with 20% fetal bovine serum, 100 U/mL penicillin, and 100  $\mu$ g/mL streptomycin (P/S), and all other cell lines were cultured in RPMI and supplemented with a 10–20% fetal bovine serum and 100 U/mL penicillin and 100  $\mu$ g/mL streptomycin. The cells were kept at 37 °C in a 5% CO<sub>2</sub> incubator. Prior to screening, the appropriate cell concentration for all cell lines was determined. For the cell lines' treatments, cells were maintained as follows: OCI-AML3 at  $0.25 \times 10^6$ /mL, OCI-AML2 and IMS-M2 at  $0.35 \times 10^6$ /mL, and SKM-1 and MOLM-13 at  $0.5 \times 10^6$ /mL. The compounds were re-suspended at 10 mM stock in DMSO. Further dilutions were performed in phosphate-buffer-saline (PBS) for pharmacological experiments. The cells were exposed to compounds at different concentrations for the indicated time points and sampled as described below. Briefly, the cells ( $4 \times 10^5$ /mL) were seeded in 384-well plate and treated for 48 h with various concentrations (0.001  $\mu$ M to 100  $\mu$ M) of either one of the compounds, **T101**, **T126**, and **T159**, or **NSC348884**, as a positive control [39]. Each plate included DMSO at 0.1% as a negative control. The metabolic cell activity was measured by using the CellTiter Blue proliferation agent (Roche) as described in the manufacturer's procedure. Briefly, CellTiter Blue solution (Resazurin) was added to each well and the plates were incubated at 37 °C with 5% CO<sub>2</sub> for 4 h. During the incubation time, the resazurin is reduced to fluorescent resorufin in metabolically and proliferating living cells. The fluorescence intensity was measured using the automated Tecan plate reader (Tecan Group Ltd., Männedorf, Switzerland) at an excitation/emission wavelength of 531/572 nm. The fluorescence readouts were reported as relative fluorescence units (RFU) and read on

a luminescence plate reader (Infinite 200 Pro, Tecan, CA, USA). The dose response curves (maximal inhibitory concentration ( $IC_{50}$ )) were obtained by non-linear regression analysis using the GraphPad Prism 5.0 program. The concentration is shown as a logarithmic function. All the experiments were performed at least in triplicate, with technical repetition. The results are expressed as mean  $\pm$  standard error of the mean (SEM). For the Colony Forming Unit (CFU) assay,  $10 \times 10^6$  CD34+ human hematopoietic progenitors were received from unique healthy donors, upon signed informed consent, and were cultured in SFEM II (Serum-free medium) and P/S at a density of  $1 \times 10^6$ /mL with cytokines that are important for cell division and self-renewal: fms-like tyrosine kinase 3 (FLT3)-ligand, FLT3L (100 ng/mL), Stem Cell Factor, SCF (100 ng/mL) and Trombopoietin, and TPO (50 ng/mL) for 48 h before plating them on a Methocult medium.

#### 2.4.2. Colony Forming Unit (CFU) Assay

For the CFU assay, 500 CD34+ human cells were plated in a MethoCult™ enriched medium (see Table S4) on a 6-well plate (untreated cells versus T126 at 1, 2.5, and 5  $\mu$ M, each condition in triplicate). The plates were then incubated for 14 days at 37 °C (5% CO<sub>2</sub>), and the images were captured and the colonies counted by STEMvision™. STEMvision™ is a bench-top instrument and computer system designed specifically for the automated imaging and counting of hematopoietic colonies in the CFU assay. This system has been optimized for use with MethoCult™ media and meniscus-free SmartDish™ culture ware. The use of this standardized platform significantly improves the accuracy and reproducibility of the human CFU assay. Mobilized peripheral blood (MPB) analysis packages have been used to accurately count colonies.

#### 2.4.3. Cell Lysates Preparation and Western Blot Analysis

Immunoblotting was conducted as described previously [37]. Briefly, fresh cell pellets (0.2–0.5  $\times 10^6$ /test for AML cell lines) were dissolved directly in 30–60  $\mu$ L of Laemmli sample buffer 1 $\times$  (1.5 M Tris-HCl pH 6.8, glycerol,  $\beta$ -mercaptoethanol, SDS, bromophenol blue) and boiled at 95 °C for 5 min. The proteins were separated by SDS-polyacrylamide gel electrophoresis (SDS-PAGE) on Precast 4–15% gradient gels (Biorad, Hercules, CA, USA) transferred onto nitrocellulose membranes (GE Healthcare, Piscataway, NJ, USA) and probed with specific primary antibodies followed by horseradish peroxidase-conjugated secondary antibodies (GE Healthcare Lifesciences). The polypeptides were visualized using enhanced chemiluminescence (Luminata Crescendo, Merck Millipore, Burlington, MA, USA) according to the manufacturer's instructions. The bands were visualized using the Biorad Chemidoc and the images were processed using the image lab software (Biorad) and Adobe Photoshop (Ps CC 2019).  $\beta$ -actin expression levels were used as a control for protein loading, as indicated.

#### 2.4.4. Cell Growth and Apoptosis Evaluation

The viable cell count was evaluated daily using the Invitrogen Countess automated cell counter (Invitrogen, Carlsbad, CA, USA) by trypan blue exclusion, and individual growth curves were generated from these data.

The cell apoptosis was assessed using Annexin V APC- or FITC-conjugated antibodies and counterstained with Propidium Iodide (PI) or 7AAD for the detection of necrotic cells (Becton Dickinson, Franklin Lakes, NJ, USA), according to the manufacturer's protocol. The data acquisition and analysis were done with a FACS Canto II flow cytometer and data were acquired and analyzed using Diva software (Becton Dickinson, Franklin Lakes, NJ, USA).

#### 2.4.5. Antibodies

The primary antibodies used for western blot analyses are the following: mouse monoclonal anti-human  $\beta$ -actin (Clone AC-15; dilution 1:5000) from Sigma Aldrich (St. Louis, MO, USA); rabbit monoclonal anti-human Cleaved poly (ADP-ribose) polymerase (c-PARP) (Clone Asp 214; dilution 1:1000); rabbit monoclonal phospho-Akt



(Ser473) (clone D9E, dilution 1:500); rabbit polyclonal phospho-mTOR (Ser2448) (dilution 1:500); rabbit polyclonal phospho-4E-BP1 (Ser65) (dilution 1:500); rabbit monoclonal Akt1 (clone D9R8K, dilution 1:500); rabbit polyclonal 4E-BP1 (dilution 1:500); and rabbit polyclonal mTOR (dilution 1:500), all from Cell Signaling (Cell Signaling Technology, Inc., Danvers, MA, USA).

#### 2.4.6. Statistical Analysis

All the experiments were performed at least in triplicate, as indicated, with technical repetition when possible. The results are expressed as mean  $\pm$  standard error of the mean (SEM). A one- or two-tailed paired Student *t*-test with a normal-based 95% CI was applied for statistical analysis, as indicated. Statistical significance was defined as  $p < 0.05$ .

### 2.5. Validation Assays to Confirm T126 as a True Hit

#### 2.5.1. Intrinsic Fluorescence Assay

Compound **T126** was serially diluted in 384-well black plates with Hepes 100 mM, DMSO 4%, Brij 0.003%, Tween 20 0.004%, MgCl<sub>2</sub> 10 mM, at a pH = 7.5 and incubated for 2 h at 37 °C. After the incubation time the intensity of fluorescence ( $\lambda_{exc}$ : 485 nm;  $\lambda_{em}$ : 535 nm) was detected in a Tecan M1000 Pro.

#### 2.5.2. Solubility Screen Assay to Determine Chemical Aggregation

The stock solutions (10–2 M) of the compound **T126** were diluted to a decreased molarity, from 100  $\mu$ M to 0.0001  $\mu$ M, in 384-well transparent plates (Greiner 781801) with 1% DMSO: 99% buffer Hepes 100 mM, DMSO 4%, Brij 0.003%, Tween 20 0.004%, MgCl<sub>2</sub> 10 mM, at a pH = 7.5. Incubation occurred at 37 °C and the results were read after 2 h in a NEPHELOstar Plus (BMG LABTECH, Ortenberg, Germany). The results were adjusted to a segmented regression to obtain the maximum concentration in which the compounds were soluble.

#### 2.5.3. UV-VIS Titration Assay with an Increasing Amount of MgCl<sub>2</sub>

The potential ability of **T126** to chelate Mg<sup>2+</sup> ions was evaluated by spectrophotometric methods using a T70+ UV-Vis Spectrometer (PG Instruments, Leicestershire, UK) and a quartz cuvette with a 1 cm optical path. MgCl<sub>2</sub> · 5H<sub>2</sub>O 1M solution was prepared from powder (VWR International, Milan, Italy). The compound **T126** was dissolved in DMSO to a final concentration of 10 mM and diluted with a milliQ water/DMSO mixture to a final concentration of 100  $\mu$ M (4% DMSO). The obtained solution was placed in a cuvette and the UV-Vis spectra was recorded between 200 and 500 nm using water milliQ (with 4% DMSO) as reference. Thereafter, small volumes of MgCl<sub>2</sub> aqueous solution were added both in the sample and in the reference cuvettes to obtain a series of solutions containing increasing concentrations of MgCl<sub>2</sub> (1.25, 2.5, 5 and 10 mM), carefully pipetted for mixing, and the UV-Vis spectra were repeated. Each experiment was performed in triplicate.

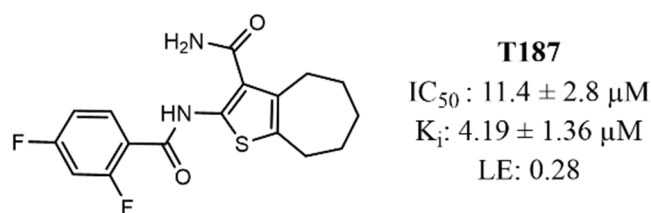
## 3. Results and Discussion

### 3.1. Computer-Aided Identification of Novel AKT1 Inhibitors

The idea of exploring AKT1 as a pharmacological target arose from serendipity during our efforts to discover new bioactive compounds against other protein kinases that were already the objects of our studies [40,41].

Among the investigated compounds, the in-house cyclohepta[*b*]thiophen-3-carboxamide derivative **T187** (Figure 1) turned out to be inactive against the desired target (i.e., p38 MAPK), showing instead an unexpected inhibitory activity towards the catalytic domain of the AKT1 protein, with a percentage of enzymatic inhibition at 10  $\mu$ M equal to 56%. This unforeseen result prompted us to better characterize the small molecule, which showed an IC<sub>50</sub> = 11.4  $\pm$  2.8  $\mu$ M and a K<sub>i</sub> = 4.19  $\pm$  1.36  $\mu$ M. Interestingly, a data literature search using SciFinder [42] pointed out that neither compound **T187** nor its chemical

scaffold *N*-(5,6,7,8-tetrahydro-4*H*-cyclohepta[*b*]thiophen-2-yl)benzamide had ever been investigated in the context of AKT1 inhibition.



**Figure 1.** Chemical structure and biological data for **T187**.  $IC_{50}$  represents the compound concentration necessary to reduce by 50% the ADP formation in the ADP-Glo Assay;  $K_i$  is the AKT1 inhibition constant; Ligand efficiency (LE) refers to the potency of a compound averaged by its non-hydrogen atom count ( $LE = 1.4 \text{ p}IC_{50}/N$ , where  $N$  is the number of heavy atoms). LE is expressed as units of  $\text{kcal mol}^{-1} \text{N}^{-1}$ .

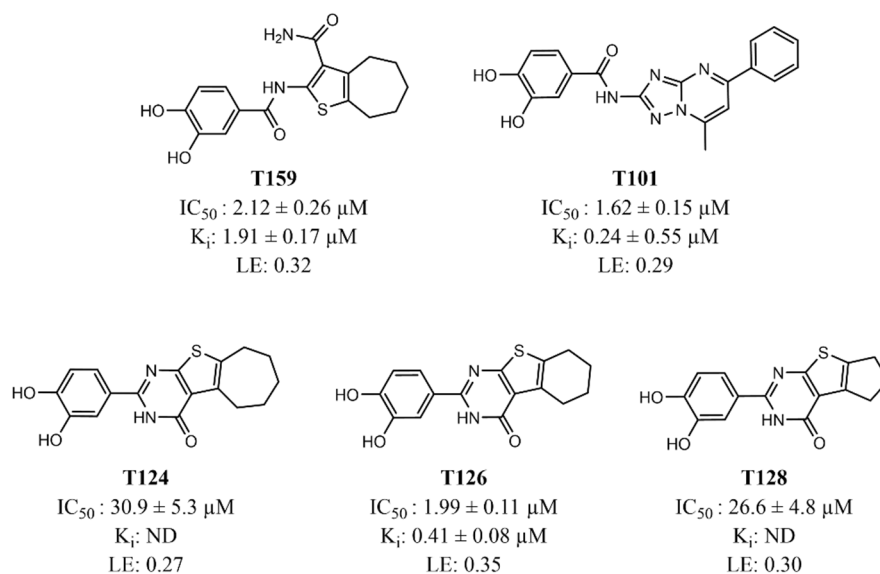
Intrigued by these results and stimulated by our interest and expertise in the field of kinases [43–45] and AML [46–48], we decided to take advantage of the serendipitous discovery of **T187** to rationally search for other AKT1 inhibitors within our in-house compound library (herein after called UNIPG-lib). Specifically, the UNIPG-lib is a chemical collection of ~3000 small molecules, including both target compounds and intermediates, synthesized and/or collected by the research team in the context of several drug discovery projects.

For our AKT1-targeted program, we carried out both ligand- and structure-based modeling studies to aid the selection of **T187**-like compounds for biological testing. First, the BioSolveIT Feature Trees (FTrees) [22] software tool was used to perform a fast 2D-similarity screening of the UNIPG-lib using **T187** as a query molecule. This ligand-based approach allowed us to select 247 available neighbors to the initial compound with a similarity threshold of at least 0.65. At this stage, to further rationalize the identification of potential AKT1 inhibitors, the collected compounds were submitted to molecular docking simulations to explore their binding potential to the investigated kinase. Within this aim, the RCSB PDB [23] was consulted to retrieve structural information on AKT1 and its ATP-site binders, highlighting that 28 crystal structures had been disclosed prior to December 2021. In particular, the most interesting co-crystallized ligands were present in the PDB structures 4EKL [25] and 4GV1 [24], showing the clinical trial inhibitors **ipatasertib** (GDC-0068) and **capivasertib** (AZD5363), respectively [20]. These small molecules shared a double interaction with the hinge region (residues Glu228 and Ala230) that anchored the ligand to the ATP-binding site (Figure S1). With such valuable structural information available, we decided to explore the ATP-binding pocket in the rational search of new potential AKT1 inhibitors. Among the two previously mentioned structures, 4GV1 showed the most favorable resolution and was thus selected as a protein model for molecular docking experiments of the previously cited 247 in-house compounds. Each molecule was docked using Glide [30] in the extra precision (XP) mode and the generated poses were then rescored with the MM-GBSA method within Prime [28]. The two co-crystallized advanced inhibitors were added to the ligand set for comparison, and the obtained binding poses were evaluated mainly based on the predicted intermolecular interactions, paying particular attention to the contacts that involved the key residues Ala230 and Glu228. The best docking conformations of **ipatasertib** and **capivasertib** agreed well with their experimental poses and in both cases the key interactions with the hinge residues were correctly reproduced (Figure S2).

Subsequently, the docking-based approach allowed the selection of 12 virtual hits as the most promising in-house AKT1 small-molecule binders (Tables S1 and S2), which were then evaluated for the anti-AKT1 activity.

In the employed biochemical assay, a compound was considered as a ‘primary active’ only when the inhibition of the AKT1 phosphorylation activity (hereinafter called %inh) was reduced by at least of 60%, employing a 10  $\mu\text{M}$  compound concentration. Among the tested virtual hits, five compounds were thus selected as primary actives and evaluated in

a dose–response assay to calculate the 50% inhibitory concentration ( $IC_{50}$ ) value (Figure 2 and Table S2).



**Figure 2.** Chemical structure and biological data for the experimentally validated in-house compounds as AKT1 inhibitors. ND = not determined.

The [1,2,4]triazolo[1,5-*a*]pyrimidine derivative **T101** [35] and the cyclohepta[*b*]thiophene-3-carboxamide **T159** [32] were previously reported as allosteric inhibitors of HIV-1 reverse transcriptase-associated ribonuclease H. Analogously, compounds **T124**, **T126**, and **T128**, showing a common [4,5]thieno[2,3-*d*]pyrimidin-4(3*H*)-one moiety, were described as HIV-1 reverse transcriptase-associated ribonuclease H inhibitors by Masaoka et al. [34], and re-synthesized by us to serve as internal reference compounds.

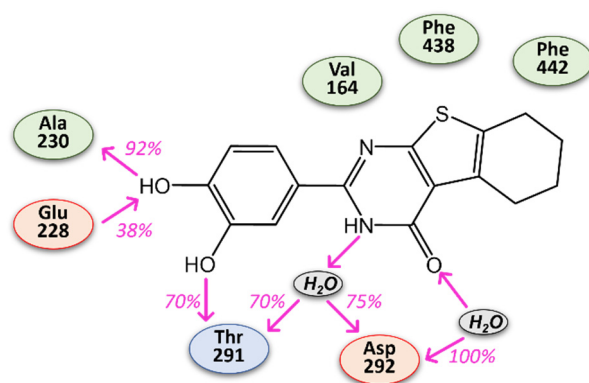
Among them, compounds **T101**, **T126**, and **T159** exhibited an AKT1 inhibitory potency higher than **T187**, displaying  $IC_{50}$  values of  $1.62 \pm 0.15 \mu\text{M}$ ,  $1.99 \pm 0.11 \mu\text{M}$ , and  $2.12 \pm 0.26 \mu\text{M}$ , respectively.

Notably, these three molecules turned out to be efficient inhibitors, as highlighted by the corresponding experimental values of LE. Particularly, **T159** and **T126** had an LE value  $\geq 0.3$  (Figure 2), which is the generally accepted lower limit of efficiency in a typical drug discovery program. It is worth noting that the 5,6,7,8-tetrahydrobenzo[4,5]thieno[2,3-*d*]pyrimidin-4(3*H*)-one derivative **T126** showed a LE value comparable to that of the clinical trial inhibitors **capivasertib** and **ipatasertib** (Figure S1). In addition, preliminary structure-activity relationships (SAR) analysis around this in-house compound can be deduced by examining the collected biological results (Table S2). First, the replacement of the amide nitrogen atom in the tricyclic core with an oxygen atom seemed to be detrimental for kinase inhibition, as highlighted by comparing **T126** (%inh = 87%,  $IC_{50}$  =  $1.99 \pm 0.11 \mu\text{M}$ ) and **T128** (%inh = 78%,  $IC_{50}$  =  $26.6 \pm 4.8 \mu\text{M}$ ) with **T125** (%inh = 9%) and **T127** (%inh = 43%), respectively. This observation underlined that, although the in silico approach was successful in identifying new AKT1 inhibitors, the different impact on the biological activity of the pyrimidin-4(3*H*)-one moiety (**T126** and **T128**) compared to that of the oxazin-4-one (**T125** and **T127**) was not predicted correctly because similar docking poses and ligand-target interactions were proposed for the two series of compounds (Figure S3).

Therefore, we carried out molecular dynamics (MD) simulations to elucidate the molecular basis of the SAR data by overcoming the limitations of ordinary molecular docking studies, where the protein is typically treated as a rigid entity and no water molecules are included in the target preparation. The docking-generated AKT1–**T126** and AKT1–**T125** complexes were thus used as starting structures for three 200 ns MD-simulation replicas us-

ing Desmond software [31], and the analysis of the produced trajectories provided valuable clues to explain the SAR observation.

Specifically, the **T126** orientation generated from the docking study was well preserved during the entire execution time, with the overall ligand stability having been reached in the last 100 ns of the MD simulations (Figure S4). Interestingly, the nitrogen of the endocyclic amide established well-conserved, water-mediated interactions with the residues Thr291 and Asp292 (Table S3 and Figure 3).



**Figure 3.** A schematic overview of the MD-derived intermolecular interactions established by **T126** within the AKT1 ATP-binding pocket. The key contacts are represented with their occurrence calculated as the average value of the three replicas in the time window 100–200 ns. The protein residues are color-coded as follows: red, charged (negative); green, hydrophobic; cyan, polar.

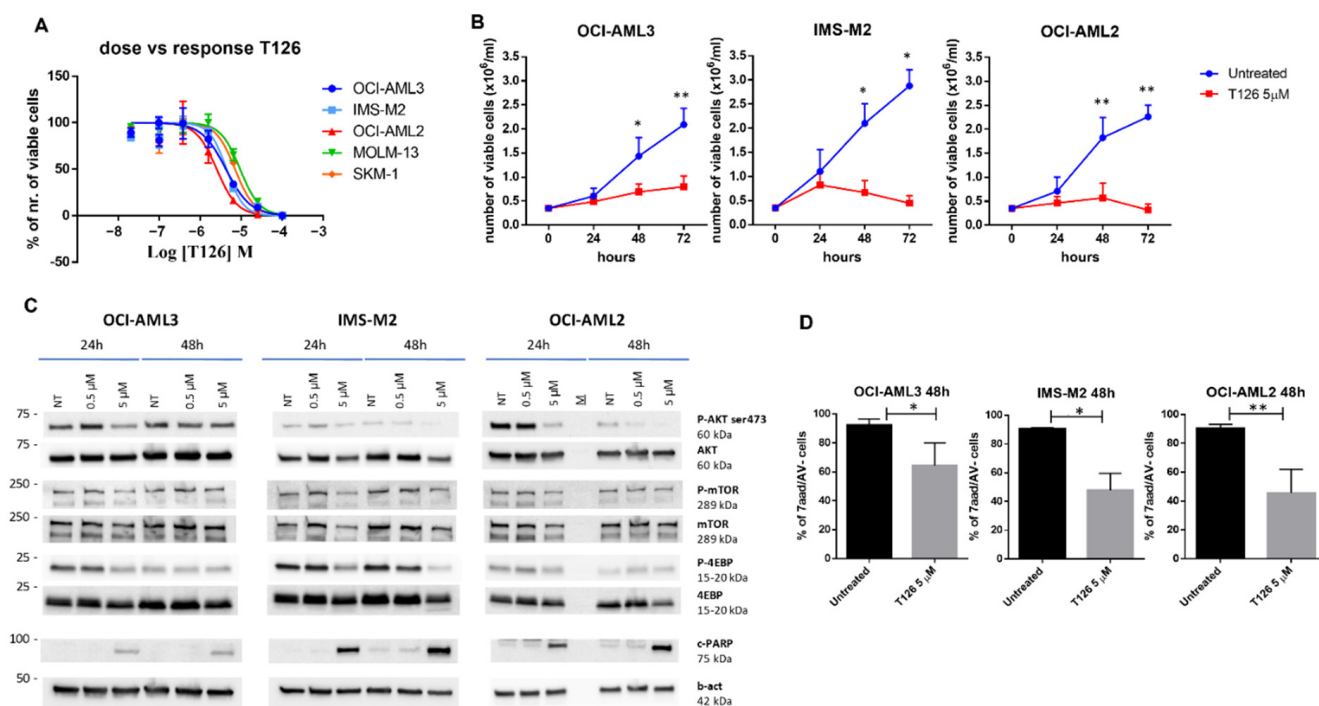
Conversely, the three generated replicas for the inactive analog **T125** (Figure S4) did not detect common stable ligand-protein contacts, with the oxygen atom of the oxazin-4-one moiety never having been involved in significantly conserved intermolecular interactions (Table S3).

As a second SAR insight, the size of the aliphatic ring of the tricyclic core appeared to be crucial to gain high inhibitory potency against AKT1. Indeed, the 6-membered ring of **T126** turned out to be the best substitution with respect to the 5-membered (**T128**) and 7-membered (**T124**, %inh = 60%,  $IC_{50}$  = 30.9  $\mu$ M) systems.

In addition, it is well known that the level of interest in kinase targets has created a crowded chemical space landscape, rendering the discovery of novel chemical entities as kinase inhibitors challenging. Against this backdrop, compounds **T126**, **T159**, and **T101** were used as inputs for a structure search in SciFinder. To the best of our knowledge prior to December 2021, none of the three explored compounds had been reported in the literature, including publications and patents, as inhibitor of AKT1 or other kinases, as well as no information on the effect of these compounds on AML has emerged from our bibliographic survey.

### 3.2. Evaluation of the Identified AKT1 Inhibitors on AML Cell Lines

Encouraged by the variety of information gathered so far, we evaluated these compounds in cellular assays of AML models. Specifically, a cell viability assay was initially performed to determine the cellular  $IC_{50}$  of **T101**, **T126**, and **T159** on different human AML cell lines, namely, OCI-AML3, IMS-M2, OCI-AML2, MOLM-13, and SKM-1, which carry some of the most recurrent AML mutations [37,38]. We measured the ability of living cells to convert a redox dye (resazurin) into a fluorescent end-product (resorufin). A dose response curve was generated for each cell line using GraphPad Prism and the  $IC_{50}$  was established. While no interesting ( $IC_{50}$  higher than 30  $\mu$ M) inhibitory activity was detected for **T101** and **T159** in all the explored cell lines, we obtained promising results for **T126** (Figure 4).



**Figure 4.** T126 induces growth arrest and apoptosis in AML cells. (A) T126 dose-response curves as generated by CellTiter Blue assay for the human AML cell lines OCI-AML3, IMS-M2, OCI-AML2, MOLM-13, and SKM-1. (B) T126 induced a significant cell growth inhibition on OCI-AML3, IMS-M2, and OCI-AML2, at 48 and 72 h from the start of the treatment at a 5 μM dose (student paired *t*-test, 48 h  $p = 0.02$  and 72 h  $p = 0.006$ , 48 h  $p = 0.04$  and 72 h  $p = 0.01$ , and 48 h  $p = 0.006$  and 72 h  $p = 0.004$ , respectively). (C) The effects of T126 at a 0.5 and 5 μM dose on phosphorylation of AKT1 and downstream signaling molecules, namely mTOR and 4E-BP1, at 24 and 48 h, in OCI-AML3, IMS-M2, and OCI-AML2 cells. Activation of the apoptotic signaling molecule cleaved-PARP (c-PARP) under the same experimental conditions. β-actin (b-act) expression levels were used as a control for protein loading. The representative results of at least three independent experiments are shown. All the original blots are reported in Figure S8. (D) T126 at a 5 μM dose induced a significant level of apoptosis (% of Annexin V negative/7aad negative cells) in OCI-AML3, IMS-M2, and OCI-AML2 cells at 48 h (Student paired *t*-test, where \* and \*\* stand for  $p = 0.01$  and  $p = 0.005$ , respectively).

Indeed, T126 IC<sub>50</sub> values were 4.2, 4.3, 2.4, 9.2, and 6.9 μM for OCI-AML3, IMS-M2, OCI-AML2, MOLM-13, and SKM-1 cell lines, respectively (Figure 4A).

It is noteworthy that the low-micromolar inhibitory activities observed in the cell-based assays were similar to those obtained for the reference compound NSC348884 [39] used as positive control (Figure S5), and were in keeping with the low-micromolar IC<sub>50</sub> of T126 on the isolated AKT1 protein (i.e., 1.99 μM).

We then investigated the effect of T126 on OCI-AML3, IMS-M2, and OCI-AML2 cell growth (0–72 h), using a concentration of 5 μM, and found that T126 was able to induce a significant growth inhibition at 48 and 72 h in all the three of the AML cell lines (Figure 4B).

To determine the effect of T126 on the AKT1 intracellular mediated signaling pathway and cell death, we exposed our cell lines to an increasing concentration of T126 and checked whether this small molecule acted upon their functional proteomic profiles. The effect of T126 on the AKT signaling pathway was assessed by western blot analysis, focusing on the key targets. Upon increasing concentrations of T126, we observed at various levels in the different AML cell lines a decreased phosphorylation of AKT1 (phospho-AKT, at site S473) as an expression of the AKT1 activity inhibition [17], and of the downstream signaling molecule mTOR (phospho-mTOR, at site S2448). As a representative target of mTOR activity,

we also analyzed the E4-BP1 protein and we noticed a reduction of its phosphorylation levels at site S65 (Figure 4C). As a marker of cell apoptosis, the apoptosis-related protein cleaved-PARP was detected upon treatment with **T126** 5  $\mu$ M at 48 h (Figure 4C). The effect of **T126** on cell apoptosis was also measured by flow cytometry using Annexin V/7AAD probes for the identification of apoptotic cells. Notably, in accordance with western blot analysis, at the concentration of 5  $\mu$ M, **T126** induced a significant level of apoptosis at 48 h in OCI-AML3, IMS-M2, and OCI-AML2 (Figure 4D), confirming in this setting, its anti-leukemic effect.

Finally, we performed a colony forming unit assay (CFU) using normal donor CD34+ hematopoietic stem/progenitor cells (HSPC) which were exposed to escalating doses of **T126** (1, 2.5 and 5  $\mu$ M) and plated in a Methocult medium for 14 days. Remarkably, at 1 and 2.5  $\mu$ M, compound **T126** did not inhibit the colony forming ability of human CD34+ HSPC, suggesting that there was no toxicity at these lower doses. Importantly, whilst a slight inhibition emerged at the maximum dose of 5  $\mu$ M, the clonogenic efficiency was not blocked, but only decreased by about 20% as compared to the untreated control (Figure S6A). The obtained results were quite encouraging considering that the inhibition of p-AKT was already observed at an early time point (4 h) at the concentrations of 1 and 2.5  $\mu$ M in the OCI-AML3 cell line (Figure S6B), suggesting that the compound could also be used at lower doses in additional biological experiments. These results confirm the pivotal role of the AKT pathway in the maintenance of cell growth and survival of AML cells, as previously reported [4,5]. Moreover, AKT pathway activation has also been implicated as a mechanism of resistance to therapy, including novel agents [18,49], pointing to AKT1 as an attractive target for AML, more specifically by using AKT1 inhibitors in combination with other drugs. Considering this, it is worth noting that the three AKT isoforms are highly conserved and share about 80% of the amino acid sequence identity [50]. As a consequence, the majority of currently developed AKT inhibitors are pan-AKT inhibitors, and this concept is evident when considering the two AKT inhibitors mentioned earlier and undergoing clinical trials (i.e., **capivasertib**  $IC_{50}$ -AKT1 = 3 nM,  $IC_{50}$ -AKT2 = 8 nM,  $IC_{50}$ -AKT3 = 8 nM, **ipatasertib**  $IC_{50}$ -AKT1 = 5 nM,  $IC_{50}$ -AKT2 = 18 nM, and  $IC_{50}$ -AKT3 = 8 nM) [51]. Based on this, we are aware that **T126** may potentially also inhibit AKT2 and AKT3. However, in the AML cell lines used in this study, AKT1 is the most expressed isoform among the AKT family members. Indeed, the analyses of RNA seq data from these cell lines (<https://cellmodelpassports.sanger.ac.uk/passports>, accessed on 14 October 2022) clearly indicate that AKT1 shows a higher degree of expression compared to the other isoforms. In the light of this information and considering that the work herein reported falls within the early-stage drug discovery process, we have focused our efforts exclusively on AKT1 to identify a hit compound. Nevertheless, during the next planned hit-to-lead steps, biological characterization studies involving the other AKT family members will be also carried out.

### 3.3. Validation of T126 as a True Hit

To further validate **T126** as a promising hit, focused studies were conducted to rule out the possibility that the inhibitory potency detected in the AKT1 assays could be related to an artifact. Indeed, this small molecule possessed a catechol moiety that seemed to be important for AKT1 binding by establishing polar interactions (Figure 3). Although the presence of the catechol by itself did not guarantee a satisfactory potency against AKT1 as the moderately active (**T124** and **T128**) and inactive (**T125**, **T127**, and **T129**) derivatives shared this feature as well, it is well-known that the mentioned chemical group has been counted as one of the Pan-Assay Interference Compounds (PAINS) motifs [52,53].

Various mechanisms of assay interference or promiscuous behaviors have been reported as responsible for PAINS activity, including compound fluorescence effect, metal chelation, and chemical aggregation [52–54].

In the AKT1 inhibition assay, the enzymatic activity was evaluated by measuring the phosphorylation of a fluorescently-labelled peptide induced by the kinase. Indeed, the detection of the substrate peptide and the product phosphorylated peptide after a microflu-

idic mobility shift was performed by measuring the fluorescence given to the substrate and the product of the kinase reaction. Based on the methodology employed for quantifying the AKT1 activity, it was not expected that the intrinsic fluorescence of the compounds could interfere with the assay. Nevertheless, we determined the intrinsic fluorescence of **T126**, which emerged as not fluorescent at the excitation/emission wavelength (485–535 nm) used in the assay.

Second, since the AKT1 inhibition assay required MgCl<sub>2</sub>, the Mg-complexation ability has been investigated for the **T126** derivative to rule out any interference. Specifically, UV-vis spectra were recorded for the compound alone and in the presence of increasing concentrations of MgCl<sub>2</sub>. The results showed no shift in the maximum of absorbance (hypsochromic effect), nor any presence of an isosbestic point (Figure S7) up to 10 mM concentration of MgCl<sub>2</sub> (as used in the biochemical assay), thus suggesting the inability of **T126** to chelate Mg<sup>2+</sup> ions.

Finally, to discard the hypothesis of chemical aggregation, the presence of aggregates was evaluated in the same buffer employed in the AKT1 activity assay by a NEPHELOstar Plus (BMG LABTECH). Compound **T126** did not aggregate at concentrations up to 100 μM, thus rejecting that the AKT1 inhibition effect may be due to aggregation.

In conclusion, the 5,6,7,8-tetrahydrobenzo[4,5]thieno[2,3-*d*]pyrimidin-4(3*H*)-one derivative **T126** showed a clear anti-AKT1 effect and the growth inhibition and induction of apoptosis in AML cells at low micromolar concentrations, making it an appealing candidate for further testing in other biological assays. Furthermore, the low molecular weight (MW = 314,37) and promising LE value of **T126** render this small molecule an attractive starting point for future medicinal chemistry efforts directed at hit-to-lead optimization.

**Supplementary Materials:** The following supporting information can be downloaded at: <https://www.mdpi.com/article/10.3390/pharmaceutics14112295/s1>. Figure S1: 2D representation of the protein-ligand interactions of **capivasertib** (A) and **ipatasertib** (B) with AKT1, Figure S2: Superimposition of the experimental and docking poses for **capivasertib** and **ipatasertib**, Figure S3: Superimposition of the pyrimidin-4(3*H*)-one derivative **T126** and the oxazin-4-one derivative **T125** binding modes, Figure S4: Ligand RMSD computed for the three MD replicas on the **T126**-AKT1 and **T125**-AKT1 complexes, Figure S5: Dose-response curves for the reference compound **NSC348884**, Figure S6: (A) CFU assay on normal donor CD34+ hematopoietic stem/progenitor cells (HSPC). (B) Effects of **T126** at 0.5, 1.5 and 2.5 μM dose on phosphorylation of AKT at 4 hours (4 h) in OCI-AML3, Figure S7: UV-vis spectra of compound **T126** measured alone and in presence of increasing concentrations of MgCl<sub>2</sub>, Figure S8: Uncropped full-length pictures of western blotting membranes, Table S1: Summary of the docking results, Table S2: Chemical structure and biological activity for the selected in-house virtual hits against AKT1, Table S3: Protein-ligand interaction occurrences observed in the three MD replicas for **T125**-AKT1 and **T126**-AKT1 complexes, Table S4: Composition of Enriched Methocult medium.

**Author Contributions:** Conceptualization, A.A. and M.L.B.; methodology, investigation, and validation: (i) computational studies, A.A., D.P. and M.L.B. (ii) chemistry, solubility screen, and UV-VIS titration assays, M.C.P., O.T. and S.M. (iii) enzymatic and intrinsic fluorescence assays, J.B. and M.I.L. (iv) cell-based assays, F.M., M.M. and M.P.M.; writing—original draft preparation, A.A., F.M., D.P., S.M. and M.L.B.; writing—review and editing, all authors; supervision, M.L.B. All authors have read and agreed to the published version of the manuscript.

**Funding:** Part of this research was funded by the ERC Cons Grant 2016, grant number 725725 (to M.P.M.).

**Institutional Review Board Statement:** Not applicable.

**Informed Consent Statement:** Not applicable.

**Data Availability Statement:** Data are contained within the article or Supplementary Materials.

**Acknowledgments:** Fondazione Umberto Veronesi—Post-doctoral Fellowships 2021 (to A.A.) and 2022 (to M.C.P.).

**Conflicts of Interest:** The authors declare no conflict of interest. M.P.M. declares an honoraria from Rasna Therapeutics, Inc. for scientific advisor activities. M.P.M. also declares an honoraria/consultancy at the scientific advisory board for Abbvie, Amgen, Celgene, Janssen, Novartis, Pfizer, Jazz Pharmaceuticals. M.L.B. is a co-founder and shareholder of the innovative start up Sibylla Biotech SRL (<https://www.sibyllabiotech.it>).

### Abbreviations

AML, acute myeloid leukemia; ATP, adenosine triphosphate; 4E-BP1, eukaryotic translation initiation factor 4E (eIF4E)-binding protein 1; FLT3, fms-like tyrosine kinase 3; LE, ligand efficiency; mTOR, mammalian target of rapamycin; p70S6K, p70 ribosomal S6 kinase; PARP, poly (ADP-ribose) polymerase; CFU, colony forming unit; HSPC, hematopoietic stem/progenitor cells; PAINS, Pan-Assay Interference Compounds; KRAS, Kirsten rat sarcoma viral oncogene; NRAS, neuroblastoma ras viral oncogene homolog; SAR, structure-activity relationship; XPO1, exportin 1.

### References

- Scheid, M.P.; Woodgett, J.R. PKB/AKT: Functional insights from genetic models. *Nat. Rev. Mol. Cell Biol.* **2001**, *2*, 760–768. [CrossRef] [PubMed]
- Vanhaesebroeck, B.; Stephens, L.; Hawkins, P. PI3K signalling: The path to discovery and understanding. *Nat. Rev. Mol. Cell Biol.* **2012**, *13*, 195–203. [CrossRef] [PubMed]
- Altomare, D.A.; Testa, J.R. Perturbations of the AKT signaling pathway in human cancer. *Oncogene* **2005**, *24*, 7455–7464. [CrossRef] [PubMed]
- Nepstad, I.; Hatfield, K.J.; Gronningsaeter, I.S.; Reikvam, H. The PI3K-Akt-mTOR Signaling Pathway in Human Acute Myeloid Leukemia (AML) Cells. *Int. J. Mol. Sci.* **2020**, *21*, 2907. [CrossRef] [PubMed]
- Sabnis, H.; Bradley, H.L.; Bunting, S.T.; Cooper, T.M.; Bunting, K.D. Capillary nano-immunoassay for Akt 1/2/3 and 4EBP1 phosphorylation in acute myeloid leukemia. *J. Transl. Med.* **2014**, *12*, 166. [CrossRef] [PubMed]
- The Cancer Genome Atlas Research Network. Genomic and epigenomic landscapes of adult de novo acute myeloid leukemia. *N. Eng. J. Med.* **2013**, *368*, 2059–2074. [CrossRef]
- Tamburini, J.; Elie, C.; Bardet, V.; Chapuis, N.; Park, S.; Broet, P.; Cornillet-Lefebvre, P.; Lioure, B.; Ugo, V.; Blanchet, O.; et al. Constitutive phosphoinositide 3-kinase/Akt activation represents a favorable prognostic factor in de novo acute myelogenous leukemia patients. *Blood* **2007**, *110*, 1025–1028. [CrossRef]
- Recher, C.; Dos Santos, C.; Demur, C.; Payrastra, B. mTOR, a new therapeutic target in acute myeloid leukemia. *Cell Cycle* **2005**, *4*, 1540–1549. [CrossRef]
- Chow, S.; Minden, M.D.; Hedley, D.W. Constitutive phosphorylation of the S6 ribosomal protein via mTOR and ERK signaling in the peripheral blasts of acute leukemia patients. *Exp. Hematol.* **2006**, *34*, 1183–1191. [CrossRef]
- Fransecky, L.; Mochmann, L.H.; Baldus, C.D. Outlook on PI3K/AKT/mTOR inhibition in acute leukemia. *Mol. Cell* **2015**, *3*, 2. [CrossRef]
- Gallay, N.; Dos Santos, C.; Cuzin, L.; Bousquet, M.; Simmonet Gouy, V.; Chaussade, C.; Attal, M.; Payrastra, B.; Demur, C.; Recher, C. The level of AKT phosphorylation on threonine 308 but not on serine 473 is associated with high-risk cytogenetics and predicts poor overall survival in acute myeloid leukaemia. *Leukemia* **2009**, *23*, 1029–1038. [CrossRef]
- Tazzari, P.L.; Cappellini, A.; Grafone, T.; Mantovani, I.; Ricci, F.; Billi, A.M.; Ottaviani, E.; Conte, R.; Martinelli, G.; Martelli, A.M. Detection of serine 473 phosphorylated Akt in acute myeloid leukaemia blasts by flow cytometry. *Br. J. Haematol.* **2004**, *126*, 675–681. [CrossRef] [PubMed]
- Min, Y.H.; Eom, J.I.; Cheong, J.W.; Maeng, H.O.; Kim, J.Y.; Jeung, H.K.; Lee, S.T.; Lee, M.H.; Hahn, J.S.; Ko, Y.W. Constitutive phosphorylation of Akt/PKB protein in acute myeloid leukemia: Its significance as a prognostic variable. *Leukemia* **2003**, *17*, 995–997. [CrossRef] [PubMed]
- Kornblau, S.M.; Womble, M.; Qiu, Y.H.; Jackson, C.E.; Chen, W.; Konopleva, M.; Estey, E.H.; Andreeff, M. Simultaneous activation of multiple signal transduction pathways confers poor prognosis in acute myelogenous leukemia. *Blood* **2006**, *108*, 2358–2365. [CrossRef] [PubMed]
- Bhutani, J.; Sheikh, A.; Niazi, A.K. Akt inhibitors: Mechanism of action and implications for anticancer therapeutics. *Infect. Agent. Cancer* **2013**, *8*, 49. [CrossRef] [PubMed]
- Huang, W.C.; Hung, M.C. Induction of Akt activity by chemotherapy confers acquired resistance. *J. Med. Assoc.* **2009**, *108*, 180–194. [CrossRef]
- Martelli, A.M.; Evangelisti, C.; Chappell, W.; Abrams, S.L.; Basecke, J.; Stivala, F.; Donia, M.; Fagone, P.; Nicoletti, F.; Libra, M.; et al. Targeting the translational apparatus to improve leukemia therapy: Roles of the PI3K/PTEN/Akt/mTOR pathway. *Leukemia* **2011**, *25*, 1064–1079. [CrossRef]



18. Lin, K.H.; Rutter, J.C.; Xie, A.; Killarney, S.T.; Vaganay, C.; Benaksas, C.; Ling, F.; Sodaro, G.; Meslin, P.A.; Bassil, C.F.; et al. P2RY2-AKT activation is a therapeutically actionable consequence of XPO1 inhibition in acute myeloid leukemia. *Nat. Cancer* **2022**, *3*, 837–851. [CrossRef]
19. Coleman, N.; Moyers, J.T.; Harbery, A.; Vivanco, I.; Yap, T.A. Clinical Development of AKT Inhibitors and Associated Predictive Biomarkers to Guide Patient Treatment in Cancer Medicine. *Pharmgenomics. Pers. Med.* **2021**, *14*, 1517–1535. [CrossRef]
20. Lazaro, G.; Kostaras, E.; Vivanco, I. Inhibitors in AKTion: ATP-competitive vs allosteric. *Biochem. Soc. Trans.* **2020**, *48*, 933–943. [CrossRef]
21. *Schrödinger Release 2019-2: LigPrep*; Schrödinger, LLC: New York, NY, USA, 2019.
22. Rarey, M.; Dixon, J.S. Feature trees: A new molecular similarity measure based on tree matching. *J. Comput. Aided Mol. Des.* **1998**, *12*, 471–490. [CrossRef] [PubMed]
23. Berman, H.M.; Battistuz, T.; Bhat, T.N.; Bluhm, W.F.; Bourne, P.E.; Burkhardt, K.; Feng, Z.; Gilliland, G.L.; Iype, L.; Jain, S.; et al. The Protein Data Bank. *Acta Cryst. D Biol. Cryst.* **2002**, *58*, 899–907. [CrossRef] [PubMed]
24. Addie, M.; Ballard, P.; Buttar, D.; Crafter, C.; Currie, G.; Davies, B.R.; Debreczeni, J.; Dry, H.; Dudley, P.; Greenwood, R.; et al. Discovery of 4-amino-N-[(1S)-1-(4-chlorophenyl)-3-hydroxypropyl]-1-(7H-pyrrolo[2,3-d]pyrimidin-4-yl)piperidine-4-carboxamide (AZD5363), an orally bioavailable, potent inhibitor of Akt kinases. *J. Med. Chem.* **2013**, *56*, 2059–2073. [CrossRef] [PubMed]
25. Lin, K.; Lin, J.; Wu, W.I.; Ballard, J.; Lee, B.B.; Gloor, S.L.; Vigers, G.P.; Morales, T.H.; Friedman, L.S.; Skelton, N.; et al. An ATP-site on-off switch that restricts phosphatase accessibility of Akt. *Sci. Signal* **2012**, *5*, ra37. [CrossRef] [PubMed]
26. Sastry, G.M.; Adzhigirey, M.; Day, T.; Annabhimoju, R.; Sherman, W. Protein and ligand preparation: Parameters, protocols, and influence on virtual screening enrichments. *J. Comput. Aided Mol. Des.* **2013**, *27*, 221–234. [CrossRef]
27. Greenwood, J.R.; Calkins, D.; Sullivan, A.P.; Shelley, J.C. Towards the comprehensive, rapid, and accurate prediction of the favorable tautomeric states of drug-like molecules in aqueous solution. *J. Comput. Aided Mol. Des.* **2010**, *24*, 591–604. [CrossRef]
28. Jacobson, M.P.; Pincus, D.L.; Rapp, C.S.; Day, T.J.F.; Honig, B.; Shaw, D.E.; Friesner, R.A. A Hierarchical Approach to All-Atom Protein Loop Prediction. *Proteins Struct. Funct. Bioinform.* **2004**, *55*, 351–367. [CrossRef]
29. Halgren, T.A.; Murphy, R.B.; Friesner, R.A.; Beard, H.S.; Frye, L.L.; Pollard, W.T.; Banks, J.L. Glide: A New Approach for Rapid, Accurate Docking and Scoring. 2. Enrichment Factors in Database Screening. *J. Med. Chem.* **2004**, *47*, 1750–1759. [CrossRef]
30. Friesner, R.A.; Murphy, R.B.; Repasky, M.P.; Frye, L.L.; Greenwood, J.R.; Halgren, T.A.; Sanschagrin, P.C.; Mainz, D.T. Extra precision glide: Docking and scoring incorporating a model of hydrophobic enclosure for protein-ligand complexes. *J. Med. Chem.* **2006**, *49*, 6177–6196. [CrossRef]
31. Bowers, K.J.; Chow, E.; Xu, H.; Dror, R.O.; Eastwood, M.P.; Gregersen, B.A.; Klepeis, J.L.; Kolossvary, I.; Moraes, M.A.; Sacerdoti, F.D.; et al. Scalable Algorithms for Molecular Dynamics Simulations on Commodity Clusters. In Proceedings of the ACM/IEEE Conference on Supercomputing (SC06), Tampa, FL, USA, 11–17 November 2006.
32. Massari, S.; Corona, A.; Distinto, S.; Desantis, J.; Caredda, A.; Sabatini, S.; Manfroni, G.; Felicetti, T.; Cecchetti, V.; Pannecouque, C.; et al. From cycloheptathiophene-3-carboxamide to oxazinone-based derivatives as allosteric HIV-1 ribonuclease H inhibitors. *J. Enzym. Inhib. Med. Chem.* **2019**, *34*, 55–74. [CrossRef]
33. Desantis, J.; Nannetti, G.; Massari, S.; Barreca, M.L.; Manfroni, G.; Cecchetti, V.; Palu, G.; Goracci, L.; Loregian, A.; Tabarrini, O. Exploring the cycloheptathiophene-3-carboxamide scaffold to disrupt the interactions of the influenza polymerase subunits and obtain potent anti-influenza activity. *Eur. J. Med. Chem.* **2017**, *138*, 128–139. [CrossRef] [PubMed]
34. Masaoka, T.; Chung, S.; Caboni, P.; Rausch, J.W.; Wilson, J.A.; Taskent-Sezgin, H.; Beutler, J.A.; Tocco, G.; Le Grice, S.F. Exploiting drug-resistant enzymes as tools to identify thienopyrimidinone inhibitors of human immunodeficiency virus reverse transcriptase-associated ribonuclease H. *J. Med. Chem.* **2013**, *56*, 5436–5445. [CrossRef] [PubMed]
35. Desantis, J.; Massari, S.; Corona, A.; Astolfi, A.; Sabatini, S.; Manfroni, G.; Palazzotti, D.; Cecchetti, V.; Pannecouque, C.; Tramontano, E.; et al. 1,2,4-Triazolo[1,5-a]pyrimidines as a Novel Class of Inhibitors of the HIV-1 Reverse Transcriptase-Associated Ribonuclease H Activity. *Molecules* **2020**, *25*, 1183. [CrossRef] [PubMed]
36. Wang, Y.D.; Johnson, S.; Powell, D.; McGinnis, J.P.; Miranda, M.; Rabindran, S.K. Inhibition of tumor cell proliferation by thieno[2,3-d]pyrimidin-4(1H)-one-based analogs. *Bioorg. Med. Chem. Lett.* **2005**, *15*, 3763–3766. [CrossRef] [PubMed]
37. Quentmeier, H.; Martelli, M.P.; Dirks, W.G.; Bolli, N.; Liso, A.; Macleod, R.A.; Nicoletti, I.; Mannucci, R.; Pucciarini, A.; Bigerna, B.; et al. Cell line OCI/AML3 bears exon-12 NPM gene mutation-A and cytoplasmic expression of nucleophosmin. *Leukemia* **2005**, *19*, 1760–1767. [CrossRef] [PubMed]
38. Chi, H.T.; Vu, H.A.; Iwasaki, R.; Nagamura, F.; Tojo, A.; Watanabe, T.; Sato, Y. Detection of exon 12 type A mutation of NPM1 gene in IMS-M2 cell line. *Leuk Res.* **2010**, *34*, 261–262. [CrossRef]
39. Balusu, R.; Fiskus, W.; Rao, R.; Chong, D.G.; Nalluri, S.; Mudunuru, U.; Ma, H.; Chen, L.; Venkannagari, S.; Ha, K.; et al. Targeting levels or oligomerization of nucleophosmin 1 induces differentiation and loss of survival of human AML cells with mutant NPM1. *Blood* **2011**, *118*, 3096–3106. [CrossRef]
40. Sancineto, L.; Iraci, N.; Massari, S.; Attanasio, V.; Corazza, G.; Barreca, M.L.; Sabatini, S.; Manfroni, G.; Avanzi, N.R.; Cecchetti, V.; et al. Computer-aided design, synthesis and validation of 2-phenylquinazolinone fragments as CDK9 inhibitors with anti-HIV-1 Tat-mediated transcription activity. *ChemMedChem* **2013**, *8*, 1941–1953. [CrossRef]
41. Astolfi, A.; Kudolo, M.; Brea, J.; Manni, G.; Manfroni, G.; Palazzotti, D.; Sabatini, S.; Cecchetti, F.; Felicetti, T.; Cannalire, R.; et al. Discovery of potent p38alpha MAPK inhibitors through a funnel like workflow combining in silico screening and in vitro validation. *Eur. J. Med. Chem.* **2019**, *182*, 111624. [CrossRef]

42. Available online: <https://scifinder.cas.org> (accessed on 15 February 2022).
43. Sabatini, S.; Manfroni, G.; Barreca, M.L.; Bauer, S.M.; Gargaro, M.; Cannalire, R.; Astolfi, A.; Brea, J.; Vacca, C.; Pirro, M.; et al. The Pyrazolobenzothiazine Core as a New Chemotype of p38 Alpha Mitogen-Activated Protein Kinase Inhibitors. *Chem. Biol. Drug Des.* **2015**, *86*, 531–545. [CrossRef]
44. Astolfi, A.; Iraci, N.; Sabatini, S.; Barreca, M.L.; Cecchetti, V. p38alpha MAPK and Type I Inhibitors: Binding Site Analysis and Use of Target Ensembles in Virtual Screening. *Molecules* **2015**, *20*, 15842–15861. [CrossRef] [PubMed]
45. Astolfi, A.; Iraci, N.; Manfroni, G.; Barreca, M.L.; Cecchetti, V. A Comprehensive Structural Overview of p38alpha MAPK in Complex with Type I Inhibitors. *ChemMedChem* **2015**, *10*, 957–969. [CrossRef] [PubMed]
46. Martelli, M.P.; Rossi, R.; Venanzi, A.; Meggendorfer, M.; Perriello, V.M.; Martino, G.; Spinelli, O.; Ciurnelli, R.; Varasano, E.; Brunetti, L.; et al. Novel NPM1 exon 5 mutations and gene fusions leading to aberrant cytoplasmic nucleophosmin in AML. *Blood* **2021**, *138*, 2696–2701. [CrossRef] [PubMed]
47. Gionfriddo, I.; Brunetti, L.; Mezzasoma, F.; Milano, F.; Cardinali, V.; Ranieri, R.; Venanzi, A.; Pierangeli, S.; Vetro, C.; Spinozzi, G.; et al. Dactinomycin induces complete remission associated with nucleolar stress response in relapsed/refractory NPM1-mutated AML. *Leukemia* **2021**, *35*, 2552–2562. [CrossRef]
48. Falini, B.; Brunetti, L.; Sportoletti, P.; Martelli, M.P. NPM1-mutated acute myeloid leukemia: From bench to bedside. *Blood* **2020**, *136*, 1707–1721. [CrossRef]
49. Grandage, V.L.; Gale, R.E.; Linch, D.C.; Khwaja, A. PI3-kinase/Akt is constitutively active in primary acute myeloid leukaemia cells and regulates survival and chemoresistance via NF-kappaB, Mapkinase and p53 pathways. *Leukemia* **2005**, *19*, 586–594. [CrossRef]
50. Toker, A.; Marmiroli, S. Signaling specificity in the Akt pathway in biology and disease. *Adv. Biol. Regul.* **2014**, *55*, 28–38. [CrossRef]
51. Martorana, F.; Motta, G.; Pavone, G.; Motta, L.; Stella, S.; Vitale, S.R.; Manzella, L.; Vigneri, P. AKT Inhibitors: New Weapons in the Fight Against Breast Cancer? *Front. Pharm.* **2021**, *12*, 662232. [CrossRef]
52. Baell, J.B.; Holloway, G.A. New substructure filters for removal of pan assay interference compounds (PAINS) from screening libraries and for their exclusion in bioassays. *J. Med. Chem.* **2010**, *53*, 2719–2740. [CrossRef]
53. Baell, J.; Walters, M.A. Chemistry: Chemical con artists foil drug discovery. *Nature* **2014**, *513*, 481–483. [CrossRef]
54. Baell, J.B. Feeling Nature's PAINS: Natural Products, Natural Product Drugs, and Pan Assay Interference Compounds (PAINS). *J. Nat. Prod.* **2016**, *79*, 616–628. [CrossRef] [PubMed]

## Article

# A ROR1 Small Molecule Inhibitor (KAN0441571C) Induced Significant Apoptosis of Mantle Cell Lymphoma (MCL) Cells

Amineh Ghaderi <sup>1</sup>, Wen Zhong <sup>1,†</sup>, Mohammad Ali Okhovat <sup>1,†</sup>, Johanna Aschan <sup>1</sup>, Ann Svensson <sup>1</sup>, Birgitta Sander <sup>2</sup>, Johan Schultz <sup>3</sup>, Thomas Olin <sup>3</sup>, Anders Österborg <sup>1,4</sup>, Mohammad Hojjat-Farsangi <sup>1,\*</sup> and Håkan Mellstedt <sup>1</sup>

<sup>1</sup> Department of Oncology-Pathology, BioClinicum, Karolinska University Hospital Solna and Karolinska Institutet, 171 64 Stockholm, Sweden

<sup>2</sup> Department of Laboratory Medicine, Division of Pathology, Karolinska Institutet, 171 77 Stockholm, Sweden

<sup>3</sup> Kancera AB, Nanna Svartz Väg 4, 171 65 Solna, Sweden

<sup>4</sup> Department of Hematology, Karolinska University Hospital Solna, 171 77 Stockholm, Sweden

\* Correspondence: mohammad.hojjat-farsangi@ki.se; Tel.: +46-735-234-706

† These authors contributed equally to this work.

**Abstract:** The receptor tyrosine kinase orphan receptor 1 (ROR1) is absent in most normal adult tissues but overexpressed in various malignancies and is of importance for tumor cell survival, proliferation, and metastasis. In this study, we evaluated the apoptotic effects of a novel small molecule inhibitor of ROR1 (KAN0441571C) as well as venetoclax (BCL-2 inhibitor), bendamustine, idelalisib (PI3K $\delta$  inhibitor), everolimus (mTOR inhibitor), and ibrutinib (BTK inhibitor) alone or in combination in human MCL primary cells and cell lines. ROR1 expression was evaluated by flow cytometry and Western blot (WB). Cytotoxicity was analyzed by MTT and apoptosis by Annexin V/PI staining as well as signaling and apoptotic proteins (WB). ROR1 was expressed both in patient-derived MCL cells and human MCL cell lines. KAN0441571C alone induced significant time- and dose-dependent apoptosis of MCL cells. Apoptosis was accompanied by decreased expression of MCL-1 and BCL-2 and cleavage of PARP and caspase 3. ROR1 was dephosphorylated as well as ROR1-associated signaling pathway molecules, including the non-canonical WNT signaling pathway (PI3K $\delta$ /AKT/mTOR). The combination of KAN0441571C and ibrutinib, venetoclax, idelalisib, everolimus, or bendamustine had a synergistic apoptotic effect and significantly prevented phosphorylation of ROR1-associated signaling molecules as compared to KAN0441571C alone. Our results suggest that targeting ROR1 by a small molecule inhibitor, KAN0441571C, should be further evaluated particularly in combination with other targeting drugs as a new therapeutic approach for MCL.

**Keywords:** MCL; ROR1; small molecules; apoptosis; targeted therapy

**Citation:** Ghaderi, A.; Zhong, W.; Okhovat, M.A.; Aschan, J.; Svensson, A.; Sander, B.; Schultz, J.; Olin, T.; Österborg, A.; Hojjat-Farsangi, M.; et al. A ROR1 Small Molecule Inhibitor (KAN0441571C) Induced Significant Apoptosis of Mantle Cell Lymphoma (MCL) Cells. *Pharmaceutics* **2022**, *14*, 2238. <https://doi.org/10.3390/pharmaceutics14102238>

Academic Editor: Gabriele Grassi

Received: 22 August 2022

Accepted: 17 October 2022

Published: 20 October 2022

**Publisher's Note:** MDPI stays neutral with regard to jurisdictional claims in published maps and institutional affiliations.



**Copyright:** © 2022 by the authors. Licensee MDPI, Basel, Switzerland. This article is an open access article distributed under the terms and conditions of the Creative Commons Attribution (CC BY) license (<https://creativecommons.org/licenses/by/4.0/>).

## 1. Introduction

Receptor tyrosine kinases (RTKs) are therapeutic targets in cancer. The RTK ROR1 plays a crucial role in the development of different tissues and organs during embryogenesis [1]. ROR1 is essentially not expressed in normal adult postpartum tissues but overexpressed in several malignancies [2]. Mutations, translocations, deletions, and overexpression of RTKs have been identified. Overexpression of ROR1 in patients was first described in chronic lymphocytic leukemia (CLL) by applying gene expression profiling [3]. ROR1 has also been shown to be overexpressed in several other hematological malignancies, including mantle cell lymphoma (MCL), as well as in solid tumors [4–12]. Small molecules and monoclonal antibodies have been used to target dysregulated RTKs in malignancies in a therapeutic approach [13,14].

In neoplastic cells, ROR1 is of importance for survival, proliferation, migration, and metastasis [15]. ROR1 mediates chemotactic and proliferative signals induced by the binding of WNT5a to ROR1 [16], resulting in the activation of guanine exchange factors

and the phosphoinositol-3 kinase (PI3K)/JNK signaling pathway [17]. Activation of the canonical and non-canonical WNT signaling pathways correlated with activated ROR1 [18]. Moreover, high expression of ROR1 was associated with disease progression and short survival in several malignancies [15,19,20].

Hematological malignancies account for around 6.5% of cancers around the world [21]. Various lymphomas, including MCL, mostly spread to the bone marrow, and different RTKs, such as focal adhesion kinase (FAK), are involved in tumor–stromal cells interaction (in the tumor microenvironment) to enhance tumor cell survival and drug resistance [22]. MCL is a rare but aggressive B-cell lymphoma characterized by the chromosomal translocation (11; 14) (q13; q32) and constitutive overexpression of cyclin D1 [23,24] contributing to the uncontrolled growth of MCL cells [25]. Despite the introduction of novel drugs such as BTK inhibitors and new therapeutic principles, including CAR-T, drug resistance and relapses occur, and MCL remains incurable [26]. Thus, there is a need for novel therapeutic approaches with other mechanisms of action (MOAs) than those in clinical use. ROR1 is an important molecule for the malignant phenotype, e.g., tumor cell proliferation, survival, epithelial–mesenchymal transition (EMT), migration, and metastasis [15,26,27], and been suggested to be an interesting target molecule for precision cancer medicine (PCM).

In the present study, the expression of ROR1 in MCL cells was characterized and the apoptotic effects of a novel ROR1 inhibitor, KAN0441571C, were evaluated in *in vitro* and *ex vivo* preclinical models as well as in combination with therapeutics with other MOAs of clinical relevance (ibrutinib, idelalisib, bendamustine, everolimus, and venetoclax) that are currently used for the treatment of patients with MCL [28] or have shown promising results in clinical trials. The results indicate that a small molecule ROR1 inhibitor might be a promising new drug candidate that warrants further evaluation in preclinical models and clinical trials in difficult-to-treat MCL patients.

## 2. Materials and Methods

### 2.1. Patients

Patients were diagnosed and treated according to the Swedish MCL guidelines at the Department of Hematology, Karolinska University Hospital, Stockholm, Sweden. The study was authorized by the National Ethics Authority ([www.etikprovningmyndigheten.se](http://www.etikprovningmyndigheten.se) (accessed on 20 December 2016)). A written consent form was collected from patients before blood sampling. Eleven patients with MCL were included, consisting of two females and nine males with a median age of 70 years (range 62–84). Five had early-stage untreated MCL and six had active MCL, and all but two were treatment-naïve. The selection was based on the availability of stored blood MCL cells (liquid nitrogen).

### 2.2. Cell Lines

Five human MCL cell lines, Granta-519 (ACC 342), Mino (ACC 687), JeKo1 (ACC 553), JVM-2 (ACC 12), and Z-138 (CRL-3001), obtained from the American Type Culture Collection (ATCC), were used. All cell lines were tested for mycoplasma contamination. The cell lines were cultured in RPMI-1640 medium (Sigma, St. Louis, MO, USA) with 10% fetal bovine serum (FBS) (Gibco, Life Technologies, Karlsruhe, Germany), 100 µg/mL penicillin/streptomycin (Biochrom KG, Berlin, Germany), and 2% glutamine (Biochrom KG) in humidified air at 37 °C with 5% CO<sub>2</sub>.

### 2.3. ROR1 Small Molecule Tyrosine Kinase Inhibitor (KAN0441571C)

The development of the first small molecule ROR1 tyrosine kinase inhibitor (KAN0439834) was reported in 2018 [29]. The second generation of a ROR1 small molecule inhibitor, KAN0441571C, with a higher cytotoxic potency against tumor cells *in vitro*, as well as longer half-time (T<sub>1/2</sub>) in a mouse model (11 h) compared to KAN0439834 (2 h), was recently described [30,31] and was applied in the present study.

#### 2.4. Cell Surface Marker Analysis (Flowcytometry)

Analysis of surface ROR1 expression was performed using an anti-ROR1 monoclonal antibody (Miltenyi Biotec, Bergisch Gladbach, Germany) [27]. Cells were analyzed by a FACS Canto II flow cytometer (BD Biosciences, San Jose, CA, USA). The FlowJo software program (Tree Star Inc., Ashland, OR, USA) was applied for analysis of cells.

#### 2.5. Annexin V/PI Apoptosis Assay

Human MCL cell lines were plated in 24-well plates at a concentration of  $5 \times 10^4$  cells per well in RPMI-1640 medium containing 10% FBS and incubated with KAN0441571C or venetoclax (BCL-2 inhibitor), ibrutinib (BTK inhibitor), idelalisib (PI3k inhibitor), everolimus (mTOR inhibitor), and bendamustine (an alkylating agent) as single drugs or in combination with KAN0441571C. After 24 h of incubation, the cells were centrifuged and resuspended in 100  $\mu$ L of Annexin V binding buffer (BD Biosciences) containing 1  $\mu$ L fluorescein isothiocyanate (FITC)-conjugated Annexin V and 1  $\mu$ L propidium iodide (PI) (BD Biosciences) and incubated for 15 min at RT.

Frozen primary MCL cells were thawed at 37 °C for 1–2 min and resuspended in 10 mL of RPMI-1640 medium with 10% FBS. Cell viability was analyzed by EVE™ Automatic Cell Counter NanoEnTek (VWR, Atlanta, GA, USA) according to the manufacturer's description. Cells were cultured in RPMI-1640 medium supplemented with 10% FBS and 20% conditioned media (CM). CM was harvested from 70% confluent HS-5 cells (CRL-11882, ATCC) grown in RPMI-1640 medium with 10% FBS for 72 h. The supernatant was collected, filtered, and used fresh. Then,  $2 \times 10^5$  MCL cells were seeded in 96-well plates and incubated at 37 °C in 5% CO<sub>2</sub> for 24 h with and without drugs. Cells were stained with Annexin V/PI gated for CD45<sup>+</sup>/ROR1<sup>+</sup>/CD3<sup>-</sup> cells, as exemplified in Figure S1. Cells were analyzed with NovoCyte Advanteon flow cytometry (Agilent, Santa Clara, CA, USA), and data were collected with the NovoExpress® 1.4.1 software program (Agilent, Santa Clara, CA, USA).

#### 2.6. MTT Cytotoxicity (or % Inhibition of Cell Proliferation or Cell Growth) Assay

MCL cell lines ( $10^4$  cells/well) were incubated in quadruplicates in 200  $\mu$ L of RPMI-1640 containing 10% FBS in 96-well plates for 24–72 h at 37 °C with 5% CO<sub>2</sub>. Then, 20  $\mu$ L MTT solution (5 mg/mL) was added to each well and incubated for another 4 h at 37 °C. Stopping solution (solubilizing reagent) (10% sodium dodecyl sulphate (SDS) in 0.01M HCL) was added to a final volume of 100  $\mu$ L/well. After overnight incubation at 37 °C, the plates were read in a microplate reader at 570 nm.

#### 2.7. Drug Combination Analyses

Zero Interaction Potency (ZIP) is a reference model [32] for evaluating drug combinations by comparing the deviation in potency of the dose–response curves between the individual agents and the combinations. A ZIP delta score ( $\Delta$ ) for each pair of drugs was used to quantify the deviation by taking the average of all delta scores over their dose combinations. Summary synergy scores are defined as the average excess response of drug interactions, e.g., a score of 20 corresponds to 20% of response above the expectation, i.e., synergism. A score close to 0 gives low confidence for synergism or antagonism. A score less than –10 indicates that the relationship between two drugs is possibly antagonistic; from –10 to 10, the relationship between two drugs might be additive; and if the score is >10, the interaction between two drugs is likely to be synergistic [32].

#### 2.8. Western Blot (WB) Analysis

Western blot was carried out as previously described [26]. MCL cells were lysed on ice for 30 min in lysis buffer containing 1% Triton X-100, 150 mM NaCl, 5 mM EDTA, and 50 mM Tris-HCl with 1% protease inhibitor cocktail (Sigma-Aldrich, St. Louis, MO, USA) and phosphatase inhibitors (Roche Ltd., Basel, Switzerland) and centrifuged at 14,000 rpm. Protein concentration was measured by Pierce™ BCA Protein Assay Kit (Thermo Fisher

Scientific, Waltham, MA, USA). Then, 10–20 µg protein was loaded into each well for WB analysis. The following antibodies were used for the detection of total (t) and phosphorylated (p) proteins: ROR1 (R & D Systems, Minneapolis, MN, USA), own produced polyclonal rabbit anti-p-ROR1 (Tyr 641 and 646, Ser 652) [26], AKT and p-AKT (Ser 473), mammalian target of rapamycin (mTOR) and p-mTOR (Ser 2448), phosphoinositide 3-kinase (PI3K) p110δ, cleaved poly ADP ribose polymerase (PARP), myeloid cell leukemia-1 B-cell lymphoma (BCL)-2, cleaved caspase 3 (Cell Signaling Technology, Danvers, MA, USA), and p-PI3K p110δ (Tyr 585) (Santa Cruz Biotechnology, Santa Cruz, CA, USA). β-actin (Sigma-Aldrich, St. Louis, MO, USA) was used as a loading control. Densitometry measurements of proteins were calculated by Image J1.44p software (National Institute of Health, Bethesda, MD, USA).

### 2.9. Statistical Analysis

Statistical analysis was performed using GraphPad Prism software (GraphPad Software, Inc., La Jolla, CA, USA). EC<sub>50</sub> values were calculated from the dose–response curve by non-linear curve fitting (HillSlope). The Mann–Whitney U test was applied for comparison of non-Gaussian distributed data. *p*-values < 0.05 were considered significant. Asterisks represent *p*-values of \* 0.01 to 0.05, \*\* 0.001 to < 0.01, \*\*\* < 0.001, and \*\*\*\* < 0.0001.

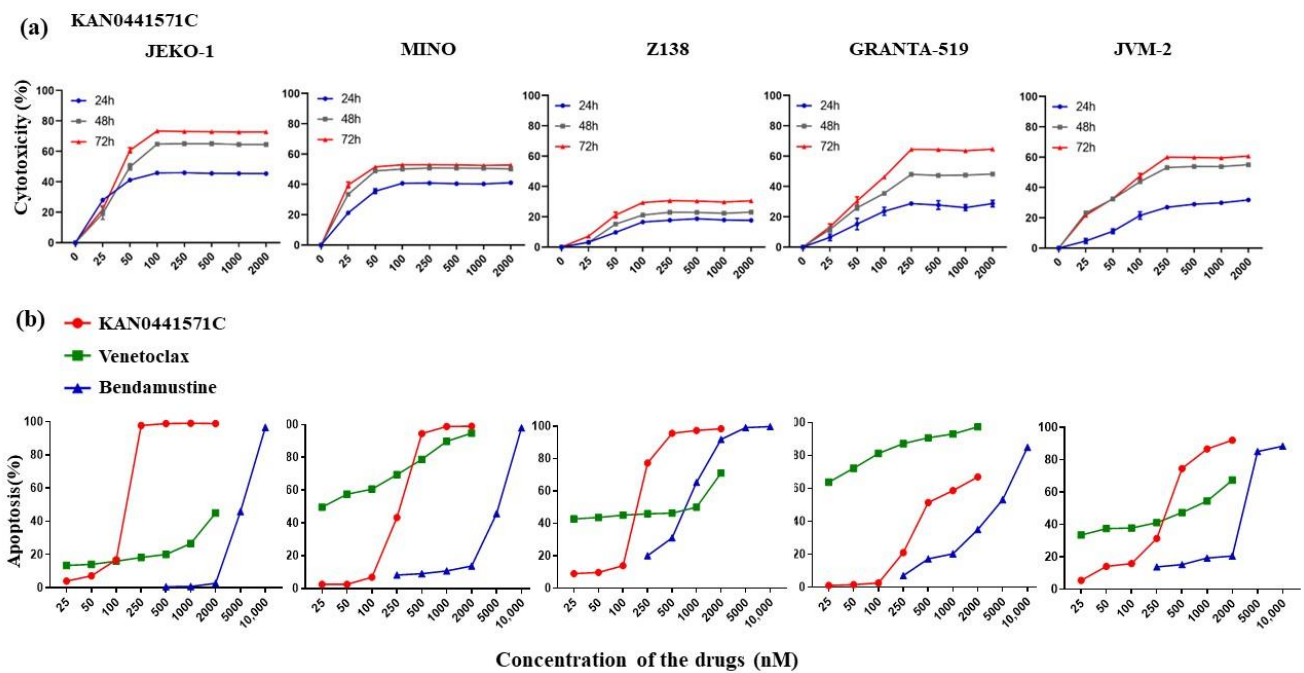
## 3. Results

### 3.1. Surface ROR1 Was Heterogeneously Expressed on MCL Cell Lines and Primary MCL Cells

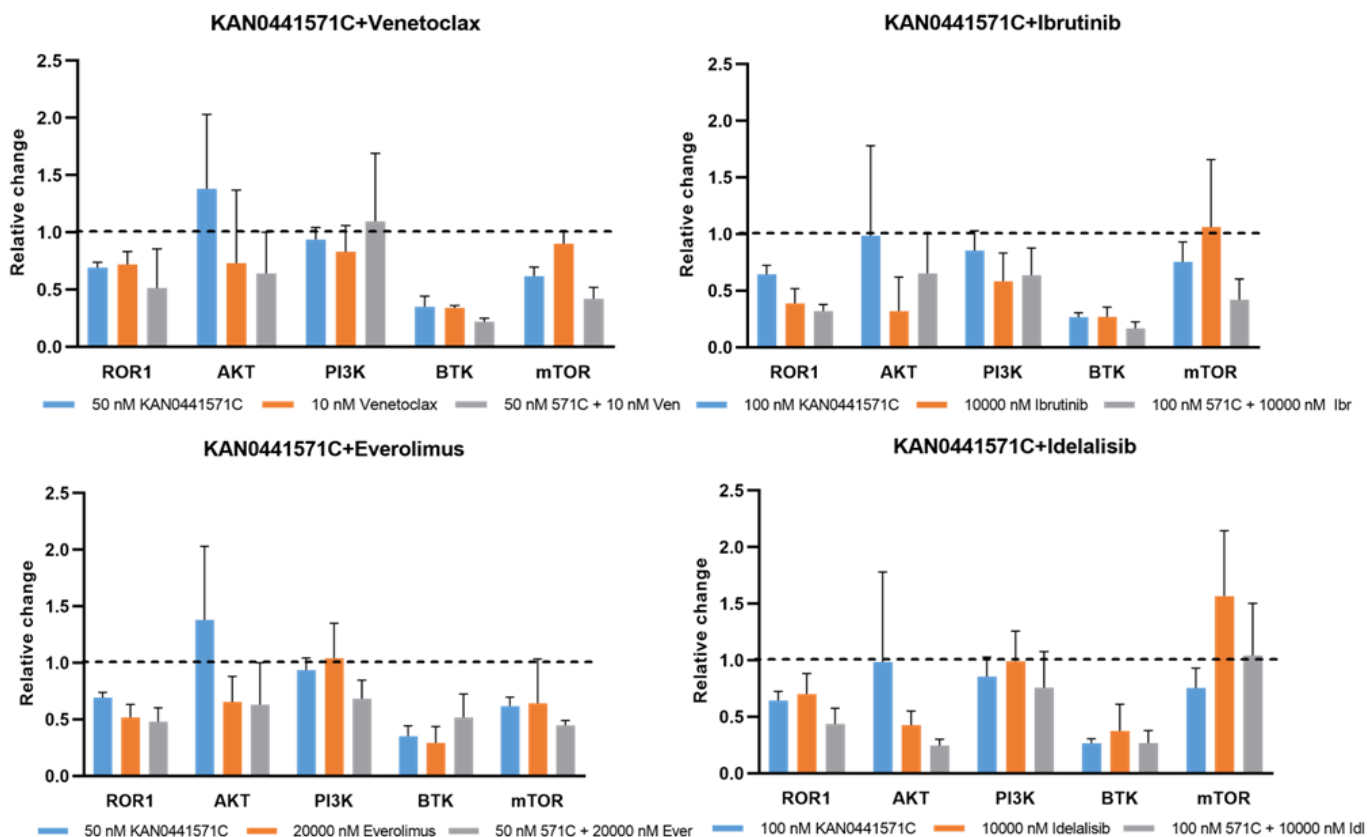
The frequency of surface ROR1-positive cells of JeKo-1, Mino, Z138, and Granta-519 cell lines was 100%, 99%, 71%, and 21%, respectively, while JVM-2 did not express surface ROR1 (Figure S2A). However, in WB, JVM-2 showed intense expression of ROR1 (Figure S2B). This indicates that JVM-2 expressed ROR1 as a splice variant lacking the extracellular part. Surface ROR1 was also analyzed in MCL cells from peripheral blood of leukemia patients (*n* = 11). MCL cells were identified as CD19<sup>+</sup>/CD5<sup>+</sup> cells. The frequency of blood CD19<sup>+</sup>/CD5<sup>+</sup> cells was 80 ± 4% (mean ± SEM), and 68 ± 10% of the blood MCL cells exhibited surface ROR1.

### 3.2. KAN0441571C Induced Significant Cell Death of MCL Cell Lines

KAN0441571C induced a time- and dose-dependent cell death (MTT) of all MCL lines but to varying degrees. Seventy-two hours of incubation were required to achieve the optimal cytotoxic effect. JeKo1 seemed to be the most sensitive cell line and Z138 the least sensitive (Figure 1A). Next, apoptosis analysis (Annexin V/PI staining) was performed after incubation with KAN0441571C, venetoclax, or bendamustine (Figures 1B and S6D). JeKo1 was again the most sensitive cell line to ROR1 inhibition, reaching almost 100% killing at 250 nM, while venetoclax and bendamustine were less effective. A similar pattern was seen for Mino, Z138, and JVM-2, while Granta-519 was the most sensitive to venetoclax. The data support the notion that ROR1 inhibition by a small molecule inhibitor seems to effectively induce death of MCL cells. We analyzed protein phosphorylation and found, as expected, that KAN0441571C prevented phosphorylation of ROR1 in a dose-dependent manner in all MCL cell lines (Figure S2B). Previous studies of ROR1 inhibitors in tumor cells from other hematological malignancies have indicated the involvement of both WNT non-canonical (PI3K/AKT/mTOR) and WNT canonical (beta-catenin) signaling pathways, as well as downregulation of the intrinsic apoptotic pathway, including cleavage of caspase 3 [12,27,28]. When primary MCL cells were analyzed, we also found that in addition to the prevention of ROR1 phosphorylation, PI3K, AKT, and mTOR were also subsequently dephosphorylated (Figure 2).



**Figure 1.** Effects of KAN0441571C, venetoclax, and bendamustine on MCL cell lines. (a) Cytotoxicity (MTT) of 5 ROR1<sup>+</sup> MCL cell lines incubated with the ROR1 inhibitor KAN0441571C for various time periods. (b) Apoptosis (Annexin V/PI) of MCL cell lines incubated with KAN0441571C, venetoclax, or bendamustine alone for 48 h. Data are shown as mean  $\pm$  SEM of triplicate samples.

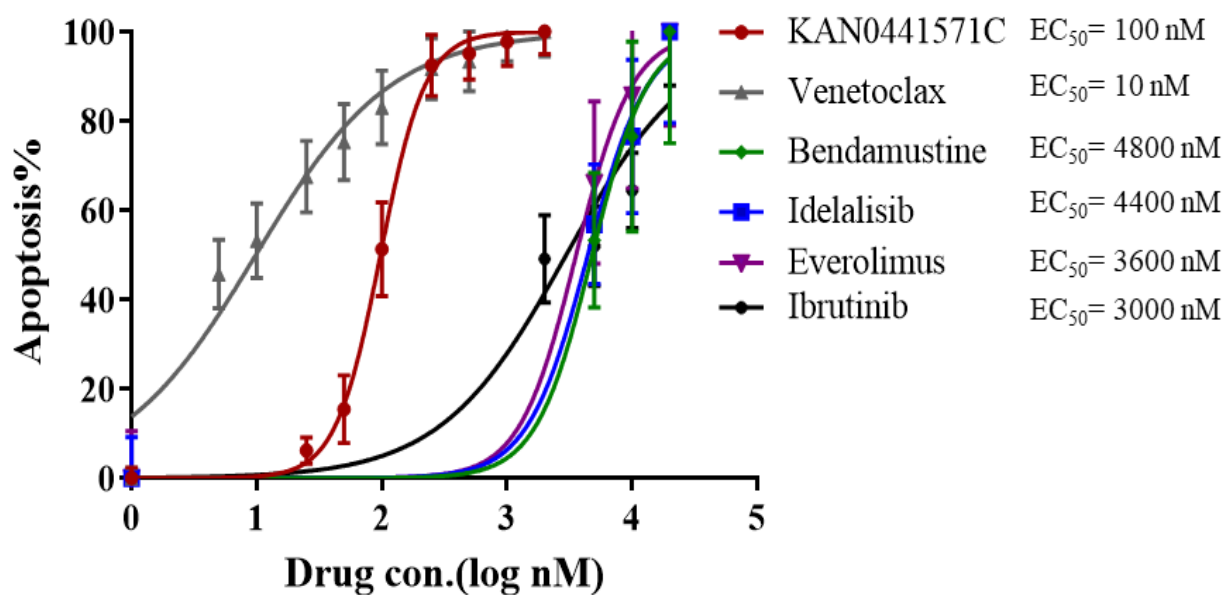


**Figure 2.** Effects of KAN0441571C, venetoclax, ibrutinib, and idelalisib as well as the combinations on intracellular signaling molecules. Relative change in primary MCL cells in the levels of phosphorylated

ROR1, AKT, PI3K, BTK, and mTOR after single-drug incubation with KAN0441571C (571C) and venetoclax (Ven), ibrutinib (Ibr), everolimus (Ever), and idelalisib (Idel), respectively, and in combination, as indicated at the bottom of the figure. The dotted lines indicate the level of the phosphorylated protein in untreated cells. The figure shows mean  $\pm$  SEM of 3 patients.

### 3.3. Effects of KAN0441571C in Combination with Other Drugs

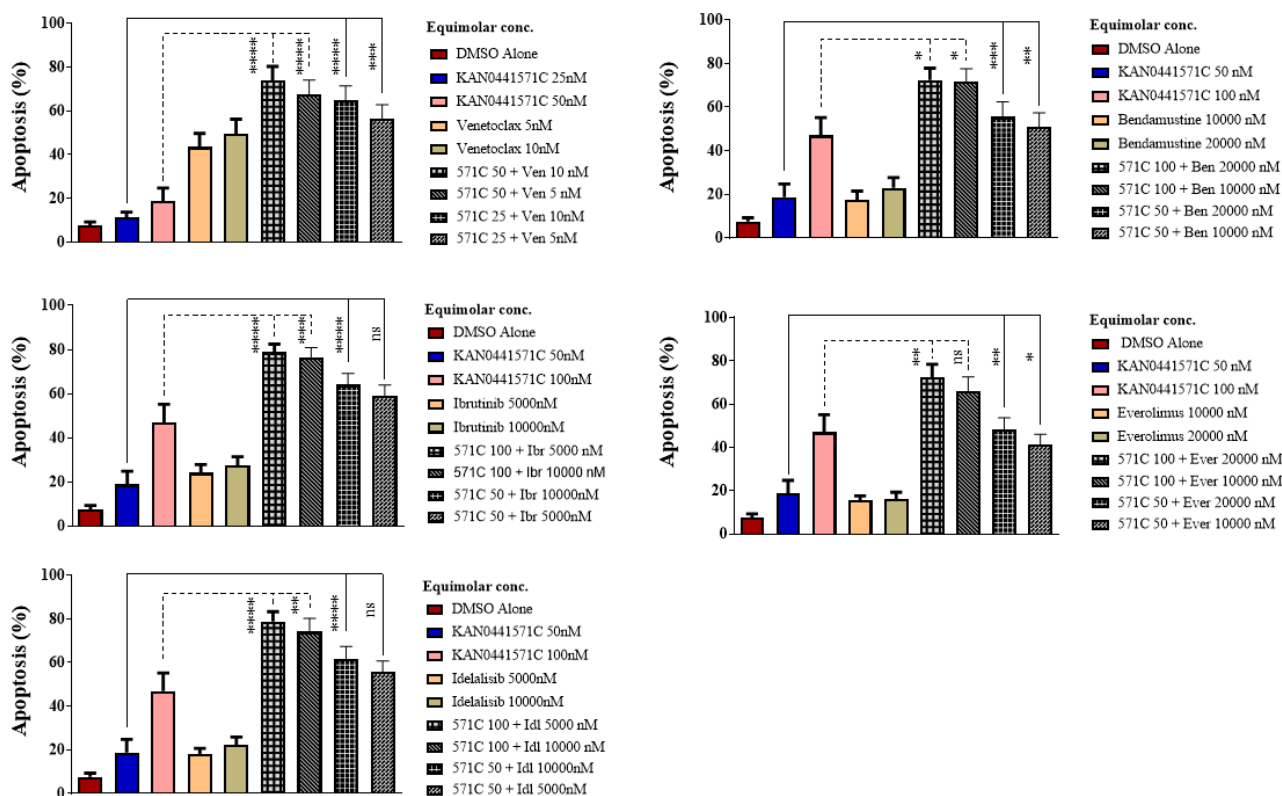
First, we evaluated the apoptotic effect of single-drug KAN0441571C, venetoclax, ibrutinib, idelalisib, everolimus, or bendamustine on patient-derived blood MCL cells ( $n = 11$ ). Dose–response curves for each individual drug, including  $EC_{50}$  values, are shown in Figure 3. Venetoclax and KAN0441571C were the most effective single agents among the tested drugs. Next, MCL cell lines were incubated with the  $EC_{50}$  concentration of KAN0441571C and equimolar concentrations of venetoclax, ibrutinib, or bendamustine, alone and in combination (Figures S3 and S6). In single-drug experiments, KAN0441571C, venetoclax, and ibrutinib were similarly effective in inducing cell death of the four different MCL cell lines, while bendamustine seemed to be inferior in two of five cell lines (Mino and Granta-519). In drug combination experiments, KAN0441571C plus venetoclax or KAN0441571C plus ibrutinib showed a statistically significant increased cytotoxic effect, indicating synergism for three cell lines (not for Granta-519) compared to each drug alone, while the combination of KAN0441571C with bendamustine showed synergism in all cell lines except for Granta-519.



**Figure 3. Dose–response curves and  $EC_{50}$  values for each individual drug.** Apoptosis (Annexin V/PI) (mean  $\pm$  SEM) of MCL cells from patients ( $n = 11$ ) incubated in vitro with KAN0441571C, venetoclax, bendamustine, idelalisib, everolimus, and ibrutinib for 24 h.  $EC_{50}$  values for each drug are shown. R-square values are 0.119, 0.6161, 0.2826, 0.3542, 0.3077, and 0.5438 for KAN0441571C, venetoclax, bendamustine, idelalisib, everolimus, and ibrutinib, respectively.

We then repeated the drug combination experiments using patient-derived MCL cells. The results are shown in Figure 4. There was a significant increase in apoptosis (Annexin V/PI) of MCL cells when KAN0441571C was incubated in combination with either venetoclax, ibrutinib, idelalisib, everolimus, or bendamustine as compared to each drug alone. Furthermore, when drugs were combined, low doses of each drug seemed to be as effective as high doses.

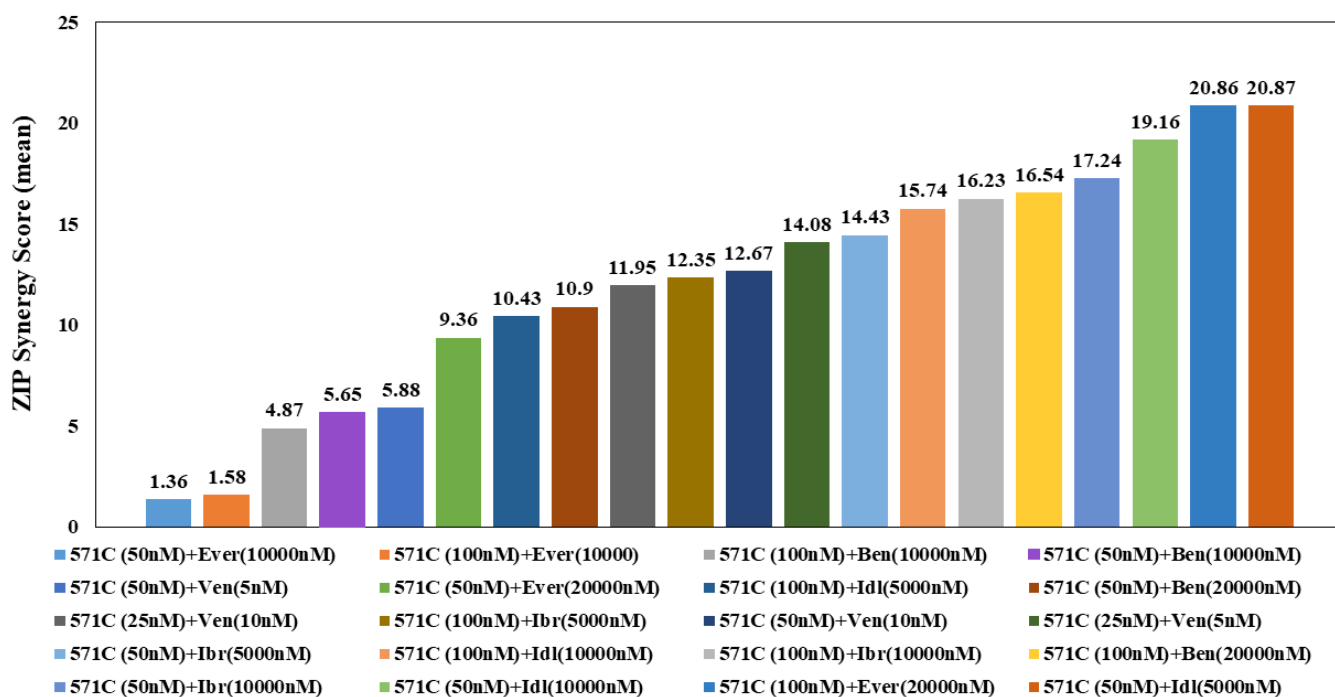




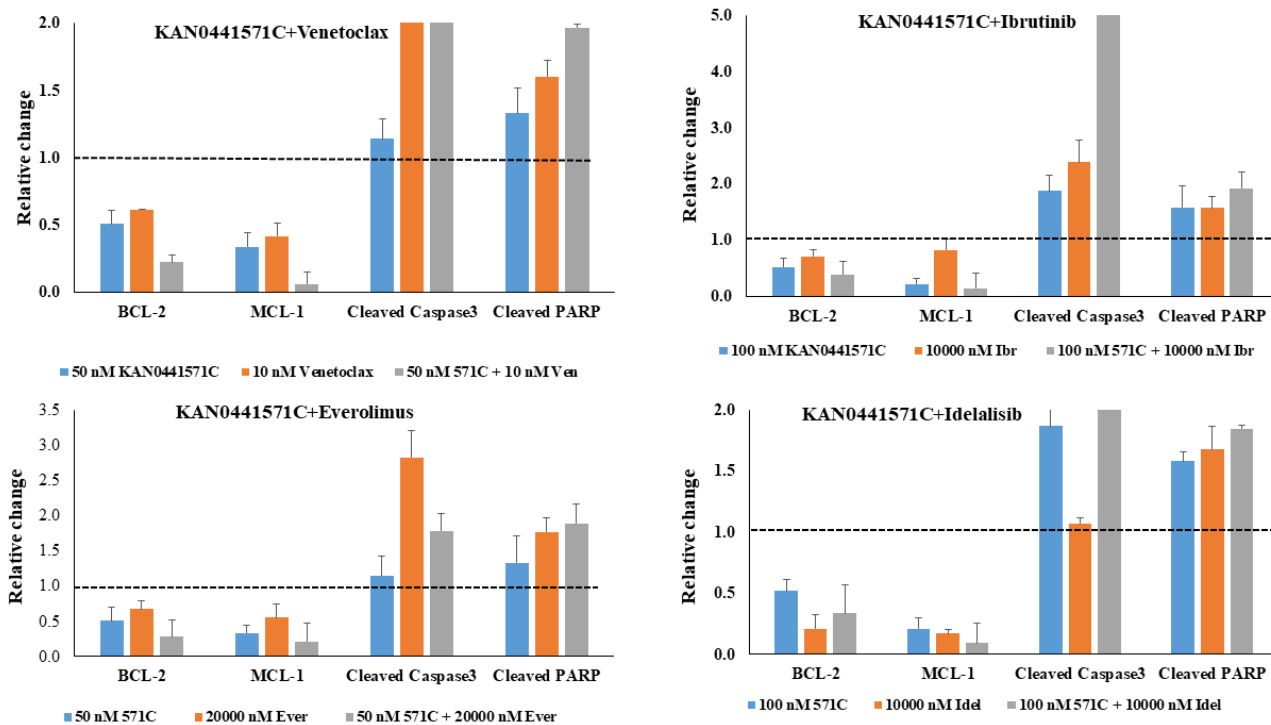
**Figure 4.** Induction of apoptosis by inhibitors alone or in combination on primary MCL cells. Apoptosis (Annexin V/PI) (mean  $\pm$  SEM) of primary MCL cells ( $n = 11$ ) incubated in vitro with equimolar concentrations of KAN0441571C (571C), ibrutinib (Ibr), venetoclax (Ven), idelalisib (Idl), everolimus (Ever), or bendamustine (Ben) alone and in combination. Statistical significances are shown at the top: \*  $p < 0.05$ , \*\*  $p < 0.01$ , \*\*\*  $p < 0.001$ , \*\*\*\*  $p < 0.0001$ ; ns: not significant (Mann–Whitney test was used for comparisons between different groups).

A summary of apoptosis ranking for all drug combinations in primary MCL cells is displayed in Figure 5. The highest synergism was seen between a low dose (50 nM) of KAN0441571C and a low dose (5000 nM) of idelalisib. Moreover, a low dose (50 nM) of KAN0441571C and a low dose (5 nM) of venetoclax showed significant synergism. A high dose (100 nM) of KAN0441571C and everolimus (20,000 nM) induced a significant synergistic effect, as well. To confirm apoptosis, we analyzed the expression of BCL-2 and MCL-1, which were markedly downregulated by the combination of drugs as compared to each drug alone, while cleaved caspase 3 and cleaved PARP were upregulated (Figures 6 and S4).

As shown above, KAN0441571C alone dephosphorylated ROR1, followed by the inactivation of AKT, BTK, and mTOR, which are involved in the ROR1 signaling pathway (Figures S2B and 2). When KAN0441571C was combined with venetoclax, ibrutinib, everolimus, or idelalisib, phosphorylation of ROR1, AKT, BTK, and mTOR was decreased as compared to single drugs (Figure 2). The most effective combination seemed to be KAN0441571C with venetoclax or ibrutinib. Interestingly, phospho-PI3K was least affected by all drugs and combinations including idelalisib (Figure 2). Overall, the pattern of phosphorylation of target proteins was less clear as compared to that of apoptotic proteins, probably reflecting the complex network of intracellular signaling.



**Figure 5.** Ranking (ZIP synergy score) for apoptosis induced by drug combinations in primary MCL cells. ZIP synergy score (mean) for apoptosis (Annexin V/PI) of drug combinations using MCL cells derived from patients (n = 11) incubated for 24 h by indicated drugs and conc. The ZIP score captures the effect of drug combinations by comparing the change in the potency of the dose–response curves between individual drugs and their combination (<https://synergyfinder.org/> (accessed on 21 August 2021)). A score between 1 and 10 indicates an additive effect and >10 synergism. KAN0441571C (571C), everolimus (Ever), ibrutinib (Ibr), idelalisib (Idl), bendamustine (Bend), venetoclax (Ven).



**Figure 6.** Induction of apoptosis following treatment of MCL primary cells with KAN0441571C, venetoclax, ibrutinib, everolimus, or idelalisib. Relative change in MCL cells from patients of BCL-2,

MCL-1, cleaved caspase 3, and cleaved PARP after incubation with single-agent KAN0441571C (571C), venetoclax (Ven), ibrutinib (Ibr), everolimus (Ever), or idelalisib (Idel) alone and in combination, as indicated at the bottom of the figure. The dotted lines indicate the level of untreated cells. The figure shows the results of one representative patient out of three.

#### 4. Discussion

The introduction of new drugs has improved the prognosis for patients with MCL. However, there is an urgent medical need for novel treatment options to increase the response rate and depth of remission and a drug with other MOAs than those currently used at clinical relapse and resistance. ROR1 has been proposed to be a druggable target [26,31] and is reported to be heterogeneously expressed in MCL [33]. In this study, we confirmed and extended the expression pattern of ROR1 in MCL cell lines and primary MCL cells. There are also splice variants of ROR1. A truncated ROR1 lacking the extracellular domain with an intact intracellular region has been described [2]. Forouzesh et al. [34] also reported a splice variant which only had the extracellular region. These results might explain the findings in JeKo1 and Mino cell lines comparing surface staining and Western blot. Different isoforms of ROR1 have also been reported with molecular weights from 100 to 130 kDa, which may represent different degrees of glycosylation [6,34].

KAN0441571C is the second generation of a small molecule ROR1 tyrosine kinase inhibitor [30]. The drug induced apoptosis of ROR1<sup>+</sup> MCL cell lines as well as primary MCL cells. The ROR1 inhibitor prevented phosphorylation of ROR1. Molecules of the non-canonical WNT signaling pathway were inactivated, which is in line with previous reports showing that ROR1 signals through at least the  $\beta$ -catenin-independent (non-canonical) WNT pathway [35–37]. Involvement of the PI3K/AKT/mTOR pathway in MCL is also supported by a previous report showing that inhibition of mTOR in MCL cells induced cell cycle arrest and apoptosis [38]. Furthermore, AKT activates mTOR through the interaction of several signaling molecules [35], including the downstream target CREB. AKT inactivation is of importance for apoptosis induced by many targeting drugs [39]. The ERK pathway, which is frequently mutated in malignancies [40], was also inactivated by ROR1 inhibition, which is in agreement with a report showing that ERK was dephosphorylated followed by treatment with KAN0441571C in small-cell lung cancer cells [41]. Moreover, ROR1 interacts with SRC, a key regulator of cancer cells. KAN0441571C prevented phosphorylation of SRC, which should also be of significance for induction of tumor cell death.

Intracellular signaling is a complex network of interactions between proteins. Malignant cells are masters to overcome signal suppression through upregulation of other signaling proteins. In MCL, various signaling pathways seemed to be used, which may vary between patients. A drug which can act on several key oncogenic signaling molecules should be of interest in a therapeutic attempt. KAN0441571C not only prevented phosphorylation of ROR1 but also inactivation of the PI3K/AKT/mTOR molecules, an important axis in tumorigenesis and a significant therapeutic target [42].

The combination of KAN0441571C with other agents had a synergistic apoptotic effect. Increased tumor cell death induced by KAN0441571C in combination with other drugs was supported by enhanced downregulation of, e.g., the anti-apoptotic MCL-1 and BCL-2 proteins, which are highly expressed in MCL cells [34]. The BCL-2 family proteins are crucial regulators of the mitochondrial apoptotic pathway. Genetic aberrations of these genes correlated with lymphomagenesis and chemotherapy resistance [33,43]. Altering the balance between anti-apoptotic and pro-apoptotic BCL-2 proteins may lead to the evasion of apoptosis and the extension of the survival of malignant cells. Targeting MCL-1 and BCL-2 might be a rewarding therapeutic approach in MCL.

Drugs which are in clinical use for MCL such as ibrutinib, venetoclax, idelalisib, everolimus, and bendamustine showed significant killing of MCL cells. The ROR1 inhibitor KAN0441571C seemed to act synergistically with these drugs, enhancing tumor cell death. Of specific interest was that low doses of KAN0441571C and low doses of venetoclax, ibrutinib, and idelalisib had a significant synergistic apoptotic effect. The increased apop-

otic effect of KAN0441571C in combination with other targeting drugs might be due to enhanced inactivation of various signaling molecules associated with ROR1 signaling.

This is the first study on the effects of a small molecule ROR1 inhibitor alone on MCL tumor cell survival and signaling. The data also indicated that combining the ROR1 inhibitor with drugs targeting other dysregulated pathways contributes to an increased anti-tumor effect. Previous studies in diffuse large B-cell lymphoma (DLBCL) and small-cell lung cancer (SCLC) have indicated that combining ROR1 inhibitors with venetoclax [30,41,44] or with erlotinib and chemotherapeutics in pancreatic carcinoma [5] acted synergistically to induce tumor cell death. This report also adds PI3K and BTK inhibitors to the group of combinatorial partners for ROR1 inhibitors. Further pre-clinical and clinical studies are warranted to evaluate this new treatment concept with respect to side effects and anti-tumor activity. As the tumor microenvironment is of importance for tumor progression [45], models where a tumor microenvironment is incorporated should be included. There is a substantial amount of data indicating the importance of the microenvironment in MCL [26]. We have previously shown that when CLL cells were cultured in the presence of stromal cells, low concentrations of the ROR1 inhibitor were not as effective in killing leukemic cells as if cultured without stromal cells. When a high concentration of the inhibitor was used, stromal cells had no preventive effect [29].

## 5. Conclusions

ROR1 is an oncogenic RTK involved in the survival of tumor cells of various origins. Due to its unique expression in tumors, ROR1 has been recognized as an interesting target for cancer treatment. ROR1 small molecule inhibitor in hematologic malignancies, including MCL, induced significant apoptosis of tumor cells *in vitro* as well as the inhibition of several important signaling pathways for tumor cell survival. In combination with other small molecules targeting MCL tumor cells, a significantly increased tumor cell death was seen.

**Supplementary Materials:** The following supporting information can be downloaded at: <https://www.mdpi.com/article/10.3390/pharmaceutics14102238/s1>, Figure S1: Dose-dependent apoptosis effects of KAN0441571C. Analysis of apoptosis in primary MCL cells from a patient using Annexin V/PI staining in CD45<sup>+</sup>/ROR1<sup>+</sup>/CD3<sup>-</sup> gated cells after incubation for 24 h with KAN0441571C (25–2000 nM); Figure S2: Analysis of ROR1 expression in MCL cell lines. Analysis of ROR1 surface expression in 5 MCL cell lines (A). Western blot analysis of total (t) ROR1 and phosphorylated (p) ROR1 proteins in 5 MCL cell lines before and after incubation (4 h) with the ROR1 inhibitor, KAN044157C (250 and 500 nM) (B). pROR1/ROR1 density has been shown under each blot; Figure S3: MTT assay on 5 MCL cell lines. Cytotoxicity (MTT) in 5 MCL cell lines incubated for 72 h with EC<sub>50</sub> concentration of KAN0441571C and equimolar concentration of venetoclax, ibrutinib, and bendamustine. *p*-values comparing cytotoxicity of KAN0441571C alone against the combination of KAN0441571C with other drugs are shown at the top. \*\* *p* < 0.01, \*\*\*\* *p* < 0.0001; ns: not significant. The Mann–Whitney test was used for comparisons; Figure S4: Western blots analysis of apoptotic proteins in patient-derived MCL cells. Western blots for apoptotic proteins in patient-derived MCL cells after incubation with KAN0441571C, venetoclax, ibrutinib, or everolimus alone and in combination, as indicated at the top. The molecular weight of protein is shown for each blot (A). Relative density of each protein band to beta actin (B); Figure S5: Effects of KAN0441571C, venetoclax, ibrutinib, idelalisib, or everolimus alone and in combination on ROR1 and intracellular signaling molecules. Western blots of total and phosphorylated proteins after incubation with KAN0441571C, venetoclax, ibrutinib, idelalisib, or everolimus alone and in combination, as indicated at the top (A). Densitometry analysis of pROR1/ROR1, pAKT/AKT, pPI3K/PI3K, and pBTK/BTK (B); Figure S6: Induction of apoptosis (flowcytometry Annexin/PI) in primary MCL cells. Representative figures of patients are shown in (A) (2013#020), (B) (2010#040), and (C) (2013#058) using a combination of KAN0441571C (25 nM) and venetoclax (5 nM). Untreated or DMSO (10 µL/mL) were used as controls (24 h). Induction of apoptosis (48 h) in the MCL cell line MINO (D) using various concentrations of KAN0441571C (25–2000 nM) and DMSO (10 µL/mL) as a negative control is also shown.

**Author Contributions:** A.G., M.A.O., W.Z., J.A. and A.S. performed experiments, analyzed data, and finalized the manuscript. J.S. and T.O. produced the small molecule and finalized the manuscript. B.S. provided clinical material, analyzed data, and finalized the manuscript. A.Ö., H.M. and M.H.-F. designed the study, performed experiments, supervised the study, and wrote the manuscript. All authors have read and agreed to the published version of the manuscript.

**Funding:** This research was funded by the Åke Olsson Foundation for Hematology Research (grant numbers 2017-00436, 2019-00396 to M.H.-F.), the Cancer and Allergy Foundation (grant numbers 2016/5, 2017/63, 2018/63, 2019/189, 2020/258 to A.Ö. and 2017/64, 2018/140, 2019/194, 2020/260 to H.M.), the Cancer Society in Stockholm (grant numbers 151313, 184203 to A.Ö. and 144142, 164122 to H.M.), the Swedish Cancer Society (grant numbers CAN 2015/408, CAN 2018/499 to A.Ö.), AFA Insurance (grant number 130054 to A.Ö.), the Karolinska Institutet Foundation (A.Ö., H.M.), and Region Stockholm (grant numbers 20150070, 20180030 to A.Ö.).

**Institutional Review Board Statement:** The study was conducted in accordance with Good Clinical Practice Guidelines and the Declaration of Helsinki. All patients or their legally acceptable representative, or both (if possible), provided written informed consent. The study was authorized by the National Ethics Authority of Sweden (www.etikprovningmyndigheten.se (accessed on 20 December 2016)) (approval code: 2016/2506-32, date of approval: 20 December 2016).

**Informed Consent Statement:** Informed consent was obtained from all subjects involved in the study.

**Data Availability Statement:** Not applicable.

**Acknowledgments:** For excellent secretarial assistance, we thank Leila Relander.

**Conflicts of Interest:** J.S. is an employee and shareholder of Kancera AB. T.O. is a founder, employee, and shareholder of Kancera AB. H.M. is a founder and shareholder of Kancera AB and received research grants and honorarium from Kancera AB. The remaining authors declare that they have no conflict of interest.

## References

1. Minami, Y.; Oishi, I.; Endo, M.; Nishita, M. Ror-family receptor tyrosine kinases in noncanonical Wnt signaling: Their implications in developmental morphogenesis and human diseases. *Dev. Dyn.* **2010**, *239*, 1–15. [CrossRef]
2. Reddy, U.R.; Phatak, S.; Pleasure, D. Human neural tissues express a truncated Ror1 receptor tyrosine kinase, lacking both extracellular and transmembrane domains. *Oncogene* **1996**, *13*, 1555–1559. [PubMed]
3. Klein, U.; Tu, Y.; Stolovitzky, G.A.; Mattioli, M.; Cattoretti, G.; Husson, H.; Freedman, A.; Inghirami, G.; Cro, L.; Baldini, L.; et al. Gene expression profiling of B cell chronic lymphocytic leukemia reveals a homogeneous phenotype related to memory B cells. *J. Exp. Med.* **2001**, *194*, 1625–1638. [CrossRef] [PubMed]
4. Baskar, S.; Kwong, K.Y.; Hofer, T.; Levy, J.M.; Kennedy, M.G.; Lee, E.; Staudt, L.M.; Wilson, W.H.; Wiestner, A.; Rader, C. Unique cell surface expression of receptor tyrosine kinase ROR1 in human B-cell chronic lymphocytic leukemia. *Clin. Cancer Res.* **2008**, *14*, 396–404. [CrossRef] [PubMed]
5. Daneshmanesh, A.H.; Hojjat-Farsangi, M.; Ghaderi, A.; Moshfegh, A.; Hansson, L.; Schultz, J.; Vågberg, J.; Byström, S.; Olsson, E.; Olin, T.; et al. A receptor tyrosine kinase ROR1 inhibitor (KAN0439834) induced significant apoptosis of pancreatic cells which was enhanced by erlotinib and ibrutinib. *PLoS ONE* **2018**, *13*, e0198038. [CrossRef] [PubMed]
6. Daneshmanesh, A.H.; Mikaelsson, E.; Jeddi-Tehrani, M.; Bayat, A.A.; Ghods, R.; Ostadkarampour, M.; Akhondi, M.; Lagercrantz, S.; Larsson, C.; Osterborg, A.; et al. Ror1, a cell surface receptor tyrosine kinase is expressed in chronic lymphocytic leukemia and may serve as a putative target for therapy. *Int. J. Cancer* **2008**, *123*, 1190–1195. [CrossRef]
7. Karvonen, H.; Niininen, W.; Murumägi, A.; Ungureanu, D. Targeting ROR1 identifies new treatment strategies in hematological cancers. *Biochem. Soc. Trans.* **2017**, *45*, 457–464. [CrossRef]
8. O’Connell, M.P.; Marchbank, K.; Webster, M.R.; Valiga, A.A.; Kaur, A.; Vultur, A.; Li, L.; Herlyn, M.; Villanueva, J.; Liu, Q.; et al. Hypoxia induces phenotypic plasticity and therapy resistance in melanoma via the tyrosine kinase receptors ROR1 and ROR2. *Cancer Discov.* **2013**, *3*, 1378–1393. [CrossRef]
9. Shabani, M.; Asgarian-Omran, H.; Jeddi-Tehrani, M.; Vossough, P.; Faranoush, M.; Sharifian, R.A.; Toughe, G.R.; Kordmahin, M.; Khoshnoodi, J.; Roohi, A.; et al. Overexpression of orphan receptor tyrosine kinase Ror1 as a putative tumor-associated antigen in Iranian patients with acute lymphoblastic leukemia. *Tumour Biol.* **2007**, *28*, 318–326. [CrossRef]
10. Shabani, M.; Asgarian-Omran, H.; Vossough, P.; Sharifian, R.A.; Faranoush, M.; Ghragozlou, S.; Khoshnoodi, J.; Roohi, A.; Jeddi-Tehrani, M.; Mellstedt, H.; et al. Expression profile of orphan receptor tyrosine kinase (ROR1) and Wilms’ tumor gene 1 (WT1) in different subsets of B-cell acute lymphoblastic leukemia. *Leuk. Lymphoma* **2008**, *49*, 1360–1367. [CrossRef]

11. Yamaguchi, T.; Yanagisawa, K.; Sugiyama, R.; Hosono, Y.; Shimada, Y.; Arima, C.; Kato, S.; Tomida, S.; Suzuki, M.; Osada, H.; et al. NKX2-1/TITF1/TTF-1-Induced ROR1 is required to sustain EGFR survival signaling in lung adenocarcinoma. *Cancer Cell* **2012**, *21*, 348–361. [CrossRef] [PubMed]
12. Zhang, S.; Chen, L.; Cui, B.; Chuang, H.Y.; Yu, J.; Wang-Rodriguez, J.; Tang, L.; Chen, G.; Basak, G.W.; Kipps, T.J. ROR1 is expressed in human breast cancer and associated with enhanced tumor-cell growth. *PLoS ONE* **2012**, *7*, e31127. [CrossRef] [PubMed]
13. Hojjat-Farsangi, M. Small-molecule inhibitors of the receptor tyrosine kinases: Promising tools for targeted cancer therapies. *Int. J. Mol. Sci.* **2014**, *15*, 13768–13801. [CrossRef]
14. Yamaoka, T.; Kusumoto, S.; Ando, K.; Ohba, M.; Ohmori, T. Receptor Tyrosine Kinase-Targeted Cancer Therapy. *Int. J. Mol. Sci.* **2018**, *19*, 3491. [CrossRef]
15. Hojjat-Farsangi, M.; Moshfegh, A.; Daneshmanesh, A.H.; Khan, A.S.; Mikaelsson, E.; Osterborg, A.; Mellstedt, H. The receptor tyrosine kinase ROR1—An oncofetal antigen for targeted cancer therapy. *Semin. Cancer Biol.* **2014**, *29*, 21–31. [CrossRef] [PubMed]
16. Vaisitti, T.; Arruga, F.; Vitale, N.; Lee, T.T.; Ko, M.; Chadburn, A.; Braggio, E.; Di Napoli, A.; Iannello, A.; Allan, J.N.; et al. ROR1 targeting with the antibody-drug conjugate VLS-101 is effective in Richter syndrome patient-derived xenograft mouse models. *Blood* **2021**, *137*, 3365–3377. [CrossRef] [PubMed]
17. Yoda, A.; Oishi, I.; Minami, Y. Expression and function of the Ror-family receptor tyrosine kinases during development: Lessons from genetic analyses of nematodes, mice, and humans. *J. Recept. Signal Transduct. Res.* **2003**, *23*, 1–15. [CrossRef]
18. Karvonen, H.; Perttilä, R.; Niininen, W.; Hautanen, V.; Barker, H.; Murumägi, A.; Heckman, C.A.; Ungureanu, D. Wnt5a and ROR1 activate non-canonical Wnt signaling via RhoA in TCF3-PBX1 acute lymphoblastic leukemia and highlight new treatment strategies via Bcl-2 co-targeting. *Oncogene* **2019**, *38*, 3288–3300. [CrossRef]
19. Cui, B.; Ghia, E.M.; Chen, L.; Rassenti, L.Z.; DeBoever, C.; Widhopf, G.F., 2nd; Yu, J.; Neuberger, D.S.; Wierda, W.G.; Rai, K.R.; et al. High-level ROR1 associates with accelerated disease progression in chronic lymphocytic leukemia. *Blood* **2016**, *128*, 2931–2940. [CrossRef]
20. Mao, Y.; Xu, L.; Wang, J.; Zhang, L.; Hou, N.; Xu, J.; Wang, L.; Yang, S.; Chen, Y.; Xiong, L.; et al. ROR1 associates unfavorable prognosis and promotes lymphoma growth in DLBCL by affecting PI3K/Akt/mTOR signaling pathway. *Biofactors* **2019**, *45*, 416–426. [CrossRef]
21. Tietsche de Moraes Hungria, V.; Chiattonne, C.; Pavlovsky, M.; Abenoza, L.M.; Agreda, G.P.; Armenta, J.; Arrais, C.; Avendano Flores, O.; Barroso, F.; Basquiera, A.L.; et al. Epidemiology of Hematologic Malignancies in Real-World Settings: Findings from the Hemato-Oncology Latin America Observational Registry Study. *J. Glob. Oncol.* **2019**, *5*, 1–19. [CrossRef] [PubMed]
22. Rudelius, M.; Rosenfeldt, M.T.; Leich, E.; Rauer-Wunderlich, H.; Solimando, A.G.; Beilhack, A.; Ott, G.; Rosenwald, A. Inhibition of focal adhesion kinase overcomes resistance of mantle cell lymphoma to ibrutinib in the bone marrow microenvironment. *Haematologica* **2018**, *103*, 116–125. [CrossRef]
23. Cheah, C.Y.; Seymour, J.F.; Wang, M.L. Mantle Cell Lymphoma. *J. Clin. Oncol.* **2016**, *34*, 1256–1269. [CrossRef]
24. Dreyling, M.; Aurer, I.; Cortelazzo, S.; Hermine, O.; Hess, G.; Jerkeman, M.; Le Gouill, S.; Ribrag, V.; Trněný, M.; Visco, C.; et al. Treatment for patients with relapsed/refractory mantle cell lymphoma: European-based recommendations. *Leuk. Lymphoma* **2018**, *59*, 1814–1828. [CrossRef]
25. Chen, R.; Chubb, S.; Cheng, T.; Hawtin, R.E.; Gandhi, V.; Plunkett, W. Responses in mantle cell lymphoma cells to SNS-032 depend on the biological context of each cell line. *Cancer Res.* **2010**, *70*, 6587–6597. [CrossRef]
26. Jain, P.; Wang, M.L. Mantle cell lymphoma in 2022—A comprehensive update on molecular pathogenesis, risk stratification, clinical approach, and current and novel treatments. *Am. J. Hematol.* **2022**, *97*, 638–656. [CrossRef]
27. Zhao, Y.; Zhang, D.; Guo, Y.; Lu, B.; Zhao, Z.J.; Xu, X.; Chen, Y. Tyrosine Kinase ROR1 as a Target for Anti-Cancer Therapies. *Front. Oncol.* **2021**, *11*, 680834. [CrossRef]
28. Wang, M.L.; Jurczak, W.; Jerkeman, M.; Trotman, J.; Zinzani, P.L.; Belada, D.; Boccomini, C.; Flinn, I.W.; Giri, P.; Goy, A.; et al. Ibrutinib plus Bendamustine and Rituximab in Untreated Mantle-Cell Lymphoma. *N. Engl. J. Med.* **2022**, *386*, 2482–2494. [CrossRef]
29. Hojjat-Farsangi, M.; Daneshmanesh, A.H.; Khan, A.S.; Shetye, J.; Mozaffari, F.; Kharaziha, P.; Rathje, L.S.; Kokhaei, P.; Hansson, L.; Vågberg, J.; et al. First-in-class oral small molecule inhibitor of the tyrosine kinase ROR1 (KAN0439834) induced significant apoptosis of chronic lymphocytic leukemia cells. *Leukemia* **2018**, *32*, 2291–2295. [CrossRef]
30. Ghaderi, A.; Daneshmanesh, A.H.; Moshfegh, A.; Kokhaei, P.; Vågberg, J.; Schultz, J.; Olin, T.; Harrysson, S.; Smedby, K.E.; Drakos, E.; et al. ROR1 Is Expressed in Diffuse Large B-Cell Lymphoma (DLBCL) and a Small Molecule Inhibitor of ROR1 (KAN0441571C) Induced Apoptosis of Lymphoma Cells. *Biomedicines* **2020**, *8*, 170. [CrossRef]
31. Hojjat-Farsangi, M.; Moshfegh, A.; Schultz, J.; Norin, M.; Olin, T.; Osterborg, A.; Mellstedt, H. Targeting the Receptor Tyrosine Kinase ROR1 by Small Molecules. *Handb. Exp. Pharmacol.* **2021**, *269*, 75–99.
32. Yadav, B.; Wennerberg, K.; Aittokallio, T.; Tang, J. Searching for Drug Synergy in Complex Dose-Response Landscapes Using an Interaction Potency Model. *Comput. Struct. Biotechnol. J.* **2015**, *13*, 504–513. [CrossRef] [PubMed]
33. Karvonen, H.; Chiron, D.; Niininen, W.; Ek, S.; Jerkeman, M.; Moradi, E.; Nykter, M.; Heckman, C.A.; Kallioniemi, O.; Murumägi, A.; et al. Crosstalk between ROR1 and BCR pathways defines novel treatment strategies in mantle cell lymphoma. *Blood Adv.* **2017**, *1*, 2257–2268. [CrossRef] [PubMed]

34. Forouzes, F.; Tabarian, S.S.; Emami, S.; Tehrani, M.J.; Hadavi, R.; Rabbani, H. Construction and Stable Expression of a Truncated Human Receptor Tyrosine Kinase Ror1 (Ror1-ECD). *Avicenna J. Med. Biotechnol.* **2012**, *4*, 41–45. [PubMed]
35. Daneshmanesh, A.H.; Hojjat-Farsangi, M.; Moshfegh, A.; Khan, A.S.; Mikaelsson, E.; Österborg, A.; Mellstedt, H. The PI3K/AKT/mTOR pathway is involved in direct apoptosis of CLL cells induced by ROR1 monoclonal antibodies. *Br. J. Haematol.* **2015**, *169*, 455–458. [CrossRef]
36. Green, J.L.; Kuntz, S.G.; Sternberg, P.W. Ror receptor tyrosine kinases: Orphans no more. *Trends Cell Biol.* **2008**, *18*, 536–544. [CrossRef]
37. Ho, H.Y.; Susman, M.W.; Bikoff, J.B.; Ryu, Y.K.; Jonas, A.M.; Hu, L.; Kuruvilla, R.; Greenberg, M.E. Wnt5a-Ror-Dishevelled signaling constitutes a core developmental pathway that controls tissue morphogenesis. *Proc. Natl. Acad. Sci. USA* **2012**, *109*, 4044–4051. [CrossRef]
38. Peponi, E.; Drakos, E.; Reyes, G.; Leventaki, V.; Rassidakis, G.Z.; Medeiros, L.J. Activation of mammalian target of rapamycin signaling promotes cell cycle progression and protects cells from apoptosis in mantle cell lymphoma. *Am. J. Pathol.* **2006**, *169*, 2171–2180. [CrossRef]
39. Rudelius, M.; Pittaluga, S.; Nishizuka, S.; Pham, T.H.; Fend, F.; Jaffe, E.S.; Quintanilla-Martinez, L.; Raffeld, M. Constitutive activation of Akt contributes to the pathogenesis and survival of mantle cell lymphoma. *Blood* **2006**, *108*, 1668–1676. [CrossRef]
40. McCubrey, J.A.; Steelman, L.S.; Chappell, W.H.; Abrams, S.L.; Wong, E.W.; Chang, F.; Lehmann, B.; Terrian, D.M.; Milella, M.; Tafuri, A.; et al. Roles of the Raf/MEK/ERK pathway in cell growth, malignant transformation and drug resistance. *Biochim. Biophys. Acta* **2007**, *1773*, 1263–1284. [CrossRef]
41. Wang, W.Z.; Shilo, K.; Amann, J.M.; Shulman, A.; Hojjat-Farsangi, M.; Mellstedt, H.; Schultz, J.; Croce, C.M.; Carbone, D.P. Predicting ROR1/BCL2 combination targeted therapy of small cell carcinoma of the lung. *Cell Death Dis.* **2021**, *12*, 577. [CrossRef] [PubMed]
42. Lien, E.C.; Dibble, C.C.; Toker, A. PI3K signaling in cancer: Beyond AKT. *Curr. Opin. Cell Biol.* **2017**, *45*, 62–71. [CrossRef] [PubMed]
43. Frenzel, A.; Grespi, F.; Chmielewskij, W.; Villunger, A. Bcl2 family proteins in carcinogenesis and the treatment of cancer. *Apoptosis* **2009**, *14*, 584–596. [CrossRef] [PubMed]
44. Ghaderi, A.; Okhovat, M.A.; Wikanthi, L.S.S.; Svensson, A.; Palma, M.; Schultz, J.; Olin, T.; Osterborg, A.; Mellstedt, H.; Hojjat-Farsangi, M. A ROR1 small molecule inhibitor (KAN0441571C) induced significant apoptosis of ibrutinib-resistant ROR1(+) CLL cells. *EJHaem* **2021**, *2*, 498–502. [CrossRef]
45. Hanahan, D. Hallmarks of Cancer: New Dimensions. *Cancer Discov.* **2022**, *12*, 31–46. [CrossRef]

## Article

# Optimization of a Novel Mandelamide-Derived Pyrrolopyrimidine Series of PERK Inhibitors

Michael E. Stokes <sup>1,\*</sup>, Matthew D. Surman <sup>2,\*</sup>, Veronica Calvo <sup>1</sup>, David Surguladze <sup>1</sup>, An-Hu Li <sup>1</sup>, Jennifer Gasperek <sup>3</sup>, Matthew Betzenhauser <sup>3</sup>, Guangyu Zhu <sup>3</sup>, Hongwen Du <sup>4</sup>, Alan C. Rigby <sup>1</sup> and Mark J. Mulvihill <sup>1</sup>

<sup>1</sup> HiberCell Inc., 619 West 54th Street, New York, NY 10019, USA

<sup>2</sup> Curia, 26 Corporate Circle, Albany, NY 12203, USA

<sup>3</sup> Curia, 1001 Main Street, Buffalo, NY 14203, USA

<sup>4</sup> Pharmaron Beijing Co., Ltd., No. 6, TaiHe Road, BDA, Beijing 100176, China

\* Correspondence: mstokes@hibercell.com (M.E.S.); matthew.surman@curiaglobal.com (M.D.S.)

† These authors contributed equally to this work.

**Abstract:** The protein kinase R (PKR)-like endoplasmic reticulum kinase (PERK) is one of three endoplasmic reticulum (ER) transmembrane sensors of the unfolded protein response (UPR) responsible for regulating protein synthesis and alleviating ER stress. PERK has been implicated in tumorigenesis, cancer cell survival as well as metabolic diseases such as diabetes. The structure-based design and optimization of a novel mandelamide-derived pyrrolopyrimidine series of PERK inhibitors as described herein, resulted in the identification of compound **26**, a potent, selective, and orally bioavailable compound suitable for interrogating PERK pathway biology in vitro and in vivo, with pharmacokinetics suitable for once-a-day oral dosing in mice.

**Keywords:** ER stress; PERK; UPR; kinase; inhibitor; cancer; diabetes; small molecule; structure-activity-relationship (SAR)

**Citation:** Stokes, M.E.; Surman, M.D.; Calvo, V.; Surguladze, D.; Li, A.-H.; Gasperek, J.; Betzenhauser, M.; Zhu, G.; Du, H.; Rigby, A.C.; et al. Optimization of a Novel Mandelamide-Derived Pyrrolopyrimidine Series of PERK Inhibitors. *Pharmaceutics* **2022**, *14*, 2233. <https://doi.org/10.3390/pharmaceutics14102233>

Academic Editor: Francesca Musumeci

Received: 2 September 2022

Accepted: 17 October 2022

Published: 19 October 2022

**Publisher's Note:** MDPI stays neutral with regard to jurisdictional claims in published maps and institutional affiliations.



**Copyright:** © 2022 by the authors. Licensee MDPI, Basel, Switzerland. This article is an open access article distributed under the terms and conditions of the Creative Commons Attribution (CC BY) license (<https://creativecommons.org/licenses/by/4.0/>).

## 1. Introduction

Cells must match the rates of protein synthesis with demand to avoid the onset of proteotoxic endoplasmic reticulum (ER) stress. In conditions of excess protein production, an accumulation of misfolded proteins in the ER lumen induces the unfolded protein response (UPR), which arrests global translation while enabling specific processes that restore protein homeostasis [1,2]. The UPR is mediated by three discrete signaling cascades, IRE1, ATF6, and EIF2AK3 (PERK) [3]. Upon activating the UPR, PERK phosphorylates eIF2a at Ser51, leading to widespread inhibition of protein translation with a few selected regulatory proteins translated to restore homeostasis and alleviate ER stress [1,3]. In cancer, acute activation of UPR enables tumors to overcome deleterious ER stress induced by rapid cell proliferation, nutrient deprivation, hypoxia, and drug treatments [4–6]. Pharmacological or genetic inhibition of PERK slows proliferation of tumor xenografts in mice [7,8], and small molecule PERK inhibitors have recently entered clinical trials for several oncology indications, including clear cell renal cell carcinoma (ccRCC) and multiple myeloma (NCT04834778; NCT05027594).

Acute ER stress and activation of UPR restores protein homeostasis and supports cell survival, whereas long-term ER stress shifts cells toward an apoptotic cell fate [9]. While intermittent ER stress occurs regularly in cell types that produce high abundance of protein, metabolic dysfunction can result in chronic ER stress that coincides with a number of metabolic and neurological diseases [9–12]. Type-1 Diabetes (T1D) is an example of a metabolic disease and autoimmune disorder characterized by PERK hyperactivation in insulin-producing  $\beta$ -cells of the pancreatic islets [11–13]. Immunohistochemistry (IHC) staining of pancreas sections from T1D patients revealed PERK pathway activation in



insulin-secreting beta cells, relative to healthy control patient samples [13], and PERK activation precedes the destructive autoimmune attack of beta cells in animal models of T1D [12,14]. Together, these findings highlight a potential role for PERK in diabetes and possible therapeutic benefit of PERK inhibitors beyond oncology.

While some cancers and metabolic diseases are characterized by PERK hyperactivation, genetic ablation of PERK results in glucose dysregulation and pancreatitis, suggesting that some basal level of PERK activity is essential to pancreatic health [15,16]. It is possible that the attenuation of PERK activity, rather than complete suppression, could provide therapeutic benefit while supporting normal pancreatic function. To enable future testing of this hypothesis, we sought to create a series of PERK inhibitors with stable PK profiles that could be administered at low doses to attenuate PERK yet tuned through higher doses to sufficiently inhibit PERK for tumor inhibition.

Previously described medicinal chemistry efforts around PERK inhibitors have made use of a variety of core hinge-binding regions, including aminopyridines, pyrrolopyrimidines, quinazolines, and quinolines [7,8,17]. Pyrrolopyrimidine cores have been developed and approved as JAK kinase inhibitors [18,19], and modifications to the core scaffold can have profound effects on stability and selectivity [17]. Here, we optimized the pyrrolopyrimidine core and leveraged extensive SAR information from our recently reported aminopyridine series of inhibitors to guide chemistry efforts aimed at optimizing the in vivo properties of pyrrolopyrimidine PERK inhibitors [7].

Our efforts were focused on developing potent and selective PERK inhibitors with suitable pharmacokinetic profiles to enable once or twice per day oral dosing in mouse models with a flat steady state exposure profile. The goal was to avoid large differences between  $C_{max}$  to  $C_{12h}$  or  $C_{24h}$  in order to achieve a constant and sustained pharmacodynamic response. This paper focuses on the structure-based design, structure–activity relationship (SAR), absorption, distribution, metabolism and excretion (ADME), and pharmacokinetic/pharmacodynamic (PK/PD) properties of a novel class of mandelamide-derived pyrrolopyrimidine PERK inhibitors leading to the identification of Compound **26**, with the desired flat steady state exposure profile. Compound **26** was characterized in a mouse pancreas assay and has been selected for further evaluation in animal models, which will be reported in due course.

## 2. Materials and Methods

### 2.1. Biochemical Assays

The inhibitory potencies of **26** inhibition against PKR, HRI, PERK and GCN2 were evaluated in cell-free biochemical assays following manufacturer’s instructions (Carna; Table 1). In brief, **26** was dissolved in DMSO and serially diluted 3-fold to generate concentrations ranging from 10  $\mu$ M to 0.2 nM in a 384-well plate using a TECAN EVO200 automated liquid handler. 10 nL stock solution was transferred into each well of a 384well assay plate by an Echo550 and an equivalent volume of DMSO was added to the control wells. To each assay well, recombinant protein was suspended in 20  $\mu$ L reaction buffer (listed below) and incubated at 25 °C for 1.5 h while shaking at 1250 rpm. Following incubation, 10  $\mu$ L of a FRET dilution buffer including 20 mM EDTA and 4 nM Tb-anti-peIF2a [pSer51] (Invitrogen, Cat# PV4815) was added to each well and incubated at 25 °C for 2 h while shaking at 600 rpm in the dark. Analysis was performed using an Envision Microplate Reader (PerkinElmer).

**Table 1.** Reagents and conditions used in biochemical characterization of ISR kinases.

Protein	Carna Cat#	Assay Buffer
GCN2	05-153	GCN2 (1 nM); DTT (2 mM); ATP (150 $\mu$ M); GFP-eIF2a (100 nM; Invitrogen Cat# PV4809)
HRI	05-154	HRI (0.12 nM); DTT (2 mM); ATP (30 $\mu$ M); GFP-eIF2a (100 nM; Invitrogen Cat# PV4809)
PERK	05-155	PERK (0.09 nM); DTT (2 mM); ATP (8 $\mu$ M); GFP-eIF2a (100 nM; Invitrogen Cat# PV4809)
PKR	05-156	PKR (0.11 nM); DTT (2 mM); ATP (6 $\mu$ M); GFP-eIF2a (100 nM; Invitrogen Cat# PV4809)

## 2.2. PERK Crystallization and Structure Determination

Human PERK (575-1094  $\Delta$ 670-874) was purified as described previously [7]. Purified PERK protein at 11 mg/mL was mixed with 10 mM compound **11**, **24**, or **26** (in DMSO) to a final protein-inhibitor molar ratio 1:2. The PERK-inhibitor mixture was incubated on ice for 2 h before crystallization. The crystals with compound **11** or **26** were grown at 20 °C in sitting drops by combining 2.0  $\mu$ L PERK-inhibitor mixture, 2.0  $\mu$ L reservoir solution (12–14% PEG3350, 4% tacsimate pH7.0), and 0.4  $\mu$ L seed stock which was equilibrated over a 500  $\mu$ L reservoir solution. The crystal with compound **24** was grown at 4 °C in a hanging drop by combining 1.5  $\mu$ L PERK-inhibitor mixture, 1.5  $\mu$ L reservoir solution (9% PEG3350, 180 mM Na/K tartrate, 100 mM HEPES pH 7.0) which was equilibrated over a 500  $\mu$ L reservoir solution. The crystals were grown to 0.2–0.5 mm over a three-week period before harvesting for analysis. The crystal was transferred stepwise to a cryo-solution with the crystallization cocktail plus 20% glycerol before being frozen in liquid nitrogen. Diffraction data were collected at the IMCA-CAT beamline 17ID for compound **11** or GMCA-CAT beamline 23IDD for compound **24** or **26** at the Advanced Photon Source at Argonne National Laboratory using a Pilatus 6M detector. The diffraction images were processed with DIALS [20] and scaled with AIMLESS [21]. The structure was solved by molecular replacement using PDB 4X7J [17] as starting model by Phaser [22]. The structure was manually built using Coot [23] and subsequently refined using Refmac5 [24]. The crystallographic figures were generated by CCP4MG [25], and the statistics of data collection and refinement are summarized in Supplemental Table S1.

## 2.3. Pharmacokinetic and Pharmacodynamic Analysis in Plasma and Pancreas

For PK analysis of pyrrolopyrimidine analogs in mouse, rat, and dog plasma, the oral formulation was prepared as a solution containing 20% (*w/v*) Captisol in 25 mM NaH<sub>2</sub>PO<sub>4</sub> buffer (pH 2). Compounds were administered orally by gavage at 10 mg/kg to female CD1 mice. After dosing, plasma samples were collected to characterize the PK profiles at 0.25, 0.5, 1, 2, 4, 8, 12 and 24 h post-dose. The plasma concentration of compound was determined by protein precipitation with acetonitrile and liquid chromatography with mass spectrometric detection (LC-MS/MS). Parameters were estimated using Phoenix (WinNonlin) pharmacokinetic software version 6.1.0 using a non-compartmental approach consistent with the oral route of administration. PK analysis of **26** in plasma and pancreas followed a similar analytical method as above, with minor modifications. Compound **26** was suspended in a vehicle consisting of 0.5% methylcellulose (400 cP) and 0.1% Tween80 in water and administered to BALB/c nude mice by oral gavage at 0.3, 1, 3, 10, 30 mg/kg. Plasma and pancreas were sampled from 5 mice per group following a single oral administration at 1, 4, 8, 12, 24 h post-dose.

Total protein was extracted from pancreas tissues sampled during PK studies described above. Frozen pancreas tissue was homogenized by polytron in lysis buffer consisting of 2x Laemmli SDS sample buffer (Novex), supplemented with 10% BME (Gibco), 1X benzonase (EMD Millipore Sigma), phosphatase inhibitors (Sigma) and Mini protease inhibitor tablet (Roche). Homogenate was incubated at room temperature for 10', then boiled for 10', followed by centrifugation for 10' at max speed on a benchtop centrifuge. Protein analysis performed using JESS high-throughput protein analysis instrument (Biotechne) using antibodies for phosphoPERK developed internally and PERK (CST).

## 2.4. Biochemical and Cell-Based Characterization of Pyrrolopyrimidine Analogs

Methods used to evaluate biochemical PERK activity are described and published elsewhere [7]. In brief, biochemical PERK activity is evaluated using a LanthaScreen™ (PerkinElmer) TR-FRET assay to detect phosphorylation of a GFP-tagged eIF2a substrate (ThermoFisher). Excitation at 340 nm of a terbium chelate donor fluorophore in an eIF2a antibody results in energy transfer to GFP acceptor fluorophore upon eIF2a phosphorylation by PERK. Reaction buffer was composed of 50 mM HEPES (pH 7.4), 10 mM MgCl<sub>2</sub>, 1 mM EGTA and 0.01% (*v/v*) Brij™-35. Reactions were initiated by the addition of substrate and

ATP, followed by incubation for 1 h at RT prior to addition of EDTA and the anti-peIF2a antibody. FRET was measured by an EnVision Plate Reader (PerkinElmer). Data were plotted as percent inhibition along a 10-point 3-fold dilution series of inhibitors. IC<sub>50</sub> values were calculated using 4-parameter logistical fitting in XLFit.

Methods used to evaluate in vitro cellular PERK inhibition are described and published elsewhere [7]. In brief, stable HEK293 cells were created using lentiviral particles harboring a GFP-eIF2a expression vector. Transfectants were selected by puromycin and enriched using fluorescent cell sorting based on GFP expression. HEK293-EGFP-eIF2a cells were plated at 5000 cells/well in 384-well assay plates and incubated overnight. The following day, pyrrolopyrimidine analogs were added to wells using an Echo acoustic dispenser and incubated for 30 min. ER stress was induced by the addition of tunicamycin to the wells at 1 mM for 2 h. Cells were lysed and peIF2a was evaluated using a TR-FRET system, as described above.

### 2.5. In Vivo Tumor Xenograft Studies

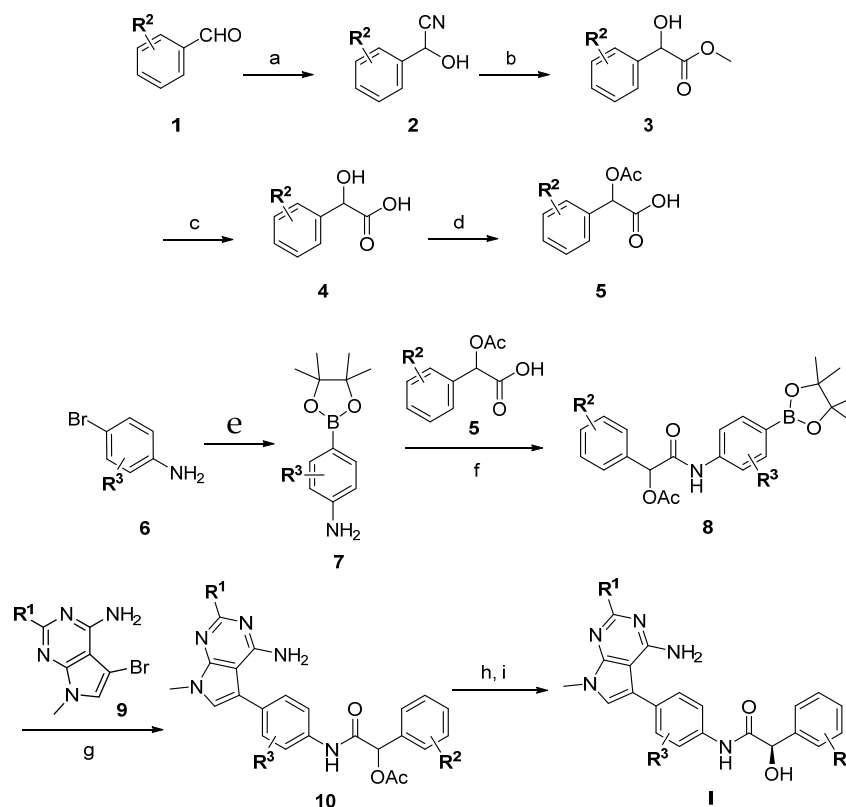
In vivo studies of the effect of pyrrolopyrimidines on 786-O xenograft inhibition follow a method published elsewhere [7]. Female BALB/c nude mice were inoculated subcutaneously with 786-O tumor cells ( $5 \times 10^6$ ) in 0.1 mL of PBS. Animals were randomized when tumors reached 100–200 mm<sup>3</sup> into treatment groups. Pyrrolopyrimidine PERK inhibitors **24**, **26** or **70** were dissolved in vehicle solution consisting of 20% (*w/v*) Captisol in 25 mM NaPO<sub>4</sub> buffer (pH2) and administered twice daily (BID) by oral gavage for 29 days. Tumor volumes were measured by caliper and the volume was expressed in mm<sup>3</sup> using the formula:  $V = (L \times W \times W)/2$ , where V, L, and W represent tumor volume, length, and width, respectively. All studies were conducted following an IACUC-approved protocol (AN-1903-05-1798). Experimental data management and reporting were in accordance with applicable Crown Bioscience's Guidelines and Standard Operating Procedures.

## 3. Results and Discussion

Small molecule PERK inhibitors across a variety of chemotypes have been previously described in the literature and captured in an earlier publication from our group around an aminopyridine series of PERK inhibition [7]. Herein, we report the synthesis and discovery of a series of novel mandelamide-derived pyrrolopyrimidines (**I**) that are highly potent, selective, and orally bioavailable PERK inhibitors. These medicinal chemistry efforts were iteratively supported by an X-ray crystallography structure-based approach to develop and refine SAR information. Collectively this approach permitted us to optimize the physiochemical and ADME/PK properties of this chemical series. Different R<sup>1</sup>, R<sup>2</sup>, R<sup>3</sup>, Ar and L groups have been introduced into our PERK small molecule series to tune the potency, selectivity and drug-like properties, such as aqueous solubility and cellular permeability.

The general synthesis for our pyrrolopyrimidine PERK inhibitors is shown in Scheme 1. The terminal ring substitution with different R<sup>2</sup> groups was introduced through the corresponding aldehyde **1**. Cyanohydrin **2** formation with TMS-cyanide and zinc(II) iodide followed by acid hydrolysis of the nitrile in methanol provided methyl mandelic ester **3**. Hydrolysis of the ester with lithium hydroxide and acylation of the benzylic alcohol gave the protected mandelic acid **5**.

The proximal ring substitution with different R<sup>3</sup> groups was introduced through bromo aniline **6**. Palladium-mediated borylation of **6** to give the aniline boronate ester **7** was followed by T<sub>3</sub>P coupling with acid **5** to provide amide **8**. Boronate ester **8** underwent Suzuki coupling with pyrrolopyrimidine bromide **9** to give racemic acetyl-protected product **10**. Deacylation under basic conditions followed by chiral separation of the enantiomers provided the final product **I**.



**Scheme 1.** General synthesis of PERK inhibitors. Reaction conditions: (a) TMS-CN (1.2 equiv.), ZnI<sub>2</sub> (0.1 equiv.), 0 °C; (b) 3M HCl in MeOH, 0 °C to rt, 60–80% over two steps; (c) LiOH·H<sub>2</sub>O (1.2 equiv.), THF, H<sub>2</sub>O, MeOH, rt, 50–85%; (d) AcCl (2 vol.), 0 °C to rt, 70–85%; (e) B<sub>2</sub>pin<sub>2</sub> (1.2 equiv.), KOAc (3 equiv.), PdCl<sub>2</sub>(PPh<sub>3</sub>)<sub>2</sub> (5 mol. %), NEt<sub>3</sub> (10 vol.), 90 °C, 50–70%; (f) **5** (1.2 equiv.), 50% propylphosphonic anhydride (T<sub>3</sub>P) in EtOAc (1.5 equiv.), DIPEA (3 equiv.), CH<sub>2</sub>Cl<sub>2</sub>, 0 °C to rt, 50–80%; (g) XPhos-Pd-G<sub>2</sub> (10 mol. %), K<sub>2</sub>CO<sub>3</sub> (3 equiv.), THF, H<sub>2</sub>O, 80 °C, 25–70%; (h) K<sub>2</sub>CO<sub>3</sub> (2 equiv.), MeOH, rt, 80–90%; (i) Chiral SFC separation.

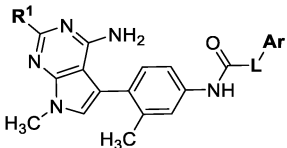
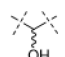
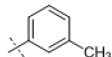
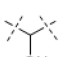
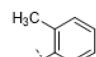

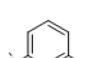

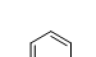
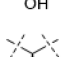
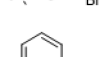
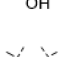
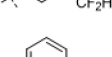
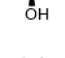
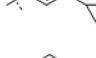
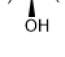
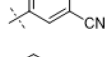
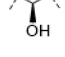
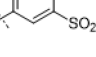
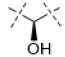
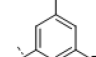

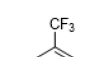
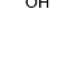
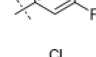
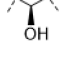
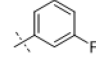

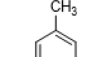

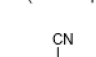
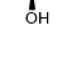
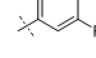
The PERK activity of analog **I** was evaluated using cell-free biochemical assays. In these assays, PERK phosphorylation of eIF2 $\alpha$  was assessed using a FRET-based labelled protein assay [7]. Compounds were then evaluated for cellular activity by quantifying inhibition of eIF2 $\alpha$  phosphorylation in HEK293 cells treated with the ER inducer tunicamycin [7]. Together, these data read out the potency of a given analog against PERK as well as the cellular permeability to enable bioactivity.

Initial SAR studies in the pyrrolopyrimidine series focused on the linker (**L**) region between the central amide and terminal aryl ring (Table 2). Hydroxyl substitution on this group was found to increase potency by 2–3-fold (**13** vs. **14**) with preference for the (*R*)-over the (*S*)-enantiomer (**11** vs. **12**). Expansion or contraction of the length of the linker **L** was not tolerated, resulting in at least 20-fold losses in PERK biochemical potency and nearly 50- to 100-fold losses in cellular potency (**14** vs. **15** and **16**, respectively). Difluoro substitution of the linker also caused a substantial loss in potency, as did replacement of the CH(OH) group with an O, NH, or NCH<sub>3</sub> group (**13** vs. **17**, **18**, **19**, and **20**, respectively). Seven-fold losses in both biochemical and cellular potency were observed when the hydroxyl group was converted to the methyl ether (**13** vs. **21**). Even more substantial losses were associated with replacement of the hydroxyl with an amino group (**13** vs. **23**). Addition of a methyl group to the linker to form a tertiary alcohol also caused a substantial loss in potency (**13** vs. **22**). Based on these findings, it was concluded that (*R*)-CH(OH) is the preferred **L** group.

**Table 2.** In vitro data of PERK inhibitors.

						PERK	p-eIF2 $\alpha$
Cmpd	R <sup>1</sup>	L	Ar	IC <sub>50</sub> ( $\mu$ M)	IC <sub>50</sub> ( $\mu$ M)		
11	H			0.0022	0.0084		
12	H			0.0078	0.057		
13	H			0.0018	0.023		
14	H			0.0052	0.041		
15	H			0.126	1.93		
16	H	---		0.168	3.96		
17	H			0.3	0.532		
18	H			3.98	>10.0		
19	H			0.021	0.211		
20	H			0.108	1.75		
21	H			0.014	0.174		
22	H			0.056	0.184		
23	H			0.033	0.581		
24	Me			0.02	0.051		
25	Me			0.102	0.303		
26	Me			0.0028	0.015		
27	Me			0.343	2.05		
28	Me			0.0018	0.016		
29	Me			0.107	0.713		

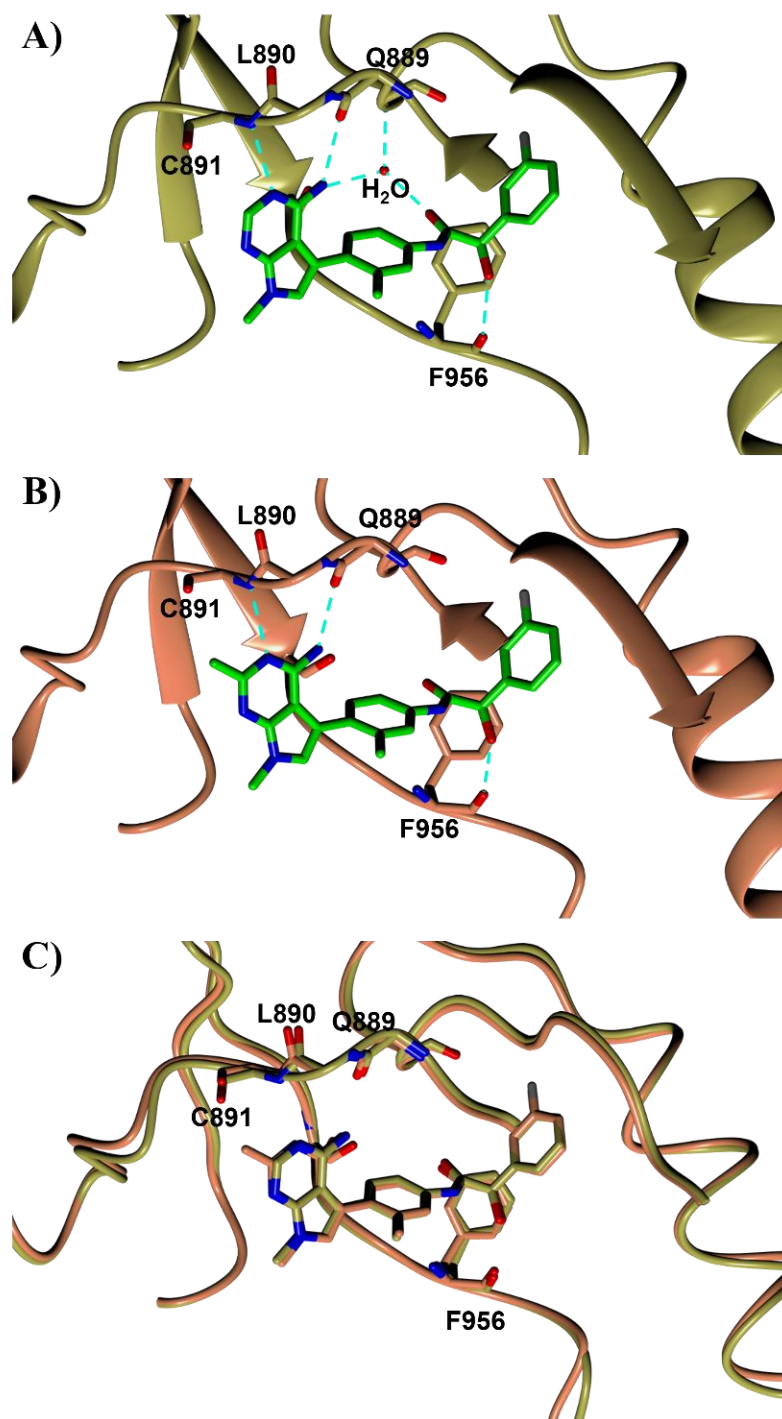
Table 2. Cont.

						PERK	p-eIF2 $\alpha$
Cmpd	R <sup>1</sup>	L	Ar	IC <sub>50</sub> ( $\mu$ M)	IC <sub>50</sub> ( $\mu$ M)		
30	Me			0.014	0.083		
31	Me			0.026	0.122		
32	Me			0.003	0.0078		
33	Me			0.003	0.014		
34	Me			0.0059	0.021		
35	Me			0.0059	0.017		
36	Me			0.008	0.325		
37	Me			>1	>10		
38	Me			0.0019	0.014		
39	Me			0.0026	0.011		
40	Me			0.0029	0.0085		
41	Me			0.0014	0.01		
42	Me			0.0042	0.032		
43	Me			0.052	0.562		
44	Me			0.017	0.129		
45	Me			0.019	0.165		

Previously reported SAR of PERK inhibitors have revealed modifications to the hinge binding region that have profound effects on binding affinity to PERK as well as selectivity versus the kinome [7,17]. Structure based design modelling was used to focus efforts on optimizing the pyrrolopyrimidine hinge-binding region of the molecule. Inhibitor **11** was co-crystallized with PERK into a trigonal space group P3<sub>2</sub>21 with comparable cell parameters as PDB 4X7O. Compound **11** formed three hydrogen bonds directly with the carbonyl of Q889, the amide of C891, and the carbonyl of F956 from PERK, respectively (Figure 1A). In addition, compound **11** forms two hydrogen bonds with a water molecule, and this molecule hydrogen bonds to the amide of V652. In the ATP binding hinge region, substitution at the C2-position (R1) of the pyrrolopyrimidine ring appeared feasible, filling a small pocket near C891. A methyl group located at the R1 position of compound **11** afforded analog **24** whose co-crystal structure with PERK confirmed the occupation of the small pocket near C891 along with the close contact of the C2-methyl group with the carbonyl of C891 with a distance of 3.14 Å (Figure 1B). Although a weak CH...O hydrogen bond is feasible, this contact appears to be more repulsive. As a result, a small rotation of the main chain amino acid Q889 and L890 of PERK, along with a minor shift of the pyrrolopyrimidine ring of inhibitor **24** are observed compared to those in the structure of **11** (Figure 1C). These shifts maintain the hydrogen bonds with similar distances. Due to a lower resolution (2.92Å) of the compound **24** structure (Table S1), the aforementioned water molecule in the compound **11** structure was not observed. This water molecule is assumed to locate at the same position, as all hydrogen bond donor and acceptor atoms are still presented at similar positions in the compound **24** structure. These observations indicate that the reduction of potency of **24** is likely caused by repulsion from the methyl group rather than the disruption of the hydrogen bonding pattern.

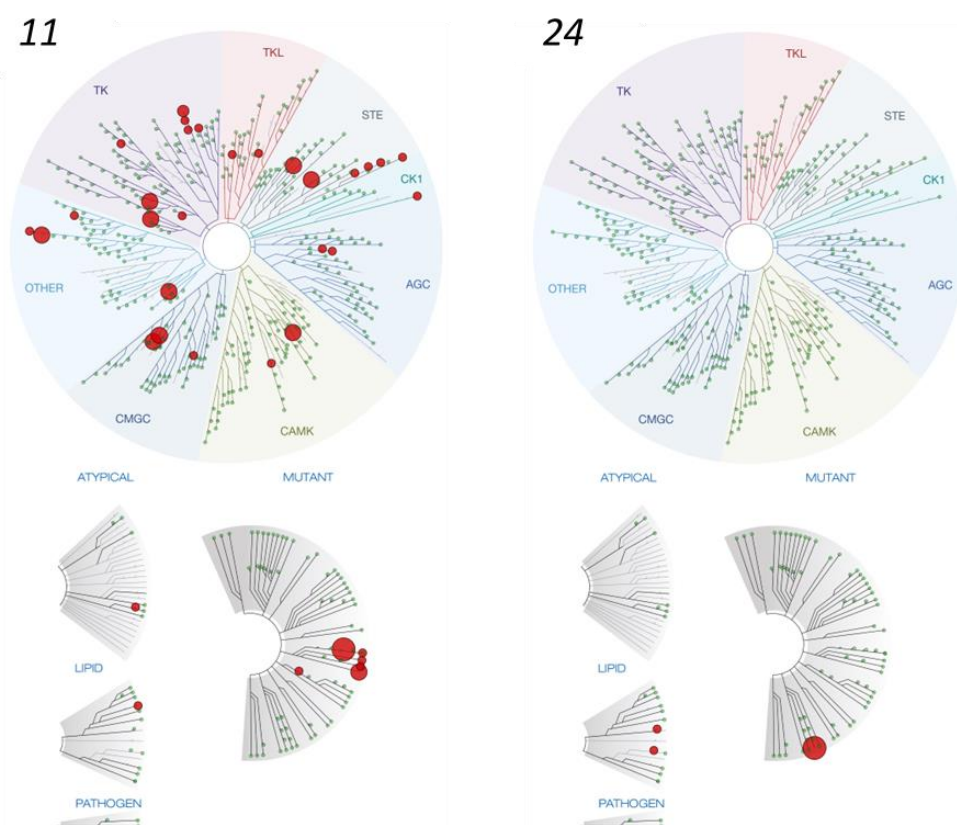
While having a minor effect on PERK potency, the methyl substituent on the pyrrolopyrimidine ring had a profound effect on the kinase selectivity. Compounds **11** and **24** were screened in the DiscoverX scanMAX<sup>SM</sup> panel of 468 kinases [26]. The resulting TREEspot<sup>TM</sup> interaction maps (Figure 2) revealed that the methyl substituent in **24** led to superior selectivity versus **11**. The S(35), S(10), and S(1) selectivity scores at a concentration of 1 µM were 0.005, 0, and 0 for **24** versus 0.072, 0.035, and 0 for **11**. Given the superior selectivity of **24** but slight loss in potency versus **11**, further optimization of the series was carried out with the 2-methyl substitution on the pyrrolopyrimidine ring to further improve potency and drug-like properties.

Exploration of the terminal aryl ring revealed several trends (Table 2): (1) Substitution at the 3-position was preferred to substitution at the 2-position of the ring (compare **24** vs. **25**, **26** vs. **27**, **28** vs. **29**, and **30** vs. **31**). (2) Lipophilic substituents, such as CF<sub>3</sub>, Cl, Br, CCH, CF<sub>2</sub>H, and *c*-Pr provided enhanced biochemical and cellular potency compared with F substitution (**24** vs. **26**, **28**, **33**, **32**, **34**, and **35**) leading to the recovery of the potency lost with the incorporation of the selectivity-enhancing 2-methyl pyrrolopyrimidine ring (compare **11** vs. **24** and **11** vs. **26**, **28**, **33**, and **32**). (3) Polar substituents were not well tolerated and resulted in substantially reduced cellular potency, as in the case of CN derivative **36**, or in complete loss of activity (biochemical and cellular activity at the concentrations tested), as in the case of sulfone analog **37**. (4) 3,5-Di-substitution with lipophilic groups provided further enhancements in potency (**38**, **39**, **40**, and **41**). Interestingly, addition of a fluorine substituent to CN on the terminal phenyl ring largely reversed the loss of cellular potency due to the CN group (**36** vs. **42**). (5) Replacement of the terminal phenyl ring with heterocycles, such as F-, Cl-, or CF<sub>3</sub>-substituted pyridines, resulted in 8- to 11-fold losses in cellular potency (compare **24** vs. **43**, **28** vs. **44**, and **26** vs. **45**).



**Figure 1.** Crystal structures of PERK with selected inhibitors **11** (A) and **24** (B). Overlay of the crystal structures of **11** and **24** (C). The same orientation is presented for all panels. The PERK backbone is shown as a ribbon or solid strand in yellow for **11** and coral for **24**. The side chains are depicted as cylinders in the same color as the main chain for carbon, blue for nitrogen, and red for oxygen atoms. Inhibitors are shown as cylinders with same color scheme except green for carbon in panels (A,B) and grey for fluorine. Hydrogen bonds are shown as cyan dashed lines.





**Figure 2.** The TREEspot™ interaction map of **11** and **24** assayed at 1000 nM in the 468-kinase scanMAXSM panel. The panel includes 403 unique wild-type kinases and 59 mutant isoforms. Note that PERK is not included in the TREEspot assay but was evaluated in separate biochemical assays. Complete tabulated results presented in Supplemental Table S2.

Next, the SAR of the proximal aryl ring was examined with new analogs incorporating the best substituted phenyl groups from the survey of the terminal aryl ring (3-F-Ph; 3-CF<sub>3</sub>-Ph; 3-Cl-Ph; 3-CH<sub>3</sub>-Ph; 3-Et-Ph; 3-F,5-CF<sub>3</sub>-Ph; and 3-F,5-CH<sub>3</sub>-Ph) was (Table 3). Replacement of the proximal ring methyl substituent with a F, Cl, or Et group was found to be well tolerated (**24** vs. **46**, **53**, and **59**). These changes to the proximal ring could be combined with modifications to the terminal ring to provide analogs with <5 nM biochemical and <15 nM cellular potency (**47**, **48**, **52**, **57**). Modest losses in cellular potency (2.5- to 4-fold) were observed for H and CF<sub>3</sub> methyl replacements on the proximal ring (**24** vs. **62** and **58**). More substantial reductions in potency (8- to 36-fold) occurred with CF<sub>3</sub>O and CH<sub>3</sub>O replacements (**24** vs. **61** and **60**). Addition of a fluorine substituent to the proximal ring of **24** resulted in the general maintenance of cellular potency with a 10-fold range in biochemical potency, depending upon the F regioisomer (**24** vs. **65**, **66**, and **67**). 3,5-Dimethyl proximal ring substitution (**68**) provided comparable in vitro potency to the 3-fluoro, 5-methyl analog **67**. Movement of the fluorine substituent from the 3-position of the proximal ring (**46**) to the 2-position (**69**) had little impact on the biochemical or cellular potency of the compounds. Addition of a second fluorine to the proximal ring of **46** similarly had little impact on the cellular potency of the compounds, although some variation in the biochemical data was observed (**46** vs. **70** and **71**). Replacement of the proximal phenyl ring of **24** with a pyridine ring resulted in modest (2- to 3-fold) losses in cellular potency (**24** vs. **72** and **74**). Some of the lost potency could be restored by replacing the terminal ring F with CF<sub>3</sub> (**73** vs. **72** and **75** vs. **74**). Replacement of the proximal phenyl ring of **24** with a pyrimidine ring was not tolerated, resulting in a 30-fold loss in biochemical potency and complete loss in cellular activity (**24** vs. **76**).

**Table 3.** In vitro data of PERK inhibitors with proximal and terminal ring modifications.

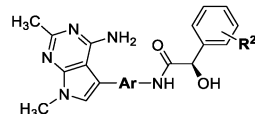
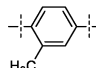
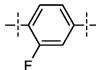
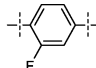
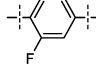
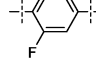
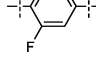
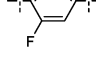
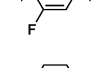
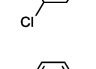
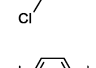
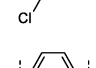
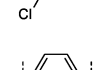
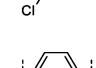
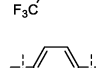
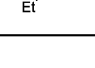
Cmpd No.			PERK IC <sub>50</sub> (μM)	p-eIF2α IC <sub>50</sub> (μM)
	Ar	R <sup>2</sup>		
24		3-F	0.020	0.051
46		3-F	0.0022	0.041
47		3-CF <sub>3</sub>	0.0051	0.011
48		3-Cl	0.0010	0.010
49		3-Me	0.0011	0.017
50		3-Et	0.0009	0.025
51		3-F, 5-CF <sub>3</sub>	0.0027	0.062
52		3-F, 5-Me	0.0011	0.011
53		3-F	0.017	0.056
54		3-CF <sub>3</sub>	0.0027	0.021
55		3-Cl	0.0016	0.017
56		3-Me	0.0041	0.018
57		3-Et	0.059	0.014
58		3-F	0.0085	0.204
59		3-F	0.0040	0.041

Table 3. Cont.

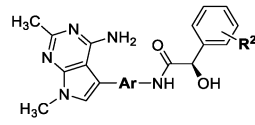
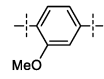
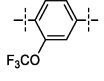
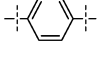
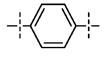
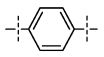
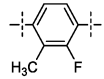
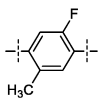
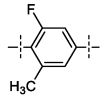
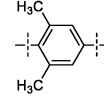
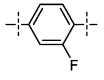
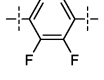
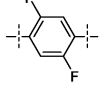
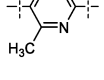
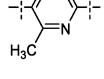
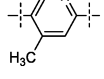
Cmpd No.			PERK IC <sub>50</sub> (μM)	p-eIF2α IC <sub>50</sub> (μM)
	Ar	R <sup>2</sup>		
60		3-F	0.236	1.85
61		3-F	0.023	0.435
62		3-F	0.0020	0.126
63		3-CF <sub>3</sub>	0.0028	0.013
64		3-Br	0.0015	0.014
65		3-F	0.0019	0.030
66		3-F	0.011	0.042
67~		3-F	0.022	0.078
68~		3-F	0.013	0.082
69		3-F	0.0010	0.026
70		3-F	0.0015	0.024
71~		3-F	0.0010	0.034
72		3-F	0.017	0.105
73		3-CF <sub>3</sub>	0.013	0.051
74		3-F	0.0083	0.146

Table 3. Cont.

Cmpd No.			PERK IC <sub>50</sub> (μM)	p-eIF2α IC <sub>50</sub> (μM)
	Ar	R <sup>2</sup>		
75		3-CF <sub>3</sub>	0.0068	0.095
76		3-F	0.647	>10

~Racemic mixture of alcohols.

The SAR campaign successfully identified a number of PERK inhibitors that demonstrated biochemical and cellular potency. These promising compounds were evaluated in vitro ADME assays (aqueous solubility, Caco-2 permeability, plasma protein binding, and hepatocyte stability) to determine their drug-like properties (Table 4). In general, the compounds showed moderate kinetic aqueous solubility in PBS at pH 7.4, ranging from 10–66 μM. The Caco-2 permeability was found to be high for all compounds ( $P_{app} \geq 9 \times 10^{-6}$  cm/s), predicting good oral absorption. Additionally, with the exception of **24** (efflux ratio of 5.2), the compounds showed little to no efflux. Plasma protein binding was found to be high across all species tested, a characteristic common for many kinase inhibitors.

Table 4. Solubility, permeability, plasma protein binding and hepatocyte clearance properties of selected PERK inhibitors.

Cmpd No.	Kinetic Aqueous Solubility (μM)	Caco-2		Plasma Protein Binding				Hepatocyte Clearance (t <sub>1/2</sub> min)			
		P <sub>app</sub> (A→B) (10 <sup>-6</sup> cm/s)	Efflux Ratio	Human	Rat	Mouse	Dog	Human	Rat	Mouse	Dog
26	19	21	2.2	99.8 ± 0.0	99.8 ± 0.0	99.9 ± 0.0	99.5 ± 0.0	194	166	118	130
28	35	23	1.9	99.8 ± 0.1	99.7 ± 0.0	>99.9	98.3 ± 0.3	778	27	62	355
65	58	26	1.6	99.6 ± 0.1	98.9 ± 0.0	99.3 ± 0.2	98.7 ± 0.1	390	22	64	567
24	76	9	5.2	99.2 ± 0.2	99.1 ± 0.2	99.4 ± 0.0	97.0 ± 0.4	733	23	31	>1000
41	24	20	2.5	99.6 ± 0.2	99.5 ± 0.2	99.9 ± 0.0	98.8 ± 0.3	68	16	24	232
39	10	16	2.0	99.9 ± 0.0	99.9 ± 0.0	>99.9	>99.9	277	252	320	223
38	19	19	1.9	99.0 ± 0.1	99.1 ± 0.3	99.2 ± 0.3	98.4 ± 0.1	897	121	805	460
48	14	24	1.6	99.9 ± 0.0	99.6 ± 0.0	99.8 ± 0.0	99.6 ± 0.1	556	25	53	215
66	61	24	1.5	99.3 ± 0.2	98.6 ± 0.1	98.8 ± 0.2	98.2 ± 0.2	358	13	167	39
70	66	29	1.7	99.4 ± 0.0	99.3 ± 0.1	99.7 ± 0.1	99.4 ± 0.1	360	15	45	268

In vitro metabolic stability was assessed in human, rat, mouse, and dog hepatocytes. In general, the compounds were found to be relatively stable in human and dog hepatocytes and exhibited long half-lives. For several compounds (**28**, **65**, **24**, **41**, **66**, and **70**), stability was reduced in rodent hepatocytes, particularly rat. Compounds with alkyl groups (i.e., Me) on the terminal phenyl ring tended to have lower stability (**41** vs. **39**). Several compounds (**26**, **39**, and **38**) maintained good metabolic stability across all species tested.

To connect the *in vitro* ADME results with the *in vivo* setting, select compounds (**26**, **28**, **65**, **24**, **41**, **39**, **38**, **48**, **66**, and **70**) were examined in mouse PK studies (Table 5). All of the compounds showed robust oral exposure with  $C_{\max}$  values for most compounds >8000 ng/mL and  $AUC_{0-\text{last}}$  values >25,000 h·ng/mL. The compounds also showed good *in vivo* half-lives of 2–3.5 h and excellent bioavailability ( $\geq 70\%$ ) apart from compound **41**. Compound **26** stood out with a particularly attractive pharmacokinetics profile with  $C_{\max}$  of 17,200 ng/mL,  $AUC_{0-\text{last}}$  of 126,019 h·ng/mL, half-life of 3.5 h, and bioavailability of 82%, a significant improvement over our earlier analog **24** and was therefore chosen as one of the key leads in this series PERK inhibitors.

**Table 5.** *In vivo* pharmacokinetics (PK) properties of selected PERK inhibitors in mice. Compounds administered at 10 mg/kg by oral gavage (PO).

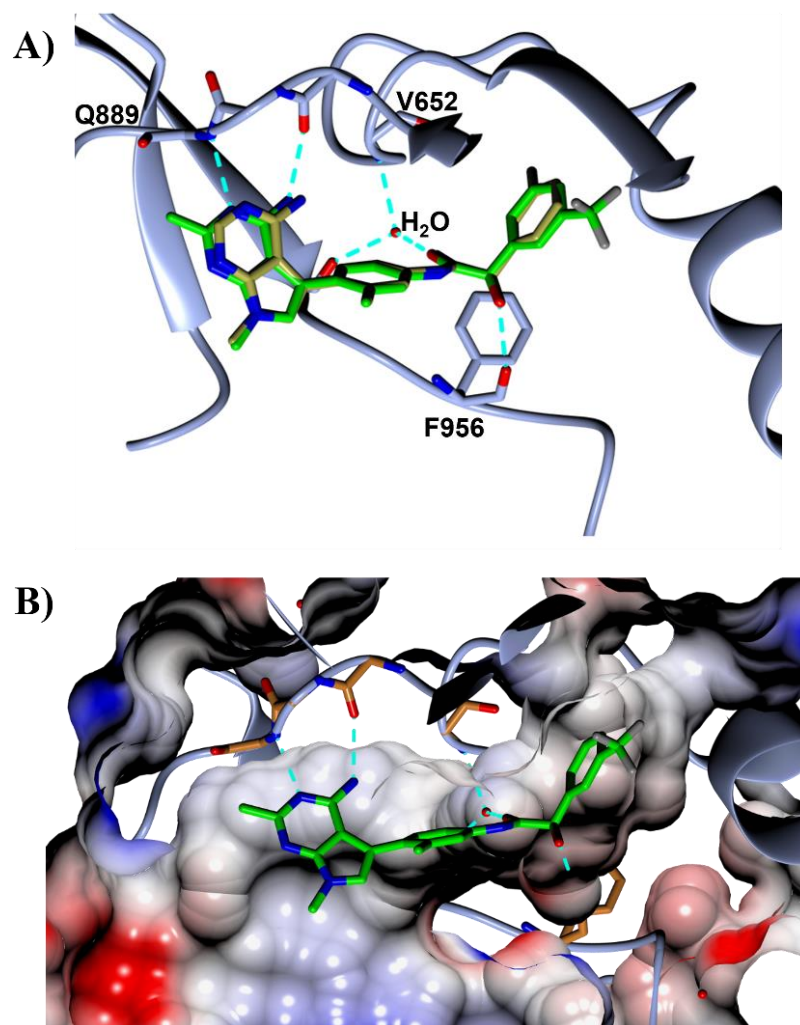
Compound	$C_{\max}$ (ng/mL)	$AUC_{0-\text{last}}$ (h·ng/mL)	$t_{1/2}$ (h)	F (%)
<b>26</b>	17,200	126,019	3.5	82
<b>28</b>	14,067	65,764	2.4	84
<b>65</b>	8150	40,105	2.2	129
<b>24</b>	13,100	37,495	2.1	77
<b>41</b>	12,467	26,010	2.7	40
<b>39</b>	14,300	86,444	2.9	78
<b>38</b>	8597	28,932	2.0	94
<b>48</b>	3017	10,889	2.1	70
<b>66</b>	9610	39,835	2.0	126
<b>70</b>	9723	32,258	2.0	117

Inhibitor **26** was co-crystallized with PERK into a trigonal space group  $P3_221$  with comparable cell parameters as previously noted with compounds **11** and **24**. Replacement of the 3-fluorine on the terminal phenyl group in **11** and **24** and with a larger  $CF_3$  group in **26** induces a flip in the phenyl ring since the enzyme position containing the fluorine cannot accommodate the bulkier  $CF_3$  group (Figures 1 and 3). The fluorine atom of **24** forms four contacts with a distance of 3.8 Å or less with residues within the back pocket region of PERK, whereas the  $CF_3$  group of **26** forms ten contacts with PERK. These extra contacts may stabilize the binding of **26** to PERK and explain the increased potency of **26** compared to **24**.

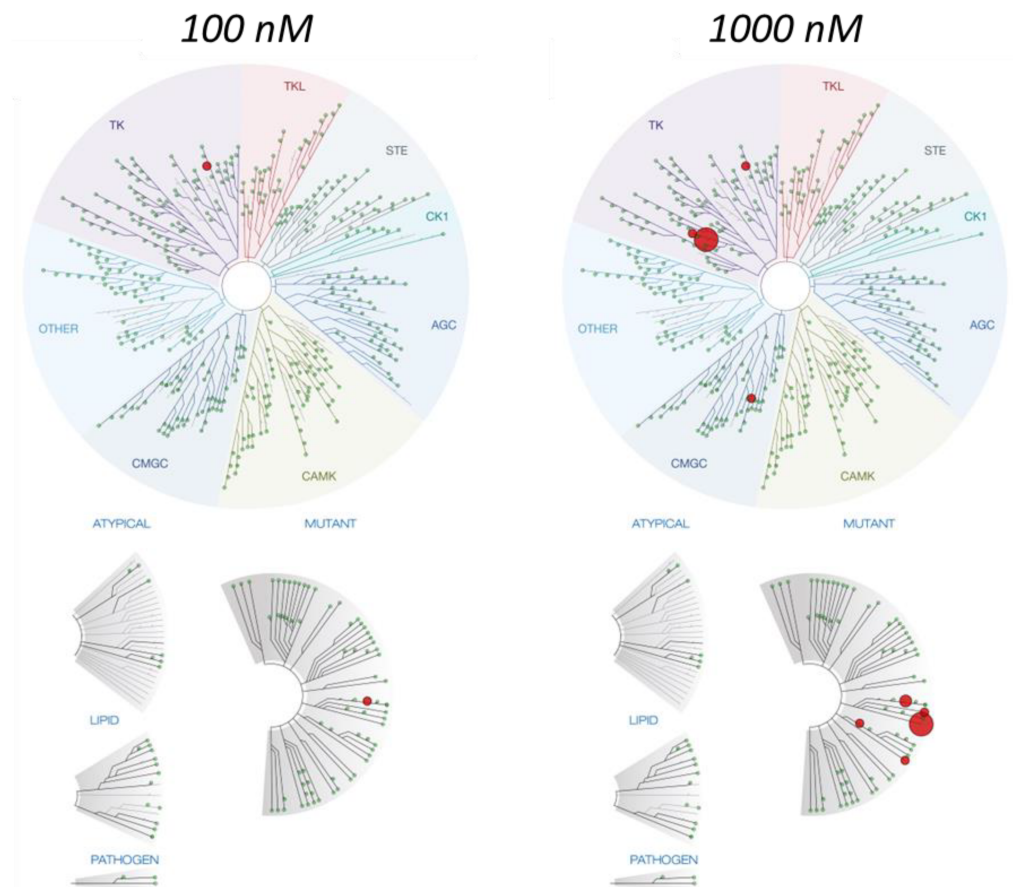
Compound **26** was found to have excellent selectivity in the DiscoverX kinase panel (Figure 4; Supplemental Table S2) comparable to that of compound **24**. The  $S(35)$ ,  $S(10)$ , and  $S(1)$  selectivity scores at a concentration of 1  $\mu\text{M}$  were 0.01, 0.002, and 0.002. Importantly, **26** demonstrated potent selectivity for PERK over the other three highly conserved ISR kinases (GCN2, HRI, and PKR; Supplemental Table S3). In biochemical assays, the  $IC_{50}$  of **26** against PERK was 4.7 nM, compared to  $IC_{50}$  values greater than 10  $\mu\text{M}$  for each of the other ISR kinases. The primary off-target activity of **26** was associated with FLT3 kinase and its mutant isoforms. Radiometric kinase assays were used to validate the kinome panel and determine the relative  $IC_{50}$  value of **26** against wild-type FLT3 and a mutant isoform (D835Y). When evaluated individually using concentrations of **26** up to 10  $\mu\text{M}$ , the relative  $IC_{50}$  against wild-type FLT3 was >1  $\mu\text{M}$ , and >10  $\mu\text{M}$  against the mutant variant FLT3 (D385Y), indicating weak to no activity against FLT3wt or the mutant form (Supplemental Table S3).

To understand the effect of **26** in target organs, the PK/PD relationship of **26** was investigated in mouse pancreas. PK analysis of plasma and pancreas samples from mice treated with **26** revealed dose-proportionate exposure at doses ranging from 0.3 to 30 mg/kg following a single administration by oral gavage (Supplemental Figure S2). Pancreas tissue was sampled to evaluate the effect of **26** on PERK autophosphorylation in pancreas, following oral administration of **26** at 0.3, 1, 3, 10, and 30 mg/kg. At 1 h following administration, phosphoPERK (T980), relative to total PERK protein (pPERK/PERK) decreased in a dose-dependent manner, reaching approximately 80% inhibition at 30 mg/kg (Figure 5A). When PERK inhibition was evaluated across time in mouse pancreas, a dose-dependent

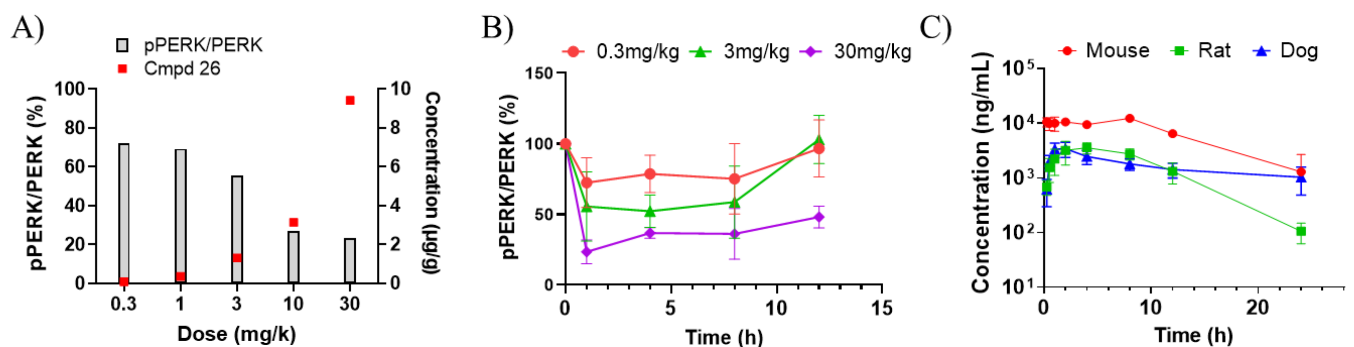
inhibition was observed which was relatively stable across a 12 h period following administration of **26** (Figure 5B). This observation was consistent with the dose-proportionate exposure and low clearance rate of **26** observed in both mouse plasma and pancreas (Supplemental Figure S2). To confirm that the PK profile of **26** in other species was suitable to enable further development, plasma concentration of **26** was quantified in mouse, rat and dog following a single oral administration at 10 mg/kg. Consistent with observations in mice, rat and dog both shared similar clearance rates as mouse, albeit with different exposure levels following administration (Figure 5C).



**Figure 3.** Crystal structure of compound **26** bound to the PERK kinase domain. (A) View of **26** in the PERK active site. PERK backbone is shown as a blue ribbon, and the side chains are shown as cylinder in brown for carbon, blue for nitrogen, and red for oxygen atoms, respectively. Compound **26** is shown as cylinder with same color scheme except green for carbon and grey for fluorine. Compound **11** is shown in a similar manner to compound **26**, except the color gold is used for carbon atoms. Hydrogen bonds for **26** are shown as cyan dashed lines. The phenyl ring is flipped due to a replacement of the 3-fluorine in **11** to CF<sub>3</sub> in **26**. (B) View of **26** in the PERK active site with surface rendering. The color intensity corresponds to the calculated electrostatic potential, from  $-20$  kT/e (red) to  $+20$  kT/e (blue).

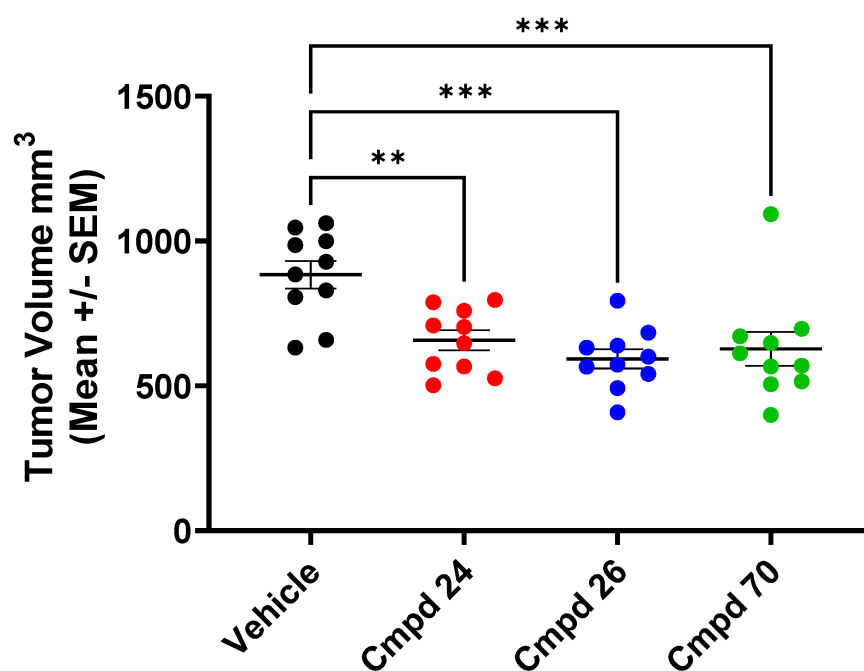


**Figure 4.** The TREEspot™ interaction map of compound **26** in the 468-kinase scanMAXSM panel at 100 and 1000 nM. The panel includes 403 unique wild-type kinases and 59 mutant isoforms. Note that PERK is not included in the TREEspot assay. Complete tabulated results presented in Supplemental Table S2.



**Figure 5.** In vivo PK/PD analysis of **26**. (A) Inhibition of pPERK relative to total PERK protein (pPERK/PERK) in pancreas following oral administration of **26**. Abundance of **26** quantified by LC-MS/MS from matching pancreas samples at C<sub>max</sub> (1 h post administration). (B) Inhibition of pPERK/PERK in pancreas following oral administration of **26** at 0.3, 3, or 30 mg/kg. Pancreas samples taken at 1, 4, 8, 12 h following oral administration of **26**. Data represent mean ± SD of four mice. (C) Plasma PK analysis of **26** in mouse, rat and dog. **26** administered orally at 10 mg/kg, and sampled across a 24-h period; **26** quantified by LC-MS/MS.

As the focus of this program was to develop a novel, highly potent, selective and orally bioavailable PERK inhibitor to probe the role of PERK biology in animal models, compounds **24**, **26** and **70** were tested for in vivo efficacy in a clear cell renal cell carcinoma (ccRCC) xenograft model, 786-O (Figure 6). The 786-O model is driven by the Von Hippel-Lindau (VHL) mutation, which leads to PERK pathway activation and is therefore a suitable model to assess the biological activity of these PERK inhibitors [17]. The compounds were dosed at 30 mg/kg, twice per day (BID) for 29 days and were well tolerated as determined by body weight measurement (Supplemental Figure S3). Treatment with pyrrolopyrimidine PERK inhibitors resulted in significant tumor growth inhibition that was in line with our previously reported aminopyridine series of PERK inhibitors [7].



**Figure 6.** PERK inhibitors **24**, **26** and **70** inhibit tumor growth of 786-O RCC xenografts. Animals were treated at 30 mg/kg BID dosing for 29 days. Statistical analysis of group means by one-way ANOVA (\*\*  $p < 0.01$ , \*\*\*  $p < 0.001$ ).

In summary, we have developed a novel class of potent pyrrolopyrimidine PERK inhibitors with excellent ADME and PK/PD properties. Robust kinase selectivity was achieved with substitution on the pyrrolopyrimidine hinge binder region driving kinase selectivity, with a methyl substitution at the 2-position of the ring resulting in exquisite selectivity for PERK over other kinases. Further optimization of the 2-methyl substituted analogs led to identification of lead molecule **26** that retained excellent potency and selectivity and had good in vitro metabolic stability across all species tested. When **26** was evaluated in vivo, high  $AUC_{last}$  values and a flat, sustained plasma exposure profile were observed in mouse plasma and pancreas tissue. A single administration of **26** resulted in stable PERK inhibition across a 12 h period in mouse pancreas. These characteristics led to the selection of **26** for further development, and evaluation in animal models is ongoing.



**Supplementary Materials:** The following supporting information can be downloaded at: <https://www.mdpi.com/article/10.3390/pharmaceutics14102233/s1>, Supplemental Table S1: Crystallography data collection and refinement statistics; Supplemental Table S2: scanMAXSM Kinome Assay Results; Supplemental Table S3: Potency of Cmpd **26** against four ISR kinases and two FLT3 isoforms; Supplemental Figure S1: Compound **26** is selective against cell lines driven by FLT3-ITD; Supplemental Figure S2: In vivo PK in plasma and pancreas; Supplemental Figure S3: Compound **26** slows growth of 786-O RCC tumor xenografts; Supplemental Scheme S1: Synthesis of (*R*)-*N*-(4-(4-amino-7-methyl-7*H*-pyrrolo[2,3-*d*]pyrimidin-5-yl)-3-methylphenyl)-2-(3-fluorophenyl)-2-hydroxyacetamide (**11**) and (*S*)-*N*-(4-(4-amino-7-methyl-7*H*-pyrrolo[2,3-*d*]pyrimidin-5-yl)-3-methylphenyl)-2-(3-fluorophenyl)-2-hydroxyacetamide (**12**); Supplemental Scheme S2: Synthesis of (*S*)-*N*-(4-(4-amino-2,7-dimethyl-7*H*-pyrrolo[2,3-*d*]pyrimidin-5-yl)-2,3-difluorophenyl)-2-(3-fluorophenyl)-2-hydroxyacetamide (**96**) and (*R*)-*N*-(4-(4-amino-2,7-dimethyl-7*H*-pyrrolo[2,3-*d*]pyrimidin-5-yl)-2,3-difluorophenyl)-2-(3-fluorophenyl)-2-hydroxyacetamide (**70**); Supplemental Scheme S3: Synthesis of (*S*)-*N*-(4-(4-amino-2,7-dimethyl-7*H*-pyrrolo[2,3-*d*]pyrimidin-5-yl)-3-fluorophenyl)-2-hydroxy-2-(3-(trifluoromethyl)phenyl)acetamide (**106**) and (*R*)-*N*-(4-(4-amino-2,7-dimethyl-7*H*-pyrrolo[2,3-*d*]pyrimidin-5-yl)-3-fluorophenyl)-2-hydroxy-2-(3-(trifluoromethyl)phenyl)acetamide (**47**). References [7,17,20–25,27] are cited in the supplementary materials.

**Author Contributions:** Conceptualization, M.J.M., A.C.R., M.E.S. and M.D.S.; methodology, M.J.M., M.E.S., J.G., M.B., V.C., D.S., A.-H.L. and M.D.S.; formal analysis, M.D.S., M.E.S., D.S. and V.C.; investigation, M.E.S., V.C., G.Z., M.B. and J.G.; resources, A.C.R. and M.J.M.; data curation, G.Z. and M.D.S.; writing—original draft preparation, M.J.M., M.E.S., M.D.S. and V.C.; writing—review and editing, M.E.S., M.J.M. and M.D.S.; visualization, H.D. and G.Z.; supervision, A.C.R., M.J.M., M.E.S., J.G., M.B. and M.D.S.; funding acquisition, A.C.R. and M.J.M. All authors have read and agreed to the published version of the manuscript.

**Funding:** All laboratory work was funded by HiberCell Inc.

**Institutional Review Board Statement:** All the procedures related to animal handling, care, and the treatment in this study were performed according to guidelines approved by the Institutional Animal Care and Use Committee (IACUC) of Pharmaron following the guidance of the Association for Assessment and Accreditation of Laboratory Animal Care (AAALAC). All animal studies were approved and carried out in accordance with Pharmaron's Institutional Animal Care and Use Committee, protocol ON-TOL-09012021 approved on 26 March 2021.

**Data Availability Statement:** Coordinates and structural factors have been deposited in the PDB under codes 8EQ9 (Compound **11**), 8EQD (Compound **24**), and 8EQE (Compound **26**).

**Acknowledgments:** We acknowledge the support of Advanced Photon Source beam lines IMCA-CAT and GMCA-CAT. The use of the IMCA-CAT beamline 17-ID at APS was supported by the companies of the Industrial Macromolecular Crystallography Association through a contract with the Hauptman-Woodward Medical Research Institute. GM/CA@APS has been funded in whole or in part with Federal funds from the NCI, National Institutes of Health, Grant ACB-12002 and NIGMS, National Institutes of Health Grant AGM-12006. This research used resources of the Advanced Photon Source, a United States Department of Energy (DOE) Office of Science User Facility operated for the DOE Office of Science by Argonne National Laboratory under Contract DE-AC02-06CH11357. We also thank Arie Zask for reviewing the manuscript and sharing thoughtful editorial feedback. HiberCell would like to thank and acknowledge the chemists at Curia, Hyderabad: Srikanth Malibhatla, Madhavarao Bandaru, Prabhakara Reddy Goluguri, Satyanarayana Yatam, Ravi Adarasandi, Madhusudhan Velmala, Durga Rama Prasad Singireddi, Mahendar Velpuri, Bhaskar Reddy Nareddy, Visweswara Sastry, Chiranjeevi Mandati, Kumaraswamy Battula, Rajashekar Reddy Chittem, Sujatha Kanuganti, Shapi Siddiqui, and Subir Sadhukhan. The authors would also like to thank technical assistance by Elena Chad, Jennifer Wolfley, Richard Miller, Kirsten Feldman, Brent Weins, and Mary Koszelak-Rosenblum.

**Conflicts of Interest:** At the time of execution, M.E.S., V.C., D.S., A.-H.L., A.C.R. and M.J.M. were employed by HiberCell Inc. As such, HiberCell was involved in all aspects of this work, including conceptualization and methodology, investigation, data analysis, resources, and writing of this manuscript. Curia Global is a contract research organization engaged by HiberCell Inc to support chemical synthesis and characterization of novel molecules. At the time of experimentation, M.D.S., M.B., J.G. and G.Z. were employed by Curia Global, which was involved in conceptualization, methodology, resources, data analysis and manuscript composition. Pharmaron Co. Ltd. is a contract research organization engaged by HiberCell to support chemical characterization of novel compounds. At the time of experimentation, H.D. was employed by Pharmaron, which was involved in data visualization and manuscript composition.

## References

- Hetz, C.; Zhang, K.; Kaufman, R.J. Mechanisms, regulation and functions of the unfolded protein response. *Nat. Rev. Mol. Cell Biol.* **2020**, *21*, 421–438. [CrossRef] [PubMed]
- Walter, P.; Ron, D. The Unfolded Protein Response: From Stress Pathway to Homeostatic Regulation. *Science* **2011**, *334*, 1081–1086. [CrossRef]
- Hetz, C. The unfolded protein response: Controlling cell fate decisions under ER stress and beyond. *Nat. Rev. Mol. Cell Biol.* **2012**, *13*, 89–102. [CrossRef] [PubMed]
- Mann, M.J.; Hendershot, L.M. UPR activation alters chemosensitivity of tumor cells. *Cancer Biol. Ther.* **2006**, *5*, 736–740. [CrossRef] [PubMed]
- Ma, Y.; Hendershot, L.M. The role of the unfolded protein response in tumour development: Friend or foe? *Nat. Rev. Cancer* **2004**, *4*, 966–977. [CrossRef] [PubMed]
- Avril, T.; Vauléon, E.; Chevet, E. Endoplasmic reticulum stress signaling and chemotherapy resistance in solid cancers. *Oncogenesis* **2017**, *6*, e373. [CrossRef] [PubMed]
- Calvo, V.; Surguladze, D.; Li, A.-H.; Surman, M.D.; Malibhatla, S.; Bandaru, M.; Jonnalagadda, S.K.; Adarasandi, R.; Velmala, M.; Singireddi, D.R.P.; et al. Discovery of 2-amino-3-amido-5-aryl-pyridines as highly potent, orally bioavailable, and efficacious PERK kinase inhibitors. *Bioorg. Med. Chem. Lett.* **2021**, *43*, 128058. [CrossRef] [PubMed]
- Atkins, C.; Liu, Q.; Minthorn, E.; Zhang, S.-Y.; Figueroa, D.J.; Moss, K.; Stanley, T.B.; Sanders, B.; Goetz, A.; Gaul, N.; et al. Characterization of a Novel PERK Kinase Inhibitor with Antitumor and Antiangiogenic Activity. *Cancer Res.* **2013**, *73*, 1993–2002. [CrossRef] [PubMed]
- Oakes, S.A.; Papa, F.R. The Role of Endoplasmic Reticulum Stress in Human Pathology. *Annu. Rev. Pathol. Mech. Dis.* **2015**, *10*, 173–194. [CrossRef]
- Sharma, R.B.; Landa-Galván, H.V.; Alonso, L.C. Living Dangerously: Protective and Harmful ER Stress Responses in Pancreatic  $\beta$ -Cells. *Diabetes* **2021**, *70*, 2431–2443. [CrossRef] [PubMed]
- Brozzi, F.; Eizirik, D.L. ER stress and the decline and fall of pancreatic beta cells in type 1 diabetes. *Upsala J. Med. Sci.* **2016**, *121*, 133–139. [CrossRef] [PubMed]
- Marré, M.L.; James, E.A.; Piganelli, J.D.  $\beta$  cell ER stress and the implications for immunogenicity in type 1 diabetes. *Front. Cell Dev. Biol.* **2015**, *3*, 67. [CrossRef] [PubMed]
- Marhfour, I.; Lopez, X.M.; Lefkaditis, D.; Salmon, I.; Allagnat, F.; Richardson, S.J.; Morgan, N.G.; Eizirik, D.L. Expression of endoplasmic reticulum stress markers in the islets of patients with type 1 diabetes. *Diabetologia* **2012**, *55*, 2417–2420. [CrossRef] [PubMed]
- Tersey, S.A.; Nishiki, Y.; Templin, A.T.; Cabrera, S.M.; Stull, N.D.; Colvin, S.C.; Evans-Molina, C.; Rickus, J.L.; Maier, B.; Mirmira, R.G. Islet  $\beta$ -Cell Endoplasmic Reticulum Stress Precedes the Onset of Type 1 Diabetes in the Nonobese Diabetic Mouse Model. *Diabetes* **2012**, *61*, 818–827. [CrossRef] [PubMed]
- Zhang, P.; McGrath, B.; Li, S.; Frank, A.; Zambito, F.; Reinert, J.; Gannon, M.; Ma, K.; McNaughton, K.; Cavener, D.R. The PERK Eukaryotic Initiation Factor 2 $\alpha$  Kinase Is Required for the Development of the Skeletal System, Postnatal Growth, and the Function and Viability of the Pancreas. *Mol. Cell. Biol.* **2002**, *22*, 3864–3874. [CrossRef] [PubMed]
- Harding, H.P.; Zeng, H.; Zhang, Y.; Jungries, R.; Chung, P.; Plesken, H.; Sabatini, D.D.; Ron, D. Diabetes Mellitus and Exocrine Pancreatic Dysfunction in Perk $^{-/-}$  Mice Reveals a Role for Translational Control in Secretory Cell Survival. *Mol. Cell* **2001**, *7*, 1153–1163. [CrossRef]
- Smith, A.L.; Andrews, K.L.; Beckmann, H.; Bellon, S.F.; Beltran, P.J.; Booker, S.; Chen, H.; Chung, Y.-A.; D'Angelo, N.D.; Dao, J.; et al. Discovery of 1H-Pyrazol-3(2H)-ones as Potent and Selective Inhibitors of Protein Kinase R-like Endoplasmic Reticulum Kinase (PERK). *J. Med. Chem.* **2015**, *58*, 1426–1441. [CrossRef] [PubMed]
- Ayala-Aguilera, C.C.; Valero, T.; Lorente-Macías, Á.; Baillache, D.J.; Croke, S.; Unciti-Broceta, A. Small Molecule Kinase Inhibitor Drugs (1995–2021): Medical Indication, Pharmacology, and Synthesis. *J. Med. Chem.* **2021**, *65*, 1047–1131. [CrossRef]
- Xing, L.; Klug-Mcleod, J.; Rai, B.; Lunney, E.A. Kinase hinge binding scaffolds and their hydrogen bond patterns. *Bioorg. Med. Chem.* **2015**, *23*, 6520–6527. [CrossRef] [PubMed]

20. Winter, G.; Waterman, D.G.; Parkhurst, J.M.; Brewster, A.S.; Gildea, R.J.; Gerstel, M.; Fuentes-Montero, L.; Vollmar, M.; Michels-Clark, T.; Young, I.D.; et al. *DIALS*: Implementation and evaluation of a new integration package. *Acta Crystallogr. Sect. D Struct. Biol.* **2018**, *74 Pt 2*, 85–97. [CrossRef]
21. Evans, P.R.; Murshudov, G.N. How good are my data and what is the resolution? *Acta Crystallogr. Sect. D Biol. Crystallogr.* **2013**, *69 Pt 7*, 1204–1214. [CrossRef] [PubMed]
22. McCoy, A.J.; Grosse-Kunstleve, R.W.; Adams, P.D.; Winn, M.D.; Storoni, L.C.; Read, R.J. Phaser crystallographic software. *J. Appl. Crystallogr.* **2007**, *40 Pt 4*, 658–674. [CrossRef] [PubMed]
23. Emsley, P.; Lohkamp, B.; Scott, W.G.; Cowtan, K. Features and development of Coot. *Acta Crystallogr. Sect. D Biol. Crystallogr.* **2010**, *66 Pt 4*, 486–501. [CrossRef]
24. Murshudov, G.N.; Skubák, P.; Lebedev, A.A.; Pannu, N.S.; Steiner, R.A.; Nicholls, R.A.; Winn, M.D.; Long, F.; Vagin, A.A. REFMAC5 for the refinement of macromolecular crystal structures. *Acta Crystallogr. Sect. D Biol. Crystallogr.* **2011**, *67 Pt 4*, 355–367. [CrossRef]
25. McNicholas, S.; Potterton, E.; Wilson, K.S.; Noble, M.E.M. Presenting your structures: TheCCP4mgmolecular-graphics software. *Acta Crystallogr. Sect. D Biol. Crystallogr.* **2011**, *67 Pt 4*, 386–394. [CrossRef] [PubMed]
26. Fabian, M.A.; Biggs, W.H., III; Treiber, D.K.; Atteridge, C.E.; Azimioara, M.D.; Benedetti, M.G.; Carter, T.A.; Ciceri, P.; Edeen, P.T.; Floyd, M.; et al. A small molecule–kinase interaction map for clinical kinase inhibitors. *Nat. Biotechnol.* **2005**, *23*, 329–336. [CrossRef]
27. Williams, C.J.; Headd, J.J.; Moriarty, N.W.; Prisant, M.G.; Videau, L.L.; Deis, L.N.; Verma, V.; Keedy, D.A.; Hintze, B.J.; Chen, V.B.; et al. MolProbity: More and better reference data for improved all-atom structure validation. *Protein Sci.* **2018**, *27*, 293–315. [CrossRef] [PubMed]

Review

# Heterocyclic Compounds as Hsp90 Inhibitors: A Perspective on Anticancer Applications

Mina Ardestani <sup>1</sup>, Zahra Khorsandi <sup>1</sup>, Fariba Keshavarzipour <sup>1</sup>, Siavash Iravani <sup>2</sup>, Hojjat Sadeghi-Aliabadi <sup>1,\*</sup> and Rajender S. Varma <sup>3,\*</sup>

<sup>1</sup> Pharmaceutical Sciences Research Center, School of Pharmacy and Pharmaceutical Sciences, Isfahan University of Medical Sciences, Isfahan 81746-73461, Iran

<sup>2</sup> School of Pharmacy and Pharmaceutical Sciences, Isfahan University of Medical Sciences, Isfahan 81746-73461, Iran

<sup>3</sup> Regional Centre of Advanced Technologies and Materials, Czech Advanced Technology and Research Institute, Palacký University in Olomouc, Šlechtitelů 27, 783 71 Olomouc, Czech Republic

\* Correspondence: sadeghi@pharm.mui.ac.ir (H.S.-A.); varma.rajender@epa.gov (R.S.V.)

**Abstract:** Heat shock proteins (Hsps) have garnered special attention in cancer therapy as molecular chaperones with regulatory/mediatory effects on folding, maintenance/stability, maturation, and conformation of proteins as well as their effects on prevention of protein aggregation. Hsp90 ensures the stability of various client proteins needed for the growth of cells or the survival of tumor cells; therefore, they are overexpressed in tumor cells and play key roles in carcinogenesis. Accordingly, Hsp90 inhibitors are recognized as attractive therapeutic agents for investigations pertaining to tumor suppression. Natural Hsp90 inhibitors comprising geldanamycin (GM), reclaimed analogs of GM including 17-AAG and DMAG, and radicicol, a natural macrocyclic antifungal, are among the first potent Hsp90 inhibitors. Herein, recently synthesized heterocyclic compounds recognized as potent Hsp90 inhibitors are reviewed along with the anticancer effects of heterocyclic compounds, comprising purine, pyrazole, triazine, quinolines, coumarin, and isoxazoles molecules.

**Keywords:** Hsp90 inhibitor; co-chaperone; heterocycle molecules; anticancer agents; heat shock proteins

**Citation:** Ardestani, M.; Khorsandi, Z.; Keshavarzipour, F.; Iravani, S.; Sadeghi-Aliabadi, H.; Varma, R.S.

Heterocyclic Compounds as Hsp90 Inhibitors: A Perspective on Anticancer Applications.

*Pharmaceutics* **2022**, *14*, 2220.

<https://doi.org/10.3390/pharmaceutics14102220>

Academic Editor: Ja-Hyoung Ryu

Received: 6 September 2022

Accepted: 17 October 2022

Published: 18 October 2022

**Publisher's Note:** MDPI stays neutral with regard to jurisdictional claims in published maps and institutional affiliations.



**Copyright:** © 2022 by the authors. Licensee MDPI, Basel, Switzerland. This article is an open access article distributed under the terms and conditions of the Creative Commons Attribution (CC BY) license (<https://creativecommons.org/licenses/by/4.0/>).

## 1. Introduction

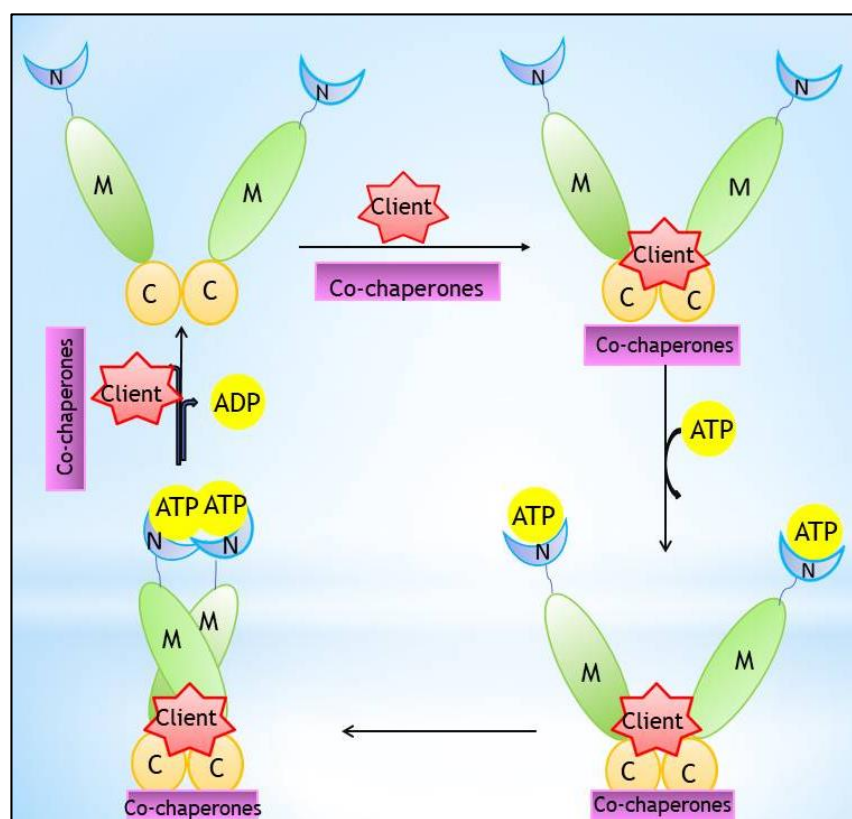
Cancer refers to a variety of diseases caused by escalating uninhibited cell proliferation, which may spread beyond tissue range. Cancer is initiated with the deformation of a normal cell caused by several hereditary factors, lifestyle, immune system defects, environmental/occupational factors, possible toxicity from medications, including the aging process, causing damage or genetic mutations [1–4]. The mechanisms of control, proliferation, and differentiation of cells are disrupted [5–9], which leads to deviation of normal cells from their regular growth path [10–12]. Tumor cells may acquire autonomy in two ways, namely activation of a growth-promoting oncogene or inactivation of a growth-inhibiting gene [13–15]. Cancer is one of the major death reasons which ranked after cardiovascular diseases; therefore, anticancer explorations have attracted much attention, especially through the evaluation of the deactivation of various proteins, such as tubulin, aromatase, and heat shock proteins [16–24].

Heat shock proteins (Hsps) inhibitors are one of the most eminent active anticancer agents with appropriate effects on several strange signaling paths in tumors; notably, these inhibitors can help to surmount several notorious problems regarding resistance cancers. Hsps act as proteins for vital cellular activities, including protein accumulation, secretion, and regulation of gene expression through direct correlation with transcription factors; the cellular expression is increased due to various stressors. Hsps are classified by their molecular weight into the Hsp110, Hsp90, Hsp70, Hsp60, Hsp40, and Hsp27; most of them being generally characterized as ATP-dependent [25–27]. Additionally, Hsp90 can regulate

the activity and stability of different client proteins with a wide range of sizes and functions as these client proteins have critical roles in proliferation, survival, protein misfolding, aggregation, and apoptosis. There are four various homologs of Hsp90: cytosolic Hsp90 (including Hsp90 $\alpha$ , Hsp90 $\beta$ ), TRAP1 (tumor necrosis factor receptor-associated protein 1) in mitochondrial, GRP94 (94 kDa glucose-regulated protein) in the endoplasmic reticulum (ER), and Hsp90C in chloroplasts [27].

The crystal formation of Hsp90 was first defined in 1996 as a homodimer with a three-part monomer. The N-terminal domain (~35-kDa) is fabricated from layers of a/b sandwich structures formed in the pocket, acting as a binding site for adenine nucleotides. The requirement of ATP in Hsp90 is associated with auto-phosphorylation with the N-terminal folding pattern; the superfamily of ATPase has shown similar activity to Hsp90 by type II topoisomerases and MutL (Mutator L) [28,29].

A client protein binding site and nuclear localization signal, Hsp90 middle domain (~35 kDa), entails precise identification of client proteins and molecular regulator chaperones to activate the appropriate substrate, such as ATP hydrolysis [30]. The C-terminal domain (~12 kDa) is the site of dimerization close to the ATP binding site and a pentapeptide domain (Met-Glu-Glu-Val-Asp or MEEVD), as well as the binding site of co-chaperones of Hsp90 consisting of Sti15 and Hop [31]; the Hsp90 ATPase cycle is depicted in Figure 1.



**Figure 1.** ATPase cycle in Hsp90.

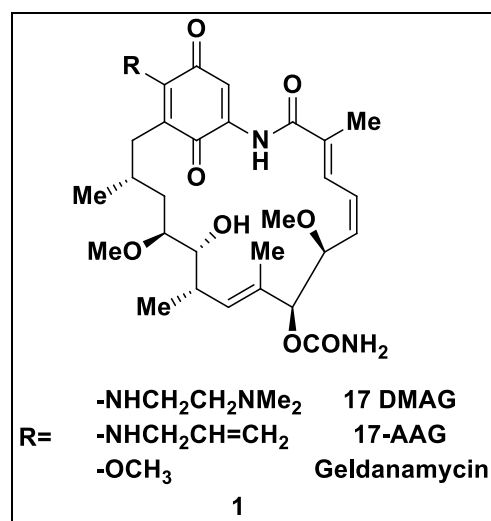
Hsp90 consists of a chaperoning subsidiary with the assistance of co-chaperones and ATP. Initially, the client protein attaches to the M domain with the co-chaperones source; afterward, the ATP binds to the N domain to dimer the Hsp90, leading to the production of “closed form” protein. The client protein is reformed, while the required energy is supplied from the bond division process, and ATP is hydrolyzed to ADP and unfastened phosphate. The release of client proteins and ADP from the complex occurs after covering the chaperoning function; ATP binds to the N terminal via a standard chaperoning cycle and then the client protein binds to Hsp90 by assisting co-chaperones [32–34].

Due to the unique effectiveness of Hsp90 inhibitors in cancer therapy, researchers have focused on them in recent decades [35–47]. Hsp90 is responsible for the conformational maturation of 500 client protein substrates embracing transcription factors, receptors, kinases, or oncoproteins, which might be overexpressed and/or mutated in most cancers [48]. Consequently, the inhibition of Hsp90 is contemplated an attractive cancer-treating strategy due to its impacts on oncoprotein and pathways, concurrently [48,49]. Herein, recent advances in potential inhibitory effects of lately synthesized heterocyclic compounds, such as purine, pyrazole, triazine, quinolines, coumarin, and isoxazoles against Hsp90, are deliberated, focusing on their anticancer and antitumor applications.

## 2. Hsp90 Inhibitors

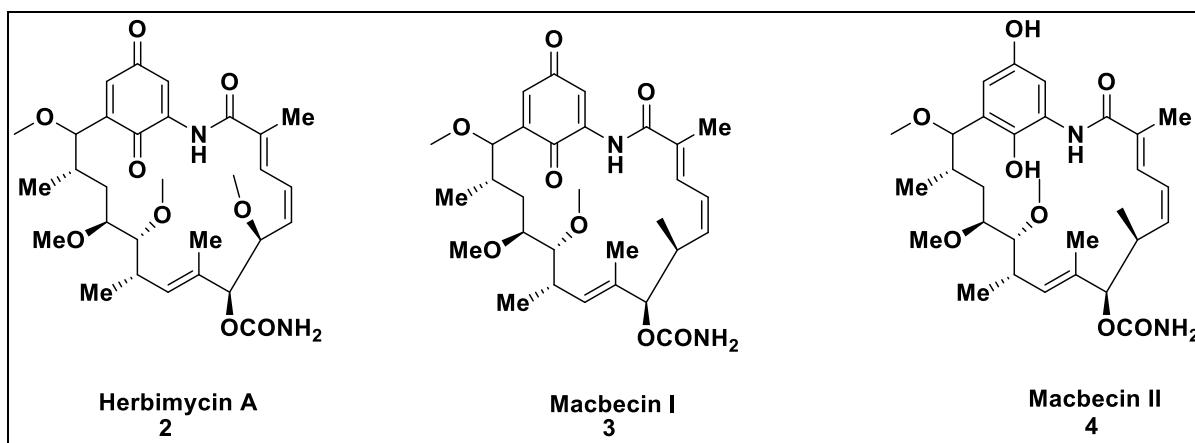
### 2.1. Natural Inhibitors

The first reported natural Hsp90 inhibitor has been a macrocyclic product called geldanamycin (**1**) (GM), extracted from the culture of *Streptomyces hygroscopicus* in 1970 which is known as an antibiotic compound (Scheme 1) [50]. Due to its unacceptable toxicological properties, the additional development of this compound was averted. However, the Hsp90 inhibitory activity of several geldanamycin analogs, namely, 17-dimethylaminoethylamino-17-demethoxygeldanamycin (17-DMAG), and 17-allylamino-17-demethoxygeldanamycin (17-AAG) are studied, but their clinical trials have been interrupted due to their poor solubility, complex formulation, and hepatotoxicity [51–56].



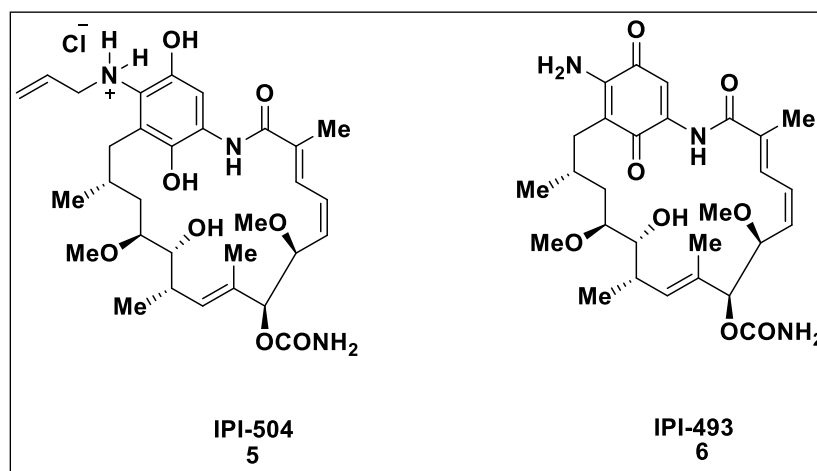
**Scheme 1.** Chemical structure of geldanamycin and its analogs.

One of the developed GM analogs is herbimycin A in which the methoxy substitution is located at positions C-11 and C-15, and the methoxy group is not present at position C-17; GM and herbimycin A (**2**) can induce Hsp70 expression in fibroblasts [57]. Macbecin I (**3**) as a GM analog has been developed with a similar structure to herbimycin A, except that the methoxy group at C-6 is replaced by a methyl group. Macbecin II (**4**) is a hydroquinone analog of macbecin I with less separation tendency due to its inferior structural instability [58,59]. The chemical structures of Herbimycin A and macbecin (I and II) are depicted in Scheme 2.



**Scheme 2.** Chemical structures of herbimycin A, macbecin I, and macbecin II.

IPI-504 (retaspimycin hydrochloride) (5) and IPI-493 (17-AG) (6) (Scheme 3) are more soluble analogs of GM and both of them inhibit Hsp90 activity through the degradation of client proteins. Several clinical trials (phase I and II) have been disclosed on different types of cancers including multiple myeloma, metastatic gastrointestinal stromal tumor (GIST), refractory non-small cell lung cancer (NSCLC), and chronic myelogenous leukemia (CML) [60]. IPI-493, equivalent to 17-AAG, obstructs the growth of SKBr3 breast cancerous cells, which may be derived from a similar major metabolite. IPI-493 exhibited highly effective results in GIST xenografts carrying heterogeneous KIT mutations in a preclinical investigation; these findings led to the start of its phase I clinical trial studies [61–63].

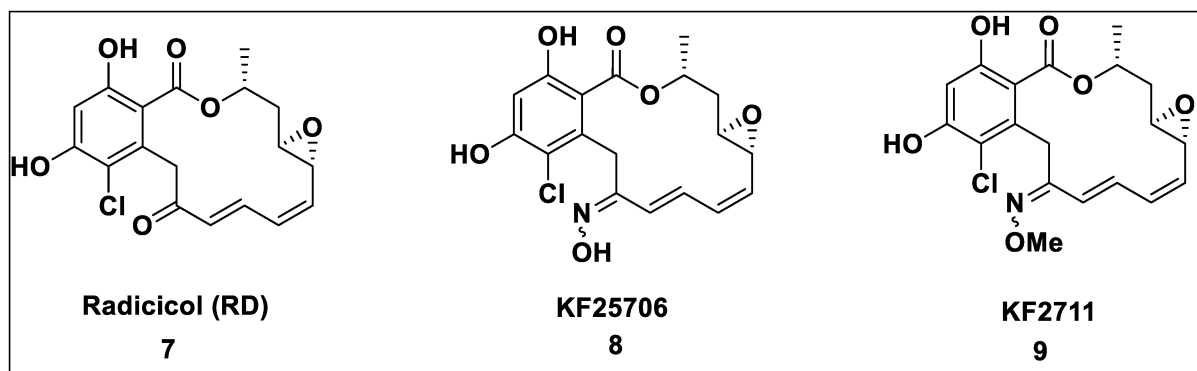


**Scheme 3.** Chemical structures of IPI-504 and IPI-493.

Benzoquinone ansamycins are also known as Hsp90 inhibitors that act as anti-malarial, antiviral, and anti-surra agents, and their efficacy in the treatment of cardiac arrest, stroke, and Alzheimer's has been explored [64]. One of the natural Hsp90 inhibitors is Radicol (RD) (7), which has been isolated from *Monosporium bonorden*, it can link to the N-terminal ATP binding site. RD is a potential cell growth inhibitor, but its unstable metabolite in the body leads to inactivity; therefore, elaborative studies have been focused on the modification of its structures to obtain analogs with better stability [65].

KF25706 (8) and KF2711(9) have been introduced as more soluble analogs of RD with significant inhibition of the Hsp90 activity. As depicted in their chemical structure (Scheme 4), the carbonyl group in RD has been replaced with the oxime group, from the point of view of chemistry; this replacement can reduce its Michael acceptor electrophilicity

thus improving the stability. However, their anticancer investigations have been limited to in vivo and animal model studies [65,66].



**Scheme 4.** Chemical structures of Radicol, KF25706, and KF2711.

## 2.2. Synthetic Hsp90 Inhibitors

### 2.2.1. Purine-Based Structures

Naturally-derived Hsp90 inhibitors may suffer from some disadvantages, including low solubility and restricted activity. To overcome these limitations, the usage of synthesized Hsp90 inhibitors has garnered much attention; for instance, purine-scaffold-based compounds were reported as effective Hsp90 inhibitors with good solubility and an acceptable level of cell permeability [67]. Purine is an aromatic heterocycle compound consisting of two fused rings. Purine derivatives have exhibited significant pharmaceutical activities such as anticancer, anti-HIV-1, and antimicrobial properties [68–72]. Purine and pyrimidine-based entities are essential natural heterocyclic compounds that have a critical role in several metabolic and cellular conversion processes in deoxyguanosine monophosphate (DGMP) nucleotide (AMP). Moreover, the chemical structure of several biologically important molecules, such as ATP, GTP, cyclic AMP, NADH, and 3'-phosphoadenosine-5'-phosphosulfate (PAPS) contain fused purine ring. In chemical terms, purine is a nitrogen-rich heterocyclic compound comprising two rings of pyrimidine and imidazole, and because of the lack of natural sources, they ought to be prepared through synthetic organic reactions [73–75].

The activity of a purine-based molecule as a synthesized Hsp90 inhibitor (PU<sub>3</sub>) has been investigated by assessing its interaction in Hsp90 K ADP/ADP binding site. As a theoretical outcome, this molecule covered all the necessary interactions with hosting protein; the Lys112 interacted with methoxy groups, and the hydrophobic pocket was occupied (Figure 2) [76]. The purine derivatives PU<sub>3</sub> and Pu24FCl (Scheme 5) have been introduced as potential small-molecule Hsp90 inhibitors through binding to the Hsp90 ADP/ATP site. The trimethoxy phenyl functional group of Pu24FCl makes it suitable to bind into the phosphate region of the host protein. Bao et al. reported a purine-based Hsp90 inhibitor with potential oral activity, named CUDC-305 (**12**), it is a unique compound due to its: ability to extremely privilege into the tissue of the brain, prolonged duration in intracranial tumors in animal models, and function in intracranial glioblastoma models; these attractive features may be raised from its fascinating high lipophilicity (clog P of 4.0) (Scheme 5) [77].



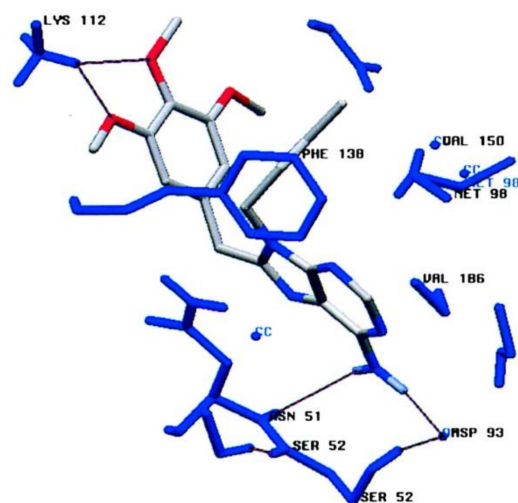
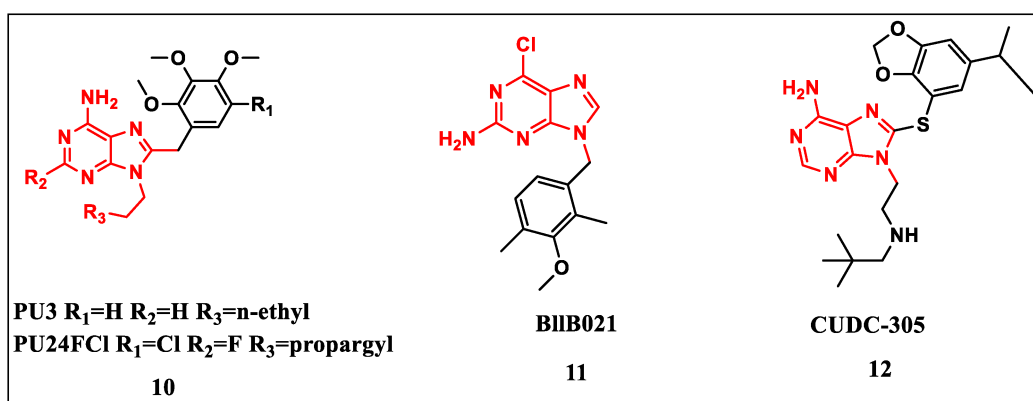


Figure 2. Molecular docking analysis of PU<sub>3</sub> in interaction with Hsp90.

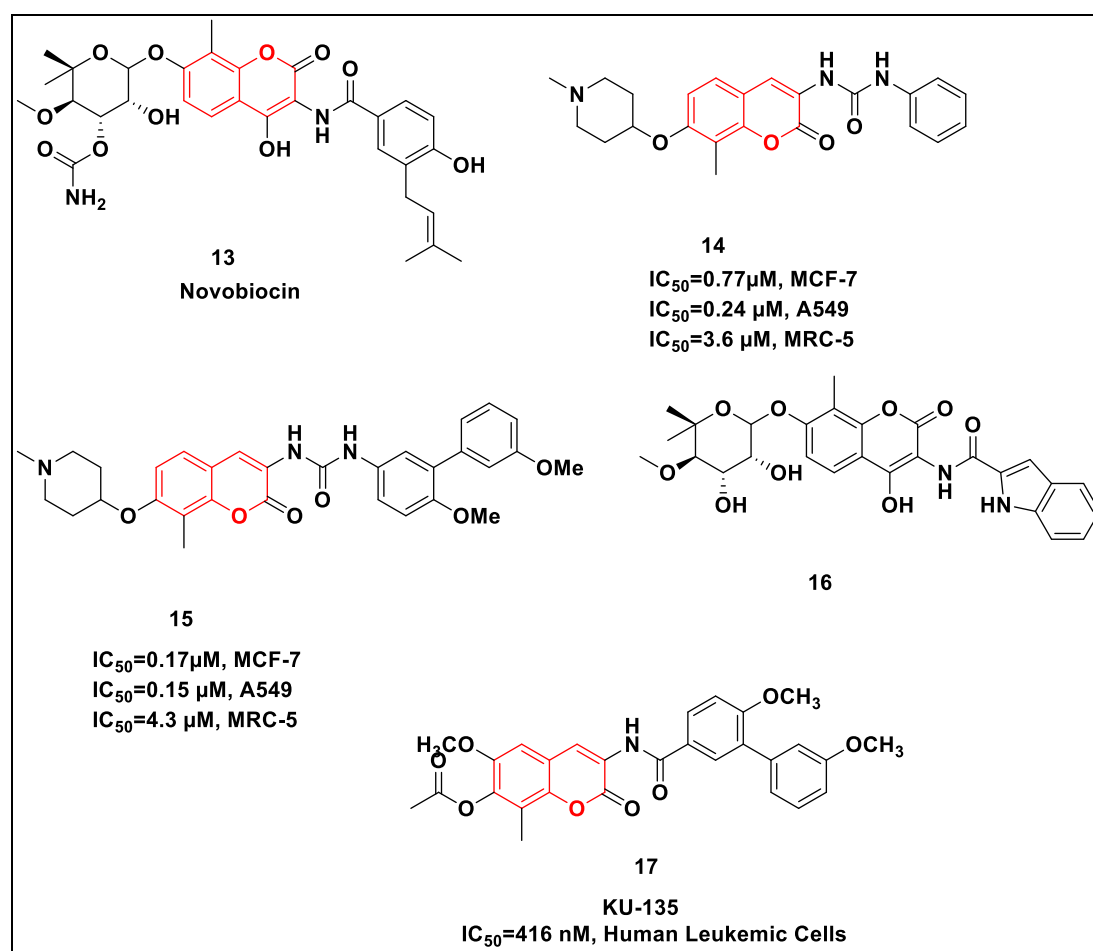


Scheme 5. Chemical structures of PU<sub>3</sub>, PU24FCI, BIIB021, and CUDC-305.

A family of 8-arylsulfonyl analogs of PU<sub>3</sub> (**10**) have been synthesized to evaluate the influence of the aryl part on inhibitory function and are being introduced as a purine-based Hsp90 inhibitor with selective activities which successfully enters clinical trials [78–81]. BIIB021 (**11**) has been the first fully synthetic Hsp90 inhibitor that moved in clinical trials endowed with its special properties that facilitated its formulation and bioavailability improvement; it binds to Hsp90 with high affinity and inhibits tumor growth. In phase I clinical trials, BIIB021 exhibited well-tolerated and good antitumor activity [82]. Therefore, this most developed purine-based compound, entered phase II clinical trials for GIST treatment. Pharmacokinetic parameters for BIIB021 600 mg, the mean C<sub>max</sub> was 1.5 μmol and the mean AUC was 2.9 μmol h; a C<sub>max</sub> > 1.5 μmol being associated with a decrease in standardized uptake value (SUV<sub>max</sub>) [83].

### 2.2.2. Coumarin-Based Structures

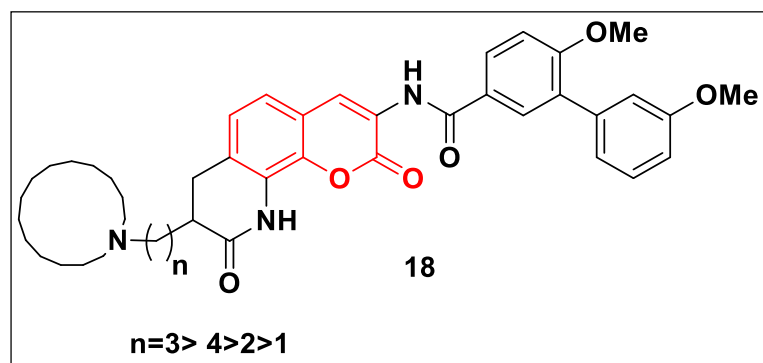
Coumarin and its derivatives are important heterocyclic molecules endowed with various biological activities, such as platelet aggregation inhibition, antibacterial effects, and anticancer activity [84–88]. Novobiocin (**13**) is one of the first established organic compounds with a coumarin core that functioned as an Hsp90 inhibitor; it is a natural product with significant antibacterial DNA gyrase activity. However, its low efficiency in degrading Hsp90 clients (IC<sub>50</sub> = ~700 μM) has discontinued more evaluations; therefore, research has mainly focused on structure-activity relationship (SAR) studies to identify other coumarin-based compounds with stronger inhibitor activity [89]. Modification of the 3-position of coumarin, from amide in novobiocin to urea, creates a new link to the hosting protein. The chemical structure of modified coumarin (**14**) is depicted in Scheme 6.



**Scheme 6.** Hsp90 inhibitors containing coumarin motif.

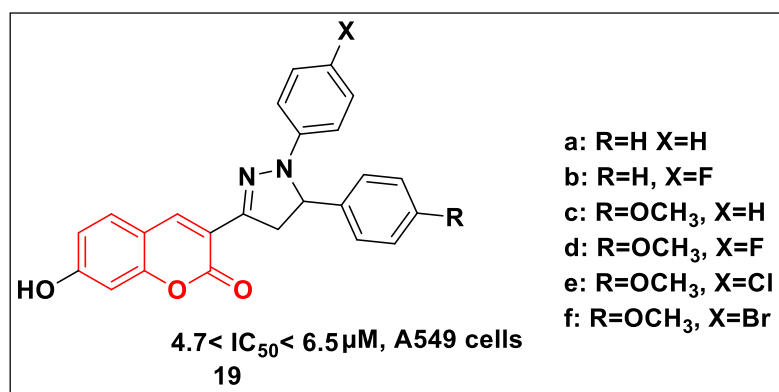
Among coumarin derivatives, compound 15 (Scheme 6) did not show any Hsp90 inhibitory activities, but additional investigations revealed its ability to interrupt MAPK signaling pathway by inhibiting the level of p-ERK and p-MEK; this function would be useful in anticancer activities [90]. Blagg et al. illustrated that the 4-hydroxyl and the 3'-carbamate functional groups of novobiocin have proven to be detrimental as their essential components for Hsp90 inhibitory activity by SAR studies. Therefore, indole moiety replacement in compound 16 significantly increased its activity (Scheme 6), more than 500 times that of novobiocin [91]. Furthermore, Shelton et al. synthesized KU135 as an Hsp90 inhibitor agent with anti-proliferative activity. The results showed that this compound can degrade Hsp90 client proteins through signaling pathways, a process that has stronger anti-proliferative effects than the N-terminal Hsp90 inhibitor 17-AAG. Notably, the explorations on this Hsp90 inhibitor demonstrated that this compound could inhibit G2/M cell cycle and have mitochondria-mediated apoptosis effects [92].

Garg et al, produced different analogs of ring-bound novobiocin (Scheme 7) wherein SAR and computational studies illustrated that when lactam was in  $\alpha$  position, it produced more effective analogs than sugars. Activity of these derivatives was assessed as anti-proliferative agents against SKBr3 and MCF-7 cell lines. Among these derivatives, the cyclohexylamine analog demonstrated the best inhibitory effect with  $IC_{50}$  compared to bicycloalkyl and tricyclic amino analogs ( $0.35\mu M$  against MCF-7 and  $0.2\mu M$  against SKBr3 cells) [93].



**Scheme 7.** Chemical structure of ring-bound novobiocin analogs synthesized and evaluated by Garg et al. [93].

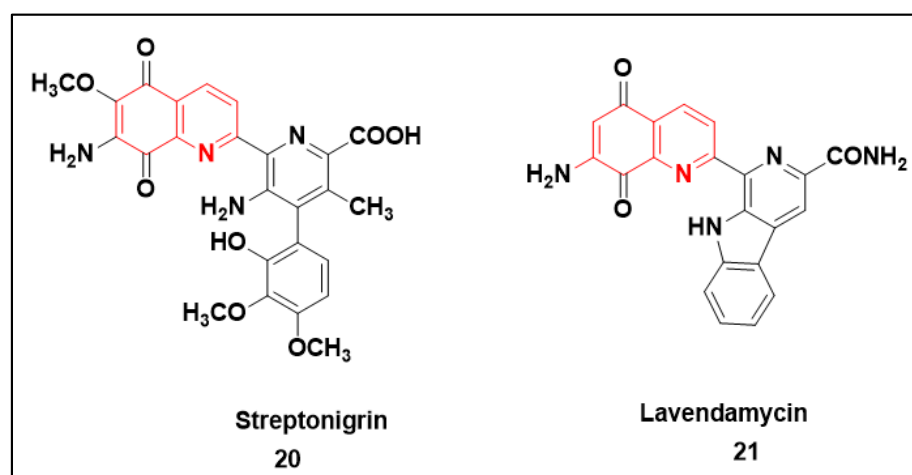
Wei et al. reported some assorted coumarin compounds comprising the pyrazoline functional group, (compound **19** (a–f), Scheme 8) and evaluated their anticancer activity through several biological assays. Based on docking study results, all of these compounds are located in the active site of the N-terminus of Hsp90. Among these six derivatives, the structure of 19a exhibited higher binding energy and Hsp90 inhibitory function ( $IC_{50} = \sim 4.7 \mu\text{M}$ ). All these derivatives reduced the viability of A549 lung cancerous cells, without any necrosis induction on them as they stimulated the apoptosis with blocking effects on the autophagic flux of HCP1 in A549 lung cancerous cells [94].



**Scheme 8.** Chemical structures of pyrazoline containing coumarin compounds, reported by Wei et al. [94].

### 2.2.3. Quinolone-Based Structures

Quinolines are one of the most important nitrogenous heterocyclic compounds that have been extensively examined due to their widespread pharmacology appliances, such as anti-malarial, antitumor, anti-parasitic, antibacterial, anti-asthma, antidiabetic, anti-inflammatory, antiplatelet, and antihypertensive activities [95–102]. Streptonigrin (isolated from *Streptomyces flocculus*) and lavendamycin have already been known as antimicrobial and antitumor compounds with quinoline skeleton (Scheme 9); they create efficient interactions with targets to act as a cancer chemotherapy agent and as Hsp90 inhibitors [103–105].



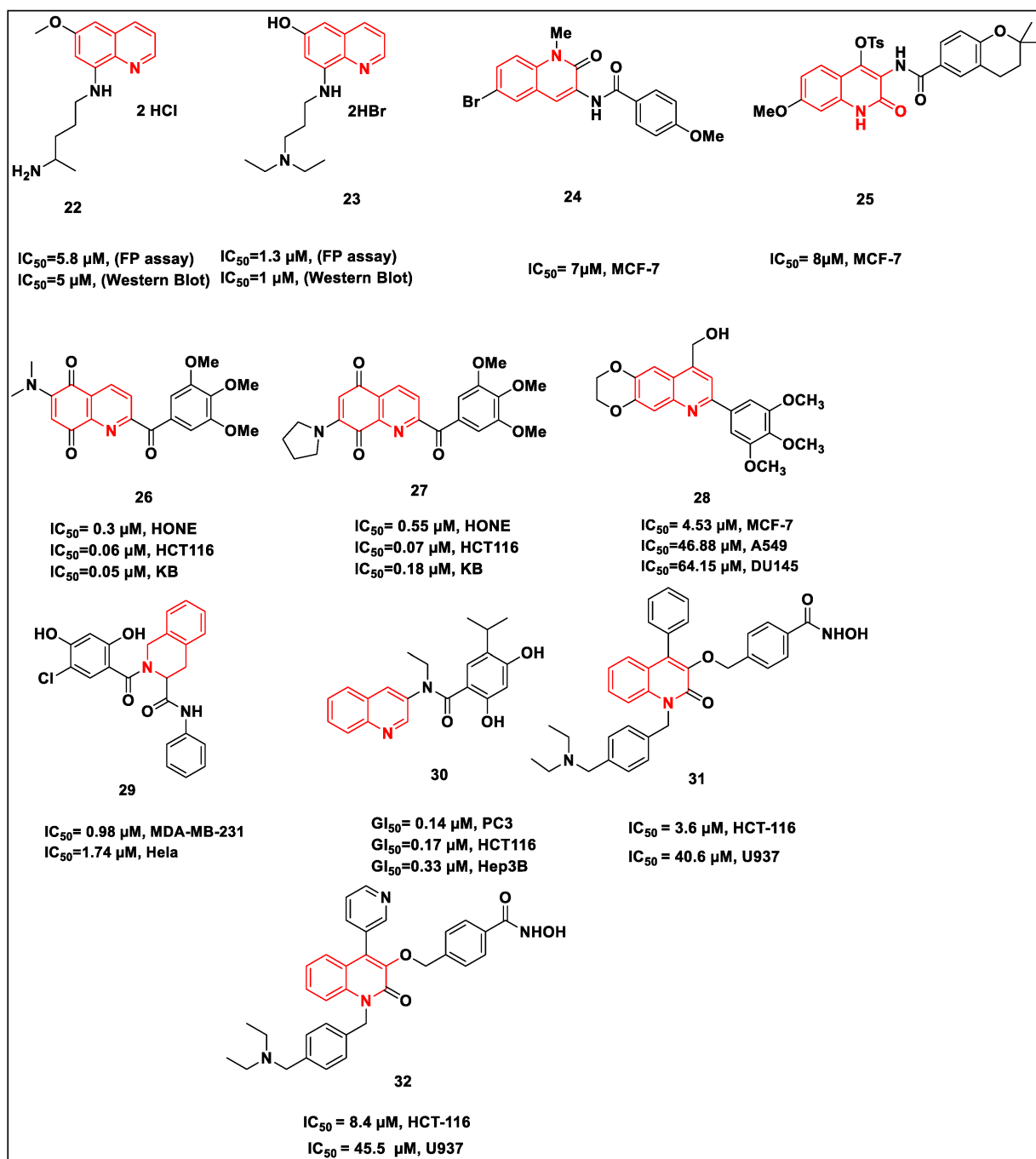
**Scheme 9.** Chemical structures of quinolones-based HSP90 inhibitors: Streptonigrin and Lavendamycin.

The chemical structures of synthesized quinolones-core organic compounds with Hsp90 inhibitory potentials properties have been investigated; their chemical structure is depicted in Scheme 10, named 22 to 32. Ganesh and co-workers reported the modest Hsp90 inhibitor activity of compound **22** (Scheme 10). Several quinoline-based organic compounds were synthesized and their activities were evaluated in micromolar concentrations using cell-based Western blot (WB) and fluorescent polarization (FP) techniques [106].

Studies of SAR, optimization of structures, and re-synthesis of several aminoquinoline compounds indicated their low Hsp90 inhibitor activity. However, the synthesized compound **23** (Scheme 10) exhibited high activity, with  $IC_{50}$  of  $\sim 0.73 \mu\text{M}$  and  $1 \mu\text{M}$  in the low micro-molar range obtained in FP and WB assays, respectively. These compounds, with their simple chemical structures and facile synthesis pathways, are recognized as a series of new Hsp90 inhibitors [106]. Audisio and co-workers synthesized a novel array of 3-(*N*-substituted) aminoquinolin-2(1H)-one derivative and evaluated their anticancer activity using cell proliferation and flow cytometry, including biological assays.

Among these synthetic derivatives, compounds **24** and **25** (Scheme 10) offered the most effective inhibitory activity against various genes, such as Raf-1, HER2, CDK4, and estrogen receptors. It was indicated that compound **24** could stimulate apoptosis in MCF-7 breast cancer cells by activating caspases and subsequent division of poly (ADP-ribose) polymerase (PARP) and inhibiting the growth of all tumor cell-independent cell lines with growth inhibition of 50% ( $GI_{50}$ ) values in the range of 2 to  $32 \mu\text{M}$ . The examined cell lines included MCF-7, T47D, IRGOV-1, Ishikawa, HT-29, Caco-2, and MDA-MB-231. In addition to these properties, only compound **24** was identified as mediated cell death inductor in a p23-independent procedure; the p23 was a small and important co-chaperone for the Hsp90 chaperoning pathway [107].

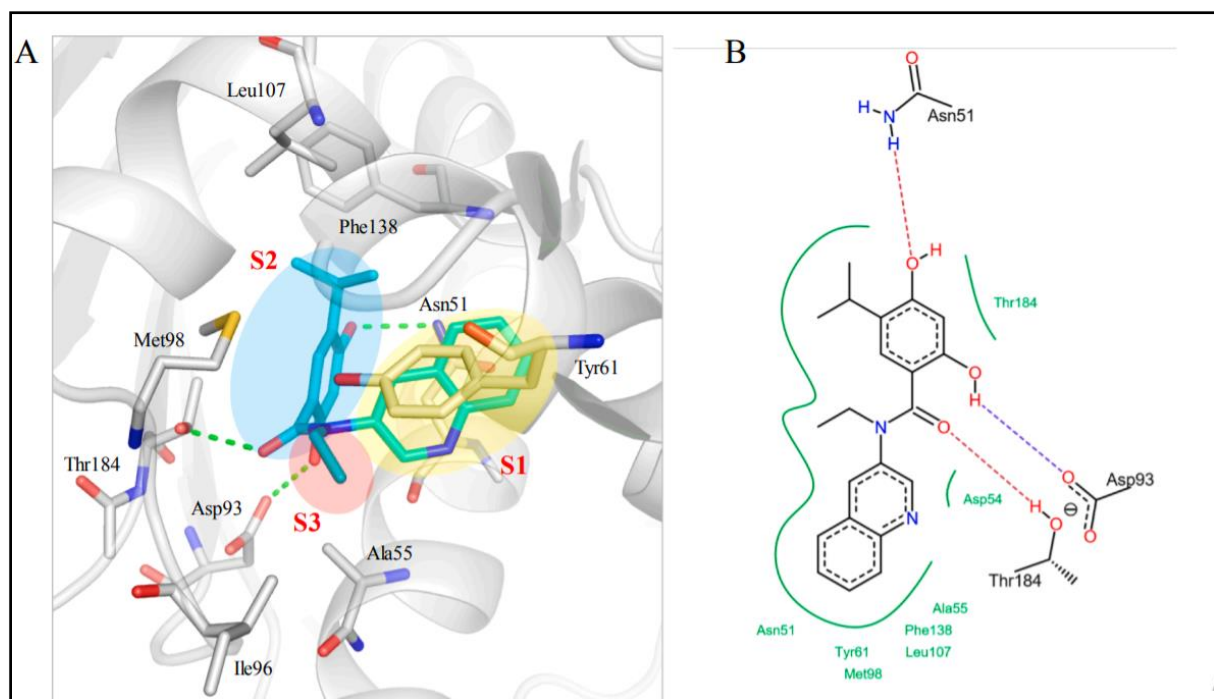
A series of 2-arylquinoline-5,8-diones have been synthesized and their potential biological activities have been evaluated by Nepali and coworkers [108]. Among these Hsp90 inhibitors, compounds **26** and **27** could inhibit the growth of cancerous cells ( $IC_{50} = \sim 0.14$  (compound **26**) and  $0.27 \mu\text{M}$  (compound **27**). Moreover, compound **27** displayed an  $IC_{50}$  of  $\sim 5.9 \mu\text{M}$  to inhibit tubulin polymerization as it persuaded the degradation of Hsp70 and Akt protein through WB analysis. Different quinoline analogs have been reported as Hsp90 inhibitors with a cytotoxic function against cancerous cell lines. Accordingly, cytotoxic derivatives encompassing alcohol functional groups exhibited significant activity against MCF-7 cells. Among these evaluated compounds with anti-proliferative activity, compound **28** distinguished itself as the most effective analog in the degradation of Her2 protein, a client protein of Hsp90. The possible state of interaction between compound **28** and the N-terminal ATP binding pocket of Hsp90 was demonstrated by molecular modeling studies [109].



Scheme 10. Hsp90 inhibitors containing quinoline motif.

Liang et al. synthesized two new series of compounds of *N*-(5-chloro-2,4-dihydroxybenzoyl)-1,2,3,4-tetrahydroisoquinoline-3-carboxamides as Hsp90 inhibitors, which illustrated acceptable anti-proliferative activities against MDA-MB-231 and HeLa cell lines. Compound **29** unveiled strong cytotoxicity with inhibitory effects against the molecular proliferation of MDA-MB-231 ( $IC_{50} \sim 0.98 \mu\text{M}$ ) and HeLa ( $IC_{50} \sim 1.74 \mu\text{M}$ ). Moreover, the effective intracellular interaction of compound **29** with Hsp90 $\alpha$  in 293T cells was confirmed through isothermal dose-response fingerprint curves. The induction activity of compound **29** in the degradation of CDK4, Her2, Cdc-2, and C-RAF Hsp90 client proteins was assessed by WB evaluation on MDA-MB-231 breast cancer cell lines [110].

Molecular docking and dynamic (MD) analyses on the complex of compound **29** and Hsp90 displayed its effective binding to Hsp90 through the interaction of its benzyl amino moiety with the residue Phe138, leading to the formation of a  $\Pi$ -stacking interaction [110]. Nepali et al. reported different fused quinoline-resorcinol compounds with powerful inhibitory activity against Hsp90. Through MD analysis of synthesized compounds in interactions with the Hsp90 chaperone protein receptor (Figure 3), compound **30** was determined as the ideal candidate. It interacted with the amino acid residues of the Hsp90 chaperone protein, resorcinol ring of compound **30**, 1,3-dihydroxybenzene, link to chaperone function through amide bond formation with 1,3-dihydroxybenzene. In vitro studies indicated the effective cell growth inhibitory effect of compound **30**, as one of the most active entities through in silico studies, against HCT-116 (colon), Hep3B (liver), and PC-3 (bone metastasis) cell lines [111].



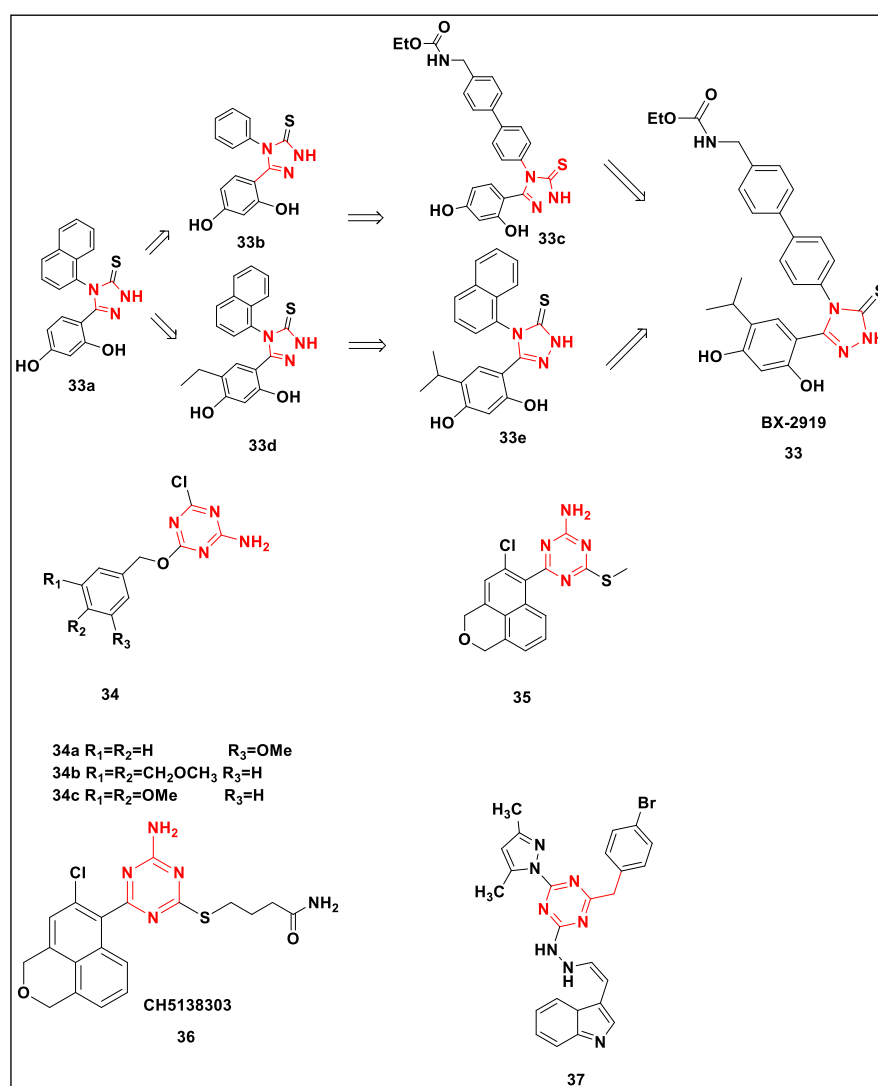
**Figure 3.** MD analysis of compound **30** in interaction with Hsp90. (A) compound **30** (blue) is anchored within the Hsp90 (gray) binding site. The three distinct sections of MPTG0G256 that are located in the S1, S2, and S3 sites, are colored as yellow, blue, and red, respectively. Interacting residues are shown as sticks and labeled as indicated. Hydrogen bonds are indicated by dotted green lines. (B) 2D representation of compound **30** docked in Hsp90. Green lines show regions of hydrophobic interactions. Interacting residues are labeled as indicated. Adapted from Ref. [111] with permission. Copyright 2019 Elsevier.

Relitti and co-workers synthesized various quinolone-based organic compounds as histone deacetylase 6 (HDAC6), wherein compounds **31** and **32** were introduced as the most promising active molecules against HDAC6. In addition, they displayed potent activity in cellular studies with development of inhibition against human cancer cell lines, HCT-116, and histiocytic lymphoma (U9347). It was an effective compound against tumor cells via apoptosis induction [112].

#### 2.2.4. Triazine and Triazolothione-Based Structures

Triazine is an organic heterocyclic compound with a 6-membered ring containing three carbon atoms and three adjacent nitrogen atoms. Pharmacology studies have revealed that triazine derivatives have significant activity as antimicrobial, antituberculosis, anticancer, antiviral, and antimalarial agent [113–117]. BX-2919 was discovered by Feldman et al.

as an Hsp90 inhibitor during HTS, through a high-throughput screening assay that was performed to identify Hsp90 inhibitors that compete with GA binding. The resorcinol **33a** analog (Scheme 11) was identified as one of Hsp90 inhibitors optimized by applying parallel paths on its aryl rings. After assessing the strength of a large number of aryl compounds, ethyl carbamate **33c** was found as one of the best candidates. Among the resorcinol ring alternatives, the ethyl analog (**33d**) increased relative strength; finally, the isopropyl analog (**33e**) was the optimal alternative in this situation. A combination of optimal alternatives with the BX-2819 was examined. This compound could bind strongly to Hsp90 ( $IC_{50} = \sim 41$  nM) to inhibit GM-Bodipy binding, which was less than both above-mentioned compounds 17AAG ( $IC_{50} = \sim 350$  nM) or radicicol ( $IC_{50} = \sim 87$  nM) [118].



**Scheme 11.** Hsp90 inhibitors containing triazine and triazolothione motif.

Seo et al. reported a set of 2-amino-1,3,5 triazines containing a tricyclic part as Hsp90 inhibitors with high activity against gefitinib-resistant H1975 cells (Scheme 11) [119]. Several derivatives of compound **34** (Scheme 11) were synthesized, most of which entailed cell multiplication in a highly dose-dependent behavior with regularity effects on cell proliferation. Among them, compound **34a** demonstrated the highest activity as an inhibitor of cell proliferation and the product containing 2,6 dimethyl phenyl was able to reach the hydrophobic part of Hsp90 by van der Waals interactions, which led to anti-proliferative activity against H1975. Miura et al. synthesized various tricyclic molecules, including 2-amino-1 and 3,5-triazines as Hsp90 inhibitors with suitable anti-proliferative

function against HCT-116 ( $IC_{50} = \sim 0.46$  mM). Among these synthesized compounds, hybrid CH5015765 (35, Scheme 11) significantly improved the binding affinity ( $K_d = 3.4$  nM) [120].

The structural properties are involved in the possible interactions with Hsp90 at the active region, thus the fabricated tricyclic molecules should be precisely analyzed. Consequently, it was indicated that the hydrogen bonds can be formed between the amino group on the two positions of the triazine core and the carboxylic group of Asp93. A hydrophobic interaction can be formed between the methyl thio group at the 4-position and Ile96/Met98. Additionally, a hydrophobic portion can interact with the side chains of Leu107, Phe138, and Val150. Finally, the ether oxygen may bind to the remnant Phe138 and Asn51 [121]. Compound 36 (CH5138303) showed potent inhibitory activity against HCT-116, *in vitro*. Its efficacy and chemical properties led to reducing the phosphorylation and protein level of several Hsp90 client proteins. By further improving the chemical structure of tricyclic molecules, a category of triazines derivatives could be produced via the functionalization of the sulfur atom in compound 36 with hydrogen bond acceptor functional groups. They are primed to interact with the Lys58, which concerned in several hydrogen bonds with geldanamycin as a natural and specific inhibitor of Hsp90. In general, the derivative of compound 36 exhibited significant antiproliferative activity, *in vitro* and *in vivo* ( $K_d = 0.48$  nM) [122].

The antitumor activity of compound 37 as an Hsp90 inhibitor agent was reported by Zhao et al. [123]. Their interaction with Hsp90 was studied by surface plasmon resonance (SPR) assay; consequently, the results indicated the binding of compound 37 into the N-terminal of the protein with a very extraordinary binding mode with respect to the old inhibitors of Hsp90. Its anti-proliferative function was evaluated *in vitro* and *in vivo*. Accordingly, the results obtained from *in vitro* assessments demonstrated that these compounds could inhibit the molecular proliferation of BT-474 ( $IC_{50} = \sim 8.9$  mM), SK-BR-3 ( $IC_{50} = \sim 7.1$  mM), A549 ( $IC_{50} = \sim 7.5$  mM), K562 ( $IC_{50} = \sim 8.6$  mM), and HCT-116 ( $IC_{50} = \sim 6.7$  mM). After *in vivo* assessments, it was revealed that these compounds could obstruct the increase in proliferation of tumors that increased with a dose-dependent behavior in the BT-474 [123].

#### 2.2.5. Isoxazole-Based Structures

One of the prominent heterocyclic organic compounds comprises the isoxazole ring, a 5-membered ring, with adjacent oxygen and nitrogen atoms. Various chemical structures/compounds encompassing the isoxazole moiety have shown attractive biomedical and pharmaceutical potentials, especially for cancer therapy [124–130]. Medicinal chemistry studies have revealed that the inclusion of isoxazole in the chemical structure of Hsp90 inhibitors could lead to improved efficacy, decreased toxicity, and enhanced pharmacokinetics profiles. Aromatase is an enzyme for the conversion of androgenic hormone into estrogen; thus, considering the high-level expression of aromatase in breast tissue, intense generation of estrogen can cause breast cancer. Isoxazole derivatives could stop the conversion of androgen into estrogen by inhibiting the aromatase enzyme, thus serving as anticancer drugs [131].

Apoptosis is an extremely regulated process enabling cells to destroy themselves and kill unwanted cells; this has a crucial role in homeostasis development. Isoxazoles as an inducer of apoptosis causes the elimination of or discontinues the progression of cancer [132]. Enzymes of protein tyrosine phosphatases are involved in mechanisms of cellular signaling by regulating the levels of phosphorylation in a clear tyrosine residue in proteins or peptides, controlling various functions of cells, including metabolism, migration, survival, adhesion, and multiplication. Mutations in proteins can cause cancers. In this context, isoxazole derivatives can attach to the ATP-binding region of the protein kinase and hinder the signaling cascade, resulting in cell cycle arrest and apoptosis [133].

Many preclinical studies have indicated that Hsp90 inhibition is associated with anti-neoplastic effects; these properties motivated researchers to find novel small-molecule containing isoxazoles as Hsp90 inhibitors. Their capability to bind with the  $NH_2$ -terminal

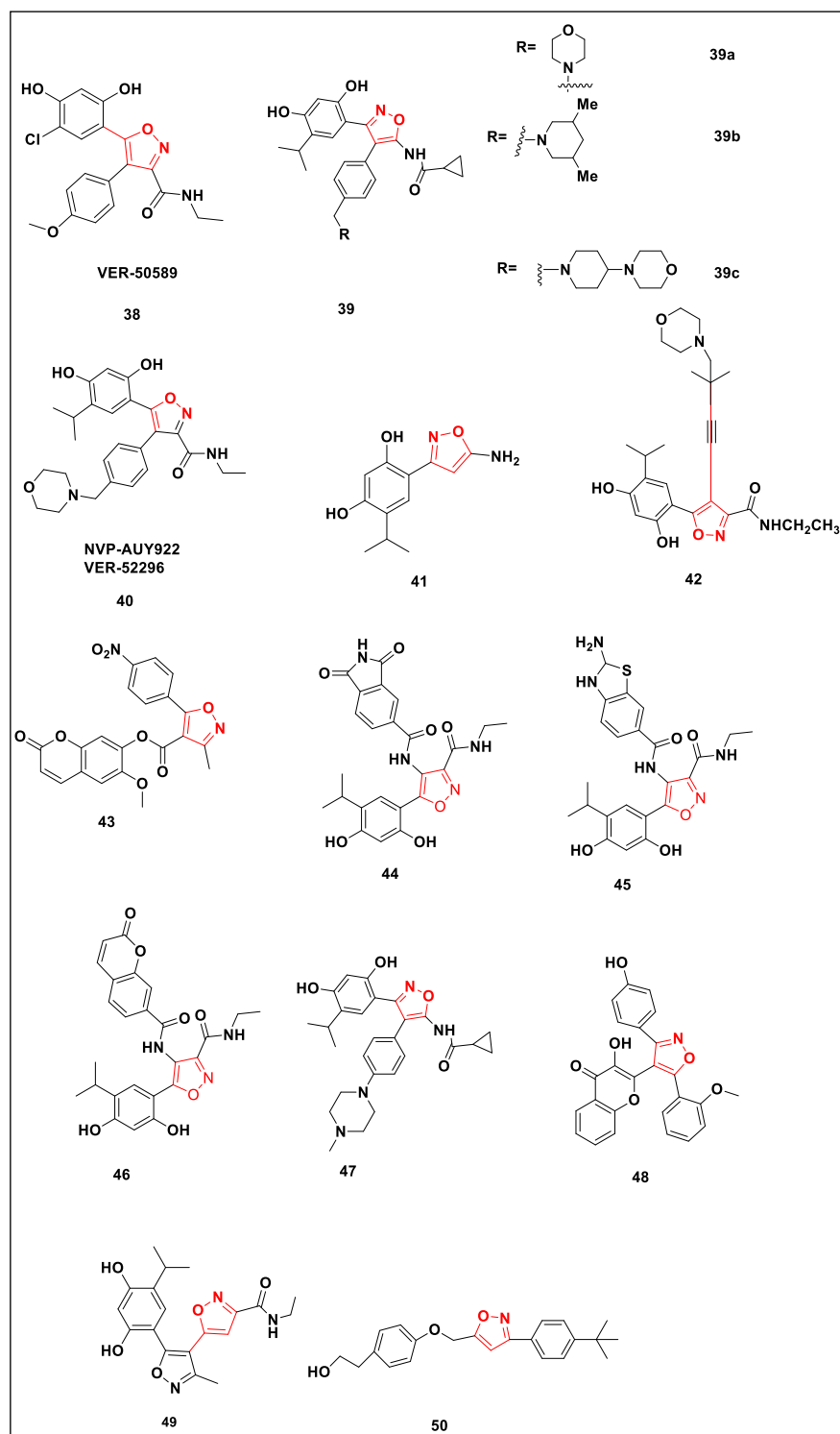


nucleotide-binding region of human Hsp90 was found extremely strong along with inhibitory effects on the multiplication of growth cells through inducing the arrest of G1-G2 and apoptosis. Pharmacological compounds containing isoxazole are active against different examined cell lines of tumors, especially breast cancer, which stimulated numerous efforts to design and synthesize innovative isoxazole derivatives [134].

Eccles et al. synthesized organic compounds containing isoxazole, such as VER-50589 (Scheme 12). Their Hsp90 inhibitory activity was assessed through *in vivo* studies, wherein these small synthetic molecules exhibited strong inhibitory activity. The results were found comparable with the activity of the clinically approved drug 17-AAG, an analog of geldanamycin; additionally, their lipophilicity renders them capable of easily penetrating the cell membrane. The encouraging outcomes illustrated the value of a structure-based design and optimization process on the way to achieve a potential clinical candidate. Prodigious findings motivated more research on the optimization of their potency, pharmacokinetic, and pharmacodynamic properties via structural modifications, which led to the discovery of VER52296 (NVP-AUY922) (Scheme 12). The anticancer activity of VER52296 was investigated against cell lines, namely, HCT-116, Hun7, and SW620, by applying 3-(4,5-dimethylthiazol-2-yl)-2,5-diphenyltetrazolium bromide tetrazolium (MTT) assay. The obtained results demonstrated high cytotoxic activity with  $IC_{50}$  values lower than  $20 \mu\text{M}$  ( $IC_{50} = \sim 21 \text{ nM}$  and  $K_d = 1.7 \text{ nM}$ ), besides the low glucuronidation metabolite levels. Thus, VER52296 was introduced as a potential anticancer drug, and it is under evaluation in a second phase clinical trial [135].

A set of Hsp90 inhibitors comprising *N*-(isoxazol-5-yl) amides structures presented unique pharmacokinetic characteristics as well as high antitumor activities (both *in vitro* and *in vivo*). Compounds **39a**, **39b**, and **39c** exhibited the  $GI_{50}$  lower than  $0.1 \mu\text{M}$ ; thus, studies have been performed on their activity against the various cell lines. They displayed potential cytotoxicity with common  $GI_{50}$  which indicated their extensive antitumor activities [135]. Chen et al. reported various small molecules comprising isoxazole rings and identified them by X-ray crystallographic techniques. Their Hsp90 inhibitory effects were evaluated, and compound **40** exhibited potent inhibitory effects on Hsp90 at cellular/molecular levels; moreover, *in vivo* assessments showed its remarkable capability for inhibiting the growth of tumors. The ratio between treated and control (T/C) value of compound **41** was equal to 18.35% at 50 mg/kg, which was found to be nearly twice as strong as NVP-AUY 922 as a traditional Hsp90 (T/C values at 50 mg/kg reach 34.06%) [136].

Sun et al. reported a set of isoxazole scaffolds associated with alkynes to study their inhibitory activity on the human Hsp90 protein as well as their anti-proliferative function against the examined cell lines of tumors. During conservation, it was found that the substitution of alkynes at C-4, in compound **42**, could induce nice cation- $\pi$  bond interaction with the Lys58 residue of the Hsp90 protein, along with the interaction of the resorcinol hydroxyl and C-3 amide groups. Based on the results, a set of 4-alkynylisoxazole structures were synthesized with 3,5-substitutes and their binding affinity to Hsp90 protein was also indicated. In addition, their anti-proliferative effects were evaluated against five cancerous cell lines, such as A549, human basal alveolar epithelial cell adenocarcinoma, K562, human immortal myeloma leukemia line, MCF-7, and the cell line of most breast cancers. Promising results were obtained, wherein compound **42** demonstrated an  $IC_{50}$  value of  $\sim 0.066 \mu\text{M}$  [137].



**Scheme 12.** Hsp90 inhibitors containing isoxazole motif.

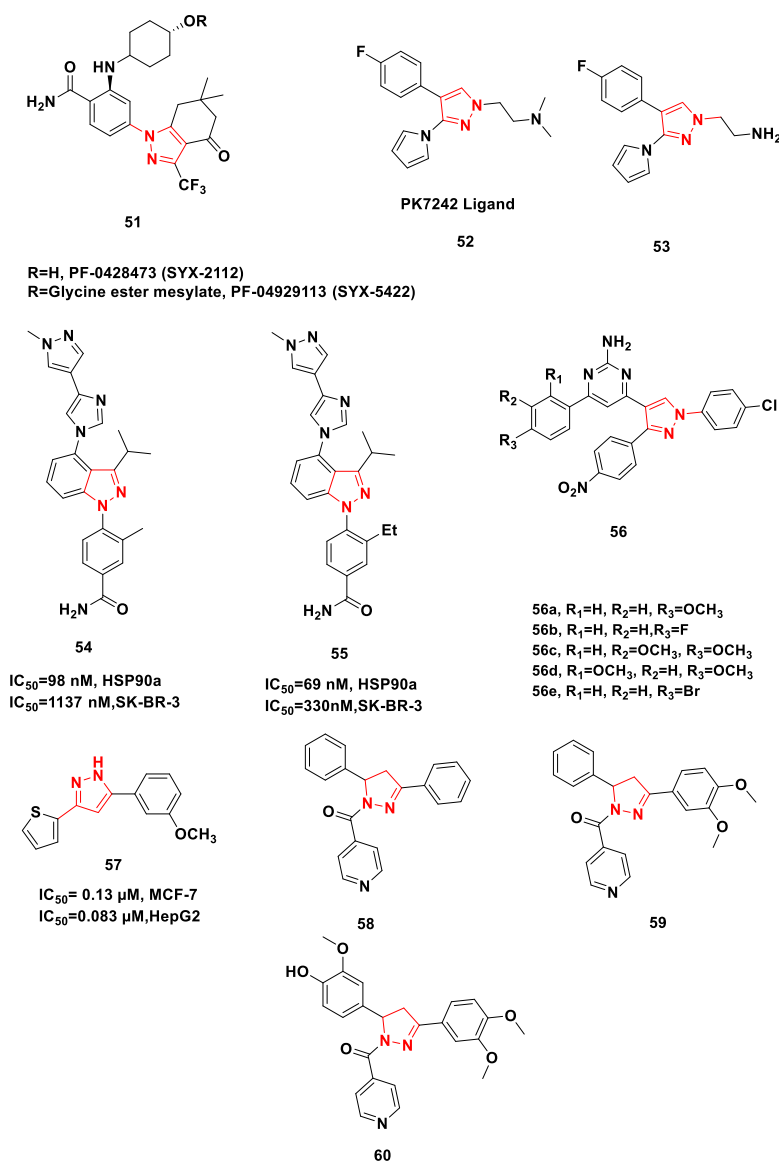
Shi et al. synthesized a set of scopoletin-isoxazole and scopoletin-pyrazole hybrids and their anticancer effects were evaluated against SW620, Hun7, and HCT-116. Scopoletin-isoxazole derivatives illustrated higher cytotoxic activity in comparison with scopoletin-pyrazole hybrids ( $IC_{50} \leq 20 \mu M$ ). Impressively, compound **43** showed anti-proliferative effects similar to sunitinib, the FDA-approved drug, with  $IC_{50} = \sim 8.76\text{--}9.83 \mu M$  against SW620, Hun7, and HCT-116, and it disclosed low toxicity on normal HFL-1 cells ( $IC_{50} = \sim 90.9 \mu M$ ) [138]. Sadeghi et al. studied the potential Hsp90 inhibitor activity of 50 organic molecules, includ-

ing 3,4-isoxazolidiamides functional groups; they discovered that three compounds, **44**, **45**, and **46**, could be considered as promising target molecules for further evaluations [139]. They also introduced compound **47** as an efficient Hsp90 inhibitor after the assessment of several isoxazoles-based compounds [140]. Additionally, several chromone-linked isoxazole compounds were synthesized, and their ER- $\alpha$  and their anti-proliferative activity against MCF-7 were evaluated. The replacement of isoxazole's positions of 3 and 5 with phenyl ring and 3-hydroxychromone increased their anticancer activity. Compound **48** displayed cytotoxicity against ER $\alpha$ -positive (MCF-7) with IC<sub>50</sub> of 32  $\mu\text{g mL}^{-1}$  by linking with a key residue of Glu353 and Arg394. These residues were stabilized by forming H-bonds of 4-hydroxyl phenyl in 4HT (4-hydroxytamoxifen) through molecular docking studies investigations [141].

Jung et al. reported a variety of isoxazole-containing compounds as Hsp90 inhibitors. Their capability of client protein degradation as well as ATPase performance was analyzed through in vitro cytotoxic assessments against cancerous cell lines. The targeted compounds were assessed for their possible antitumor effects in tumor xenograft models in vivo. Molecular modeling studies demonstrated the binding mode inside the inhibitors and N-terminal ATP binding pocket. To evaluate the antitumor effects of isoxazole-containing compounds, their cytotoxicity was analyzed against A2780 (ovarian cancer) and HCT-116 (colon cancer). Consequently, the IC<sub>50</sub> of compound **49** for ATPase, Her2, A2780, and HCT-116 were found to be 0.284, 0.028, 0.043, and 0.014  $\mu\text{g}$ , respectively [142]. Aissa and co-workers reported the synthesis of 3, 5-disubstituted isoxazoles and 1,4-disubstituted triazoles and evaluated their possible anticancer/hemolytic activities. The anticancer derivatives of isoxazole exhibited an active apoptotic trend in the glioma U251-MG and T98G. These derivatives illustrated significant anti-proliferative function against most human glioblastoma cancerous cell lines (U87) in a dose-dependent manner wherein compound **50** (IC<sub>50</sub> 15.2  $\pm$  1.0  $\mu\text{g mL}^{-1}$ ) exhibited stronger anticancer activity. Notably, the hemolytic activity of compound **53** caused hemolysis up to 40% at a concentration of 400  $\mu\text{g mL}^{-1}$ . These results revealed that isoxazole derivatives did not damage red blood cells and release hemoglobin, which strengthened the potential of these compounds as innovatively synthesized anticancer prototypes with low toxicity [143].

#### 2.2.6. Pyrazole-Based Structure

Pyrazole is a 5-membered ring heterocycle compound consisting of three carbon atoms and two adjacent nitrogen atoms. Pyrazole derivatives have significant activities, such as high efficacy as partial agonists in G protein-coupled and cannabinoid receptors [144–147]. Synthetic small pyrazole-fused heterocycle molecules, PF-04929113 and PF-04929113, were developed as inhibitors of Hsp90, but their restrictions/disadvantages, such as poor solubility and cytotoxicity prompted a search for the structural improvement of pyrazole-based compounds (Scheme 13) [148]. Bai et al. synthesized various fluorescent pyrazoline coumarin derivatives and investigated their anticancer activity against lung cancer cell lines in vitro. As a result, compound **52** had the strongest growth inhibition (IC<sub>50</sub> =  $\sim$ 7.9 mM), with a strong fluorescence strip; subsequently, it was introduced as a potential and promising fluorescent Hsp90 inhibitor [149].



**Scheme 13.** Hsp90 inhibitors containing pyrazole motif.

Sadeghi et al. predicted dual agents as mutant P53 activators and Hsp90 inhibitors by using docking and MD analysis; according to their published results, compound **53** was proposed as a dual-mode agent, P53 activator, and Hsp90 inhibitor [150]. Uno et al. reported various pyrazolo [3,4-b]pyridine derivatives as potential Hsp90 $\alpha$  and Hsp90 $\beta$  inhibitory agents with oral availability properties. Compound **55** exhibited the same binding state of Hsp90 as an analog of pyrazole compound **54** via X-ray crystallography. Oral administration of compound **54** demonstrated potent antitumor effects on human lung cancer (NCI-H1975) in a xenograft mouse model [151]. Mettu et al. innovatively synthesized a variety of pyrazolyl 2-aminopyrimidine derivatives and evaluated their Hsp90 inhibitory and anticancer activity. Among them, compound **56e** established the highest binding affinity to Hsp90 (20 nM) with anti-proliferative function against MCF7 (IC<sub>50</sub> = ~2.4 μM), MDA-MB-231 (IC<sub>50</sub> = ~0.8 μM), and HCT-116 (IC<sub>50</sub> = ~4.8 μM), in vitro. According to Western blotting (WB) analysis, two compounds (**56b**, **56e**) generated dose-dependent degradation of two client proteins (pHER2 and pERK1/2) [152]. Molecular docking studies demonstrated that the compounds **56b**–**56e** were significant Hsp90 inhibitors. These studies revealed that the para substitution on pyrazole rings A and B, especially with the p-nitro group on ring B and 2 amino groups on the pyrimidine ring, had unique consequences on the development of new Hsp90 inhibitors. The binding potential of the disubstituted

pyrazolyl pyrimidine scaffold and pocket of Hsp90 had effective interactions with Thr184, Asn51, and AsH93 (a protonated form of Asp93), Asp54, and Lys58 [152]. According to the results reported by Mettu et al. compound **56e** was the most active compound; the apoptosis potential of this compound was recognized by the Annexin V assay, where it could induce mitochondrial stress that increases membrane permeability, causing induction of apoptosis in MCF-7 cells. This was demonstrated by increasing the generation of J-monomer by applying JC-1 stain. Furthermore, a change in mitochondrial membrane potential could inevitably give rise to ROS strains as evidenced by DCFDA staining. In addition, this compound could stop the subG1 phase cell cycle. Thus, compound **56e** could serve as a potential compound with anticancer activity [153].

Mohamady et al. synthesized and evaluated possible biological activities of 3,5-diarylpyrazoles derivatives against HepG2 and MCF-7 cancerous cells. Among them, compound **57** exhibited the highest cytotoxic activity on HepG2 ( $IC_{50} = \sim 0.083 \mu M$ ) and MCF7 ( $IC_{50} = \sim 0.13 \mu M$ ) cells, with efficient anti-proliferation effectiveness. Compound **57** induced the inhibition of tumor cell proliferation by stimulating G2 phase inhibition, obstructing client proteins, such as c-Raf, EGFR, Akt, and c-Met and increasing the levels of Hsp70 [154]. Kadasi et al. reported the preparation of a novel series of *N*-pyridoyl-2-pyrazolines and evaluated their Hsp90 inhibitory activities for possible anticancer effects. The docking simulations revealed the binding potential of the synthesized compounds in the N-terminal ATP in Hsp90; moreover, the optimized compounds had significant interactions with Asp93 and Thr184. Consequently, compounds **58**, **59**, and **60** demonstrated an effective cytotoxic activity against MDA-MB-468 with  $IC_{50}$  of 1.60, 2.8, and 12  $\mu M$ , respectively. Compound **58** exhibited efficient inhibitory effect as well ( $IC_{50} = \sim 7.7 \mu M$ ) against A375 as human melanoma cells [155].

### 3. Conclusions and Future Outlook

Several investigations have focused on the design of inhibitors with heterocyclic structures to bring down the increased level of Hsp90 proteins in cancer or tumor cells, thus providing promising treatment strategies for cancer therapy with higher targeting and efficiency/efficacy. Hsp90 proteins have crucial roles in regulatory activity: folding, maintenance, function, and stability of various vital proteins, especially in client proteins. The inhibition of Hsp90s overexpressed in tumor cells can be considered an effective treatment strategy for various cancers. Numerous natural products and rationally designed synthetic Hsp90 inhibitors encompassing purine, pyrazole, triazine, quinolines, coumarin, and isoxazole structures can be viable candidates for further anticancer evaluations as deliberated. However, more systematic analyses and explorations are still needed for clinical applications and formulations of these compounds. Hsp90 proteins have serious roles with regulatory activity in folding, maintenance, function, and stability of various vital proteins, especially, client proteins, which make them attractive candidates for cancer therapy targets. The inhibition of these Hsp90s overexpressed in tumor cells can be considered as an effective treatment strategy for various cancers and malignancies.

In past years, several investigations have focused on heterocyclic structures, which are capable of inhibiting Hsp90 proteins, which are overexpressed in cancer or tumor cells, providing promising treatment strategies for cancer therapy with high targeting and efficiency. These Hsp90 inhibitors are attractive candidates due to their inhibitory effect against several cellular signaling pathways simultaneously in cancer cells or tumors. Natural compounds (**1–9**) were proposed as Hsp90 inhibitors, and some compounds were selected for animal and in-vivo studies. Compounds based on the purine structure (**10–12**) were synthesized which are claimed to bind to the Hsp90 inhibitors strength and inhibit tumor growth, these compounds were known as good candidates for clinical phase studies. Coumarin and its derivatives (**13–19**) have different biological activities such as platelet aggregation inhibition, antibacterial effects, and anticancer activity, these scaffolds also act as Hsp90 inhibitors. Modification of 4-hydroxyl and the 3'-carbamate functional groups

of novobiocin in compound **16** led to an increase in its activity more than 500 times from novobiocin.

Compounds aroylquinolone-based compounds were also categorized as Hsp90 inhibitors that prevent significant growth of cancerous cells. For example, compound **27** displayed an IC<sub>50</sub> of ~5.9 μM to inhibit tubulin polymerization and degradation of Hsp70 and Akt protein through WB analysis. Compound **35**, hybrid CH5015765, containing the 2-amino-1,3,5-triazines was recognized as an Hsp90 inhibitor with good anti-proliferative activity against HCT-116 and excellent binding affinity (K<sub>d</sub> = 3.4 nM). Triazines were also known as Hsp90 inhibitors with high activity and good anti-proliferative activity against HCT-116. In general, the triazine derivatives showed significant anti-proliferative activity in vitro and in vivo. Medicinal chemistry studies showed that the inclusion of isoxazole in the chemical structure of Hsp90 inhibitors can lead to improved efficacy. Isoxazole derivatives (**38–53**) can block the signaling cascade by binding to the ATP of the kinase protein and cause cell cycle arrest and apoptosis, investigations exposed that the isoxazole derivatives did not damage red blood cells, which strengthened the potential of these compounds as synthesized anticancer prototypes with low toxicity. Pyrazole derivatives (**54–64**) have remarkable activities, such as high efficiency as partial agonists at G protein and cannabinoid receptors, which make these properties useful inhibitors. This combination inhibits the proliferation of tumor cells by stimulating G2 phase inhibition. However, more systematic analyses are still needed for clinical applications and formulations of these compounds.

**Author Contributions:** M.A., Z.K. and F.K.: contributed equally to conceptualization and writing—review; S.I., H.S.-A. and R.S.V.: conceptualization, writing—review, and editing. All authors have read and agreed to the published version of the manuscript.

**Funding:** This work was supported by Projects 298121, 140192 and 988767 of the Pharmaceutical Sciences Research Center; National Institute for Medical Research Development.

**Institutional Review Board Statement:** Not applicable.

**Informed Consent Statement:** Not applicable.

**Data Availability Statement:** Not applicable.

**Acknowledgments:** The authors are thankful to National Institute for Medical Research Development for providing necessary research facilities. NIMAD (Project No. 988767) and the Pharmaceutical Sciences Research Center (Projects No. 298121, No. 140192).

**Conflicts of Interest:** There are no conflict of interest.

## References

- Mahboubi-Rabbani, M.; Zarghi, A. Lipoxygenase Inhibitors as Cancer Chemopreventives: Discovery, Recent Developments and Future Perspectives. *Curr. Med. Chem.* **2021**, *28*, 1143–1175. [CrossRef] [PubMed]
- Schopf, F.H.; Biebl, M.M.; Buchner, J. The Hsp90 chaperone machinery. *Nat. Rev. Mol. Cell Biol.* **2017**, *18*, 345–360. [CrossRef] [PubMed]
- Mahalingam, D.; Swords, R.; Carew, J.S.; Nawrocki, S.T.; Bhalla, K.; Giles, F.J. Targeting HSP90 for cancer therapy. *Br. J. Cancer* **2009**, *100*, 1523–1529. [CrossRef] [PubMed]
- Ischia, J.; So, A.I. The role of heat shock proteins in bladder cancer. *Nat. Rev. Urol.* **2013**, *10*, 386–395. [CrossRef]
- Davenport, J.; Manjarrez, J.R.; Peterson, L.; Krumm, B.; Blagg, B.S.J.; Matts, R.L. Gambogic Acid, a Natural Product Inhibitor of Hsp90. *J. Nat. Prod.* **2011**, *74*, 1085–1092. [CrossRef] [PubMed]
- Bhat, R.; Tummalapalli, S.R.; Rotella, D.P.J. Progress in the Discovery and Development of Heat Shock Protein 90 (Hsp90) Inhibitors: Miniperspective. *Med. Chem.* **2014**, *57*, 8718–8728. [CrossRef] [PubMed]
- Jaeger, A.M.; Whitesell, L. Hsp90: Enabler of Cancer Adaptation. *Annu. Rev. Cancer Biol.* **2019**, *3*, 275–297. [CrossRef]
- Gupta, S.D.; Bommaka, M.K.; Banerjee, A. Inhibiting protein-protein interactions of Hsp90 as a novel approach for targeting cancer. *Eur. J. Med. Chem.* **2019**, *178*, 48–63. [CrossRef]
- Wang, L.; Zhang, Q.; You, Q. Targeting the HSP90–CDC37–kinase chaperone cycle: A promising therapeutic strategy for cancer. *Med. Res. Rev.* **2022**, *42*, 156–182. [CrossRef]
- Li, L.; Chen, N.-N.; You, Q.-D.; Xu, X.-L. An updated patent review of anticancer Hsp90 inhibitors (2013–present). *Expert Opin. Ther. Patents* **2021**, *31*, 67–80. [CrossRef]

11. Niu, M.; Song, S.; Su, Z.; Wei, L.; Li, L.; Pu, W.; Zhao, C.; Ding, Y.; Wang, J.; Cao, W.; et al. Inhibition of heat shock protein (HSP) 90 reverses signal transducer and activator of transcription (STAT) 3-mediated muscle wasting in cancer cachexia mice. *Br. J. Pharmacol.* **2021**, *178*, 4485–4500. [CrossRef] [PubMed]
12. Jafari, A.; Rezaei-Tavirani, M.; Farhadhosseinabadi, B.; Taranejoo, S.; Zali, H. HSP90 and Co-chaperones: Impact on Tumor Progression and Prospects for Molecular-Targeted Cancer Therapy. *Cancer Investig.* **2020**, *38*, 310–328. [CrossRef] [PubMed]
13. Sanchez, J.; Carter, T.R.; Cohen, M.S.; Blagg, B.S.J. Old and New Approaches to Target the Hsp90 Chaperone. *Curr. Cancer Drug Targets* **2020**, *20*, 253–270. [CrossRef] [PubMed]
14. Trepel, J.; Mollapour, M.; Giaccone, G.; Neckers, L. Targeting the dynamic HSP90 complex in cancer. *Nat. Rev. Cancer* **2010**, *10*, 537–549. [CrossRef]
15. Nazarpour, E.; Mousazadeh, F.; Moghadam, M.D.; Najafi, K.; Borhani, F.; Sarani, M.; Ghasemi, M.; Rahdar, A.; Iravani, S.; Khatami, M. Biosynthesis of lead oxide and cerium oxide nanoparticles and their cytotoxic activities against colon cancer cell line. *Inorg. Chem. Commun.* **2021**, *131*, 108800. [CrossRef]
16. Iravani, S.; Varma, R.S. MXenes for Cancer Therapy and Diagnosis: Recent Advances and Current Challenges. *ACS Biomater. Sci. Eng.* **2021**, *7*, 1900–1913. [CrossRef]
17. Delfi, M.; Sartorius, R.; Ashrafzadeh, M.; Sharifi, E.; Zhang, Y.; De Berardinis, P.; Zarrabi, A.; Varma, R.S.; Tay, F.R.; Smith, B.R.; et al. Self-assembled peptide and protein nanostructures for anti-cancer therapy: Targeted delivery, stimuli-responsive devices and immunotherapy. *Nano Today* **2021**, *38*, 101119. [CrossRef]
18. Alavi, M.; Varma, R.S. Overview of Novel Strategies for the Delivery of Anthracyclines to Cancer Cells by Liposomal and Polymeric Nano Formulations. *Int. J. Biol. Macromol.* **2020**, *164*, 2197–2203. [CrossRef]
19. Makvandi, P.; Baghbantaraghdari, Z.; Zhou, W.; Zhang, Y.; Manchanda, R.; Agarwal, T.; Wu, A.; Maiti, T.K.; Varma, R.S.; Smith, B.R. Gum polysaccharide/nanometal hybrid biocomposites in cancer diagnosis and therapy. *Biotechnol. Adv.* **2021**, *48*, 107711. [CrossRef]
20. Hajipour, A.R.; Khorsandi, Z.; Mortazavi, M.; Farrokhpour, H. Green, efficient and large-scale synthesis of benzimidazoles, benzoxazoles and benzothiazoles derivatives using ligand-free cobalt-nanoparticles: As potential anti-estrogen breast cancer agents, and study of their interactions with estrogen receptor by molecular docking. *RSC Adv.* **2015**, *5*, 107822–107828. [CrossRef]
21. Khorsandi, Z.; Hajipour, A.R.; Sarfjoo, M.R.; Varma, R.S. A Pd/Cu-Free magnetic cobalt catalyst for C–N cross coupling reactions: Synthesis of abemaciclib and fedratinib. *Green Chem.* **2021**, *23*, 5222–5229. [CrossRef]
22. Khorsandi, Z.; Keshavarzipour, F.; Varma, R.S.; Hajipour, A.R.; Sadeghi-Aliabadi, H. Sustainable synthesis of potential antitumor new derivatives of Abemaciclib and Fedratinib via C-N cross coupling reactions using Pd/Cu-free Co-catalyst. *Mol. Catal.* **2021**, *517*, 112011. [CrossRef]
23. Whitesell, L.; Lindquist, S.L. HSP90 and the chaperoning of cancer. *Nat. Rev. Cancer.* **2005**, *5*, 761–772. [CrossRef] [PubMed]
24. Jego, G.; Hazoumé, A.; Seigneuric, R.; Garrido, C. Targeting heat shock proteins in cancer. *Cancer Lett.* **2013**, *332*, 275–285. [CrossRef]
25. Calderwood, S.K.; Khaleque, M.A.; Sawyer, D.B.; Ciocca, D.R. Heat Shock Proteins in Cancer: Chaperones of Tumorigenesis. *J. Pet. Sci. Eng.* **2006**, *31*, 164–172.
26. Patel, H.J.; Patel, P.D.; Ochiana, S.O.; Yan, P.; Sun, W.; Patel, M.R.; Shah, S.K.; Tramentozzi, E.; Brooks, J.; Bolaender, A.J. Structure–Activity Relationship in a Purine-Scaffold Compound Series with Selectivity for the Endoplasmic Reticulum Hsp90 ParalogGrp94. *Med. Chem.* **2015**, *58*, 3922–3943. [CrossRef]
27. Johnson, J.L. Evolution and function of diverse Hsp90 homologs and cochaperone proteins. *Biochim. Biophys. Acta Mol. Cell Res.* **2012**, *1823*, 607–613. [CrossRef]
28. Csermely, P.; Miyata, Y.; Schneider, T.; Yahara, I. Autophosphorylation of grp94 (Endoplasmic). *J. Biol. Chem.* **1995**, *270*, 6381–6388. [CrossRef]
29. Mishra, P.; Bolon, D.N. Designed Hsp90 Heterodimers Reveal an Asymmetric ATPase-Driven Mechanism In Vivo. *Mol. Cell* **2014**, *53*, 344–350. [CrossRef]
30. Meyer, P.; Prodromou, C.; Hu, B.; Vaughan, C.; Roe, S.M.; Panaretou, B.; Piper, P.W.; Pearl, L.H. Structural and Functional Analysis of the Middle Segment of Hsp90: Implications for ATP Hydrolysis and Client Protein and Cochaperone Interactions. *Mol. Cell* **2003**, *11*, 647–658. [CrossRef]
31. Gupta, S.D. Hsp90 Flexibility and Development of its Inhibitors for the Treatment of Cancer. *Curr. Chem. Biol.* **2018**, *12*, 53–64. [CrossRef]
32. Gupta, S.D. Novel Anti-Cancer Drugs Based on Hsp90 Inhibitory Mechanisms: A Recent Report. In *Medicinal Chemistry with Pharma-Ceutical Product Development*; Apple Academic Press: New York, NY, USA, 2019; pp. 57–104.
33. Gupta, S.D.; Pan, C.H. Recent update on discovery and development of Hsp90 inhibitors as senolytic agents. *Int. J. Biol. Macromol.* **2020**, *161*, 1086–1098. [CrossRef] [PubMed]
34. Hanahan, D.; Weinberg, R.A. The Hallmarks of Cancer. *Cell* **2000**, *100*, 57–70. [CrossRef]
35. Hanahan, D.; Weinberg, R.A. Hallmarks of cancer: The next generation. *Cell* **2011**, *144*, 646–674. [CrossRef]
36. Vartholomaiou, E.; Echeverría, P.C.; Picard, D. Unusual Suspects in the Twilight Zone Between the Hsp90 Interactome and Carcinogenesis. *Adv. Cancer Res.* **2016**, *129*, 1–30. [CrossRef]

37. Hayat, U.; Elliott, G.T.; Olszanski, A.J.; Altieri, D.C. Feasibility and safety of targeting mitochondria for cancer therapy—preclinical characterization of gamitrinib, a first-in-class, mitochondrial-targeted small molecule Hsp90 inhibitor. *Cancer Biol. Ther.* **2022**, *23*, 117–126. [CrossRef]
38. Biondini, M.; Kiepas, A.; El-Houjeiri, L.; Annis, M.G.; Hsu, B.E.; Fortier, A.-M.; Morin, G.; Martina, J.A.; Sirois, I.; Aguilar-Mahecha, A.; et al. HSP90 inhibitors induce GPNMB cell-surface expression by modulating lysosomal positioning and sensitize breast cancer cells to glembatumumab vedotin. *Oncogene* **2022**, *41*, 1701–1717. [CrossRef]
39. Epp-Ducharme, B.; Dunne, M.; Fan, L.; Evans, J.C.; Ahmed, L.; Bannigan, P.; Allen, C. Heat-activated nanomedicine formulation improves the anticancer potential of the HSP90 inhibitor luminespib in vitro. *Sci. Rep.* **2021**, *11*, 11103. [CrossRef]
40. Wu, Y.-W.; Chao, M.-W.; Tu, H.-J.; Chen, L.-C.; Hsu, K.-C.; Liou, J.-P.; Yang, C.-R.; Yen, S.-C.; HuangFu, W.-C.; Pan, S.-L. A novel dual HDAC and HSP90 inhibitor, MPT0G449, downregulates oncogenic pathways in human acute leukemia in vitro and in vivo. *Oncogenesis* **2021**, *10*, 39. [CrossRef]
41. Mshaik, R.; Simonet, J.; Georgievski, A.; Jamal, L.; Bechoua, S.; Ballerini, P.; Bellaye, P.-S.; Mlaml, Z.; de Barros, J.-P.P.; Geissler, A.; et al. HSP90 inhibitor NVP-BEP800 affects stability of SRC kinases and growth of T-cell and B-cell acute lymphoblastic leukemias. *Blood Cancer J.* **2021**, *11*, 61. [CrossRef]
42. Abdelmoaty, A.A.A.; Zhang, P.; Lin, W.; Fan, Y.-J.; Ye, S.-N.; Xu, J.-H. C0818, a novel curcumin derivative, induces ROS-dependent cytotoxicity in human hepatocellular carcinoma cells in vitro via disruption of Hsp90 function. *Acta Pharmacol. Sin.* **2022**, *43*, 446–456. [CrossRef] [PubMed]
43. Zhao, S.; Zhou, L.; Dicker, D.T.; Lev, A.; Zhang, S.; Ross, E.; El-Deiry, W.S. Anti-Cancer Efficacy Including Rb-Deficient Tumors and VHL-Independent HIF1 $\alpha$  Proteasomal Destabilization by Dual Targeting of CDK1 or CDK4/6 and Hsp90. *Sci. Rep.* **2021**, *11*, 20871. [CrossRef] [PubMed]
44. Chen, X.-L.; Liu, P.; Zhu, W.-L.; Lou, L.-G. DCZ5248, a novel dual inhibitor of Hsp90 and autophagy, exerts antitumor activity against colon cancer. *Acta Pharmacol. Sin.* **2021**, *42*, 132–141. [CrossRef] [PubMed]
45. Cheng, C.-J.; Liu, K.-X.; Zhang, M.; Shen, F.-K.; Ye, L.-L.; Wu, W.-B.; Hou, X.-T.; Hao, E.-W.; Hou, Y.-Y.; Bai, G. Okicamelliaside targets the N-terminal chaperone pocket of HSP90 disrupts the chaperone protein interaction of HSP90-CDC37 and exerts antitumor activity. *Acta Pharmacol. Sin.* **2021**, *43*, 1046–1058. [CrossRef] [PubMed]
46. Konstantinopoulos, P.A.; Cheng, S.-C.; Supko, J.G.; Polak, M.; Wahner-Hendrickson, A.E.; Ivy, S.P.; Bowes, B.; Sawyer, H.; Basada, P.; Hayes, M.; et al. Combined PARP and HSP90 inhibition: Preclinical and Phase 1 evaluation in patients with advanced solid tumours. *Br. J. Cancer* **2021**, *126*, 1027–1036. [CrossRef]
47. Magwenyane, A.M.; Lawal, M.M.; Amoako, D.G.; Somboro, A.M.; Agoni, C.; Khan, R.B.; Mhlongo, N.N.; Kumalo, H.M. Exploring the inhibitory mechanism of resorcinylic isoxazole amine NVP-AUY922 towards the discovery of potential heat shock protein 90 (Hsp90) inhibitors. *Sci. Afr.* **2022**, *15*, e01107. [CrossRef]
48. Serwetnyk, M.A.; Blagg, S.J. The Disruption of Protein–Protein Interactions with Co-chaperones and Client Substrates as a Strategy Towards Hsp90 Inhibition. *Acta. Pharm. Sin. B* **2021**, *11*, 1446–1468. [CrossRef]
49. Roe, S.M.; Prodromou, C.; O'Brien, R.; Ladbury, J.E.; Piper, P.W.; Pearl, L.H. Structural Basis for Inhibition of the Hsp90 Molecular Chaperone by the Antitumor Antibiotics Radicol and Geldanamycin. *J. Med. Chem.* **1999**, *42*, 260–266. [CrossRef]
50. Supko, J.G.; Hickman, R.L.; Grever, M.R.; Malspeis, L. Preclinical Pharmacologic Evaluation of Geldanamycin as an Antitumor Agent. *Cancer Chemother. Pharmacol.* **1995**, *36*, 305–315. [CrossRef]
51. Banerji, U.; O'Donnell, A.; Scurr, M.; Benson, C.; Hanwell, J.; Clark, S.; Raynaud, F.; Turner, A.; Walton, M.; Workman, P.; et al. Phase I Trial of the Heat Shock Protein 90 (Hsp90) Inhibitor 17-Allylamino 17-Demethoxygeldanamycin (17AAG). Pharmacokinetic (PK) Profile and Pharmacodynamic (PD) Endpoints. *Proc. Am. Soc. Clin. Oncol.* **2001**, *20*, 326.
52. Egorin, M.J.; Zuhowski, E.G.; Rosen, D.M.; Sentz, D.L.; Covey, J.M.; Eiseman, J.L. Plasma pharmacokinetics and tissue distribution of 17-(allylamino)-17-demethoxygeldanamycin (NSC 330507) in CD2F1 mice. *Cancer Chemother. Pharmacol.* **2001**, *47*, 291–302. [CrossRef] [PubMed]
53. Egorin, M.J.; Lagattuta, T.F.; Hamburger, D.R.; Covey, J.M.; White, K.D.; Musser, S.M.; Eiseman, J.L. Pharmacokinetics, tissue distribution, and metabolism of 17-(dimethylaminoethylamino)-17-demethoxygeldanamycin (NSC 707545) in CD2F1 mice and Fischer 344 rats. *Cancer Chemother. Pharmacol.* **2002**, *49*, 7–19. [CrossRef] [PubMed]
54. Munster, P.N.; Tong, L.; Schwartz, L.; Larson, S.; Kenneson, K.; De La Cruz, A.; Rosen, N.; Scher, H. Phase I Trial of 17(Allylamino)-17-demethoxygeldanamycin (17AAG) in Patients (Pts) with Advanced Solid Malignancies. *Proc. Am. Soc. Clin. Oncol.* **2001**, *20*, 83–91.
55. Soga, S.; Sharma, S.V.; Shiotsu, Y.; Shimizu, M.; Tahara, H.; Yamaguchi, K.; Ikuina, Y.; Murakata, C.; Tamaoki, T.; Kurebayashi, J.; et al. Stereospecific antitumor activity of radicol oxime derivatives. *Cancer Chemother. Pharmacol.* **2001**, *48*, 435–445. [CrossRef] [PubMed]
56. Johnson, V.A.; Singh, E.K.; Nazarova, L.A.; Alexander, L.D.; McAlpine, S.R. Macrocyclic inhibitors of hsp90. *Curr. Top. Med. Chem.* **2010**, *10*, 1380–1402. [CrossRef] [PubMed]
57. Porter, J.R.; Ge, J.; Lee, J.; Normant, E.; West, K. Ansamycin Inhibitors of Hsp90: Nature's Prototype for Anti-chaperone Therapy. *Curr. Top. Med.* **2009**, *9*, 1386–1418. [CrossRef]
58. Tanida, S.; Hasegawa, T.; Higashide, E.; Macbecins, I.; Macbecins, I.I. New Antitumor Antibiotics. I. Producing Organism, Fermentation and Antimicrobial Activities. *J. Antibiot.* **1980**, *33*, 199–204. [CrossRef]



59. Tian, Z.-Q.; Liu, Y.; Zhang, D.; Wang, Z.; Dong, S.D.; Carreras, C.W.; Zhou, Y.; Rastelli, G.; Santi, D.V.; Myles, D.C. Synthesis and biological activities of novel 17-aminogeldanamycin derivatives. *Bioorg. Med. Chem.* **2004**, *12*, 5317–5329. [CrossRef]
60. Wagner, A.J.; Chugh, R.; Rosen, L.S.; Morgan, J.A.; George, S.; Gordon, M.; Dunbar, J.; Normant, E.; Grayzel, D.; Demetri, G.D. A Phase I Study of the HSP90 Inhibitor Retaspimycin Hydrochloride (IPI-504) in Patients with Gastrointestinal Stromal Tumors or Soft-Tissue Sarcomas. *Clin. Cancer Res.* **2013**, *19*, 6020–6029. [CrossRef]
61. Floris, G.; Debiec-Rychter, M.; Wozniak, A.; Stefan, C.; Normant, E.; Faa, G.; Machiels, K.; Vanleeuw, U.; Sciot, R.; Schöffski, P. The Heat Shock Protein 90 Inhibitor IPI-504 Induces KIT Degradation, Tumor Shrinkage, and Cell Proliferation Arrest in Xenograft Models of Gastrointestinal Stromal Tumors. *Mol. Cancer Ther.* **2011**, *10*, 1897–1908. [CrossRef]
62. Floris, G.; Sciot, R.; Wozniak, A.; Van Looy, T.; Wellens, J.; Faa, G.; Normant, E.; Debiec-Rychter, M.; Schöffski, P. The Novel Hsp90 inhibitor, IPI-493, is Highly Effective in Human Gastrointestinal Stromal Tumor Xenografts Carrying Heterogeneous KIT Mutations. *Clin. Cancer Res.* **2011**, *17*, 5604–5614. [CrossRef] [PubMed]
63. Whitesell, L.; Mimnaugh, E.G.; De Costa, B.; Myers, C.E.; Neckers, L.M. Inhibition of heat shock protein HSP90-pp60v-src heteroprotein complex formation by benzoquinone ansamycins: Essential role for stress proteins in oncogenic transformation. *Proc. Natl. Acad. Sci. USA* **1994**, *91*, 8324–8328. [CrossRef] [PubMed]
64. Stebbins, C.E.; Russo, A.A.; Schneider, C.; Rosen, N.; Hartl, F.; Pavletich, N.P. Crystal Structure of an Hsp90–Geldanamycin Complex: Targeting of a Protein Chaperone by an Antitumor Agent. *Cell* **1997**, *89*, 239–250. [CrossRef]
65. Soga, S.; Shiotsu, Y.; Akinaga, S.; Sharma, S. Development of Radicicol Analogues. *Curr. Cancer Drug Targets* **2003**, *3*, 359–369. [CrossRef] [PubMed]
66. Miyata, Y. Hsp90 Inhibitor Geldanamycin and Its Derivatives as Novel Cancer Chemotherapeutic Agents. *Curr. Pharm. Des.* **2005**, *11*, 1131–1138. [CrossRef]
67. Chiosis, G.; Lucas, B.; Huez, H.; Solit, D.; Basso, A.; Rosen, N. Development of Purine-Scaffold Small Molecule Inhibitors of Hsp90. *Curr. Cancer Drug Targets* **2003**, *3*, 371–376. [CrossRef]
68. Conejo-García, A.; García-Rubiño, M.E.; Marchal, J.A.; Núñez, M.C.; Ramírez, A.; Cimino, S.; García, M.; Aránega, A.; Gallo, M.A.; Campos, J.M. Synthesis and anticancer activity of (RS)-9-(2,3-dihydro-1,4-benzoxaheteroin-2-ylmethyl)-9H-purines. *Eur. J. Med. Chem.* **2011**, *46*, 3795–3801. [CrossRef]
69. Pelliccia, S.; Amato, J.; Capasso, D.; Di Gaetano, S.; Massarotti, A.; Piccolo, M.; Irace, C.; Tron, G.C.; Pagano, B.; Randazzo, A.J. Bio-Inspired Dual-Selective BCL-2/c-MYC G-Quadruplex Binders: Design, Synthesis, and Anticancer Activity of Drug-like Imidazo [2,1-i] purine Derivatives. *Med. Chem.* **2019**, *63*, 2035–2050. [CrossRef]
70. Ashour, F.A.; Rida, S.M.; El-Hawash, S.A.; ElSemaary, M.M.; Badr, M.H. Synthesis, Anticancer, Anti-HIV-1, and Antimicrobial Activity of Some Tricyclic Triazino and Triazolo [4,3-e] purine Derivatives. *Cancer Causes Control* **2012**, *21*, 1107–1119. [CrossRef]
71. Kinali-Demirci, S.; İdil, Ö.; Dişli, A. Synthesis of Some Novel Purine Derivatives Incorporating Tetrazole Ring and Investigation of their Antimicrobial Activity and DNA Interactions. *Cancer Cell Int. J. Mol. Histol.* **2015**, *24*, 1218–1225. [CrossRef]
72. Abdallah, A.E.; Elgemeie, G.H. Development; Therapy, Design, Synthesis, Docking, and Antimicrobial Evaluation of Some Novel Pyrazolo [1,5-a] Pyrimidines and their Corresponding Cycloalkane Ring-fused Derivatives as Purine Analogs. *Drug Des. Devel. Ther.* **2018**, *12*, 1785–1798. [CrossRef] [PubMed]
73. Rosemeyer, H. The Chemodiversity of Purine as a Constituent of Natural Products. *Chem. Biodivers.* **2004**, *1*, 361–401. [CrossRef] [PubMed]
74. Kaneko, K.; Aoyagi, Y.; Fukuuchi, T.; Inazawa, K.; Yamaoka, N. Total Purine and Purine Base Content of Common Foodstuffs for Facilitating Nutritional Therapy for Gout and Hyperuricemia. *Biol. Pharm. Bull.* **2014**, *37*, 709–721. [CrossRef] [PubMed]
75. Yin, J.; Ren, W.; Huang, X.; Deng, J.; Li, T.; Yin, Y. Potential Mechanisms Connecting Purine Metabolism and Cancer Therapy. *Front. Immunol.* **2018**, *9*, 1697. [CrossRef] [PubMed]
76. Chiosis, G.; Timaull, M.N.; Lucas, B.; Munster, P.N.; Zheng, F.F.; Sepp-Lorenzino, L.; Rosen, N. A small molecule designed to bind to the adenine nucleotide pocket of Hsp90 causes Her2 degradation and the growth arrest and differentiation of breast cancer cells. *Chem. Biol.* **2001**, *8*, 289–299. [CrossRef]
77. Bao, R.; Lai, C.-J.; Qu, H.; Wang, D.; Yin, L.; Zifcak, B.; Atoyan, R.; Wang, J.; Samson, M.; Forrester, J.; et al. CUDC-305, a Novel Synthetic HSP90 Inhibitor with Unique Pharmacologic Properties for Cancer Therapy. *Clin. Cancer Res.* **2009**, *15*, 4046–4057. [CrossRef]
78. Zhang, H.; Neely, L.; Lundgren, K.; Yang, Y.-C.; Lough, R.; Timple, N.; Burrows, F. BIIB021, a synthetic HSP90 inhibitor, has broad application against tumors with acquired multidrug resistance. *Int. J. Cancer* **2010**, *126*, 1226–1234. [CrossRef]
79. Yin, X.; Zhang, H.; Lundgren, K.; Wilson, L.; Burrows, F.; Shores, C.G. BIIB021, a novel HSP90 inhibitor, sensitizes head and neck squamous cell carcinoma to radiotherapy. *Int. J. Cancer* **2010**, *126*, 1216–1225. [CrossRef]
80. Chaurasiya, A.; Wahan, S.K.; Sahu, C.; Chawla, P.A. An insight into the rational design of recent purine-based scaffolds in targeting various cancer pathways. *J. Mol. Struct.* **2022**, 134308. [CrossRef]
81. Wang, X.-T.; Bao, C.-H.; Jia, Y.-B.; Wang, N.; Ma, W.; Liu, F.; Wang, C.; Wang, J.-B.; Song, Q.-X.; Cheng, Y.-F. BIIB021, a novel Hsp90 inhibitor, sensitizes esophageal squamous cell carcinoma to radiation. *Biochem. Biophys. Res. Commun.* **2014**, *452*, 945–950. [CrossRef]
82. ElFiky, A.; Saif, M.W.; Beeram, M.; Brien, S.O.; Lammanna, N.; Castro, J.E.; Woodworth, J.; Perea, R.; Storgard, C.; Von Hoff, D.D. BIIB021, an oral, synthetic non-ansamycin Hsp90 inhibitor: Phase I experience. *J. Clin. Oncol.* **2008**, *26*, 2503. [CrossRef]

83. Dickson, M.A.; Okuno, S.H.; Keohan, M.L.; Maki, R.G.; D'Adamo, D.R.; Akhurst, T.J.; Antonescu, C.R.; Schwartz, G.K. Phase II study of the HSP90-inhibitor BIIB021 in gastrointestinal stromal tumors. *Ann. Oncol.* **2013**, *24*, 252–257. [CrossRef] [PubMed]
84. Emami, S.; Dadashpour, S. Current developments of coumarin-based anti-cancer agents in medicinal chemistry. *Eur. J. Med. Chem.* **2015**, *102*, 611–630. [CrossRef] [PubMed]
85. Zhang, L.; Xu, Z. Coumarin-containing hybrids and their anticancer activities. *Eur. J. Med. Chem.* **2019**, *181*, 111587. [CrossRef] [PubMed]
86. Al-Warhi, T.; Sabt, A.; Elkaeed, E.B.; Eldehna, W.M. Recent advancements of coumarin-based anticancer agents: An up-to-date review. *Bioorg. Chem.* **2020**, *103*, 104163. [CrossRef] [PubMed]
87. Song, X.; Fan, J.; Liu, L.; Liu, X.; Gao, F. Coumarin derivatives with anticancer activities: An update. *Arch. Pharm.* **2020**, *353*, 2000025. [CrossRef]
88. Qin, H.-L.; Zhang, Z.-W.; Ravindar, L.; Rakesh, K. Antibacterial activities with the structure-activity relationship of coumarin derivatives. *Eur. J. Med. Chem.* **2020**, *207*, 112832. [CrossRef]
89. Keshavarzipour, F.; Tavakol, H. The synthesis of coumarin derivatives using choline chloride/zinc chloride as a deep eutectic solvent. *J. Iran. Chem. Soc.* **2016**, *13*, 149–153. [CrossRef]
90. Ahmed, E.Y.; Elserwy, W.S.; El-Mansy, M.F.; Serry, A.M.; Salem, A.M.; Abdou, A.M.; Abdelrahman, B.A.; Elsayed, K.H.; Elaziz, M.R.A. Angiokinase inhibition of VEGFR-2, PDGFR and FGFR and cell growth inhibition in lung cancer: Design, synthesis, biological evaluation and molecular docking of novel azaheterocyclic coumarin derivatives. *Bioorg. Med. Chem. Lett.* **2021**, *48*, 128258. [CrossRef]
91. Burlison, J.A.; Neckers, L.; Smith, A.B.; Maxwell, A.A.; Blagg, B.S.J. Novobiocin: Redesigning a DNA Gyrase Inhibitor for Selective Inhibition of Hsp90. *J. Am. Chem. Soc.* **2006**, *128*, 15529–15536. [CrossRef]
92. Shelton, S.N.; Shawgo, M.E.; Matthews, S.B.; Lu, Y.; Donnelly, A.C.; Szabla, K.; Tanol, M.; Vielhauer, G.A.; Rajewski, R.A.; Matts, R.L.; et al. KU135, a Novel Novobiocin-Derived C-Terminal Inhibitor of the 90-kDa Heat Shock Protein, Exerts Potent Antiproliferative Effects in Human Leukemic Cells. *Mol. Pharmacol.* **2009**, *76*, 1314–1322. [CrossRef] [PubMed]
93. Garg, G.; Zhao, H.; Blagg, B.S.J. Design, Synthesis, and Biological Evaluation of Ring-Constrained Novobiocin Analogues as Hsp90 C-Terminal Inhibitors. *ACS Med. Chem. Lett.* **2015**, *6*, 204–209. [CrossRef] [PubMed]
94. Wei, Q.; Ning, J.-Y.; Dai, X.; Gao, Y.-D.; Su, L.; Zhao, B.-X.; Miao, J.-Y. Discovery of novel HSP90 inhibitors that induced apoptosis and impaired autophagic flux in A549 lung cancer cells. *Eur. J. Med. Chem.* **2018**, *145*, 551–558. [CrossRef] [PubMed]
95. Kouznetsov, V.V.; Méndez, L.Y.V.; Galvis, C.E.P.; Villamizar, M.C.O. The direct C–H alkenylation of quinoline *N*-oxides as a suitable strategy for the synthesis of promising antiparasitic drugs. *New J. Chem.* **2020**, *44*, 12–19. [CrossRef]
96. Keshavarzipour, F.; Tavakol, H. Zinc Cation Supported on Carrageenan Magnetic Nanoparticles: A Novel, Green and Efficient Catalytic System for One-pot Three-Component Synthesis of Quinoline Derivatives. *Appl. Organomet. Chem.* **2017**, *31*, 3682–3692. [CrossRef]
97. Insuasty, D.; García, S.; Abonia, R.; Insuasty, B.; Quiroga, J.; Nogueras, M.; Laali, K.K. Design, Synthesis, and Molecular Docking Study of Novel Quinoline-Based Bis-Chalcones as Potential Antitumor Agents. *Arch. Pharm.* **2021**, *354*, 2100094–2100103. [CrossRef]
98. Jin, G.; Li, Z.; Xiao, F.; Qi, X.; Sun, X. Optimization of activity localization of quinoline derivatives: Design, synthesis, and dual evaluation of biological activity for potential antitumor and antibacterial agents. *Bioorg. Chem.* **2020**, *99*, 103837. [CrossRef]
99. Mishra, S.; Salahuddin, R.K.; Majumder, A.; Kumar, A.; Singh, C.; Tigiani, D. Updates on Synthesis and Biological Activities of Quinoline Derivatives: A Review. *Int. J. Pharm. Sci. Rev. Res.* **2021**, *13*, 3941–3960.
100. Goyal, S.; Binnington, B.; McCarthy, S.D.; Desmaële, D.; Férié, L.; Figadère, B.; Loiseau, P.M.; Branch, D.R. Inhibition of in vitro Ebola infection by anti-parasitic quinoline derivatives. *F1000Research* **2020**, *9*, 268. [CrossRef]
101. Verma, C.; Quraishi, M.; Ebenso, E.E. Quinoline and its derivatives as corrosion inhibitors: A review. *Surfaces Interfaces* **2020**, *21*, 100634. [CrossRef]
102. Kayamba, F.; Malimabe, T.; Ademola, I.K.; Poee, O.J.; Kushwaha, N.D.; Mahlalela, M.; van Zyl, R.L.; Gordon, M.; Mudau, P.T.; Zininga, T.; et al. Design and synthesis of quinoline-pyrimidine inspired hybrids as potential plasmodial inhibitors. *Eur. J. Med. Chem.* **2021**, *217*, 113330. [CrossRef] [PubMed]
103. Rao, K.V.; Cullen, W.P. Streptonigrin, an Antitumor Substance. I. Isolation and Characterization. *Antibiot. Annu.* **1959**, *7*, 950–953.
104. Chirigos, M.A.; Pearson, J.W.; Papas, T.S.; Woods, W.A.; Wood, H.B., Jr.; Spahn, G. Effect of Three Strains of BeG Against a Murine Leukemia After Drug Therapy. *Cancer Chemother. Rep.* **1973**, *57*, 305–309.
105. Balitz, D.M.; Bush, J.A.; Bradner, W.T.; Doyle, T.W.; O'Herron, F.A.; Nettleton, D.E. Isolation of lavendamycin. A new antibiotic from *Streptomyces lavendulae*. *J. Antibiot.* **1982**, *35*, 259–265. [CrossRef] [PubMed]
106. Ganesh, T.; Min, J.; Thepchatrri, P.; Du, Y.; Li, L.; Lewis, I.; Wilson, L.; Fu, H.; Chiosis, G.; Dingleline, R.; et al. Discovery of aminoquinolines as a new class of potent inhibitors of heat shock protein 90 (Hsp90): Synthesis, biology, and molecular modeling. *Bioorg. Med. Chem.* **2008**, *16*, 6903–6910. [CrossRef] [PubMed]
107. Audisio, D.; Messaoudi, S.; Cegiolkowski, L.; Peyrat, J.-F.; Brion, J.-D.; Methy-Gonnot, D.; Radanyi, C.; Renoir, J.-M.; Alami, M. Discovery and Biological Activity of 6BrCaQ as an Inhibitor of the Hsp90 Protein Folding Machinery. *Chem. Med. Chem.* **2011**, *6*, 804–815. [CrossRef]

108. Nepali, K.; Kumar, S.; Huang, H.-L.; Kuo, F.-C.; Lee, C.-H.; Kuo, C.-C.; Yeh, T.-K.; Li, Y.-H.; Chang, J.-Y.; Liou, J.-P.; et al. 2-Aroylquinoline-5,8-diones as potent anticancer agents displaying tubulin and heat shock protein 90 (HSP90) inhibition. *Org. Biomol. Chem.* **2015**, *14*, 716–723. [CrossRef]
109. Malayeri, S.O.; Abnous, K.; Arab, A.; Akaberi, M.; Mehri, S.; Zarghi, A.; Ghodsi, R. Design, Synthesis and Biological Evaluation of 7-(Aryl)-2,3-dihydro-[1,4] dioxino [2,3-g] Quinoline Derivatives as Potential Hsp90 Inhibitors and Anticancer Agents. *Bioorg. Med. Chem.* **2017**, *25*, 1294–1302. [CrossRef]
110. Liang, C.; Hao, H.; Wu, X.; Li, Z.; Zhu, J.; Lu, C.; Shen, Y. Design and synthesis of N-(5-chloro-2,4-dihydroxybenzoyl)-(R)-1,2,3,4-tetrahydroisoquinoline-3-carboxamides as novel Hsp90 inhibitors. *Eur. J. Med. Chem.* **2016**, *121*, 272–282. [CrossRef]
111. Nepali, K.; Lin, M.-H.; Chao, M.-W.; Peng, S.-J.; Hsu, K.-C.; Lin, T.E.; Chen, M.-C.; Lai, M.-J.; Pan, S.-L.; Liou, J.-P. Amide-tethered quinoline-resorcinol conjugates as a new class of HSP90 inhibitors suppressing the growth of prostate cancer cells. *Bioorg. Chem.* **2019**, *91*, 103119. [CrossRef]
112. Relitti, N.; Saraswati, A.P.; Chemi, G.; Brindisi, M.; Brogi, S.; Herp, D.; Schmidtkunz, K.; Saccoccia, F.; Ruberti, G.; Ulivieri, C.; et al. Novel quinolone-based potent and selective HDAC6 inhibitors: Synthesis, molecular modeling studies and biological investigation. *Eur. J. Med. Chem.* **2021**, *212*, 112998. [CrossRef] [PubMed]
113. Liu, H.; Long, S.; Rakesh, K.P.; Zha, G.F. Structure-Activity Relationships (SAR) of Triazine Derivatives: Promising Antimicrobial Agents. *Eur. J. Med. Chem.* **2020**, *185*, 111804. [CrossRef] [PubMed]
114. Gavade, S.N.; Markad, V.L.; Kodam, K.M.; Shingare, M.S.; Mane, D.V. Synthesis and Biological Evaluation of Novel 2, 4, 6-Triazine Derivatives as Antimicrobial Agents. *Bioorg. Med. Chem. Lett.* **2012**, *22*, 5075–5077. [CrossRef]
115. Cascioferro, S.; Parrino, B.; Spanò, V.; Carbone, A.; Montalbano, A.; Barraja, P.; Diana, P.; Cirrincione, G. An overview on the recent developments of 1,2,4-triazine derivatives as anticancer compounds. *Eur. J. Med. Chem.* **2017**, *142*, 328–375. [CrossRef] [PubMed]
116. Singla, P.; Luxami, V.; Paul, K. Triazine as a Promising Scaffold for its Versatile Biological Behavior. *Eur. J. Med. Chem.* **2015**, *102*, 39–57. [CrossRef]
117. Patel, P.K.; Patel, R.V.; Mahajan, D.H.; Parikh, P.A.; Mehta, G.N.; Pannecouque, C.; Chikhaliya, K.H. Different Heterocycles Functionalized s-Triazine Analogues: Design, Synthesis and In Vitro Antimicrobial, Antituberculosis, and Anti-HIV Assessment. *J. Heterocycl. Chem.* **2014**, *51*, 1641–1658. [CrossRef]
118. Feldman, R.I.; Mintzer, B.; Zhu, D.; Wu, J.M.; Biroc, S.L.; Yuan, S.; Emayan, K.; Chang, Z.; Chen, D.; Arnaiz, D.O.; et al. Potent Triazolothione Inhibitor of Heat-Shock Protein-90. *Oncol. Lett.* **2009**, *74*, 43–50. [CrossRef]
119. Lee, T.; Seo, Y.H. Targeting the hydrophobic region of Hsp90's ATP binding pocket with novel 1,3,5-triazines. *Bioorg. Med. Chem. Lett.* **2013**, *23*, 6427–6431. [CrossRef]
120. Miura, T.; Fukami, T.A.; Hasegawa, K.; Ono, N.; Suda, A.; Shindo, H.; Yoon, D.-O.; Kim, S.-J.; Na, Y.-J.; Aoki, Y.; et al. Lead generation of heat shock protein 90 inhibitors by a combination of fragment-based approach, virtual screening, and structure-based drug design. *Bioorg. Med. Chem. Lett.* **2011**, *21*, 5778–5783. [CrossRef]
121. Suda, A.; Koyano, H.; Hayase, T.; Hada, K.; Kawasaki, K.-I.; Komiyama, S.; Hasegawa, K.; Fukami, T.A.; Sato, S.; Miura, T.; et al. Design and synthesis of novel macrocyclic 2-amino-6-arylpyrimidine Hsp90 inhibitors. *Bioorg. Med. Chem. Lett.* **2012**, *22*, 1136–1141. [CrossRef]
122. Suda, A.; Kawasaki, K.-I.; Komiyama, S.; Isshiki, Y.; Yoon, D.-O.; Kim, S.-J.; Na, Y.-J.; Hasegawa, K.; Fukami, T.A.; Sato, S.; et al. Design and synthesis of 2-amino-6-(1H,3H-benzo[de]isochromen-6-yl)-1,3,5-triazines as novel Hsp90 inhibitors. *Bioorg. Med. Chem.* **2014**, *22*, 892–905. [CrossRef] [PubMed]
123. Zhao, Z.; Zhu, J.; Quan, H.; Wang, G.; Li, B.; Zhu, W.; Xie, C.; Lou, L. X66, a novel N-terminal heat shock protein 90 inhibitor, exerts antitumor effects without induction of heat shock response. *Oncotarget* **2016**, *7*, 29648–29663. [CrossRef] [PubMed]
124. Ali, I.; Lone, M.; Al-Othman, Z.; Al-Warthan, A.; Sanagi, M. Heterocyclic Scaffolds: Centrality in Anticancer Drug Development. *Curr. Drug Targets* **2015**, *16*, 711–734. [CrossRef]
125. Çalışkan, B.; Sinoplu, E.; İbiş, K.; Akhan Güzelcan, E.; Atalay, R.Ç.; Banoglu, E. Synthesis and Cellular Bioactivities of Novel Isoxazole Derivatives Incorporating an Arylpiperazine Moiety as Anticancer Agents. *J. Enzym. Inhib. Med. Chem.* **2018**, *33*, 1352–1361. [CrossRef] [PubMed]
126. Shaik, A.; Bhandare, R.R.; Palleapati, K.; Nissankararao, S.; Kancharlapalli, V.; Shaik, S. Antimicrobial, Antioxidant, and Anticancer Activities of Some Novel Isoxazole Ring Containing Chalcone and Dihydropyrazole Derivatives. *Molecules* **2020**, *25*, 1047. [CrossRef] [PubMed]
127. Barmade, M.A.; Murumkar, P.R.; Sharma, M.K.; Yadav, M.R. Medicinal Chemistry Perspective of Fused Isoxazole Derivatives. *Curr. Top. Med. Chem.* **2016**, *16*, 2863–2883. [CrossRef] [PubMed]
128. Galenko, A.V.; Khlebnikov, A.F.; Novikov, M.S.; Pakalnis, V.V.; Rostovskii, N.V. Recent advances in isoxazole chemistry. *Russ. Chem. Rev.* **2015**, *84*, 335–377. [CrossRef]
129. Sysak, A.; Obmińska-Mrukowicz, B. Isoxazole ring as a useful scaffold in a search for new therapeutic agents. *Eur. J. Med. Chem.* **2017**, *137*, 292–309. [CrossRef]
130. Arya, G.C.; Kaur, K.; Jaitak, V. Isoxazole derivatives as anticancer agent: A review on synthetic strategies, mechanism of action and SAR studies. *Eur. J. Med. Chem.* **2021**, *221*, 113511. [CrossRef]
131. Fernald, K.; Kurokawa, M. Evading apoptosis in cancer. *Trends Cell Biol.* **2013**, *23*, 620–633. [CrossRef]

132. Tonks, N.K. Protein Tyrosine Phosphatases: From Genes, to Function, to Disease. *Nat. Rev. Mol. Cell Biol.* **2006**, *7*, 833–846. [CrossRef] [PubMed]
133. Taldone, T.; Gozman, A.; Maharaj, R.; Chiosis, G. Targeting Hsp90: Small-molecule inhibitors and their clinical development. *Curr. Opin. Pharmacol.* **2008**, *8*, 370–374. [CrossRef] [PubMed]
134. Sharp, S.Y.; Prodromou, C.; Boxall, K.; Powers, M.V.; Holmes, J.L.; Box, G.; Workman, P. Inhibition of The Heat Shock Protein 90 Molecular Chaperone in vitro and in vivo by Novel, Synthetic, Potent Resorcinylic Pyrazole/isoxazole Amide Analogues. *Mol. Cancer Ther.* **2007**, *6*, 1198–1211. [CrossRef] [PubMed]
135. Eccles, S.A.; Massey, A.; Raynaud, F.I.; Sharp, S.Y.; Box, G.; Valenti, M.; Patterson, L.; de Haven Brandon, A.; Gowan, S.; Boxall, F.; et al. NVP-AUY922: A Novel Heat Shock Protein 90 Inhibitor Active against Xenograft Tumor Growth, Angiogenesis, and Metastasis. *Cancer Res.* **2008**, *68*, 2850–2860. [CrossRef] [PubMed]
136. Chen, D.; Shen, A.; Li, J.; Shi, F.; Chen, W.; Ren, J.; Liu, H.; Xu, Y.; Wang, X.; Yang, X.; et al. Discovery of potent N-(isoxazol-5-yl)amides as HSP90 inhibitors. *Eur. J. Med. Chem.* **2014**, *87*, 765–781. [CrossRef] [PubMed]
137. Sun, J.; Lin, C.; Qin, X.; Dong, X.; Tu, Z.; Tang, F.; Chen, C.; Zhang, J. Synthesis and biological evaluation of 3,5-disubstituted-4-alkynylisoxazoles as a novel class of HSP90 inhibitors. *Bioorg. Med. Chem. Lett.* **2015**, *25*, 3129–3134. [CrossRef]
138. Shi, W.; Hu, J.; Bao, N.; Li, D.; Chen, L.; Sun, J. Design, synthesis and cytotoxic activities of scopoletin-isoxazole and scopoletin-pyrazole hybrids. *Bioorg. Med. Chem. Lett.* **2017**, *27*, 147–151. [CrossRef]
139. Abbasi, M.; Sadeghi-Aliabadi, H.; Amanlou, M. Prediction of New Hsp90 Inhibitors Based on 3, 4-Isoxazolidiamide Scaffold Using QSAR Study, Molecular Docking and Molecular Dynamic Simulation. *Daru J. Pharm. Sci.* **2017**, *25*, 17. [CrossRef]
140. Abbasi, M.; Sadeghi-Aliabadi, H.; Amanlou, M. 3D-QSAR, Molecular Docking, and Molecular Dynamic Simulations for Prediction of New Hsp90 Inhibitors Based on Isoxazole Scaffold. *J. Biomol. Struct. Dyn.* **2018**, *36*, 1463–1478. [CrossRef]
141. Kaushik, S.; Sanawar, R.; Lekshmi, A.; Chandrasekhar, L.; Nair, M.; Bhatnagar, S.; Santhoshkumar, T.R. ER alpha selective chromone, isoxazolylchromones, induces ROS-mediated cell death without autophagy. *Chem. Biol. Drug Des.* **2019**, 1352–1367.
142. Jung, J.; Kwon, J.; Hong, S.; Moon, A.-N.; Jeong, J.; Kwon, S.; Kim, J.-A.; Lee, M.; Lee, H.; Lee, J.H.; et al. Discovery of novel heat shock protein (Hsp90) inhibitors based on luminespib with potent antitumor activity. *Bioorg. Med. Chem. Lett.* **2020**, *30*, 127165. [CrossRef] [PubMed]
143. Aissa, I.; Abdelkafi-Koubaa, Z.; Chouaïb, K.; Jalouli, M.; Assel, A.; Romdhane, A.; Harrath, A.H.; Marrakchi, N.; Ben Jannet, H. Glioblastoma-specific anticancer activity of newly synthesized 3,5-disubstituted isoxazole and 1,4-disubstituted triazole-linked tyrosol conjugates. *Bioorg. Chem.* **2021**, *114*, 105071. [CrossRef] [PubMed]
144. Chaudhary, M.; Kumar, N.; Baldi, A.; Chandra, R.; Babu, M.A.; Madan, J. Chloro and bromo-pyrazole curcumin Knoevenagel condensates augmented anticancer activity against human cervical cancer cells: Design, synthesis, in silico docking and in vitro cytotoxicity analysis. *J. Biomol. Struct. Dyn.* **2020**, *38*, 200–218. [CrossRef] [PubMed]
145. Rai, G.; Urban, D.J.; Mott, B.T.; Hu, X.; Yang, S.-M.; Benavides, G.A.; Johnson, M.S.; Squadrito, G.L.; Brimacombe, K.R.; Lee, T.D.; et al. Pyrazole-Based Lactate Dehydrogenase Inhibitors with Optimized Cell Activity and Pharmacokinetic Properties. *J. Med. Chem.* **2020**, *63*, 10984–11011. [CrossRef]
146. Azimi, F.; Azizian, H.; Najafi, M.; Hassanzadeh, F.; Sadeghi-Aliabadi, H.; Ghasemi, J.B.; Mahdavi, M. Design and Synthesis of Novel Quinazolinone-Pyrazole Derivatives as Potential  $\alpha$ -Glucosidase Inhibitors: Structure-activity Relationship, Molecular Modeling and Kinetic Study. *Bioorg. Chem.* **2021**, *114*, 105127–105134. [CrossRef]
147. Abbasi, M.; Amanlou, M.; Aghaei, M.; Bakherad, M.; Doosti, R.; Sadeghi-Aliabadi, H. New heat shock protein (Hsp90) inhibitors, designed by pharmacophore modeling and virtual screening: Synthesis, biological evaluation and molecular dynamics studies. *J. Biomol. Struct. Dyn.* **2020**, *38*, 3462–3473. [CrossRef]
148. Bennani, F.E.; Doudach, L.; Cherrah, Y.; Ramli, Y.; Karrouchi, K.; Ansar, M.; Faouzi, M.E.A. Overview of recent developments of pyrazole derivatives as an anticancer agent in different cell line. *Bioorg. Chem.* **2020**, *97*, 103470. [CrossRef]
149. Bai, S.-Y.; Dai, X.; Zhao, B.-X.; Miao, J.-Y. Discovery of a novel fluorescent HSP90 inhibitor and its anti-lung cancer effect. *RSC Adv.* **2014**, *4*, 19887–19890. [CrossRef]
150. Abbasi, M.; Sadeghi-Aliabadi, H.; Hassanzadeh, F.; Amanlou, M. Prediction of dual agents as an activator of mutant p53 and inhibitor of Hsp90 by docking, molecular dynamic simulation and virtual screening. *J. Mol. Graph. Model.* **2015**, *61*, 186–195. [CrossRef]
151. Uno, T.; Kawai, Y.; Yamashita, S.; Oshiumi, H.; Yoshimura, C.; Mizutani, T.; Kitade, M. Discovery of 3-Ethyl-4-(3-isopropyl-4-(4-(1-methyl-1H-pyrazol-4-yl)-1H-imidazol-1-yl)-1H-pyrazolo [3,4-b] pyridin-1-yl) benzamide (TAS-116) as a Potent, Selective, and Orally Available Hsp90 Inhibitor. *J. Med. Chem.* **2018**, *62*, 531–551. [CrossRef]
152. Mettu, A.; Talla, V.; Bajaj, D.M.; Subhashini, N.J. Design, Synthesis, Molecular Docking Studies of Novel Pyrazolyl 2-Aminopyrimidine Derivatives as Hsp90 Inhibitors. *Arch. Pharm.* **2019**, *352*, 1900063. [CrossRef] [PubMed]
153. Mettu, A.; Talla, V.; Naikal, S.J.P. Novel anticancer Hsp90 inhibitor disubstituted pyrazolyl 2-aminopyrimidine compound 7t induces cell cycle arrest and apoptosis via mitochondrial pathway in MCF-7 cells. *Bioorg. Med. Chem. Lett.* **2020**, *30*, 127470. [CrossRef] [PubMed]
154. Mohamady, S.; Ismail, M.; Mogheith, S.M.; Attia, Y.M.; Taylor, S.D. Discovery of 5-aryl-3-thiophen-2-yl-1H-pyrazoles as a new class of Hsp90 inhibitors in hepatocellular carcinoma. *Bioorg. Chem.* **2020**, *94*, 103433. [CrossRef] [PubMed]
155. Kadasi, S.; Yerroju, R.; Gaddam, S.; Pullanagiri, N.; Chary, M.; Pingili, D.; Raghavendra, N.M. Discovery of N-Pyridoyl- $\Delta$ 2-pyrazolines as Hsp90 Inhibitors. *Arch. Der Pharm.* **2020**, *353*, 190019. [CrossRef]

## Article

# Bruton's Tyrosine Kinase Inhibitor Zanubrutinib Effectively Modulates Cancer Resistance by Inhibiting Anthracycline Metabolism and Efflux

Lucie Čermáková<sup>1</sup>, Jakub Hofman<sup>2</sup>, Lenka Laštovičková<sup>1</sup>, Lucie Havlíčková<sup>1</sup>, Ivona Špringrová<sup>1</sup>,  
Eva Novotná<sup>1</sup> and Vladimír Wsól<sup>1,\*</sup>

<sup>1</sup> Department of Biochemical Sciences, Faculty of Pharmacy, Charles University, Akademika Heyrovského 1203, 50005 Hradec Kralove, Czech Republic

<sup>2</sup> Department of Pharmacology and Toxicology, Faculty of Pharmacy, Charles University, Akademika Heyrovského 1203, 50005 Hradec Kralove, Czech Republic

\* Correspondence: wsol@faf.cuni.cz

**Abstract:** Zanubrutinib (ZAN) is a Bruton's tyrosine kinase inhibitor recently approved for the treatment of some non-Hodgkin lymphomas. In clinical trials, ZAN is often combined with standard anthracycline (ANT) chemotherapy. Although ANTs are generally effective, drug resistance is a crucial obstacle that leads to treatment discontinuation. This study showed that ZAN counteracts ANT resistance by targeting aldo-keto reductase 1C3 (AKR1C3) and ATP-binding cassette (ABC) transporters. AKR1C3 catalyses the transformation of ANTs to less potent hydroxy-metabolites, whereas transporters decrease the ANT-effective concentrations by pumping them out of the cancer cells. In our experiments, ZAN inhibited the AKR1C3-mediated inactivation of daunorubicin (DAUN) at both the recombinant and cellular levels. In the drug combination experiments, ZAN synergistically sensitised AKR1C3-expressing HCT116 and A549 cells to DAUN treatment. Gene induction studies further confirmed that ZAN did not increase the intracellular level of AKR1C3 mRNA; thus, the drug combination effect is not abolished by enzyme induction. Finally, in accumulation assays, ZAN was found to interfere with the DAUN efflux mediated by the ABCB1, ABCG2, and ABCC1 transporters, which might further contribute to the reversal of ANT resistance. In summary, our data provide the rationale for ZAN inclusion in ANT-based therapy and suggest its potential for the treatment of tumours expressing AKR1C3 and/or the above-mentioned ABC transporters.

**Keywords:** zanubrutinib; anthracycline; drug resistance; aldo-keto reductase 1C3; ABC drug efflux transporter

**Citation:** Čermáková, L.; Hofman, J.; Laštovičková, L.; Havlíčková, L.; Špringrová, I.; Novotná, E.; Wsól, V. Bruton's Tyrosine Kinase Inhibitor Zanubrutinib Effectively Modulates Cancer Resistance by Inhibiting Anthracycline Metabolism and Efflux. *Pharmaceutics* **2022**, *14*, 1994. <https://doi.org/10.3390/pharmaceutics14101994>

Academic Editor:  
Francesca Musumeci

Received: 5 August 2022

Accepted: 14 September 2022

Published: 21 September 2022

**Publisher's Note:** MDPI stays neutral with regard to jurisdictional claims in published maps and institutional affiliations.



**Copyright:** © 2022 by the authors. Licensee MDPI, Basel, Switzerland. This article is an open access article distributed under the terms and conditions of the Creative Commons Attribution (CC BY) license (<https://creativecommons.org/licenses/by/4.0/>).

## 1. Introduction

In recent decades, an understanding of the processes related to the pathogenesis of cancer has given rise to targeted therapy. Anticancer drugs target a wide range of cellular structures and signalling pathway components involved in cancer cell growth and survival. One such important target is Bruton's tyrosine kinase (BTK), belonging to non-receptor tyrosine kinases of the TEC family [1,2]. BTK has been recognised as a key player in the B-cell receptor signalling pathway, the dysregulation of which is implicated in B-cell malignancies [3,4]. Abundant expression of BTK has been identified in B-cell chronic lymphocytic leukaemia (CLL) and B-cell lymphomas, making it a promising target for the development of new small-molecule inhibitors [5–7].

The first BTK inhibitor that was given accelerated approval by the U.S. Food and Drug Administration (FDA) was ibrutinib (IBR) in 2013, followed by acalabrutinib (ACA) in 2017 [8,9]. The incorporation of IBR into cancer therapy is a milestone that has changed the fate of many patients with CLL, Waldenström's macroglobulinaemia, and some non-Hodgkin lymphomas [10–14]. IBR and ACA are strong BTK inhibitors that covalently

and irreversibly interact with Cys-481 in the ATP-binding domain of BTK. The inhibitory activity of IBR has also been demonstrated in other kinases containing homologous cysteine residues such as Itk and Tec [6,15,16]. The combined inhibition of different kinases may contribute to some adverse effects of IBR, such as bleeding and cardiovascular complications [17,18]. Thus, although IBR and ACA are the most effective agents for treating several B-cell malignancies, treatment-limiting adverse effects and emerging cases of cancer resistance [19,20] have encouraged the search for new BTK inhibitors. Various compounds (e.g., vecabrutinib, fenebrutinib, and tirabrutinib) have been identified as BTK inhibitors and have entered clinical trials in recent years [21,22]. However, in addition to IBR and ACA, only zanubrutinib (ZAN) has been approved by the FDA [23–25].

In clinical trials, IBR, ACA, and ZAN have been tested alone and in combination with anthracycline (ANT)-containing standard chemotherapy [26–29]. ANTs, even in the era of targeted therapy, represent the gold standard for the treatment of haematological malignancies. Daunorubicin (DAUN) and doxorubicin (DOX) are routinely used to treat acute myeloid leukaemia (AML), acute lymphoblastic leukaemia, and aggressive lymphomas. Therefore, emerging ANT resistance is a serious complication that is often responsible for the failure of cancer therapy. The decreased cancer sensitivity to ANTs may be due to several mechanisms. Metabolic drug inactivation by anthracycline reductases and increased efflux mediated by ATP-binding cassette (ABC) transporters are known to contribute significantly to this phenomenon [30–33].

Recently, we reported that IBR and ACA interact with aldo-keto reductase 1C3 (AKR1C3) [34], an enzyme that is overexpressed in several malignancies [35–38]. AKR1C3 catalyses the two-electron reduction of DAUN and DOX, converting them to alcohol metabolites that possess lower anticancer activities than their parent drugs [32,39,40]. In our previous experiments, IBR and ACA inhibited the AKR1C3-mediated inactivation of DAUN, leading to an increase in its effectiveness against cancer cells [34]. Furthermore, IBR sensitises cancer cells to DOX by inhibiting the ABCC1 transporter [41]. Knowing these off-target activities of IBR and ACA and considering their structural similarities within BTK inhibitors, we aimed to investigate whether there might be a rationale for combining the novel second-generation BTK inhibitor ZAN and ANTs for therapeutic purposes. The assumption that targeting AKR1C3 and/or ABC transporters may improve the clinical outcome of ANTs [42,43] allowed us to investigate whether ZAN interacts with these resistance mediators and counteracts their activities. First, we performed inhibitory studies on recombinant enzymes at the cellular level. Next, drug combination studies were performed to examine whether ZAN acts as a dual-activity resistance modulator. As AKR1C3 may influence the resistance phenotype of cancer cells, we performed induction studies focusing on the expression of this enzyme.

## 2. Materials and Methods

### 2.1. Material

ZAN was purchased from MedChemExpress LLC (Monmouth Junction, NJ, USA). Nicotinamide adenine dinucleotide phosphate (NADP<sup>+</sup>), glucose-6-phosphate, glucose-6-phosphate dehydrogenase (Roche), fetal bovine serum (FBS), and high-performance liquid chromatography (HPLC) grade solvents were obtained from Merck (Prague, Czech Republic). Phenazine methosulfate (PMS) and 2,3-Bis-(2-Methoxy-4-Nitro-5-Sulphophenyl)-2H-Tetrazolium-5-Carboxanilide (XTT) tetrazolium salt were purchased from BioTech (Prague, Czech Republic). DAUN was supplied by SelleckChem (Houston, TX, USA). Daunorubicinol (DAUN-OL), a C13-hydroxy-metabolite of DAUN, was obtained from Toronto Research Chemicals (Toronto, ON, Canada). JetPrime transfection reagent (Polyplus Transfection, Illkirch, France) was provided by VWR International Ltd. (Radnor, PA, USA). Cell culture reagents were obtained from Lonza (Walkersville, MD, USA) and Merck (St. Louis, MO, USA). TRI reagent solution was purchased from Molecular Research Center Inc. (Cincinnati, OH, USA). The RNA extraction kit was supplied by Zymo Research (Irvine, CA, USA). AKR1C3-specific primers (Forward primer: 5'-GCCAGGTGAGGAACTTTCAC-

3', Reverse primer: 5'-AGTTTGACACCCCAATGGAC-3') and oligo-dT were purchased from Generi Biotech (Hradec Králové, Czech Republic). ProtoScript II buffer, dithiothreitol (DTT), dNTP mix, and ProtoScript II Reverse Transcriptase were obtained from New England BioLabs (Ipswich, MA, USA). The qPCR SG mix was acquired from the Institute of Applied Biotechnologies (Prague, Czech Republic).

## 2.2. Cell Culture

Human colorectal carcinoma HCT116 cell line and human bone marrow AML KG1 $\alpha$  cells were purchased from the European Collection of Authenticated Cell Cultures (Salisbury, UK). Human liver carcinoma HepG2 and human non-small cell lung carcinoma A549 cells were obtained from the American Type Culture Collection (Manassas, VA, USA). HCT116, HepG2, and A549 cells were cultured in Dulbecco's modified Eagle's medium (DMEM) with 10% FBS. KG1 $\alpha$  leukaemia cells were maintained in Iscove's modified Dulbecco's medium (IDMEM) supplemented with 20% FBS and 2 mM L-glutamine. All cells were cultured under standard conditions (37 °C, 5% CO<sub>2</sub>) and examined for mycoplasma infections. Routine cultivation and all experiments were performed in an antibiotic-free medium. Cell passages of 10–25 were used in the experiments. ZAN was dissolved in dimethyl sulfoxide (DMSO), and the concentration of DMSO in the experiments did not exceed 0.5% (*v/v*). The effect of DMSO on cell viability was observed to be negligible in the validation experiments. Furthermore, possible interfering effects on other biological processes were eliminated by using of vehicle controls.

## 2.3. Cloning, Overexpression, and Purification of Recombinant Enzymes

As described previously, human recombinant AKR1C3 was prepared in *E. coli* BL21(DE3) [44] and purified using NGC chromatography system equipped with a 1 ml HisTrap FF column (GE Healthcare Life Sciences, Marlborough, MA, USA) [45].

## 2.4. Inhibitory Assays

To determine the value of half-maximal inhibitory concentration (IC<sub>50</sub>), human recombinant AKR1C3 (1.5  $\mu$ g) was incubated with ZAN (0.01–100  $\mu$ M) or vehicle DMSO. The reaction was carried out in 0.1 M sodium phosphate buffer (pH 7.4) containing NADP<sup>+</sup> regeneration system (2.54 mM NADP, 19.72 mM glucose-6-phosphate, 10 mM MgCl<sub>2</sub>, and 0.88 U glucose-6-phosphate-dehydrogenase), as described previously [45]. After 10 min of pre-incubation, the reactions were started with a DAUN (500  $\mu$ M) addition, and the solution was further incubated for 30 min. Methanol (300  $\mu$ L) was used to stop the reactions, and the samples were cooled on ice and allowed to precipitate for 1 h at 4 °C. After centrifugation (9050 $\times$  *g*, 10 min), the solution was filtered through a 0.2  $\mu$ m PTFE membrane (Whatman, GE Healthcare, Uppsala, Sweden). The amount of DAUN-OL was analysed using ultra-high-performance liquid chromatography (UHPLC). To determine the mode of interaction between AKR1C3 and ZAN, AKR1C3 was incubated with DAUN (200–2000  $\mu$ M) and ZAN (1, 5, 10  $\mu$ M) or DMSO, and the Michaelis–Menten kinetic parameters were calculated and transformed into a Lineweaver–Burk plot using GraphPad Prism 9.3.1 (GraphPad Software, Inc., La Jolla, CA, USA).

## 2.5. Inhibition of AKR1C3 in Transiently Transfected HCT116 Cells

Vector coding for AKR1C3 (pCI\_AKR1C3) and pCI empty vector (EV) was generated, purified from *E. coli* HB101, and used to transfect HCT116 cells, as described previously [43,46]. In brief, HCT116 cells (approximately 30  $\times$  10<sup>4</sup> cells/well) were seeded into 24-well plates and cultured for 24 h under standard conditions (5% CO<sub>2</sub>, 37 °C). The transfection mixture (0.25  $\mu$ g plasmid and 0.75  $\mu$ L jetPRIME<sup>®</sup> Transfection Reagent in jetPRIME buffer) was prepared according to the manufacturer's protocol (Polyplus Transfection, Illkirch, France). After 24 h, the culture medium was refreshed, the transfection mixture (37.5  $\mu$ L) was added dropwise to each well, and the cells were incubated (37 °C, 5% CO<sub>2</sub>) for 24 h before being used for subsequent experiments. The functional expression of AKR1C3 was verified, as previously described [43].

To study the inhibition of AKR1C3 in HCT116-transfected cells, the culture medium was harvested and replaced with fresh medium containing DAUN (1  $\mu$ M) and ZAN (1, 5, 10, and 50  $\mu$ M) or DMSO (vehicle). HCT116 cells harbouring EV (HCT116-EV) or pCI\_AKR1C3 (HCT116-AKR1C3) were incubated with DAUN and ZAN, or its vehicle DMSO, for 2 and 4 h (37 °C, 5% CO<sub>2</sub>). At specified intervals, the culture medium was collected and cells were lysed with 200  $\mu$ L of lysis buffer (25 mM Tris, 150 mM NaCl, and 1% Triton X-100, pH 7.8) for 15 min at room temperature (25 °C). The medium was mixed with the cell lysate, DAUN and DAUN-OL were extracted twice with 1 mL of ethyl acetate, and the organic phases were evaporated under vacuum. These residues were then dissolved in the mobile phase and analysed using UHPLC.

## 2.6. UHPLC

The amount of DAUN-OL was determined using UHPLC with fluorescence detection. Briefly, an Agilent 1290 Series UHPLC chromatographic system equipped with a Zorbax C18 Eclipse Plus (2.1  $\times$  50 mm, 1.8  $\mu$ m) column and a 1290 Infinity inline filter (Agilent, Santa Clara, CA, USA) was used. The mobile phase was a mixture of 0.1% formic acid in water and acetonitrile at a ratio of 74:26 (*v/v*). Isocratic elution and a flow rate of 0.7 mL/min were used. The excitation and emission wavelengths of the detector were 480 and 560 nm, respectively.

## 2.7. Drug Combination Assays

Prior to drug combination studies, HCT116 cells were transfected using the same procedure as described above, but optimised for the 96-well plate. In detail, HCT116 cells (approximately 8  $\times$  10<sup>3</sup> cells/well) were seeded in 96-well plates and cultured for 24 h (5% CO<sub>2</sub>, 37 °C). The next day, the cells were transfected with pCI\_AKR1C3 or EV, according to the manufacturer's protocol (Polyplus Transfection, Illkirch, France). In each well of the 96-well plate, a mixture of 0.10  $\mu$ g plasmid and 0.20  $\mu$ L jetPRIME<sup>®</sup> Transfection Reagent in jetPRIME buffer was added and incubated for 10 min at room temperature (25 °C). The polyplexes (5  $\mu$ L) were then added dropwise to HCT116 cells cultured in 100  $\mu$ L of fresh DMEM supplemented with 10% FBS and further incubated for 24 h (5% CO<sub>2</sub>, 37 °C). A549 cells (approximately 5  $\times$  10<sup>3</sup> cells/well) were seeded into 96-well plates, cultured under standard conditions (37 °C, 5% CO<sub>2</sub>) for 24 h, and then directly used for the experiments. To determine whether ZAN counteracts AKR1C3-mediated DAUN resistance, the culture medium was changed to a fresh medium containing DAUN (0.1–5  $\mu$ M for HCT116-AKR1C3 and HCT116-EV; 0.01–1  $\mu$ M for A549) and ZAN (5 and 10  $\mu$ M for HCT116-AKR1C3 and HCT116-EV; 1 and 5  $\mu$ M for A549), or DMSO (a vehicle). The cells were incubated for 72 h under standard conditions (37 °C, 5% CO<sub>2</sub>) before their viability assessment by XTT assay. Apart from these combinations, the cytotoxicity of ZAN itself (0.1–50  $\mu$ M) was also determined for both cell lines. The Chou–Talalay method was used to quantify combination effects [47,48].

## 2.8. XTT Cell Proliferation Assay

An XTT solution consisting of XTT powder (1 mg/mL) and phenazine methosulfate (3 mg/mL) in phosphate-buffered saline (PBS) was added to HCT116, A549, HepG2, and KG1 $\alpha$  cells and incubated for 1.5 h (HCT116, A549, HepG2) or 4 h (KG1 $\alpha$ ). Absorbance was measured at 450 nm using a microplate reader (Infinite M200; Tecan, Salzburg, Austria). This method was used to verify the lack of ZAN toxicity in cellular inhibitory assays, drug combination studies, and induction experiments.

## 2.9. Accumulation Studies in KG1 $\alpha$ and A549 Cells

To study the effect of ZAN on DAUN accumulation, KG1 $\alpha$  (approximately 50  $\times$  10<sup>4</sup> cells/well) and A549 cells (approximately 35  $\times$  10<sup>4</sup> cells/well) were seeded into 24- and 12-well plates, respectively. After 24 h, ZAN (1, 5, 10, and 25  $\mu$ M), LY335979 (2  $\mu$ M), Ko143 (2  $\mu$ M), and MK571 (25  $\mu$ M) (selective inhibitors of the ABC transporters ABCB1, ABCG2, and ABCC1, respectively) were added to the cells and incubated for 15 min. Then,



2 and 1  $\mu\text{M}$  DAUN were pipetted into A549 and KG1 $\alpha$  cell cultures, respectively. Following 1 h of incubation, the cells were washed twice with cold PBS and used for further analysis of DAUN accumulation using a Sony SA3800 Spectral Cell Analyser (Sony Biotechnology, San Jose, CA, USA) flow cytometer with a laser set to 488 nm. The SA3800 software (Sony Biotechnology, San Jose, CA, USA) was used to evaluate the data.

#### 2.10. Determination of ZAN Cytotoxicity in HepG2 and KG1 $\alpha$ Cells

Prior to the induction studies, the cytotoxicity of ZAN alone was tested to determine a relatively non-toxic concentration suitable for subsequent experiments. HepG2 (approximately  $18 \times 10^3$  cells/well) and KG1 $\alpha$  (approximately  $25 \times 10^3$  cells/well) cells were seeded into 96-well plates, and either on the same day (KG1 $\alpha$ ), or after a 24 h-incubation (HepG2 cells), were treated with ZAN (0.1–50  $\mu\text{M}$ ) or DMSO (vehicle). After incubation for 48 h under standard conditions (37  $^\circ\text{C}$ , 5%  $\text{CO}_2$ ), the effect of ZAN on cancer cell viability was measured using the XTT assay.

#### 2.11. Induction Studies in HepG2 and KG1 $\alpha$ Cells

Induction studies were performed as previously described [46]. HepG2 (approximately  $20 \times 10^4$  cells/well) and KG1 $\alpha$  (approximately  $35 \times 10^4$  cells/well) cells were seeded into 48-well plates. While the KG1 $\alpha$  cells were immediately treated with ZAN (0.5  $\mu\text{M}$ ) or DMSO (a vehicle), the HepG2 cells were first cultured for 24 h and then treated with 0.5  $\mu\text{M}$  ZAN or a vehicle control. After 24 and 48 h of incubation, the medium was removed, the cells were lysed in TriReagent, and the total RNA was isolated using the Zymo Research Direct-zol<sup>TM</sup> RNA Miniprep kit and transcribed into cDNA, according to the manufacturer's instructions (ProtoScript<sup>®</sup> II Reverse Transcriptase, New England Biolabs, Ipswich, MA, USA). AKR1C3 mRNA levels were quantified using quantitative real-time PCR (qRT-PCR). The PCR contained 1x concentrated XCEED qPCR SG Mix, AKR1C3-specific primers (1  $\mu\text{M}$ ), and 20 ng of cDNA. qPCR was performed using QuantStudio 6flex (Applied Biosystems by Life Technologies, Carlsbad, CA, USA) set to the following conditions: initial denaturation at 95  $^\circ\text{C}$  for 10 min, followed by 40 cycles at 95  $^\circ\text{C}$  for 15 s and 65  $^\circ\text{C}$  for 1 min. Absolute quantification of AKR1C3 expression was achieved by comparing samples with the concomitantly amplified AKR1C3 standard, which was generated as described previously [43].

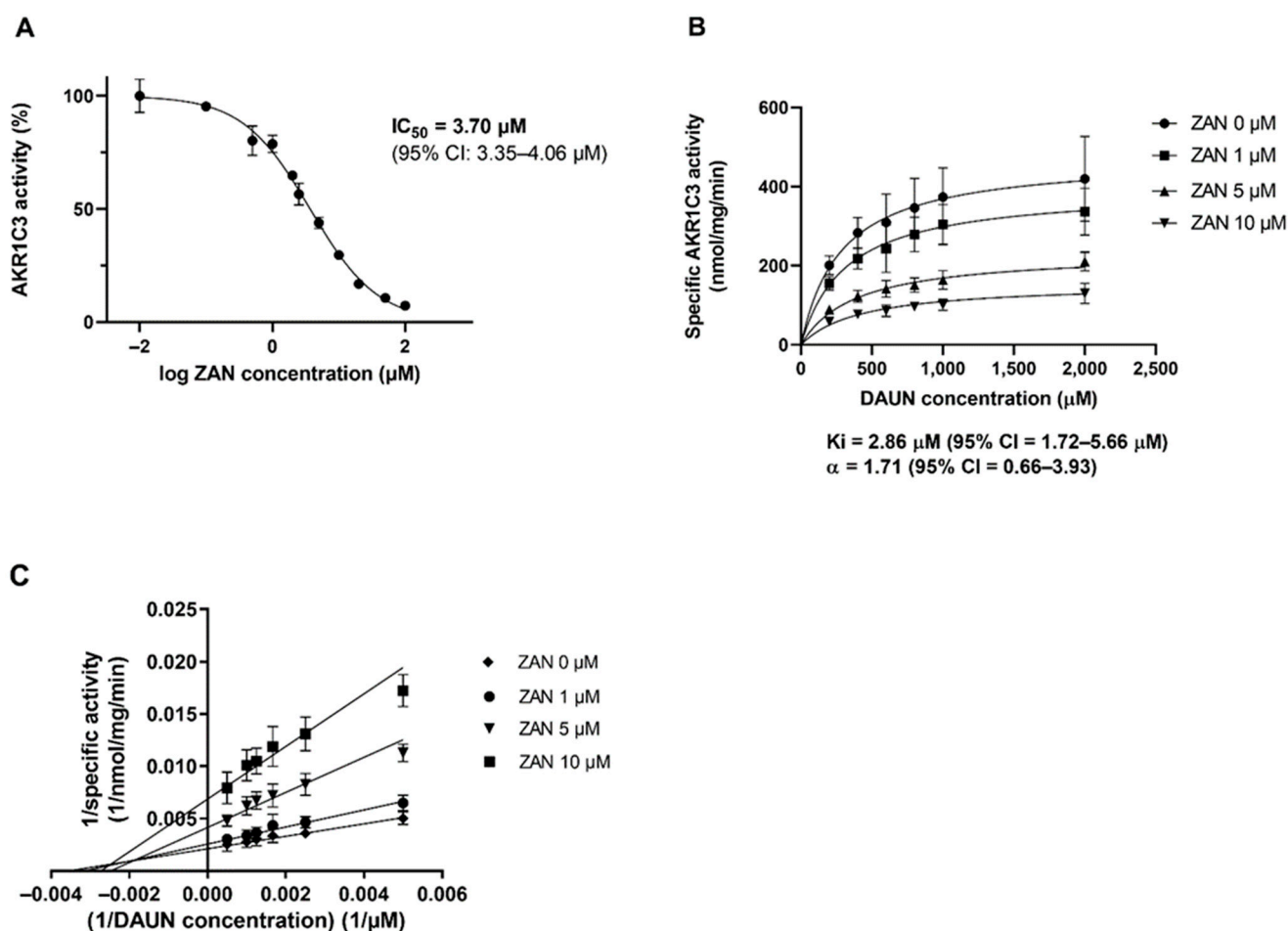
#### 2.12. Statistical Analysis

Statistical analysis of the data was performed using GraphPad Prism software version 9.3.1 (GraphPad Software Inc., La Jolla, CA, USA) using ordinary one-way analysis of variance (ANOVA) followed by Dunnett's post hoc test or unpaired t-test with Welch's correction, as specified in the respective figure legends. Statistical significance was set at  $p < 0.05$ . In the case of drug combination studies, the combination indices (CI) were used to distinguish between synergism (CI < 0.9), additivity (CI = 0.9–1.1), and antagonism (CI > 1.1), which were calculated using CompuSyn software (version 1.0; ComboSyn Inc., Paramus, NJ, USA).

### 3. Results

#### 3.1. ZAN Inhibits the Recombinant AKR1C3-Mediated DAUN Reduction In Vitro

First, we investigated whether ZAN could inhibit ANT metabolism using the recombinant enzyme. AKR1C3 was incubated with the substrate DAUN, with or without ZAN. As can be seen from the half-maximal inhibitory concentration ( $\text{IC}_{50}$ ) (Figure 1A), ZAN interacted with AKR1C3 and potently inhibited the reduction of DAUN to C13-hydroxy-metabolite daunorubicinol (DAUN-OL) in a dose-dependent manner. Furthermore, Michaelis–Menten kinetics and the Lineweaver–Burk double reciprocal plot provided evidence of a mixed-type mode of inhibition (inhibition constant ( $K_i$ ) = 2.9  $\mu\text{M}$ ,  $\alpha > 1.0$ ) (Figure 1B,C).



**Figure 1.** Zanubrutinib (ZAN) inhibits daunorubicin (DAUN) reduction catalysed by human recombinant AKR1C3. (A)  $\text{IC}_{50}$  of AKR1C3 inhibition. (B) Determination of the inhibition constant ( $\text{K}_i$ ). (C) Mode of inhibition graphically represented by the Lineweaver–Burk plot. All data are expressed as the mean  $\pm$  standard deviation (SD) from at least three independent experiments. 95% CI = 95% confidence interval.

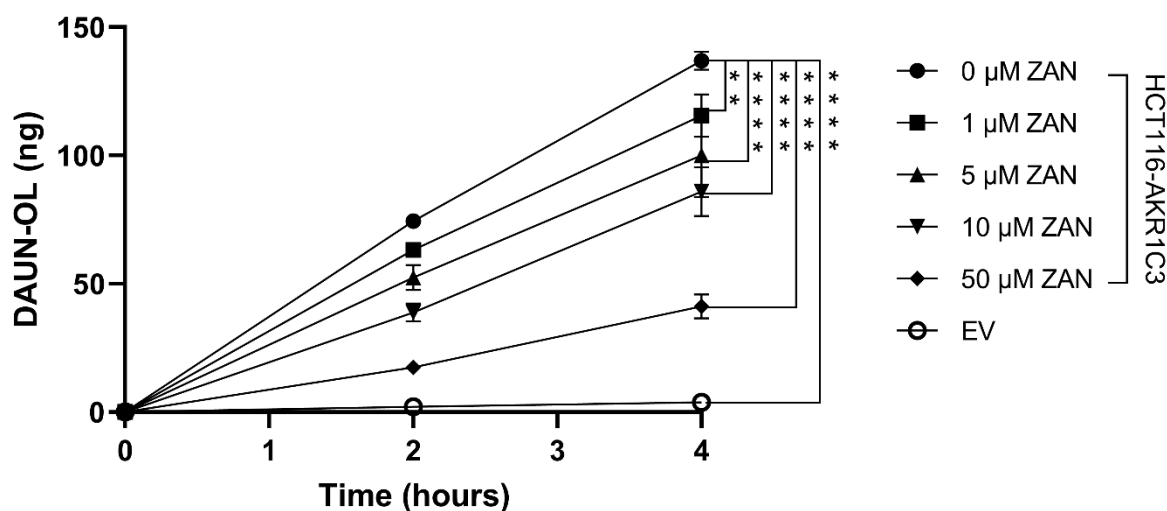
### 3.2. Effect of ZAN on AKR1C3-Mediated DAUN Metabolism in Transfected HCT116 Cells

Next, we investigated the effect of ZAN on AKR1C3-mediated DAUN metabolism in intact cells. HCT116 cells were chosen because of their negligible endogenous expression of AKR1C3 and high transfectability [43]. HCT116 cells were transfected with pCI\_AKR1C3 or an EV. Transfected cells were treated with DAUN (1  $\mu\text{M}$ ) and ZAN (or vehicle control), which were used at concentrations that were non-toxic to HCT116 cells, at a reaction interval of 2 and 4 h (data not shown). Figure 2 shows that ZAN, at all concentrations tested, significantly inhibited the conversion of DAUN to DAUN-OL in HCT116-AKR1C3 cells, proving that ZAN can influence the intracellular activity of the enzyme.

### 3.3. ZAN Overcomes DAUN Resistance in A549 and Transfected HCT116 Cells

After confirming that ZAN inhibits AKR1C3 intracellularly, we analysed whether a decrease in DAUN metabolism modulates ANT resistance in HCT116 cells. HCT116-AKR1C3 and HCT116-EV cells were treated with various combinations of DAUN and ZAN. In HCT116 cells expressing AKR1C3, the value of  $\text{IC}_{50}$  for DAUN alone was almost two times higher than the value of  $\text{IC}_{50}$  obtained from experiments with HCT116-EV cells. These data demonstrate that the expression of AKR1C3 protects cancer cells from DAUN toxicity. Importantly, as can be seen from the shifts in  $\text{IC}_{50}$  values, the DAUN resistance of HCT116-AKR1C3 cells was reversed when ZAN (5 or 10  $\mu\text{M}$ ) was added to the culture

(Figure 3A). No such significant changes in  $IC_{50}$  were found in experiments with HCT116-EV cells (Figure 3B), confirming the critical role of the ZAN-AKR1C3 interaction in the DAUN resistance reversal effect. Combination effects were precisely quantified using the Chou–Talalay method [47,48]. Combination index (CI) vs. fraction of cells affected ( $F_A$ ) plots were created. Cells that survived the treatment were considered unaffected. The values of CI for DAUN with ZAN (5 or 10  $\mu$ M) resulted in synergism (CI = 0.3–0.9) in HCT116-AKR1C3 cells. The lowest value of CI was detected when 10  $\mu$ M ZAN was combined with 0.25  $\mu$ M DAUN (CI =  $0.33 \pm 0.11$ ). In contrast, additivity to antagonism was detected when the examined drug combinations were tested in HCT116-EV cells (CI = 0.9–10) (Figure 3C,D).



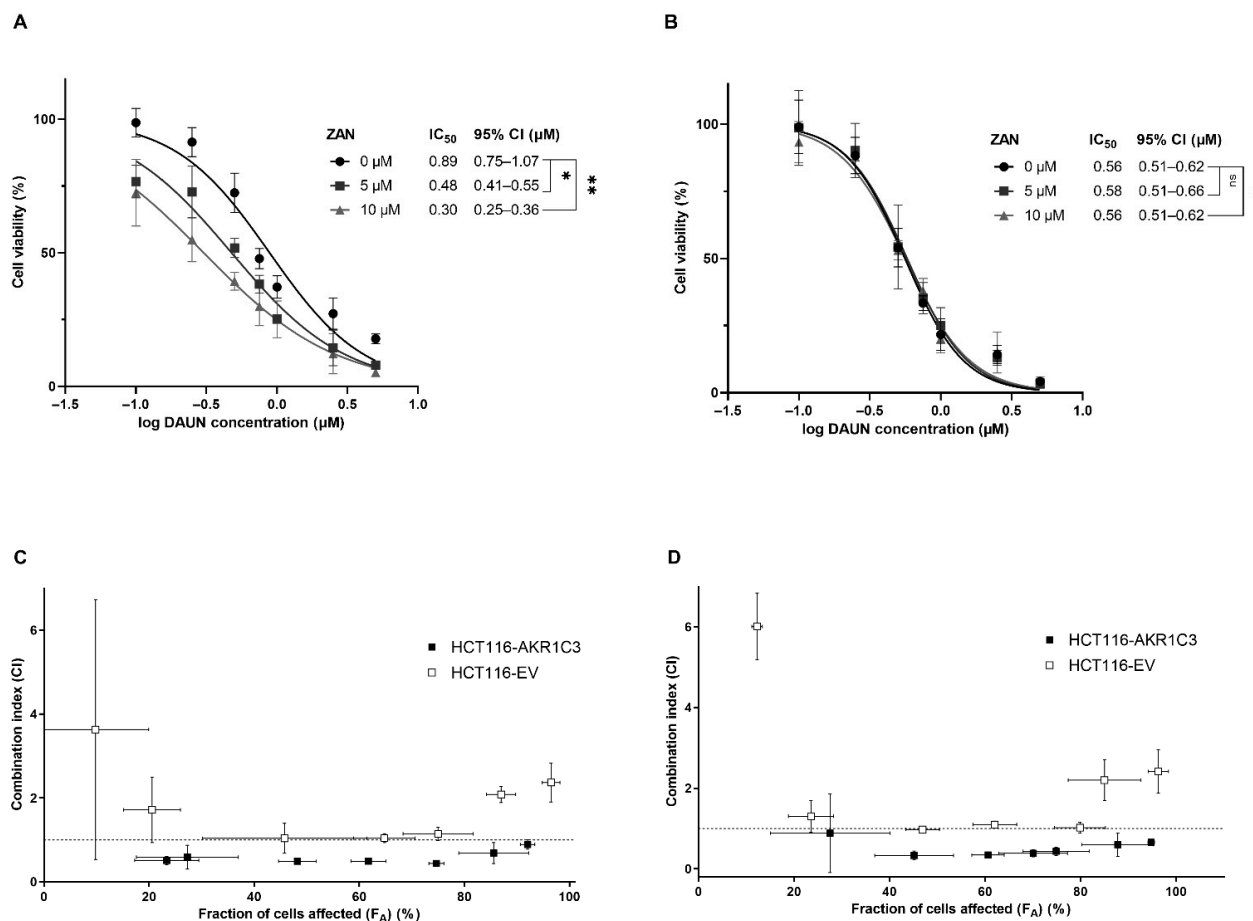
**Figure 2.** Zanubrutinib (ZAN) inhibits AKR1C3-mediated daunorubicin (DAUN) metabolism in intact cells. Transfected HCT116 cells were incubated with DAUN (1  $\mu$ M) in combination with ZAN (1, 5, 10 and 50  $\mu$ M) or its vehicle dimethyl sulfoxide (DMSO) for 2 and 4 h. DAUN-OL was then extracted and its amount was analysed by ultra-high-performance liquid chromatography (UHPLC). Data were evaluated with one-way analysis of variance (ANOVA), followed by Dunnett's post hoc test. \*\*  $p < 0.01$  and \*\*\*\*  $p < 0.0001$  compared to DMSO vehicle control. The values are expressed as mean  $\pm$  standard deviation (SD) from three independent experiments.

After confirming that the inhibition of AKR1C3 remains beyond the synergy between DAUN and ZAN in transfected cells, combination studies were performed with the lung adenocarcinoma cell line A549, which naturally expresses considerable amounts of AKR1C3 [43]. Similar to HCT116-AKR1C3 cells, significant shifts in  $IC_{50}$  values were detected when A549 cells were treated with a combination of DAUN and ZAN (1 and 5  $\mu$ M) (Figure 4A). Using the Chou–Talalay method, a synergistic effect was detected over the entire range  $F_A$ , with the lowest CI value detected for the combination of 5  $\mu$ M ZAN + 0.75  $\mu$ M DAUN (CI =  $0.06 \pm 0.05$ ) (Figure 4B).

### 3.4. ZAN Increases DAUN Accumulation by Inhibiting the Efflux Activity of ABC Transporters

As mentioned in the Introduction, not only AKR1C3, but also ABC transporters are IBR off-targets [41,49]. ABC transporters actively pump ANTs out of cancer cells, decreasing their effective concentration and contributing to drug resistance [50]. The fact that IBR re-sensitises drug-resistant ABCC1-overexpressing leukaemia cells to DOX [41] inspired us to investigate whether a similar interaction could be observed with ZAN. A549 and KG1 $\alpha$  leukaemia cells were selected for our experiments because of their high ABC transporter expression. Using selective modulators LY335979 (inhibitor of ABCB1), Ko143 (ABCG2 inhibitor), and MK571 (ABCC1 inhibitor), along with substrate DAUN, we demonstrated the functional presence of the ABCB1 transporter in KG1 $\alpha$  and the existence of ABCG2 and ABCC1 in the A549 cell line (Figure 5A,B). Furthermore, both the cell lines were incubated

with a combination of DAUN and ZAN. The obtained data showed that ZAN at 10 and 25  $\mu\text{M}$  inhibited DAUN efflux in A549 cells, while 5, 10, and 25  $\mu\text{M}$  ZAN interacted with the ABCB1 transporter expressed in KG1 $\alpha$  cells (Figure 5). Importantly, our results with model inhibitors correlate well with previous reports on the expressions and/or functional activities of examined transporters in selected cellular models [51–54].

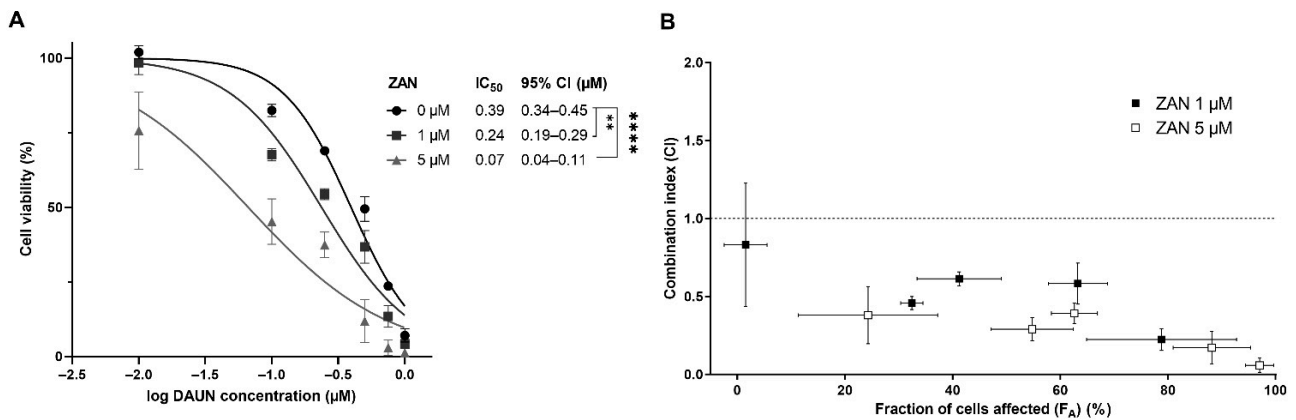


**Figure 3.** Zanubrutinib (ZAN) counteracts AKR1C3-mediated daunorubicin (DAUN) resistance in cancer cells. HCT116-AKR1C3 (A) and HCT116-EV (B) cells were treated with dimethyl sulfoxide (DMSO) (a vehicle) or ZAN (5 and 10  $\mu\text{M}$ ) and increasing concentrations of DAUN (0.1–5  $\mu\text{M}$ ). After 72 h of incubation, cell viability was evaluated using the XTT test. GraphPad Prism 9.3.1. was used for one-way analysis of variance (ANOVA), followed by Dunnett’s post hoc test. ns = non-significant, \*  $p < 0.05$ , and \*\*  $p < 0.01$  compared to DMSO vehicle control. 95% CI = 95% confidence interval. Chou–Talalay analysis was conducted to create combination index (CI) vs. fraction of cells affected (F<sub>A</sub>) plots for 5 (C) and 10  $\mu\text{M}$  ZAN (D) in order to distinguish between synergism (<0.9), additivity (0.9–1.1), and antagonism (>1.1). The dotted line was positioned at CI = 1 for better orientation. Data are presented as mean  $\pm$  standard deviation (SD) from three independent experiments.

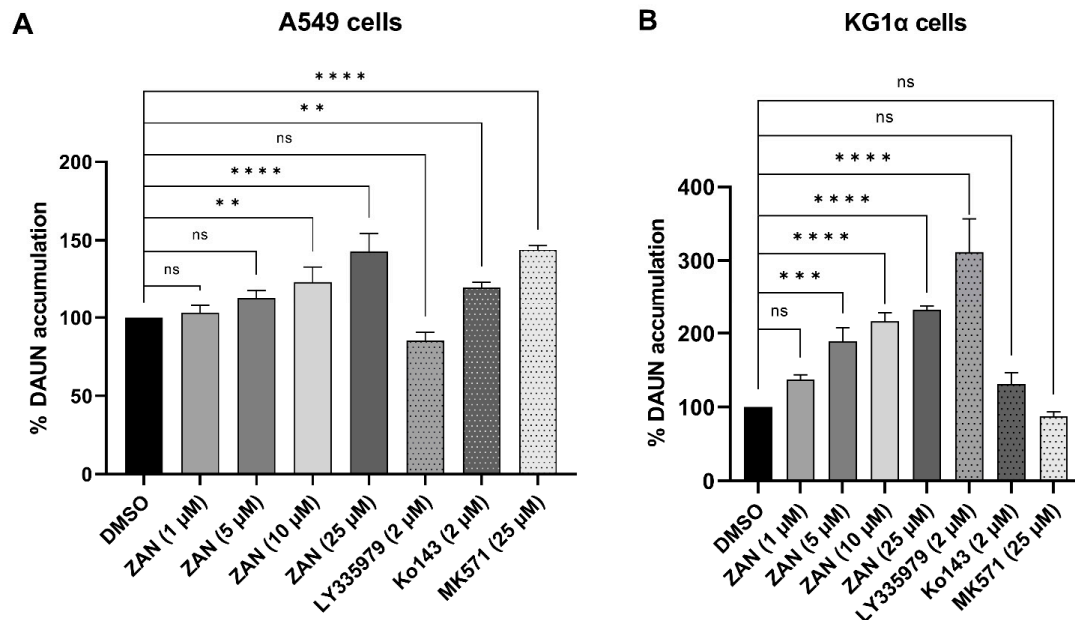
### 3.5. ZAN Does Not Affect AKR1C3 Expression

In addition to inhibition, changes in AKR1C3 expression may affect the pharmacological fate of ANTs. Therefore, in the last part of our study, we investigated how ZAN affects the intracellular levels of AKR1C3 mRNA. Along with the KG1 $\alpha$  leukaemia cells, the HepG2 hepatocarcinoma cell line was used as a liver model to evaluate whether ZAN has the potential to influence whole-body DAUN pharmacokinetics. First, we tested the effects of ZAN on the viability of HepG2 and KG1 $\alpha$  cells to determine the concentration with tolerable cytotoxicity. Based on these experiments (Figure 6A,B), a pharmacologically relevant [55] and negligibly cytotoxic concentration of 0.5  $\mu\text{M}$  ZAN was used for induction studies. The qRT-PCR results showed that ZAN did not cause any significant changes in

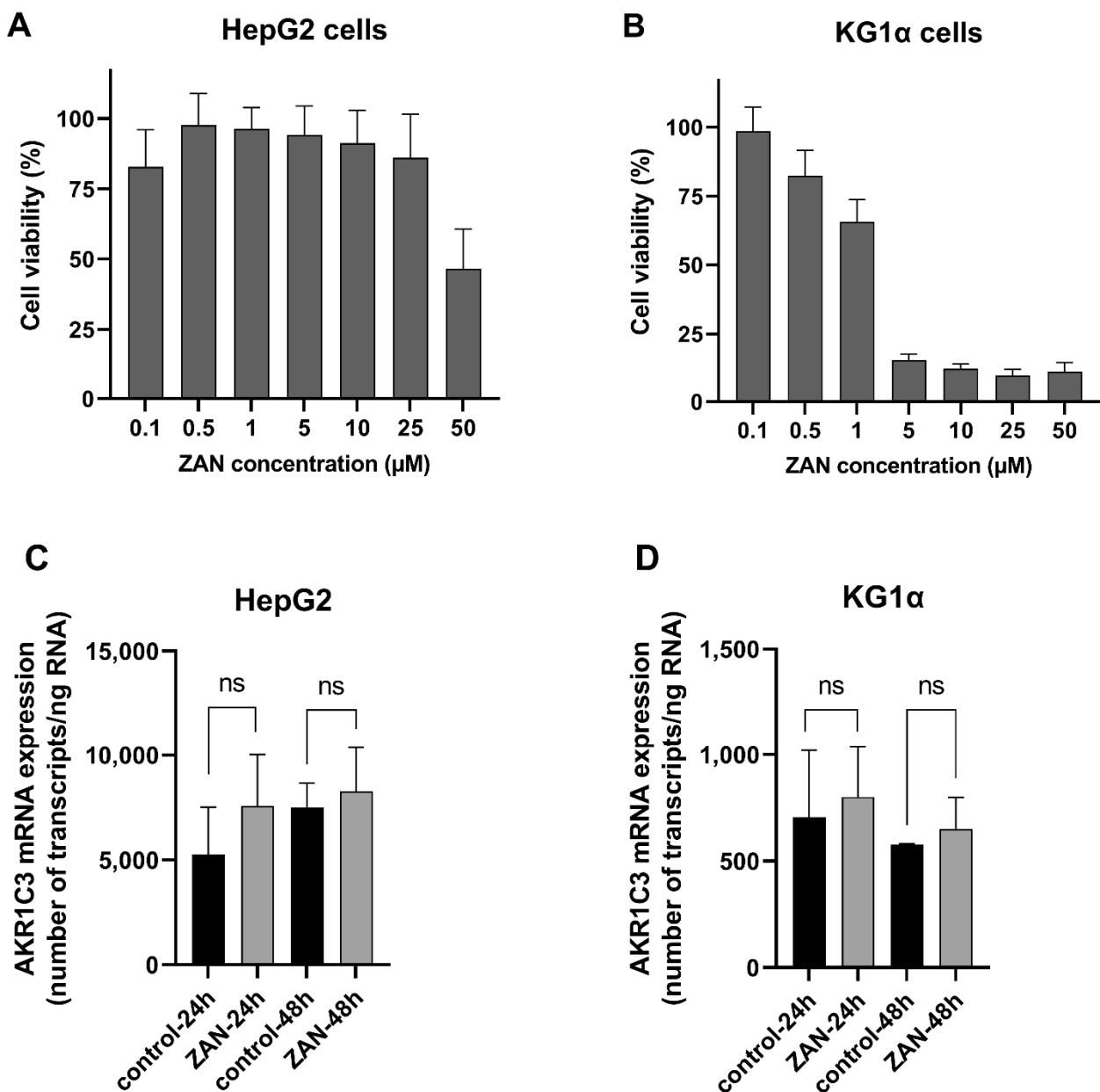
AKR1C3 mRNA expression in either the KG1 $\alpha$  or HepG2 cells (Figure 6C,D). These results confirmed that exposure to ZAN does not strengthen the resistance phenotype inside the cancer cells or force DAUN elimination from the body.



**Figure 4.** Zanubrutinib (ZAN) counteracts daunorubicin (DAUN) resistance in A549 cells. **(A)** A549 cells were treated with dimethyl sulfoxide (DMSO) (a vehicle) or ZAN (1 and 5  $\mu$ M) and increasing concentrations of DAUN (0.01–1  $\mu$ M), incubated for 72 h, and then cell viability was evaluated using the XTT test. GraphPad Prism 9.3.1. was used for one-way analysis of variance (ANOVA), followed by Dunnett’s post hoc test. \*\*  $p < 0.01$  and \*\*\*\*  $p < 0.0001$  in regards to DMSO vehicle control. 95% CI = 95% confidence interval. **(B)** Chou–Talalay analysis was performed to create the combination index (CI) vs. fraction of cells affected ( $F_A$ ) plot for 1 and 5  $\mu$ M ZAN and to distinguish synergism (<0.9) from additivity (0.9–1.1) and antagonism (>1.1). The dotted line was positioned at CI = 1 for better orientation. Data are presented as mean  $\pm$  standard deviation (SD) from three independent experiments.



**Figure 5.** Flow cytometry analysis of daunorubicin (DAUN) accumulation in A549 **(A)** and KG1 $\alpha$  cells **(B)**. A549 and KG1 $\alpha$  cells were preincubated with zanubrutinib (ZAN) (1, 5, 10, and 25  $\mu$ M) or selective inhibitors of ABC transporters: LY335979 (inhibitor of ABCB1), Ko143 (inhibitor of ABCG2), or MK571 (inhibitor of ABCC1). After preincubation, 2  $\mu$ M (A549) or 1  $\mu$ M DAUN (KG1 $\alpha$ ) were added to the cells. The bar graphs represent the DAUN accumulation in % relative to the dimethyl sulfoxide (DMSO) vehicle control. Data were analysed by one-way analysis of variance (ANOVA), followed by Dunnett’s post hoc test; ns = non-significant, \*\*  $p < 0.01$ , \*\*\*  $p < 0.001$ , and \*\*\*\*  $p < 0.0001$ . Data are presented as mean  $\pm$  standard deviation (SD) from three independent experiments.



**Figure 6.** Effect of zanubrutinib (ZAN) on AKR1C3 mRNA expression in HepG2 and KG1 $\alpha$  cell lines. To find a non-toxic ZAN concentration, HepG2 (A) and KG1 $\alpha$  (B) cells were treated with ZAN (0.1–50  $\mu$ M) or dimethyl sulfoxide (DMSO) (a vehicle) for 48 h, and the cell viability was evaluated by the XTT test. Furthermore, determination of AKR1C3 mRNA following ZAN (0.5  $\mu$ M) exposure was performed in HepG2 (C) and KG1 $\alpha$  (D) cells. qRT-PCR was used to monitor changes in AKR1C3 mRNA expression following a 24 and 48 h incubation. The Student's unpaired t-test with Welch's correction was used to assess statistical significance; ns = non-significant. The data represent mean  $\pm$  standard deviation (SD) from at least three independent experiments.

#### 4. Discussion

The FDA approved ZAN as a second-line therapy for relapsed/refractory marginal zone lymphoma (MZL) and mantle cell lymphoma (MCL), and as a first-line treatment for Waldenström's macroglobulinaemia [23–25]. Currently, ZAN, either alone or in combination with other drugs, is being studied in 66 clinical trials, of which 48 are currently recruiting, or have not started recruiting yet [56]. In addition to FDA-approved indications, the effectiveness of ZAN has been tested in other B-cell malignancies, such as CLL/small

lymphocytic lymphoma (SLL), diffuse large B-cell lymphoma (DLBCL), CNS lymphoma, and follicular lymphoma [57–61]. CLL/SLL and indolent lymphomas are typically characterised by slow growth rates that allow a “watch and wait” strategy, if no symptoms are present [62–65]. However, genetic alterations leading to blastic transformations, such as Richter’s syndrome in B-CLL, can cause serious complications. They drive the aggression of cancer cells, and the disease progression requires immediate treatment [66,67]. Although rituximab + cyclophosphamide + ANT + vincristine + prednisone (R-CHOP) and other ANT-containing chemotherapy regimens are generally effective in such cases, some patients do not respond to the therapy. Patients who are naturally insensitive or resistant to drug therapy during treatment require new strategies to overcome resistance issues and prevent disease relapse [68].

Several factors that impair the effectiveness of ANT treatment in cancer cells have been identified. Metabolic inactivation and drug efflux, mediated by ABC transporters, are among the most important factors. AKR1C3 reduces DAUN and DOX to less potent C13-hydroxy-metabolites, whereas ABC transporters pump ANTs out of cancer cells, decreasing their effective concentration [30–33]. In our experiments, ZAN inhibited AKR1C3 at the level of a recombinant enzyme in AKR1C3-overexpressing intact cells. Synergism between DAUN and ZAN was detected in HCT116-AKR1C3 cells when ZAN was tested at concentrations of 5 and 10  $\mu$ M. In A549 cells, a similar effect was observed with ZAN, even at a concentration of 1  $\mu$ M, which can be explained by the dual inhibition of both AKR1C3 and ABC transporters. In a phase 1 study, a therapeutic dose of 320 mg resulted in a ZAN plasma  $C_{max}$  of 1.4  $\mu$ M [55]. Therefore, it is presumed that the effects observed in our *in vitro* experiments could also be manifested in patients with cancer. Importantly, no upregulation of AKR1C3 mRNA was detected upon ZAN treatment of HepG2 or KG1 $\alpha$  cells, suggesting that ZAN does not affect systemic DAUN metabolism or influence the resistance of cancer cells to DAUN by promoting changes in AKR1C3 expression.

There are several lines of evidence regarding the role of AKR1C3 and ABC transporters in aggressive lymphomas and their sensitivity to ANT therapy, identifying them as potential drug targets. First, AKR1C3 expression was detected in samples obtained from patients with DLBCL treated with anthracycline-based therapy. Second, the AKR1C3 single nucleotide polymorphism may influence the survival outcomes of patients receiving the CHOP regimen [69]. Finally, the role of ABC transporters in cancer responses to ANT-containing chemotherapy has been suggested in DLBCL [70], MCL [71], and Burkitt lymphoma [72]. In addition to the primary indication of BTK inhibitors in CLL and lymphomas, their efficacy has recently been demonstrated in AML and solid tumours [73–76]. Rushworth et al. (2014) discovered that BTK is phosphorylated (p-BTK), and is thus constitutively active in the majority of samples obtained from patients with AML. Importantly, ibrutinib was found to enhance the cytotoxic effect of DAUN in high p-BTK-expressing AML cells and in the U937 cell line, but not in CD34+ non-malignant cells [75]. However, the mechanism of DAUN-IBR synergism may potentially be BTK-independent [77]. Our current results suggest that inhibition of DAUN metabolism and/or its cellular efflux may help to explain the ANT-sensitising effects of the BTK inhibitor ZAN. Importantly, AKR1C3 is not only an ANT-reductase, but is also involved in the production of sex hormones and pro-proliferative prostaglandins [78–80]. The association between AKR1C3 expression and poor patient prognosis has been proven many times in different solid tumours (e.g., breast, prostate, and liver) [35,81–83]. Several studies have further pointed to a potential link between AKR1C3 and leukaemogenesis [78,80,84]. Moreover, maternal and offspring polymorphisms of AKR1C3 were found to be associated with an increased risk of the development of childhood leukaemia [85], contributing to the FDA’s list of AKR1C3 as a relevant target in paediatric oncology [86,87]. Therefore, by targeting AKR1C3, ZAN may affect both leukaemia- and hormone-dependent, as well as independent, cancers. This further supports the rationale for combining ZAN with ANT therapy in cancers with a high expression of AKR1C3 and/or ABC transporters. If confirmed *in vivo*, this information

may be translated into an effective therapeutic strategy beneficial for a significant number of patients.

**Author Contributions:** Conceptualization, V.W., J.H. and E.N.; data curation, L.Č., L.L., I.Š. and L.H.; funding acquisition, V.W. and J.H.; investigation, L.Č., L.L. and L.H.; methodology, E.N. and J.H.; project administration, V.W.; supervision, V.W. and J.H.; writing—original draft, L.Č. and E.N.; writing—review and editing, J.H., L.L. and V.W. All authors have read and agreed to the published version of the manuscript.

**Funding:** This work was supported by the InoMed (project no. CZ.02.1.01/0.0/0.0/18\_069/0010046), co-funded by the European Union, by the Czech Science Foundation (project no. 20-20414Y), by the Grant Agency of Charles University (project no. 315221), and finally by the Charles University (SVV 260 550).

**Institutional Review Board Statement:** Not applicable.

**Informed Consent Statement:** Not applicable.

**Data Availability Statement:** Not applicable.

**Conflicts of Interest:** The authors declare no conflict of interest.

## References

1. Uckun, F.M.; Tibbles, H.E.; Vassilev, A.O. Bruton's tyrosine kinase as a new therapeutic target. *Anticancer Agents Med. Chem.* **2007**, *7*, 624–632. [CrossRef] [PubMed]
2. Mano, H. Tec family of protein-tyrosine kinases: An overview of their structure and function. *Cytokine Growth Factor Rev.* **1999**, *10*, 267–280. [CrossRef]
3. Niemann, C.U.; Wiestner, A. B-cell receptor signaling as a driver of lymphoma development and evolution. *Semin. Cancer Biol.* **2013**, *23*, 410–421. [CrossRef] [PubMed]
4. Buggy, J.J.; Elias, L. Bruton tyrosine kinase (BTK) and its role in B-cell malignancy. *Int. Rev. Immunol.* **2012**, *31*, 119–132. [CrossRef] [PubMed]
5. Davis, R.E.; Ngo, V.N.; Lenz, G.; Tolar, P.; Young, R.M.; Romesser, P.B.; Kohlhammer, H.; Lamy, L.; Zhao, H.; Yang, Y.; et al. Chronic active B-cell-receptor signalling in diffuse large B-cell lymphoma. *Nature* **2010**, *463*, 88–92. [CrossRef]
6. Honigberg, L.A.; Smith, A.M.; Sirisawad, M.; Verner, E.; Loury, D.; Chang, B.; Li, S.; Pan, Z.; Thamm, D.H.; Miller, R.A.; et al. The Bruton tyrosine kinase inhibitor PCI-32765 blocks B-cell activation and is efficacious in models of autoimmune disease and B-cell malignancy. *Proc. Natl. Acad. Sci. USA* **2010**, *107*, 13075–13080. [CrossRef]
7. Herman, S.E.; Gordon, A.L.; Hertlein, E.; Ramanunni, A.; Zhang, X.; Jaglowski, S.; Flynn, J.; Jones, J.; Blum, K.A.; Buggy, J.J.; et al. Bruton tyrosine kinase represents a promising therapeutic target for treatment of chronic lymphocytic leukemia and is effectively targeted by PCI-32765. *Blood* **2011**, *117*, 6287–6296. [CrossRef]
8. FDA (US Food and Drug Administration). FDA Approves Imbruvica. Available online: <https://www.drugs.com/newdrugs/fda-approves-imbruvica-ibrutinib-mantle-cell-lymphoma-3960.html> (accessed on 8 July 2022).
9. FDA (US Food and Drug Administration). FDA Approves New Treatment for Adults with Mantle Cell Lymphoma. Available online: <https://www.fda.gov/news-events/press-announcements/fda-approves-new-treatment-adults-mantle-cell-lymphoma> (accessed on 8 July 2022).
10. Byrd, J.C.; Furman, R.R.; Coutre, S.E.; Burger, J.A.; Blum, K.A.; Coleman, M.; Wierda, W.G.; Jones, J.A.; Zhao, W.; Heerema, N.A.; et al. Three-year follow-up of treatment-naive and previously treated patients with CLL and SLL receiving single-agent ibrutinib. *Blood* **2015**, *125*, 2497–2506. [CrossRef]
11. Castillo, J.J.; Meid, K.; Gustine, J.N.; Leventoff, C.; White, T.; Flynn, C.A.; Sarosiek, S.; Demos, M.G.; Guerrero, M.L.; Kofides, A.; et al. Long-term follow-up of ibrutinib monotherapy in treatment-naive patients with Waldenström macroglobulinemia. *Leukemia* **2022**, *36*, 532–539. [CrossRef]
12. Rusconi, C.; Cheah, C.Y.; Eyre, T.A.; Tucker, D.L.; Klener, P.; Gine, E.; Crucitti, L.; Muzi, C.; Iadecola, S.; Infante, G.; et al. Ibrutinib improves survival compared to chemotherapy in mantle cell lymphoma with central nervous system relapse. *Blood* **2022**, in press. [CrossRef]
13. Noy, A.; de Vos, S.; Coleman, M.; Martin, P.; Flowers, C.R.; Thieblemont, C.; Morschhauser, F.; Collins, G.P.; Ma, S.; Peles, S.; et al. Durable ibrutinib responses in relapsed/refractory marginal zone lymphoma: Long-term follow-up and biomarker analysis. *Blood Adv.* **2020**, *4*, 5773–5784. [CrossRef] [PubMed]
14. Byrd, J.C.; Hillmen, P.; O'Brien, S.; Barrientos, J.C.; Reddy, N.M.; Coutre, S.; Tam, C.S.; Mulligan, S.P.; Jaeger, U.; Barr, P.M.; et al. Long-term follow-up of the RESONATE phase 3 trial of ibrutinib vs ofatumumab. *Blood* **2019**, *133*, 2031–2042. [CrossRef] [PubMed]
15. Pan, Z.; Scheerens, H.; Li, S.J.; Schultz, B.E.; Sprengeler, P.A.; Burrill, L.C.; Mendonca, R.V.; Sweeney, M.D.; Scott, K.C.; Grothaus, P.G.; et al. Discovery of selective irreversible inhibitors for Bruton's tyrosine kinase. *ChemMedChem* **2007**, *2*, 58–61. [CrossRef] [PubMed]



16. Barf, T.; Covey, T.; Izumi, R.; van de Kar, B.; Gulrajani, M.; van Lith, B.; van Hoek, M.; de Zwart, E.; Mittag, D.; Demont, D.; et al. Acalabrutinib (ACP-196): A Covalent Bruton Tyrosine Kinase Inhibitor with a Differentiated Selectivity and In Vivo Potency Profile. *J. Pharmacol. Exp. Ther.* **2017**, *363*, 240–252. [CrossRef]
17. Von Hundelshausen, P.; Siess, W. Bleeding by Bruton Tyrosine Kinase-Inhibitors: Dependency on Drug Type and Disease. *Cancers* **2021**, *13*, 1103. [CrossRef]
18. Ahn, I.E. Cardiovascular adverse events of ibrutinib. *Blood* **2019**, *134*, 1881–1882. [CrossRef]
19. Woyach, J.A.; Furman, R.R.; Liu, T.M.; Ozer, H.G.; Zapatka, M.; Ruppert, A.S.; Xue, L.; Li, D.H.; Steggerda, S.M.; Versele, M.; et al. Resistance mechanisms for the Bruton's tyrosine kinase inhibitor ibrutinib. *N. Engl. J. Med.* **2014**, *370*, 2286–2294. [CrossRef]
20. Burger, J.A.; Landau, D.A.; Taylor-Weiner, A.; Bozic, I.; Zhang, H.; Sarosiek, K.; Wang, L.; Stewart, C.; Fan, J.; Hoellenriegel, J.; et al. Clonal evolution in patients with chronic lymphocytic leukaemia developing resistance to BTK inhibition. *Nat. Commun.* **2016**, *7*, 11589. [CrossRef]
21. Bond, D.A.; Woyach, J.A. Targeting BTK in CLL: Beyond Ibrutinib. *Curr. Hematol. Malig. Rep.* **2019**, *14*, 197–205. [CrossRef]
22. Byrd, J.C.; Smith, S.; Wagner-Johnston, N.; Sharman, J.; Chen, A.I.; Advani, R.; Augustson, B.; Marlton, P.; Renee Commerford, S.; Okrah, K.; et al. First-in-human phase 1 study of the BTK inhibitor GDC-0853 in relapsed or refractory B-cell NHL and CLL. *Oncotarget* **2018**, *9*, 13023–13035. [CrossRef]
23. FDA (US Food and Drug Administration). FDA Approves Therapy to Treat Patients with Relapsed and Refractory Mantle Cell Lymphoma Supported by Clinical Trial Results Showing High Response Rate of Tumor Shrinkage. Available online: <https://www.fda.gov/news-events/press-announcements/fda-approves-therapy-treat-patients-relapsed-and-refractory-mantle-cell-lymphoma-supported-clinical> (accessed on 8 July 2022).
24. FDA (US Food and Drug Administration). FDA Approves Zanubrutinib for Waldenström's Macroglobulinemia. Available online: <https://www.fda.gov/drugs/resources-information-approved-drugs/fda-approves-zanubrutinib-waldenstroms-macroglobulinemia> (accessed on 8 July 2022).
25. FDA (US Food and Drug Administration). FDA Grants Accelerated Approval to Zanubrutinib for Marginal Zone Lymphoma. Available online: <https://www.fda.gov/drugs/resources-information-approved-drugs/fda-grants-accelerated-approval-zanubrutinib-marginal-zone-lymphoma> (accessed on 8 July 2022).
26. Younes, A.; Thieblemont, C.; Morschhauser, F.; Flinn, I.; Friedberg, J.W.; Amorim, S.; Hivert, B.; Westin, J.; Vermeulen, J.; Bandyopadhyay, N.; et al. Combination of ibrutinib with rituximab, cyclophosphamide, doxorubicin, vincristine, and prednisone (R-CHOP) for treatment-naïve patients with CD20-positive B-cell non-Hodgkin lymphoma: A non-randomised, phase 1b study. *Lancet Oncol.* **2014**, *15*, 1019–1026. [CrossRef]
27. Younes, A.; Sehn, L.H.; Johnson, P.; Zinzani, P.L.; Hong, X.; Zhu, J.; Patti, C.; Belada, D.; Samoilo, O.; Suh, C.; et al. Randomized Phase III Trial of Ibrutinib and Rituximab Plus Cyclophosphamide, Doxorubicin, Vincristine, and Prednisone in Non-Germinal Center B-Cell Diffuse Large B-Cell Lymphoma. *J. Clin. Oncol.* **2019**, *37*, 1285–1295. [CrossRef] [PubMed]
28. Davies, A.; Caddy, J.; Mercer, K.; Saunders, G.N.; Stanton, L.; Collins, G.P.; Cummin, T.E.C.; Schuh, A.; Ardeschna, K.M.; McMillan, A.; et al. Acalabrutinib in Combination with Rituximab, Cyclophosphamide, Doxorubicin, Vincristine and Prednisolone (R-CHOP) As First Line Therapy for Patients with Diffuse Large B-Cell Lymphoma (DLBCL): The Accept Phase Ib/II Single Arm Study. *Blood* **2020**, *136*, 38–39. [CrossRef]
29. Zhu, H.; Sha, Y.; Wu, W.; Chen, R.; Yang, Y.; Qiu, J.; Mi, H.; Peng, C.; Ding, C.; Wang, Z.; et al. Zanubrutinib, Lenalidomide Plus R-CHOP (ZR2-CHOP) as the Treatment for Diffused Large B-Cell Lymphoma (DLBCL). *Hematol. Oncol.* **2021**, *39*, 425–427. [CrossRef]
30. Xiao, H.; Zheng, Y.; Ma, L.; Tian, L.; Sun, Q. Clinically-Relevant ABC Transporter for Anti-Cancer Drug Resistance. *Front. Pharmacol.* **2021**, *12*, 648407. [CrossRef] [PubMed]
31. Bains, O.S.; Grigliatti, T.A.; Reid, R.E.; Riggs, K.W. Naturally occurring variants of human aldo-keto reductases with reduced in vitro metabolism of daunorubicin and doxorubicin. *J. Pharmacol. Exp. Ther.* **2010**, *335*, 533–545. [CrossRef]
32. Bains, O.S.; Szeitz, A.; Lubieniecka, J.M.; Cragg, G.E.; Grigliatti, T.A.; Riggs, K.W.; Reid, R.E. A correlation between cytotoxicity and reductase-mediated metabolism in cell lines treated with doxorubicin and daunorubicin. *J. Pharmacol. Exp. Ther.* **2013**, *347*, 375–387. [CrossRef]
33. Penning, T.M.; Jonnalagadda, S.; Trippier, P.C.; Rizner, T.L. Aldo-Keto Reductases and Cancer Drug Resistance. *Pharmacol. Rev.* **2021**, *73*, 1150–1171. [CrossRef]
34. Morell, A.; Cermakova, L.; Novotna, E.; Lastovickova, L.; Haddad, M.; Haddad, A.; Portillo, R.; Wsol, V. Bruton's Tyrosine Kinase Inhibitors Ibrutinib and Acalabrutinib Counteract Anthracycline Resistance in Cancer Cells Expressing AKR1C3. *Cancers* **2020**, *12*, 3731. [CrossRef]
35. Wang, B.; Gu, Y.; Hui, K.; Huang, J.; Xu, S.; Wu, S.; Li, L.; Fan, J.; Wang, X.; Hsieh, J.T.; et al. AKR1C3, a crucial androgenic enzyme in prostate cancer, promotes epithelial-mesenchymal transition and metastasis through activating ERK signaling. *Urol. Oncol.* **2018**, *36*, 472.e411–472.e420. [CrossRef]
36. Yamashita, N.; Kanno, Y.; Saito, N.; Terai, K.; Sanada, N.; Kizu, R.; Hiruta, N.; Park, Y.; Bujo, H.; Nemoto, K. Aryl hydrocarbon receptor counteracts pharmacological efficacy of doxorubicin via enhanced AKR1C3 expression in triple negative breast cancer cells. *Biochem. Biophys. Res. Commun.* **2019**, *516*, 693–698. [CrossRef] [PubMed]

37. Miller, V.L.; Lin, H.K.; Murugan, P.; Fan, M.; Penning, T.M.; Brame, L.S.; Yang, Q.; Fung, K.M. Aldo-keto reductase family 1 member C3 (AKR1C3) is expressed in adenocarcinoma and squamous cell carcinoma but not small cell carcinoma. *Int. J. Clin. Exp. Pathol.* **2012**, *5*, 278–289. [PubMed]
38. Bortolozzi, R.; Bresolin, S.; Rampazzo, E.; Paganin, M.; Maule, F.; Mariotto, E.; Boso, D.; Minuzzo, S.; Agnusdei, V.; Viola, G.; et al. AKR1C enzymes sustain therapy resistance in paediatric T-ALL. *Br. J. Cancer* **2018**, *118*, 985–994. [CrossRef] [PubMed]
39. Bernardini, N.; Giannesi, F.; Bianchi, F.; Dolfi, A.; Lupetti, M.; Zaccaro, L.; Malvaldi, G.; Del Tacca, M. Comparative activity of doxorubicin and its major metabolite, doxorubicinol, on fibroblasts: A morphofunctional study. *Exp. Mol. Pathol.* **1991**, *55*, 238–250. [CrossRef]
40. Heibein, A.D.; Guo, B.; Sprowl, J.A.; Maclean, D.A.; Parissenti, A.M. Role of aldo-keto reductases and other doxorubicin pharmacokinetic genes in doxorubicin resistance, DNA binding, and subcellular localization. *BMC Cancer* **2012**, *12*, 381. [CrossRef]
41. Zhang, H.; Patel, A.; Ma, S.L.; Li, X.J.; Zhang, Y.K.; Yang, P.Q.; Kathawala, R.J.; Wang, Y.J.; Anreddy, N.; Fu, L.W.; et al. In vitro, in vivo and ex vivo characterization of ibrutinib: A potent inhibitor of the efflux function of the transporter MRP1. *Br. J. Pharmacol.* **2014**, *171*, 5845–5857. [CrossRef]
42. Kosztyu, P.; Bukvova, R.; Dolezel, P.; Mlejnek, P. Resistance to daunorubicin, imatinib, or nilotinib depends on expression levels of ABCB1 and ABCG2 in human leukemia cells. *Chem. Biol. Interact.* **2014**, *219*, 203–210. [CrossRef]
43. Hofman, J.; Malcekova, B.; Skarka, A.; Novotna, E.; Wsol, V. Anthracycline resistance mediated by reductive metabolism in cancer cells: The role of aldo-keto reductase 1C3. *Toxicol. Appl. Pharmacol.* **2014**, *278*, 238–248. [CrossRef]
44. Skarydova, L.; Tomanova, R.; Havlikova, L.; Stambergova, H.; Solich, P.; Wsol, V. Deeper insight into the reducing biotransformation of bupropion in the human liver. *Drug Metab. Pharmacokinet.* **2014**, *29*, 177–184. [CrossRef]
45. Bukum, N.; Novotna, E.; Morell, A.; Zelazkova, J.; Lastovickova, L.; Cermakova, L.; Portillo, R.; Solich, P.; Wsol, V. Inhibition of AKR1B10-mediated metabolism of daunorubicin as a novel off-target effect for the Bcr-Abl tyrosine kinase inhibitor dasatinib. *Biochem. Pharmacol.* **2021**, *192*, 114710. [CrossRef]
46. Tavares, T.S.; Hofman, J.; Lekesova, A.; Zelazkova, J.; Wsol, V. Olaparib Synergizes the Anticancer Activity of Daunorubicin via Interaction with AKR1C3. *Cancers* **2020**, *12*, 3127. [CrossRef] [PubMed]
47. Chou, T.C. Drug combination studies and their synergy quantification using the Chou-Talalay method. *Cancer Res.* **2010**, *70*, 440–446. [CrossRef] [PubMed]
48. Chou, T.C. Theoretical basis, experimental design, and computerized simulation of synergism and antagonism in drug combination studies. *Pharmacol. Rev.* **2006**, *58*, 621–681. [CrossRef] [PubMed]
49. Zhang, H.; Patel, A.; Wang, Y.J.; Zhang, Y.K.; Kathawala, R.J.; Qiu, L.H.; Patel, B.A.; Huang, L.H.; Shukla, S.; Yang, D.H.; et al. The BTK Inhibitor Ibrutinib (PCI-32765) Overcomes Paclitaxel Resistance in ABCB1- and ABCG2-Overexpressing Cells and Tumors. *Mol. Cancer Ther.* **2017**, *16*, 1021–1030. [CrossRef] [PubMed]
50. Juan-Carlos, P.M.; Perla-Lidia, P.P.; Stephanie-Talia, M.M.; Monica-Griselda, A.M.; Luz-Maria, T.E. ABC transporter superfamily. An updated overview, relevance in cancer multidrug resistance and perspectives with personalized medicine. *Mol. Biol. Rep.* **2021**, *48*, 1883–1901. [CrossRef] [PubMed]
51. Shi, B.; Xu, F.F.; Xiang, C.P.; Jia, R.; Yan, C.H.; Ma, S.Q.; Wang, N.; Wang, A.J.; Fan, P. Effect of sodium butyrate on ABC transporters in lung cancer A549 and colorectal cancer HCT116 cells. *Oncol. Lett.* **2020**, *20*, 148. [CrossRef]
52. Lainey, E.; Sebert, M.; Thepot, S.; Scoazec, M.; Bouteloup, C.; Leroy, C.; De Botton, S.; Galluzzi, L.; Fenaux, P.; Kroemer, G. Erlotinib antagonizes ABC transporters in acute myeloid leukemia. *Cell Cycle* **2012**, *11*, 4079–4092. [CrossRef]
53. Grundy, M.; Seedhouse, C.; Russell, N.H.; Pallis, M. P-glycoprotein and breast cancer resistance protein in acute myeloid leukaemia cells treated with the aurora-B kinase inhibitor barasertib-hQPA. *BMC Cancer* **2011**, *11*, 254. [CrossRef]
54. Hauswald, S.; Duque-Afonso, J.; Wagner, M.M.; Schertl, F.M.; Lubbert, M.; Peschel, C.; Keller, U.; Licht, T. Histone deacetylase inhibitors induce a very broad, pleiotropic anticancer drug resistance phenotype in acute myeloid leukemia cells by modulation of multiple ABC transporter genes. *Clin. Cancer Res.* **2009**, *15*, 3705–3715. [CrossRef]
55. Tam, C.S.; Trotman, J.; Opat, S.; Burger, J.A.; Cull, G.; Gottlieb, D.; Harrup, R.; Johnston, P.B.; Marlton, P.; Munoz, J.; et al. Phase 1 study of the selective BTK inhibitor zanubrutinib in B-cell malignancies and safety and efficacy evaluation in CLL. *Blood* **2019**, *134*, 851–859. [CrossRef]
56. ClinicalTrials.gov. Available online: <https://clinicaltrials.gov/ct2/home> (accessed on 21 July 2022).
57. Hillmen, P.; Brown, J.R.; Eichhorst, B.F.; Lamanna, N.; O'Brien, S.M.; Qiu, L.; Salmi, T.; Hilger, J.; Wu, K.; Cohen, A.; et al. ALPINE: Zanubrutinib versus ibrutinib in relapsed/refractory chronic lymphocytic leukemia/small lymphocytic lymphoma. *Future Oncol.* **2020**, *16*, 517–523. [CrossRef] [PubMed]
58. Tam, C.S.; Giannopoulos, K.; Jurczak, W.; Šimkovič, M.; Shadman, M.; Österborg, A.; Laurenti, L.; Walker, P.; Opat, S.; Chan, H.; et al. SEQUOIA: Results of a Phase 3 Randomized Study of Zanubrutinib versus Bendamustine + Rituximab (BR) in Patients with Treatment-Naïve (TN) Chronic Lymphocytic Leukemia/Small Lymphocytic Lymphoma (CLL/SLL). *Blood* **2021**, *138*, 396. [CrossRef]
59. Yang, H.; Xiang, B.; Song, Y.; Zhang, H.; Zhao, W.; Zou, D.; Lv, F.; Guo, W.; Liu, A.; Li, C.; et al. Zanubrutinib monotherapy for relapsed or refractory non-germinal center diffuse large B-cell lymphoma. *Blood Adv.* **2022**, *6*, 1629–1636. [CrossRef] [PubMed]
60. Phillips, T.; Chan, H.; Tam, C.S.; Tedeschi, A.; Johnston, P.; Oh, S.Y.; Opat, S.; Eom, H.S.; Allewelt, H.; Stern, J.C.; et al. Zanubrutinib monotherapy in relapsed/refractory indolent non-Hodgkin lymphoma. *Blood Adv.* **2022**, *6*, 3472–3479. [CrossRef]

61. Zhang, Y.; Li, Y.; Zhuang, Z.; Wang, W.; Wei, C.; Zhao, D.; Zhou, D.; Zhang, W. Preliminary Evaluation of Zanubrutinib-Containing Regimens in DLBCL and the Cerebrospinal Fluid Distribution of Zanubrutinib: A 13-Case Series. *Front. Oncol.* **2021**, *11*, 760405. [CrossRef]
62. Armitage, J.O.; Longo, D.L. Is watch and wait still acceptable for patients with low-grade follicular lymphoma? *Blood* **2016**, *127*, 2804–2808. [CrossRef]
63. Brieghel, C.; Galle, V.; Agius, R.; da Cunha-Bang, C.; Andersen, M.A.; Vlummens, P.; Mattsson, M.; Rosenquist, R.; Smedby, K.E.; Herling, C.D.; et al. Identifying patients with chronic lymphocytic leukemia without need of treatment: End of endless watch and wait? *Eur. J. Haematol.* **2022**, *108*, 369–378. [CrossRef]
64. Sindel, A.; Al-Juhaishi, T.; Yazbeck, V. Marginal Zone Lymphoma: State-of-the-Art Treatment. *Curr. Treat. Options Oncol.* **2019**, *20*, 90. [CrossRef]
65. Durot, E.; Delmer, A. Watch and wait in Waldenstrom macroglobulinaemia: Looking for who to watch carefully and who can wait without worrying. Is it that simple? *Br. J. Haematol.* **2021**, *195*, 155–157. [CrossRef]
66. Rossi, D.; Spina, V.; Gaidano, G. Biology and treatment of Richter syndrome. *Blood* **2018**, *131*, 2761–2772. [CrossRef]
67. Gonzalez-Rincon, J.; Mendez, M.; Gomez, S.; Garcia, J.F.; Martin, P.; Bellas, C.; Pedrosa, L.; Rodriguez-Pinilla, S.M.; Camacho, F.I.; Quero, C.; et al. Unraveling transformation of follicular lymphoma to diffuse large B-cell lymphoma. *PLoS ONE* **2019**, *14*, e0212813. [CrossRef] [PubMed]
68. Coiffier, B.; Sarkozy, C. Diffuse large B-cell lymphoma: R-CHOP failure-what to do? *Hematol. Am. Soc. Hematol. Educ. Program* **2016**, *2016*, 366–378. [CrossRef] [PubMed]
69. Gustafson, H.L.; Yao, S.; Goldman, B.H.; Lee, K.; Spier, C.M.; LeBlanc, M.L.; Rimsza, L.M.; Cerhan, J.R.; Habermann, T.M.; Link, B.K.; et al. Genetic polymorphisms in oxidative stress-related genes are associated with outcomes following treatment for aggressive B-cell non-Hodgkin lymphoma. *Am. J. Hematol.* **2014**, *89*, 639–645. [CrossRef] [PubMed]
70. Liu, D.; Wu, N.; Sun, H.; Dong, M.; Guo, T.; Chi, P.; Li, G.; Sun, D.; Jin, Y. ABCG2 and NCF4 polymorphisms are associated with clinical outcomes in diffuse large B-cell lymphoma patients treated with R-CHOP. *Oncotarget* **2017**, *8*, 58292–58303. [CrossRef] [PubMed]
71. Takimoto-Shimomura, T.; Nagoshi, H.; Maegawa, S.; Fujibayashi, Y.; Tsukamoto, T.; Matsumura-Kimoto, Y.; Mizuno, Y.; Chinen, Y.; Mizutani, S.; Shimura, Y.; et al. Establishment and Characteristics of a Novel Mantle Cell Lymphoma-derived Cell Line and a Bendamustine-resistant Subline. *Cancer Genom. Proteom.* **2018**, *15*, 213–223. [CrossRef]
72. Tabata, M.; Tsubaki, M.; Takeda, T.; Tateishi, K.; Tsurushima, K.; Imano, M.; Satou, T.; Ishizaka, T.; Nishida, S. Dasatinib reverses drug resistance by downregulating MDR1 and Survivin in Burkitt lymphoma cells. *BMC Complement Med. Ther.* **2020**, *20*, 84. [CrossRef]
73. Molina-Cerrillo, J.; Alonso-Gordoa, T.; Gajate, P.; Grande, E. Bruton's tyrosine kinase (BTK) as a promising target in solid tumors. *Cancer Treat. Rev.* **2017**, *58*, 41–50. [CrossRef]
74. Szklener, K.; Michalski, A.; Zak, K.; Piwonski, M.; Mandziuk, S. Ibrutinib in the Treatment of Solid Tumors: Current State of Knowledge and Future Directions. *Cells* **2022**, *11*, 1338. [CrossRef]
75. Rushworth, S.A.; Murray, M.Y.; Zaitseva, L.; Bowles, K.M.; MacEwan, D.J. Identification of Bruton's tyrosine kinase as a therapeutic target in acute myeloid leukemia. *Blood* **2014**, *123*, 1229–1238. [CrossRef]
76. Yeh, C.T.; Chen, T.T.; Satriyo, P.B.; Wang, C.H.; Wu, A.T.H.; Chao, T.Y.; Lee, K.Y.; Hsiao, M.; Wang, L.S.; Kuo, K.T. Bruton's tyrosine kinase (BTK) mediates resistance to EGFR inhibition in non-small-cell lung carcinoma. *Oncogenesis* **2021**, *10*, 56. [CrossRef]
77. Rotin, L.E.; Gronda, M.; Hurren, R.; Wang, X.; Minden, M.D.; Slassi, M.; Schimmer, A.D. Investigating the synergistic mechanism between ibrutinib and daunorubicin in acute myeloid leukemia cells. *Leuk. Lymphoma* **2016**, *57*, 2432–2436. [CrossRef]
78. Birtwistle, J.; Hayden, R.E.; Khanim, F.L.; Green, R.M.; Pearce, C.; Davies, N.J.; Wake, N.; Schrewe, H.; Ride, J.P.; Chipman, J.K.; et al. The Aldo-Keto Reductase AKR1C3 contributes to 7,12-dimethylbenz(a)anthracene-3,4-dihydrodiol mediated oxidative DNA damage in myeloid cells: Implications for leukemogenesis. *Mutat. Res.* **2009**, *662*, 67–74. [CrossRef]
79. Byrns, M.C.; Duan, L.; Lee, S.H.; Blair, I.A.; Penning, T.M. Aldo-keto reductase 1C3 expression in MCF-7 cells reveals roles in steroid hormone and prostaglandin metabolism that may explain its over-expression in breast cancer. *J. Steroid Biochem. Mol. Biol.* **2010**, *118*, 177–187. [CrossRef]
80. Desmond, J.C.; Mountford, J.C.; Drayson, M.T.; Walker, E.A.; Hewison, M.; Ride, J.P.; Luong, Q.T.; Hayden, R.E.; Vanin, E.F.; Bunce, C.M. The Aldo-Keto Reductase AKR1C3 is a novel suppressor of cell differentiation that provides a plausible target for the non-cyclooxygenase-dependent antineoplastic actions of nonsteroidal anti-inflammatory drugs. *Cancer Res.* **2003**, *63*, 505–512.
81. Oduwole, O.O.; Li, Y.; Isomaa, V.V.; Mantyniemi, A.; Pulkka, A.E.; Soini, Y.; Vihko, P.T. 17beta-hydroxysteroid dehydrogenase type 1 is an independent prognostic marker in breast cancer. *Cancer Res.* **2004**, *64*, 7604–7609. [CrossRef]
82. Zhu, P.; Feng, R.; Lu, X.; Liao, Y.; Du, Z.; Zhai, W.; Chen, K. Diagnostic and prognostic values of AKR1C3 and AKR1D1 in hepatocellular carcinoma. *Aging* **2021**, *13*, 4138–4156. [CrossRef] [PubMed]
83. Zhao, S.F.; Wang, S.G.; Zhao, Z.Y.; Li, W.L. AKR1C1-3, notably AKR1C3, are distinct biomarkers for liver cancer diagnosis and prognosis: Database mining in malignancies. *Oncol. Lett.* **2019**, *18*, 4515–4522. [CrossRef]
84. Mahadevan, D.; DiMento, J.; Croce, K.D.; Riley, C.; George, B.; Fuchs, D.; Mathews, T.; Wilson, C.; Lobell, M. Transcriptome and serum cytokine profiling of an atypical case of myelodysplastic syndrome with progression to acute myelogenous leukemia. *Am. J. Hematol.* **2006**, *81*, 779–786. [CrossRef]

85. Liu, C.Y.; Hsu, Y.H.; Pan, P.C.; Wu, M.T.; Ho, C.K.; Su, L.; Xu, X.; Li, Y.; Christiani, D.C.; Kaohsiung Leukemia Research, G. Maternal and offspring genetic variants of AKR1C3 and the risk of childhood leukemia. *Carcinogenesis* **2008**, *29*, 984–990. [CrossRef]
86. FDA (US Food and Drug Administration). U.S. Food & Drug Administration: List of the Relevant Molecular Targets in Paediatric Oncology. Available online: <https://www.fda.gov/about-fda/oncology-center-excellence/pediatric-oncology> (accessed on 16 July 2022).
87. FDA (US Food and Drug Administration). U.S. Food & Drug Administration: List of the Relevant Molecular Targets in Paediatric Oncology. Available online: <https://www.fda.gov/media/120332/download> (accessed on 16 July 2022).

## Article

# Vitamin E TPGS-Poloxamer Nanoparticles Entrapping a Novel PI3K $\alpha$ Inhibitor Potentiate Its Activity against Breast Cancer Cell Lines

Suhair Sunoqrot \*, Sundos Aliyeh, Samah Abusulieh and Dima Sabbah

Department of Pharmacy, Faculty of Pharmacy, Al-Zaytoonah University of Jordan, Amman 11733, Jordan

\* Correspondence: suhair.sunoqrot@zuj.edu.jo; Tel.: +962-64291511 (ext. 197)

**Abstract:** N-(2-fluorophenyl)-6-chloro-4-hydroxy-2-quinolone-3-carboxamide (R19) is a newly synthesized phosphatidylinositol 3-kinase alpha (PI3K $\alpha$ ) inhibitor with promising activity against cancer cells. The purpose of this study was to develop a polymeric nanoparticle (NP) formulation for R19 to address its poor aqueous solubility and to facilitate its future administration in preclinical and clinical settings. NPs were prepared by nanoprecipitation using two polymers: D- $\alpha$ -tocopheryl polyethylene glycol 1000 succinate (vitamin E TPGS) and the poloxamer Pluronic P123 in different ratios. Physicochemical characterization of the NPs revealed them to be around 100 nm in size with high monodispersity, a spherical morphology, and an almost neutral surface charge. The NPs achieved ~60% drug loading efficiency and sustained release of R19 for up to 96 h, with excellent colloidal stability in serum-containing cell culture media. NPs containing TPGS enhanced R19's potency against MCF-7 and MDA-MB-231 breast cancer cells in vitro, with half-maximal inhibitory concentrations (IC<sub>50</sub>) ranging between 1.8 and 4.3  $\mu$ M compared to free R19, which had an IC<sub>50</sub> of 14.7–17.0  $\mu$ M. The NPs also demonstrated low cytotoxicity against human dermal fibroblasts and more significant induction of apoptosis compared to the free drug, which was correlated with their cellular uptake efficiency. Our findings present a biocompatible NP formulation for the delivery of a cancer-targeted PI3K $\alpha$  inhibitor, R19, which can further enhance its potency for the treatment of breast cancer and potentially other cancer types.

**Keywords:** breast cancer; nanomedicine; PI3K $\alpha$ ; poloxamers; polymeric nanoparticles; TPGS

**Citation:** Sunoqrot, S.; Aliyeh, S.; Abusulieh, S.; Sabbah, D. Vitamin E TPGS-Poloxamer Nanoparticles Entrapping a Novel PI3K $\alpha$  Inhibitor Potentiate Its Activity against Breast Cancer Cell Lines. *Pharmaceutics* **2022**, *14*, 1977. <https://doi.org/10.3390/pharmaceutics14091977>

Academic Editor: Francesca Musumeci

Received: 4 August 2022

Accepted: 13 September 2022

Published: 19 September 2022

**Publisher's Note:** MDPI stays neutral with regard to jurisdictional claims in published maps and institutional affiliations.



**Copyright:** © 2022 by the authors. Licensee MDPI, Basel, Switzerland. This article is an open access article distributed under the terms and conditions of the Creative Commons Attribution (CC BY) license (<https://creativecommons.org/licenses/by/4.0/>).

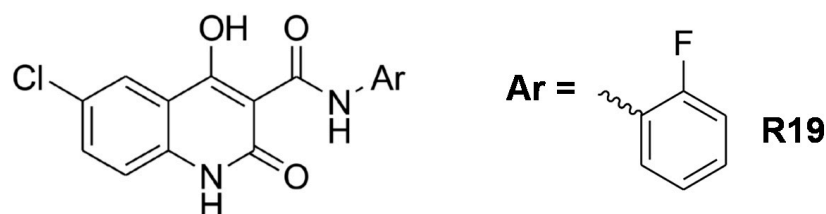
## 1. Introduction

Despite advances in early detection and medical treatments, cancer remains one of the leading causes of death globally [1]. Cancer treatment regimens typically include surgery, radiotherapy, and chemotherapy [2]. Chemotherapy involves the use of cytotoxic agents, which are accompanied by immediate and chronic side effects that can significantly impact cancer patients' quality of life. The side effects are mainly attributed to the systemic distribution of the cytotoxic agent and a lack of selectivity in killing normal and cancer cells alike [3]. For this reason, significant efforts have been dedicated to the discovery of targeted therapies that can reduce the systemic side effects of chemotherapy.

Protein kinases are important enzymes that modify other proteins by phosphorylation, which consequently regulates the function of these proteins and their downstream signaling pathways. Several kinases have been found to be dysregulated in various cancers, which has inspired the development of kinase inhibitors as cancer-targeted therapies [4]. The phosphatidylinositol-3-kinases (PI3Ks) are a family of lipid kinases that are important for the regulation of cell metabolism, proliferation, migration, and survival [5]. PI3Ks are part of a signaling pathway that includes Akt and the mammalian target of rapamycin (mTOR). The PI3K/Akt/mTOR signaling pathway regulates the growth of both normal and cancer cells and has been shown to be hyperactivated in cancer cells [6–8]. Three classes of PI3Ks are known; class I, II, and III. Class I can be divided into Class I<sub>A</sub> and

Class I<sub>B</sub>. Class I<sub>A</sub> is the class of concern since it is directly linked to cancer progression. Class I<sub>A</sub> PI3K consists of  $\alpha$ ,  $\beta$ , and  $\delta$  isoforms, which are encoded by the genes PIK3CA, PIK3CB, and PIK3CD, respectively [5,9]. Several cancers have demonstrated abnormal PI3K $\alpha$ /Akt/mTOR signaling pathway activation, in which PIK3CA gene expression has been implicated [9].

N-phenyl-6-chloro-4-hydroxy-2-quinolone-3-carboxamides (Figure 1) are a group of newly developed anticancer agents with inhibitory activity against PI3K $\alpha$ . A series of different analogues were recently synthesized to achieve the maximum inhibition of cancer cells with the lowest possible toxicity on normal cells. N-(2-fluorophenyl)-6-chloro-4-hydroxy-2-quinolone-3-carboxamide (R19) was found to be an effective inhibitory agent against human colon carcinoma (HCT-116) and human epithelial colorectal adenocarcinoma (Caco-2) cell lines, with half-maximal inhibitory concentrations (IC<sub>50</sub>) of 5.3 and 17.0  $\mu$ M, respectively. Moreover, R19 was tested for its activity on the PI3K/Akt/mTOR signaling pathway, where gene expression analysis revealed a significant reduction in the expression of PI3K and Akt genes and a significant increase in the pro-apoptotic gene Bcl-2-associated death promoter (BAD) [9]. Despite its promising anticancer potency, R19 and its newly developed analogs suffer from poor aqueous solubility, which will be a limiting factor in the clinical translation of this class of compounds.



**Figure 1.** Chemical structure of the N-phenyl-6-chloro-4-hydroxy-2-quinolone-3-carboxamide series and R19 [9].

Nanotechnology has revolutionized the way that we treat diseases, especially cancer. Nanosized drug carriers or nanoparticles (NPs) can improve the solubility, permeability, absorption, delivery, and targeting of drug molecules to the site of action [10–12]. Polymeric NPs are a particularly attractive delivery approach due to their highly tunable properties, which can be leveraged to achieve better solubility, bioavailability, controlled release, and targeting of drug candidates by passive and active targeting mechanisms [13–16].

Poloxamers are amphiphilic triblock copolymers composed of poly(ethylene oxide) (PEO) and poly(propylene oxide) (PPO) (PEO-PPO-PEO) [17,18]. They are biocompatible polymers that are used in various applications, especially as nanocarriers for hydrophobic drugs [19]. Poloxamers have also been combined with other polymers to improve drug loading, impart NP stability, and enhance drug solubility [18]. On the other hand, D- $\alpha$ -tocopheryl polyethylene glycol 1000 succinate (vitamin E TPGS or TPGS) is a water-soluble form of vitamin E that is used in drug delivery to prolong the circulation half-life, enhance the bioavailability, improve the cytotoxicity, and synergize with other anticancer drugs [20–23]. TPGS is used as a nanocarrier for hydrophobic and poorly water-soluble drugs due to its amphiphilic nature [24,25].

In this study, we hypothesized that two biocompatible polymers, TPGS and a poloxamer (Pluronic P123), can be used as nanocarriers for R19 encapsulation and delivery, combining the benefits of both TPGS and poloxamers. To verify our hypothesis, R19 NPs at different ratios of TPGS and Pluronic P123 were prepared and characterized for their physicochemical properties. The NPs were also tested on breast cancer cell lines to evaluate their bioactivity and biocompatibility.

## 2. Materials and Methods

### 2.1. Materials

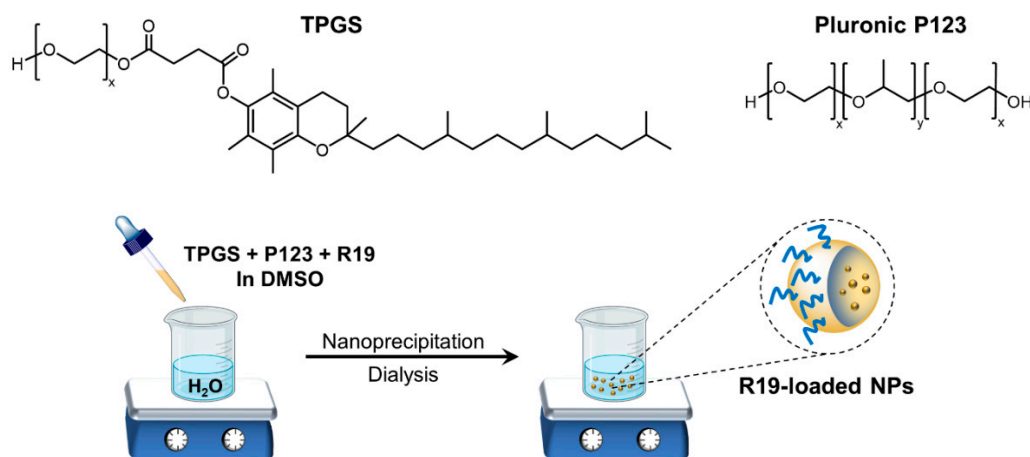
N-(2-fluorophenyl)-6-chloro-4-hydroxy-2-quinolone-3-carboxamide (R19) was synthesized and characterized as previously described [9]. Pluronic P123 (P123), TPGS, and Nile red (NR) were purchased from Sigma-Aldrich (St. Louis, MO, USA). Phosphate buffered saline solution (PBS, 10×, pH 7.4), potassium bromide (KBr), and dimethyl sulfoxide (DMSO) were procured from Fisher Chemicals (Pittsburgh, PA, USA). Spectra/Por dialysis membranes with 3500 and 12,000–14,000 Da molecular weight cut-offs (MWCO) were obtained from Repligen (Waltham, MA, USA). Ultrapure water was prepared using a Millipore Direct-Q 5UV system (EMD Millipore, Burlington, MA, USA).

### 2.2. Preparation of R19-Loaded NPs

R19-loaded NPs were produced via the nanoprecipitation technique, as previously described [26]. Different NP formulations were prepared by varying the P123: TPGS ratio (Table 1), and each batch was prepared in triplicate. Stock solutions of each polymer (P123 and TPGS) were first prepared at 20 mg/mL in DMSO. Each batch consisted of a 20 mg polymer or polymer mixture, and the amount of drug was fixed at 2 mg. The organic phase was prepared by mixing the appropriate volumes of polymer solutions in a microtube (total volume 1 mL), to which 2 mg of R19 powder was added, and the mixture was vortexed until the drug was completely dissolved. The resultant organic phase was then added dropwise to 10 mL of ultrapure water under continuous stirring. After 30 min of stirring, the NP dispersion was transferred to a dialysis membrane (3500 MWCO) and was dialyzed against 2 L of deionized water under gentle stirring for 24 h. After 24 h, the dialysis bag was emptied into a vial, and the samples were either used directly or were stored at 4 °C for further characterization. Blank NPs were prepared as described above but without the addition of R19. NR-labeled NPs were prepared by replacing R19 with NR (0.2 mg per NP formulation), and the NPs were purified by dialysis, as described above. A schematic of the NP preparation process is presented in Figure 2.

**Table 1.** Composition of R19-loaded NPs.

NP	R19 (mg)	Pluronic P123 (mg)	TPGS (mg)
100% TPGS	2	0	20
25% P123/75% TPGS	2	5	15
50% P123/50% TPGS	2	10	10
75% P123/25% TPGS	2	15	5
100% P123	2	20	0



**Figure 2.** Structures of TPGS and P123 and a schematic of R19 NP preparation by nanoprecipitation.

### 2.3. Particle Size and Zeta Potential Measurements

Dynamic light scattering (DLS) was used for the measurement of the particle size and polydispersity index (PDI) of the NPs. Electrophoretic light scattering was used for zeta potential measurements. Samples were analyzed using a Nicomp<sup>®</sup> Nano Z3000 instrument (Entegris, Billerica, MA, USA). For the analysis, fresh NPs (200  $\mu$ L) were diluted at a ratio of 1:1 with ultrapure water to obtain a scattering intensity between 200 and 300 kHz. Results were expressed as the mean  $\pm$  standard deviation (SD), and each formulation was prepared in triplicate.

### 2.4. Drug Loading Efficiency Determination

The amount of R19 loaded in the NPs and the drug loading efficiency were determined by UV-Vis (UV-1800 spectrophotometer, Shimadzu, Kyoto, Japan). Fresh NPs (100  $\mu$ L) were diluted 10 $\times$  in DMSO, and their UV absorbance was measured at 309 nm ( $\lambda_{\max}$  for R19). The concentration of loaded R19 was then calculated based on a calibration curve of drug absorbance at 309 nm versus concentration in DMSO. The concentration was multiplied by the total volume of each formulation to obtain the total amount of loaded drug; then, the drug loading efficiency (DL%) was calculated according to Equation (1):

$$\text{Drug loading efficiency (DL\%)} = (\text{Actual amount of drug loaded}) / (\text{Initial amount of drug added}) \times 100\% \quad (1)$$

NR-labeled NPs were also diluted 10 $\times$  in DMSO, and the absorbance was measured at 552 nm. A calibration curve of NR in DMSO was prepared at 552 nm and was used to determine the NR concentration in the labeled NPs.

### 2.5. Transmission Electron Microscopy (TEM) Imaging

R19-loaded NPs were visualized by transmission electron microscopy (TEM). Samples were prepared and were imaged as previously described [27].

### 2.6. Characterization by Fourier Transform-Infrared (FTIR) Spectroscopy

For analysis by FTIR, fresh R19-loaded NPs were lyophilized (FreeZone 4.5 L, Lab-conco, Kansas City, MO, USA) and transformed into KBr pellets. The FTIR spectra of R19, Pluronic P123, TPGS, and the R19-loaded NPs were acquired using an IR Affinity-1 spectrometer (Shimadzu, Kyoto, Japan) within a wavenumber range of 3600–500  $\text{cm}^{-1}$ .

### 2.7. Differential Scanning Calorimetry (DSC)

The thermal transitions of the R19-loaded NPs were examined using a Netzsch DSC 204 F1 instrument (Selb, Germany). Approximately 10 mg of lyophilized NPs, individual polymers, and R19 were used for the analysis. The samples' thermal behavior was investigated by heating from ambient temperature to 250  $^{\circ}\text{C}$  at a rate of 10  $^{\circ}\text{C}/\text{min}$  under a nitrogen atmosphere.

### 2.8. Colloidal Stability of R19-Loaded NPs

The stability of the prepared NPs was evaluated upon incubation in cell culture media for 24 h at 37  $^{\circ}\text{C}$  by monitoring the changes in particle size and in the PDI. In total, 200  $\mu$ L of each sample were diluted with 200  $\mu$ L of cell culture medium supplemented with 10% fetal bovine serum (FBS), and the samples were incubated for 24 h with shaking at 100 rpm and 37  $^{\circ}\text{C}$  (Biosan ES-20 Orbital Shaker-Incubator, Riga, Latvia). Particle size and PDI of the NPs were measured before and after 24 h incubation by DLS. The experiment was performed in triplicate, and the results were reported as the mean  $\pm$  SD.

### 2.9. In Vitro Release of R19 from R19-Loaded NPs

The in vitro release of R19 was evaluated using the dialysis method. Briefly, 1-mL aliquots of fresh NPs were transferred to a dialysis bag (12,000–14,000 MWCO) in triplicate and were inserted into vials containing 30 mL of phosphate-buffered saline (PBS, pH 7.4)



supplemented with 0.5% *w/v* Tween 80 to maintain sink conditions [25]. The samples were incubated under shaking at 100 rpm and 37 °C (Biosan ES-20 Orbital Shaker-Incubator). At the designated sampling time points, 10 mL of each release medium was withdrawn and replaced with 10 mL of fresh buffer. At the 24, 48, 72, and 96 h time points, 10 mL samples were withdrawn, and the remaining release medium was replaced with 30 mL of fresh buffer. The collected samples were lyophilized, redissolved in 1 mL of DMSO, and centrifuged for 5 min at 4000 rpm to precipitate the undissolved buffer salts. The amount of R19 released was then measured by analyzing the UV absorbance of the supernatant based on the calibration curve of R19 in DMSO. Results were expressed as the average cumulative release (%) versus time (h). The release profiles were compared by calculating the similarity factor ( $f_2$ ) between each of the two formulations according to Equation (2) [28]:

$$f_2 = 50 \times \log[(1 + 1/n \sum (R_t - T_t)^2)^{-0.5} \times 100] \quad (2)$$

where  $n$  is the number of sampling time points, and  $R_t$  and  $T_t$  are the cumulative amounts released from every two formulations at each time point  $t$ .

### 2.10. Cell Viability Assays

Cell viability assays were conducted on the MCF-7 and MDA-MB-231 breast cancer cells as well as on human dermal fibroblasts (HDFs) as normal cells. Cell lines were obtained from the American Type Culture Collection (ATCC, Manassas, VA, USA). MCF-7 cells were grown in Minimum Essential Medium (MEM; Gibco, Thermo Fisher Scientific, Waltham, MA, USA). MDA-MB-231 cells were grown in Roswell Park Memorial Institute (RPMI) 1640 medium (Euroclone SpA, Milan, Italy). HDFs were grown in Dulbecco's Modified Eagle's Medium (DMEM; Euroclone SpA). All media were supplemented with 10% heat-inactivated fetal bovine serum (FBS; Capricorn Scientific, Ebsdorfergrund, Germany) and penicillin–streptomycin (100 U/mL–100 µg/mL; Euroclone SpA). Cells were maintained at 37 °C in a humidified 5% CO<sub>2</sub> incubator. For the viability assays, cells were seeded in 96-well plates at a density of 10,000 cells/well (MCF-7 and MDA-MB-231) or 7000 cells/well (HDFs) and were incubated overnight. The next day, cells ( $n = 5$  per treatment group) were treated with R19 (from a 20 mg/mL stock solution in DMSO) and R19-loaded NPs (freshly prepared and dispersed in water) at concentrations between 0 and 300 µM of R19 diluted in complete culture medium for 48 h. Another group of cells was treated with blank NP formulations at concentrations equivalent to the concentrations used for R19-loaded NPs. At the end of the incubation period, the medium was removed, and 100 µL of fresh medium containing 0.5 mg/mL of 3-(4,5-dimethylthiazol-2-yl)-2,5-diphenyltetrazolium bromide (MTT, Wheeling, IL, USA) was added to each well. Following incubation for 2 h, the medium was removed, and 100 µL of DMSO was added to each well to dissolve the formazan crystals. The optical density of each well was measured at 540 nm using a BioTek Synergy HTX Multi-Mode Reader. Cell viability was expressed as the % relative to the untreated cells. IC<sub>50</sub> values were determined by a non-linear regression analysis of cell viability versus concentration curves using GraphPad Prism software version 7.00 (San Diego, CA, USA).

### 2.11. Mitochondrial Membrane Potential Assay

The mitochondrial membrane potential of MCF-7 and MDA-MB-231 cells treated with R19 and the R19-loaded NPs was measured using the JC-1 probe (Abcam, Cambridge, UK) [29]. Briefly, cells were seeded in 96-well plates at a density of 10,000 cells/well overnight. The next day, cells were treated with 20 µM of free R19 or an equivalent concentration of R19-loaded NPs for 24 h in triplicate (100 µL per well). After 24 h, JC-1 was diluted in PBS to a concentration of 20 µM, and 100 µL of the dye solution was added to each well. The cells were incubated with JC-1 for 10 min at 37 °C, and the fluorescence intensity of the wells was then measured using a BioTek Synergy HTX Multi-Mode Reader at 485 nm/528 nm excitation/emission wavelengths for the detection of the green JC-1 monomers and at 540 nm/620 nm excitation/emission wavelengths for the detection of the

red JC-1 aggregates. The results were expressed as the ratio of green/red fluorescence after subtracting the background fluorescence of the unstained cells.

#### 2.12. Cellular Uptake of NR-Labeled NPs

Cellular uptake assays were conducted in MCF-7 and MDA-MB-231 cells using NR-labeled NPs. Briefly, cells were seeded in 24-well plates at a density of 50,000 cells/well. The next day, cells were treated with NR dissolved in complete culture medium (MEM for MCF-7 cells or RPMI 1640 for MDA-MB-231 cells) at a concentration of 1 µg/mL or at an equivalent concentration of NR NPs for 1 h ( $n = 3$ ). Then, the medium was removed, the cells were washed with PBS twice, and 500 µL of PBS was added to each well. NR fluorescence was quantified using a BioTek Synergy HTX Multi-Mode Reader at 540 nm/620 nm excitation/emission wavelengths. Untreated cells were used as background controls, and cell-associated fluorescence was normalized relative to the untreated cells.

#### 2.13. Statistical Analysis

All data are presented as mean  $\pm$  SD of at least three different trials. Differences between sample means were compared using one- or two-way analysis of variance (ANOVA) followed by Tukey's or Sidak's multiple comparison test, respectively, where a  $p$ -value of 0.05 was considered statistically significant. All analyses were performed in GraphPad Prism version 7.00.

### 3. Results and Discussion

#### 3.1. Preparation and Characterization of R19-Loaded NPs

Here, we investigated the feasibility of incorporating R19 in a polymeric NP formulation to ensure its solubility, stability, and potential targeting ability when applied in vivo due to the enhanced permeability and retention (EPR) effect [15,30]. NPs were prepared by nanoprecipitation, as it is a simple and convenient method for entrapping hydrophobic drugs in polymeric NPs (Figure 2) [31]. R19 was formulated using two types of biocompatible polymers to evaluate the loading capacity of the NPs for the drug, the size of the NPs produced, and the effectiveness and safety toward cancer and normal cells.

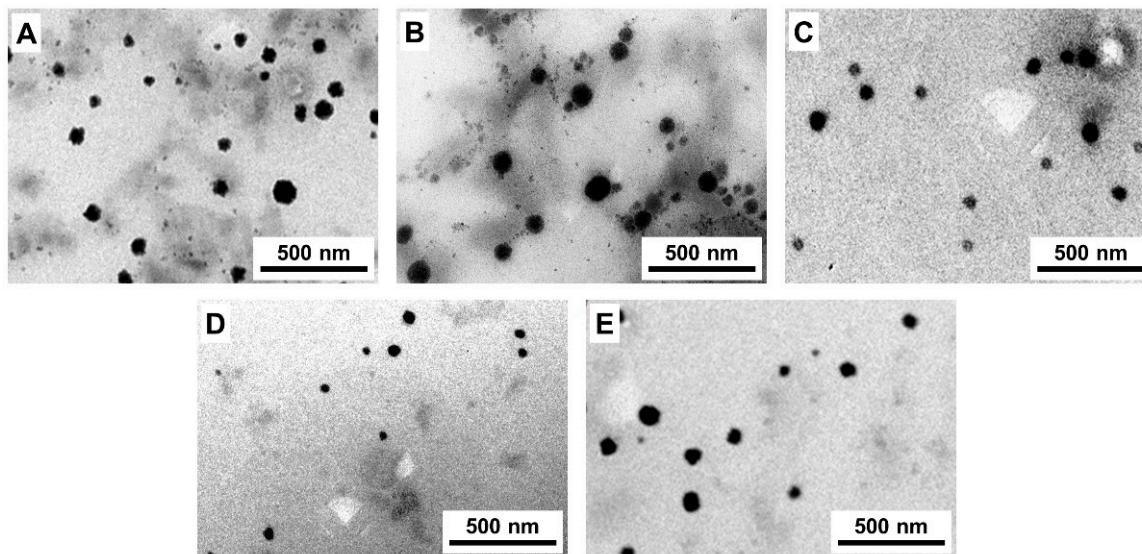
Several formulations were prepared using different ratios of P123: TPGS (Table 1), and the characteristics of the NPs in terms of particle size, PDI, and DL% are presented in Table 2. The R19-loaded NPs were initially prepared using 100% P123. The average DL% was 59%, and the average particle size of the NPs was 100 nm, with a PDI of 0.17. Then, TPGS was used in combination with P123 to evaluate its effect on the DL% and particle size. Different ratios of both polymers were prepared: 100% TPGS (0% P123), 25% P123/75% TPGS, 50% P123/50% TPGS, and 75% P123/25% TPGS. Interestingly, as shown in Table 2, the different NP formulations showed similar average particle sizes ranging between 92 and 112 nm. With respect to the DL%, it ranged between 57 and 61%. Overall, the different ratios of P123 with TPGS did not reveal a significant difference with regard to the DL% nor the particle size of the NPs obtained. Likewise, the PDI of the formulations was relatively small and ranged between 0.14 and 0.20. PDI is a measure of the uniformity of the particle size distribution [32]. The PDI results revealed a narrow particle size distribution in all of the NP formulations as the values were close to 0, reflecting the excellent monodispersity of the NPs. Furthermore, the NPs were characterized by a spherical morphology when observed under TEM (Figure 3).

Zeta potential is used as an indicator of a colloidal dispersion's stability that is based on the surface charge of the particles in contact with water [33]. The zeta potential values for all of the NP formulations ranged between  $-30$  mV and  $+30$  mV, indicating that the NPs carried an almost neutral surface charge. Since this may affect their aggregation tendency, particularly when in contact with biological fluids, this led us to investigate the stability of the R19-loaded NPs in cell culture media, as described later.

**Table 2.** Characteristics of R19-loaded NPs reported as the mean  $\pm$  SD of at least three different batches of each NP.

NP	Particle Size * (nm)	PDI	Zeta Potential (mV)	DL%
100% TPGS	108 $\pm$ 8	0.20 $\pm$ 0.06	−1.7 $\pm$ 5.0	60 $\pm$ 6
25% P123/75% TPGS	92 $\pm$ 7	0.20 $\pm$ 0.03	−6.6 $\pm$ 19.6	57 $\pm$ 7
50% P123/50% TPGS	111 $\pm$ 8	0.14 $\pm$ 0.01	−5.4 $\pm$ 15.3	59 $\pm$ 10
75% P123/25% TPGS	112 $\pm$ 8	0.15 $\pm$ 0.05	16.0 $\pm$ 2.9	59 $\pm$ 6
100% P123	100 $\pm$ 8	0.17 $\pm$ 0.02	−10.5 $\pm$ 17.1	59 $\pm$ 7

\* Intensity-weighted.

**Figure 3.** TEM images of R19-loaded NPs prepared using (A) 100% TPGS, (B) 25% P123/75% TPGS, (C) 50% P123/50% TPGS, (D) 75% P123/25% TPGS, and (E) 100% P123.

The five NP formulations were characterized by FTIR spectroscopy and were compared to free R19 and the individual polymers P123 and TPGS (Figure 4). TPGS displayed characteristic bands at  $1750\text{ cm}^{-1}$  and at  $2900\text{--}3000\text{ cm}^{-1}$ , corresponding to the O–C=O stretching of its ester groups and C–H stretching, respectively [34]. The O–C=O stretching band appeared in the R19 NP formulation prepared with 100% TPGS and in the other formulations containing TPGS but with lower intensities due to the lower concentration. Moreover, this band disappeared in the formulations containing 100% P123. Pluronic P123 is a polyether characterized by a broad C–O–C stretching band between  $1000$  and  $1100\text{ cm}^{-1}$  [35]. P123 also showed a C–H stretching band at  $2900\text{--}3000\text{ cm}^{-1}$ , which is related to asymmetric C–H stretching in the methyl groups in PPO in addition to the band at  $1300\text{--}1400\text{ cm}^{-1}$  [36]. R19 NPs exhibited the same bands at  $1300\text{--}1400\text{ cm}^{-1}$ . R19 and TPGS showed similar bands that overlapped with P123. In addition to a broad –OH stretching band between  $2600$  and  $3200\text{ cm}^{-1}$ , R19 displayed a sharp band at  $1660\text{ cm}^{-1}$  corresponding to the amide C=O stretching. This band was present in the NP formulations but had a weaker intensity, most likely due to the low % of R19 in the formulations (around 6% *w/w*). Overall, no new peaks were formed, which indicated no drug–excipient interaction.

The thermal transitions of the NP formulations were examined by DSC. As shown in Figure 5A, R19 displayed broad endothermic melting peaks between  $80$  and  $100\text{ }^{\circ}\text{C}$  and between  $150$  and  $270\text{ }^{\circ}\text{C}$ , indicating the nearly amorphous nature of the compound. Neat TPGS (Figure 5B) exhibited a sharp endothermic melting peak at around  $45.9\text{ }^{\circ}\text{C}$ , which is close to the literature value [37]. The R19-loaded NPs prepared using 100% TPGS (Figure 5C) showed a reduction in the TPGS melting peak to  $40.9\text{ }^{\circ}\text{C}$ , suggesting an interaction between the drug and the polymer, most likely representing van der Waals and potentially H-bonding interactions. As P123 was added to the formulation, the melting

peak of TPGS was slightly lowered to 38.2–39.5 °C in the R19 NPs composed of 25% P123/75% TPGS (Figure 5D) and 50% P123/50% TPGS (Figure 5E), reflecting additional polymer–polymer and polymer–drug interactions. Notably, the peaks that were originally present in R19 disappeared in all of the NP formulations, suggesting that it is contained in the NPs in an amorphous state. The neat P123 and NPs with 75% and 100% P123 could not be analyzed due to the liquification of the polymer upon heating and the technical limitations of the DSC instrument. However, according to the literature, P123 is known for its thermal stability, with a weak endothermic peak appearing at 75 °C corresponding to the melting of PEO chains and a strong endothermic peak at around 400 °C due to polymer decomposition [38].

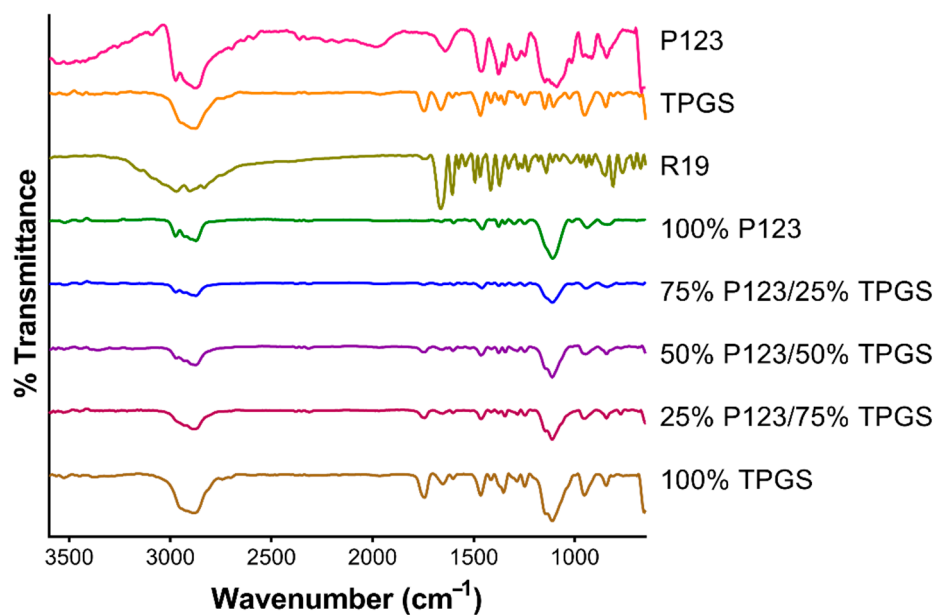


Figure 4. FTIR spectra of R19, P123, TPGS, and R19-loaded NPs.

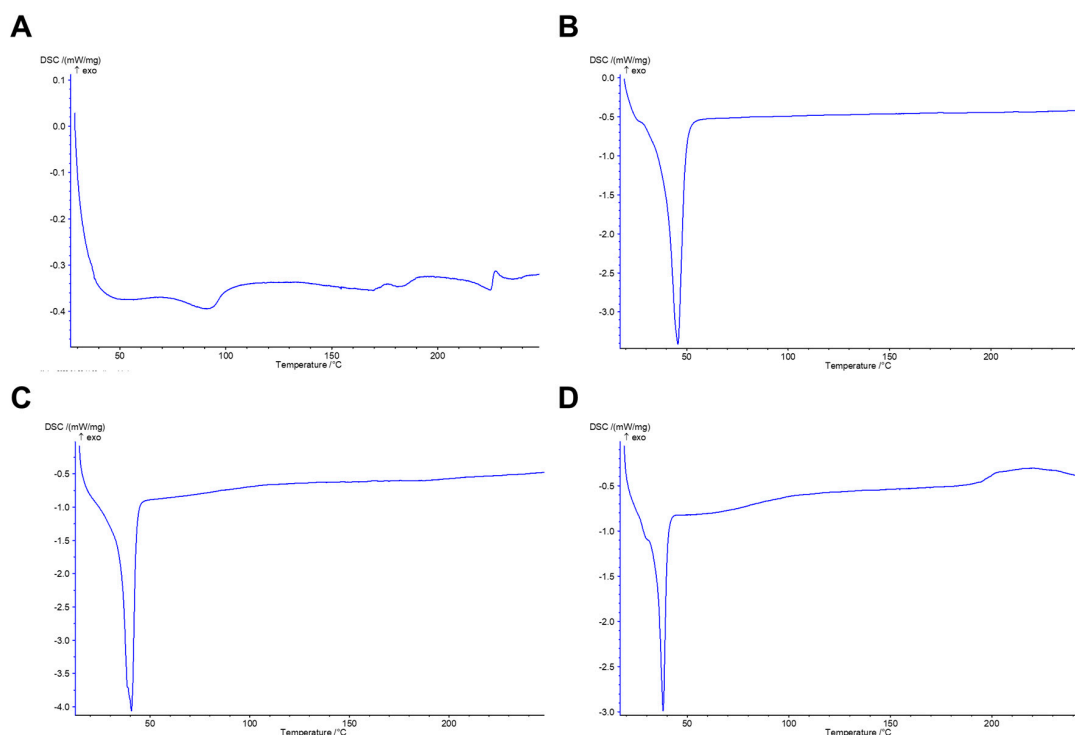
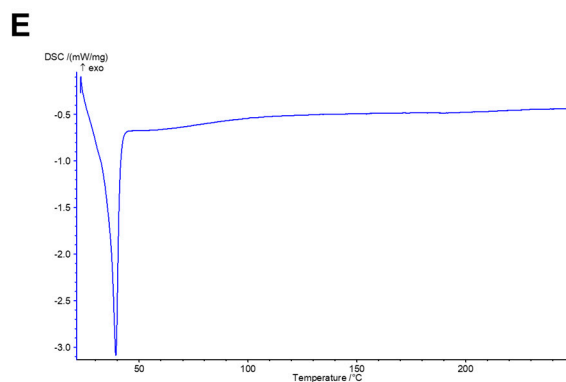


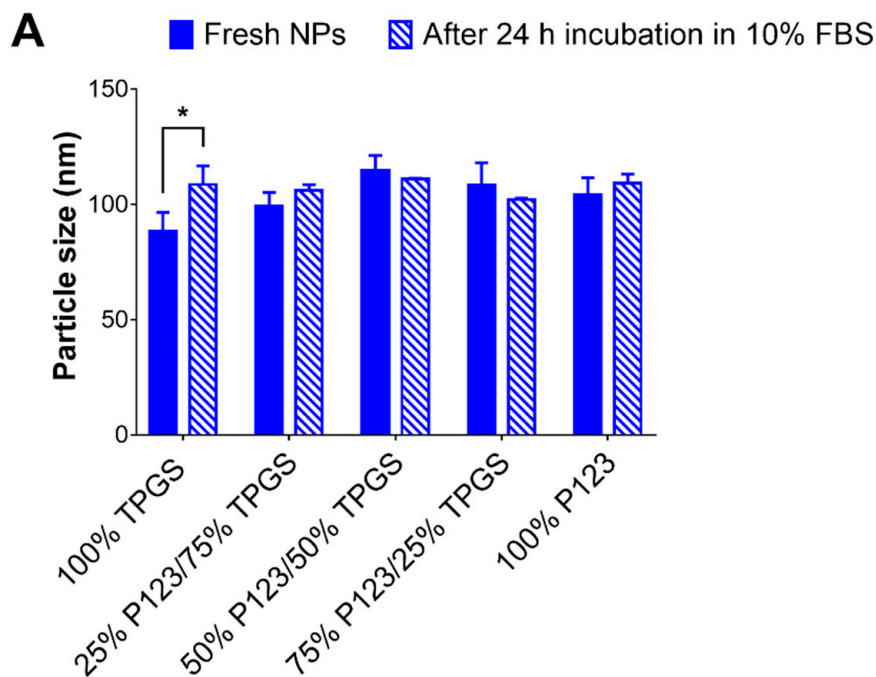
Figure 5. Cont.



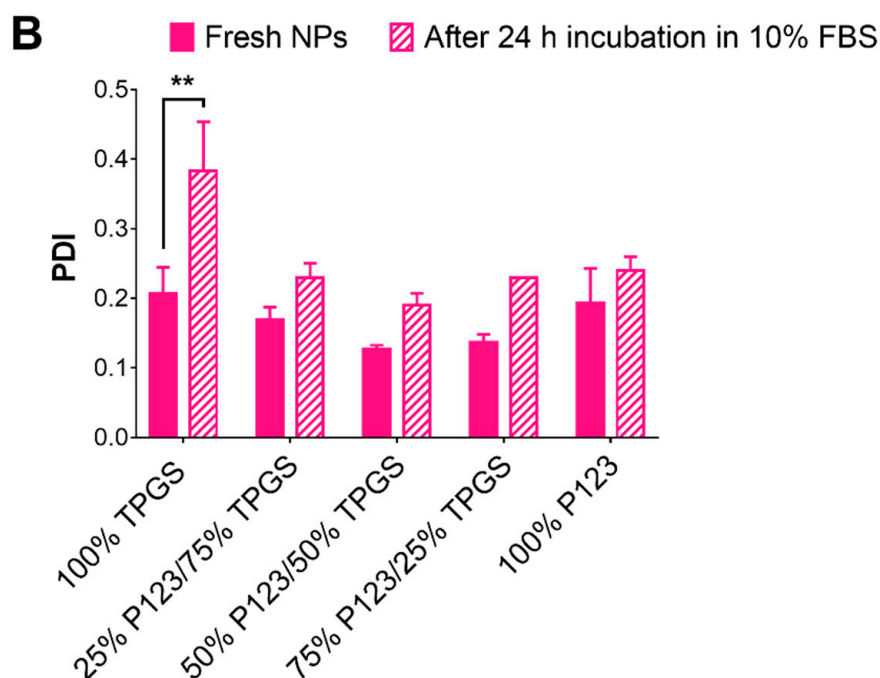
**Figure 5.** DSC thermograms of (A) R19, (B) neat TPGS, and R19-loaded NPs composed of (C) 100% TPGS, (D) 25% P123/75% TPGS, and (E) 50% P123/50% TPGS.

### 3.2. Stability of R19-Loaded NPs

As mentioned earlier, the R19-loaded NPs may have a tendency toward aggregation due to their low surface charge. It is challenging to maintain a stabilized particle size distribution of the NPs in a colloidal dispersion, particularly in biological fluids. Since the NPs were going to be evaluated in in vitro cell culture, we tested the colloidal stability of the NPs in a serum-supplemented cell culture medium for 24 h. Figure 6 represents the particle sizes of the samples before and after 24 h of incubation at 37 °C in the cell culture medium. Interestingly, all of the NPs, except for those prepared using 100% TPGS, showed no significant changes in the particle size nor in the PDI upon incubation. On the other hand, the NPs composed of 100% TPGS underwent a significant size increase ( $p < 0.05$ ) from 88 nm to 108 nm that was accompanied by a marked increase in the PDI from 0.21 to 0.38 ( $p < 0.01$ ). These results strongly indicate that the presence of P123, even at small percentages, can make the NPs more stable against aggregation when applied in biological systems.



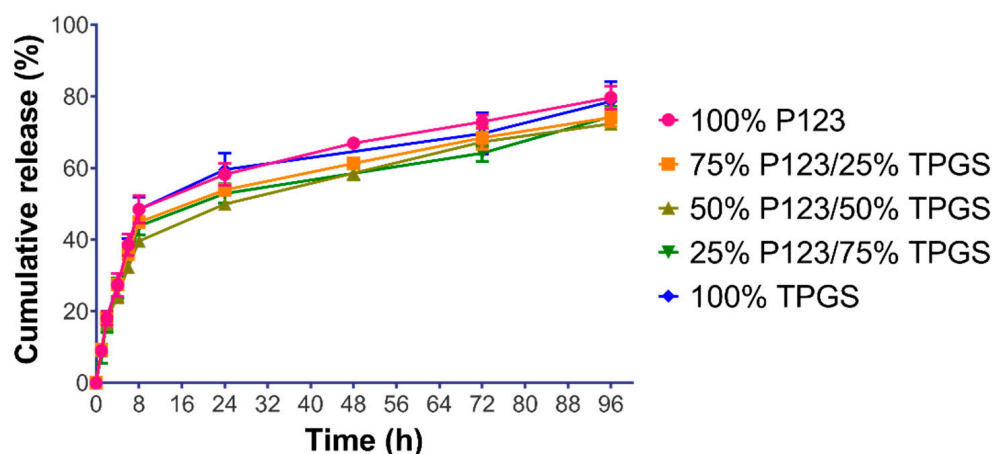
**Figure 6.** Cont.



**Figure 6.** Change in (A) particle size and (B) PDI of R19-loaded NPs after 24 h incubation in cell culture medium supplemented with 10% FBS at 37 °C. Results are presented as the mean  $\pm$  SD ( $n = 3$ ). \*  $p < 0.05$  and \*\*  $p < 0.01$  based on two-way ANOVA followed by Sidak's multiple comparison test.

### 3.3. In Vitro Release of R19 from R19-Loaded NPs

The different formulations of the R19-loaded NPs were subjected to release testing in PBS buffer with a pH of 7.4 at 37 °C to mimic physiological conditions. As shown in Figure 7, the cumulative drug release from all of the formulations was almost superimposable. All of the profiles were characterized by a biphasic release pattern, with a relatively fast release phase within the first 8 h followed by a more sustained release phase up to 96 h. The first phase may be related to the drug release from the surface of the NPs, whereas the second phase may be attributed to the slow diffusion of the drug from inside the NPs. Within the first 8 h of incubation, the cumulative drug release across all of the formulations was between 40 and 49%. After 24 h, the cumulative drug release increased more gradually to 50–58%. The same trend was observed at 48 and 72 h. After 96 h, the cumulative drug release reached 72–79% among the various formulations. Our results are in line with previous work on similar polymeric systems. For example, TPGS-formulated liposomes or NPs have been studied to determine in vitro release and showed a relatively slow release and a cumulative release of 82% after 48 h [39,40]. As for P123-based nanoformulations, the release of different drugs was affected by the percentage of P123 and ranged between 50 and 80% [41]. On the other hand, formulations with P123/TPGS mixtures showed a slow in vitro release that ranged between 40 and 50%, which was believed to be caused by the micelles formed from P123/TPGS and the preference of the hydrophobic drug to remain in the hydrophobic core of the micelles due to its low solubility in the release medium [42]. The similarity factor ( $f_2$ ) was calculated between the various NP formulations to examine the differences between the release profiles. As shown in Table 3,  $f_2$  was greater than 50 in all of the formulations, confirming their similar release behavior [28].



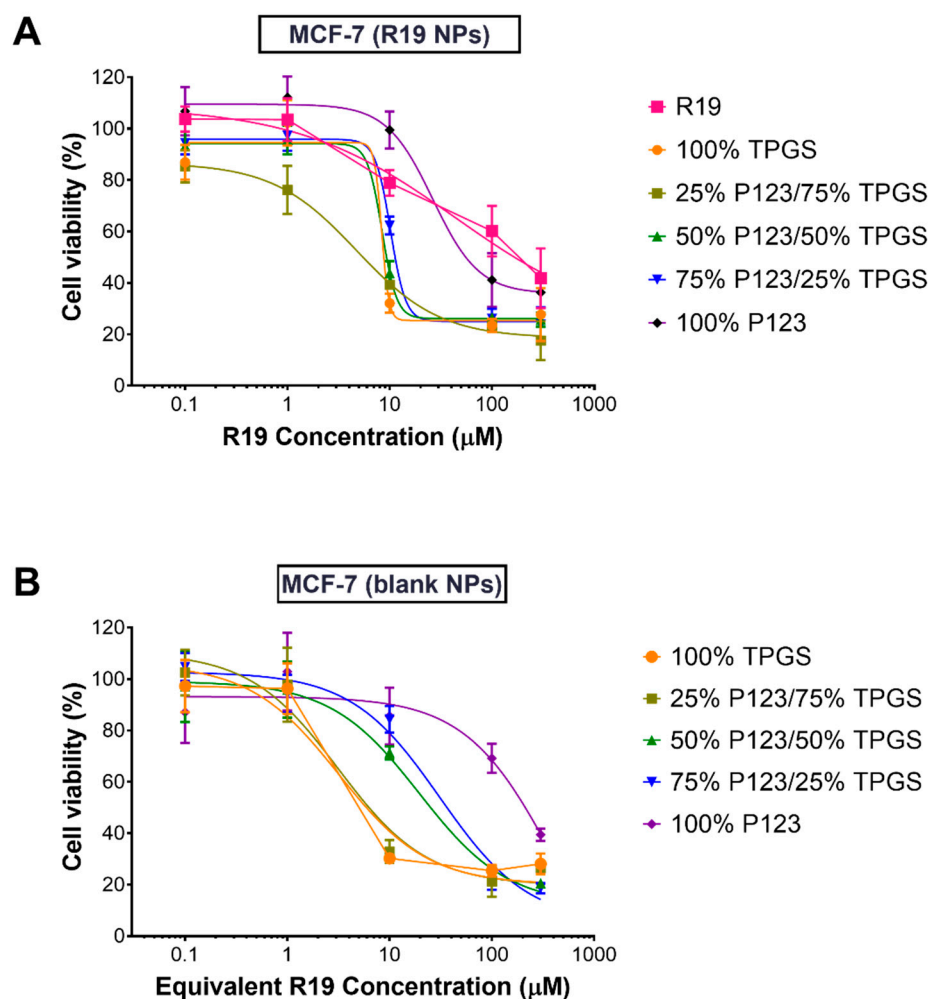
**Figure 7.** In vitro release of R19 from R19-loaded NPs in PBS pH 7.4 at 37 °C, demonstrating sustained drug release up to 96 h. Results are expressed as the mean cumulative release %  $\pm$  SD ( $n = 3$ ) plotted against time (h).

**Table 3.** Similarity factor ( $f_2$ ) results for R19-loaded NPs.

Sample 1	Sample 2	$f_2$
100% P123	75% P123/25% TPGS	71
	50% P123/50% TPGS	60
	25% P123/75% TPGS	66
	100% TPGS	88
75% P123/25% TPGS	50% P123/50% TPGS	75
	25% P123/75% TPGS	84
	100% TPGS	75
50% P123/50% TPGS	25% P123/75% TPGS	78
	100% TPGS	62
25% P123/75% TPGS	100% TPGS	69

### 3.4. Cell Viability Assays

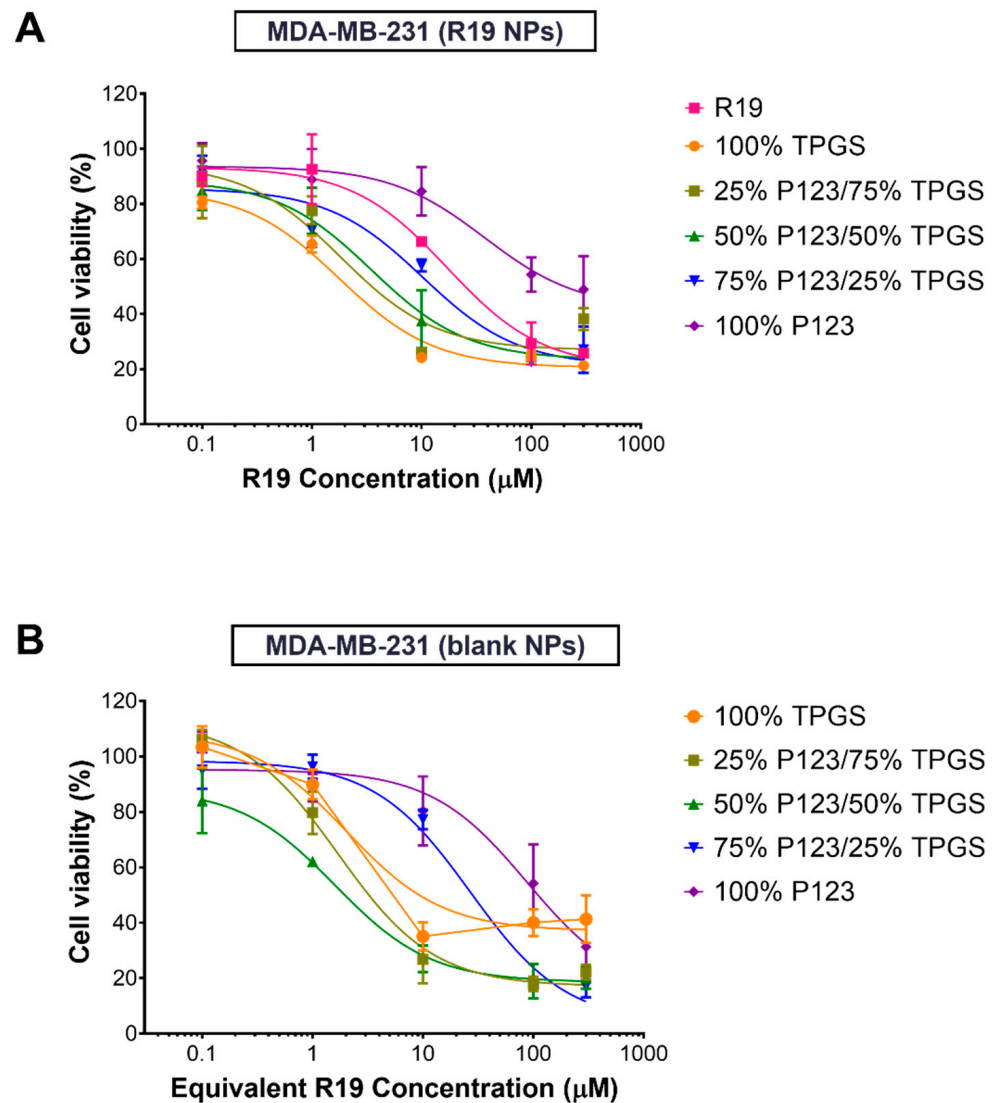
The anticancer activity of R19 and R19-loaded NPs was evaluated against two breast cancer cell lines: MCF-7 and MDA-MB-231, because breast cancer is the most common malignancy affecting women and accounts for the highest percentage of cancer-related deaths [43]. Cells were treated with increasing concentrations of R19 and the NPs for 48 h, followed by the MTT assay. As shown in Figures 8A and 9A, all of the treatments caused a dose-dependent inhibition of cell growth, but with varying degrees. The dose-response curves were fitted by non-linear regression analysis to obtain the  $IC_{50}$  values, which correspond to the treatments' potency. As shown in Table 4, R19 displayed similar potency against both cell lines, with  $IC_{50}$  values of 14.7 and 17.0  $\mu$ M in the MCF-7 and MDA-MB-231 cells, respectively. These values were similar to the R19 potency in colorectal cancer cells [9]. Since the PI3K/Akt/mTOR pathway is dysregulated in these cancer cell lines, it was expected that R19 would show similar inhibitory activity. The potent anticancer effect of R19 in breast cancer cell lines strongly support its application as a potential targeted therapy in hormone receptor-positive and triple-negative breast cancer.



**Figure 8.** Percentage viability of MCF-7 cells treated with (A) R19 and R19-loaded NPs and (B) blank NPs for 48 h ( $n = 5$ ).

As for the R19 NP formulations, lower  $\text{IC}_{50}$  values were obtained compared to the free drug in both cell lines, with the exception of 100% P123 NPs. The highest potency was observed for the R19 NPs prepared using 100% TPGS and 25% P123/75% TPGS in both the MCF-7 and MDA-MB-231 cells, with almost a three-fold reduction in the  $\text{IC}_{50}$  values in MCF-7 cells and a two- to nine-fold reduction in MDA-MB-231 cells. Generally, the  $\text{IC}_{50}$  value increased as the % of TPGS decreased, and the NPs with 100% P123 displayed the highest  $\text{IC}_{50}$  values and the poorest fit to the dose–response curve ( $R^2 < 0.9$ ). The enhancement of anticancer potency in the NP formulations can likely be attributed to the polymeric carriers, particularly TPGS. TPGS has been reported to inhibit cancer cell proliferation through cell cycle arrest and the induction of apoptosis [44,45]. In addition, TPGS has been shown to overcome cancer drug resistance by downregulating the expression of P-glycoprotein efflux pumps [46,47]. These findings were confirmed by testing equivalent concentrations of the NPs without the drug under the same conditions. As shown in Table 4, blank NPs containing more than 50% TPGS were almost equally potent as the drug-loaded formulations. However, as the % of P123 increased, a reduction in potency was observed, similar to the drug-loaded NPs. These results provide a promising approach for the application of TPGS-containing R19 NPs, not only in breast cancer but also in multidrug-resistant cancer types.





**Figure 9.** Percentage viability of MDA-MB-231 cells treated with (A) R19 and R19-loaded NPs and (B) blank NPs for 48 h (*n* = 5).

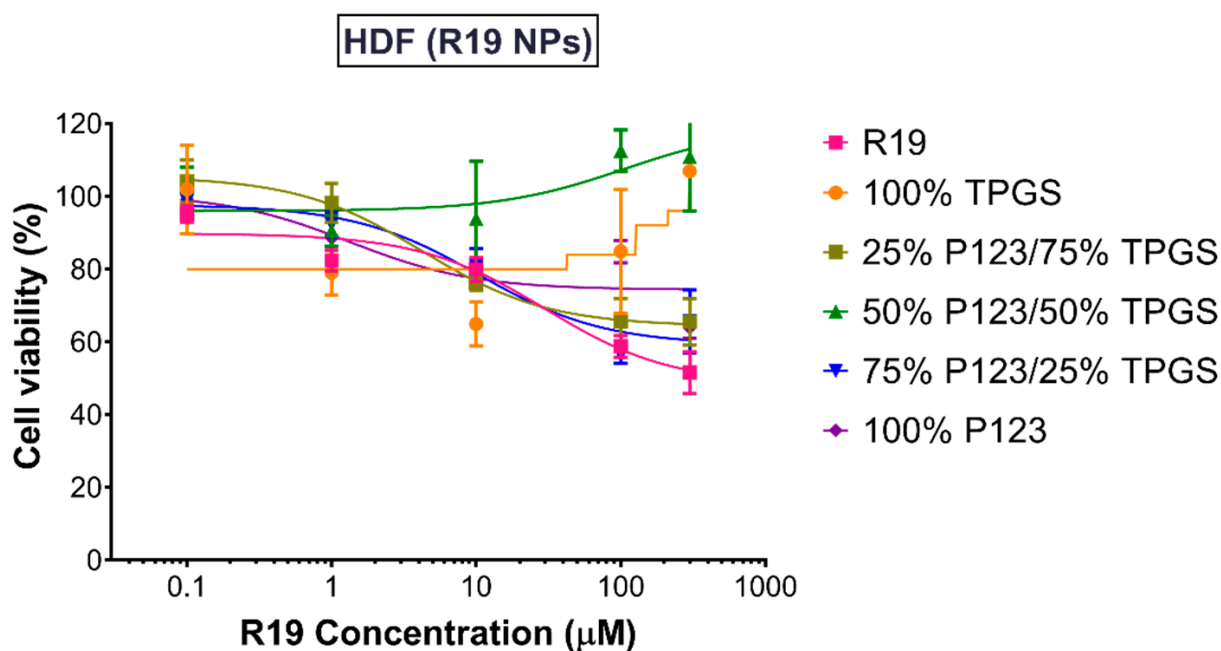
**Table 4.** IC<sub>50</sub> values of R19 and R19-loaded NPs and equivalent concentrations of blank NPs in MCF-7 and MDA-MB-231 cells after 48 h of incubation.

Treatment	IC <sub>50</sub> (μM; Mean ± SEM *)	
	MCF-7	MDA-MB-231
R19	14.7 ± 5.3	17.0 ± 4.2
100% TPGS	4.3 ± 1.9	1.8 ± 0.4
25% P123/75% TPGS	4.7 ± 1.0	1.8 ± 0.7
50% P123/50% TPGS	4.9 ± 1.1	3.5 ± 1.0
75% P123/25% TPGS	12.3 ± 2.4	10.2 ± 3.2
100% P123	45.4 ± 18.6	37.5 ± 24.3
Blank 100% TPGS	3.2 ± 1.1	2.0 ± 0.8
Blank 25% P123/75% TPGS	3.1 ± 1.0	1.7 ± 0.3
Blank 50% P123/50% TPGS	19.5 ± 4.9	1.6 ± 0.4
Blank 75% P123/25% TPGS	31.0 ± 7.2	26.8 ± 5.8
Blank 100% P123	415.1 ± 448.8	87.1 ± 52.0

\* SEM: standard error.

Having shown excellent activity against cancer cells, equivalent concentrations of R19-loaded NPs were also tested in HDF to determine their selectivity and biocompatibility.

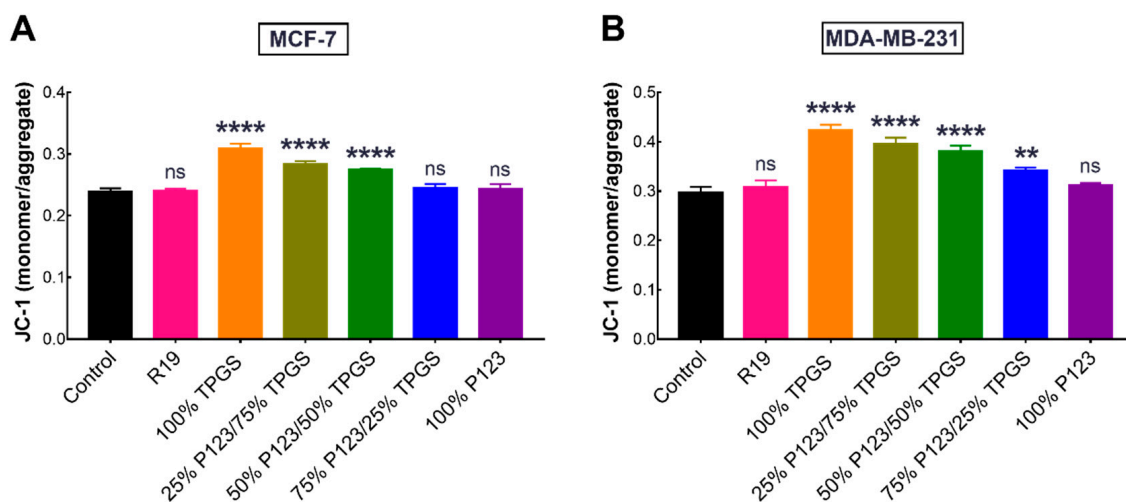
As depicted in Figure 10, the NPs exhibited more than 60% cell viability at the highest concentration tested (300  $\mu\text{M}$ ), whereas the free drug caused an almost 50% reduction in cell viability at the same concentration. Moreover, the NPs prepared using 100% TPGS and 50% P123/50% TPGS maintained a cell viability of  $\sim 100\%$  at the highest concentration, indicating their superior biocompatibility. As all of the groups resulted in more than 50% cell viability, the  $\text{IC}_{50}$  values could not be accurately determined. Altogether, the results clearly demonstrate the selectivity of R19 in killing cancer cells, which was enhanced upon incorporation into the NPs. Moreover, the low  $\text{IC}_{50}$  values obtained for the TPGS-containing NPs in the MDA-MB-231 cells, which represent the more aggressive type of breast cancer, represent a highly promising result for the potential clinical application of the NP formulation as a breast cancer nanomedicine.



**Figure 10.** Percentage viability of HDF treated with R19 and R19-loaded NPs for 48 h ( $n = 5$ ).

### 3.5. Mitochondrial Membrane Potential Assay of R19-Treated Cells

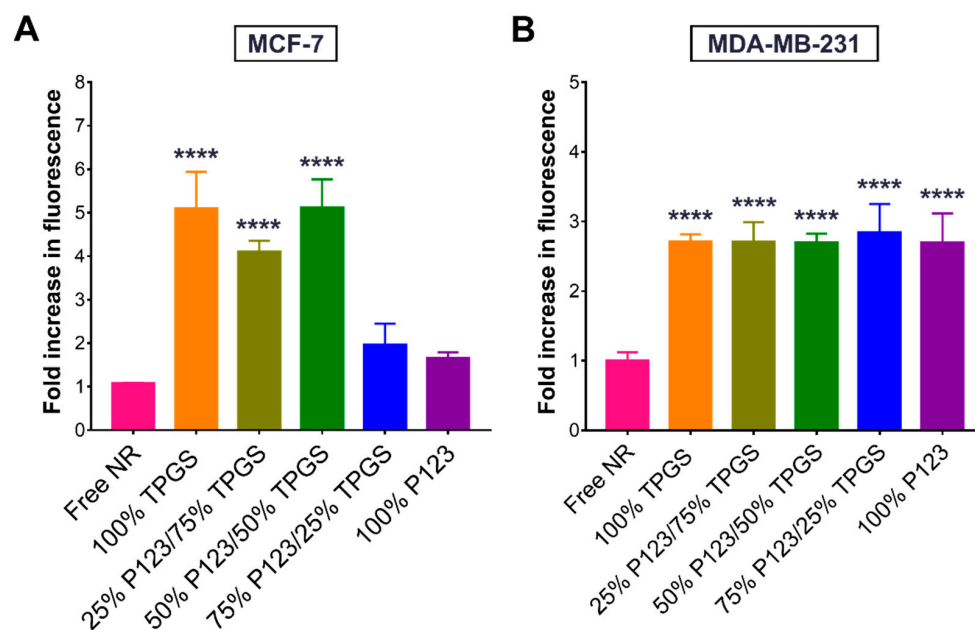
Mitochondrial depolarization is one of the early signs of apoptosis and can be conveniently detected by JC-1. Under normal conditions, JC-1 exists in an aggregated state within the mitochondrial matrix and emits red fluorescence. As the mitochondrial transmembrane potential dissipates in cells undergoing apoptosis, JC-1 is effluxed to the cytoplasm, where it dissociates into monomers that emit green fluorescence. Therefore, the change in the ratio of green/red fluorescence may be used as an indicator of apoptosis induction [48]. As seen in Figure 11A, MCF-7 cells treated with free R19 and R19 NPs composed of 75% P123/25% TPGS and 100% P123 did not show a significant difference in the JC-1 monomer/aggregate ratio compared to the control (untreated cells). Likewise, the mitochondrial membrane potential of MDA-MB-231 cells treated with R19 and R19 NPs composed of 100% P123 was similar to that of the control (Figure 11B). On the other hand, cells treated with the R19 NPs containing TPGS displayed a significantly higher JC-1 monomer/aggregate ratio, signifying that these formulations were able to induce a greater degree of apoptosis compared to the free drug and R19 NPs composed entirely of P123.



**Figure 11.** Change in mitochondrial membrane potential of (A) MCF-7 and (B) MDA-MB-231 cells after 24 h of treatment with 20  $\mu$ M of R19 and R19-loaded NPs. Results are expressed as the ratio of the green/red fluorescence signals of the JC-1 monomers and aggregates, respectively (mean  $\pm$  SD;  $n = 3$ ). \*\*  $p < 0.01$ , \*\*\*\*  $p < 0.0001$ , and ns: not significantly different, compared to the control (untreated cells), based on one-way ANOVA followed by Tukey's multiple comparisons test.

### 3.6. Cellular Uptake of NR-Labeled NPs

The observed enhancement in the bioactivity of R19 upon incorporation into the NP formulations may in part be attributed to an enhancement in cellular uptake. To test this hypothesis, R19 was replaced with NR, and the NR-labeled NPs were incubated with the cells. As depicted in Figure 12A, in MCF-7 cells, the NPs composed of high percentages of TPGS (100%, 75%, and 50%) were associated with the highest increase in intracellular fluorescence compared to the free dye, denoting enhanced cellular uptake. As for MDA-MB-231 cells (Figure 12B), all of the NPs exhibited a significant increase in intracellular fluorescence compared to the free dye regardless of their composition. Interestingly, the TPGS-containing NPs achieved a four- to five-fold increase in fluorescence compared to the control in MCF-7 cells, whereas in the MDA-MB-231 cells, the NPs averaged around a 2.7-fold increase in fluorescence. These results are most likely attributed to differences in the membrane permeability between the two cell lines. Nonetheless, the results strongly support the ability of the NP formulations, particularly those containing TPGS, to enhance the cellular uptake of hydrophobic molecules such as R19, consistent with the cell viability and JC-1 assays.



**Figure 12.** Normalized fluorescence intensities (mean  $\pm$  SD;  $n = 3$ ) of (A) MCF-7 and (B) MDA-MB-231 cells treated with free NR or NR-labeled NPs for 1 h. \*\*\*\*  $p < 0.0001$  based on one-way ANOVA followed by Tukey's multiple comparison test.

#### 4. Conclusions

R19 is a new chemical entity that has been found to be an effective anticancer agent. In this work, R19 was successfully formulated in NPs composed of different combinations of TPGS and Pluronic P123. The NPs had particle sizes of approximately 100 nm and high monodispersity. Additionally, the DL% reached about 60% in the different polymer combinations and all of the NPs sustained the release of the drug up to 96 h. The NPs were highly stable in serum-supplemented cell culture medium, with the exception of the formulations composed of 100% TPGS, which exhibited a tendency for aggregation. Cell viability assays in MCF-7 and MDA-MB-231 breast cancer cell lines revealed an enhanced potency of R19 when it was incorporated into TPGS-containing NPs with reduced cytotoxicity against HDE, most likely by enhancing its cellular uptake and promoting apoptosis. The observed cancer cell selectivity and high biocompatibility of the NP formulations emphasize the positive attributes of the designed polymeric NPs as a promising delivery approach for R19 and its analogs, bringing them one step closer to clinical translation.

**Author Contributions:** Conceptualization, S.S. and D.S.; methodology, S.S.; software, S.S.; validation, S.A. (Sundos Aliyeh), S.A. (Samah Abusulieh) and S.S.; formal analysis, S.A. (Sundos Aliyeh) and S.S.; investigation, S.A. (Sundos Aliyeh), S.A. (Samah Abusulieh) and S.S.; resources, S.S.; data curation, S.A. (Sundos Aliyeh), S.A. (Samah Abusulieh) and S.S.; writing—original draft preparation, S.A. (Sundos Aliyeh); writing—review and editing, D.S. and S.S.; visualization, S.S.; supervision, D.S. and S.S.; project administration, S.S.; funding acquisition, S.S. All authors have read and agreed to the published version of the manuscript.

**Funding:** This research was funded by Al-Zaytoonah University of Jordan, grants number 11/18/2018-2019 and 14/08/2021-2022. The APC was funded by the authors.

**Institutional Review Board Statement:** Not applicable.

**Informed Consent Statement:** Not applicable.

**Data Availability Statement:** Not applicable.

**Acknowledgments:** The authors thank Faten Alregeb (University of Jordan) for the assistance with the DSC analysis.

**Conflicts of Interest:** The authors declare no conflict of interest. The funders had no role in the design of the study; in the collection, analyses, or interpretation of data; in the writing of the manuscript; or in the decision to publish the results.

## References

- World Health Organization (WHO). Cancer Fact Sheet. Available online: <https://www.who.int/news-room/fact-sheets/detail/cancer> (accessed on 14 July 2022).
- Rallis, K.S.; Lai Yau, T.H.; Sideris, M. Chemoradiotherapy in cancer treatment: Rationale and clinical applications. *Anticancer Res.* **2021**, *41*, 1. [CrossRef] [PubMed]
- Schirrmacher, V. From chemotherapy to biological therapy: A review of novel concepts to reduce the side effects of systemic cancer treatment (Review). *Int. J. Oncol.* **2019**, *54*, 407–419.
- Kannaiyan, R.; Mahadevan, D. A comprehensive review of protein kinase inhibitors for cancer therapy. *Expert Rev. Anticancer Ther.* **2018**, *18*, 1249–1270. [CrossRef] [PubMed]
- Andrs, M.; Korabecny, J.; Jun, D.; Hodny, Z.; Bartek, J.; Kuca, K. Phosphatidylinositol 3-inase (PI3K) and phosphatidylinositol 3-kinase-related kinase (PIKK) inhibitors: Importance of the morpholine ring. *J. Med. Chem.* **2015**, *58*, 41–71. [CrossRef] [PubMed]
- Zhang, Y.; Kwok-Shing Ng, P.; Kucherlapati, M.; Chen, F.; Liu, Y.; Tsang, Y.H.; de Velasco, G.; Jeong, K.J.; Akbani, R.; Hadjipanayis, A.; et al. A Pan-cancer proteogenomic atlas of PI3K/Akt/mTOR pathway alterations. *Cancer Cell* **2017**, *31*, 820–832.e823. [CrossRef]
- Yu, J.S.; Cui, W. Proliferation, survival and metabolism: The role of PI3K/Akt/mTOR signalling in pluripotency and cell fate determination. *Development* **2016**, *143*, 3050–3060. [CrossRef]
- Hamadneh, L.; Bahader, M.; Abuarqoub, R.; AlWahsh, M.; Alhusban, A.; Hikmat, S. PI3K/AKT and MAPK1 molecular changes preceding matrix metalloproteinases overexpression during tamoxifen-resistance development are correlated to poor prognosis in breast cancer patients. *Breast Cancer* **2021**, *28*, 1358–1366. [CrossRef]
- Sabbah, D.A.; Haroon, R.A.; Bardaweel, S.K.; Hajjo, R.; Sweidan, K. N-phenyl-6-chloro-4-hydroxy-2-quinolone-3-carboxamides: Molecular docking, synthesis, and biological investigation as anticancer agents. *Molecules* **2020**, *26*, 73. [CrossRef]
- Zhong, Y.; Su, T.; Shi, Q.; Feng, Y.; Tao, Z.; Huang, Q.; Li, L.; Hu, L.; Li, S.; Tan, H.; et al. Co-administration of iRGD enhances tumor-targeted delivery and anti-tumor effects of paclitaxel-loaded PLGA nanoparticles for colorectal cancer treatment. *Int. J. Nanomed.* **2019**, *14*, 8543–8560. [CrossRef]
- Jin, C.; Wang, K.; Oppong-Gyebi, A.; Hu, J. Application of nanotechnology in cancer diagnosis and therapy—A mini-review. *Int. J. Med. Sci.* **2020**, *17*, 2964–2973. [CrossRef]
- Sunoqrot, S.; Hamed, R.; Abdel-Halim, H.; Tarawneh, O. Synergistic interplay of medicinal chemistry and formulation strategies in nanotechnology—From drug discovery to nanocarrier design and development. *Curr. Top. Med. Chem.* **2017**, *17*, 1451–1468. [CrossRef] [PubMed]
- Gagliardi, A.; Giuliano, E.; Venkateswararao, E.; Fresta, M.; Bulotta, S.; Awasthi, V.; Cosco, D. Biodegradable polymeric nanoparticles for drug delivery to solid tumors. *Front. Pharmacol.* **2021**, *12*, 601626. [CrossRef] [PubMed]
- Kamaly, N.; Yameen, B.; Wu, J.; Farokhzad, O.C. Degradable controlled-release polymers and polymeric nanoparticles: Mechanisms of controlling drug release. *Chem. Rev.* **2016**, *116*, 2602–2663. [CrossRef] [PubMed]
- Nakamura, H.; Jun, F.; Maeda, H. Development of next-generation macromolecular drugs based on the EPR effect: Challenges and pitfalls. *Expert Opin. Drug Deliv.* **2015**, *12*, 53–64. [CrossRef]
- Sunoqrot, S.; Alsadi, A.; Tarawneh, O.; Hamed, R. Polymer type and molecular weight dictate the encapsulation efficiency and release of Quercetin from polymeric micelles. *Colloid Polym. Sci.* **2017**, *295*, 2051–2059. [CrossRef]
- Parmar, A.; Singh, K.; Bahadur, A.; Marangoni, G.; Bahadur, P. Interaction and solubilization of some phenolic antioxidants in Pluronic® micelles. *Colloids Surf. B Biointerfaces* **2011**, *86*, 319–326. [CrossRef] [PubMed]
- Zhao, L.; Du, J.; Duan, Y.; Zang, Y.n.; Zhang, H.; Yang, C.; Cao, F.; Zhai, G. Curcumin loaded mixed micelles composed of Pluronic P123 and F68: Preparation, optimization and in vitro characterization. *Colloids Surf. B Biointerfaces* **2012**, *97*, 101–108. [CrossRef]
- Nguyen, V.T.; Nguyen, T.H.; Dang, L.H.; Vu-Quang, H.; Tran, N.Q. Folate-conjugated chitosan-pluronic P123 nanogels: Synthesis and characterizations towards dual drug delivery. *J. Nanomater.* **2019**, *2019*, 1067821. [CrossRef]
- Gan, H.; Chen, L.; Sui, X.; Wu, B.; Zou, S.; Li, A.; Zhang, Y.; Liu, X.; Wang, D.; Cai, S.; et al. Enhanced delivery of sorafenib with anti-GPC3 antibody-conjugated TPGS-b-PCL/Pluronic P123 polymeric nanoparticles for targeted therapy of hepatocellular carcinoma. *Mater. Sci. Eng. C* **2018**, *91*, 395–403. [CrossRef]
- Zou, T.; Gu, L. TPGS emulsified zein nanoparticles enhanced oral bioavailability of daidzin: In vitro characteristics and in vivo performance. *Mol. Pharm.* **2013**, *10*, 2062–2070. [CrossRef]
- Gaonkar, R.; Ganguly, S.; Dewanjee, S.; Sinha, S.; Gupta, A.; Ganguly, S.; Chattopadhyay, S.; Debnath, C. Garcinol loaded vitamin E TPGS emulsified PLGA nanoparticles: Preparation, physicochemical characterization, in vitro and in vivo studies. *Sci. Rep.* **2017**, *7*, 530–544. [CrossRef] [PubMed]
- Zhu, D.; Tao, W.; Zhang, H.; Liu, G.; Wang, T.; Zhang, L.; Zeng, X.; Mei, L. Docetaxel (DTX)-loaded polydopamine-modified TPGS-PLA nanoparticles as a targeted drug delivery system for the treatment of liver cancer. *Acta Biomater.* **2016**, *30*, 144–154. [CrossRef] [PubMed]

24. Zhang, J.; Tao, W.; Chen, Y.; Chang, D.; Wang, T.; Zhang, X.; Mei, L.; Zeng, X.; Huang, L. Doxorubicin-loaded star-shaped copolymer PLGA-vitamin E TPGS nanoparticles for lung cancer therapy. *J. Mater. Sci. Mater. Med.* **2015**, *26*, 165. [CrossRef] [PubMed]
25. Mu, L.; Feng, S.S. PLGA/TPGS nanoparticles for controlled release of paclitaxel: Effects of the emulsifier and drug loading ratio. *Pharm. Res.* **2003**, *20*, 1864–1872. [CrossRef]
26. Sunoqrot, S.; Orainee, B.; Alqudah, D.A.; Daoud, F.; Alshaer, W. Curcumin-tannic acid-poloxamer nanoassemblies enhance curcumin's uptake and bioactivity against cancer cells in vitro. *Int. J. Pharm.* **2021**, *610*, 121255. [CrossRef]
27. Sunoqrot, S.; Al-Shalabi, E.; Al-Bakri, A.G.; Zalloum, H.; Abu-Irmaileh, B.; Ibrahim, L.H.; Zeno, H. Coffee bean polyphenols can form biocompatible template-free antioxidant nanoparticles with various sizes and distinct colors. *ACS Omega* **2021**, *6*, 2767–2776. [CrossRef]
28. Duan, J.Z.; Riviere, K.; Marroum, P. In vivo bioequivalence and in vitro similarity factor (f<sub>2</sub>) for dissolution profile comparisons of extended release formulations: How and when do they match? *Pharm. Res.* **2011**, *28*, 1144–1156. [CrossRef]
29. Sivanzade, F.; Bhalerao, A.; Cucullo, L. Analysis of the Mitochondrial Membrane Potential Using the Cationic JC-1 Dye as a Sensitive Fluorescent Probe. *Bio-Protocol* **2019**, *9*, e3128. [CrossRef]
30. Kalyane, D.; Raval, N.; Maheshwari, R.; Tambe, V.; Kalia, K.; Tekade, R.K. Employment of enhanced permeability and retention effect (EPR): Nanoparticle-based precision tools for targeting of therapeutic and diagnostic agent in cancer. *Mater. Sci. Eng. C* **2019**, *98*, 1252–1276. [CrossRef]
31. Martínez Rivas, C.J.; Tarhini, M.; Badri, W.; Miladi, K.; Greige-Gerges, H.; Nazari, Q.A.; Galindo Rodríguez, S.A.; Román, R.Á.; Fessi, H.; Elaissari, A. Nanoprecipitation process: From encapsulation to drug delivery. *Int. J. Pharm.* **2017**, *532*, 66–81. [CrossRef]
32. Danaei, M.; Dehghankhold, M.; Ataei, S.; Hasanzadeh Davarani, F.; Javanmard, R.; Dokhani, A.; Khorasani, S.; Mozafari, M.R. Impact of particle size and polydispersity index on the clinical applications of lipidic nanocarrier systems. *Pharmaceutics* **2018**, *10*, 57. [CrossRef] [PubMed]
33. Ferraris, S.; Cazzola, M.; Peretti, V.; Stella, B.; Spriano, S. Zeta potential measurements on solid surfaces for in vitro biomaterials testing: Surface charge, reactivity upon contact with fluids and protein absorption. *Front. Bioeng. Biotechnol.* **2018**, *6*, 60. [CrossRef] [PubMed]
34. Khare, V.; Sakarchi, W.A.; Gupta, P.N.; Curtis, A.D.M.; Hoskins, C. Synthesis and characterization of TPGS–gemcitabine prodrug micelles for pancreatic cancer therapy. *RSC Adv.* **2016**, *6*, 60126–60137. [CrossRef]
35. Dehvari, K.; Lin, K.-S.; Hammouda, B. Small-angle neutron scattering studies of microenvironmental and structural changes of Pluronic micelles upon encapsulation of paclitaxel. *J. Taiwan Inst. Chem. Eng.* **2017**, *71*, 405–413. [CrossRef]
36. Su, Y.-L.; Wang, J.; Liu, H.-Z. FTIR spectroscopic study on effects of temperature and polymer composition on the structural properties of PEO–PPO–PEO block copolymer micelles. *Langmuir* **2002**, *18*, 5370–5374. [CrossRef]
37. Mu, L.; Feng, S.S. A novel controlled release formulation for the anticancer drug paclitaxel (Taxol<sup>®</sup>): PLGA nanoparticles containing vitamin E TPGS. *J. Control. Release* **2003**, *86*, 33–48. [CrossRef]
38. Zhang, G.; Chen, X.; Zhao, Y.; Ma, F.; Jing, B.; Qiu, H. Lyotropic liquid-crystalline phases formed by pluronic p123 in ethylammonium nitrate. *J. Phys. Chem. B* **2008**, *112*, 6578–6584. [CrossRef]
39. Mu, L.; Feng, S.S. Vitamin E TPGS used as emulsifier in the solvent evaporation/extraction technique for fabrication of polymeric nanospheres for controlled release of paclitaxel (Taxol<sup>®</sup>). *J. Control. Release* **2002**, *80*, 129–144. [CrossRef]
40. Farooq, M.A.; Xinyu, H.; Jabeen, A.; Ahsan, A.; Seidu, T.A.; Kutoka, P.T.; Wang, B. Enhanced cellular uptake and cytotoxicity of vorinostat through encapsulation in TPGS-modified liposomes. *Colloids Surf. B Biointerfaces* **2021**, *199*, 111523. [CrossRef]
41. Jindal, N.; Mehta, S.K. Nevirapine loaded Poloxamer 407/Pluronic P123 mixed micelles: Optimization of formulation and in vitro evaluation. *Colloids Surf. B Biointerfaces* **2015**, *129*, 100–106. [CrossRef]
42. Duan, Y.; Cai, X.; Du, H.; Zhai, G. Novel in situ gel systems based on P123/TPGS mixed micelles and gellan gum for ophthalmic delivery of curcumin. *Colloids Surf. B Biointerfaces* **2015**, *128*, 322–330. [CrossRef]
43. Lei, S.; Zheng, R.; Zhang, S.; Wang, S.; Chen, R.; Sun, K.; Zeng, H.; Zhou, J.; Wei, W. Global patterns of breast cancer incidence and mortality: A population-based cancer registry data analysis from 2000 to 2020. *Cancer Commun.* **2021**, *41*, 1183–1194. [CrossRef]
44. Neophytou, C.M.; Constantinou, C.; Papageorgis, P.; Constantinou, A.I. D-alpha-tocopheryl polyethylene glycol succinate (TPGS) induces cell cycle arrest and apoptosis selectively in Survivin-overexpressing breast cancer cells. *Biochem. Pharmacol.* **2014**, *89*, 31–42. [CrossRef]
45. Ruiz-Moreno, C.; Jimenez-Del-Rio, M.; Sierra-Garcia, L.; Lopez-Osorio, B.; Velez-Pardo, C. Vitamin E synthetic derivate-TPGS-selectively induces apoptosis in Jurkat T cells via oxidative stress signaling pathways: Implications for acute lymphoblastic leukemia. *Apoptosis* **2016**, *21*, 1019–1032. [CrossRef]
46. Guan, Y.-Y.; Zeng, S.-Q.; Qin, Y.; Mu, Y.; Liu, H. Vitamin E-tocopheryl polyethylene glycol succinate decorated drug delivery system with synergistic antitumor effects to reverse drug resistance and immunosuppression. *Colloids Surf. A Physicochem. Eng. Asp.* **2021**, *628*, 127387. [CrossRef]
47. Yan, H.; Du, X.; Wang, R.; Zhai, G. Progress in the study of D- $\alpha$ -tocopherol polyethylene glycol 1000 succinate (TPGS) reversing multidrug resistance. *Colloids Surf. B Biointerfaces* **2021**, *205*, 111914. [CrossRef]
48. Tusskorn, O.; Khunluck, T.; Prawan, A.; Senggunprai, L.; Kukongviriyapan, V. Mitochondrial division inhibitor-1 potentiates cisplatin-induced apoptosis via the mitochondrial death pathway in cholangiocarcinoma cells. *Biomed. Pharmacother.* **2019**, *111*, 109–118. [CrossRef]

## Article

# Fragment-Based and Structural Investigation for Discovery of JNK3 Inhibitors

Men Thi Hoai Duong and Hee-Chul Ahn \*

College of Pharmacy, Dongguk University-Seoul, Goyang, Gyeonggi 10326, Korea

\* Correspondence: hcahn@dongguk.edu; Tel.: +82-31-961-5221

**Abstract:** The c-Jun N-terminal kinases (JNKs) are members of the mitogen-activated protein kinase (MAPK) family and are related to cell proliferation, gene expression, and cell death. JNK isoform 3 (JNK3) is an important therapeutic target in varieties of pathological conditions including cancers and neuronal death. There is no approved drug targeting JNKs. To discover chemical inhibitors of JNK3, virtual fragment screening, the saturation transfer difference (STD) NMR, in vitro kinase assay, and X-ray crystallography were employed. A total of 27 fragments from the virtually selected 494 compounds were identified as initial hits via STD NMR and some compounds showed the inhibition of the activity of JNK3 in vitro. The structures of JNK3 with a fragment and a potent inhibitor were determined by X-ray crystallography. The fragment and inhibitor shared a common JNK3-binding feature. The result shows that fragment screening by NMR spectroscopy is a very efficient method to screen JNK3 binders and the structure of JNK3-inhibitor complex can be used to design and develop more potent inhibitors.

**Keywords:** JNK3; fragment; saturation transfer difference NMR; X-ray crystallography

**Citation:** Duong, M.T.H.; Ahn, H.-C. Fragment-Based and Structural Investigation for Discovery of JNK3 Inhibitors. *Pharmaceutics* **2022**, *14*, 1900. <https://doi.org/10.3390/pharmaceutics14091900>

Academic Editor:  
Francesca Musumeci

Received: 29 July 2022

Accepted: 5 September 2022

Published: 8 September 2022

**Publisher's Note:** MDPI stays neutral with regard to jurisdictional claims in published maps and institutional affiliations.



**Copyright:** © 2022 by the authors. Licensee MDPI, Basel, Switzerland. This article is an open access article distributed under the terms and conditions of the Creative Commons Attribution (CC BY) license (<https://creativecommons.org/licenses/by/4.0/>).

## 1. Introduction

JNKs are the serine/threonine kinases and one of the members of the mitogen-activated protein kinases [1,2]. JNK phosphorylates several substrates, such as c-Jun and activating transcription factor 2 in response to environmental stress and pro-inflammatory cytokines [2]. JNKs are involved in varieties of physiological processes including neuronal function, immune activity, and embryonic development [3,4]. Thus, it is implicated that the JNK pathway is related to various pathological conditions, including neurodegenerative diseases, cancer, and inflammation [5–7]. Since the JNK signaling pathway is involved in numerous inflammatory diseases, the inhibition of JNK signaling could decrease the expression of pro-inflammatory cytokines [8,9]. In cancer, some isoforms of JNKs are pro-oncogenic [10], whereas others act as tumor suppressors [11,12]. These findings imply the necessity of isoform-specific JNK inhibitors in the development of the cancer therapeutics.

Particularly, JNK3 is almost exclusively expressed in the brain, with very low levels in the kidneys and the testis, while JNK1 and JNK2 are widely expressed in a variety of tissues [3]. The level of the phosphorylated JNKs increased in postmortem brain tissue samples of Alzheimer's disease (AD) patients [13] and was connected to the rate of cognitive decline [14]. Several studies demonstrated that JNKs are activated in Parkinson's disease (PD) mouse models [15–17] and dopaminergic neurons were protected from apoptosis due to the inhibition of JNK by its specific inhibitor, SP600125 [18]. This evidence supports JNK3 as a promising target for the treatment of neurodegenerative diseases.

There have been great efforts to design and develop pan- and isoform-specific JNK inhibitors. Particularly, the structure determination of the JNK-inhibitor complex aided the pursuit of the development of novel and potent JNK inhibitors. Recently, we reviewed most of the available structures of JNK-inhibitor complexes [19]. Several hinge-binding scaffolds, such as aminopyrimidine, (iso)quinoline, quinazoline, and other scaffolds similar to purine,

were frequently utilized for the development of ATP-competitive kinase inhibitors and 63 ATP competitive kinase inhibitors were FDA-approved till in the year 2021 [20,21]. Even though great efforts were paid to develop JNK inhibitors, there are no clinically available drug molecules as JNK therapeutics until now.

Fragment-based drug discovery (FBDD) has been an important paradigm for new drug discovery and is actively used in many pharmaceutical companies [22,23]. FBDD starts with the fragment screening in which weak binders to a target protein are selected and followed by creating lead compounds based on the fragment hits. Therefore, the screening methods generally rely on the biophysical methods to observe the weak interaction between the fragments and proteins. Those include the fluorescence-based method, NMR, surface plasmon resonance (SPR), isothermal titration calorimetry (ITC), mass spectroscopy, and X-ray crystallography. FBDD can be applied to the discovery of new drugs against most of the therapeutic targets, regardless of the types and characteristics of the proteins. Therefore, by using this method, several drugs have already entered the market, and many drug candidates are in clinical trials [24–26]. In discovering new kinase inhibitors, the fragment-based approaches have provided powerful insights into the selectivity enhancement and the lead optimization [27,28].

Compared with other methods, the NMR method has many advantages. The NMR spectroscopy is versatile and includes various methods of measurements to identify the weak binders to proteins. For example, STD NMR [29–31], relaxation filter experiments [32,33], and waterLOGSY [34] are commonly used for a ligand-based approach. A protein-based method is also utilized to identify protein binders, where the chemical shifts of the backbone  $^1\text{H}$ - $^{15}\text{N}$  heteronuclear single quantum correlation (HSQC) spectrum are monitored in the absence and presence of fragments. If the backbone chemical shift assignments are completed, the ligand binding “hot spot” can be identified without the knowledge of the detailed three-dimensional (3D) structure of the target. This provides an important information to create more potent compounds based on the fragments [22,23]. Even though the NMR methods are some of the most popular tools in FBDD campaign, it is not a stand-alone method and should be used complementarily with other methods to reduce the false positives, such as with X-ray crystallography for the identification of the exact binding mode and the assessment of structural novelty of the binding fragment. In this work, we present a collection of a fragment library by virtual screening, STD NMR spectroscopy, in vitro kinase assay, and the 3D structures of JNK3 in complex with fragments and an inhibitor, cyclopropyl[(3R)-3-((4-[6-hydroxy-2-(naphthalen-2-yl)-1H-benzimidazol-1-yl]pyrimidin-2-yl)amino)piperidine-1-yl]methanone, which previously showed a strong binding affinity to JNK3 and presented a potency of the cell protective effect in neuronal cell apoptosis [35]. In the structural investigation, we found a common JNK3-binding feature of the fragment and inhibitor, which occurred in the solvent-exposed region near the ATP binding site. We suppose this interaction potentiates the affinity of a chemical binder to JNK3 and could be utilized to design novel JNK3 inhibitors.

## 2. Materials and Methods

### 2.1. Fragment Library

The collection of compounds for the fragment library was conducted by virtual screening with the known structure of JNK3 (PDB ID, 1JNK) [36]. The bound molecules such as AMP-PNP, magnesium ions, and water were removed for the docking simulation. Docking simulations were performed on the ATP binding site of JNK3 by using the software Autodock vina [37] with the standard protocol provided by developer. The chemicals for the docking simulation were collected virtually from the various vendors' websites (Asinex, Winston-Salem, NC, USA; Maybridge, Waltham, MA, USA; ChemiDive, San Diego, CA, USA) with the molecular weight being less than 300 Da. A total of 15,000 compounds were screened, and top-scored molecules were chosen. Of those commercially available,



494 compounds were purchased from Asinex. The information of the fragments is provided in the Supplementary Files S1 (list) and S2 (structure data file, sdf).

## 2.2. Preparation of JNK3

The gene encoding the catalytic domain of human JNK3 which spans the amino acid residues from Ser40 to was amplified by PCR and inserted into the pET-15b expression vector between NcoI and BamHI restriction sites. The plasmid was transformed into the *Escherichia coli* strain BL21 (DE3) (Merck KGaA, Darmstadt, Germany). Cells were grown at 37 °C until OD<sub>600</sub> reached to ~0.6–0.7 and induced with a final concentration of 0.5 mM isopropyl-β-D-thiogalactopyranoside (IPTG) for 16–20 h at 18 °C. Cells were harvested by centrifugation 4000 rpm at 4 °C. The cell pellet was re-suspended in 20 mL lysis buffer (20 mM Hepes, pH = 7.0, 20 mM NaCl, 10% (v/v) glycerol, 2 mM dithiothreitol (DTT)). Cell membranes were disrupted by sonication on ice. The lysate was clarified by centrifugation at 18,000 rpm for 40 min. The supernatant was used for the following steps of purification.

Ion exchange chromatography using SP-Sephacrose FF 16/10 (GE Healthcare, Chicago, IL, USA) and size-exclusion chromatography using HiLoad 16/600 Superdex 75 prep-grade (GE Healthcare) were applied sequentially to purify JNK3. The purity of JNK3 was more than 95% judged by SDS-PAGE. The purified JNK3 was collected and concentrated using an Amicon (Merck KGaA, Darmstadt, Germany) centrifugal filter with MWCO 10,000 to 10 mg/mL. The protein was frozen under liquid nitrogen and finally stored at –80 °C.

## 2.3. NMR Experiments

All NMR data were measured at 25 °C on Agilent DD2 600 MHz NMR spectrometer with TR<sup>TM</sup> probe (Agilent, Santa Clara, CA, USA). The 494 compounds were respectively dissolved in d<sub>6</sub>-DMSO for the preparation of stock solutions. The stock was diluted into d<sub>11</sub>-Tris-HCl buffer (in D<sub>2</sub>O), pH 7.5 with the final concentration of 320 μM in 500 μL. The simple <sup>1</sup>H NMR spectrum of each compound was recorded with the sweep widths, 8370.5 Hz, and the time-domain points, 32K, for all experiments. Eight compounds were mixed, and the mixture was put to a single NMR tube, followed by the <sup>1</sup>H NMR measurement. The final concentration of a single compound was 160 μM.

The purified JNK3 was added to an NMR tube containing 8 compounds to the final concentration of 4 μM. In this way, a total of 62 NMR tubes containing 8 compounds (in the last tube, 6 compounds) and JNK were prepared. <sup>1</sup>H and STD NMR spectra were recorded, respectively. For STD NMR, the reference spectrum was acquired with the off-resonance saturation at 30 ppm, and the saturation spectrum was acquired with the on-resonance saturation at 0.5 ppm. The duration of the saturations was 3 s for both on- and off-resonance experiments. All data were processed and analyzed with the software Mnova (Mestrelab Research, Santiago de Compostela, Spain).

## 2.4. Crystallization and Data Collection

The recombinant human JNK3 (10 mg/mL) solution containing 0.02% n-octyl-glucopyranoside was mixed with ATP to a final concentration of 2 mM and crystallized as described previously [38] with some modification. The JNK3-AMP crystal was obtained by vapor diffusion in hanging drops at 4 °C with a reservoir solution containing 16% PEG MME 550, 10% ethylene glycol, 0.1 M HEPES pH 7.25, and 10 mM TCEP. JNK3-fragment (or inhibitor) crystals were obtained by micro-seeding the JNK3-AMP crystal under the addition of the fragment (or inhibitor) to the crystallization solution. The inhibitor was cyclopropyl[(3R)-3-({4-[6-hydroxy-2-(naphthalen-2-yl)-1H-benzimidazol-1-yl]pyrimidin-2-yl}amino)piperidine-1-yl]methanone (inhibitor, here after), which bound very strongly to JNK3 (*K<sub>d</sub>*, 46 nM) [35]. The diffraction data were collected at the 7A and 5C beamline of Pohang Light Source, Korea. The raw data were processed with HKL2000 [39]. The crystals belonged to space group of P212121, and the asymmetric unit contained one monomer (Table 1).

### 2.5. Structure Determination and Refinement

The structures were solved by the molecular replacement method using the program PHASER [40] with the template model PDB ID 3OY1, one of the JNK3 structure in complex with a selective inhibitor [41]. A manual model was built using the program COOT [42], and the resulting models were refined with the program REFMAC5 [43]. The quality of the refined models was evaluated by the program MolProbity [44]. Data collection and refinement statistics are summarized in Table 1. All figures representing the structure were generated by the PyMOL molecular-graphics program (The PyMOL Molecular Graphics System, Schrödinger, LLC., New York, NY, USA) [45] and by UCSF Chimera program [46]. The atomic coordinate and structure factors have been deposited in the Protein Data Bank (<http://www.rcsb.org>) with accession number of 4KKH and 7YL1 for fragment- and inhibitor-bound JNK3, respectively.

**Table 1.** Data collection and refinement statistics.

Crystals	3A8	Inhibitor
PDB ID	7YL1	4KKH
Data collection		
Space group	P212121	P212121
Cell dimensions		
a, b, c (Å)	50.15, 71.98, 107.16	52.32, 71.50, 107.08
$\alpha$ , $\beta$ , $\gamma$ (°)	90, 90, 90	90, 90, 90
Wavelength (Å)	0.97951	0.97951
Resolution (Å) *	59.75–2.48 (2.55–2.49)	50–2.0 (2.03–2.00)
Redundancy *	13.3 (12.5)	13.5 (12.8)
Completeness (%) *	99.1 (99.4)	100 (100)
$I/\sigma_I$ *	33.6 (3.7)	58.9 (9.4)
$R_{\text{merge}}$ (%) <sup>a,*</sup>	9.0 (35.3)	9.0 (44.2)
Refinement		
Resolution (Å)	36.61–2.49	37.45–2.0
No. of reflections	13,406	26,471
$R_{\text{work}}/R_{\text{free}}$ (%) <sup>b</sup>	20.4/29.4	22.9/27.7
No. of atoms	2925	2942
Average B-factors	Protein/water/3A8 43.139/42.040/48.722	Protein/water/inhibitor 43.774/47.582/35.827
R.m.s. deviations		
Bond lengths (Å)	0.007	0.007
Bond angle (°)	1.157	1.109
Ramachandran plot		
Residues in		
favoured/allowed/ disallowed regions (%) <sup>c</sup>	93.9/5.5/0.6	97.4/2.6/0/0

\* Values in the parentheses refer to the highest resolution shells. <sup>a</sup>  $R_{\text{merge}} = \frac{\sum_i \sum_j |I(h)_i - \langle I(h) \rangle|}{\sum_i \sum_j I(h)_i}$ , where  $I(h)$  is the intensity of reflection  $h$ ,  $\sum_i$  is the sum over all reflections, and  $\sum_j$  is the sum over  $i$  measurements of reflection  $h$ . <sup>b</sup>  $R_{\text{work}} = \frac{\sum |F_{\text{obs}} - F_{\text{calc}}|}{\sum F_{\text{obs}}}$ , 5% of the data was set aside for  $R_{\text{free}}$  calculation. <sup>c</sup> Statistics according to MolProbity Ramachandran analysis [44].

### 2.6. In Vitro Kinase Assay

The in vitro kinase assay was carried out with ADP-Glo™ Kinase assay kit (Promega, Madison, WI). The assay was prepared with the final concentration of 2 ng of active JNK3, 50  $\mu$ M ATP, 100  $\mu$ M fragments, 1X reaction buffer, and 0.04  $\mu$ g/ $\mu$ L p38 substrate. The experiments were set up with three control experiments including without ATP, without active JNK3, and without compound.

The mixture was incubated for 1 h at room temperature. The incubated solution was then supplied with 50  $\mu$ L ADP-Glo reagent, centrifuged with 6000 rpm at 26 °C for 30 s, and incubated for 40 min at room temperature. The samples were transferred to a 96-white plate and added kinase-detection reagent with the ratio of 1:1. After incubating for 40 min

at room temperature, the luminescence signals were recorded using the GloMax<sup>®</sup>-Multi Microplate Reader (Promega, Madison, WI, USA). The kinase assays were duplicated for each fragment.

### 3. Results

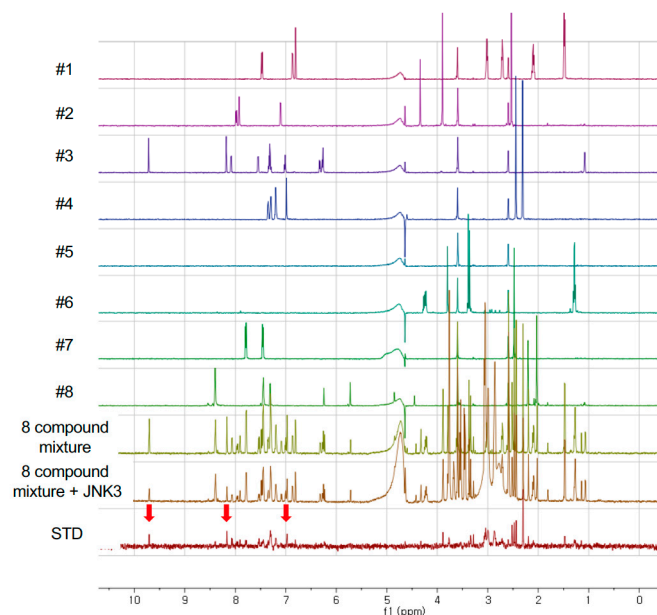
#### 3.1. Virtual Screening

To build a fragment library to screen potential JNK3 inhibitors, about 15,000 compounds with molecular weights less than 300 Da from the vendors Asinex, Maybridge, and ChemiDive were collected virtually. We performed structure-based virtual screening using the 3D structure of JNK3 (PDB ID, 3DA6) retrieved from Protein Data Bank (PDB) (<http://www.rcsb.org>). AutoDock Vina [37] was utilized for the molecular docking. The docking site of fragments was set at the ATP-binding site of JNK3. From the simulation, 494 compounds presenting docking scores less than  $-7$  kcal/mol were chosen. The structure data file of 494 compounds is available in the Supplementary File S2.

#### 3.2. Fragment Screening

First, the individual <sup>1</sup>H NMR spectra of 494 compounds were measured and used as 'reference spectra' of the fragment library. Since we performed the NMR experiments in an aqueous buffer, the NMR spectra of almost 100 compounds were not able to be measured because of the poor solubility of those chemicals. To reduce the time of NMR measurements, we added eight compounds in a single NMR tube and recorded <sup>1</sup>H NMR spectrum. Since the number of compounds in the library was 494, the number of 8 chemical mixtures in total were 62, where 61 contained 8 compounds, and the last tube contained 6 compounds.

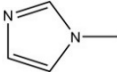
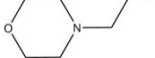
If there is no reaction or interaction between compounds in a single NMR tube, the NMR spectrum of the mixture is a simple sum of the spectra of each compound. In Figure 1, it is clear that the spectra of 8 compound mixtures is exactly the same of the overlay of individual spectrum of 8 compounds. When JNK3 was added to the 8 compound mixtures, the NMR spectrum was crowded in the region 2–4 ppm since the added protein solution contained some additives such as buffer ingredients, Hepes, and DTT; however most of the compound signals were clearly shown. In the STD NMR spectrum, we found several NMR signals which were the signals of possible JNK3-binding molecules. In this way, we found that compound #3 would have the possibility to bind to JNK3 (bottom of Figure 1).



**Figure 1.** Reference NMR spectra of fragments and STD NMR spectrum. The spectra from #1 to #8 were the individual spectrum of fragment in a single NMR tube, respectively. STD NMR spectrum showed that compound #3 might bind to JNK3 (indicated by red arrow).

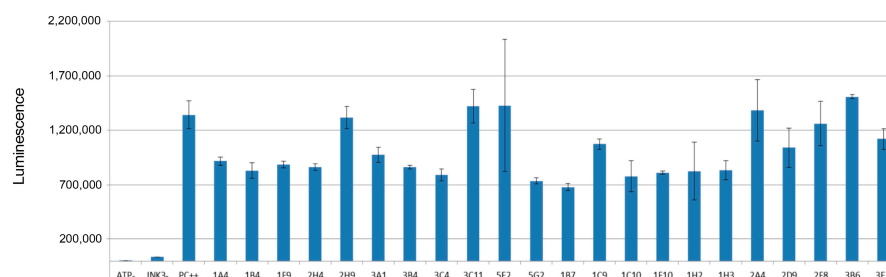
Through STD NMR experiments, we chose 27 compounds which might bind to JNK3; thus, the hit rate was about 6.9% when we excluded the insoluble compounds. Some of the selected compounds shared a common chemical structure which is similar to purine (Table 2). Among them, aliphatic chains at R<sub>1</sub> position and sulfur at R<sub>2</sub> are in common.

**Table 2.** Compounds sharing a common structure.

Code	R <sub>1</sub>	R <sub>2</sub>	R <sub>3</sub>
1A4	-CH <sub>3</sub>	-SCH <sub>2</sub> COOH	-H
2H4	-CH <sub>2</sub> -CH=CH <sub>2</sub>	-SCH <sub>2</sub> COOH	-H
1F9	-CH <sub>3</sub>		-CH <sub>3</sub>
2D5	-CH <sub>2</sub> -CH(CH <sub>3</sub> ) <sub>2</sub>	-NH-NH <sub>2</sub>	-H
2D8	-CH <sub>2</sub> -CH=CH-CH <sub>3</sub>	-SH	-H
3A1	-CH <sub>3</sub>	-SH	-H
3A8	-CH <sub>2</sub> -CH <sub>2</sub> - CH <sub>2</sub> -CH <sub>2</sub> -CH <sub>2</sub> -CH <sub>3</sub>	-SH	-H
3B11	-CH <sub>2</sub> -CO-CH <sub>3</sub>	-H	-CH <sub>3</sub>
3B7		-H	-H
1C9	-CH(CH <sub>3</sub> ) <sub>2</sub>	-S-CH <sub>2</sub> -CO-NH <sub>2</sub>	-H
2A4	-CH <sub>2</sub> -CH <sub>2</sub> -CH <sub>3</sub>	-S-CH <sub>2</sub> -CO-NH <sub>2</sub>	-H

### 3.3. In Vitro Kinase Assay

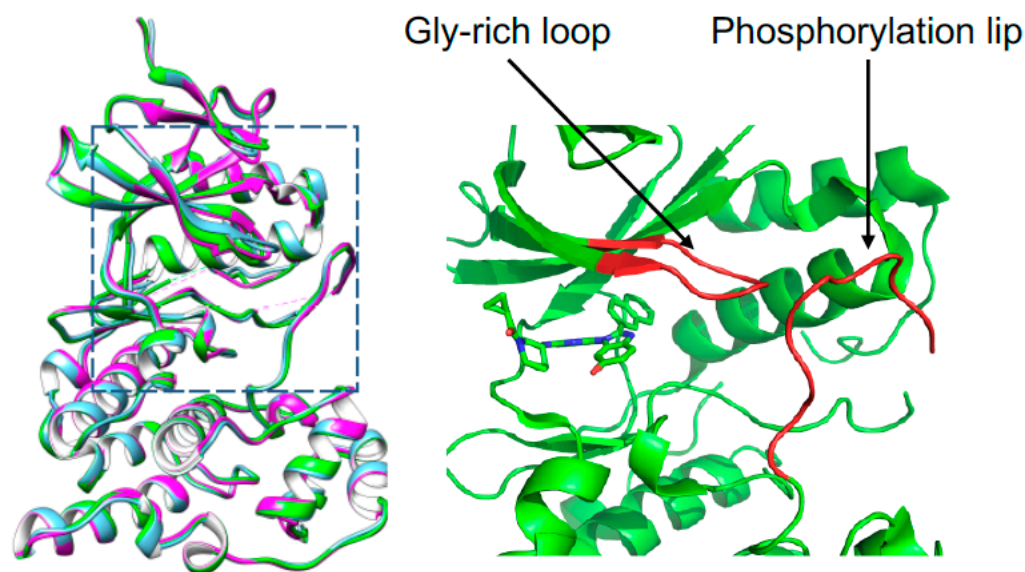
The in vitro kinase assay was performed in the presence of the selected compounds to check whether those compounds were able to inhibit the catalytic activity of JNK3. For the fragments 2D5, 2D8, 3A8, 3B7, and 3B11, it was not possible to measure the inhibitory effects, possibly because of the solubility issue of those compounds in the reaction condition. The positive control without the treatment of any fragments showed significant luminescence since in ADP-Glo™ assay ADP converted from ATP by active JNK3 was monitored by luminescence. Thus, if any fragmented molecules inhibited the enzymatic activity of JNK3, the production of ADP would be reduced, resulting in the decrease of luminescence signal. In Figure 2, the summary of the inhibitory effects of selected 22 fragments was provided. Some of those did not show any inhibitory effect against JNK3; however, several fragments including 1B7 showed about 40–50% inhibition of JNK3 activity at the fragment concentration of 100 μM.



**Figure 2.** In vitro kinase assay and the inhibitory effects of selected fragments. PC++ stands for the positive control without any fragment molecules. The experiments were duplicated, and the errors were indicated.

### 3.4. Overall Structure of JNK3 in Complex with Fragment and Inhibitor

We tried the crystallization of JNK3 with all the selected fragments by using the micro-seeding or fragment-soaking methods, but a limited number of crystals was acquired. Of those, only the structure with a fragment 3A8 (7-hexyl-3-methyl-8-sulfanylidene-9H-purine-2,6-dione) was determined, since other complex crystals gave rise to poor diffraction. Another crystal structure of human JNK3 in a complex with a potent inhibitor, cyclopropyl[(3R)-3-({4-[6-hydroxy-2-(naphthalen-2-yl)-1H-benzimidazol-1-yl]pyrimidin-2-yl}amino)piperidin-1-yl]methanone was also determined by molecular replacement. The Ramachandran plot of 3A8 bound JNK3 shows that 93.9% of non-glycine and non-proline residues are in the most favored regions; 5.5% of residues are in the additional allowed regions; and two residues, Arg212 and Asp381, in the disallowed regions. For the inhibitor-bound JNK3, those values were 97.4, 2.6, and 0%, respectively. The data and refinement statistics are summarized in Table 2. The structures of JNK3 were almost identical to the previously reported structures of JNK3. The root mean square (r. m. s.) deviation between the 3A8 bound JNK3 and AMP-PNP-bound JNK3 (PDB ID, 1JNK) was 0.392 Å for 343 C $\alpha$  atom pairs and the r. m. s. deviation between the inhibitor-bound forms and AMP-PNP-bound JNK3 was 0.495 Å for 340 C $\alpha$  atom pairs. The r. m. s. deviation of the two structures determined in this work was 0.533 Å for 345 C $\alpha$  atom pairs (Figure 3). Very subtle differences were found in the glycine-rich region (Gly71-Ser-Gly-Ala-Gln-Gly-Ile-Val78) and the phosphorylation lip (Ser217-Thr226). In the inhibitor-bound structure, the glycine-rich loop and the phosphorylation lip moved little bit toward ATP-binding site.

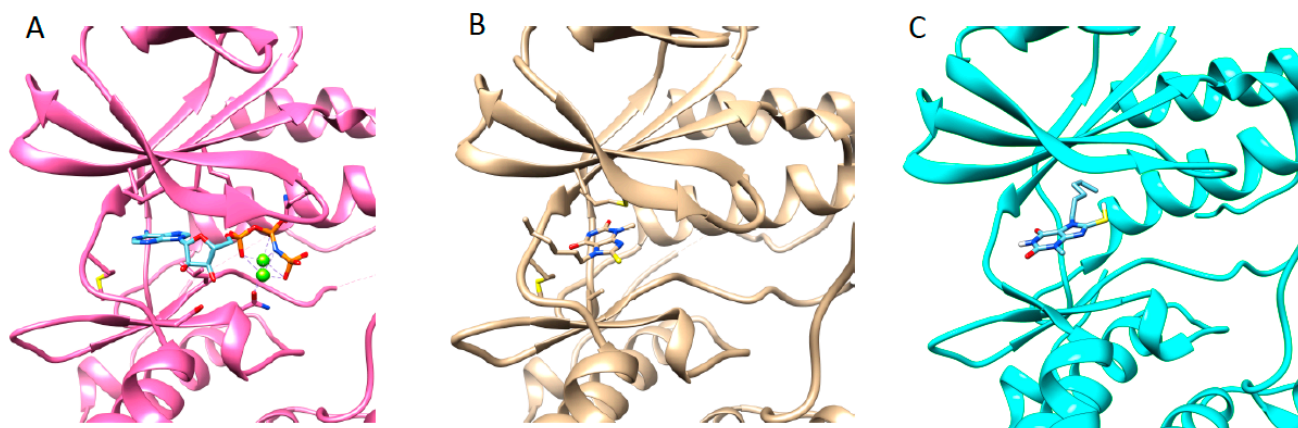


**Figure 3.** Overall structure of apo-(purple), fragment-bound (cyan), and inhibitor-bound (green) JNK3. The structural difference occurred at glycine-rich region and phosphorylation lip, which were enlarged on right and indicated. In the overlaid structures, the bound molecules were removed for the clarity of structural comparison.

### 3.5. Structure of JNK3 in Complex with Fragment 3A8

The ATP-binding site of JNK3 is located between N-terminal lobe (residues 45–149) and C-terminal lobe (residues 150–211 and 217–374) [36]. The fragment 3A8 bound to the ATP binding site of JNK3. Since 3A8 contained a similar structure to purine, the binding mode of 3A8 was thought to be similar to AMP-PNP. The 3A8 was positioned at the adenine binding site of AMP-PMP, but the orientations of the pyrine moiety of 3A8 and the adenine of AMP-PNP were different by almost 90° degrees (Figure 4A,B). 3A8 binding to JNK3 was completely opposite to the docking pose. In virtual screening, the lowest energy docking pose of 3A8 to JNK3 scored  $-7.0$  kcal/mol and the hexyl chain penetrated deeply into the hydrophobic region of the ATP binding site (Figure 4C). The hexyl chain of 3A8 in JNK3

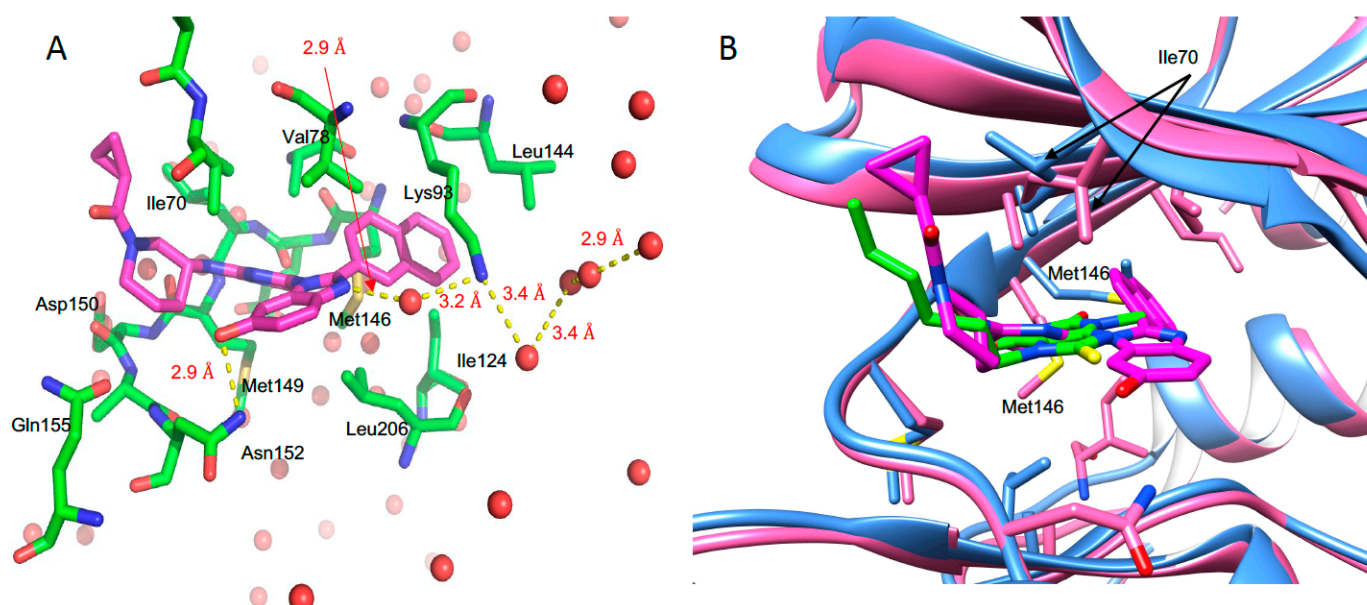
crystal structure protruded from the ATP binding site toward the surface of the protein. The hydrophobic interaction between the hexyl group of 3A8 with residues in  $\beta$ -strands above the ATP binding site might contribute to the binding of fragment to enzyme.



**Figure 4.** Structure of JNK3 in complex with AMP-PNP ((A), PDB ID, 1JNK) and fragment 3A8 (B), and docking simulated structure of JNK3 with 3A8 (C). Small molecules were presented by stick. In AMP-PNP bound structure, two magnesium ions were involved in the complex.

### 3.6. Structure JNK3 in Complex with a Potent Inhibitor

In the previous study, 1-Heteroaryl-2-aryl-1H-benzimidazole derivatives showed the inhibitory effect against JNK3 [35]. Cyclopropyl[(3R)-3-({4-[6-hydroxy-2-(naphthalen-2-yl)-1H-benzimidazol-1-yl]pyrimidin-2-yl}amino)piperidin-1-yl]methanone was one of the derivatives of those inhibitors with a high binding affinity ( $K_d$ , 46 nM) and inhibitory potency ( $IC_{50}$ , 27.7 nM) to JNK3 (Figure S1). In this work, we solved the crystal structure of JNK3 in complex with this inhibitor. The binding of inhibitor to JNK3 is illustrated in Figure 5A.



**Figure 5.** Structure of JNK3 in complexed with cyclopropyl[(3R)-3-({4-[6-hydroxy-2-(naphthalen-2-yl)-1H-benzimidazol-1-yl]pyrimidin-2-yl}amino)piperidin-1-yl]methanone (A). The residues involved in the interaction were indicated. Water molecules were indicated as red dots and hydrogen bonds as yellow broken lines. The lengths of hydrogen bonds are labeled in red. (B) Overlaid structure of JNK3 with 3A8 and inhibitor. Ile70 were indicated by arrow. Different positioning of Met146 in both structures are also indicated. JNK3 were colored blue for 3A8 bound form and pink for inhibitor bound form, respectively.

The inhibitor resided on the ATP binding site of JNK3, and the naphthalene moiety penetrated deeply into the interior of ATP binding pocket, where ATP or AMP-PNP did not interact. The naphthalene ring moiety interacted with Met 146. A naphthalene ring-binding induced the movement of the side chain of Met146 (gatekeeper in JNK3), which had a different orientation in AMP-PNP bound JNK3 structures. The naphthalene ring moiety possessed hydrophobic interaction with Lys93, Met146, Ile124, Val78, Ala91, and Leu144. Met149 formed a hydrogen bond with a 2-aminopyrimidine moiety of the inhibitor, and Ile70 interacted with piperidine and 1-cyclopropyl moieties of inhibitor. The side chain of Ile70 was rotated for stable interaction with 1-cyclopropyl. Leu206, Asn152, Val78, and Ile70 interacted with the 6-Hydroxy-1H-benzimidazole moiety of inhibitor. The side chain of Asn152 formed a direct hydrogen bond with the hydroxyl group of the 6-Hydroxy-1H-benzimidazole moiety that formed water-mediated hydrogen bond with Lys93. Several water molecules were coordinated in the vicinity of Lys93, which interacted with the naphthalene ring moiety.

When we compare the structures of JNK3 with a fragment and inhibitor, it was noticeable that the binding of 3A8 to JNK3 very much resembled the binding to the inhibitor, even though two chemicals did not share structural similarities, and the bicyclic rings of the two molecules were different. In the 3A8-bound structure, the 6-membered ring was outward from ATP binding site; however, in the inhibitor-bound one, 5-membered ring was outward and 6-membered ring inward. The common feature was the orientation and interaction of the hexyl group of 3A8 and the 1-cyclopropyl moiety of the inhibitor. Those two moieties protruded from the ATP binding site and presented hydrophobic interactions with the  $\beta$ -strand region of JNK3, where Ile 90 played a role. The importance of the hydrophobic interaction involving the 1-cyclopropyl moiety of the inhibitor on the binding and inhibitory activity to JNK3 are discussed below.

#### 4. Discussion

We have conducted the *in silico*, *in vitro*, and structural investigations for the discovery of JNK3 inhibitors by adapting the fragment-based approach. 494-membered fragment library was constructed, and the library of NMR spectra was also built, even though about 20% of compounds did not give rise to the spectrum, because of the solubility problem. The hit rate from the screening from the STD NMR experiments was 6.9%, which is a relatively high value in a drug discovery campaign. In a drug repurposing project, we have shown that the longitudinal ( $T_1$ ) and transverse ( $T_2$ ) relaxation experiments and the STD NMR spectroscopy detected the JNK3 binding of azelastine, which has an original indication for anti-allergy and anti-inflammation effects and proven that azelastine binds to ATP binding pocket of JNK3 via competition STD experiment with AMP-PNP [47]. In this regard, we have shown that NMR spectroscopy is very efficient in drug discovery process, especially in initial fragment screening.

The kinase assay presented that most of the selected compounds had the inhibitory activity against JNK3, even though the effects were not potent. Since fragments are small and have simple structures, it is very hard to find potent molecules from a fragment-based approach. In this work, we just checked the inhibitory effects of the screened fragments to see whether those could inhibit the activity of JNK3 or not. The versatility of the fragment-based approach in drug discovery would be whether the screened fragment compounds could be used for designing and creating potent inhibitors. In this context, the structural information between fragments and the target proteins are very valuable. We have determined a structure of JNK3 in complex with one of the screened fragments as well as with a potent inhibitor. The fragment 3A8 had limited water solubility, thus, it was impossible to run the kinase assay. However, in the crystallization, certain additives such as 0.02% n-octyl-glucopyranoside might enhance the solubility of 3A8 in an aqueous solution. The 3A8 shared structural similarities to the adenine of ATP; however, the binding pattern was completely different from the adenine moiety of ATP. The hydrophobic hexyl group of 3A8 protruded from the ATP binding site and gave

rise to additional interactions with the glycine-rich region of JNK3. We focused on the hydrophobic interaction to discover an isoform-specific JNK3 inhibitors. Every kinase shares a common ATP binding mode, which hampers the discovery of the specific kinase inhibitor, especially ATP-competitive inhibitors. For the discovery of potent and selective ATP-competitive JNK inhibitors, targeting hydrophobic interactions in combination with the interaction on ATP-binding sites was suggested [38]. Those interactions were ones with solvent-exposed hydrophobic regions, including a glycine-rich loop and another with deep hydrophobic region where the naphthalene moiety of inhibitor in this work penetrated. In the previous work, among 1-Heteroaryl-2-aryl-1H-benzimidazole derivatives, the inhibitor cyclopropyl[(3R)-3-((4-[6-hydroxy-2-(naphthalen-2-yl)-1H-benzimidazol-1-yl]pyrimidin-2-yl)amino)piperidin-1-yl]methanone showed the strongest binding affinity to JNK3. The binding affinity of this inhibitor was 60-fold stronger than the derivatives without 1-cyclopropyl moiety [35]. We performed the measurement of the inhibitory activity of the 1-Heteroaryl-2-aryl-1H-benzimidazole derivatives (Figure S1). The compound with the 1-cyclopropyl moiety (inhibitor in this work) showed the  $IC_{50}$  of 27 nM, whereas the compound without the moiety showed the  $IC_{50}$  of 1.41 mM, which coincides very well with previous binding experiments. When the naphthalene moiety was replaced by the dichlorophenyl moiety, the  $IC_{50}$  increased 178-fold. We confirmed experimentally that the importance of targeting hydrophobic interactions in discovering JNK inhibitors. We suppose that those interactions would be related to the selectivity of JNK inhibitors. In Figure S2, the inhibitory activity of cyclopropyl[(3R)-3-((4-[6-hydroxy-2-(naphthalen-2-yl)-1H-benzimidazol-1-yl]pyrimidin-2-yl)amino)piperidin-1-yl]methanone against several MAPKs is shown. The inhibitor in this work had potency against JNK3, JNK1, p38 $\alpha$ , and p38 $\beta$ , and showed none or little inhibitory effects on p38 $\gamma$ , and p38 $\delta$ , ERK, and GSK. We suppose that the hydrophobic interaction mentioned above would provide the selectivity. Thus, we suggest that keeping this hydrophobic interaction is very important for the discovery of novel and potent JNK3 inhibitors.

## 5. Conclusions

We presented the fragment-based approach in discovering JNK3 kinase with the structural investigation. We showed that virtual screening and in vitro assay supported by the NMR-based fragment screening were very efficient in early drug-discovery projects. In the structural investigation, we have identified the hydrophobic interaction between a fragment and the enzyme and presented the importance of this interaction in the potency and selectivity of the JNK3 inhibitors. We believe that this work provides valuable insight in designing lead compounds based on the fragment in the discovery of kinase inhibitors.

**Supplementary Materials:** The following supporting information can be downloaded at: <https://www.mdpi.com/article/10.3390/pharmaceutics14091900/s1>, Figure S1: Structures and inhibitory activities of 1-Heteroaryl-2-aryl-1H-benzimidazole derivatives; Figure S2: Inhibitory activity of cyclopropyl[(3R)-3-((4-[6-hydroxy-2-(naphthalen-2-yl)-1H-benzimidazol-1-yl]pyrimidin-2-yl)amino)piperidin-1-yl]methanone against various kinases; File S1: list\_fragments.xlsx; File S2: SDF\_fragments.sdf.

**Author Contributions:** Conceptualization, H.-C.A.; methodology, M.T.H.D.; software, M.T.H.D.; validation, H.-C.A.; formal analysis, M.T.H.D.; resources, H.-C.A.; writing—original draft preparation, M.T.H.D.; writing—review and editing, H.-C.A.; visualization, M.T.H.D.; supervision, H.-C.A.; project administration, H.-C.A.; funding acquisition, H.-C.A. All authors have read and agreed to the published version of the manuscript.

**Funding:** This work was supported by the National Research Foundation of Korea (NRF), grants funded by the Korean Government (MSIT) (NRF-2018R1D1A1B07050975 and 2021R1F1A1063558 to H.-C.A.), Korea.

**Institutional Review Board Statement:** Not applicable.

**Informed Consent Statement:** Not applicable.

**Data Availability Statement:** Not applicable.



**Acknowledgments:** We thank the staff at the Pohang Light Source (beamlines 5C and 7A) for their assistance with synchrotron data collection.

**Conflicts of Interest:** The authors declare no conflict of interest.

## References

1. Johnson, G.L.; Lapadat, R. Mitogen-activated protein kinase pathways mediated by ERK, JNK, and p38 protein kinases. *Science* **2002**, *298*, 1911–1912. [CrossRef]
2. Ip, Y.T.; Davis, R.J. Signal transduction by the c-Jun N-terminal kinase (JNK)—From inflammation to development. *Curr. Opin. Cell Biol.* **1998**, *10*, 205–219. [CrossRef]
3. Mohit, A.A.; Martin, J.H.; Miller, C.A. p493F12 kinase: A novel MAP kinase expressed in a subset of neurons in the human nervous system. *Neuron* **1995**, *14*, 67–78. [CrossRef]
4. Chang, L.; Karin, M. Mammalian MAP kinase signalling cascades. *Nature* **2001**, *410*, 37–40. [CrossRef] [PubMed]
5. Zeke, A.; Misheva, M.; Remenyi, A.; Bogoyevitch, M.A. JNK Signaling: Regulation and Functions Based on Complex Protein-Protein Partnerships. *Microbiol. Mol. Biol. Rev.* **2016**, *80*, 793–835. [CrossRef] [PubMed]
6. Tournier, C.; Dong, C.; Turner, T.K.; Jones, S.N.; Flavell, R.A.; Davis, R.J. MKK7 is an essential component of the JNK signal transduction pathway activated by proinflammatory cytokines. *Genes Dev.* **2001**, *15*, 1419–1426. [CrossRef]
7. Graczyk, P.P. JNK inhibitors as anti-inflammatory and neuroprotective agents. *Future Med. Chem.* **2013**, *5*, 539–551. [CrossRef]
8. Assi, K.; Pillai, R.; Gomez-Munoz, A.; Owen, D.; Salh, B. The specific JNK inhibitor SP600125 targets tumour necrosis factor- $\alpha$  production and epithelial cell apoptosis in acute murine colitis. *Immunology* **2006**, *118*, 112–121. [CrossRef]
9. Hefetz-Sela, S.; Stein, I.; Klieger, Y.; Porat, R.; Sade-Feldman, M.; Zreik, F.; Nagler, A.; Pappo, O.; Quagliata, L.; Dazert, E.; et al. Acquisition of an immunosuppressive protumorigenic macrophage phenotype depending on c-Jun phosphorylation. *Proc. Natl. Acad. Sci. USA* **2014**, *111*, 17582–17587. [CrossRef]
10. Das, M.; Garlick, D.S.; Greiner, D.L.; Davis, R.J. The role of JNK in the development of hepatocellular carcinoma. *Genes Dev.* **2011**, *25*, 634–645. [CrossRef]
11. Shibata, W.; Maeda, S.; Hikiba, Y.; Yanai, A.; Sakamoto, K.; Nakagawa, H.; Ogura, K.; Karin, M.; Omata, M. c-Jun NH2-terminal kinase 1 is a critical regulator for the development of gastric cancer in mice. *Cancer Res.* **2008**, *68*, 5031–5039. [CrossRef] [PubMed]
12. Han, M.S.; Barrett, T.; Brehm, M.A.; Davis, R.J. Inflammation Mediated by JNK in Myeloid Cells Promotes the Development of Hepatitis and Hepatocellular Carcinoma. *Cell Rep.* **2016**, *15*, 19–26. [CrossRef] [PubMed]
13. Zhu, X.; Raina, A.K.; Rottkamp, C.A.; Aliev, G.; Perry, G.; Boux, H.; Smith, M.A. Activation and redistribution of c-jun N-terminal kinase/stress activated protein kinase in degenerating neurons in Alzheimer’s disease. *J. Neurochem.* **2001**, *76*, 435–441. [CrossRef] [PubMed]
14. Gourmaud, S.; Paquet, C.; Dumurgier, J.; Pace, C.; Bouras, C.; Gray, F.; Laplanche, J.-L.; Meurs, E.F.; Mouton-Liger, F.; Hugon, J. Increased levels of cerebrospinal fluid JNK3 associated with amyloid pathology: Links to cognitive decline. *J. Psychiatry Neurosci.* **2015**, *40*, 151–161. [CrossRef] [PubMed]
15. Pan, J.; Li, H.; Zhang, B.; Xiong, R.; Zhang, Y.; Kang, W.-Y.; Chen, W.; Zhao, Z.-B.; Chen, S.D. Small peptide inhibitor of JNK3 protects dopaminergic neurons from MPTP induced injury via inhibiting the ASK1-JNK3 signaling pathway. *PLoS ONE* **2015**, *10*, e0119204. [CrossRef]
16. Badshah, H.; Ali, T.; Rehman, S.-U.; Amin, F.-U.; Ullah, F.; Kim, T.H.; Kim, M.O. Protective Effect of Lupeol Against Lipopolysaccharide-Induced Neuroinflammation via the p38/c-Jun N-Terminal Kinase Pathway in the Adult Mouse Brain. *J. Neuroimmune Pharmacol.* **2016**, *11*, 48–60. [CrossRef]
17. Zhang, S.; Gui, X.-H.; Huang, L.-P.; Deng, M.-Z.; Fang, R.-M.; Ke, X.-H.; He, Y.-P.; Li, L.; Fang, Y.-Q. Neuroprotective Effects of beta-Asarone Against 6-Hydroxy Dopamine-Induced Parkinsonism via JNK/Bcl-2/Beclin-1 Pathway. *Mol. Neurobiol.* **2016**, *53*, 83–94. [CrossRef]
18. Wang, W.; Ma, C.; Mao, Z.; Li, M. JNK inhibition as a potential strategy in treating Parkinson’s disease. *Drug News Perspect.* **2004**, *17*, 646–654. [CrossRef]
19. Duong, M.T.H.; Lee, J.-H.; Ahn, H.-C. C-Jun N-terminal kinase inhibitors: Structural insight into kinase-inhibitor complexes. *Comput. Struct. Biotechnol. J.* **2020**, *18*, 1440–1457. [CrossRef]
20. Attwood, M.M.; Fabbro, D.; Sokolov, A.V.; Knapp, S.; Schioth, H.B. Trends in kinase drug discovery: Targets, indications and inhibitor design. *Nat. Rev. Drug Discov.* **2021**, *20*, 839–861. [CrossRef]
21. Roskoski, R., Jr. Properties of FDA-approved small molecule protein kinase inhibitors: A 2021 update. *Pharmacol. Res.* **2021**, *165*, 105463. [CrossRef] [PubMed]
22. Hajduk, P.J.; Greer, J. A decade of fragment-based drug design: Strategic advances and lessons learned. *Nat. Rev. Drug Discov.* **2007**, *6*, 211–219. [CrossRef] [PubMed]
23. Erlanson, D.A.; Fesik, S.W.; Hubbard, R.E.; Jahnke, W.; Jhoti, H. Twenty years on: The impact of fragments on drug discovery. *Nat. Rev. Drug Discov.* **2016**, *15*, 605–619. [CrossRef] [PubMed]
24. Wang, P.-F.; Qiu, H.-Y.; Wang, Z.-F.; Zhang, Y.-J.; Wang, Z.-C.; Li, D.-D.; Zhu, H.-L. Identification of novel B-Raf(V600E) inhibitors employing FBDD strategy. *Biochem. Pharmacol.* **2017**, *132*, 63–76. [CrossRef] [PubMed]

25. Lamoree, B.; Hubbard, R.E. Current perspectives in fragment-based lead discovery (FBLD). *Essays Biochem.* **2017**, *61*, 453–464. [CrossRef]
26. Irie, T.; Sawa, M. 7-Azaindole: A Versatile Scaffold for Developing Kinase Inhibitors. *Chem. Pharm. Bull.* **2018**, *66*, 29–36. [CrossRef] [PubMed]
27. Mortenson, P.N.; Berdini, V.; O'Reilly, M. Fragment-based approaches to the discovery of kinase inhibitors. *Methods Enzymol.* **2014**, *548*, 69–92. [CrossRef]
28. Zhang, J.; Yang, P.L.; Gray, N.S. Targeting cancer with small molecule kinase inhibitors. *Nat. Rev. Cancer* **2009**, *9*, 28–39. [CrossRef]
29. Meyer, B.; Peters, T. NMR spectroscopy techniques for screening and identifying ligand binding to protein receptors. *Angew. Chem. Int. Ed. Engl.* **2003**, *42*, 864–890. [CrossRef]
30. Mayer, M.; Meyer, B. Group epitope mapping by saturation transfer difference NMR to identify segments of a ligand in direct contact with a protein receptor. *J. Am. Chem. Soc.* **2001**, *123*, 6108–6117. [CrossRef]
31. Streiff, J.H.; Juranic, N.O.; Macura, S.I.; Warner, D.O.; Jones, K.A.; Perkins, W.J. Saturation transfer difference nuclear magnetic resonance spectroscopy as a method for screening proteins for anesthetic binding. *Mol. Pharmacol.* **2004**, *66*, 929–935. [CrossRef] [PubMed]
32. Peng, C.; Frommlet, A.; Perez, M.; Cobas, C.; Blechschmidt, A.; Dominguez, S.; Lingel, A. Fast and Efficient Fragment-Based Lead Generation by Fully Automated Processing and Analysis of Ligand-Observed NMR Binding Data. *J. Med. Chem.* **2016**, *59*, 3303–3310. [CrossRef]
33. Johnson, J.A.; Olson, N.M.; Tooker, M.J.; Bur, S.K.; Pomerantz, W.C.K. Combined Protein- and Ligand-Observed NMR Workflow to Screen Fragment Cocktails against Multiple Proteins: A Case Study Using Bromodomains. *Molecules* **2020**, *25*, 3949. [CrossRef] [PubMed]
34. Dalvit, C.; Fogliatto, G.; Stewart, A.; Veronesi, M.; Stockman, B. WaterLOGSY as a method for primary NMR screening: Practical aspects and range of applicability. *J. Biomol. NMR* **2001**, *21*, 349–359. [CrossRef]
35. Kim, M.-H.; Lee, J.; Jung, K.; Kim, M.; Park, Y.-J.; Ahn, H.; Kwon, Y.H.; Hah, J.-M. Syntheses and biological evaluation of 1-heteroaryl-2-aryl-1H-benzimidazole derivatives as c-Jun N-terminal kinase inhibitors with neuroprotective effects. *Bioorganic Med. Chem.* **2013**, *21*, 2271–2285. [CrossRef] [PubMed]
36. Xie, X.; Gu, Y.; Fox, T.; Coll, J.T.; Fleming, M.A.; Markland, W.; Caron, P.R.; Wilson, K.P.; Su, M.S. Crystal structure of JNK3: A kinase implicated in neuronal apoptosis. *Structure* **1998**, *6*, 983–991. [CrossRef]
37. Trott, O.; Olson, A.J. AutoDock Vina: Improving the speed and accuracy of docking with a new scoring function, efficient optimization, and multithreading. *J. Comput. Chem.* **2010**, *31*, 455–461. [CrossRef]
38. Scapin, G.; Patel, S.B.; Lisnock, J.; Becker, J.W.; LoGrasso, P.V. The structure of JNK3 in complex with small molecule inhibitors: Structural basis for potency and selectivity. *Chem. Biol.* **2003**, *10*, 705–712. [CrossRef]
39. Otwinowski, Z.; Minor, W. Processing of X-ray diffraction data collected in oscillation mode. *Methods Enzymol.* **1997**, *276*, 307–326.
40. McCoy, A.J.; Grosse-Kunstleve, R.W.; Adams, P.D.; Winn, M.D.; Storoni, L.C.; Read, R.J. Phaser crystallographic software. *J. Appl. Crystallogr.* **2007**, *40*, 658–674. [CrossRef]
41. Probst, G.D.; Bowers, S.; Sealy, J.M.; Truong, A.P.; Hom, R.K.; Galemno, R.A., Jr.; Konradi, A.W.; Sham, H.L.; Quincy, D.A.; Pan, H.; et al. Highly selective c-Jun N-terminal kinase (JNK) 2 and 3 inhibitors with in vitro CNS-like pharmacokinetic properties prevent neurodegeneration. *Bioorg. Med. Chem. Lett.* **2011**, *21*, 315–319. [CrossRef] [PubMed]
42. Emsley, P.; Cowtan, K. Coot: Model-building tools for molecular graphics. *Acta Cryst. D* **2004**, *60*, 2126–2132. [CrossRef] [PubMed]
43. Murshudov, G.N.; Skubak, P.; Lebedev, A.A.; Pannu, N.S.; Steiner, R.A.; Nicholls, R.A.; Winn, M.D.; Long, F.; Vagin, A.A. REFMAC5 for the refinement of macromolecular crystal structures. *Acta Cryst. D* **2011**, *67*, 355–367. [CrossRef] [PubMed]
44. Davis, I.W.; Leaver-Fay, A.; Chen, V.B.; Block, J.N.; Kapral, G.J.; Wang, X.; Murray, L.W.; Arendall, W.B., 3rd; Snoeyink, J.; Richardson, J.S.; et al. MolProbity: All-atom contacts and structure validation for proteins and nucleic acids. *Nucleic Acids Res.* **2007**, *35*, W375–W383. [CrossRef] [PubMed]
45. Schrödinger, L.; DeLano, W. PyMOL. Available online: <http://www.pymol.org/pymol> (accessed on 28 July 2022).
46. Pettersen, E.F.; Goddard, T.D.; Huang, C.C.; Couch, G.S.; Greenblatt, D.M.; Meng, E.C.; Ferrin, T.E. UCSF Chimera—A visualization system for exploratory research and analysis. *J. Comput. Chem.* **2004**, *25*, 1605–1612. [CrossRef]
47. Nguyen, P.L.; Bui, B.P.; Duong, M.T.H.; Lee, K.; Ahn, H.-C.; Cho, J. Suppression of LPS-Induced Inflammation and Cell Migration by Azelastine through Inhibition of JNK/NF-kappaB Pathway in BV2 Microglial Cells. *Int. J. Mol. Sci.* **2021**, *22*, 9061. [CrossRef]

## Article

# Kinase Inhibitor Screening Displayed *ALK* as a Possible Therapeutic Biomarker for Gastric Cancer

Felipe Pantoja Mesquita <sup>1</sup>, Pedro Filho Noronha Souza <sup>1,2</sup>, Emerson Lucena da Silva <sup>1</sup>, Luina Benevides Lima <sup>1</sup>, Lais Lacerda Brasil de Oliveira <sup>1</sup>, Caroline Aquino Moreira-Nunes <sup>1,3,\*</sup>, William J. Zuercher <sup>4</sup>, Rommel Mario Rodríguez Burbano <sup>3,5,6</sup>, Maria Elisabete Amaral de Moraes <sup>1</sup> and Raquel Carvalho Montenegro <sup>1,\*</sup>

<sup>1</sup> Department of Medicine, Pharmacogenetics Laboratory, Drug Research and Development Center (NPDM), Federal University of Ceará, Fortaleza 60430-275, CE, Brazil

<sup>2</sup> Department of Biochemistry and Molecular Biology, Federal University of Ceará, Fortaleza 60430-275, CE, Brazil

<sup>3</sup> Department of Biological Sciences, Oncology Research Center, Federal University of Pará, Belém 66073-005, PA, Brazil

<sup>4</sup> Division of Chemical Biology and Medicinal Chemistry, University of North Carolina at Chapel Hill, Chapel Hill, NC 27599, USA

<sup>5</sup> Laboratory of Human Cytogenetics, Institute of Biological Sciences, Federal University of Pará, Belém 66073-005, PA, Brazil

<sup>6</sup> Molecular Biology Laboratory, Ophir Loyola Hospital, Belém 66073-005, PA, Brazil

\* Correspondence: carolfam@gmail.com (C.A.M.-N.); rcm.montenegro@gmail.com (R.C.M.)

**Citation:** Mesquita, F.P.; Souza, P.F.N.; da Silva, E.L.; Lima, L.B.; de Oliveira, L.L.B.; Moreira-Nunes, C.A.; Zuercher, W.J.; Burbano, R.M.R.; de Moraes, M.E.A.; Montenegro, R.C. Kinase Inhibitor Screening Displayed *ALK* as a Possible Therapeutic Biomarker for Gastric Cancer. *Pharmaceutics* **2022**, *14*, 1841. <https://doi.org/10.3390/pharmaceutics14091841>

Academic Editor: Murali Mohan Yallapu

Received: 20 July 2022

Accepted: 30 August 2022

Published: 1 September 2022

**Publisher's Note:** MDPI stays neutral with regard to jurisdictional claims in published maps and institutional affiliations.



**Copyright:** © 2022 by the authors. Licensee MDPI, Basel, Switzerland. This article is an open access article distributed under the terms and conditions of the Creative Commons Attribution (CC BY) license (<https://creativecommons.org/licenses/by/4.0/>).

**Abstract:** Despite advances in cancer chemotherapy, gastric cancer (GC) continues to have high recurrence rates and poor prognosis with limited treatment options. Understanding the etiology of GC and developing more effective, less harmful therapeutic approaches are vital and urgent. Therefore, this work describes a novel kinase target in malignant gastric cells as a potential therapeutic strategy. Our results demonstrate that among 147 kinase inhibitors (KI), only three molecules were significantly cytotoxic for the AGP-01 cell line. Hence, these three molecules were further characterized in their cellular mode of action. There was significant cell cycle impairment due to the expression modulation of genes such as *TP53*, *CDKN1A*, *CDC25A*, *MYC*, and *CDK2* with subsequent induction of apoptosis. In fact, the Gene Ontology analysis revealed a significant enrichment of pathways related to cell cycle regulation (GO:1902749 and GO:1903047). Moreover, the three selected KIs significantly reduced cell migration and Vimentin mRNA expression after treatment. Surprisingly, the three KIs share the same target, *ALK* and *INSR*, but only the *ALK* gene was found to have a high expression level in the gastric cancer cell line. Additionally, lower survival rates were observed for patients with high *ALK* expression in TCGA-STAD analysis. In summary, we hypothesize that *ALK* gene overexpression can be a promising biomarker for prognosis and therapeutic management of gastric adenocarcinoma.

**Keywords:** gastric cancer; kinase inhibitor; *ALK*; targeted therapy

## 1. Introduction

Gastric cancer (GC) is the second major cause of cancer-related deaths worldwide and the third leading cause in industrialized nations [1,2]. Despite improvements in the management of GC patients with distant metastases, significant recurrence rates and a poor prognosis persist, with limited treatment choices and a median survival around one year [3,4]. Another problem is that GC is a very complex illness with a complicated etiology involving complex host genetic and environmental variables [5,6].

Until now, only a few targeted therapeutic agents, such as trastuzumab and ramucirumab, have been approved by the US Food and Drug Administration for gastric cancer patients identified with the respective genetic defects [7]. However, only 7–34% of GC patients have the altered molecular target for these agents and therefore most GC patients

must continue to depend on cytotoxic chemotherapy and/or surgical resection as the current standard of care [8]. As a result, a greater number of patients evolve with poor prognostic and low survival rate because of therapeutic failure [9,10]. Therefore, understanding the etiology of GC and the development of more effective, less hazardous therapy techniques are critical and urgent.

In this sense, protein kinases are central actors in most of signal transduction pathways. Because their function is frequently disrupted in signal transduction networks leading to illnesses like cancer and inflammation, several of the 518 protein kinases encoded by the human genome have emerged as potential therapeutic targets [11]. Nowadays, there are around 250 kinase inhibitors (KIs) in clinical studies, with 37 of them being authorized for human usage [12]. Thus, it is critical to search new compounds' targets in depth in order to comprehend their molecular and cellular modes of action (MoA).

Thus, several kinase activity and binding screens have been published in the past few years. Among them, Elkins and co-workers reported a comprehensive characterization of 367 tool compounds screened against 224 recombinant kinases [13]. Despite the considerable value of these studies, the cellular or clinical evaluation of KIs has not yet been systematically analyzed. Therefore, the published kinase inhibitors library (PKIS) can be a useful tool for target screening in different cancer models. Taking all together, the present study aimed to evaluate possible novel kinase targets in malignant gastric cells in order to identify a new therapeutic strategy based on kinase inhibition using PKIs library.

## 2. Materials and Method

### 2.1. Cell Culture

Leal and co-workers (2009) developed a cell line from a patient with metastasis of gastric adenocarcinoma (AGP-01) as an alternative model for the anticancer drug screening model. A normal gastric mucosa cell line MNP-01 was used as normal cellular control [14,15]. Cells were cultured in sterilized flasks containing filtered Dulbecco's modified Eagle's medium (DMEM; Gibco<sup>®</sup>, New York, NY, USA) supplemented with 10% fetal bovine serum (Gibco<sup>®</sup>), 100 U/mL penicillin, and 100 µg/mL streptomycin. The culture flasks were maintained in a 5% CO<sub>2</sub> air-humidified atmosphere at 37 °C.

### 2.2. Alamar Blue Method

The growth inhibitory activity of 147 kinase inhibitors (KI) against the AGP-01 cell line was first evaluated at 10 µM concentration (72 h of treatment) using the Alamar Blue method. The growth inhibition (%) was calculated as comparing both KIs based on the cellular viability of treated and KI-untreated AGP-01 cells. Then, relevant KIs that obtained >80% of growth inhibition were selected for IC<sub>50</sub> determination by a concentration-response curve. KI screening was carried out on 384-well plate (Corning<sup>®</sup>, Glendale, AZ, USA). Firstly, 300 cells per well were seeded and incubated overnight at 37 °C and 5% CO<sub>2</sub>. Then, KIs were diluted with DMEM medium and subsequently added in the plate to achieve final desired concentration (10 µM). After 72 h of incubation, Alamar Blue reagent was added to measure cell viability. Fluorescence intensity (560/590 nm) was measured using Beckman Coulter Microplate Reader DTX 880. Cells treated with 0.1% dimethyl sulfoxide (DMSO) were used as negative control and doxorubicin (Doxo, Milan, Italy) was used as positive control.

### 2.3. Cell Cycle Progression

AGP-01 cells were seeded at  $2 \times 10^3$  cells per well in a 96-well plate and treated with a single concentration (1 µM) of each KI selected in the screening. After 72 h of exposure, cells were harvested, washed with PBS 1X, and fixed with ice-cold 80% ethanol for 1 h. Then, cells were incubated with RNase A (200 µg/mL) and propidium iodide (50 µg/mL) for 30 min. DNA content was analyzed using flow cytometry (BD FACSVerser<sup>™</sup>, BD Biosciences, East Rutherford, NJ, USA). In total, 10,000 events were acquired, and data

were analyzed using FlowJo<sup>®</sup> software (Version 10.5.3, FlowJo LLC, Ashland, Wilmington, DE, USA).

#### 2.4. Caspase 3/7 Activity

The caspase-3 and caspase-7 activities were evaluated using the CellEvent<sup>®</sup> Caspase-3/7 kit according to the manufacturer's protocol (Invitrogen<sup>™</sup>, Waltham, MA, USA). AGP-01 cells were plated ( $3 \times 10^3$  cells/well) in a 96-well plate and treated with KIs (1  $\mu$ M) for 72 h. Then, cells were incubated in 5  $\mu$ M of CellEvent<sup>®</sup> reagent for 30 min and evaluated in Cytation<sup>™</sup> with absorption and fluorescence emission spectra of 511/533 nm. Apoptotic cells were labelled with bright fluorescent green nuclei.

#### 2.5. Wound Healing Assay

The migratory potential of AGP-01 cells were evaluated by the wound healing assay as previously described by Mesquita et al. (2021) [16]. Cells were seeded ( $2 \times 10^4$  cells/well) in a 96-well plate and scratches were made in each well with a sterile pipette tip. Then, cells were treated with KIs (1  $\mu$ M) for 24 h. Pictures were taken at time 0 and 24 h from wells, and the scratch area was measured using ImageJ software (National Institutes of Health, Rockville, MD, USA).

#### 2.6. Gene Expression by Quantitative Real-Time PCR

Quantitative real-time PCR (qPCR) analyses were performed with QuantStudio5 Real-Time PCR system (Applied Biosystems<sup>®</sup>, Waltham, MA, USA) in a 96-well PCR plate using 3  $\mu$ L of cDNA obtained after reverse-transcription of total RNA (control and treated sample) using High-Capacity cDNA Reverse Transcription Kit (Applied Biosystems<sup>™</sup>), 1  $\mu$ L of each primer/probe in forward and reverse, 12.5  $\mu$ L of PowerUp SYBR<sup>®</sup> Master Mix (Life Technologies, Carlsbad, CA, USA), and 8.5  $\mu$ L of ultra-pure sterile water. The thermocycling was applied according to the manufacturer's protocol of PowerUp SYBR<sup>®</sup> Master Mix. Each assay was performed at least three times according to Minimum Information for Publication of Quantitative Real-Time PCR Experiments Guidelines [17]. The gene expression levels were based on relative analyses and calculated using the  $2^{-\Delta\Delta CT}$  (delta-delta threshold cycle) method [18].

#### 2.7. PPI Network and GENE Ontology Enrichment

The Protein-Protein interaction (PPI) Network and Gene Ontology (GO) enrichment analyses of the differentially expressed genes were constructed using the string (<https://string-db.org/> (accessed on 9 March 2022) freely available and yfile plug-in in Cytoscape software to analyze the interactions between them. False discovery rate was setup in  $<0.005$ .

#### 2.8. Survival Analysis

The GEPIA database (<http://gepia.cancer-pku.cn/> (accessed on 22 March 2022) was used to perform in silico correlation between gene expression and survival analyses [19]. The Cancer Genome Atlas-Stomach Adenocarcinoma (TCGA-STAD) is one of the cancer transcriptome data sets available through the GEPIA server. The database was used to compare the expression profiles of the *ALK* gene in normal and tumor tissue from gastric adenocarcinoma patients, categorizing them as high or low expression, which was then correlated with patient survival probability.

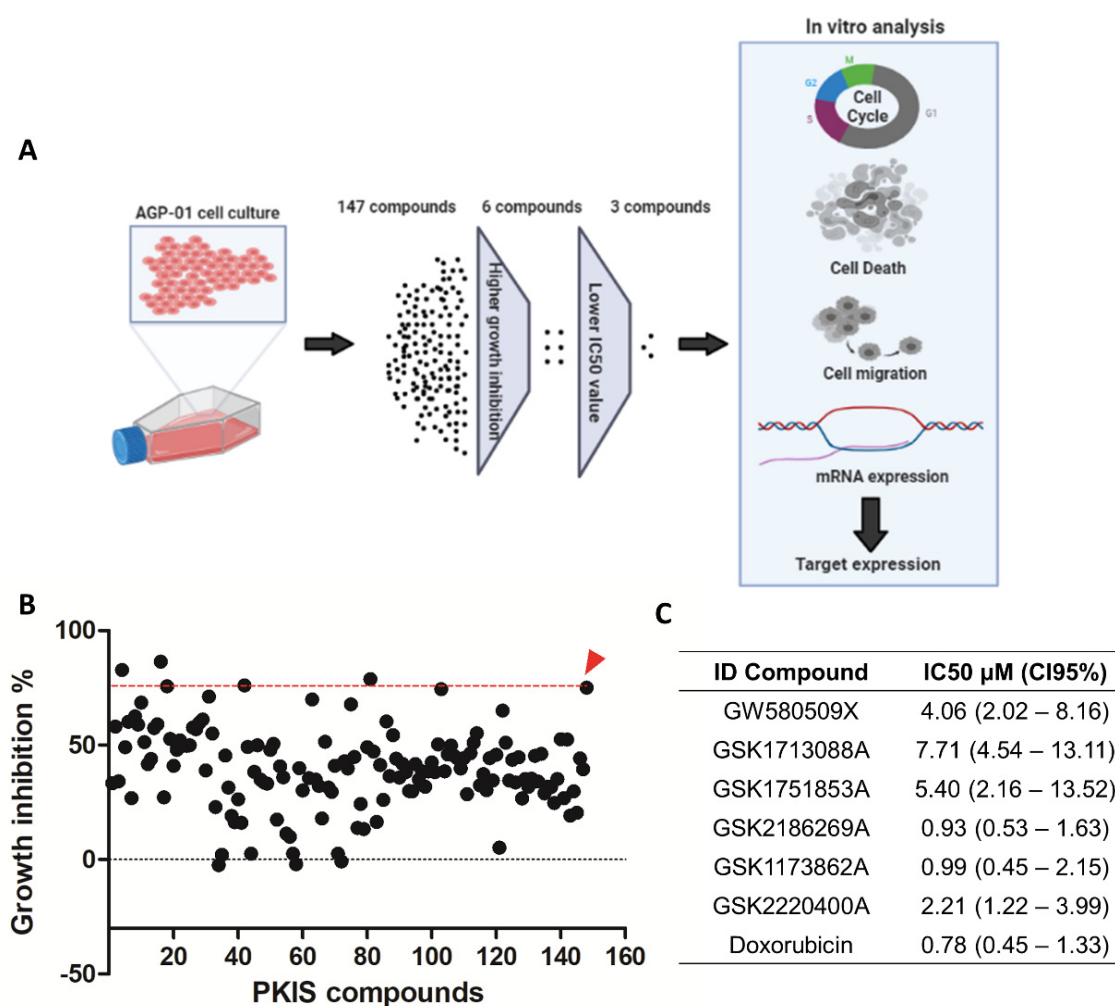
#### 2.9. Statistical Analysis

All tests were performed in three independent experiments in triplicate and shown as a mean  $\pm$  standard deviation (SD). The treated groups (KIs) were compared to the untreated group (DMSO) by Analysis of Variance (ANOVA) followed by Bonferroni's posttest or by the *t*-test, considering significant differences with an interval of confidence of 95% ( $p < 0.05$ ). GraphPad Prism 5.01 (GraphPad Software, San Diego, CA, USA) was used for data analysis and graph design.

### 3. Results

#### 3.1. Screening of KIs Compounds against Metastatic Gastric Cancer Cell Line

AGP-01 cells were treated with a single concentration (10  $\mu$ M) of 147 PKIS compounds to search for the most potent inhibitor based on cell growth inhibition (Figure 1). Among all, only six compounds suppressed the cell growth equally or even higher than the positive control doxorubicin (87% of growth inhibition): GW580509X, GSK1713088A, GSK1751853A, GSK2186269A, GSK1173862A, GSK2220400A (Figure 1B). Then, the non-linear regression was performed to assess the  $IC_{50}$  values of these inhibitors (Figure 1C), which confirmed that only three compounds had highly cytotoxic potential, in the micromolar range, GSK2186269A, GSK1173862A, and GSK2220400A ( $IC_{50} < 2.2 \mu$ M). Therefore, these three compounds were selected to proceed with further analyses.

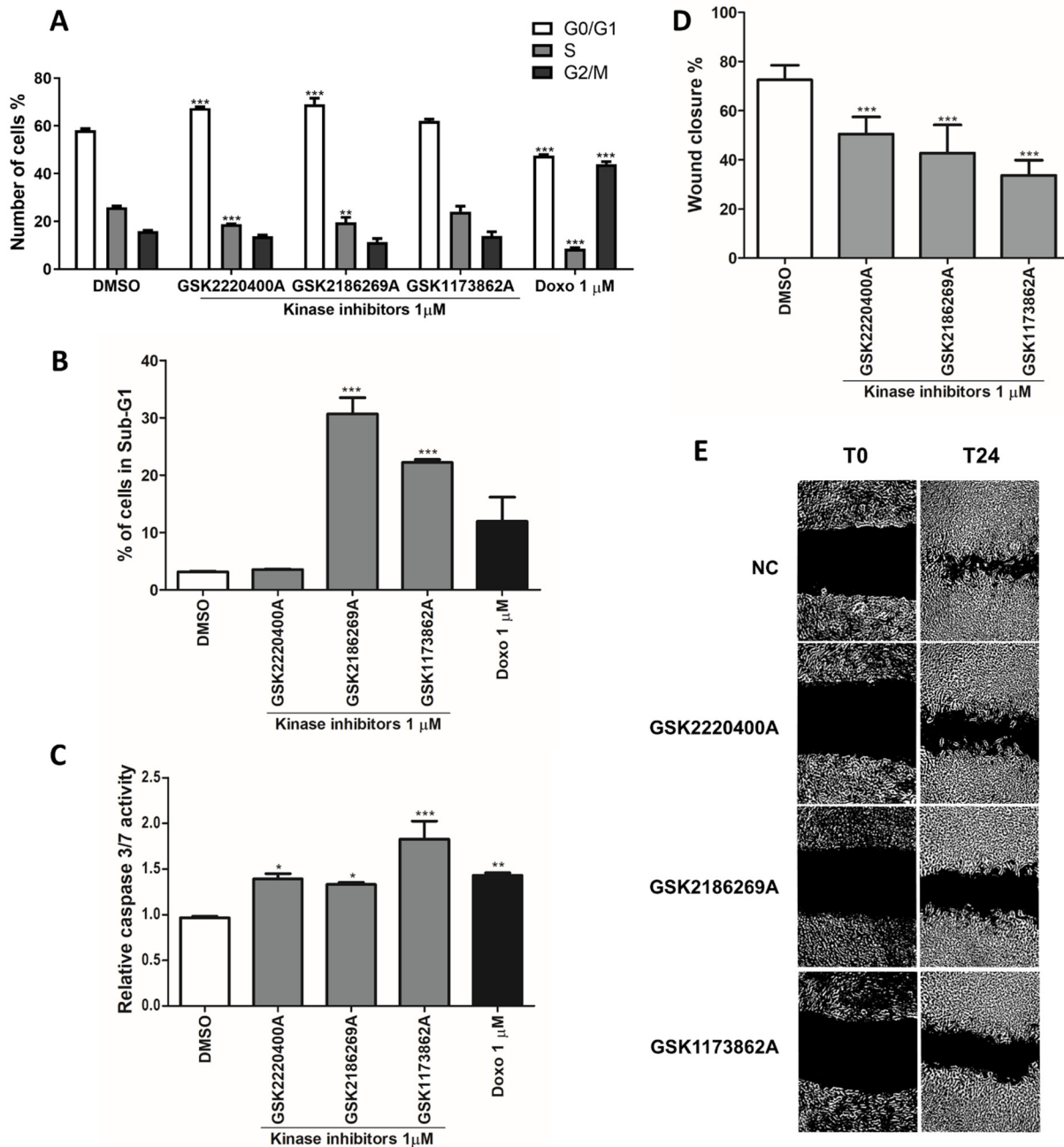


**Figure 1.** Cytotoxicity of 147 published kinase inhibitor set (PKIS) against metastatic gastric cancer cells (AGP-01). (A) Experimental design. After exposure to 147 published kinase inhibitors set (PKIS), only three kinase inhibitors were selected for further analyses based on their highly cytotoxic effect (lowest  $IC_{50}$  values). (B) Growth inhibition normalized by the untreated control (DMSO) of 147 kinase inhibitors after 72 h of treatment. The red head arrow represents the positive control doxorubicin. (C)  $IC_{50}$  values obtained from non-linear regression of curve concentration-response for the kinase with  $IC_{50}$  values higher than doxorubicin.

#### 3.2. Kinase Inhibitors Act as Anti-Cancer Agents by Regulating Cell Cycle and Mesenchymal Genes

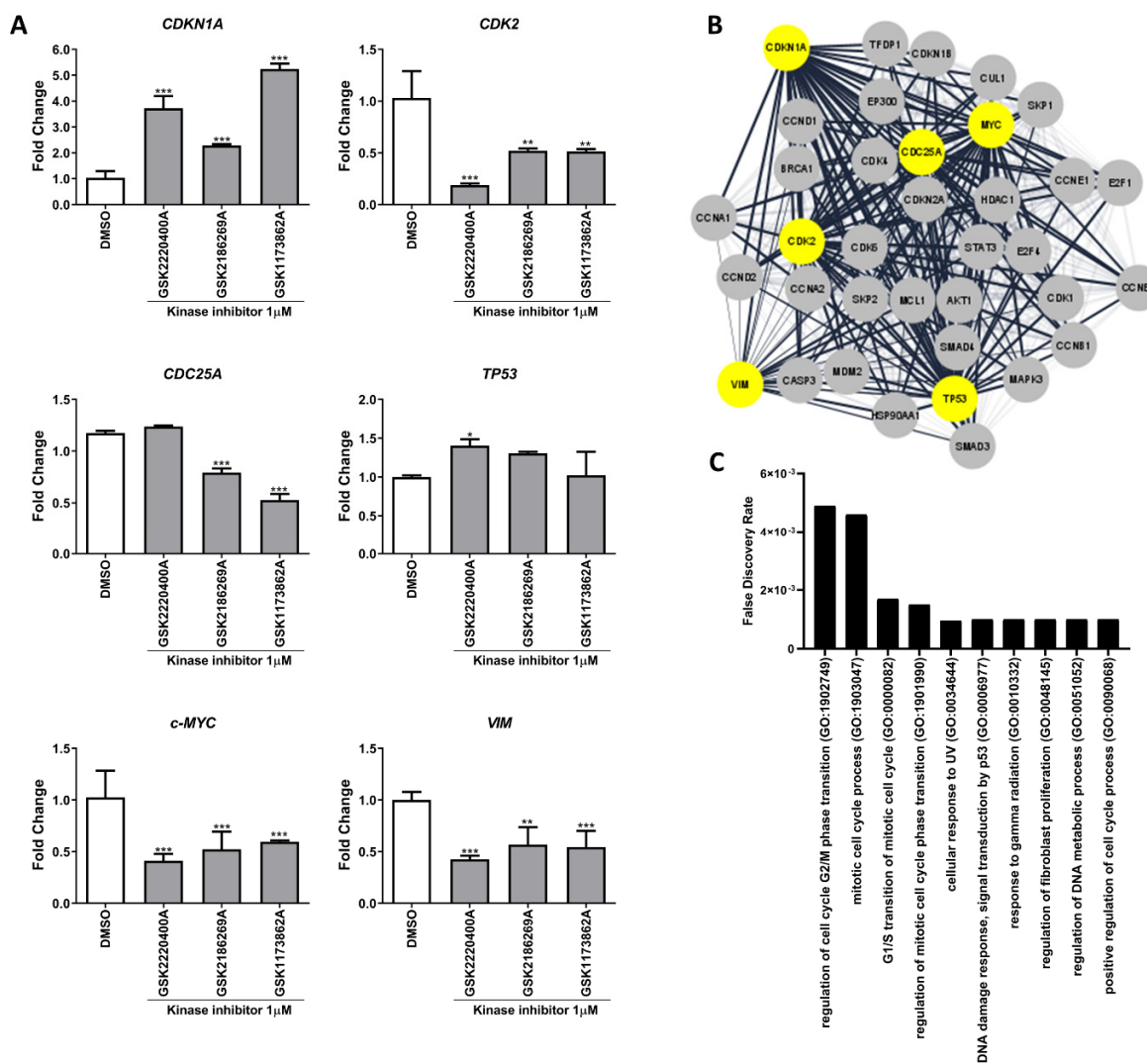
The anti-proliferative effects of GSK2186269A, GSK1173862A and GSK2220400A were then evaluated by the cell cycle interaction on flow cytometry. GSK2220400A (1  $\mu$ M) induced a significant G0/G1-phase arrest compared to the untreated control, while the

GSK2186269A (1  $\mu$ M) and GSK1173862A (1  $\mu$ M) compounds triggered extensive nuclei fragmentation, considered a sub-G1 phase alteration (Figure 2A,B). Furthermore, the three compounds significantly increased caspase 3 and 7 activity, suggesting the induction of apoptosis (Figure 2C). Another cancer hallmark significantly inhibited by the selected KIs was the cell migration. All three inhibitors (1  $\mu$ M) were capable of preventing the wound closure by the AGP-01 cells (Figure 2D,E).



**Figure 2.** Anti-cancer effects of the three selected kinase inhibitors. (A) Cell cycle phase distribution of metastatic gastric cancer cells after 72 h of kinase inhibitors treatment. (B) Percentage of cells in sub-G1 phase after kinase inhibitors treatment. (C) Caspase 3 and 7 activities after 72 h of 1  $\mu$ M kinase inhibitors exposure against metastatic gastric cancer cells. (D,E) Inhibitory effect on cell migration after 24 h of kinase inhibitors treatment. Mean  $\pm$  standard deviation. Significant differences compared to untreated control: \*  $p < 0.05$ , \*\*  $p < 0.01$ , \*\*\*  $p < 0.001$ .

Furthermore, after KI exposure, an alteration in gene expression involved in the cell cycle regulation, cell death, and migration was observed. In AGP-01 cells, the treatment with KIs led to the suppression of *CDK2*, *c-MYC*, *CDC25A*, and *VIM* expression while increasing *CDK1A* expression (Figure 3A). On the other hand, GSK2220400A did not influence the expression of *CDC25A*, but it was the only drug that increased *TP53* levels. The analysis of PPI networks produced by those were involved in processes such as *cell cycle*, *mitotic processes*, *UV and radiation response*, *DNA damage process*, and *DNA metabolic process* with an FDR < 0.05 (Figure 3B,C).



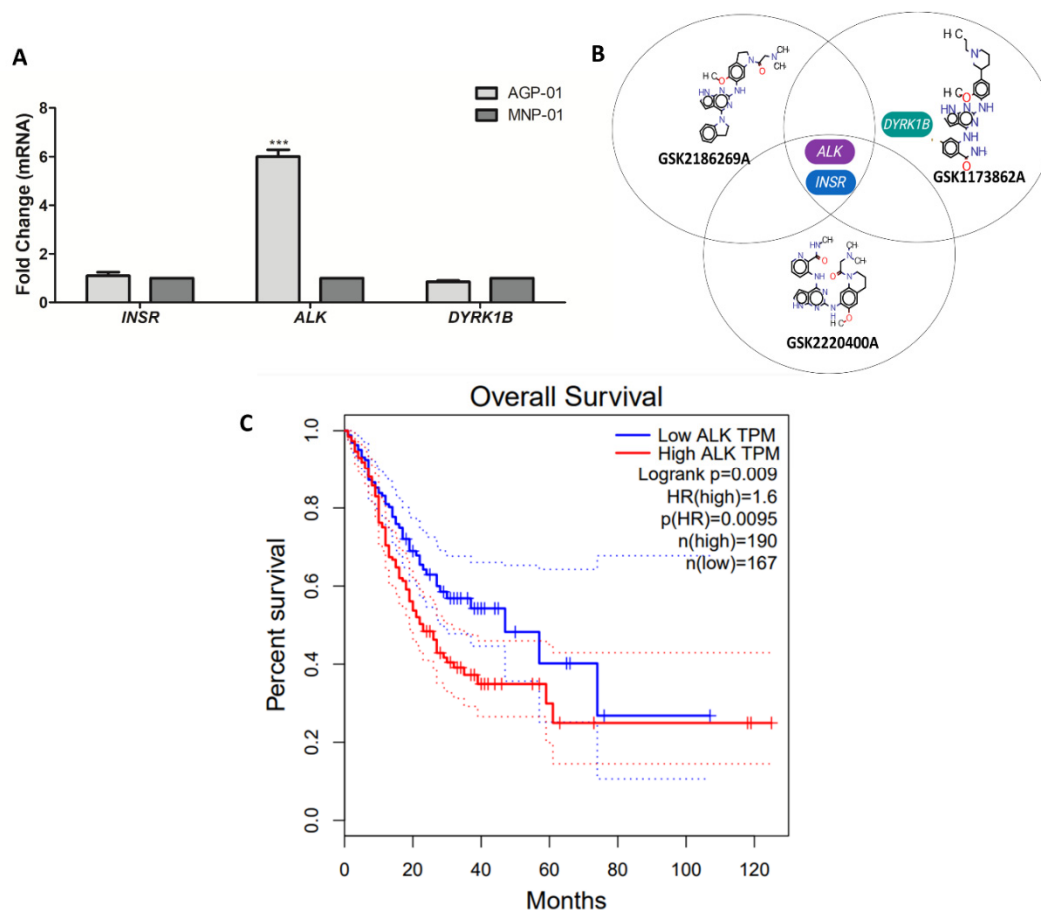
**Figure 3.** Gene expression pattern of oncogenes and tumor suppressors genes in metastatic gastric cancer cells after kinase inhibitors treatment (1 μM). (A) Mean ± standard deviation of mRNA expression fold change of *CDK1A*, *CDK2*, *CDC25A*, *TP53*, *c-MYC*, and *VIM* after KI exposure. (B) Protein–protein interaction network analysis of the modulated genes after kinase inhibitor treatment. Analyzed genes by RT-qPCR after treatment are represented with yellow color. (C) False Discovery Rate (FDR) of functional analysis with GO biological processes gene set. The top 10 GO processes are sorted by the FDR. Significant differences compared to the untreated control: \*  $p < 0.05$ , \*\*  $p < 0.01$ , \*\*\*  $p < 0.001$ .

### 3.3. Kinase Target Expression in the Metastatic Gastric Cancer Cells

Gene expression of AGP-01 cells and non-neoplastic gastric mucosa MNP-01 (normal cell) revealed that the *ALK* gene is overexpressed in the gastric cancer cells when compared



to the normal cell line. As shown in Figure 4A, among the three kinases identified as the target for the three studied compounds [13], only the *ALK* gene was overexpressed in the gastric cancer cells compared to the normal cell line. Moreover, we performed the GEPIA analysis to determine the impact of high expression on patients' survival. Gastric adenocarcinoma patients with higher expression of *ALK* gene had a lower survival probability compared to the low expression of *ALK* group ( $p = 0.0045$ ).



**Figure 4.** Overexpression of the *ALK* gene in the metastatic gastric cancer cells AGP-01. **(A)** Gene expression of the three-target kinase for the three selected inhibitors were assessed by RT-qPCR. The comparative expression between AGP-01 cells (metastatic gastric cancer cell) and MNP-01 cells (non-malignant gastric mucosa) are shown as mean  $\pm$  standard deviation (SD). **(B)** Diagram showing the three molecules selected in this study and their targets. **(C)** GEPIA server analysis for *ALK* expression on Cancer Genome Atlas Stomach Adenocarcinoma (TCGA-STAD) comparing tumor samples and normal samples. Red and blue dotted lines represent high and low *ALK* expression, respectively. Significant differences compared to untreated control: \*\*\*  $p < 0.001$ .

#### 4. Discussion

*ALK* is considered to play a key role in the nervous system's development and function, where it regulates the basic principles of cell proliferation, survival, and differentiation in response to extracellular stimuli [20,21]. Besides chromosome rearrangements, gene overexpression has been described as the relevant abnormal alterations in the *ALK* gene in neuroblastoma, lung, and oesophageal cancer [22–24]. Chen et al. (2012) also showed *ALK* overexpression in non-small cell lung cancer detected by immunohistochemical techniques [25]. Another recent evidence demonstrated that the ovarian high-grade serous carcinoma (HGSC) had significantly higher cytoplasmic *ALK* expression without chromosomal rearrangement or gene alterations compared to non-HGSC ovarian carcinomas [26]. However, *ALK* overexpression in gastric adenocarcinoma has not been well investigated.

To our knowledge, Fan and co-workers (2020) described the first case of gastrointestinal stromal tumor (GIST) with *ALK* overexpression; however, GIST are a different cancer identity when compared to gastric adenocarcinoma [27].

Our study aimed to screen 147 different kinase inhibitors identified and characterized by Elkins et al. (2016) in a metastatic gastric adenocarcinoma model in order to identify a possible kinase target with therapeutic relevance. After the initial screening, only six compounds suppressed the cell growth as much as the positive control and only three compounds (GSK2186269A, GSK1173862A, and GSK2220400A) continued to be investigated regarding their mode of action and to confirm their anti-cancer properties. The results were clear in demonstrating the cell cycle blockage, apoptosis induction, and the inhibitory effect on migration as well as in gene expression modulation. In fact, based on the gene expression of *CDKN1A*, *CDK2*, *CDC25A*, *TP53*, and *MYC*, the GO biological analysis revealed that the regulation of the cell cycle (GO:1902749, GO:1903047, GO:0000082, GO:1901990) and DNA damage response (GO:0034644, GO:0006977, GO:0010332) were induced after treatment with the three kinase inhibitors, which resulted in the eventual cell death [28–31]. The *VIM* gene suppression also revealed that the kinase inhibitors probably induced mesenchymal-epithelium transition which corroborated with the inhibition on cell migration [32]. A single study by [27] showed a decrease in cell viability and cell cycle progression, as well as tumor growth in a xenograft model of gastric cancer after *ALK* inhibition [33]. Therefore, our study corroborates with the possibility of the use of *ALK* target therapy against gastric cancer.

Evaluating the three compounds with high cytotoxic potency, compounds GSK2186269A, GSK2220400A, and GSK1173862A share the same targets [13], Anaplastic Lymphoma Receptor Tyrosine Kinase (*ALK*) and Insulin Receptor (*INSR*). Additionally, the GSK1173862A molecule also interacts with Dual Specificity Tyrosine Phosphorylation Regulated Kinase 1B (*DYRK1B*). These findings suggest that the gastric cancer cells probably overexpress these genes and therefore could be a relevant therapeutic target for gastric cancer management. Moreover, we performed the gene expression analysis of these targets on gastric cancer cells (AGP-01) and, interestingly, only the *ALK* gene showed a high expression level in gastric cancer cells when compared to the non-malignant cell line (sixfold changes). Looking for another evidence that *ALK* can be a biomarker for gastric cancer, we identified a lower survival rate for patients with gastric cancer with high levels of *ALK* expression in TCGA-STAD analysis [19]. Our hypothesis is that *ALK* gene overexpression can be a therapeutic target and/or a prognosis biomarker for patients with high-grade gastric adenocarcinoma. However, further studies are needed to confirm this hypothesis.

To our knowledge, only one study evaluated the *ALK* expression and this was in four Asian gastric cancer cell lines and a single Asian cohort of gastric cancer patients. *ALK* gene amplification and protein overexpression were not seen in any of these samples [34]. It is worth it to notice that gastric carcinogenesis differs between Asian and Caucasian tumors [35–38]. A few studies have described other *ALK* molecular alterations in gastric tumors which do not include gene overexpression. For example, a study showed 2.3% positive cases of *ALK* translocation by FISH using the standard criteria of at least 15% positive cells for the break-apart signal in signet ring cell carcinoma of the gastrointestinal tract [39].

Interestingly, a novel form of *ALK* gene fusion was identified, being the first gastric adenocarcinoma case with *RAB10-ALK* fusion [40]. On the contrary, another study did not find *ALK* fusions by FISH and gene sequencing methods in gastric adenocarcinoma [41]. Therefore, it seems to have a relevant difference among the population tested or genetic alteration found within *ALK* gene in those studies. Indeed, the genetic background can affect the molecular analysis of the cell line or cohorts [42]. Small-molecule *ALK* tyrosine kinase inhibitors are very effective against a group of cancers defined by chromosomal rearrangements involving the anaplastic lymphoma kinase (*ALK*) gene. The first- and second-generation of *ALK* inhibitors was designed to act by inhibiting the *ALK* chromosomal rearrangements, and currently, treatment resistance and recurring illness have gained

importance [43]. Therefore, there is still a need for the discovery of new *ALK* gene-related alterations and the development of new inhibitors. There is ample evidence that *ALK* overexpression may be a promising therapeutic biomarker for other populations in different continents, which could benefit gastric cancer patients.

## 5. Conclusions

In conclusion, in vitro screening of a kinase inhibitor library reveals three potential kinase inhibitors against gastric cancer cell model. These three molecules showed significant anticancer activity by inhibiting cell proliferation and migration, as well as provoking cell death. Interestingly, the three molecules share the same targets, *ALK* and *INSR*, in which only the *ALK* gene is overexpressed in the gastric cancer cell line. Looking for a possible impact on clinical aspects, we identified that higher *ALK* expression reduces patients' survival rate in TCGA-STAD data. We hypothesize that *ALK* gene overexpression can be a promising biomarker for gastric adenocarcinoma. However, further studies, in particular clinical studies, need to be conducted to prove this hypothesis.

**Author Contributions:** Invitation received, C.A.M.-N.; Conceptualization, F.P.M. and R.C.M.; Provision of data and subsequent analysis and interpretation, F.P.M., P.F.N.S., E.L.d.S., L.L.B.d.O., L.B.L., C.A.M.-N. and R.C.M.; Data Validation, F.P.M., E.L.d.S. and W.J.Z.; Writing—original draft preparation, F.P.M., P.F.N.S. and R.C.M.; Writing—review and editing, F.P.M., P.F.N.S. and C.A.M.-N., R.M.R.B. and R.C.M.; Supervision, M.E.A.d.M. and R.C.M.; Funding acquisition, R.C.M. All authors have read and agreed to the published version of the manuscript.

**Funding:** This study was supported by Brazilian funding agencies: Coordination for the Improvement of Higher Education Personnel (CAPES; to F.P.M.), National Council of Technological and Scientific Development (CNPq grant number 404213/2021-9 to C.A.M.-N.; CNPQ/MCTI/FNDCT no. 18/2021—no. 403493/2021-8 to R.C.M. and R.M.R.B., and Productivity in Research PQ to M.E.A.d.M., R.M.R.B. and R.C.M.) We also would like to thank PROPEP/UFPA for publication payment.

**Institutional Review Board Statement:** Not applicable.

**Informed Consent Statement:** Not applicable.

**Acknowledgments:** We are grateful to the Brazilian Agencies CNPq, CAPES, and FUNCAP, along with the Federal University of Ceará and the Structural Genomics Consortium for fellowships and research grants. We also thank the staff of the Multi-User Facility of the Drug Research and Development Center of Federal University of Ceará for technical support.

**Conflicts of Interest:** The authors declare no conflict of interest. The funders had no role in the design of the study; in the collection, analyses, or data interpretation; in the writing of the manuscript, or in the decision to publish the results.

## References

1. Sung, H.; Ferlay, J.; Siegel, R.L.; Laversanne, M.; Soerjomataram, I.; Jemal, A.; Bray, F. Global Cancer Statistics 2020: GLOBOCAN Estimates of Incidence and Mortality Worldwide for 36 Cancers in 185 Countries. *CA Cancer J. Clin.* **2021**, *71*, 209–249. [CrossRef] [PubMed]
2. Bray, F.; Ferlay, J.; Soerjomataram, I.; Siegel, R.L.; Torre, L.A.; Jemal, A. Global Cancer Statistics 2018: GLOBOCAN Estimates of Incidence and Mortality Worldwide for 36 Cancers in 185 Countries. *CA Cancer J. Clin.* **2018**, *68*, 394–424. [CrossRef]
3. Lee, J.; Bass, A.J.; Ajani, J.A. Gastric Adenocarcinoma: An Update on Genomics, Immune System Modulations, and Targeted Therapy. *Am. Soc. Clin. Oncol. Educ. book. Am. Soc. Clin. Oncol. Annu. Meet.* **2016**, *35*, 104–111. [CrossRef]
4. Eusebi, L.H.; Telese, A.; Marasco, G.; Bazzoli, F.; Zagari, R.M. Gastric Cancer Prevention Strategies: A Global Perspective. *J. Gastroenterol. Hepatol.* **2020**, *35*, 1495–1502. [CrossRef] [PubMed]
5. Yin, J.; Wu, X.; Li, S.; Guo, Z. Impact of Environmental Factors on Gastric Cancer: A Review of the Scientific Evidence, Human Prevention and Adaptation. *J. Environ. Sci.* **2020**, *89*, 65–79. [CrossRef]
6. Bass, A.J.; Thorsson, V.; Shmulevich, I.; Reynolds, S.M.; Miller, M.; Bernard, B.; Hinoue, T.; Laird, P.W.; Curtis, C.; Shen, H.; et al. Comprehensive Molecular Characterization of Gastric Adenocarcinoma. *Nature* **2014**, *513*, 202–209.
7. Jácome, A.A.; Coutinho, A.K.; Lima, E.M.; Andrade, A.C.; Dos Santos, J.S. Personalized Medicine in Gastric Cancer: Where Are We and Where Are We Going? *World J. Gastroenterol.* **2016**, *22*, 1160–1171. [CrossRef] [PubMed]
8. Catalano, V.; Labianca, R.; Beretta, G.D.; Gatta, G.; de Braud, F.; Van Cutsem, E. Gastric Cancer. *Crit. Rev. Oncol. Hematol.* **2009**, *71*, 127–164. [CrossRef]

9. Bang, Y.J.; Van Cutsem, E.; Feyereislova, A.; Chung, H.C.; Shen, L.; Sawaki, A.; Lordick, F.; Ohtsu, A.; Omuro, Y.; Satoh, T.; et al. Trastuzumab in Combination with Chemotherapy versus Chemotherapy Alone for Treatment of HER2-Positive Advanced Gastric or Gastro-Oesophageal Junction Cancer (ToGA): A Phase 3, Open-Label, Randomised Controlled Trial. *Lancet* **2010**, *376*, 687–697. [CrossRef]
10. Wagner, A.D.; Syn, N.L.; Moehler, M.; Grothe, W.; Yong, W.P.; Tai, B.C.; Ho, J.; Unverzagt, S. Chemotherapy for Advanced Gastric Cancer. *Cochrane Database Syst. Rev.* **2017**, *8*. [CrossRef] [PubMed]
11. Bhullar, K.S.; Lagarón, N.O.; McGowan, E.M.; Parmar, I.; Jha, A.; Hubbard, B.P.; Rupasinghe, H.P.V. Kinase-Targeted Cancer Therapies: Progress, Challenges and Future Directions. *Mol. Cancer* **2018**, *17*, 48. [CrossRef]
12. Wu, P.; Nielsen, T.E.; Clausen, M.H. FDA-Approved Small-Molecule Kinase Inhibitors. *Trends Pharmacol. Sci.* **2015**, *36*, 422–439. [CrossRef]
13. Elkins, J.M.; Fedele, V.; Szklarz, M.; Abdul Azeez, K.R.; Salah, E.; Mikolajczyk, J.; Romanov, S.; Sepetov, N.; Huang, X.P.; Roth, B.L.; et al. Comprehensive Characterization of the Published Kinase Inhibitor Set. *Nat. Biotechnol.* **2016**, *34*, 95–103. [CrossRef] [PubMed]
14. Leal, M.F.; do Nascimento, J.L.M.; da Silva, C.E.A.; Lamarão, M.F.V.; Calcagno, D.Q.; Khayat, A.S.; Assumpção, P.P.; Cabral, I.R.; Smith, M.D.A.C.; Burbano, R.R. Establishment and Conventional Cytogenetic Characterization of Three Gastric Cancer Cell Lines. *Cancer Genet. Cytogenet.* **2009**, *195*, 85–91. [CrossRef]
15. Leal, M.F.; Ribeiro, H.F.; Rey, J.A.; Pinto, G.R.; Smith, M.C.; Moreira-Nunes, C.A.; Assumpção, P.P.; Lamarão, L.M.; Calcagno, D.Q.; Montenegro, R.C.; et al. YWHAE Silencing Induces Cell Proliferation, Invasion and Migration through the up-Regulation of CDC25B and MYC in Gastric Cancer Cells: New Insights about YWHAE Role in the Tumor Development and Metastasis Process. *Oncotarget* **2016**, *7*, 85393–85410. [CrossRef] [PubMed]
16. Mesquita, F.P.; Silva, E.L.; Souza, P.F.N.; Lima, L.B.; Amaral, J.L.; Zuercher, W.; Albuquerque, L.M.; Rabenhorst, S.H.B.; Moreira-Nunes, C.A.; Moraes, M.E.; et al. Kinase Inhibitor Screening Reveals Aurora-a Kinase Is a Potential Therapeutic and Prognostic Biomarker of Gastric Cancer. *J. Cell. Biochem.* **2021**, *122*, 1376–1388. [CrossRef]
17. Bustin, S.A.; Benes, V.; Garson, J.A.; Hellemans, J.; Huggett, J.; Kubista, M.; Mueller, R.; Nolan, T.; Pfaffl, M.W.; Shipley, G.L.; et al. The MIQE Guidelines: Minimum Information for Publication of Quantitative Real-Time PCR Experiments. *Clin. Chem.* **2009**, *55*, 611–622. [CrossRef]
18. Livak, K.J.; Schmittgen, T.D. Analysis of Relative Gene Expression Data Using Real-Time Quantitative PCR and the 2<sup>(-Delta Delta C(T))</sup> Method. *Methods* **2001**, *25*, 402–408. [CrossRef]
19. Tang, Z.; Li, C.; Kang, B.; Gao, G.; Li, C.; Zhang, Z. GEPIA: A Web Server for Cancer and Normal Gene Expression Profiling and Interactive Analyses. *Nucleic Acids Res.* **2017**, *45*, W98–W102. [CrossRef]
20. Holla, V.R.; Elamin, Y.Y.; Bailey, A.M.; Johnson, A.M.; Litztenburger, B.C.; Khotskaya, Y.B.; Sanchez, N.S.; Zeng, J.; Shufean, M.A.; Shaw, K.R.; et al. ALK: A Tyrosine Kinase Target for Cancer Therapy. *Cold Spring Harb. Mol. Case Stud.* **2017**, *3*, a001115. [CrossRef]
21. Hallberg, B.; Palmer, R.H. The Role of the ALK Receptor in Cancer Biology. *Ann. Oncol. Off. J. Eur. Soc. Med. Oncol.* **2016**, *27* (Suppl. 3), iii4–iii15. [CrossRef] [PubMed]
22. Schönherr, C.; Ruuth, K.; Yamazaki, Y.; Eriksson, T.; Christensen, J.; Palmer, R.H.; Hallberg, B. Activating ALK Mutations Found in Neuroblastoma Are Inhibited by Crizotinib and NVP-TAE684. *Biochem. J.* **2011**, *440*, 405–413. [CrossRef]
23. Murugan, A.K.; Xing, M.M. Anaplastic Thyroid Cancers Harbor Novel Oncogenic Mutations of the ALK Gene. *Cancer Res.* **2011**, *71*, 4403–4411. [CrossRef] [PubMed]
24. Schoppmann, S.F.; Streubel, B.; Birner, P. Amplification but Not Translocation of Anaplastic Lymphoma Kinase Is a Frequent Event in Oesophageal Cancer. *Eur. J. Cancer* **2013**, *49*, 1876–1881. [CrossRef] [PubMed]
25. Huang, S.-F.; Chen, T.-D.; Chang, I.-C.; Chen, Y.-T.; Liu, H.-P.; Wu, Y.-C.; Wang, C.-L.; Chen, Y.-R. Correlation of Anaplastic Lymphoma Kinase Overexpression and the EML4-ALK Fusion Gene in Non-Small Cell Lung Cancer by Immunohistochemical Study. *Chang Gung Med. J.* **2012**, *35*, 309–317. [CrossRef]
26. Matsumoto, T.; Oda, Y.; Hasegawa, Y.; Hashimura, M.; Oguri, Y.; Inoue, H.; Yokoi, A.; Tochimoto, M.; Nakagawa, M.; Jiang, Z.; et al. Anaplastic Lymphoma Kinase Overexpression Is Associated with Aggressive Phenotypic Characteristics of Ovarian High-Grade Serous Carcinoma. *Am. J. Pathol.* **2021**, *191*, 1837–1850. [CrossRef]
27. Fan, J.; Yang, M.; Huang, B.; Wang, Z.; Luo, D.; Zhang, J.; Zhang, P.; Shi, H.; Li, Y.; Nie, X. ALK Expressed in a Gastrointestinal Stromal Tumor Harboring PDGFRA p. D842V Mutation: A Case Report. *Diagn. Pathol.* **2020**, *15*, 8. [CrossRef]
28. Suski, J.M.; Braun, M.; Strmiska, V.; Sicinski, P. Targeting Cell-Cycle Machinery in Cancer. *Cancer Cell* **2021**, *39*, 759–778. [CrossRef]
29. Strasser, A.; Vaux, D.L. Cell Death in the Origin and Treatment of Cancer. *Mol. Cell* **2020**, *78*, 1045–1054. [CrossRef]
30. Razaghi, A.; Heimann, K.; Schaeffer, P.M.; Gibson, S.B. Negative Regulators of Cell Death Pathways in Cancer: Perspective on Biomarkers and Targeted Therapies. *Apoptosis* **2018**, *23*, 93–112. [CrossRef]
31. Carneiro, B.A.; El-Deiry, W.S. Targeting Apoptosis in Cancer Therapy. *Nat. Rev. Clin. Oncol.* **2020**, *17*, 395–417. [CrossRef] [PubMed]
32. Debnath, P.; Huiem, R.S.; Dutta, P.; Palchaudhuri, S. Epithelial-Mesenchymal Transition and Its Transcription Factors. *Biosci. Rep.* **2022**, *42*, BSR20211754. [CrossRef]
33. Chen, X.; Ji, J.; Chen, W.; Lian, W.; Chen, R.; Yang, J.; Zhang, Q.; Weng, Q.; Khan, Z.; Hu, J.; et al. (S)-Crizotinib Reduces Gastric Cancer Growth through Oxidative DNA Damage and Triggers pro-Survival Akt Signal. *Cell Death Dis.* **2018**, *9*, 660.

34. Yang, Y.; Wu, N.; Shen, J.; Teixido, C.; Sun, X.; Lin, Z.; Qian, X.; Zou, Z.; Guan, W.; Yu, L.; et al. MET Overexpression and Amplification Define a Distinct Molecular Subgroup for Targeted Therapies in Gastric Cancer. *Gastric Cancer* **2016**, *19*, 778–788. [CrossRef]
35. Montenegro, R.C.; Clark, P.G.K.; Howarth, A.; Wan, X.; Ceroni, A.; Siejka, P.; Nunez-Alonso, G.A.; Monteiro, O.; Rogers, C.; Gamble, V.; et al. BET Inhibition as a New Strategy for the Treatment of Gastric Cancer. *Oncotarget* **2016**, *7*, 43997. [CrossRef] [PubMed]
36. Wang, J.; Sun, Y.; Bertagnolli, M.M. Comparison of Gastric Cancer Survival between Caucasian and Asian Patients Treated in the United States: Results from the Surveillance Epidemiology and End Results (SEER) Database. *Ann. Surg. Oncol.* **2015**, *22*, 2965–2971. [CrossRef] [PubMed]
37. Jin, H.; Pinheiro, P.S.; Callahan, K.E.; Altekruse, S.F. Examining the Gastric Cancer Survival Gap between Asians and Whites in the United States. *Gastric Cancer* **2017**, *20*, 573–582. [CrossRef] [PubMed]
38. Trumbull, D.; Lemini, R.; Attwood, K.; Kukar, M.; Gabriel, E. Gastric Cancer Disparities Among Asian American Subpopulations. *Anticancer Res.* **2020**, *40*, 6381–6385. [CrossRef]
39. Alese, O.B.; Rayes, B.F.; Zhang, G.; Khuri, F.R.; Sica, G.; Adsay, N.V.; Alexis, D.; Rosa, F.G.; Varella Garcia, M.; Chen, Z.; et al. Anaplastic Lymphoma Kinase (ALK) Gene Alteration in Signet Ring Cell Carcinoma of the Gastrointestinal Tract. *Ther. Adv. Med. Oncol.* **2015**, *7*, 56–62. [CrossRef]
40. Wen, Z.; Xiong, D.; Zhang, S.; Liu, J.; Li, B.; Li, R.; Zhang, H. Case Report: RAB10-ALK: A Novel ALK Fusion in a Patient With Gastric Cancer. *Front. Oncol.* **2021**, *11*, 645370. [CrossRef]
41. Ying, J.; Lin, C.; Wu, J.; Guo, L.; Qiu, T.; Ling, Y.; Shan, L.; Zhou, H.; Zhao, D.; Wang, J.; et al. Anaplastic Lymphoma Kinase Rearrangement in Digestive Tract Cancer: Implication for Targeted Therapy in Chinese Population. *PLoS ONE* **2015**, *10*, e0144731.
42. Turajlic, S.; Sottoriva, A.; Graham, T.; Swanton, C. Resolving Genetic Heterogeneity in Cancer. *Nat. Rev. Genet.* **2019**, *20*, 404–416. [CrossRef] [PubMed]
43. Shaw, A.T.; Bauer, T.M.; de Marinis, F.; Felip, E.; Goto, Y.; Liu, G.; Mazieres, J.; Kim, D.-W.; Mok, T.; Polli, A.; et al. First-Line Lorlatinib or Crizotinib in Advanced ALK -Positive Lung Cancer. *N. Engl. J. Med.* **2020**, *383*, 2018–2029. [CrossRef] [PubMed]

Review

# Kinase Inhibition in Multiple Myeloma: Current Scenario and Clinical Perspectives

Igor Valentim Barreto <sup>1,†</sup>, Caio Bezerra Machado <sup>1,†</sup>, Davi Benevides Almeida <sup>2,†</sup>, Flávia Melo Cunha de Pinho Pessoa <sup>1</sup>, Renan Brito Gadelha <sup>1</sup>, Laudreísa da Costa Pantoja <sup>3</sup>, Deivide de Sousa Oliveira <sup>4</sup>, Rodrigo Monteiro Ribeiro <sup>4</sup>, Germison Silva Lopes <sup>5</sup>, Manoel Odorico de Moraes Filho <sup>1</sup>, Maria Elisabete Amaral de Moraes <sup>1</sup>, André Salim Khayat <sup>3</sup>, Edivaldo Herculano Correa de Oliveira <sup>6,7</sup> and Caroline Aquino Moreira-Nunes <sup>1,3,8,\*</sup>

<sup>1</sup> Pharmacogenetics Laboratory, Department of Medicine, Drug Research and Development Center (NPDM), Federal University of Ceará, Fortaleza 60430-275, CE, Brazil

<sup>2</sup> Unichristus University Center, Faculty of Biomedicine, Fortaleza 60430-275, CE, Brazil

<sup>3</sup> Department of Biological Sciences, Oncology Research Center, Federal University of Pará, Belém 66073-005, PA, Brazil

<sup>4</sup> Department of Hematology, Fortaleza General Hospital (HGF), Fortaleza 60150-160, CE, Brazil

<sup>5</sup> Department of Hematology, César Cals General Hospital, Fortaleza 60015-152, CE, Brazil

<sup>6</sup> Faculty of Natural Sciences, Institute of Exact and Natural Sciences, Federal University of Pará (UFPA), Rua Augusto Correa, 01, Belém 66075-990, PA, Brazil

<sup>7</sup> Laboratory of Cytogenomics and Environmental Mutagenesis, Environment Section (SAMAM), Evandro Chagas Institute (IEC), BR 316, KM 7, s/n, Levilândia, Ananindeua 67030-000, PA, Brazil

<sup>8</sup> Northeast Biotechnology Network (RENORBIO), Itaperi Campus, Ceará State University, Fortaleza 60740-903, CE, Brazil

\* Correspondence: carolfam@gmail.com

† These authors contributed equally to this work.

**Citation:** Barreto, I.V.; Machado, C.B.;

Almeida, D.B.; Pessoa, F.M.C.d.P.;

Gadelha, R.B.; Pantoja, L.d.C.;

Oliveira, D.d.S.; Ribeiro, R.M.; Lopes,

G.S.; de Moraes Filho, M.O.; et al.

Kinase Inhibition in Multiple Myeloma: Current Scenario and Clinical Perspectives. *Pharmaceutics* **2022**, *14*, 1784. <https://doi.org/10.3390/pharmaceutics14091784>

Academic Editor: Ross McKinnon

Received: 21 July 2022

Accepted: 23 August 2022

Published: 25 August 2022

**Publisher's Note:** MDPI stays neutral with regard to jurisdictional claims in published maps and institutional affiliations.



**Copyright:** © 2022 by the authors. Licensee MDPI, Basel, Switzerland. This article is an open access article distributed under the terms and conditions of the Creative Commons Attribution (CC BY) license (<https://creativecommons.org/licenses/by/4.0/>).

**Abstract:** Multiple myeloma (MM) is a blood cell neoplasm characterized by excessive production of malignant monoclonal plasma cells (activated B lymphocytes) by the bone marrow, which end up synthesizing antibodies or antibody fragments, called M proteins, in excess. The accumulation of this production, both cells themselves and of the immunoglobulins, causes a series of problems for the patient, of a systemic and local nature, such as blood hyperviscosity, renal failure, anemia, bone lesions, and infections due to compromised immunity. MM is the third most common hematological neoplasm, constituting 1% of all cancer cases, and is a disease that is difficult to treat, still being considered an incurable disease. The treatments currently available cannot cure the patient, but only extend their lifespan, and the main and most effective alternative is autologous hematopoietic stem cell transplantation, but not every patient is eligible, often due to age and pre-existing comorbidities. In this context, the search for new therapies that can bring better results to patients is of utmost importance. Protein tyrosine kinases (PTKs) are involved in several biological processes, such as cell growth regulation and proliferation, thus, mutations that affect their functionality can have a great impact on crucial molecular pathways in the cells, leading to tumorigenesis. In the past couple of decades, the use of small-molecule inhibitors, which include tyrosine kinase inhibitors (TKIs), has been a hallmark in the treatment of hematological malignancies, and MM patients may also benefit from TKI-based treatment strategies. In this review, we seek to understand the applicability of TKIs used in MM clinical trials in the last 10 years.

**Keywords:** multiple myeloma; tyrosine kinase; treatment; ibrutinib

## 1. Introduction

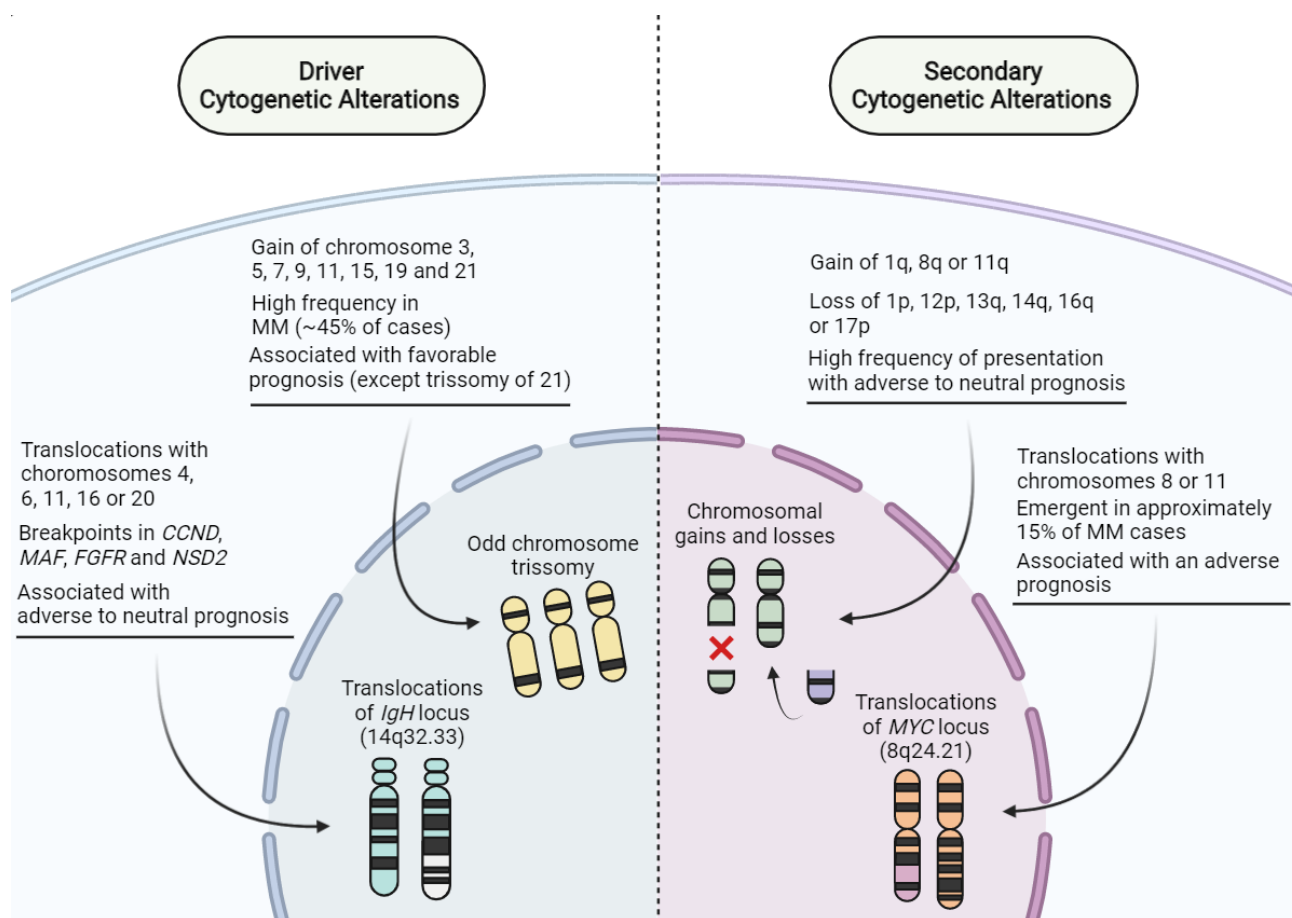
Multiple myeloma (MM) is a systemic hematological neoplasm in which there is an abnormal proliferation of malignant monoclonal plasmocytes that release antibodies or antibody fragments, called M proteins, in excess [1–5]. This feature is responsible for a range of symptoms of MM such as blood hyperviscosity and damage to the renal tubules. Along with this accumulation, the interaction of malignant plasma cells with other cells in the bone marrow (BM) causes several problems for patients such as anemia, destructive bone lesions, and infections due to compromised immunity [5–7].

MM is the third most reported neoplasm representing approximately 1% of all cancers and approximately 10% of all hematological malignancies, with risk factors for MM development involving gender, age, family history of malignancies, and ethnicity [1,8,9]. MM is more commonly reported in men than in women with a ratio of 1.5 to 1 and being twice as common in African Americans compared to Caucasians [2,10,11]. The median age at diagnosis tends to be around 65 years [2,12].

MM emerges from molecular changes caused by DNA damage and failures in DNA repair mechanisms [13]. As a genetically complex disease, MM development is a process composed of several stages, with initial mutations appearing in hematopoietic stem cells (HSC) of the bone marrow (BM), the site most affected by the disease [14]. With the onset of malignant transformations, patients enter a pre-malignant stage called smoldering multiple myeloma (SMM) or monoclonal gammopathy of undetermined significance (MGUS) that occurs due to genetic events such as chromosomal translocations involving immunoglobulin heavy chain (*IgH*) genes and aneuploidy [15]. Secondary genetic events, such as copy number abnormalities and acquired mutations, are linked to tumor progression [16–19]. With the accumulation of mutations that guarantee competitive advantages, HSCs evolve into malignant cells and begin to proliferate causing accumulation of malignant plasma cells in the BM [19]. This proliferation is sustained also due to the release of cytokines, such as interleukin 6 (IL-6), carried out by BM stromal cells [5,20,21]. The genetic alterations found in the MGUS stage are involved in tumor development, while the events present in the MM stages that were not found in MGUS are responsible for tumor progression [12,17].

MGUS is an asymptomatic pre-malignant phase, preceding most cases of MM and being present in approximately 3–4% of the population over 50 years of age. Of the total number of MGUS cases, only 1% per year has a chance of progression to MM [22–25]. Patients with translocation t(4;14), del(17p), gain(1q), and trisomies have a higher risk of progression from the SMM stage to MM, reaching 10% per year. This being also a risk factor for progression from MGUS to MM [26–28].

Regarding genetic alterations, MM is known to present a great heterogeneity; however, mutations that could be considered precursors of the disease are now well known, and these genetic alterations can be used as a prognostic factor. An example of this would be mutations in the *IgH* gene locus, responsible for producing the heavy chains of immunoglobulins, which are considered to be early precursor mutations [3,29,30]. Chromosomal translocations involving *IgH* and other genes such as *Nuclear Receptor Binding SET Domain Protein (NSD2)*, *Fibroblast Growth Factor Receptor 3 (FGFR3)*, *Cyclin D3 (CCND3)*, *Cyclin D1 (CCND1)*, *MAF bZIP Transcription Factor (MAF)*, and *MAF bZIP Transcription Factor B (MAFB)*, resulting in the translocations t(4;14), t(6;14), t(11;14), t(14;16), and t(14;20), respectively, are also an important clinical finding, as they deregulate checkpoints of the cell cycle due to increased gene transcription under the activity of *IgH* transcription enhancer (Figure 1) [14,31–34].



**Figure 1.** Cytogenetic alterations associated with multiple myeloma (MM). In pre-malignant settings, driver alterations correlate with deregulation of oncogene activity and carcinogenesis onset. At later disease stages, secondary alterations emerge due to genomic instability in malignant clones, and MM cells from the same patient may even harbor different secondary alterations, following the concepts of linear and branching evolution. Created with BioRender.com.

## 2. Current Clinical MM Treatment Options

Overall survival of MM cases has more than doubled in recent decades due to the introduction of new combinations of chemotherapy, small molecule inhibitors, and the use of monoclonal antibodies [35–38].

Hematopoietic stem cell transplantation (HSCT) is still the most recommended treatment for MM, being the first choice in most cases, although not all patients are eligible. Non-eligibility can happen for a variety of reasons, including age, which is an important cut-off point for inclusion criteria, pre-existing comorbidities, and performance score, which is used to predict poor outcomes in patients with MM [39–41].

When eligible for HSCT, patients are submitted to one of two induction regimens: VTD, which includes bortezomib, thalidomide, and dexamethasone, or VRD, which includes bortezomib, lenalidomide, and dexamethasone, being the most adopted pre-transplant induction regimens available [42]. The role of induction chemotherapy is to reduce the neoplastic burden at the patient's BM in order to increase response rates and effectiveness of an autologous transplantation graft [43–46]. Satisfactory response rates can be seen in young, transplant-eligible patients receiving high-dose melphalan therapy with autologous stem cell transplantation achieving a >60% effective response [47].

Most patients afflicted with MM end up relapsing and those who relapse and are not eligible for a new HSCT require a triple therapy regimen that varies from case to case.



Although highly cytotoxic, triple therapy regimens should be continued until the toxicity outweighs the benefits or until patients are eligible for autologous HSCT [35,38]

On the other hand, the use of proteasome inhibitors revolutionized the management of hematological malignancies emerging as one of the most important agents for the treatment of MM [48]. Tumor cells are proteasome-dependent to eliminate excess proteins that arise due to the continuous production of monoclonal immunoglobulin chains. Proteasome hyperactivity in MM results in the degradation of important proteins such as the nuclear factor kappa B (NF $\kappa$ B), the enzymatic complex of inhibitors of nuclear factor kappa B ( $\kappa$ B), tumor protein p53 (TP53) suppressor proteins, among other proteins responsible for the cell cycle [49,50]. Its inhibition leads to cellular stress induced by high protein load in the endoplasmic reticulum due to the accumulation of intracellular proteins, leading to cell death in MM cells [51,52]. Three agents in this class are approved by the Food and Drug Administration (FDA) for use, bortezomib, carfilzomib, and ixazomib [53–57].

Approved in 2003, bortezomib was the first proteasome inhibitor to be used for the treatment of relapsed and refractory multiple myeloma. Reversibly binding with high affinity to the 20S proteolytic core with the 26S proteasome without inhibiting other types of proteases commonly present in the human body, bortezomib inhibits the ubiquitin–proteasome pathway, triggering a series of events such as induction of apoptosis, cell cycle inhibition, angiogenesis and adhesion, and cell proliferation. Despite being highly potent and effective, bortezomib has a limitation during treatment: the dose that will be used is limited by the toxicity of the drug that is often associated with peripheral neuropathy [52,55,56,58,59].

Carfilzomib is a second-generation proteasome inhibitor approved in 2012 for use in monotherapy or doublet or triplet combination regimens, especially for patients with relapsed or refractory multiple myeloma. Unlike bortezomib, which binds reversibly, carfilzomib binds irreversibly and highly selectively to the 20S proteasome, precisely in the chymotrypsin-like  $\beta$ 5 subunit. The inhibition of this subunit is enough to cause apoptosis due to the accumulation of proteasome substrates inside the cell, which could explain the high sensitivity of MM cells to this drug, use of carfilzomib being possible in a monotherapy regimen aiming to reduce adverse effects. In this context, the drug has lower neurotoxicity compared to bortezomib, but there is a higher possibility of causing hypertension, congestive heart failure, and coronary artery disease, not being recommended for patients with heart diseases [54–56].

Ixazomib was approved in 2015 for use in combination with lenalidomide and dexamethasone (Rd) in patients who have received at least one therapy regimen previously. It is the first proteasome inhibitor that can be administered orally. Ixazomib is a potent and selective inhibitor of 20S proteasome, also binding in the chymotrypsin-like  $\beta$ 5 subunit, as carfilzomib, but reversibly, as bortezomib. In addition, at high concentrations, the drug can also bind in two other subunits of this proteasome:  $\beta$ 1 caspase-like and  $\beta$ 2 trypsin-like, increasing the selectivity of ixazomib by proteasome 20S. Ixazomib has no cardiotoxic effects, but neurotoxicity is present, although at a lower level when compared to bortezomib. The most reported adverse effects are thrombocytopenia, skin rash, and GI symptoms—diarrhea, nausea, and vomiting [54,55,60–62].

Another important therapy in the treatment of MM is the use of immunomodulators (IMiDs), such as thalidomide, pomalidomide, and lenalidomide. In general, immunomodulators act by inhibiting cell growth by inducing apoptosis in MM cells through the inhibition of interferon regulatory factor 4 (IRF4), thus, affecting expression of the *MYC* proto-oncogene (*MYC*). The overexpression of these two factors is linked to oncogenesis in several types of cancer, including MM, as they are involved in the processes of regulation of cell growth and metabolism, differentiation, apoptosis, angiogenesis, DNA repair, protein translation, and hematopoietic cell formation. In MM, they act by regulating the immune response and the development of immune cells [63–66].

In addition, IMiDs act favoring the production of interleukin-2 (IL-2) and interferon-gamma (IFN- $\gamma$ ), activating T lymphocytes and natural-killer (NK) cells, on the other hand

also inhibiting the production of the tumor necrosis (TNF)- $\alpha$ . The discovery of the inhibitory effects of thalidomide on tumor progression led to the development of two other analogues, lenalidomide and pomalidomide, which were authorized and released for use in MM after clinical trials in 2006 and 2013 [64,67–69].

Daratumumab is a new kind of drug that has been used since 2015 for the treatment of MM and it has been promoting an incredible improvement in the efficiency of the treatment [70]. Daratumumab is an anti-CD38 monoclonal antibody, which is a pleiotropic glycoprotein highly expressed on plasma cells and MM cells, acting as a transmembrane receptor on these cells [70,71]. The role of CD38 as a receptor involves signaling for cell activation and proliferation and inducing cell adhesion processes [72], which may explain its high expression in MM tumor cells. Therefore, the daratumumab's monoclonal antibodies directly target and destroy tumor cells due to several mechanisms, including antibody-dependent cell-mediated cytotoxicity, complement-dependent cytotoxicity, antibody-dependent phagocytosis, and immune cell depletion or inhibition of immunosuppressive cells, constituting a specific type of immunotherapy for patients with multiple myeloma [46,73–76]. Initially, it was only used as a monotherapy regimen for patients with relapsed or refractory MM, but its low toxicity allowed it to be added to other drugs in several different combinations, both in triple and quadruple therapies [70,71].

Emerging therapies with better outcomes involve immunotherapy and personalized medicine based on the molecular characteristics of the patient's tumor [33,71,77]. Specific antibodies against B-cell maturation antigen (BCMA) have shown promise in the treatment of MM, since it is an antigen whose expression is higher in myeloma cells than in healthy plasma cells, having an essential role in the process of maturation and differentiation of B-cells, being only expressed on antibody-producing B lymphocytes [78,79]. Antibodies with dual specificity are also under development, the central idea of which is to bind a T cell to a tumor cell, with the antibody acting as a binding bridge, and thus induce the destruction of the tumor cell by the T lymphocyte connected to it [71,77].

Due to the evolution of molecular profiling techniques, it is possible to identify several genetic and molecular abnormalities that constitute the neoplastic clones of a specific patient. The knowledge of the existing mutations helps guide the best available treatment based on the genetic characteristics of each patient, in addition to assessing the patient's prognosis, thus, determining whether a more aggressive drug therapy is necessary or if the patient is in a situation of good prognosis and may be eligible for autologous HSCT [31,33,80].

With the understanding that MM is a disease still treated with a non-curative approach, the constant development of new therapeutic strategies is one of the main goals in oncologic investigations and routine clinical practice. In the past couple of decades, the use of small-molecule inhibitors, which include tyrosine kinase inhibitors (TKI), has been a hallmark in the treatment of hematological malignancies, and MM patients may also benefit from TKI-based treatment strategies [31,32].

### 3. Tyrosine Kinase Inhibitors in MM

Protein tyrosine kinases (PTKs) are part of a large, multigene family and their main functions are to coordinate cellular behavior, regulate mitosis, differentiation, apoptosis, and a series of physiological and biochemical processes [81–83]. Structurally, PTKs can be divided into receptor PTKs (RTK), acting as receptors for external signals of growth and survival factors and phosphorylating other protein residues in the intracellular compartment, and non-receptor PTKs (NRTK), which are cytoplasmic or nuclear proteins that act as second messengers. Examples of both classes include insulin-like growth factor 1 receptor (IGFR), mast/stem cell growth factor receptor Kit (KIT), hepatocyte growth factor receptor (MET), fibroblast growth factor receptor (FGFR3), vascular endothelial growth factor receptor (VEGFR), and platelet derived growth factor receptor (PDGFR), as RKTs, and Bruton's tyrosine kinase (BTK), Janus kinase (JAK), SRC proto-oncogene (SRC), ABL proto-oncogene (ABL), and FA complementation group (FAC), as NRTKs [81,84–87].

Several groups of diseases present alterations linked to PTK, as their abnormal expression is linked to disorders in the regulation of cell proliferation, leading to the process of tumorigenesis, and their overexpression is also related to invasion and metastasis, tumor neovascularization, and resistance to chemotherapy [81,85,86,88,89].

There are currently 71 TKIs approved by the FDA for the treatment of neoplasms (<http://www.brimr.org/PKI/PKIs.htm>, accessed on 21 July 2022). Acquired resistance remains a problem in cancer-targeted therapies as a variety of resistance mechanisms are described in TKI treatment protocols, such as amplification of target receptor expression, mutations in tyrosine kinase inhibitor binding receptors, overactivation of alternative cell survival pathways, and activation of downstream signaling effectors linked to cell proliferation [82,90]

Table 1 is composed of a series of clinical trials over the last 10 years using TKIs as monotherapy or in combination with other cytotoxic agents to treat patients afflicted with refractory multiple myeloma and their results with degrees of efficacy.

**Table 1.** TKIs used in clinical trials to treat refractory multiple myeloma in the last 10 years.

Clinical Study Phase	Targeted Kinase	Kinase Inhibitor	Associated Treatment	Clinical Outcome	Adverse Events	References
I	BTK	Ibrutinib	Carfilzomib/Dexamethasone	ORR of 67% and a PFS of 7.2 months.	Hypertension, anemia, pneumonia, fatigue, diarrhea, and thrombocytopenia.	[91]
I/IIb	BTK	Ibrutinib	Carfilzomib/Dexamethasone	Acceptable safety profiles with PFS and ORR of 7.7 months and 71%, respectively. The average one-year OS rate was 77%.	Thrombocytopenia, anemia, diarrhea, fatigue, nausea, and hypertension.	[92]
II	BTK	Ibrutinib	Bortezomib/Dexamethasone	The drug combination initially increased the levels of infections and risk minimization measures were necessary. Clinical response was observed in 57% of patients with a duration of 9.5 months.	Thrombocytopenia, diarrhea, anemia, asthenia, and pneumonia.	[93]
II	BTK	Ibrutinib	Dexamethasone	The highest CBR was achieved in the combination of ibrutinib 840 mg with dexamethasone 40 mg. With CBR of 28%, ORR of 5%, sustained SD of 23%, and median PFS of 4.6 months.	Diarrhea, fatigue, nausea, anemia, and thrombocytopenia.	[94]
I	JAK	Ruxolitinib	Lenalidomide and methylprednisolone	The drug showed the ability to abrogate resistance to lenalidomide. Featuring CBR of 46% and ORR of 38%.	Anemia, thrombocytopenia and lymphopenia, sepsis, and pneumonia.	[95]
Ib	HGF and MET	Cabozantinib	NR	The drug alone has no significant activity in patients with refractory MM. The study was interrupted, and the rates were not calculated.	Grade 2 congestive heart failure and grade 3 APN. The remaining AEs were related to intestinal events.	[96]
Ib	JAK1	INCB052793	NR	No significant responses were observed. ORR of 24% and OS of 6.7 months.	Thrombocytopenia, anemia, fatigue, nausea, and vomiting.	[97]
II	c-MET	Tivantinib	NR	In isolation, the drug did not present a satisfactory response in refractory patients. SD of 36% and PD of 63% were obtained.	Neutropenia, hypertension, syncope, infection, and pain.	[98]
II	MEK and AKT	Trametinib and Afuresertib	NR	MTDs were found, being concentrations that are below the monotherapy concentration of each drug. However, these doses were considered subtherapeutic.	Diarrhea, acneiform dermatitis, maculopapular rash, fatigue, dry skin, nausea, dyspnea, and vomiting.	[99]

Table 1. Cont.

Clinical Study Phase	Targeted Kinase	Kinase Inhibitor	Associated Treatment	Clinical Outcome	Adverse Events	References
II	VEGF	Sorafenib	NR	Only one patient completed the 13 cycles of treatment and achieved PR, another 7 patients remained in PD.	Fatigue, nausea, hypertension, dermal toxicity, hematologic toxicity, and heart attack.	[100]
II	FGFR3	Dovitinib	NR	The SD rate in t(4;14)-positive patients was higher, being 61.5%, compared with 34.6% rates for those translocation-negative	Diarrhea, nausea, vomiting, and fatigue.	[101]

Legend: NR: not reported; SD: stable disease; PR: partial response; ORR: overall response rate; PD: patients showed progression; OS: median overall survival; PFS: progression-free survival; CBR: clinical benefit rate; MTD: maximum tolerated dose.

Of the 11 articles described in Table 1, 36.4% (4) addressed the treatment with ibrutinib as a major option for MM. The other studies addressed treatments with other kinase inhibitors, such as Ruxolitinib, Cabozantinib, INCB052793, Tivantinib, Trametinib, Afuresertibe, Sorafenib, and Dovitinib. In total, 36.4% (4) of the articles described in the table are phase I clinical trials, while the other 63.6% (7) are phase II clinical trials [92–101].

#### 4. Ibrutinib: A BTK Inhibition Approach

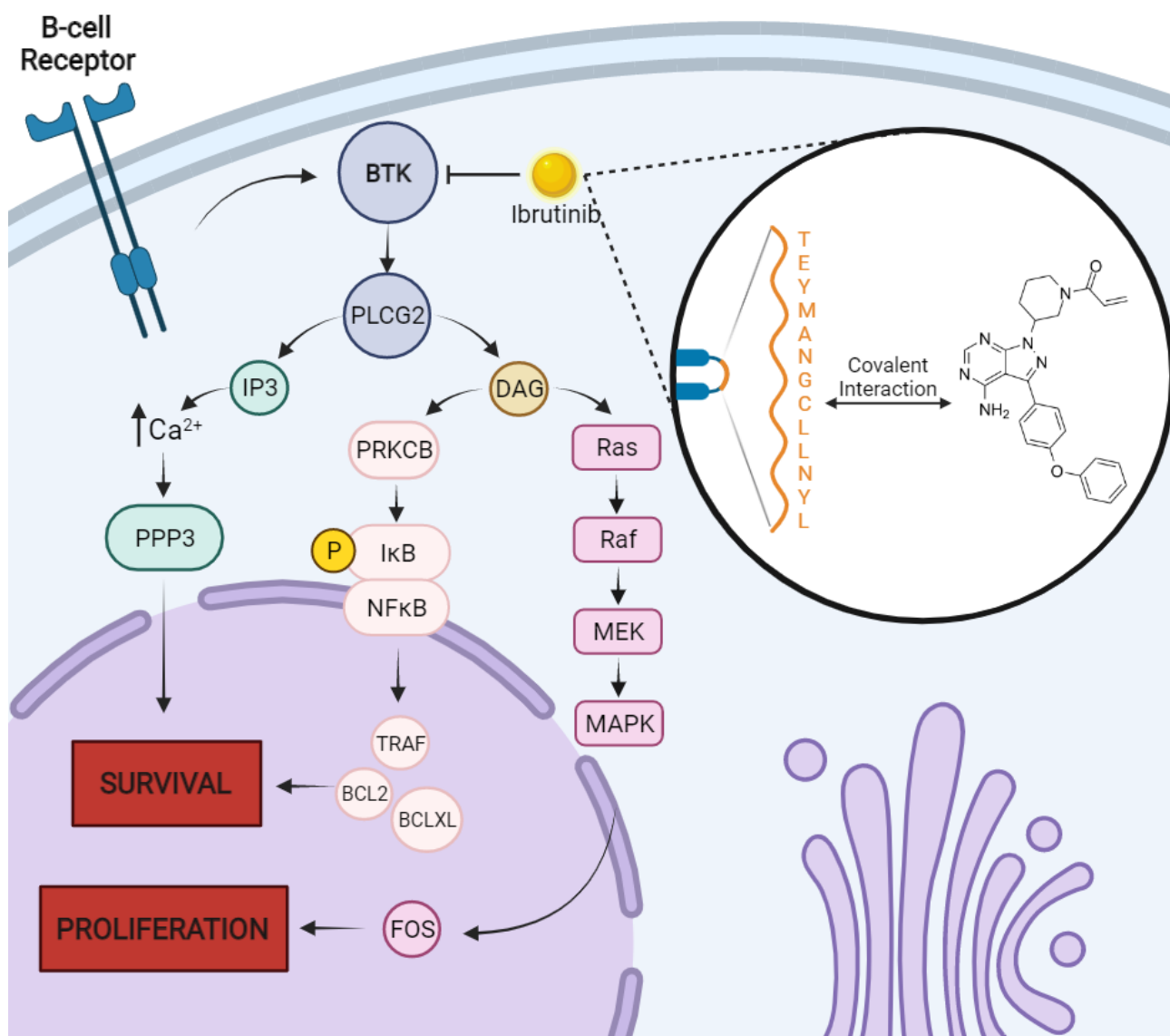
BTK inhibitors (BTKi) are one of the most popular and advanced approaches to targeting the BCR pathway. In addition to having revolutionized the treatment of B-lymphocyte malignancy, they also have a high level of efficacy in relation to chronic lymphocytic leukemia (CLL) patients, especially those with high-risk mutations [102,103]. Among these inhibitors, Ibrutinib stands out, already showing robust and durable efficacy in the treatment of refractory CLL and being one of the first inhibitors of the pathway to be approved by the FDA [104,105].

Ibrutinib is an FDA-approved drug for the treatment of B-cell malignancies [106], it works by irreversibly binding BTK through a covalent bond with a cysteine residue at position 481 (C481) [107]. It has demonstrated clinical responses mainly related to refractory CLL and mantle cell lymphoma (MCL), but it also has approval for use in cases of Waldenström's macroglobulinemia, small lymphocytic lymphoma, and marginal zone lymphoma. Chronic inhibition of BTK has been shown to be so effective in terms of its anticancer activity that its drugs are being widely tested in hematologic malignancies and solid malignancies [108,109]. Since overexpression of BTK is present in 85% of MM cases, ibrutinib appears as a promising therapy for MM patients, and the roles of BTK in the development of bone resorption by osteoclasts, as well as in cell migration, are characteristics that support BTK's research in the context of MM development [108,110–113].

BTK belongs to the Tec tyrosine kinase family that is involved in the B-cell antigen receptor (BCR) signaling pathway, being related to the survival, proliferation, and progression of malignancies in these cells. In MM, BTK is related to drug resistance, bone disease, and increased cell proliferation [114]. BTK activity, together with tyrosine phosphorylation, triggers the action of protein kinase B (AKT) which in turn will mediate transcription factors for proliferation, differentiation, and signaling cascades for survival—RAS/RAF/MEK/ERK and PI3K/AKT/mTOR (Figure 2) [110,114–117].

In the four studies presented in Table 1 in which ibrutinib was used, satisfactory results were reported, reaching conclusions where the clinical response to the use of ibrutinib encourages its use. This can also be seen in the statistical data of these articles, such as ORR above 60% [91,92], clinical response of 57% [93], and CBR of 28% [94]. The number of patients presented in the studies totaled 268, with an average age above 60 years. The preferred dose of ibrutinib was 840 mg, which is the limit dose for patients with MM, in addition to being a higher dose than that used in the treatment of other diseases such as lymphoma and chronic lymphocytic leukemia (CLL), which already have approved doses of 560 and 420 mg, respectively. It is worth mentioning that patients with CLL do not

usually use doses of 840 mg due to the risk of discontinuation caused by adverse effects (AEs) [118].



**Figure 2.** Bruton’s tyrosine kinase (BTK) survival and proliferation pathways and interaction with ibrutinib. In multiple myeloma (MM), B-cell receptors of malignant plasma cells signal for BTK cascade to begin, which is highly overexpressed and induces survival and proliferation of neoplastic clones. Downstream activity happens mainly through phospholipases which catalyze formation of IP3 (inositol 1-4-5 trisphosphate) and DAG (diacylglycerol), being effectors of intracellular calcium signaling pathways, in the case of IP3, and NFκB and MAPK signaling pathways, in the case of DAG. Inhibition of BTK by ibrutinib, however, can drastically disrupt the metabolism of MM cells and happens through the covalent and irreversible interaction of ibrutinib with the cysteine residue on position 481 of the BTK active domain. Created with BioRender.com.

All four studies [91–94] utilized drugs which are standards for MM therapies in combination with ibrutinib, varying between carfilzomib and bortozomib, but the association of ibrutinib with dexamethasone was unanimous among all groups. The association of the BTK inhibitor with other drugs seeks to potentiate the therapeutic action and increase rates such as overall response rates (ORR) and progression-free survival (PFS) [94]. This association is also observed in cases of CLL, since BTKis in monotherapy are not enough to obtain profound responses and are therefore used in combination with other drugs to increase

efficiency and not lose their effects due to resistance mechanisms [103,105]. In the study carried out by Richardson et al. [94], the combination of ibrutinib with dexamethasone demonstrated better results when compared to ibrutinib monotherapy. Chari et al. [91] observed that the combination of ibrutinib with carfilzomib and dexamethasone showed a promising response.

In studies using ibrutinib, among the AEs suffered by patients, the presence of anemia, diarrhea, and thrombocytopenia was constant [91–94]. AEs related to BTKi inhibitors are still being described, however, cardiac effects are the main concern due to the risk of combining these with hemorrhagic effects [108]. In *in vitro* studies, ibrutinib has already been demonstrated to interact with collagen-dependent platelet activation and von Willebrand factor, and it has been linked to an increased incidence of ventricular arrhythmia, hypertension, and neutropenia [110,111,118,119].

Dickerson et al. [54] observe that 78.3% of the patients who were using ibrutinib developed or worsened hypertension in an average period of 30 months. Although the causal relationship between ibrutinib and cardiotoxicity has not yet been fully elucidated, there are some theories, one of which would be the ability of ibrutinib to bind with other Tec kinases [120]. Despite cases of cardiotoxicity such as atrial fibrillation (AF), as long as the patient is benefiting from the therapy, they may continue with the treatment, with follow-up and medication to control the possible AEs. Next-generation BTK inhibitors, with less capacity to cause cardiotoxicity, are being studied and considered for MM treatment [120–122].

## 5. Clinical Perspectives with Other TKIs

In general, the use of tyrosine kinase inhibitors alone does not present a satisfactory response in patients with refractory MM [123]. The use of sorafenib alone in 7 out of 11 patients did not stop progression of MM, presenting a PFS of 2.6 months [100], while the isolated use of tivantinib was shown to be well tolerated, but in a clinical trial with 11 patients the agent was only able to stabilize 4 of 11 (36%) patients with progressive myeloma [124].

Other studies show that isolated administration of trametinib and afuresertib presented a significant clinical improvement in patients with MM, but when they are associated with other medications patients have even better responses [125,126]. Since trametinib is a drug also used to treat melanoma, its mechanism is based on MEK inhibition [127] and afuresertib is an AKT inhibitor that can also be used in the treatment of ovarian cancer [128]. However, the association between these two kinase inhibitors for the treatment of refractory MM patients performed in the study by Tolcher et al. [99] did not show such promising results, because despite having obtained maximum tolerated dose (MTD) values, these were compatible with subtherapeutic doses, thus, rendering the maintenance of the drugs in clinically significant concentrations for a long period of time impossible due to the AEs.

In the study carried out by Scheid et al. [101], the activity of dovitinib, which acts on the fibroblast growth factor receptor 3 (*FGFR3*), was evaluated in MM patients. *FGFR3* is an RTK of the FGFR family that is responsible for cell growth, differentiation, and migration in a wide variety of cell types and is present in MM and a variety of cancers. Upon ligand stimulation, a dimerization of the receptor occurs followed by transphosphorylation of tyrosine residues in the intracellular domain signaling mainly through extracellular signal-regulated kinase (ERK) 1 and 2 pathways, PI3K and PLC [129–134].

Better results from dovitinib were observed in patients with MM with the presence of t(4;14). This translocation is associated with a worse prognosis, causing the overexpression of the *MMSET* (multiple myeloma SET domain protein) and *FGFR3* genes [135,136]. Thus, the interaction between genetic abnormalities can be further explored, bringing new insights into personalized therapy.

It was possible to perceive a wide variety of occurrences in the AEs manifested by the patients participating in the analyzed studies. In general, the most recurrent AEs were diarrhea, nausea, fatigue, dermal toxicity, anemia, leukopenia, thrombocytopenia, infections, hypertension, and congestive heart failure [95–100].

Due to many clinical difficulties in the treatment of refractory MM, it is important to point out that the search for newer effective therapies extends also to the promising use of TKIs, which demonstrated the positive ability to prevent the progression of the disease in several studies described here. However, it is worth emphasizing the importance of follow-up studies and clinical trials with different drug combinations to obtain better clinical results and avoiding AEs [137].

A new alternative to this would be other BTK inhibitors that are already approved by the FDA and even those in the study phase. Ibrutinib, despite its satisfactory results, presents the problem, already discussed, regarding the AE profile and its susceptibility to resistance pathways. However, since its mechanism of action demonstrates benefits, drugs that act in a similar way appear as a good proposal for future research and treatment. An example would be zanubrutinib and acalabrutinib, which are already approved by the FDA, and despite having irreversible links in their sites of action, are able to be more selective and show fewer problems related to platelet dysfunction and bleeding. Another proposal that has been showing good prospects is the non-covalent, reversible BTK inhibitors, that, among their advantages, have a greater selectivity for the site of action and are also effective in patients with resistance to ibrutinib [138–141].

## 6. Conclusions

In this review, we observed that among the TKIs tested in the last 10 years for the treatment of refractory MM, Ibrutinib was the most used and presented better clinical results, mainly when administered in association with other drugs to avoid the emergence of resistance mechanisms that have already been found in other hematological neoplasms. Although AEs emerging from TKI's clinical administration is a major problem, when properly addressed and managed, treatment-emergent AEs are not considered serious, and the patient benefit versus risk ratio must be measured and taken into account individually from case to case.

**Author Contributions:** Invitation received, C.B.M. and C.A.M.-N.; conceptualization, I.V.B., C.B.M., F.M.C.d.P.P. and C.A.M.-N.; provision of data and sub-sequent analysis and interpretation, I.V.B., C.B.M., D.B.A., F.M.C.d.P.P., R.B.G., L.d.C.P., D.d.S.O., R.M.R., G.S.L., M.O.d.M.F., M.E.A.d.M., E.H.C.d.O. and A.S.K.; writing—original draft preparation, I.V.B., C.B.M., D.B.A., F.M.C.d.P.P., R.B.G. and C.A.M.-N.; writing—review and editing, I.V.B., C.B.M., D.B.A. and C.A.M.-N.; funding acquisition, A.S.K., E.H.C.d.O. and C.A.M.-N. All authors have read and agreed to the published version of the manuscript.

**Funding:** This study was supported by Brazilian funding agencies: Coordination for the Improvement of Higher Education Personnel (CAPES; to C.B.M), National Council of Technological and Scientific Development (CNPq grant number 404213/2021-9 to C.A.M.-N.; and Productivity in Research PQ scholarships to M.O.d.M.F., M.E.A.d.M., R.C.M., E.H.C.d.O. and A.S.K.), Cearense Foundation of Scientific and Technological Support (FUNCAP grant number P20-0171-00078.01.00/20 to F.M.C.d.P.P., M.O.d.M.F. and to C.A.M.-N.) and we also thank PROPEP/UFPB for publication payment.

**Conflicts of Interest:** The authors declare no conflict of interest. The funders had no role in the design of the study; in the collection, analyses, or data interpretation; in the writing of the manuscript, or in the decision to publish the results.

## References

1. Tsang, M.; Le, M.; Ghazawi, F.M.; Cyr, J.; Alakel, A.; Rahme, E.; Lagacé, F.; Netchiporouk, E.; Moreau, L.; Zubarev, A.; et al. Multiple Myeloma Epidemiology and Patient Geographic Distribution in Canada: A Population Study. *Cancer* **2019**, *125*, 2435–2444. [CrossRef] [PubMed]
2. Padala, S.A.; Barsouk, A.; Barsouk, A.; Rawla, P.; Vakiti, A.; Kolhe, R.; Kota, V.; Ajebo, G.H. Epidemiology, Staging, and Management of Multiple Myeloma. *Med. Sci.* **2021**, *9*, 3. [CrossRef] [PubMed]
3. Bird, S.; Cairns, D.; Menzies, T.; Boyd, K.; Davies, F.; Cook, G.; Drayson, M.; Gregory, W.; Jenner, M.; Jones, J.; et al. Sex Differences in Multiple Myeloma Biology but Not Clinical Outcomes: Results from 3894 Patients in the Myeloma XI Trial. *Clin. Lymphoma Myeloma Leuk.* **2021**, *21*, 667–675. [CrossRef] [PubMed]

4. Marinac, C.R.; Ghobrial, I.M.; Birmann, B.M.; Soiffer, J.; Rebbeck, T.R. Dissecting Racial Disparities in Multiple Myeloma. *Blood Cancer J.* **2020**, *10*, 19. [CrossRef]
5. Brigle, K.; Rogers, B. Pathobiology and Diagnosis of Multiple Myeloma. *Semin. Oncol. Nurs.* **2017**, *33*, 225–236. [CrossRef]
6. Cowan, A.J.; Green, D.J.; Kwok, M.; Lee, S.; Coffey, D.G.; Holmberg, L.A.; Tuazon, S.; Gopal, A.K.; Libby, E.N. Diagnosis and Management of Multiple Myeloma: A Review. *JAMA J. Am. Med. Assoc.* **2022**, *327*, 464–477. [CrossRef]
7. Firth, J. Haematology: Multiple Myeloma. *Clin. Med.* **2019**, *19*, 58–60. [CrossRef]
8. Joshi, H.; Lin, S.; Fei, K.; Renteria, A.S.; Jacobs, H.; Mazumdar, M.; Jagannath, S.; Bickell, N.A. Multiple Myeloma, Race, Insurance and Treatment. *Cancer Epidemiol.* **2021**, *73*, 101974. [CrossRef]
9. Rajkumar, S.V. Multiple Myeloma: 2022 Update on Diagnosis, Risk Stratification, and Management. *Am. J. Hematol.* **2022**, *97*, 1086–1107. [CrossRef]
10. Landgren, O.; Weiss, B.M. Patterns of Monoclonal Gammopathy of Undetermined Significance and Multiple Myeloma in Various Ethnic/Racial Groups: Support for Genetic Factors in Pathogenesis. *Leukemia* **2009**, *23*, 1691–1697. [CrossRef]
11. Bunce, C.M.; Drayson, M.T. Dissecting Racial Disparities in Multiple Myeloma—Clues from Differential Immunoglobulin Levels. *Blood Cancer J.* **2020**, *10*, 44. [CrossRef] [PubMed]
12. Joshua, D.E.; Bryant, C.; Dix, C.; Gibson, J.; Ho, J. Biology and Therapy of Multiple Myeloma. *Med. J. Aust.* **2019**, *210*, 375–380. [CrossRef] [PubMed]
13. Huang, R.; Zhou, P.K. DNA Damage Repair: Historical Perspectives, Mechanistic Pathways and Clinical Translation for Targeted Cancer Therapy. *Signal Transduct. Target. Ther.* **2021**, *6*, 254. [CrossRef] [PubMed]
14. Castaneda, O.; Baz, R. Multiple Myeloma Genomics—A Concise Review. *Acta Med. Acad.* **2019**, *48*, 57–67. [CrossRef] [PubMed]
15. Wallington-Beddoe, C.T.; Mynott, R.L. Prognostic and Predictive Biomarker Developments in Multiple Myeloma. *J. Hematol. Oncol.* **2021**, *14*, 151. [CrossRef] [PubMed]
16. Kumar, S.K.; Rajkumar, V.; Kyle, R.A.; van Duin, M.; Sonneveld, P.; Mateos, M.-V.; Gay, F.; Anderson, K.C. Multiple Myeloma. *Nat. Rev. Dis. Primers* **2017**, *3*, 17046. [CrossRef]
17. Manier, S.; Salem, K.Z.; Park, J.; Landau, D.A.; Getz, G.; Ghobrial, I.M. Genomic Complexity of Multiple Myeloma and Its Clinical Implications. *Nat. Rev. Clin. Oncol.* **2017**, *14*, 100–113. [CrossRef]
18. Zingone, A.; Kuehl, W.M. Pathogenesis of Monoclonal Gammopathy of Undetermined Significance and Progression to Multiple Myeloma. *Semin. Hematol.* **2011**, *48*, 4–12. [CrossRef]
19. Furukawa, Y.; Kikuchi, J. Molecular Basis of Clonal Evolution in Multiple Myeloma. *Int. J. Hematol.* **2020**, *111*, 496–511. [CrossRef]
20. Barwick, B.G.; Gupta, V.A.; Vertino, P.M.; Boise, L.H. Cell of Origin and Genetic Alterations in the Pathogenesis of Multiple Myeloma. *Front. Immunol.* **2019**, *10*, 1121. [CrossRef]
21. Maura, F.; Rustad, E.H.; Boyle, E.M.; Morgan, G.J. Reconstructing the Evolutionary History of Multiple Myeloma. *Best Pr. Res. Clin. Haematol.* **2020**, *33*, 101145. [CrossRef] [PubMed]
22. Dispenzieri, A.; Katzmann, J.A.; Kyle, R.A.; Larson, D.R.; Melton, L.J.; Colby, C.L.; Therneau, T.M.; Clark, R.; Kumar, S.K.; Bradwell, A.; et al. Prevalence and Risk of Progression of Light-Chain Monoclonal Gammopathy of Undetermined Significance: A Retrospective Population-Based Cohort Study. *Lancet* **2010**, *375*, 1721–1728. [CrossRef]
23. Kyle, R.A.; Therneau, T.M.; Rajkumar, S.V.; Larson, D.R.; Plevak, M.F.; Offord, J.R.; Dispenzieri, A.; Katzmann, J.A.; Melton, L.J. Prevalence of Monoclonal Gammopathy of Undetermined Significance. *N. Engl. J. Med.* **2006**, *354*, 1362–1369. [CrossRef] [PubMed]
24. Kyle, R.A.; Therneau, T.M.; Rajkumar, S.V.; Offord, J.R.; Larson, D.R.; Plevak, M.F.; Melton, L.J. A Long-Term Study of Prognosis in Monoclonal Gammopathy of Undetermined Significance. *N. Engl. J. Med.* **2002**, *346*, 564–569. [CrossRef]
25. Greenberg, A.J.; Vachon, C.M.; Rajkumar, S. v Disparities in the Prevalence, Pathogenesis and Progression of Monoclonal Gammopathy of Undetermined Significance and Multiple Myeloma between Blacks and Whites. *Leukemia* **2012**, *26*, 609–614. [CrossRef]
26. Lakshman, A.; Paul, S.; Rajkumar, S.V.; Ketterling, R.P.; Greipp, P.T.; Dispenzieri, A.; Gertz, M.A.; Buadi, F.K.; Lacy, M.Q.; Dingli, D.; et al. Prognostic Significance of Interphase FISH in Monoclonal Gammopathy of Undetermined Significance. *Leukemia* **2018**, *32*, 1811–1815. [CrossRef]
27. Neben, K.; Jauch, A.; Hielscher, T.; Hillengass, J.; Lehnert, N.; Seckinger, A.; Granzow, M.; Raab, M.S.; Ho, A.D.; Goldschmidt, H.; et al. Progression in Smoldering Myeloma Is Independently Determined by the Chromosomal Abnormalities Del(17p), t(4;14), Gain 1q, Hyperdiploidy, and Tumor Load. *J. Clin. Oncol.* **2013**, *31*, 4325–4332. [CrossRef]
28. Rajkumar, S.V.; Gupta, V.; Fonseca, R.; Dispenzieri, A.; Gonsalves, W.I.; Larson, D.; Ketterling, R.P.; Lust, J.A.; Kyle, R.A.; Kumar, S.K. Impact of Primary Molecular Cytogenetic Abnormalities and Risk of Progression in Smoldering Multiple Myeloma. *Leukemia* **2013**, *27*, 1738–1744. [CrossRef]
29. Avet-Loiseau, H.; Attal, M.; Moreau, P.; Charbonnel, C.; Garban, F.; Hulin, C.; Leyvraz, S.; Michallet, M.; Yakoub-Agha, I.; Garderet, L.; et al. Genetic Abnormalities and Survival in Multiple Myeloma: The Experience of the Intergroupe Francophone Du Myélome. *Blood* **2007**, *109*, 3489–3495. [CrossRef]
30. Chretien, M.-L.; Corre, J.; Lauwers-Cances, V.; Magrangeas, F.; Cleynen, A.; Yon, E.; Hulin, C.; Leleu, X.; Orsini-Piocelle, F.; Blade, J.-S.; et al. Understanding the Role of Hyperdiploidy in Myeloma Prognosis: Which Trisomies Really Matter? *Blood* **2015**, *126*, 2713–2719. [CrossRef]



31. Willenbacher, W.; Seeber, A.; Steiner, N.; Willenbacher, E.; Gatalica, Z.; Swensen, J.; Kimbrough, J.; Vranic, S. Towards Molecular Profiling in Multiple Myeloma: A Literature Review and Early Indications of Its Efficacy for Informing Treatment Strategies. *Int. J. Mol. Sci.* **2018**, *19*, 2087. [CrossRef] [PubMed]
32. Ziogas, D.C.; Dimopoulos, M.A.; Kastritis, E. Prognostic Factors for Multiple Myeloma in the Era of Novel Therapies. *Expert Rev. Hematol.* **2018**, *11*, 863–879. [CrossRef] [PubMed]
33. Pawlyn, C.; Davies, F.E. Toward Personalized Treatment in Multiple Myeloma Based on Molecular Characteristics. *Blood* **2019**, *133*, 660–675. [CrossRef]
34. Hanamura, I. [Advances in Multiple Myeloma Molecular Biology Research]. [*Rinsho Ketsueki*] *Jpn. J. Clin. Hematol.* **2019**, *60*, 1236–1242.
35. Rajkumar, S.V. Multiple Myeloma: 2020 Update on Diagnosis, Risk-stratification and Management. *Am. J. Hematol.* **2020**, *95*, 548–567. [CrossRef] [PubMed]
36. Usmani, S.Z.; Hoering, A.; Cavo, M.; Miguel, J.S.; Goldschmidt, H.; Hajek, R.; Turesson, I.; Lahuerta, J.J.; Attal, M.; Barlogie, B.; et al. Clinical Predictors of Long-Term Survival in Newly Diagnosed Transplant Eligible Multiple Myeloma—An IMWG Research Project. *Blood Cancer J.* **2018**, *8*, 123. [CrossRef] [PubMed]
37. Child, J.A.; Morgan, G.J.; Davies, F.E.; Owen, R.G.; Bell, S.E.; Hawkins, K.; Brown, J.; Drayson, M.T.; Selby, P.J. High-Dose Chemotherapy with Hematopoietic Stem-Cell Rescue for Multiple Myeloma. *N. Engl. J. Med.* **2003**, *348*, 1875–1883. [CrossRef]
38. Rajkumar, S.V. Multiple Myeloma: Every Year a New Standard? *Hematol. Oncol.* **2019**, *37*, 62–65. [CrossRef]
39. Gonsalves, W.I.; Buadi, F.K.; Ailawadhi, S.; Bergsagel, P.L.; Chanan Khan, A.A.; Dingli, D.; Dispenzieri, A.; Fonseca, R.; Hayman, S.R.; Kapoor, P.; et al. Utilization of Hematopoietic Stem Cell Transplantation for the Treatment of Multiple Myeloma: A Mayo Stratification of Myeloma and Risk-Adapted Therapy (MSMART) Consensus Statement. *Bone Marrow Transplant.* **2019**, *54*, 353–367. [CrossRef]
40. Saad, A.; Mahindra, A.; Zhang, M.-J.; Zhong, X.; Costa, L.J.; Dispenzieri, A.; Drobyski, W.R.; Freytes, C.O.; Gale, R.P.; Gasparetto, C.J.; et al. Hematopoietic Cell Transplant Comorbidity Index Is Predictive of Survival after Autologous Hematopoietic Cell Transplantation in Multiple Myeloma. *Biol. Blood Marrow Transplant.* **2014**, *20*, 402–408.e1. [CrossRef]
41. Rajkumar, S.V.; Sonneveld, P. Front-Line Treatment in Younger Patients with Multiple Myeloma. *Semin. Hematol.* **2009**, *46*, 118–126. [CrossRef]
42. Hus, I.; Mańko, J.; Jawniak, D.; Jurczyszyn, A.; Charliński, G.; Poniewierska-Jasak, K.; Usnarska-Zubkiewicz, L.; Sawicki, M.; Druzd-Sitek, A.; Świdarska, A.; et al. High Efficacy and Safety of VTD as an Induction Protocol in Patients with Newly Diagnosed Multiple Myeloma Eligible for High Dose Therapy and Autologous Stem Cell Transplantation: A Report of the Polish Myeloma Study Group. *Oncol. Lett.* **2019**, *18*, 5811–5820. [CrossRef]
43. Attal, M.; Lauwers-Cances, V.; Hulin, C.; Leleu, X.; Caillot, D.; Escoffre, M.; Arnulf, B.; Macro, M.; Belhadj, K.; Garderet, L.; et al. Lenalidomide, Bortezomib, and Dexamethasone with Transplantation for Myeloma. *N. Engl. J. Med.* **2017**, *376*, 1311–1320. [CrossRef] [PubMed]
44. al Hamed, R.; Bazarbachi, A.H.; Malard, F.; Harousseau, J.-L.; Mohty, M. Current Status of Autologous Stem Cell Transplantation for Multiple Myeloma. *Blood Cancer J.* **2019**, *9*, 44. [CrossRef] [PubMed]
45. Cavo, M.; Tacchetti, P.; Patriarca, F.; Petrucci, M.T.; Pantani, L.; Galli, M.; di Raimondo, F.; Crippa, C.; Zamagni, E.; Palumbo, A.; et al. Bortezomib with Thalidomide plus Dexamethasone Compared with Thalidomide plus Dexamethasone as Induction Therapy before, and Consolidation Therapy after, Double Autologous Stem-Cell Transplantation in Newly Diagnosed Multiple Myeloma: A Randomised Phase 3 Study. *Lancet* **2010**, *376*, 2075–2085. [CrossRef]
46. Ghandili, S.; Weisel, K.C.; Bokemeyer, C.; Leyboldt, L.B. Current Treatment Approaches to Newly Diagnosed Multiple Myeloma. *Oncol. Res. Treat.* **2021**, *44*, 690–699. [CrossRef] [PubMed]
47. Attal, M.; Harousseau, J.-L.; Stoppa, A.-M.; Sotto, J.-J.; Fuzibet, J.-G.; Rossi, J.-F.; Casassus, P.; Maisonneuve, H.; Facon, T.; Ifrah, N.; et al. A Prospective, Randomized Trial of Autologous Bone Marrow Transplantation and Chemotherapy in Multiple Myeloma. *N. Engl. J. Med.* **1996**, *335*, 91–97. [CrossRef] [PubMed]
48. Ito, S. Proteasome Inhibitors for the Treatment of Multiple Myeloma. *Cancers* **2020**, *12*, 265. [CrossRef]
49. Hideshima, T.; Mitsiades, C.; Akiyama, M.; Hayashi, T.; Chauhan, D.; Richardson, P.; Schlossman, R.; Podar, K.; Munshi, N.C.; Mitsiades, N.; et al. Molecular Mechanisms Mediating Antimyeloma Activity of Proteasome Inhibitor PS-341. *Blood* **2003**, *101*, 1530–1534. [CrossRef]
50. Besse, A.; Besse, L.; Kraus, M.; Mendez-Lopez, M.; Bader, J.; Xin, B.T.; de Bruin, G.; Maurits, E.; Overkleeft, H.S.; Driessen, C. Proteasome Inhibition in Multiple Myeloma: Head-to-Head Comparison of Currently Available Proteasome Inhibitors. *Cell Chem. Biol.* **2019**, *26*, 340–351.e3. [CrossRef]
51. Niewerth, D.; Jansen, G.; Assaraf, Y.G.; Zweegman, S.; Kaspers, G.J.L.; Cloos, J. Molecular Basis of Resistance to Proteasome Inhibitors in Hematological Malignancies. *Drug Resist. Updates* **2015**, *18*, 18–35. [CrossRef] [PubMed]
52. Adams, J. The Proteasome: A Suitable Antineoplastic Target. *Nat. Rev. Cancer* **2004**, *4*, 349–360. [CrossRef] [PubMed]
53. Nunes, A.T.; Annunziata, C.M. Proteasome Inhibitors: Structure and Function. *Semin. Oncol.* **2017**, *44*, 377–380. [CrossRef] [PubMed]
54. Gandolfi, S.; Laubach, J.P.; Hideshima, T.; Chauhan, D.; Anderson, K.C.; Richardson, P.G. The Proteasome and Proteasome Inhibitors in Multiple Myeloma. *Cancer Metastasis Rev.* **2017**, *36*, 561–584. [CrossRef]

55. Groen, K.; van de Donk, N.W.C.J.; Stege, C.A.M.; Zweegman, S.; Nijhof, I.S. Carfilzomib for Relapsed and Refractory Multiple Myeloma. *Cancer Manag. Res.* **2019**, *11*, 2663–2675. [CrossRef]
56. Tan, C.R.C.; Abdul-Majeed, S.; Cael, B.; Barta, S.K. Clinical Pharmacokinetics and Pharmacodynamics of Bortezomib. *Clin. Pharmacokinet.* **2018**, *58*, 157–168. [CrossRef]
57. Zinatizadeh, M.R.; Schock, B.; Chalbatani, G.M.; Zarandi, P.K.; Jalali, S.A.; Miri, S.R. The Nuclear Factor Kappa B (NF-KB) Signaling in Cancer Development and Immune Diseases. *Genes Dis.* **2021**, *8*, 287–297. [CrossRef]
58. Chauhan, D.; Bianchi, G.; Anderson, K.C. Targeting the UPS as Therapy in Multiple Myeloma. *BMC Biochem.* **2008**, *9*, S1. [CrossRef]
59. Richardson, P.G.; Sonneveld, P.; Schuster, M.W.; Irwin, D.; Stadtmauer, E.A.; Facon, T.; Harousseau, J.-L.; Ben-Yehuda, D.; Lonial, S.; Goldschmidt, H.; et al. Bortezomib or High-Dose Dexamethasone for Relapsed Multiple Myeloma. *N. Engl. J. Med.* **2005**, *352*, 2487–2498. [CrossRef]
60. Richardson, P.G.; Zweegman, S.; O'Donnell, E.K.; Laubach, J.P.; Raje, N.; Voorhees, P.; Ferrari, R.H.; Skacel, T.; Kumar, S.K.; Lonial, S. Ixazomib for the Treatment of Multiple Myeloma. *Expert Opin. Pharmacother.* **2018**, *19*, 1949–1968. [CrossRef]
61. Touzeau, C.; Moreau, P. Ixazomib in the Management of Relapsed Multiple Myeloma. *Future Oncol.* **2018**, *14*, 2013–2020. [CrossRef]
62. Zanwar, S.; Abeykoon, J.P.; Kapoor, P. Ixazomib: A Novel Drug for Multiple Myeloma. *Expert Rev. Hematol.* **2018**, *11*, 761–771. [CrossRef] [PubMed]
63. Lopez-Girona, A.; Heintel, D.; Zhang, L.-H.; Mendy, D.; Gaidarova, S.; Brady, H.; Bartlett, J.B.; Schafer, P.H.; Schreder, M.; Bolomsky, A.; et al. Lenalidomide Downregulates the Cell Survival Factor, Interferon Regulatory Factor-4, Providing a Potential Mechanistic Link for Predicting Response. *Br. J. Haematol.* **2011**, *154*, 325–336. [CrossRef] [PubMed]
64. Martinez-Høyer, S.; Karsan, A. Mechanisms of Lenalidomide Sensitivity and Resistance. *Exp. Hematol.* **2020**, *91*, 22–31. [CrossRef] [PubMed]
65. Agnarelli, A.; Chevassut, T.; Mancini, E.J. IRF4 in Multiple Myeloma—Biology, Disease and Therapeutic Target. *Leuk. Res.* **2018**, *72*, 52–58. [CrossRef] [PubMed]
66. Duffy, M.J.; O'Grady, S.; Tang, M.; Crown, J. MYC as a Target for Cancer Treatment. *Cancer Treat. Rev.* **2021**, *94*, 102154. [CrossRef] [PubMed]
67. Sampaio, E.P.; Sarno, E.N.; Galilly, R.; Cohn, Z.A.; Kaplan, G. Thalidomide Selectively Inhibits Tumor Necrosis Factor Alpha Production by Stimulated Human Monocytes. *J. Exp. Med.* **1991**, *173*, 699–703. [CrossRef]
68. Davies, F.E.; Raje, N.; Hideshima, T.; Lentzsch, S.; Young, G.; Tai, Y.-T.; Lin, B.; Podar, K.; Gupta, D.; Chauhan, D.; et al. Thalidomide and Immunomodulatory Derivatives Augment Natural Killer Cell Cytotoxicity in Multiple Myeloma. *Blood* **2001**, *98*, 210–216. [CrossRef]
69. Abe, Y.; Ishida, T. Immunomodulatory Drugs in the Treatment of Multiple Myeloma. *Jpn. J. Clin. Oncol.* **2019**, *49*, 695–702. [CrossRef]
70. Goldsmith, S.R.; Foley, N.; Schroeder, M.A. Daratumumab for the Treatment of Multiple Myeloma. *Drugs Today* **2021**, *57*, 591. [CrossRef]
71. Hosoya, H.; Sidana, S. Antibody-Based Treatment Approaches in Multiple Myeloma. *Curr. Hematol. Malign. Rep.* **2021**, *16*, 183–191. [CrossRef] [PubMed]
72. Nooka, A.K.; Kaufman, J.L.; Hofmeister, C.C.; Joseph, N.S.; Heffner, T.L.; Gupta, V.A.; Sullivan, H.C.; Neish, A.S.; Dhodapkar, M.V.; Lonial, S. Daratumumab in Multiple Myeloma. *Cancer* **2019**, *125*, 2364–2382. [CrossRef] [PubMed]
73. Kastiritis, E.; Palladini, G.; Minnema, M.C.; Wechalekar, A.D.; Jaccard, A.; Lee, H.C.; Sanchorawala, V.; Gibbs, S.; Mollee, P.; Venner, C.P.; et al. Daratumumab-Based Treatment for Immunoglobulin Light-Chain Amyloidosis. *N. Engl. J. Med.* **2021**, *385*, 46–58. [CrossRef] [PubMed]
74. Petrucci, M.T.; Vozella, F. The Anti-CD38 Antibody Therapy in Multiple Myeloma. *Cells* **2019**, *8*, 1629. [CrossRef]
75. Vozella, F.; Fazio, F.; Lapietra, G.; Petrucci, M.T.; Martinelli, G.; Cerchione, C. Monoclonal Antibodies in Multiple Myeloma. *Panminerva Med.* **2021**, *63*, 21–27. [CrossRef] [PubMed]
76. D'Agostino, M.; Boccadoro, M.; Smith, E.L. Novel Immunotherapies for Multiple Myeloma. *Curr. Hematol. Malign. Rep.* **2017**, *12*, 344–357. [CrossRef]
77. Minnie, S.A.; Hill, G.R. Immunotherapy of Multiple Myeloma. *J. Clin. Investig.* **2020**, *130*, 1565–1575. [CrossRef]
78. Tan, C.R.; Shah, U.A. Targeting BCMA in Multiple Myeloma. *Curr. Hematol. Malign. Rep.* **2021**, *16*, 367–383. [CrossRef]
79. Mateos, M.-V.; Masszi, T.; Grzasko, N.; Hansson, M.; Sandhu, I.; Pour, L.; Viterbo, L.; Jackson, S.R.; Stoppa, A.-M.; Gimsing, P.; et al. Impact of Prior Therapy on the Efficacy and Safety of Oral Ixazomib-Lenalidomide-Dexamethasone vs. Placebo-Lenalidomide-Dexamethasone in Patients with Relapsed/Refractory Multiple Myeloma in TOURMALINE-MM1. *Haematologica* **2017**, *102*, 1767–1775. [CrossRef]
80. Venezian Pova, L.; Ribeiro, C.H.C.; Silva, I.T. da Machine Learning Predicts Treatment Sensitivity in Multiple Myeloma Based on Molecular and Clinical Information Coupled with Drug Response. *PLoS ONE* **2021**, *16*, e0254596. [CrossRef]
81. Lemmon, M.A.; Schlessinger, J. Cell Signaling by Receptor Tyrosine Kinases. *Cell* **2010**, *141*, 1117–1134. [CrossRef] [PubMed]
82. Esteban-Villarrubia, J.; Soto-Castillo, J.J.; Pozas, J.; Román-Gil, M.S.; Orejana-Martín, I.; Torres-Jiménez, J.; Carrato, A.; Alonso-Gordo, T.; Molina-Cerrillo, J. Tyrosine Kinase Receptors in Oncology. *Int. J. Mol. Sci.* **2020**, *21*, 8529. [CrossRef] [PubMed]

83. Tibes, R.; Trent, J.; Kurzrock, R. Tyrosine Kinase Inhibitors and the Dawn of Molecular Cancer Therapeutics. *Annu. Rev. Pharmacol. Toxicol.* **2005**, *45*, 357–384. [CrossRef] [PubMed]
84. Krause, D.S.; van Etten, R.A. Tyrosine Kinases as Targets for Cancer Therapy. *N. Engl. J. Med.* **2005**, *353*, 172–187. [CrossRef] [PubMed]
85. Wang, Z.; Cole, P.A. Catalytic Mechanisms and Regulation of Protein Kinases. In *Methods in Enzymology*; Elsevier: Amsterdam, The Netherlands, 2014; Volume 548.
86. Regad, T. Targeting RTK Signaling Pathways in Cancer. *Cancers* **2015**, *7*, 1758–1784. [CrossRef]
87. Lind, J.; Czernilofsky, F.; Vallet, S.; Podar, K. Emerging Protein Kinase Inhibitors for the Treatment of Multiple Myeloma. *Expert Opin. Emerg. Drugs* **2019**, *24*, 133–152. [CrossRef]
88. Knösel, T.; Kampmann, E.; Kirchner, T.; Altendorf-Hofmann, A. Tyrosinkinase in Weichgewebstumoren. *Pathologe* **2014**, *35*, 198–201. [CrossRef]
89. Drake, J.M.; Lee, J.K.; Witte, O.N. Clinical Targeting of Mutated and Wild-Type Protein Tyrosine Kinases in Cancer. *Mol. Cell. Biol.* **2014**, *34*, 1722–1732. [CrossRef]
90. Jiao, Q.; Bi, L.; Ren, Y.; Song, S.; Wang, Q.; Wang, Y.S. Advances in Studies of Tyrosine Kinase Inhibitors and Their Acquired Resistance. *Mol. Cancer* **2018**, *17*, 1–12. [CrossRef]
91. Chari, A.; Larson, S.; Holkova, B.; Cornell, R.F.; Gasparetto, C.; Karanes, C.; Matous, J.V.; Niesvizky, R.; Valent, J.; Lunning, M.; et al. Phase 1 Trial of Ibrutinib and Carfilzomib Combination Therapy for Relapsed or Relapsed and Refractory Multiple Myeloma. *Leuk. Lymphoma* **2018**, *59*, 2588–2594. [CrossRef]
92. Chari, A.; Cornell, R.F.; Gasparetto, C.; Karanes, C.; Matous, J.V.; Niesvizky, R.; Lunning, M.; Usmani, S.Z.; Anderson, L.D.; Chhabra, S.; et al. Final Analysis of a Phase 1/2b Study of Ibrutinib Combined with Carfilzomib/Dexamethasone in Patients with Relapsed/Refractory Multiple Myeloma. *Hematol. Oncol.* **2020**, *38*, 353–362. [CrossRef]
93. Hajek, R.; Pour, L.; Ozcan, M.; Martín Sánchez, J.; García Sanz, R.; Anagnostopoulos, A.; Oriol, A.; Cascavilla, N.; Terjung, A.; Lee, Y.; et al. A Phase 2 Study of Ibrutinib in Combination with Bortezomib and Dexamethasone in Patients with Relapsed/Refractory Multiple Myeloma. *Eur. J. Haematol.* **2020**, *104*, 435–442. [CrossRef]
94. Richardson, P.G.; Bensinger, W.I.; Huff, C.A.; Costello, C.L.; Lendvai, N.; Berdeja, J.G.; Anderson, L.D.; Siegel, D.S.; Lebovic, D.; Jagannath, S.; et al. Ibrutinib Alone or with Dexamethasone for Relapsed or Relapsed and Refractory Multiple Myeloma: Phase 2 Trial Results. *Br. J. Haematol.* **2018**, *180*, 821–830. [CrossRef]
95. Berenson, J.R.; To, J.; Spektor, T.M.; Martinez, D.; Turner, C.; Sanchez, A.; Ghermezi, M.; Eades, B.M.; Swift, R.A.; Schwartz, G.; et al. A Phase I Study of Ruxolitinib, Lenalidomide, and Steroids for Patients with Relapsed/Refractory Multiple Myeloma. *Clin. Cancer Res.* **2020**, *26*, 2346–2353. [CrossRef] [PubMed]
96. Lendvai, N.; Yee, A.J.; Tsakos, I.; Alexander, A.; Devlin, S.M.; Hassoun, H.; Korde, N.; Lesokhin, A.M.; Landau, H.; Mailankody, S.; et al. Phase IB Study of Cabozantinib in Patients with Relapsed and/or Refractory Multiple Myeloma. *Blood* **2016**, *127*, 2355–2356. [CrossRef] [PubMed]
97. Zeidan, A.M.; Cook, R.J.; Bordoni, R.; Berenson, J.R.; Edenfield, W.J.; Mohan, S.; Zhou, G.; Asatiani, E.; Srinivas, N.; Savona, M.R. A Phase 1/2 Study of the Oral Janus Kinase 1 Inhibitors INCB052793 and Itacitinib Alone or in Combination with Standard Therapies for Advanced Hematologic Malignancies. *Clin. Lymphoma Myeloma Leuk.* **2022**, *22*, 523–534. [CrossRef] [PubMed]
98. Baljevic, M.; Zaman, S.; Baladandayuthapani, V.; Lin, Y.H.; de Partovi, C.M.; Berkova, Z.; Amini, B.; Thomas, S.K.; Shah, J.J.; Weber, D.M.; et al. Phase II Study of the C-MET Inhibitor Tivantinib (ARQ 197) in Patients with Relapsed or Relapsed/Refractory Multiple Myeloma. *Ann. Hematol.* **2017**, *96*, 977–985. [CrossRef]
99. Tolcher, A.W.; Patnaik, A.; Papadopoulos, K.P.; Rasco, D.W.; Becerra, C.R.; Allred, A.J.; Orford, K.; Aktan, G.; Ferron-Brady, G.; Ibrahim, N.; et al. Phase I Study of the MEK Inhibitor Trametinib in Combination with the AKT Inhibitor Afuresertib in Patients with Solid Tumors and Multiple Myeloma. *Cancer Chemother. Pharmacol.* **2015**, *75*, 183–189. [CrossRef]
100. Yordanova, A.; Hose, D.; Neben, K.; Witzens-Harig, M.; Gütgemann, I.; Raab, M.S.; Moehler, T.; Goldschmidt, H.; Schmidt-Wolf, I.G. Sorafenib in Patients with Refractory or Recurrent Multiple Myeloma. *Hematol. Oncol.* **2013**, *31*, 197–200. [CrossRef]
101. Scheid, C.; Reece, D.; Beksac, M.; Spencer, A.; Callander, N.; Sonneveld, P.; Kalimi, G.; Cai, C.; Shi, M.; Scott, J.W.; et al. Phase 2 Study of Dovitinib in Patients with Relapsed or Refractory Multiple Myeloma with or without t(4;14) Translocation. *Eur. J. Haematol.* **2015**, *95*, 316–324. [CrossRef]
102. Estupiñán, H.Y.; Boudierlique, T.; He, C.; Berglöf, A.; Gupta, D.; Saher, O.; Daza Cruz, M.Á.; Peña-Perez, L.; Yu, L.; Zain, R.; et al. Novel Mouse Model Resistant to Irreversible BTK Inhibitors: A Tool Identifying New Therapeutic Targets and Side Effects. *Blood Adv.* **2020**, *4*, 2439–2450. [CrossRef] [PubMed]
103. Ahn, I.E.; Brown, J.R. Targeting Bruton’s Tyrosine Kinase in CLL. *Front. Immunol.* **2021**, *12*, 687458. [CrossRef] [PubMed]
104. Munir, T.; Brown, J.R.; O’Brien, S.; Barrientos, J.C.; Barr, P.M.; Reddy, N.M.; Coutre, S.; Tam, C.S.; Mulligan, S.P.; Jaeger, U.; et al. Final Analysis from RESONATE: Up to Six Years of Follow-up on Ibrutinib in Patients with Previously Treated Chronic Lymphocytic Leukemia or Small Lymphocytic Lymphoma. *Am. J. Hematol.* **2019**, *94*, 1353–1363. [CrossRef]
105. Lipsky, A.; Lamanna, N. Managing Toxicities of Bruton Tyrosine Kinase Inhibitors. *Hematology* **2020**, *2020*, 336–345. [CrossRef] [PubMed]
106. Pan, Z.; Scheerens, H.; Li, S.-J.; Schultz, B.E.; Sprengeler, P.A.; Burrill, L.C.; Mendonca, R.V.; Sweeney, M.D.; Scott, K.C.K.; Grothaus, P.G.; et al. Discovery of Selective Irreversible Inhibitors for Bruton’s Tyrosine Kinase. *ChemMedChem* **2007**, *2*, 58–61. [CrossRef]

107. Bender, A.T.; Gardberg, A.; Pereira, A.; Johnson, T.; Wu, Y.; Grenningloh, R.; Head, J.; Morandi, F.; Haselmayer, P.; Liu-Bujalski, L. Ability of Bruton's Tyrosine Kinase Inhibitors to Sequester Y551 and Prevent Phosphorylation Determines Potency for Inhibition of Fc Receptor but Not B-Cell Receptor Signaling. *Mol. Pharmacol.* **2017**, *91*, 208–219. [CrossRef]
108. Pal Singh, S.; Dammeijer, F.; Hendriks, R.W. Role of Bruton's Tyrosine Kinase in B Cells and Malignancies. *Mol. Cancer* **2018**, *17*, 57, Erratum in *Mol. Cancer* **2019**, *18*, 79. [CrossRef]
109. Burger, J.A. Bruton Tyrosine Kinase Inhibitors. *Cancer J.* **2019**, *25*, 386–393. [CrossRef]
110. von Suskil, M.; Sultana, K.N.; Elbezanti, W.O.; Al-Odat, O.S.; Chitren, R.; Tiwari, A.K.; Challagundla, K.B.; Srivastava, S.K.; Jonnalagadda, S.C.; Budak-Alpdogan, T.; et al. Bruton's Tyrosine Kinase Targeting in Multiple Myeloma. *Int. J. Mol. Sci.* **2021**, *22*, 5707. [CrossRef]
111. Lampson, B.L.; Yu, L.; Glynn, R.J.; Barrientos, J.C.; Jacobsen, E.D.; Banerji, V.; Jones, J.A.; Walewska, R.; Savage, K.J.; Michaud, G.F.; et al. Ventricular Arrhythmias and Sudden Death in Patients Taking Ibrutinib. *Blood* **2017**, *129*, 2581–2584. [CrossRef]
112. Edwards, C.M. BTK Inhibition in Myeloma: Targeting the Seed and the Soil. *Blood* **2012**, *120*, 1757–1759. [CrossRef] [PubMed]
113. Tai, Y.T.; Chang, B.Y.; Kong, S.Y.; Fulciniti, M.; Yang, G.; Calle, Y.; Hu, Y.; Lin, J.; Zhao, J.J.; Cagnetta, A.; et al. Bruton Tyrosine Kinase Inhibition Is a Novel Therapeutic Strategy Targeting Tumor in the Bone Marrow Microenvironment in Multiple Myeloma. *Blood* **2012**, *120*, 1877–1887. [CrossRef] [PubMed]
114. Tai, Y.T.; Anderson, K.C. Bruton's Tyrosine Kinase: Oncotarget in Myeloma. *Oncotarget* **2012**, *3*, 913–914. [CrossRef] [PubMed]
115. Liu, Y.; Dong, Y.; Jiang, Q.L.; Zhang, B.; Hu, A.M. Bruton's Tyrosine Kinase: Potential Target in Human Multiple Myeloma. *Leuk. Lymphoma* **2014**, *55*, 177–181. [CrossRef]
116. Campbell, R.; Chong, G.; Hawkes, E.A. Novel Indications for Bruton's Tyrosine Kinase Inhibitors, beyond Hematological Malignancies. *J. Clin. Med.* **2018**, *7*, 62. [CrossRef]
117. Mohamed, A.J.; Yu, L.; Bäckesjö, C.M.; Vargas, L.; Faryal, R.; Aints, A.; Christensson, B.; Berglöf, A.; Vihinen, M.; Nore, B.F.; et al. Bruton's Tyrosine Kinase (Btk): Function, Regulation, and Transformation with Special Emphasis on the PH Domain. *Immunol. Rev.* **2009**, *228*, 58–73. [CrossRef]
118. de Weerd, I.; Koopmans, S.M.; Kater, A.P.; van Gelder, M. Incidence and Management of Toxicity Associated with Ibrutinib and Idelalisib: A Practical Approach. *Haematologica* **2017**, *102*, 1629–1639. [CrossRef]
119. Tang, C.P.S.; McMullen, J.; Tam, C. Cardiac Side Effects of Bruton Tyrosine Kinase (BTK) Inhibitors. *Leukemia and Lymphoma* **2018**, *59*. [CrossRef]
120. Ahn, I.E. Cardiovascular Adverse Events of Ibrutinib. *Blood* **2019**, *134*, 1881–1882. [CrossRef]
121. Dickerson, T.; Wiczer, T.; Waller, A.; Philippon, J.; Porter, K.; Haddad, D.; Guha, A.; Rogers, K.A.; Bhat, S.; Byrd, J.C.; et al. Hypertension and Incident Cardiovascular Events Following Ibrutinib Initiation. *Blood* **2019**, *134*, 1919–1928. [CrossRef]
122. Castillo, J.J.; Meid, K.; Gustine, J.N.; Leventoff, C.; White, T.; Flynn, C.A.; Sarosiek, S.; Demos, M.G.; Guerrera, M.L.; Kofides, A.; et al. Long-Term Follow-up of Ibrutinib Monotherapy in Treatment-Naive Patients with Waldenström Macroglobulinemia. *Leukemia* **2022**, *36*, 532–539. [CrossRef] [PubMed]
123. Srkalovic, G.; Hussein, M.A.; Hoering, A.; Zonder, J.A.; Popplewell, L.L.; Trivedi, H.; Mazzoni, S.; Sexton, R.; Orłowski, R.Z.; Barlogie, B. A Phase II Trial of BAY 43-9006 (Sorafenib) (NSC-724772) in Patients with Relapsing and Resistant Multiple Myeloma: SWOG S0434. *Cancer Med.* **2014**, *3*, 1275–1283. [CrossRef] [PubMed]
124. Orłowski, R.Z.; Zaman, S.; Thomas, S.K.; Alexanian, R.; Shah, J.J.; Weber, D.M.; Wang, M.; Holloway, A.N.; Baladandayuthapani, V.; Lin, H.Y.; et al. Phase II Study of The C-MET Inhibitor ARQ 197 (Tivantinib) In Patients With Relapsed Or Relapsed/Refractory Multiple Myeloma (RRMM). *Blood* **2013**, *122*, 1953. [CrossRef]
125. Spencer, A.; Yoon, S.S.; Harrison, S.J.; Morris, S.R.; Smith, D.A.; Brigandi, R.A.; Gauvin, J.; Kumar, R.; Opalinska, J.B.; Chen, C. The Novel AKT Inhibitor Afuresertib Shows Favorable Safety, Pharmacokinetics, and Clinical Activity in Multiple Myeloma. *Blood* **2014**, *124*, 2190–2195. [CrossRef] [PubMed]
126. Trudel, S.; Bahlis, N.J.; Venner, C.P.; Hay, A.E.; Kis, O.; Chow, S.; Li, Z.H.; Wei, E.N.; Wang, L.; Tran, C.; et al. Biomarker Driven Phase II Clinical Trial of Trametinib in Relapsed/Refractory Multiple Myeloma with Sequential Addition of the AKT Inhibitor, GSK2141795 at Time of Disease Progression to Overcome Treatment Failure: A Trial of the Princess Margaret Phase II Consortium. *Blood* **2016**, *128*, 4526. [CrossRef]
127. Hoffner, B.; Benchich, K. Trametinib: A Targeted Therapy in Metastatic Melanoma. *J. Adv. Pract. Oncol.* **2018**, *9*, 741. [CrossRef]
128. Blagden, S.P.; Hamilton, A.L.; Mileshekin, L.; Wong, S.; Michael, A.; Hall, M.; Goh, J.C.; Lisyanskaya, A.S.; DeSilvio, M.; Frangou, E.; et al. Phase IB Dose Escalation and Expansion Study of Akt Inhibitor Afuresertib with Carboplatin and Paclitaxel in Recurrent Platinum-Resistant Ovarian Cancer. *Clin. Cancer Res.* **2019**, *25*, 1472–1478. [CrossRef]
129. Moreau, P.; Attal, M.; Garban, F.; Hulin, C.; Facon, T.; Marit, G.; Michallet, M.; Doyen, C.; Leyvraz, S.; Mohty, M.; et al. Heterogeneity of t(4;14) in Multiple Myeloma. Long-Term Follow-up of 100 Cases Treated with Tandem Transplantation in IFM99 Trials. *Leukemia* **2007**, *21*, 2020–2024. [CrossRef]
130. Hart, K.C.; Robertson, S.C.; Donoghue, D.J. Identification of Tyrosine Residues in Constitutively Activated Fibroblast Growth Factor Receptor 3 Involved in Mitogenesis, Stat Activation, and Phosphatidylinositol 3-Kinase Activation. *Mol. Biol. Cell* **2001**, *12*, 931–942. [CrossRef] [PubMed]
131. Kanai, M.; Göke, M.; Tsunekawa, S.; Podolsky, D.K. Signal Transduction Pathway of Human Fibroblast Growth Factor Receptor 3. *J. Biol. Chem.* **1997**, *272*, 6621–6628. [CrossRef] [PubMed]

132. Xin, X.; Abrams, T.J.; Hollenbach, P.W.; Rendahl, K.G.; Tang, Y.; Oei, Y.A.; Embry, M.G.; Swinarski, D.E.; Garrett, E.N.; Pryer, N.K.; et al. CHIR-258 Is Efficacious in a Newly Developed Fibroblast Growth Factor Receptor 3-Expressing Orthotopic Multiple Myeloma Model in Mice. *Clin. Cancer Res.* **2006**, *12*, 4908–4915. [CrossRef] [PubMed]
133. Chell, V.; Balmanno, K.; Little, A.S.; Wilson, M.; Andrews, S.; Blockley, L.; Hampson, M.; Gavine, P.R.; Cook, S.J. Tumour Cell Responses to New Fibroblast Growth Factor Receptor Tyrosine Kinase Inhibitors and Identification of a Gatekeeper Mutation in FGFR3 as a Mechanism of Acquired Resistance. *Oncogene* **2013**, *32*, 3059–3070. [CrossRef] [PubMed]
134. Chesi, M.; Brents, L.A.; Ely, S.A.; Bais, C.; Robbiani, D.F.; Mesri, E.A.; Kuehl, W.M.; Bergsagel, P.L. Activated Fibroblast Growth Factor Receptor 3 Is an Oncogene That Contributes to Tumor Progression in Multiple Myeloma. *Blood* **2001**, *97*, 729–736. [CrossRef] [PubMed]
135. Chesi, M.; Bergsagel, P.L. Advances in the Pathogenesis and Diagnosis of Multiple Myeloma. *Int. J. Lab. Hematol.* **2015**, *37*, 108–114. [CrossRef]
136. Cardona-Benavides, I.J.; de Ramón, C.; Gutiérrez, N.C. Genetic Abnormalities in Multiple Myeloma: Prognostic and Therapeutic Implications. *Cells* **2021**, *10*, 336. [CrossRef]
137. Richter, J.; Ramasamy, K.; Rasche, L.; Bladé, J.; Zweegman, S.; Davies, F.; Dimopoulos, M. Management of Patients with Difficult-to-Treat Multiple Myeloma. *Futur. Oncol.* **2021**, *17*, 2089–2105. [CrossRef]
138. Palma, M.; Mulder, T.A.; Österborg, A. BTK Inhibitors in Chronic Lymphocytic Leukemia: Biological Activity and Immune Effects. *Front. Immunol.* **2021**, *12*, 686768. [CrossRef]
139. Brullo, C.; Villa, C.; Tasso, B.; Russo, E.; Spallarossa, A. Btk Inhibitors: A Medicinal Chemistry and Drug Delivery Perspective. *Int. J. Mol. Sci.* **2021**, *22*, 7641. [CrossRef]
140. Tasso, B.; Spallarossa, A.; Russo, E.; Brullo, C. The Development of Btk Inhibitors: A Five-Year Update. *Molecules* **2021**, *26*, 7411. [CrossRef]
141. Lewis, K.L.; Cheah, C.Y. Non-Covalent Btk Inhibitors—The New Btkids on the Block for b-Cell Malignancies. *J. Pers. Med.* **2021**, *11*, 764. [CrossRef]

## Article

# Anti-Survival Effect of SI306 and Its Derivatives on Human Glioblastoma Cells

Lorenzo Monteleone <sup>1,†</sup>, Barbara Marengo <sup>1,2,†</sup>, Francesca Musumeci <sup>3,†</sup>, Giancarlo Grossi <sup>3</sup>, Anna Carbone <sup>3</sup>, Giulia E. Valenti <sup>1</sup>, Cinzia Domenicotti <sup>1,2,\*</sup> and Silvia Schenone <sup>3</sup>

<sup>1</sup> Department of Experimental Medicine (DIMES), General Pathology Section, University of Genoa, 16132 Genoa, Italy; lorenzomonteleone94@gmail.com (L.M.); barbara.marengo@unige.it (B.M.); giuliaelda.valenti@edu.unige.it (G.E.V.)

<sup>2</sup> Inter-University Center for the Promotion of the 3Rs Principles in Teaching & Research (Centro 3R), 56122 Pisa, Italy

<sup>3</sup> Department of Pharmacy, University of Genoa, 16132 Genoa, Italy; francesca.musumeci@unige.it (F.M.); grossi@difar.unige.it (G.G.); carbone@difar.unige.it (A.C.); schenone@difar.unige.it (S.S.)

\* Correspondence: cinzia.domenicotti@unige.it; Tel.: +39-010-353-8830

† These authors contributed equally to this work.

**Abstract:** Glioblastoma (GBM) is the most common adult brain tumor and, although many efforts have been made to find valid therapies, the onset of resistance is the main cause of recurrence. Therefore, it is crucial to identify and target the molecular mediators responsible for GBM malignancy. In this context, the use of Src inhibitors such as SI306 (C1) and its prodrug (C2) showed promising results, suggesting that SI306 could be the lead compound useful to derivate new anti-GBM drugs. Therefore, a new prodrug of SI306 (C3) was synthesized and tested on CAS-1 and U87 human GBM cells by comparing its effect to that of C1 and C2. All compounds were more effective on CAS-1 than U87 cells, while C2 was the most active on both cell lines. Moreover, the anti-survival effect was associated with a reduction in the expression of epidermal growth factor receptor (EGFR)<sup>WT</sup> and EGFR-vIII in U87 and CAS-1 cells, respectively. Collectively, our findings demonstrate that all tested compounds are able to counteract GBM survival, further supporting the role of SI306 as progenitor of promising new drugs to treat malignant GBM.

**Keywords:** glioblastoma; Src; pyrazolo [3,4-*d*]pyrimidine scaffold; EGFR

**Citation:** Monteleone, L.; Marengo, B.; Musumeci, F.; Grossi, G.; Carbone, A.; Valenti, G.E.; Domenicotti, C.; Schenone, S. Anti-Survival Effect of SI306 and Its Derivatives on Human Glioblastoma Cells. *Pharmaceutics* **2022**, *14*, 1399. <https://doi.org/10.3390/pharmaceutics14071399>

Academic Editor: Gabriele Grassi

Received: 6 June 2022

Accepted: 30 June 2022

Published: 1 July 2022

**Publisher's Note:** MDPI stays neutral with regard to jurisdictional claims in published maps and institutional affiliations.

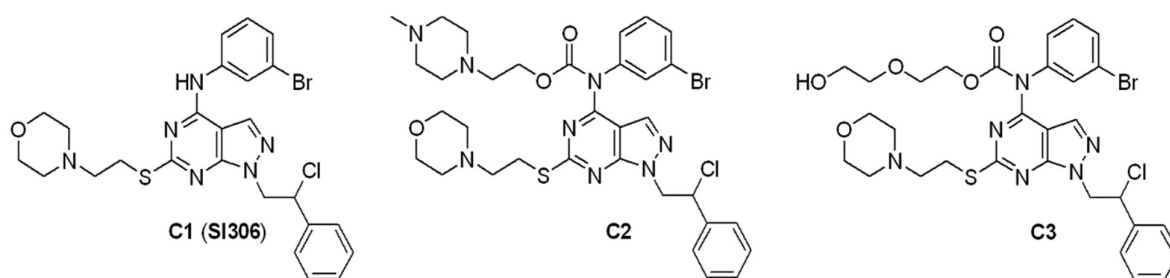


**Copyright:** © 2022 by the authors. Licensee MDPI, Basel, Switzerland. This article is an open access article distributed under the terms and conditions of the Creative Commons Attribution (CC BY) license (<https://creativecommons.org/licenses/by/4.0/>).

## 1. Introduction

Glioblastomas (GBM) are malignant and aggressive astrocytic tumors, classified grade IV according to the World Health Organization [1]. They are the most common adult brain tumors, with an annual incidence of about 1/33.330 and with a current median survival of 15 months [2].

Current therapy includes surgery, radiotherapy, and chemotherapy but, unfortunately, in many cases such approaches are ineffective and facilitate the onset of relapse and the development of therapy resistance [3]. Therefore, there is a great need to identify new treatments capable of improving the prognosis of patients. In recent years, several genetic alterations and pathways responsible for GBM malignancy were identified and indicated as targets for new therapies [4–6]. In this context, Src-Family Kinases (SFKs), having a key role in the development, tumorigenicity, invasion, and progression of GBM [7], have received particular attention. In this regard, our research group has recently developed new Src inhibitors endowed with a pyrazolo[3,4-*d*]pyrimidine scaffold [8–13]. Among this series of compounds, SI306 (compound 1, C1, Figure 1) showed significant efficacy against U87 human GBM cells [14–16]. Based on these successful results, we decided to study this compound further by synthesizing prodrugs potentially endowed with improved pharmacokinetic (PK) properties and testing them on U87 and CAS-1 GBM cells in order to evaluate their efficacy.



**Figure 1.** Structures of C1, C2, and C3.

In particular, we selected compound 2 (C2, Figure 1), an SI306 prodrug that already showed an improved activity in biological assays [13,16], and the ethylene glycol derivative 3 (C3, Figure 1) as a potential valuable prodrug of a new synthesis. Indeed, a careful analysis of the literature highlighted that introducing a poly(ethylene glycol) (PEG) chain can successfully modulate drug delivery [17]. As different studies pointed out that the activity of many small molecules is improved by PEGylation [18], we synthesized compound 3 (Figure 1), which bears two ethylene glycol units on the carbamate moiety. We chose this short PEG chain driven by the rationale to balance a feasible synthesis with the chance to afford a compound characterized by improved ADME (Absorption, Distribution, Metabolism, Excretion) properties. Compound 3, and previous analog compounds 1 and 2, were tested on CAS-1 and U87 cells, and their activities were compared.

The obtained results showed that all tested compounds exhibited a more significant anti-survival effect on CAS-1 than on U87 cells and that C2 was the most active on both cancer cell lines.

Given that Src has been demonstrated to interact and activate epidermal growth factor receptor (EGFR) [19,20], an oncogene frequently amplified and mutated in GBM [21–24], the action of SI306 (C1) and its derivatives (C2 and C3) on the expression of both wild type (wt) and mutated (vIII) EGFR was evaluated. In this regard, our results showed that CAS-1 cells express EGFR-vIII while U87 cells express EGFR<sup>WT</sup>. Moreover, 48 h exposure to the highest dose (10  $\mu$ M) of all inhibitors markedly reduced the expression of EGFR<sup>WT</sup> and EGFR-vIII in U87 and CAS-1 cells, respectively.

Collectively, our findings demonstrate that SI306 and its prodrugs are able to counteract GBM survival by inhibiting Src, as expected. Moreover, for the first time to our knowledge, we have shown that this event is accompanied by a reduction in EGFR<sup>WT</sup> and EGFR-vIII expression.

## 2. Materials and Methods

### 2.1. Chemistry

All commercially available chemicals were used as purchased from Sigma-Aldrich (St. Louis, MO, USA). DCM was dried over molecular sieves (3 Å, 10% *m/v*). TLC was carried out using Merck TLC silica gel 60 F254. Chromatographic purifications were performed on columns packed with Merck silica gel 60, 23–400 mesh, for flash technique. <sup>1</sup>H-NMR and <sup>13</sup>C-NMR spectra were recorded on a JEOL JNM ECZ-400S/L1 FT (400 MHz). Chemical shifts were reported relative to tetramethylsilane at 0.00 ppm. Elemental analysis for C, H, N, and S was determined using Thermo Scientific Flash 2000 and results were within  $\pm 0.4\%$  of the theoretical value. All target compounds possessed a purity of  $\geq 95\%$  verified by elemental analysis. Compounds 1 and 2 were previously synthesized by us [13,25,26].

### 2.2. Synthesis of 2-(2-hydroxyethoxy)ethyl (3-bromophenyl)(1-(2-chloro-2-phenylethyl)-6-((2-morpholinoethyl)thio)-1H-pyrazolo[3,4-d]pyrimidin-4-yl)carbamate (C3)

A solution of triphosgene (0.45 mmol, 133 mg) in anhydrous CH<sub>2</sub>Cl<sub>2</sub> (8 mL) was added dropwise to a mixture of NaHCO<sub>3</sub> (2.25 mmol, 189 mg) and N-(3-bromophenyl)-1-(2-chloro-2-phenylethyl)-6-((2-morpholinoethyl)thio)-1H-pyrazolo[3,4-d]pyrimidin-4-amine 1

(0.45 mmol, 258 mg) in anhydrous  $\text{CH}_2\text{Cl}_2$  (8 mL) precooled at  $0^\circ\text{C}$  in an ice bath. After 30 min, the reaction was allowed to warm to room temperature and stirred for 5 h. Then, a solution of ethylene glycol (20.00 mmol, 1.9 mL) in anhydrous  $\text{CH}_2\text{Cl}_2$  (8 mL) was added and the mixture stirred at room temperature for 16 h. Cold water (25 mL) was added, and the two phases were separated. The aqueous phase was extracted twice with  $\text{CH}_2\text{Cl}_2$  ( $2 \times 25$  mL). The organic phase was dried over anhydrous  $\text{Na}_2\text{SO}_4$  and evaporated. The crude oil was purified through two flash chromatographies on silica gel, eluting first with THF/EP 1:1 and then with ethyl acetate/acetone (1:1) affording the desired C3 as a pure light amber oil. Yield 54%.  $^1\text{H-NMR}$  ( $\text{CDCl}_3$ ):  $\delta$  2.48–2.57 (m, 6H,  $2\text{CH}_2\text{N}$  morph +  $\text{NCH}_2\text{CH}_2$ ), 2.98–3.13 (m, 2H,  $\text{CH}_2\text{S}$ ), 3.47 (t,  $J = 8$  Hz, 2H,  $\text{HOCH}_2\text{CH}_2\text{O}$ ), 3.64–3.72 (m, 8H,  $2\text{CH}_2\text{O}$  morph +  $\text{HOCH}_2 + \text{COO-CH}_2\text{CH}_2$ ), 4.41 (t,  $J = 4$  Hz, 2H,  $\text{COO-CH}_2$ ), 4.68–4.72 and 4.92–4.98 (2m, 2H,  $\text{CH}_2\text{N}$  pyraz), 5.48–5.52 (m, 1H,  $\text{CHCl}$ ), 7.16–7.18 (m, 1H Ar), 7.25–7.34 (m, 4H Ar), 7.41–7.43 (m, 3H Ar), 7.49–7.51 (m, 1H Ar), and 7.98 (s, 1H, H-3).  $^{13}\text{C-NMR}$  ( $\text{CDCl}_3$ ):  $\delta$  NMR (101 MHz),  $\delta = 31.87, 53.45, 53.93, 54.32, 57.66, 60.29, 61.70, 66.58, 66.82, 68.74, 72.62, 76.85, 77.16, 77.48, 103.66, 122.36, 127.44, 127.56, 128.88, 129.17, 130.49, 131.33, 131.93, 135.39, 137.88, 140.98, 153.45, 154.27, 156.07, \text{ and } 168.36$ . Anal. calcd. for  $\text{C}_{30}\text{H}_{34}\text{N}_6\text{O}_5\text{SClBr}$ : C 51.03, H 4.85, N 11.90, and S 4.54; found: C 50.77, H 5.19, N 11.57, and S 4.09.

### 2.3. Cell Cultures

U87 and CAS-1 human GBM cell lines were obtained from Ospedale Policlinico San Martino (Genova, Italy). Cells were periodically tested for mycoplasma contamination (Mycoplasma Reagent Set, Aurogene s.p.a, Pavia, Italy). Cells were maintained in DMEM low glucose medium (Euroclone SpA, Pavia, Italy) supplemented with 10% fetal bovine serum (FBS; Euroclone), 2 mM of glutamine (Euroclone).

### 2.4. Treatments

U87 and CAS-1 cells were treated with C1, C2, and C3 for 24, 48, and 72 h with increasing concentrations (1–10  $\mu\text{M}$ ) of each compound. The stock solutions of the three compounds were prepared in DMSO (Sigma-Aldrich Co., Saint Louis, MO, USA) and pilot experiments demonstrated that final DMSO doses did not affect any cell response analyzed.

### 2.5. Cell Viability Assay

Cell viability was determined by using the CellTiter 96<sup>®</sup> AQueous One Solution Cell Proliferation Assay (Promega, Madison, WI, USA), as previously described [27]. Briefly, cells ( $9 \times 10^4$  cells/well) were seeded in 96-well plates (Corning Incorporate, Corning, NY, USA) and then treated. Next, the cells were incubated with MTT solution according to manufacturer's instructions and the absorbance at 570/630 nm was recorded using a microplate reader (EL-808, BIO\_TEK Instruments Inc., Winooski, VT, USA). The relative IC50 values for were calculated by non-linear regression analysis using GraphPad Prism 6.0 software (GraphPad Software, La Jolla, CA, USA).

### 2.6. Blot Analyses

Immunoblots were performed according to standard methods [28] using rabbit antibody anti-human anti-Src (#2109), anti-Phospho-Src (Tyr527, #2105) corresponding in humans to tyrosine 530 residue, anti-Phospho-Src (Tyr416, #2101) corresponding in humans to tyrosine 419 residue, anti PARP (#9542), anti-EGFR (#4267), and anti-EGFR-vIII (#2232; Cell Signaling Technology Inc., Danvers, MA, USA, Upstate, Lake Placid, NY, USA). Anti-rabbit secondary antibody coupled with horseradish peroxidase (Cell Signaling Technologies, Danvers, MA, USA) was utilized.



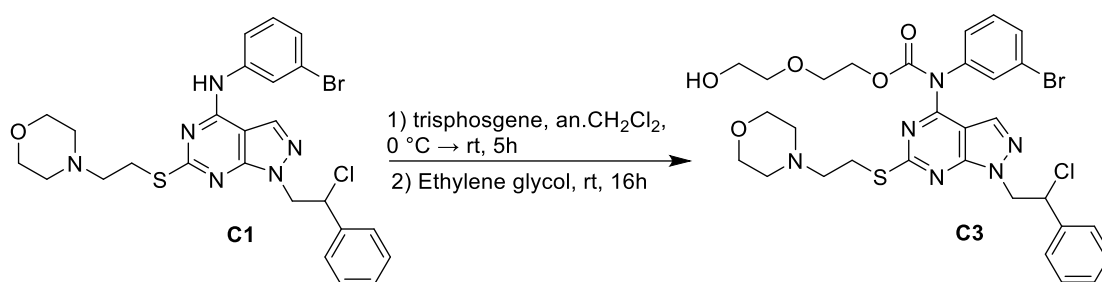
## 2.7. Statistical Analyses

Data are expressed as means  $\pm$  S.E.M. Statistical significance of differences was determined by one-way analysis of variances (ANOVA) followed by Tukey's test.  $p < 0.05$  was considered statistically significant.

## 3. Results

### 3.1. Chemistry

Synthesis of C1 and C2 was already reported by us [13,25,26]. C3 was synthesized starting from SI306 with a one-pot two-step procedure. First, trisphosgene was added to a pre-cooled solution of SI306, then ethylene glycol was added, and the reaction was stirred at room temperature affording C3 with good yield (Figure 2).



**Figure 2.** Synthesis of C3.

### 3.2. U87 Cells Are Less Sensitive Than CAS1 to the Effect of SI306- and SI306-Derived Drugs and Show a Major Susceptibility to Compound 2

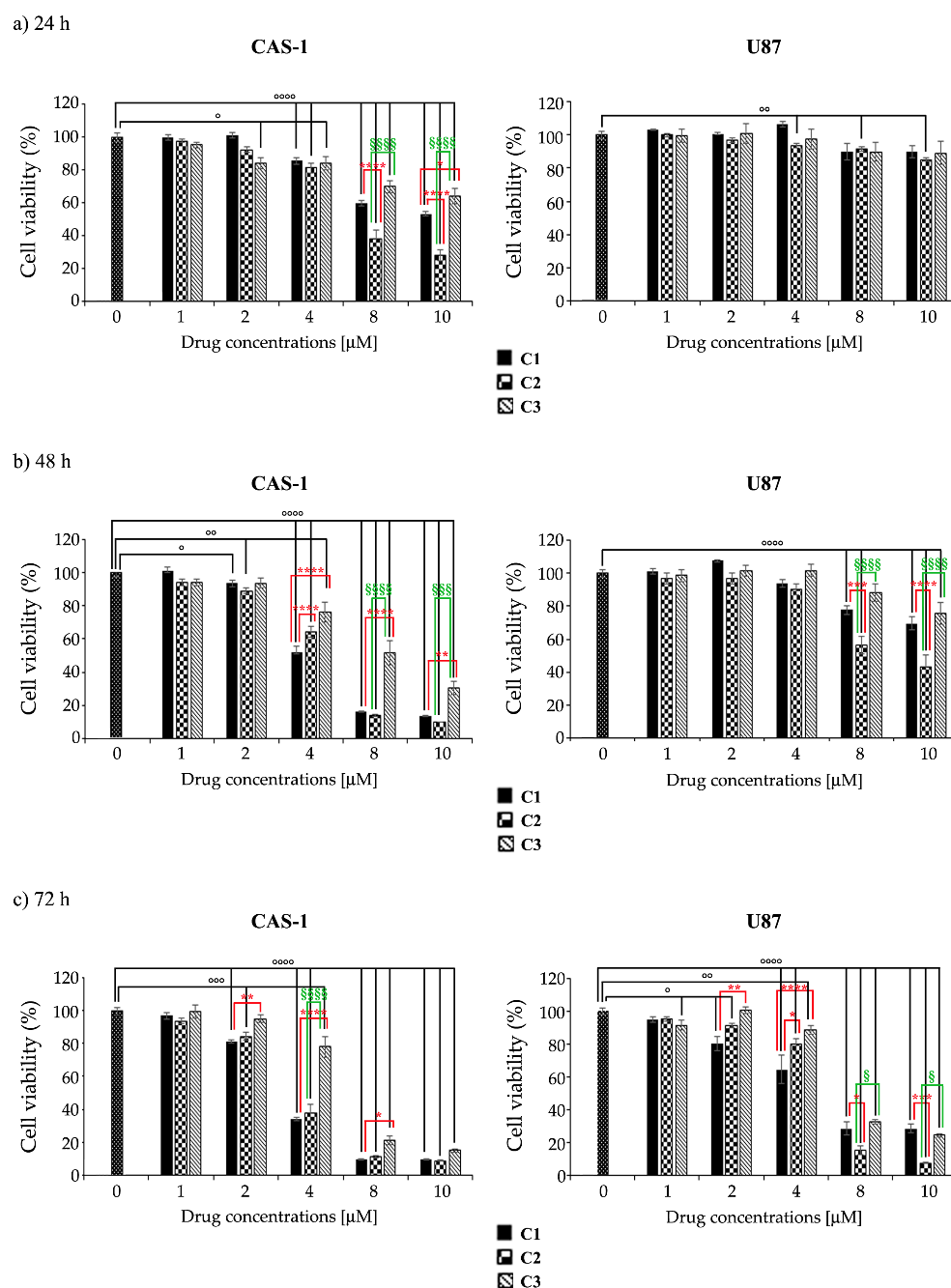
In order to compare the effects of C2 and C3 with those of SI306, two human GBM cell lines (U87 and CAS-1) were exposed to increasing concentrations of compounds for 24–72 h.

The analysis of cell viability showed that all compounds, at the same doses and time exposure, induced a major anti-survival effect on CAS-1 cells. In fact, as reported in Table 1, the  $IC_{50}$  of all three compounds was lower in CAS-1 than in U87 cells. Moreover, C2 was the most effective on both cell lines, while C3 exerted a lower activity (Table 1).

**Table 1.**  $IC_{50}$  evaluated in CAS-1 and U87 cell lines treated with increasing doses (1–10  $\mu$ M) of C1 (SI306), C2, and C3 for 24, 48, and 72 h. The data are the means  $\pm$  S.E.M. of five independent experiments. Statistical significance of differences was determined by ANOVA followed by Tukey's test. \*\*  $p < 0.01$  vs. C1; \*\*\*  $p < 0.001$  vs. C1; \*\*\*\*  $p < 0.0001$  vs. C1;  $^{\circ\circ\circ}$   $p < 0.001$  vs. C2; and  $^{\circ\circ\circ\circ}$   $p < 0.0001$  vs. C2.

Compound	CAS-1			U87		
	24 h	48 h	72 h	24 h	48 h	72 h
C1	11.74 $\pm$ 0.34	3.88 $\pm$ 0.15	3.03 $\pm$ 0.1	52.46 $\pm$ 1.24	18.63 $\pm$ 0.32	5.28 $\pm$ 0.35
C2	6.05 $\pm$ 0.15 ***	3.66 $\pm$ 0.28 ***	3.13 $\pm$ 0.16 ***	46.46 $\pm$ 0.8 ***	9.24 $\pm$ 0.14 ****	3.77 $\pm$ 0.15 **
C3	13.92 $\pm$ 0.42 $^{\circ\circ\circ\circ}$	6.97 $\pm$ 0.27 ***/ $^{\circ\circ\circ}$	4.47 $\pm$ 0.2 ***/ $^{\circ\circ\circ}$	54.51 $\pm$ 1.16 $^{\circ\circ\circ\circ}$	28.36 $\pm$ 0.2 ****/ $^{\circ\circ\circ\circ}$	5.79 $\pm$ 0.11 $^{\circ\circ\circ}$

In detail, SI306 induced a concentration-dependent decrease in the viability of CAS-1 cells, reaching a 40% reduction at 10  $\mu$ M after 24 h-exposure (Figure 3a, left panel). Instead, no effects on cell viability of U87 were induced by 24 h-treatment with SI306 (Figure 3a, right panel). Analyzing the viability at 48 h, the highest doses of SI306 (8  $\mu$ M and 10  $\mu$ M) reduced the viability of CAS1 and U87 by 85% and 25%, respectively (Figure 3b,c, respectively). Moreover, after 72 h, the highest doses decreased the viability of U87 cells by over 70% (Figure 3c), while no further changes were observed in CAS-1 in respect to those observed after 48 h.



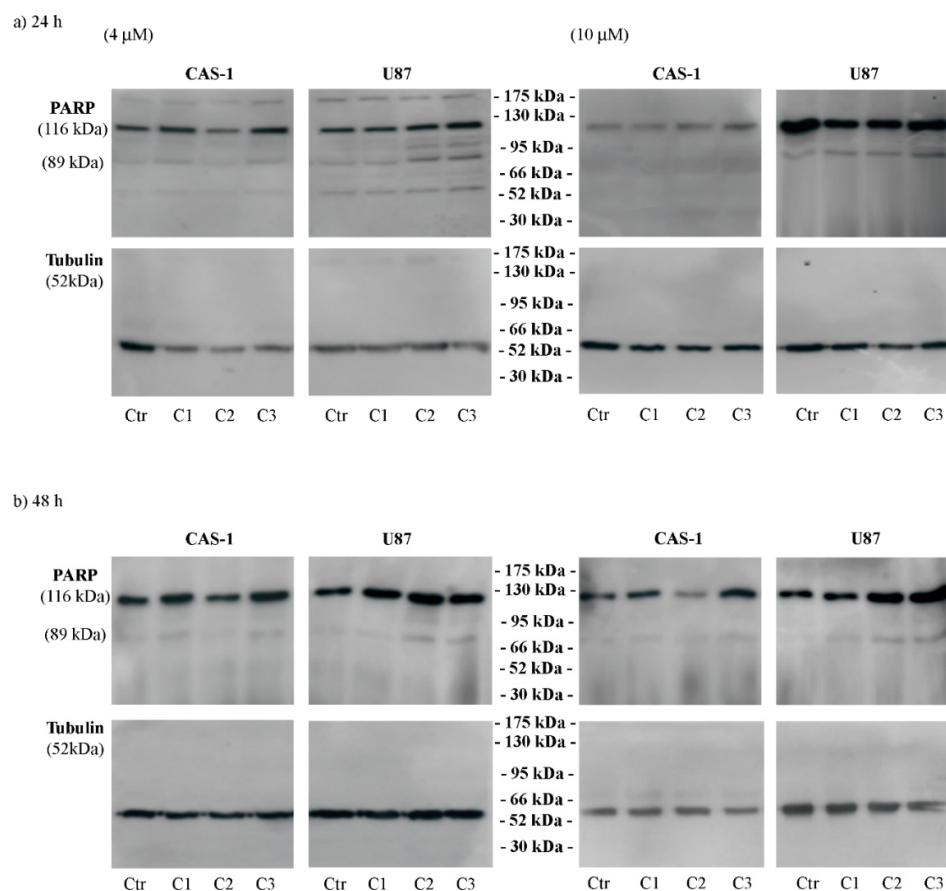
**Figure 3.** U87 cells are less sensitive than CAS1 to the anti-survival effect of SI306- and SI306-derived drugs. CAS-1 (left panels) and U87 (right panels) cells were exposed to increasing concentrations (1–10 μM) of compound 1 (C1, SI306), compound 2 (C2), and compound 3 (C3) for 24 h (a), 48 h (b), and 72 h (c). Cell viability was evaluated by MTS assay. Histograms summarize quantitative data of the means  $\pm$  S.E.M. of five independent experiments. Statistical significance of differences was determined by ANOVA followed by Tukey's test. °  $p < 0.05$  vs. untreated cells; °°  $p < 0.01$  vs. untreated cells; °°°  $p < 0.001$  vs. untreated cells; °°°°  $p < 0.0001$  vs. untreated cells; \*  $p < 0.05$  vs. compound 1; \*\*  $p < 0.01$  vs. compound 1; \*\*\*  $p < 0.001$  vs. compound 1; \*\*\*\*  $p < 0.0001$  vs. compound 1; §  $p < 0.05$  vs. compound 2; §§§  $p < 0.001$  vs. compound 2; and §§§§  $p < 0.0001$  vs. compound 2.

With regard to SI306-derived drugs, in both cell lines it has been observed that C2 had a major anti-survival action than SI306 (Figure 3), whilst C3 was less active than SI306 and C2 (Figure 3). In detail, after 24 h-treatment, the highest doses (8 μM and 10 μM) of C2 were able to reduce cell viability more effectively than SI306 (Figure 3b, right panel).

Instead, after 48 and 72 h, the highest doses of C2 and SI306 analogously decreased CAS1 cell viability by 85% and 92%, respectively (Figure 3b,c, respectively, left panels). The viability of U87 cells was significantly impaired after 48 h and, in particular, C2 was more active than SI306 and C3. Interestingly, after 72 h, the highest doses (8  $\mu$ M and 10  $\mu$ M) of C2 reduced U87 cell viability by about 90% (Figure 3, right panels).

Moreover, C3 at these highest doses (8  $\mu$ M and 10  $\mu$ M) exerted an anti-survival effect on U87 cells comparable to that of SI306, while it was found less effective on CAS1 (Figure 3).

In order to shed light on the kind of cell death, the levels of full length (116 kDa) and cleaved (89 kDa) PARP, a known marker of apoptosis [29], were evaluated. As reported in Figure 4, C1, at 10  $\mu$ M, and C2 and C3, at 4 and 10  $\mu$ M, induced apoptosis of U87 cells after 24 and 48 h. The same treatments did not induce PARP cleavage in CAS-1 cells (Figure 4).

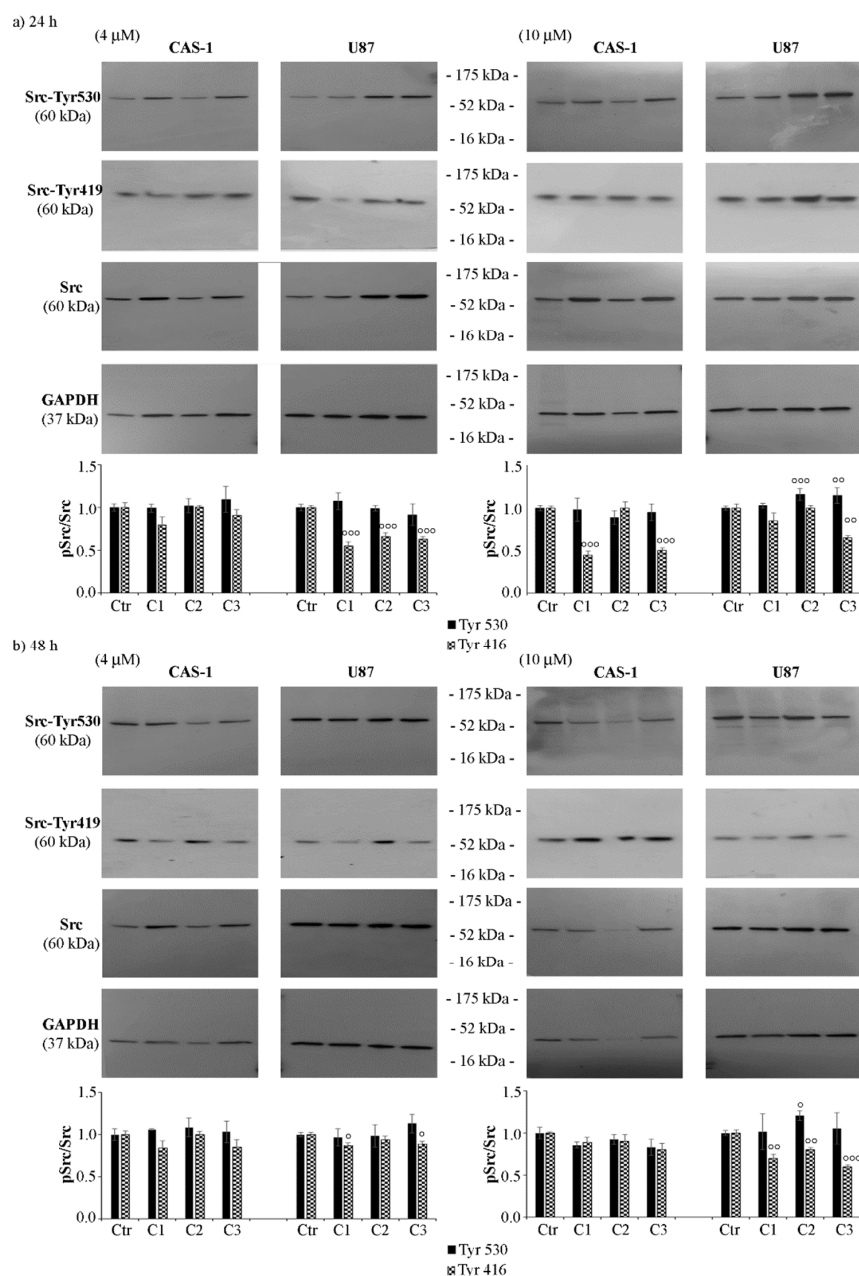


**Figure 4.** C2 and C3 induce apoptotic death of U87 cells. The expression levels of full length (116 kDa) and cleaved (89 kDa) PARP were evaluated in CAS-1 (left panels) and U87 (right panels) cells exposed to 4  $\mu$ M and 10  $\mu$ M of compound 1 (SI306, C1), compound 2 (C2), and compound 3 (C3) for 24 h (a) and 48 h (b). Immunoblots shown are representative of three independent experiments. Tubulin is the internal loading control.

### 3.3. SI306 Derivatives Inhibit Src Activity in U87 Cells

Considering that SI306 [25,30] is a Src inhibitor [8,10,11,14–16], the inhibitory ability of its derivatives was tested by evaluating the expression levels of Src phosphorylated at Tyr530, a marker of Src inactivation [31], and at Tyr416 (Tyr419 in humans), a marker of Src activation [32]. As shown in Figure 5, in U87 cells, C2 (10  $\mu$ M) increased the p-Tyr530/Src ratio by 15% and by 20% at 24 and 48 h, respectively (Figure 5, right panels), while C3 (10  $\mu$ M) induced a 15% increase after 24 h. The analysis of the expression of Src phosphorylated at Tyr416 (Tyr419) showed that 24 h-treatment of U87 cells with all compounds at 4  $\mu$ M reduced the p-Src/Src ratio by 45% (Figure 5a, left panel). After 48 h,

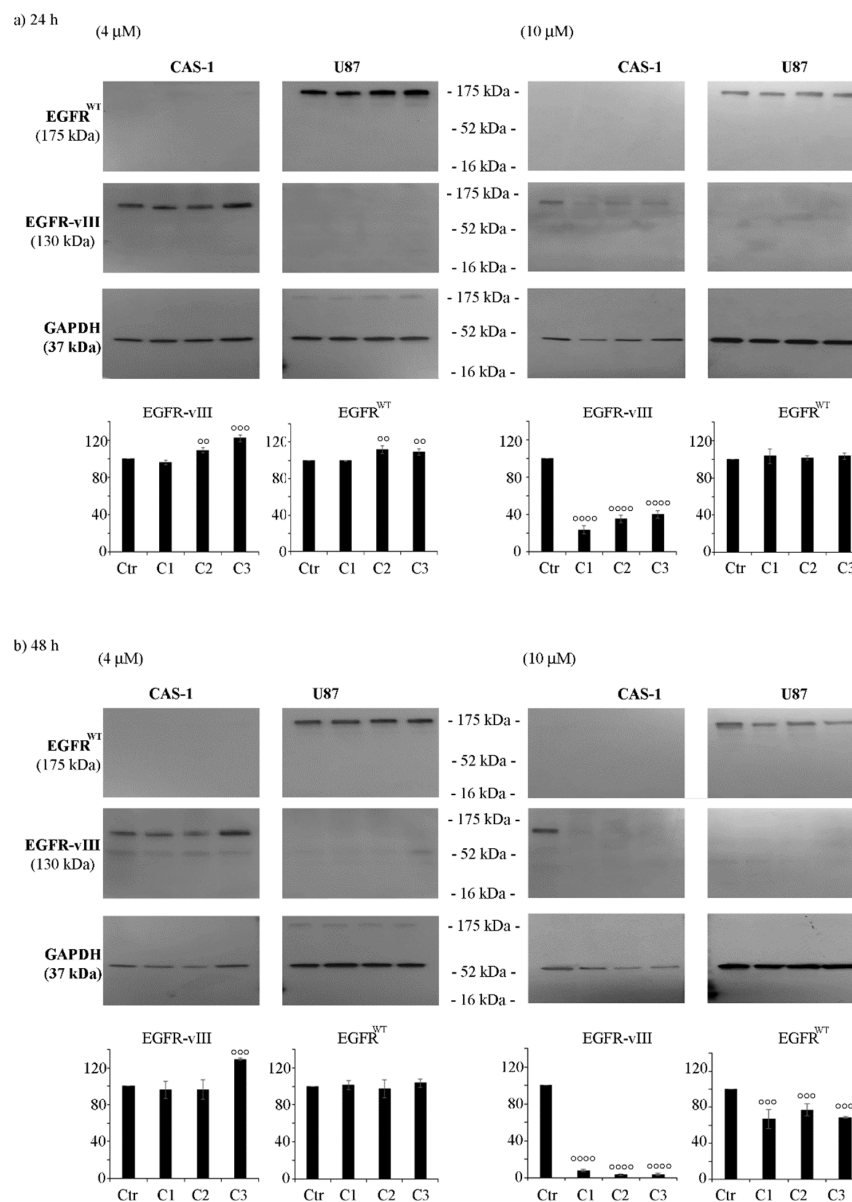
only C1 and C3 reduced the ratio by 20% (Figure 5b, left panel). No significant changes were observed in CAS-1 cells exposed to 4  $\mu\text{M}$  C1, C2, or C3 (Figure 5a,b, left panels). However, 10  $\mu\text{M}$  C1 or C3 reduced the p-Src/Src ratio by 55% in CAS-1 cells treated for 24 h, while only C3 reduced the ratio in U87 cells by 35% (Figure 5a, right panel). After 48 h, C1 and C2 also decreased the p-Src/Src ratio by 30% in U87 cells, while no significant changes were found in CAS-1 cells (Figure 5b, right panel).



**Figure 5.** SI306 derivatives inhibit Src activity in U87 cells. Src inactivation was evaluated by immunoblot analyses of p-Src (Tyr530 and Tyr419) and total Src. The expression levels of p-Src and Src were evaluated in CAS-1 (left panels) and U87 (right panels) cells exposed to 4  $\mu\text{M}$  and 10  $\mu\text{M}$  of compound 1 (SI306, C1), compound 2 (C2), and compound 3 (C3) for 24 h (a) and 48 h (b). Immunoblots shown are representative of three independent experiments. GAPDH is the internal loading control. Histograms summarize quantitative data of means  $\pm$  S.E.M. of three independent experiments. Statistical significance of differences was determined by ANOVA followed by Tukey's test. Data are expressed as a ratio of the levels of p-Src to the levels of total Src. °  $p < 0.05$  vs. untreated cells; °°  $p < 0.01$  vs. untreated cells; and °°°  $p < 0.001$  vs. untreated cells.

### 3.4. CAS-1 Cells Express EGFR-vIII While U87 Cells Express EGFR<sup>WT</sup> and the Exposure to SI306 or Its Derivatives Has a Different Impact on Their Expression Levels

As it has been demonstrated that progression of GBM is related to Src up-regulation [33] and it is also a consequence of EGFR mutations [34], the expression of both wild type EGFR (EGFR<sup>WT</sup>) and EGFR-vIII, the most common mutant found in GBM, was investigated. Firstly, as shown in Figure 6, EGFR<sup>WT</sup> was found in U87 while EGFR-vIII was detected in CAS-1 cells.



**Figure 6.** CAS-1 and U87 cells show a different type of EGFR, and treatment with SI306 or its derivatives differently alters their expression levels. The expression of EGFR<sup>WT</sup> or EGFR-vIII was evaluated by immunoblot analyses performed on protein extracts obtained by CAS-1 (left panels) and U87 (right panels) cells exposed to 4 μM and 10 μM of compound 1 (SI306, C1), compound 2 (C2), and compound 3 (C3) for 24 h (a) and 48 h (b). Immunoblots shown are representative of three independent experiments. GAPDH is the internal loading control. Histograms summarize quantitative data of means ± S.E.M. of three independent experiments. Statistical significance of differences was determined by ANOVA followed by Tukey's test. °°  $p < 0.01$  vs. untreated cells; °°°  $p < 0.001$  vs. untreated cells; °°°°  $p < 0.0001$  vs. untreated cells.

Notably, 24 h-treatment with 4  $\mu\text{M}$  of C2 or C3 increased the expression of EGFR<sup>WT</sup> in U87 cells by 10%, while it enhanced EGFR<sup>vIII</sup> levels in CAS-1 by about 15%, in respect to control cells (Figure 6a, left panels). However, 48 hour-exposure to C3 induced a 30% increase in EGFR-vIII protein levels in CAS-1 cells (Figure 6b, left panel), while 24 h-treatment with 4  $\mu\text{M}$  of SI306 did not significantly change the expression of either EGFR<sup>WT</sup> or EGFR-vIII in either cell population (Figure 6a,b, respectively, left panels).

Surprisingly, all compounds at the dose of 10  $\mu\text{M}$  reduced the expression of EGFR-vIII in CAS-1 cells by 70% and 95% after 24 and 48 h, respectively (Figure 6b, right panels), and a 30–35% decrease in EGFR<sup>WT</sup> protein levels was observed in U87 cells only after 48 h of treatment (Figure 6b, right panels).

#### 4. Discussion

Despite ongoing efforts to find valid therapies, GBM remains a highly aggressive tumor with low recovery expectations. In fact, today, the standard cure for GBM is surgery, followed by radiotherapy and/or chemotherapy [2]. However, such approaches are not currently curative, and the onset of resistance is the main cause of recurrence. Therefore, it is crucial to identify the molecular mediators responsible for therapeutic resistance in order to develop targeted strategies capable of overcoming this obstacle. In this regard, several studies have attributed a crucial role to the Src family, both in GBM carcinogenesis and in the mechanisms involved in therapeutic failure [14,35,36]. This evidence suggests that targeting Src could be a valuable approach to improve the life expectancy of GBM patients. Most of the Src inhibitors available today are non-specific and offer cross-reactivity [37]. Moreover, the particular location of GBM makes necessary to develop drugs able to cross the Blood–brain barrier (BBB), and to over-express ATP-binding cassette (ABC) transporters, preventing the drug supply and accumulation in the brain. Many FDA-approved drugs are directed towards these transporters [7] but, although they induce an adequate intake of the drug to the brain, are not effective for GBM treatment [38–40].

Therefore, based on these considerations, an effective therapy must hit GBM acting on several fronts and target the molecular pathways involved in the resistance. In recent years, our research team developed an extensive library of pirazolo[3,4-*d*]pyrimidines able to cross the BBB [9,10]. Among these compounds, SI306 (namely C1 in the paper), by inhibiting Src [41,42] and the ABC transporter Pgp [9,10], has demonstrated a powerful antitumor action in vitro and in vivo, both as monotherapy and combined therapy [8,10,13,14]. Similar results were obtained with the prodrug of SI306 (namely C2) [10,13]. Starting from these promising results, a new SI306 derivative (namely C3) was designed and synthesized in order to extend our knowledge on the effect of a different polar chain on the carbamate moiety. C3 was decorated with an ethylene glycol unit in place of the *N*-methyl piperazine fragment present in C2. Both prodrugs were tested on two human GBM cell lines and their effects compared with those of the parent drug SI306. The obtained results herein demonstrate that the anti-survival action of SI306 and its derivatives is both time- and concentration-dependent. In fact, the lowest doses (2 and 4  $\mu\text{M}$ ) of all compounds were able to reduce cell survival after 48 h while the highest ones (8 and 10  $\mu\text{M}$ ) decreased cell survival already at 24 h with a progressive reduction at 48 and 72 h.

However, although an MTT test revealed that U87 cells are less sensitive than CAS-1, PARP cleavage, as a recognized marker of apoptosis [43], was detected only in U87 treated cells, suggesting that in CAS-1 cells other death pathways occur and further investigation is needed. Interestingly, the pro-apoptotic effect of these compounds on U87 cells is accompanied by Src inactivation measured by evaluating the phosphorylation of Tyr530 and 416 (Tyr419 in humans) [31,32].

With regard to CAS-1 cells, the reduction in cell viability is not related to Src activity and might be due to other mechanisms that deserve further investigation. However, the data demonstrates that Src phosphorylation status does not predict the drug sensitivity in agreement with a recent study reporting that patients with different GBM subtypes expressed similar levels of the unphosphorylated and phosphorylated Src [44]. In the

present study, the different sensitivity of two GBM cells to the tested compounds could be related to their pharmacokinetic profile, but also to the fact that CAS-1 cells express EGFR-vIII while U87 cells express EGFR<sup>WT</sup>. This result is in contradiction with a previous data reporting that U87 cells express EGFR-vIII [45] and we believe that this discrepancy could be due to the different specificity of the antibody used in Western blotting analysis.

However, to investigate if all tested compounds are effective on GBM with a different status of EGFR could have important therapeutic implications. In fact, considering that patients with EGFR-vIII have a reduced survival rate [46] and that EGFR-vIII is not expressed in healthy tissues, EGFR-vIII could be considered an excellent target for therapy [47]. To date, drugs developed to treat patients with EGFR-vIII or EGFR have proven to be ineffective due to the inability of such drugs to overcome the BBB, to tumor heterogeneity, and to the activation of compensatory pathways such as Src [21–24]. Although further investigations are needed, our studies demonstrate that SI306 and its derivatives impact GBM cell survival and that this event is accompanied by a reduction in the expression of EGFR<sup>WT</sup> and EGFR-vIII in U87 and Cas-1 cells, respectively. These results lead us to believe that these compounds could represent a promising alternative approach to treat GBM.

**Author Contributions:** Conceptualization, B.M., F.M., S.S. and C.D.; methodology, B.M., L.M. and G.G.; validation, B.M. and C.D.; visualization, B.M., L.M., F.M. and C.D.; investigation, B.M., L.M., G.G. and G.E.V.; formal analysis, B.M., L.M. and G.E.V.; writing—original draft preparation, B.M., L.M. and G.E.V.; writing—review and editing, B.M., F.M., A.C., S.S. and C.D.; resources, S.S. and C.D.; supervision, S.S. and C.D.; project administration, S.S. and C.D.; and funding acquisition, S.S. All authors have read and agreed to the published version of the manuscript.

**Funding:** This research was funded by the AIRC Foundation for Cancer Research in Italy (Fondazione AIRC per la Ricerca sul Cancro, AIRC), Grant IG-2019, project code 23725, PI Silvia Schenone.

**Informed Consent Statement:** Not applicable.

**Acknowledgments:** We would like to thank Giuseppe Catalano (DIMES-University of Genoa) for his technical assistance.

**Conflicts of Interest:** The authors declare no conflict of interest.

## References

1. Louis, D.N.; Perry, A.; Wesseling, P.; Brat, D.J.; Cree, I.A.; Figarella-Branger, D.; Hawkins, C.; Ng, H.K.; Pfister, S.M.; Reifenberger, G.; et al. The 2021 WHO Classification of Tumors of the Central Nervous System: A summary. *Neuro-Oncology* **2021**, *23*, 1231–1251. [CrossRef] [PubMed]
2. Tan, A.C.; Ashley, D.M.; López, G.Y.; Malinzak, M.; Friedman, H.S.; Khasraw, M. Management of glioblastoma: State of the art and future directions. *CA Cancer J. Clin.* **2020**, *70*, 299–312. [CrossRef] [PubMed]
3. Olar, A.; Aldape, K.D. Using the molecular classification of glioblastoma to inform personalized treatment. *J. Pathol.* **2014**, *232*, 165–177. [CrossRef] [PubMed]
4. Martins, T.A.; Schmassmann, P.; Shekarian, T.; Boulay, J.L.; Ritz, M.F.; Zanganeh, S.; Vom Berg, J.; Hutter, G. Microglia-Centered Combinatorial Strategies Against Glioblastoma. *Front. Immunol.* **2020**, *11*, 571951. [CrossRef]
5. Majc, B.; Novak, M.; Kopitar-Jerala, N.; Jewett, A.; Breznik, B. Immunotherapy of Glioblastoma: Current Strategies and Challenges in Tumor Model Development. *Cells* **2021**, *10*, 265. [CrossRef] [PubMed]
6. Liu, E.K.; Sulman, E.P.; Wen, P.Y.; Kurz, S.C. Novel Therapies for Glioblastoma. *Curr. Neurol. Neurosci. Rep.* **2020**, *20*, 19. [CrossRef] [PubMed]
7. Cirotti, C.; Contadini, C.; Barilà, D. SRC Kinase in Glioblastoma News from an Old Acquaintance. *Cancers* **2020**, *12*, 1558. [CrossRef] [PubMed]
8. Calgani, A.; Vignaroli, G.; Zamperini, C.; Coniglio, F.; Festuccia, C.; Di Cesare, E.; Gravina, G.L.; Mattei, C.; Vitale, F.; Schenone, S.; et al. Suppression of SRC Signaling Is Effective in Reducing Synergy between Glioblastoma and Stromal Cells. *Mol. Cancer Ther.* **2016**, *15*, 1535–1544. [CrossRef] [PubMed]
9. Ceccherini, E.; Indovina, P.; Zamperini, C.; Dreassi, E.; Casini, N.; Cutaia, O.; Forte, I.M.; Pentimalli, F.; Esposito, L.; Polito, M.S.; et al. SRC family kinase inhibition through a new pyrazolo[3,4-*d*]pyrimidine derivative as a feasible approach for glioblastoma treatment. *J. Cell Biochem.* **2015**, *116*, 856–863. [CrossRef] [PubMed]
10. Fallacara, A.L.; Zamperini, C.; Podolski-Renić, A.; Dinić, J.; Stanković, T.; Stepanović, M.; Mancini, A.; Rango, E.; Iovenitti, G.; Molinari, A.; et al. A New Strategy for Glioblastoma Treatment: In Vitro and In Vivo Preclinical Characterization of Si306, a Pyrazolo[3,4-*d*]Pyrimidine Dual Src/P-Glycoprotein Inhibitor. *Cancers* **2019**, *11*, 848. [CrossRef] [PubMed]

11. Greco, C.; Taresco, V.; Pearce, A.K.; Vasey, C.E.; Smith, S.; Rahman, R.; Alexander, C.; Cavanagh, R.J.; Musumeci, F.; Schenone, S. Development of Pyrazolo[3,4-*d*]pyrimidine Kinase Inhibitors as Potential Clinical Candidates for Glioblastoma Multiforme. *ACS Med. Chem. Lett.* **2020**, *11*, 657–663. [CrossRef] [PubMed]
12. Musumeci, F.; Fallacara, A.L.; Brullo, C.; Grossi, G.; Botta, L.; Calandro, P.; Chiariello, M.; Kissova, M.; Crespan, E.; Maga, G.; et al. Identification of new pyrrolo[2,3-*d*]pyrimidines as Src tyrosine kinase inhibitors in vitro active against Glioblastoma. *Eur. J. Med. Chem.* **2017**, *127*, 369–378. [CrossRef] [PubMed]
13. Vignaroli, G.; Iovenitti, G.; Zamperini, C.; Coniglio, F.; Calandro, P.; Molinari, A.; Fallacara, A.L.; Sartucci, A.; Calgani, A.; Colecchia, D.; et al. Prodrugs of Pyrazolo[3,4-*d*]pyrimidines: From Library Synthesis to Evaluation as Potential Anticancer Agents in an Orthotopic Glioblastoma Model. *J. Med. Chem.* **2017**, *60*, 6305–6320. [CrossRef] [PubMed]
14. Cammarata, F.P.; Torrisi, F.; Forte, G.I.; Minafra, L.; Bravatà, V.; Pisciotta, P.; Savoca, G.; Calvaruso, M.; Petringa, G.; Cirrone, G.A.P.; et al. Proton Therapy and Src Family Kinase Inhibitor Combined Treatments on U87 Human Glioblastoma Multiforme Cell Line. *Int. J. Mol. Sci.* **2019**, *20*, 4745. [CrossRef]
15. Kostić, A.; Jovanović Stojanov, S.; Podolski-Renić, A.; Nešović, M.; Dragoj, M.; Nikolić, I.; Tasić, G.; Schenone, S.; Pešić, M.; Dinić, J. Pyrazolo[3,4-*d*]pyrimidine Tyrosine Kinase Inhibitors Induce Oxidative Stress in Patient-Derived Glioblastoma Cells. *Brain Sci* **2021**, *11*, 884. [CrossRef] [PubMed]
16. Nešović, M.; Divac Rankov, A.; Podolski-Renić, A.; Nikolić, I.; Tasić, G.; Mancini, A.; Schenone, S.; Pešić, M.; Dinić, J. Src Inhibitors Pyrazolo[3,4-*d*]pyrimidines, Si306 and Pro-Si306, Inhibit Focal Adhesion Kinase and Suppress Human Glioblastoma Invasion In Vitro and In Vivo. *Cancers* **2020**, *12*, 1570. [CrossRef]
17. Greenwald, R.B.; Choe, Y.H.; McGuire, J.; Conover, C.D. Effective drug delivery by PEGylated drug conjugates. *Adv. Drug Deliv. Rev.* **2003**, *55*, 217–250. [CrossRef]
18. Wu, T.; Chen, K.; He, S.; Liu, X.; Zheng, X.; Jiang, Z.X. Drug Development through Modification of Small Molecular Drugs with Monodisperse Poly(ethylene glycol)s. *Org. Process Res. Dev.* **2020**, *24*, 1364–1372. [CrossRef]
19. Cvrljević, A.N.; Akhavan, D.; Wu, M.; Martinello, P.; Furnari, F.B.; Johnston, A.J.; Guo, D.; Pike, L.; Cavenee, W.K.; Scott, A.M.; et al. Activation of Src induces mitochondrial localisation of de2-7EGFR (EGFRvIII) in glioma cells: Implications for glucose metabolism. *J. Cell Sci.* **2011**, *124*, 2938–2988. [CrossRef]
20. Eskilsson, E.; Rosland, G.V.; Talasila, K.M.; Knappskog, S.; Keunen, O.; Sottoriva, A.; Foerster, S.; Solecki, G.; Taxt, T.; Jirik, R.; et al. EGFRvIII mutations can emerge as late and heterogenous events in glioblastoma development and promote angiogenesis through Src activation. *Neuro-Oncology* **2016**, *18*, 1644–1655. [CrossRef] [PubMed]
21. An, Z.; Aksoy, O.; Zheng, T.; Fan, Q.W.; Weiss, W.A. Epidermal growth factor receptor and EGFRvIII in glioblastoma: Signaling pathways and targeted therapies. *Oncogene* **2018**, *37*, 1561–1575. [CrossRef] [PubMed]
22. Banisadr, A.; Eick, M.; Beri, P.; Parisian, A.D.; Yeoman, B.; Placone, J.K.; Engler, A.J.; Furnari, F. EGFRvIII uses intrinsic and extrinsic mechanisms to reduce glioma adhesion and increase migration. *J. Cell Sci.* **2020**, *133*, jcs247189. [CrossRef] [PubMed]
23. Rutkowska, A.; Stoczyńska-Fidelus, E.; Janik, K.; Włodarczyk, A.; Rieske, P. EGFR<sup>vIII</sup>: An Oncogene with Ambiguous Role. *J. Oncol.* **2019**, *2019*, 1092587. [CrossRef] [PubMed]
24. Sigismund, S.; Avanzato, D.; Lanzetti, L. Emerging functions of the EGFR in cancer. *Mol. Oncol.* **2018**, *12*, 3–20. [CrossRef] [PubMed]
25. Tintori, C.; Fallacara, A.L.; Radi, M.; Zamperini, C.; Dreassi, E.; Crespan, E.; Maga, G.; Schenone, S.; Musumeci, F.; Brullo, C.; et al. Combining X-ray crystallography and molecular modeling toward the optimization of pyrazolo[3,4-*d*]pyrimidines as potent c-Src inhibitors active in vivo against neuroblastoma. *J. Med. Chem.* **2015**, *58*, 347–361. [CrossRef] [PubMed]
26. Vignaroli, G.; Zamperini, C.; Dreassi, E.; Radi, M.; Angelucci, A.; Sanità, P.; Crespan, E.; Kissova, M.; Maga, G.; Schenone, S.; et al. Pyrazolo[3,4-*d*]pyrimidine prodrugs: Strategic optimization of the aqueous solubility of dual Src/Abl inhibitors. *ACS Med. Chem. Lett.* **2013**, *4*, 622–626. [CrossRef] [PubMed]
27. Marengo, B.; De Ciucis, C.; Ricciarelli, R.; Passalacqua, M.; Nitti, M.; Zingg, J.M.; Marinari, U.M.; Pronzato, M.A.; Domenicotti, C. PKC $\delta$  sensitizes neuroblastoma cells to L-buthionine-sulfoximine and etoposide inducing reactive oxygen species overproduction and DNA damage. *PLoS ONE* **2011**, *6*, e14661. [CrossRef] [PubMed]
28. Monteleone, L.; Speciale, A.; Valenti, G.E.; Traverso, N.; Ravera, S.; Garbarino, O.; Leardi, R.; Farinini, E.; Roveri, A.; Ursini, F.; et al. PKC $\alpha$  Inhibition as a Strategy to Sensitize Neuroblastoma Stem Cells to Etoposide by Stimulating Ferroptosis. *Antioxidants* **2021**, *10*, 691. [CrossRef] [PubMed]
29. Boulares, A.H.; Yakovlev, A.G.; Ivanova, V.; Stoica, B.A.; Wang, G.; Iyer, S.; Smulson, M. Role of poly(ADP-ribose) polymerase (PARP) cleavage in apoptosis. Caspase 3-resistant PARP mutant increases rates of apoptosis in transfected cells. *J. Biol. Chem.* **1999**, *274*, 22932–22940. [CrossRef]
30. Tintori, C.; Laurenzana, I.; La Rocca, F.; Falchi, F.; Carraro, F.; Ruiz, A.; Esté, J.A.; Kissova, M.; Crespan, E.; Maga, G.; et al. Identification of Hck inhibitors as hits for the development of antileukemia and anti-HIV agents. *ChemMedChem* **2013**, *8*, 1353–1360. [CrossRef] [PubMed]
31. Ayrapetov, M.K.; Wang, Y.H.; Lin, X.; Gu, X.; Parang, K.; Sun, G. Conformational basis for SH2-Tyr(P)527 binding in Src inactivation. *J. Biol. Chem.* **2006**, *281*, 23776–23784. [CrossRef] [PubMed]
32. Boczek, E.E.; Luo, Q.; Dehling, M.; Röpke, M.; Mader, S.L.; Seidl, A.; Kaila, V.R.I.; Buchner, J. Autophosphorylation activates c-Src kinase through global structural rearrangements. *J. Biol. Chem.* **2019**, *294*, 13186–13197. [CrossRef]



33. Lewis-Tuffin, L.J.; Feathers, R.; Hari, P.; Durand, N.; Li, Z.; Rodriguez, F.J.; Bakken, K.; Carlson, B.; Schroeder, M.; Sarkaria, J.N.; et al. Src family kinases differentially influence glioma growth and motility. *Mol. Oncol.* **2015**, *9*, 1783–1798. [CrossRef] [PubMed]
34. Frederick, L.; Wang, X.Y.; Eley, G.; James, C.D. Diversity and frequency of epidermal growth factor receptor mutations in human glioblastomas. *Cancer Res.* **2000**, *60*, 1383–1387. [PubMed]
35. Stettner, M.R.; Wang, W.; Nabors, L.B.; Bharara, S.; Flynn, D.C.; Grammer, J.R.; Gillespie, G.Y.; Gladson, C.L. Lyn kinase activity is the predominant cellular SRC kinase activity in glioblastoma tumor cells. *Cancer Res.* **2005**, *65*, 5535–5543. [CrossRef]
36. Du, J.; Bernasconi, P.; Clauser, K.R.; Mani, D.R.; Finn, S.P.; Beroukhim, R.; Burns, M.; Julian, B.; Peng, X.P.; Hieronymus, H.; et al. Bead-based profiling of tyrosine kinase phosphorylation identifies SRC as a potential target for glioblastoma therapy. *Nat. Biotechnol.* **2009**, *27*, 77–83. [CrossRef]
37. Knight, Z.A.; Lin, H.; Shokat, K.M. Targeting the cancer kinome through polypharmacology. *Nat. Rev. Cancer* **2010**, *10*, 130–137. [CrossRef]
38. Agarwal, S.; Mittapalli, R.K.; Zellmer, D.M.; Gallardo, J.L.; Donelson, R.; Seiler, C.; Decker, S.A.; Santacruz, K.S.; Pokorny, J.L.; Sarkaria, J.N.; et al. Active efflux of Dasatinib from the brain limits efficacy against murine glioblastoma: Broad implications for the clinical use of molecularly targeted agents. *Mol. Cancer Ther.* **2012**, *11*, 2183–2192. [CrossRef]
39. Lassman, A.B.; Pugh, S.L.; Gilbert, M.R.; Aldape, K.D.; Geinoz, S.; Beumer, J.H.; Christner, S.M.; Komaki, R.; DeAngelis, L.M.; Gaur, R.; et al. Phase 2 trial of dasatinib in target-selected patients with recurrent glioblastoma (RTOG 0627). *Neuro-Oncology* **2015**, *17*, 992–998. [CrossRef]
40. Galanis, E.; Anderson, S.K.; Twohy, E.L.; Carrero, X.W.; Dixon, J.G.; Tran, D.D.; Jeyapalan, S.A.; Anderson, D.M.; Kaufmann, T.J.; Feathers, R.W.; et al. A phase 1 and randomized, placebo-controlled phase 2 trial of bevacizumab plus dasatinib in patients with recurrent glioblastoma: Alliance/North Central Cancer Treatment Group N0872. *Cancer* **2019**, *125*, 3790–3800. [CrossRef]
41. Molinari, A.; Fallacara, A.L.; Di Maria, S.; Zamperini, C.; Poggialini, F.; Musumeci, F.; Schenone, S.; Angelucci, A.; Colapietro, A.; Crespan, E.; et al. Efficient optimization of pyrazolo[3,4-d]pyrimidines derivatives as c-Src kinase inhibitors in neuroblastoma treatment. *Bioorg. Med. Chem. Lett.* **2018**, *28*, 3454–3457. [CrossRef] [PubMed]
42. Radi, M.; Tintori, C.; Musumeci, F.; Brullo, C.; Zamperini, C.; Dreassi, E.; Fallacara, A.L.; Vignaroli, G.; Crespan, E.; Zanolli, S.; et al. Design, synthesis, and biological evaluation of pyrazolo[3,4-d]pyrimidines active in vivo on the Bcr-Abl T315I mutant. *J. Med. Chem.* **2013**, *56*, 5382–5394. [CrossRef] [PubMed]
43. Colla, R.; Izzotti, A.; De Ciucis, C.; Fenoglio, D.; Ravera, S.; Speciale, A.; Ricciarelli, R.; Furfaro, A.L.; Pulliero, A.; Passalacqua, M.; et al. Glutathione-mediated antioxidant response and aerobic metabolism: Two crucial factors involved in determining the multi-drug resistance of high-risk neuroblastoma. *Oncotarget* **2016**, *7*, 70715–70737. [CrossRef] [PubMed]
44. Alhalabi, O.T.; Fletcher, M.N.C.; Hielscher, T.; Kessler, T.; Lokumcu, T.; Baumgartner, U.; Wittmann, E.; Schlue, S.; Rahman, M.G.; Hai, L.; et al. A novel patient stratification strategy to enhance the therapeutic efficacy of dasatinib in glioblastoma. *Neuro-Oncology* **2022**, *24*, 39–51. [CrossRef]
45. Nishikawa, R.; Ji, X.D.; Harmon, R.C.; Lazar, C.S.; Gill, G.N.; Cavenee, W.K.; Huang, H.J. A mutant epidermal growth factor receptor common in human glioma confers enhanced tumorigenicity. *Proc. Natl. Acad. Sci. USA* **1994**, *91*, 7727–7731. [CrossRef]
46. Shinojima, N.; Tada, K.; Shiraishi, S.; Kamiryo, T.; Kochi, M.; Nakamura, H.; Makino, K.; Saya, H.; Hirano, H.; Kuratsu, J.; et al. Prognostic value of epidermal growth factor receptor in patients with glioblastoma multiforme. *Cancer Res.* **2003**, *63*, 6962–6970.
47. Congdon, K.L.; Gedeon, P.C.; Suryadevara, C.M.; Caruso, H.G.; Cooper, L.J.; Heimberger, A.B.; Sampson, J.H. Epidermal growth factor receptor and variant III targeted immunotherapy. *Neuro-Oncology* **2014**, *16* (Suppl. 8), viii20–5. [CrossRef]

## Article

# Choline Kinase $\alpha$ Inhibitors MN58b and RSM932A Enhances the Antitumor Response to Cisplatin in Lung Tumor Cells

Juan Carlos Lacal<sup>1,2,\*</sup>, Rosario Perona<sup>1,2</sup>, Javier de Castro<sup>2</sup> and Arancha Cebrián<sup>1,3</sup>

<sup>1</sup> Instituto de Investigaciones Biomédicas, CSIC/UAM, 28029 Madrid, Spain; rperona@iib.uam.es (R.P.); arancha.cebrian@quironsalud.es (A.C.)

<sup>2</sup> Instituto de Investigación Sanitaria Hospital La Paz, IDIPAZ, 28046 Madrid, Spain; javier.decastro@salud.madrid.org

<sup>3</sup> Instituto de Investigación Sanitaria Fundación Jiménez Díaz, 28040 Madrid, Spain

\* Correspondence: jclacal@iib.uam.es; Tel.: +34-914-975-438

**Abstract:** Lung cancer is one of the main causes of death in developed countries, and non-small cell lung cancer (NSCLC) is the most frequent type (80% of patients). In advanced NSCLC, platinum-based chemotherapy is the frontline palliative treatment, but less than 5% of patients achieve prolonged survival. Immunotherapy has recently been proposed as the standard of care (SoC) as either monotherapy or in combination with chemotherapy for advanced NSCLC. The levels of expression of PD-L1 are the only predictive biomarkers for patient assessment. Although around 30% of patients receiving immunotherapy achieve 5-year survival, a significant number does not benefit from this novel therapeutic approach. Therefore, there is a need for novel strategies to improve clinical outcomes. The expression level of choline kinase  $\alpha$  (ChoK $\alpha$ ) is increased in a large number of human tumors, including NSCLC tumors, and constitutes an independent prognostic factor for early-stage NSCLC patients. Thus, ChoK $\alpha$  has been postulated as a new target drug in cancer therapy. The combination of cisplatin with novel targeted drugs such as choline kinase inhibitors may improve both the survival rates and the quality of life of NSCLC patients and may serve as the basis for the development of new therapeutic approaches. To that aim, we developed several in vitro and in vivo approaches to assess the antitumor activity of a novel combination regimen using cisplatin and ChoK $\alpha$  inhibitors. Our results suggest that a proper combination of specific inhibitors of the NSCLC prognostic factor ChoK $\alpha$  and platinum-based conventional chemotherapy might constitute a new, efficient treatment approach for NSCLC patients. This novel approach may help reduce the toxicity profile associated with cisplatin since, despite the advances in NSCLC management in recent years, the overall 5-year survival rate is still poor.

**Citation:** Lacal, J.C.; Perona, R.; de Castro, J.; Cebrián, A. Choline Kinase  $\alpha$  Inhibitors MN58b and RSM932A Enhances the Antitumor Response to Cisplatin in Lung Tumor Cells. *Pharmaceutics* **2022**, *14*, 1143. <https://doi.org/10.3390/pharmaceutics14061143>

Academic Editor: Francesca Musumeci

Received: 7 April 2022

Accepted: 24 May 2022

Published: 27 May 2022

**Publisher's Note:** MDPI stays neutral with regard to jurisdictional claims in published maps and institutional affiliations.



**Copyright:** © 2022 by the authors. Licensee MDPI, Basel, Switzerland. This article is an open access article distributed under the terms and conditions of the Creative Commons Attribution (CC BY) license (<https://creativecommons.org/licenses/by/4.0/>).

**Keywords:** choline kinase; lipid metabolism; cisplatin; lung tumors; combinatorial chemotherapy

## 1. Introduction

Over 2.2 million cases of lung cancer are diagnosed each year worldwide, constituting the leading cause of cancer-related mortality, with 1.8 million deaths in 2020 (Globocan, 2020; see [https://gco.iarc.fr/today/online-analysis-table?v=2020&mode=cancer&mode\\_population=continents&population=900&populations=900&key=asr&sex=0&cancer=39&type=1&statistic=5&prevalence=0&population\\_group=0&ages\\_group%5B%5D=0&ages\\_group%5B%5D=17&group\\_cancer=1&include\\_nmsc=0&include\\_nmsc\\_other=1](https://gco.iarc.fr/today/online-analysis-table?v=2020&mode=cancer&mode_population=continents&population=900&populations=900&key=asr&sex=0&cancer=39&type=1&statistic=5&prevalence=0&population_group=0&ages_group%5B%5D=0&ages_group%5B%5D=17&group_cancer=1&include_nmsc=0&include_nmsc_other=1), accessed on 23 May 2022). Over 80% of all lung cancers belong to the “non-small cell” histological subgroup, known as non-small cell lung cancer (NSCLC). A total of 20–25% of NSCLC patients present with stage III, and 35–40% are stage IV. For this advanced disease, firstline treatment options have evolved in recent years with immunotherapy in patients with high levels of PD-L1. This approach has rendered an impressive 30% survival rate at 5 years; however, the remaining 70% experience no benefit, and the mainstay still consists of platinum-based chemotherapy doublets. Furthermore, concurrent chemoradiotherapy is still the therapeutic approach used in patients with unresectable stage III and good

performance status. However, a wide range of side effects are associated with this regimen, including nausea, vomiting, and myelosuppression, as well as oto-, neuro-, and nephro-toxicity, accounting for a strong decrease in quality of life [1,2].

In order to reduce the toxicity profile of cisplatin-based regimens, the use of new generations of platinum drugs, including carboplatin and oxaliplatin, has been introduced in the backbone of systemic chemotherapy in NSCLC, but adverse events still display a relevant impact on the quality of life of these patients. Subsequently, the introduction of third-generation cytotoxic drugs to platinum agents (known as doublets), including paclitaxel, docetaxel, gemcitabine, pemetrexed, and vinorelbine, has yielded higher response rates, maintaining the use of platinum doublets as standard therapy for NSCLC treatment [3,4].

More recently, new targeted, personalized therapies based on identified oncogenic drivers usually alone, but also combined with platinum doublets, with the introduction of patient selection procedures, have been explored with the main goals of improving clinical outcomes and minimizing side effects of treatments within drug optimization. Among these, interferences with EGFR, ALK, ROS 1, BRAF, NTRK, RET, and MET signaling have provided improved outcome in these patients [5]. Finally, the advent of immunotherapy based on specific antibodies against the programmed death (PD-1) receptor, the programmed death-ligand 1 (PD-L1), and the cytotoxic T-lymphocyte-associated protein 4 receptor (CTLA-4) has had a great impact on survival for some NSCLC patients. In metastatic tumors, recent clinical trials favored the use of these immune checkpoint inhibitors (ICIs) as first- or second-line treatments alone or in combination with chemotherapy [6]. The levels of expression of PD-L1 in tumor cells are the reference biomarkers for patient assessment of this approach. However, despite these advances, a significant number of patients cannot benefit from these therapies. Therefore, there is still a need for testing new targets and new combinatorial regimens.

Choline kinase alpha (ChoK $\alpha$ ), the first enzyme of the Kennedy pathway for the biosynthesis of the major phospholipid of the plasma membrane, phosphatidylcholine (PC), has been described as a novel oncogene [7] whose gene expression levels constitute a new prognostic factor in NSCLC patients [8]. Consequently, ChoK $\alpha$ -specific inhibitors have been designed and showed strong *in vitro* antiproliferative activity against human lung-cancer-derived models, as well as efficient antitumor activity *in vivo* in nude mice against different human xenografts [9]. These results were further confirmed using siRNA-driven interference molecules [10–12]. The development of RSM-932A/TCD-717, a highly specific ChoK $\alpha$  inhibitor [13] allowed entrance into a Phase I clinical trial as a new “first in class” targeted therapy (<http://clinicaltrials.gov/ct2/show/NCT01215864>; accessed on 6 April 2022). Here, we present *in vitro* and *in vivo* approaches to assess the antitumor activity of a novel combination regimen using cisplatin and ChoK $\alpha$  inhibitors.

## 2. Materials and Methods

### 2.1. Patients

Specimens of lung cancer tissue from 63 randomly selected patients who underwent surgical resection for NSCLC between 2001 and 2004 and who were followed up on by the Medical Oncology division at La Paz Hospital in Madrid were used for this analysis. No adjuvant therapy was administered to these patients. The institutional review board of the hospital approved the study, and written informed consent was obtained from all the patients.

### 2.2. Primary Cultures of NSCLC Tumors

The resected tissues from the NSCLC patients were enzymatically and chemically dissociated (Cell dissociation sieve-tissue grinder Kit, SIGMA-Aldrich, Madrid, Spain), and the obtained cells were seeded into 96-well plates (BD, Falcon, Bioscience, San Jose, CA, USA), as previously described [14]. The cells were treated with increasing concentrations (0, 0.5, 1, 5, 10, and 20  $\mu$ M) of cDDP, taxol, vinorelbine, gemcitabine, or MN58b for 10 days

in DMEM:F12HAM (Ref:D8437, SIGMA-Aldrich) supplemented with 10% fetal bovine serum (FBS) (Life Technologies, Grand Island, NY, USA). The final persistent population in each well was quantified with an Alamar blue assay, as previously described [14]. Alamar blue was added directly into the culture media at a final concentration of 10%, and the plate was returned to the incubator. The optical density of the plate was measured at 570 and 600 nm with a standard spectrophotometer at 3 h after adding Alamar blue. The cell viability was calculated according to the manufacturer's protocol (Biosource Europe, Nivelles, Belgium).

### 2.3. Cell Lines and Chemicals

All the cell lines used in this study were maintained under standard conditions of temperature (37 °C), humidity (95%), and carbon dioxide (5%). Epithelial non-small lung cancer H460 cells (generated from a pleural effusion of a patient with large cell lung cancer) and H1299 cells (derived from an NSCLC carcinoma) were maintained in RPMI supplemented with 10% fetal bovine serum (FBS) (Life Technologies, Grand Island, NY, USA). Cell lines resistant to the ChoK $\alpha$ -specific inhibitors MN58b or RSM-932A/TCD-717 were generated by prolonged continuous exposure to increasing concentrations of each drug and were maintained in RPMI supplemented with 10% FBS. A parallel control (H460 stock) of the cell line in the absence of the compounds was kept in culture for the same time. In-house-generated MN58b and RSM-932A/TCD-717 were dissolved in PBS and DMSO: PBS 2:1, respectively. Cisplatin was obtained from Ferrer Farma (EGF speciality).

### 2.4. Cell Proliferation Assays and Combined Index Evaluation

An amount of 6000 cells/well was seeded into 96-well flat-bottomed plates (BD, Falcon, Bioscience, San Jose, CA, USA) and incubated for 24 h under standard conditions. The cells were then treated with different concentrations of ChoK $\alpha$  inhibitors and cisplatin either concomitantly or in a sequential manner, with cisplatin for 5 h followed by a ChoK $\alpha$  inhibitor (MN58b or RSM-932A/TCD-717) for the next 40 h. Quantification of the number of cells remaining in each well was carried out using the MTT (3-(4,5-dimethylthiazol-2-yl)-2,5-diphenyltetrazolium bromide) method. The absorbance was read at 560 nm with a VersaMax Microplate Reader (Molecular Devices, Sunnyvale, CA, USA). Drug interaction between the ChoK $\alpha$  inhibitors and cisplatin was assessed using a combination index (CI) [15] where  $CI < 1$ ,  $CI = 1$ , and  $CI > 1$  indicated synergistic, additive, and antagonistic effects, respectively. The CI value was calculated as  $CI = D_1/Df_1 + D_2/Df_2$ , where  $Df_1$  and  $Df_2$  are the concentrations of MN58b or RSM-932A/TCD-717 and cisplatin, respectively, required to inhibit cell growth by 50%, and  $D_1$  and  $D_2$  are the drugs' concentrations in the combination treatment that also inhibited cell growth by 50%. The data analysis was performed with Calcsyn software (Biosoft, Oxford, UK).

### 2.5. Flow Cytometric Assay

The cell cycle distribution was determined by DNA content analysis after propidium iodide staining. The cells were treated with ChoK $\alpha$  inhibitors and cisplatin alone or in combination for 45 h. The cells were then harvested, stained, and incubated with 50  $\mu$ L detergent and 1 mL IP (50  $\mu$ g/mL) containing RNase (20  $\mu$ g/mL). The DNA content of approximately  $4 \times 10^5$  stained cells was analyzed using a Coulter XL-MZL flow cytometer. The fractions of cells in apoptosis, G0-G1, S, and G2-M phases were analyzed with DNA program software.

### 2.6. Western Blot Analysis

The cells were incubated with ChoK $\alpha$  inhibitors and cisplatin alone or in combination. Equal amounts of protein (30  $\mu$ g) were loaded into 15% SDS-PAGE acrylamide gels, and the resolved proteins were transferred onto nitrocellulose membranes. The following antibodies were used: anti-p-JNK (Promega, v7932), anti-p-p38 (Cell Signaling 9211S), and anti-P38 (Santa Cruz sc-535), with anti- $\alpha$ -tubulin (Sigma T9026) as a load control.

### 2.7. *In Vivo* Antitumoral Assays

Female athymic BALB/C nude mice were supplied by Jackson. The animal care and surgery protocols were approved by the Animal Care Committee. The mice were maintained with autoclaved water and sterile food ad libitum. The mice were inoculated subcutaneously with injections of  $1 \times 10^6$  H460 cells in the flank of each mouse mixed 1:1 with matrigel (354234, BD Bioscience, Haryana, India). The tumor sizes were determined using micrometer calipers, and when the size of the tumors was approximately  $0.1 \text{ cm}^3$ , the mice were divided into 8 different groups: control (vehicle); 2 mg MN58b/kg for 3 days/week; 1 mg cisplatin/kg for 2 days/week; 2 mg RSM-932A/TCD-717/kg for 2 days/week; and MN58b-cisplatin or RSM-932A/TCD-717-cisplatin combinations following both a sequential and concomitant schedule. MN58b and cisplatin were dissolved in PBS and injected i.p. in the amount of 0.1 mL/mouse. RSM-932A/TCD-717 was dissolved in DMSO:PBS 2:1 and diluted with PBS to give appropriate concentrations. The tumor sizes were measured twice a week at their greatest lengths and widths, and the volumes were calculated as  $(\text{tumor width}^2 \times \text{tumor length})/2$ .

### 2.8. Statistical Analysis

The correlations in responsiveness to the different treatments in the tumor samples of patients with NSCLC were performed following Pearson's correlations ( $r$ ) to measure the linear correlation between two different treatments. This is achieved by determining the ratio between their covariance and the product of their standard deviations according to the following formula:

$$r_{x,y} = \text{COV}(x,y) / \sigma_x \sigma_y$$

where  $\text{COV}$  is the covariance,  $\sigma_x$  is the standard deviation of  $x$ , and  $\sigma_y$  is the standard deviation of  $y$ . This rendered a normalized measurement of the covariance, such that the result always had a value between  $-1$  and  $+1$ . A Pearson's correlation of ( $r = -1$ ) meant a negative perfect correlation, while ( $r = 1$ ) was a perfect positive alignment. A value of 0 implied that there was no linear dependency between the variables. The values for  $r$  represented comparisons between pairs of the drugs used in the study and are reflected in Figure 1. The dispersion graphics are also reported.

Comparisons in the tumor volumes between the untreated and treated groups were performed using a nonparametric Mann–Whitney test. Two-sided  $p$ -values less than 0.05 were considered statistically significant. All the calculations were performed using SPSS software, version 20.0 (SPSS Inc., Chicago, IL, USA).

## 3. Results

### 3.1. Cisplatin-Intrinsic-Resistant NSCLC Tumors Are Sensitive to ChoK $\alpha$ Inhibition

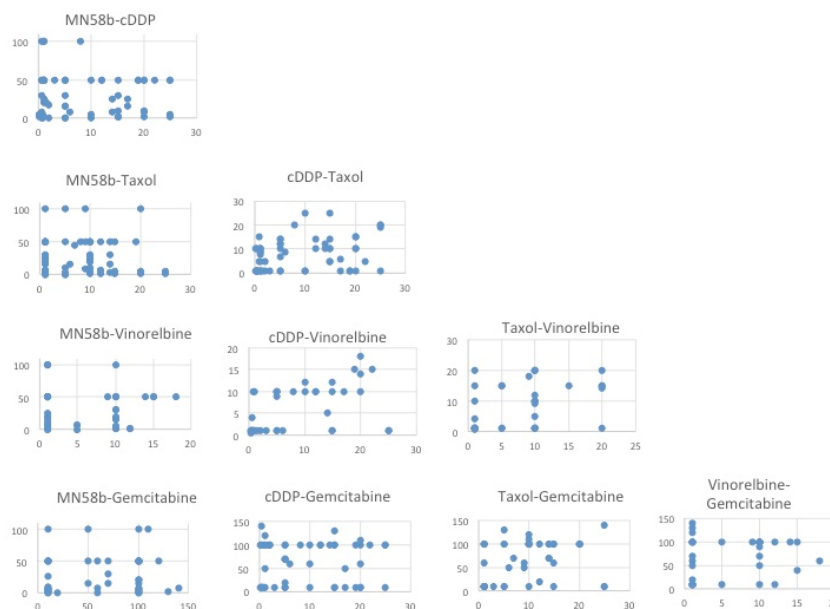
The primary cultures from 63 resected NSCLC tumors were established and cultivated for 10 days, during which they were treated with increasing concentrations of the ChoK $\alpha$ -specific inhibitor MN58b, cisplatin (cDDP), taxol, vinorelbine, or gemcitabine. Considering resistance when nearly 100% of the cells remained alive for the maximum concentration of the drug at day 10, different resistance rates to the treatments were found. As shown in Table 1, more than 50% of the samples were resistant independently to the treatment, in keeping with the lack of response to chemotherapy observed in the clinic.

A correlation analysis of the responsiveness of these tumors to the different treatments was then performed (Figure 1). Pearson's correlation indicated significant cross-resistance among cisplatin, taxol, vinorelbine, and gemcitabine. By contrast, MN58b showed no significant cross-resistance to any of the chemotherapeutic drugs tested, consistent with its different mechanism of action [16,17].

**Table 1.** Responsiveness of NSCLC primary cultures to different antitumor agents. Resected tissues from NSCLC patients were dissociated to obtain primary cultures that were treated for 10 days with different concentrations of the indicated drugs. Cell viability was determined by Alamar blue. The number of total samples examined in each case and the number of samples sensitive or resistant to each treatment are reported with their proportions (%).

Drug	NSCLC Samples	Sensitive (%)	Resistant (%)
MN58b	63	35 (55.6)	28 (44.4)
cDDP	62	31 (50.0)	31 (50.0)
Taxol	62	27 (43.5)	35 (56.5)
Vinorelbine	39	15 (38.5)	24 (61.5)
Gemcitabine	52	18 (34.6)	34 (65.4)

MN58b	r	1				
	s					
	n	63				
cDDP	r	-0.096	1			
	s	0.46				
	n	62	62			
Taxol	r	-0.09	0.319(*)	1		
	s	0.488	0.012			
	n	62	62	62		
Vinorelbine	r	-0.124	0.469(**)	0.421(**)	1	
	s	0.45	0.003	0.008		
	n	39	39	39	39	
Gemcitabine	r	0.133	0.074	0.364(**)	0.174	1
	s	0.346	0.603	0.008	0.304	
	n	52	52	52	37	52
		<b>MN58b</b>	<b>cDDP</b>	<b>Taxol</b>	<b>Vinorelbine</b>	<b>Gemcitabine</b>



**Figure 1.** Pearson's correlation analysis of intrinsic resistance of primary tumors of patients with NSCLC to different antitumoral agents. Upper panel: the statistical analysis was performed as indicated in Material and Methods for the response rate of the samples to the different treatments. MN58b was the only drug whose response did not correlate in responsiveness to any other agent. *r*: Pearson's correlations coefficient; *s*: significant correlation, bilateral (\*  $p \leq 0.05$ ; \*\*  $p \leq 0.01$ ); *n*: number of primary tumors analyzed. Lower panel: dispersion graphs for each pair of drugs.

To further confirm the absence of cross-resistance between ChoK $\alpha$  inhibitors and cisplatin, resistant H460 cells were generated by exposure to increasing doses of MN58b or RSM-932A/TCD717. The cell lines acquired drug resistance over a long-term period of 9–10 months, after which their sensitivity to both ChoK $\alpha$  inhibitors and cisplatin was determined (Table 2). The fold resistance was from 7–8 for RSM-932A/TCD-717 and from 49–73 for MN58b. A control cell line (H460 stock) was maintained in culture for the same time without treatment and was included as a comparison with the parental cell line. As a consequence of the similar mechanisms of action of the two ChoK $\alpha$  inhibitors, resistant cells to either MN58b (H460 MN58R) or to RSM-932A/TCD-717 (H460 TCD717R) showed an important cross-resistance between them. By contrast and consistent with a different mechanism of resistance acquisition, a significant lack of cross-resistance was found with cisplatin in both cases. In fact, cells resistant to the ChoK $\alpha$  inhibitors were slightly more sensitive to cisplatin.

**Table 2.** Absence of cross-resistance between cisplatin and ChoK $\alpha$  inhibitors. NSCLC H460 cells and H460 cells made resistant to ChoK $\alpha$  inhibitors MN58b (H460 MN58R) or RSM-932A/TCD-717 (H460 TCD717R) were treated with different concentrations of MN58b, RSM-932A/TCD-717, and cisplatin. The concentration where 50% of the cell proliferation was inhibited (IC<sub>50</sub>) was determined by MTT method. Data represent the mean  $\pm$  SD of 3 to 9 independent experiments, each performed in quadruplicate. The fold induction of resistance is shown within parentheses.

Cell Line	IC <sub>50</sub> MN58b ( $\mu$ M)	IC <sub>50</sub> TCD-717 ( $\mu$ M)	IC <sub>50</sub> cDDP ( $\mu$ M)
H460	0.28 $\pm$ 0.12	1.11 $\pm$ 0.4	16.60 $\pm$ 1.8
H460 Stoc	0.39 $\pm$ 0.19	1.32 $\pm$ 0.43	14.95 $\pm$ 2.6
H460 MN58R	19.2 $\pm$ 2.6 (49)	9.5 $\pm$ 1.19 (7)	6.60 $\pm$ 1.2 (0.4)
H460 TCD717R	28.8 $\pm$ 10.5 (73)	10.8 $\pm$ 2.26 (8)	4.98 $\pm$ 0.9 (0.3)

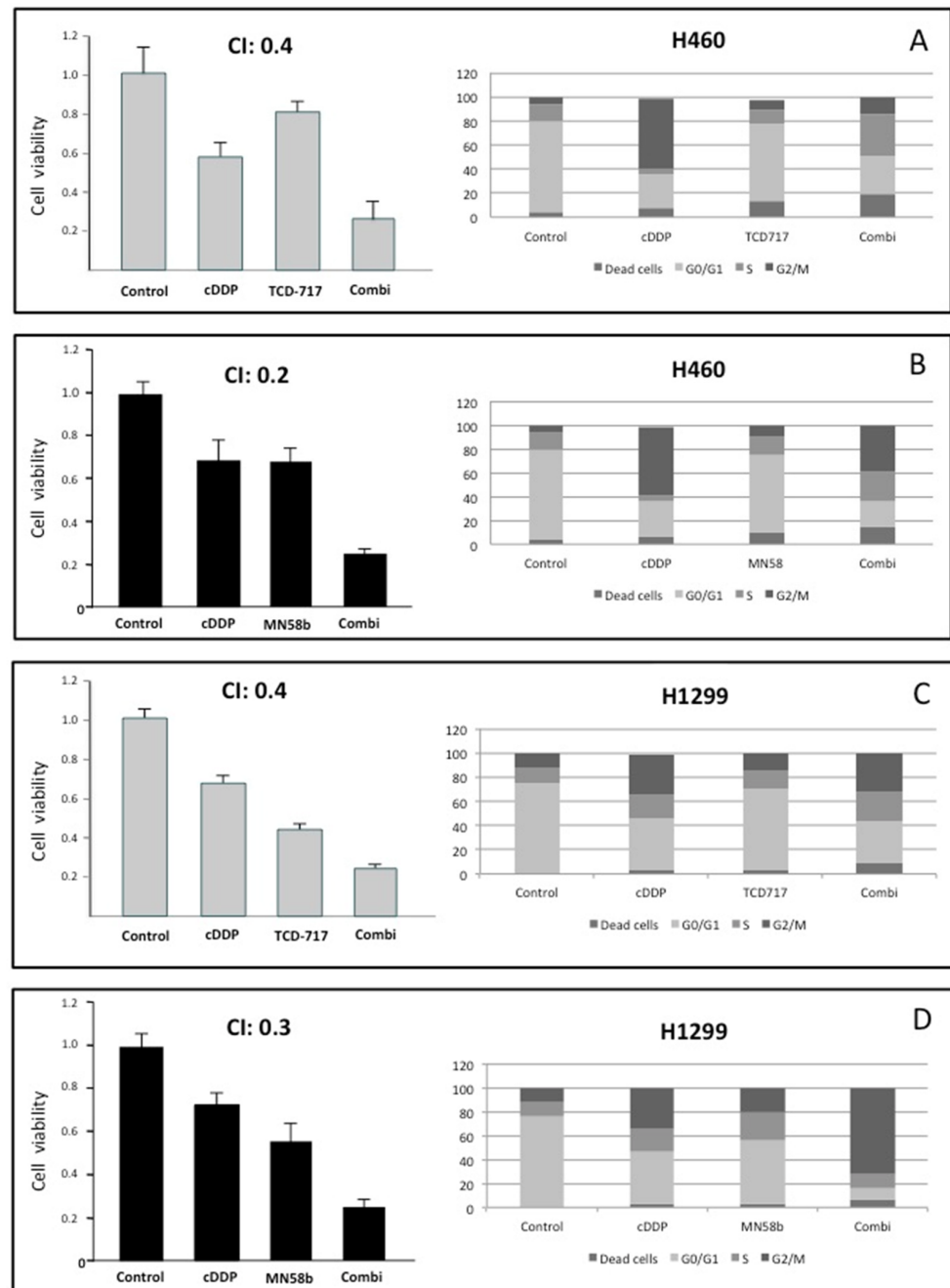
### 3.2. Synergism of Cisplatin and ChoK $\alpha$ Inhibitors against NSCLC Cells

The results shown above suggest the putative effectiveness of combined therapy between cisplatin and ChoK $\alpha$  inhibitors. In order to address this issue, the cytotoxic effects of combinations of cisplatin and the ChoK $\alpha$  inhibitors MN58b or RSM-932A/TCD-717 were determined in the human NSCLC H460 cell line (Figure 2A,B). To this end, cell viability was determined after treatment with different drug concentrations and schedules. Strong synergism (combination index, CI  $\leq$  0.4) was observed when the cells were treated following a sequential treatment initiated with cisplatin for a short period of time (5 h), followed by treatment with RSM-932A/TCD-717 (Figure 2A) or MN58b (Figure 2B) for longer times. Synergism was observed in the different timepoints analyzed, treating with ChoK $\alpha$  inhibitors from 24 to 72 h. A moderate synergistic effect was also found with both agents following a concomitant treatment (CI = 0.5–0.8) (data not shown). These results were confirmed using a second NSCLC cell line, H1299 (Figure 2C,D).

With the aim of further validating these results, we investigated the effect of this combination on cell cycle distribution using flow cytometry analysis. As shown in Figure 2, the combination of these agents displayed a stronger antiproliferative effect than when treating with these drugs separately. Furthermore, the promotion of cell death mediated by the combination was observed even under conditions when these agents separately displayed a minimum effect.

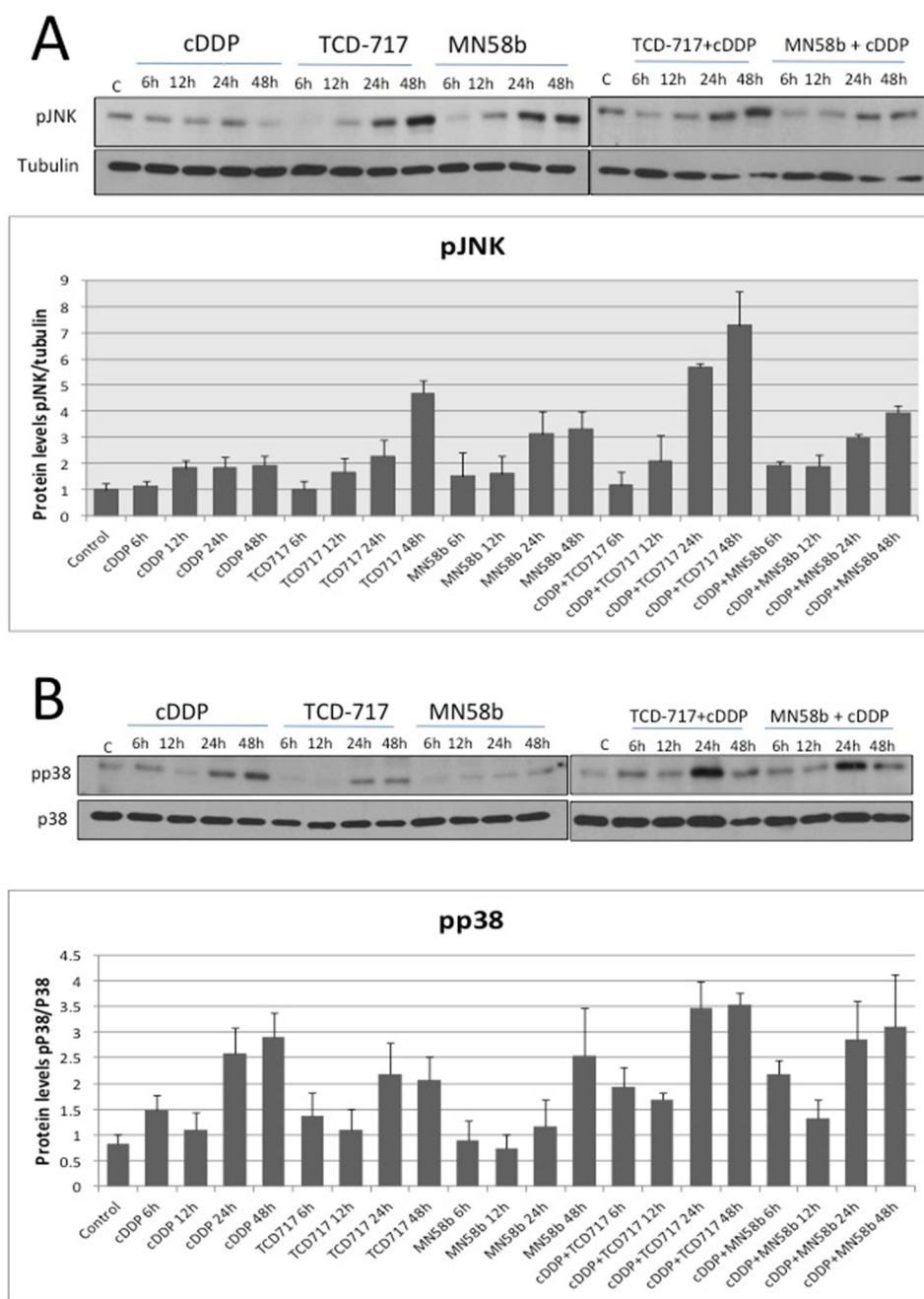
With the aim of elucidating the mechanism of this synergism, the putative modulation mediated by ChoK $\alpha$  inhibitors of JNK and p38 known to be involved in cell death induced by cisplatin [18] was investigated. As shown in Figure 3A, a two-fold activation of JNK was promoted by cisplatin after 12 h of treatment. ChoK $\alpha$  inhibitors induced a significant greater increase of activation of this pathway (3–4 fold). However, the major effect was observed after the combination of cisplatin and RSM-932A/TCD-717, increasing basal levels of p-JNK up to seven-fold induction. On the other hand, the p38 pathway was significantly more affected by cisplatin than by the ChoK $\alpha$  inhibitors (Figure 3B), also

with greater effects after combination. These results suggested that the p38 pathway is mainly activated by cisplatin, whereas JNK is mostly modulated by the ChoK $\alpha$  inhibitors, suggesting that the synergistic effect may be a consequence of a complementary increase in both pathways of the combinatory regimen.



**Figure 2.** Synergistic effect of ChoK $\alpha$  inhibitors and cisplatin in H460 and H1299 cells. (A,B) H460 cells were exposed to cisplatin for 5 h. Then, cells were treated with RSM-932A/TCD-717 (A) or MN58b (B) for 40 h. Cytotoxicity was evaluated by MTT assay (left panels). Combinations of the two drugs was also tested using flow cytometry analysis (right panels). (C,D) H1299 cells were treated as indicated for H460 cells with either RSM932A/TCD-717 (C) or MN58b (D). Represented CI value in each case is the mean of three independent experiments for each concentration in quadruplicate. As shown for both drugs, a CI < 1 indicated a strong synergistic effect. Furthermore, combination of the two drugs increased cell death compared to the two drugs alone, as determined by flow cytometry analysis. As shown, similar results were obtained with both cell lines.





**Figure 3.** MAPK pathway activation in response to treatment with cisplatin combined with ChoK $\alpha$  inhibitors. H460 human NSCLC cells were exposed to cisplatin, ChoK $\alpha$  inhibitors, or both treatments following a sequential schedule and showing a synergistic effect (cisplatin followed by ChoK $\alpha$  inhibitors). p-JNK (A) and p-p38 (B) levels were analyzed by Western blotting at different timepoints. Tubulin or total p38 protein were used to normalize. Results are the means of three independent experiments. Western blots are representative of one single experiment.

### 3.3. ChoK $\alpha$ Inhibitors Potentiate the Antitumoral Efficacy of Cisplatin In Vivo against NSCLC Xenografts, Reducing the Toxicity Associated with Cisplatin Treatment

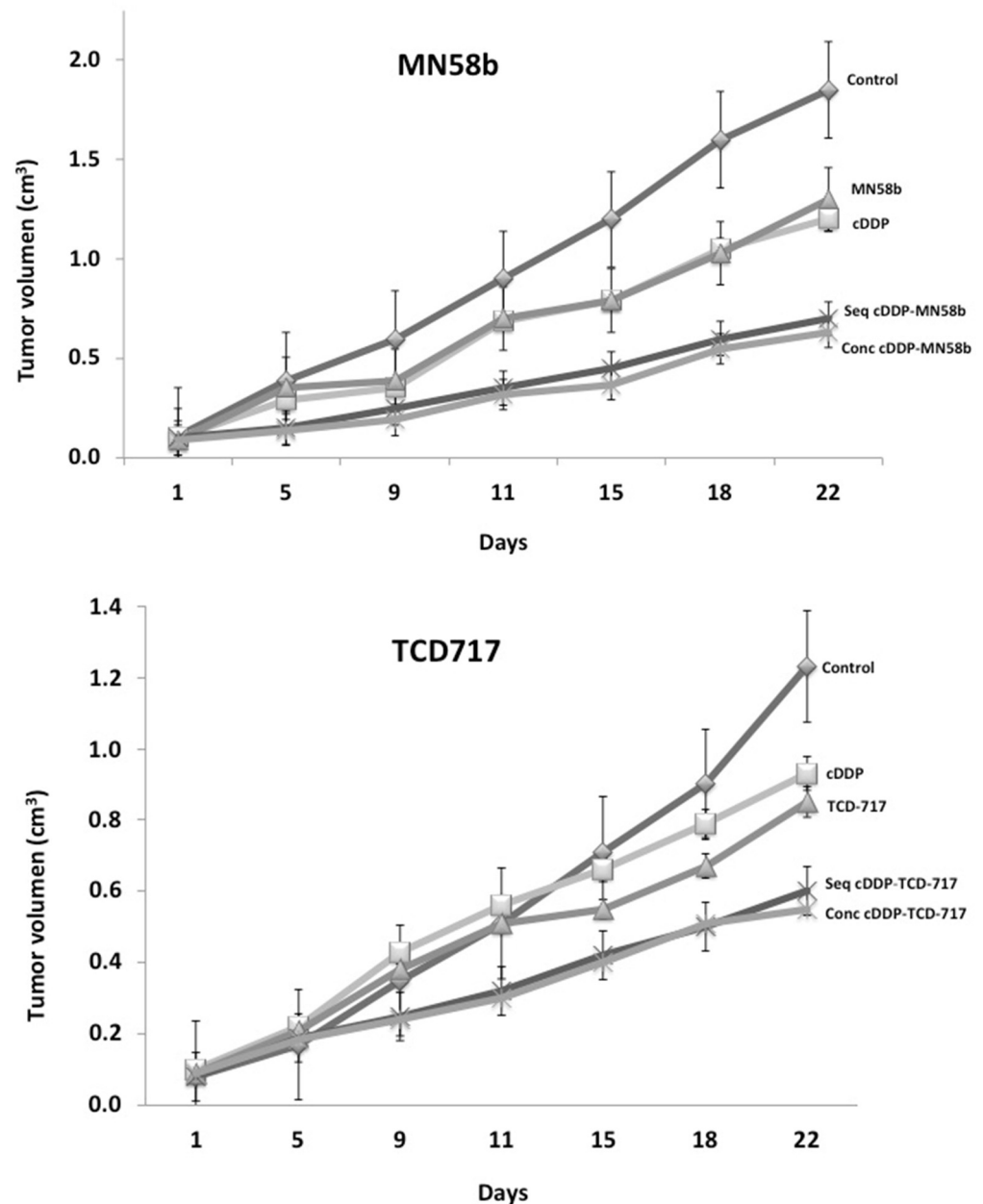
Cisplatin is still used in firstline chemotherapeutic regimens for NSCLC patients. As shown above, synergistic effects were observed when this agent was combined with ChoK $\alpha$  inhibitors in vitro in NSCLC cells. In order to further evaluate the potential therapeutic effect of these combinations, a series of experiments was carried out in vivo using human NSCLC H460 xenografts. Mice were inoculated subcutaneously with an injection of

$1 \times 10^6$  H460 cells in the flank mixed with Matrigel, as described in Material and Methods. When tumor volumes reached  $0.1 \text{ cm}^3$ , the animals were randomly distributed in groups ( $n = 8$ ), and treatments were assayed according to the in vitro regimens. The schedules of the treatments were determined when the maximum efficacy was reached following sequential treatment regimes initiated by cisplatin. A schematic representation of the followed treatments is shown in Table 3. Treatment of the NSCLC H460 tumors with ChoK $\alpha$  inhibitors in combination with cisplatin resulted in a significant reduction in tumor growth compared to these drugs alone (Figure 4).

**Table 3.** Synergistic antitumoral effect of cisplatin and ChoK $\alpha$  inhibitors in vivo. The antitumoral effect of the combination of cisplatin and MN58b or RSM932A/TCD-717 was evaluated in vivo using NSCLC xenografts. H460 cells were injected in nude mice, and when tumor volumes reached  $0.1 \text{ cm}^3$ , animals were randomly distributed in groups ( $n = 8$ ) to start treatments according to the schedules described in Material and Methods (indicated as the days treatment was performed for each drug or vehicle (DMSO)). Tumor growth inhibition, mean body weight, and statistical significance are shown. More similar efficacy was observed with the combinations than with much higher concentrations of cisplatin alone, significantly reducing toxicity. \* statistical significance  $p < 0.05$ .

MN58b	Drug	Schedule (Days)	Mean Body Weighth (Day 22)	Tumor Growth Inhibition (Day 22)	<i>p</i>
Control-1	Vehicle	1,3,4,5,8,10,11,12,15,17,18,19	23.4		
cDDP	cDDP (1 mg/kg)	1,4,8,11,15,18	23	33%	0.3
MN58b	MN58b (2 mg/kg)	1,3,5,8,10,12,15,17,19	24.4	35%	0.09
Sequential	cDDP (1 mg/kg)	1,4	23.9	67%	0.017 *
	MN58b (2 mg/kg)	8,10,12,15,17,19			
Concomitant	cDDP (1 mg/kg)	1,4,8,11,15,18	22.5	66%	0.160 *
	MN58b (2 mg/kg)	1,3,5,8,10,12,15,17,19			
Control cDDP	cDDP (4 mg/kg)	1,3,5,8,10,12,15,17,19	17.4 *	69%	0.014 *
TCD-717	Drug	Schedule (Days)	Mean Body Weighth (Day 22)	Tumor Growth Inhibition (Day 22)	<i>p</i>
Control-2	Vehicle	1,4,8,11,15,18	20.6		
cDDP	cDDP (1 mg/kg)	1,4,8,11,15,18	20.9	24%	0.4
TCD-717	TCD717 (2 mg/kg)	1,4,8,11,15,18	19.9	31%	0.16
Sequential	cDDP (1 mg/kg)	1,4	21.2	51%	0.03 *
	TCD717 (2 mg/kg)	8,11,15,18			
Concomitant	cDDP (1 mg/kg)	1,4,8,11,15,18	20.1	55%	0.04 *
	TCD717 (2 mg/kg)	1,4,8,11,15,18			

With this combination therapy, no external signs of toxicity were observed during the treatment, as indicated by the maintenance of body weight. The concomitant treatment of MN58b reached the same efficacy as that of the sequential group, but much higher doses of cytotoxic agents were required. By contrast, to obtain similar effectiveness in the inhibition of tumor growth (65%) using cisplatin as a single agent, its dosage had to be increased from 1 to 4 mg/kg, conditions in which clear signs of toxicity were observed, including a significant reduction in body weight (Table 3). Similar results were obtained when the RSM-932A/TCD-717 inhibitor was used (Table 3).



**Figure 4.** Tumor growth inhibition on H460 xenografts by combination of MN58b or RSM-932A/TCD-717 and cisplatin. H460 cells were injected in nude mice, and when tumor volumes reached  $0.1 \text{ cm}^3$ , animals were randomly distributed in groups ( $n = 8$ ) to start treatments. Mice were treated with the indicated ChoK $\alpha$  and cisplatin (cDDP) either alone or following sequential or concomitant schedules. A significant synergistic effect was observed with the combined therapy in both cases: MN58b (upper) and RSM-932A/TCD-717 (lower).

#### 4. Discussion

NSCLC accounts for 80–85% of all bronchogenic malignancies. Included in this category are squamous cell carcinoma (25%), adenocarcinoma (40%), and large cell carcinoma (10%). Extensive research has been performed in the last decade using newly developed drugs as an important attempt to improve clinical outcomes, aiming at achieving higher responses and longer survival rates. In this sense, although the introduction of new, active agents, including paclitaxel, docetaxel, gemcitabine, pemetrexed, and vinorelbine, was promising, the finding of strong cross-resistances is a serious drawback [4]. Furthermore, cancer embraces different diseases, and specific drugs and regimens are required for each

specific tumor type. Currently, among the different drugs approved by the FDA as anti-cancer agents, only a few are related to NSCLC. Bevacizumab, a monoclonal antibody that binds to the vascular endothelial growth factor (VEGF), blocking interaction with its receptors on endothelial cells, prevents the initiation of new blood vessel growth. Some studies have demonstrated that the addition of bevacizumab to platinum-based chemotherapy in addition to gemcitabine or paclitaxel improves chemotherapy response, progression-free survival, and overall survival. The use of the tyrosine kinase inhibitor gefitinib first and, more recently, osimertinib proved to be efficient as a first therapy for NSCLC harbouring EGFR mutations [5].

Efforts have been dedicated in recent years to immunotherapy based on specific antibodies against PD-1, its ligand (PD-L1), and CTLA-4. This effort has translated into improved survival for NSCLC patients. Both first- and second-line treatments have been intensively explored, either alone or in combination with diverse chemotherapy treatments. As a result of this search for improved protocols and regimens, the use of these ICIs along with chemotherapy seems to be most promising and has translated into improved survival for NSCLC patients [6]. However, for 70% of these NSCLC patients, the OS is still in very poor figures and makes it necessary to investigate further alternative targets and new combinatorial regimens. Keeping with this, the use of drugs with different mechanisms of action may be useful for overcoming drug resistance to individual treatments. Here, we reported the successful combination of platinum-based chemotherapy with a novel targeted therapy approach as an innovative strategy against solid tumors, such as inhibition of an enzyme that is critical for phospholipid metabolism.

Both primary and acquired resistance is one of the major problems in cancer treatment. The mechanism of action for cisplatin consists of the interaction with N7 sites of purine bases to form inter- and intrastrand crosslinks. The main mechanisms of resistance to cisplatin are reduction in the accumulation of cisplatin by changing uptake or efflux; inactivation of the drug by glutathione, metallothionein, or other sulphur-containing molecules; increased repair of adducts; and increased cisplatin adduct tolerance [19–23]. In contrast, the mechanism of action for ChoK $\alpha$  has been related to the metabolic disbalance produced by the inhibition of phosphatidylcholine synthesis. The inhibition of this enzyme by pharmacological or siRNA approaches produces a loss of mitochondrial potential and cytochrome c release, increased ceramide production, ER stress, unfold protein response (UPR), and ROS homeostasis via glutathione levels. Additional effects due to mitochondria function render a reduction in citrate synthase expression and AMPK activation. Finally, this cascade of events induces an increase in glucose and acetate uptake to overcome the metabolic stress. All these events induce apoptosis or necrosis, specifically in cancer cells (reviewed in [9]).

Resistance to ChoK $\alpha$  has been related to an increase in acid ceramidase, which drains the elevated levels of ceramides and allows cancer cells to keep proliferating [16]. This effect was found in primary NSCLC cultures and in ChoK $\alpha$ -resistant H460 cells, and it was reverted by acid ceramidase inhibitors [24]. However further studies are needed to define precisely a complete set of biomarkers to define ChoK $\alpha$  inhibitor resistance. This will allow efficient selection for NSCLC patients who are potentially resistant to the proposed combination.

In this study, we demonstrated that neither cisplatin nor other drugs usually taking part in platinum-based chemotherapy of NSCLC patients displayed cross-resistance with ChoK $\alpha$  inhibitors. These results may be explained by the differential mechanisms of action of these novel drugs, whose activities rely on inhibiting ChoK $\alpha$ , the first enzyme of the biosynthesis of the major phospholipid component of cell membranes [16,17], or interfering with the replication of DNA [20]. This effect is reflected in the responsiveness of primary tumors from NSCLC patients, and also in tumor-derived cell lines [24]. Therefore, when cells are promoted to division, they are simultaneously blocked at two different phases of the cell cycle, increasing the possibilities to overcome resistance to any of these agents when used alone. This is further supported by the evidence presented in our study where the

p38 and the JNK pathways were differentially activated by cisplatin and ChoK $\alpha$  inhibitors, while the combination of both drugs triggered a complementary increase in both pathways.

We also demonstrated here, both in vitro and in vivo, that the use of this combined therapy achieved another important aim of a combination regimen: obtaining similar efficacy using lower concentrations of the chemotherapeutic agents and, therefore, reducing their associated toxicities. ChoK $\alpha$  inhibitors have entered Phase I clinical trials, in part based on the involvement of this enzyme and the effect of its inhibitors on NSCLC. In this sense, ChoK $\alpha$  gene expression levels are independent prognosis factors for early-stage NSCLC patients [8], suggesting an easy molecular method for identifying patients that could benefit from this treatment. Therefore, since platinum-based chemotherapy continues to constitute a key tool in the management of NSCLC and ChoK $\alpha$  inhibition constitutes a “first in class” targeted therapy for NSCLC patients, our study provides the basis for a promising new alternative of combination treatment therapy for patients with this disease.

## 5. Conclusions

Cancer is a multifactorial disease with a large diversity of clinical manifestations. Lung cancer represents one of the most devastating types of cancer, being responsible for over 1.8 million deaths every year worldwide. NSCLC represents over 80% of all lung cancers. Significant improvements in clinical management have been achieved in the last decade with the introduction of third-generation cytotoxic drugs, targeted personalized therapies, and immune checkpoint inhibitors (ICIs). However, the clinical outcome of a 5-year survival rate is still poor. New therapeutic approaches are urgently needed for these patients. We provided evidence that ChoK $\alpha$  is a bona fide new target for NSCLC patients and that its inhibitors are potent therapeutic agents that can be efficiently combined with cisplatin-based chemotherapeutic regimens. A limitation of our study is that we presented this effect in two established NSCLC cell lines, H460 (derived from a large cell lung cancer) and H1299 (derived from a carcinoma), which represent only 50% of the NSCLC types. This novel strategy requires confirmation in appropriate Phase II clinical trials.

**Author Contributions:** Conceptualization, J.C.L.; methodology, J.C.L., R.P., J.d.C. and A.C.; resources, J.C.L., R.P. and J.d.C.; writing—original draft preparation, J.C.L.; writing—review and editing, J.C.L., R.P., J.d.C. and A.C.; supervision, J.C.L.; funding acquisition, J.C.L. and R.P. All authors have read and agreed to the published version of the manuscript.

**Funding:** This research was funded by MCIN/AEI/10.13039/501100011033, Grant PID2020-116165RB-C21 and Fondo de Investigaciones Sanitarias, Instituto de Salud Carlos III, Spain, Grant PI20-00335 supported by FEDER funds.

**Institutional Review Board Statement:** The study was conducted in accordance with the Declaration of Helsinki and approved by the Institutional Ethics Committee of the La Paz Hospital (HULP: PI-1409) on 10 December 2012. The animal study protocol was approved by the Institutional Ethics Committee of CSIC (CEEA-CNB: 080025) on 18 February 2008.

**Informed Consent Statement:** Informed consent was obtained from all subjects involved in the study.

**Acknowledgments:** We acknowledge Ana Ramírez de Molina for discussion of the research design, as well as Ana de la Cueva, Rosario Machado-Pinilla, and Vanessa Rodríguez-Fanjul for their excellent technical contributions.

**Conflicts of Interest:** The authors declare no conflict of interest. The funders had no role in the design of the study; in the collection, analysis, or interpretation of data; in the writing of the manuscript; or in the decision to publish the results.

## References

1. Chaitanya Thandra, K.; Barsouk, A.; Saginala, K.; Sukumar Aluru, J.; Barsouk, A. Epidemiology of Lung Cancer. *Contemp. Oncol.* **2021**, *25*, 45–52. [CrossRef]
2. Griesinger, F.; Korol, E.E.; Kayaniyil, S.; Varol, N.; Ebner, T.; Goring, S.M. Efficacy and safety of first-line carboplatin-versus cisplatin-based chemotherapy for non-small cell lung cancer: A meta-analysis. *Lung Cancer* **2019**, *135*, 196–204. [CrossRef] [PubMed]

3. Schiller, J.H.; Harrington, D.; Belani, C.; Langer, C.; Sandler, A.; Krook, J.; Zhu, J.; Johnson, D.H. Comparison of Four Chemotherapy Regimens for Advanced Non-Small-Cell Lung Cancer. *N. Engl. J. Med.* **2002**, *346*, 92–98. [CrossRef] [PubMed]
4. Baxevanos, P.; Mountzios, G. Novel chemotherapy regimens for advanced lung cancer: Have we reached a plateau? *Ann. Transl. Med.* **2018**, *6*, 139. [CrossRef] [PubMed]
5. Remon, J.; Hendriks, L.E.L. Targeted therapies for unresectable stage III non-small cell lung cancer. *Mediastinum* **2021**, *5*, 22. [CrossRef]
6. Reck, M.; Remon, J.; Hellmann, M.D. First-Line Immunotherapy for Non-Small-Cell Lung Cancer. *J. Clin. Oncol.* **2022**, *40*, 586–597. [CrossRef]
7. Ramirez de Molina, A.; Gallego-Ortega, D.; Sarmentero, J.; Bañez-Coronel, M.; Martin-Cantalejo, Y.; Lacal, J.C. Choline kinase is a novel oncogene that potentiates RhoA-induced carcinogenesis. *Cancer Res.* **2005**, *65*, 5647–5653. [CrossRef]
8. Ramirez de Molina, A.; Sarmentero-Estrada, J.; Belda-Iniesta, C.; Taron, M.; Ramirez de Molina, V.; Cejas, P.; Skrzypski, M.; Gallego-Ortega, D.; de Castro, J.; Casado, E.; et al. Expression of choline kinase alpha to predict outcome in patients with early-stage non-small-cell lung cancer: A retrospective study. *Lancet Oncol.* **2007**, *8*, 889–897. [CrossRef]
9. Lacal, J.; Zimmerman, T.; Campos, J. Choline Kinase: An Unexpected Journey for a Precision Medicine Strategy in Human Diseases. *Pharmaceutics* **2021**, *13*, 788. [CrossRef]
10. Banez-Coronel, M.; de Molina, A.; Rodriguez-Gonzalez, A.; Sarmentero, J.; Ramos, M.; Garcia-Cabezas, M.; Garcia-Oroz, L.; Lacal, J. Choline Kinase Alpha Depletion Selectively Kills Tumoral Cells. *Curr. Cancer Drug Targets* **2008**, *8*, 709–719. [CrossRef]
11. Glunde, K.; Raman, V.; Mori, N.; Bhujwalla, Z.M. RNA interference-mediated choline kinase suppression in breast cancer cells induces differentiation and reduces proliferation. *Cancer Res.* **2005**, *65*, 11034–11043. [CrossRef]
12. Yalcin, A.; Clem, B.; Makoni, S.; Clem, A.; Nelson, K.; Thornburg, J.; Siow, D.; Lane, A.N.; E Brock, S.; Goswami, U.; et al. Selective inhibition of choline kinase simultaneously attenuates MAPK and PI3K/AKT signaling. *Oncogene* **2009**, *29*, 139–149. [CrossRef]
13. Lacal, J.C.; Campos, J. Preclinical Characterization of RSM-932A, a Novel Anticancer Drug Targeting the Human Choline Kinase Alpha, an Enzyme Involved in Increased Lipid Metabolism of Cancer Cells. *Mol. Cancer Ther.* **2015**, *14*, 31–39. [CrossRef]
14. De Cáceres, I.I.; Cortés-Sempere, M.; Moratilla, C.; Machado-Pinilla, R.; Rodriguez-Fanjul, V.; Manguan-García, C.; Cejas, P.; Lopez-Rios, F.; Paz-Ares, L.; de CastroCarpeño, J.; et al. IGFBP-3 hypermethylation-derived deficiency mediates cisplatin resistance in non-small-cell lung cancer. *Oncogene* **2010**, *29*, 1681–1690. [CrossRef]
15. Chou, T.C.; Talalay, P. Quantitative analysis of dose-effect relationships: The combined effects of multiple drugs or enzyme inhibitors. *Adv. Enzym. Regul.* **1984**, *22*, 27–55. [CrossRef]
16. Rodríguez-González, A.; de Molina, A.R.; Fernández, F.; Lacal, J.C. Choline kinase inhibition induces the increase in ceramides resulting in a highly specific and selective cytotoxic antitumoral strategy as a potential mechanism of action. *Oncogene* **2004**, *23*, 8247–8259. [CrossRef]
17. Rodríguez-González, A.; de Molina, R.; Fernández, F.; Ramos, M.A.; Núñez, M.D.C.; Campos, J.; Lacal, J.C. Inhibition of choline kinase as a specific cytotoxic strategy in oncogene-transformed cells. *Oncogene* **2003**, *22*, 8803–8812. [CrossRef]
18. Sánchez-Pérez, I.; Perona, R. Lack of c-Jun activity increases survival to cisplatin. *FEBS Lett.* **1999**, *453*, 151–158. [CrossRef]
19. Kelland, L. The resurgence of platinum-based cancer chemotherapy. *Nat. Rev. Cancer* **2007**, *7*, 573–584. [CrossRef]
20. Lai, G.-M.; Ozols, R.F.; Young, R.C.; Hamilton, T.C. Effect of Glutathione on DNA Repair in Cisplatin-Resistant Human Ovarian Cancer Cell Lines. *JNCI J. Natl. Cancer Inst.* **1989**, *81*, 535–539. [CrossRef]
21. Zeng-Rong, N.; Paterson, J.; Alpert, L.; Tsao, M.; Viallet, J.; Alaoui-Jamali, M.A. Elevated DNA repair capacity is associated with intrinsic resistance of lung cancer to chemotherapy. *Cancer Res.* **1995**, *55*, 4760–4764.
22. Komatsu, M.; Sumizawa, T.; Mutoh, M.; Chen, Z.S.; Terada, K.; Furukawa, T.; Yang, X.L.; Gao, H.; Miura, N.; Sugiyama, T.; et al. Copper-transporting P-type adenosine triphosphatase (ATP7B) is associated with cisplatin resistance. *Cancer Res.* **2000**, *60*, 1312–1316.
23. Mamenta, E.L.; Poma, E.E.; Kaufmann, W.K.; Delmastro, D.A.; Grady, H.L.; Chaney, S.G. Enhanced replicative bypass of platinum-DNA adducts in cisplatin-resistant human ovarian carcinoma cell lines. *Cancer Res.* **1994**, *54*, 3500–3505.
24. Ramírez de Molina, A.; de la Cueva, A.; Machado-Pinilla, R.; Rodríguez-Fanjul, V.; Gómez del Pulgar, T.; Cebrián, A.; Perona, R.; Lacal, J.C. Acid ceramidase as a chemotherapeutic target to overcome resistance to the antitumoral effect of choline kinase  $\alpha$  inhibition. *Curr. Cancer Drug Targets* **2012**, *12*, 617–624. [CrossRef]

Review

# A Comprehensive Overview of Globally Approved JAK Inhibitors

Ahmed M. Shawky<sup>1</sup>, Faisal A. Almalki<sup>2,\*</sup>, Ashraf N. Abdalla<sup>3,4</sup>, Ahmed H. Abdelazeem<sup>5,6</sup>  
and Ahmed M. Gouda<sup>5,\*</sup>

<sup>1</sup> Science and Technology Unit (STU), Umm Al-Qura University, Makkah 21955, Saudi Arabia; amesmail@uqu.edu.sa

<sup>2</sup> Department of Pharmaceutical Chemistry, Faculty of Pharmacy, Umm Al-Qura University, Makkah 21955, Saudi Arabia

<sup>3</sup> Department of Pharmacology and Toxicology, Faculty of Pharmacy, Umm Al-Qura University, Makkah 21955, Saudi Arabia; anabdrabo@uqu.edu.sa

<sup>4</sup> Department of Pharmacology and Toxicology, Medicinal and Aromatic Plants Research Institute, National Center for Research, Khartoum 2404, Sudan

<sup>5</sup> Department of Medicinal Chemistry, Faculty of Pharmacy, Beni-Suef University, Beni-Suef 62514, Egypt; ahmed.haasn77@yahoo.com

<sup>6</sup> Department of Pharmacy, College of Pharmacy, Riyadh Elm University, Riyadh 11681, Saudi Arabia

\* Correspondence: famalki@uqu.edu.sa (F.A.A.); ahmed.gouda@pharm.bsu.edu.eg (A.M.G.)

**Abstract:** Janus kinase (JAK) is a family of cytoplasmic non-receptor tyrosine kinases that includes four members, namely JAK1, JAK2, JAK3, and TYK2. The JAKs transduce cytokine signaling through the JAK-STAT pathway, which regulates the transcription of several genes involved in inflammatory, immune, and cancer conditions. Targeting the JAK family kinases with small-molecule inhibitors has proved to be effective in the treatment of different types of diseases. In the current review, eleven of the JAK inhibitors that received approval for clinical use have been discussed. These drugs are abrocitinib, baricitinib, delgocitinib, fedratinib, filgotinib, oclacitinib, pacritinib, peficitinib, ruxolitinib, tofacitinib, and upadacitinib. The aim of the current review was to provide an integrated overview of the chemical and pharmacological data of the globally approved JAK inhibitors. The synthetic routes of the eleven drugs were described. In addition, their inhibitory activities against different kinases and their pharmacological uses have also been explained. Moreover, their crystal structures with different kinases were summarized, with a primary focus on their binding modes and interactions. The proposed metabolic pathways and metabolites of these drugs were also illustrated. To sum up, the data in the current review could help in the design of new JAK inhibitors with potential therapeutic benefits in inflammatory and autoimmune diseases.

**Keywords:** JAK; synthesis; kinase inhibitory activity; pharmacological uses; binding mode/interactions

**Citation:** Shawky, A.M.; Almalki, F.A.; Abdalla, A.N.; Abdelazeem, A.H.; Gouda, A.M. A Comprehensive Overview of Globally Approved JAK Inhibitors. *Pharmaceutics* **2022**, *14*, 1001. <https://doi.org/10.3390/pharmaceutics14051001>

Academic Editor: Francesca Musumeci

Received: 1 April 2022

Accepted: 28 April 2022

Published: 6 May 2022

**Publisher's Note:** MDPI stays neutral with regard to jurisdictional claims in published maps and institutional affiliations.



**Copyright:** © 2022 by the authors. Licensee MDPI, Basel, Switzerland. This article is an open access article distributed under the terms and conditions of the Creative Commons Attribution (CC BY) license (<https://creativecommons.org/licenses/by/4.0/>).

## 1. Introduction

Janus kinases (JAKs) are intracellular, non-receptor tyrosine kinases [1]. The JAK family consists of four members, including JAK1, JAK2, JAK3, and TY2K. Since the first discovery of JAKs by Wilks thirty years ago [2], great efforts have been made to understand their structure and functions. The four JAKs play an essential role in the transduction of the cytokine-mediated signals, which takes place through the JAK-signal transducers and activators of the transcription (STAT) pathway [3]. Four members of the JAK family have emerged as potential drug targets in different types of diseases [4].

In the current review, we aimed to provide an integrated overview of the chemical and pharmacological data of the globally approved JAK inhibitors that were approved for the treatment of inflammatory, autoimmune, and myeloproliferative diseases. Highlighting the differences in chemical structure, binding interactions, kinase inhibitory activities,

pharmacological activities, and metabolic pathways of these drugs could help in the design of new, more potent, and safer JAK inhibitors.

### 1.1. Structure of JAKs

The structure of JAKs (Figure 1) consists of 7 domains, JH1-JH7 [5]. The four JAKs have the same domains with an overall similarity of 48% [6]. The first domain is JH1, which exists at the C-terminal. This domain is also called the kinase domain because it is responsible for the enzymatic activity of the kinase. The second domain, JH2, is the pseudo-kinase domain, which lacks the tyrosine kinase activity [7]. However, JH2 plays an important role in the regulation of kinase activity [8]. JAKs also include two domains, JH3-JH4, which share homology with the Src-homology-2 (SH2) domain, while the fourth region of JAKs is the FERM domain, which exists at the N-terminal and plays a role in the binding of JAKs with cytokine receptors [9].

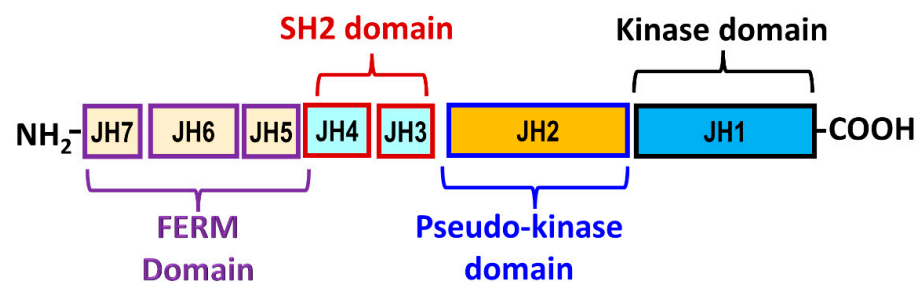


Figure 1. Domain structure of JAKs.

### 1.2. JAK-STAT Pathway

Several ligands such as cytokines and growth factors have been reported to activate the JAK-STAT pathway [10]. Following the activation of JAKs, phosphorylation and dimerization of STATs take place (Figure 2). The phosphorylated STATs enter the nucleus, where they initiate a suitable transcriptional response in the genes that regulate immunity, inflammation, and hematopoiesis [10–12].

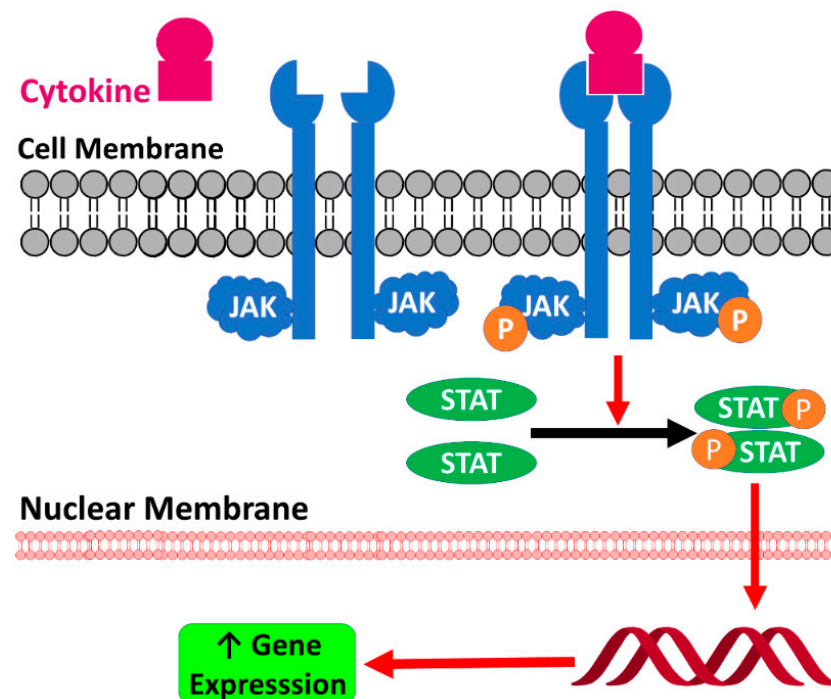


Figure 2. JAK-STAT pathway.



### 1.3. Therapeutic Potential of JAK Inhibition

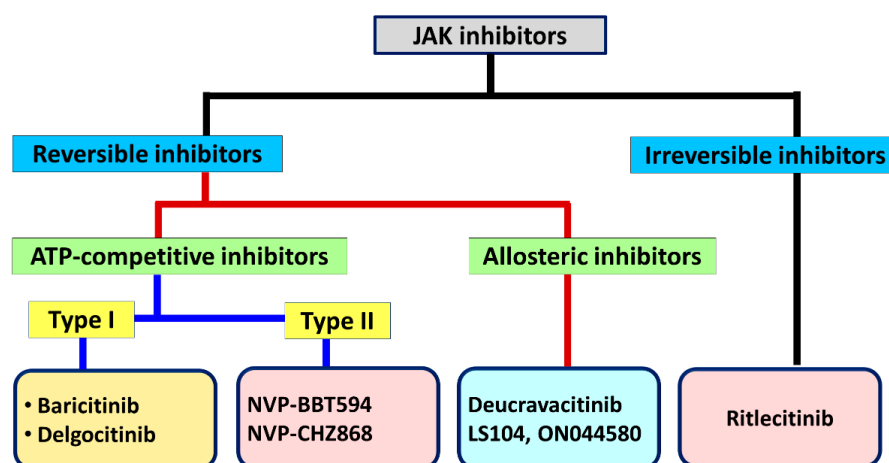
The JAK-STAT pathway is responsible for the transduction of cytokines and growth factor signals that play a crucial role in inflammation and autoimmune diseases [13]. Among these kinases, JAK1 seems to play a crucial role in pruritic dermatitis [14], allergic rhinitis [15], asthma [16], and inflammatory bowel disease [17]. Targeting JAK1 with small-molecule inhibitors has proved efficacy in the treatment of these diseases [16,18,19]. Moreover, several small molecules with JAK1 and JAK2 inhibitory activity have also provided therapeutic benefits in the treatment of rheumatoid arthritis, psoriasis, and pruritis [20]. In addition, several JAK3 selective inhibitors have been evaluated for their efficacy in the treatment of rheumatoid arthritis [20]. In addition, JAK1/TYK2 dual inhibitors have also been developed with potential therapeutic options in inflammatory diseases [21]. Furthermore, TYK2 selective inhibitors may also be useful in the treatment of autoimmune diseases [20,22].

On the other hand, excessive activation of JAKs has also been reported in different types of cancer [23]. The JAK/STAT3 pathway plays an important role in the proliferation and angiogenesis of solid tumors [23]. In 2005, the discovery of JAK2 mutation (JAK2V617F) in myeloproliferative neoplasms has attracted much attention [24,25]. This discovery led to a better understanding of these diseases. In addition, JAK2V617F has emerged as a potential therapeutic target for myeloproliferative neoplasms [26,27]. In addition, the JAK1/JAK2 inhibitor, ruxolitinib, has also been approved for the treatment of myelofibrosis and polycythemia vera [28,29]. Moreover, the dual inhibition of JAK2 and FLT3 could also provide therapeutic option in the treatment of acute myelogenous leukemia and myeloproliferative neoplasms [30–32].

### 1.4. Classification of JAK Inhibitors

JAK inhibitors can be divided into two generations [33]. The first-generation includes small molecules such as baricitinib and tofacitinib, which act as non-selective inhibitors of JAKs. On the other hand, second-generation drugs such as filgotinib and upadacitinib have selective inhibitory activity against JAKs [33]. This difference in the selectivity of the two generations is associated with some differences in their safety and efficacy.

One the other hand, JAK inhibitors may also be classified based on their binding mode and the type of interactions with the amino acids in JAKs into reversible (competitive) and irreversible (covalent) inhibitors (Figure 3).



**Figure 3.** Classification of JAK inhibitors with representative examples for each type.

#### 1.4.1. Reversible JAK Inhibitors

Competitive JAK inhibitors form reversible (non-covalent) binding interactions with the amino acids in the four JAKs. The binding interactions formed by this type of JAK

inhibitors include hydrogen bonds and hydrophobic interactions. The class of reversible JAK inhibitors can also be classified into two sub-classes.

#### ATP-Competitive Inhibitors

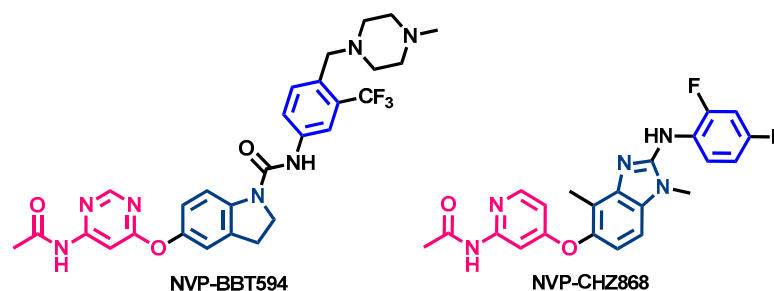
The mechanism of action of these inhibitors depends on their competition with ATP for the catalytic ATP-binding site in JAKs [27,34]. These inhibitors may also be classified based on the conformation of the kinase domain to which they bind:

- Type I JAK Inhibitors

These inhibitors bind to the ATP-binding site of the JAKs under the active conformation of the kinase domain [27,34]. This includes clinically approved drugs such as filgotinib, which acts and is classified as a selective JAK1, while fedratinib exhibits the selective inhibition of JAK2 [20,35]. On the other hand, tofacitinib and peficitinib act by blocking multiple JAKs [20,36]. The ability of type I JAK inhibitors to bind to multiple kinases and act as non-selective inhibitors could be due to the highly conserved structure of the ATP-binding site in the four JAKs [18].

- Type II JAK Inhibitors

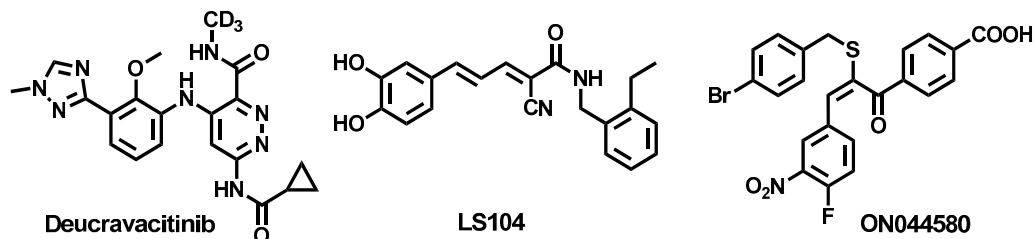
Type II JAK inhibitors also bind to the ATP-binding site of the kinase domain in the inactive conformation of JAKs [27,34]. NVP-BBT594 and NVP-CHZ868 (Figure 4) are representative examples of type II inhibitor, which target JAK2 [37,38].



**Figure 4.** JAK2 inhibitors, NVP-BBT594 and NVP-CHZ868.

- Allosteric JAK Inhibitors

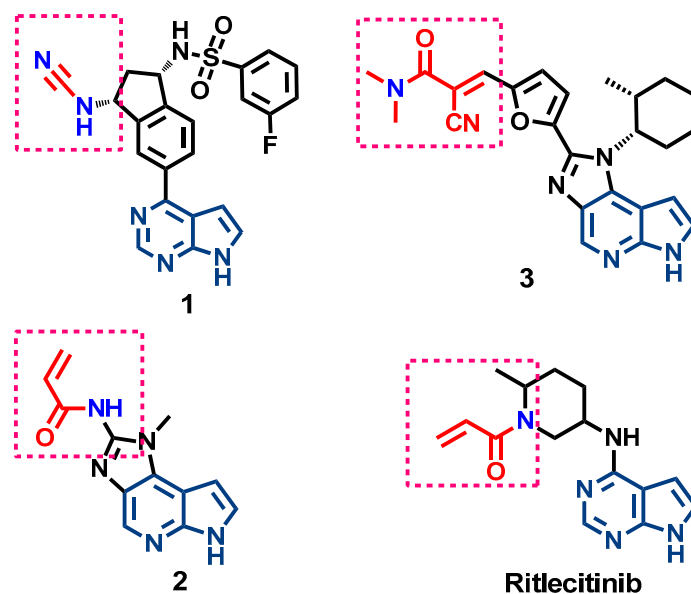
The allosteric JAK inhibitors (Figure 5) include small molecule inhibitors that bind to a site other than the ATP-binding site in JAKs [27,34]. Among these inhibitors, deucravacitinib (BMS-986165) act as a selective allosteric inhibitor of TYK2 [39]. In addition, LS104, and ON044580 are examples of JAK2 allosteric inhibitors [34,40–42].



**Figure 5.** Allosteric JAKs inhibitors.

#### 1.4.2. Irreversible JAK3 Inhibitors

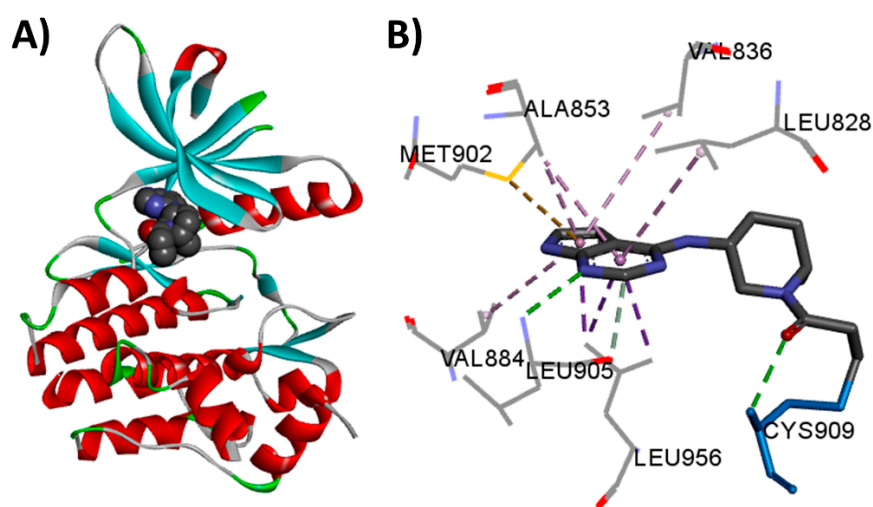
This class of irreversible JAK inhibitors (Figure 6) that target JAK3 was also reported [43–45]. The mechanism of action of these inhibitors depends on the covalent interaction with the unique Cys909 residue in JAK3 [43]. The chemical structure of these inhibitors has a covalent-bond forming group such as acrylamide and  $\alpha$ -cyanoacrylamide, which can bind covalently with Cys909 residue (Figure 6).



**Figure 6.** JAK3 covalent inhibitors.

Compound 1 was reported among a series of cyanamide-based JAK3 covalent inhibitors [43]. Moreover, compounds 2 ( $IC_{50} = 0.003 \mu M$ ) and 3 ( $IC_{50} = 154 pM$ ) were also reported with potent and selective inhibitory activity against JAK3 [44,45].

Ritlecitinib (Figure 6) is an irreversible inhibitor of JAK3, which is currently under evaluation in clinical trials in humans [43,46]. The inhibitory activity of ritlecitinib was mediated by a covalent interaction with Cys909 residue in JAK3 [43]. The binding mode and interaction of ritlecitinib in JAK3 (pdb: 5TOZ) are visualized in Figure 7. The crystal structure was downloaded from the protein data bank (<https://www.rcsb.org/>, accessed on 11 November, 2021). In this work, the crystal structures of JAK kinases were visualized using the Discovery Studio Visualizer [47]. The crystals were prepared by removing water molecules following the previous reports [48,49]. Moreover, 2/3D binding modes of the JAK inhibitors into the co-crystallized kinases were visualized according to the previous report [50].



**Figure 7.** JAK3 (pdb: 5TOZ) bound to ritlecitinib: (A) 3D representation of JAK3 bound to ritlecitinib (shown as CPK); (B) 3D binding mode of ritlecitinib showing one covalent bond with Cys909, hydrogen bonds (shown as green-dotted lines), and multiple hydrophobic interactions, this figure was generated using Discovery Studio Visualizer (V16.1.0.15350).

### 1.5. Mutation of JAKs

Besides the role of wild-type of JAKs in autoimmune and inflammatory diseases, JAK mutants also play crucial roles in myeloproliferative, lymphomas, and leukemias diseases [6]. JAK1 mutation has been found in acute lymphoblastic leukemia [51]. In addition, JAK2 mutation (JAK2V617F) has been associated with the incidence of myeloproliferative neoplasms [24,52]. The occurrence of JAK2 mutation was reported in nearly all patients with polycythaemia vera (PV) [53].

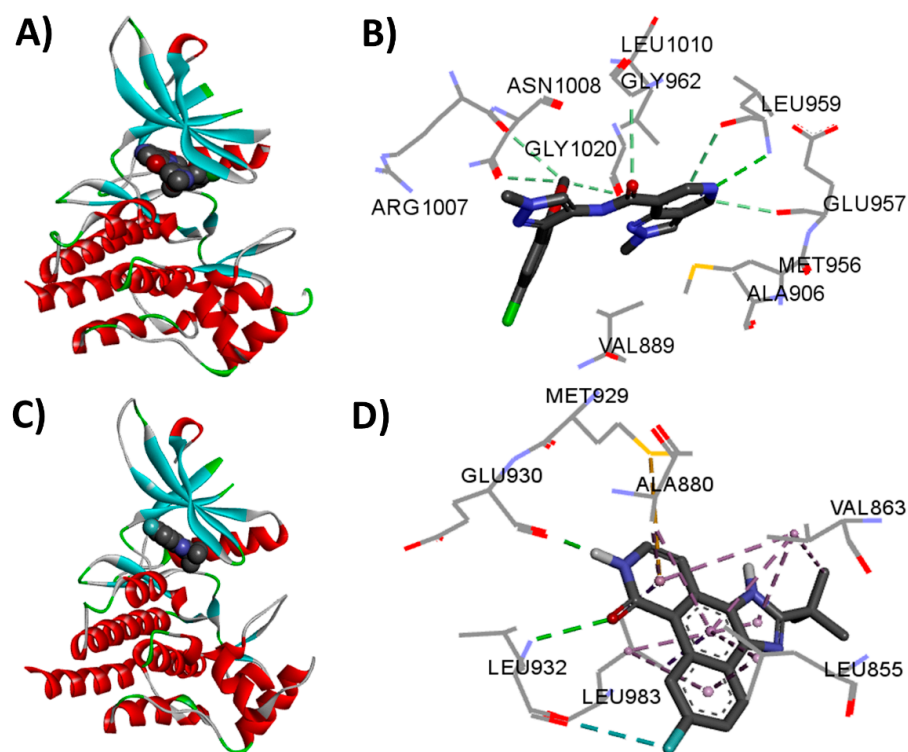
Moreover, the expression of the JAK3 mutant was associated with the induction of leukemia in mice [54]. JAK3 mutation was also reported in small percent of patient with T-cell acute lymphoblastic leukemia. It was also associated with the occurrence of severe combined immunodeficiency [55].

On the other hand, TYK2 mutations were also associated with immunodeficiency with T-cell lymphopenia [56]. It was also associated with increased susceptibility to bacterial and/or viral infections. The deficiency of TYK2 was associated with recurrent respiratory infection [57].

### 1.6. Crystal Structure of JAKs

The advances in X-ray crystallography have provided a lot of data about the structure and function of different members of the JAK family. This data has helped in the design of selective JAK inhibitors [58]. Many of the crystal structures of different JAKs are available from the protein data bank (<https://www.rcsb.org/>). Visualization of the binding modes and interactions of the different small molecules inhibitors into the four JAKs was done using the Discovery Studio Visualizer [47].

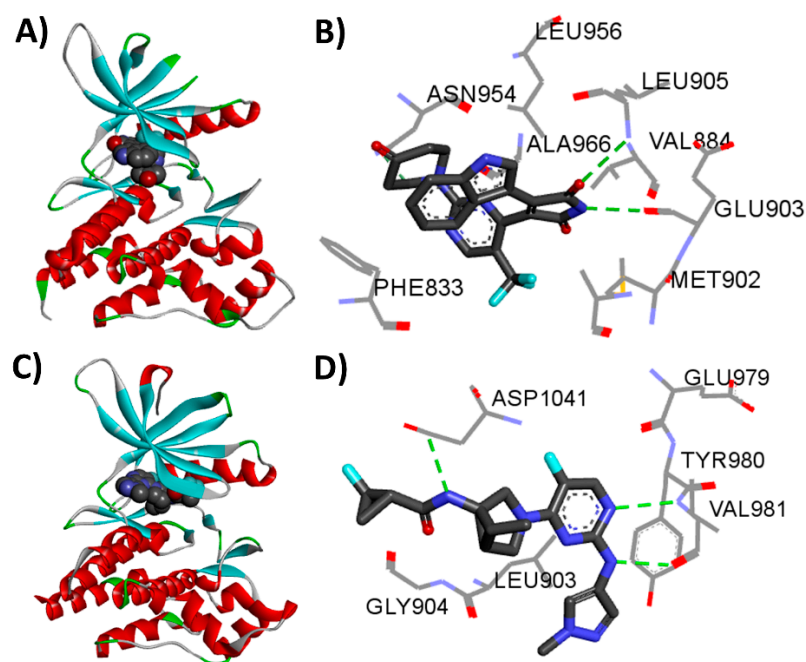
The binding mode and interactions of KEV, a pyrazolopyridine inhibitor with JAK1 kinase (pdb: 6N7A) [19], were visualized in Figure 8. KEV displays hydrogen bond interactions with Glu957 and Leu959 in the hinge region of JAK1.



**Figure 8.** JAK1 (pdb: 6N7A) and JAK2 (pdb: 2B7A) kinases bound to small-molecule inhibitors: (A) 3D representation of JAK1 bound to KEV (shown as CPK); (B) 3D binding mode of KEV into JAK1 showing the hydrogen bond interactions; (C) 3D representation of JAK2 bound to IZA (shown as CPK); (D) 3D binding mode of IZA into JAK2, hydrogen bonds are shown as green-dotted lines, this figure was generated using Discovery Studio Visualizer (V16.1.0.15350).

In addition, many small molecules of diverse chemical nature were reported as co-crystallized ligands with JAK2 [59,60]. Among these ligands, IZA is an isoquinoline derivative with potent and pan-JAK inhibitory activity. The binding interactions of IZA show two conventional hydrogen bonds with Leu932 and Glu930 in the hinge region in JAK2 (Figure 8).

The crystal structure of JAK3 (pdb: 3PJC) in complex with PJC, a pyrazolopyridine inhibitor [61] was visualized in Figure 9. PJC shows hydrogen bond interactions with Leu905 and Glu903. On the other hand, the crystal structure of TYK2 kinase (pdb: 6VNX) in complex with R4V, a pyrimidine inhibitor [62] was also visualized in Figure 9. R4V shows one conventional hydrogen bond with Asp1041.

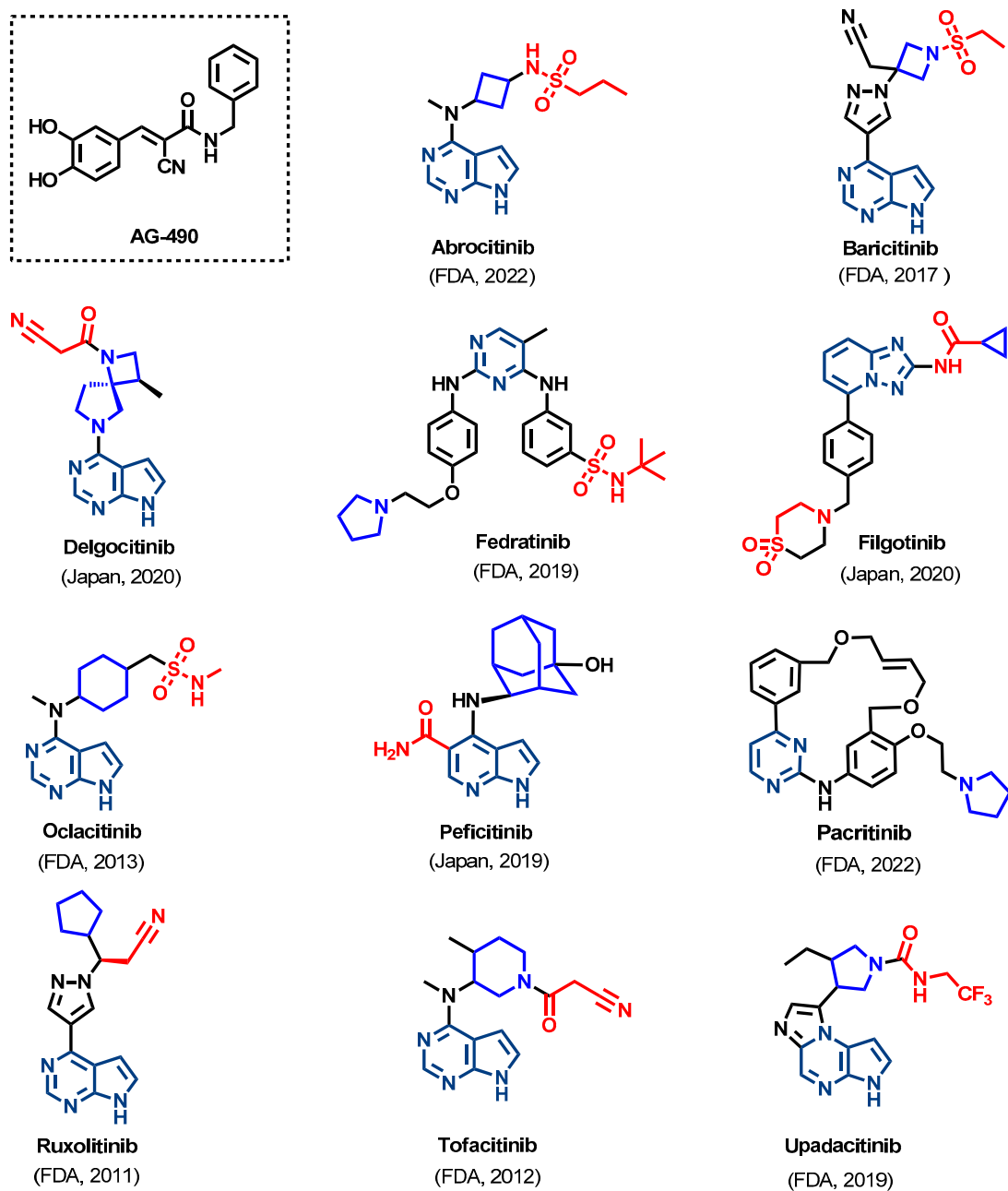


**Figure 9.** JAK3 (pdb: 3PJC) and TYK2 (pdb: 6VNX) kinases bound to small-molecule inhibitors: (A) 3D representation of JAK3 bound to PJC (shown as CPK); (B) 3D binding mode of PJC into JAK3; (C) 3D representation of TYK2 bound to R4V (shown as CPK); (D) 3D binding mode of R4V into TYK2, this figure was generated using Discovery Studio Visualizer (V16.1.0.15350).

### 1.7. JAK Inhibitors Approved for Clinical Use

In 1996, Meydan et al. reported AG-490 (Figure 10), a JAK2 inhibitor with antileukemic activity [63]. Following this discovery, great efforts have been made in the last two decades to develop potent and selective JAK inhibitors.

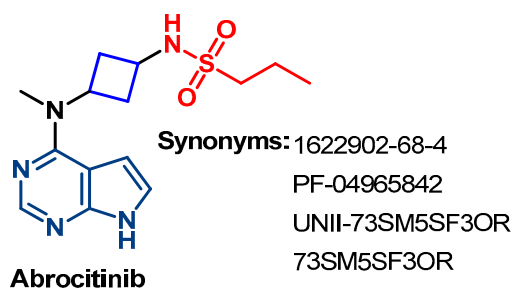
In 2011, the FDA-approved ruxolitinib (Figure 10) became the first JAK inhibitor [64]. One year later, tofacitinib was also approved for the treatment of rheumatoid arthritis [64]. In 2017, baricitinib was approved by the FDA for rheumatoid arthritis [65]. However, in 2019, three JAK inhibitors were approved for clinical use [66–68]. These drugs include fedratinib and upadacitinib, which were approved by the FDA, whereas peficitinib had already been approved in Japan for rheumatoid arthritis. In 2020, delgocitinib and filgotinib were also approved in Japan for the treatment of atopic dermatitis and rheumatoid arthritis, respectively [69,70].



**Figure 10.** Chemical structure of AG-490 and the globally proven JAK inhibitors with the dates of their first approval.

### 1.7.1. Abrocitinib Approval History

Abrocitinib (Figure 11) is a JAK1 kinase inhibitor [71,72]. It was approved by the FDA in January 2020 for the treatment of refractory, moderate-to-severe atopic dermatitis [72].

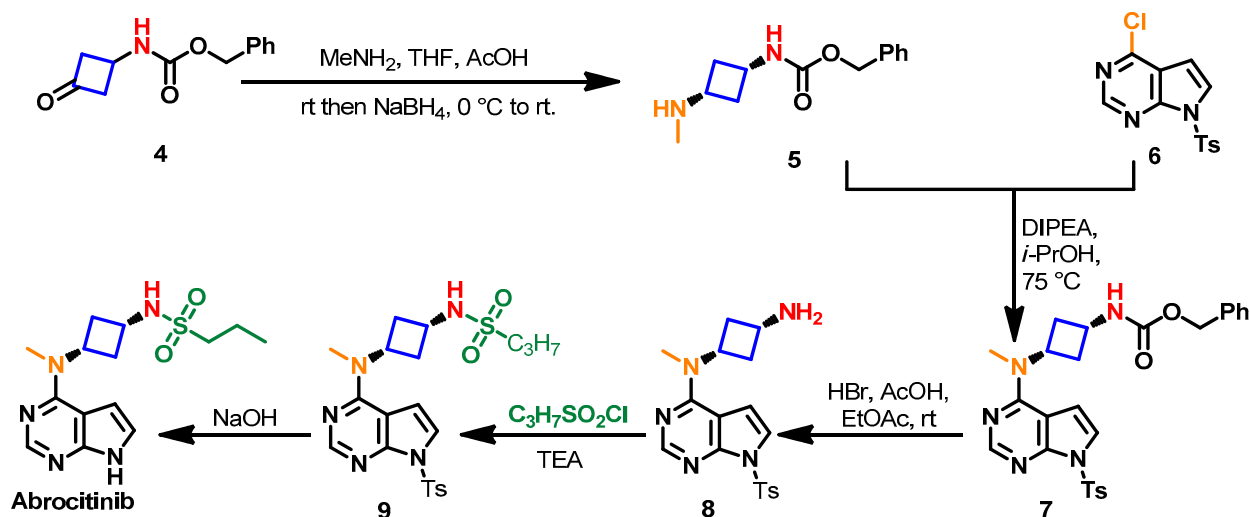
**Abrocitinib**

**Chem. name:** *N*-(3-(methyl(7*H*-pyrrolo[2,3-*d*]pyrimidin-4-yl)amino)cyclobutyl)propane-1-sulfonamide

**Figure 11.** Chemical structure/name/synonyms of abrocitinib.

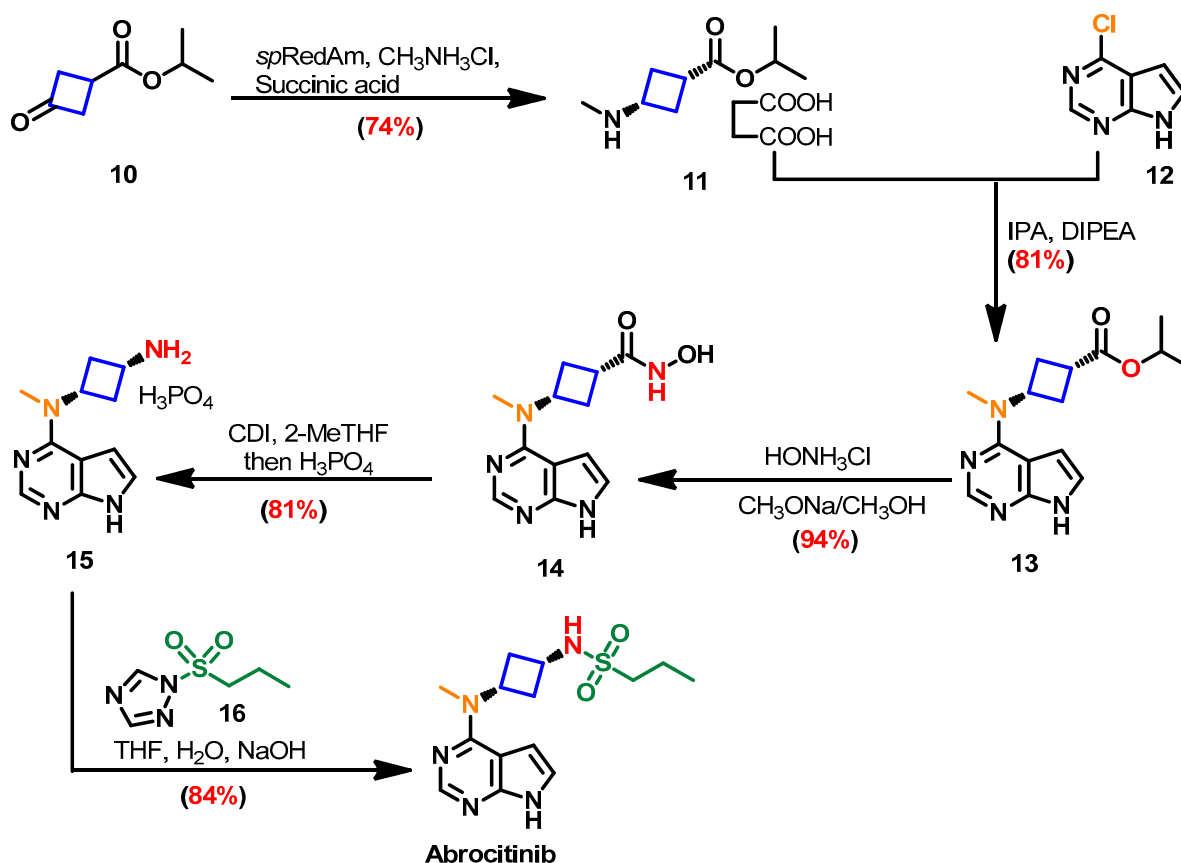
## Synthesis

Vazquez et al. [59] have reported the synthesis of abrocitinib from cyclobutyl carbamate **4**, Scheme 1. The ketone group in **4** was condensed with methylamine and reduced with sodium borohydride to give **5**. The coupling of **6** with the *cis*-isomer of **5** afforded **7**, which underwent the acid-catalyzed hydrolysis of the carbamate group to give **8**. The base-catalyzed sulfonylation of **8** with propane-1-sulfonyl chloride afforded **9**, which underwent deprotection to remove the tosyl moiety and give abrocitinib.



**Scheme 1.** Synthesis of abrocitinib (route 1).

Connor et al. [71] have also developed a commercial route for the synthesis of abrocitinib. The synthesis takes place through a nitrene-type rearrangement, Scheme 2. Compound **10** underwent biocatalytic reductive amination using the wild-type *SpRedAm* enzyme from *S. purpureus*, which gave the *cis*-amino ester compound **11** in 74% yield. The reaction of **11** and **12** afforded the isopropyl ester **13**. The reaction of **13** with hydroxylamine hydrochloride afforded the hydroxamic acid derivative **14**, which underwent Lossen rearrangement on the reaction with 1,1-carbonyldiimidazole (CDI) to give **15**. The sulfonylation of **15** was achieved using the triazole derivative **16** to avoid the sulfonylation of the pyrrole nitrogen.



Scheme 2. Synthesis of abrocitinib (route 2).

### Target Kinases

The inhibitory activity of abrocitinib against JAK kinases was evaluated by Vazquez et al. [59]. The results revealed inhibitory activity against JAK1 and JAK2 at  $\text{IC}_{50}$  values of 0.029 and 0.803  $\mu\text{M}$ , respectively (Figure 12).

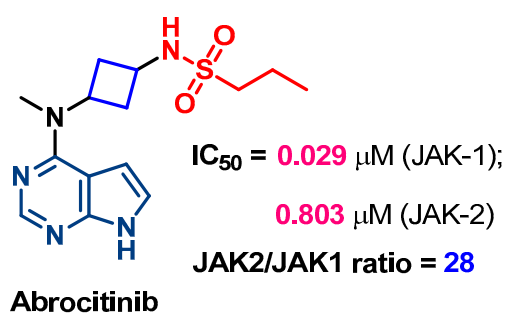


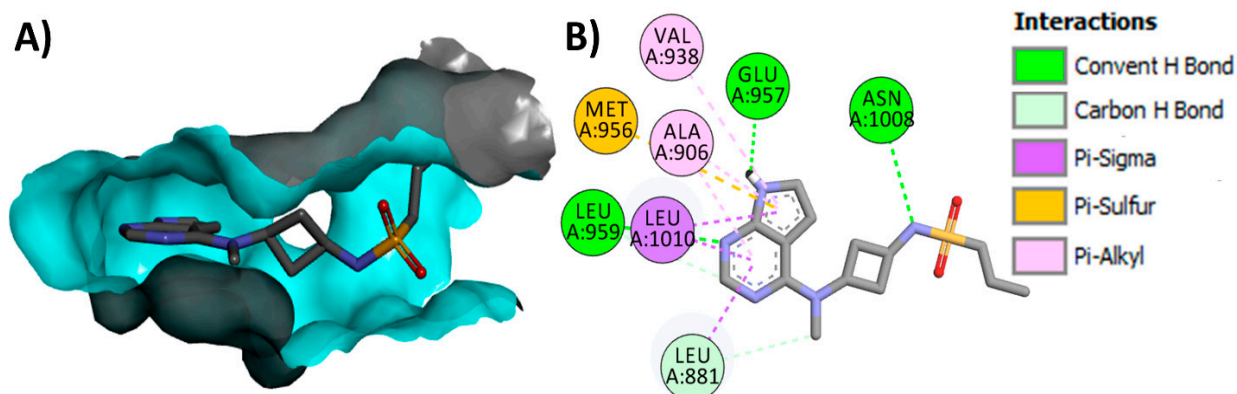
Figure 12. JAKs inhibitory activities of abrocitinib.

### Crystal Structures

Abrocitinib exists as a co-crystallized ligand in two crystal structures, including its crystal structure with JAK1 (pdb: 6BBU) and JAK2 (pdb: 6BBV) [59].

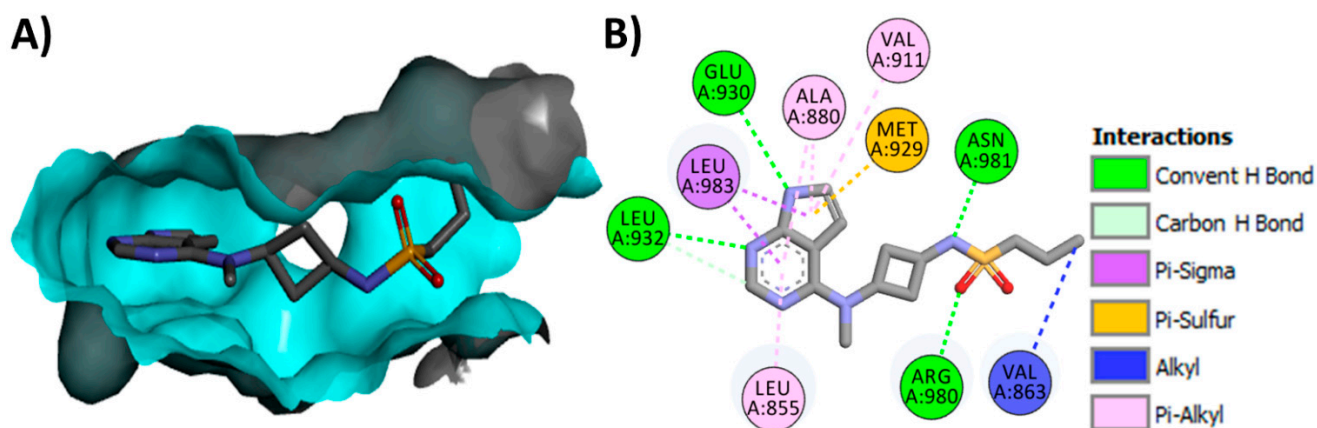
The binding mode of abrocitinib in the active site of JAK1 is illustrated in Figure 13. Abrocitinib shows three conventional hydrogen bonds with Glu957, Leu959, and Asn1008. In addition, abrocitinib shows three carbon–hydrogen bonds with LEU881 and Leu959. Several hydrophobic interactions were also observed between abrocitinib and amino acids in JAK1.





**Figure 13.** Binding modes of abrocitinib (shown as sticks) into JAK1 (pdb: 6BBU): (A) 3D binding mode, receptor shown as a hydrogen bond surface; (B) 2D binding mode showing different types of binding interactions with amino acids in JAK1; this figure was generated using Discovery Studio Visualizer (V16.1.0.15350).

On the other hand, abrocitinib exhibited four conventional hydrogen bonding interactions with Glu930, Leu932, Arg980, and Asn981, Figure 14. The binding interactions of abrocitinib also included one carbon–hydrogen bond with Leu932 and several hydrophobic interactions, with Leu855, Val863, Ala880, Val911, and Leu983.



**Figure 14.** Binding modes of abrocitinib (shown as sticks) into JAK2 (pdb: 6BBV): (A) 3D binding mode, receptor shown as a hydrogen bond surface; (B) 2D binding mode showing different types of binding interactions with amino acids in JAK2; this figure was generated using Discovery Studio Visualizer (V16.1.0.15350).

#### Pharmacological Activities and Uses

Abrocitinib combined with topical therapy displayed higher effectiveness in the treatment of atopic dermatitis compared to the placebo [73]. In another clinical trial (NCT03720470), abrocitinib showed higher therapeutic benefits regarding the symptoms of atopic dermatitis compared to the placebo [74].

The abrocitinib-induced response in patients with moderate-to-severe atopic dermatitis was also evaluated by Blauvelt et al. [75]. The results revealed the effectiveness of the induction treatment with abrocitinib, as most responders did not flare.

#### Metabolism

The metabolic study of abrocitinib in humans revealed the formation of several oxidative metabolites, in addition to the parent drug (26%) [76,77]. The results of the in vitro metabolic study of abrocitinib revealed that it undergoes metabolism by several CYP450 enzymes, where CYP2C19 and CYP2C9 were the major metabolizing enzymes. Among these

metabolites, the 3-hydroxypropyl M1 (PF-06471658) and the 2-hydroxypropyl metabolite M2 (PF-07055087) were retrieved in 11% and 12%, respectively, Figure 15. Both M1 and M2 exhibited JAK inhibitory activity similar to the parent drug with higher selectivity toward JAK1 over the other JAKs. On the other hand, a third oxidative metabolite M4 (PF-07054874) that lacks JAK inhibitory activity was also isolated [77].

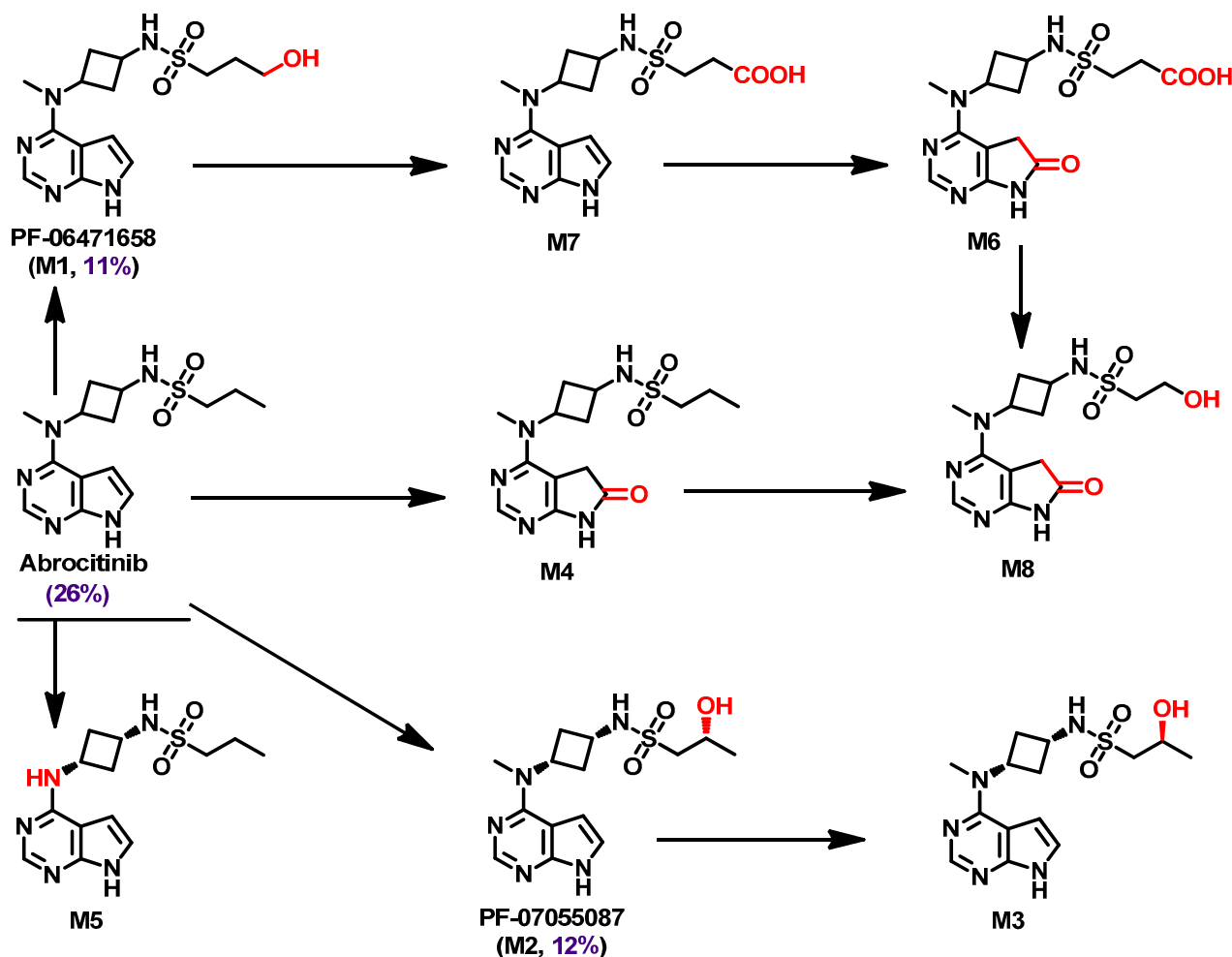


Figure 15. Proposed metabolic pathways and metabolites of abrocitinib.

### 1.7.2. Baricitinib Approval History

Baricitinib (Figure 16) is an orally active small-molecule inhibitor of JAK1/2. It was approved by the European Medicine Agency (EMA) in 2017 for the treatment of rheumatoid arthritis [65]. In June, 2018, baricitinib was approved by the FDA for the treatment of moderate-to-severe rheumatoid arthritis in adults [64]. Recently, the FDA issued an emergency use authorization for the combination of baricitinib and remdesivir to treat hospitalized patients with COVID-19 [78].

### Synthesis

The original synthesis of baricitinib was reported by Rodgers et al. [79]. In the first step, 3-oxoazetidone-1-carboxylate **18** underwent a Horner–Emmons reaction with diethyl (cyanomethyl)phosphonate **17** to give **19**, Scheme 3. Treatment of **19** with hydrochloric acid resulted in the removal of the protective group and produced **20**. The reaction of compound **20** with ethane sulfonyl chloride **21** afforded **22**.

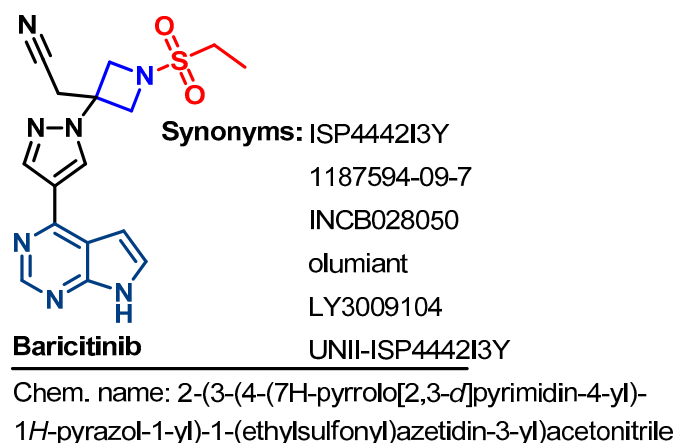
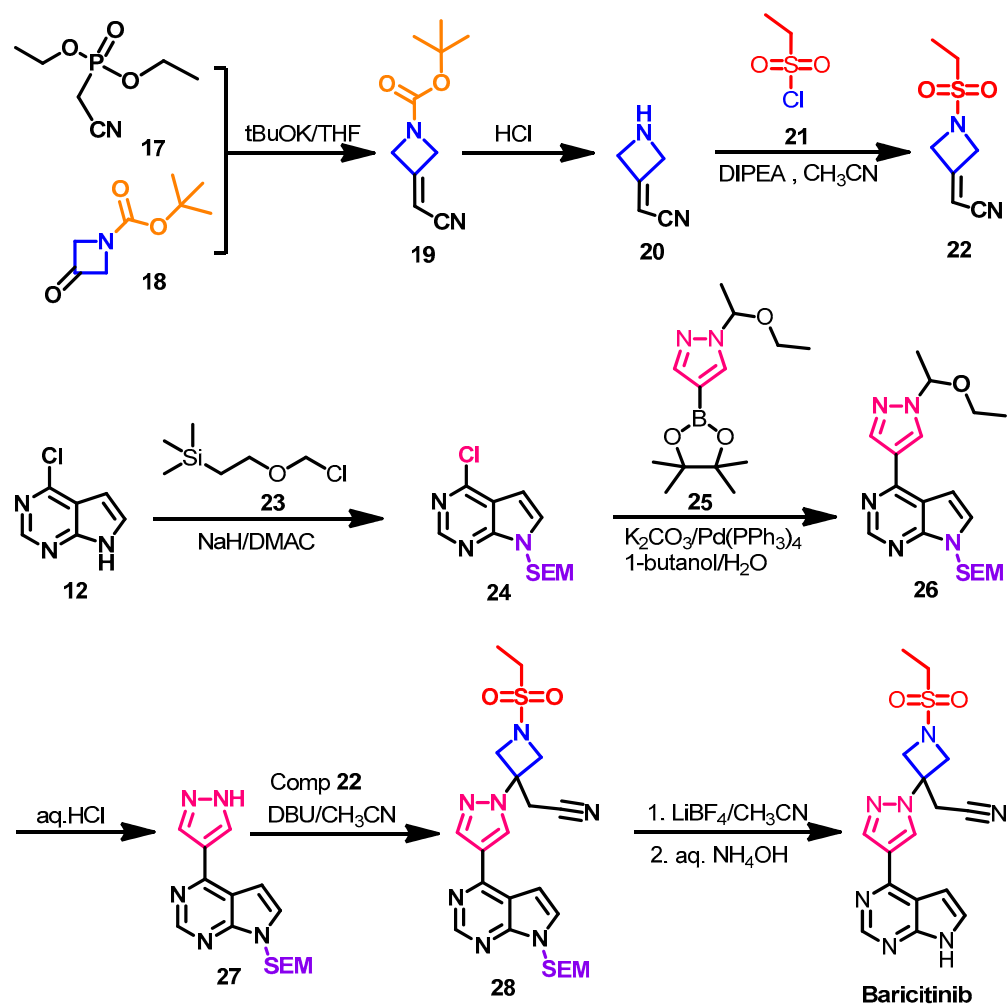


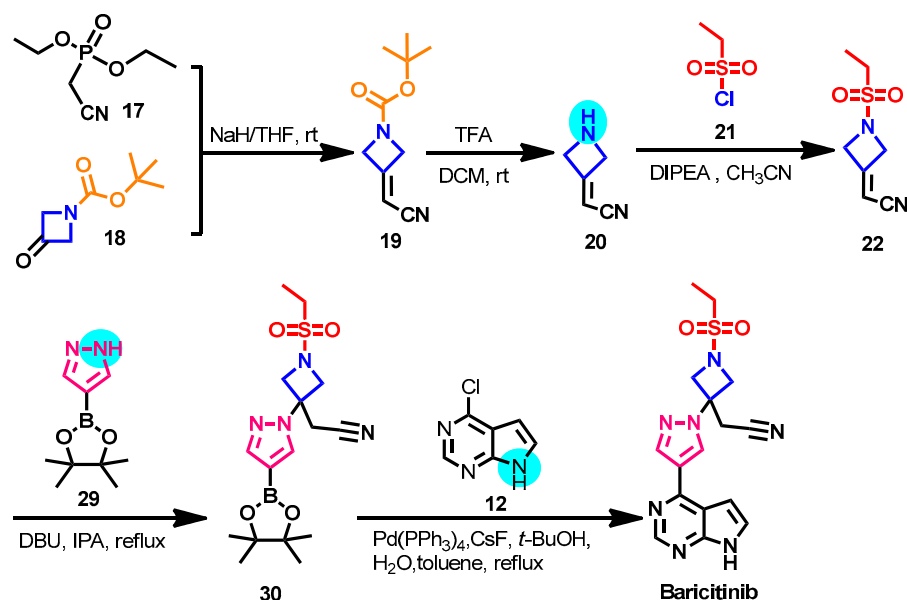
Figure 16. Chemical structure/name/synonyms of baricitinib.



Scheme 3. Synthesis of baricitinib (route 1).

On the other hand, protection of the pyrrole nitrogen in **12** was achieved on the reaction of **12** with (2-(chloromethoxy)ethyl)trimethylsilane (SEM) **23**, which gave **24**. Compound **24** underwent Suzuki coupling with 4-(1,3,2-dioxaborolan-2-yl)-1H-pyrazole **25** to give **26**, Scheme 3. The acid hydrolysis of **26** afforded **27**, which was then reacted with **22** to give compound **28**. Compound **28** was treated with lithium tetrafluoroborate followed by ammonia solution to give baricitinib.

Xu et al. [80] have reported an efficient five-step synthetic route of baricitinib (Scheme 4) with an overall yield of 49% compared to the eight-step method reported by Rodgers et al. [79]. Both methods share the first 3 steps. In the fourth step of Xu et al.'s method, a nucleophilic addition of **29** to the double bond in **22** afforded compound **30**. Suzuki coupling of **30** with compound **12** gave baricitinib. This method may be suitable for industrial synthesis due to its low cost and simple operating requirements [80].

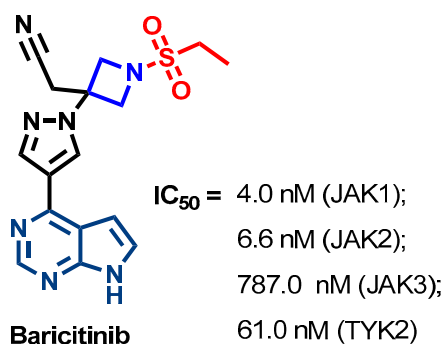


**Scheme 4.** Synthesis of baricitinib (route 2).

Furthermore, several other methods have been reported, describing alternative synthetic routes of baricitinib using the key intermediates **12** and **22** [81,82]. Among these methods, Cui et al. [82] reported a green and facile synthesis of the azetidene intermediate **22** using inexpensive and environmentally friendly starting materials.

#### Target Kinases

The inhibitory activity of baricitinib against JAKs was evaluated by Clark et al. [83]. These results revealed high inhibitory activity against JAK1/2 (Figure 17). However, baricitinib also exhibited moderate inhibitory activity against TYK2 ( $IC_{50} = 61$  nM).

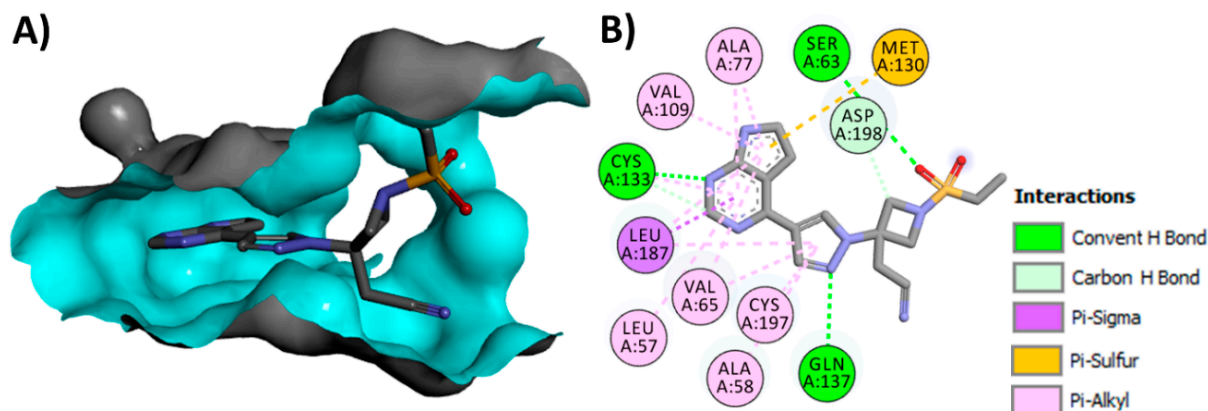


**Figure 17.** JAKs inhibitory activities of baricitinib.

#### Crystal Structures

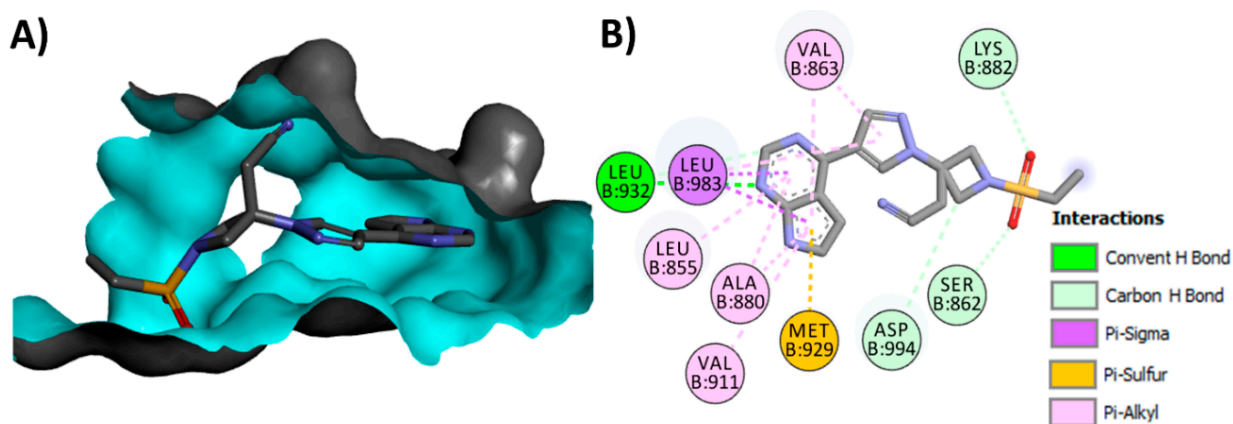
Baricitinib is found in three crystal structures in the protein data bank. The first is the crystal structure of baricitinib with BMP-2-inducible kinase (pdb: 4W9X) [84]. In addition baricitinib also exists as a co-crystallized ligand in two crystal structures of JAK2 [85,86].

The bone morphogenic proteins (BMPs) are involved in skeletal morphogenesis [87]. The binding mode of baricitinib into BMP-2-inducible kinase is visualized in Figure 18. The binding interactions of baricitinib into BMP-2-inducible kinase include 3 conventional hydrogen bonds with Ser63, Cys133 and Gln137. Baricitinib also shows one carbon hydrogen bond with Asp198 and one pi-sulfur interaction with Met130. Several hydrophobic interactions could also be observed between baricitinib and the hydrophobic residues in the kinase.



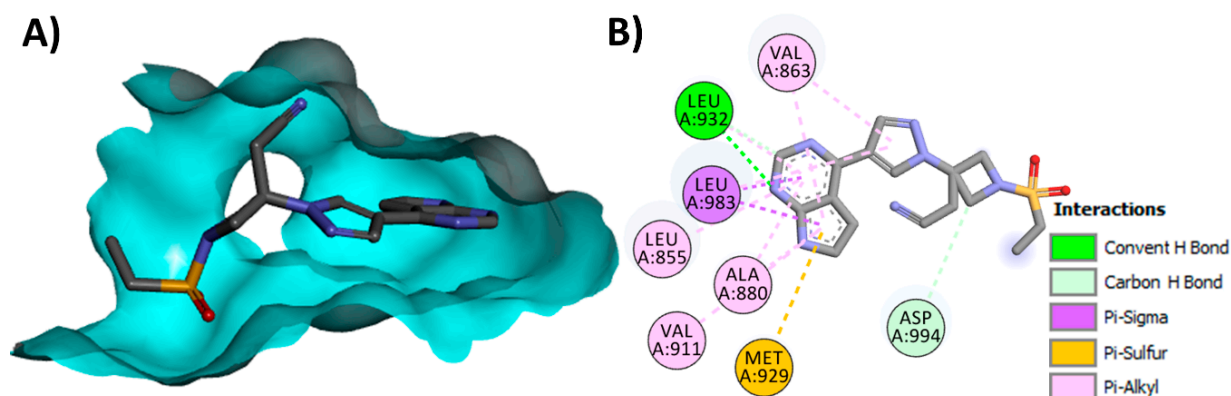
**Figure 18.** Binding modes of baricitinib (shown as sticks) into BMP-2-inducible kinase (pdb: 4W9X): (A) 3D binding mode, receptor shown as a hydrogen bond surface; (B) 2D binding mode showing different types of binding interactions with amino acids in BMP-2-inducible kinase; this figure was generated using Discovery Studio Visualizer (V16.1.0.15350).

Visualization of the binding mode/interactions of baricitinib into JAK2 JH1 (pdb: 6VN8) shows one conventional hydrogen bond with Leu932 [85]. Baricitinib also shows three carbon hydrogen bonds with Ser862, Lys882, and Asp994 (Figure 19). Baricitinib also shows one pi-sulfur interaction with Met929 and several hydrophobic interactions of the pi-sigma and pi-alkyl types.



**Figure 19.** Binding modes of baricitinib (shown as sticks) into JAK2 JH1 (pdb: 6VN8): (A) 3D binding mode, receptor shown as a hydrogen bond surface; (B) 2D binding mode showing different types of interactions with JAK2 JH1; the figure was generated using Discovery Studio Visualizer (V16.1.0.15350).

In addition, the binding mode of baricitinib into human JAK2 JH1 was also reported in another crystal structure (pdb: 6WTO) [86]. Visualization of the binding mode/interactions (Figure 20) shows identical hydrogen bonds and hydrophobic interactions with those of the above crystal (pdb: 6VN8), Figure 19.



**Figure 20.** Binding modes of baricitinib (shown as sticks) into human JAK2 JH1 (pdb: 6WTO): (A) 3D binding mode, receptor shown as a hydrogen bond surface; (B) 2D binding mode showing different types of interactions with JAK2 JH1; the figure was generated using Discovery Studio Visualizer (V16.1.0.15350).

#### Pharmacological Activities and Uses

Baricitinib was the second JAK inhibitor to be approved for rheumatoid arthritis after the approval of ruxolitinib. It showed rapid and long-lasting therapeutic benefits in the treatment of rheumatoid arthritis [88].

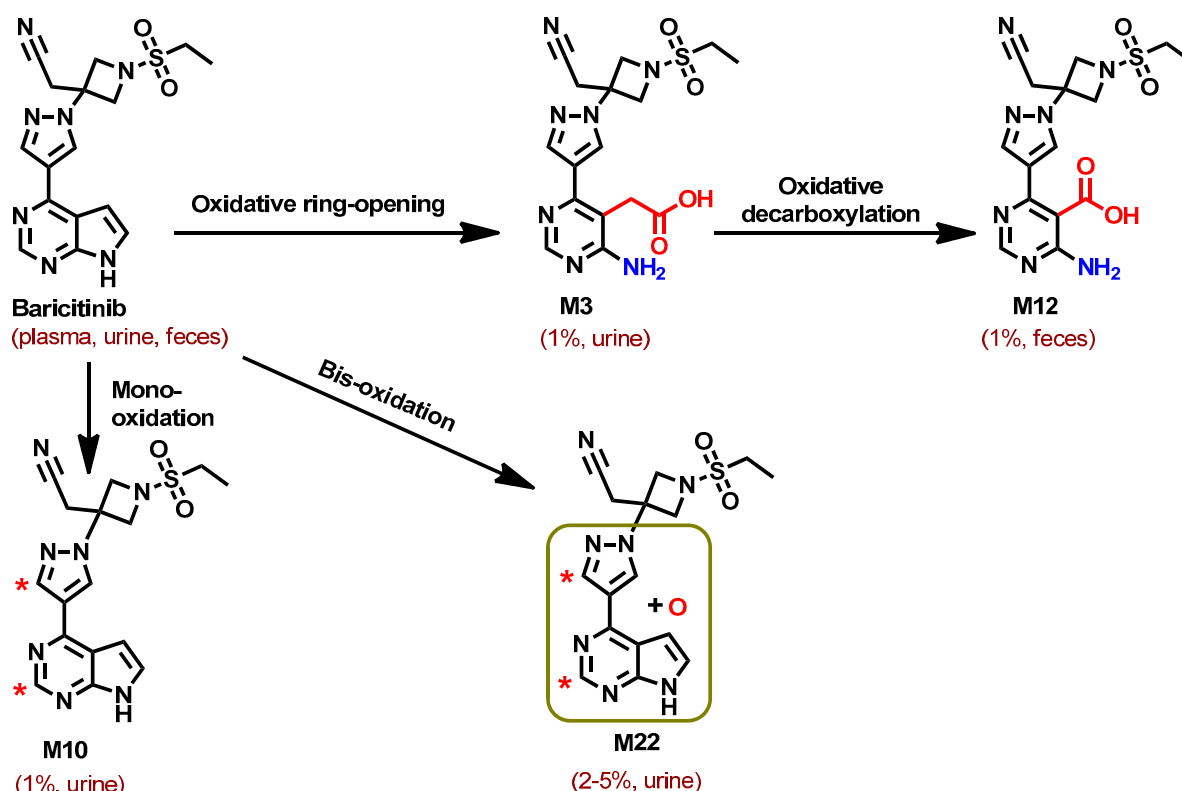
Baricitinib also improved the signs and symptoms of systemic lupus erythematosus in a double-blind study [89]. Moreover, baricitinib decreased inflammation/pruritus in atopic dermatitis patients when used with topical corticosteroids [90].

On the other hand, The inhibition of JAK1/2 by baricitinib leads to the inhibition of the JAK-STAT signaling pathway and subsequent inhibition of the production of the pro-inflammatory cytokines that could be useful for patients with COVID-19 [91]. The results of the clinical trial of baricitinib in combination with remdesivir (NCT04401579) revealed superior activity in reducing the recovery period compared to remdesivir alone [92]. Similar results were also obtained when using a combination of dexamethasone with baricitinib/remdesivir [93]. Finally, the combination of baricitinib and remdesivir received an Emergency Use Authorization (EUA) from the FDA to treat hospitalized patients with COVID-19.

#### Metabolism

The *in vivo* metabolism of baricitinib was performed in mice, rats, and dogs using [ $^{14}\text{C}$ ]-baricitinib [94,95]. The metabolic pathways include mono- and bis-oxidation, oxidative ring opening, and oxidative decarboxylation. The *in vitro* metabolism of baricitinib incubated with human liver enzymes was also very limited, with the formation of four metabolites.

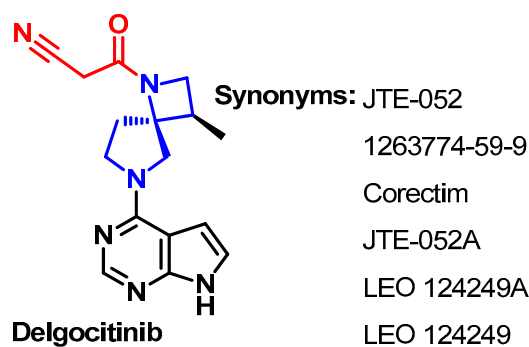
Baricitinib undergoes minor *in vivo* metabolic transformation mediated by the CYP3A4 enzyme [94,95]. Nearly 6–10% of baricitinib undergoes metabolism, producing four oxidative metabolites (Figure 21). Accordingly, it is excreted mainly as an unchanged drug in urine (69%) and feces (15%), while no circulating metabolites were identified in human plasma. The proposed metabolite M3 was formed through oxidative ring opening of the pyrrole ring, which undergoes oxidative decarboxylation giving M12. On the other hand, mono- or bis-oxidation of baricitinib affords the oxidative metabolites M10 and M22, respectively. The metabolic profile of baricitinib in animals was similar to that observed in humans.



**Figure 21.** Proposed metabolic pathways and major metabolites of baricitinib in human, asterisks indicate the sites of oxidation.

### 1.7.3. Delgocitinib Approval History

Delgocitinib (Figure 22) is a pan-JAK inhibitor that was approved for atopic dermatitis in 2020 in Japan [69]. Delgocitinib demonstrated inhibitory activity against the four JAKs [96].



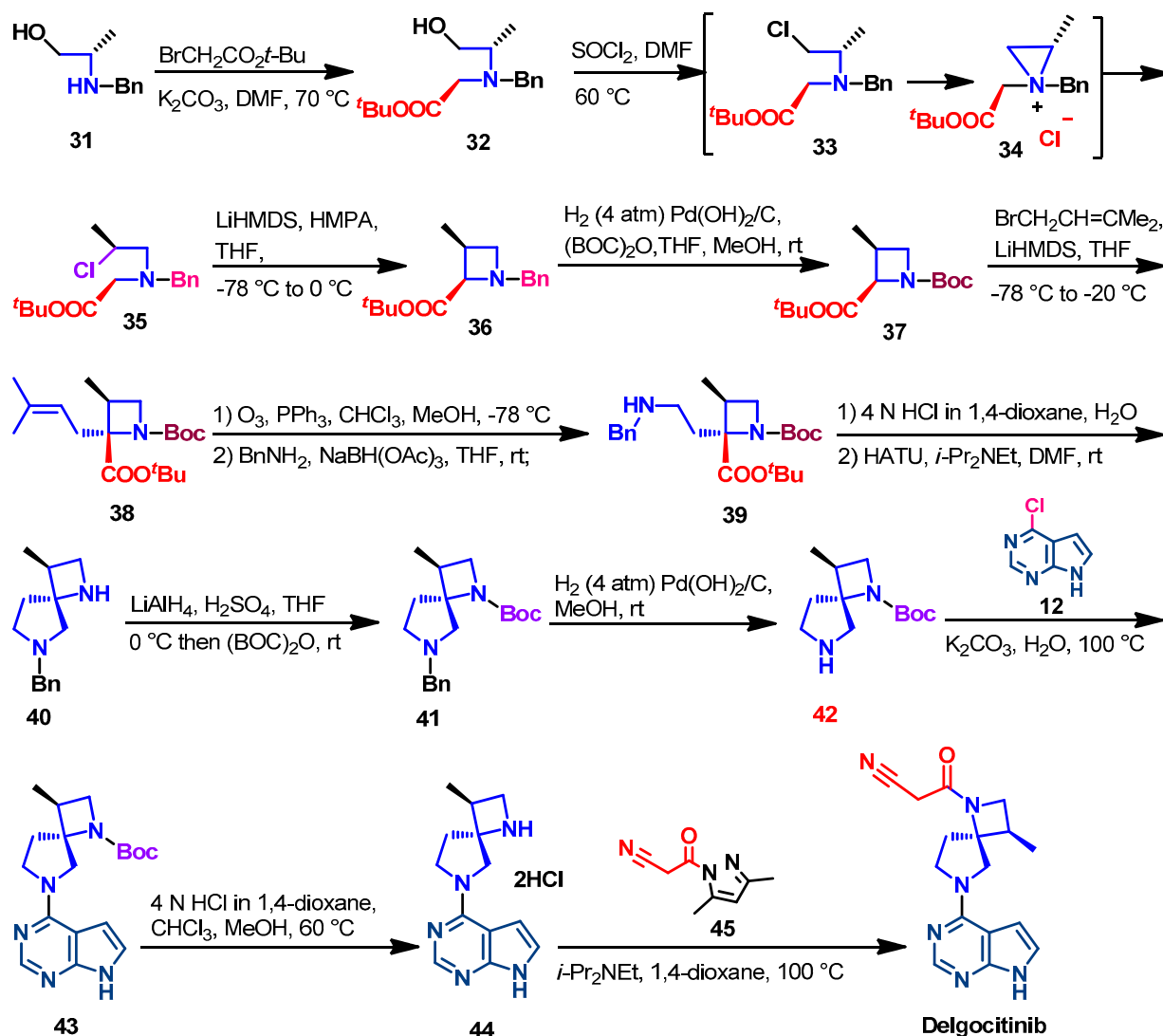
**Chem. name:** 3-((3*R*,4*S*)-3-methyl-6-(7*H*-pyrrolo[2,3-*d*]pyrimidin-4-yl)-1,6-diazaspiro[3.4]octan-1-yl)-3-oxopropanenitrile

**Figure 22.** Chemical structure/name/synonyms of delgocitinib.

### Synthesis

Noji et al. have reported the original stereoselective synthesis of delgocitinib [96]. In the first step, compound **31** was alkylated with *t*-butyl bromoacetate to give **32**, Scheme 5. The chlorination of **32** resulted in the formation of the reactive aziridinium intermediate **34**, which gave **35** on heating. Compound **35** underwent intramolecular cyclization to afford **36** as a single enantiomer. The protecting group in **36** was replaced by *t*-butyloxycarbonyl protecting (Boc) in **37**. Compound **37** underwent  $\alpha$ -alkylation to give **38**, which underwent

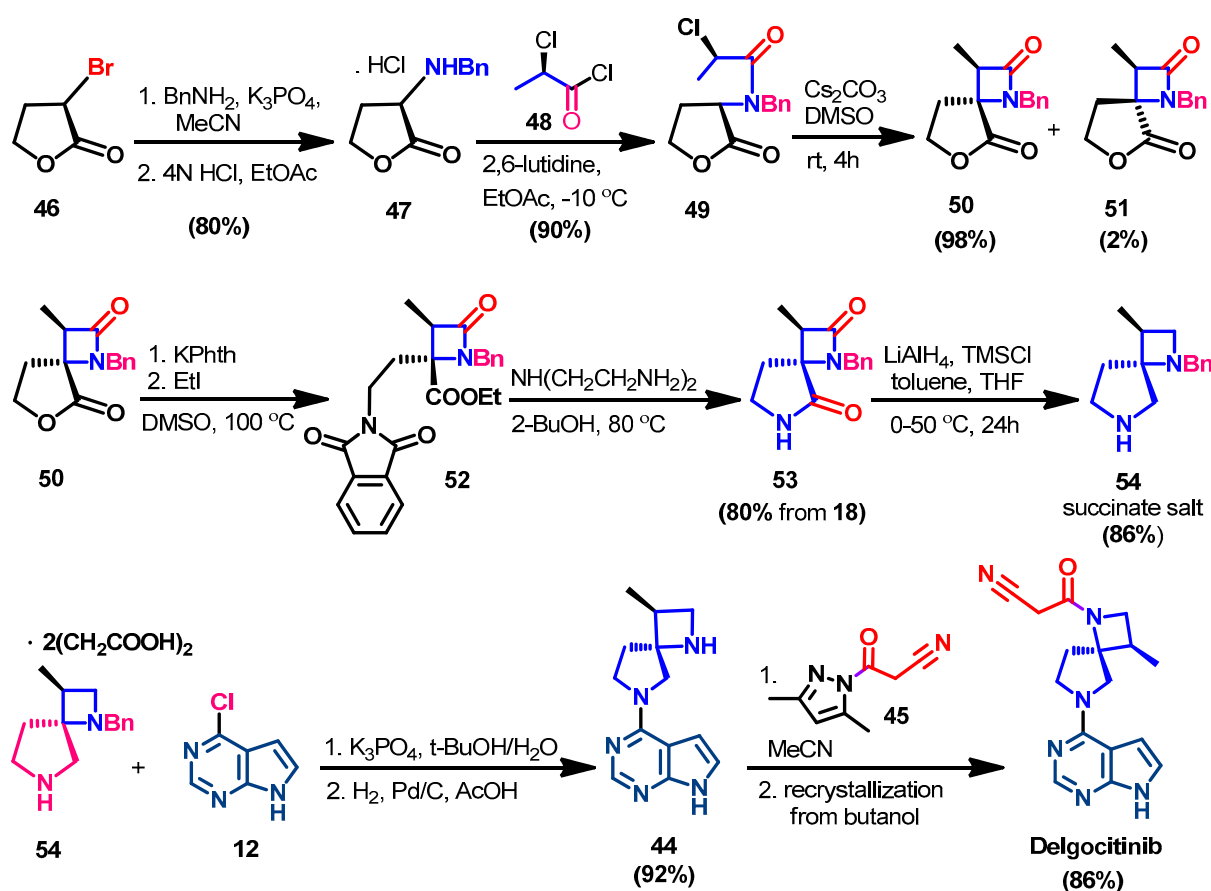
ozonolysis and reductive amination to give **39**. Removal of the Boc group and intramolecular cyclization of **39** afforded **40**, which was reacted with di-*tert*-butyl dicarbonate to protect the azetidine nitrogen, resulting in **41**. The debenzoylation of **41** followed by reaction with 4-chloro-7*H*-pyrrolo[2,3-*d*]pyrimidine **12** afforded **43**, which underwent deprotection by the removal of the Boc group, followed by cyanoacetylation, using **45** to give delgocitinib.



Scheme 5. Synthesis of delgocitinib (route 1).

In addition, Takiguchi et al. have also reported the stereocontrolled synthesis of delgocitinib [97]. The synthesis was started with 3-bromodihydrofuran-2(3*H*)-one **46**, which was converted to **49** in a three-step synthesis, Scheme 6. Compound **49** underwent intramolecular cyclization catalyzed by  $\text{Cs}_2\text{CO}_3$  to afford a diastereomixture of **50** and **51** in 98% and 2% yield, respectively. Compound **50** was isolated chromatographically and reacted with potassium phthalimide, followed by esterification with ethyl iodide to give the intermediate **52**. Dephthaloylation of compound **52** gave the dilactam derivative **53**. The  $\text{LiAlH}_4/\text{TMSCl}$ -catalyzed reduction of **53** afforded **54**, which was isolated as a stereochemically pure succinate salt in 86% yield. The reaction of **12** with **54** afforded compound **44**, which was reacted with the cyanoacetyl pyrazole derivative **45** to give delgocitinib.





Scheme 6. Synthesis of delgocitinib (route 2).

## Target Kinases

Noji et al. [96] have investigated the kinase inhibitory activity of delgocitinib. The results (Figure 23) show potent activities against the four JAKs ( $IC_{50} = 2.6\text{--}58\text{ nM}$ ). Delgocitinib also exhibited inhibitory activity against lymphocyte-specific protein tyrosine kinase (LCK) at  $IC_{50}$  value of  $5.8\ \mu\text{M}$ .

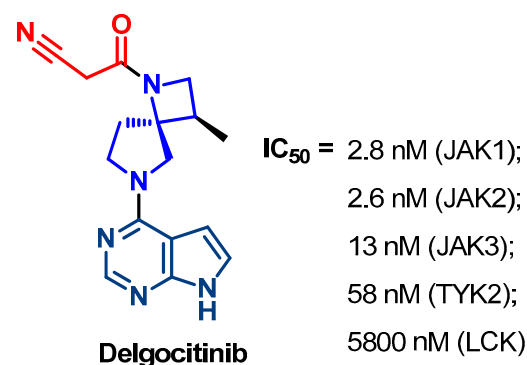
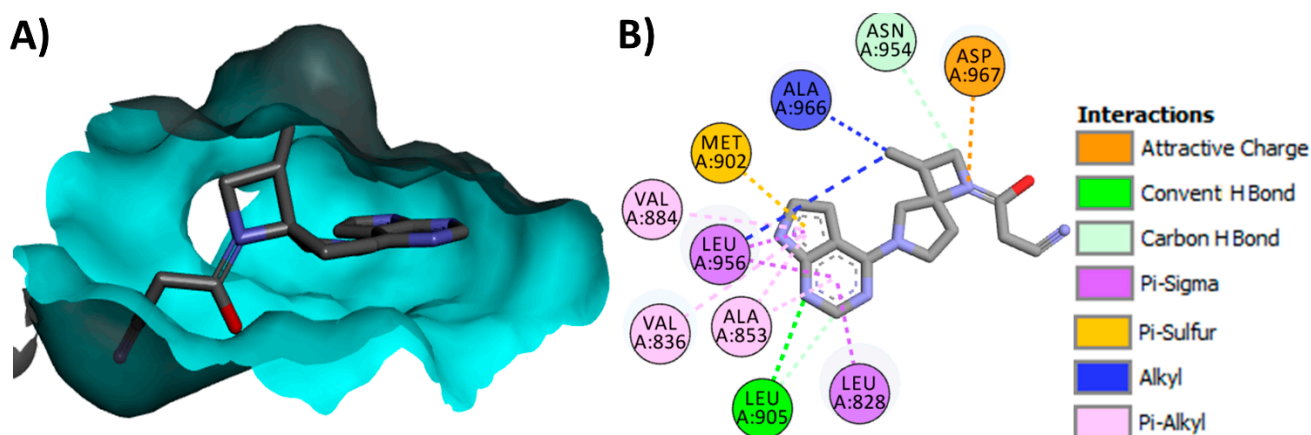


Figure 23. Kinase inhibitory activity of delgocitinib.

## Crystal Structures

One crystal structure of delgocitinib in complex with JAK3 (pdb: 7C3N) is available on the protein data bank [96]. The binding mode of delgocitinib into JAK3 is visualized in Figure 24. Delgocitinib shows one conventional hydrogen bond with Leu905 and an electrostatic interaction (attractive charge) with Asp967.



**Figure 24.** Binding modes of delgocitinib (shown as sticks) into JAK3 (pdb: 7C3N): (A) 3D binding mode, receptor shown as a hydrogen bond surface; (B) 2D binding mode showing different types of interactions with JAK3; this figure was generated using Discovery Studio Visualizer (V16.1.0.15350).

#### Pharmacological Activities and Uses

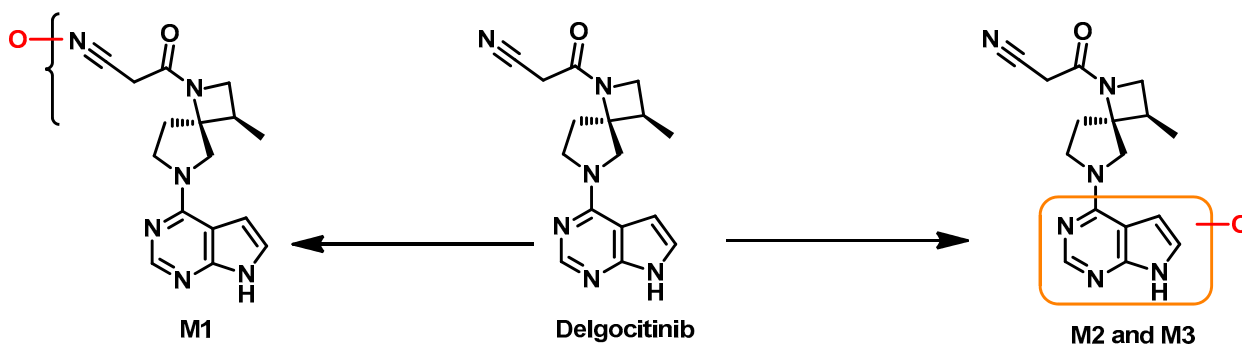
Delgocitinib displayed therapeutic efficacy in the treatment of patients with atopic dermatitis [98]. Delgocitinib was approved in Japan for atopic dermatitis [69].

Due to its pan-JAK inhibitory activity, the pharmacological effects of delgocitinib depend on the competitive inhibition of the four JAKs, which plays an important role in the pathophysiology of chronic inflammatory skin diseases [69]. Delgocitinib also inhibited the activation of inflammatory cells such as mast cells and T cells [99].

Delgocitinib was also evaluated for the treatment of psoriasis and chronic hand eczema (CHE) [69]. After 8 weeks of topical treatment, delgocitinib showed clearance of CHE in a significant number of patients compared to the vehicle [100]. On the other hand, the clinical trial of delgocitinib for discoid lupus erythematosus (NCT03958955) was terminated [101].

#### Metabolism

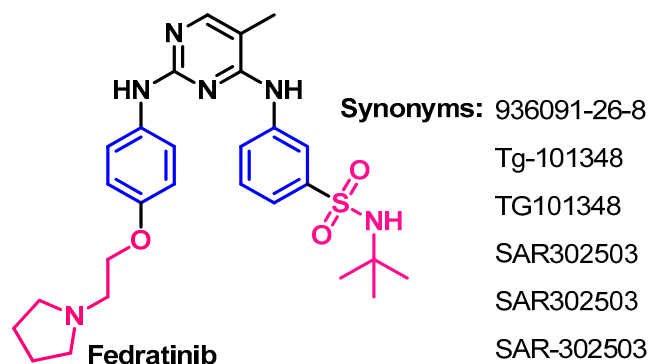
The pharmacokinetic study of delgocitinib (JTE-052) revealed that it is excreted mainly as the parent drug in urine, which indicates its stability to metabolism [102]. Delgocitinib also has higher stability values in human cells compared to animal cells [96,103]. The *in vitro* metabolic study performed using mouse, rat, rabbit, and dog hepatocytes revealed the recovery of the parent drug in 95.5–97.7%. These results indicate that less than 5% of the total dose was metabolized. The metabolic study was performed using animal microsomes and revealed the formation of three metabolites, M1 (oxidative metabolites of the side chain), M2, and M3 (oxidative metabolites of pyrrolopyrimidine), Figure 25.



**Figure 25.** Proposed metabolic pathways and major metabolites of delgocitinib based on the data of the deliberation results [103].

### 1.7.4. Fedratinib Approval History

Fedratinib (Figure 26) is a competitive inhibitor of JAK2, BRD4, and FMS-like tyrosine kinase 3 (FLT3) [35]. Fedratinib was approved by the FDA in August 2019 to treat patients with intermediate-2 or high-risk primary or secondary myelofibrosis [66].

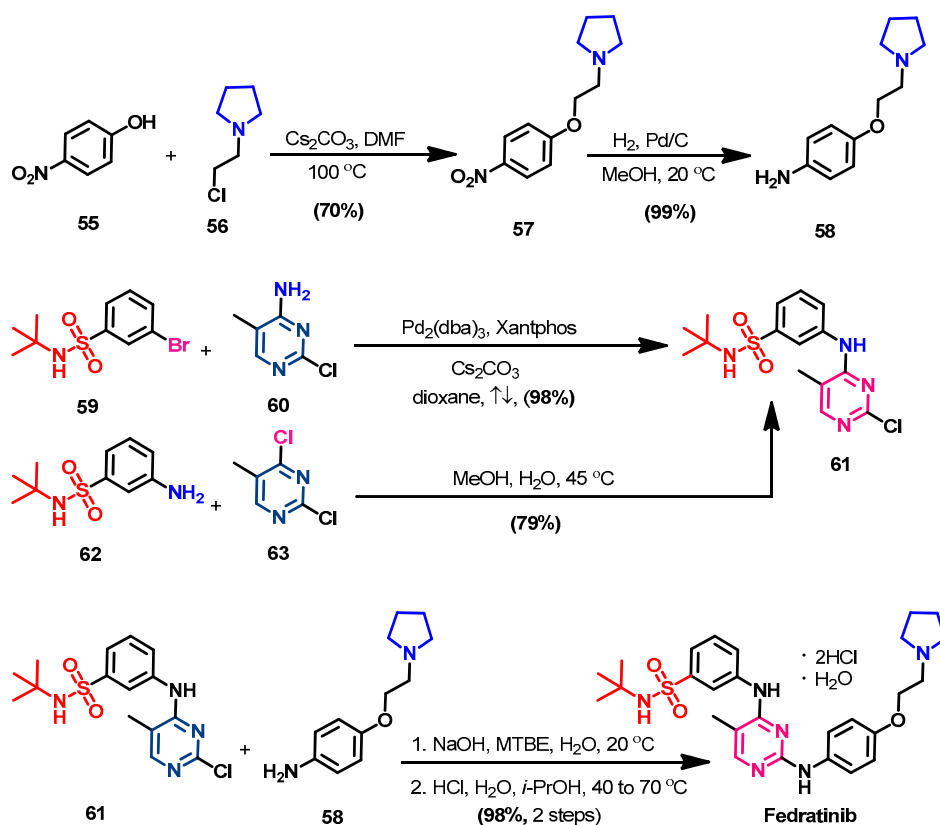


**Chem name:** *N*-(*tert*-butyl)-3-((5-methyl-2-((4-(2-(pyrrolidin-1-yl)ethoxy)phenyl)amino)pyrimidin-4-yl)amino)benzenesulfonamide

**Figure 26.** Chemical structure/name/synonyms of fedratinib.

### Synthesis

The synthesis of fedratinib could be achieved by the reaction of the intermediates **58** and **61** [104]. Firstly, compound **58** was obtained from the reaction of *p*-nitrophenol **55** and 1-(2-chloroethyl)pyrrolidine **56** in the presence of CsCO<sub>3</sub> according to the previous report [105]. The reduction of the nitro group in **57** afforded the amino ether **58**, Scheme 7.

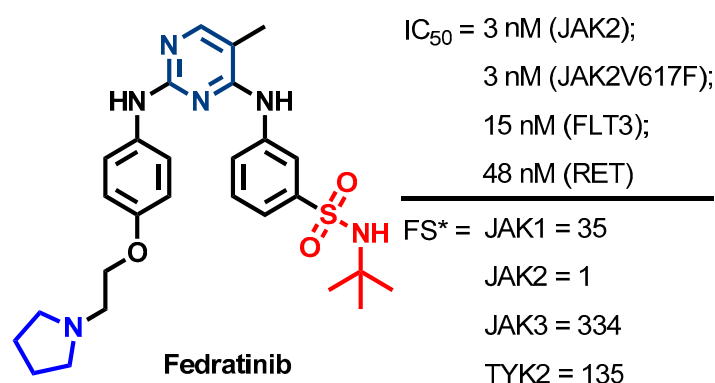


**Scheme 7.** Synthesis of fedratinib.

On the other hand, compound **61** was obtained in 98% yield from the Pd-catalyzed coupling of **59** and **60** [104,106,107]. Compound **61** could also be prepared in 79% yield from the reaction of **62** with **63** in methanol. The reaction of **58** and **61** in the presence of sodium hydroxide followed by treatment with acidic isopropyl alcohol gave fedratinib, Scheme 7.

### Target Kinases

Wernig et al. investigated the kinase inhibitory activity of fedratinib [35]. The results revealed the highest inhibitory activity against JAK2 and JAK2V617F at  $IC_{50}$  3 nM against the two kinases, Figure 27. On the other hand, fedratinib exhibited weak inhibitory activity against JAK3. Fedratinib also showed inhibitory activity against FLT3 and RET kinases with  $IC_{50}$  values of 15 nM and 48 nM, respectively. In addition, fedratinib exhibited potent bromodomain inhibitory activity at  $IC_{50}$  value in the nanomolar range [108].

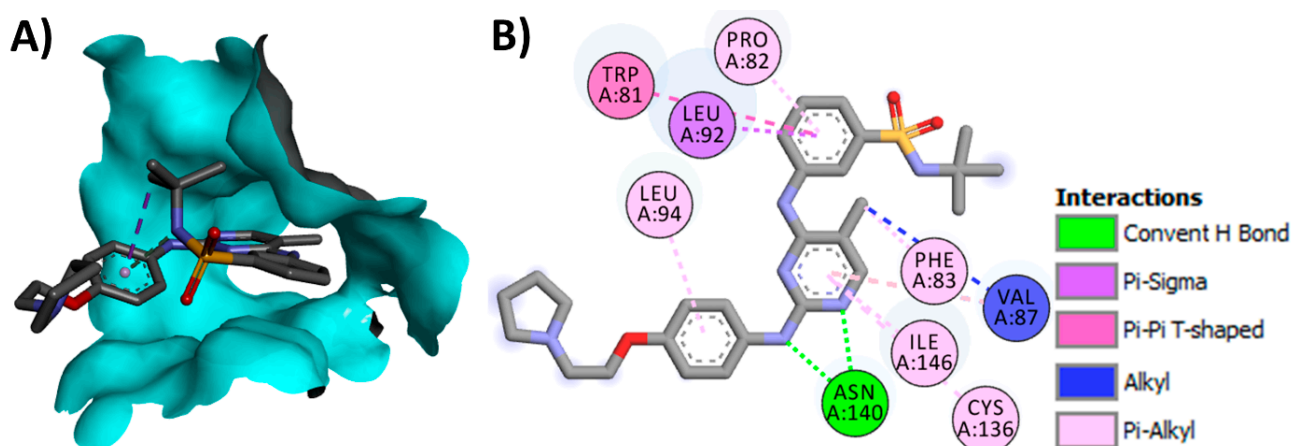


**Figure 27.** Kinase inhibitory activity of fedratinib (\* fold selectivity compared with JAK2).

### Crystal Structures

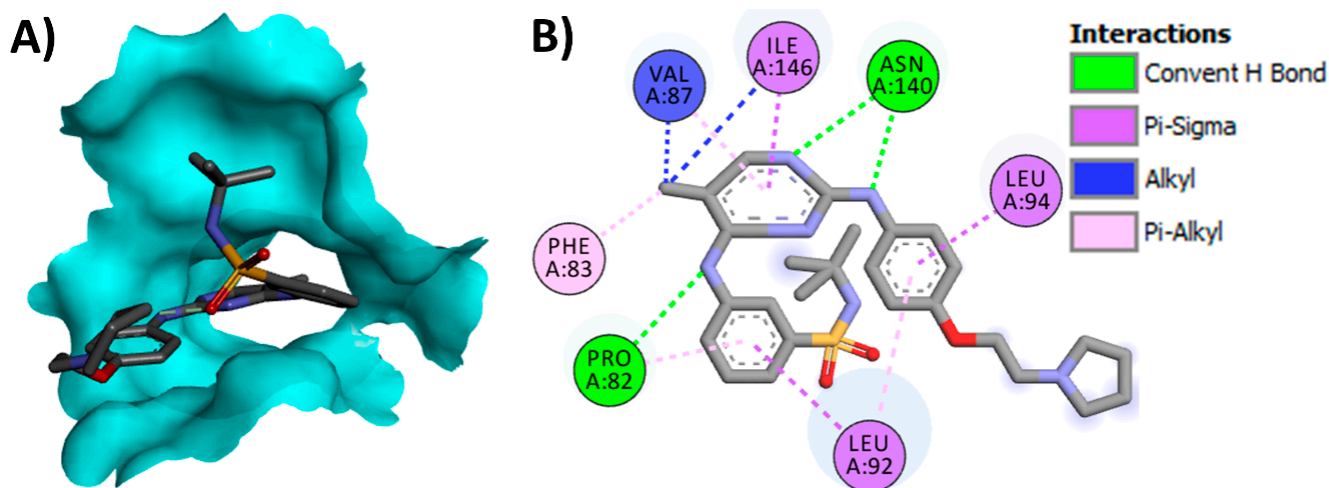
Three crystal structures of fedratinib are available on the protein data bank. Two of these crystals are bromodomain of human dual kinase-bromodomain (BRD4) in complex with fedratinib (pdb: 4OGJ and 4PS5) [108,109], while the third crystal is a complex of fedratinib with JAK2 JH1 (pdb: 6VNE) [85].

The binding mode of fedratinib into human bromodomain BRD4 was visualized in Figure 28. Fedratinib shows two conventional hydrogen bonds with Asn140 and multiple hydrophobic interactions with BRD4.



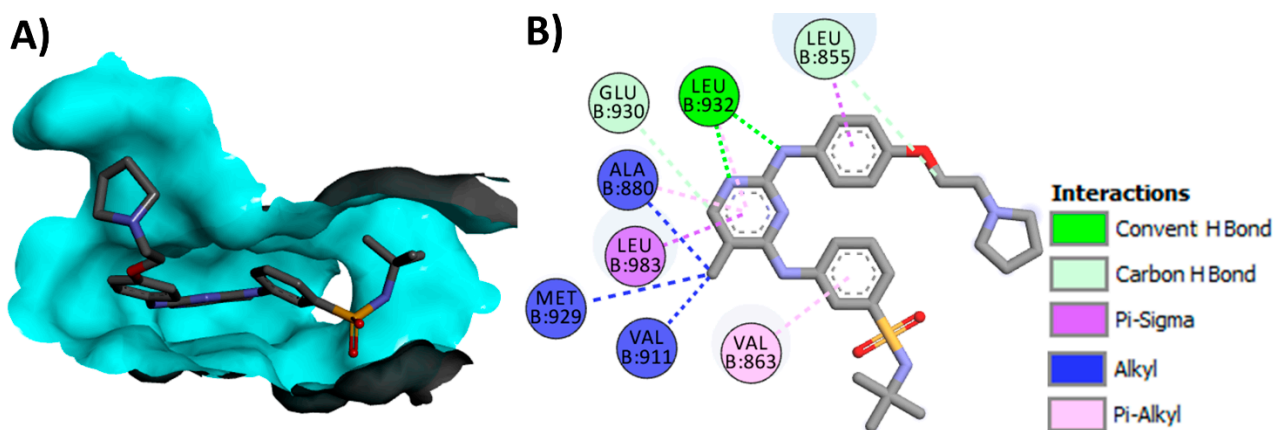
**Figure 28.** Binding modes of fedratinib (shown as sticks) into human bromodomain BRD4 (pdb: 4OGJ): (A) 3D binding mode, receptor shown as a hydrogen bond surface; (B) 2D binding mode showing different types of interactions with BRD4; the figure was generated using Discovery Studio Visualizer (V16.1.0.15350).

On the other hand, fedratinib displays two conventional hydrogen bond and Asn140 into human bromodomain BRD4 (pdb: 4PS5). However, fedratinib also shows an additional hydrogen bond with Pro82 (Figure 29).



**Figure 29.** Binding modes of fedratinib (shown as sticks) into human bromodomain BRD4 (pdb: 4PS5): (A) 3D binding mode, receptor shown as a hydrogen bond surface; (B) 2D binding mode showing different types of interactions with BRD4; the figure was generated using Discovery Studio Visualizer (V16.1.0.15350).

In addition, the binding mode of fedratinib into JAK2 JH1 was visualized in Figure 30. Fedratinib exhibits two conventional hydrogen bonds with Leu932 in JAK2 JH1. Moreover, two carbon hydrogen bonds could be observed with Leu855 and Glu930.



**Figure 30.** Binding modes of fedratinib (shown as sticks) into JAK2 JH1 (pdb: 6VNE): (A) 3D binding mode, receptor shown as a hydrogen bond surface; (B) 2D binding mode showing different types of interactions with JAK2 JH1; the figure was generated using Discovery Studio Visualizer.

#### Pharmacological Activities and Uses

Fedratinib has equal inhibitory activity against the wild-type JAK2 and its mutated form, JAK2V617F [110]. It was approved for the treatment of myelofibrosis in adult patients [66].

Moreover, fedratinib displayed inhibitory activity against other kinases such as FLT3 and RET kinases (Figure 27). The overexpression of FLT3 has been reported in acute leukaemia [111]. In addition, the overexpression of BRD proteins has been reported in different types of cancers [112]. Accordingly, the inhibition of BRD4 by fedratinib could contribute to its pharmacological activity [110].

## Metabolism

Ogasawara et al. evaluated the metabolic transformation of [ $^{14}\text{C}$ ]-labeled fedratinib in healthy subjects [113]. The results revealed that nearly 80% of the radioactivity in plasma was due to the parent compound. Among the identified metabolites, SAR317981, a metabolite obtained through oxidation of the pyrrolidine ring, was retrieved in 9.4%, Figure 31. In addition, the *N*-butyric acid derivative (SAR318031) was retrieved at 5.7%. Fedratinib and its metabolites are eliminated mainly through feces (50–70%) and partly in urine (~3%). The amino ethanoic acid derivatives (M17 and M21b) were also detected among 19 different metabolites identified in feces.

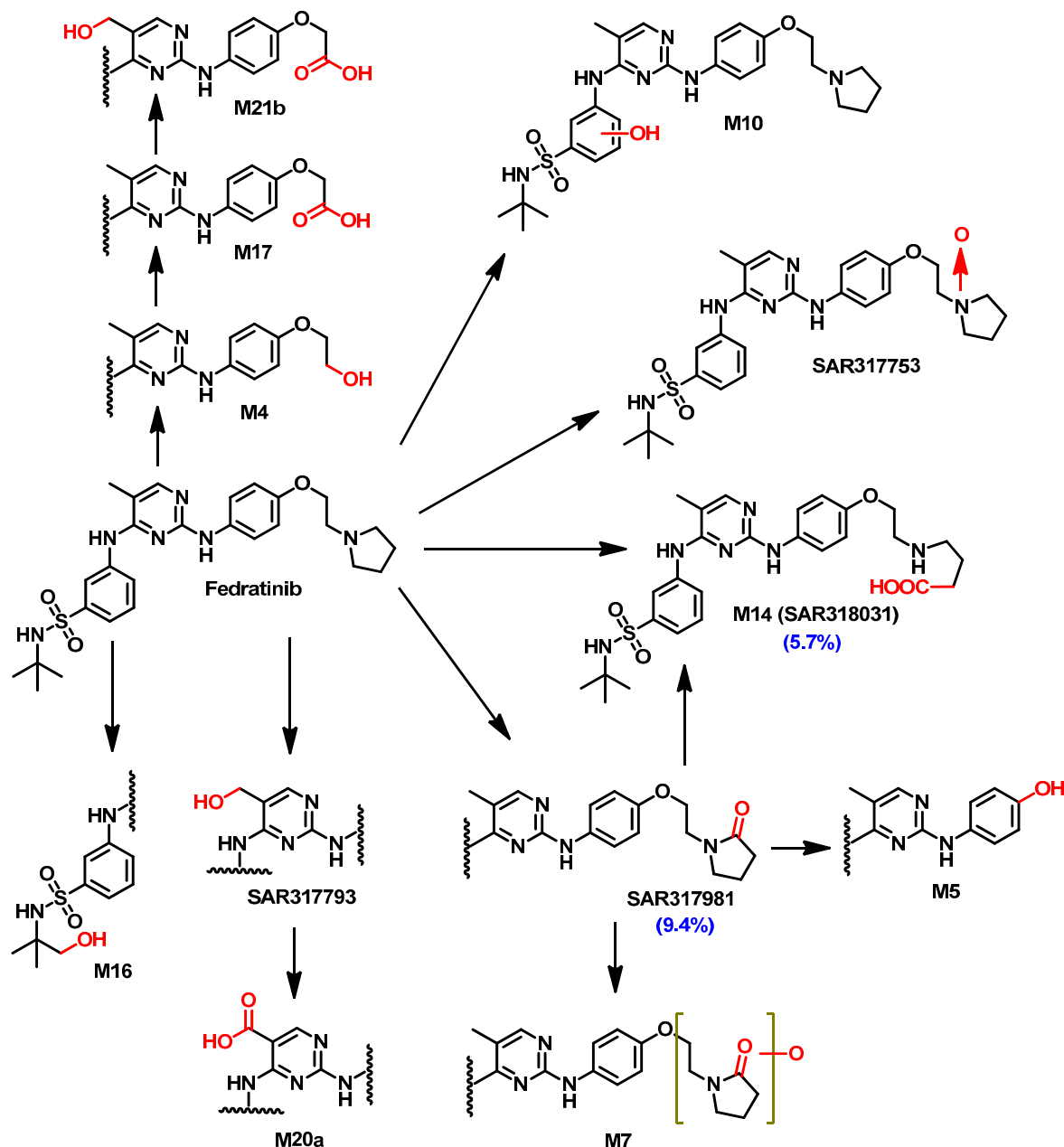


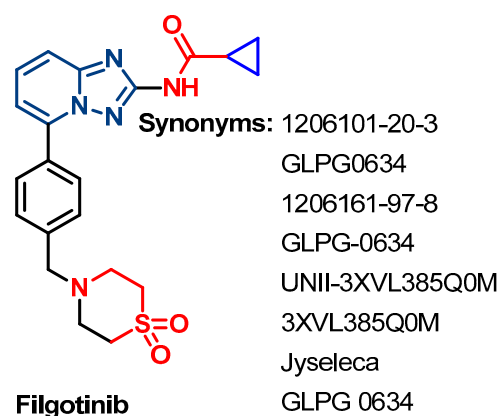
Figure 31. Proposed metabolic pathway and metabolites of fedratinib in humans.

## 1.7.5. Filgotinib

## Approval History

Filgotinib (Figure 32) is classified as a selective, ATP-competitive inhibitor of JAK1 [70]. Filgotinib was approved by the European Medicines Agency (EMA) in September 2020, for

adult patients with moderate to severely active rheumatoid arthritis [70]. Filgotinib was also approved for the treatment of rheumatoid arthritis in Japan [70].

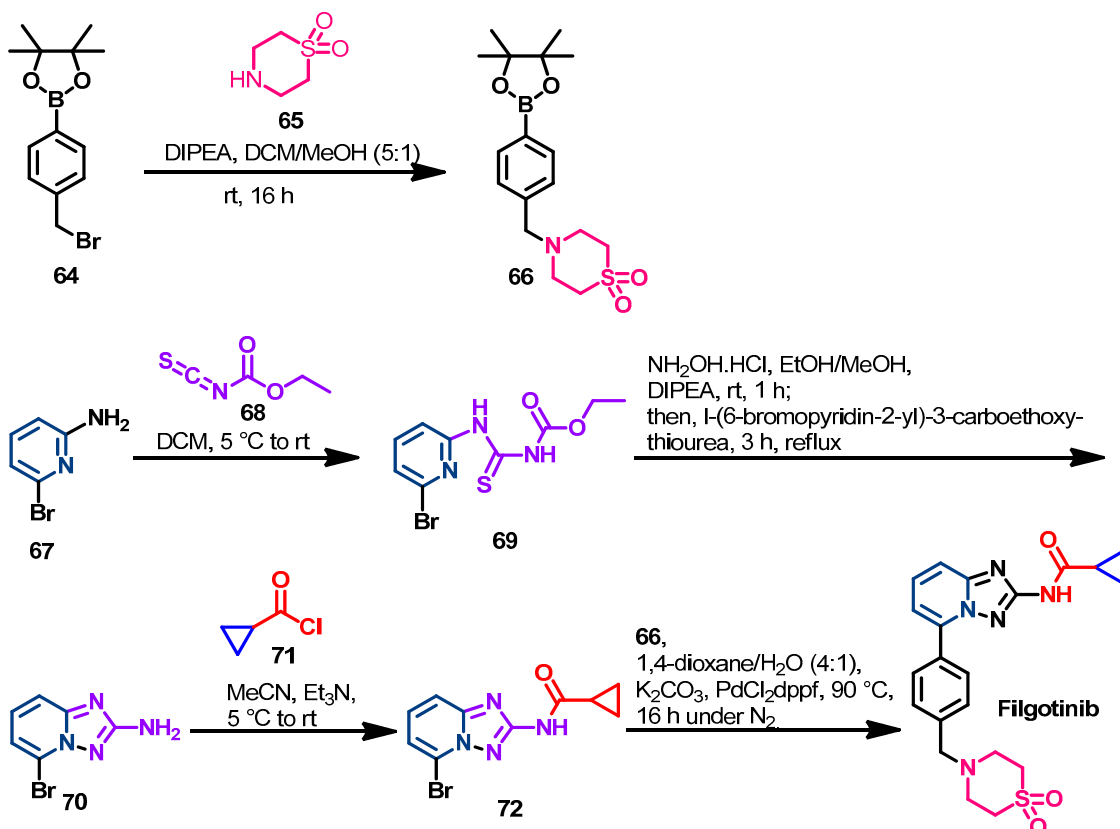


**Chemical name:** *N*-(5-(4-((1,1-dioxidothiomorpholino)methyl)phenyl)-[1,2,4] triazolopyridin-2-yl)cyclopropanecarboxamide

**Figure 32.** Chemical structure/name/synonyms of filgotinib.

### Synthesis

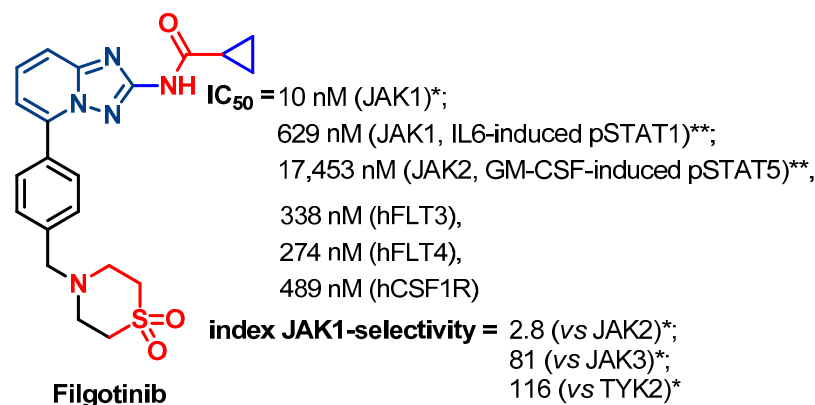
The synthesis of filgotinib (Scheme 8) was achieved in a five-step synthesis [114,115]. Initially, compound **64** was reacted with thiomorpholine 1,1-dioxide **65** to give **66**. On the other hand, the triazolopyridine **70** was prepared from compound **67** in a two-step synthesis. The first step involved the reaction of **67** with ethoxycarbonyl isothiocyanate **68** to give **69**, which underwent intramolecular cyclization with the hydrolysis of the carbamate group to give compound **70**. Acylation of the amino group in **70** with cyclopropanecarbonyl chloride **71** afforded **72**. Finally, filgotinib was obtained from the reaction between **66** and **72**.



**Scheme 8.** Synthesis of filgotinib.

### Target Kinases

The inhibitory activity of filgotinib was evaluated using recombinant JAKs and whole blood assay [116,117]. The results revealed the highest inhibitory activity against JAK1 ( $IC_{50} = 10$  nM), Figure 33. In addition, filgotinib exhibited 2.8-, 81-, and 116-fold selectivity for JAK1 over JAK2, JAK3, and TYK2, respectively.

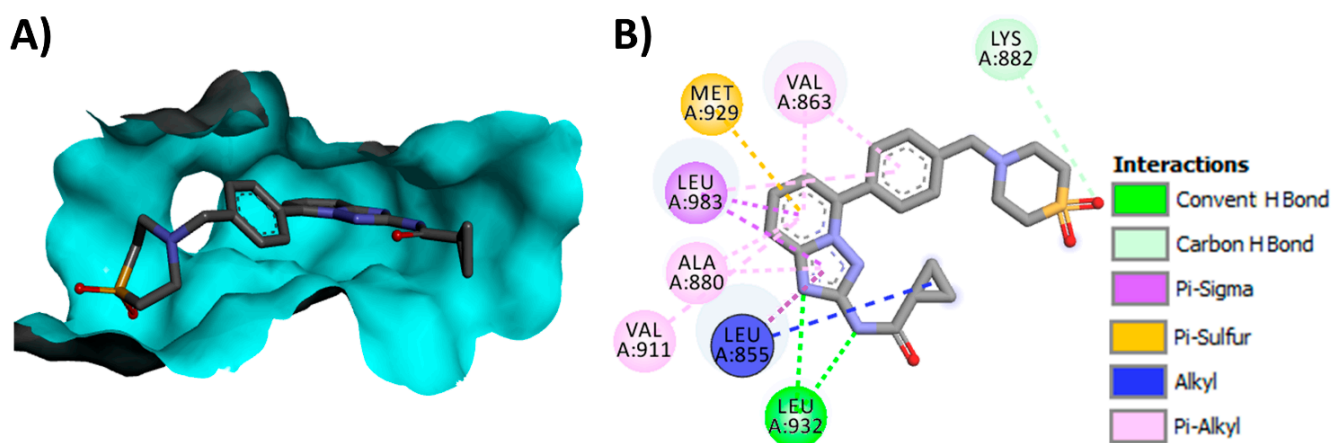


**Figure 33.** Kinase inhibitory activity of filgotinib, \* indicates the  $IC_{50}$  and index selectivity values determined using recombinant JAKs, \*\* indicates the  $IC_{50}$  values determined using a human whole blood assay [116,117].

Filgotinib was also tested against a panel of 170 kinases [117]. The results revealed weak inhibitory activities against hFLT3, hFLT4 and hCSF1R (Figure 33).

### Crystal Structures

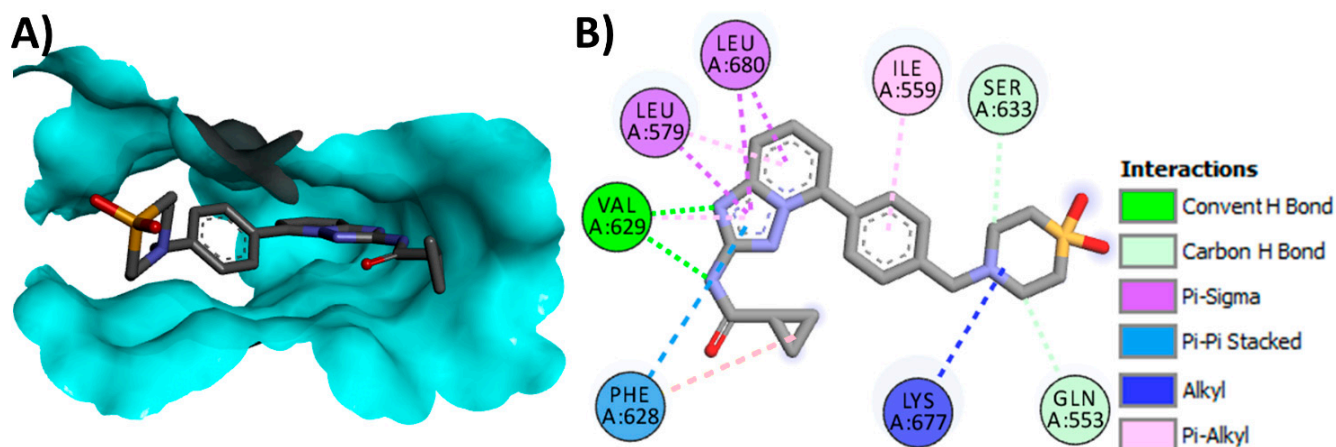
Filgotinib exists in two crystal structures with JAKs protein in the protein data bank. The first crystal (pdb: 4P7E) [117] was refined at a resolution of 2.40 Å, while the second (pdb: 5UT5) [118] was refined at 1.90 Å resolution. The binding mode/interactions of filgotinib into the ATP-binding site of JAK1 (pdb: 4P7E) shows two conventional hydrogen bonds with Leu932 and one carbon hydrogen bond Lys882, Figure 34.



**Figure 34.** Binding modes of filgotinib (shown as sticks) into JAK1 (pdb: 4P7E): (A) 3D binding mode, receptor shown as a hydrogen bond surface; (B) 2D binding mode showing different types of interactions with JAK1; the figure was generated using Discovery Studio Visualizer (V16.1.0.15350).

On the other hand, the binding mode of filgotinib into the JH2 domain of JAK2 was visualized in Figure 35. Filgotinib shows two conventional hydrogen bonds with Val629 and two carbon hydrogen bonds with Gln553 and Ser633.





**Figure 35.** Binding modes of filgotinib (shown as sticks) into JAK2 JH2 (pdb: 5UT5): (A) 3D binding mode, receptor shown as a hydrogen bond surface; (B) 2D binding mode showing different types of interactions with JAK2 JH2; the figure was generated using Discovery Studio Visualizer (V16.1.0.15350).

#### Pharmacological Activities and Uses

Filgotinib was first investigated for the treatment of rheumatoid arthritis, where the clinical results proved that rheumatoid arthritis can be treated with a selective inhibitor of JAK1 [119]. Later, filgotinib showed promising efficacy in the treatment of rheumatoid arthritis in two randomized phase IIa trials of filgotinib that were performed by Vanhoutte et al. [120]. In addition, filgotinib showed a rapid improvement in the signs and symptoms of rheumatoid arthritis [121]. In 2020, filgotinib was approved for the treatment of moderate-to-severe rheumatoid arthritis. It acts as a selective inhibitor of JAK1, which leads to the prevention of STAT phosphorylation and activation [3].

Filgotinib was also evaluated in a phase-II study for the treatment of Crohn's disease [122]. The results obtained from this study were also promising for patients with moderate-to-severe Crohn's disease. Moreover, the clinical remission induced by filgotinib in patients with active Crohn's disease was associated with an acceptable safety profile [123].

Moreover, the efficacy of filgotinib in the treatment of ulcerative colitis was also evaluated in a clinical trial (NCT02914522) [124]. The results revealed the efficacy of filgotinib in the treatment of ulcerative colitis.

In addition, the safety and efficacy of filgotinib were also evaluated in a clinical trial (NCT03101670) for the treatment of active psoriatic arthritis [125].

#### Metabolism

Namour et al. [126] investigated the pharmacokinetics of filgotinib and its active metabolite in healthy male volunteers. The results revealed the formation of an active metabolite, aminotriazolopyridine metabolite (Figure 36), which contributes to the inhibitory activity against JAKs [119,127]. In addition, the active metabolite of filgotinib undergoes further metabolism by glucuronidation of the free amino group to give a glucuronide metabolite.

The aminotriazolopyridine active metabolite of filgotinib (Figure 36) exhibited an inhibitory activity against human JAK1 ( $IC_{50} = 307$  nM) using human recombinant JAK1 [117,127]. On the other hand, the inhibitory activity of this metabolite against JAK1 was observed at  $IC_{50}$  of  $11.9$   $\mu$ M in a whole blood assay (IL6-induced pSTAT1).

In another study, Namour et al. identified the aminotriazolopyridine active metabolite of filgotinib in three animals (mouse, monkey, and dog) and humans [128]. The study revealed a significant interaction between filgotinib or its active metabolite with CYP450, glucuronosyltransferases, or drug transporters. This study suggests that filgotinib can be combined with the other drugs used for rheumatoid arthritis.

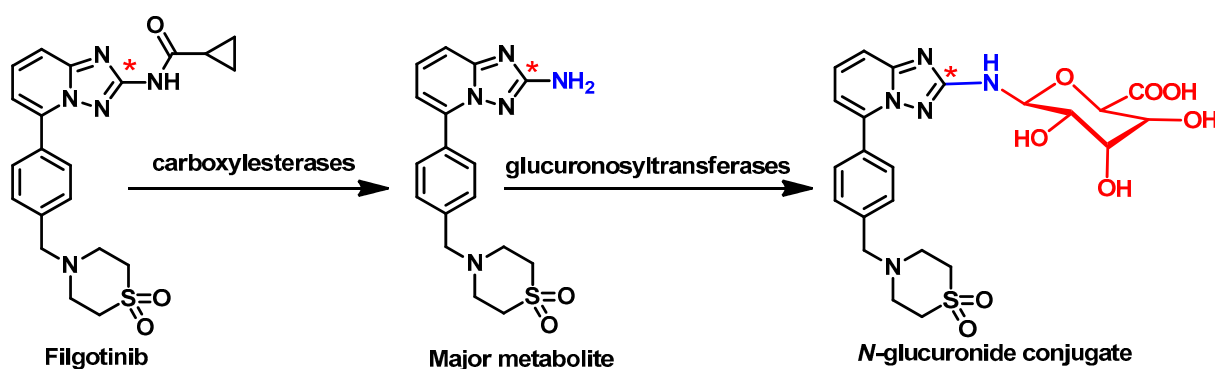


Figure 36. Proposed metabolic pathway of filgotinib.

#### 1.7.6. Oclacitinib

##### Approval History

In 2013, oclacitinib (Figure 37) was approved by the FDA to treat dogs with atopic dermatitis and pruritus associated with allergic dermatitis [129].

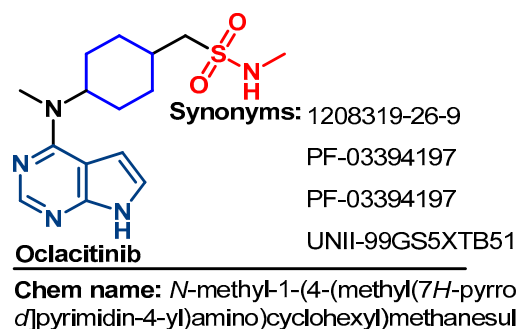


Figure 37. Chemical structure/name/synonyms of oclacitinib.

##### Synthesis

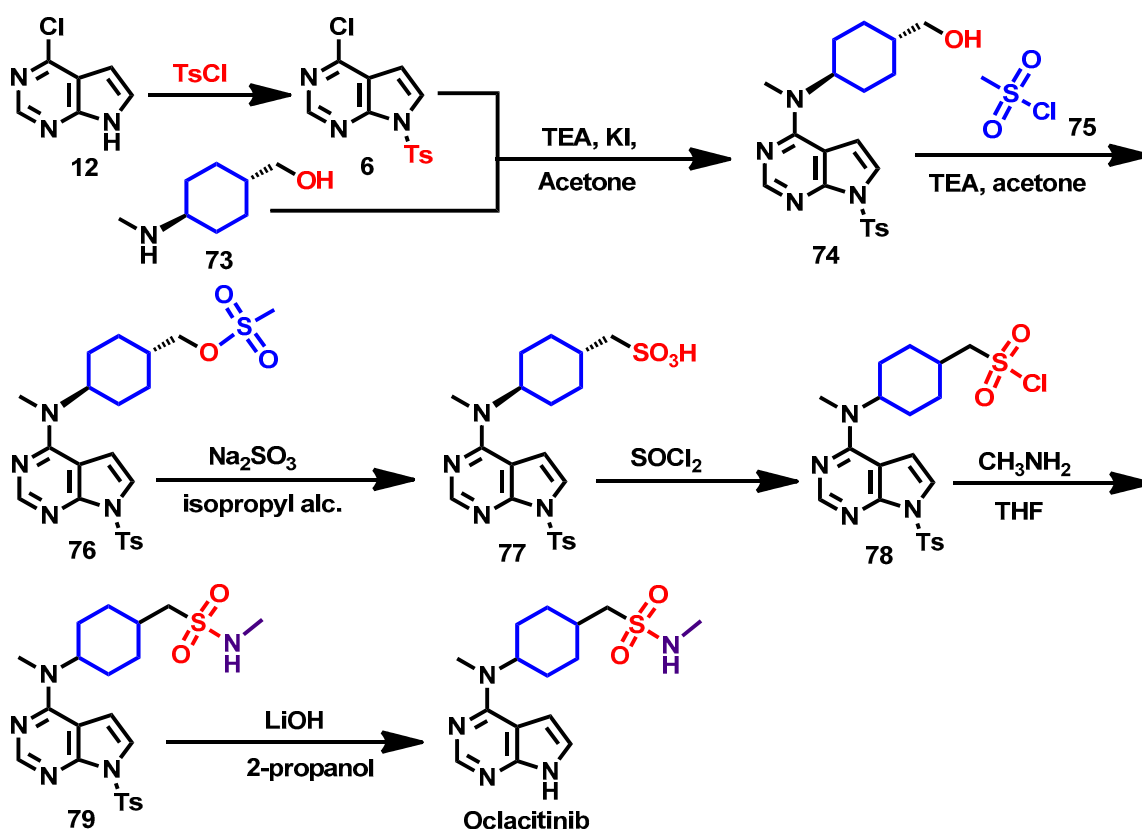
The preparation of oclacitinib was patented by Berlinski et al. [130]. The synthetic route depends on the reaction of the commercially available 4-chloro-7*H*-pyrrolo[2,3-*d*]pyrimidine **12** with tosyl chloride to give compound **6**, Scheme 9.

In addition, compound **6** was reacted with **73** to afford **74**, which underwent sulfonylation with methanesulfonyl chloride **75** to give **76**, Scheme 9. The reaction of **76** with sodium sulfite gave **77**, which was treated with thionyl chloride to give **78**. Finally, the reaction of compound **78** with methylamine gave **79**, which was treated with lithium hydroxide to liberate oclacitinib as a free base.

##### Target Kinases

Gonzales et al. evaluated the inhibitory activity of oclacitinib against the four JAKs using isolated enzymes [129]. The results revealed inhibitory activity against the four kinases at IC<sub>50</sub> values in the range of 10–99 nM, Figure 38. The highest inhibitory activity of oclacitinib was observed against JAK1 (IC<sub>50</sub> = 10 nM) with 1.8- and 9.9-fold selectivity toward JAK1 compared to JAK2 and JAK3, respectively.

Oclacitinib was also evaluated for its inhibitory activity against a panel of 38 non-JAK kinases [129]. The results revealed 32%–42% inhibition in the activity of aurora-related kinase 1 (ARK1), serine/threonine protein kinase MARK, high-affinity nerve growth factor receptor (TRK-A), and vascular endothelial growth factor receptor 2 (VEGFR-2/FLK1), Figure 38.



Scheme 9. Synthesis of oclacitinib.

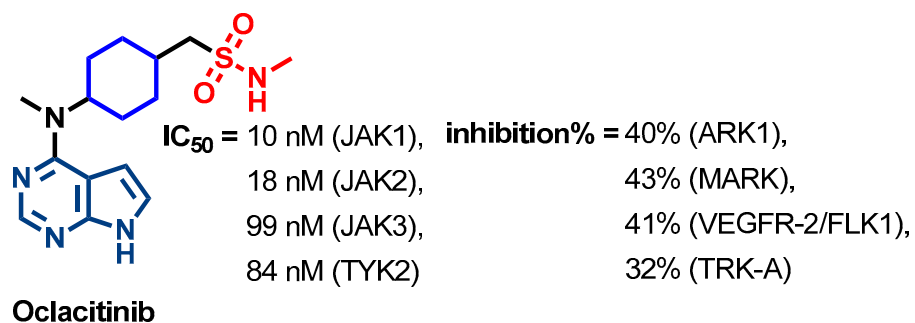


Figure 38. Kinase inhibitory activity of oclacitinib.

### Crystal Structures

Oclacitinib has not yet been reported in a crystal structure with any of its target kinases.

### Pharmacological Activities and Uses

Gonzales et al. evaluated the effect of oclacitinib on the function of different cytokines in canine and human cell model systems [129]. The results revealed the inhibition of IL-2, IL-4, IL-6, IL-13, and IL-31, which play an essential role in inflammation, allergy, and pruritus at IC<sub>50</sub> values in the range of 36–249 nm. In 2013, oclacitinib was approved by the FDA to treat dogs ≥12 months old with atopic dermatitis and pruritus associated with allergic dermatitis [129]. Moreover, Haugh et al. also reported the first use of oral oclacitinib in the treatment of a man with atopic dermatitis [131].

Oclacitinib also showed safe and effective control in the treatment of dogs with pruritus associated with allergic dermatitis [132].

Rynhoud et al. investigated the association between the use of oclacitinib and antibacterial therapy [133]. The results suggested a reduction of the antibacterial use when combined with oclacitinib, compared to other antipruritic agents.

Banovic et al. [134] have reported an immunosuppressive effect of oclacitinib in dogs when used at a dose higher than that used in the treatment of allergic pruritus. However, an increase in CD4+ lymphocyte populations in dogs was observed after long-term treatment with oclacitinib [135].

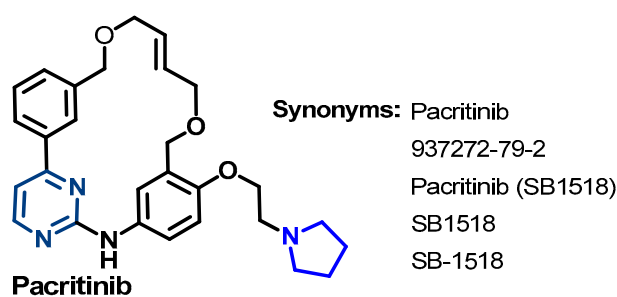
### Metabolism

Oclacitinib maleate has rapid oral absorption with 89% absolute bioavailability and a low clearance rate in dogs [136]. It undergoes metabolism into several metabolites. Among these metabolites, one major oxidative metabolite was detected in plasma and urine [137]. However, oclacitinib exhibited very weak inhibitory activity against Cyp450 enzymes, which indicates a low potential for drug–drug interaction.

### 1.7.7. Pacritinib

#### Approval History

Pacritinib (Figure 39), a JAK2/FLT3 inhibitor, was approved by the FDA for the treatment of myelofibrosis in adult patients with thrombocytopenia [138].



Chemical name: 11-(2-pyrrolidin-1-yl-ethoxy)-14,19-dioxo-5,7,26-triaza-tetracyclo [19.3.1.1(2,6).1(8,12)]heptacos-1(25),2(26),3,5,8,10,12(27),16,21,23-decaene

**Figure 39.** Chemical structure, name, and synonyms of pacritinib.

#### Synthesis

The synthesis of pacritinib was reported by William et al. [139]. It depends on the reaction of the intermediate compounds **83** and **88**, Scheme 10.

At the first step (Scheme 10), compound **80** was reacted with **81** to give **82**, which underwent a base-catalyzed alkylation using allyl bromide to give **83** [139].

On the other hand, 2-hydroxy-5-nitrobenzaldehyde **84** was reacted with dichloroethane, followed by a reduction in the resulting product **85** to give the corresponding alcohol **86** [139]. Compound **86** was alkylated using allyl bromide to give **87**, which saw a decrease in the nitro group to give **87**. The reaction of **88** with **83** afforded **89**, which was reacted with pyrrole to give pacritinib, Scheme 10.

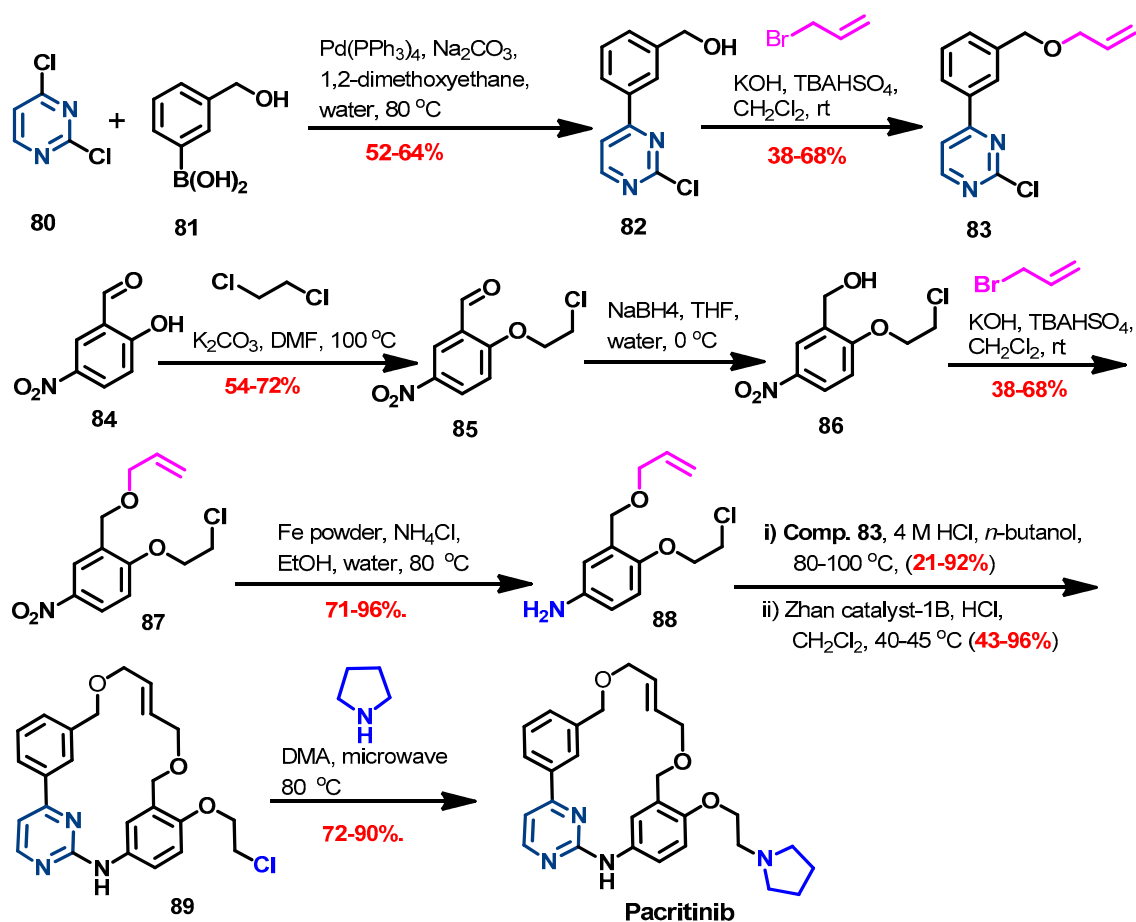
#### Target Kinases

The kinase inhibitory activity of pacritinib was evaluated by William et al. [139]. The results revealed inhibitory activity against JAK2 and JAK2<sup>V617F</sup>, at IC<sub>50</sub> values of 22 and 19 nM, respectively, Figure 40.

Pacritinib also showed weaker inhibitory activity against the other types of JAK kinases. It also showed potent inhibitory activity against FLT3 (IC<sub>50</sub> = 22 nM) [139]. In addition, only weak inhibitory activity was observed against CDK2, Figure 40.

Pacritinib also underwent extensive evaluation of its inhibitory activity against 439 recombinant kinases [140]. Besides the inhibition of JAK2, JAK2V617F, and FLT3, pacritinib

also showed inhibitory activity against colony-stimulating factor 1 receptor, and interleukin-1 receptor-associated kinase 1 at  $IC_{50} < 50$  nM.



Scheme 10. Synthesis of pacritinib.

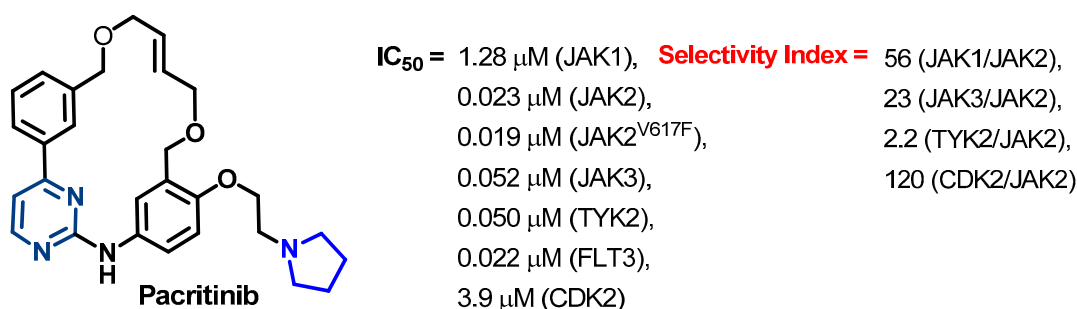
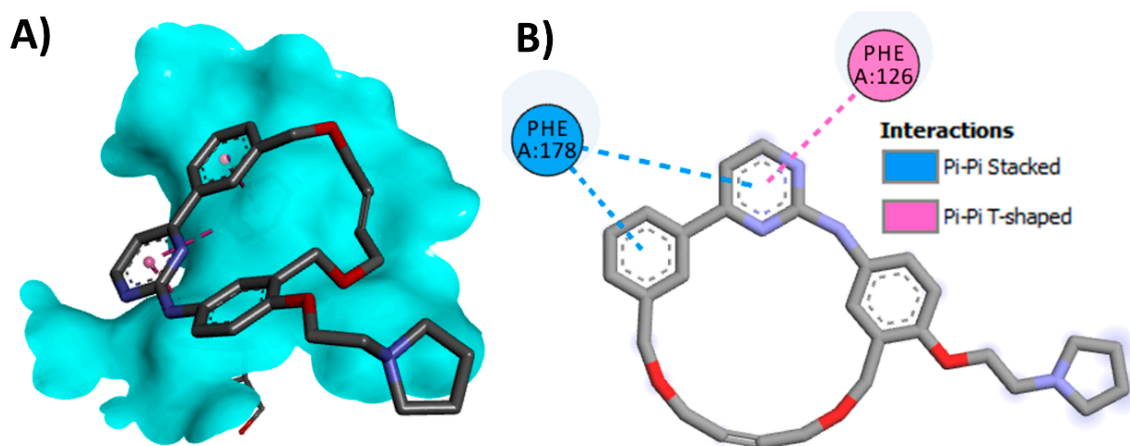


Figure 40. Kinase inhibitory activities of pacritinib.

#### Crystal Structures

Pacritinib exists in only one crystal structure in the protein data bank. This crystal includes pacritinib in complex with human quinone reductase 2 (NQO2) (pdb: 5LBZ) [141]. Pacritinib shows only multiple hydrophobic interactions of the pi-pi stacked and pi-pi T-shaped types with Phe126 and Phe178 in this reductase enzyme, Figure 41. However, no crystal structure with any of the target JAKs has been reported yet.



**Figure 41.** Binding modes of pacritinib (shown as sticks) into human quinone reductase 2 (NQO2) (pdb: 5LBZ): (A) 3D binding mode, receptor shown as a hydrogen bond surface; (B) 2D binding mode showing different types of binding interactions; this figure was generated using Discovery Studio Visualizer (V16.1.0.15350).

#### Pharmacological Activities and Uses

Pacritinib acts as an inhibitor of both JAK2 and FLT3 that could be used to overcome the resistance problems in patients with acute myeloid leukaemia (AML) [30]. The dual activity against the two kinases could enable pacritinib to overcome the resistance mediated by the upregulation of JAK2 in FLT3-TKI-resistant AML cells [30].

Pacritinib was later tested for its activity in the treatment of myelofibrosis in several clinical trials [142,143]. The efficacy of pacritinib was evaluated against the best available therapy in patients with myelofibrosis (NCT01773187) [142]. The results revealed a significant reduction in the volume of the spleen (SVR) in patients receiving pacritinib therapy, indicating that it could be used in the treatment of myelofibrosis.

In addition, pacritinib also showed higher efficacy in reducing splenomegaly than the best available therapy in patients with myelofibrosis and thrombocytopenia (NCT02055781) [143].

Pacritinib also showed potential anti-leukemic activity when combined with chemotherapeutic agents [144,145].

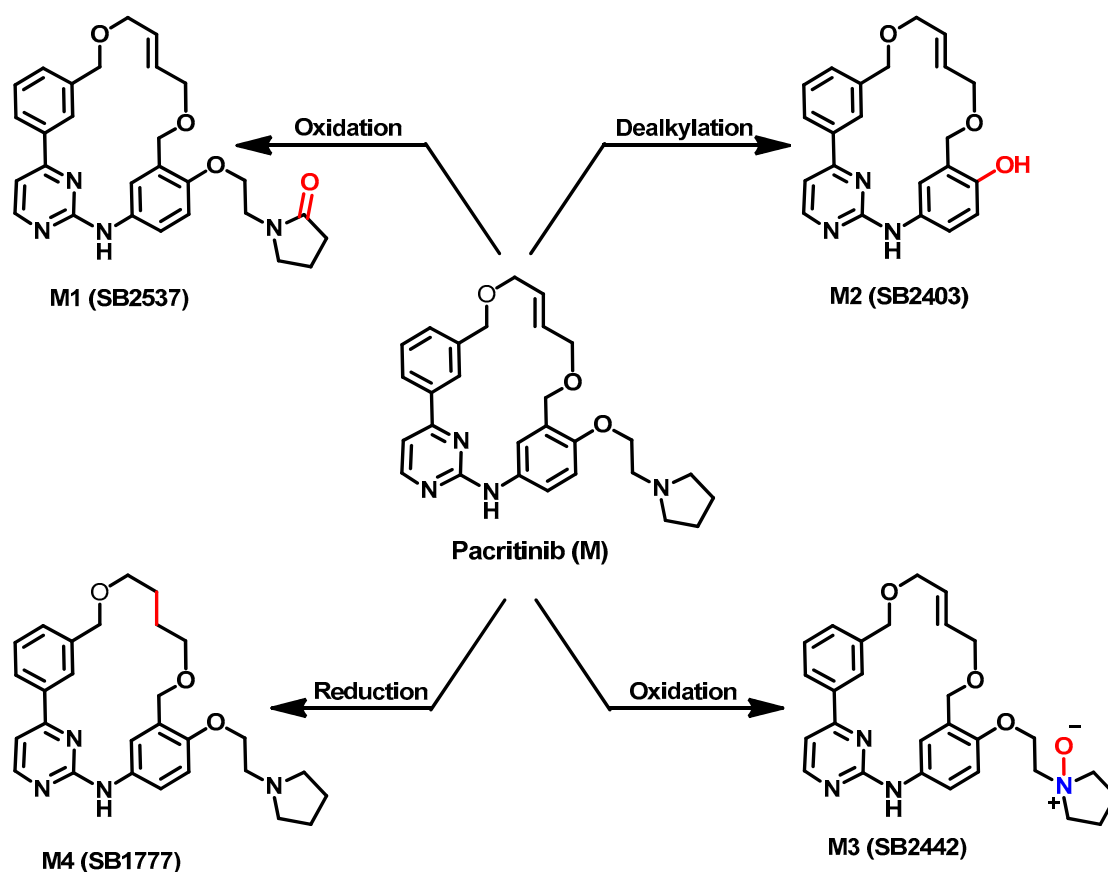
The efficacy of pacritinib in the treatment of patients with glioblastoma multiforme was also reported when combined with temozolomide [146].

#### Metabolism

The preliminary results of the metabolic study of pacritinib revealed that CYP3A4 is the main metabolizing enzyme [139]. However, no inhibitory activity was observed against the other isoenzymes.

On the other hand, the metabolism of pacritinib was investigated *in vitro/in vivo* by Jayaraman et al. [147]. The results revealed the formation of four metabolites by liver microsomes in both humans and mice, Figure 42.

The detected metabolites include two oxidation metabolites formed by oxidation of the pyrrole ring (M1) and pyrrole nitrogen (M3) [147]. In addition, the third metabolite (M2) formed by *O*-dealkylation of the pyrrole-bearing side chain, while the fourth one (M4) was formed by reduction of the double bond, Figure 42.

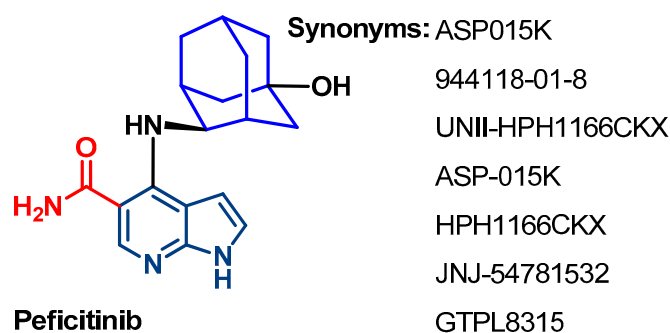


**Figure 42.** Proposed metabolic pathways and metabolites of pacritinib in human and mouse plasma.

### 1.7.8. Peficitinib

#### Approval History

Peficitinib (Figure 43) is a pan-JAK inhibitor. It was approved in 2019 in Japan for the treatment of rheumatoid arthritis [68].



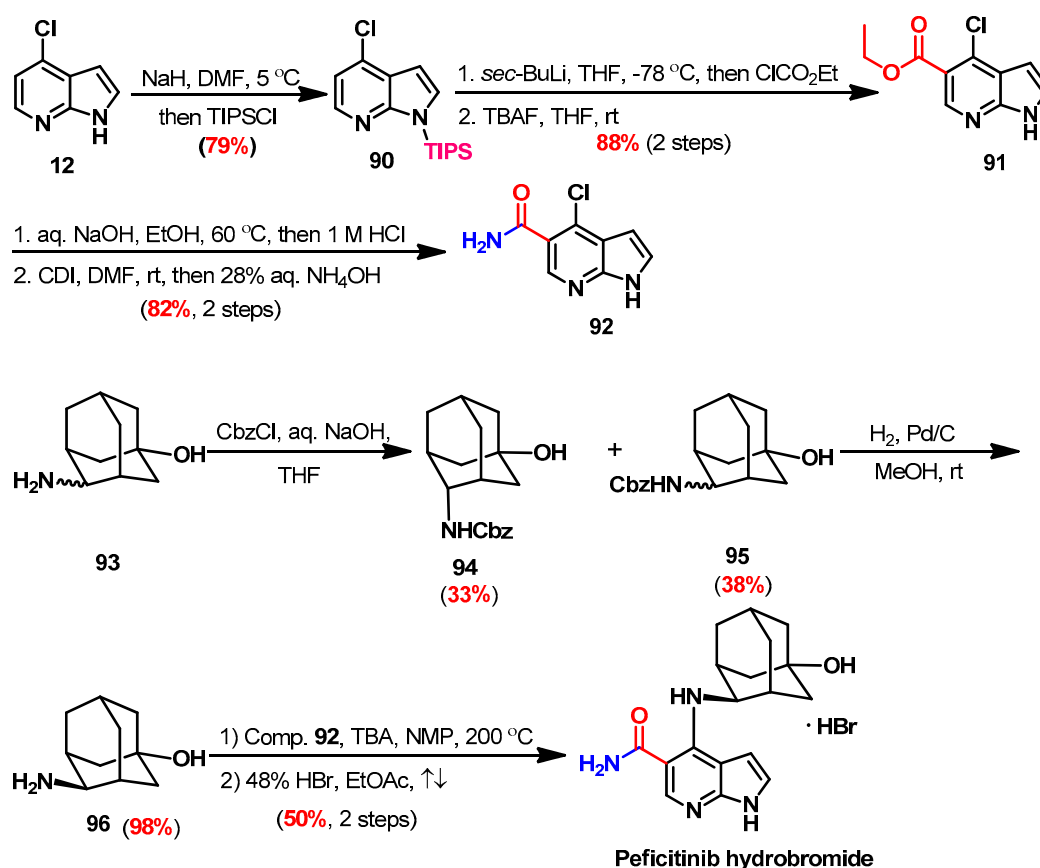
#### Peficitinib

**Chem. name:** 4-(((1*R*,2*s*,3*S*,5*s*,7*s*)-5-hydroxyadamantan-2-yl)amino)-1*H*-pyrrolo[2,3-*b*]pyridine-5-carboxamide

**Figure 43.** Chemical structure/name/synonyms of peficitinib.

#### Synthesis

Peficitinib was obtained from pyrrolo[2,3-*b*]pyridine **7** in a seven-step synthesis [104,148]. In the first step, *N*-protected pyrrolo[2,3-*b*]pyridine **90** was obtained from the reaction of **12** with triisopropylsilyl chloride (TIPSCl). Compound **91** was obtained from the reaction of **90** with *sec*-BuLi and ethyl chloroformate followed by treatment with *tetra*-butylammonium fluoride (TBAF) to remove the TIPS group, Scheme 11.



Scheme 11. Synthesis of peficitinib.

Conversion of the ethyl ester group in **91** to the corresponding amide group in **92** was achieved in two steps (Scheme 11). The first step proceeded through hydrolysis of the ester group in **91** to liberate the corresponding carboxylic acid derivative, which was reacted with ammonium hydroxide in the presence of CDI to give the amide derivative **92**.

On the other hand, the diastereomeric mixture of **93** was reacted with benzyl chloroformate followed by chromatographic separation to isolate the *trans*-isomer **95**. Pd/C-catalyzed hydrogenation of **95** yielded *trans*-4-aminoadamantan-1-ol **96**. The reaction between **92** and **96** afforded peficitinib as a free base. Treatment of peficitinib with hydrobromic acid afforded peficitinib hydrobromic acid salt, Scheme 11.

#### Target Kinases

The kinase inhibitory activity of peficitinib was evaluated against the four JAKs [149,150]. The results (Figure 44) revealed inhibitory activity against the four kinases with  $\text{IC}_{50}$  values in the range of 0.70–5.0 nM [149]. These results indicate that the highest inhibitory activity of peficitinib was against JAK3.

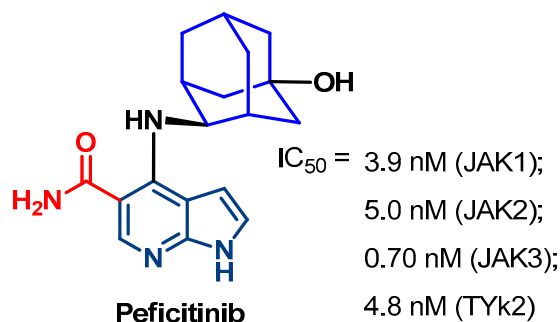
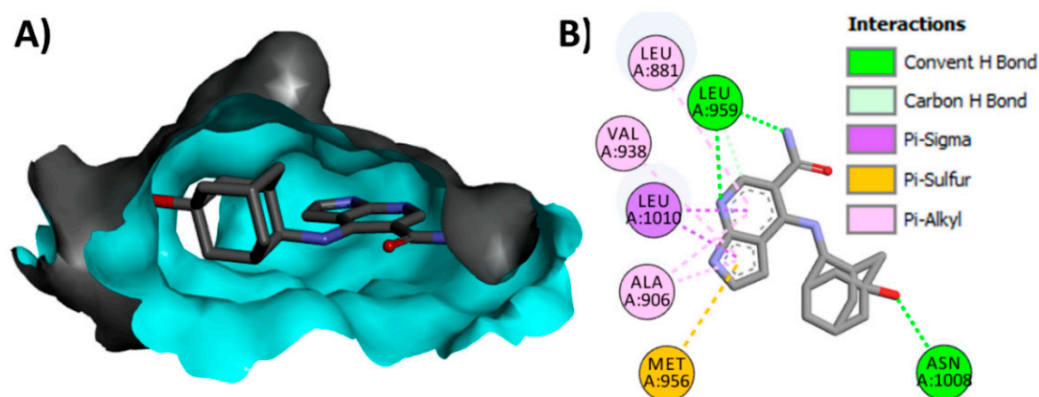


Figure 44. Kinase inhibitory activities of peficitinib.



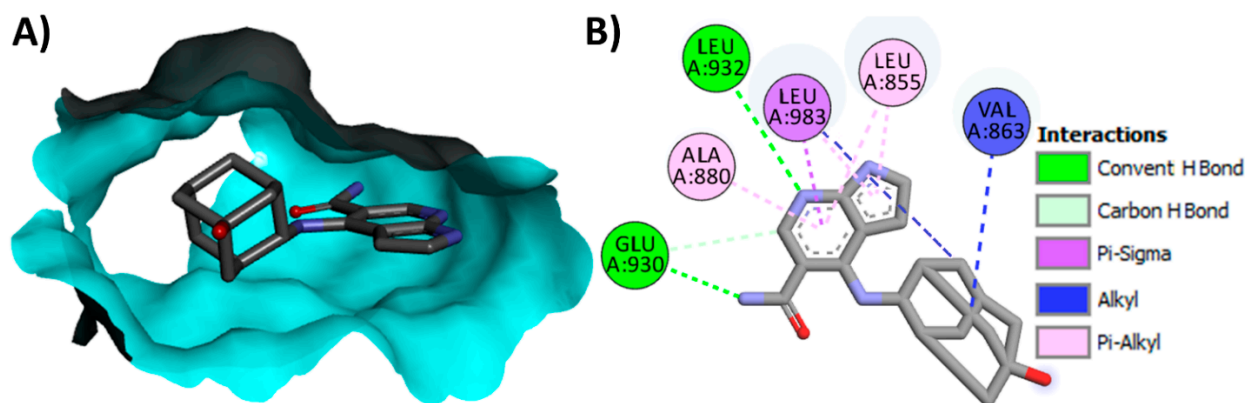
### Crystal Structures

Peficitinib is available as a co-crystallized ligand in four crystal structures with JAKs in the protein data bank. These crystals include the crystal structure of peficitinib bound to JAK1 (pdb: 6AAH) [151], JAK2 (pdb: 6AAJ) [151], JAK3 (pdb: 6AAK) [151], and TYK2 (6AAM) [151]. All at 1.83–2.67 Å resolution. The binding mode and interactions of peficitinib with JAK1 (pdb: 6AAH) are presented in Figure 45. Peficitinib shows three conventional hydrogen bonds with Leu959 and Asn1008.



**Figure 45.** Binding modes of peficitinib (shown as sticks) into JAK1 (pdb: 6AAH): (A) 3D binding mode, receptor shown as a hydrogen bond surface; (B) 2D binding mode showing different types of interactions with JAK1; the figure was generated using Discovery Studio Visualizer (V16.1.0.15350).

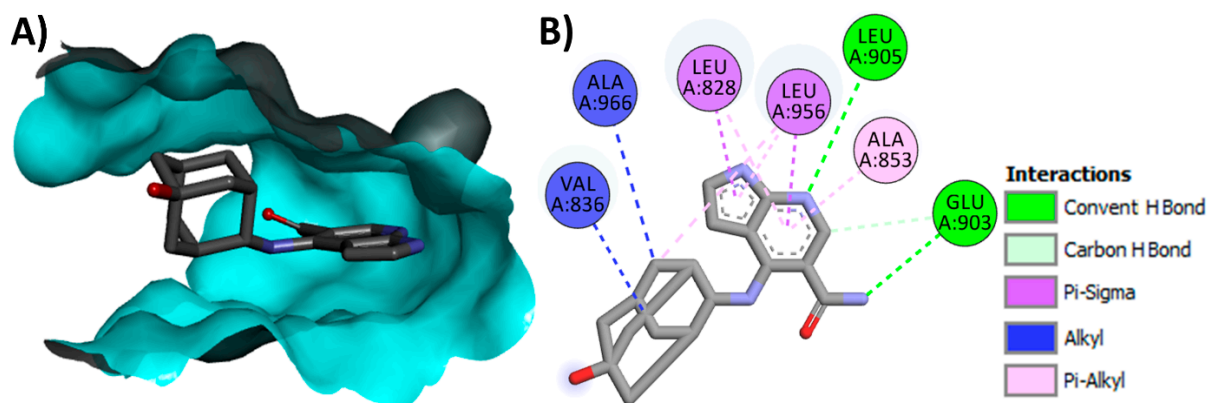
The binding interactions of peficitinib in JAK2 (pdb: 6AAJ) show two conventional hydrogen bonds with Glu930 and Leu932, Figure 46. In addition, peficitinib forms one carbon hydrogen bond with Glu930.



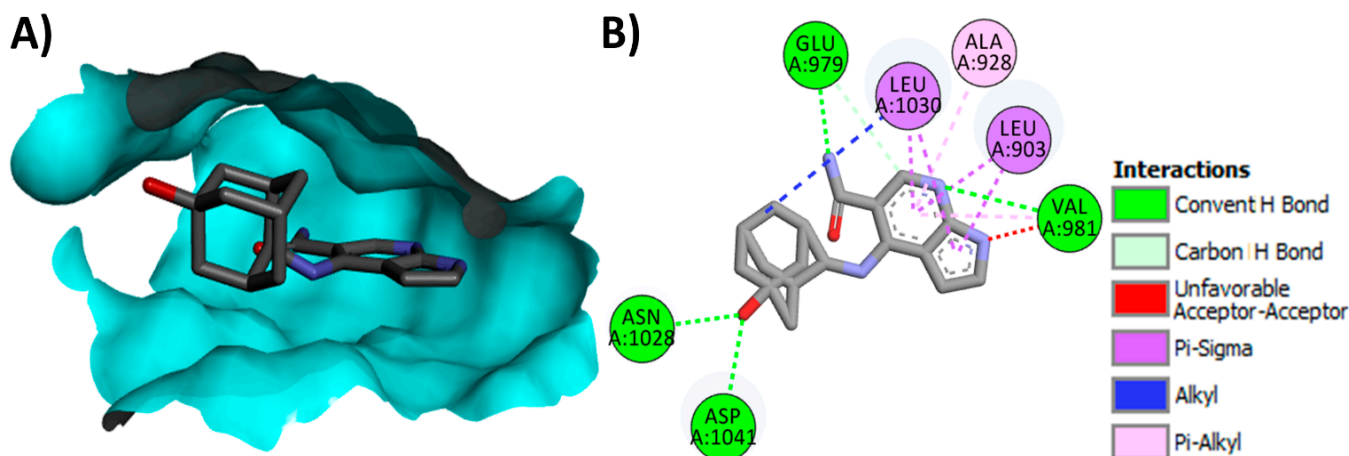
**Figure 46.** Binding modes of peficitinib (shown as sticks) into JAK2 (pdb: 6AAJ): (A) 3D binding mode, receptor shown as a hydrogen bond surface; (B) 2D binding mode showing different types of interactions with JAK2; hydrogen atoms were omitted for clarity; this figure was generated using Discovery Studio Visualizer (V16.1.0.15350).

The binding mode and interactions of peficitinib are presented in Figure 47. Peficitinib shows two conventional hydrogen bonds with Glu903 and Leu905, as well as one carbon–hydrogen bond with Glu903.

On the other hand, the binding orientation, and interactions of peficitinib with TYK2 are presented in Figure 48. Peficitinib shows four conventional hydrogen bonds: Val981, Glu979, Asn1028, and Asp1041.



**Figure 47.** Binding modes of peficitinib (shown as sticks) into JAK3 (pdb: 6AAK): (A) 3D binding mode, receptor shown as a hydrogen bond surface; (B) 2D binding mode showing different types of interactions with JAK3; hydrogen atoms were omitted for clarity; this figure was generated using Discovery Studio Visualizer (V16.1.0.15350).



**Figure 48.** Binding modes of peficitinib (shown as sticks) into TYK2 (pdb: 6AAM): (A) 3D binding mode, receptor shown as a hydrogen bond surface; (B) 2D binding mode showing different types of interactions with TYK2; hydrogen atoms were omitted for clarity; this figure was generated using Discovery Studio Visualizer (V16.1.0.15350).

#### Pharmacological Activities and Uses

Cytokines play an important role in pain, inflammatory reactions, and nerve sensitization [152]. The pan-JAK inhibitor, peficitinib, was evaluated for the treatment of rheumatoid arthritis, which is characterized by joint destruction and inflammation [153]. Peficitinib suppressed bone destruction and paw swelling in rats with adjuvant-induced arthritis [149].

In a clinical trial (NCT01565655), peficitinib exhibited a dose-dependent ACR20 response rate when given orally to patients with moderate-to-severe rheumatoid arthritis [154]. Peficitinib also demonstrated clinical efficacy and prevention of joint destruction in Asian patients who displayed an inadequate response to conventional DMARDs [155]. In addition, no drop in the effectiveness of peficitinib was observed after long-term use [156]. However, the use of peficitinib was also associated with a risk of herpes zoster infection, similar to other JAK inhibitors [157].

#### Metabolism

Oda et al. investigated the metabolism of peficitinib in healthy male subjects using [ $^{14}\text{C}$ ]-labelled peficitinib [158]. The results revealed the formation of a sulfate-conjugated metabolite (M2). The sulfate conjugate and the parent drug constituted the major compo-

nents in plasma and urine, Figure 49. On the other hand, peficitinib was metabolized to give the *N*-methylated derivative (M4), which was identified in feces.

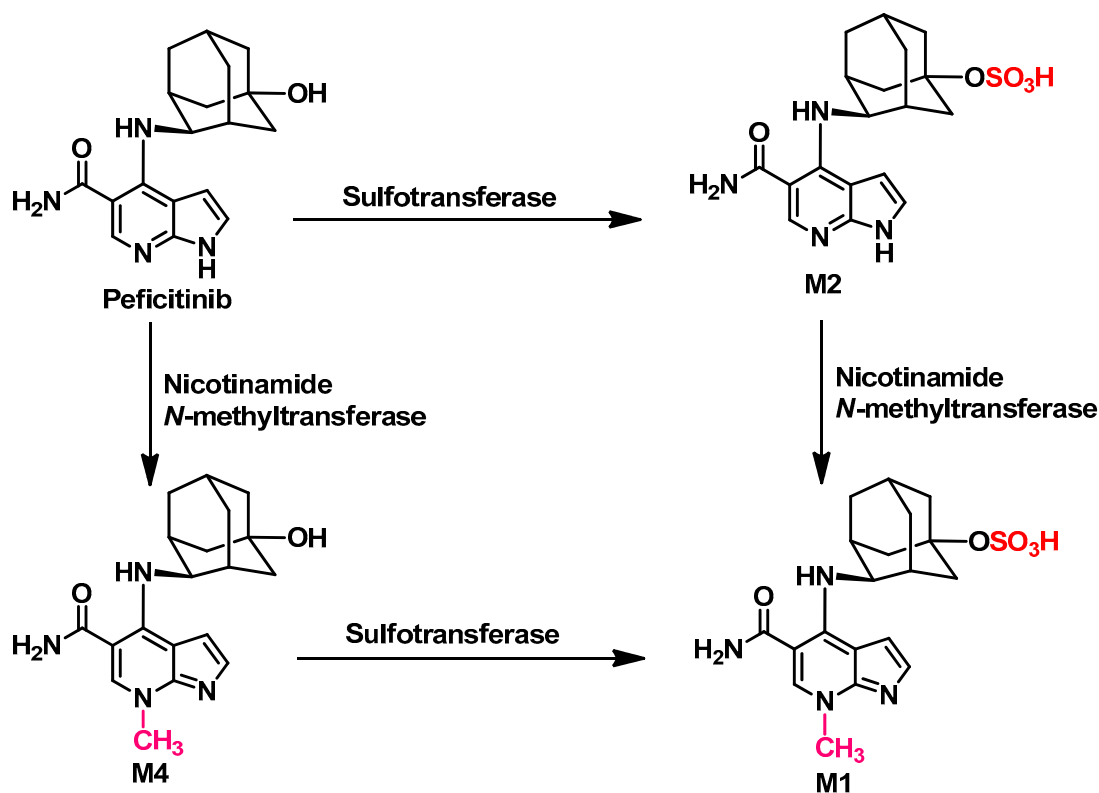


Figure 49. Proposed metabolic pathways and metabolites of peficitinib.

Miyatake et al. investigated the effect of hepatic impairment on the pharmacokinetic profile of peficitinib [159]. The results of this study suggest a decrease in the dose of peficitinib in patients with moderate hepatic impairment.

#### 1.7.9. Ruxolitinib

##### Approval History

Ruxolitinib (Figure 50) was approved by the FDA in November 2011 to treat myelofibrosis [28]. The FDA also approved ruxolitinib in December 2014 for the treatment of patients with polycythemia vera [29]. In addition, ruxolitinib received approval in 2019 and 2021 for the treatment of acute and chronic graft-versus-host disease, respectively [160].

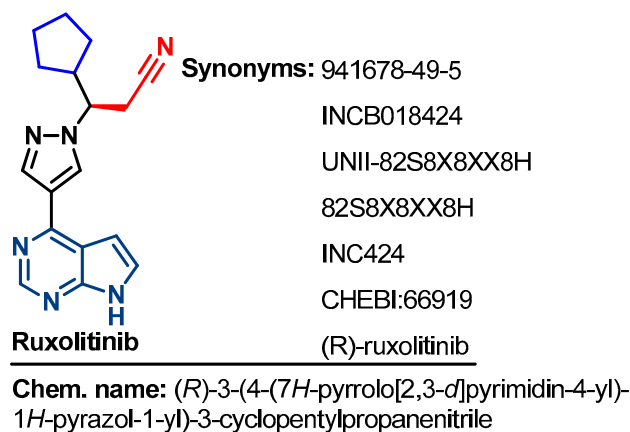
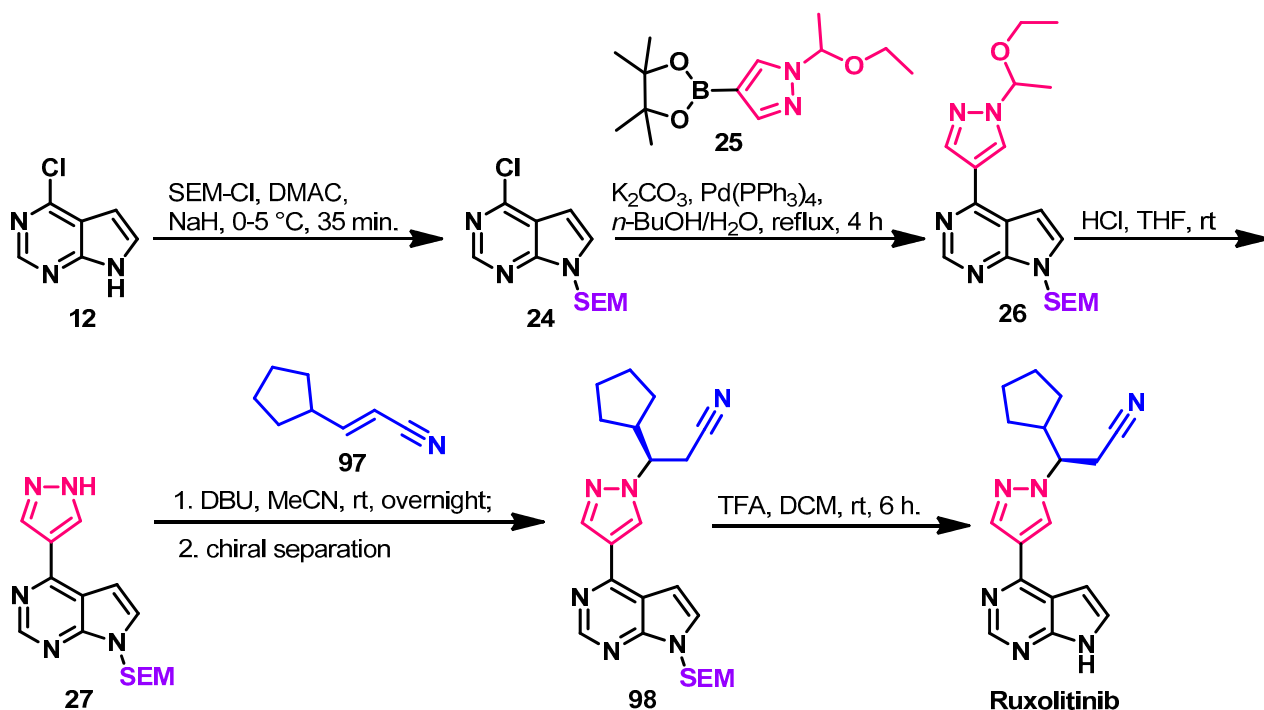


Figure 50. Chemical structure/name/synonyms of ruxolitinib.

## Synthesis

The synthesis of ruxolitinib (Scheme 12) was achieved from compound **12** in a five-step synthesis [115,161]. Compound **12** was first reacted with 2-(trimethylsilyl)ethoxyethyl chloride (SEM-Cl) to give **24**.



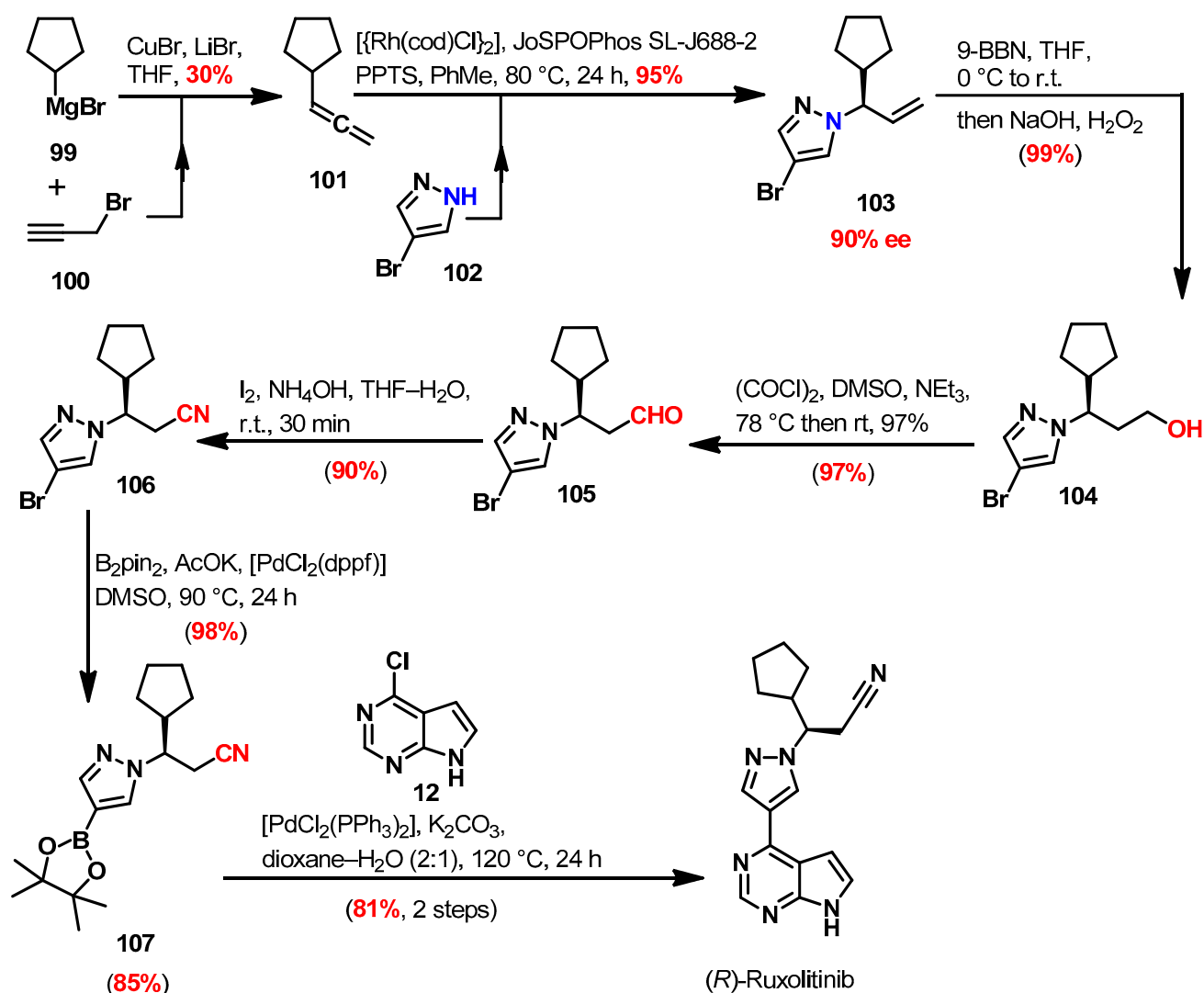
Scheme 12. Synthesis of ruxolitinib (route 1).

In addition, compound **27** was prepared from compound **24** via two steps, Scheme 12. The first step is a Suzuki coupling of **24** and **25** to give **26**. In the second step, compound **26** underwent acid-catalyzed hydrolysis to give **27**. The reaction of **27** with 3-cyclopentylacrylonitrile **97** afforded a mixture of *R*- and *S*-enantiomers **98**, which underwent chiral separation. The *R*-enantiomer of **98** was treated with trifluoroacetic acid to give ruxolitinib.

Haydl et al. [162] reported a regio- and enantioselective synthesis of *N*-substituted pyrazoles that can be used in the synthesis of ruxolitinib, Scheme 13. Compound **101** was prepared from the reaction of cyclopentyl magnesium bromide **99** and 3-bromoprop-1-yne **100**.

Asymmetric addition reaction of the substituted pyrazole **102** to the cyclohexylallene **101** afforded **103**; Scheme 13. Hydroboration of **103** using 9-borabicyclo(3.3.1)nonane followed by the Swern oxidation of the alcoholic group afforded **105**. Compound **105** was then reacted with hydroxylamine in the presence of iodine to give the corresponding nitrile **106**, which was then reacted with bis(pinacolato)diboron to give **107**. The Suzuki coupling of compounds **12** and **107** afforded (*R*)-ruxolitinib.

Lin et al. [163] have also reported an enantioselective synthesis of ruxolitinib (INCB018424). This synthesis depends on the addition of a substituted pyrazole to (*E*)-3-cyclopentylacrylaldehyde, which was catalyzed by diarylprolinol silyl ether.



Scheme 13. Synthesis of ruxolitinib (route 2).

## Target Kinases

Clark et al. investigated the inhibitory activity of ruxolitinib against JAKs [83]. The results (Figure 51) revealed the highest inhibitory activity against JAK1 and JAK2 with  $\text{IC}_{50}$  values of 6.4 and 8.8 nM, respectively.

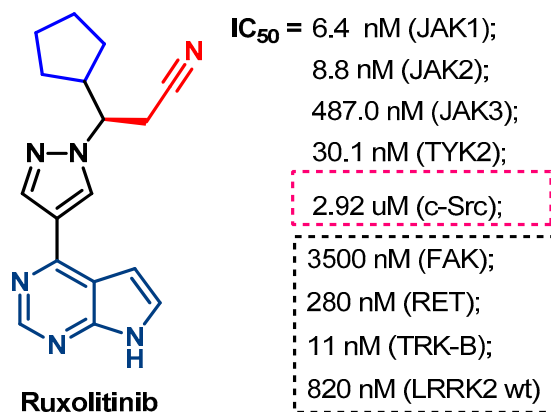


Figure 51. Kinases inhibitory activity of ruxolitinib.

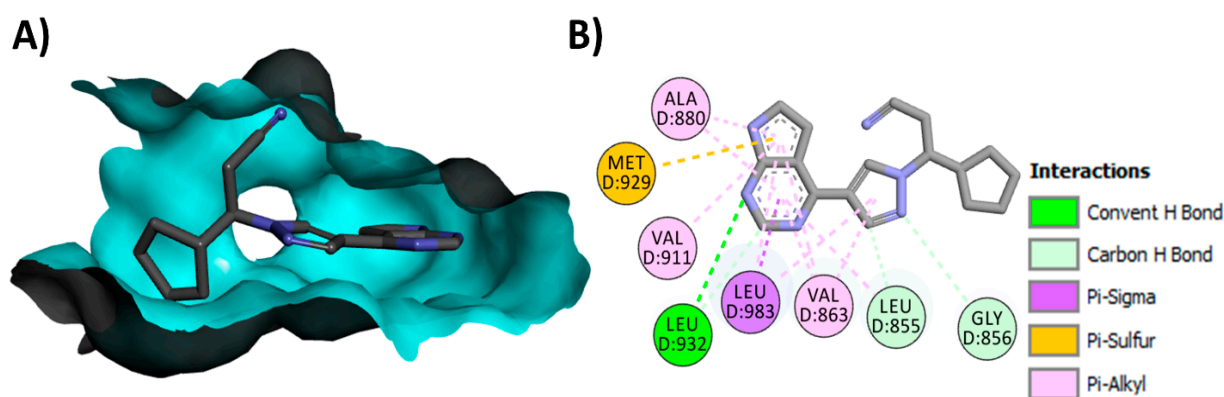
The kinase inhibitory activity of ruxolitinib was also evaluated against 368 kinases by Zhou et al. [164]. At 1  $\mu\text{M}$ , ruxolitinib displayed 96%–100% inhibition in the activity of the four JAKs. Ruxolitinib also showed inhibitory activity against other kinases such as FAC, RET, TRK-B, and LRRK2 (wild-type), Figure 51. Ruxolitinib also exhibited inhibitory activity against c-Src kinase at  $\text{IC}_{50}$  value of 2.92 nM [165].

In another study performed by Quintás-Cardama et al. [166], ruxolitinib displayed inhibitory activity against the four JAKs at  $\text{IC}_{50}$  in the range of 2.8–428 nM. The results of this study revealed the inhibitory activity of ruxolitinib against JAK1 ( $\text{IC}_{50}$  = 3.3 nM) and JAK2 ( $\text{IC}_{50}$  = 2.8 nM). Ruxolitinib also exhibited moderate inhibitory activity against TYK2 ( $\text{IC}_{50}$  = 19 nM). In addition, high efficacy of ruxolitinib was also observed in tumour cells with JAK2V617F mutation.

Ruxolitinib was also evaluated for its inhibitory activity against CHK2 and c-Met kinases, where the results revealed  $\text{IC}_{50}$  values exceeding 1000 nM [166].

### Crystal Structures

Ruxolitinib exists as a co-crystallized ligand in five crystal structures in the protein data bank. Three of these crystals include complexes of ruxolitinib with the JH1 domain of JAK2 (pdb: 6VGL, 6WTN, and 6VNK) [85,86]. Ruxolitinib also exists as a co-crystallized ligand with c-Src (pdb: 4U5J) [165] and DRLK1 (pdb: 7F3G). The binding mode and interactions of ruxolitinib into JAK2 JH1 (pdb: 6VGL) are visualized in Figure 52. Ruxolitinib shows one conventional hydrogen bond with Leu932 and two carbon hydrogen bonds with Leu855 and Gly856.

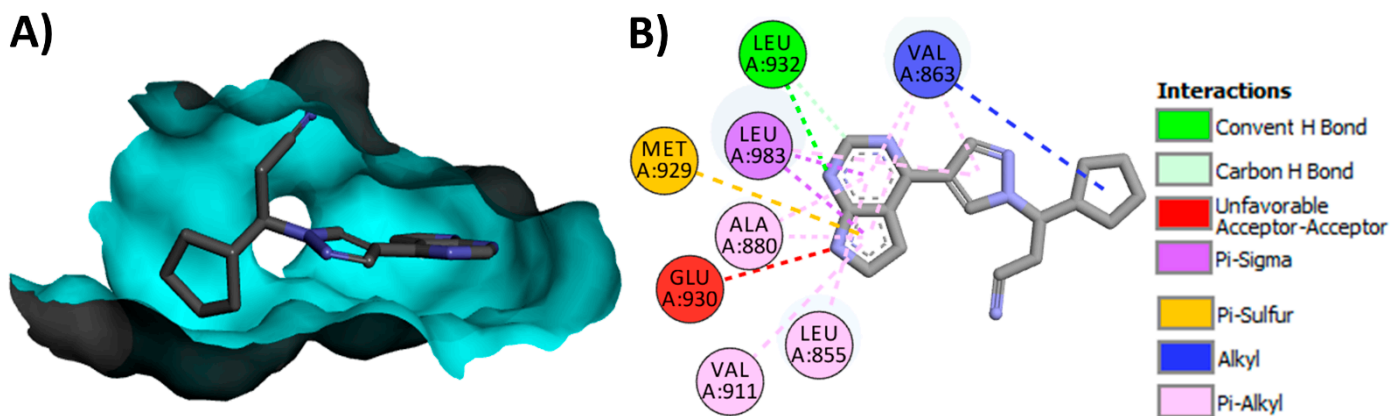


**Figure 52.** Binding modes of ruxolitinib (shown as sticks) into JAK2 JH1 (pdb: 6VGL): (A) 3D binding mode, receptor shown as a hydrogen bond surface; (B) 2D binding mode showing different types of interactions with JAK2 JH1; hydrogen atoms were omitted for clarity; this figure was generated using Discovery Studio Visualizer (V16.1.0.15350).

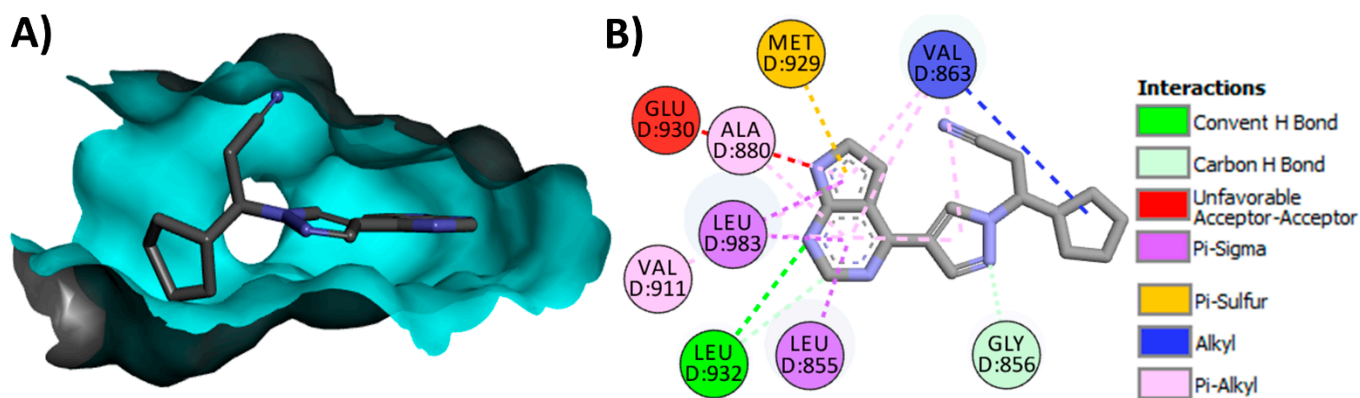
Ruxolitinib also exists as a co-crystallized ligand into the JH1 domain of human JAK2 (pdb: 6WTN) at 1.83 Å resolution. Visualization of the binding mode and interactions of ruxolitinib shows one conventional and one carbon hydrogen bond with Leu932, Figure 53.

In addition, ruxolitinib was also isolated as a co-crystallized ligand with JAK2 JH1 (pdb: 6VNK) at 2.00 Å resolution [85]. The binding interactions also shows one conventional hydrogen bond with Leu932 and one carbon hydrogen bond with Gly856, Figure 54.

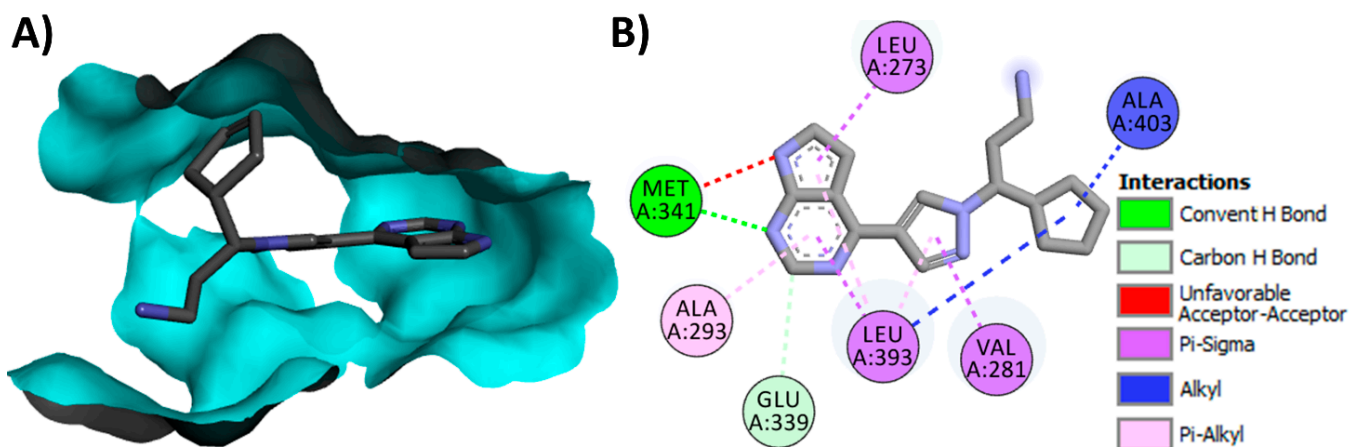
The Src and JAK family kinases share ~34% sequence identity in the kinase domain [165]. Ruxolitinib was also refined in a crystal structure with c-Src (pdb: 4U5J) [165]. The binding interactions of ruxolitinib with c-Src show one conventional hydrogen bond with Met341 and one carbon–hydrogen bond with Glu339, Figure 55.



**Figure 53.** Binding modes of ruxolitinib (shown as sticks) into human JAK2 JH1 (pdb: 6WTN): (A) 3D binding mode, receptor shown as a hydrogen bond surface; (B) 2D binding mode showing different types of interactions with JAK2 JH1; hydrogen atoms were omitted for clarity; this figure was generated using Discovery Studio Visualizer (V16.1.0.15350).

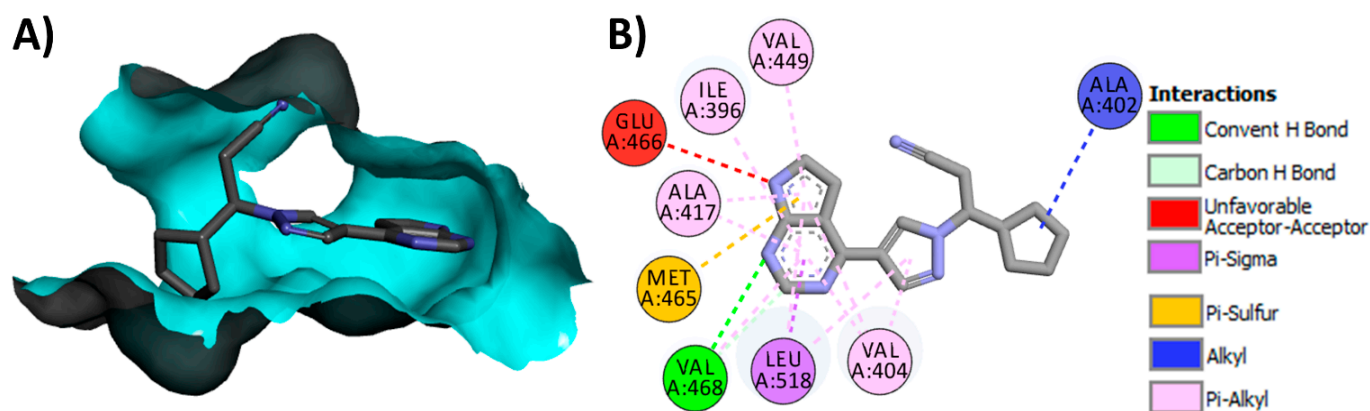


**Figure 54.** Binding modes of ruxolitinib (shown as sticks) into JAK2 JH1 (pdb: 6VNK): (A) 3D binding mode, receptor shown as a hydrogen bond surface; (B) 2D binding mode showing different types of interactions with JAK2 JH1; hydrogen atoms were omitted for clarity; this figure was generated using Discovery Studio Visualizer (V16.1.0.15350).



**Figure 55.** Binding modes of ruxolitinib (shown as sticks) into c-Src (pdb: 4U5J): (A) 3D binding mode, receptor shown as a hydrogen bond surface; (B) 2D binding mode showing different types of interactions with c-Src; hydrogen atoms were omitted for clarity; this figure was generated using Discovery Studio Visualizer (V16.1.0.15350).

Ruxolitinib also exists as a co-crystallized ligand with DCLK1 kinase (pdb: 7F3G). Visualization of the binding mode/interactions of ruxolitinib into DCLK1 shows one conventional hydrogen bond with Val468, Figure 56.



**Figure 56.** Binding modes of ruxolitinib (shown as sticks) into the DCLK1 kinase domain (pdb: 7F3G): (A) 3D binding mode, receptor shown as a hydrogen bond surface; (B) 2D binding mode showing different types of interactions with DCLK1 kinase domain; hydrogen atoms were omitted for clarity; this figure was generated using Discovery Studio Visualizer (V16.1.0.15350).

#### Pharmacological Activities and Uses

Ruxolitinib is a JAK1/2 inhibitor which showed the strong inhibition of JAK2V617F-positive Ba/F3 cells [167]. The efficacy of ruxolitinib in the treatment of myelofibrosis was evaluated in several clinical trials [167,168]. The results of the clinical trial (NCT00952289) revealed significant therapeutic outcomes compared to placebo [168].

In addition to its inhibitory activity against JAKs, ruxolitinib also targets other kinases such as CHK2 and c-Met [166]. Furthermore, ruxolitinib exhibited antiproliferative activity against JAK2V617F+ Ba/F3 cells at  $IC_{50}$  127 nM [166]. The combination of ruxolitinib and ERBB1/2/4 inhibitors also displayed synergistic anticancer activity against lung, breast, and ovarian cancer cells [169].

In 2019, Kim et al. [170] investigated the efficacy of ruxolitinib cream in the treatment of atopic dermatitis in a phase 2 study. A fast improvement in the symptoms of atopic dermatitis was observed, which persisted for up to 12 weeks without significant site reactions. Papp et al. also reported similar findings in another study [171]. Ruxolitinib cream was later approved by the FDA for the treatment of atopic dermatitis [172].

Furthermore, ruxolitinib has also displayed therapeutic benefits in the treatment of acute or chronic graft-versus-host disease (a/cGVHD) [173,174].

#### Metabolism

Shilling et al. [175] investigated the metabolic profile of ruxolitinib in healthy human subjects using [ $^{14}C$ ]-labeled ruxolitinib. The results revealed that the parent drug constitutes the major circulating component in plasma (58–74%). Ruxolitinib underwent extensive metabolism, mainly through oxidative pathways that occurred preferentially at the 2- or 3-position of the cyclopentyl ring and resulted in a series of hydroxy/oxo-metabolites, Figure 57. In addition, *O*-glucuronide conjugates (M28 and M51) were also identified. Among these metabolites, the 2-hydroxycyclopentyl derivative of ruxolitinib (M18) was the major one.

Shi et al. [176] evaluated the impact of the CYP3A4 inhibitor and inducer on the pharmacokinetics of ruxolitinib. The results of this study revealed an increase of the plasma concentration of ruxolitinib by the CYP3A4 inhibitors, ketoconazole, and erythromycin. On the other hand, a decrease in total ruxolitinib was observed on co-administration with the CYP3A4 inducer rifampin.



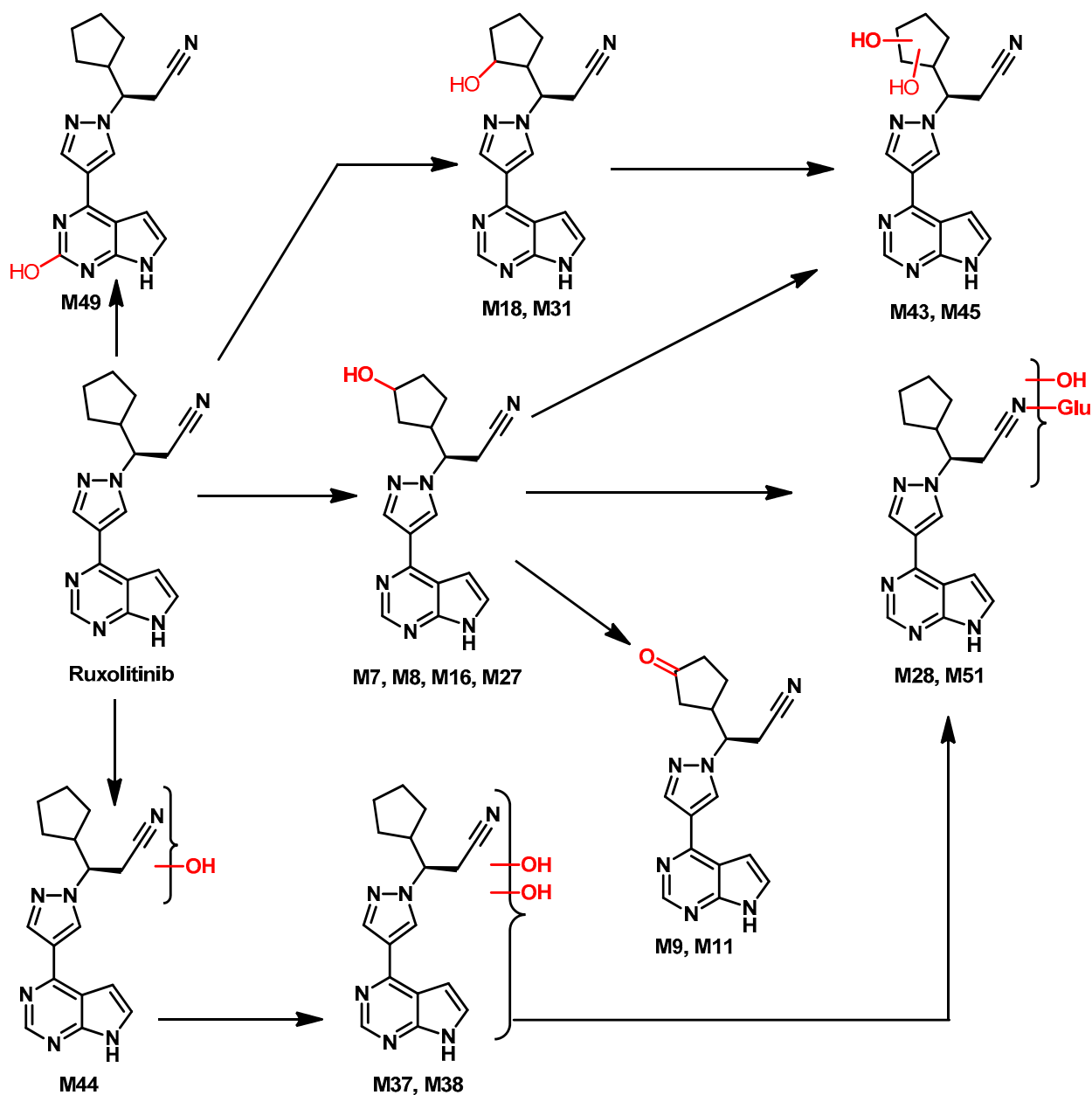


Figure 57. Proposed metabolic pathways and metabolites of ruxolitinib in humans.

#### 1.7.10. Tofacitinib

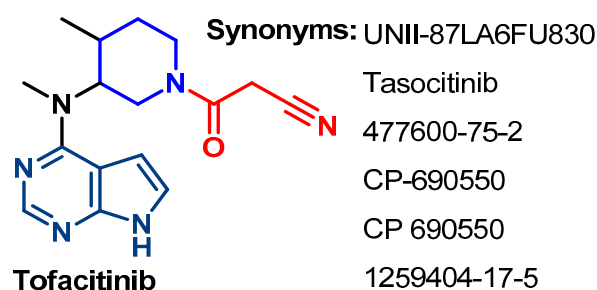
##### Approval History

Tofacitinib (Figure 58) is a JAK inhibitor that was approved by the FDA for rheumatoid arthritis in 2012 [64,177,178]. It was also approved for the treatment of psoriatic arthritis and ulcerative colitis in 2017 and 2018, respectively [115]. In addition, tofacitinib has received FDA approval for the treatment of juvenile idiopathic arthritis in 2020 [179]. In December 2021, tofacitinib was approved for the treatment of active ankylosing spondylitis [180].

##### Synthesis

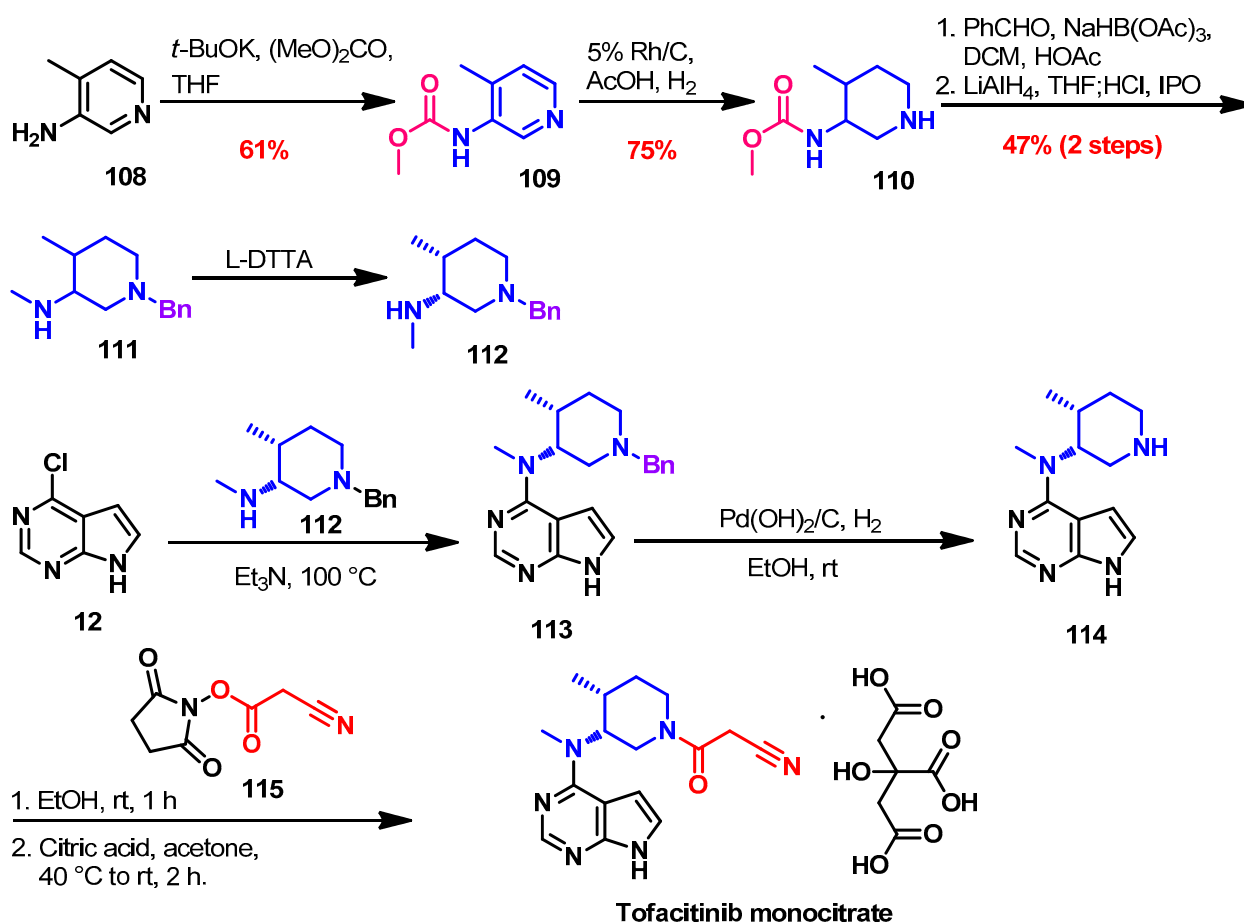
Tofacitinib was obtained from the reaction of compound **12** and (3*R*,4*R*)-1-benzyl-*N*,4-dimethylpiperidin-3-amine **112** [115,181]. Preparation of the substituted piperidine **112** could be prepared from different starting materials using diverse reaction conditions [64,182]. Among these materials, the 4-methylpyridin-3-amine **108** was reacted with dimethyl carbonate to give **109**, Scheme 14. Rhodium-catalyzed hydrogenation of **109** gave **110**, which underwent reductive amination to give **111** as a racemic mixture. The (3*R*,4*R*)-1-benzyl-*N*,4-

dimethylpiperidin-3-amino enantiomer of **111** was resolved using L-di-*p*-toluoyl-tartaric acid (L-DTTA) to give **112**.



**Chem. name:** 3-(4-methyl-3-(methyl(7H-pyrrolo[2,3-d]pyrimidin-4-yl)amino)piperidin-1-yl)-3-oxopropanenitrile

Figure 58. Chemical structure/name/synonyms of tofacitinib.



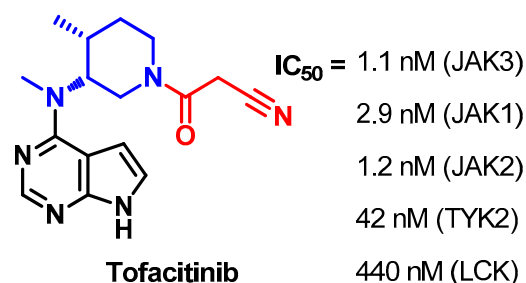
Scheme 14. Synthesis of tofacitinib citrate.

The reaction of compound **12** with the piperidine derivative **112** afforded compound **113**, Scheme 14. Removal of the benzyl group in **113** was achieved using Pd/C-catalyzed hydrogenation, which gave **114**. Tofacitinib was then obtained from the reaction of **114** with cyanoacetic acid 2,5-dioxopyrrolidin-1-yl ester **115**, while treatment of tofacitinib with citric acid afforded the citrate salt.

#### Target Kinases

The kinase inhibitory activity of tofacitinib was evaluated in several studies [83,96]. The results (Figure 59) revealed the inhibitory activity of tofacitinib against the four JAKs

at  $IC_{50}$  values in the range of 1.1–42 nM, where the highest inhibitory activity was against JAK3 [96]. In addition, tofacitinib inhibited JAK1 and JAK2 at  $IC_{50}$  values of 2.9 nM and 1.2 nM, respectively.

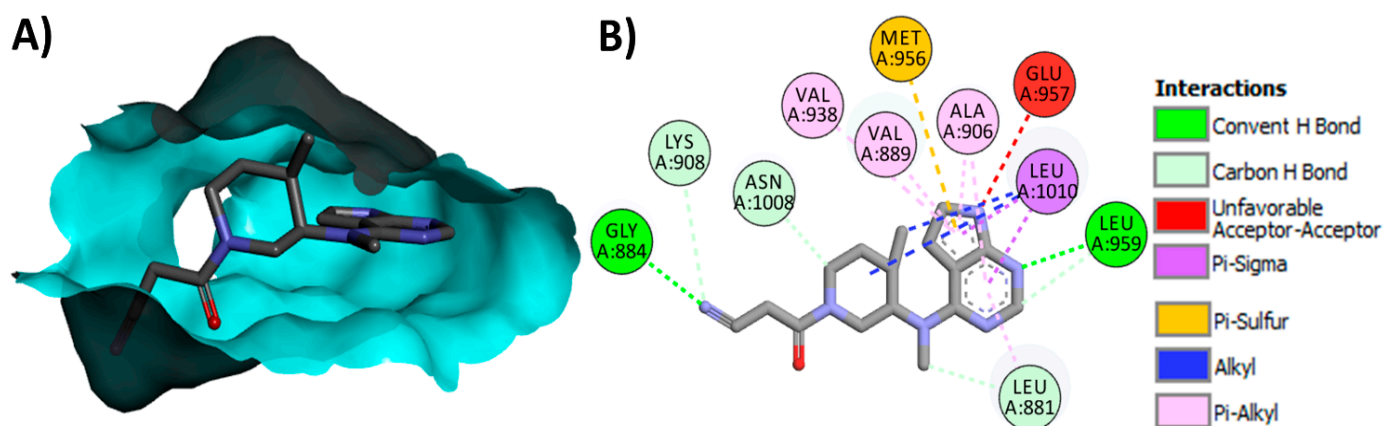


**Figure 59.** Kinase inhibitory activity of tofacitinib.

On the other hand, the inhibitory activity of tofacitinib against JAKs was also evaluated by Clark et al. [83]. The results of that study revealed its inhibitory activity against JAK3 at  $IC_{50}$  of 55 nM. In addition, tofacitinib inhibited the enzymatic activity of JAK1 and JAK2 at  $IC_{50}$  values of 15.1 nM and 77.4 nM, respectively.

#### Crystal Structures

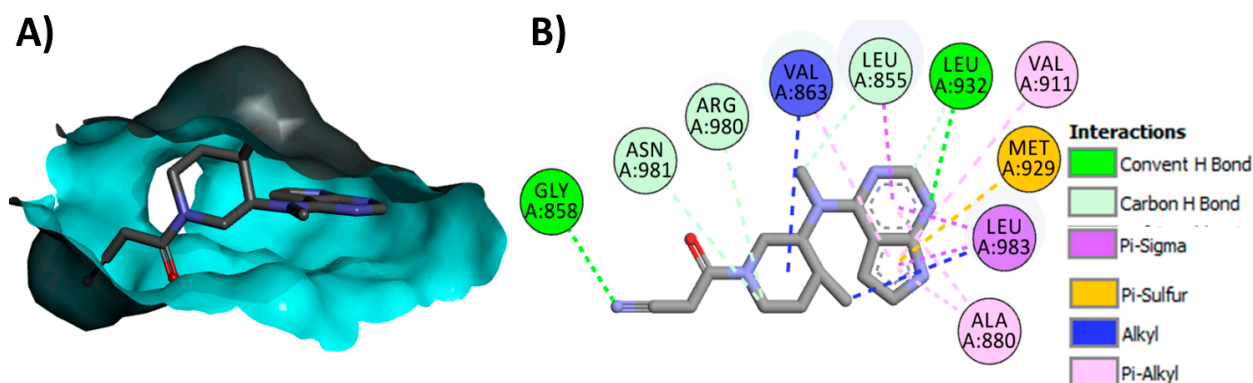
Tofacitinib exists as a co-crystallized ligand in five crystal structures. These crystals include tofacitinib in complex with JAK1 (pdb: 3EYG) [183], JAK2 (pdb: 3FUP) [183], JAK3 (pdb: 3LXK) [184], TYK2 (pdb: 3LXN) [184], and PRK1 (pdb: 4OTI) [185]. The binding interactions of tofacitinib into JAK1 (pdb: 3EYG) are depicted in Figure 60. Tofacitinib shows two conventional hydrogen bonds with Gly884 and Leu959.



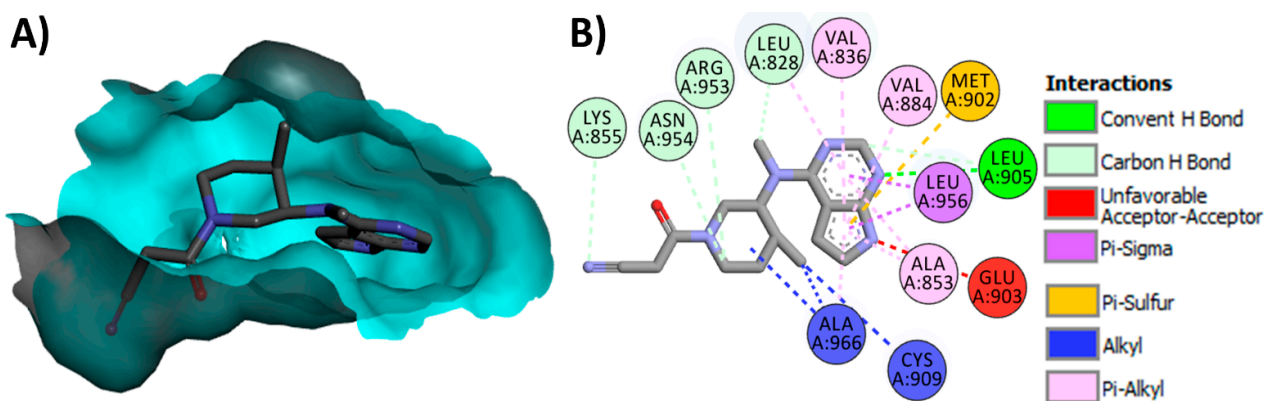
**Figure 60.** Binding modes of tofacitinib (shown as sticks) into JAK1 (pdb: 3EYG): (A) 3D binding mode, receptor shown as a hydrogen bond surface; (B) 2D binding mode showing different types of interactions with JAK1; hydrogen atoms were omitted for clarity; this figure was generated using Discovery Studio Visualizer (V16.1.0.15350).

The binding mode and interactions of tofacitinib with JAK2 (pdb: 3FUP) are depicted in Figure 61. Tofacitinib shows two conventional hydrogen bonds with Gly858 and Leu932. In addition, tofacitinib forms three carbon hydrogen bonds with Leu855, Arg980, and Asn981.

In addition, the binding mode, and interactions of tofacitinib with JAK3 (pdb: 3LXK) are visualized in Figure 62. Tofacitinib shows one conventional hydrogen bond with Leu905. In addition, tofacitinib displays four carbon hydrogen bonds with Leu828, Lys855, Arg953, and Asn954 amino acids in JAK3.

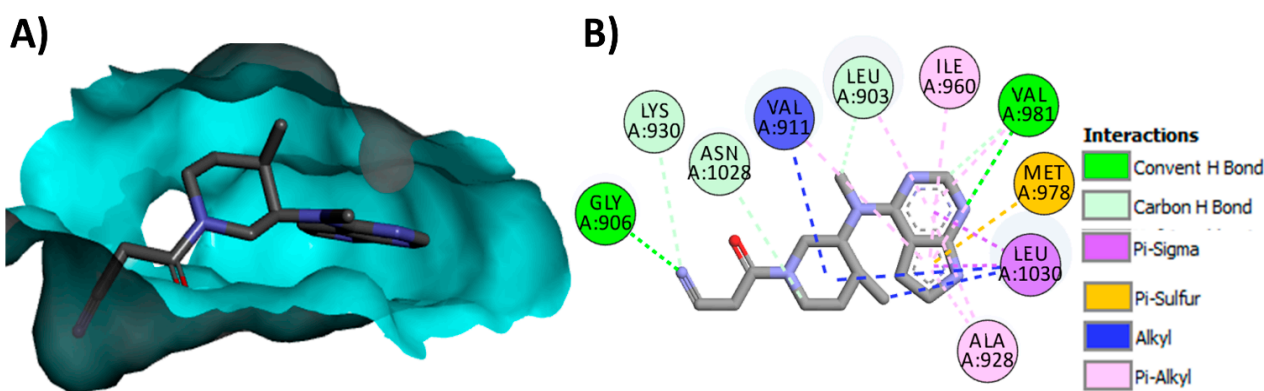


**Figure 61.** Binding modes of tofacitinib (shown as sticks) into JAK2 (pdb: 3FUP): (A) 3D binding mode, receptor shown as a hydrogen bond surface; (B) 2D binding mode showing different types of interactions with JAK2; hydrogen atoms were omitted for clarity; this figure was generated using Discovery Studio Visualizer (V16.1.0.15350).



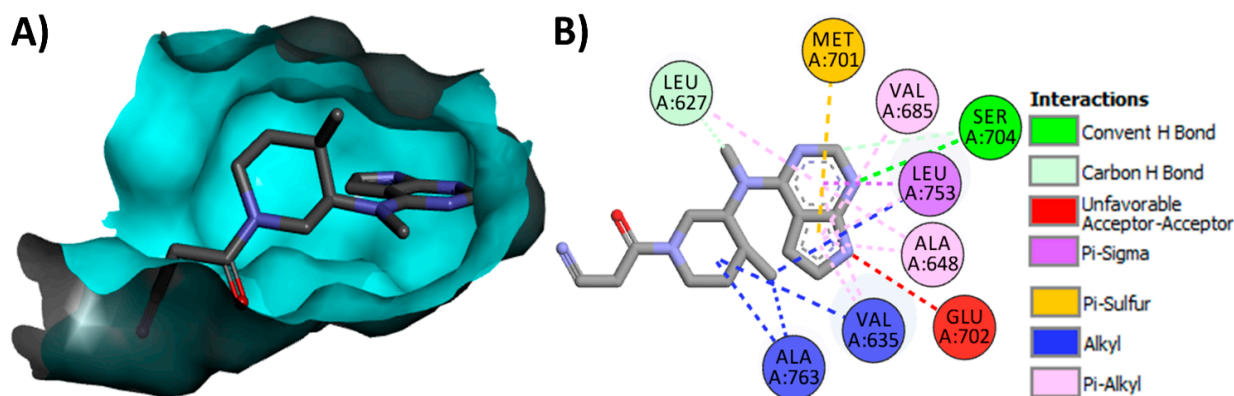
**Figure 62.** Binding modes of tofacitinib (shown as sticks) into JAK3 (pdb: 3LXK): (A) 3D binding mode, receptor depicted as a hydrogen bond surface; (B) 2D binding mode showing different types of interactions with JAK3; hydrogen atoms were omitted for clarity; this figure was generated using Discovery Studio Visualizer (V16.1.0.15350).

On the other hand, the orientation of tofacitinib into TYK2 (pdb: 3LXN) is visualized in Figure 63. Tofacitinib shows two conventional hydrogen bonds with Gly906 and Val981.



**Figure 63.** Binding modes of tofacitinib (shown as sticks) into TYK2 (pdb: 3LXN): (A) 3D binding mode, receptor shown as a hydrogen bond surface; (B) 2D binding mode showing different types of interactions with TYK2; hydrogen atoms were omitted for clarity; this figure was generated using Discovery Studio Visualizer (V16.1.0.15350).

In addition, the binding mode/interactions of tofacitinib into PRK1 (pdb: 4OTI) are visualized in Figure 64. Tofacitinib shows one conventional hydrogen bond with Ser704 and one carbon hydrogen bond with Leu627.



**Figure 64.** Binding modes of tofacitinib (shown as sticks) into the PRK1 catalytic domain (pdb: 4OTI): (A) 3D binding mode, receptor shown as a hydrogen bond surface; (B) 2D binding mode showing different types of interactions with PRK1 catalytic domain; hydrogen atoms were omitted for clarity; this figure was generated using Discovery Studio Visualizer (V16.1.0.15350).

#### Pharmacological Activities and Uses

Several clinical trials were performed to evaluate the efficacy of tofacitinib in the treatment of rheumatoid arthritis. In 2008, the results of a clinical trial (NCT00814307) of tofacitinib revealed improvement in the signs and symptoms of rheumatoid arthritis [186].

In another clinical trial (NCT00853385), tofacitinib showed similar efficacy to adalimumab in patients with rheumatoid arthritis [187]. In patients receiving methotrexate, tofacitinib also stopped the progression of structural damage [188]. By the end of 2012, tofacitinib received the first approval for the treatment of rheumatoid arthritis.

Since the first approval of tofacitinib in 2012 for rheumatoid arthritis, several studies have been performed to evaluate its efficacy in several types of inflammatory and immune diseases. In a clinical trial (NCT01882439), tofacitinib reduced active psoriatic arthritis in patients who had an inadequate response to TNF inhibitors [189]. Mease et al. also evaluated the efficacy of tofacitinib in patients with psoriatic arthritis who had an inadequate response to DMARDs [190].

In another clinical trial (NCT00787202), tofacitinib was investigated for the treatment of patients with severely active ulcerative colitis [191]. The results showed that clinical response and remission were more expected in the treated patients than in those receiving placebo. In addition, Huang et al. also reported an improvement in arthritis in a 13-year-old girl, with complete remission within three months [192]. Tofacitinib was approved by the FDA for the treatment of active psoriatic arthritis, ulcerative colitis, and juvenile idiopathic arthritis [177,178].

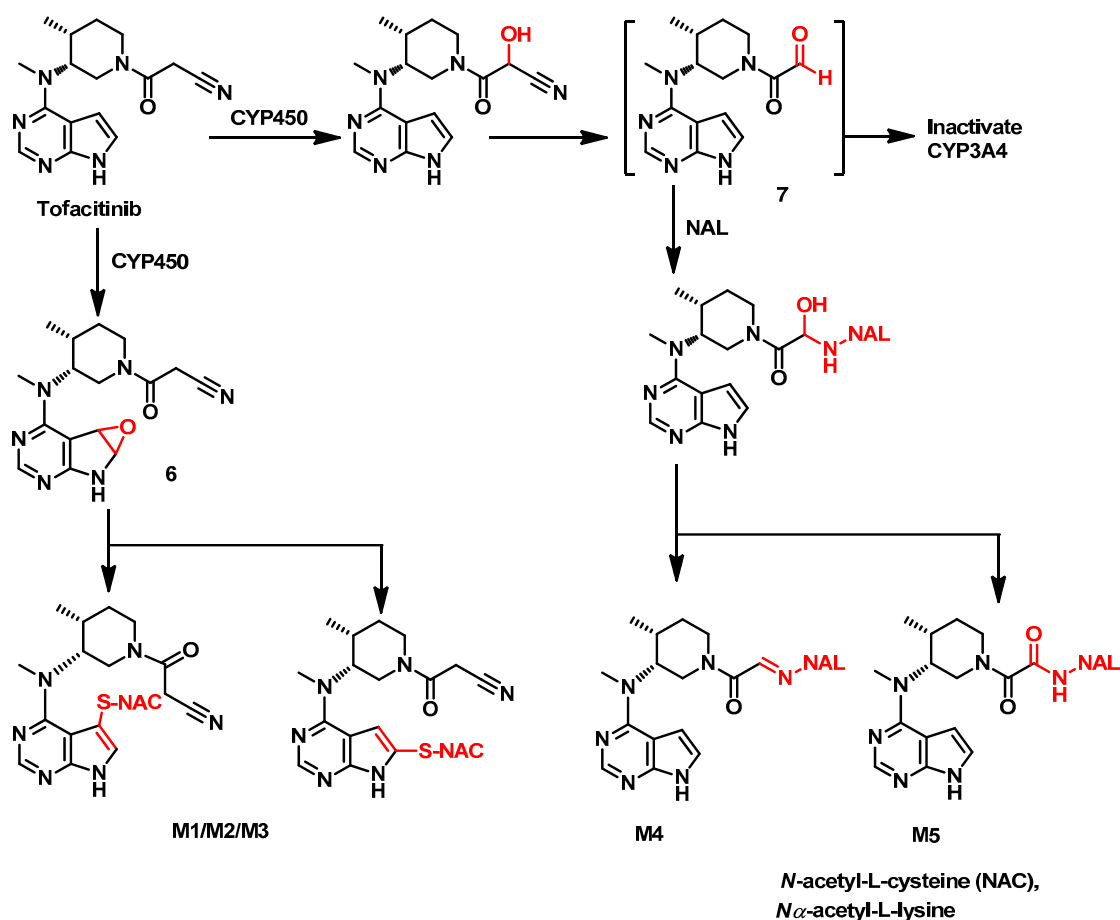
On the other hand, tofacitinib displayed inhibitory activity against LCK, which could also contribute to its pharmacological activities [64].

#### Metabolism

The pharmacokinetics parameters of tofacitinib were evaluated by Dowty et al. [193] using [ $^{14}\text{C}$ ]-labeled tofacitinib in healthy males. The results showed rapid absorption with the parent drug forming ~70% of the circulating activity in plasma.

Guo et al. investigated the metabolism of tofacitinib in vitro using a recombinant CYP3A4 enzyme [194]. Tofacitinib was incubated with mixed male human liver microsomes (HLMs) or individual human recombinant P450 enzymes. The results revealed the formation of a tofacitinib epoxide metabolite which was trapped by *N*-acetyl-L-cysteine (NAC), Figure 65. On the other hand, the metabolism of tofacitinib afforded also an  $\alpha$ -keto-

aldehyde metabolite, which was catalyzed by CYP3A4. This metabolite was trapped with *N* $\alpha$ -acetyl-L-lysine.

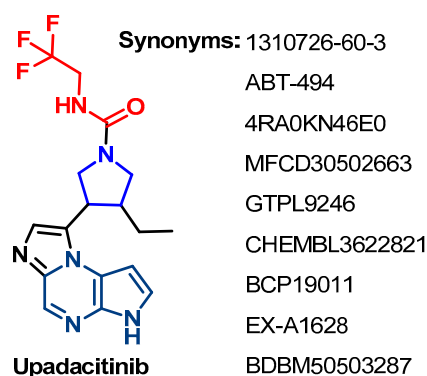


**Figure 65.** Proposed metabolic pathways and metabolites of tofacitinib.

### 1.7.11. Upadacitinib

#### Approval History

Upadacitinib (Figure 66) is a JAK1 inhibitor that was approved to treat rheumatoid arthritis by the FDA in August 2019 [67]. It was also approved for the treatment of patients with psoriatic arthritis [195]. In 2022, upadacitinib was approved for treatment of atopic dermatitis [196]. In addition, it was approved in March 2022 to treat patients with moderate-to-severe active ulcerative colitis [197].

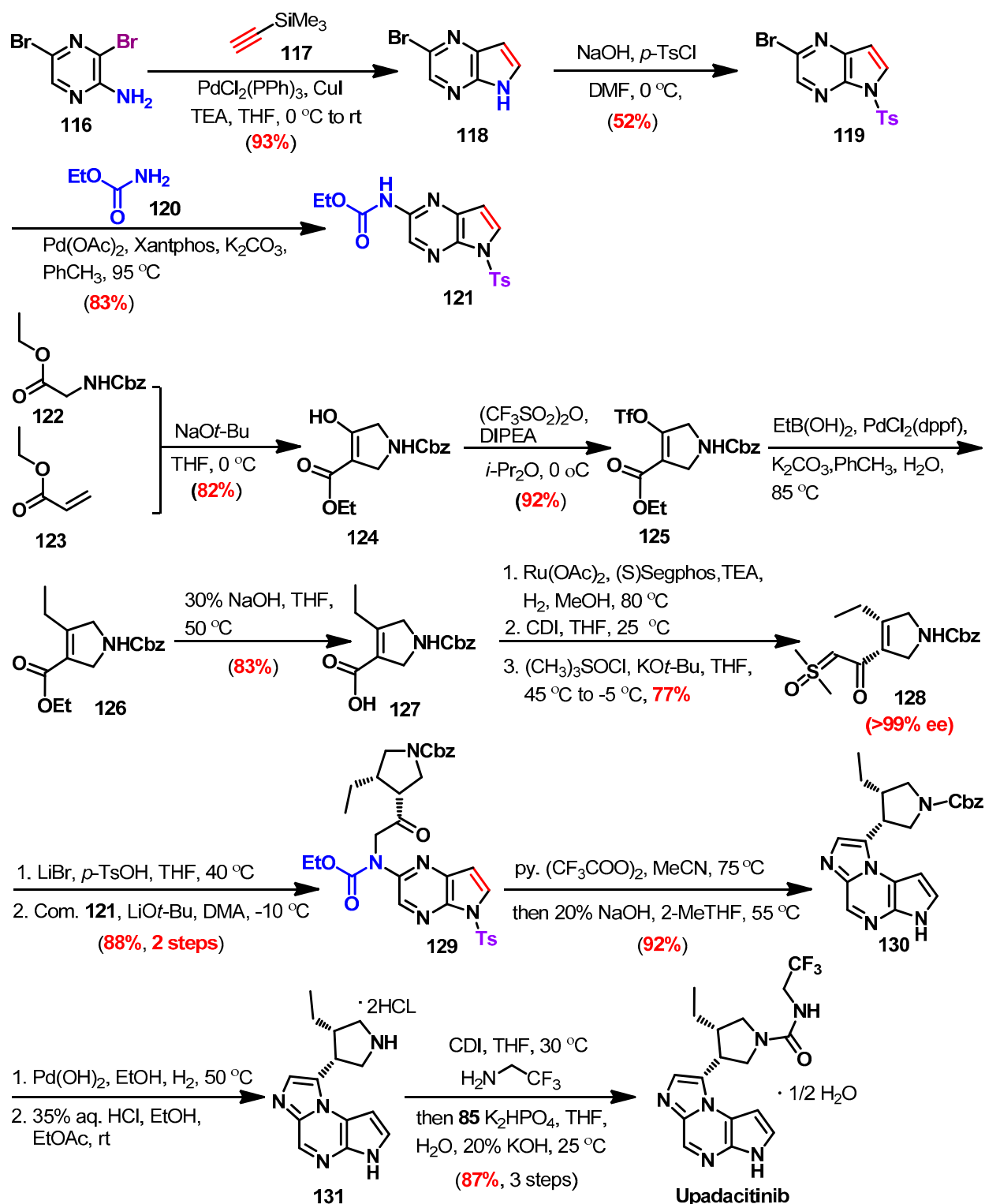


**Chem. name:** 3-ethyl-4-(3*H*-imidazo[1,2-*a*]pyrrolo[2,3-*e*]pyrazin-8-yl)-*N*-(2,2,2-trifluoroethyl)pyrrolidine-1-carboxamide

**Figure 66.** Chemical structure/name/synonyms of upadacitinib.

## Synthesis

Upadacitinib was synthesized from the coupling of compounds **121** and **128** [104,198]. Compound **121** was obtained **116** in a three steps synthesis. In the first step, 3,5-dibromopyrazin-2-amine **116** was reacted with ethynyltrimethylsilane **117** to afford **118**, which was reacted with *p*-toluenesulfonyl chloride to give **119**. Palladium-catalyzed amination of **119** with ethyl carbamate **120** afforded **121**. Scheme 15.



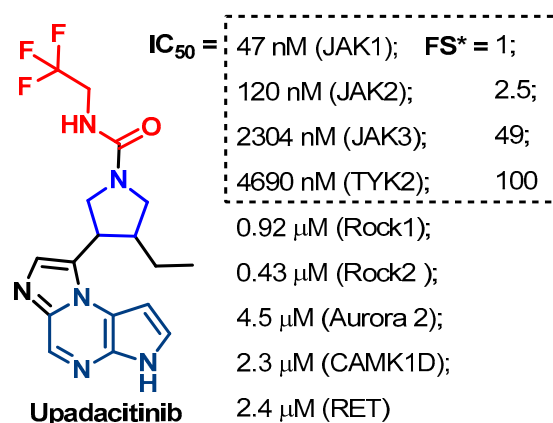
Scheme 15. Synthesis of upadacitinib.

To prepare compound **128**, the ethyl acrylate **123** was first reacted with compound **122** to give **124**, which was then reacted with triflic anhydride to give **125**, Scheme 15. The reaction of **125** with ethyl boronic acid gave **126**, which underwent alkaline hydrolysis to give **127**. Compound **128** was obtained from **127** in a three-step synthesis, which included ruthenium-catalyzed hydrogenation, reaction with carbonyldiimidazole (CDI), and reaction with trimethyl sulfoxonium chloride.

The coupling of **121** and **128** afforded **129**, which underwent intramolecular cyclization to give the tricyclic imidazo[1,2-*a*]pyrrolo[2,3-*e*]pyrazine **130**, Scheme 15. Palladium-catalyzed hydrogenation of **130** was performed to remove the protecting group, followed by treatment with hydrochloric acid to give the salt **131**. The reaction of **131** with CDI and trifluoroethylamine afforded upadacitinib.

### Target Kinases

The JAKs inhibitory activity of upadacitinib was evaluated by Parmentier et al. [199]. The results revealed the highest inhibitory activity against JAK1 ( $IC_{50} = 47$  nM), Figure 67. The study also revealed inhibitory activity for upadacitinib against JAK2 at  $IC_{50}$  120 nM, which indicates 2.5-fold lower inhibitory activity compared to JAK1.



**Figure 67.** Kinase inhibitory activity of upadacitinib (\* FS, fold selectivity compared to JAK1).

In addition, the results of the kinase inhibitory assay of upadacitinib against 70 kinases revealed weak inhibitory activity against kinases other than JAKs [199].

### Crystal Structures

Upadacitinib has not yet been reported in a crystal structure with any of its target kinases.

### Pharmacological Activities and Uses

Upadacitinib is a second-generation selective JAK inhibitor that was evaluated for the treatment of different types of inflammatory and immune diseases [200–203]. Evaluation of the efficacy of upadacitinib in the treatment of rheumatoid arthritis revealed a fast and favorable efficacy profile [202]. In addition, Smolen et al. [204] evaluated the efficacy of upadacitinib monotherapy in rheumatoid arthritis. The results also revealed significant therapeutic outcomes compared to methotrexate. The medical use of upadacitinib, either alone or in combination therapy for the treatment of rheumatoid arthritis, was associated with lower direct medical costs [203]. In August 2019, upadacitinib was approved for the treatment of moderate-to-severe rheumatoid arthritis.

Moreover, several clinical trials were also performed to evaluate the efficacy of upadacitinib in the treatment of psoriatic arthritis. In a clinical trial (NCT03104400.) for treatment of psoriatic arthritis, upadacitinib produced a rapid and sustained improvement in patient outcomes [201]. Upadacitinib was also evaluated in a 24-week, phase 3 trial to treat psoriatic arthritis [205]. The results revealed a significantly higher number of patients with ACR20 compared to the placebo. In addition, upadacitinib at a daily dose of 30 mg showed



superior results to those of adalimumab. Furthermore, no significant safety signals were observed when upadacitinib was evaluated in patients with psoriatic arthritis. Burmester et al. [206] also evaluated the safety of upadacitinib in patients with psoriatic arthritis for up to 3 years, where the results revealed a safety profile similar to that observed in rheumatoid arthritis. Currently, upadacitinib has been approved by the FDA and EMA for the treatment of patients with active psoriatic arthritis [195,207].

Furthermore, upadacitinib was also studied in adult patients with atopic dermatitis, where the results showed superior efficacy compared to the human monoclonal antibody dupilumab [208]. In January 2022, upadacitinib was also approved by the FDA to treat refractory, moderate to severe atopic dermatitis in children aged  $\geq 12$  years.

#### Metabolism

The results of the in vitro metabolic study of upadacitinib suggested that it undergoes metabolism by cytochrome P450 [209]. On the other hand, the contribution of CYP2D6 in the metabolism of upadacitinib was very minor [209]. Coadministration of upadacitinib with the CYP3A4 inhibitor, ketoconazole, resulted in a weak effect on its concentration [210]. However, coadministration of upadacitinib with rifampin, a broad CYP inducer, resulted in a decrease in upadacitinib concentration by  $\sim 50\%$  [211].

In conclusion, the target kinases of the eleven JAK inhibitors and the approval data including the approval date and the disease for which these inhibitors were approved are presented in Table 1.

**Table 1.** The globally approved JAK inhibitors, their target kinase, clinical trials, and the approval data.

Drug	Target JAKs	Disease	Approval Date	Reference	Clinical Trials
Abrocitinib	JAK1, JAK2	Atopic dermatitis	2022	[72]	NCT03627767, NCT03720470
Baricitinib	JAK1, JAK2	Rheumatoid arthritis	2017 (EMA) 2018 (FDA)	[64,65]	NCT02265705, NCT01710358
		COVID-19	2020 (EUA)	[78]	NCT04421027, NCT04401579
Delgocitinib	Nonselective	Atopic dermatitis	2020 (Japan)	[69]	NCT03826901, NCT03725722
Fedratinib	JAK2, JAK2V617F	Myelofibrosis	2019 (FDA)	[66]	NCT00724334, NCT00631462 NCT01437787
Filgotinib	JAK1	Rheumatoid arthritis	2020 (EMA)	[70]	NCT02873936, NCT02886728
Oclacitinib	JAK1	Canine allergic dermatitis	2013	[129]	NA *
Pacritinib	JAK2, JAK2V617F	Myelofibrosis	2022 (FDA)	[138]	NCT04884191
Peficitinib	Pan-JAK inhibitor	Rheumatoid arthritis	2019 (Japan)	[68]	NCT01565655, NCT02308163
Ruxolitinib	JAK1, JAK2 JAK2V617F	Myelofibrosis	2011	[28]	NCT00952289
		Polycythemia vera	2014	[29]	NCT02038036
		Acute and chronic graft-versus-host disease	2019, 2021	[160]	NCT03112603 NCT03147742

Table 1. Cont.

Drug	Target JAKs	Disease	Approval Date	Reference	Clinical Trials
Tofacitinib	JAK1, JAK2, JAK3	Rheumatoid arthritis	2012 (FDA)	[64]	NCT02187055
		Psoriatic arthritis	2017	[115]	NCT01877668
		Ulcerative colitis	2018	[115]	NCT03281304
		Juvenile idiopathic arthritis	2020	[179]	NCT02592434
		Ankylosing spondylitis	2021	[180]	NCT03502616
Upadacitinib	JAK1	Rheumatoid arthritis	2019	[67]	NCT02706847
		Psoriatic arthritis	2021	[195]	NCT03104400
		Atopic dermatitis	2022	[196]	NCT03738397
		Ulcerative colitis	2022	[197]	NCT02819635

\* NA, not applicable.

## 2. Conclusions

In the current review, eleven of the JAK inhibitors that received approval for the treatment of inflammatory, autoimmune, and myeloproliferative neoplasms were discussed. These drugs are abrocitinib, baricitinib, delgocitinib, fedratinib, filgotinib, oclacitinib, pacritinib, peficitinib, ruxolitinib, tofacitinib, and upadacitinib. The synthetic routes of these drugs, including the original and/or alternative pathways, were described. The crystal structures of these drugs in various kinases were also listed. Their binding modes and interactions were visualized, where two key hydrogen-bonding interactions were observed with Leu959 and Leu932 in JAK1 and JAK2, respectively. Furthermore, the kinase inhibitory activities and pharmacological uses of the eleven drugs were also summarized. Based on their inhibitory activity against the target kinases, these drugs could be classified as either selective or nonselective JAK inhibitors. Among these drugs, several JAK1 inhibitors have been approved for the treatment of inflammatory and autoimmune conditions. On the other hand, the drugs approved for treatment of myeloproliferative neoplasms target JAK2 and its mutant form (JAK2V617F). In addition, the metabolic studies of the eleven drugs revealed the formation of several oxidation metabolites, which were mediated by CYP450 enzymes. On the other hand, few conjugation metabolites such as glucuronide acid and sulfate conjugates were detected among the metabolites of filgotinib and peficitinib, respectively. To sum up, the data in this review may assist in the design of new JAK inhibitors with potential therapeutic benefits.

## 3. Perspective

The high efficacy of the clinically approved JAK inhibitors in the treatment of inflammatory and autoimmune diseases has attracted much attention. However, most of them are non-selective inhibitors, which may account for some of their adverse effects, such as anemia, thrombocytopenia, upper respiratory tract infection, and herpes infection [212–216]. Accordingly, design and development of new potent, selective, and more safe JAK inhibitors could provide a solution to these adverse effects [217].

Currently, several nonselective JAK inhibitors, including brepocitinib, cerdulatinib, gusacitinib, and momelotinib (Figure 68), are being investigated for their efficacy in inflammatory and cancer diseases [218–221]. In addition, the efficacy and safety of several selective JAK inhibitors are being investigated in clinical trials. Among these inhibitors, the selective JAK1 inhibitor, itacitinib showed promising efficacy when evaluated in patients with aGVHD [222].

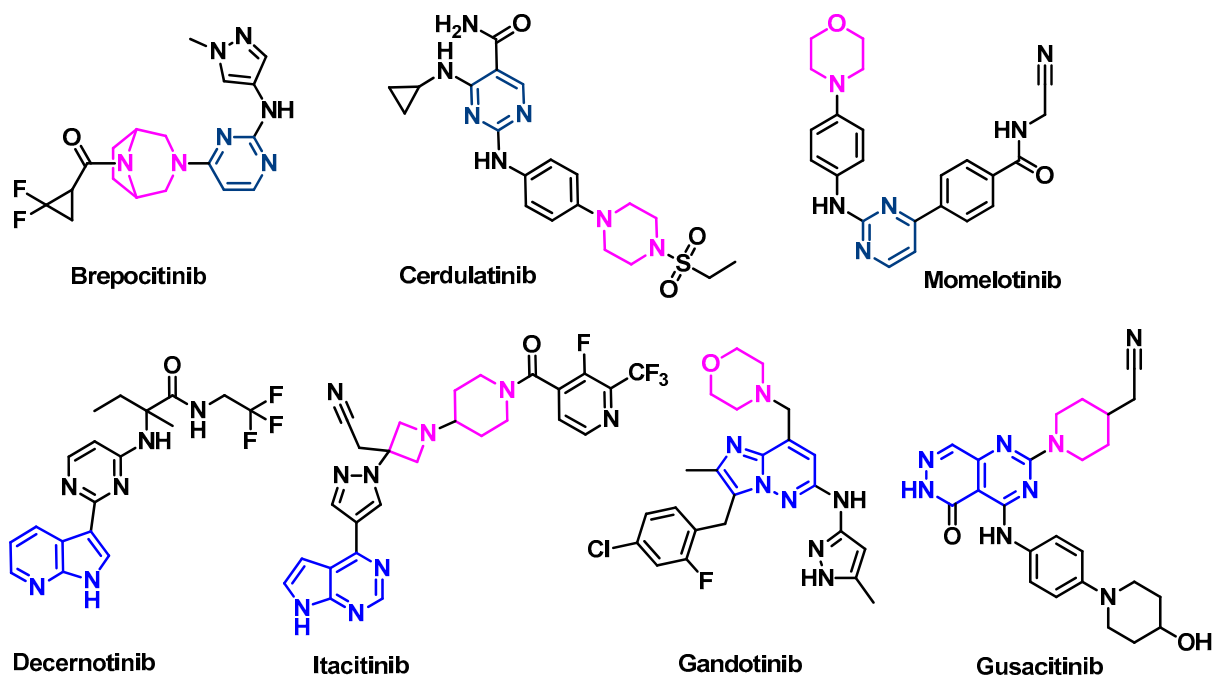


Figure 68. JAK inhibitors under development.

The JAK2 inhibitor, gandotinib (Figure 68), showed high potency toward the JAK2V617F mutation and showed promising potential in the treatment of myeloproliferative disorders [223]. In addition, JAK2/FLT3 dual inhibitors could provide better therapeutic option for acute myeloid leukemia [30,224]. Currently, it is seeking FDA approval for the treatment of myelofibrosis. On the other hand, the JAK3 inhibitor, decernotinib also showed a high potential activity in the treatment of rheumatoid arthritis [225].

Several JAK inhibitors have been reported to bind reversibly to allosteric sites in JAKs [34,42]. Among these inhibitors, deucravacitinib and LS104 are being investigated in clinical trials. This type of JAK inhibitor could provide advantages over the currently used ATP-competitive inhibitors [27]. However, none of these allosteric inhibitors has been approved for clinical use. Future research in this area could lead to approval of the allosteric inhibitors for clinical use.

Development of irreversible JAK3 inhibitors that can bind covalently with the unique Cys909 residue has attracted a great attention in the last few years [43]. Several small molecules have displayed potent and selective inhibition of JAK activity [43,44,226]. The design of new JAK3 covalent inhibitors could be supported by the success of ritlecitinib in reaching the clinical trial (NCT04517864). In addition, advances in X-ray and covalent docking may also play a crucial role in the design of this type of JAK inhibitors.

Recently, JAK inhibitors showed promising potential in the treatment of COVID-19-related cytokine storm [227]. However, among several drug combinations evaluated in the treatment of COVID-19 [228,229], the combination of baricitinib plus remdesivir has received EUA by the FDA [92,230,231]. Moreover, the clinical trials of tofacitinib (NCT04469114) and nezulcitinib (NCT04402866) are being performed in patients with COVID-19 related lung problems [36,232]. Although these results also support the investigation of other JAK inhibitors in the treatment of COVID-19 related problems, the adverse effects of these inhibitors on the immune responses must be evaluated [233].

**Author Contributions:** Conceptualization, A.M.S., F.A.A., A.N.A., A.H.A. and A.M.G.; methodology, F.A.A., A.N.A., A.M.S., A.H.A. and A.M.G.; software, A.M.S., F.A.A., A.N.A., A.H.A. and A.M.G.; validation, F.A.A., A.N.A., A.M.S., A.H.A. and A.M.G.; formal analysis, A.M.S., F.A.A., A.N.A. and A.M.G.; investigation, F.A.A., A.N.A., A.M.S., A.H.A. and A.M.G.; resources, A.M.S., F.A.A., A.N.A. and A.M.G.; data curation, F.A.A., A.N.A., A.M.S. and A.M.G.; writing—original draft preparation,

A.M.S., F.A.A., A.N.A., A.H.A. and A.M.G.; writing—review and editing, F.A.A., A.N.A., A.M.S. and A.M.G.; visualization, F.A.A., A.N.A., A.M.S., A.H.A. and A.M.G.; supervision, A.M.S., F.A.A., A.N.A. and A.M.G.; Project administration, A.M.S.; funding acquisition, A.M.S. All authors have read and agreed to the published version of the manuscript.

**Funding:** The authors would like to thank the Deanship of Scientific Research at Umm Al-Qura University for supporting this work by Grant Code: (22UQU4331174DSR08).

**Institutional Review Board Statement:** Not applicable.

**Informed Consent Statement:** Not applicable.

**Conflicts of Interest:** Authors declared that there is no conflict of interest and have approved the article.

## References

1. Yamaoka, K.; Saharinen, P.; Pesu, M.; Holt, V.E.T., 3rd; Silvennoinen, O.; O’Shea, J.J. The Janus kinases (Jaks). *Genome Biol.* **2004**, *5*, 253. [CrossRef] [PubMed]
2. Wilks, A.F. Two putative protein-tyrosine kinases identified by application of the polymerase chain reaction. *Proc. Natl. Acad. Sci. USA* **1989**, *86*, 1603–1607. [CrossRef] [PubMed]
3. Banerjee, S.; Biehl, A.; Gadina, M.; Hasni, S.; Schwartz, D.M. JAK-STAT signaling as a target for inflammatory and autoimmune diseases: Current and future prospects. *Drugs* **2017**, *77*, 521–546. [CrossRef]
4. Aittomäki, S.; Pesu, M. Therapeutic targeting of the Jak/STAT pathway. *Basic Clin. Pharmacol. Toxicol.* **2014**, *114*, 18–23. [CrossRef] [PubMed]
5. Abroun, S.; Saki, N.; Ahmadvand, M.; Asghari, F.; Salari, F.; Rahim, F. STATs: An old story, yet mesmerizing. *Cell J.* **2015**, *17*, 395–411. [CrossRef]
6. Liao, N.P.D.; Laktyushin, A.; Morris, R.; Sandow, J.J.; Nicola, N.A.; Kershaw, N.J.; Babon, J.J. Enzymatic characterization of wild-type and mutant janus kinase 1. *Cancers* **2019**, *11*, 1701. [CrossRef]
7. Min, X.; Ungureanu, D.; Maxwell, S.; Hammarén, H.; Thibault, S.; Hillert, E.-K.; Ayres, M.; Greenfield, B.; Eksterowicz, J.; Gabel, C.; et al. Structural and functional characterization of the JH2 pseudokinase domain of JAK family tyrosine kinase 2 (TYK2). *J. Biol. Chem.* **2015**, *290*, 27261–27270. [CrossRef]
8. Garrido-Trigo, A.; Salas, A. Molecular structure and function of Janus kinases: Implications for the development of inhibitors. *J. Crohns. Colitis* **2020**, *14*, S713–S724. [CrossRef]
9. Ferrao, R.; Lupardus, P.J. The Janus kinase (JAK) FERM and SH2 domains: Bringing specificity to JAK-receptor interactions. *Front. Endocrinol.* **2017**, *8*, 71. [CrossRef]
10. Kiu, H.; Nicholson, S.E. Biology and significance of the JAK/STAT signalling pathways. *Growth Factors* **2012**, *30*, 88–106. [CrossRef]
11. Bryan, M.C.; Rajapaksa, N.S. Kinase inhibitors for the treatment of immunological disorders: Recent advances. *J. Med. Chem.* **2018**, *61*, 9030–9058. [CrossRef] [PubMed]
12. Xu, P.; Shen, P.; Yu, B.; Xu, X.; Ge, R.; Cheng, X.; Chen, Q.; Bian, J.; Li, Z.; Wang, J. Janus kinases (JAKs): The efficient therapeutic targets for autoimmune diseases and myeloproliferative disorders. *Eur. J. Med. Chem.* **2020**, *192*, 112155. [CrossRef] [PubMed]
13. Hammarén, H.M.; Virtanen, A.T.; Raivola, J.; Silvennoinen, O. The regulation of JAKs in cytokine signaling and its breakdown in disease. *Cytokine* **2019**, *118*, 48–63. [CrossRef]
14. Yasuda, T.; Fukada, T.; Nishida, K.; Nakayama, M.; Matsuda, M.; Miura, I.; Dainichi, T.; Fukuda, S.; Kabashima, K.; Nakaoka, S.; et al. Hyperactivation of JAK1 tyrosine kinase induces stepwise, progressive pruritic dermatitis. *J. Clin. Investig.* **2016**, *126*, 2064–2076. [CrossRef] [PubMed]
15. Shen, Y.; Liu, Y.; Ke, X.; Kang, H.-Y.; Hu, G.-H.; Hong, S.-L. Association between JAK1 gene polymorphisms and susceptibility to allergic rhinitis. *Asian Pac. J. Allergy Immunol.* **2016**, *34*, 124–129. [CrossRef] [PubMed]
16. Wills-Karp, M.; Luyimbazi, J.; Xu, X.; Schofield, B.; Neben, T.Y.; Karp, C.L.; Donaldson, D.D. Interleukin-13: Central mediator of allergic asthma. *Science* **1998**, *282*, 2258–2261. [CrossRef] [PubMed]
17. Harris, C.; Cummings, J.R.F. JAK1 inhibition and inflammatory bowel disease. *Rheumatology* **2021**, *60*, ii45–ii51. [CrossRef] [PubMed]
18. Virtanen, A.T.; Haikarainen, T.; Raivola, J.; Silvennoinen, O. Selective JAKinibs: Prospects in inflammatory and autoimmune diseases. *BioDrugs* **2019**, *33*, 15–32. [CrossRef]
19. Zak, M.; Hanan, E.J.; Lupardus, P.; Brown, D.G.; Robinson, C.; Siu, M.; Lyssikatos, J.P.; Romero, F.A.; Zhao, G.; Kellar, T.; et al. Discovery of a class of highly potent Janus Kinase 1/2 (JAK1/2) inhibitors demonstrating effective cell-based blockade of IL-13 signaling. *Bioorg. Med. Chem. Lett.* **2019**, *29*, 1522–1531. [CrossRef]
20. Schwartz, D.M.; Kanno, Y.; Villarino, A.; Ward, M.; Gadina, M.; O’Shea, J.J. JAK inhibition as a therapeutic strategy for immune and inflammatory diseases. *Nat. Rev. Drug Discov.* **2017**, *16*, 843–862. [CrossRef]
21. Menet, C.J. A dual inhibition, a better solution: Development of a JAK1/TYK2 inhibitor. *J. Med. Chem.* **2018**, *61*, 8594–8596. [CrossRef] [PubMed]

22. Wroblewski, S.T.; Moslin, R.; Lin, S.; Zhang, Y.; Spergel, S.; Kempson, J.; Tokarski, J.S.; Strnad, J.; Zupa-Fernandez, A.; Cheng, L.; et al. Highly selective inhibition of tyrosine kinase 2 (TYK2) for the treatment of autoimmune diseases: Discovery of the allosteric inhibitor BMS-986165. *J. Med. Chem.* **2019**, *62*, 8973–8995. [CrossRef] [PubMed]
23. Buchert, M.; Burns, C.J.; Ernst, M. Targeting JAK kinase in solid tumors: Emerging opportunities and challenges. *Oncogene* **2016**, *35*, 939–951. [CrossRef] [PubMed]
24. Kilpivaara, O.; Levine, R.L. JAK2 and MPL mutations in myeloproliferative neoplasms: Discovery and science. *Leukemia* **2008**, *22*, 1813–1817. [CrossRef] [PubMed]
25. Trelinski, J.; Robak, T. JAK inhibitors: Pharmacology and clinical activity in chronic myeloproliferative neoplasms. *Curr. Med. Chem.* **2013**, *20*, 1147–1161. [CrossRef] [PubMed]
26. Nielsen, C.; Birgens, H.S.; Nordestgaard, B.G.; Kjaer, L.; Bojesen, S.E. The JAK2 V617F somatic mutation, mortality and cancer risk in the general population. *Haematologica* **2011**, *96*, 450–453. [CrossRef]
27. Leroy, E.; Constantinescu, S.N. Rethinking JAK2 inhibition: Towards novel strategies of more specific and versatile Janus kinase inhibition. *Leukemia* **2017**, *31*, 1023–1038. [CrossRef]
28. Mascarenhas, J.; Hoffman, R. Ruxolitinib: The first FDA approved therapy for the treatment of myelofibrosis. *Clin. Cancer Res. Off. J. Am. Assoc. Cancer Res.* **2012**, *18*, 3008–3014. [CrossRef]
29. Raedler, L.A. Jakafi (Ruxolitinib): First FDA-approved medication for the treatment of patients with polycythemia vera. *Am. Health Drug Benefits* **2015**, *8*, 75–79.
30. Hart, S.; Goh, K.C.; Novotny-Diermayr, V.; Tan, Y.C.; Madan, B.; Amalini, C.; Ong, L.C.; Kheng, B.; Cheong, A.; Zhou, J.; et al. Pacritinib (SB1518), a JAK2/FLT3 inhibitor for the treatment of acute myeloid leukemia. *Blood Cancer J.* **2011**, *1*, e44. [CrossRef]
31. Yang, T.; Hu, M.; Qi, W.; Yang, Z.; Tang, M.; He, J.; Chen, Y.; Bai, P.; Yuan, X.; Zhang, C.; et al. Discovery of potent and orally effective dual Janus kinase 2/FLT3 inhibitors for the treatment of acute myelogenous leukemia and myeloproliferative neoplasms. *J. Med. Chem.* **2019**, *62*, 10305–10320. [CrossRef] [PubMed]
32. Hu, X.; Li, J.; Fu, M.; Zhao, X.; Wang, W. The JAK/STAT signaling pathway: From bench to clinic. *Signal Transduct. Target. Ther.* **2021**, *6*, 402. [CrossRef] [PubMed]
33. Angelini, J.; Talotta, R.; Roncato, R.; Fornasier, G.; Barbiero, G.; Dal Cin, L.; Brancati, S.; Scaglione, F. JAK-Inhibitors for the treatment of rheumatoid arthritis: A focus on the present and an outlook on the future. *Biomolecules* **2020**, *10*, 1002. [CrossRef] [PubMed]
34. Vainchenker, W.; Leroy, E.; Gilles, L.; Marty, C.; Plo, I.; Constantinescu, S.N. JAK inhibitors for the treatment of myeloproliferative neoplasms and other disorders. *F1000Research* **2018**, *7*, 82. [CrossRef] [PubMed]
35. Wernig, G.; Kharas, M.G.; Okabe, R.; Moore, S.A.; Leeman, D.S.; Cullen, D.E.; Gozo, M.; McDowell, E.P.; Levine, R.L.; Doukas, J.; et al. Efficacy of TG101348, a selective JAK2 inhibitor, in treatment of a murine model of JAK2V617F-induced polycythemia vera. *Cancer Cell* **2008**, *13*, 311–320. [CrossRef]
36. Singh, D.; Bogus, M.; Moskalenko, V.; Lord, R.; Moran, E.J.; Crater, G.D.; Bourdet, D.L.; Pfeifer, N.D.; Woo, J.; Kaufman, E.; et al. A phase 2 multiple ascending dose study of the inhaled pan-JAK inhibitor nezulcitinib (TD-0903) in severe COVID-19. *Eur. Respir. J.* **2021**, *58*, 2100673. [CrossRef]
37. Andraos, R.; Qian, Z.; Bonenfant, D.; Rubert, J.; Vangrevelinghe, E.; Scheufler, C.; Marque, F.; Régnier, C.H.; De Pover, A.; Ryckelynck, H.; et al. Modulation of activation-loop phosphorylation by JAK inhibitors is binding mode dependent. *Cancer Discov.* **2012**, *2*, 512–523. [CrossRef]
38. Wu, S.-C.; Li, L.S.; Kopp, N.; Montero, J.; Chapuy, B.; Yoda, A.; Christie, A.L.; Liu, H.; Christodoulou, A.; van Bodegom, D.; et al. Activity of the type II JAK2 inhibitor CHZ868 in B cell acute lymphoblastic leukemia. *Cancer Cell* **2015**, *28*, 29–41. [CrossRef]
39. Burke, J.R.; Cheng, L.; Gillooly, K.M.; Strnad, J.; Zupa-Fernandez, A.; Catlett, I.M.; Zhang, Y.; Heimrich, E.M.; McIntyre, K.W.; Cunningham, M.D.; et al. Autoimmune pathways in mice and humans are blocked by pharmacological stabilization of the TYK2 pseudokinase domain. *Sci. Transl. Med.* **2019**, *11*, eaaw1736. [CrossRef]
40. Lipka, D.B.; Hoffmann, L.S.; Heidel, F.; Markova, B.; Blum, M.-C.; Breitenbuecher, F.; Kasper, S.; Kindler, T.; Levine, R.L.; Huber, C.; et al. LS104, a non-ATP-competitive small-molecule inhibitor of JAK2, is potently inducing apoptosis in JAK2V617F-positive cells. *Mol. Cancer Ther.* **2008**, *7*, 1176–1184. [CrossRef]
41. Jatiani, S.S.; Cosenza, S.C.; Reddy, M.V.R.; Ha, J.H.; Baker, S.J.; Samanta, A.K.; Olnes, M.J.; Pfannes, L.; Sloand, E.M.; Arlinghaus, R.B.; et al. A non-ATP-competitive dual inhibitor of JAK2 and BCR-ABL kinases: Elucidation of a novel therapeutic spectrum based on substrate competitive inhibition. *Genes Cancer* **2010**, *1*, 331–345. [CrossRef] [PubMed]
42. Alexander, M.; Luo, Y.; Raimondi, G.; O’Shea, J.J.; Gadina, M. Jakinibs of all trades: Inhibiting cytokine signaling in immune-mediated pathologies. *Pharmaceutics* **2022**, *15*, 48. [CrossRef] [PubMed]
43. Casimiro-Garcia, A.; Trujillo, J.I.; Vajdos, F.; Juba, B.; Banker, M.E.; Aulabaugh, A.; Balbo, P.; Bauman, J.; Chrencik, J.; Coe, J.W.; et al. Identification of cyanamide-based Janus kinase 3 (JAK3) covalent inhibitors. *J. Med. Chem.* **2018**, *61*, 10665–10699. [CrossRef] [PubMed]
44. Goedken, E.R.; Argiriadi, M.A.; Banach, D.L.; Fiamengo, B.A.; Foley, S.E.; Frank, K.E.; George, J.S.; Harris, C.M.; Hobson, A.D.; Ihle, D.C.; et al. Tricyclic covalent inhibitors selectively target Jak3 through an active site thiol. *J. Biol. Chem.* **2015**, *290*, 4573–4589. [CrossRef] [PubMed]

45. Forster, M.; Chaikuad, A.; Bauer, S.M.; Holstein, J.; Robers, M.B.; Corona, C.R.; Gehringer, M.; Pfaffenrot, E.; Ghoreschi, K.; Knapp, S.; et al. Selective JAK3 Inhibitors with a covalent reversible binding mode targeting a new induced fit binding pocket. *Cell Chem. Biol.* **2016**, *23*, 1335–1340. [CrossRef]
46. Telliez, J.-B.; Dowty, M.E.; Wang, L.; Jussif, J.; Lin, T.; Li, L.; Moy, E.; Balbo, P.; Li, W.; Zhao, Y.; et al. Discovery of a JAK3-selective inhibitor: Functional differentiation of JAK3-selective inhibition over pan-JAK or JAK1-selective inhibition. *ACS Chem. Biol.* **2016**, *11*, 3442–3451. [CrossRef]
47. Dassault Systems BIOVIA. *Discovery Studio Visualizer*, version 16.1.0.15350; Dassault Systems: San Diego, CA, USA, 2016.
48. Almalki, F.A.; Shawky, A.M.; Abdalla, A.N.; Gouda, A.M. Icotinib, almonertinib, and olmutinib: A 2D similarity/docking-based study to predict the potential binding modes and interactions into EGFR. *Molecules* **2021**, *26*, 6423. [CrossRef]
49. Abourehab, M.A.S.; Alqahtani, A.M.; Almalki, F.A.; Zaher, D.M.; Abdalla, A.N.; Gouda, A.M.; Beshr, E.A.M. Pyrrolizine/indolizine-NSAID hybrids: Design, synthesis, biological evaluation, and molecular docking studies. *Molecules* **2021**, *26*, 6582. [CrossRef]
50. Abourehab, M.A.S.; Alqahtani, A.M.; Youssif, B.G.M.; Gouda, A.M. Globally approved EGFR inhibitors: Insights into their syntheses, target kinases, biological activities, receptor interactions, and metabolism. *Molecules* **2021**, *26*, 6677. [CrossRef]
51. Arulogun, S.O.; Choong, H.-L.; Taylor, D.; Ambrosoli, P.; Magor, G.; Irving, I.M.; Keng, T.-B.; Perkins, A.C. JAK1 somatic mutation in a myeloproliferative neoplasm. *Haematologica* **2017**, *102*, e324–e327. [CrossRef]
52. Musumeci, F.; Greco, C.; Giacchello, I.; Fallacara, A.L.; Ibrahim, M.M.; Grossi, G.; Brullo, C.; Schenone, S. An update on JAK inhibitors. *Curr. Med. Chem.* **2019**, *26*, 1806–1832. [CrossRef] [PubMed]
53. Levine, R.L.; Pardanani, A.; Tefferi, A.; Gilliland, D.G. Role of JAK2 in the pathogenesis and therapy of myeloproliferative disorders. *Nat. Rev. Cancer* **2007**, *7*, 673–683. [CrossRef] [PubMed]
54. Degryse, S.; Bornschein, S.; de Bock, C.E.; Leroy, E.; Vanden Bempt, M.; Demeyer, S.; Jacobs, K.; Geerdens, E.; Gielen, O.; Soulier, J.; et al. Mutant JAK3 signaling is increased by loss of wild-type JAK3 or by acquisition of secondary JAK3 mutations in T-ALL. *Blood* **2018**, *131*, 421–425. [CrossRef] [PubMed]
55. O’Shea, J.J.; Husa, M.; Li, D.; Hofmann, S.R.; Watford, W.; Roberts, J.L.; Buckley, R.H.; Changelian, P.; Candotti, F. JAK3 and the pathogenesis of severe combined immunodeficiency. *Mol. Immunol.* **2004**, *41*, 727–737. [CrossRef]
56. Nemoto, M.; Hattori, H.; Maeda, N.; Akita, N.; Muramatsu, H.; Moritani, S.; Kawasaki, T.; Maejima, M.; Ode, H.; Hachiya, A.; et al. Compound heterozygous TYK2 mutations underlie primary immunodeficiency with T-cell lymphopenia. *Sci. Rep.* **2018**, *8*, 6956. [CrossRef]
57. Wu, P.; Chen, S.; Wu, B.; Chen, J.; Lv, G. A TYK2 gene mutation c.2395G>A leads to TYK2 deficiency: A case report and literature review. *Front. Pediatr.* **2020**, *8*, 253. [CrossRef]
58. Menet, C.J.; van Rompaey, L.; Geney, R. Advances in the discovery of selective JAK inhibitors. *Prog. Med. Chem.* **2013**, *52*, 153–223. [CrossRef]
59. Vazquez, M.L.; Kaila, N.; Strohbach, J.W.; Trzupek, J.D.; Brown, M.F.; Flanagan, M.E.; Mitton-Fry, M.J.; Johnson, T.A.; Ten-Brink, R.E.; Arnold, E.P.; et al. Identification of N-[cis-3-[Methyl(7H-pyrrolo[2,3-d]pyrimidin-4-yl)amino]cyclobutyl]propane-1-sulfonamide (PF-04965842): A selective JAK1 clinical candidate for the treatment of autoimmune diseases. *J. Med. Chem.* **2018**, *61*, 1130–1152. [CrossRef]
60. Lucet, I.S.; Fantino, E.; Styles, M.; Bamert, R.; Patel, O.; Broughton, S.E.; Walter, M.; Burns, C.J.; Treutlein, H.; Wilks, A.F.; et al. The structural basis of Janus kinase 2 inhibition by a potent and specific pan-Janus kinase inhibitor. *Blood* **2006**, *107*, 176–183. [CrossRef]
61. Thoma, G.; Nuninger, F.; Falchetto, R.; Hermes, E.; Tavares, G.A.; Vangrevelinghe, E.; Zerwes, H.-G. Identification of a potent Janus kinase 3 inhibitor with high selectivity within the Janus kinase family. *J. Med. Chem.* **2011**, *54*, 284–288. [CrossRef]
62. Fensome, A.; Ambler, C.M.; Arnold, E.; Banker, M.E.; Clark, J.D.; Dowty, M.E.; Efremov, I.V.; Flick, A.; Gerstenberger, B.S.; Gifford, R.S.; et al. Design and optimization of a series of 4-(3-azabicyclo[3.1.0]hexan-3-yl)pyrimidin-2-amines: Dual inhibitors of TYK2 and JAK1. *Bioorg. Med. Chem.* **2020**, *28*, 115481. [CrossRef] [PubMed]
63. Meydan, N.; Grunberger, T.; Dadi, H.; Shahar, M.; Arpaia, E.; Lapidot, Z.; Leeder, J.S.; Freedman, M.; Cohen, A.; Gazit, A.; et al. Inhibition of acute lymphoblastic leukaemia by a JAK-2 inhibitor. *Nature* **1996**, *379*, 645–648. [CrossRef] [PubMed]
64. Coricello, A.; Mesiti, F.; Lupia, A.; Maruca, A.; Alcaro, S. Inside perspective of the synthetic and computational toolbox of JAK inhibitors: Recent updates. *Molecules* **2020**, *25*, 3321. [CrossRef] [PubMed]
65. Markham, A. Baricitinib: First global approval. *Drugs* **2017**, *77*, 697–704. [CrossRef]
66. Blair, H.A. Fedratinib: First approval. *Drugs* **2019**, *79*, 1719–1725. [CrossRef]
67. Duggan, S.; Keam, S.J. Upadacitinib: First approval. *Drugs* **2019**, *79*, 1819–1828. [CrossRef]
68. Markham, A.; Keam, S.J. Peficitinib: First global approval. *Drugs* **2019**, *79*, 887–891. [CrossRef]
69. Dhillon, S. Delgocitinib: First approval. *Drugs* **2020**, *80*, 609–615. [CrossRef]
70. Dhillon, S.; Keam, S.J. Filgotinib: First approval. *Drugs* **2020**, *80*, 1987–1997. [CrossRef]
71. Connor, C.G.; DeForest, J.C.; Dietrich, P.; Do, N.M.; Doyle, K.M.; Eisenbeis, S.; Greenberg, E.; Griffin, S.H.; Jones, B.P.; Jones, K.N.; et al. Development of a nitrene-type rearrangement for the commercial route of the JAK1 inhibitor abrocitinib. *Org. Process Res. Dev.* **2021**, *25*, 608–615. [CrossRef]
72. Deeks, E.D.; Duggan, S. Abrocitinib: First approval. *Drugs* **2021**, *81*, 2149–2157. [CrossRef] [PubMed]

73. Eichenfield, L.F.; Flohr, C.; Sidbury, R.; Siegfried, E.; Szalai, Z.; Galus, R.; Yao, Z.; Takahashi, H.; Barbarot, S.; Feeney, C.; et al. Efficacy and safety of abrocitinib in combination with topical therapy in adolescents with moderate-to-severe atopic dermatitis: The JADE TEEN randomized clinical trial. *JAMA Dermatol.* **2021**, *157*, 1165–1173. [CrossRef] [PubMed]
74. Bieber, T.; Simpson, E.L.; Silverberg, J.I.; Thaçi, D.; Paul, C.; Pink, A.E.; Kataoka, Y.; Chu, C.-Y.; DiBonaventura, M.; Rojo, R.; et al. Abrocitinib versus placebo or dupilumab for atopic dermatitis. *N. Engl. J. Med.* **2021**, *384*, 1101–1112. [CrossRef]
75. Blauvelt, A.; Silverberg, J.I.; Lynde, C.W.; Bieber, T.; Eisman, S.; Zdybski, J.; Gubelin, W.; Simpson, E.L.; Valenzuela, F.; Criado, P.R.; et al. Abrocitinib induction, randomized withdrawal, and retreatment in patients with moderate-to-severe atopic dermatitis: Results from the JAK1 Atopic dermatitis efficacy and safety (JADE) REGIMEN phase 3 trial. *J. Am. Acad. Dermatol.* **2022**, *86*, 104–112. [CrossRef]
76. Wang, E.Q.; Le, V.; O’Gorman, M.; Tripathy, S.; Dowty, M.E.; Wang, L.; Malhotra, B.K. Effects of hepatic impairment on the pharmacokinetics of abrocitinib and its metabolites. *J. Clin. Pharmacol.* **2021**, *61*, 1311–1323. [CrossRef] [PubMed]
77. European Medicines Agency EMA/MB/69923/2010, Abrocitinib Assessment Report. Available online: [https://www.ema.europa.eu/en/documents/assessment-report/cibinqo-epar-public-assessment-report\\_en.pdf](https://www.ema.europa.eu/en/documents/assessment-report/cibinqo-epar-public-assessment-report_en.pdf) (accessed on 14 February 2022).
78. FDA Fact Sheet for Healthcare Providers Emergency use Authorization (EUA) of Baricitinib. Available online: <https://www.fda.gov/media/143823/download> (accessed on 20 April 2022).
79. Rodgers, J.D.; Shepard, S. Azetidine and Cyclobutane Derivatives as JAK Inhibitors. US Patent 8,158,616, 17 April 2012.
80. Xu, J.; Cai, J.; Chen, J.; Zong, X.; Wu, X.; Ji, M.; Wang, P. An efficient synthesis of baricitinib. *J. Chem. Res.* **2016**, *40*, 205–208. [CrossRef]
81. Azad, M.A.K.; Pandey, G.; Singh, K.; Prasad, M. Process for the Preparation of Baricitinib and an Intermediate Thereof. U.S. Patent US10526350B2, 7 January 2020.
82. Cui, X.; Du, J.; Jia, Z.; Wang, X.; Jia, H. A green and facile synthesis of an industrially important quaternary heterocyclic intermediates for baricitinib. *BMC Chem.* **2019**, *13*, 123. [CrossRef] [PubMed]
83. Clark, J.D.; Flanagan, M.E.; Telliez, J.-B. Discovery and development of Janus kinase (JAK) inhibitors for inflammatory diseases. *J. Med. Chem.* **2014**, *57*, 5023–5038. [CrossRef]
84. Sorrell, F.J.; Szklarz, M.; Abdul Azeez, K.R.; Elkins, J.M.; Knapp, S. Family-wide structural analysis of human numb-associated protein kinases. *Structure* **2016**, *24*, 401–411. [CrossRef]
85. Davis, R.R.; Li, B.; Yun, S.Y.; Chan, A.; Nareddy, P.; Gunawan, S.; Ayaz, M.; Lawrence, H.R.; Reuther, G.W.; Lawrence, N.J.; et al. Structural insights into JAK2 inhibition by ruxolitinib, fedratinib, and derivatives thereof. *J. Med. Chem.* **2021**, *64*, 2228–2241. [CrossRef]
86. Chang, Y.; Min, J.; Jarusiewicz, J.; Actis, M.; Bradford, S.Y.-C.; Mayasundari, A.; Yang, L.; Chepyala, D.; Alcock, L.J.; Roberts, K.G.; et al. Degradation of Janus kinases in CRLF2-rearranged acute lymphoblastic leukemia. *Blood.* **2021**, *138*, 2313–2326. [CrossRef] [PubMed]
87. Wan, M.; Cao, X. BMP signaling in skeletal development. *Biochem. Biophys. Res. Commun.* **2005**, *328*, 651–657. [CrossRef] [PubMed]
88. Al-Salama, Z.T.; Scott, L.J. Baricitinib: A review in rheumatoid arthritis. *Drugs* **2018**, *78*, 761–772. [CrossRef] [PubMed]
89. Wallace, D.J.; Furie, R.A.; Tanaka, Y.; Kalunian, K.C.; Mosca, M.; Petri, M.A.; Dörner, T.; Cardiel, M.H.; Bruce, I.N.; Gomez, E.; et al. Baricitinib for systemic lupus erythematosus: A double-blind, randomised, placebo-controlled, phase 2 trial. *Lancet* **2018**, *392*, 222–231. [CrossRef]
90. Guttman-Yassky, E.; Silverberg, J.I.; Nemoto, O.; Forman, S.B.; Wilke, A.; Prescilla, R.; de la Peña, A.; Nunes, F.P.; Janes, J.; Gamalo, M.; et al. Baricitinib in adult patients with moderate-to-severe atopic dermatitis: A phase 2 parallel, double-blinded, randomized placebo-controlled multiple-dose study. *J. Am. Acad. Dermatol.* **2019**, *80*, 913–921.e9. [CrossRef]
91. Hasan, M.J.; Rabbani, R.; Anam, A.M.; Huq, S.M.R. Additional baricitinib loading dose improves clinical outcome in COVID-19. *Open Med.* **2021**, *16*, 41–46. [CrossRef]
92. Kalil, A.C.; Patterson, T.F.; Mehta, A.K.; Tomashek, K.M.; Wolfe, C.R.; Ghazaryan, V.; Marconi, V.C.; Ruiz-Palacios, G.M.; Hsieh, L.; Kline, S.; et al. Baricitinib plus remdesivir for hospitalized adults with COVID-19. *N. Engl. J. Med.* **2020**, *384*, 795–807. [CrossRef]
93. Izumo, T.; Kuse, N.; Awano, N.; Tone, M.; Sakamoto, K.; Takada, K.; Muto, Y.; Fujimoto, K.; Saiki, A.; Ito, Y.; et al. Clinical impact of combination therapy with baricitinib, remdesivir, and dexamethasone in patients with severe COVID-19. *Respir. Investig.* **2021**, *59*, 799–803. [CrossRef]
94. Eli Lilly & Co. Baricitinib. U.S. Food and Drug Administration Website. Available online: [https://www.accessdata.fda.gov/drugsatfda\\_docs/nda/2018/207924Orig1s000PharmR.pdf](https://www.accessdata.fda.gov/drugsatfda_docs/nda/2018/207924Orig1s000PharmR.pdf) (accessed on 16 February 2022).
95. Eli Lilly Australia Pty Ltd. Olumiant Australian Public Assessment Report for Baricitinib. Available online: <https://www.tga.gov.au/sites/default/files/auspar-baricitinib-190321.pdf> (accessed on 16 February 2022).
96. Noji, S.; Hara, Y.; Miura, T.; Yamanaka, H.; Maeda, K.; Hori, A.; Yamamoto, H.; Obika, S.; Inoue, M.; Hase, Y.; et al. Discovery of a Janus kinase inhibitor bearing a highly three-dimensional spiro scaffold: JTE-052 (delgocitinib) as a new dermatological agent to treat inflammatory skin disorders. *J. Med. Chem.* **2020**, *63*, 7163–7185. [CrossRef]
97. Takiguchi, H.; Higashi, A.; Watanabe, T.; Takeichi, T.; Shimazaki, T.; Inaba, T. Stereocontrolled synthesis of delgocitinib, a JAK inhibitor for the treatment of atopic dermatitis. *Org. Process Res. Dev.* **2021**, *25*, 342–348. [CrossRef]

98. Nakagawa, H.; Nemoto, O.; Igarashi, A.; Saeki, H.; Kaino, H.; Nagata, T. Delgocitinib ointment, a topical Janus kinase inhibitor, in adult patients with moderate to severe atopic dermatitis: A phase 3, randomized, double-blind, vehicle-controlled study and an open-label, long-term extension study. *J. Am. Acad. Dermatol.* **2020**, *82*, 823–831. [CrossRef] [PubMed]
99. Tanimoto, A.; Ogawa, Y.; Oki, C.; Kimoto, Y.; Nozawa, K.; Amano, W.; Noji, S.; Shiozaki, M.; Matsuo, A.; Shinozaki, Y.; et al. Pharmacological properties of JTE-052: A novel potent JAK inhibitor that suppresses various inflammatory responses in vitro and in vivo. *Inflamm. Res.* **2015**, *64*, 41–51. [CrossRef] [PubMed]
100. Worm, M.; Bauer, A.; Elsner, P.; Mahler, V.; Molin, S.; Nielsen, T.S.S. Efficacy and safety of topical delgocitinib in patients with chronic hand eczema: Data from a randomized, double-blind, vehicle-controlled phase IIa study. *Br. J. Dermatol.* **2020**, *182*, 1103–1110. [CrossRef] [PubMed]
101. Xie, Z.; Yang, X.; Duan, Y.; Han, J.; Liao, C. Small-molecule kinase inhibitors for the treatment of nononcologic diseases. *J. Med. Chem.* **2021**, *64*, 1283–1345. [CrossRef]
102. Nakagawa, H.; Nemoto, O.; Yamada, H.; Nagata, T.; Ninomiya, N. Phase 1 studies to assess the safety, tolerability and pharmacokinetics of JTE-052 (a novel Janus kinase inhibitor) ointment in Japanese healthy volunteers and patients with atopic dermatitis. *J. Dermatol.* **2018**, *45*, 701–709. [CrossRef]
103. Japan Tobacco Inc. Report on the Deliberation Results, Corectim Ointment 0.5% (Delgocitinib). Available online: <https://www.pmda.go.jp/files/000240793.pdf> (accessed on 16 February 2022).
104. Flick, A.C.; Leverett, C.A.; Ding, H.X.; McInturff, E.; Fink, S.J.; Mahapatra, S.; Carney, D.W.; Lindsey, E.A.; DeForest, J.C.; France, S.P.; et al. Synthetic approaches to the new drugs approved during 2019. *J. Med. Chem.* **2021**, *64*, 3604–3657. [CrossRef]
105. Wang, Y.; Li, H. Diphenylaminopyrimidine Compound for Inhibiting Kinase Activity. U.S. Patent US20200071303A1, 5 March 2020.
106. Noronha, G.; Mak, C.C.; Cao, J.; Renick, J.; McPherson, A.; Zeng, B.; Pathak, V.P.; Lohse, D.L.; Hood, J.D.; Soll, R.M. Preparation of Pyrimidine Derivatives as JAK Kinases Inhibitors. U.S. Patent US20110212077A1, 1 September 2011.
107. Tefferi, A. N-tert-Butyl-3-[(5-methyl-2-[[4-(2-pyrrolidin-1-yl)ethoxy]phenyl]amino)pyrimidin-4-yl]amino]benzenesulfonamide for treating myelofibrosis. WO2012060847A1, 10 May 2012.
108. Ciceri, P.; Müller, S.; O'Mahony, A.; Fedorov, O.; Filippakopoulos, P.; Hunt, J.P.; Lasater, E.A.; Pallares, G.; Picaud, S.; Wells, C.; et al. Dual kinase-bromodomain inhibitors for rationally designed polypharmacology. *Nat. Chem. Biol.* **2014**, *10*, 305–312. [CrossRef]
109. Ember, S.W.J.; Zhu, J.-Y.; Olesen, S.H.; Martin, M.P.; Becker, A.; Berndt, N.; Georg, G.I.; Schönbrunn, E. Acetyl-lysine binding site of bromodomain-containing protein 4 (BRD4) interacts with diverse kinase inhibitors. *ACS Chem. Biol.* **2014**, *9*, 1160–1171. [CrossRef]
110. Talpaz, M.; Kiladjian, J.-J. Fedratinib, a newly approved treatment for patients with myeloproliferative neoplasm-associated myelofibrosis. *Leukemia* **2021**, *35*, 1–17. [CrossRef]
111. Poubel, C.P.; Mansur, M.B.; Boroni, M.; Emerenciano, M. FLT3 overexpression in acute leukaemias: New insights into the search for molecular mechanisms. *Biochim. Biophys. Acta Rev. Cancer* **2019**, *1872*, 80–88. [CrossRef]
112. Muller, S.; Filippakopoulos, P.; Knapp, S. Bromodomains as therapeutic targets. *Expert Rev. Mol. Med.* **2011**, *13*, e29. [CrossRef] [PubMed]
113. Ogasawara, K.; Xu, C.; Kanamaluru, V.; Siebers, N.; Surapaneni, S.; Ridoux, L.; Palmisano, M.; Krishna, G. Excretion balance and pharmacokinetics following a single oral dose of [<sup>14</sup>C]-fedratinib in healthy subjects. *Cancer Chemother. Pharmacol.* **2020**, *86*, 307–314. [CrossRef] [PubMed]
114. Menet, C.J.M.; van Rompaey, L.J.C.; Robert, S.; Blanc, J.; Jouannigot, N.; Hodges, A.J.; Smits, K.K. Novel Compounds Useful for the Treatment of Degenerative and Inflammatory Diseases. WO2010010190A1, 28 January 2021.
115. Ayala-Aguilera, C.C.; Valero, T.; Lorente-Macías, Á.; Baillache, D.J.; Croke, S.; Unciti-Broceta, A. Small molecule kinase inhibitor drugs (1995–2021): Medical indication, pharmacology, and synthesis. *J. Med. Chem.* **2021**, *65*, 1047–1131. [CrossRef] [PubMed]
116. Van Rompaey, L.; Galien, R.; van der Aar, E.M.; Clement-Lacroix, P.; Nelles, L.; Smets, B.; Lepescheux, L.; Christophe, T.; Conrath, K.; Vandeghinste, N.; et al. Preclinical characterization of GLPG0634, a selective inhibitor of JAK1, for the treatment of inflammatory diseases. *J. Immunol.* **2013**, *191*, 3568–3577. [CrossRef] [PubMed]
117. Menet, C.J.; Fletcher, S.R.; Van Lommen, G.; Geney, R.; Blanc, J.; Smits, K.; Jouannigot, N.; Deprez, P.; van der Aar, E.M.; Clement-Lacroix, P.; et al. Triazolopyridines as selective JAK1 inhibitors: From hit identification to GLPG0634. *J. Med. Chem.* **2014**, *57*, 9323–9342. [CrossRef] [PubMed]
118. Newton, A.S.; Deiana, L.; Puleo, D.E.; Cisneros, J.A.; Cutrona, K.J.; Schlessinger, J.; Jorgensen, W.L. JAK2 JH2 Fluorescence polarization assay and crystal structures for complexes with three small molecules. *ACS Med. Chem. Lett.* **2017**, *8*, 614–617. [CrossRef]
119. Norman, P. Selective JAK inhibitors in development for rheumatoid arthritis. *Expert Opin. Investig. Drugs* **2014**, *23*, 1067–1077. [CrossRef] [PubMed]
120. Vanhoutte, F.; Mazur, M.; Voloshyn, O.; Stanislavchuk, M.; Van der Aa, A.; Namour, F.; Galien, R.; Meuleners, L.; van 't Klooster, G. Efficacy, safety, pharmacokinetics, and pharmacodynamics of filgotinib, a selective JAK-1 inhibitor, after short-term treatment of rheumatoid arthritis: Results of two randomized phase IIa trials. *Arthritis Rheumatol.* **2017**, *69*, 1949–1959. [CrossRef] [PubMed]



121. Westhovens, R.; Taylor, P.C.; Alten, R.; Pavlova, D.; Enríquez-Sosa, F.; Mazur, M.; Greenwald, M.; Van der Aa, A.; Vanhoutte, F.; Tasset, C.; et al. Filgotinib (GLPG0634/GS-6034), an oral JAK1 selective inhibitor, is effective in combination with methotrexate (MTX) in patients with active rheumatoid arthritis and insufficient response to MTX: Results from a randomised, dose-finding study (DARWIN 1). *Ann. Rheum. Dis.* **2017**, *76*, 998–1008. [CrossRef] [PubMed]
122. Labetoulle, R.; Paul, S.; Roblin, X. Filgotinib for the treatment of Crohn's disease. *Expert Opin. Investig. Drugs* **2018**, *27*, 295–300. [CrossRef] [PubMed]
123. Vermeire, S.; Schreiber, S.; Petryka, R.; Kuehbacher, T.; Hebuterne, X.; Roblin, X.; Klopocka, M.; Goldis, A.; Wisniewska-Jarosinska, M.; Baranovsky, A.; et al. Clinical remission in patients with moderate-to-severe Crohn's disease treated with filgotinib (the FITZROY study): Results from a phase 2, double-blind, randomised, placebo-controlled trial. *Lancet* **2017**, *389*, 266–275. [CrossRef]
124. Feagan, B.G.; Danese, S.; Loftus, E.V.J.; Vermeire, S.; Schreiber, S.; Ritter, T.; Fogel, R.; Mehta, R.; Nijhawan, S.; Kempinski, R.; et al. Filgotinib as induction and maintenance therapy for ulcerative colitis (SELECTION): A phase 2b/3 double-blind, randomised, placebo-controlled trial. *Lancet* **2021**, *397*, 2372–2384. [CrossRef]
125. Mease, P.; Coates, L.C.; Helliwell, P.S.; Stanislavchuk, M.; Rychlewska-Hanczewska, A.; Dudek, A.; Abi-Saab, W.; Tasset, C.; Meuleners, L.; Harrison, P.; et al. Efficacy and safety of filgotinib, a selective Janus kinase 1 inhibitor, in patients with active psoriatic arthritis (EQUATOR): Results from a randomised, placebo-controlled, phase 2 trial. *Lancet* **2018**, *392*, 2367–2377. [CrossRef]
126. Namour, F.; Diderichsen, P.M.; Cox, E.; Vayssière, B.; Van der Aa, A.; Tasset, C.; Van't Klooster, G. Pharmacokinetics and pharmacokinetic/pharmacodynamic modeling of filgotinib (GLPG0634), a selective JAK1 inhibitor, in support of phase IIB dose selection. *Clin. Pharmacokinet.* **2015**, *54*, 859–874. [CrossRef] [PubMed]
127. Van't Klooster, G.A.E.; Brys, R.C.X.; Van Rompaey, L.J.C.; Namour, F.S. Aminotriazolopyridine for Use in the Treatment of Inflammation, and Pharmaceutical Compositions Thereof. WO2013189771A1, 27 December 2013.
128. Namour, F.; Desrivot, J.; Van der Aa, A.; Harrison, P.; Tasset, C.; van't Klooster, G. Clinical confirmation that the selective JAK1 inhibitor filgotinib (GLPG0634) has a low liability for drug-drug interactions. *Drug Metab. Lett.* **2016**, *10*, 38–48. [CrossRef] [PubMed]
129. Gonzales, A.J.; Bowman, J.W.; Fici, G.J.; Zhang, M.; Mann, D.W.; Mitton-Fry, M. Oclacitinib (APOQUEL®) is a novel Janus kinase inhibitor with activity against cytokines involved in allergy. *J. Vet. Pharmacol. Ther.* **2014**, *37*, 317–324. [CrossRef] [PubMed]
130. Berlinski, P.J.; Birchmeier, M.J.; Bowman, J.W.; Gonzales, A.J.; Kamerling, S.G.; Mann, D.W.; Mitton-Fry, M.J. Pyrrolo[2,3-d]Pyrimidine Compounds. WO2010020905A1, 25 February 2010.
131. Haugh, I.M.; Watson, I.T.; Alan Menter, M. Successful treatment of atopic dermatitis with the JAK1 inhibitor oclacitinib. *Bayl. Univ. Med. Cent. Proc.* **2018**, *31*, 524–525. [CrossRef] [PubMed]
132. Cosgrove, S.B.; Wren, J.A.; Cleaver, D.M.; Martin, D.D.; Walsh, K.F.; Harfst, J.A.; Follis, S.L.; King, V.L.; Boucher, J.F.; Stegemann, M.R. Efficacy and safety of oclacitinib for the control of pruritus and associated skin lesions in dogs with canine allergic dermatitis. *Vet. Dermatol.* **2013**, *24*, 479–e114. [CrossRef] [PubMed]
133. Rynhoud, H.; Gibson, J.S.; Meler, E.; Soares Magalhães, R.J. The association between the use of oclacitinib and antibacterial therapy in dogs with allergic dermatitis: A retrospective case-control study. *Front. Vet. Sci.* **2021**, *8*, 631443. [CrossRef] [PubMed]
134. Banovic, F.; Tarigo, J.; Gordon, H.; Barber, J.P.; Gogal, R.M.J. Immunomodulatory in vitro effects of oclacitinib on canine T-cell proliferation and cytokine production. *Vet. Dermatol.* **2019**, *30*, 17–e6. [CrossRef] [PubMed]
135. De Caro Martins, G.; da Costa-Val, A.P.; Coura, F.M.; Diamantino, G.M.L.; Nogueira, M.M.; de Oliveira Melo-Junior, O.A.; Giunchetti, R.C.; da Silveira-Lemos, D.; Melo, M.M. Immunomodulatory effect of long-term oclacitinib maleate therapy in dogs with atopic dermatitis. *Vet. Dermatol.* **2021**, *33*, 142–e40. [CrossRef] [PubMed]
136. Collard, W.T.; Hummel, B.D.; Fielder, A.F.; King, V.L.; Boucher, J.F.; Mullins, M.A.; Malpas, P.B.; Stegemann, M.R. The pharmacokinetics of oclacitinib maleate, a Janus kinase inhibitor, in the dog. *J. Vet. Pharmacol. Ther.* **2014**, *37*, 279–285. [CrossRef] [PubMed]
137. Zoetis.com APOQUEL®(Oclacitinib Tablet): Fast-Acting and Safe Itch Relief for Dogs. Available online: [https://www.zoetis.com/products/dogs/apoquel/assets/downloadable-resources/1413113\\_m03r\\_apl\\_infosheet\\_fda\\_labelupdate-1\\_\\_new2019.pdf](https://www.zoetis.com/products/dogs/apoquel/assets/downloadable-resources/1413113_m03r_apl_infosheet_fda_labelupdate-1__new2019.pdf) (accessed on 14 February 2022).
138. FDA Approves Drug for Adults with Rare Form of Bone Marrow Disorder. Available online: <https://www.fda.gov/drugs/news-events-human-drugs/fda-approves-drug-adults-rare-form-bone-marrow-disorder> (accessed on 17 April 2022).
139. William, A.D.; Lee, A.C.-H.; Blanchard, S.; Poulsen, A.; Teo, E.L.; Nagaraj, H.; Tan, E.; Chen, D.; Williams, M.; Sun, E.T.; et al. Discovery of the macrocycle 11-(2-pyrrolidin-1-yl-ethoxy)-14,19-dioxo-5,7,26-triaza-tetracyclo[19.3.1.1(2,6).1(8,12)]heptacosal(25),2(26),3,5,8,10,12(27),16,21,23-decaene (SB1518), a potent Janus kinase 2/fms-like tyrosine kinase-3 (JAK2/FLT3) inhibitor. *J. Med. Chem.* **2011**, *54*, 4638–4658. [CrossRef] [PubMed]
140. Singer, J.W.; Al-Fayoumi, S.; Ma, H.; Komrokji, R.S.; Mesa, R.; Verstovsek, S. Comprehensive kinase profile of pacritinib, a nonmyelosuppressive Janus kinase 2 inhibitor. *J. Exp. Pharmacol.* **2016**, *8*, 11–19. [CrossRef]
141. Klaeger, S.; Heinzlmeier, S.; Wilhelm, M.; Polzer, H.; Vick, B.; Koenig, P.-A.; Reinecke, M.; Ruprecht, B.; Petzoldt, S.; Meng, C.; et al. The target landscape of clinical kinase drugs. *Science* **2017**, *358*, eaan4368. [CrossRef] [PubMed]
142. Mesa, R.A.; Vannucchi, A.M.; Mead, A.; Egyed, M.; Szoke, A.; Suvorov, A.; Jakucs, J.; Perkins, A.; Prasad, R.; Mayer, J.; et al. Pacritinib versus best available therapy for the treatment of myelofibrosis irrespective of baseline cytopenias (PERSIST-1): An international, randomised, phase 3 trial. *Lancet. Haematol.* **2017**, *4*, e225–e236. [CrossRef]

143. Mascarenhas, J.; Hoffman, R.; Talpaz, M.; Gerds, A.T.; Stein, B.; Gupta, V.; Szoke, A.; Drummond, M.; Pristupa, A.; Granston, T.; et al. Pacritinib vs best available therapy, including ruxolitinib, in patients with myelofibrosis: A randomized clinical trial. *JAMA Oncol.* **2018**, *4*, 652–659. [CrossRef]
144. Hosseini, M.M.; Kurtz, S.E.; Abdelhamed, S.; Mahmood, S.; Davare, M.A.; Kaempf, A.; Elferich, J.; McDermott, J.E.; Liu, T.; Payne, S.H.; et al. Inhibition of interleukin-1 receptor-associated kinase-1 is a therapeutic strategy for acute myeloid leukemia subtypes. *Leukemia* **2018**, *32*, 2374–2387. [CrossRef]
145. Jeon, J.Y.; Zhao, Q.; Buelow, D.R.; Phelps, M.; Walker, A.R.; Mims, A.S.; Vasu, S.; Behbehani, G.; Blachly, J.; Blum, W.; et al. Preclinical activity and a pilot phase I study of pacritinib, an oral JAK2/FLT3 inhibitor, and chemotherapy in FLT3-ITD-positive AML. *Investig. New Drugs* **2020**, *38*, 340–349. [CrossRef]
146. Jensen, K.V.; Cseh, O.; Aman, A.; Weiss, S.; Luchman, H.A. The JAK2/STAT3 inhibitor pacritinib effectively inhibits patient-derived GBM brain tumor initiating cells in vitro and when used in combination with temozolomide increases survival in an orthotopic xenograft model. *PLoS ONE* **2017**, *12*, e0189670. [CrossRef]
147. Jayaraman, R.; Pasha, M.K.; Williams, A.; Goh, K.C.; Ethirajulu, K. Metabolism and disposition of pacritinib (SB1518), an orally active Janus kinase 2 inhibitor in preclinical species and humans. *Drug Metab. Lett.* **2015**, *9*, 28–47. [CrossRef] [PubMed]
148. Inoue, T.; Tanaka, A.; Nakai, K.; Sasaki, H.; Takahashi, F.; Shirakami, S.; Hatanaka, K.; Nakajima, Y.; Mukoyoshi, K.; Hamaguchi, H.; et al. Heterocyclic Janus Kinase 3 Inhibitors. WO2007077949A1, 12 July 2007.
149. Ito, M.; Yamazaki, S.; Yamagami, K.; Kuno, M.; Morita, Y.; Okuma, K.; Nakamura, K.; Chida, N.; Inami, M.; Inoue, T.; et al. A novel JAK inhibitor, peficitinib, demonstrates potent efficacy in a rat adjuvant-induced arthritis model. *J. Pharmacol. Sci.* **2017**, *133*, 25–33. [CrossRef] [PubMed]
150. Takeuchi, T.; Tanaka, Y.; Iwasaki, M.; Ishikura, H.; Saeki, S.; Kaneko, Y. Efficacy and safety of the oral Janus kinase inhibitor peficitinib (ASP015K) monotherapy in patients with moderate to severe rheumatoid arthritis in Japan: A 12-week, randomised, double-blind, placebo-controlled phase IIb study. *Ann. Rheum. Dis.* **2016**, *75*, 1057–1064. [CrossRef] [PubMed]
151. Hamaguchi, H.; Amano, Y.; Moritomo, A.; Shirakami, S.; Nakajima, Y.; Nakai, K.; Nomura, N.; Ito, M.; Higashi, Y.; Inoue, T. Discovery and structural characterization of peficitinib (ASP015K) as a novel and potent JAK inhibitor. *Bioorg. Med. Chem.* **2018**, *26*, 4971–4983. [CrossRef] [PubMed]
152. Zhang, J.-M.; An, J. Cytokines, inflammation, and pain. *Int. Anesthesiol. Clin.* **2007**, *45*, 27–37. [CrossRef]
153. Takeuchi, T.; Tanaka, Y.; Tanaka, S.; Kawakami, A.; Song, Y.-W.; Chen, Y.-H.; Rokuda, M.; Izutsu, H.; Ushijima, S.; Kaneko, Y. Safety and effectiveness of peficitinib (ASP015K) in patients with rheumatoid arthritis: Final results (32 months of mean peficitinib treatment) from a long-term, open-label extension study in Japan, Korea, and Taiwan. *Rheumatol. Ther.* **2021**, *8*, 425–442. [CrossRef]
154. Genovese, M.C.; Greenwald, M.; Codding, C.; Zubrzycka-Sienkiewicz, A.; Kivitz, A.J.; Wang, A.; Shay, K.; Wang, X.; Garg, J.P.; Cardiel, M.H. Peficitinib, a JAK inhibitor, in combination with limited conventional synthetic disease-modifying antirheumatic drugs in the treatment of moderate-to-severe rheumatoid arthritis. *Arthritis Rheumatol.* **2017**, *69*, 932–942. [CrossRef]
155. Tanaka, Y.; Izutsu, H. Peficitinib for the treatment of rheumatoid arthritis: An overview from clinical trials. *Expert Opin. Pharmacother.* **2020**, *21*, 1015–1025. [CrossRef]
156. Takeuchi, T.; Tanaka, Y.; Tanaka, S.; Kawakami, A.; Song, Y.-W.; Chen, Y.-H.; Rokuda, M.; Izutsu, H.; Ushijima, S.; Kaneko, Y.; et al. Safety and effectiveness of peficitinib (ASP015K) in patients with rheumatoid arthritis: Interim data (22.7 months mean peficitinib treatment) from a long-term, open-label extension study in Japan, Korea, and Taiwan. *Arthritis Res. Ther.* **2020**, *22*, 47. [CrossRef]
157. Kaneko, Y. Efficacy and safety of peficitinib in rheumatoid arthritis. *Mod. Rheumatol.* **2020**, *30*, 773–778. [CrossRef]
158. Oda, K.; Cao, Y.J.; Sawamoto, T.; Nakada, N.; Fisniku, O.; Nagasaka, Y.; Sohda, K.-Y. Human mass balance, metabolite profile and identification of metabolic enzymes of [<sup>14</sup>C]ASP015K, a novel oral janus kinase inhibitor. *Xenobiotica* **2015**, *45*, 887–902. [CrossRef] [PubMed]
159. Miyatake, D.; Shibata, T.; Toyoshima, J.; Kaneko, Y.; Oda, K.; Nishimura, T.; Katashima, M.; Sakaki, M.; Inoue, K.; Ito, T.; et al. Pharmacokinetics and safety of a single oral dose of peficitinib (ASP015K) in Japanese subjects with normal and impaired hepatic function. *Clin. Pharmacol. Drug Dev.* **2020**, *9*, 699–708. [CrossRef] [PubMed]
160. Yang, W.; Zhu, G.; Qin, M.; Li, Z.; Wang, B.; Yang, J.; Wang, T. The effectiveness of ruxolitinib for acute/chronic graft-versus-host disease in children: A retrospective study. *Drug Des. Devel. Ther.* **2021**, *15*, 743–752. [CrossRef] [PubMed]
161. Rodgers, D.J.; Shepard, S. Heteroaryl Substituted Pyrrolo[2,3-b]pyridines and Pyrrolo[2,3-b]pyrimidines as Janus Kinase Inhibitors. U.S. Patent US7598257B2, 16 October 2009.
162. Haydl, A.M.; Xu, K.; Breit, B. Regio- and enantioselective synthesis of N-substituted pyrazoles by rhodium-catalyzed asymmetric addition to allenes. *Angew. Chemie Int. Ed.* **2015**, *54*, 7149–7153. [CrossRef] [PubMed]
163. Lin, Q.; Meloni, D.; Pan, Y.; Xia, M.; Rodgers, J.; Shepard, S.; Li, M.; Galya, L.; Metcalf, B.; Yue, T.-Y.; et al. Enantioselective synthesis of Janus kinase inhibitor INCB018424 via an organocatalytic Aza-Michael reaction. *Org. Lett.* **2009**, *11*, 1999–2002. [CrossRef] [PubMed]
164. Zhou, T.; Georgeon, S.; Moser, R.; Moore, D.J.; Caflisch, A.; Hantschel, O. Specificity and mechanism-of-action of the JAK2 tyrosine kinase inhibitors ruxolitinib and SAR302503 (TG101348). *Leukemia* **2014**, *28*, 404–407. [CrossRef]
165. Duan, Y.; Chen, L.; Chen, Y.; Fan, X. c-Src binds to the cancer drug Ruxolitinib with an active conformation. *PLoS ONE* **2014**, *9*, e106225. [CrossRef]

166. Quintás-Cardama, A.; Vaddi, K.; Liu, P.; Manshouri, T.; Li, J.; Scherle, P.A.; Caulder, E.; Wen, X.; Li, Y.; Waeltz, P.; et al. Preclinical characterization of the selective JAK1/2 inhibitor INCB018424: Therapeutic implications for the treatment of myeloproliferative neoplasms. *Blood* **2010**, *115*, 3109–3117. [CrossRef]
167. Arana Yi, C.; Tam, C.S.; Verstovsek, S. Efficacy and safety of ruxolitinib in the treatment of patients with myelofibrosis. *Future Oncol.* **2015**, *11*, 719–733. [CrossRef]
168. Verstovsek, S.; Mesa, R.A.; Gotlib, J.; Levy, R.S.; Gupta, V.; DiPersio, J.F.; Catalano, J.V.; Deininger, M.; Miller, C.; Silver, R.T.; et al. A double-blind, placebo-controlled trial of ruxolitinib for myelofibrosis. *N. Engl. J. Med.* **2012**, *366*, 799–807. [CrossRef]
169. Tavallai, M.; Booth, L.; Roberts, J.L.; Poklepovic, A.; Dent, P. Rationally repurposing ruxolitinib (Jakafi (®)) as a solid tumor therapeutic. *Front. Oncol.* **2016**, *6*, 142. [CrossRef]
170. Kim, B.S.; Howell, M.D.; Sun, K.; Papp, K.; Nasir, A.; Kuligowski, M.E. Treatment of atopic dermatitis with ruxolitinib cream (JAK1/JAK2 inhibitor) or triamcinolone cream. *J. Allergy Clin. Immunol.* **2020**, *145*, 572–582. [CrossRef] [PubMed]
171. Papp, K.; Szepietowski, J.C.; Kircik, L.; Toth, D.; Eichenfield, L.F.; Leung, D.Y.M.; Forman, S.B.; Venturanza, M.E.; Sun, K.; Kuligowski, M.E.; et al. Efficacy and safety of ruxolitinib cream for the treatment of atopic dermatitis: Results from 2 phase 3, randomized, double-blind studies. *J. Am. Acad. Dermatol.* **2021**, *85*, 863–872. [CrossRef]
172. Witkoff, B.; Logas, C.M.; Glick, B.P.; Del Rosso, J.Q. JAK inhibitors in the treatment of atopic dermatitis. *Dermatol. Rev.* **2022**, *3*, 20–28. [CrossRef]
173. Sarmiento Maldonado, M.; Ramírez Villanueva, P.; Bertín Cortes-Monroy, P.; Jara Arias, V.; Soto Donoso, K.; Uribe Gonzalez, P.; Ocqueteau Tachini, M.; Perez-Simón, J.A. Compassionate use of ruxolitinib in acute and chronic graft versus host disease refractory both to corticosteroids and extracorporeal photopheresis. *Exp. Hematol. Oncol.* **2017**, *6*, 32. [CrossRef]
174. Przepiorka, D.; Luo, L.; Subramaniam, S.; Qiu, J.; Gudi, R.; Cunningham, L.C.; Nie, L.; Leong, R.; Ma, L.; Sheth, C.; et al. FDA approval summary: Ruxolitinib for treatment of steroid-refractory acute graft-versus-host disease. *Oncologist* **2020**, *25*, e328–e334. [CrossRef] [PubMed]
175. Shilling, A.D.; Nedza, F.M.; Emm, T.; Diamond, S.; McKeever, E.; Punwani, N.; Williams, W.; Arvanitis, A.; Galya, L.G.; Li, M.; et al. Metabolism, excretion, and pharmacokinetics of [14C]INCB018424, a selective Janus tyrosine kinase 1/2 inhibitor, in humans. *Drug Metab. Dispos.* **2010**, *38*, 2023–2031. [CrossRef]
176. Shi, J.G.; Chen, X.; Emm, T.; Scherle, P.A.; McGee, R.F.; Lo, Y.; Landman, R.R.; McKeever, E.G.J.; Punwani, N.G.; Williams, W.V.; et al. The effect of CYP3A4 inhibition or induction on the pharmacokinetics and pharmacodynamics of orally administered ruxolitinib (INCB018424 phosphate) in healthy volunteers. *J. Clin. Pharmacol.* **2012**, *52*, 809–818. [CrossRef]
177. Aschenbrenner, D.S. Tofacitinib trial prompts FDA review of adverse effects. *Am. J. Nurs.* **2019**, *119*, 25. [CrossRef]
178. Berbert Ferreira, S.; Berbert Ferreira, R.; Neves Neto, A.C.; Assef, S.M.C.; Scheinberg, M. Topical tofacitinib: A Janus kinase inhibitor for the treatment of vitiligo in an adolescent patient. *Case Rep. Dermatol.* **2021**, *13*, 190–194. [CrossRef]
179. Kostik, M.M.; Raupov, R.K.; Suspitsin, E.N.; Isupova, E.A.; Gaidar, E.V.; Gabrusskaya, T.V.; Kaneva, M.A.; Snegireva, L.S.; Likhacheva, T.S.; Miulkidzhan, R.S.; et al. The safety and efficacy of tofacitinib in 24 cases of pediatric rheumatic diseases: Single centre experience. *Front. Pediatr.* **2022**, *10*, 820586. [CrossRef] [PubMed]
180. Mohanakrishnan, R.; Beier, S.; Deodhar, A. Tofacitinib for the treatment of active ankylosing spondylitis in adults. *Expert Rev. Clin. Immunol.* **2022**, *18*, 273–280. [CrossRef] [PubMed]
181. Blumenkopf, T.A.; Flanagan, M.E.; Munchhof, M.J. Pyrrolo[2,3-d]pyrimidine Compounds. U.S. Patent US6956041B2, 18 October 2005.
182. Cai, W.; Colony, J.L.; Frost, H.; Hudspeth, J.P.; Kendall, P.M.; Krishnan, A.M.; Makowski, T.; Mazur, D.J.; Phillips, J.; Ripin, D.H.B.; et al. Investigation of practical routes for the kilogram-scale production of cis-3-methylamino-4-methylpiperidines. *Org. Process Res. Dev.* **2005**, *9*, 51–56. [CrossRef]
183. Williams, N.K.; Bamert, R.S.; Patel, O.; Wang, C.; Walden, P.M.; Wilks, A.F.; Fantino, E.; Rossjohn, J.; Lucet, I.S. Dissecting specificity in the Janus kinases: The structures of JAK-specific inhibitors complexed to the JAK1 and JAK2 protein tyrosine kinase domains. *J. Mol. Biol.* **2009**, *387*, 219–232. [CrossRef] [PubMed]
184. Chrencik, J.E.; Patny, A.; Leung, I.K.; Korniski, B.; Emmons, T.L.; Hall, T.; Weinberg, R.A.; Gormley, J.A.; Williams, J.M.; Day, J.E.; et al. Structural and thermodynamic characterization of the TYK2 and JAK3 kinase domains in complex with CP-690550 and CMP-6. *J. Mol. Biol.* **2010**, *400*, 413–433. [CrossRef]
185. Chamberlain, P.; Delker, S.; Pagarigan, B.; Mahmoudi, A.; Jackson, P.; Abbasian, M.; Muir, J.; Raheja, N.; Cathers, B. Crystal structures of PRK1 in complex with the clinical compounds lestaurtinib and tofacitinib reveal ligand induced conformational changes. *PLoS ONE* **2014**, *9*, e103638. [CrossRef]
186. Fleischmann, R.; Kremer, J.; Cush, J.; Schulze-Koops, H.; Connell, C.A.; Bradley, J.D.; Gruben, D.; Wallenstein, G.V.; Zwillich, S.H.; Kanik, K.S. Placebo-controlled trial of tofacitinib monotherapy in rheumatoid arthritis. *N. Engl. J. Med.* **2012**, *367*, 495–507. [CrossRef]
187. Van Vollenhoven, R.F.; Fleischmann, R.; Cohen, S.; Lee, E.B.; García Meijide, J.A.; Wagner, S.; Forejtova, S.; Zwillich, S.H.; Gruben, D.; Koncz, T.; et al. Tofacitinib or Adalimumab versus Placebo in Rheumatoid Arthritis. *N. Engl. J. Med.* **2012**, *367*, 508–519. [CrossRef] [PubMed]
188. Van der Heijde, D.; Tanaka, Y.; Fleischmann, R.; Keystone, E.; Kremer, J.; Zerbini, C.; Cardiel, M.H.; Cohen, S.; Nash, P.; Song, Y.-W.; et al. Tofacitinib (CP-690,550) in patients with rheumatoid arthritis receiving methotrexate: Twelve-month data from a twenty-four-month phase III randomized radiographic study. *Arthritis Rheum.* **2013**, *65*, 559–570. [CrossRef]

189. Gladman, D.; Rigby, W.; Azevedo, V.F.; Behrens, F.; Blanco, R.; Kaszuba, A.; Kudlacz, E.; Wang, C.; Menon, S.; Hendrikx, T.; et al. Tofacitinib for psoriatic arthritis in patients with an inadequate response to TNF inhibitors. *N. Engl. J. Med.* **2017**, *377*, 1525–1536. [CrossRef]
190. Mease, P.; Hall, S.; FitzGerald, O.; van der Heijde, D.; Merola, J.F.; Avila-Zapata, F.; Cieślak, D.; Graham, D.; Wang, C.; Menon, S.; et al. Tofacitinib or adalimumab versus placebo for psoriatic arthritis. *N. Engl. J. Med.* **2017**, *377*, 1537–1550. [CrossRef] [PubMed]
191. Sandborn, W.J.; Ghosh, S.; Panes, J.; Vranic, I.; Su, C.; Rousell, S.; Niezychowski, W. Tofacitinib, an oral Janus kinase inhibitor, in active ulcerative colitis. *N. Engl. J. Med.* **2012**, *367*, 616–624. [CrossRef] [PubMed]
192. Huang, Z.; Lee, P.Y.; Yao, X.; Zheng, S.; Li, T. Tofacitinib treatment of refractory systemic juvenile idiopathic arthritis. *Pediatrics* **2019**, *143*, e20182845. [CrossRef] [PubMed]
193. Dowty, M.E.; Lin, J.; Ryder, T.F.; Wang, W.; Walker, G.S.; Vaz, A.; Chan, G.L.; Krishnaswami, S.; Prakash, C. The pharmacokinetics, metabolism, and clearance mechanisms of tofacitinib, a Janus kinase inhibitor, in humans. *Drug Metab. Dispos.* **2014**, *42*, 759–773. [CrossRef]
194. Guo, X.; Li, W.; Li, Q.; Chen, Y.; Zhao, G.; Peng, Y.; Zheng, J. Tofacitinib is a mechanism-based inactivator of cytochrome P450 3A4. *Chem. Res. Toxicol.* **2019**, *32*, 1791–1800. [CrossRef]
195. Muensterman, E.; Engelhardt, B.; Gopalakrishnan, S.; Anderson, J.K.; Mohamed, M.-E.F. Upadacitinib pharmacokinetics and exposure-response analyses of efficacy and safety in psoriatic arthritis patients—Analyses of phase III clinical trials. *Clin. Transl. Sci.* **2022**, *15*, 267–278. [CrossRef]
196. AbbVie U.S. FDA Approves RINVOQ®(Upadacitinib) to Treat Adults and Children 12 Years and Older with Refractory, Moderate to Severe Atopic Dermatitis. Available online: <https://news.abbvie.com/news/press-releases/us-fda-approves-rinvoq-upadacitinib-to-treat-adults-and-children-12-years-and-older-with-refractory-moderate-to-severe-atopic-dermatitis.htm#:~:text=14%2C2022%2FPRNewswire%2F> (accessed on 20 April 2022).
197. AbbVie RINVOQ®(Upadacitinib) Receives FDA Approval for the Treatment of Adults with Moderately to Severely Active Ulcerative Colitis. Available online: <https://news.abbvie.com/news/press-releases/rinvoq-upadacitinib-receives-fda-approval-for-treatment-adults-with-moderately-to-severely-active-ulcerative-colitis.htm> (accessed on 19 April 2022).
198. Allian, A.; Jayanth, J.; Mohamed, M.-E.; Mulhern, M.; Nordstroem, L.F.; Othman, A.; Rozema, M.; Bhagavatula, L.; Marroum, P.J.; Mayer, P.T. Processes for the Preparation of (3S,4R)-3-Ethyl-4-(3H-Imidazo[1,2-a]Pyrrolo[2,3-e]-Pyrazin-8-yl)-N-(2,2,2-Trifluoroethyl)Pyrrolidine-1-Carboxamide and Solid State Forms Thereof. WO2017066775A1, 20 April 2017.
199. Parmentier, J.M.; Voss, J.; Graff, C.; Schwartz, A.; Argiriadi, M.; Friedman, M.; Camp, H.S.; Padley, R.J.; George, J.S.; Hyland, D.; et al. In vitro and in vivo characterization of the JAK1 selectivity of upadacitinib (ABT-494). *BMC Rheumatol.* **2018**, *2*, 23. [CrossRef]
200. Padda, I.S.; Bhatt, R.; Parmar, M. *Upadacitinib*; StatPearls Publishing: Treasure Island, FL, USA, 2021.
201. Strand, V.; Mease, P.J.; Soriano, E.R.; Kishimoto, M.; Salvarani, C.; Saffore, C.D.; Zueger, P.; McDearmon-Blondell, E.; Kato, K.; Gladman, D.D. Improvement in patient-reported outcomes in patients with psoriatic arthritis treated with upadacitinib versus placebo or adalimumab: Results from SELECT-PsA 1. *Rheumatol. Ther.* **2021**, *8*, 1789–1808. [CrossRef]
202. Serhal, L.; Edwards, C.J. Upadacitinib for the treatment of rheumatoid arthritis. *Expert Rev. Clin. Immunol.* **2019**, *15*, 13–25. [CrossRef]
203. Bergman, M.; Tundia, N.; Yang, M.; Orvis, E.; Clewell, J.; Bensimon, A. Economic benefit from improvements in quality of life with upadacitinib: Comparisons with tofacitinib and methotrexate in patients with rheumatoid arthritis. *Adv. Ther.* **2021**, *38*, 5649–5661. [CrossRef]
204. Smolen, J.S.; Pangan, A.L.; Emery, P.; Rigby, W.; Tanaka, Y.; Vargas, J.I.; Zhang, Y.; Damjanov, N.; Friedman, A.; Othman, A.A.; et al. Upadacitinib as monotherapy in patients with active rheumatoid arthritis and inadequate response to methotrexate (select-monotherapy): A randomised, placebo-controlled, double-blind phase 3 study. *Lancet* **2019**, *393*, 2303–2311. [CrossRef]
205. McInnes, I.B.; Anderson, J.K.; Magrey, M.; Merola, J.F.; Liu, Y.; Kishimoto, M.; Jeka, S.; Pacheco-Tena, C.; Wang, X.; Chen, L.; et al. Trial of upadacitinib and adalimumab for psoriatic arthritis. *N. Engl. J. Med.* **2021**, *384*, 1227–1239. [CrossRef]
206. Burmester, G.R.; Winthrop, K.; Blanco, R.; Nash, P.; Goupille, P.; Azevedo, V.F.; Salvarani, C.; Rubbert-Roth, A.; Lesser, E.; Lippe, R.; et al. Safety profile of upadacitinib up to 3 years in psoriatic arthritis: An integrated analysis of two pivotal phase 3 trials. *Rheumatol. Ther.* **2021**, *9*, 521–539. [CrossRef] [PubMed]
207. Funk, P.J.; Perche, P.O.; Singh, R.; Kelly, K.A.; Feldman, S.R. Comparing available JAK inhibitors for treating patients with psoriasis. *Expert Rev. Clin. Immunol.* **2022**, *18*, 281–294. [CrossRef]
208. Blauvelt, A.; Teixeira, H.D.; Simpson, E.L.; Costanzo, A.; De Bruin-Weller, M.; Barbarot, S.; Prajapati, V.H.; Lio, P.; Hu, X.; Wu, T.; et al. Efficacy and safety of upadacitinib vs dupilumab in adults with moderate-to-severe atopic dermatitis: A randomized clinical trial. *JAMA Dermatol.* **2021**, *157*, 1047–1055. [CrossRef] [PubMed]
209. Mohamed, M.-E.F.; Camp, H.S.; Jiang, P.; Padley, R.J.; Asatryan, A.; Othman, A.A. Pharmacokinetics, safety and tolerability of ABT-494, a novel selective JAK 1 inhibitor, in healthy volunteers and subjects with rheumatoid arthritis. *Clin. Pharmacokinet.* **2016**, *55*, 1547–1558. [CrossRef] [PubMed]
210. Mohamed, M.-E.F.; Jungerwirth, S.; Asatryan, A.; Jiang, P.; Othman, A.A. Assessment of effect of CYP3A inhibition, CYP induction, OATP1B inhibition, and high-fat meal on pharmacokinetics of the JAK1 inhibitor upadacitinib. *Br. J. Clin. Pharmacol.* **2017**, *83*, 2242–2248. [CrossRef]

211. Mohamed, M.-E.F.; Klünder, B.; Othman, A.A. Clinical pharmacokinetics of upadacitinib: Review of data relevant to the rheumatoid arthritis indication. *Clin. Pharmacokinet.* **2020**, *59*, 531–544. [CrossRef]
212. Vainchenker, W.; Favale, F. Myelofibrosis, JAK2 inhibitors and erythropoiesis. *Leukemia* **2013**, *27*, 1219–1223. [CrossRef]
213. Wood, H.; Chandler, A.; Nezamololama, N.; Papp, K.; Gooderham, M.J. Safety of Janus kinase (JAK) inhibitors in the short-term treatment of atopic dermatitis. *Int. J. Dermatol.* **2021**. [CrossRef]
214. Minshawi, F.; Lanvermann, S.; McKenzie, E.; Jeffery, R.; Couper, K.; Papoutsopoulou, S.; Roers, A.; Muller, W. The generation of an engineered interleukin-10 protein with improved stability and biological function. *Front. Immunol.* **2020**, *11*, 1794. [CrossRef] [PubMed]
215. Almoallim, H.M.; Alharbi, L.A. Rheumatoid arthritis in Saudi Arabia. *Saudi Med. J.* **2014**, *35*, 1442–1454. [PubMed]
216. Hussain, W.; Janoudi, N.; Noorwali, A.; Omran, N.; Baamer, M.; Assiry, E.H.; Alrayes, H.; Alosaimi, H.; Ibrahim, A.; Gohary, S.; et al. Effect of adalimumab on work ability assessed in rheumatoid arthritis disease patients in Saudi Arabia (AWARDS). *Open Rheumatol. J.* **2015**, *9*, 46–50. [CrossRef]
217. O’Shea, J.J.; Gadina, M. Selective Janus kinase inhibitors come of age. *Nat. Rev. Rheumatol.* **2019**, *15*, 74–75. [CrossRef] [PubMed]
218. Pardanani, A.; Lasho, T.; Smith, G.; Burns, C.J.; Fantino, E.; Tefferi, A. CYT387, a selective JAK1/JAK2 inhibitor: In vitro assessment of kinase selectivity and preclinical studies using cell lines and primary cells from polycythemia vera patients. *Leukemia* **2009**, *23*, 1441–1445. [CrossRef]
219. Sideris, N.; Vakirlis, E.; Tsentemidou, A.; Kourouklidou, A.; Ioannides, D.; Sotiriou, E. Under development JAK inhibitors for dermatologic diseases. *Mediterr. J. Rheumatol.* **2020**, *31*, 137–144. [CrossRef]
220. Ma, J.; Xing, W.; Coffey, G.; Dresser, K.; Lu, K.; Guo, A.; Raca, G.; Pandey, A.; Conley, P.; Yu, H.; et al. Cerdulatinib, a novel dual SYK/JAK kinase inhibitor, has broad anti-tumor activity in both ABC and GCB types of diffuse large B cell lymphoma. *Oncotarget* **2015**, *6*, 43881–43896. [CrossRef]
221. Nogueira, M.; Puig, L.; Torres, T. JAK inhibitors for treatment of psoriasis: Focus on selective TYK2 inhibitors. *Drugs* **2020**, *80*, 341–352. [CrossRef]
222. Schroeder, M.A.; Khoury, H.J.; Jagasia, M.; Ali, H.; Schiller, G.J.; Staser, K.; Choi, J.; Gehrs, L.; Arbushites, M.C.; Yan, Y.; et al. A phase 1 trial of itacitinib, a selective JAK1 inhibitor, in patients with acute graft-versus-host disease. *Blood Adv.* **2020**, *4*, 1656–1669. [CrossRef]
223. Verstovsek, S.; Mesa, R.A.; Salama, M.E.; Li, L.; Pitou, C.; Nunes, F.P.; Price, G.L.; Giles, J.L.; D’Souza, D.N.; Walgren, R.A.; et al. A phase 1 study of the Janus kinase 2 (JAK2)(V617F) inhibitor, gandotinib (LY2784544), in patients with primary myelofibrosis, polycythemia vera, and essential thrombocythemia. *Leuk. Res.* **2017**, *61*, 89–95. [CrossRef]
224. Verstovsek, S.; Odenike, O.; Singer, J.W.; Granston, T.; Al-Fayoumi, S.; Deeg, H.J. Phase 1/2 study of pacritinib, a next generation JAK2/FLT3 inhibitor, in myelofibrosis or other myeloid malignancies. *J. Hematol. Oncol.* **2016**, *9*, 137. [CrossRef] [PubMed]
225. Genovese, M.C.; van Vollenhoven, R.F.; Pacheco-Tena, C.; Zhang, Y.; Kinnman, N. VX-509 (decernotinib), an oral selective JAK-3 inhibitor, in combination with methotrexate in patients with rheumatoid arthritis. *Arthritis Rheumatol.* **2016**, *68*, 46–55. [CrossRef] [PubMed]
226. Tan, L.; Akahane, K.; McNally, R.; Reyskens, K.M.S.E.; Ficarro, S.B.; Liu, S.; Herter-Sprie, G.S.; Koyama, S.; Pattison, M.J.; Labella, K.; et al. Development of selective covalent Janus kinase 3 inhibitors. *J. Med. Chem.* **2015**, *58*, 6589–6606. [CrossRef] [PubMed]
227. Tanaka, Y.; Luo, Y.; O’Shea, J.J.; Nakayamada, S. Janus kinase-targeting therapies in rheumatology: A mechanisms-based approach. *Nat. Rev. Rheumatol.* **2022**, *18*, 133–145. [CrossRef]
228. Jin, W.; Stokes, J.M.; Eastman, R.T.; Itkin, Z.; Zakharov, A.V.; Collins, J.J.; Jaakkola, T.S.; Barzilay, R. Deep learning identifies synergistic drug combinations for treating COVID-19. *Proc. Natl. Acad. Sci. USA* **2021**, *118*, e2105070118. [CrossRef] [PubMed]
229. Sayed Ahmed, H.A.; Merrell, E.; Ismail, M.; Joudeh, A.I.; Riley, J.B.; Shawkat, A.; Habeb, H.; Darling, E.; Goweda, R.A.; Shehata, M.H.; et al. Rationales and uncertainties for aspirin use in COVID-19: A narrative review. *Fam. Med. Community Health* **2021**, *9*, e000741. [CrossRef]
230. Marconi, V.C.; Ramanan, A.V.; de Bono, S.; Kartman, C.E.; Krishnan, V.; Liao, R.; Piruzeli, M.L.B.; Goldman, J.D.; Alatorre-Alexander, J.; de Cassia Pellegrini, R.; et al. Efficacy and safety of baricitinib for the treatment of hospitalised adults with COVID-19 (COV-BARRIER): A randomised, double-blind, parallel-group, placebo-controlled phase 3 trial. *Lancet Respir. Med.* **2021**, *9*, 1407–1418. [CrossRef]
231. Kmietowicz, Z. COVID-19: WHO recommends baricitinib and sotrovimab to treat patients. *BMJ* **2022**, *376*, o97. [CrossRef]
232. Guimarães, P.O.; Quirk, D.; Furtado, R.H.; Maia, L.N.; Saraiva, J.F.; Antunes, M.O.; Kalil Filho, R.; Junior, V.M.; Soeiro, A.M.; Tognon, A.P.; et al. Tofacitinib in patients hospitalized with COVID-19 pneumonia. *N. Engl. J. Med.* **2021**, *385*, 406–415. [CrossRef] [PubMed]
233. Seror, R.; Camus, M.; Salmon, J.-H.; Roux, C.; Dernis, E.; Basch, A.; Germain, V.; Leske, C.; Brousseau, S.; Truchetet, M.-E.; et al. Do JAK inhibitors affect immune response to COVID-19 vaccination? Data from the MAJIK-SFR Registry. *Lancet. Rheumatol.* **2022**, *4*, e8–e11. [CrossRef]

MDPI  
St. Alban-Anlage 66  
4052 Basel  
Switzerland  
[www.mdpi.com](http://www.mdpi.com)

*Pharmaceutics* Editorial Office  
E-mail: [pharmaceutics@mdpi.com](mailto:pharmaceutics@mdpi.com)  
[www.mdpi.com/journal/pharmaceutics](http://www.mdpi.com/journal/pharmaceutics)



Disclaimer/Publisher's Note: The statements, opinions and data contained in all publications are solely those of the individual author(s) and contributor(s) and not of MDPI and/or the editor(s). MDPI and/or the editor(s) disclaim responsibility for any injury to people or property resulting from any ideas, methods, instructions or products referred to in the content.





Academic Open  
Access Publishing

[mdpi.com](http://mdpi.com)

ISBN 978-3-7258-1289-9